

Online ISSN : 2395-602X

Print ISSN : 2395-6011

www.ijrst.com



**Conference
Proceedings**

**National Conference on Development Trends
and Techniques In Chemical and Material**

DTTCMS-2025

10th January 2025

Organized By

**Department of Chemistry, Meharabpura, Tehsil Road,
Achalpur, Dist: Amaravti, Maharashtra, India**

VOLUME 12, ISSUE 7, JANUARY-FEBRUARY-2025

**INTERNATIONAL JOURNAL OF SCIENTIFIC
RESEARCH IN SCIENCE AND TECHNOLOGY**

PEER REVIEWED AND REFEREED INTERNATIONAL SCIENTIFIC RESEARCH JOURNAL

Scientific Journal Impact Factor : 8.627

Email : editor@ijrst.com Website : <http://ijrst.com>



Hon'ble Late. Dadasaheb Alias Shankarrao Sherkar

Shri Jagadamba Vinkar Shikshan Sanstha's
Jagadamba Mahavidyalaya, Achalpur
(NAAC Re-accredited with B Grade)



National Conference on Development Trends and Techniques in Chemical and Material

10th January 2025

Organized by

Shri Jagadamba Vinkar Shikshan Sanstha's
Jagadamba Mahavidyalaya
Department of Chemistry, Meharabpura, Tehsil Road, Achalpur, Dist:
Amaravti, Maharashtra, India

Published By



International Journal of Scientific Research in Science and Technology
Print ISSN: 2395-6011 Online ISSN: 2395-602X

Volume 12, Issue 7, January-February-2025

International Peer Reviewed, Open Access Journal

Published By
Technoscience Academy

website: www.technoscienceacademy.com



Our Inspiration
Hon'ble Late. Dadasaheb Alias Shankarrao Sherkar



Shri Jagadamba Vinkar Shikshan Sanstha's
Jagadamba Mahavidyalaya, Achalpur

(NAAC Re-accredited with B Grade)

Department of Chemistry

Organizes

National Conference

On

Development Trends and Techniques in Chemical and Material Sciences

(DTTCMS-2025)

10th January, 2025

Time- 9 am to 6 pm

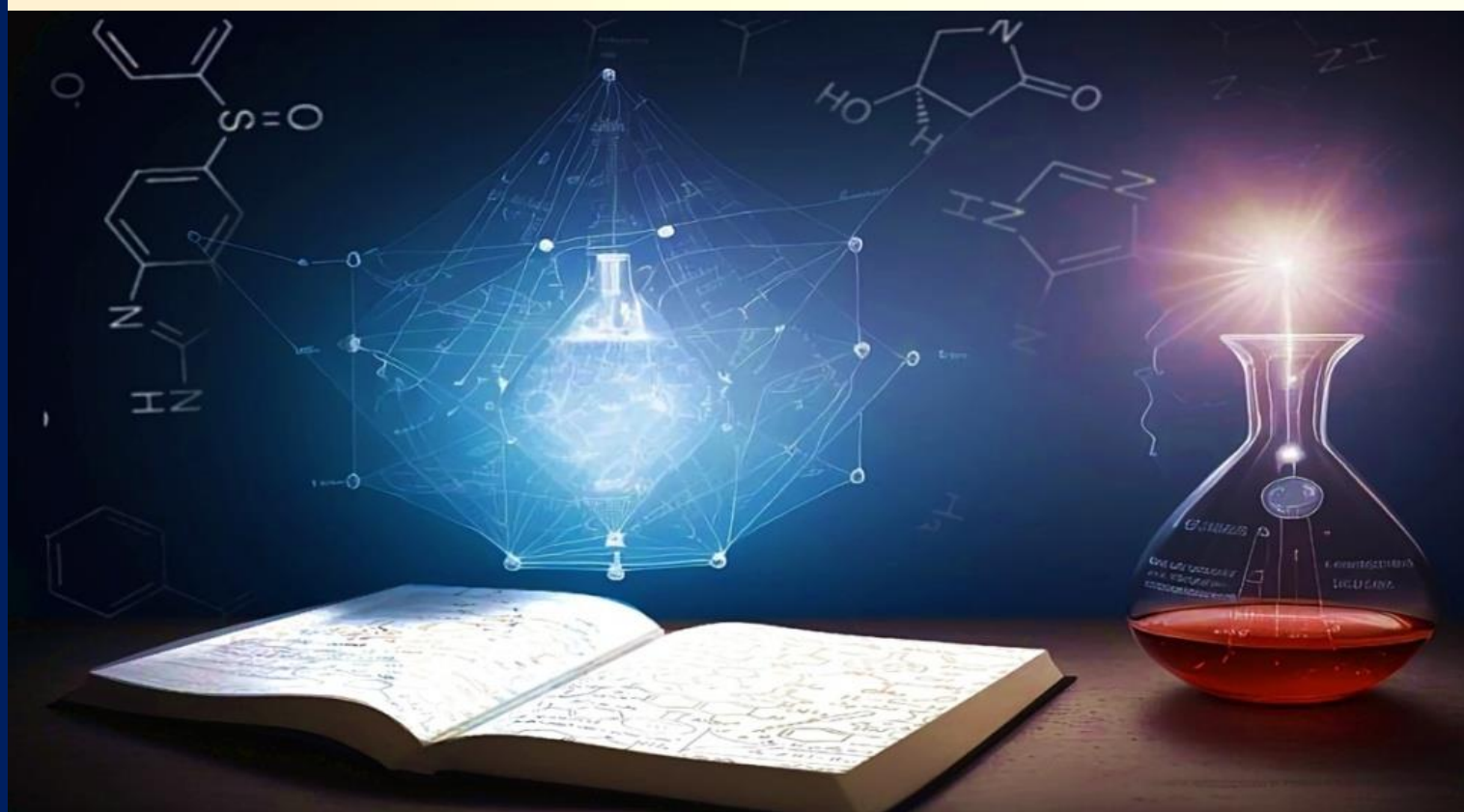
Venue

Conference Hall

Jagadamba Mahavidyalaya, Achalpur (City),

Meharabpura, Tehsil Road, Achalpur

Dist: Amaravti - 444806 (M.S.)



Our Patron



Hon'ble Shri R. S. Sherkar

President, JVSS, Achalpur

Chief Organizer



Dr. A. M. Kohale

**Principal
JMV Achalpur**

Organizing Secretary

Dr. M. S. Lunge

Convener

Dr. P. P. Kalbende

Co-conveners

**Ms. M. H. Shaikh
Dr. N. B. Jadhav
Dr. P. K. Tawalare**

**Dr. P. V. Raut
Dr. D. A. Pund
Dr. S. P. Ingole**

Coordinator

Dr. A. G. Khanderao

Dr. S. S. Padhen

Co-coordinator

**Dr. S. G. Khobragade
Dr. S. A. Waghmare
Dr. A. B. Wadekar**

About Conference:

This conference, "Development Trends and Techniques in Chemistry and Material Sciences", will delve into the forefront of molecular synthesis, exploring the latest advancements and innovative techniques shaping the field. We will study emerging trends in catalyst design and utilization, novel synthetic methodologies for complex molecules, and the application of artificial intelligence and machine learning to accelerate and optimize synthetic pathways. Discussions will encompass a wide range of topics, including green chemistry approaches, flow chemistry and the synthesis of functional materials with tailored properties. The conference aims to foster a collaborative environment where leading researchers, industry experts and students can exchange knowledge and inspire future breakthroughs in molecular synthesis. In addition to the rich exploration of molecular synthesis techniques, the conference will also host workshops and panel discussions designed to engage participants in hands-on learning and collaborative brainstorming. Moreover, the conference will highlight the crucial role of sustainable practices in molecular synthesis. As environmental considerations take center stage in scientific research, participants will engage in discussions about the principles of green chemistry, waste reduction strategies, and the design of safer, more efficient synthetic routes. Sessions will feature case studies demonstrating successful implementations of these principles in real-world applications, providing attendees with valuable insights into how sustainability can be effectively integrated into their work. By prioritizing sustainability alongside technological advancement, the conference will generate meaningful dialogue on the ethical responsibilities of chemists in driving innovation while respecting ecological boundaries.



Celebrating Academic & Research Contribution of Prof. Dr. D.T.Tayade on his Superannuation

Themes of Conference

- Recent Trends and Techniques in Organic, Inorganic and Complex molecules' synthesis.
- Green Synthesis
- Investigations in the studies of effect of synthesized molecules on various microorganism, plants and animals
- Recent Trends and Techniques in Nanotechnology and Nanomolecule Synthesis
- Phytochemistry and Proximate Analysis
- Chemistry of Natural Product
- Medicinal and Pharmaceutical Chemistry
- Recent Trends in Forensic Sciences
- Biological Investigations of Isolated or Synthesized Molecules
- Recent Trends in Computational Chemistry
- Recent Trends and Techniques in Physico-chemical Investigations of Molecules
- Polymer Science and Technology
- Solar and Fuel Cell, Green Energy
- Optoelectronics and Non-Linear Optics
- Luminescence, LED, Photonics
- Magnetism and Spintronics
- Crystal growth
- Quantum Computing and Modeling

Abstract Submission:

Only abstracts from registered candidates will be considered for presentation. Please indicate your choice of presentation format (oral or poster).

Abstract and Full length research paper should be sent to the following email address: dtcms2025@gmail.com.

National Advisory Committee

- Prof. M.V. Basveshwarao, (A.P.)
- Prof. S.G. Warkar (Delhi)
- Prof. S.V. Mohril (M.S.)
- Dr. Dileep Kumar (M.P.)
- Prof. J.J.Bhatt (Gujarat)
- Prof. M. Chand Jaipur (R.J.)
- Prof. M.K. Dwivedi (M.P.)
- Dr. Uma Shankar (Punjab)
- Dr. T.C.Nagawe (M.P.)
- Dr. Raja Ram (R.J.)
- Dr. S.K.Sikarwar (M.P.)
- Dr. S.T.Kozhikode (Kerla)
- Dr. D.S. Turuveli (T.S.)
- Dr. V.V. Wagh (U.P.)
- Dr. Bashir Lone (Kashmir)
- Prof. S.G. Shankarwar (M.S.)
- Prof. S. A. Waghuley (M.S.)
- Prof. S.T. Gaikwad (M.S.)
- Prof. N.S.Karde (M.S.)
- Dr.M.N.Lokande (A.P.)
- Dr. B.J.Lokhande (M.S.)
- Prof. M.R.Lanjewar (M.S.)
- Dr. Mazhar Farooqui (M.S.)
- Prof. Sayyad Husain (M.S.)
- Prof. M. V. Kalambe(M.S.)
- Prof. A. S. Goswami-Giri (M.S.)
- Prof. B.B. Shingte (M.S.)
- Dr. P.R.Rajput (M.S.)
- Prof. A.S.Aswar (M.S.)
- Prof. G.G.Muley (M.S.)
- Dr. S.S. Aswale (M.S.)
- Prof. P.B.Raghuvanshi (M.S.)
- Prof. H. S. Chandak (M.S.)
- Prof. G. R. Dhokane (M.S.)
- Prof. N.S.Thakre (M.S.)
- Dr. M Trivdi (Gujrat)
- Prof. R.G.Weginwar (M.S.)
- Prof. P.K.Rahangdale (M.S.)
- Prof. S.S. Rajput (M.S.)
- Prof. Nitin Dongarwal (M.S.)
- Prof. P.E.Ajamire (M.S.)
- Dr. K.M.Kulkarni (M.S.)
- Dr. N. S. Ugemuge (M.S)

Regional Advisory Committee

- Prof. S.V.Kolhe
- Prof. S.D.Thakur
- Prof. P.S.Bodkhe
- Prof. J.V.Bharad
- Prof. R.P.Ganorkar
- Dr. A.B.Dhote
- Dr. Samreen Farooqui
- Dr. D. M. Nagrik
- Dr. Zakir Khan
- Dr. N. V. Gandhare
- Dr. M.E. Shelke
- Dr. R.S. Shaikh
- Dr. R.C. Panpaliya
- Dr. S.P.Dhakite
- Dr. M.R. Raghuwanshi
- Dr. R.A.Bhagwatkar
- Dr. J.S. Waghmare
- Dr V.M.Raut
- Dr. M. M. Kodape
- Dr. A.M. Kshirsagar
- Dr. A.K.Bhagvatkar
- Dr. K.P. Jumde
- Dr. N.J. Meshram
- Dr. A.S. Shendge
- Dr. A.A. Dhande
- Dr. R.D. Thombare
- Dr. R.D.Isankar
- Dr.S.O.Mohod
- Dr. P.P.Barange
- Dr. P.R. Kale
- Dr. S.R. Khan
- Mr. S.E.Quazi
- Mr. M. Zade
- Dr. M.B.Dhande
- Dr. N.S. Dixit
- Dr. M.P.Wadekar

Local Advisory Committee

- Mr. L.R.Muley
- Dr.G.U.Khapekar
- Dr.P.G.Khapekar
- Dr.S.R.Pande
- Dr.A.S.Rawankar
- Dr.V.P.Deshmukh
- Dr.B.Y.Fugare
- Ms. M.S.Dixit
- Dr.T.A.Khadse
- Mr.D.M.Raut
- Mr.A.A.Pakhare
- Mr.S.C.Darunde
- Mr.D.G.Parate
- Dr.M.S.Shingrup
- Mr.P.S.Dhore
- Prof.B.G.Wankhade
- Dr.S.G.Charjan
- Dr.Imran Ali
- Dr.A.A.Pakhare
- Dr.M.D.Tayade
- Mr.P.A.Tale
- Dr.M.R.Datir
- Dr.K.B.Jogi
- Dr.S.G.Joshi
- Mr.T.K.Wahane
- Dr.V.B.Patil
- Mr.S.G.Gayakwad
- Dr.S.D.Gawali
- Dr.P.A.Vairalkar
- Dr.P.S.Barbde

About the College:

Jagadamba Mahavidyalaya was established by “Shri Jagadamba Vinkar Shikshan Sanstha, Achalpur City” in 1962 with Arts and Commerce faculties with the noble cause of imparting quality higher education to the students in the historical city of Achalpur and the adjoining rural belt, situated at the hilly area and bottom of Melghat region of Satpuda ranges. The hard laboring and visionary weaver community understood the educational need of the region, realized the importance of higher education and took the initiative to establish the college for the promising, poor and students belonging to underprivileged sections of the society. Science faculty was introduced in the college in 1971. The college runs UG and PG courses in Arts, commerce and Science faculties. In order to equip students with entrepreneurial skills and to encourage them for self employment, the college has also started 4 career oriented courses in Instrumentation, Agricultural Marketing, Fish Culture and Tissue Culture. The college boasts of a rich central library with more than 40,000 books. As per the mission statement “*Duritanche Timir Jao*” the Colleges work of imparting education is going on ceaselessly and the college is trying to make itself competent to face the new educational challenges. Our students regularly feature in the University Merit List, bags University Color Coats and participate in various competitions and bring laurels for the college. Jagadamba Mahavidyalaya has helped students to realize their dreams.

About Chemistry Department

The department of Chemistry was established in 1971 is one of the leading department in the field of teaching and research in Chemical sciences. Initially with B.Sc. Programme, keeping pace with advances in various aspects of Chemical sciences, P. G. programme was started in 2010 with organic chemistry specialization. In 2011 department had been recognized as Research Centre for Ph.D. Degree. Since its inception the progress of the department has been inextricably linked with the efforts of former Faculty members to name a few Hon’ble Prof. W. G. Gurharikar, Prof. R. M. Avinashe, Prof. P. J. Bahad, Prof. R. G. Bhangale and Dr. P.G.Rohankar . Even though the department has significantly contributed in various academic and research areas it continuous to strive for excellence. Recently 04 faculties are working in this department namely Dr. P. P. Kalbende, Ms. M. H. Shaikh, Dr. N. B. Jadhao, and Dr. M. S. Lunge.

About the Chikhaldara and Tiger Reserve of Melghat

The sole hill station in the Vidarbha region, it is situated at an altitude of 1118 meters with highest elevation point 1188 meters and has the added dimension of being the only coffee-growing area in Maharashtra. Also, it is well known as Nandanwan of Vidarbha. Next to Chikhaldara, Melghat Tiger Reserve is situated on Gavilgarh Hill, a southern branch of Central India’s Satpuda Hill Range. It is 30 kilometres away from Achalpur. It was founded in 1967 as a wildlife sanctuary and



designated as a tiger reserve in 1974. It was one of the original nine tiger reserves recognised in 1973–1974 as part of Project Tiger, an effort to conserve wildlife launched in India in 1972 with the goal of preserving Bengal tigers. It was Maharashtra’s first tiger reserve. In terms of acreage, it is still one of the largest known as tiger reserves in

the nation. The term “Melghat” refers to the meeting of many “ghats” or valleys, which describes the characteristic topography of this tiger reserve. You can travel to Melghat by road, rail, and air (the nearest airport- is Nagpur). From a tourist’s perspective, Semadoh is the primary location. Another tourist destination in the Melghat Tiger Reserve is Narnala Sanctuary (base camp: Shahnur in the Akola district), where you may go on a jungle safari and see a fortification that dates back at least 600 years.



DTT CMS-2025

CONTENT

SR. NO	ARTICLE/PAPER	PAGE NO
1	Spectral Characterization of Newly Synthesized Azopyrazole Derivatives from Toluidine A P Thakare, A D Bansod	01-05
2	Viscosity and Density Analysis of 1-((4-Methoxy-3, 5- Dimethylpyridin-2-Yl) Methyl) Thiourea in Ethanol- Water Binary Mixtures A. P. Pachkawade, S. A. Wani, R. N. Bhagat	06-10
3	Determination of ΔH, ΔS and ΔG of [MDA] and [EDA] by Conductometric Studies A. B. Dhote, K. P. Jumde, S. H. Shrirame	11-16
4	Thin-Layer Chromatography Separation and Identification of Heavy Metals from Ore Water Sample Ashish Bansod, Amol Thakare, Rajesh Gulhane	17-26
5	Plant Based Green Synthesis of Lead Acetate NPs A.K. Maladhure, M.S. Chavan, S.A. Thakare, M.J. Pawar	27-33
6	COD Removal from Industrial Waste Water from Palghar MIDC Area Using Low-Cost Technique A.K. Wanjari, S.R. Kolteke, R.D. Ghodile	34-38
7	Green Synthesis of Copper Oxide Nanoparticle and Their Potent Antioxidant Application Thakare A. R, Padole P. D, Ghodile R. D, Deshmukh G. S	39-48
8	Synthesis of Some Substituted Azomethine Drug in Medicinal Chemistry: Green and Eco-Friendly Approach A. V. Kawalkar, P. P. Choudhari, M. P. Wadekar	49-55
9	Removal of Heavy Metals from Wastewater Using Nanotechnology : A Review Amritpal Singh S., Swapnil S. Kosalge, Sandhya Bharambe, Pushpinder G. Bhatia	56-77
10	Geochemical Characterization of Trace Metal in Estuarine Water and Sediment of Ratnagiri Coast: Sources, Patterns, and Environmental Risk Analysis Ashutosh Nirbhavane, Amol Pund, Dr. Anil Kurhe	78-83

11	Systematic Evaluation of Ultrasonic Properties of Substituted Thiocarbamidophenol In 80% Mixed Solvent Media Prof. Bhagyashri Bodkhe, Prof. Gayatri Tayade, Dr. Sanjay Kolhe	84-87
12	Sovereign Synthesis and Study of Alkyl Substituted 1, 3-Thiazole and Its Nanoparticles as Antibacterial Agents Chhaya D. Badnakhe	88-96
13	Protonation Dynamics and Metal-Ligand Stability of Beta-Ketone Ligands: Insights from pKa, nA, and LogK Constants Choudhari P. P., Wadekar M. P., Kawalkar A. V., Yawale P. R., Dongapure A. C.	97-102
14	Synthesis, Characterization and Catalytic Performance of Metal Inserted Al-MCM-41 Mesoporous Material Dr. Gaur S.R.	103-110
15	Natural Dyeing Cotton Fabric with Black Catechu and Quebracho Wood Dye Powder Using Different Mordant– Their Colour Fastness Test & FTIR Analysis Dr (Ms) Swaroopa Rani N. Gupta	111-130
16	Natural Dyeing Cotton Fabric with Annatto Seed and Heena Leaf Dye Powder Using Different Mordant– Their Colour Fastness Test & FTIR Analysis Dr (Ms) Swaroopa Rani N. Gupta	131-150
17	Acoustical Study of Molecular Interaction of 3,4-Dihydro-2H-1,2,4-Benzothiadiazine 1, 1-Dioxide in Aqueous Solution at Different Temperatures Nita P. Mohabansi, Monali Sabane	151-155
18	Medico-ethnobotany and Phytochemical Screening of Leonotis nepetifolia, Colebrookea oppositifolia from Melghat Region, Amravati District (M.S.) Dr. Nitin A. Khandare, Nandkishor K. More	156-159
19	Easy Fabrication of a Combination of Polyaniline and Graphene Oxide for Use as Electrode Materials and Its Characterization Dr. Prachi R. Bonde	160-166
20	Synthesis, Characterization and Biological Evaluation of 4-(4-Chloro-1-Hydroxy Naphthalen-2-Yl)-6-(3, 4-Dimethoxy Phenyl)-5, 6-Dihydropyrimidine-2(1h)-On Dr. Vinod M. Sherekar	167-170
21	Physicochemical and Thermodynamic Studies of the Schiff Base Ligands in Binary Polar and Nonpolar Solvent System Y. S. Thakare	171-178

22	Study of Acoustic Properties of Some Synthesized Thiazolyl Substituted Schiff Bases in Acetone-Water Mixture At 303.15 K Using Ultrasonic Velocity Measurement Dr. R. S. Talegaonkar	179-185
23	Studies on the Viscometric Measurements of 4-P- Phenylthi-Carbamidinonaphol at Various Moles and Temperatures of 70% Ethanol-Water Mixture Dr. Saleem. R. Khan, Dr. Quazi Saifuddin Ejazuddin	186-188
24	Synthesis, Characterization and In Vitro Antimicrobial Screening of Novel Substituted Aurone Gajanan Ingle, Dr. Sanjay Kolhe	189-195
25	Cutting-Edge Developments in 1,3,4-Oxadiazole Derivatives: Synthesis, Properties, and Applications Gajanan M. Amle, Rajendra K. Wanare	196-199
26	Investigation of Thermodynamic Parameters Substituted Thiocarbamidonaphthol Prof. Chetan Soye, Prof. Gayatri Harne, Prof.Divya Sherkar, Dr. Sanjay Kolhe	200-203
27	pH-Metric Studied Stability Constant of 5-P-Hydroxyphenyl-Thiocarbamido-1-Naphthol with Various Metal Ions in 60 % Ethanol-Water Mixture I.R. Dhoke, G.S. Rathod, A.G. Mule, S.N. Jadhav, P.S. Bodkhe	204-207
28	Acoustic, Volumetric, and Excess Properties for Binary Mixture of BTX and Ethyl Alcohol K.P. Belsare, N.B. Selukar	208-214
29	Investigation of Ultrasonic Properties of 2- Ethylthiocarbamidophenol K. P. Jumde, A. B. Dhote	215-218
30	Role of Graphene Oxide Cadmium Oxide Nanocomposite as a Photo Catalyst in Synthesis of Heterocyclic Compounds M. N. Zade, D. T. Tayade	219-226
31	The Study of Alterations in Tissue Cholesterol in Reproductive Organs of Female Albino Rats Fed With Steroidal and Non-Steroidal Contraceptive Pills M. P. Chikhale	227-232
32	Synthesis and Microbial Evaluation of Some of 1,2,4-Thiadiazole Derivatives M. R. Raghuvanshi	233-238
33	Impact of Substituted Flavones in Medicinal field Dr. S. L. Sayre, Dr. P. B. Raghuvanshi	239-241

34	Evaluation of Proximate Composition in Leaves Extract of Catharanthus Roseus Plant From Gondwadi Area of Dharni in Maharashtra State Pavan Raut, Vishala Patil, Maya Soham, Monali Shahakar	242-245
35	Awareness of Micronutrient Level in the Water and Soil for Integrated Farming in Rural Area: A Case Study of Varakute-Mhaswad Tal-Man Dist-Satara (Maharashtra) Mr. Chavan Mahendra Sadashiv, Mr. Kalel Kailaspati Pandurang, Mr. Salunkhe Popat Bhanudas	246-251
36	Developments in Synthesis of Nanomaterials of Tungsten and Molybdenum Disulfides for Supercapacitive Applications - A Review Mr. N. A. Barwat, Prof. G. N. Chaudhary	252-258
37	Polymer Composites Doped With Rare-Earth Elements : A Review of Luminescent, Electrical, and Optical Properties Ms. Riya R. Tekade, Dr. Shilpa G. Vidhale, Ms. Chitralekha A. Kolhe	259-264
38	Bio-Inspired Synthesis and Characterisation of Sulphur Nanoparticles Synthesized By Using (Azadiracta Indica) Neem Leaves Extract N. S. Dixit, S. G. Khobragade, M. S. Dixit, A. S. Dixit, Pratiksha Ardak	265-269
39	Versatile Applications of Polyaniline Polyvinylacetate Blends : A Comprehensive Review N.D. Kolekar, A.V. Kohale, B.T. Kumbhare	270-273
40	Effect of Zinc Oxide Nanoparticles on the Growth of Mungbean (Vigna Radiata) Seedlings P. C. Pandit, Dr. M. M. Kulkarni	274-283
41	Viscosity and Density Characterization of 1-((4-Methoxy-3, 5-Dimethylpyridin-2-Yl) Methyl)-3-Methyl Thiourea in Ethanol-Water Mixtures P. R. Kute, N.D. Chaudhari, S. U. Shinde, G. B. Andhale, A. M. Kute, S. S. Padhen	284-288
42	Approach of Graph Theory in Material Science P. B. Deshmukh	289-295
43	Recent Biological Applications and Chemical Synthesis of Aurones Dr. Prashant A. Gotmare, Dr. Sanjay V. Kolhe	296-301
44	Rosa Rubiginosa Mediated Green Synthesis of Silver Nanoparticles Prashant B. Lihitkar, Panu Upare	302-310

45	Multi-Decadal Changes of Konkan Region Mangrove Forest Coast of Maharashtra and Its Response to the Tidal Dynamics, Spatial and Temporal Changes Pund A. R., Nirbhavane A. M., Dr. Kurhe A. R	311-318
46	Estimation of Proximate Contents of Trigonella Foenum-Graecum Stem in Aurangabad City of Maharashtra, India Quazi Saifuddin, Saleem Khan	319-322
47	Red Phosphor Materials: Synthesis, Characterization, and Luminescence Analysis R. S. Palaspagar, S. R. Khandekar	323-327
48	Facile Synthesis of MgO Nanoparticles and MgO/PANI NCS as a Promising Photocatalyst towards Waste Water Treatment Ramdas S. Suralkar, Deepak M. Nagrik, Vivek C. Badgujar	328-338
49	Phytochemicals and GC-MS Analysis of Bioactive Compounds Present In Methanolic Leaves Extract of Justicia Adhatoda L Anil F. Bobade, Rahul P. Rahate	339-344
50	Antimicrobial and Pharmacological Evaluation of Propane 1, 3-Diones Derivatives Containing P-Formyl Phenol Moiety Rajendra M. Pathade, Pravin S. Bodkhe, R. D. Isankar	345-351
51	Green Synthesis of Copper Oxide Nanoparticles from Plant Extract and Their Biological Applications : A Review Ruqqaiya Shaikh, D.T.Tayade, Pathan Mohd Arif, Mohd. Anis, R. D. Isankar	352-360
52	Novel Synthesis of Flavanones and Its Impact on Seed Germination S. P. Rathod	361-364
53	Conduction Mechanism and DC Conductivity of Solid Polymer Electrolyte S. R. Jadhao, S. P. Bakde	365-367
54	Geological Application of VO(IV), Zr(IV) and UO₂(VI) Complexes Derived From Thiazole Schiff Base S. R. Kelode, D. B. Dupare	368-371
55	Synthesis and Characterization of Heterocyclic Active Functionalities of Pyrazoles with Their Importance S. A. Ikhe, P. M. Dahikar, D.A. Pund	372-376
56	Bio-Green Synthesis of AgNPs from Moringaoleiferaleaves Extract and Its Antibacterial Application S.D. Chavan, R. D. More, S. P. Moharir, S. S. Paden	377-382

57	Sustainable Phytofabrication of Sulfur Nanoparticles from Orange Peel Extract: Structural, Morphological, and Antibacterial Insights S. G. Khobragade, N. S. Dixit, S. B. Bansod, M. S. Dixit, D. C. Deshmukh, A. S. Dixit	383-388
58	Extraction and Isolation of Vanillic Acid from Catharanthus Roseus Plant and Synthesis of Their Analogues S. S. Padhen, S. P. Gahukar	389-392
59	Harnessing Photophysical Properties of Schiff Base Cyclometallated Complexes for Advanced Applications: A Review S. R. Khandekar, S. R. Kelode, R. S. Palaspagar	393-398
60	Investigation On Inter Ferometric Study of 4-(p-Bromo) Phenylthiocarbamidophenolin Mixed Solvent Media Mr. S. U. Patil	399-401
61	The Role of Optical Properties in Enhancing Electromagnetic Interference (EMI) Shielding S.V. Tayade, A.P. Bangar, S.A. Waghuley	402-407
62	Interferometric Investigation of 2-EthylThiocarbamido- phenol in 65% Mixed Solvent Media S.Z.Jadhao, B. M.Theete	408-411
63	Green Synthesis and Characterization of Copper Nanoparticles Using Raphanus sativus Leaf Extract Sachin S. Bangade, Vivek M. Raut, R.S. Shaikh, Ram.D. Isankar, M.E. Shelke, D.P. Gulwade	412-422
64	Synthesis and Characterization of Schiff Base ligand for Corrosion Inhibition of Mild Steel in Sulphuric Acid Medium Prashant Ashtaputrey, Sampada Payal, Ashok Kalambe, Kavita Gour, Rohit Chunarkar	423-434
65	Spectroscopic Studies and Combustion Synthesis of LiAlO₈:Gd³⁺ Phosphor for Optical Applications Sandip M. Parkhi, S.A.Shah, Shruti Dhale, Avinash M. Nannaware, N.S.Ugemuge	434-443
66	Comparative Study of the Effect of a Foreign Particle on Binding Interaction of Chiral Drugs 2BMCA with BSA by Equilibrium Dialysis Shrikant B. Thakare	444-449
67	Synthesis, Characterization and Antimicrobial Activity of Plant Pathogens : A Study of 4,5-Dihydro Isoxazole Derivatives Shubhangi Y. Deshmukh, Mithilesh M. Rathor, Nilesh S. Padole	450-455

68	Viscosity and Density Evaluation Of [(2z, 4z) -2-(Ethylimino)-N-(4-Methoxy-3, 5-Dimethylpyridin-2-Yl) Methyl)-4-Phenylimino)]-4h-1, 3, 5-Dithiazin-6-Amine in Ethanol-Water Mixture S.S. Padhen, P.C. Sawarkar, S.P. Gahukar, D. B. Dupare	456-460
69	Application of Ultrasound in Synthesis of Heterocyclic Compound: A Green Chemistry Perspective Abhimanyu P. Pawar, Kishor S. Naktode, Arvind J. Mungole, Dalesh M. Parshuramkar	461-467
70	Novel Synthesis and Antimicrobial Study Of (E)-1-(4-Substituted Phenyl)-N-(4- Chlorophenyl) Methanamine Derivative D S Warbhe, O K Kapse, R M More	468-472
71	Chemical Synthesis and Optical Characterization of Anatase TiO₂ Nanoparticles Nikita Subhash Jaiswal, Sanjeev Jagtap	473-479
72	Sustainable Approach to 1, 3-Dithiazine Derivative Synthesis via Fruit Juice Catalysis and Synthetic Organic Acids Pradnya Nalawade	480-483
73	Synthesis and Characterization of Copper Oxide Nanoparticles Using Precipitation Method Dr. Priya Sachin Deole, Miss. Ravi P. Raut	484-489
74	Synthesis and Characterization of Some Chromene Derivatives Sharad N. Pawar, Deepak M. Nagrik	490-494
75	Understanding the Properties and Behaviour of Group Theory in Molecular Chemistry S. C. Darunde	495-498
76	A Comprehensive Review of Storage Principles and Electrode Materials in Supercapacitors Vaibhav R. Shrikhande, Anjali B. Bodade	499-506
77	Computational Analysis of 5-N-Substituted-2-(Substituted Benzenesulphonyl) Glutamine Derivatives as Potential Inhibitors of the Kinase Domain in Imatinib-Resistant Abl Mutant Enzyme Asita Ganatra, Neetu Gupta, Satyen Patil, Sunil Ganatra	507-517
78	Synthesis and Optical Studies of Magnesium Pyrophosphate Z. S. Khan, S. P. Chavhan, V. K. Bhosle, P. P. Rathod, S. H. Sharma	518-522
79	Revolutionizing Chemistry : Applications and Innovations of Artificial Intelligence in Chemical Research and Development Mr. Ankit Gotmare	523-527

80	Green Synthesis and Characterization of Copper Nanoparticles Using Raphanus sativus Leaf Extract Sachin S. Bangade, Vivek M. Raut, R.S. Shaikh, Ram. D. Isankar, M.E. Shelke, D.P. Gulwade	528-537
81	Review on Effect of Synthesis Process and Quantum Efficiency of Luminescence Material Mr. U. T. Bhati	539-541
82	Various Disorders Can Be Effectively Treated With Wild Vegetables Dr. Prerana Pramod Bhatkar	542-544
83	Effect of Synthetic Pyrethroid on enzyme of freshwater fish Ophiocephalus orientalis Dr. Shruti R. Pande	545-548
84	Boosting DSSC Efficiency Using Conducting Polymer-Decorated Hybrid Counter Electrodes and Tio2 Nanocrystalline Photoanode Sensitized With Bixa Orellana Dye M.S. Dixit, A. P. Deshmukh, S. P. Tiwari, S. P. Yawale	549-557
85	Estimation of Proximate Contents of Andrographis paniculate Leaves in Yavatmal District of Maharashtra, India Anjali Sarkate, Rupali Biradar, Vishnudas Bhosle, Vikas Gambhire	558-561
86	Novel Synthesis, Characterization and Biological Evaluation Copper Nanoparticles from Goat Bile Juice Nilesh B. Jadhav, Pawan P. Kalbende, Mithun S. Lunge, Sandip B. Chaudhari, Ramesh T. Parihar, Nandkishor J. Suryawanshi, Dharmendra B. Dupare, Mrs. M. H. Shaikh	562-570
87	Synthesis and Biological Study of Cu, Zn, Ag Nanoparticles from Plant Extracts of Ehretia laevisRoxb and Carissa carandas- A Review Tejan D. Gajbhiye, Bhavna Khobragade, Subodh Bhandarkar	571-575
88	Photocatalytic Behavior of Synthesized and Characterized Graphene Oxide Pravin Rathod, Vishnudas Bhosle, Ashok Ubale, Zakir Khan	576-580
89	Conductivity Analysis of (1-X)BFO - xBT Ceramics Prepared by Sol Gel Method Rajesh R.Raut	581-586
90	Exploration of Phytochemical Constituents and Antimicrobial Properties of some Medicinal plants of Jhabua District Dr. Sunil Kumar Sikarwar, Kajal Dasondhi	587-591
91	Elaboration and Applications of Nanostructured Metal Oxides : Synthesis,	592-595

	Properties, and Prospects V. R. Hiranwale, R. B. Pedhekar, G. B. Harde, V. D. Wankhade, S. P. Patil	
92	Fabrication and Performance Evaluation of Spherical Stannic Oxide Nano Particles for H₂S, CO₂, NH₃, and LPG Detection Swapnil S. Kosalge, Fulsingh C. Raghuwanshi, Digambar N. Sapkal, Pushpinder G. Bhatia	596-603
93	Effect of Invasive Species on Fish Fauna in Freshwater Bodies in and Around Morshi Taluka, District-Amravati (Maharashtra), India Mr. Vinayak Vishwanathrao Tathod, Dr. Mrs. D. S. Kulkarni	604-606
94	Analysis of Collective Creativity : Gender, Power, and the Cultural Significance of Fanfiction Shradha Upadhya	607-614
95	Media Optimization for Maximum Azoreductase Enzyme Azo-LM1 Production by Lysinibacillus macrolides LMG 16474 Mr. Mayur J. Thakare, Dr. A. M. Garode	615-620
96	Diversity of Phytoplankton and Zooplankton of Nilona Dam Dist. Yavatmal Ninad Dharkar, M. A. Shahezad, Kisor Suradkar, Sangita Khadse	621-624
97	Synthesis, Characterization and Biological Evaluation of 4-(5-Chloro-8-Hydroxynaphthalen-2-Yl)-6-(3, 4-Dimethoxyphenyl)-5, 6-Dihydropyrimidin-2(1h)-One Mr. Nilesh S. Padole	625-629
98	Molecular Properties of Skeletal Muscle Protein of Vertebrates Gajanan B. Santape	630-633
99	pH-Metric Studies on Stability Constants of the Complexes of Some New Substituted Pyrazoles and Isoxazoles with Cu(II) and Fe(III) Transition Metal Ions in 70% Dioxane-Water Mixture Sushil K. Pagariya, P. S. Bodkhe	634-645
100	A Study on Acoustical Parameters of Isradipine Drug in Different Binary Mixture of Solvents At 313 K Wasnik Usha	646-650
101	Interaction of 1(4-Chlorophenyl)-2(P-Tolylthiocarbamido)-1-Ethanolwithmn (II), Fe (II) and Cu (II) Ions Deliberate Ph-Metrically R. J. Deshmukh, A. B. Wadekar, S. A. Ikhe, P. M. Dahikar, RD. Kakade	651-655
102	pH-Metric Studied Stability Constant of 5-P-Hydroxyphenyl - Thiocarbamido-1-Naphthol with Various Metal Ionsin 60 % Ethanol-Water	656-660

	Mixture Y. P. Wayal, N. D. Dahake, P. M. Deshmukh, P. S. Bodkhe, R. T. Parihar	
103	One Pot Synthesis of 1(4-Chlorophenyl)-2-(P-Tolylthiocarbamido)-1-Ethanol A. B. Wadekar, A. P. Nagrale, D. L. Bhade, V. G. Bhagat, M. M. Rathore	661-664
104	Evaluation of Thermodynamic Parameters of Substituted Naphthol Aditya D. Joshi, Vaishnavi A. Petkar, Gopal S. Bharambe, Dr. Sanjay V. Kolhe	665-668
105	Preliminary phytochemical analysis of Clematis triloba B. Heyne ex Roth Abhijeet A. Pakhare, Radhika Dhurve, Shumaila Taqdees, Misbah Anjum and Vishal P. Deshmukha	669-673
106	Adsorptive Removal of Heavy Metal-Cr from Aqueous Solution using Banana Peel Powder as a Bio Adsorbent Manoj A. Pande	674-676
108	Evaluation of the corrosion inhibition properties of Bouhunia Racemose Leaves Extracts for mild steel in 1 M H₂SO₄ solution on basis of Thermodynamics and adsorption study. Yogesh Pawar, Dhanashri Panchbhai	677-688

Spectral Characterization of Newly Synthesized Azopyrazole Derivatives from Toluidine

A P Thakare, A D Bansod

Department of Chemistry, Rajarshree Shahu Science College, Chandur Rly, Maharashtra, India

ARTICLE INFO

Article History:

Accepted : 01 Jan 2025

Published : 10 Jan 2025

Publication Issue :

Volume 12, Issue 7

January-February-2025

Page Number :

01-05

ABSTRACT

The given paper describe the synthesis 3-(2-(p-tolyl)hydrazono)pentane-2,4-dione from toluidine and acetyl acetone in presence of sodium nitrite. These synthesized compound then reacts with the 4-methyl phenyl hydrazine and 4-chloro phenyl hydrazine for the synthesis 3,5-dimethyl-1-(p-tolyl)-4-(p-tolyldiazenyl)-1H-pyrazole and 1-(4-chlorophenyl)-3,5-dimethyl-4-(p-tolyldiazenyl)-1H-pyrazole. All the newly synthesized compounds are characterized on the basis of Elemental, IR, ¹H-NMR and Mass spectral data. The spectral data obtained is in good agreement with the suggested structure of compounds.

Keywords: Aniline, acetyl acetone, 4-chloro phenyl hydrazine, 4-methyl phenyl hydrazine, ¹H-NMR

I. INTRODUCTION

Heterocyclic compounds are organic chemical compounds with a ring-like structure that contains one or more heteroatoms. The most common heterocycles have five- or six-membered rings and contain heteroatoms of nitrogen (N), oxygen (O), or sulfur (S). Among them pyrazoles are five-membered heterocycles that constitute a class of compounds particularly useful in organic synthesis. They are one of the most studied groups of compounds among the azole family. The presence of the pyrazole nucleus in different structures leads to diversified applications in different areas such as technology, medicine and agriculture. In particular, they are described as inhibitors of protein glycation, antibacterial, antifungal, anticancer, antidepressant, antiinflammatory, anti-tuberculosis, antioxidant as well as antiviral agents.

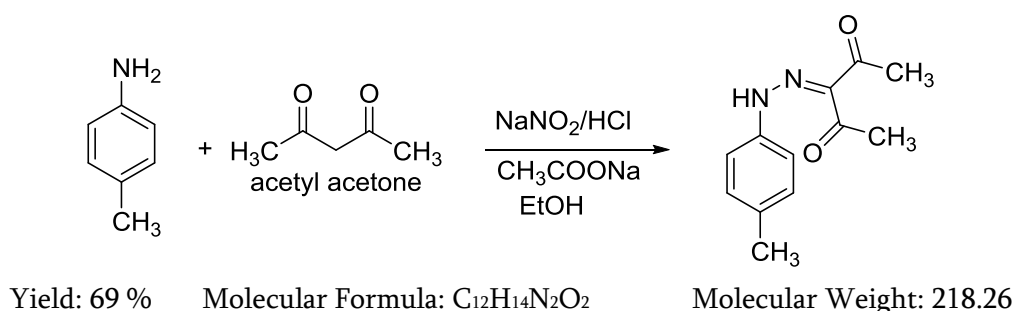
By considering the biological activities of azopyrazole compounds given paper describe their synthesis and characterization. [1-3]

II. METHODS AND MATERIAL

All chemicals used were of the analytical reagent grade and of the highest purity available. It includes, 4-chloro aniline, p-toluidine, 4-methoxy aniline, acetyl acetone, 4-methyl phenyl hydrazine and 4-chloro phenyl hydrazine. Melting points were taken in open capillaries on a Cintex melting point apparatus and are uncorrected. Purity of the compounds was checked by TLC. IR spectra were recorded in KBr on a Perkin-Elmer RX-IFTIR spectrophotometer and ^1H NMR spectra on a Avance Neo (Bruker) 500 MHz spectrometer using TMS as internal standard. Mass spectra were recorded on a Jeol JMS 0-300 instrument at 70 eV.

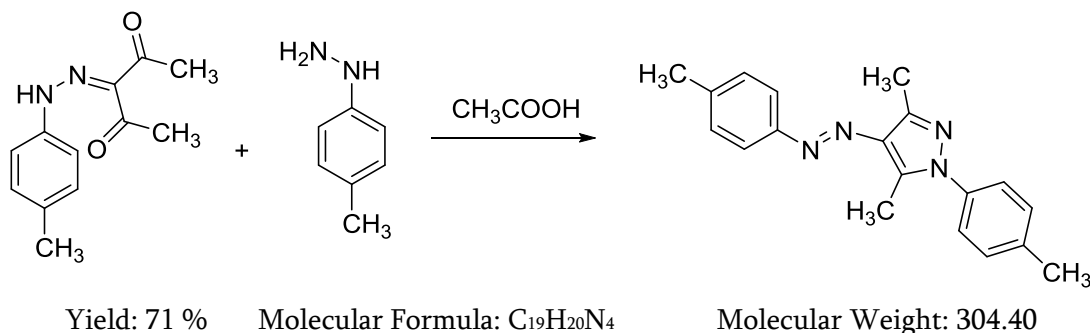
Synthesis of 3-(2-(p-tolyl)hydrazono)pentane-2,4-dione

4-substituted aniline was dissolved in a mixture of concentrated HCl and water and cooled to 0 °C on ice bath. A cold aqueous solution of sodium nitrite was added. The cold diazonium salt solution was filtered into a cooled solution of acetyl acetone in presence of sodium nitrite and sodium acetate in ethanol and stirred for 4-5 hours. The resulting solid was filtered, dried and purified by recrystallization from ethanol to afford compound.



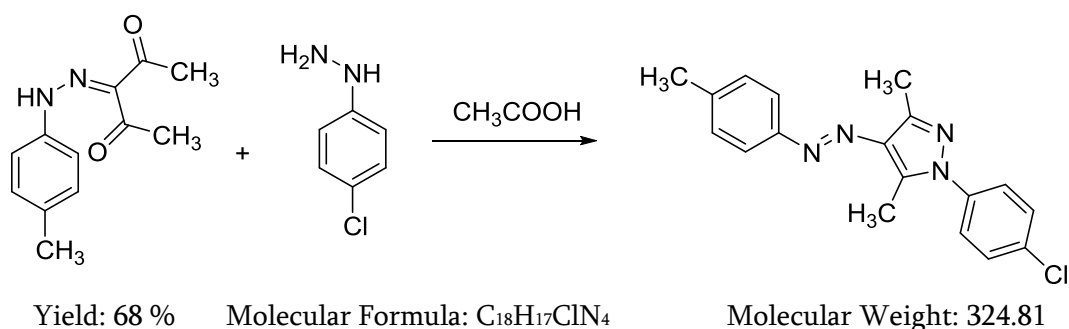
Synthesis of 3,5-dimethyl-1-(p-tolyl)-4-(p-tolyldiazenyl)-1H-pyrazole

A mixture of 3-(2-(p-tolyl)hydrazono)pentane-2,4-dione (0.01 mole) and 4-methyl phenyl hydrazine (0.1mole) in glacial acetic acid (15 mL) is refluxed for 4-5 hours. The resulting mixture was concentrated and allowed to cool. The resulting solid was filtered, washed, dried & recrystallized from ethanol to afford compound.



Synthesis of 1-(4-chlorophenyl)-3,5-dimethyl-4-(p-tolyldiazenyl)-1H-pyrazole

A mixture of 3-(2-(p-tolyl)hydrazono)pentane-2,4-dione (0.01 mole) and 4-chloro phenyl hydrazine (0.1mole) in glacial acetic acid (15 mL) is refluxed for 4-5 hours. The resulting mixture was concentrated and allowed to cool. The resulting solid was filtered, washed, dried & recrystallized from ethanol to afford compound.



III.RESULTS AND DISCUSSIONS

All new compounds were characterized on the basis of elemental analysis IR, ¹H –NMR and mass data.

Spectral data of 3-(2-(p-tolyl)hydrazono)pentane-2,4-dione

% C – 66.04 % H – 6.47 % N – 12.84 % O – 14.66

IR (KBr, cm⁻¹): 3180 (N-H), 3050 (Ar C-H), 1675 (C=O), 1605 (C=N), 1520 (C=C), 1130 (C-O)

¹H-NMR: (CDCl₃, 500 MHz): δ 7.45, m (4H, Ar-H) δ 13.24 s (1H, NH) δ 2.51 s (6H CH₃CO) δ 2.32 s (3H, ArCH₃)

Mass: m/z 218.11, 219.11.

Spectral data of 3,5-dimethyl-1-(p-tolyl)-4-(p-tolyldiazenyl)-1H-pyrazole

% C – 74.97 % H – 6.62 % N – 18.41

IR (KBr, cm⁻¹): 1458 (N=N), 3050 (Ar C-H), 1480 (C=C), 1605 (C=N)

¹H-NMR: (CDCl₃, 500 MHz): δ 2.34 s (6H, ArCH₃) δ 7.40 d (2H, Ar-H) δ 7.79 d (2H, Ar-H) δ 7.28 d (2H, Ar-H) δ 7.56 d (2H, Ar-H) δ 2.75 s (6H, ArCH₃)

Mass: m/z 304.17, 305.17, 306.18.

Spectral data of 1-(4-chlorophenyl)-3,5-dimethyl-4-(p-tolyldiazenyl)-1H-pyrazole

% C – 66.56 % H – 5.28 % N – 17.25

IR (KBr, cm⁻¹): 1455 (N=N), 3090 (Ar C-H), 1483 (C=C), 1605 (C=N)

¹H-NMR: (CDCl₃, 500 MHz): δ 2.34 s (6H, ArCH₃) δ 7.40 d (2H, Ar-H) δ 7.79 d (2H, Ar-H) δ 7.40 d (2H, Ar-H) δ 7.35 d (2H, Ar-H) δ 2.75 s (6H, ArCH₃)

Mass: m/z 324.11, 326.11, 325.12.

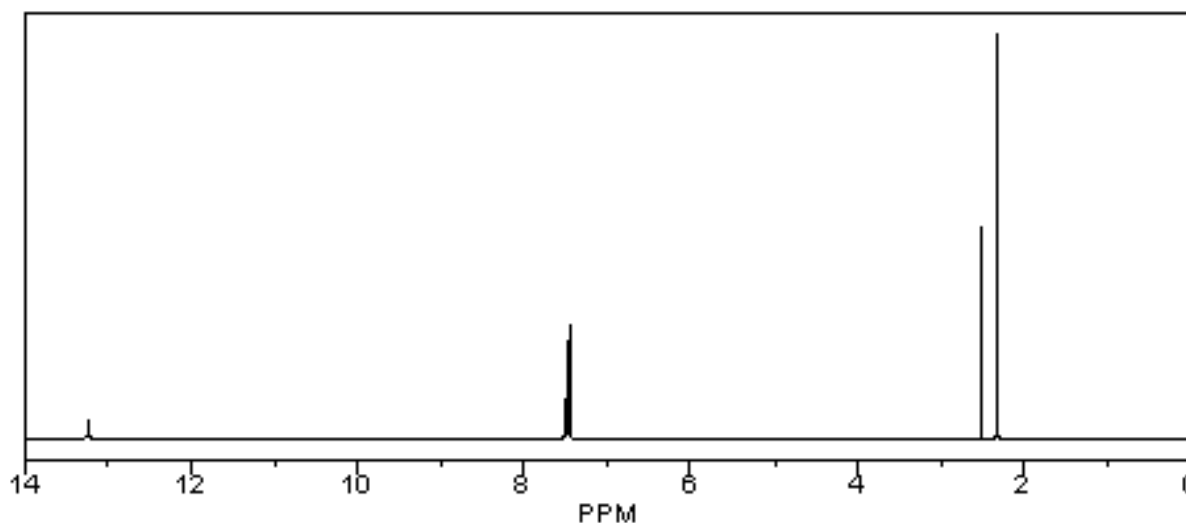


Fig: ¹H-NMR Spectrum of 3-(2-(p-tolyl)hydrazono)pentane-2,4-dione

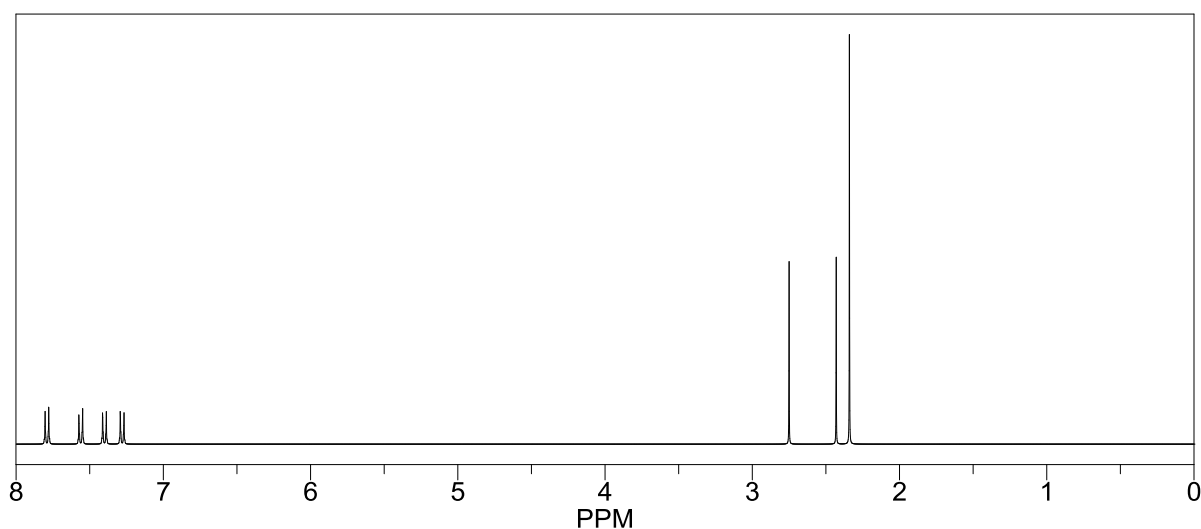


Fig: ^1H -NMR Spectrum of 3,5-dimethyl-1-(p-tolyl)-4-(p-tolyldiazenyl)-1H-pyrazole

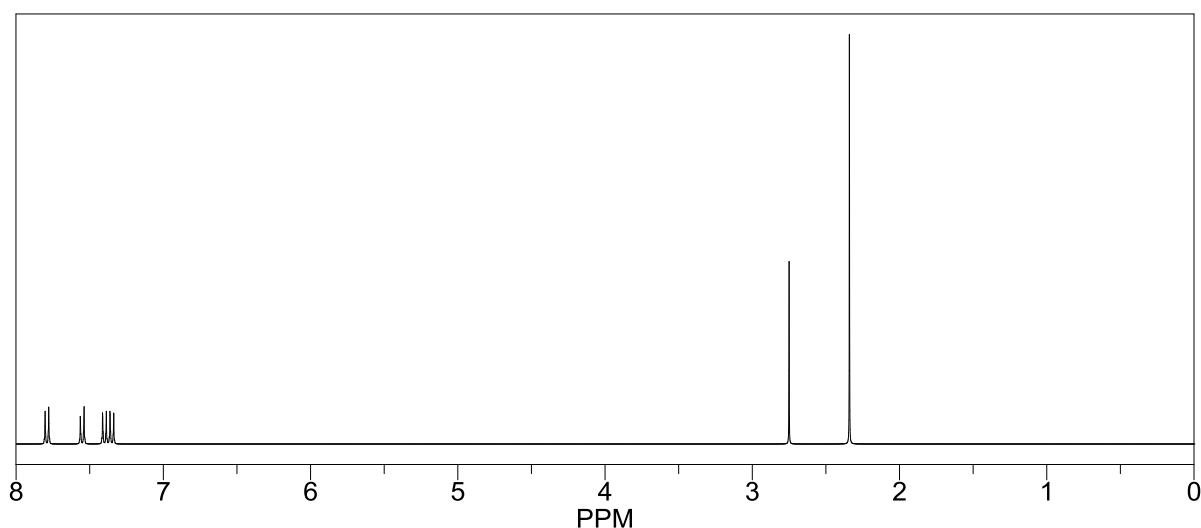


Fig: ^1H -NMR Spectrum of 1-(4-chlorophenyl)-3,5-dimethyl-4-(p-tolyldiazenyl)-1H-pyrazole

Antibacterial activities of all the compounds were studied against Gram-positive Bacteria (*Bacillus subtilis*) and Gram-negative Bacteria (*E. coli*) at a concentration of 50 $\mu\text{g/ml}$ by Agar cup plate method. Methanol system was used as control in this method. The area of inhibition of zone was measured in mm. All compounds were found more active against the above microbes.

IV. CONCLUSION

The given study contains the synthesis of azopyrazole derivatives. The spectral data obtained matches with the probable structure of compound.

V. REFERENCES

- [1]. N. Depa and H. Erothu. 2022. *Rasayan J. Chem.* 15, 3, 1709-1717.
- [2]. M. Faisal, A Saeed, S Hussain, P Dar and A Larik. 2019. *J. Chem. Sci.* 131,70.

- [3]. S Katke. 2023. Environmental Science: An Indian Journal. 19, 01, 1-11.
- [4]. G Bheema Raju, M. Mahesh, G. Manjunath and P. Venkata Ramana. 2016. Chemical Science Transaction. 5(1), 125136.
- [5]. S. Dhonnar, B. Jagdale, A Sawant, T. Pawar and S. Chobe. 2016. Der Pharma Chemica. 8(17), 119128.
- [6]. B. Chandrakantha, A.M. Isloor, S.K. Peethamber ,P. Shetty. 2012. Der Pharma Chemica, 4, 1723.
- [7]. M. Amir, S. Kumar. 2005. Ind. J Chem. 44B, 2532.
- [8]. A. B. Patel, K. S. Nimawat and K. B. Vyas. 2013. Archives of Applied Science Research. 5(1), 120-123.

Viscosity and Density Analysis of 1-((4-Methoxy-3, 5-Dimethylpyridin-2-yl) Methyl) Thiourea in Ethanol- Water Binary Mixtures

A. P. Pachkawade, S. A. Wani*, R. N. Bhagat

Department of Physics, Rajarshee Shahu Science College Chandur Railway, Dist.-Amravati, 444 904, Maharashtra, India

ARTICLE INFO

Article History:

Accepted : 01 Jan 2025

Published : 10 Jan 2025

Publication Issue :

Volume 12, Issue 7

January-February-2025

Page Number :

06-10

ABSTRACT

For the purpose of so many applications also heterocyclic molecules play a vital role in medicinal chemistry, with heterocyclic rings forming the backbone of numerous drugs on the market. Pyridine, a six- member heteroaromatic ring, is a key component of many natural compounds, such as vitamins and alkaloids, and its derivatives are highly valued for their versatility in developing new medications. Recently, we conducted a study in our laboratory to assess the viscosity and density of theorem under controlled concentrations at varying temperatures. The experimental data provided insights into solute- solvent interactions and the effects of solvent dilution. Results indicated that relative viscosity decreases with increasing temperature, suggesting enhanced salvation effects. This research contributes valuable knowledge about the physicochemical properties of pyridine derivatives, aiding the development of more effective pharmaceutical compounds.

KEYWORDS: Heterocyclic molecules, Pyridine derivatives, Viscosity and density, 1-((4-Methoxy-3,5- dimethylpyridin-2-yl)methyl)theorem, Solvent dilution, Temperature effects.

I. INTRODUCTION

to Pyridine derivatives are known for their diverse biological applications. Due to its pharmacological properties, the heterocyclic pyridine ring is extensively utilized in the creation of new drugs. Pyridine-based compounds serve as key components in medications with anti-inflammatory, antibacterial, antiviral, anticancer, antioxidant, antihypertensive, ant diabetic, and ant malarial activities. Additionally, the strong affinity of pyridine derivatives for various ions and neutral species makes them highly effective as chemosensory, enabling the detection and differentiation of a wide range of species [1]. Substitutions on the

pyridine nucleus target a broad spectrum of biological challenges, including microbial infections, viral conditions, and various cancerous cells. Pyridine derivatives interact with enzymes, proteins, and DNA to tackle a wide range of biological problems effectively [2]. The biological targets of pyridine nucleus replacements include a variety of malignant cells, viral problems, and microbial disorders. Pyridine derivatives address a range of biological problems via interacting with proteins, enzymes, and DNA [3]. Heterocyclic molecules containing nitrogen and sulfur are essential to life. These substances, which come in a range of ring configurations, are essential to numerous biological processes and systems. These rings have special chemical characteristics and reactivity profiles because they contain nitrogen and sulfur atoms, which are necessary for their biological roles [4,5]. Thiocarbamide, commonly known as thiourea $\text{CS}(\text{NH}_2)_2$, is a vital organic chemistry chemical due to its unique structure and reactivity. We are synthesizing the thiocarbamide derivatives of pyridine-based moiety. Its relevance is explained by its many applications as a reagent, intermediate, and functional group in a variety of chemical processes. Thioureas have numerous therapeutic applications in addition to their non-medical applications in metallurgy, analytical chemistry, and industrial. Numerous thioureas have a range of medical applications and are utilized in clinical settings. Over time, more and more thioureas are being employed in medicine. In agriculture, thioureas are used as insect growth regulators, enzymatic inhibitors, herbicides, rodenticides, and antifungal agents [6-15]. Both aqueous and non-aqueous solutions include interactions between the solute and the solvent. This important information is obtained from measurements of viscometrical parameters. A drug's behavior, including absorption, transmission, and effects, will be directly influenced by measurements of its viscosity and interactions with solvents in the human body [16].

Water and alcohol mixtures are intriguing systems due to their complex dynamics, driven by hydrogen bonding and the presence of hydrophobic groups. These mixtures are widely studied, both theoretically and experimentally, because of their extensive use as solvents. Viscosity in a liquid can be influenced by various factors, including temperature, molecular size, molecular weight, intermolecular interactions, and the presence of impurities. Analyzing viscosity provides valuable insights into the molecular interactions and characteristics of binary and ternary liquid systems. Notably, favorable interactions within these systems can lead to an increase in viscosity. Density, on the other hand, is a critical property for determining whether a material will float or sink in a liquid. Specifically, a substance will float if its density is lower than that of the liquid. Furthermore, density plays a key role in determining other physical and acoustic properties, such as surface tension, molar refraction, dipole moment, and boiling point.

Many pharmacological and biochemical characteristics of pyridine derivatives, such as antiviral, antibacterial, anti-inflammatory, anesthetizing, and mydriatic agents, have been reported in the literature review. These compounds have antiviral, antifungal, antibacterial, anti-helminthic, and anti-tuberculostatic properties. Given these factors, measuring the viscometry concentration of 1-((4-methoxy-3,5-dimethylpyridin-2-yl)methyl)thiourea at various temperatures is quite relevant. All things considered, this kind of research advances the field of drug science and helps create pharmaceutical goods that are more dependable and effective, which eventually improves patient outcomes [4,5,18].

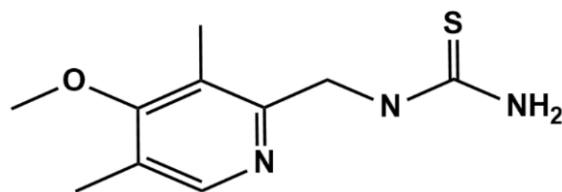


Fig. 1-1-((4-methoxy-3,5-dimethylpyridin-2-yl)methyl)thiourea

II. EXPERIMENTAL

In this study, double-distilled water and analytical grade (A.R.) chemicals were employed. The weights of the compounds were determined using a digital balance with a precision of ± 0.001 grams. Viscosity measurements were conducted using an Ostwald viscometer, with the temperature maintained at a constant 29°C ($\pm 0.1^\circ\text{C}$) using an Elite thermostatic water bath. Density measurements were carried out using a bicapillary tube with an internal diameter of 1 mm. Prior to measurement, the viscometer and water bath were allowed sufficient time to reach thermal equilibrium. The compound 1-((4-methoxy-3,5-dimethylpyridin-2-yl)methyl)thiourea was studied viscometrically at a concentration of 0.1 M in a 60% ethanol-water mixture across various temperatures. Freshly prepared solutions were utilized for the analysis, and viscosity readings were taken following established literature protocols.

III. OBSERVATIONS AND CALCULATIONS

Molecular interactions were analyzed using the solute's β -coefficient, derived from the data obtained in this study. The results are presented in Table 1. Based on the Jones-Dole equation: $C(\eta_r - 1) = A + BC$, values were calculated for various temperatures at a concentration of 0.1 M. The computed A and β -coefficients are summarized in Table 2.

TABLE No.1 The Determination of Relative and Specific Viscosities at Different Temperatures at 0.1 Millimeters, As Well As Measurements of Viscosity at Constant Concentrations

MEDIUM - 60% ETHANOL-WATER							
Conc.	Temp. ($^\circ\text{C}$)	\sqrt{C}	Time	Density $\rho \times 10^3$ ($\text{kg} \cdot \text{cm}^{-3}$)	η_r	$\eta_{sp} = \eta_r - 1$	$(\eta_r - 1)/\sqrt{C} (\text{pa}^{-1}\text{s})$
0.1 M	22	0.314	69	0.9823	0.069421	-0.930579	-2.96362
	24	0.314	59	0.9763	0.058214	-0.941786	-2.99931
	26	0.314	51	0.9876	0.052143	-0.947857	-3.01779
	28	0.314	45	0.9535	0.049125	-0.950875	-3.02826

TABLE No.- 2 The values of a and β for the 60% coefficient are displayed references to 1-((4-methoxy-3,5-dimethylpyridin-2-yl)methyl)thiourea

W-E Mixture (%)	Temp $^\circ\text{C}$	Mean "A"	β (Slope "m")
60	27	-3.00233	0.0069

IV. RESULT AND DISCUSSION

$$\eta_r = D_s \times t_s / D_w \times t_w.$$

The relative viscosities were analyzed using the

Jones-Dole equation, $(\eta_r - 1)/\sqrt{C} = A + B\sqrt{C}$ Where,

A = Falkenhagen coefficient

B = Jones-Dole coefficient

C = concentration of solutions

The Jones-Dole coefficient (B) was used to evaluate solute-solvent interactions, while the Falkenhagen coefficient (A) assessed solute-solute interactions. A graph was plotted between \sqrt{C} and $(\eta_r - 1)/\sqrt{C}$, showing a linear relationship for each system with a corresponding β -coefficient value.

V. CONCLUSION

The density and relative viscosity of the current work monitor decrease with increasing temperature. The finding that the solute-solvent interaction rises with temperature, intensifying the solvation effect, lends credence to this. The public benefits from and learns from studies on a drug's pharmacodynamics and pharmacokinetics.

VI. ACKNOWLEDGEMENT

I would like to express my sincere gratitude to Dr. D. T. Tayade, a respected professor at GVISH College in Amravati, for his invaluable support and guidance. His expertise and dedication have played a crucial role in assisting me throughout this research.

VII. REFERENCES

- [1]. Mohammad Abu-Taweel G, Ibrahim MM, Khan S, Al-Saidi HM, Alshamrani M, Alhumaydhi FA, Alharthi SS. Medicinal Importance and Chemosensing Applications of Pyridine Derivatives: A Review. *Crit Rev Anal Chem.* 2022 Jun 20:1-18.
- [2]. Ataf Ali Altaf, Adnan Shahzad, Zarif Gul, Nasir Rasool, Amin Badshah, Bhajan Lal, Ezzat Khan. A Review on the Medicinal Importance of Pyridine Derivatives. *Journal of Drug Design and Medicinal Chemistry.* Vol. 1, No. 1, 2015, pp. 1-11.
- [3]. Ataf Ali Altaf, Adnan Shahzad, Zarif Gul, Nasir Rasool, Amin Badshah, Bhajan Lal, Ezzat Khan. A Review on the Medicinal Importance of Pyridine Derivatives. *Journal of Drug Design and Medicinal Chemistry.* Vol. 1, No. 1, 2015, pp. 1-11. doi:10.11648/j.jddmc.20150101.11.
- [4]. Solanki, A. and Thakur, I. (2007). *Indian Journal of Chemistry.* 45(B): 517.
- [5]. Saleem, F. (2008). *Eur. Pot., CHAPPL.* 87: 19. [6] Shakeel, A., Altaf, A. A., Qureshi, A. M., & Badshah, A. (2016). Thiourea derivatives in drug design and medicinal chemistry: A short review. *J. drug des. med. chem*, 2(1), 10.
- [6]. Yuan, Y. F., Wang, J. T., Gimeno, M. C., Laguna, A., & Jones, P. G. (2001). Synthesis and characterisation of copper complexes with N-ferrocenoyl-N'-aryl (alkyl) thioureas. *Inorganica Chimica Acta*, 324(1-2), 309-317.
- [7]. Y.M. Zhang, T.B. Wei, L. Xian, L.M. Gao, *Phosphorus, Sulphur Silicon Relat. Elem.* 179 (2004) 2007–2013.
- [8]. Y.M. Zhang, T.B. Wei, X.C. Wang, S.Y. Yang, *Indian J. Chem., Sect. B* 37 (1998) 604–606. [10] Weiqun, Z., Baolong, L., Jiangang, D., Yong, Z., Lude, L., & Xujie, Y. (2004). Structural and spectral studies on N-(4-chloro) benzoyl-N'-(4-tolyl) thiourea. *Journal of molecular structure*, 690(1-3), 145-150.
- [9]. Eweis, M., Elkholy, S. S., & Elsabee, M. Z. (2006). Antifungal efficacy of chitosan and its thiourea derivatives upon the growth of some sugar-beet pathogens. *International Journal of Biological Macromolecules*, 38(1), 1-8..

- [10]. Saeed, S., Bhatti, M. H., Tahir, M. K., & Jones, P. G. (2008). Ethyl 4-(3-butyrylthioureido) benzoate. *Acta Crystallographica Section E: Structure Reports Online*, 64(7), o1369-o1369.
- [11]. Walpole, C., Ko, S. Y., Brown, M., Beattie, D., Campbell, E., Dickenson, F., ... & Urban, L. (1998). 2-Nitrophenylcarbamoyl-(S)-prolyl- (S)-3-(2-naphthyl) alanyl-N-benzyl-N- methylamide (SDZ NKT 343), a potent human NK1 tachykinin receptor antagonist with good oral analgesic activity in chronic pain models. *Journal of medicinal chemistry*, 41(17), 3159-3173.
- [12]. Gan, S. F., Wan, J. P., Pan, Y. J., & Sun, C. R. (2011). Highly efficient and catalyst-free synthesis of substituted thioureas in water. *Molecular diversity*, 15, 809-815.
- [13]. Makhsumov, A. G., Safaev, A. S., & Abidova, S. V. (1969). Katal Pererab. Uglevodordn. Syrya 1968, 101. In *Chem. Abstr* (Vol. 71, p.101668v).
- [14]. Vibhute, Y.B. and Basser, M.A. (2003). *Ind. J. of Chem.* 42(B): 202-205.
- [15]. Padmanaban, R.; Gayathri, A.; Gopalan, A.I.; Lee, D.-E.; Venkatramanan, K. Comparative Evaluation of Viscosity, Density and Ultrasonic Velocity Using Deviation Modelling for Ethyl-Alcohol Based Binary Mixtures. *Appl. Sci.* 2023, 13, 7475.
- [16]. Zhang, L.X. Zhang, A.J. Hu, M.L. and Lei, X.X. (2003). *Acta Chim.Sinica*. 61(6): 917.

Determination of ΔH , ΔS and ΔG of [MDA] and [EDA] by Conductometric Studies

A.B.Dhote, K.P.Jumde, S.H.Shrirame

Department of Chemistry, N. S. Science and Arts College, Bhadrawati 442 902, Maharashtra, India

ARTICLE INFO

Article History:

Accepted : 01 Jan 2025

Published : 10 Jan 2025

Publication Issue :

Volume 12, Issue 7

January-February-2025

Page Number :

11-16

ABSTRACT

Conductivity play vital role in molecule; diffusion, transmission, metabolism (molecule activity and molecule effect) and excretion in pharmacokinetics and pharmacodynamics of molecules. Thermodynamic parameters affected by substituent's of molecule. Considering these facts recently in this laboratory, conductometrically thermodynamic parameters of 5-(1-methylamino-2,4-dithiobiureto)aminoindole [MDA] and 5-(1-ethylamino-2,4-dithiobiureto)aminoindole [EDA] were investigated at different molar concentrations and different percentage compositions. This work mainly highlights on investigation of G , K and μ values. The thermodynamic parameters viz. ΔH , ΔS and ΔG for ion pair formation were determined from the value of ion association constant at 303.15 K. This technique is suitable and accurate to study pharmacokinetics and pharmacodynamics parameters.

Keywords: Conductometric measurements, thermodynamic parameters, [MDA], [EDA]

I. INTRODUCTION

Organic chemistry of 2,4-dithiobiureto nuclei contain heterocycles and heteroacycles revealed distinct effects of these compounds are due to their strong biological activities¹⁻¹². Indoles showed antimicrobial, anti-inflammatory, anti-cancer and anti-oxidant activities¹³⁻¹⁵. These 2,4-dithiobiurets can also be used as intermediates for synthesis of numerous heterocycles with notable biological activities¹⁶⁻¹⁹. The biological uses of 2,4-dithiobiuret are altered by different substitutions on its nitrogen atom. Numerous 2,4-dithiobiurests were produced as part of a larger lab program to manufacture heteroacycles, and these were then converted into 5, 6, and 7 member heterocycles²⁰.

With conductometric measurements G , K and μ values, ΔH , ΔS and ΔG can be determined and which provided theoretical information about medicine/molecule activity²¹.

Conductance measurements provide very important and valuable information regarding ion-ion and ion-solvent interactions^{22,23}. Conductance of alkali metal in different mixtures mixed solvents were reported^{24,25}. The

thermodynamic parameters and Walden products of different complexes were studied by few researcher and they also determined the comparison of transition metal complexes among the halide groups²⁶. Interaction between sodium sulphate and 1-propanol, 1-butanol, 1-pentanol and 1-hexanol at different temperatures were determined by conductometric technique²⁷.

The present study deals with an investigation of conductometric properties, thermodynamic behaviour and Walden product of 5-(1-methylamino-2,4-dithiobiureto)aminoindole [MDA] and 5-(1-ethylamino-2,4-dithiobiureto)aminoindole [EDA] in ethanol-water mixture at different concentrations and different percentage compositions at constant temperature 303.15 K.

II. EXPERIMENTAL

All the chemicals and solvents used for the synthesis were of A.R. grade. All the freshly prepared solutions were used for investigations. Different concentration solutions of 0.1M of 5-(1-methylamino-2,4-dithiobiureto)aminoindole [MDA] and 5-(1-ethylamino-2,4-dithiobiureto)aminoindole [EDA] were prepared. 0.1M solution of [MDA] and [EDA] was prepared and then by serial dilution method, 0.075 M, 0.050 M and 0.025 M were prepared in 100% water and ethanol-water mixture respectively. Similar solutions were prepared for 80% and 70% water-ethanol mixture. All the solutions of molecule were always used a fresh in the present investigation.

In 50 ml glass beaker [MDA] solution was taken and it was kept inside the thermostat for 15-20 minutes to attain the thermal equilibrium 303.15 K. After achieving the thermal equilibrium, the conductivity was measured. Similar procedure was adopted for [EDA].

III. RESULTS AND DISCUSSION:

During this investigation conductometric measurements of 100%, 80%, and 70% mixtures of water-ethanol were prepared. In first set 0.1M solution of [MDA] and in second set 0.1M solution of [EDA] was prepared in conductivity water and by serial dilution method 0.075M, 0.050M and 0.025M solutions were prepared. At 303.15 K the conductance of each solution was measured by conductivity bridge and result are cited in **Table 1** and **Table 2**. From the data observed conductance (G), specific conductance (k) and molar conductance (μ) were determined by known literature method.

Table 1: Conductometric Measurements of [MDA] at different concentration				
Determination of G, k and μ on different Concentrations at 303.15 K				
% of solution (Water-ethanol)	Concentration (M)	Observed conductance (G)	Specific conductance (k)	Molar conductance (μ)
100%	0.1 M	0.58×10^{-3}	0.550961×10^{-3}	5.689606
	0.075 M	0.49×10^{-3}	0.465317×10^{-3}	6.450887
	0.050 M	0.35×10^{-3}	0.332092×10^{-3}	7.021847
	0.025 M	0.19×10^{-3}	0.179836×10^{-3}	7.973448
80%	0.1 M	0.71×10^{-3}	0.674669×10^{-3}	6.926687
	0.075 M	0.68×10^{-3}	0.646121×10^{-3}	8.861609

70%	0.050 M	0.59×10^{-3}	0.560477×10^{-3}	11.58953
	0.025 M	0.39×10^{-3}	0.370156×10^{-3}	15.58626
	0.1 M	0.23×10^{-3}	0.2179×10^{-3}	2.359003
	0.075 M	0.2×10^{-3}	0.189352×10^{-3}	2.771363
	0.050 M	0.18×10^{-3}	0.17032×10^{-3}	3.786404
	0.025 M	0.12×10^{-3}	0.113224×10^{-3}	5.308966

Table 2: Conductometric Measurements of [EDA] at different concentration				
Determination of G, k and μ on different Concentrations at 303.15 K				
% of solution (Water-ethanol)	Concentration (M)	Observed conductance (G)	Specific conductance (k)	Molar conductance (μ)
100%	0.1 M	0.20×10^{-3}	0.189352×10^{-3}	2.07352
	0.075 M	0.15×10^{-3}	0.141772×10^{-3}	2.13696
	0.050 M	0.1×10^{-3}	0.094192×10^{-3}	2.26384
	0.025 M	0.06×10^{-3}	0.056128×10^{-3}	3.02512
80%	0.1 M	0.14×10^{-3}	0.132256×10^{-3}	1.50256
	0.075 M	0.13×10^{-3}	0.12274×10^{-3}	1.8832
	0.050 M	0.1×10^{-3}	0.09419×10^{-3}	2.26384
	0.025 M	0.06×10^{-3}	0.056128×10^{-3}	3.02512
70%	0.1 M	0.13×10^{-3}	0.1227×10^{-3}	1.4074
	0.075 M	0.11×10^{-3}	0.103708×10^{-3}	1.62944
	0.050 M	0.09×10^{-3}	0.084676×10^{-3}	2.07352
	0.025 M	0.05×10^{-3}	0.046612×10^{-3}	2.64448

From **Table-1 to Table-2**, it was observed that the observed conductance (G) and specific conductance (k) were decreases from [MDA] to [EDA] continuously while molar conductance (μ) increases. In [MDA] observed conductance continuously decreases from 0.1M concentration to 0.025M concentration continuously. Same pattern was observed in percentage compositions of the mixture. Specific conductance of [MDA] decreases when the molar concentration and percentage composition of water decreases but the specific conductance increases at the same temperature. In [EDA] it was also observed that molar conductance increases from 0.1M concentration to 0.025M concentration as well as it increases in all percentage compositions. In 100% water molar conductance is highest while it will decreases from 100% to 70% water-ethanol percentage compositions. Molar conductance in 100% water is highest in all molar concentrations. Above results showed that [MDA] and [EDA] can give good medicinal activities. Same patterns of observed conductance, molar conductance and specific conductance were observed for [EDA]. These results throw light on pharmacokinetics of [MDA] and [EDA]. During this investigation it was observed that the molar conductance of [MDA] is more than [EDA] which clearly indicates the pharmacokinetic effect of [MDA] is comparatively good than [EDA]. It means that the absorption, transformation and metabolism of [MDA] is better than [EDA], so [MDA] possesses best metabolic activity than [EDA].

The specific constant (K_{sp}), $\log(K_{sp})$ and thermodynamics parameter viz. change in free energy (ΔG), change in entropy (ΔS) and change in enthalpy (ΔH) of [MDA] and [EDA] were determined by known literature method at various molar concentration, percentage compositions and temperatures and result are cited in **Table 1** to **Table 8**.

Table 3 : Conductometric Measurements of [MDA] at different concentration					
Determination of K_{sp}, $\log K_{sp}$, ΔG, ΔH and ΔS at different Concentrations at 303.15 K					
SYSTEM: [MDH]			MEDIUM - 100% WATER		
Conc. (M)	K_{sp}	$\log K_{sp}$	ΔG	ΔH	ΔS
0.100	0.07979	-1.02091	5749.358	-580158	-1953.05
0.075	0.054843	-1.14585	6467.024	-580158	-1955.44
0.050	0.029895	-1.32194	7478.517	-580158	-1958.81
0.025	0.004948	-1.62297	9207.676	-580158	-1964.57

Table 4 : Conductometric Measurements of [MDA] at different concentration					
Determination of K_{sp}, $\log K_{sp}$, ΔG, ΔH and ΔS at different Concentrations at 303.15 K					
SYSTEM: [MDA]			MEDIUM - 80% WATER		
Conc. (M)	K_{sp}	$\log K_{sp}$	ΔG	ΔH	ΔS
0.100	0.059832	-1.11782	6306.023	-580158	-1954.9
0.075	0.039874	-1.24276	7023.689	-580158	-1957.25
0.050	0.019916	-1.41885	8035.182	-580158	-1960.67
0.025	-4.2E-05	-1.71988	9764.341	-580158	-1966.43

Table 5 : Conductometric Measurements of [MDA] at different concentration					
Determination of K_{sp}, $\log K_{sp}$, ΔG, ΔH and ΔS at different Concentrations at 303.15 K					
SYSTEM: MOLECULE [MDA]			MEDIUM - 70% WATER		
Conc. (M)	K_{sp}	$\log K_{sp}$	ΔG	ΔH	ΔS
0.100	0.049853	-1.17581	6639.137	-580158	-1956.01
0.075	0.03239	-1.30075	7356.803	-580158	-1958.4
0.050	0.014927	-1.47684	8368.296	-580158	-1961.78
0.025	-0.00254	-1.77787	10097.46	-580158	-1967.54

Table 6: Conductometric Measurements of [EDA] at different concentration					
Determination of K_{sp}, $\log K_{sp}$, ΔG, ΔH and ΔS at different Concentrations at 303.15 K					
SYSTEM: MOLECULE [EDA]			MEDIUM - 100% WATER		
Conc. (M)	K_{sp}	$\log K_{sp}$	ΔG	ΔH	ΔS
0.100	3.905965	0.573946	-3411.73	-580158	-1922.51
0.075	2.924472	0.449008	-2694.07	-580158	-1924.9
0.050	1.942983	0.272916	-1682.57	-580158	-1928.27
0.025	0.961491	-0.02811	46.58543	-580158	-1934.04

Table 7: Conductometric Measurements of [EDA] at different concentration					
Determination of K_{sp}, log K_{sp}, ΔG, ΔH and ΔS at different Concentrations at 303.15 K					
SYSTEM:LIGAND [EDA]			MEDIUM - 80% WATER		
Conc. (M)	K_{sp}	Log K_{sp}	ΔG	ΔH	ΔS
0.100	3.120772	0.477036	-2855.07	-580158	-1924.36
0.075	2.335579	0.352098	-2137.4	-580158	-1926.76
0.050	1.550386	0.176006	-1125.91	-580158	-1930.13
0.025	0.765193	-0.12502	603.2504	-580158	-1935.89

Table 8 : Conductometric Measurements of [EDA] at different concentration					
Determination of K_{sp}, log K_{sp}, ΔG, ΔH and ΔS at different Concentrations at 303.15 K					
SYSTEM:MOLECULE [EDA]			MEDIUM - 70% WATER		
Conc. (M)	K_{sp}	Log K_{sp}	ΔG	ΔH	ΔS
0.100	2.728176	0.419044	-2521.95	-580158	-1925.47
0.075	2.041132	0.294106	-1804.29	-580158	-1927.87
0.050	1.354088	0.118014	-792.795	-580158	-1931.24
0.025	0.667044	-0.70704	936.3644	-580158	-1937

From **Table-3** to **Table-8** it was observed for these molecules K_{sp}, log K_{sp}, ΔH and ΔS decreases continuously while ΔG increases when we go from 0.1M concentration solution to 0.025M concentration. Same pattern was observed in percentage composition of the mixture i.e. these thermodynamic parameters are highest in 100% water while least in 70% water-ethanol solvent. In [EDA] the values of all thermodynamic parameter as well as K_{sp} and log K_{sp} are the greatest than [MDA].

IV. CONCLUSION:

From this investigation it is clear that various functional groups such as electron donating, electron withdrawing, acidic, basic and various functional groups present in the molecule directly affect conductance, specific conductance, molar conductance, K_{sp}, ΔH, ΔS and ΔG values of that molecule. The structure of the molecule as well as nature of that molecule directly affects these parameters. The temperature molar concentrations and percentage compositions are also responsible for changing the values of these parameters. The solute (molecule)-solvent interactions, solvent-solvent interactions, solvent-solvent-solute interactions and solute-solute-solvent interactions are another factor which directly hamper these parameters. The internal geometry as well as internal and intra hydrogen bonding affect these parameters.

During this investigation it was also observed that the molar conductance of [MDA] is highest than [EDA] which clearly indicates the molecule effect of [MDA] is comparatively more than [EDA].

V. DISCLOSURE OF CONFLICT OF INTEREST:

Authors wish to state that there is no conflict of interest on this work.

VI. REFERENCES

- [1]. Tayade D.T., Waghmare S.A., Am. J. Pharm, Res., 6(3), 2016, 605-612.
- [2]. Tayade D.T., Bhagwatkar A.K., D.M. Nagrik, J. App. Chem., 2(4), 2013, 993-997.
- [3]. Tayade D.T., Mohammad F.Z., Ind. J. Pharma. Sci. Res., 4(4), 2014, 1-3.
- [4]. Tayade D.T., Thombare R.D., Eur. J. Pharm. Med. Res., 3(3), 2016, 443-446.
- [5]. Lunge M.S., Shaikh R.S., Tayade D.T., Int. J. Adv. Res., 4(1), 2016, 908-912.
- [6]. Tayade D.T., Padhen S.S., Eur. J. Pharm. Med. Res. 3(8), 2016, 538-540.
- [7]. Tayade D.T., Kale P.R., Int. J. App. Res., 3(3), 2016, 370-374.
- [8]. Tayade D.T., Ingole S.P., Eur. J. Pharm. Med. Res., 3(7), 2016, 214-219.
- [9]. Tayade D.T., Raghuvanshi M.R., Bhagwatkar A.K., Aswale S.R., Canadian Int. J. Chem., 3(2), 2011, 74-78.
- [10]. Murhekar M. M., Padghan P.D., Mhaske S.S., Khadsan R.E., Der pharma Chemica, 2011, 396-399.
- [11]. Paranjpe M.G., J. Ind. Chem. Soc., 4(10), 1996, 42-45.
- [12]. Chigwada T. R., Chikwana E., Ruwana T., Olagunju O., J. of Phys. Chem. 4,111(45), 2007, 11552-11561.
- [13]. Isankar R. D., Tayade D. T., Journal of medicinal chemistry and molecule discovery, 2017, 02, 541-545.
- [14]. Bodkhe P. S., Wadekar A.B. Isankar R.D. and Tayade D.T., Journal of chemistry and chemical sciences, 2019, 9(2), 45-48.
- [15]. Tayade K. D., Pund D. A., Isankar R. D., Patil S. U., Journal of Medicinal chemistry and Molecule discovery, 2016, 1, 15-19.
- [16]. Tayade D.T., Bhagwatkar A.K., Int. J. of Pharm Pharmaceutical Sci Res, 3(3), 2013, 91-93.
- [17]. Sing A.K., Mishra G., Joyti K., J. App. Pharm. Sci., 01(5), 2011, 44-49.
- [18]. Ekhallas N., J Am. Sci., 6(8), 2010, 54-57.
- [19]. Sharma P.C., Kharb R., Yar M.S., Kaur P., Int. J. Pharm Sci. Res. 2(4), 2011, 758-771.
- [20]. Padghan P. D., Baldaniya B. B., Khadson R. E., Mhaske S. S. Der Pharma Chemica, 3(6), 2011, 243-246.
- [21]. S.Chakraborty, D.Shukla, A.Jain, B.Mishra and S.Singh, J.Coll.Int.Sci., 355, 242-249, (2009).
- [22]. E. A. Gomaa, B. M. Al-Jahdalli, Conductometric Studies of Ionic Association of Divalent Asymmetric Electrolyte $\text{Cu}(\text{NO}_3)_2$ with Kryptofix -22 in Mixed (MeOH-DMF) Solvents at Different Temperatures, American Journal of Condensed Matter Physics, Vol. 2 No. 1, 2012, pp. 16-21. doi: 10.5923/j.ajcmp.20120201.03.
- [23]. W.A.L. Izonfuo, C.C. Obunwa, Ind. J. Chem., 38A, 939, (1999).
- [24]. G.C. Bag, N.M. Singh, N.R. Singh, J. Ind. Chem. Soc., 77, 146, (2000).
- [25]. N. Dubey, J. Surface Sci. Technol., 24, 139-148, (2008).
- [26]. A.B. Wadekar, D. T. Tayade, [2016], Conductometric Study of Substituted thiocarbamidonaphthols in 70% Ethanol- Water Mixture at Different Molar Concentrations at Constant Temperature, International Journal of Science and Research 5(1), 678-680
- [27]. Agnieszka Boruń, Conductance and ionic association of selected imidazolium ionic liquids in various solvents: A review, Journal of Molecular Liquids, 276, 2019, 214-224, <https://doi.org/10.1016/j.molliq.2018.11.140>.

Thin-Layer Chromatography Separation and Identification of Heavy Metals from Ore Water Sample

Ashish Bansod¹, Amol Thakare¹, Rajesh Gulhane²

¹Department of Chemistry, Rajarshee Shahu Science College, Chandur Rail, District Amravati, Maharashtra, India

²Department of Chemistry, Hutatma Rashtriya Arts & Science College Ashti District Wardha, Maharashtra, India

ARTICLE INFO

Article History:

Accepted : 01 Jan 2025

Published : 10 Jan 2025

Publication Issue :

Volume 12, Issue 7

January-February-2025

Page Number :

17-26

ABSTRACT

Heavy metal cations have been chromatographed on silica gel thin-layer chromatography plates with pure organic, mixed organic and mixed aqueous-organic mobile phases. Mobile phases such aqueous mixture of acetic acid, minchloro acetic acid, dichloroacetic acid and trichloroacetic acid were found most suitable for rapid separation and identification of mixtures of Fe(II), Mn(II) and Zn(II) respectively. The effect of impurities such as inorganic ions was investigated at different sample solution pH. The proposed method was successfully used for identification of Fe(II), Mn(II) and Zn(II) from a variety of ore water samples.

I. INTRODUCTION

Heavy metals have recently received considerable attention from analysts, because of their physical and environmental importance [1,2]. Metals such as Pb, Cd, Hg, Ni, Cu, Zn and As are toxic and harmful to human health. They can form stable complexes with bio-ligands containing oxygen, nitrogen, or sulphur atoms [3] which control several redox processes in living organisms. The substantial increase in the use of heavy metals over the past few decades has inevitably resulted in an increased flux of metallic substances in aquatic life. Industrial waste is the major source of different kinds of metal pollution in aqueous systems. The major sources of chromium in the aquatic environment are electroplating and metal-finishing industrial effluents, sewage and wastewater treatment plant discharge, and chromates from cooling water.

The different analytical techniques available for the detection, determination, and separation of heavy metal include normal-phase and reversed-phase thin-layer chromatography [4-6], ion chromatography [7,8], extraction chromatography [9], ion-exchange chromatography [10,11], reversed-phase high-performance liquid chromatography [12,13], micellar electro kinetic chromatography [14], precipitation flotation [15], solid-phase extraction [16], titrimetry [17,18], capillary electrophoresis [19,20], spectro-photometry [21,22], atomic-absorption spectroscopy [23-25], graphite furnace atomic-absorption spectroscopy [26,27], atomic emission

spectroscopy [28], neutron activation analysis [29,30], and hyphenated techniques such as ion-exchange chromatography–flame atomic absorption spectroscopy [31], ion-chromatography–thermal lens spectrometry [32,33], gas chromatography–neutron activation analysis [34], inductively coupled plasma mass spectroscopy [35,36], inductively coupled plasma mass spectroscopy–atomic emission spectroscopy [37,38], ion-exchange chromatography–flame atomic absorption spectroscopy [39], solid-phase extraction–flame atomic emission spectroscopy [40], liquid chromatography–inductively coupled plasma mass spectroscopy [41], high-performance liquid chromatography–inductively coupled plasma mass spectroscopy [42], and ion chromatography–inductively coupled plasma mass spectroscopy [43]. Of the different separation procedures, thin-layer chromatography (TLC) is probably the most versatile, because it can be used for the selective separation of metal cations on the micro and macro scales. The use of TLC plates has further enhanced the efficiency of this technique. An exhaustive survey of the literature published in the last thirty years [44] shows that much progress has been made in developing rapid and selective TLC methods for separation of toxic heavy metals (Cu, Ni, Co, Pb, Cd, Zn, Hg, Cr, Fe, and Al) from interfering elements, by use of a variety of acidic developers containing mineral or carboxylic acids as one of the components. Systematic examination of published data on the use of acidic mobile phases for analysis of metal cations shows that the number of applications of the acids decreases in the order: $\text{HCl} > \text{HNO}_3 > \text{H}_2\text{SO}_4 > \text{H}_3\text{PO}_4 > \text{CH}_3\text{COOH} > \text{HCOOH} > \text{other carboxylic acids}$. That HCl is used most frequently is understandable, because it forms chloro complexes with almost all heavy metal cations. Use of formic acid as a mobile phase component in the TLC of metal cations has received little attention [45–49] despite several favorable properties:

- i) It does not result in oxidation of cations during analysis;
- ii) formic acid-containing mobile phases are less affected by the properties of silica gel than those containing other acids [50];
- iii) It enables excellent resolution of aflatoxins [50] and metal cations [45–49]; and
- iv) It is sufficiently acidic ($K_a(\text{H}_2\text{O})$ at $25^\circ\text{C} = 1.77 \times 10^{-4}$) to prevent hydrolysis of salts.

Considering the relevance and significance here we reported studied deals with the thin layer chromatographic behaviors of three metal ions like Fe, Zn and Mn. The metals were separated in different solvents systems using unimpregnated layers of silica Gel – as an adsorbent. The developing solvents include the aqueous solution of acetic acid and its sodium salt. The effect of chloro substituent group in acetic acid i.e. mono, di and tri chloro on the migrations of above mentioned metal ions is also studied. The optimum conditions for the separation of metal ions in ternary component mixture are established. The effect of pH and concentration of mobile phase on the R_f values of different metal ions are studied. The R_f values of each ion are graphically presented.

The method developed for the separation of metal ions present in synthetic mixture was applied to the separation of metal ions in tube well water and also to water samples from lake.

II. METHODS AND MATERIAL

Experimental Apparatus.

Ordinary glass plates of 5X 20 cm size were used as chromatoplates for coating silica gel–G. The chromatography was performed in 15 x 30 cm chromatography glass jar. Systronic pH meter 305 was used for adjusting the pH of the solution, small borosil glass spray of 100 ml capacity were used for spraying the chromatograms with different detecting reagents.

Chemicals and Reagents.

The chemicals used were all analytical grade, double distilled water used for the preparation of solution and slurry. Silica Gel –G (E. Merck) was used for preparation of thin layers. The stock solution (0.05M) of Fe(II), Zn(II) and Mn(II) were prepared by dissolving their chlorides, nitrates and sulphate in 0.1 M HCl. The difference solvents used in the systems as mobile phase are aqueous acetic acid, monoacetic acid, dichloroacetic acid, trichloroacetic acid aqueous sodium acetate etc.

Detection Reagents.

The detecting agents used for detection of metal ions are listed as follows.

- 1) 0.05 % dithizone in carbontetrachloride.
- 2) 3 % aqueous potassium ferrocyanide
- 3) 0.1% aqueous solution of 4-(2-pyridylazo)-resorcinol.

Preparation of Thin Layer Plates.

Slurry was prepared by mixing silica –gel G and double distilled water in the ration 1:3 with constant shaking for 10 minutes. It was then immediately applied to the glass plates by the dipping method. The plates were allowed to dry overnight at room temperature and were used next day for thin layer chromatography.

Solvent system.

The aqueous solution of acetic acid, monoacetic acid, dichloroacetic acid, trichloroacetic acid aqueous. Sodium acetate etc. are used as mobile phase in the range of concentration from 0.01 M to 0.2 M.

Procedure.

The stock solution prepared above were standardized by established method. The test solution was spotted on the chromate plates with capillary tube and the spot were blown dried with hot air. The solution of chosen solvents systems with a particular concentration was adjusted to desire pH using NaOH or HCl solution. The chromatograms were devolved by ascending technique for 15 minutes in the glass jar containing 20 ml of developing solvents. The plates were again dried with a hot air blower. Solvent's front was marked and cations were detected by spraying suitable spot test reagents. The solution of dithizone was used for Zn(II) potassium ferrocyanide for Fe(III) and 4(2-pyridylazo)-resorcinol for Mn(II) as spraying reagent for detection of metal ions lastly the R values were measured.

All experiments are carried out at room temperature. The R_f values were measured in triplicate for each set of detererminations various experiments were carried out to study the effect of pH and concentration of mobile phase on R_f values of individual cation. The different metal included iron, zinc and manganese. The conditions were established where there was maximum difference between the R_f values of different ions. The binary and ternary mixtures of metal ions were prepared. These mixtures were spotted on the plates and chromatograms were developed using particular solvent system under study. The similar procedures were to the various solvent system of the present study.

Application to tube well water.

Tube well water samples were taken form sandur village (dist-Bellary Karantaka state which is manganese and iron ore area). Metals were separated in these samples by present method 100 ml of sample was evaporated to

dryness at a low flame. The residue was cooled and extracted with 0.1 N HCl. The extract containing mixture of different metal ions was then spotted on chromatoplates and the chromatogram was developed using aqueous sodium acetate as mobile phase separated metals were detected by using various spot reagents. The chromatogram was also developed by using aqueous acetic acid, aqueous monochloro acetic acid, aqueous dichloro acetic acid and aqueous trichloro acetic acid as mobile phases separated metal were detected by using various spot detecting reagents.

Application to water from lake.

The water samples were taken from lake from sandur region (dist-Bellary, Karanataka) same procedures were applied which was applied for sample from tube well water.

III.RESULTS AND DISCUSSIONS

The results of various experiments conducted to achieve the separation Fe(II) Zn(II) and Mn(II) metal ions from their mixture. The study includes the use of aqueous solution of acetic acid and its sodium salt and also the effect of chloro substituent of acetic acid on the migration Fe(II) Zn(II) and Mn(II) of is also studied.

In present work R_f values of different metal ions are discussed. The different separation achieved in (binary and ternary) component mixture in various systems. The optimum conditions for several binary, ternary mixtures are established by performing various experiments. The present study emphasizes the use of unimpregnated silica Gel-G, thin layers as adsorbents and use of different ion exchanges, inorganic salts and organic ion exchange for impregnation of silica Gel -G is totally avoided. The present method is also applied to the separation of metal ions from the water samples.

Part A

Separation studies of Fe(III), Mn(II) and (II) metal ions in aqueous sodium acetate etc.

Choice of proper adsorbent.

Many new sorbent phases have been developed by impregnation silica gel-G with different inorganic salts for separations of metal ions by thin Layer chromatography using carboxylic acids as media for the preparation of thin layer chromatographic plates, impregnates on silica gel by the use of ammonium chloride, barium nitrates has also been reported. It has been observed that the previous workers tried to reduce the development time and aimed at economical TLC method. The use of acetic acid and its salt as mobile phase has been reported with many separation. The system included the separation of metal ions Fe(III), Zn(II), Ni(II), Cu(II), Cd(II), Pb(II), Al(II) and Ag(II), In binary and ternary mixture with development time with 12 minute. They used silica Gel-G impregnated with inorganic salts. It was thought worthwhile to reduce the time of separation still further and hence the present system was undertaken. The section includes the use of unimpregnated silica Gel-G thin layer as an adsorbent and aqueous solution of sodium acetate as a mobile phase.

Effect of development time.

Various experiments were carried out to develop the present method. The R_f measurements at different migration time were done for Fe(II), Zn(II) and Mn(II) ,metal ions .The result obtained are presented in table 3.1

The results of variation in the R_f values with development time are given in table 3.1 .It is evident from the table 3.1 that though there is a little effect of development time on the R_f values of metal ions .It is seen that binary and also ternary separation of metal ions are possible in less than five minutes. However the effect of time on the R_f values of metal ions has been studied up to 20 minutes as development time. Finally 10 minutes time was fixed as optimum development time for the migration of metal ions.

Effect of pH.

The results of effect of pH on the R_f values of all the three metal ions are illustrated in fig 3.1 .The effect of pH on the R_f values of different metal ions was studied in the range of 1.0 to 10.0 .It is observed that Fe(II), Zn(II) and Mn(II) showed R_f between 0.39 and 0.55 at pH 1.0 Fe(III) remain near base line between 5.0 to 10.0 .The increase in pH from 3.0 to 10.0 did not solvent front at low pH value .The cation showed little separation tendency until PH 4.0 it is also observed that beyond pH 5.0 Fe(III) and Zn (II) remain near the base line. It is observed that though metal ions travel with solvent front at low pH the maximum difference in the R_f optimum pH for further R_f measurements in sodium acetate media.

Effect of Concentration.

The effect of sodium acetate concentration on the R_f values of different metal ions is also show in the table 3.2 .It is revealed form table 3.2 that at 0.01 M acetate concentration the different metal ions showed very close R_f values and hence it was not possible to separate them at 0.01 M acetate concentration.From table 3.2 it is reveled that at 0.05 M concentration metal ions showed little separation tendencies .The increase in sodium acetate concentration to 0.1 M as revealed form table3.2 helped in concluding that 0.1 M could be fixed as optimum concentration because there was a maximum difference in the R values of metal ions leading to satisfactory separation. Thus 0.1M was fixed as optimum concentration for all R measurements in sodium acetate system.

Application to environmental sample.

The different qualitative synthetic mixture within 10 minutes are shown in table 3.3 .The method was further applied to the separation and detections of metal ions in tube well water samples and water from lake .Result are tabulated in table 3.4

Table 1.1 Variation R_f values with developments time.

Absorbent – silica Gel –G

Mobile Phase- 0.1M sodium Acetate pH -5.0

Metal ions	Development time in minutes			
	5	10	15	20
	Rf Values			
Fe(II)	0.06	0.12	0.10	0.06
Zn(II)	0.37	0.34	0.30	0.4
Mn(II)	0.60	0.62	0.64	0.66

Table 1.2 Variation R_f values with developments time.

Absorbent – silica Gel –G
Mobile Phase- 0.1M sodium Acetate pH -5.0 developing
Time -10 minutes

Metal ions	Cinc, of Sodium Acetate	R _f values
Fe(II)	0.01 M	0.12
Zn(II)		0.36
Mn(II)		0.24
Fe(II)	0.05	0.05
Zn(II)		0.50
Mn(II)		0.41
Fe(II)	0.1M	0.10.
Zn(II)		0.62
Mn(II)		0.34
Fe(II)	0.2M	0.27
Zn(II)		0.56
Mn(II)		0.40

Table 1.3 Qualitive separation of metal ions in synthetic mixtures.

Variation R_f values with developments time

Absorbent – silica Gel –G

Mobile Phase-0.1M sodium Acetate pH -5.0 developing

Time -10 minutes

Composition mixture	Metal ions detected with R _f values
Fe(II) , Mn(II)	Fe (0.09) ,Mn(0.60)
Fe(II) ,Zn(II)	Fe (0.09) ,Zn(0.33)
Mn(II) , Zn(II)	Mn(0.61) , Zn(0.31)
Fe(II) , Mn(II), Zn(II)	Fe(0.10) , Mn(0.60), Zn(0.33)

Table 1.4 Qualitive separation of metal ions in Water samples.

Variation R_f values with developments time

Absorbent – silica Gel –G

Mobile Phase- 0.1M sodium Acetate pH -5.0 developing

Time -10 minutes

Water sample	Composition	Metal ions detected by present method with R _f values
1) Tube well water sample	Fe(II), Mn(II), Zn(II)	Fe(0.09) Mn(0.61) Zn(0.34)
2) Water sample from lake	Fe(II), Mn(II), Zn(II)	Fe(0.10) Mn(0.69) Zn(0.33)

Part B: -

Separation studies of Fe(III), Mn(II) and (II) metal ions in acetic acid and chloro substituted acetic acid media.

Choice of proper adsorbent.

This section also includes the use of unimpregnated silica Gel-Ge thin layer as an adsorbent and aqueous solution acetic acid and chlorosubstituted acetic acid as a mobile phase.

Effect of development time.

The R measurements at different migration time were done for Fe(III) ,Zn(II) and Mn(II) ions. The results obtained are presented in table 4.1 to 4.4 .it is evident form the table that there is a little effect of development time on the R values of metal ions. The effect of time on the R_f values of metal ions has been studied up to 20 minutes as development time. Finally, 10 minutes time was fixed as optimum development time of the migration of metal ions.

Effect of pH.

The result of effect of pH on the R values of all the three metal ions are illustrated in fig 4.1 to 4.4. The effect of pH on the R_f values of different metal ions was studied in the range of 1.0 to 7.0 .

In acetic acid media it is observed that Fe(III) ,Zn(II) and Mn(II) showed R between 0.65 and 0.80 at pH 1.0 Fe(III) remain near base line between 5.0 to 7.0 .The increase in pH from 3.0 to 7.0 did not have any effect on the R_f values of metal ions Fe(III) and Mn(II).It is seen that most of the metal ions moved with solvent front at low pH .But the maximum difference in the R_f values of the metal ion are shown at pH 5.0 .So it was conclude that pH-5.0 as the optimums pH for further R_f measurements in acetic acid media.

In monochloro acetic acid media. It seen that Fe(III), Zn(II) and Mn(II) showed R_f between 0.70 and 0.90 at pH 1.0.The increase in pH from 3.0 to 7.0 did not have any effect on the R_f values of metal ions. It is observed that though metal ions travel with solvent front at low pH. The maximum difference in the R_f value of the metal ions are shown at pH-3.5 as the optimum pH for further R_f measurements in mono chloro acetic acid media

In dichloro acetic acid media. It is observed that Fe(III), Zn(II) and Mn(II) showed R_f between 0.55 and 0.60 at pH 1.0 .The increase in pH from 3.0 to 7.0 showed that Fe(III) and Mn(II) remain near the base line. It is observed that though metal ions travel with solvent front at low pH. The maximum difference in the R_f values of metal ions are shown at pH-2. It was thus concluding to fix pH-2.0 as the optimum pH for further R_f measurements in dichloro acetic acid media.

In trichloro acetic acid media. It is observed that Fe(III), Zn(II) and Mn(II) showed R_f between 0.80 to 0.95. The increase in pH from 2 to 7 showed that Fe(III) and Mn(II) remain near the base line .It is observed that enough metal ions travel with solvent front at low pH .The maximum difference in R_f values of metal ions are shown at pH-1.5 .It was thus conclude to fix pH-1.5 as the optimum pH for further R measurements in trichloroacetic acid media.

The effect of concentrations.

The effect of acetic acid, mono chloroacetic acid, dichloro acetic acid and trichloro acetic acid on the R_f values of different metal ions are observed and cited in table 4.5 .It is revealed from table 4.5 that at 0.01 M concentration of acetic acid ,monchloro acetic acid dichloro acetic acid and trichloro acetic acid. The different metal ions showed very close R_f values and hence it was not possible to separate them at 0.01 M concentration. Also it is revealed from table that at 0.05M concentration metal ions showed little separations tendencies. The increase in concentration of acetic acid, monchloro acetic acid, dichloro acetic acid and trichloro acetic acid to

0.1 M as revealed from table-4.5 helped in concluding that 0.1 M could be fixed as optimum concentration because there was a maximum difference in the R_f values of the metal ions leading to satisfactory separations. Thus 0.1 M was fixed as optimum concentration for all the R_f measurements in acetic acid, mono, di and tri chloro acetic acid system.

Application to environmental sample.

The different qualitative separations achieved in synthetic mixture within 10 minutes are shown in table 4.6. The method was further applied to the separation and detection of metal ions in tube well water samples and water samples from lake which are tabulated in table 4.7 and 4.8

Table 2.1 Variation R_f values with developments time.

Mobile Phase- 0.1M acetic acid pH -5.0

Metal ions	Development time in minutes			
	5	10	15	20
	R_f Values			
Fe(II)	0.36	0.24	0.20	0.12
Zn(II)	0.76	0.64	0.63	0.64
Mn(II)	0.92	0.90	0.87	0.88

Table 2.2 Variation R_f values with developments time.

Mobile Phase- 0.1M Mino chloroacetic acid pH -5.0

Metal ions	Development time in minutes			
	5	10	15	20
	R_f Values			
Fe(II)	0.36	0.18	0.13	0.11
Zn(II)	0.71	0.67	0.62	0.55
Mn(II)	0.87	0.88	0.84	0.87

Table 2.3 Qualitive separation of metal ions in synthetic mixtures.

Variation R_f values with developments time

Mobile Phase-0.1M Dichloroacetic acid pH -5.0

Metal ions	Development time in minutes			
	5	10	15	20
	R_f Values			
Fe(II)	0.54	0.44	0.38	0.37
Zn(II)	0.62	0.60	0.52	0.56
Mn(II)	0.78	0.91	0.89	0.90

Table 2.4 Qualitive separations of metal ions in Water samples.

Variation R_f values with developments time
Mobile Phase- 0.1M Trichloroacetic acid pH -5.0 developing

Metal ions	Development time in minutes			
	5	10	15	20
	R _f Values			
Fe(II)	0.53	0.51	0.47	0.41
Zn(II)	0.75	0.55	0.55	0.51
Mn(II)	0.85	0.91	0.83	0.83

Table 2.5 Variation in R_f values with change concentration.

Mobile Phase	Concentration	pH	Metal ions separated with R _f values
Acetic acid	0.1	5.0	Fe ²⁺ (0.04) , Mn ²⁺ (0.40), Zn ²⁺ (0.68)
	0.01	5.0	Fe ²⁺ (0.10) , Mn ²⁺ (0.40), Zn ²⁺ (0.38)
	0.05	5.0	Fe ²⁺ (0.38) , Mn ²⁺ (0.25), Zn ²⁺ (0.30)
Minochloroacetic acid	0.1	5.0	Fe ²⁺ (0.09) , Mn ²⁺ (0.92), Zn ²⁺ (0.57)
	0.01	5.0	Fe ²⁺ (0.16) , Mn ²⁺ (0.59), Zn ²⁺ (0.52)
	0.05	5.0	Fe ²⁺ (0.06) , Mn ²⁺ (0.70), Zn ²⁺ (0.57)
Dichloroacetic acid	0.1	5.0	Fe ²⁺ (0.41) , Mn ²⁺ (0.89), Zn(0.60)
	0.01	5.0	Fe ²⁺ (0.42),Mn ²⁺ (0.54), Zn ²⁺ (0.50)
	0.05	5.0	Fe ²⁺ (0.21) , Mn ²⁺ (0.60), Zn ²⁺ (0.41)
Trichloroacetic acid	0.1	5.0	Fe ²⁺ (0.57) , Mn ²⁺ (0.92), Zn ²⁺ (0.71)
	0.01	5.0	Fe ²⁺ (0.45) , Mn ²⁺ (0.62), Zn ²⁺ (0.55)
	0.05	5.0	Fe ²⁺ (0.31) , Mn ²⁺ (0.65), Zn ²⁺ (0.48)

Table 2.6 Separation of metal ions in synthetic mix.

Development time -10 minutes.

Solvents	pH	Metal ions separated with R _f values
Acetic acid	5.0	Fe ²⁺ (0.03) , Zn ²⁺ (0.69)
	5.0	Fe ²⁺ (0.04) , Mn ²⁺ (0.90)
	5.0	Mn ²⁺ (0.89), Zn ²⁺ (0.68)
	5.0	Fe ²⁺ (0.04) , Mn ²⁺ (0.90), Zn ²⁺ (0.68)
Minochloroacetic acid	5.0	Fe ²⁺ (0.05) , Zn ²⁺ (0.79)
	5.0	Fe ²⁺ (0.09) , Mn ²⁺ (0.95),
	5.0	Mn ²⁺ (0.91), Zn ²⁺ (0.57)
	5.0	Fe ²⁺ (0.08) , Mn ²⁺ (0.93), Zn ²⁺ (0.58)
Dichloroacetic acid	5.0	Fe ²⁺ (0.56) , Zn ²⁺ (0.87)
	5.0	Fe ²⁺ (0.40) , Mn ²⁺ (0.90)
	5.0	Mn ²⁺ (0.87), Zn ²⁺ (0.67)
	5.0	Fe ²⁺ (0.41) , Mn ²⁺ (0.87), Zn ²⁺ (0.61)
Trichloroacetic acid	5.0	Fe ²⁺ (0.57) , Zn ²⁺ (0.66)
	5.0	Fe ²⁺ (0.56) , Mn ²⁺ (0.88)
	5.0	Mn ²⁺ (0.86), Zn ²⁺ (0.69)
	5.0	Fe ²⁺ (0.47) , Mn ²⁺ (0.90), Zn ²⁺ (0.71)

Table 2.7 Qualitive separation of metal ions in Tube Water samplesVariation R_f values with developments time

Concentration 0.1M Developing Time -10 minutes

Mobile Phase	pH	Metal ions separated with R_f values
Acetic acid	5.0	Fe^{2+} (0.04) , Mn^{2+} (0.89), Zn^{2+} (0.67)
Minochloroacetic acid	5.0	Fe^{2+} (0.09) , Mn^{2+} (0.92), Zn^{2+} (0.56)
Dichloroacetic acid	2.0	Fe^{2+} (0.40) , Mn^{2+} 0.87), Zn^{2+} (0.61)
Trichloroacetic acid	1.5	Fe^{2+} (0.56) , Mn^{2+} (0.91), Zn^{2+} (0.72)

Table 2.8 Qualitive separation of metal ions in Tube Water samples from lakeVariation R_f values with developments time

Concentration 0.1M Developing Time -10 minutes

Mobile Phase	pH	Metal ions separated with R_f values
Acetic acid	5.0	Fe^{2+} (0.03) , Mn^{2+} (0.90), Zn^{2+} (0.68)
Minochloroacetic acid	5.0	Fe^{2+} (0.08) , Mn^{2+} (0.91), Zn^{2+} (0.57)
Dichloroacetic acid	2.0	Fe^{2+} (0.41) , Mn^{2+} (0.88), Zn^{2+} (0.12)
Trichloroacetic acid	1.5	Fe^{2+} (0.54) , Mn^{2+} (0.92), Zn^{2+} (0.76)

IV.ACKNOWLEDGMENT

The authors are wish thankful to university authority for providing research facility in Department of Chemistry, Sant Gadge Baba Amravati University, Amravati

V. REFERENCES

- [1]. H. Siegel, Metal Ions in Biological Systems, Vols. I and II, Marcel Dekker, New York, USA, 1986
- [2]. V. Venngopal and T. Luckey, Metal Toxicity of Metals and Metalloids, Plenum, New York, USA, 1987.
- [3]. M. Bukowska – Strzyżewska, W. Maniukewicz, G. Bazylak, and J. Masłowska, J. Crystallogr. Spectrosc. Res., 21, 157 (1991)
- [4]. G. Schubert, V. Alan, J. Zirko – Babic, and S. Turina, J. Planar Chromatogr., 1998, 11, 460.
- [5]. S. Przeszlakowski and M. Maliszewska, Chem. Anal., 1992, 37, 547.
- [6]. S.D. Sharma and S.C. Sharma, J. Chromatogr., A, 1999, 841, 263.
- [7]. M. Mizobuchi, Y. Horie, and K. Saito, Nara-ken Eisei Kenkyusho Nenpo, 26, 56, (1991) (Published 1992); Chem. Abstr., 1993, 118, 20248q.
- [8]. Y. Zhou, G. Shao, and S. Mu, Huanjing Huaxue, 15, 446 (1996); Chem Abstr., 1997, 126, 36660.
- [9]. R.O. Crubellati and A.G. Ledesma, Analyst, 1993, 118, 529.
- [10]. S.A. Nabi, A. Gupta, and A. Sikarwar, Ann. Chim., 1999, 89, 419.
- [11]. M. Ghannadi – Marageh, S.W. Husain, A.R. Khanchi, and S.J. Ahmady, Sep. Sci. Technol., 34, 219 (1999)
- [12]. M.L. Marina, P. Andres, and J.C. Diez – Masa, Chromatographia, 35, 621 (1993)
- [13]. Y. Tomita, Y. Aoyama, and E. Aoyama, Ibaraki Kogyo Koto Senmon Gakko Kenkyu Iho, 36, 65 (2001); Chem. Abstr., 135, 50686e (2001)

- [14]. E.F. Hilder, M. Macka, and P.R. Haddad, *Analyst*, 123, 2865 (1998)
- [15]. K.S. Lee, H.S. Choi, and Y.S. Kim, *Anal. Sci. Technol.*, 3, 419 (1990)
- [16]. V. Ostruba, J. Pivnicka, and V. Kanicky, *Collect. Czech. Chem. Commun.*, 2000, 65, 1865.
- [17]. L. Zheng and S. Wang, *Yejin Fenxi*, 16, 49 (1996); *Chem. Abstr.*, 126, 165878a (1997)
- [18]. K.K. Paliwal, D.K. Gorji, S. Kumar, N. Naulakha, A.K. Goswami, and D.N. Purohit, *Asian J. Chem.*, 2001, 13, 299.
- [19]. M.C. Mehra and C.A. Lucy, *Orient. J. Chem.*, 1996, 12, 231.
- [20]. Z. Chen, R. Naidu, and A. Subramanian, *J. Chromatogr. A*, 2001, 927, 219.
- [21]. W. Shi and T. Hu, *Huaxue Fence*, 34, 447 (1998); *Chem. Abstr.*, 1999, 130, 85763b.
- [22]. Z.G. Xu, X.H. Wen, and Q.Z. Wu, *Chin. Chem. Lett.*, 2001, 12, 635.
- [23]. Z. Shen, Y. Li, and Y. Li, *Guangdong Weiliang Yuansu Kexue*, 1998, 5, 69, *Chem. Abstr.*, 1999, 130, 147940.
- [24]. D. Qin, Z. Lin, and J. Wang, *Huaxue Fenxi Jiliang*, 9, 17 (2002); *Chem. Abstr.* 2001, 135, 24284.
- [25]. A. Gaspar, C. Songor, and J. Posta, *Fresenius J. Anal. Chem.*, 1999, 363, 480.
- [26]. S.T. Sauerhoff, Z.A. Grosser, and G.R. Carnrick, *At. Spectrosc.*, 1996, 17, 225.
- [27]. T.W. Lin and S.D. Huang, *Anal. Chem.*, 2001, 73, 4319.
- [28]. E.S. Zolotovitskaya, L.V. Glushkova, Z.V. Shititelman, and A.B. Blank, *Khim. Tekhnol. Vody*, 1993, 15, 255.
- [29]. T.M. Bahrainwala and Z.R. Tural, *J. Radioanal. Nucl. Chem.*, 1996, 214, 199.
- [30]. H. Rausch and T. Braun, *Fullerene Sci. Technol.*, 1997, 5, 407.
- [31]. B. Demirata, I. Tar, H. Filik, and H. Afsar, *Fresenius J. Anal. Chem.*, 1996, 356, 375.
- [32]. M. Sikovec, M. Franko, and M. Novic, *AIP Conf. Proc.*, 1999, 463, 682.
- [33]. M. Sikovec, M. Franko, M. Novic, and M. Veber, *J. Chromatogr. A*, 2001, 920, 119.
- [34]. G.S. Sattarov and A.A. Kist, *Czech. J. Phys.*, 1999, 49, 303.
- [35]. T. Etoh, M. Yamada, and M. Matsubara, *Kankyo Kagaku*, 3, 398 (1993); *Chem. Abstr.*, 119, 102860 (1993)
- [36]. J.C. Yu, X.-J. Wu, and Z. Chen, *Anal. Chim. Acta*, 2001, 436, 59.
- [37]. J. Guan, Y. Shi, B. Gao, and Y. Liu, *Yuanzineng Kexue Jishu*, 1991, 25, 8 *Chem. Abstr.*, 1993, 118, 15539.
- [38]. H. Chen, *Huaxue Shijie*, 41, 488 (2000); *Chem. Abstr.*, 2001, 134, 36428.
- [39]. V. Stresko, J. Polakovicova, and A. Celkova, *Chem. Pap.*, 2001, 55, 100.
- [40]. V. Ostruba, J. Pivnicka, and V. Kanicky, *Proc. – Semin. At. Spectrochem.*, 1998, 14, 247.
- [41]. Y.-L. Chang and S.J. Jiang, *J. Anal. At. Spectrom.*, 2001, 16, 858.
- [42]. Y. Martinez – Bravo, A.F. Roig – Navaro, F.J. Lopez, and F. Hernandez, *J. Chromatogr. A*, 2001, 926, 256.
- [43]. H. Guerleyuek and D. Wallschlaeger, *J. Anal. At. Spectrom.*, 2001, 16, 926.
- [44]. A. Mohammad, M. Ajmal, S. Anwar, and E. Iraqi, *J. Planar Chromatogr.*, 1996, 9, 318.
- [45]. N. Fatima and A. Mohammad, *Sep. Sci. Technol.*, 1994, 19, 429.
- [46]. M. Ajmal, A. Mohammad, and N. Fatima, *Microchem. J.* 1988, 37, 314.
- [47]. A. Mohammad and N. Fatima, *Chromatographia*, 1986, 22, 109.
- [48]. A. Mohammad and M.A.M. Khan, *J. Planar Chromatogr.*, 1995, 8, 134.
- [49]. A. Mohammad, M. Ajmal, and S. Anwar, *Acta Chromatogr.*, 1999, 9, 113.
- [50]. I. Balzer, C. Bogdanic, and C. Pepeljnjak, *J. Assoc. Anal. Chem.*, 1978, 61, 584.
- [51]. M. Ajmal, A. Mohammad, N. Fatima, and J. Ahmad, *J. Planar Chromatogr.*, 1988, 1, 329

Plant Based Green Synthesis of Lead Acetate NPs

A.K. Maldhure, M.S. Chavan, S.A. Thakare, M.J. Pawar

Department of Chemistry, Smt. Narsamma Arts, Commerce and Science College, Amravati, Maharashtra, India

ARTICLE INFO

Article History:

Accepted : 01 Jan 2025

Published : 10 Jan 2025

Publication Issue :

Volume 12, Issue 7

January-February-2025

Page Number :

27-33

ABSTRACT

In the current study, lead acetate nanoparticles were synthesized using NEEM and PAPAYA leaf extracts as stabilizing agents. The structural and optical properties of the nanoparticles were examined using FT-IR and XRD techniques. The particle size, determined using the Debye-Scherrer equation, ranged from 9 to 13 nm. The results demonstrated that the green-synthesized lead acetate nanoparticles are stable, and the green synthesis method is more cost-effective compared to traditional chemical methods. X-ray diffraction analysis confirmed that the as-synthesized lead acetate nanoparticles exhibited a simple monoclinic structure.

Keywords: Nanoparticles; Green Synthesis; Lead Acetate; X-ray Diffraction;

I. INTRODUCTION

Various physical and chemical techniques have been developed for the synthesis of metallic nanoparticles. In addition, nanotechnology plays a crucial role in creating clean, non-toxic, and environmentally friendly methods for the fabrication and assembly of these nanoparticles [1]. One promising approach is the biosynthesis of metallic nanoparticles using plant extracts, which offers an eco-friendly solution for producing nanoparticles with well-defined sizes, shapes, and controlled uniformity. Metal oxide nanoparticles (NPs) are gaining significant interest due to their potential applications in optoelectronics, nano-sensors, nano devices, nanoelectronics, information storage, and catalysis [2].

Green synthesis provides an environmentally friendly approach for the production of nanoparticles. Natural products, such as those derived from the neem plant, play a significant role in disease prevention and treatment by enhancing antioxidant activity, inhibiting bacterial growth, and modulating genetic pathways. The therapeutic potential of various plants in disease management is actively being researched due to their minimal side effects and cost-effectiveness. In contrast, allopathic drugs are often expensive and can have toxic effects on normal tissues and other biological functions. It is widely acknowledged that many pharmacologically active drugs are sourced from natural resources, including medicinal plants [3]. Several methods have been developed for the synthesis of metal nanoparticles, including photocatalytic reduction, radiolytic reduction, solvent

extraction reduction, microemulsion technique, polyol process, and alcohol reduction. Due to their excellent antibacterial and anti-inflammatory properties, these nanoparticles are increasingly used in the field of biomedicine [3].

Nanoparticles (NPs) are extremely small units, typically ranging from 1 to 100 nanometers in size. Due to their tiny dimensions, they are highly mobile and chemically reactive, owing to the large surface area relative to their volume. It is well-established that the properties of atoms and molecules in metals or non-metals at the nanoscale significantly differ from those of the bulk material [4]. These unique characteristics enable nanoparticles to have a wide range of practical applications in fields such as medicine, industry, and environmental remediation. Nanoparticles can also help in controlling potentially harmful metal concentrations. Furthermore, the interaction of nanoparticles with various materials is notably different from that of their larger counterparts. The production of nanoparticles is steadily increasing due to their diverse applications and benefits. In the last decade, nanoparticle production has surged, with a reported 25-fold increase between 2005 and 2010 (PEN, 2013). However, chemical synthesis of nanoparticles is associated with several challenges. Studies have indicated that the preparation of certain nanoparticles requires thermal processing, which can alter their physicochemical properties, including density, crystal structure, and the presence of surface contaminants. When these chemically synthesized nanoparticles, also known as engineered nanomaterials (ENMs), are used for biological applications, there is a risk of toxicity. The release of these particles into the environment must also be handled with caution. *Karakoti et al.* (2013) observed that even small changes in room temperature during synthesis or storage could lead to unpredictable and non-reproducible properties in nanoparticles [5].

According to the investigation by *Sahoo et al.*, the synthesis of lead acetate nanoparticles using papaya leaf extract as both a reducing and capping agent resulted in the formation of stable, monodisperse nanoparticles with a spherical shape. These nanoparticles had an average size of 27 nm [6]. A study conducted by *Singh et al.* proposed the green synthesis of lead acetate nanoparticles using papaya leaf extract and sodium hydroxide [7]. The synthesized nanoparticles were reported to have a spherical shape and a size range of 6-15 nm. Additionally, the study highlighted that these nanoparticles exhibited antimicrobial activity against both gram-positive and gram-negative bacteria. A study by *Sharma et al.* reported the green synthesis of lead acetate nanoparticles using papaya leaf extract and sodium hydroxide [8]. The synthesized nanoparticles were found to have a spherical shape and a size range of 50-80 nm. Additionally, the study demonstrated that these nanoparticles exhibited both antioxidant and antibacterial activities.

The present investigation, focused on the green synthesis of lead acetate nanoparticles using extract of *Azadirachta indica* and Papaya leaves. The synthesized samples were characterized by using X-ray diffraction (XRD), UV-Vis spectroscopy, Scanning electron microscopy (SEM) etc.

II. MATERIALS AND METHOD

2.1. Materials

Lead Acetate (Extra Pure) Tetrahydrated, Fresh and healthy leaves of *Azadirachta indica* leaves, Papaya leaves
Distilled water and Ethanol.

2.2. Method

2.2.1. Green Synthesis Method

2.2.1.1. Preparation of Leaf Extract.

For the synthesis of lead acetate nanoparticles, *Azadirachta indica* (neem) leaves and papaya leaves were used. Approximately 15 g of leaves were collected, washed thoroughly with running tap water to remove debris and other contaminants, then rinsed with distilled water and air-dried at room temperature for 2-3 days in the shade. The leaves were then cut into small pieces and crushed using a mortar and pestle. A Soxhlet apparatus was employed for the extraction of the leaf material.

2.2.1.2. Synthesis of Lead Acetate nanoparticles

For the synthesis of lead acetate nanoparticles, 150 mL of leaf extract was prepared. Then, 50 mL of lead acetate solution was mixed with 50 mL of water in a beaker using a stirrer. This mixture was added to the 150 mL of leaf extract in a 250 mL conical flask. Upon mixing, a dark green-colored precipitate began to settle. The mixture was left overnight to allow for the full formation of the precipitate. The next day, the obtained precipitate was filtered using Whatman Filter Paper No. 1, washed with distilled water, and left to dry overnight. The following day, the lead acetate nanoparticles were collected and labeled as LA-N (lead acetate nanoparticles prepared using neem leaves extract) and LA-P (lead acetate nanoparticles prepared using papaya leaves extract).

2.2.2. Characterization of Nanoparticles

Characterization techniques are essential for understanding the specific properties of the nanoparticles, providing accurate and reliable data for interpreting the measured values. The synthesized nanoparticles were subjected to various characterization studies to examine properties such as optical behavior, structure, morphology, elemental composition, particle size, and functional groups. The characterization of the green-synthesized nanoparticles was performed using several techniques, including UV-Vis spectrophotometry, Fourier Transform Infrared Spectroscopy (FTIR), and X-ray Diffraction (XRD). These methods help in analyzing the nanoparticles in detail and confirmation of their properties.

III. RESULT DISCUSSION

3.1. FT-IR Spectrum

3.1.1. FT-IR Spectrum of LA-N

FTIR analysis is conducted to identify the potential biomolecules present in neem leaf extract and to determine the functional groups or organic compounds involved in the synthesis of lead acetate nanoparticles. The FTIR analysis is performed within a range of 4000 cm^{-1} to 400 cm^{-1} . The FTIR spectra show peaks between 1000 cm^{-1} and 400 cm^{-1} , with significant peaks at 614.35 cm^{-1} , 663.54 cm^{-1} , 786.99 cm^{-1} , 883.44 cm^{-1} , 935.52 cm^{-1} , and 1020.39 cm^{-1} . A sharp peak at 663.54 cm^{-1} is attributed to Pb-O stretching vibrations, which suggests the formation of Pb-O bonds in the nanoparticles. The other peaks observed are likely due to organic compounds derived from the neem leaf extract, which play a role in the nanoparticle synthesis process.



Figure 1 FT-IR of Lead acetate nanoparticles obtained by using NEEM leaves extract.

3.1.2. FT-IR Spectrum of LA-P

FTIR analysis is conducted to identify the potential biomolecules present in the neem leaf extract and to determine the functional groups or organic compounds responsible for the synthesis of lead acetate nanoparticles. The analysis is performed within a range of 4000 cm^{-1} to 400 cm^{-1} . The FTIR spectrum shows peaks between 1000 cm^{-1} and 400 cm^{-1} , with notable peaks at 615.32 cm^{-1} , 662.58 cm^{-1} , 773.49 cm^{-1} , 843.89 cm^{-1} , and 1019.42 cm^{-1} . A sharp peak at 615.32 cm^{-1} is attributed to Pb-O stretching vibrations, indicating the formation of Pb-O bonds in the nanoparticles. The other peaks observed are associated with organic compounds derived from the papaya leaf extract, which plays a role in the synthesis process of the nanoparticles.

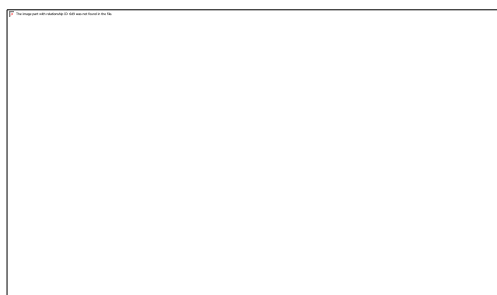


Figure 2. Figure 1 FT-IR of Lead acetate nanoparticles obtained by using Papaya leaves extract.

3.2. X-ray Diffraction analysis

3.2.1. X-ray Diffraction analysis of LA-N

X-ray diffraction (XRD) is a key technique for characterizing material properties such as crystal structure, crystallite size, and strain. Its application in pharmaceutical research is growing due to its versatility. XRD operates on the principle of Bragg's law, which describes the reflection of a collimated X-ray beam off crystal planes in the sample being analyzed. This technique relies on wide-angle elastic scattering and is typically used for materials with long-range order, particularly crystalline substances, making it less suitable for disordered or amorphous materials. When the X-ray beam passes through the sample, it interacts with the atoms, causing scattering. The resulting interference patterns, measured using Bragg's law and detected by a positioned detector, provide insights into the material's crystalline structure. XRD measurements are usually expressed in angstroms ($1\text{ Å} = 0.1\text{ nm}$ or 10^{-10} m). To verify the results from XRD, they can be compared with other techniques like microscopy or other solid-state characterization methods.

Table 1 XRD analysis of as synthesized lead acetate

Sample	Two Theta	d-space	FWHM	(hkl)	Participle size (nm)
LA-N	26.11	3.410	6.63	1 1 1	12.8
	44.7	2.026	7.5	2 2 0	12.0
	73.0	1.295	5.8	3 3 1	18
LA-P	29.34	3.042	6.90	3 1 0	12.43
	44.8	2.02	10.0	3 3 2	9.0
	47.6	1.911	6.5	4 2 2	13.9

The powder XRD diffraction patterns of the lead acetate are presented in Figure 4.3 The crystallite sizes of the complexes were calculated by following Debye-Scherrer equation.

$$D = \frac{K\lambda}{\beta \cos \theta}$$

Where, D is particle size, k is shape correction factor, λ is wavelength of light used in X-ray diffraction process, β is FWHM and θ is angle of diffraction.

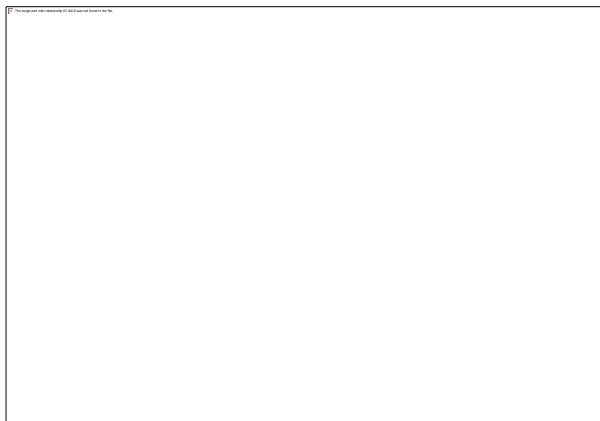


Figure 3 XRD analysis of LA-N nanoparticles.

The synthesized Lead acetate compound exhibits distinctive peaks with notable intensity, identified as (11-3), (51-1), and (51-6), which align well with the data from PDF Card No. 9009850. The particle size, determined using the Debye-Scherrer equation, is provided in Table 1. Based on the XRD results, the structure of Lead acetate was confirmed to be simple monoclinic. The average particle size of Pb in the extract was calculated to be 47.77 nm.

The powder diffraction pattern of the NEEM leaves extract was recorded over the range of $2\theta = 10^\circ$ to 80° . The crystal data and structure refinement of the nanoparticles are provided in the table. The X-ray diffraction pattern corresponds well with JCPDS (PDF) card number 9009850. The diffraction pattern clearly indicates the well-defined crystalline nature of the nanoparticles, confirming that they belong to the cubic crystal system ($a = b = c$; $\alpha = \beta = \gamma$).

3.2.2. X-ray Diffraction analysis of LA-P

X-ray diffraction (XRD) is a key technique used for the characterization of material properties, such as crystal structure, crystallite size, and strain (presented in Table 1). Its application in pharmaceutical research has been growing due to its versatility and wide range of uses. XRD operates based on Bragg's law, which describes the reflection of a collimated X-ray beam incident on the crystal planes of a sample. This allows for the characterization of the material's internal structure.

XRD is primarily suited for ordered materials, especially crystalline substances that exhibit long-range order, and is not typically used for disordered materials. In the XRD process, an X-ray beam is directed through the specimen, where it is scattered by the atoms within the sample. The interference resulting from the scattering of X-rays is analyzed by applying Bragg's law, with a detector positioned at the appropriate angle. This process reveals the crystalline structure characteristics of the material.

All measurements in XRD are expressed in angstroms ($1 \text{ \AA} = 0.1 \text{ nm}$ or 10^{-10} m). To validate the results obtained from XRD analysis, they are often compared with other techniques, such as microscopy or other solid-state characterization methods.



Figure 4 XRD analysis of LA-P nanoparticles.

IV. CONCLUSION

From the above results we can able to conclude that, Azardirachta Indica extract and Papaya extract can synthesis Lead acetate nanoparticle in an easy, less toxic, ecofriendly and cost-effective manner. In this study very less amount of chemicals was used for the synthesis of Lead acetate nanoparticle and hence it is a green technology. The characterization of lead nanoparticle was done by FTIR, XRD analysis. The synthesized Pb NP will be used for further analysis of bioactivities they possess. Further studies are required using SEM for the structure analysis of synthesized lead nanoparticles and a comparison in structure and properties of nanoparticles synthesized at various temperatures. The particle size calculated by using Debye Scherrer equation is presented in Table 1. From XRD data, the structure of the Lead acetate was conferred as simple monoclinic. The average Size of the Pb in extract was found to respectively 47.77 nm, 35.66 nm

V. REFERENCES

- [1]. Yang GW, Prog Mater Sci, 2007, 52(4), 648-698.
- [2]. Nagaraj B, Krishnamurthy N B, Liny P, Divya TK and Dinesh R, Int J Pharma Bio Sci., 2011, 2, 557-565.
- [3]. Pandian CJ, Palanivel R and Dhananasekaran S, Chine J Chem Engg., 2015, 23(8), 1307-1315.
- [4]. Sudhasree S, Shakila Banu A, Brindha P and Kurian G A, Toxicological Environ Chem., 2014, 96(5), 743-754.
- [5]. Krishnamurthy N, Vallinayagam P and Madhavan D, Engineering Chemistry, PHI Learning Pvt. Ltd, 2014.
- [6]. Hyeon T, Chem Commun., 2003, 9, 927-934.
- [7]. Karmhag R, Tesfamichael T, Wackelgard E, Niklasson G A and Nygren M, Solar Energy., 2000, 68(8), 329-333; DOI:10.1016/S0038-092X (00)00025-6.
- [8]. Mariam A A, Kashif M, Arokiyaraj S, Bououdina M, Sankaracharyulu MGV, Jayachandran M and Hashim U, Dig J NanomaterBiostruct., 2014, 9(3), 1007- 1019.
- [9]. Saxena A, Kumar A and Mozumdar S, J Mole Catal A: Chem., 2007, 269(1-2), 35-40.
- [10]. Alonso F, Riente P and Yus M, Tetrahedron, 2008, 64(8), 1847-1852.
- [11]. Dhakshinamoorthy A and Pitchumani K, Tetrahedron Lett., 2008, 49(11), 1818-1823.
- [12]. Alonso F, Riente P and Yus M, Eur J Organic Chem., 2009, 2009, 6034-6042.
- [13]. Alonso F, Riente P and Yus M, Eur J Org Chem., 2008, 2008, 4908-4914.
- [14]. Li X K, Ji W J, Zhao J, Wang S J and Au CT, J Catal., 2005, 236(2), 181-189.

- [15]. Li Y, Zhang B, Xie X, Liu J, Xu Y and Bali R., N. Razak, A. Lumb & A. T. Harris. (2006). The synthesis of metallic nanoparticles inside live plants. Int.
- [16]. Usha S., K.T. Ramappa, Sharanagouda Hiregoudar, G. D. Vasanthkumar & D. S. Aswathanarayana. (2017) Biosynthesis and Characterization of Copper Nanoparticles from Tulasi (*Ocimum sanctum* L.) Leaves, Int.J. Curr.Microbiol. App.Sci 6(11): 2219-2228.
- [17]. Vasudev D. Kulkarni & Pramod S. Kulkarni, (2013). Green Synthesis of Copper Nanoparticles Using *Ocimum Sanctum* Leaf Extract, International Journal of Chemical Studies, 1-4.
- [18]. Rui H, Xing R, Xu Z, Hou Y, Goo S and Sun S, Adv Mater., 2010, 22, 2729-2742.
- [19]. Brigger I, Dubernet C and Couvreur P, Adv Drug Delivery Rev., 2002, 54(5), 631-651.
- [20]. Gupta A. K and Gupta M, Biomaterials, 2005, 26(13), 1565-1573.
- [21]. Basak S, Chen D R and Biswas P, Chem Engg Sci., 2007, 62(4), 1263-1268;

COD Removal from Industrial Waste Water from Palghar MIDC Area Using Low-Cost Technique

A.K. Wanjari^{*1}, S.R. Kolteke¹, R.D. Ghodile²

¹Department of Chemistry, Mahatma Fule Arts, Commerce and Sitaramji Chaudhari Science College, Warud, Dist-Amravati, Amravati University, Maharashtra, India

²S.P.M. Science and Gilani Arts, Commerce College, Ghatanji, Dist-Yawatmal, Amravati University, Maharashtra, India

ARTICLE INFO

Article History:

Accepted : 01 Jan 2025

Published : 10 Jan 2025

Publication Issue :

Volume 12, Issue 7

January-February-2025

Page Number :

34-38

ABSTRACT

Rapid urbanization and industrialization increase organic pollutants in river and dam water which ultimately effects on water quality level. This research papers deals with the study of analysis of water parameters like pH, COD, presence of heavy metal and to treat this waste water by using low-cost technique. In this study, water samples from three different industries were analyse and treated by using batch experiment process using Fenton`s reagent followed by charcoal treatment. Effect of pH, dose of Fenton`s reagent and charcoal were examined in order to optimize the COD reduction.

Keywords: Fenton`s reagent, industrial wastewater, chemical oxygen demand

I. INTRODUCTION

The water effluents from pulp and paper industries are often very complex, and it is almost impossible to characterize all types of constituents. Chemical and mechanical pulping processes will generate different wastewaters because different quantities of water and/or additives are used [1-5]. The wastewater will generally contain carbohydrates (glucose, xylose, galactose, manose, arabinose etc.), extractives (fatty acids, resin acids, triglycerides) and low molecular weight compounds (formic acid, acetic acid, oxalic acid). In textile and paper colouration industries synthetic dyes from residual dye baths are released in to waste streams. It is estimated about 10-15% of dyes goes unused in textile effluents [6-7]. Conventional high-technology wastewater treatment systems are in many situations not a suitable solution in developing countries because it is not sustainable to install wastewater systems which require guaranteed power supply, replaceable spare parts and a skilled labour for operation and maintenance. Improved process engineering, process closures and use of external treatments have in recent years drastically lowered the BOD [8-9]. However, the COD emissions have

not decreased to the same extent and must therefore be further reviewed. Chemical precipitation, which can bind large parts of the remaining COD into solid matter, making it possible to be removed from the effluent by various separation technologies, contributes to an efficient COD removal. However, a major drawback with this type of treatment is the generation of large quantities of sludge which is difficult to dewater (consumes a lot of energy) and generates large quantities of waste [10-13]. A cheap and more effectively methods for treating liquid waste before discharging it into any other water systems is required [14-16]. A lot of wastewater technologies are known which include physicochemical treatment processes and biological treatment processes. COD is a parameter that represents the amount of oxygen needed for complete decomposition of organic matter. In terms of pulp and paper production, COD originates from dissolved raw materials, process aids and all substances formed during pulp cooking that are not removed with the black liquor [17-18]. These types of substances are often very persistent and cannot be removed efficiently, causing negative effects on environment. Therefore, industrial effluents containing dyes must be treated before their release into the environment.

II. EXPERIMENTAL

Collection of wastewater sample

The wastewater sample is collected from different industries from Palghar MIDC area which is a town in Konkan division of Maharashtra state.

Preparation of Fenton solutions

Fenton's reagents were prepared by dissolving 150 gm of solid Ferrous sulphate and hydrogen peroxide 50% m/w in 500 ml deionized water.

EXPERIMENTAL SETUP AND PROCEDURE

Effect of pH

In order to study at what pH range COD level will decrease it is important to study effect of pH for COD removal. As Fenton's reagent more effectively work in acidic range, first the pH of the solution adjusted between 2 to 5 using 0.1 N H_2SO_4 solution. For the study of effect of pH 200 ml of waste water from each industry were put in three different shaking bottles. After that, the various amounts of hydrogen peroxide solutions and $FeSO_4 \cdot 7H_2O$ (in a solid state) were added and shaken for 1hr. after that resultant solution were filter off and treated with 0.1 gm of charcoal followed by filtration. The obtained results were depicted in table no.1 and fig no.1. COD was determined in accordance with standard methods [APHA, 1992], while pH was measured using a pH meter.

Effect of Contact time

In order to optime the reaction time for the removal of COD, 200 ml of waste water from each industry were put in three different shaking bottles and shaken for 2 hr by adding adequate amount of Fenton's reagent followed by charcoal treatment and examine the effect of contact time. Results are depicted in table no.1 and figure no. 2

Effect of Temperature

H_2O_2 decomposes into oxygen and water above the $40^\circ C$ temperature. So, in order to estimate the effect of temperature, temperature of the solution was set in between 25 to $35^\circ C$ and examine the effect of temperature for the removal of COD and results are depicted in table no.1 and figure no.3.

Industrial Waste water	Fe^{2+} ml	H_2O_2 (ml)	pH	Temp. ($^\circ C$)	Time (min)	Initial COD	Final after charcoal	COD Removal %
------------------------	--------------	---------------	----	----------------------	------------	-------------	----------------------	---------------

(Palghar MIDC)						(ppm)	treatment	
Pharmaceutical industry	8	12	3.2	30	60	1825	845	53.70
	10	15	3.8	35	60	1762	912	48.25
Dye industry	8	12	3.5	30	60	3254	895	72.49
	10	15	4.0	35	60	3120	1035	66.82
Textile industry	8	12	3.4	30	60	2024	654	67.68
	10	15	3.8	35	60	2125	623	70.68

III.RESULTS AND DISCUSSION

In the first part of the investigations, optimization of Fenton's reaction was carried out for the three types of wastewater like dyes, textile and pharmaceutical wastewater. Different doses of H_2O_2 , as well as concentrations of Fe^{+2} ions and pH were reduced from 8-10 to 3-4 and residence time about 60 min. The wastewater sample is collected from primary tank or collection tank or equalization tank. The optimum COD reduction by this process is in the range of 60% to 85%. The comparison between raw water COD and after Fenton Process can be visualized by the following chart.

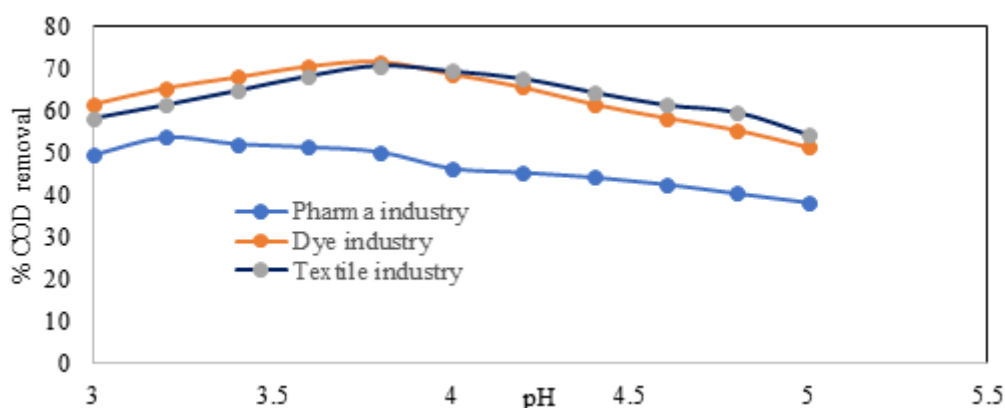


Figure No.1 Effect of pH on COD removal

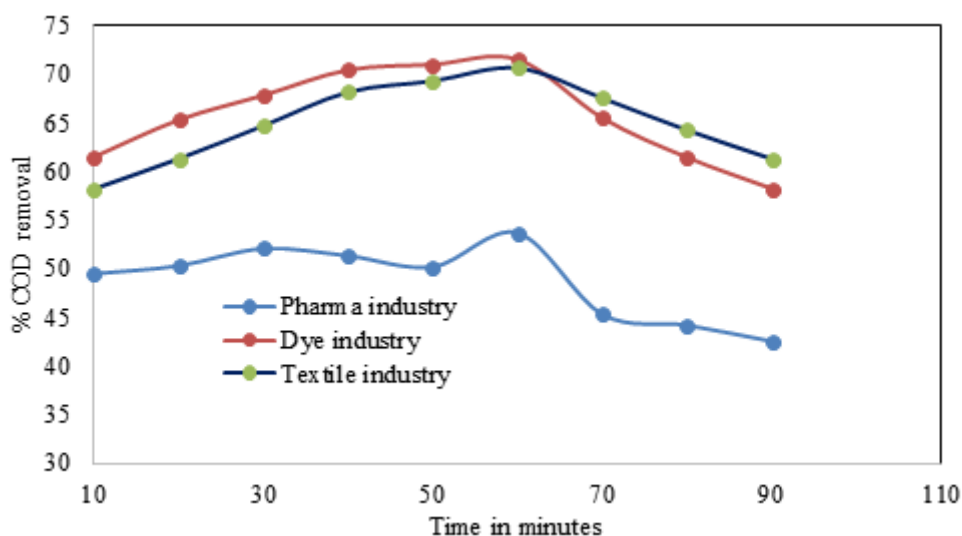


Figure No.2 Effect of contact time on COD removal

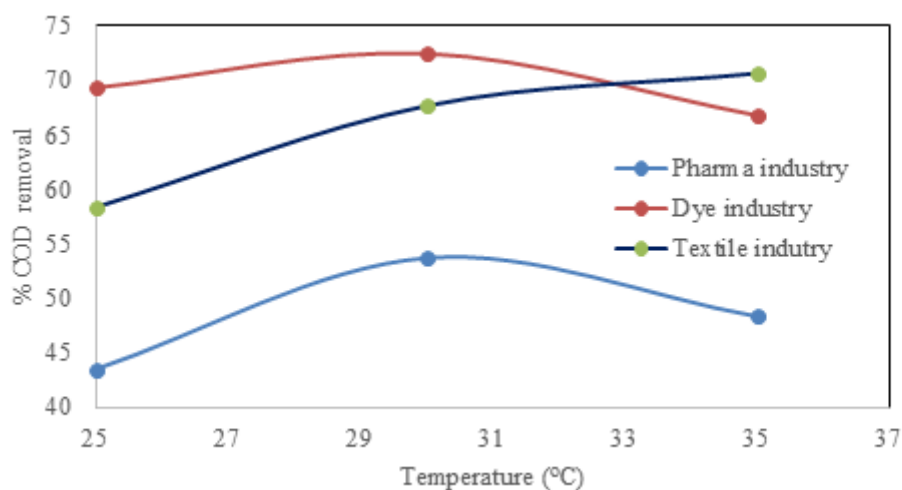


Figure No.3 Effect of temperature on COD removal

IV. CONCLUSION

The study concluded that pH, contact time and temperature have a significant influence on Chemical oxygen demand (COD) removal efficiency by using Fenton's reagent followed by charcoal treatment. This shows that these Fenton's reagent followed by charcoal treatment have enormous potential to degrade the COD from pharmaceutical industry, dye industry and textile industry and resolve the problem of unnecessary high COD present in the effluents of industries. Further pilot scale studies are required with these strains for actual industrial applications, and detailed study is needed to explore the mechanism involved.

V. REFERENCES

- [1]. Es S, S., Im Ne , Contrer S, S., Sc , E. Rodr E , M. Comparison of different advanced oxidation processes for phenol degradation. Water Research, 36, 1034-1042.
- [2]. Gogate, P. R. & Pandit, A. B. 2004. A review of imperative technologies for wastewater treatment I: Oxidation technologies at ambient conditions. Advances in Environmental Research, 8, 501-551.
- [3]. Jamil, T. S., Ghaly, M. Y., El-Seesy, I. E., Souaya, E. R. & Nasr, R. A. 2011. A comparative study among different photochemical oxidation processes to enhance the biodegradability of paper mill wastewater. Journal of Hazardous Materials, 185, 353-358.
- [4]. Rai, P.K. (2009). Heavy metals in water, sediments and wetland plants in an aquatic ecosystem of tropical industrial region India. Environment Monitoring and Assessment, 158, 433-457.
- [5]. Salomons W., Forstner, U. and Mader, P. "Heavy metals: problems and solutions", Springer-VerlagB, erlin (1995).
- [6]. Moore J. W. and Ramamoorthy S. "Heavy metals in natural waters: applied monitoringandimpactassessment"S, pringer-Verlag New York (1984).
- [7]. Dilek, F.B.,Gokcay C.F., Yetis, U. (1998). Combined effects of Ni (II) and Cr (IV) on activated sludge. Water Resources,32 (2), 303-312.
- [8]. FergussonJ . E. "The heavyelements:chemistry, environmentalimpact and health effects", Pergamon Press, Oxford (1990).

- [9]. Mahdi, Ahmad., Azni, Idris., Aofah, Adam. (2007). Combined anaerobic-aerobic system for treatment for textile wastewater. *Journal of engineering science and technology*, April 2 (1), 55-69.
- [10]. Nriagu, J.O. (1979). Global inventory of natural and anthropogenic emission of trace metals to the atmosphere. *Nature*, 279, 409–411.
- [11]. Saxena, S., and D'souza S.F. (2005). Heavy metal pollution abatement using rock phosphate mineral. *Founder's Day Special Issue*, 94-99.
- [12]. Gupta, V.K., Pathania, D., Sharma, S., Singh, P. (2013). Preparation of bio-based porous carbon by microwave assisted phosphoric acid activation and its use for adsorption of Cr (VI). *Journal of colloid and interface science*, July 1 (401), 125-132.
- [13]. UN-Water. UN-Water statement on water quality. www.unwater.org. (2010).
- [14]. Azizullah, A., Khattak, M.N., Richter, P., Hader, D.P. (2011). Water pollution in Pakistan and its impact on public health - A review. *Environmental International*, February 37 (2), 479–497.
- [15]. Rai, P.K. (2008). Phytoremediation of Hg and Cd from industrial effluents using an aquatic free floating macrophyte *azolla pinnata*. *International Journal of Phytoremediation*, 10 (5), 430–439.
- [16]. Khan, A.G., Kuek, C., Chaudhry, T.M., Khoo, C.S., Hayes W.J. (2000). Role of mycorrhizae and phytochelators in heavy metal contaminated land remediation. *Chemosphere*, 41 (1-2), 197–207.
- [17]. Goel, Jyotsna, Kadirvelu, K., Rajagopal, C., and Garg, V.K. (2005). Removal of lead (II) by adsorption using treated granular activated carbon: Batch and column studies. *Journal of Hazardous Material*, B125, 211-220.
- [18]. Kadirvelu, K., Thamaraiselvi, K., Namasivayam, C. (2001). Removal of heavy metals from industrial wastewaters by adsorption onto activated carbon prepared from an agricultural solid waste. *Bioresource Technology*, 76 (1), 63-65.

Green Synthesis of Copper Oxide Nanoparticle & Their Potent Antioxidant Application

Thakare A. R^{1*}, Padole P. D², Ghodile R. D², Deshmukh G. S³

¹Department of Chemistry, Shankarlal Agrawal Science College Salekasa, Gondia, Maharashtra, India

²Department of Chemistry, Shri Shivaji Science College Amravati, Maharashtra, India

³Department of Chemistry, S. P. M. Science & Gilani Arts, Commerce College, Ghatanji, Yavatmal, Maharashtra, India

ARTICLE INFO

Article History:

Accepted : 01 Jan 2025

Published : 10 Jan 2025

Publication Issue :

Volume 12, Issue 7

January-February-2025

Page Number :

39-48

ABSTRACT

The manufacture of metallic nanoparticles utilizing plants, enzymes, and microbes has been acknowledged as an environmentally friendly alternative to more conventional physical and chemical methods. The biological generation of nanoparticles has garnered significant interest from scientists and researchers recently due to its simple process, inexpensive cost, non-toxicity, and environmental friendliness. Thus, copper oxide nanoparticles (CuO-NPs) were synthesized using a reduction agent obtained from fruit pulp extract of *Abelmoscus Manihot*, as reported in this work. The biosynthesized CuO-NPs were characterized by means of an X-ray diffraction (XRD), UV-visabsorption spectroscopy, and a scanning electron microscope (SEM) and EDX. The average size of the nanoparticles was found to range from 25 to 52 nm.

Keywords:- Green synthesis, Copper oxide nanoparticles, *Abelmoscusmanihot*, Antioxidants property

I. INTRODUCTION

The objective of nanomaterial research is to comprehend and utilize the unique morphological and physicochemical characteristics of small particles with an average size ranging from 1 to 100 nm for a wide range of applications across various scientific and technological disciplines (Pourmadadi et al 2022, Hassanisaadi et al 2022). This area of study is highly esteemed in the realms of engineering, chemistry, physics, biology, material science, and medicine (Bayda et al 2022). Nanotechnology research delves into diverse synthesis methods, alterations in nanoparticle structure, and adjustments in nanoparticle sizes. Nanoparticles are defined as materials that are less than 100 nm in size, existing at the nanoscale. They exhibit remarkable thermal stability, a high surface-to-volume ratio, and exceptional electrical, mechanical, optical, and magnetic properties (Chandrakala et al 2022). The synthesis of nanostructured materials can be achieved through

physical, chemical, and biological methods (Rotti et al 2023). Chemical synthesis methods such as pyrolysis, micelle, hydrothermal, sol-gel, and precipitation processes are known to pose risks to the environment and ecology (Manjula et al 2023). To address this issue, green synthesis has emerged as a solution to minimize the negative impact on the environment. Utilizing microorganisms, algae, and plants as biological building blocks for green synthesis can help mitigate the environmental hazards associated with traditional chemical synthesis methods (Ying et al 2022). Recently, there has been a significant focus among material scientists on developing environmentally friendly methods for producing nanoscale materials. One area of interest in green chemistry is the utilization of plant-derived extracts for the green synthesis of nanoparticles. This approach is considered to be both accessible and cost-effective (Iravani et al 2011, Duan et al 2015, Bala et al 2015). Moreover, the green synthesis method is recognized for its ability to stabilize and reduce potential risks, making it a safer and more sustainable option for nanoparticle creation (Ishwarya et al 2017). Various metals, including copper (Cu) (Kiriyanthan et al 2020), gold (Au) (Suganya et al 2017), and silver (Ag) (Ishwarya et al 2017), as well as trace elements (Rekha et al 2019), have been utilized as reduction and coating agents in the production of nanoparticles. Nevertheless, concerns regarding the toxicity of Ag, Au, and Cu nanoparticles have been raised, limiting their potential therapeutic applications (Rajeshkumar et al 2023). Nanotechnology has not only addressed numerous challenges in areas such as energy sustainability, climate change, and industries like beauty, textiles, and healthcare, but has also significantly improved the quality of life by advancing treatments for serious illnesses such as cancer and Alzheimer's (Hasan et al 2015, Barzinjy et al 2020). Nanoparticles (NPs) possess the potential to exert both advantageous and detrimental impacts on the growth and development of plants. The magnitude and nature of these effects are contingent upon various factors, including the dimensions, configuration, and characteristics of both the plant species and the NPs involved (Ghodake et al 2011).

Copper (Cu), a microelement located in block D of the periodic table, plays a crucial role in enhancing plant development and progression. It serves as a cofactor for superoxide phenol oxidases and ascorbate oxidase, while also being a component of regulatory proteins. Additionally, copper actively participates in the electron transport chain during both photosynthesis and respiration processes (Nekrasova et al 2011, Yruela et al 2005). Cu in the form of nanomaterial exhibits exceptional characteristics due to its small size and large surface area, resulting in chemical reactivity, physical durability, magnetism, and optical properties (Hong et al 2015). These unique attributes make copper nanoparticles (CuNPs) suitable for a wide range of applications such as bioactive coatings, air and liquid filtration, sensors, ceramics, films, skincare products, lubricants, inks, wood preservation, and textiles. Current estimates indicate that the global production of CuNPs, or Cu-based nanoparticles, has reached 200 tons per year (White et al 2006). The widespread use and engineering of CuNPs have led to their introduction into the environment, where they interact with agricultural systems. The impact of CuNPs on plants can vary from positive to negative, depending on the concentration of nanoparticles and the plant species. Therefore, there is an urgent need to investigate the effects of CuNPs on crops, as limited studies have explored this relationship. CuNPs can be synthesized using various methods, including physical, chemical, and biological techniques. However, physical and chemical methods are time-consuming and involve the use of hazardous chemicals, making them less desirable (Buazar et al 2012, Kassaei et al 2010, Buazar et al 2019). In contrast, biological methods, such as green synthesis, offer advantages such as being environmentally friendly, cost-effective, and high yielding (Murugan et al 2014). The emphasis on green synthesis is driven by environmental concerns, aiming to establish a sustainable and pollution-free approach to nanoparticle synthesis (Mohammed et al 2022).

Biological synthesis, whether occurring extracellularly or intracellularly in higher plants or microbes, has emerged as a superior alternative to chemical methods due to its higher productivity, eco-friendliness, reduced

capital requirements, and absence of toxicity (Shobha et al 2014). The global significance of biological synthesis is being increasingly highlighted. The application of nanoscience in agriculture has primarily remained theoretical. From its inception, it is poised to have a substantial impact on disease detection, improvement of nutrient absorption, and targeted delivery. Moreover, it has the potential to increase crop yield by administering pesticides for precise treatment against diseases, thereby advancing our comprehension of "the biology of different crops" (Chinnamuthu et al 2009). Over the past decade, a multitude of exploratory studies have been carried out to assess the tangible influence of nanotechnology on enhancing crops (Chittaranjan et al 2013). Recent investigations on Nanoparticles (Nps) in various crops such as corn, wheat, ryegrass, alfalfa, soybean, tomato, radish, lettuce, spinach, onion, pumpkin, bitter melon, and cucumber have demonstrated improvements in seedling growth, germination, photosynthetic activity, nitrogen metabolism, protein levels, mRNA expression, and alterations in gene expression, underscoring their potential for crop enhancement (Chittaranjan et al 2013, Cyren et al 2011, Yang et al 2007).

In this study, the synthesis of CuNPs was conducted by utilizing a plant extract, taking into consideration the significance and advantages of green synthesis. Using aqueous extracts of the fruit from *Abelmoschus manihot*, we demonstrate here the production of copper oxide nanoparticles from plants. Environmentally produced CuO-NPs will be employed in numerous biological activities. During the manufacture of biogenic CuO-NPs, the metabolites in the aqueous extract of *Abelmoschus manihot* fruit serve as a capping and reducing agent. The green synthesised nanoparticles were characterised using contemporary techniques such as scanning electron microscopy (SEM), X-ray diffraction (XRD), and Fourier transform infrared (FTIR) spectroscopy. We'll look at the NPs' antiviral, antioxidant, antilarvicidal, and anti-inflammatory qualities.

II. METHOD AND MATERIALS

2.1. Preparation of *Abelmoschus manihot* subsp. *tetraphyllus* fruit extract.

The process of preparing the fruit extract of *Abelmoschus manihot* involved several steps. Initially, ripe fruits of *Abelmoschus manihot* subsp. *tetraphyllus* were collected from the Salekasa region in GondiaMaharashtra, with geographical coordinates of latitude 21.30 and longitude 80.48. These fruits were carefully cleaned and cut into small pieces. Subsequently, 20 g of the fruit pieces were added to 50 mL of distilled water. To facilitate the extraction process, the mixture was then subjected to agitation for duration of two hours at a temperature of 60 °C. Following this, the extract was filtered using filter paper, ensuring the removal of any impurities or solid particles. Finally, the obtained fruit extract was stored in a refrigerator, ready for further research studies.

2.2. Green synthesis of copper oxide nanoparticle.

To synthesize the green CuO nanoparticles, a combination of 20 ml of fruit pulp extract from *Abelmoschus manihot* subsp. *tetraphyllus* and 50 ml of 0.1 mol/L copper sulphate (Himedia, purity = 99.6%) was prepared in a conical flask. The resulting mixture was subjected to magnetic stirring for a period of 1 hour. Subsequently, the mixture was slowly blended with 0.1 mol/L sodium hydroxide solution to adjust the pH to 10. The liquid was then magnetically stirred for 2 hours. After the reaction, the products were centrifuged at 2000 rpm for 10 minutes. The supernatant was removed, and the precipitates were washed twice with ethanol before being dried at 70 °C.

2.3. Characterization of zinc oxide nanoparticles.

2.3.1. Ultraviolet spectroscopy;-

The confirmation of CuONPs synthesis was confirmed by observing a change in color within the solution. Furthermore, UV-Vis spectrophotometry was utilized for analysis. The absorption spectrum of the resulting

sample was then recorded using a BMS UV-2600 spectrophotometer within the wavelength range of 200–1100 nm.

2.3.2. Fourier transform infrared (FTIR) spectroscopy;-

It was necessary to examine the capping agents on the surface of CuONPs by utilizing FTIR analysis with a prepared sample. CuONPs in a dried powder state were essential for this procedure. The FTIR analysis of the dry powder was carried out using Shimadzu: IRTracer-100, with specific conditions including a reduction in the overall reflection mode, a resolution of four cm⁻¹, and a spectral range of 4000–400 cm⁻¹.

2.3.3. Scanning electron microscopy (SEM);-

copper oxide nanoparticles underwent morphological analysis with the assistance of an electron scanning microscope (EVO-LS10). The electron beam was utilized to capture the picture and measure the size of the CuONPs from the dried sample.

2.3.4. Characterization using XRD;-

X-ray diffraction was utilized to characterize the green-synthesized copper oxide nanoparticles. The X-ray diffraction data was collected with a PANalyticaX'pert X-ray diffractometer. Scherer's equation was applied to calculate the size of the crystallites (Winter et al 1962).

$$D_k = \lambda \beta / \cos \theta$$

The given equation represents the relationship between various parameters in X-ray diffraction (XRD). In this equation, λ represents the X-ray wavelength, which is measured in units of 1.5421 Å. The parameter D corresponds to the half peak height of an XRD line that arises from a specific crystallographic plane. The form factor, denoted by k , has a value of 0.94. Additionally, β represents the Full Width at Half Maximum (FWHM) in terms of Bragg's angle, while θ is the same FWHM but measured in radians.

Antioxidant assay

2,2-Diphenyl-1-picryl hydrazyl (DPPH) radical scavenging activity

The antioxidant activity of the methanolic extract and CuO nanoparticles of *Abelmoschus manihot subsp. tetraphyllus* was measured on the basis of the scavenging activity of the stable DPPH free radical according to the method described by Blois, M.S. (1958). An aliquot of 0.5 ml of the sample solution in methanol was mixed with 2.5 ml of 0.5 mM methanolic solution of DPPH. The mixture was shaken vigorously and incubated for 30 min in the dark at room temperature. The absorbance was measured at 517 nm using UV spectrophotometer. The same procedure was adapted for CuO nanoparticles. Ascorbic acid was used as a positive control. DPPH free radical scavenging ability (%) was calculated by using the formula [Blois, M. S. 1958].

$$\text{Percent Inhibition} = \frac{\text{Absorbance Control} - \text{Absorbance Extract}}{\text{Absorbance Control}} \times 100$$

III.RESULTS AND DISCUSSION

3.1. Characterization of zinc oxide nanoparticles.

3.1.1. Ultraviolet—Visible (UV-Vis) Spectroscopy; -

The prepared sample was subjected to UV-vis examination in order to verify the presence of CuO nanoparticles. The produced spectra, which are shown in Figure 1, show that the absorption peak of CuO nanoparticles is at about 466 nm, demonstrating that the intended CuO nanoparticles were formed. Generally, the absorption peak of CuO is found between 200 and 500 nm, depending on the particle size. The absorption peak in bulk

CuO is redshifted, meaning it appears at longer wavelengths. In contrast, the position of the absorption peaks shifts towards shorter wavelengths (blue-shifted) when the particle size decreases (Dagher et al). CuO nanoparticles were made from *P. marsupium* heartwood extract in a prior study, and the UV absorption peak was noted.

3.2. Fourier transform infrared (FTIR) spectroscopy; -

Since separate chemical bonds usually show discrete energy absorption bands, FTIR spectroscopy works well for characterising functional groups inside molecules. Researchers can obtain important structural and bonding information about complicated compounds using this technique, which makes it easier to analyse the type and strength of bonds (N. Li et al). The Cu-O stretching phenomena in the monoclinic phase of CuO is responsible for the detection of absorption bands with a wavenumber of 507 cm⁻¹ (Fan et al. Peaks 795 cm⁻¹ and 1121 cm⁻¹ indicate different types of bending vibration in the Cu-O bond.

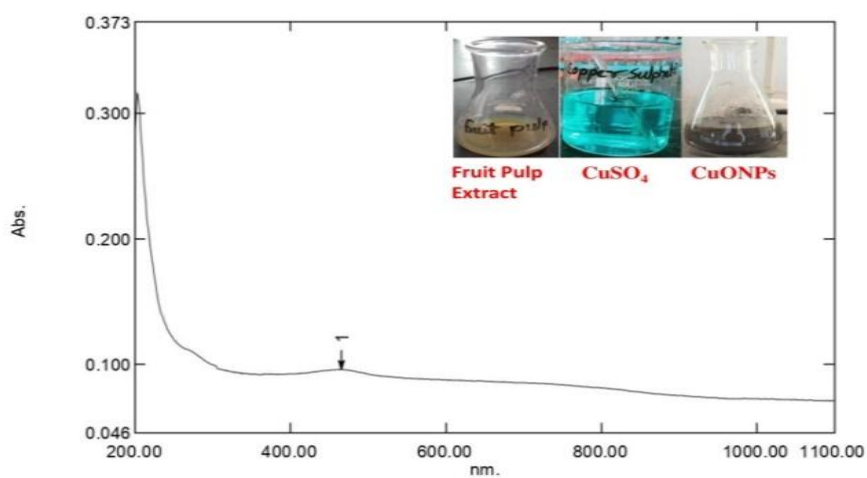


Figure 2 UV absorption spectra for AMCuO Nanoparticle

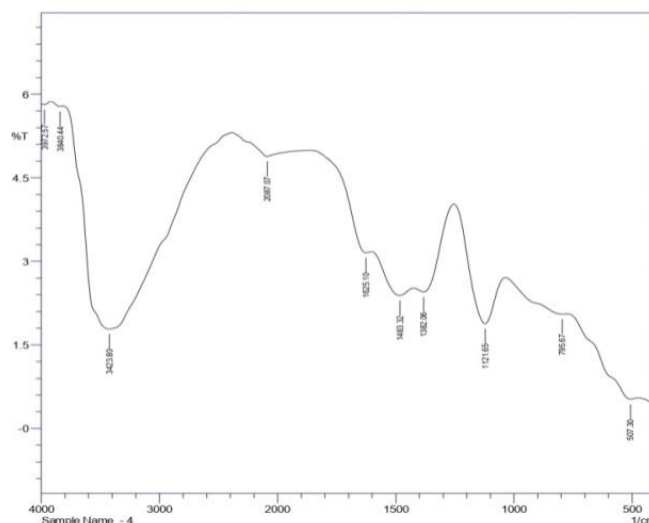


Figure 3 FTIR spectra for AMCuO Nanoparticles

The stretching vibration of the Cu-O bond in copper (II) oxide nanoparticles is indicated by the appearance of a peak at 1695 cm⁻¹. The band area at 1483 cm⁻¹ is caused by the stretching mode of the antisymmetric carbonate species present in the interlayer, while the free CO₃⁻ ion in the interlayer region was seen to have a sharper band region at 1382 cm⁻¹ (Sánchez-cantú et al). The bands seen at 3432 cm⁻¹ are indicative of the asymmetric stretching vibration of the O-H bond.

3.3. Scanning electron microscopy (SEM):-

Figure 4's SEM study shows how CuO nanoparticles are shaped. On the surface, these nanoparticles appear as microscopic needle-like structures. This finding clearly suggests that the CuO nanoparticles are securely bonded to the phytochemicals' surface. 1. It has been noted that hydrogen bonds and electrostatic interactions cause bioorganic capping agents and nanoparticles to agglomerate. Furthermore, the scanning electron microscope image's lack of direct contact with CuO nanoparticles indicates that the capping molecules have successfully stabilised the nanoparticles.

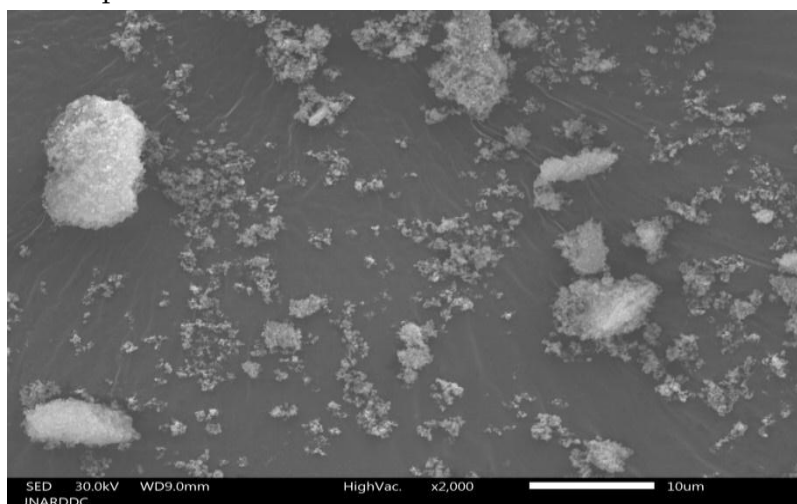


Figure 4 SEM image for AMCuO Nanoparticles

3.4. XRD analysis:-

The creation of a single-phase CuO with a monoclinic structure is suggested by the X-ray diffraction pattern acquired in this investigation, which closely mimics that of pure CuO (JCPDS-05-0661). This investigation's diffraction peaks at $2\theta = 32.48, 35.41, 38.69, 46.19, 48.66, 53.53, 58.25,$ and 61.46 were ascribed to the monoclinic CuO nanoparticles' reflection lines. The diffraction patterns of the CuO nanoparticles that Das et al. synthesised are in good agreement with these experimental results.

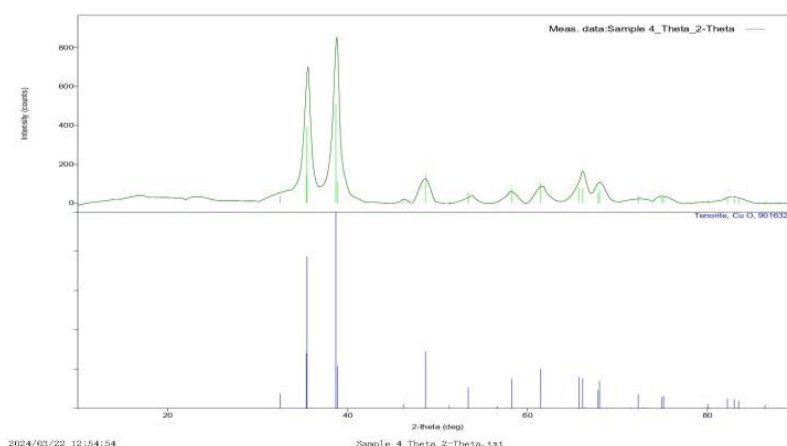


Figure 5.XRD image for AMCuO Nanoparticles

Antioxidant assay

2,2-Diphenyl-1-picryl hydrazyl (DPPH) radical scavenging activity

The antioxidant activities of ZnO nanoparticle synthesized from *Abelmoschus manihot* plant extract assessed by DPPH activity. The DPPH activity of different concentration of ZnO nanoparticle (50–250 μg/ml) along with standard ascorbic acid is presented in the [Table 6]. With the increasing concentrations, positive

scavenging activity was noted. The percentage of scavenging activity is increasing with the increasing concentration in ZnO nanoparticles. Among the five different concentration (50–250 µg/ml) tested, the ZnO nanoparticles showed higher inhibition (75.4 ± 0.86) was observed in 250 µg/ml concentration against ascorbic acid (85.2 ± 0.92). The ZnO nanoparticles showed higher inhibition (72.1 ± 0.94) in 200 µg/ml concentration against the ascorbic acid showed (78.8 ± 0.92) in 200 µg/m concentration. DPPH free radicals have the ability to take electron from the antioxidants that is why it is used for the antioxidant scavenging assays of the nanoparticle for its estimation.

Table 1 DPPH radical scavenging activity of ZnO nanoparticle synthesized by using *Abelmoschus manihot*

SN		% of inhibition				
		50 µg/ml	100 µg/ml	150 µg/ml	2000 µg/ml	250 µg/ml
1	ZnO Nanoparticle	57.6 ± 0.88	60.8 ± 0.94	68.8 ± 0.94	72.1 ± 0.94	75.4 ± 0.86
2	Ascorbic acid	61.0 ± 0.93	66.3 ± 0.88	$74. \pm 0.96$	78.8 ± 0.92	85.2 ± 0.92

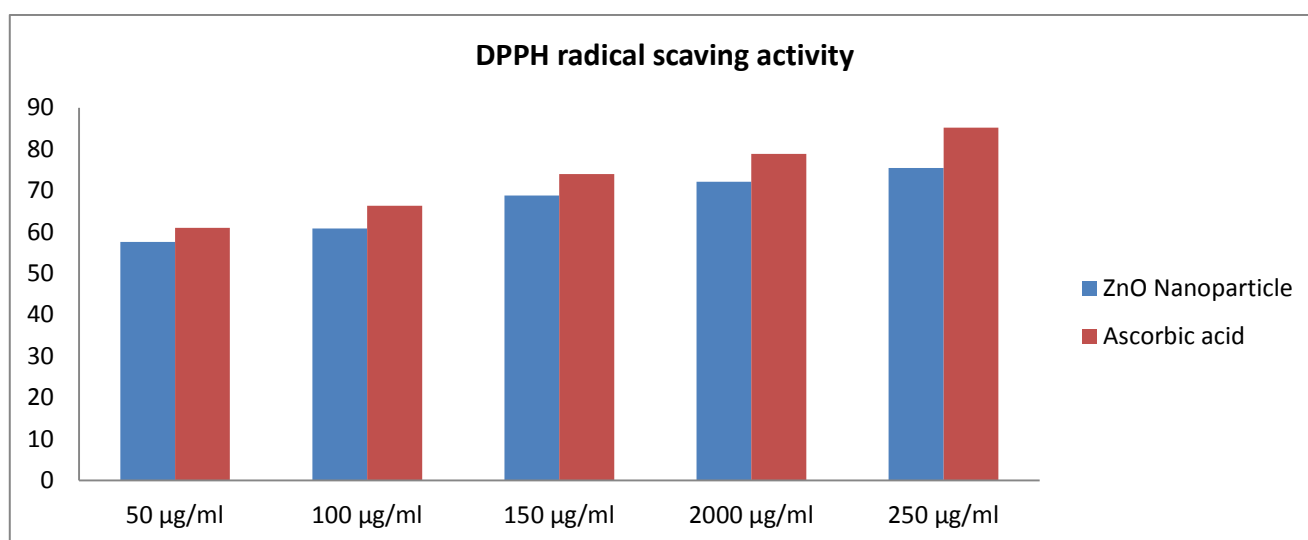


Figure 6 DPPH radical scavenging activity of ZnO nanoparticle synthesized by using *H. Pubescens*

IV. CONCLUSION

This work successfully produced copper oxide nanoparticles using an extract from the *Abelmoschus manihot*, providing a simple, inexpensive, and efficient way for doing so. FTIR, XRD, SEM, and UV-Vis spectroscopy were used to characterize the CuO NPs. To verify the antioxidant activity of the biosynthesized CuONPs, DPPH method was employed. These nanoparticles were very stable and have potent antioxidant qualities. The study successfully demonstrates the convenient utilization of *Abelmoschus manihot* extract as a fuel to get structurally and morphologically interesting and potentially antioxidant CuO nanoparticles.

V. REFERENCES

- [1]. M. Pourmadadi, M. M. Eshaghi, S. Ostovar et al., "UiO-66 metal–organic framework nanoparticles as gifted MOFs to the biomedical application: a comprehensive review," *Journal of Drug Delivery Science and Technology*, vol. 76, Article ID 103758, 2022.
- [2]. M. Hassanisaadi, A. H. S. Bonjar, A. Rahdar, R. S. Varma, N. Ajalli, and S. Pandey, "Eco-friendly biosynthesis of silver nanoparticles using *Aloysia citrodora* leaf extract and evaluations of their bioactivities," *Materials Today Communications*, vol. 33, Article ID 104183, 2022
- [3]. S. Bayda, M. Adeel, T. Tuccinardi, M. Cordani, and F. Rizzolio, "The history of nanoscience and nanotechnology: from chemical–physical applications to nanomedicine," *Molecules*, vol. 25, no. 1, Article ID 112, 2020.
- [4]. Chandrakala, V.; Aruna, V.; Angajala, G. Review on metal nanoparticles as nanocarriers: Current challenges and perspectives in drug delivery systems. *Emergent Mater.* 2022, 5, 1593–1615.
- [5]. Rotti RB, Sunitha DV, Manjunath R, Roy A, Mayegowda SB, Gnanaprakash AP, Alghamdi S, Almehmadi M, Abdulaziz O, Allahyani M, Aljuaid A, Alsaiari AA, Ashgar SS, Babalghith AO, Abd El-Lateef AE and Khidir EB (2023), Green synthesis of MgO nanoparticles and its antibacterial properties. *Front. Chem.* 11:1143614. doi: 10.3389/fchem.2023.1143614
- [6]. Manjula, N. G., Sarma, G., Mayegowda Shilpa, B., and Suresh Kumar, K. (2022). Environmental applications of green engineered copper nanoparticles. *Phyt. Ed. by Maulin P. Shah Arpita Roy.*, 255–276. doi:10.1007/978-981-19-4811-4_7
- [7]. S. Ying, Z. Guan, P.C. Ofoegbu et al. *Environmental Technology & Innovation* 26 (2022) 102336 4.1.
- [8]. Iravani, S. Green synthesis of metal nanoparticles using plants. *Green Chem.* 2011, 13, 2638–2650.
- [9]. Duan, H.; Wang, D.; Li, Y. Green chemistry for nanoparticle synthesis. *Chem. Soc. Rev.* 2015, 44, 5778–5792.
- [10]. Bala, N.; Saha, S.; Chakraborty, M.; Maiti, M.; Das, S.; Basu, R.; Nandy, P. Green synthesis of zinc oxide nanoparticles using *Hibiscus subdariffa* leaf extract: effect of temperature on synthesis, antibacterial activity and anti-diabetic activity. *RSC Adv.* 2015, 5, 4993– 5003.
- [11]. Ishwarya, R.; Vaseeharan, B.; Anuradha, R.; Rekha, R.; Govindarajan, M.; Alharbi, N.S.; Kadaikunnan, S.; Khaled, J.M.; Benelli, G. Eco-friendly fabrication of Ag nanostructures using the seed extract of *Pedaliu murex*, an ancient Indian medicinal plant: Histopathological effects on the Zika virus vector *Aedes aegypti* and inhibition of biofilm-forming pathogenic bacteria. *J. Photochem. Photobiol. B Biol.* 2017, 174, 133–143.
- [12]. Suganya, P.; Vaseeharan, B.; Vijayakumar, S.; Balan, B.; Govindarajan, M.; Alharbi, N.S.; Kadaikunnan, S.; Khaled, J.M.; Benelli, G. Biopolymer zein-coated gold nanoparticles: Synthesis, antibacterial potential, toxicity and histopathological effects against the Zika virus vector *Aedes aegypti*. *J. Photochem. Photobiol. B Biol.* 2017, 173, 404–411.
- [13]. Kiriyanthan, R.M.; Sharmili, S.A.; Balaji, R.; Jayashree, S.; Mahboob, S.; Al-Ghanim, K.A.; Al-Misned, F.; Ahmed, Z.; Govindarajan, M.; Vaseeharan, B. Photocatalytic, antiproliferative and antimicrobial properties of copper nanoparticles synthesized using *Manilkara zapota* leaf extract: A photodynamic approach. *Photodiagnosis Photodyn. Ther.* 2020, 32, 102058.
- [14]. Rekha, R.; Vaseeharan, B.; Vijayakumar, S.; Abinaya, M.; Govindarajan, M.; Alharbi, N.S.; Kadaikunnan, S.; Khaled, J.M.; Al-anbr, M.N. Crustin-capped selenium nanowires against microbial pathogens and

- Japanese encephalitis mosquito vectors—Insights on their toxicity and internalization. *J. Trace Elem. Med. Biol.* 2019, 51, 191–203.
- [15]. Rajeshkumar, S.; Parameswari, R.P.; Sandhiya, D.; Al-Ghanim, K.A.; Nicoletti, M.; Govindarajan, M. Green Synthesis, Characterization and Bioactivity of *Mangifera indica* Seed-Wrapped Zinc Oxide Nanoparticles. *Molecules* 2023, 28, 2818. <https://doi.org/10.3390/molecules28062818>
- [16]. Hasan, S. A review on nanoparticles: their synthesis and types. *Res. J. Recent Sci* 2015, 4, 1–3.
- [17]. Ghodake G, Seo YD, Lee DS. Hazardous phytotoxic nature of cobalt and zinc oxide nanoparticles assessed using *Allium cepa*. *J Hazard Mater.* 2011; 186:952–955. <https://doi.org/10.1016/j.jhazmat.2010.11.018> PMID: 21122986
- [18]. Nekrasova GF, Ushakova OS, Ermakov AE, Uimin MA, Byzov IV. Effects of copper (II) ions and copper oxide nanoparticles on *Elodea densa* Planch. *Russ J Ecol.* 2011; 42(6):458–463. <https://doi.org/10.1134/S1067413611060117>
- [19]. Yruela I. Copper in plants. *Braz J Plant Physiol.* 2005; 17(1):145–156. <https://doi.org/10.1590/S1677-04202005000100012>
- [20]. Hong J, Rico C, Zhao L, Adeleye AS, Keller AA, Peralta-Videa JR, et al. Toxic effects of copper-based nanoparticles or compounds to lettuce (*Lactuca sativa*) and alfalfa (*Medicago sativa*). *Environ Sci: Proc Imp.* 2015; 17:177–185. <https://doi.org/10.1039/C4EM00551A> PMID: 25474419
- [21]. White B, Yin M, Hall A, Le D, Stolbov S, Rahman T, et al. Complete CO oxidation over Cu₂O nanoparticles supported on silica gel. *Nano Lett.* 2006; 6(9):2095–2098. <https://doi.org/10.1021/nl061457v> PMID: 16968032
- [22]. Buazar F, Cheshmehkani A, Kassaei MZ. Nanosteel synthesis via arc discharge: media and current effects. *J Iran Chem Soc.* 2012; 9(2):151–156. <https://doi.org/10.1007/s13738-011-0038-3>
- [23]. Kassaei MZ, Buazar F, Motamedi E. Effects of current on arc fabrication of Cu nanoparticles. *J Nanomater.* 2010; 2010: 403197. <https://doi.org/10.1155/2010/403197>
- [24]. Buazar F, Sweidi S, Badri M, Kroushawi F. Biofabrication of highly pure copper oxide nanoparticles using wheat seed extract and their catalytic activity: A mechanistic approach. *Green Process Synth.* 2019; 8(1):691–702. <https://doi.org/10.1515/gps-2019-0040>
- [25]. Winter CA, Risley EA, Nuss WG. Carrageenin-induced edema in hind paws of the rats as an assay for antiinflammatory drugs. *Proceed Soc for Exp Biol and Med*, 1962, 111: 544–547.
- [26]. BLOIS, M. S. (1958). Antioxidant Determinations by the Use of a Stable Free Radical. *Nature*, 181(4617), 1199–1200. doi:10.1038/1811199a0
- [27]. Murugan K, Senthilkumar B, Senbagam D, Al-Sohaibani S. Biosynthesis of silver nanoparticles using *Acacia leucophloea* extract and their antibacterial activity. *Int J Nanomed.* 2014; 9:2431–2438. <https://doi.org/10.2147/IJN.S61779> PMID: 24876776
- [28]. Mohammed SA, Khashan KS, Jabir MS, Abdulameer FA, Sulaiman GM, Al-Omar MS, et al. Copper Oxide Nanoparticle-Decorated Carbon Nanoparticle Composite Colloidal Preparation through Laser Ablation for Antimicrobial and Antiproliferative Actions against Breast Cancer Cell Line, MCF-7. *BioMed Res Int.* 2022; 2022:9863616. <https://doi.org/10.1155/2022/9863616> PMID: 35299896
- [29]. Shobha G, Vinutha Moses & Ananda S *International Journal of Pharmaceutical Science Invention* ISSN (Online): 2319 – 6718, ISSN (Print): 2319 – 670X www.ijpsi.org Volume 3 Issue 8 | August 2014 | PP.06-28-38
- [30]. C.R. Chinnamuthu and P. Murugesu Boopathi, Nanotechnology and Agroecosystem, *Madras Agric. J.*, 96(1-6), 2009, 17-31.

- [31]. Chittaranjan Kole, Phullara Kole, K Manoj Randunu, Poonam Choudhary, Ramakrishna Podila, Pu Chun Ke, Apparao M Rao, and Richard K Marcus, Nanobiotechnology can boost crop production and quality: first evidence from increased plant biomass, fruit yield and phytomedicine content in bitter melon (*Momordica charantia*), *BMC Biotechnology*, 13(37),2013, 1-10.
- [32]. Cyren M. Rico, Sanghamitra Majumdar, Maria Duarte-Gardea, Jose R. Peralta-Videa and Jorge L. Gardea-Torresdey, Interaction of nanoparticles with edible plants and their possible implications in the food chain, *J Agric Food Chem.*, 59(8),2011, 3485–3498.
- [33]. F. Yang, C. Liu ,F. Gao F, M. Su , X. Wu , L. Zheng , F. Hong and P. Yang, The improvement of spinach growth by nano-anatase TiO₂ treatment is related to nitrogen photoreduction, *Biol Trace Elem Res.*, 119, 2007, 77–88.
- [34]. Fernandez-Escobar, R., Benlloch, M., Herrera, E., et al.: ‘Effect of traditional and slow-release N fertilizers on growth of olive nursery plants and N losses by leaching’, *Sci. Horticulturae*, 2004, 101, (1), pp. 39–49
- [35]. Savci, S.: ‘An agricultural pollutant: chemical fertilizer’, *Int. J. Environ. Sci. Dev.*, 2012, 3, p. 73

Synthesis of Some Substituted Azomethine Drug in Medicinal Chemistry: Green and Eco-Friendly Approach

A.V. Kawalkar¹, P.P. Choudhari², M.P. Wadekar³

¹Department of Chemistry, Amolakhchand Mahavidyalaya Yavatmal, Maharashtra, India

²Department of Chemistry, G. S. Tompe Arts Commerce and Science College, Chandur Bazar, Amravati, Maharashtra, India

³Department of Applied Chemistry division, Govt. Vidarbha Institute of Science and Humanity Amravati, Maharashtra, India

ARTICLE INFO

Article History:

Accepted : 01 Jan 2025

Published : 10 Jan 2025

Publication Issue :

Volume 12, Issue 7

January-February-2025

Page Number :

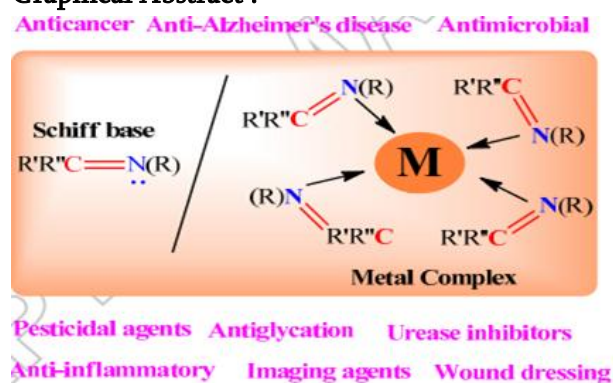
49-55

ABSTRACT

Schiff bases are synthesized and structurally diverse compounds, by different methods by the condensation between primary aromatic amines and aldehyde or ketones. The reaction of primary aromatic amines with aryl aldehydes is found to be catalyzed by lemon juice as natural acid under solvent-free conditions to give the corresponding Azomethine in good yields. This eco-friendly reaction has many advantages like economical, environmental, mild reaction conditions and simple work-up with high product yield. The naturally available fruit juice as a biocatalyst in synthesis fulfills almost all the terms and conditions of green chemistry and attracted the interest of researchers. The best thing is that most of fruits are easily available, cheap and can be easily extracted. The purpose of this review is to look out present aspects of fruit juice in organic transformations.

Keywords: Azomethine, Green Synthesis, lemon juice, natural acid.

Graphical Abstract :



I. INTRODUCTION

Azomethine is a nitrogen analog of an aldehyde or ketone in which the C=O group is replaced by RC=N group. It is usually formed by condensation of an aldehyde or ketone with a primary amine. Azomethine have a large number of synthetic uses in organic chemistry. The research on the chemistry of azomethine has been a focus of attention for chemists for several years; due to their wide spread diversified biological activities. It play an important roles in biological systems. The main aim of this concept is to develop the smooth and nonpolluting pathways and to find creative ways to reduce the use of toxic reagents, solvents, harsh reaction conditions and expensive catalysts [1-3]. The experimental trials of new catalyst in an environmentally benign manner have become much more important in recent years [4]. The conventional synthesis of chemicals produces large amount of toxic wastes and by-products [5]. These threats indicate that it must be important to develop methods which satisfy green principles [6-7]. The growing concern for the environment demands the development of eco-friendly and economic processes where in even less hazardous byproducts are not desirable. Organic reactions under solvent-free conditions have gained in popularity in recent years [8]. The formation of Schiff bases in this method depends upon the rate of removal of water from reaction mixture.

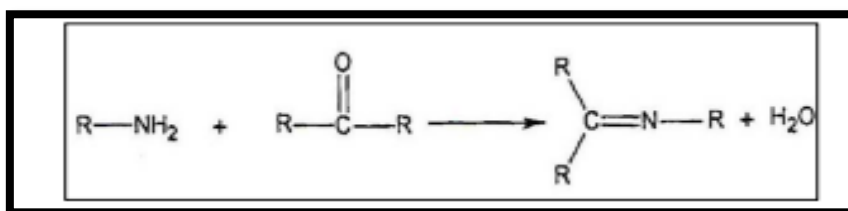


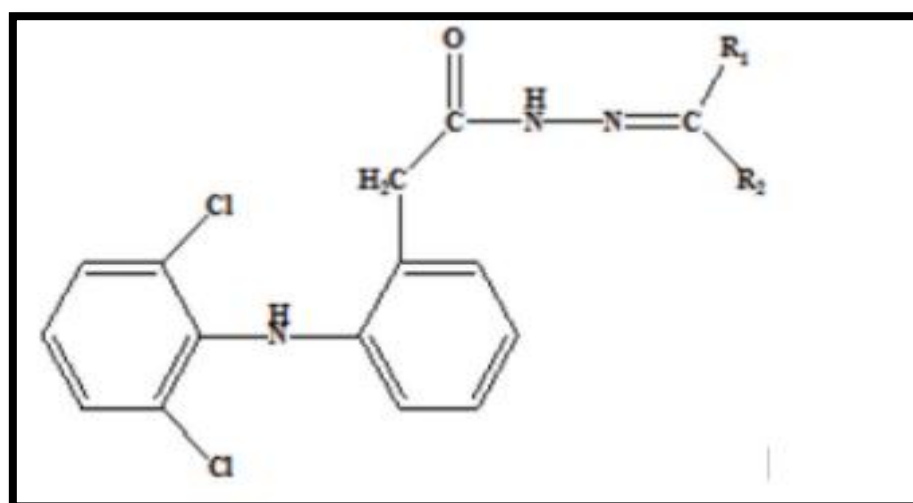
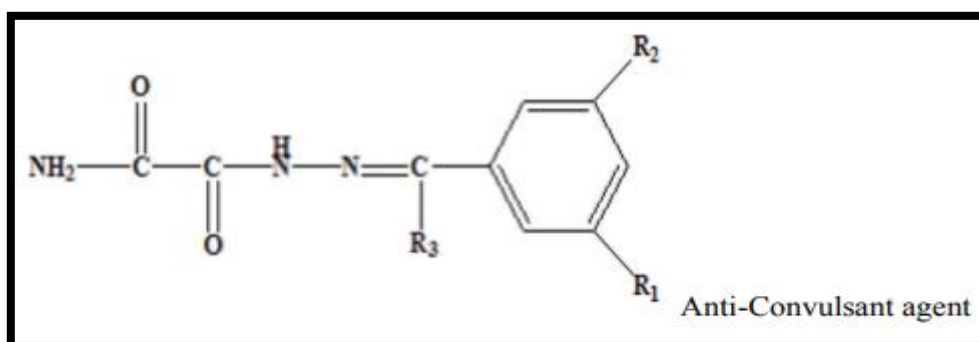
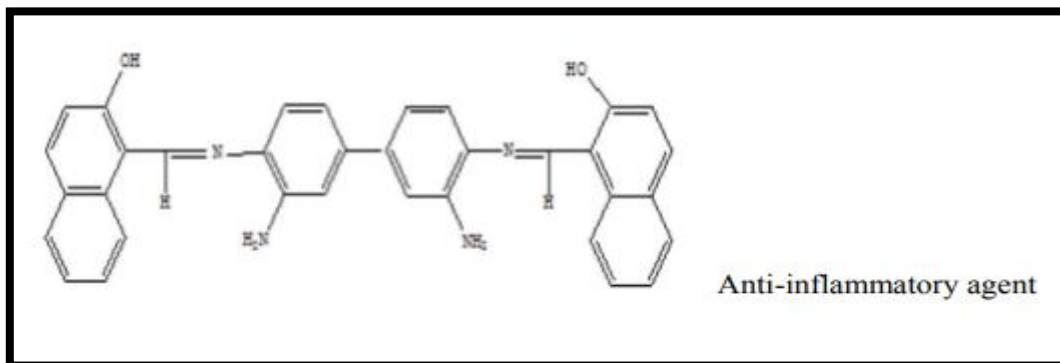
Fig 1 : Formation of Schiff base by condensation reaction.

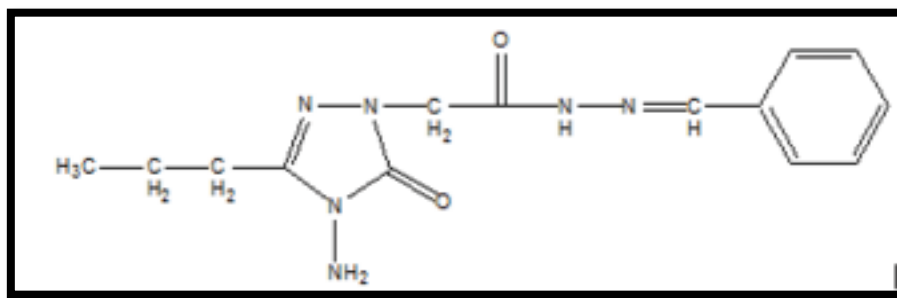
Originally, the classical synthetic route for synthesis of Schiff bases was reported by Hugo Schiff [9] which involves condensation of primary amines with carbonyl compounds under azeotropic distillation [10] with the simultaneous removal of water. The formation of carbon–nitrogen double bond plays an important role in organic synthesis. This can be achieved by the reaction of aldehydes and amines in acidic medium which leads to synthesis of Schiff bases (imines). Schiff bases have attracted considerable attention of organic chemists due to their significant biological activities like anticancer [11], antitumor [12], anti-inflammatory agents [13], insecticidal [14], antibacterial [15], antituberculosis [16], antimicrobial [17], anticonvulsant [18] activity. The Schiff bases are also used as versatile components in nucleophilic addition with organometallic reagents [19] and in cycloaddition reactions [20,21].

The methodologies reported above have some disadvantages such as prolonged reaction time, the high reaction temperatures, an excess of costly dehydrating reagents/catalysts, moisture sensitive catalysts, and special apparatus, etc. Considering these facts, we have decided to synthesize Schiff bases of various substituted aldehydes and aromatic amines by employing Mango juice, Grape juice, Lemon juice as green catalyst for green approach. *Citrus aurantium*, *Citrus indica*, *Citrus limonium* are some important species of citrus family commonly known as lemon. The lemon is indigenous to the north-west regions of India. It is now widely grown in all tropical and subtropical countries. In India it is also cultivated in home gardens. For the present work, we have used extract of *Citrus limonium* species of lemon as natural catalyst for synthesis of Schiff bases.

The synthesis of Schiff Base by using lemon juice (*Citrus limonium*) as an effective and mild acid catalyst for condensation reaction [22]. This synthesis shows the formation of selective imine by the reaction of aryl aldehyde and aromatic primary amine. This method provides a cost effective idea and benefits from the

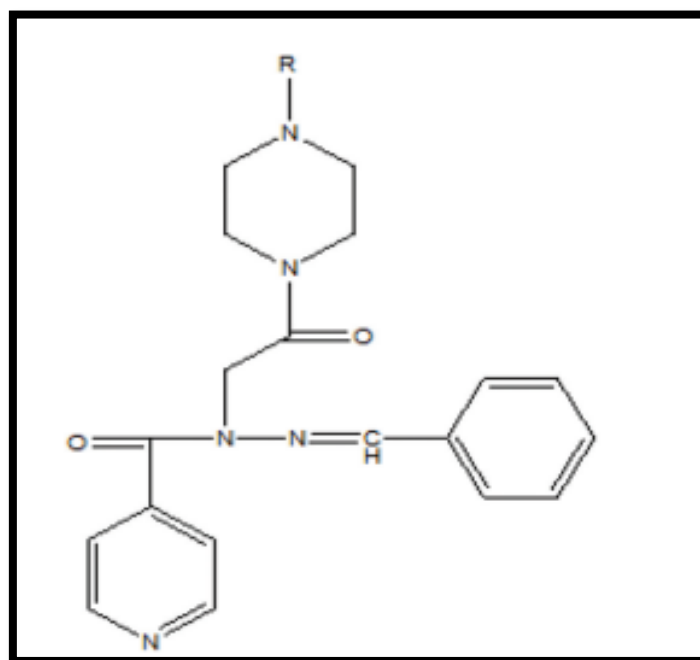
elimination of production of acidic waste. A green procedure for Knoevenagel condensation was reported [23]. They showed that lemon juice (*Citrus limonium*) act as environmentally benign acid catalyst for the reaction between aldehydes and nitriles. The mixture was stirred at room temperature for 30-60 minutes. This is new procedure by lemon juice qualifying it is a green method.





Anti-tumour agent

The halogenated solvents chloroform and dichloromethane (DCM) are now used instead. It is important to emphasise that these measures have proven to be short sighted with respect to increasingly strict chemical controls worldwide. Toluene is in fact suspected of damaging the unborn child and of organ damage through prolonged exposure [24, 25]. Chloroform and DCM are likely to be carcinogenic to humans according to the World Health Organization IARC evaluations. In addition to DCM, even as a short-lived halogenated substance has now been shown to be ozone depleting as well [26].



Hydrazide Derivative

Hazardous solvents	Issues	Green solvents (alternate solvents)
Pentane	Lower flash point than other similar solvents	Heptane
Diethyl ether	Lower flash point than other similar solvents	2-MeTHF, TME
Diisopropyl ether	Powerful peroxide formation compared to similar solvents	2-MeTHF, TME
Hexane	More toxic than other similar solvents	Heptane
Benzene	Carcinogen	Toluene
Chloroform	Carcinogen	DCM
1,2-DCE	Carcinogen	DCM
1,2-DME	Carcinogen	2-MeTHF, TME
Pyridine	Carcinogenicity (not classifiable)	Triethylamine (base)
1,4-Dioxane	Carcinogenicity (not classifiable)	2-MeTHF, TME
DCM	Emissions	Application dependent
Carbon tetrachloride	Emissions	DCM
DMF	Reproductive toxicity	Acetonitril
DMAc	Reproductive toxicity	Acetonitril
NMP	Reproductive toxicity	Acetonitril

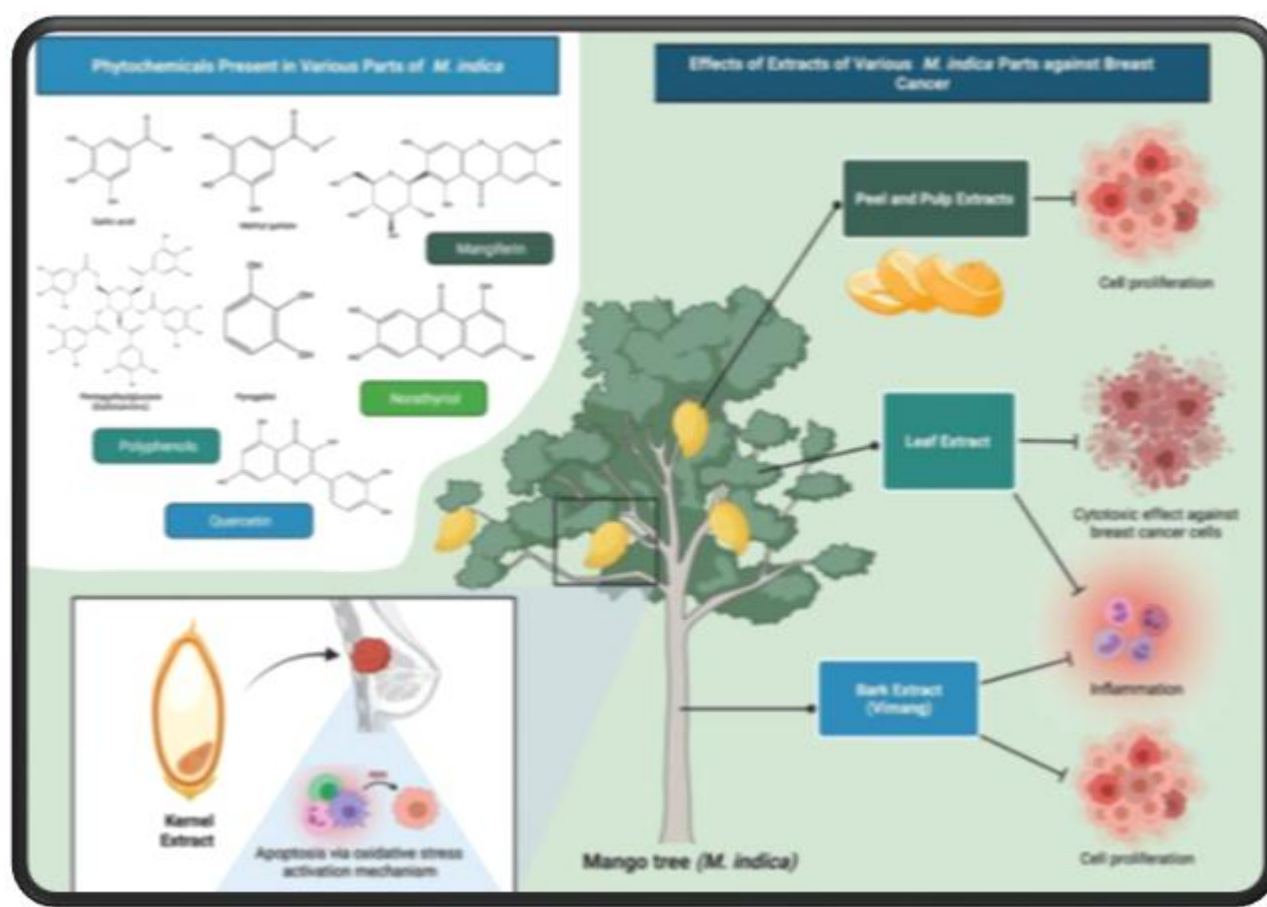
II. CONCLUSION

Green chemistry has come a long way since its birth in 1991, growing from a small grassroots idea into a new approach to scientifically based environmental protection. All over the world, governments and industries are working with “green” chemists to transform the economy into a sustainable enterprise. Green chemistry includes the technologies of the invention, design and application of chemical products and processes to reduce or to eliminate the use and generation of hazardous substances and where possible utilize renewable raw materials. Replacement by natural or less hazardous reagent to the harmful reagents makes environment pollution free.

In organic synthesis various newly discover solvent and catalyst help to reduce long reaction time. Computer aided designing also provide important tools to reduce reaction time. By the use of appropriating methods and handling of chemicals there is reduced risk of environmental contamination reactions. Implementation of suitable technologies and methods also help to improve the green chemistry some examples are microwave synthetic tools to the preparation of chemical compounds and drugs, computer aided drug design, using green

solvents, green catalyst etc. These procedures offer advantages such as reduced reaction time, mild reaction condition, productivity and higher yield, ease of execution and economic viability.

In this article, we are reporting a new eco-friendly route with good yield for the synthesis of Schiff bases by using sweet Mango Juice, Grapes juice and Lemon juice. The catalytic activity including the application of fruit juice in various organic transformations such as formation of C-C, C-N bonds and breaking of C-O, C-N bonds in different synthetically important organic compounds have been studied. Although many observations have not received by application of fruit juice in synthesis of natural products or complex structured molecules in details, it is believed that in near future the fruit juice chemistry will continue to attract significant research activity. Therefore, the present review would serve the need of organic chemists in searching new applications of fruit juice for organic synthesis.



III. REFERENCES

- [1]. Brahmachari G, Banerjee B. Catalyst free organic synthesis at room temperature in aqueous and non-aqueous media: An emerging field of green chemistry practice and sustainability. *Curr Green Chem.* 2015;2:274-305.
- [2]. Trost BM. On inventing reactions for atom economy. *AccChem Res.* 2002;35:695-705.
- [3]. Sankar M, Dimitratos N, Miedziak PJ, Wells PP, Kiely CJ. Designing bimetallic catalysts for a green and sustainable future. *ChemSoc Rev.* 2012;41:8099-8139.
- [4]. Maruoka K, List B, Yamamoto H, Gong LZ. Organocatalysis: A web collection. *ChemCommun.* 2012;48:10703-10703.

- [5]. Aken KV, Strekowski L, PatinyL.EcoScale, a semi-quantitative tool to selectan organic preparation based on economical and ecological parameters, Beilist J.Org Chem. 2006;2:3.
- [6]. Anastas PT, Warner JC. Green chem. theory and practice. Oxford Univ. Press,New York; 1998.
- [7]. Anastas PT, Kirchoff MM. Origins, currentstatus, and future challenges of greenchemistry. Acc. Chem. Res. 2002;35(9):686-694.
- [8]. (a) J.O. Metzger, Angew.Chem. Int. Ed., 1998, 37, 2975; (b) C.J. Li, T.H. Chan, Tetrahedron, 1999, 55, 11149.
- [9]. H. Schiff, Ann. Chem., 1864, 131, 118.
- [10]. R. B. Moffett and N. Rabjohn, Editor, Organic Synthesis; John Wiley &Sons, Inc., New York, 1963, 4, 605.
- [11]. F.D.Popp, J. Org. Chem., 1961, 26, 1566.
- [12]. D. Kong, X. Zhang, Q. Zhu, J. Xie, X. Zhou, ZhongguoYaowenHuaxueZazhi, 1998, 8(4), 245.
- [13]. D. J. Hadjipavlou-litina, A. A. Geronikaki, Drug Des. Discov.,1996, 15,199.
- [14]. S. S. Murthy, A. Kaur, B. Sreenivasalu, R.N. Sarma, Indian J. Exp. Biol., 1998, 36, 724.
- [15]. K.N. Venugopala, V.A.Jayashree, Indian J. Pharm. Sci., 2008, 70, 88.
- [16]. N. Solak, S. Rollas, Arkivoc, 2006, xii, 173.
- [17]. S.J. Wadher, M.P. Puranik, N.A.Karande, P.G.Yeole, Int. J. Pharm. Tech. Res., 2009, 1, 22.
- [18]. A. L. Cates, S. M. Rasheed, Pharm. Res., 1984, 6, 271.
- [19]. V. V. Kuznetsov, A. R. Palma, A. E. Aliev, A. V. Varlamov, N. S. Prostakov, Zh. Org. Khim. 1991, 127, 1579.
- [20]. A. E. Taggi, A. M. Hafez, H. Wack, B. Young, D. Ferraris, T. Lectka, J. Am. Chem. Soc., 2002, 124, 6626.
- [21]. (a) O. Tsuge, R. Kanemasa, Adv. Heterocycl. Chem., 1989, 45, 231; (b) M. F. Aly, M. I. Younes, S. A. M.Metwally, Tetrahedron, 1994, 50, 3159.
- [22]. Patil S, Jadhav SD, Patil UP. Natural acid catalyzed synthesis of Schiff base under solvent-free condition: As a Green approach. Arch. Appl. Sci. Res. 2012;4(2): 1074-1078.
- [23]. Deshmukh MB, Patil SS, Jadhav SD, Pawar PB. Green approach forKnoevenagel condensation of aromatic aldehydes with active methylene group.Synth.Commun.2012;42(8):1177-1183.
- [24]. Finnish Safety and Chemicals Agency. Toluene substance evaluation report2013
- [25]. European Chemicals Agency (ECHA) Classification and labellinginventory, 2015
- [26]. Hossaini R, Chipperfield MP, Montzka SA, Rap A, Dhomse S, FengW Efficiency of short-lived halogens at influencing climate throughdepletion of stratospheric ozone. Nat Geosci, 2015;8:186–190

Removal of Heavy Metals from Wastewater Using Nanotechnology: A Review

Amritpal Singh S.^{1*}, Swapnil S. Kosalge¹, Sandhya Bharambe², Pushpinder G. Bhatia¹

¹Department of Physics, Guru Nanak College of Arts, Science & Commerce, Mumbai, Maharashtra, India

²Department of Humanities and Applied Sciences, SIES Graduate School of Technology, Navi Mumbai, Maharashtra, India

ARTICLE INFO

Article History:

Accepted : 01 Jan 2025

Published : 10 Jan 2025

Publication Issue :

Volume 12, Issue 7

January-February-2025

Page Number :

56-77

ABSTRACT

Water pollution refers to the contamination of water sources by substances which make the water unusable for drinking, cooking, cleaning, swimming, and other activities. Pollutants include chemicals, trash, bacteria, and parasites. All these forms of pollution, directly or indirectly, make their way to water. Millions of people have lost their lives due to consumption of contaminated water. Due to rapid increase in population, development of new industries, there has been increase in water contamination. Major sources of water contaminants are in the form of organic pollutants, inorganic & biological pollutants. Inorganic pollutants include heavy metals like Pb, Cr, Cd, As, Cr, Hg etc. These heavy metals are harmful if consumed above their safety limits. Heavy metal-based industries have grown rapidly, and this has resulted in serious environmental problems with local dumping and wastewater from these industries. Nanotechnology is a rapidly expanding science with noteworthy outcomes in practically all areas of life. In recent years, active researchers are mostly interested in nanomaterials because of their distinctive characteristics, such as excellent reactivity and better catalysis. This review article, firstly, emphasizes on the methods employed for removal of Heavy Metal Ions from wastewater. Also, different types of nanomaterials used in the removal of Heavy Metal Ions & their future prospects are discussed further.

Keywords: Nanomaterial's, Heavy Metal Ions, Contamination, Magnetic nanoparticles, Wastewater, Adsorption

I. INTRODUCTION

Water can be contaminated by a variety of human activities or existing natural features, such as mineral-rich geologic formations. Chemical pollution from agriculture, industry, cities, and mining endangers the quality of the water[1]. These activities' air pollutants can also enter bodies of water via dry deposition, precipitation, and runoff. Some chemical pollutants have substantial and well-known health impacts, whilst many others have long-term health effects that are unknown[2]. Dangerous metals have contaminated the environment due to human progress and excessive activities, regardless of the fact that these metals are naturally present in the earth's crust. The preservation of wood and dyes, the photochemical and steel industries, smelting, synthetic chemicals, coating, mineral extraction, atmospheric build-up, sewage irrigation, textiles, alloy fabrication, fertilizer production, and battery building are some of these operations[3]. Heavy metal contamination has increased substantially in recent years, owing to the ongoing development of urban, industrial, and agricultural activity[4][5]. In general, fertilizers, metallic ferrous ores, sewage sludge, pesticides, combustion of fossil fuels, and municipal wastes are the primary causes of heavy metal toxicity. Contaminated (also referred as waste) water has various forms of organic, inorganic & biological pollutants[6]. Herbicides and pesticides, medications, fuel (such as oil spills), industrial solvents and cleansers, and synthetic dyes connected with pharmaceuticals are all examples of organic pollutants in water[7]. Nutrients such as nitrate and phosphate, heavy metals, chloride, and radioactive isotopes released from mining or nuclear accidents (such as caesium, iodine, uranium, and radon gas) are examples of inorganic pollutants. Some nutrients can be derived from geologic material, such as phosphorus-rich rock, although they are most obtained from fertilizer, animal and human waste. Heavy metals such as arsenic, mercury, lead, cadmium, and chromium can bioaccumulate and biomagnified throughout the food chain[8][9]. Pollutants from land cultivation, mining operations, agricultural chemicals, viruses & bacteria etc. are all pollutants present in water. Among the biological pollutants are Pathogens (infectious bacteria or viruses) enter water mostly through faecal waste from humans and animals due to insufficient sewage treatment[10]. *Fig. 1 shows the major pollutants present in water.* Many physiological and biological processes require trace levels of heavy metals as molybdenum (Mo), nickel (Ni), manganese (Mn), selenium (Se), zinc (Zn), magnesium (Mg), iron (Fe), chromium (Cr), copper (Cu), and cobalt (Co). Some trace metals are regarded vital, whereas others are deemed non-essential[11]. However, high amounts of these trace elements are detrimental to both individuals and the environment. High lead levels in drinking water have been linked to a variety of negative effects, including nervous system diseases, anaemia, renal failure, and cancer[12]. Due to their high toxicity, several metals, such as arsenic, mercury, lead, chromium, cadmium, are of utmost concern for public health because even little exposures can cause organ damage.[13]

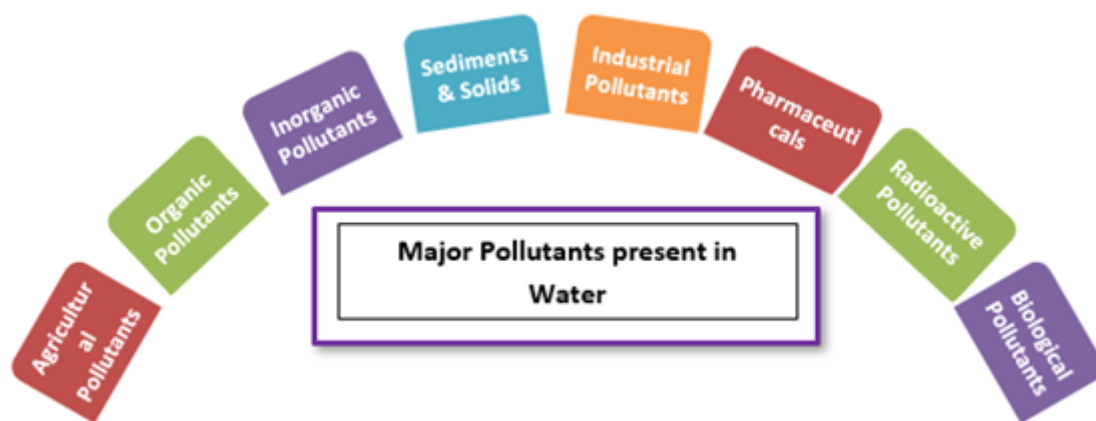


Fig. 1: Types of Pollutants in water

This review mainly focusses on heavy metals as pollutants in water bodies. Heavy metal Ions (HMI) in water are metallic elements that, when present in high concentrations, (density $> 5\text{g/cm}^3$ i.e., 5 times more than density of water) can endanger human and environmental health[14][15]. Lead, mercury, and cadmium are examples of common heavy metals. There are permissible values below which the heavy metals in water are considered safe. According to Ministry of Jal Shakti, in India, Arsenic (As) & Lead (Pb) should not exceed 0.01 mg/L whereas for Cadmium (Cd) it is 0.003 mg/L & Chromium, (Cr) it is 0.005 mg/L, Copper (Cu) 0.25 mg/L, Nickel (Ni) 0.20 mg/L (1). According to the ministry reports, in 2021 it was found that these heavy metals exceed their permissible values & Arsenic (As) content in ground water in India is found in fewParts of 154 districts in 21 states & Union Territories (UTs), Lead (Pb) in parts of 92 districts in 14 states, Cadmium (Cd) in parts of 24 districts in 9 states, Chromium (Cr) in parts of 29 districts in 10 states. As per World Health Organisation's (WHO) report the permissible limits for As, Pb, Cd, Cr are 0.05, 0.05. 0.005, 0.05 ppm respectively[16].(parts per million)*Fig. 2 shows various sources of heavy metal ions with their harmful impact on humans.*

Heavy metals disrupt the proper development and function of organs at concentrations greater than a few mg/L, poisoning the human body and destroying internal organs and tissues by diverse mechanisms such as enzyme denaturation, ion replacement, and protein inactivation[17]. Heavy metals have a variety of acute and chronic harmful effects on various human organs. In addition to neurological abnormalities, skin infections, vascular damage, immunological dysfunction, birth deformities, and cancer, heavy metal exposure can also cause problems with the kidneys and gastrointestinal tract.[18]. Exposure to high levels of heavy metals, particularly mercury and lead, can result in serious problems such as stomach colic pain, bloody diarrhoea, and kidney failure[19]. The fact that a number of metals have been identified as potential human carcinogens is yet another crucial component of long-term exposure.[20].

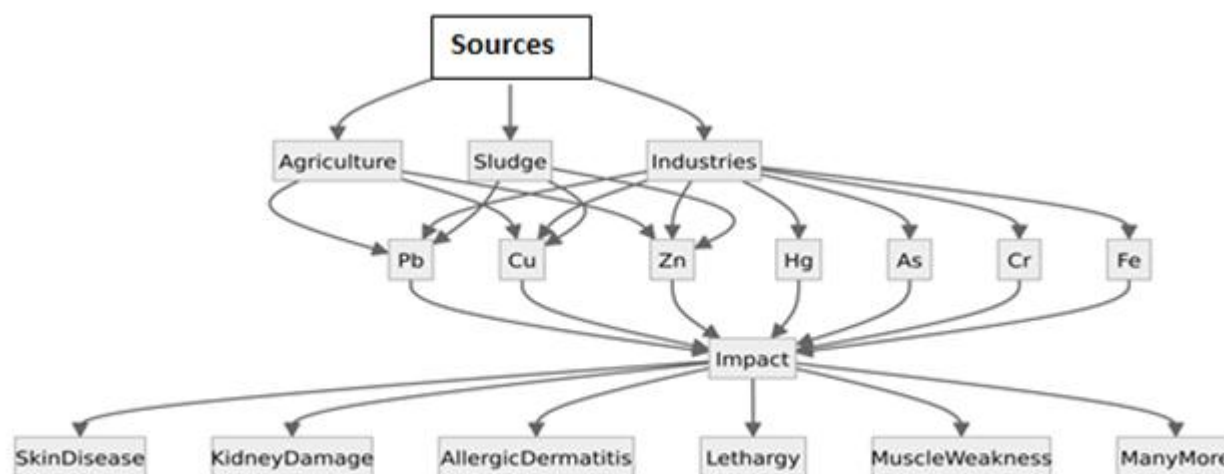


Fig. 2: Various sources of heavy metal ions with their harmful impact on humans.

II. METHODS ADOPTED FOR REMOVAL OF HEAVY METAL ION FROM WASTEWATER:

The most common ways for removing HMI from water are divided into three categories: physical, biological, and chemical procedures. The physical approach of wastewater treatment is primarily concerned with solid-liquid separations, and filtration plays a vital role.[21]. Chemical treatment methods rely on chemical interactions between contaminants and the operator of the chemical application to assist in either eliminating

contaminants from water or neutralizing adverse effects connected with contaminants[22]. Although biological wastewater treatment appears simple since it depends on natural processes to aid in the decomposition of organic contaminants, it is quite complex. Adsorption is one the most useful and largely used technique. A great adsorbent for wastewater treatment should meet the following standards[23][24]:

- 1) Pollutants can be effectively removed from the surface.
- 2) Environmentally friendly
- 3) Recyclable.
- 4) Validate excellent selectivity and sorption capacity, particularly for low-concentration contaminants in water.

Each method is briefly described below. Their advantages & disadvantages are mentioned in Table 1. [25][26][27][28]

A. Physical Methods:

- Adsorption: Process where impurities in water are attracted to a solid surface.
- Ion exchange: Process that swaps ions in water using an exchanger.
- Nanofiltration: Filtration process that uses nanoporous membranes.
- Reverse osmosis membrane: Membrane process that uses pressure to push water through a semipermeable membrane.
- Solvent extraction: Process that uses a solvent to extract impurities from water.
- Ultrafiltration: Filtration process that uses a semipermeable membrane to remove large particles.

B. Chemical Methods:

- Coagulation & Flocculation: Process that initially destabilizes the collides by neutralizing the forces and then agglomerating the destabilized particles.
- Electrodeposition: Process that uses electricity to deposit a substance onto a surface.
- Electrodialysis: Process that uses electricity to drive the movement of ions through a membrane.
- Electrolysis: Chemical decomposition of water into hydrogen and oxygen using an electric current.
- Chemical precipitation: Process that uses chemicals like phosphates, sulphides, hydroxides to precipitate out impurities.
- Insoluble salt precipitation: Process that causes salts to form insoluble precipitates.
- Neutralization precipitation: Process that causes a chemical reaction to form precipitates.

C. Biological Methods:

- Bio-flocculation: Process that uses microorganisms to aggregate particles.
- Bio-sorption: Process that uses microorganisms to bind and remove contaminants from water.
- Phytoremediation: Process that uses plants to remove contaminants from soil, water, or air.
- Bio-precipitation: Process that uses microorganisms to precipitate out impurities.
- Biotransformation: Process that uses microorganisms to transform contaminants into less harmful substances.

These methods are used in various applications such as wastewater treatment, drinking water purification, and industrial processes.

Table 1: The advantages & disadvantages of Physical, Chemical & Biological methods.

Method	Advantages	Disadvantages	Reference
PHYSICAL			
1. Adsorption	<ul style="list-style-type: none"> • Cost effective • Easy availability of raw materials • Excellent removal efficiency • No generation of toxic elements 	<ul style="list-style-type: none"> • Not suitable for automation • Regeneration of adsorbents 	[29]
2. Ion exchange	<ul style="list-style-type: none"> • Can remove metals in low concentration • High removal efficiency is possible; Fast kinetics • Selective ion removal is possible using right ion exchanger 	<ul style="list-style-type: none"> • Extremely sensitive to the pH of the solution • Has long production cycle 	[30]
3. Nano filtration	<ul style="list-style-type: none"> • Can be operated continuously • High rate of removal • High separation efficiency • Simple & Reliable 	<ul style="list-style-type: none"> • Low production volume • High pH requirements 	[31]
4. Reverse Osmosis (RO)	<ul style="list-style-type: none"> • High efficiency in removal of ions • Water is used for drinking 	<ul style="list-style-type: none"> • Backwash requirements • High cost • No regeneration 	[32]
5. Solvent extraction	<ul style="list-style-type: none"> • Suitable for treating low concentrations of ions • High selectivity for specific ions 	<ul style="list-style-type: none"> • Limited scalability for large scale applications • Adverse effect on environment due to used solvents & extraction by-products. 	[33]
6. Ultra-filtration	<ul style="list-style-type: none"> • Easy separation of small sized particles/contaminants • Minimal use of chemicals; environment friendly 	<ul style="list-style-type: none"> • High operational costs • Chances of membrane fouling • Limited removal efficiency 	[34]
CHEMICAL			
1. Coagulation & Flocculation	<ul style="list-style-type: none"> • Efficient for wide pH range • Cost effective 	<ul style="list-style-type: none"> • High operating cost of chemical addition • Large amount of sludge is produced • Not 100% efficient 	[35]
2. Electro deposition	<ul style="list-style-type: none"> • Low cost • Less chemicals used • Selective process 	<ul style="list-style-type: none"> • Inclination towards non-conformal development on surfaces. 	[36]

Method	Advantages	Disadvantages	Reference
	<ul style="list-style-type: none"> • Simple set-up 		
3. Electrodialysis	<ul style="list-style-type: none"> • Low operating pressure • Can remove metals in low concentration • Simple set-up 	<ul style="list-style-type: none"> • Metal precipitation occurs • More energy consumption 	[37]
4. Electrolysis	<ul style="list-style-type: none"> • High efficiency can be achieved 	<ul style="list-style-type: none"> • Large operational cost • High energy consumption 	[38]
5. Chemical precipitation (using hydroxides, sulphides etc.)	<ul style="list-style-type: none"> • Ease of operation; Cheap • Could be performed at suitable temperature • Can remove metals which are in high concentration • High selectivity 	<ul style="list-style-type: none"> • High amount of precipitating agents are used • Large amount of sludge is generated • Does not remove complex metals • Slow method 	[39]
6. Insoluble salt precipitation	<ul style="list-style-type: none"> • Effective removal • Cost effectiveness 	<ul style="list-style-type: none"> • Sludge disposal • Selective precipitation 	[40]
7. Neutralization precipitation	<ul style="list-style-type: none"> • Effective removal • Good pH adjustment 	<ul style="list-style-type: none"> • Chemicals involved in huge amount • Limited applicability 	[41]
BIOLOGICAL			
1. Bio flocculation	<ul style="list-style-type: none"> • Environmentally friendly • Cost effective 	<ul style="list-style-type: none"> • Slow process 	[42]
2. Biosorption	<ul style="list-style-type: none"> • Environmentally friendly • Cost effective 	<ul style="list-style-type: none"> • Limited metal specificity 	[43]
3. Photo remediation	<ul style="list-style-type: none"> • Environmentally friendly • Efficient removal of few ions 	<ul style="list-style-type: none"> • Energy intensive • Limited depth of penetration 	[44]
4. Bio precipitation	<ul style="list-style-type: none"> • Environmentally friendly • Low operating cost • Selective removal 	<ul style="list-style-type: none"> • Limited scalability 	[45]
e) Biotransformation	<ul style="list-style-type: none"> • Environmentally friendly • Efficient method 	<ul style="list-style-type: none"> • Slow process 	[46]

III.NANOMATERIALS USED FOR REMOVAL OF HMI FROM WASTEWATER:

A. Zeolites:

Zeolites are naturally occurring or synthetic hydrated aluminosilicate minerals with a porous structure[47]. These minerals have a three-dimensional crystalline structure with cavities and channels that can trap and exchange cations, water, and other molecules. Cost effectiveness, environmentally friendly, High efficiency are some of the advantages of using zeolites for removal of HMI's. Fig. 3 shows different types of nanomaterials used for removing HMI from wastewater.

Zeolites are known for their high surface area, adsorption capacity, and ion-exchange properties, making them valuable in various applications such as: Adsorbents in wastewater treatment for removing pollutants & heavy metals. Due to their acidic property, they are also used as catalysts. Also used in gas separation techniques to remove or separate certain gases from a mixture. For cleaning purposes, they are also used in detergents. Zeolites are commonly used to remove heavy metal ions from wastewater due to their remarkable adsorption capabilities. These naturally plentiful minerals are very selective towards heavy metals. Zeolites' negatively charged frameworks enable the exchange of cations with heavy metal ions in water, making them efficient adsorbents[48]. Zeolites' adsorption ability for heavy metal ions can be enhanced by a variety of means, including the addition of surfactants or polymers. Studies have demonstrated that zeolites may successfully remove heavy metals such as lead, copper, cadmium, zinc, and nickel from industrial effluent, greatly improving water quality for agricultural usage[49]. Furthermore, thermal activation of natural zeolites increases their adsorption efficacy for certain heavy metals, making them a cost-effective and environmentally benign solution for water filtration. [50][51]

N. Elboughdiriet al. [52] reported use of natural zeolites for adsorption behaviour of Cu, Pb & Cd in synthetic wastewater. Natural zeolites like clinoptilolite, chabazite, mordenite, jordanian and other varieties are recognized for their ion-exchange and adsorption properties, rendering them effective for the elimination of heavy metals. The key findings regarding the adsorption behaviour of Cu (II), Pb (II), and Cd (II) using natural zeolites are :The study indicated the suitability of zeolite for the removal of Cu (II), Pb (II), and Cd (II) ions from synthetic wastewater. Factors influencing the rate of adsorption include adsorbent mass, initial solution concentration, initial solution pH, adsorbent particle size, and agitation speed. It was observed that the removal efficiency of Cu(II) increased with increase in adsorbent mass, initial solution concentration, initial solution pH. It was also observed that the adsorption capacity of the adsorbents for heavy metals is directly related to the mass of adsorbent, initial solution pH, agitation speed, and initial solution concentration. Z.Z. Tasic et al. [53] reported that natural zeolites have been found effective in removing organic compounds, HMI, from wastewater. Clinoptilolite shows good selectivity & sorption for metals like Ni, Fe, Pb in wastewater. Chabazite is one of the most common zeolite used in removing HMI. The most frequent natural zeolites include analcime, chabazite, clinoptilolite, erionite, mordenite, and phillipsite. Clinoptilolite stood out among them as it is commonly used as an adsorbent for wastewater purification. Because of their strong adsorptive capabilities, they may effectively remove various pollutants like heavy metals, oil, and organic contaminants. Natural zeolites are low-cost adsorbents with high selectivity for different cations and ion exchange capacity. T.P Belova [54] reported model solutions with concentrations ranging from 0.5 to 3.5 mg-eq/L were used in removing HMI using zeolites. The sorption capacity of zeolite rises with metal ion concentration. The sorption capacity of heavy metal ions increases in the following order: $\text{Cu}^{2+} > \text{Fe}^{2+} > \text{Ni}^{2+} > \text{Co}^{2+}$. Langmuir and Freundlich equations were used to calculate sorption properties for each ion under study. [55]



Fig. 3: Types of nanomaterials used for removing HMI from wastewater

B. Carbon based Nanomaterials:

Carbon nanotubes (CNTs) are allotropes of carbon & are widely used to remove heavy metal ions from wastewater due to their superior physicochemical features. CNTs have a vast surface area, nanoscale size, and a variety of functions, making them extremely effective at adsorbing heavy metals[56]. Functionalizing CNTs with organic ligands improves their metal ion removal effectiveness by up to almost 100%. Furthermore, CNT composites including metal nanoparticles, graphene oxide, and zeolites have exhibited exceptional potential for removing heavy metals from wastewater due to their increased active surface area and adsorption sites[57]. The usage of CNTs and their composites not only aids in environmental monitoring and pollution control, but also in metal recovery and enrichment, emphasizing their importance in tackling heavy metal contamination in water. Functionalized multiwalled carbon nanotubes (MWCNTs) have been successfully utilized for the adsorptive removal of heavy metals like Pb^{2+} from synthetic wastewater, displaying high sorption capacity and efficiency[58]. The treatment of CNTs with active groups boosts their sorption ability and selectivity, making them useful in isolating and preconcentrating $Pb(II)$ from complicated matrices. Furthermore, the use of CNTs as adsorbents for heavy metals such as hexavalent chromium, lead, manganese and cadmium has been studied, suggesting their potential for water purification. Overall, CNTs provide a cost-effective and efficient option for removing heavy metal ions from wastewater, thereby dramatically improving water quality[59].

Ibrahim Elghamry and colleagues [60]discovered a new substance called 2-aminobenzimidazole, which is based on a heterocyclic molecule. It was anchored and connected directly to MWCNTs- CO_2H through the carbonyl group utilizing simple procedures. The material was examined for its ability to adsorb hazardous metal ions, including Cd^{2+} and Pb^{2+} , from contaminated water solutions. Abdel Majid Adam and collaborators [61]found

that crushing fullerene CNTs with the ZnFe_2O_4 composite improved the adsorption characteristics of free fullerene CNTs towards the tested heavy metal ions by 25%. Mostafa R. Abukhadra et al. [62] developed kaolinite nanotubes (KNTs) and described them as an adsorbent for metal ions such as Zn^{2+} , Cd^{2+} , Pb^{2+} , and Cr^{6+} . The synthesized KNTs effectively eliminated metal ions five times, resulting in significant reductions in removal percentages of 20.5%, 15.12%, 22.8%, and 23.16% for Zn^{2+} , Cd^{2+} , Pb^{2+} , and Cr^{6+} , respectively. Inadequate functional groups in raw CNTs cause easy aggregation, poor water dispersion, and insufficient metal adsorption capacity and selectivity. Adsorption efficacy of CNTs can be increased by adding functional groups such as hydroxyl, carboxyl, amine, and amino, all of which have strong chemical and electrostatic interactions with heavy metals. The aforementioned purification techniques can introduce oxygen-containing groups; however they may cause structural damage and reduce CNT stability. O^2 -plasma oxidation has been demonstrated to be an effective, efficient, and environmentally friendly alternative approach for adding hydrophilic carbonyl and carboxyl groups without producing obvious structural damage [63]. Furthermore, it was revealed that $-\text{COOH}$ can boost Pb(II) adsorption via ion exchange and surface precipitation, resulting in 93% elimination at pH 2.

C. Polymer based nanomaterials:

Heavy metal ion removal from wastewater has showed great potential for polymer-based nanomaterials. These materials have benefits including strong sorption activity, stability, and affordability. They include polymer nanocomposites and sorbents. These polymer-based materials have improved qualities such as improved permeability and antibacterial capabilities by integrating nanotechnology. These materials are now useful instruments in water remediation procedures due to their modification with additives such as metal nanoparticles, activated charcoal, and nano-fillers, which has increased removal efficiency. The advantages of polymer-based nanomaterials for removing heavy metal ions are:

- a. **Efficient Adsorption:** Polymer-based nanomaterials have excellent adsorption effectiveness for heavy metal ions in wastewater, which improves removal procedures.
- b. **Tailored qualities:** These nanomaterials can be designed to have specialized qualities for removing heavy metal ions with greater efficiency and selectivity.
- c. **Regenerability:** Polymer-based nanocomposites have a high degree of regenerability, which is important for practical wastewater treatment applications.
- d. **Cost-Effectiveness:** When compared to other technologies, polymer-based nanomaterials can provide a less expensive alternative for removing heavy metal ions from wastewater.
- e. **Environmental friendliness:** The usage of polymer-based nanoparticles is ecologically friendly, in line with the demand for sustainable and eco-friendly wastewater treatment methods.

Research has indicated that polymer nanocomposites are a useful tool for the adsorption of heavy metals from contaminated water, including Cr^{3+} , Ni^{2+} , Zn^{2+} , Cd^{2+} , Cu^{2+} , Hg , and Pb^{2+} . For example, [64] the production of polymeric nanocomposites such as HNTs@PDA/ZIF-8 has shown efficient adsorption capabilities for heavy metal ions, with amounts of 285.00 mg/g for Cu^{2+} and 515 mg/g for Pb^{2+} . Furthermore, heavy metal ions from wastewater have been effectively removed by the use of nanofiltration (NF) membranes, which can be made from cutting-edge materials like glutaraldehyde (GA) and polyvinyl amine (PVAM) [65]. Additionally, using a carbon magnetic nanocomposite as an adsorbent has demonstrated excellent removal efficiency for zinc, lead, and copper ions, with lead adsorption capacities reaching as high as 83.54 mg/g. These investigations demonstrate how well polymer-based nanoparticles extract heavy metal ions from tainted water sources. A special sulphur-rich microporous polymer with a sulphur content of 31.4 weight percent can be used to extract

mercury from water. It has a high concentration of easily accessible sulphur atoms and a large surface area. The as manufactured polymer (SMP) for Hg^{2+} shown significant binding affinity, high adsorption capacities, fast adsorption kinetics, and outstanding recyclability. The adsorption capacity of SMP is 595.2 mg/g. Ibrahim HotanAlsohaimi& group[66] showed that the adsorption capacity of the composite (which consisted of a chitosan-polymer)for Pb^{2+} ions increased as the pH increased until it reached pH 5.5. The maximum adsorption capacity was observed at an initial Pb^{2+} level of 20 mg/L and a contact time of 150 min.

D. Silica based nanomaterials:

Silica-based nanomaterials have demonstrated promising performance in the removal of heavy metal ions from wastewater. These nanomaterials, created using diverse approaches such as sol-gel procedures and surface modifications, have significant adsorption capabilities for metals such as lead, chromium, cobalt, and manganese[67]. According to studies, silica-based nanoparticles are effective at removing hazardous metals due to the presence of Si-OH groups on the surfaces, as well as their porosity and large surface area. However, material aggregation remains a concern for scientists, which can be solved by surface modification techniques such as functionalizing silica materials with nanoparticles. The functionalization of silica with various groups increases its adsorption efficacy, making it a long-term solution for water clean-up[68]. Studies have shown that these materials are effective at removing heavy metals using kinetic and equilibrium models, with spontaneous and thermodynamically beneficial adsorption processes. Furthermore, the recyclability and stability of silica-based nanoparticles have been emphasized, indicating their potential for repeated usage in heavy metal removal, hence contributing to environmental sustainability.

Several investigations [69]have demonstrated the efficacy of these materials in adsorbing contaminants such as Pb^{2+} and Cr(VI). The production of nano-silica oxide and mesoporous silica nanoparticles showed high adsorption capabilities for lead and cadmium ions, with removal efficiencies of up to 89%. Furthermore, the functionalization of silica nanoparticles with materials such as iron phthalocyanine and chitosan improved their adsorption capabilities, resulting in outstanding adsorption capacities of 150.33 mg/g for Pb^{2+} and 126.26 mg/g for Cd^{2+} . These important results highlight the potential use of silica-based nanoparticles as effective adsorbents for heavy metal removal in wastewater treatment applications. Nano-silica oxide (nano- SiO_2) has been successfully produced and used to adsorb lead Pb (II) and chromium Cr (VI) from aqueous solutions, with high removal efficiency.

E. Magnetic Nanoparticles (MNPs) :

Because of their efficacy and recyclability, magnetic nanoparticles are increasingly being used to remove heavy metal ions from wastewater. These nanoparticles, including magnetite nanoparticles, have excellent adsorption capabilities for heavy metals such as copper, lead, and zinc[70]. Functionalized magnetite nanoparticles can successfully remove heavy metal ions such as Pb^{2+} and Cd^{2+} from water, indicating potential adsorption capacities. Nanoparticles' unique qualities, such as a high surface-to-volume ratio and configurable band edges, allow them to effectively remove harmful contaminants from industrial and domestic wastes. Nano bioremediation, which involves microorganism-assisted nanoparticle synthesis, is a sustainable and environmentally benign technique to heavy metal removal, with benefits such as increased catalytic performance and cost-effectiveness[71]. Several studies have demonstrated the efficacy of various magnetic nanomaterials in adsorbing heavy metals such as copper, lead, zinc, chromium, and others from aqueous solutions. These magnetic nanocomposites, which include carbon magnetic nanocomposites, nanofiltration membranes, nanoparticles such as Ferrihydrite and magnetic iron nanocomposites, and iron oxide nanoparticles

generated from coal fly ash, have shown excellent removal efficiencies ranging from 40% to over 99%. The usage of magnetic nanoparticles has advantages such as high adsorption capacities, quick kinetics, and easy separation from the solution, making them a promising solution for heavy metal wastewater treatment[72]. Spinel ferrite (SFs) are a significant class of ferric-ion-containing composite metal oxides with the general structural formula $M^{2+}Fe_2^{3+}O_4$ (where $M = Mg^{2+}, Co^{2+}, Ni^{2+}, Zn^{2+}, Fe^{2+}, Mn^{2+}$, etc.)[73]. They have exceptional magnetic properties, a high chemical stability, high specific surface area, tunable shape and size, surface active sites, and are simple to modify or functionalize. Chitosan-coated $MnFe_2O_4$ nanoparticles with uniform size displayed strong adsorption for Cu (II) and Cr (VI) at 22.6 mg/g and 15.4 mg/g, respectively[74]. A cobalt ferrite-chitosan-graphene composite was recently created using graphene and chitosan and it has a higher adsorption capacity of 361 mg/g for Hg (II)[75]. *Fig. 4 shows removal of HMI using magnetic nanoparticles.*

Muntean et al. [76] created a novel nanocomposite material from magnetic iron oxide, silver, and activated carbon by an innovative combustion method. The specific surface area of the nanocomposite (NC) is quite close to that of the activated carbon, but the significant advantage comes from its magnetic properties. The Langmuir model showed that the nanocomposite had maximal adsorption capacities of 81.36 mg/g for copper, 83.54 mg/g for lead, and 57.11 mg/g for zinc ions. M.M. Arman[77] used the citrate auto-combustion approach to create Ho-doped $SmFeO_3$ multiferroics in a single phase. This sample has the highest anisotropy constant and magnetization, making it ideal for applications including sensors, catalysis, and heavy metal removal. The Freundlich isotherm accurately reflects the adsorption of Cr^{6+} ions from water using Ho-doped $SmFeO_3$. Empirical studies published in the literature provides interesting scientific insights into the significantly varying characteristics of the adsorption kinetics of various adsorbate-magnetic nanoadsorbent combinations. For example, [78] depositing Ag ions onto Fe_3O_4 nanoparticles reduced particle size while improving the magnetic properties of the nanocomposites. In another investigation, a Fe^{3+} stabilized magnetic polydopamine composite displayed outstanding adsorption performance for methylene blue in single adsorbate aqueous solutions for pH ranging from 3 to 10 at 45 degrees Celsius. A study examined the effectiveness of magnetite particles in treating wastewater samples from a wastewater treatment facility. In general, magnetite particles had a promising behaviour in terms of reducing detergents and chemical oxygen demand, whereas removals of total nitrogen and phosphates, as well as most heavy metals examined (which included chromium, zinc, lead, copper, and cobalt), were high to moderate[79].

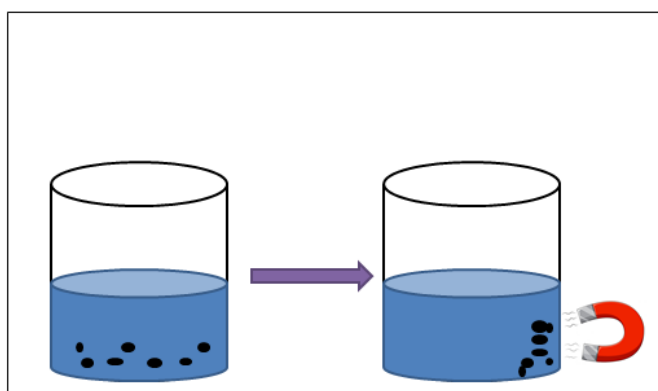


Fig. 4. Use of magnetic nanoparticles in removal of HMI from synthetic water

Due to restrictions on using bare hematite, magnetite, and maghemite nanoparticles, researchers typically create modified nanoparticles from iron oxide[80]. Over the years, nanoparticles have been synthesized using chemical processes such as coprecipitation, microemulsions, sol-gel synthesis, sonochemical reactions,

hydrothermal reactions, hydrolysis, and so on. Furthermore, various factors influence nanoparticle size and stability, including pH and temperature. The methods described above could be used to create nanoparticles of various sizes and forms[81]. In order to produce pure synthetic materials, they are isolated using a magnetic field, washed multiple times with ultrapure water, and dried in a vacuum oven to eliminate diamines. To achieve optimal adsorption capacity, nanoparticles must be well-defined across several parameters. These criteria define and affect the application of nanoparticles, such as size, shape, size distribution, degree of aggregation, surface charge, and surface area. Christos Liosis and group [82]revealed the primary findings in the recent decade on the usage of magnetic nanoparticles.Metal oxide nanoparticles are synthesized from pure metal precursors. These nanoparticles have a wide range of applications in physics, chemistry, and materials research. Table 2 shows the usage of MNP to remove HMI from wastewater. Thermal elements are capable of manufacturing a diverse range of oxide compounds. These can have a variety of structural shapes, with an electrical structure that can exhibit insulator, semiconductor, or metallic characteristics. These nanoparticles have unique optoelectronic features due to their well-known localized surface plasmon resonance properties. Metal oxide nanomaterials include manganese oxides, nanosized iron oxides, titanium oxides, cerium oxides, zinc oxides, magnesium oxides, aluminum oxides, and zirconium oxides.

T. Naseem and colleague [83]presented a complete overview of five metal oxide nanoparticles: copper oxide, silver oxide, zinc oxide, iron oxide, and titanium oxide.

Table 2: Advantages & Disadvantages of using magnetic nanoparticles to remove heavy metal ions from wastewater:[84]

Advantages	Disadvantages
<p>a) High removal efficiency: Magnetic nanoparticles have been proven to remove heavy metal ions such as Pb and Cr with efficiencies ranging from 40-70%.</p> <p>b) Cost-effective: Iron oxide nanoparticles may be synthesized from waste materials such as coal fly ash, making it an inexpensive form of wastewater treatment. Iron oxide nanoparticles recovered from waste sources are reusable, giving them eco-friendly solutions for adsorption operations.</p> <p>c) Strong Adsorption Capacity: Magnetic carbon nanocomposites have shown strong adsorption capacities for metal ions such as copper, lead, and zinc, with removal efficiencies greater than 75%.</p>	<p>(a) Fouling: Nanofiltration membranes, notably those containing nanoparticles, are susceptible to fouling, which can diminish their efficiency over time.</p> <p>(b) Membrane Cleaning: Repeated cleaning of membranes affects their lifespan, providing issues for long-term use.</p>

F. Graphene based nanomaterials:

Graphene-based nanoparticles have emerged as powerful adsorbents for removing HMI from wastewater. These nanomaterials, which include graphene oxides and their composites, have high adsorption capabilities, chemical stability, and recyclability, making them ideal for water treatment applications[85]. Studies have demonstrated that graphene-based nanocomposites may effectively remove over 90% of heavy metal ions and synthetic dyes, with certain materials attaining up to 100% decontamination. Furthermore, density functional theory (DFT) studies have shown that nanographene is effective at capturing heavy metal ions such as Pb^{2+} , Hg^{2+} , and Cd^{2+} from wastewater, indicating its potential for practical applications in water treatment. Several studies [86]have demonstrated the efficacy of these materials. For example, graphene oxide (GO) functionalized with 3,5-diaminobenzoic acid (DABA) displayed improved adsorption performance for heavy metal ions such

as Pb^{2+} and Al^{+3} , exceeding standard GO due to its large surface area and dentate functional groups. Furthermore, polyethyleneimine-grafted graphene oxide (PEI/GO) had a high adsorption capacity for lead ions (Pb^{2+}), with a maximum adsorption capacity of 64.94 mg/g, indicating that it is a viable adsorbent for heavy metal removal from industrial effluent. Furthermore, a long-lasting graphene-based water filter was created, capable of regenerating when treated with hot water or mild acid and eliminating heavy metals such as lead, cadmium, and mercury. These findings highlight the importance of graphene-based nanomaterials in sustainable heavy metal removal techniques. Graphene-based materials outperform typical materials in terms of heavy metal ion adsorption due to their high surface area, huge porosity, and functional groups. Graphene oxide typically interacts with heavy metals via precipitation, ion exchange, and surface complexation. Oxygen functional groups are commonly used to remove heavy metals due to their negative surface charge, which can effectively adsorb positively charged metals[87].

G. Nanophotocatalysts:

Nanophotocatalysts are sophisticated nanostructures utilized for heavy metal adsorption and photocatalytic reduction. They are often made up of semiconductor oxides such as titanium oxide (TiO_2), zinc oxide (ZnO), or binary nanomaterials that combine both oxides. When exposed to a suitable wavelength of light, nano photocatalysts induce photocatalytic ion reduction, which results in heavy metal removal from contaminated water[88].

Pollutants that are frequently encountered in wastewater along with heavy metal ions include polybrominated diphenyl ether, phthalates, phenolic chemicals, pharmaceuticals, antibiotics, and dyes. Metal-doping enhances the breakdown efficiency of several chemicals, including titanium, copper, zinc, and iron[89]. The efficiency of the photocatalyst is essentially determined by fundamental elements such as pH, doping, catalyst loading, light intensity, and stability. These factors contribute significantly to the degradation of contaminants. C. Sivaraman and group provides a detailed explanation of how these parameters affect photocatalytic degradation efficiency rates. Nanophotocatalysts' performance in heavy metal reduction can be improved through strategies such as dye sensitization, atom doping, defect introduction, and connecting multiple semiconductors[90]. The use of nanomaterials in photocatalysis provides physically and chemically customizable properties that improve heavy metal adsorption and ion reduction capabilities. The synthesis technique, surface area, defect concentration, and particle size all have an impact on nanophotocatalyst effectiveness, indicating the need for additional research to enhance their efficiency. Overall, nano photocatalysts offer a viable and environmentally benign solution to heavy metal contamination in water sources. Cheng et al. [91] employed a hydrothermal technique to create $\text{TiO}_2/\text{Fe}_2\text{O}_3$ hybrids, which were then used as a photocatalyst to degrade RhB.

H. Multifunctional Magnetic Nanoparticles (MFMNPs)

Multifunctional nanoparticles (MFMNPs) are nanoparticles that have many capabilities within a single particle, making them useful for a variety of applications. MFMNPs are highly efficient at adsorbing heavy metal ions from wastewater due to their increased adsorption sites and active surface area[92]. These nanoparticles can have varying porosity, enabling for customisation based on particular removal needs. These nanoparticles serve an important role in human healthcare monitoring because they protect water quality and reduce the health hazards associated with heavy metal contamination. Magnetic nanoparticles can be functionalized with a variety of inorganic materials, including silica, metal oxides, and nonmetal compounds, to remove metals from water or wastewater. Coating nanoparticles with these materials stabilizes them in aqueous solution and enhances their binding to certain ligands on their surfaces[93]. They facilitate the covalent binding

of ligands on the surface of nanoparticles. Traditional adsorbents, such as activated carbon, clays, silica beads, and biosorbent, have limitations in terms of permeability, selectivity, temperature dependence, pH dependence, and secondary waste. To avoid potential harm from harmful substances in the environment and biological systems, magnetic oxide nanoparticles must be released with precision and accuracy[94]. To prevent bursts and leaks, the superparamagnetic particles are coated to block undesirable potentials. Coating materials include: organic-inorganic shells (e.g., $\text{Fe}_3\text{O}_4@\text{SiO}_2\text{-NH}_2$) ; organic molecules (e.g., EDTAD- Fe_3O_4 , $\text{Fe}_3\text{O}_4@\text{C}$; polymers (e.g., $\text{Fe}_3\text{O}_4@\text{APS}@AA\text{-Co-CA}$); metal oxides (e.g., $\text{MgO-Fe}_3\text{O}_4$) ; surfactants ($\text{Fe}_3\text{O}_4\text{-oleic acid}$); inorganic molecules (e.g., $\text{Fe}_3\text{O}_4@\text{SiO}_2$); and multi-shells ($\text{Fe}_3\text{O}_4@\text{SiO}_2@\text{CS}@pyropheophorbide$) . Ebenezer C. Nnadozie and team reviewed Multifunctional Magnetic Oxide Nanoparticle (MNP) Core-Shell[95].

Magnetic oxide nanoparticles (MIONs) are frequently used to shield the core magnetic component from weakening and improve stability in aquatic environments. Following thermalization, the protective coating acts as a sacrificial layer, providing additional functionality. Several authors employed silicon(IV) oxide in the form of tetraethyl orthosilicate (TEOS) for surface coating. Silicon(IV) oxide is frequently utilized for its chemical inertness, hydrophilicity, non-toxicity, and ease of modification. [96].

I. Multicomponent Hybrid Nanoparticles:

Multicomponent hybrid nanoparticles provide more active sites for heavy metal ion adsorption, resulting in larger adsorption capabilities. The use of various nanomaterials in multicomponent hybrids improves the effectiveness of heavy metal ion removal methods. The synergistic effects of diverse components in multicomponent nanoparticles can lead to better adsorption and photocatalytic reduction of heavy metal ions in wastewater[97].

L. Jiao and group studied and concluded that Halloysite@polydopamine/ZIF-8 nanocomposites effectively remove heavy metal ions. The parameters influencing heavy metal ion (Pb^{2+} , Cd^{2+} , Cu^{2+} , and Ni^{2+}) adsorption by HNTs@PDA/ZIF-8 were explored. The Langmuir model accurately described the adsorption of HNTs@PDA/ZIF-8. The maximum adsorption capacity was 285.00 mg/g for Cu^{2+} , 515.00 mg/g for Pb^{2+} , 185 mg/g for Cd^{2+} , and 112.5 mg/g for Ni^{2+} [98]. Furthermore, HNTs@PDA/ZIF-8 has a high regenerability, which is important in practical applications. The key interactions between adsorbents and heavy metal ions were discovered as electrostatic attraction, coordination processes, and ion exchange during the adsorption mechanism analysis.

Mantovani et al. [99] studied whether microalgae were suitable for the hydrothermal carbonization process, which is regarded as an environmentally acceptable method for producing iron nanoparticles. Laboratory tests demonstrated that microalgal biomass grown on municipal sewage sludge centrates can be used to manufacture iron nanoparticles for cleaning effluent. Marganovici et al. [100] investigated the chemical $\text{Ca}[\text{O}_2\text{P}(\text{CH}_2\text{CH}_2\text{COOH})(\text{C}_6\text{H}_5)_2]$ (CaCEPPA), which has a layered structure with phenyl groups orientated into the interlayer space and crystallizes in the monoclinic system. The compound $\text{Co}_2[(\text{O}_2\text{P}(\text{CH}_2\text{CH}_2\text{COO})(\text{C}_6\text{H}_5)(\text{H}_2\text{O}))_2 \cdot 2\text{H}_2\text{O}]$ (CoCEPPA) has a 1D structure made of zig-zag chains. CaCEPPA and CoCEPPA materials were investigated for their ability to remove lead and cadmium from aqueous solutions.

J. Nanocomposite Membranes:

Due to their superior characteristics and effectiveness, nanocomposite membranes play an important role in the removal of heavy metal ions from wastewater[101]. These membranes, which are frequently manufactured employing modern materials and modification processes such as interfacial polymerization, grafting, and the insertion of nano-fillers, have excellent treatment efficiency, reaching up to 99.90% for certain heavy metals

such as Cr^{3+} . The addition of novel materials to the membrane structure, such as Zn-based metal-organic frameworks or functionalized halloysite nanotube nanoparticles, improves their effectiveness in heavy metal ion removal[102]. Furthermore, nanocomposite membranes have superior anti-fouling capabilities, higher water permeability, and high rejection rates for heavy metal ions, making them a suitable solution for effective wastewater treatment.

It is observed that Nanofiltration (NF) is a membrane-based separation technology that uses hydrostatic pressure to move molecules across semipermeable membranes. This approach permits low-molecular-weight solutes and solvents to pass through the barrier, while bigger molecules remain trapped[103]. NF has various advantages over other membrane technologies, including improved rejection of higher flux and divalent ions, less energy usage, and lower operating pressure. This technology may successfully remove oil, grease, suspended particles, heavy metals, dyes, and other contaminants from industrial effluents and drinking water. Membrane desalination, a highly efficient strategy for treating saline water and wastewater, has received a lot of attention recently.. The primary issue in membrane research is to develop highly permeable and stable membranes with outstanding selectivity and desirable physicochemical features[104]. A. A. Alotaibi and group reported that modifying mesoporous silica nanoparticles (MSNs) with amine and sulphonic groups improved the performance of mixed matrix polysulfone (PSU) nanocomposite membranes. Chemical alteration of MSNs improved membrane characteristics, resulting in higher water permeability[105]. The inclusion of functional groups on nanoparticles increased the efficacy of heavy metal ion removal, particularly cadmium and zinc. The elimination efficiency of these heavy metal ions increased by more than 90%.

The developed functionalized-MSNs/PSU nanocomposite membrane has excellent potential for industrial wastewater removal applications. It provides a viable alternative for the treatment of wastewater containing heavy metal ions. The study shown that using surface-functionalized mesoporous silica nanoparticles in membrane technology improves water treatment applications[106]. MoS_2 nanosheets of few layers were prepared through a surfactant assisted hydrothermal method. The prepared sheets were further used as an efficient adsorbent for removal of Hg from wastewater. The prepared nanosheets had high stability and negative zeta potential which made the material efficient for adsorption of mercury from wastewater. Novel 2D sheets made of graphene can be used as a very good adsorbent for the purification of heavy metals. Fu et al studied about the unique advances on 2D materials and also showed their composition and crystal structures .[107]

IV.CONCLUSION

Water is a crucial resource for life, yet maintaining its accessibility, affordability, and dependability is a significant challenge for our world. Heavy metal ions (HMIs) are among of the most hazardous contaminants. This review presents the use of nanotechnology and different types of nanomaterials used in removing heavy metal ions from wastewater. Each type of nanomaterials has some advantage and disadvantage depending upon its use. These different types of nanomaterials reported in literature are reported in this paper with few important results which are of great importance. As far as synthesis methods are concerned, this paper covers almost all types of physical, chemical and biological methods for synthesis of nanomaterials. Nanomaterials have potential for heavy metal removal from water due to some key physicochemical properties, such as larger surface areas than bulk particles, the ability to functionalize with different chemical groups to enhance their affinity to a given compound, and the ability to be reused multiple times. The preferential attraction of

different heavy metals for the adsorbent determines their ability to be removed from water. Significant growth has been observed in use of adsorption method which produce great results.

V. FUTURE OUTLOOKS & CHALLENGES

The materials described above have limits regarding cost effectiveness and efficiency. The minimization of costs and environmental implications from waste products will be an important component to investigate for the widespread use of innovative materials in wastewater treatment. Although most novel materials have high adsorption performance in theoretical simulations, a large number of empirically manufactured novel materials are still required. Furthermore, considerable inconsistencies between practical and theoretical absorption capacities frequently result in non-ideal surface conditions, which appear to be a barrier to the widespread use of innovative materials in wastewater treatment. Some research found that modifying adsorbents improved their ability to remove heavy metals. Therefore, it is assumed that there are still numerous functionalized or modified new materials that are worth investigating in future.

More research on introducing easy synthesis methods to reduce costs, as well as investigating structural modifications by ligands, should be conducted. Cost-effective recycling techniques, environmentally friendly disposable options, and durability are also required for the practical application of innovative materials on a large scale. Clarification of the actual process causing the loss in performance following recycled usage is essential. Currently, no nanoparticles are environmentally friendly as well as non-hazardous. Their discharge throughout the synthesis, application, and disposal management processes can raise the risk of environmental contamination. As a result, there is an urgent need to establish a safe and appropriate method for their disposal. The development of more competent, low-cost, and recyclable nanoparticles may lead to safer water treatment in the near future.

VI. CONFLICT OF INTEREST

The authors declare no conflict of interest.

VII. REFERENCES

- [1]. G. Amo-Duodu, E. Kweinor Tetteh, S. Rathilal, and M. N. Chollom, "Synthesis and characterization of magnetic nanoparticles: Biocatalytic effects on wastewater treatment," *Mater. Today Proc.*, vol. 62, pp. S79–S84, 2022, doi: 10.1016/j.matpr.2022.02.091.
- [2]. A. S. Mahmoud, M. K. Mostafa, and R. W. Peters, "A prototype of textile wastewater treatment using coagulation and adsorption by Fe/Cu nanoparticles: Techno-economic and scaling-up studies," *Nanomater. Nanotechnol.*, vol. 11, pp. 1–21, 2021, doi: 10.1177/18479804211041181.
- [3]. S. Ethaib, S. Al-Qutaifia, N. Al-Ansari, and S. L. Zubaidi, "Function of Nanomaterials in Removing Heavy Metals for Water and Wastewater Remediation: A Review," *Environ. - MDPI*, vol. 9, no. 10, 2022, doi: 10.3390/environments9100123.
- [4]. K. Gupta, P. Joshi, R. Gusain, and O. P. Khatri, "Recent advances in adsorptive removal of heavy metal and metalloid ions by metal oxide-based nanomaterials," *Coord. Chem. Rev.*, vol. 445, p. 214100, 2021, doi: 10.1016/j.ccr.2021.214100.

- [5]. J. Nikić et al., "Synthesis, characterization and application of magnetic nanoparticles modified with Fe-Mn binary oxide for enhanced removal of As(III) and As(V)," *Environ. Technol. (United Kingdom)*, vol. 42, no. 16, pp. 2527–2539, 2021, doi: 10.1080/09593330.2019.1705919.
- [6]. T. Patil, J. A. C. Eng, and B. B. T. Patil, "Journal of Advanced Wastewater Treatment Using Nanoparticles," vol. 5, no. 3, 2015, doi: 10.4172/2090-4568.1000131.
- [7]. F. M. Alzahrani, N. S. Alsaiari, K. M. Katubi, A. Amari, F. Ben Rebah, and M. A. Tahooun, "Synthesis of polymer-based magnetic nanocomposite for multi-pollutants removal from water," *Polymers (Basel)*, vol. 13, no. 11, 2021, doi: 10.3390/polym13111742.
- [8]. R. Ramadan, "Preparation, characterization and application of Ni-doped magnetite," *Appl. Phys. A Mater. Sci. Process.*, vol. 125, no. 9, pp. 1–8, 2019, doi: 10.1007/s00339-019-2887-z.
- [9]. F. Almomani, R. Bhosale, M. Khraisheh, A. kumar, and T. Almomani, "Heavy metal ions removal from industrial wastewater using magnetic nanoparticles (MNP)," *Appl. Surf. Sci.*, vol. 506, p. 144924, 2020, doi: 10.1016/j.apsusc.2019.144924.
- [10]. K. Anbalagan, M. M. Kumar, J. S. Sudarsan, and S. Nithiyanantham, "Removal of heavy metal ions from industrial wastewater using magnetic nanoparticles," *J. Eng. Res.*, vol. 10, no. 4, pp. 59–71, 2022, doi: 10.36909/jer.6924.
- [11]. M. F. Horst, M. Alvarez, and V. L. Lassalle, "Removal of heavy metals from wastewater using magnetic nanocomposites: Analysis of the experimental conditions," *Sep. Sci. Technol.*, vol. 51, no. 3, pp. 550–563, 2016, doi: 10.1080/01496395.2015.1086801.
- [12]. A. Buccolieri et al., "Synthesis and Characterization of Mixed Iron-Manganese Oxide Nanoparticles and Their Application for Efficient Nickel Ion Removal from Aqueous Samples," *J. Anal. Methods Chem.*, vol. 2017, 2017, doi: 10.1155/2017/9476065.
- [13]. Renu, M. Agarwal, and K. Singh, "Heavy metal removal from wastewater using various adsorbents: A review," *J. Water Reuse Desalin.*, vol. 7, no. 4, pp. 387–419, 2017, doi: 10.2166/wrd.2016.104.
- [14]. M. A. Tahooun, S. M. Siddeeg, N. S. Alsaiari, W. Mnif, and F. Ben Rebah, "Effective Heavy Metals Removal from Water Using Nanomaterials : A Review," pp. 1–24.
- [15]. M. O. Usman, G. Aturagaba, M. Ntale, and G. W. Nyakairu, "A review of adsorption techniques for removal of phosphates from wastewater," *Water Sci. Technol.*, vol. 86, no. 12, pp. 3113–3132, 2022, doi: 10.2166/wst.2022.382.
- [16]. Y. Tao, C. Zhang, T. Lü, and H. Zhao, "Removal of Pb(II) ions from wastewater by using polyethyleneimine-functionalized Fe₃O₄ magnetic nanoparticles," *Appl. Sci.*, vol. 10, no. 3, 2020, doi: 10.3390/app10030948.
- [17]. S. M. Ansari et al., "Eco-Friendly Synthesis, Crystal Chemistry, and Magnetic Properties of Manganese-Substituted CoFe₂O₄ Nanoparticles," *ACS Omega*, vol. 5, no. 31, pp. 19315–19330, 2020, doi: 10.1021/acsomega.9b02492.
- [18]. C. Nilsson, C. Nilsson, R. Lakshmanan, and G. Renman, "Efficacy of reactive mineral-based sorbents for phosphate, bacteria, nitrogen and TOC removal- Column experiment in recirculation batch mode Efficacy of reactive mineral-based sorbents for phosphate, bacteria, nitrogen and TOC removal e Column experime," *Water Res.*, no. May 2014, 2013, doi: 10.1016/j.watres.2013.05.056.
- [19]. A. Singh, S. Chaudhary, and B. S. Dehiya, "Fast removal of heavy metals from water and soil samples using magnetic Fe₃O₄ nanoparticles," 2020.

- [20]. M. Ul-Islam et al., "Current advancements of magnetic nanoparticles in adsorption and degradation of organic pollutants," *Environ. Sci. Pollut. Res.*, vol. 24, no. 14, pp. 12713–12722, 2017, doi: 10.1007/s11356-017-8765-3.
- [21]. K. Singh, N. A. Renu, and M. Agarwal, "Methodologies for removal of heavy metal ions from wastewater: an overview," *Interdiscip. Environ. Rev.*, vol. 18, no. 2, p. 124, 2017, doi: 10.1504/ier.2017.10008828.
- [22]. V. Dhiman and N. Kondal, "ZnO Nanoadsorbents: A potent material for removal of heavy metal ions from wastewater," *Colloids Interface Sci. Commun.*, vol. 41, no. October 2020, p. 100380, 2021, doi: 10.1016/j.colcom.2021.100380.
- [23]. S. Singh Rathore, S. Tejasvi, and V. Gupta, "Elimination of Heavy Metal Ions from Industrial Wastewater: A Review," *Eur. Chem. Bull*, vol. 2023, no. 1, pp. 1052–1065.
- [24]. N. Ghosh, S. Das, G. Biswas, and P. K. Halder, "Review on some metal oxide nanoparticles as effective adsorbent in wastewater treatment," vol. 85, no. 12, pp. 3370–3395, 2022, doi: 10.2166/wst.2022.153.
- [25]. G. H. Chala, "Review on Green Synthesis of Iron-Based Nanoparticles for Environmental Applications," *J. Chem. Rev.*, vol. 5, no. 1, pp. 1–14, 2023, [Online]. Available: <https://doi.org/10.22034/JCR.2023.356745.1184>
- [26]. F. S. A. Khan et al., "Magnetic nanoparticles incorporation into different substrates for dyes and heavy metals removal—A Review," *Environ. Sci. Pollut. Res.*, vol. 27, no. 35, pp. 43526–43541, 2020, doi: 10.1007/s11356-020-10482-z.
- [27]. R. Asadi, H. Abdollahi, M. Gharabaghi, and Z. Boroumand, "Effective removal of Zn (II) ions from aqueous solution by the magnetic MnFe₂O₄ and CoFe₂O₄ spinel ferrite nanoparticles with focuses on synthesis, characterization, adsorption, and desorption," *Adv. Powder Technol.*, vol. 31, no. 4, pp. 1480–1489, 2020, doi: 10.1016/j.appt.2020.01.028.
- [28]. F. Asghar and A. Mushtaq, "The Future of Nanomaterial in Wastewater Treatment: A Review," *Int. J. Chem. Biochem. Sci.*, vol. 23, no. 1, pp. 150–157, 2023.
- [29]. M. K. Bharti, S. Gupta, S. Chalia, I. Garg, P. Thakur, and A. Thakur, "Potential of Magnetic Nanoferrites in Removal of Heavy Metals from Contaminated Water: Mini Review," *J. Supercond. Nov. Magn.*, vol. 33, no. 12, pp. 3651–3665, 2020, doi: 10.1007/s10948-020-05657-1.
- [30]. A. Predescu, E. Matei, A. Berbecaru, and R. Vidu, "Synthesis of Magnetic Nanoparticles for the removal of heavy metal ions from wastewaters," *Proc. 38th Annu. Congr. ARA*, no. JULY 2014, pp. 37–42, 2015, doi: 10.14510/araproc.v0i0.1270.
- [31]. S. M. Abdelbasir and A. E. Shalan, "An overview of nanomaterials for industrial wastewater treatment," *Korean J. Chem. Eng.*, vol. 36, no. 8, pp. 1209–1225, 2019, doi: 10.1007/s11814-019-0306-y.
- [32]. T. D. Chaemiso, "Removal Methods of Heavy Metals from Laboratory Wastewater," *J. Nat. Sci. Res.*, vol. 9, no. 2, pp. 36–42, 2019, doi: 10.7176/jnsr/9-2-04.
- [33]. G. N. Hlongwane, P. T. Sekoai, M. Meyyappan, and K. Moothi, "Simultaneous removal of pollutants from water using nanoparticles: A shift from single pollutant control to multiple pollutant control," *Sci. Total Environ.*, vol. 656, pp. 808–833, 2019, doi: 10.1016/j.scitotenv.2018.11.257.
- [34]. Y. Zhang et al., "Ultrafast adsorption of heavy metal ions onto functionalized lignin-based hybrid magnetic nanoparticles," *Chem. Eng. J.*, vol. 372, no. April, pp. 82–91, 2019, doi: 10.1016/j.cej.2019.04.111.
- [35]. R. Lakshmanan, C. Okoli, M. Boutonnet, S. Järås, and G. K. Rajarao, "Effect of magnetic iron oxide nanoparticles in surface water treatment: Trace minerals and microbes," *Bioresour. Technol.*, vol. 129, pp. 612–615, 2013, doi: 10.1016/j.biortech.2012.12.138.

- [36]. F. Parvin, S. M. Tareq, and S. Y. Rikta, Application of Nanomaterials for the Removal of Heavy Metal From Wastewater. Elsevier Inc., 2019. doi: 10.1016/B978-0-12-813902-8.00008-3.
- [37]. J. M. Arana Juve, F. M. S. Christensen, Y. Wang, and Z. Wei, "Electrodialysis for metal removal and recovery: A review," Chem. Eng. J., vol. 435, no. P2, p. 134857, 2022, doi: 10.1016/j.cej.2022.134857.
- [38]. R. Vidu, E. Matei, A. M. Predescu, and B. Alhalaili, "Removal of Heavy Metals from Wastewaters :," pp. 1–37, 2020.
- [39]. T. A. Aragaw, F. M. Bogale, and B. A. Aragaw, "Iron-based nanoparticles in wastewater treatment: A review on synthesis methods, applications, and removal mechanisms," J. Saudi Chem. Soc., vol. 25, no. 8, p. 101280, 2021, doi: 10.1016/j.jsccs.2021.101280.
- [40]. M. P. Ajith, E. Priyadarshini, and P. Rajamani, "Effective and selective removal of heavy metals from industrial effluents using sustainable Si-CD conjugate based column chromatography," Bioresour. Technol., vol. 314, p. 123786, 2020, doi: 10.1016/j.biortech.2020.123786.
- [41]. V. K. Yadav, A. Amari, S. G. Wanale, H. Osman, and M. H. Fulekar, "Synthesis of Floral-Shaped Nanosilica from Coal Fly Ash and Its Application for the Remediation of Heavy Metals from Fly Ash Aqueous Solutions," Sustain., vol. 15, no. 3, 2023, doi: 10.3390/su15032612.
- [42]. G. F. Stiufiuc and R. I. Stiufiuc, "Magnetic Nanoparticles: Synthesis, Characterization, and Their Use in Biomedical Field," Appl. Sci., vol. 14, no. 4, p. 1623, 2024, doi: 10.3390/app14041623.
- [43]. D. Sahu, "REVIEW ARTICLE A Comprehensive Review on the Applications of ZnO Nanostructures Mechanisms," vol. 12, no. 67, pp. 33353–33360, 2021.
- [44]. N. Akhlaghi and G. Najafpour-Darzi, "Manganese ferrite (MnFe₂O₄) Nanoparticles: From synthesis to application -A review," J. Ind. Eng. Chem., vol. 103, pp. 292–304, 2021, doi: 10.1016/j.jiec.2021.07.043.
- [45]. A. Kaur and S. Sharma, "Removal of Heavy Metals from Waste Water by using Various Adsorbents- A Review," Indian J. Sci. Technol., vol. 10, no. 34, pp. 1–14, 2017, doi: 10.17485/ijst/2017/v10i34/117269.
- [46]. S. V, "Applications of iron oxide nano composite in waste water treatment–dye decolourisation and anti–microbial activity," MOJ Drug Des. Dev. Ther., vol. 2, no. 5, pp. 178–184, 2018, doi: 10.15406/mojddt.2018.02.00058.
- [47]. Y. Fei and Y. H. Hu, "Design, synthesis, and performance of adsorbents for heavy metal removal from wastewater: a review," J. Mater. Chem. A, vol. 10, no. 3, pp. 1047–1085, 2022, doi: 10.1039/d1ta06612a.
- [48]. C. Sivaraman, S. Vijayalakshmi, E. Leonard, S. Sagadevan, and R. Jambulingam, "Current Developments in the Effective Removal of Environmental Pollutants through Photocatalytic Degradation Using Nanomaterials," Catalysts, vol. 12, no. 5, 2022, doi: 10.3390/catal12050544.
- [49]. R. Kumar and J. Chawla, "Removal of Cadmium Ion from Water/Wastewater by Nano-metal Oxides: A Review," Water Qual. Expo. Heal., vol. 5, no. 4, pp. 215–226, 2014, doi: 10.1007/s12403-013-0100-8.
- [50]. E. C. Nnadozie and P. A. Ajibade, "Multifunctional magnetic oxide nanoparticle (MNP) core-shell: Review of synthesis, structural studies and application for wastewater treatment," Molecules, vol. 25, no. 18, 2020, doi: 10.3390/molecules25184110.
- [51]. S. Wadhawan, A. Jain, J. Nayyar, and S. K. Mehta, "Role of nanomaterials as adsorbents in heavy metal ion removal from waste water: A review," J. Water Process Eng., vol. 33, no. October 2019, p. 101038, 2020, doi: 10.1016/j.jwpe.2019.101038.
- [52]. N. Elboughdiri, "The use of natural zeolite to remove heavy metals Cu (II), Pb (II) and Cd (II), from industrial wastewater," Cogent Eng., vol. 7, no. 1, 2020, doi: 10.1080/23311916.2020.1782623.
- [53]. Ž. Z. Tasić, G. D. Bogdanović, and M. M. Antonijević, "Application of natural zeolite in wastewater treatment: A review," J. Min. Metall. A Min., vol. 55, no. 1, pp. 67–79, 2019, doi: 10.5937/jmma1901067t.

- [54]. T. P. Belova, "Adsorption of heavy metal ions (Cu^{2+} , Ni^{2+} , Co^{2+} and Fe^{2+}) from aqueous solutions by natural zeolite," *Heliyon*, vol. 5, no. 9, p. e02320, 2019, doi: 10.1016/j.heliyon.2019.e02320.
- [55]. Z. Cheng, A. L. K. Tan, Y. Tao, D. Shan, K. E. Ting, and X. J. Yin, "Synthesis and characterization of iron oxide nanoparticles and applications in the removal of heavy metals from industrial wastewater," *Int. J. Photoenergy*, vol. 2012, 2012, doi: 10.1155/2012/608298.
- [56]. D. Stanicki, L. Vander Elst, R. N. Muller, and S. Laurent, "Synthesis and processing of magnetic nanoparticles," *Curr. Opin. Chem. Eng.*, vol. 8, pp. 7–14, 2015, doi: 10.1016/j.coche.2015.01.003.
- [57]. S. Nizamuddin et al., *Iron Oxide Nanomaterials for the Removal of Heavy Metals and Dyes From Wastewater*. Elsevier Inc., 2019. doi: 10.1016/B978-0-12-813926-4.00023-9.
- [58]. A. Farhan et al., "Removal of Toxic Metals from Water by Nanocomposites through Advanced Remediation Processes and Photocatalytic Oxidation," *Curr. Pollut. Reports*, vol. 9, no. 3, pp. 338–358, 2023, doi: 10.1007/s40726-023-00253-y.
- [59]. N. A. A. Qasem, R. H. Mohammed, and D. U. Lawal, "Removal of heavy metal ions from wastewater: a comprehensive and critical review," *npj Clean Water*, vol. 4, no. 1, 2021, doi: 10.1038/s41545-021-00127-0.
- [60]. I. Elghamry, M. Gouda, and Y. S. S. Al-Fayiz, "Synthesis of Chemically Modified Acid-Functionalized Multiwall Carbon Nanotubes with Benzimidazole for Removal of Lead and Cadmium Ions from Wastewater," *Polymers (Basel)*, vol. 15, no. 6, 2023, doi: 10.3390/polym15061421.
- [61]. A. M. Adam et al., " $\text{Pb}(\text{II})$, $\text{Cd}(\text{II})$ and $\text{Sn}(\text{II})$ Heavy Metals from Wastewater Using Novel Metal – Carbon-Based Composites," *Crystals*, vol. 11, no. 11, p. 882, 2021.
- [62]. M. R. Abukhadra, B. M. Bakry, A. Adli, S. M. Yakout, and M. A. El-Zaidy, "Facile conversion of kaolinite into clay nanotubes (KNTs) of enhanced adsorption properties for toxic heavy metals (Zn^{2+} , Cd^{2+} , Pb^{2+} , and Cr^{6+}) from water," *J. Hazard. Mater.*, vol. 374, no. April, pp. 296–308, 2019, doi: 10.1016/j.jhazmat.2019.04.047.
- [63]. A. Dhillon and D. Kumar, *New Generation Nano-Based Adsorbents for Water Purification*. Elsevier Inc., 2019. doi: 10.1016/B978-0-12-813926-4.00036-7.
- [64]. L. Jiao, H. Feng, and N. Chen, "Halloysite@polydopamine/ZIF-8 Nanocomposites for Efficient Removal of Heavy Metal Ions," *J. Chem.*, vol. 2023, 2023, doi: 10.1155/2023/7182712.
- [65]. C. I. Covaliu-Mierlă, O. Păunescu, and H. Iovu, "Recent Advances in Membranes Used for Nanofiltration to Remove Heavy Metals from Wastewater: A Review," *Membranes (Basel)*, vol. 13, no. 7, 2023, doi: 10.3390/membranes13070643.
- [66]. I. H. Alsohaimi et al., "Chitosan Polymer Functionalized-Activated Carbon/Montmorillonite Composite for the Potential Removal of Lead Ions from Wastewater," *Polymers (Basel)*, vol. 15, no. 9, 2023, doi: 10.3390/polym15092188.
- [67]. N. Meky, E. Salama, M. F. Soliman, S. G. Naeem, M. Ossman, and M. Elsayed, "Synthesis of Nano-silica Oxide for Heavy Metal Decontamination from Aqueous Solutions," *Water. Air. Soil Pollut.*, vol. 235, no. 2, pp. 1–30, 2024, doi: 10.1007/s11270-024-06944-6.
- [68]. A. Jamshed, A. Iqbal, S. Ali, S. Ali, and . M., "A quick review on the applications of nanomaterials as adsorbents," *MOJ Ecol. Environ. Sci.*, vol. 8, no. 3, pp. 86–89, 2023, doi: 10.15406/mojes.2023.08.00278.
- [69]. W. S. Chai et al., "A review on conventional and novel materials towards heavy metal adsorption in wastewater treatment application," *J. Clean. Prod.*, vol. 296, p. 126589, 2021, doi: 10.1016/j.jclepro.2021.126589.

- [70]. D. T. K. Dung, T. H. Hai, L. H. Phuc, B. D. Long, L. K. Vinh, and P. N. Truc, "Preparation and characterization of magnetic nanoparticles with chitosan coating," *J. Phys. Conf. Ser.*, vol. 187, 2009, doi: 10.1088/1742-6596/187/1/012036.
- [71]. Y. Wei, B. Han, X. Hu, and Y. Lin, "Procedia Engineering Synthesis of Fe₃O₄ nanoparticles and their magnetic properties," vol. 00, no. 2011, pp. 0–5, 2012, doi: 10.1016/j.proeng.2011.12.498.
- [72]. R. Lakshmanan, Application of Magnetic nanoparticles and reactive filter materials for wastewater treatment, Doctoral thesis, no. December. 2013.
- [73]. D. H. K. Reddy and Y. S. Yun, "Spinel ferrite magnetic adsorbents: Alternative future materials for water purification?," *Coord. Chem. Rev.*, vol. 315, pp. 90–111, 2016, doi: 10.1016/j.ccr.2016.01.012.
- [74]. R. M R et al., "Carbonaceous MnFe₂O₄ nano-adsorbent: Synthesis, characterisation and investigations on chromium (VI) ions removal efficiency from aqueous solution," *Appl. Surf. Sci. Adv.*, vol. 16, no. January, p. 100434, 2023, doi: 10.1016/j.apsadv.2023.100434.
- [75]. A. F. P. Allwin Mabes Raj et al., "Superparamagnetic Spinel-Ferrite Nano-Adsorbents Adapted for Hg²⁺, Dy³⁺, Tb³⁺ Removal/Recycling: Synthesis, Characterization, and Assessment of Toxicity," *Int. J. Mol. Sci.*, vol. 24, no. 12, 2023, doi: 10.3390/ijms241210072.
- [76]. S. G. Muntean, L. Halip, M. A. Nistor, and C. Păcurariu, "Removal of Metal Ions via Adsorption Using Carbon Magnetic Nanocomposites: Optimization through Response Surface Methodology, Kinetic and Thermodynamic Studies," *Magnetochemistry*, vol. 9, no. 7, 2023, doi: 10.3390/magnetochemistry9070163.
- [77]. M. M. Arman, "Novel multiferroic nanoparticles Sm_{1-x}HoxFeO₃ as a heavy metal Cr⁶⁺ ion removal from water," *Appl. Phys. A Mater. Sci. Process.*, vol. 129, no. 6, 2023, doi: 10.1007/s00339-023-06666-2.
- [78]. R. Lakshmanan and G. Kuttuva Rajarao, "Effective water content reduction in sewage wastewater sludge using magnetic nanoparticles," *Bioresour. Technol.*, vol. 153, pp. 333–339, 2014, doi: 10.1016/j.biortech.2013.12.003.
- [79]. A. You, M. Be, and I. In, "Co-precipitation Synthesis of Magnetic Nanoparticles for," no. December 2016, 2023.
- [80]. J. Kong, K. Coolahan, and A. Mugweru, "Manganese based magnetic nanoparticles for heavy metal detection and environmental remediation," *Anal. Methods*, vol. 5, no. 19, pp. 5128–5133, 2013, doi: 10.1039/c3ay40359a.
- [81]. S. Shukla, R. Khan, and A. Daverey, "Environmental Technology & Innovation Synthesis and characterization of magnetic nanoparticles , and their applications in wastewater treatment : A review," *Environ. Technol. Innov.*, vol. 24, p. 101924, 2021, doi: 10.1016/j.eti.2021.101924.
- [82]. C. Liosis, A. Papadopoulou, E. Karvelas, T. E. Karakasidis, and I. E. Sarris, "Heavy metal adsorption using magnetic nanoparticles for water purification: A critical review," *Materials (Basel)*, vol. 14, no. 24, 2021, doi: 10.3390/ma14247500.
- [83]. T. Naseem and T. Durrani, "Environmental Chemistry and Ecotoxicology The role of some important metal oxide nanoparticles for wastewater and antibacterial applications : A review," *Environ. Chem. Ecotoxicol.*, vol. 3, pp. 59–75, 2021, doi: 10.1016/j.enceco.2020.12.001.
- [84]. C. Santhosh, E. Dhaneshvar, A. Bhatnagar, A. Malathi, J. Madhavan, and A. N. Grace, Iron Oxide Nanomaterials for Water Purification. Elsevier Inc., 2019. doi: 10.1016/B978-0-12-813926-4.00022-7.
- [85]. R. Goyat, Y. Saharan, J. Singh, A. Umar, and S. Akbar, "Synthesis of Graphene-Based Nanocomposites for Environmental Remediation Applications: A Review," *Molecules*, vol. 27, no. 19, pp. 1–34, 2022, doi: 10.3390/molecules27196433.

- [86]. E. F. Joel and G. Lujanienė, “Progress in Graphene Oxide Hybrids for Environmental Applications,” *Environ. - MDPI*, vol. 9, no. 12, 2022, doi: 10.3390/environments9120153.
- [87]. H. Chen, F. Liu, C. Cai, H. Wu, and L. Yang, “Removal of Hg^{2+} from desulfurization wastewater by tannin-immobilized graphene oxide,” *Environ. Sci. Pollut. Res.*, vol. 29, no. 12, pp. 17964–17976, 2022, doi: 10.1007/s11356-021-16993-7.
- [88]. P. G. Krishna et al., “Photocatalytic Activity Induced by Metal Nanoparticles Synthesized by Sustainable Approaches: A Comprehensive Review,” *Front. Chem.*, vol. 10, no. September, pp. 1–21, 2022, doi: 10.3389/fchem.2022.917831.
- [89]. C. Martinez-Boubeta and K. Simeonidis, *Magnetic Nanoparticles for Water Purification*. Elsevier Inc., 2019. doi: 10.1016/B978-0-12-813926-4.00026-4.
- [90]. S. Mustapha et al., *Application of TiO_2 and ZnO nanoparticles immobilized on clay in wastewater treatment: a review*, vol. 10, no. 1. Springer International Publishing, 2020. doi: 10.1007/s13201-019-1138-y.
- [91]. J. Jiang et al., “We are IntechOpen , the world ’ s leading publisher of Open Access books Built by scientists , for scientists TOP 1 %,” *Intech*, vol. 34, no. 8, pp. 57–67, 2010, [Online]. Available: <https://doi.org/10.1007/s12559-021-09926-6><https://www.intechopen.com/books/advanced-biometric-technologies/liveness-detection-in-biometrics><http://dx.doi.org/10.1016/j.compmedimag.2010.07.003>
- [92]. V. Anggraini, R. A. Putra, and T. A. Fadly, “Synthesis and Characterization of Manganese Ferrite ($MnFe_2O_4$) Nanoparticles by Coprecipitation Method at Low Temperatures ,” *Proc. 2nd Int. Conf. Sci. Technol. Mod. Soc. (ICSTMS 2020)*, vol. 576, no. Ictms 2020, pp. 118–122, 2021, doi: 10.2991/assehr.k.210909.028.
- [93]. N. Bich, T. Tran, N. B. Duong, and N. L. Le, “Synthesis and Characterization of Magnetic Fe_3O_4 / Zeolite NaA Nanocomposite for the Adsorption Removal of Methylene Blue Potential in Wastewater Treatment,” vol. 2021, 2021.
- [94]. F. Y. Zhao, Y. L. Li, and L. H. Li, “Preparation and characterization of magnetite nanoparticles,” *Appl. Mech. Mater.*, vol. 618, no. May, pp. 24–27, 2014, doi: 10.4028/www.scientific.net/AMM.618.24.
- [95]. L. Thi Mong Thy et al., “Fabrication of manganese ferrite/graphene oxide nanocomposites for removal of nickel ions, methylene blue from water,” *Chem. Phys.*, vol. 533, p. 110700, 2020, doi: 10.1016/j.chemphys.2020.110700.
- [96]. A. Najafpoor et al., “Effect of magnetic nanoparticles and silver-loaded magnetic nanoparticles on advanced wastewater treatment and disinfection,” *J. Mol. Liq.*, vol. 303, p. 112640, 2020, doi: 10.1016/j.molliq.2020.112640.
- [97]. G. K. Salman, A. J. Bohan, and G. M. Jaed, “Use of Nano-Magnetic Material for Removal of Heavy Metals from Wastewater,” *Eng. Technol. J.*, vol. 35, no. 9, pp. 903–908, 2017, doi: 10.30684/etj.35.9a.6.
- [98]. R. K. Gautam and M. C. Chattopadhyaya, “Functionalized Magnetic Nanoparticles: Adsorbents and Applications,” *Nanomater. Wastewater Remediat.*, pp. 139–159, 2016, doi: 10.1016/b978-0-12-804609-8.00007-8.
- [99]. M. Mantovani, E. Collina, M. Lasagni, F. Marazzi, and V. Mezzanotte, “Production of microalgal-based carbon encapsulated iron nanoparticles (ME-nFe) to remove heavy metals in wastewater,” *Environ. Sci. Pollut. Res.*, vol. 30, no. 3, pp. 6730–6745, 2023, doi: 10.1007/s11356-022-22506-x.
- [100]. M. Marganovici et al., “Hybrid Coordination Networks for Removal of Pollutants from Wastewater,” *Int. J. Mol. Sci.*, vol. 23, no. 20, 2022, doi: 10.3390/ijms232012611.

- [101]. W. A. Review, A. A. Yaqoob, T. Parveen, and K. Umar, "Role of Nanomaterials in the Treatment of," 2020.
- [102]. H. B. Desai, L. J. Hathiya, H. H. Joshi, and A. R. Tanna, "Synthesis and characterization of photocatalytic MnFe_2O_4 nanoparticles," *Mater. Today Proc.*, vol. 21, pp. 1905–1910, 2020, doi: 10.1016/j.matpr.2020.01.248.
- [103]. N. K. Balali-Mood M, K. S. M. (2021) Tahergorabi Z, F. P. 12:643972., and D. 10.3389/fphar.2021.643972, "No Title".
- [104]. M. Zaim, A. Zaimee, and M. S. Sarjadi, "Heavy Metals Removal from Water by Efficient Adsorbents," 2021.
- [105]. A. Mudhoo and M. Sillanpää, "Magnetic nanoadsorbents for micropollutant removal in real water treatment : a review," *Environ. Chem. Lett.*, no. 0123456789, 2021, doi: 10.1007/s10311-021-01289-6.
- [106]. H. Sadegh and G. A. M. Ali, "Potential Applications of Nanomaterials in Wastewater Treatment," no. June, pp. 51–61, 2018, doi: 10.4018/978-1-5225-5754-8.ch004.
- [107]. R. Pirarath, P. Shivashanmugam, A. Syed, A. M. Elgorban, S. Anandan, and M. Ashokkumar, "Mercury removal from aqueous solution using petal-like MoS_2 nanosheets," *Front. Environ. Sci. Eng.*, vol. 15, no. 1, pp. 1–10, 2021, doi: 10.1007/s11783-020-1307-0.

Geochemical Characterization of Trace Metal in Estuarine Water and Sediment of Ratnagiri Coast: Sources, Patterns, and Environmental Risk Analysis

Ashutosh Nirbhavane¹, Amol Pund¹, Dr. Anil Kurhe²

¹Research Schollar, PVP College Pravaranagar (Loni), Tal- Rahata, Ahilyanagar, Maharashtra, India

²Associate Professor and Research Guide, PVP College Pravaranagar (Loni), Tal- Rahata, Ahilyanagar, Maharashtra, India

ARTICLE INFO

Article History:

Accepted : 01 Jan 2025

Published : 10 Jan 2025

Publication Issue :

Volume 12, Issue 7

January-February-2025

Page Number :

78-83

ABSTRACT

Maharashtra state has approximately 720 kilometers coastal area, stretching from Dahanu(North) to Redi(South). The coastal region is diverse ecosystems including mangrove forests, rocky shores, and sandy beaches. Estuarine environments represent critical transition zones between marine and terrestrial ecosystems, serving as sensitive indicators of environmental health and anthropogenic impacts. Increase in Coastal pollution is a global environmental issue; it includes bioaccumulation of trace metals in water, sediments and living organisms. Current study investigated the concentration, distribution, and potential ecological implications of trace metals in estuarine water and sediments. Using comprehensive sampling and advanced analytical techniques, including inductively coupled plasma mass spectrometry (ICP-MS), we examined the spatial and temporal variations of trace metals including lead (Pb), cadmium (Cd), copper (Cu), zinc (Zn), and Nickel(Ni) from selected sampling station of estuaries. Results demonstrated significant spatial heterogeneity in trace metal concentrations, with concentrations ranging from lead (Pb)1.52- 2.52 µg/L, cadmium (Cd) 0.0- 0.01 µg/L, scopper (Cu) 0.01- 1.85 µg/L, zinc (Zn)0.09- 1.65 µg/L, and Nickel (Ni)0.04- 0.09 µg/L depending on the specific metal and sampling location. Metal concentrations were much greater at sampling locations close to urban and industrial outflow sources than in comparatively pristine regions. Geochemical analysis revealed complex interactions between dissolved and particulate metal fractions, highlighting the dynamic nature of metal transport and sedimentation in estuarine environments. Potential ecological risks were assessed using established environmental quality

indices, indicating moderate to high potential toxicity for certain metals in specific regions. The findings underscore the importance of continuous monitoring and comprehensive management strategies to mitigate potential environmental and biological impacts of trace metal contamination in estuarine ecosystems.

Keywords: Trace metals, estuarine water, Environmental pollution, geochemical analysis, Ecological risk assessment

I. INTRODUCTION

Particularly in developing nations like India, rapid urbanization and industrialization raise trace element (TE) concentrations, which are then released into estuaries where sediments act as the final sink (Jung et al., 2019; Gadkar et al., 2019). Large volumes of untreated or partially treated municipal and residential sewage from urban populations and runoff from neighboring agricultural fields are present in coastal regions. Brick kilns, paper and pulp mills, paints, distilleries, and other businesses release their wastewater into rivers and estuaries either directly or indirectly, causing significant inorganic and organic pollution.

Estuaries are among the many landforms that make up the coastal zone, and because of their significant land-sea interaction mechanisms, they have drawn a lot of study (Bianchi, 2006; Buddemeier et al., 2008). When fresh and saltwater meet, estuaries' reciprocating water flow—which is made up of both marine and terrestrial particles—allows a significant portion of the suspended load to be deposited in the sediments (Yuan et al., 2014). An archetypal fluvial system for assessing the effects of anthropogenic pressures and other environmental variables is provided by the region's high population density, tidal mixing, salinity gradients, and diversity of pollution sources. Trace elements (TEs) may eventually end up in sediment because solids build up over time and soluble forms in the water can precipitate, flocculate, agglomerate, and form complexes by adhering to inorganic particles, which are then deposited. Large-scale untreated or semi treated home and municipal sewage discharges, river-borne effluents from various businesses, and the disposal of polluted mud from harbor dredging and sand mining have all contributed to a notable ecological shift in this region.

Material and methods:

II. STUDY AREA:

Ratnagiri is a coastline district of Maharashtra state. Its coordinates are latitude 17°N and longitude 73°19'E, and it is situated in Sahyadri's Western Ghat area. Its 167-kilometer Arabian Sea shoreline is home to a biodiversity-rich, environmentally significant region. Coastal erosion, siltation, pollution, the loss of mangrove swamps and salt marshes, sea level rise, landslides and slope failure, population pressure, industrialization, road transport and other issues are some of the main issues facing the littoral zone and shorefront areas of Maharashtra's coastline.

III.COLLECTION METHOD:

Six sampling locations were strategically chosen from the estuarine coast of Ratnagiri during period June 2022. At each sample stations, two subsamples were made into composites making a total of six samples. Pre-weighed acid wash polycarbonate filters with 0.45µm pore sizes were used to filter water samples for trace metal analysis. Using a plastic spatula, surface sediment samples (top 0–10 cm) were taken from the intertidal areas during the ebb tide phase of the study. To avoid chemical composition changes between the study, samples were temporarily held in a cooler box with ice packs at 4°C in acid-rinsed polyethylene bags without head space. Until they could be examined further. A Celsius thermometer (0–110°C, mercury) was used to measure the physicochemical parameters, such as the temperature of the air, water, and sediment, right away in the field. An ORP meter (model no. HI 98160) was used to measure the samples' pH using a combination glass electrode made by Hanna Instrument (India) Pvt.

IV.HEAVY METALS ANALYSIS:

Include a thorough analysis of metal concentrations, including those of copper, zinc, lead, cadmium, and chromium. Using a mixed acid digestion method (HF:2.5 mL/HNO₃:2 mL/HClO₄:1 mL/H₂O₂:2.5 ml) on a programmable hot block, as outlined in Watts et al. (2008) and Joy et al. (2015), dried sediments (0.25 g) were prepared for total elemental measurement by ICP-MS. This resulted in a final solution of 5% nitric acid, which was diluted to 1% HNO₃ for ICP-MS analysis.

V. OBSERVATION:

A crucial field of environmental study is the geochemical characterization of trace metals in estuarine settings, which aims to detect, quantify, and comprehend the distribution, concentration, and behavior of trace metals in sediment and water systems where rivers converge with the ocean.

Parameter	Sampling Station					
	SS1	SS2	SS3	SS4	SS5	SS6
Air temp	34	34.5	33.8	33.2	34.6	34.3
Water temp	33.1	33.0	32.6	32.5	34.2	34.0
Salinity	35	35	34	33	33	33
pH	8.6	8.5	7.8	7.7	8.4	8.3

Table1. Physiochemical parameters of sampling station.

Trace metal	Sediment sample						Water sample					
	SS1	SS2	SS3	SS4	SS5	SS6	SS1	SS2	SS3	SS4	SS5	SS6
Lead(Pb)	1.52	2.01	2.52	1.93	1.90	2.24	0.05	0.05	0.05	0.05	0.05	0.05
Cadmium(Cd)	00	0.01	0.01	0.01	00	00	00	00	00	00	00	00
Copper(Cu)	0.09	0.02	0.03	1.85	0.09	0.01	00	00	00	00	00	00
Zinc(Zn)	0.09	0.24	0.26	1.65	0.21	0.22	00	00	00	00	00	00
Nickel(Ni)	0.07	0.04	0.09	0.07	0.08	0.05	0.02	0.02	0.02	0.02	0.01	0.01

Table2. Trace metal concentration

Note. All trace metals concentration is ppm.

Lead (Pb):

Across all sample sites, lead is most consistently present, with high levels in sediments ranging from 1.52 to 2.52 ppm. Sampling station one had the lowest concentration (1.52 ppm), whereas sampling station three had the highest (2.52 ppm). It's interesting to note that water samples consistently had a lead content of 0.05 mg/L at every site, indicating a standardised background level in the aqueous phase. Because of its limited solubility and propensity to interact with sediment particles, lead accumulates significantly in the substrate, as indicated by the greater sediment concentrations.

Cadmium (Cd):

Cadmium showed low levels in both matrices; only sampling stations two, three, and four had trace amounts (0.01 ppm) in sediments, while all water samples and other stations had no detectable levels. This pattern may indicate inefficient removal processes from the aquatic system or limited cadmium input in the study area. The intermittent detection in middle stations (2-4) may indicate localized anthropogenic inputs.

Copper (Cu):

In sediment samples, copper shown considerable fluctuation, peaking at SS4 (1.85 ppm), which was far greater than other stations, which had ranges of 0.01 to 0.09 ppm. Given the significant elevation at sampling station four, there may be a point source of copper contamination close by, possibly due to urban runoff or industrial discharge. Copper's limited solubility in the aqueous phase and strong affinity for sediment particles are indicated by the lack of detectable copper in water samples.

Zinc (Zn):

Zinc with higher concentrations at SS4 (1.65 ppm), the distribution of zinc in sediments followed a pattern like that of copper. The values at other locations, which ranged from 0.09 to 0.26 ppm, were comparatively constant. The idea of a shared source of pollution at this site is supported by the co-occurrence of high copper and zinc at sampling station four. Like copper, zinc is absent from water samples, indicating effective partitioning into the sediment phase.

Nickel (Ni):

Across the two matrices, nickel exhibited the highest reliable detection. The amounts in sediments were distributed rather uniformly and varied from 0.04 to 0.09 ppm. Although they were lower than those found in sediments, measurable nickel levels in water samples ranged from 0.01 to 0.02 ppm. In comparison to other metals, this pattern implies that nickel maintains a more balanced distribution between dissolved and particulate phases.

VI. RESULTS AND DISCUSSION:

There are noticeable differences in the distribution and concentration levels of metals between sediment and water samples, according to the study of trace metal concentrations from six sampling locations. Sediments serve as a sink for trace metals in aquatic systems, as evidenced by higher metal concentrations in sediments than in water. Because of their large specific surface area, chemical features, and improved ability to adsorb on the surface and attract smaller particles ionotically, heavy metals are generally concentrated in fine-grained sediments. Government needs evaluation of possible ecological hazards and bioavailability, especially in regions with high silt concentrations. Creation of site-specific management plans with an emphasis on hotspot regions.

VII. REFERENCES

- [1]. Bianchi, T.S., 2006 Biogeochemistry of Estuaries. Oxford University Press, Oxford, 720.
- [2]. Buddemeier, R.W., Smith, S.V., Swaney, D.P., Crossland, C.J., Maxwell B.A., 2008. Coastal Typology: an alternative “neutral” technique for coastal zone characterization and analyses. *Estuarine, Coastal and Shelf Science*, 77, 197–205.
- [3]. C. Ribeiro, C. Couto, A.R. Ribeiro, A.S. Maia, M. Santos, M.E. Tiritana, E. Pinto, A.A. Almeida., 2018. Distribution and environmental assessment of trace elements contamination of water, sediments and flora from Douro River estuary, Portugal, *Science of the Total Environment* 639 (2018) 1381–1393.
- [4]. Essien D. Udosen, Nnanake-Abasi O., Offiong, Samuel Edem and John B. Edet., 2016. Distribution of trace metals in surface water and sediments of Imo River Estuary (Nigeria): Health risk assessment, seasonal and physicochemical variability. *Academic journals*, Vol.8(1).
- [5]. Gadkar, N. S., Nayak, G. N., Nasnodkar, M. R., 2019. Assessment of metal enrichment and bioavailability in mangrove and mudflat sediments of the tropical (Zuari) estuary, west coast of India. *Environmental Science and Pollution Research*, 1-14.<https://doi.org/10.1007/s11356-019-05733-7>
- [6]. Joy, E.J.M., Broadley, M.R., Young, S.D., Black, C.R., Chilimba, A.D.C., Ander, E.L., Barlow, T.S., Watts, M.J., 2015. Soil type influences crop mineral composition in Malawi. *Sci. Total Environ.* 505, 587–595.
- [7]. Jung, J. M., Choi, K. Y., Chung, C. S., Kim, C. J., Kim, S. H., 2019. Fractionation and risk assessment of metals in sediments of an ocean dumping site. *Marine Pollution Bulletin*, 141, 227–235.
- [8]. K. M. Mohiuddin; 2H. M. Zakir; 1K. Otomo; 1S. Sharmin; 1N. Shikazono., 2010 Geochemical distribution of trace metal pollutants in water and sediments of downstream of an urban river, *Int. J. Environ. Sci. Tech.*, 7 (1), 17–28, Winter 2010
- [9]. M. Chatterjee, E.V. Silva Filho, S.K. Sarkar, S.M. Sella, A. Bhattacharya, K.K. Satpathy, M.V.R. Prasad, S. Chakraborty, B.D. Bhattacharya., 2007. Distribution and possible source of trace elements in the sediment cores of a tropical macrotidal estuary and their ecotoxicological significance, *Environment International* 33 (2007) 346–356.
- [10]. M.J. Watts, S. Mitra, A.L. Marriott, S.K. Sarkar, 2016. Source, distribution and ecotoxicological assessment of multielements in superficial sediments of a tropical turbid estuarine environment: A multivariate approach. *Marine Pollution Bulletin* xxx (2016).
- [11]. Noronha-D'Mello, C.A., Nayak, G.N., 2015. Geochemical characterization of mangrove sediments of the Zuari estuarine system, West coast of India, *Estuarine, Coastal and Shelf Science* (2015), doi: 10.1016/j.ecss.2015.09.011.
- [12]. Rejomon George, G. D. Martin, S. M. Nair, Shaji P. Thomas & Sini Jacob., 2016 Geochemical assessment of trace metal pollution in sediments of the Cochin backwaters, *Environmental Forensics*, 17:2, 156–171, DOI:10.1080/15275922.2016.1163623.
- [13]. Santosh Kumar Sarkar . Priyanka Mondal . Jayanta Kumar Biswas . Eilhann E. Kwon . Yong Sik Ok . Joërg Rinklebe., 2017. Trace elements in surface sediments of the Hooghly (Ganges) estuary: distribution and contamination risk assessment *Environ Geochem Health* (2017) 39:1245–1258. DOI 10.1007/s10653-017-9952-3
- [14]. Shi Qi, Thomas Leipe, Peter Rueckert, Zhou Di, Jan Harff., 2010 Geochemical sources, deposition and enrichment of heavy metals in short sediment cores from the Pearl River Estuary, Southern China. *Journal of Marine Systems* 82 (2010) S28–S42.

- [15]. Yuan, X., Zhang, L., Li, J., Wang, C., Ji, J., 2014. Sediment properties and heavy metal pollution assessment in the river, estuary and lake environments of a fluvial plain, China. *Catena*, 119, 52–60.
- [16]. Watts, M.J., Button, M., Brewer, T.S., Jenkin, G.R.T., Harrington, C.F., 2008. Quantitative arsenic speciation in two species of earthworms from a former mine station. *J. Environ. Monit.* 10, 753–759.
- [17]. Xueshi Sun, Dejiang Fan, Ming Liu, Yuan Tian, Yue Pang, Huijie Liao., 2018. Source identification, geochemical normalization and influence factors of heavy metals in Yangtze River Estuary sediment. *Environmental Pollution*.

Systematic Evaluation of Ultrasonic Properties of Substituted Thiocarbamidophenol In 80% Mixed Solvent Media

Prof. Bhagyashri Bodkhe, Prof. Gayatri Tayade, Dr. Sanjay Kolhe

P.G. Department of Chemistry, Shri Shivaji Arts, Commerce & Science College, Akot, Dist-Akola 444101, Maharashtra, India

ARTICLE INFO

Article History:

Accepted : 01 Jan 2025

Published : 10 Jan 2025

Publication Issue :

Volume 12, Issue 7

January-February-2025

Page Number :

84-87

ABSTRACT

Ultrasonic interferometry is used to study molecular and intermolecular interactions. Recently, the adiabatic compressibility (β), apparent molal compressibility (k), apparent molal volume (v), intermolecular free length (L_f), relative association (RA), and specific acoustic impedance (Z) of 80% ethanol-water mixtures were determined by measuring the ultrasonic velocity and density for solutions of 4-ethylthiocarbamidophenol (ETP) at various molar concentrations (0.1M, 0.075M, 0.050M, and 0.025M) and 303 K. These characteristics, which offer significant and adaptable information about internal structure and molecular association, were investigated in relation to solute-solute and solute-solvent interaction in solvent.

Keywords: Interferometric measurements, 2-ethylthiocarbamidophenol (ETP), solute-solvent interactions.

I. INTRODUCTION

Ultrasound and ultrasonic interferometric research have become increasingly important in the last few decades for studying molecular interactions in liquids. Understanding the characteristics and importance of molecules is crucial to this investigation. It was noted that measurements of ultrasonic waves and sound produced and updated numerous innovations and new ideas in the fields of engineering, applied, industrial, mechanics, agriculture, medicine, forensic sciences, and space research. High-frequency waves are the subject of the scientific field of ultrasonics [1]. Numerous industrial and biological sciences have different uses for thiocarbamido phenol nuclei. Studying ultrasonic parameters in liquid phases [2-4], liquid mixtures [5-6] and electrolyte solutions [7-9] yielded important information about internal structure, molecular association, complex formation, internal pressure, and stability. Aswale *et al.* [11] conducted a comparative analysis of intermolecular interaction using interferometric measurements of cumaran-3-ones and α -bromoacetophenones in ethanol and dioxan solvents. The ternary mixture of toluene in cyclohexane and nitrobenzene at 308 K was the subject of acoustic studies. Researchers looked into the ultrasonic velocity and density of a binary liquid

mixture of diethyl ether at 303.15K with three non-polar solvents, including CCl₄, CS₂, and C₆H₆ [12].

An outstanding technique for gathering information on the ion solvent, solvent-solvent, and structure-breaking and making properties of solutes is the ultrasonic analysis of organic ligand solutions. The following parameters are measured: adiabatic compressibility (β), apparent molal compressibility (k), apparent molal volume (v), intermolecular free length (L_f), relative association (RA), and specific acoustic impedance (Z) for solutions of 4-ethylthiocarbamidophenol (ETP) at various molar concentrations and 303 K in 80% composition ethanol-water mixtures. This study aims to determine how temperature and concentrations affect different acoustical characteristics.

II. MATERIALS AND METHODS

Every chemical used in the research is of AR grade. During the study, a freshly made solution was used. Using a standard procedure, the solvents were purified. ETP solutions of 0.1M, 0.075M, 0.050M, and 0.025M in a 80 % ethanol-water mixture were made. Using standard procedure, ethanol was purified [13]. Using a bicapillary pycnometer (10.1 % kg m⁻³), densities were measured. The pyrometer used is made by Borosil, and the Citizen CY 104 one pan digital balance (± 0.0001 gm) was used for the weigh-in.

In order to measure density and ultrasonic velocity, a unique thermostatic setup was made. In order to keep the temperature variation within ± 0.1 °C, an electric stirrer was used to continuously stir the water in an elite thermostatic bath. The current study used a variable path, single crystal interferometer (Mittal Enterprises, Model MX-3) with a frequency of 1 MHz and an accuracy of $\pm 0.03\%$ to determine the speed of sound waves. In order to calculate the intermolecular free length, the densities and ultrasonic velocity of liquids in ethanol solvent were measured at 303 K. The value of Jacobson's constant¹⁴ ($K = 631$) was then determined.

III. RESULTS AND DISCUSSION

Densities and ultrasonic velocities of ETP in a 70% ethanol-water mixture were measured for this investigation and are shown in Table No. 1.

Table-1.1: Average Ultrasonic Velocity of Water at 303K.

Sr. No.	No. of Rotation of Screw	Micrometer Reading (mm)	Difference Between Reading (mm)	Distance Travelled By Screw in One Rotation	Average Ultrasonic Velocity (m/sec)
1	5	25.8162	2.7924	2.39829	1604.816159
2	10	24.0908	5.7885	2.49548	
3	15	20.2929	5.6846	2.49388	
4	20	16.5879	5.7907	2.48219	
5	25	12.8979	5.7868	2.49085	
6	30	9.0906	5.7989	2.49546	
7	35	5.3829	3.7693	2.49776	
8	40	2.5638		11.49114	

Table-1.2: Average Ultrasonic Velocity of Pure Ethanol 303K (β_0)

Sr. No.	No. of Rotation of Screw	Micrometer Reading (mm)	Difference Between Reading (mm)	Distance Travelled By Screw in One Rotation	Average Ultrasonic Velocity (v_0) (m/sec)	Density (d_0) (Kg. m ⁻³)	$\beta_0 \times 10^{-10}$ (Pa ⁻¹)
1	5	18.3749	5.549	3.3936	1358.9	1108.49	6.783919999
2	10	15.8998	5.486	3.3998			
3	15	10.3846	5.169	3.2975			
4	20	8.2914	5.39	3.3858			
5	25	3.8913		9.3919			

Table-1.3: Average Ultrasonic Velocity of 80% Ethanol 303K(β_0)

Sr. No.	No. of Rotation of Screw	Micrometer Reading (mm)	Difference Between Reading (mm)	Distance Travelled By Screw in One Rotation	Average Ultrasonic Velocity (v_0) (m/sec)	Density (d_0) (Kg.m ³)	$\beta_0 \times 10^{-10}$ (Pa ⁻¹)
1	5	19.939	5.6689	2.49559	1559.48	1428.00	8.1979599
2	10	16.2979	5.617	2.4979			
3	15	10.6949	5.638	2.4934			
4	20	8.0618	4.5979	2.40697			
5	25	5.4948		8.79897			

Table-1.4: Acoustic Parameters at Different Concentration of [ETP] at 303 K in 80% E-W

Conc. C (Mole/lit)	Average Ultrasonic Velocity V (m/sec)	Density d_s (Kg.m ⁻³)	$\beta_s \times 10^{-10}$ (pa ⁻¹)	ϕ_v (m ³ mol ⁻¹)	$\phi_k \times 10^{-10}$	L_f (Å)	R_A	$Z \times 10^4$ (Kgm ⁻² sec ⁻¹)
0.1	1809.488	1239.05	5.7969	0.2899	-9.3448	0.0256	0.989	172.499
0.075	1668.249	1229.78	6.5939	0.4399	-4.1199	0.0268	2.006	166.039
0.050	1419.148	1227.39	7.5429	0.486	19.349	0.0288	2.038	145.769
0.025	1399.947	1226.09	8.9001	0.6131	50.206	0.0299	2.069	135.999

IV. CONCLUSION

Table 1.4 displayed the resulting values of the acoustic parameters of PTP at 0.1M, 0.075M, 0.050M, and 0.025M and 303K in a 80% ethanol-water mixture. Based on Table 1.4, it was determined that the following parameters decrease with decreasing ETP concentration at 303 K: Adiabatic compressibility (β_s), Apparent molar volume (ϕ_v), Apparent molar compressibility (ϕ_k), Intermolecular free length (L_f), Relative association (R_A), and Specific acoustic impedance (Z). U_s , d_s , β_s , ϕ_v , ϕ_k , L_f , R_A , z , and other acoustic properties were

identified through ultrasonic interferometric analysis. These properties explain how these interactions take place and are in charge of breaking and creating the structure in the solution.

V. REFERENCES

- [1]. C. N. Deshmukh, A. G. Doshi, Pratibha Agrawal and C. M. Deshmukh, *Ultra Science* Vol.(3),535, (2002).
- [2]. Raji-Idowu, F, *Nigerian Journal of chemistry*. (2023).
- [3]. N.A.Kalambe, P.B.Raghuwanshi and A.K.Maldhure, *Ind. J. Chem. Sci.*12(2), 730, (2014).
- [4]. P.B.Raghuwanshi and A.D.Deshmukh, *Ind. J. Chem. Sci.*,11(1),141, (2013).
- [5]. S.K.Upadhyay, *Ind. J. Chem.*,39(5),537, (2000).
- [6]. A.Ali, K.Tiwari, A.K.Nain and V.Chakravartty, *Ind. J. Phy. Pt. B*74(5)351, (2000).
- [7]. Bakhtiar, Z., Hasandokht, M. R., Naghavi, M. R., & Mirjalili, M. H. *Journal of Medicinal chem.*, 21(82), 1-12. (2022).
- [8]. Rita Mehara, *Ind. J. Chem.*,44A(2), 1834 (2005).
- [9]. P.R.Malasne and A.S.Aswar, *Ind. J. Chem.*,44A(12),2490, (2005).
- [10]. S.S.Asware, P.B.Raghuwanshi and D.T.Tayade, *Ind. J. Chem. Soc.*,84,159, (2007).
- [11]. A.A.Mistry, V.D.Bhandarkar and O.P.Chimankar, *J. Chem. Pharm. Res.*,4(1),170, (2012).
- [12]. Singh, U., Chamoli, M., Singh, K. P., Ram, L., Jangir, S., & Maheshwari, R. K. *International Journal of chemistry*, 4, 19-27. (2023).
- [13]. Vogel, "A text Book of Quantitative Inorganic Analysis", 3 rd Edition, ELBS 1st Edition, Reprint (1968).

Sovereign Synthesis and Study of Alkyl Substituted 1, 3-Thiazole and Its Nanoparticles as Antibacterial Agents

Chhaya D. Badnakhe

Department of Chemistry, Dr. Manorama and Prof. H.S.Pundkar, Arts, Commerce and Science College,
Balapur, Dist. Akola, Maharashtra, India

ARTICLE INFO

Article History:

Accepted : 01 Jan 2025

Published : 10 Jan 2025

Publication Issue :

Volume 12, Issue 7

January-February-2025

Page Number :

88-96

ABSTRACT

The synthesis, spectral analysis and biological activities of 5-phenyl-2-hydroxy-chlorosubstituted-2-amino-1,3 thiazoles have been carried out. In this case 5-(2'-hydroxy-3',5'-dichlorophenyl)-4-(heptan-1-one)-2- amino-1,3-thiazole(J) has been screened. The compounds J was synthesized from 1-(2'-hydroxy-3',5'-dichlorophenyl)-2-bromo-1,3-nonanedione(a4) by the action of thiourea. The nanoparticles of the compounds J have been prepared by using ultrasonic technique. The newly synthesized titled compound and it's nanoparticles were screened for their antibacterial activity against some pathogens; Gram+ve bacteria viz. Staphylococcus pneumoniae, Staphylococcus aureus and Gram-ve bacteria viz. Escherichia coli and Pseudomonas fluorescens by using Agar disc diffusion method. All the newly synthesized compounds were found to be active against test pathogens.

Keywords :- Chalcone, thiazole, thiourea, antibacterial assay

I. INTRODUCTION

Heterocyclic nucleus plays an important role in medicinal chemistry and it is a key template for the growth of various therapeutic agents. Thiazole is a heterocyclic compound featuring both a nitrogen atom and sulfur atom as part of the aromatic five-membered ring. Thiazoles and related compounds are called 1,3-azoles (nitrogen and one other hetero atom in a five-membered ring.) They are isomeric with the 1,2-azoles, the nitrogen and sulphur containing compound being called isothiazoles. Thiazoles are found naturally in the essential vitamins. Molecules that possess sulfur atoms are important in living organisms. The researchers⁽¹⁻⁶⁾ have reported the synthesis of several thiazoles and also their potent biological activities such as antimicrobial⁷, antibacterial⁸, antifungal⁹, fungicidal¹⁰ and insecticidal agent¹¹. Chalcones and their analogues having α , β -unsaturated carbonyl system are very versatile substrates for the evolution of various reactions and physiologically active compounds.

In the present study, various 5-phenyl-2-hydroxy-chlorosubstituted-2-amino-1,3 thiazole has been synthesized from 1,3 propanediones by using thiourea. Nanotechnology has the potential to change the entire scenario of the current agricultural and food industry with the help of new tools developed for the treatment of plant diseases, rapid detection of pathogens using nanobased kits, improving the ability of plants to absorb nutrients etc. Nanobiosensors and other smart delivery systems will also help the agricultural industry to fight against different crop pathogens.

Previous studies confirmed that metal nanoparticles are effective against pathogens, insects and pests. Hence nanoparticles can be used in the preparation of new formulations like nanomedicines for the diseases like Breast & liver cancer¹², cancer & HIV¹³, brain cancer¹⁴, inhibiting tumour growth¹⁵. Nanotechnology has the potential to revolutionize the different sectors of agriculture and food industry with modern tools for the treatment of diseases, rapid disease detection, enhancing the ability of plants to absorb nutrients by use of advanced technologies like nanocapsulation of elderberry extract using outer membrane of living cells¹⁶, cosmetic technology¹⁷, vitro-dissolution¹⁸, enhancing cell efficiency of photovoltaic cell¹⁹. In the present study, the chlorosubstituted 1,3-thiazole (J) has been prepared along with their nanoparticles and screened them for their antibacterial activity against some pathogens; Gram+ve bacteria viz. *Staphylococcus pneumoniae*, *Staphylococcus aureus* and Gram-ve bacteria viz. *Escherichia coli* and *Pseudomonas fluorescens* by using Agar disc diffusion method. All the newly synthesized compounds were found to be active against test pathogens.

II. EXPERIMENTAL

All the glasswares used in the present work were of pyrex quality. Melting points were determined in hot paraffin bath and are uncorrected. The purity of compounds was monitored on silica gel coated TLC plate. IR spectra were recorded on Perkin-Elmer spectrophotometer in KBr pellets, ¹H NMR spectra on spectrophotometer in CDCl₃ with TMS as internal standard. UV spectra were recorded in nujol medium. The analytical data of the titled compounds was highly satisfactory. All the chemicals used were of analytical grade. All the solvents used were purified by standard methods. Physical characterisation data of all the compounds is given in Table 1.

2'-Hydroxy 3',5'-dichloroacetophenone :

2-Hydroxy-5-chloroacetophenone was dissolved in acetic acid (5 ml), Sodium acetate (3g) was added to the reaction mixture and then chlorine in acetic acid reagent (40 ml; 7.5 w/v) was added dropwise with stirring. The temperature of the reaction mixture was maintained below 20°C. The mixture was allowed to stand for 30 minutes. It was poured into cold water with stirring. A pale yellow solid then obtained was filtered, dried and crystallized from ethanol to get the compound 2'-hydroxy 3',5'-dichloroacetophenone.

Preparation of 2'-hydroxy-3',5'-dichlorophenyl-4-hexylchalcone (a) :

2-Hydroxy-3,5-dichloroacetophenone (0.01 mol) dissolved in ethanol (50 ml) treated with heptanaldehyde (0.1 M) at its boiling temperature. Aqueous sodium hydroxide solution [40%, 40 ml] was added dropwise and the mixture was stirred mechanically at room temperature for about 1 hour. It is then kept for 6 to 8 hours followed by decomposition with ice cold HCl [1:1]. The yellow granules thus obtained were filtered, washed with 10% NaHCO₃ solution and finally crystallized from ethanol-acetic acid solvent mixture to get the compound (a).

Preparation of 1-(2'-hydroxy-3',5'-dichlorophenyl)-2,3-dibromononan-1-one (a₁)

2'-Hydroxy-3',5'-dichlorophenyl-4-hexylchalcone (a) (0.01 M) was suspended in bromine-glacial acid reagent [25% w/v] [6.4 ml]. The reagent was added dropwise with constant stirring. After complete addition of reagent

the reaction mixture was kept at room temperature for about 30 minutes. The solid product, thus separated, was filtered and washed with a little petroleum ether to get the compound (a₁).

Preparation of 2-(4''-hexyl)- 6,8-dichloroflavone (a₂) :

1-(2'-Hydroxy-3',5'-dichlorophenyl)-2,3-dibromo-nonan-1-one (a₁) (0.01 mol) was dissolved in ethanol (25 ml). To this, aqueous solution of KOH (25 ml) was added. The reaction mixture was refluxed for 1 hour, cooled and diluted with water. The product, thus separated, was filtered and crystallized from ethanol to get the compound (a₂).

Preparation of 1-(2'-hydroxy-3',5'-dichlorophenyl)-1,3-nonanedione (a₃) :

2-(4''-Hexyl)-6,8-dichloroflavone (a₂) (0.01 mol) was dissolved in ethanol (25 ml). To this, aqueous solution of HCl (25 ml) was added. The reaction mixture was then refluxed for one hour, cooled and diluted with water. The solid product, thus obtained, filtered and crystallized from ethanol to get the compound (a₃).

Preparation of 1-(2'-hydroxy-3',5'-dichlorophenyl)-2-bromo-1,3-nonanedione (a₄) :

1-(2'-Hydroxy-3',5'-dichlorophenyl)-1,3-nonanedione (a₃) (0.01 mol) was dissolved in a mixture of ethanol (10 ml) and dioxane (10 ml). To this, calculated amount of liquid bromine (0.5 ml) was added. The product was not separated even after standing for one hour. It was then diluted with water and washed with water several times and extracted with ether. The solvent was removed under reduced pressure to get the white solid of the compound (a₄).

Preparation of 5-(2'-hydroxy-3',5'-dichlorophenyl)-4-(heptan-1-one)-2- amino-1,3-thiazole (J) :

1-(2'-Hydroxy-3',5'-dichlorophenyl)-2-bromo-1,3-nonanedione (a₄) (0.01 mol) and thiourea (0.01 mol) were dissolved in ethanol (25 ml). To this, aqueous KOH solution (0.01 mol) was added. The reaction mixture was then refluxed for three hours, cooled, diluted with water and acidified with conc HCl. The product, thus separated, was filtered and crystallized from ethanol to get the compound (J).

The newly synthesized compound was characterised on the basis of elemental analysis, molecular determination, UV, IR, NMR. spectral data.

The UV, IR, and NMR spectral data :-

Compound (J) :

UV :Spectrum No. 1

The UV-Vis spectrum of the compound (J) reported in dioxane showed λ_{\max} value 410 nm corresponding to $n \rightarrow \pi^*$ transition.

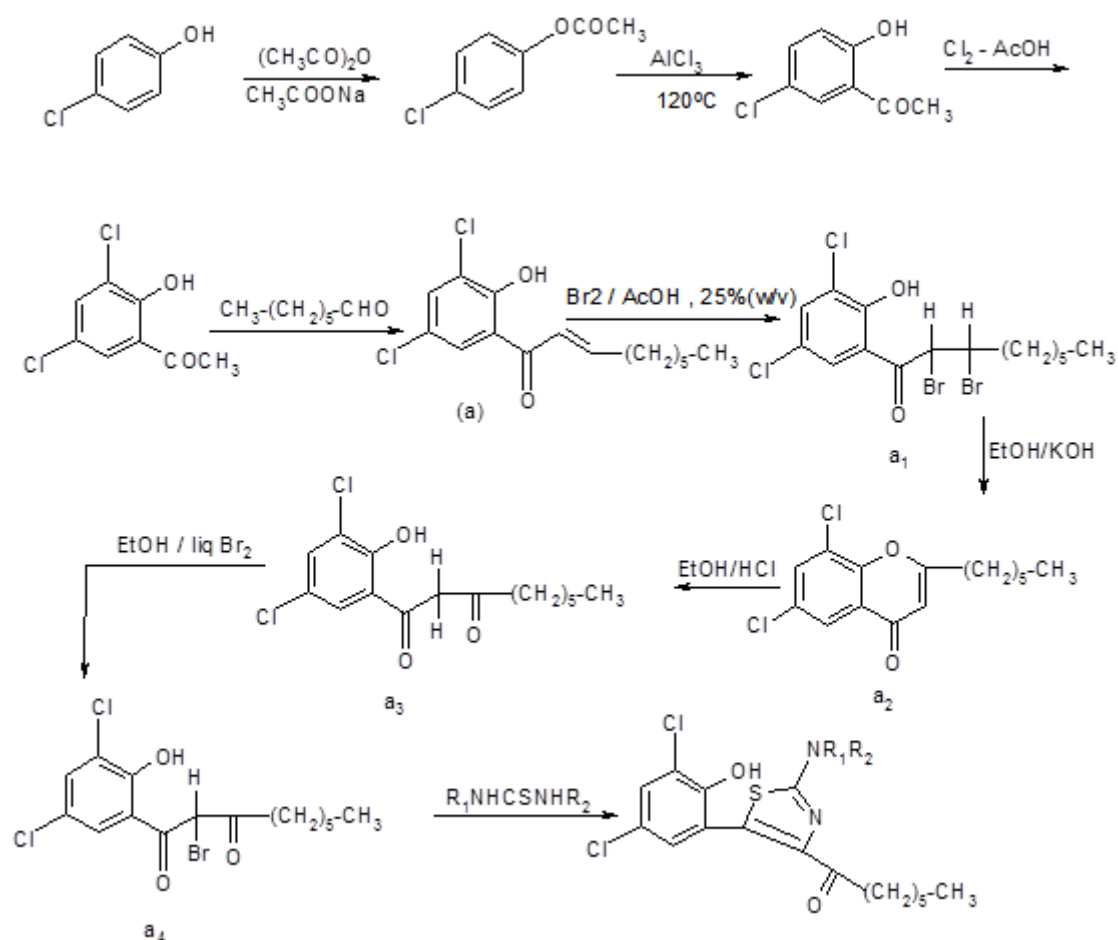
IR (KBr) :-Spectrum No. 2

3036.60 cm^{-1} (-OH phenolic), 2955.55 cm^{-1} (aliphatic -C-H stretching), 3208.58 cm^{-1} (aromatic -C-H stretching), 3797.72 cm^{-1} (-N-H stretching), 1228.56 cm^{-1} (-C=N- stretching), 756.57 cm^{-1} (-C-Cl stretching in aliphatic), 1073.66 cm^{-1} (C-Cl stretching in aromatic).

PMR :-Spectrum No. 3

δ 5.2 (hump, 2H, (-N-H) ; δ 6.7 (d, 1H, -CH=C-H-) ; δ 6.8 (d, 1H, -CH=C-H-) ; δ 7.0 to 7.8 (m, 2H, Ar-H) ; δ offset, (region not observed, observed, O-H)

Scheme:



Where :

- 1) $\text{R}_1 = -\text{H}$,
- 2) $\text{R}_2 = -\text{H}$,

Preparation of nanoparticles of the titled compounds:

Ultrasonic Processor Sonapros PR-250MP was used to produce nanoparticles of the test compounds. The test compound was dissolved in dioxane to prepare 0.1 M solution. This solution was taken in a beaker and the probe of the sonapras 250 MP was dipped in solution. This solution was exposed to sonopros MP 250 for 10 minutes separately. The test compound was converted to nanoparticles. The solvent dioxane was evaporated by conventional heating method. The size of nanoparticles of the test compound was confirmed by X-ray diffraction studies using Benchtop x-ray diffraction (XRD) instrument (Miniflex).

The thin film of the nanoparticles of the test compound was prepared on glass slide. This slide was introduced to the X-ray diffraction instrument to get graphical information which was used for the calculation of the crystal size of test compounds.

Characterisation of size of nanoparticles of the test compounds :-

The crystal size of nanoparticles of the test compounds calculated by using Debye-Scherrer equation.

$$D = \frac{0.94 \lambda}{\beta \cdot \cos \theta}$$

Where,

D = The average crystalline size.

0.94 = The particle shape factor which depends on the shape and size of the particle.

λ = is the wavelength.

β = is the full width at half maximum [FWHM] of the selected diffraction peaks ($\beta = 0.545$)

θ = is the Bragg's angle obtained from 2θ values which was corresponding to the maximum intensity peak in XRD pattern ($\theta = 0.7501$ rad).

III.EXPERIMENTAL DETAILS AND DISCUSSION OF RESULTS

Antibacterial Assay :

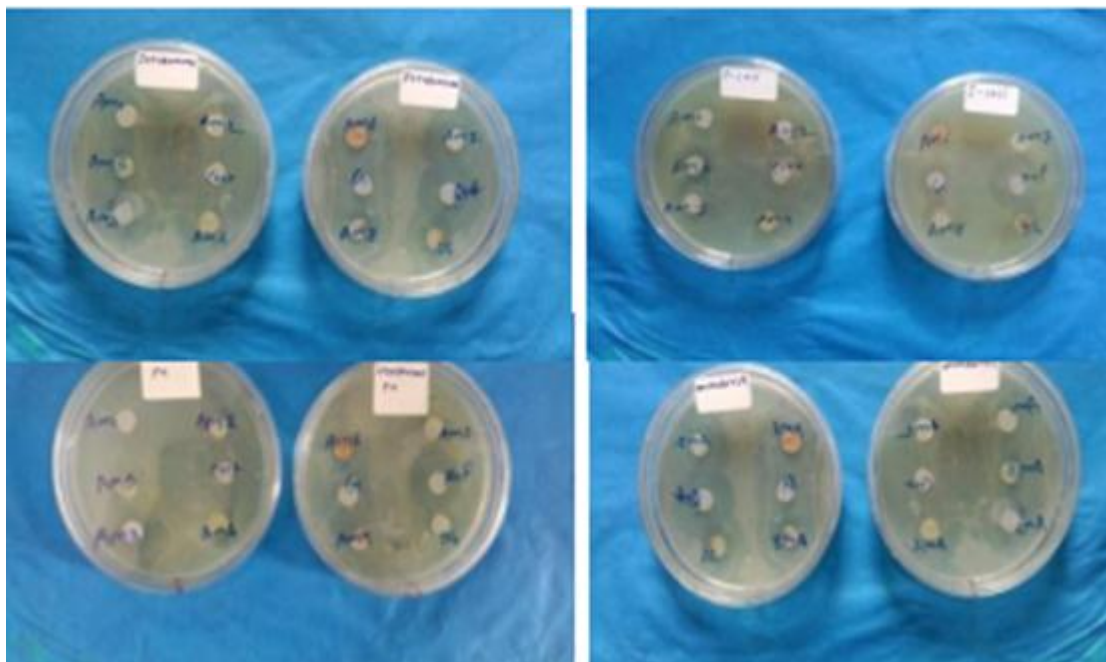
All the newly synthesised compound (a-J) and its nanoparticles were screened for their antibacterial activity against Gram+ve bacteria viz. Staphylococcus pneumoniae, Staphylococcus aureus and Gram-ve bacteria viz. Escherichia coli and Pseudomonas fluorescens at conc. of 1000 ppm by using Agar disc diffusion method. Ofloxacin used as a standard and chloroform as solvent control. The zones of inhibition formed were measured in mm and are shown in Table No.2.

The zones of inhibition formed were measured in mm and are shown in table -2.

Table No.2- Impact of test compounds against plant pathogens :

Sample Code	(Gram positive)		(Gram Negative)	
	Staphylococcus pneumoniae	Staphylococcus aureus	Escherichia coli	Pseudomonas fluorescens
a	11	14	15	12
a1	14	13	14	11
a2	12	11	13	-
a3	-	15	12	15
a4	12	15	11	14
J	14	12	15	12
Reference Antibiotic	(Ofloxacin)	(Ofloxacin)	(Ofloxacin)	(Ofloxacin)

Diameter of inhibition zone (mm)



IV. RESULT AND DISCUSSION :

The newly synthesized compound (a - j) and its nanoparticles were found to be active against test pathogens. However a further detailed study in the light of Medical sciences is advised.

Most of the test compounds have shown remarkable and very encouraging antibacterial activities. A further detailed study in the light of plant pathology is advised.

V. ACKNOWLEDGEMENTS

The author is thankful to Dr.D.H.Pundkar, Principal, Dr.Manorama & Prof.H. S.Pundkar, Arts, Commerce & Science College, Balapur, Dr.B.B.Wankhade, Principal, Malkapur Vidnyan Mahavidyalaya, Malkapur, and Shri Shankarlal Khandelwal College, Akola for providing help in carrying out the antibacterial activities & for providing necessary facilities to carry out the research work.

VI. REFERENCES

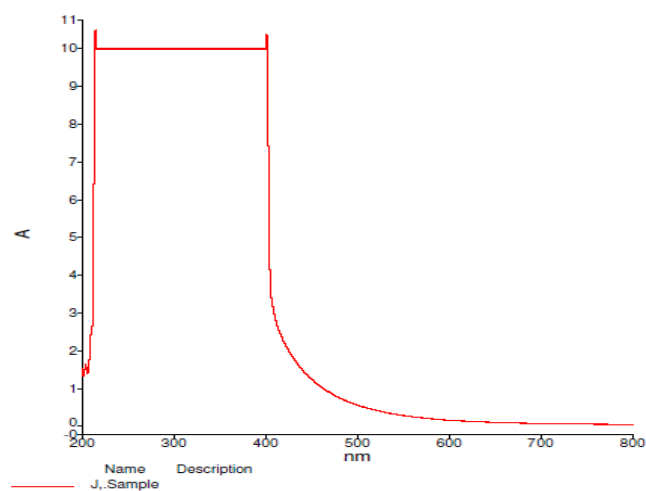
- [1]. Baviskar B, Patel S., Baviskar B., Khadabadi S.S., Shiradkar M, Design and synthesis of some novel chalcones as Potent Antimicrobial Agent Asian J. Research Chem. 1, 2008.
- [2]. Saravanan G., Alagarsamy V., Pavitra T.G.V., Kumar C.G., Savithri Y., Naresh L., Avinash P. Synthesis, characterisation and antimicrobial activities of novel thiazole derivatives. International Journal of Pharma and Bio – Sciences 2010 : 1 : 3 : 1-8.
- [3]. Vicini P. Geronikaki A, Anastasia K, Incer ti M, Zani F. Synthesis and Antimicrobial activity of novel-2-thiazolyl-imino-5-arylidene-4- thiazolidonones Bio. org. Med. Chem. 2006, 14 ; 3859-3864.
- [4]. Pathan S., Alagwadi K., Bhat A., Reddy V., Patthan J., Khade A., Bhat K., Ind. drugs 2007 ; 45 (7) : 532-535.
- [5]. Patthan S., Reddy V., Manvi F., Desai B., Bhat A., Ind. J. Chem. 2006 ; 45 B, 1778-1781.

- [6]. Andreni A., Granajola M., Leoni A., Locatelli A., Morigi R., Rambaldi M., Eur. J. Med. Chem. 2001 : 36 : 743-746.
- [7]. Azam,A.,A.S.Ahmed,M.Oves,M.S.Khan and A.Memic,(2012).Size-dependent antimicrobial properties of CuO nanoparticles against Gram positive and Gram negative bacterial strains.Int.J.Nanomed.,7:3527-3535.
- [8]. Jayaseelan C.,A.A.Rahuman,A.V.Kirthi,S.Marimuthu and T.Santoshkumar (2012).Novel microbial route to synthesize ZnO nanoparticles using Aeromonas hydrophila and their activity against pathogenic bacteria and fungi. Spectrochimica Acta A: Mol.Biomol.Spectrosc.,90:78-84.
- [9]. Singh,D.,A.Kumar,A.K.Singh and H.S.Tripathi,(2013).Induction of resistance in field pea against rust disease through various chemicals/micronutrients and their impact on growth and yield.Plant Pathol.J.,12:36-49.
- [10]. Bryaskova,R.,D. Pencheva,S. Nnikolov and T. Kantardjiev,(2011).Synthesis and comparative study on antimicrobial activity of hybrid materials based on silver nanoparticles (AgNps) stabilized by polyvinylpyrrolidone (PVP). J.Chem.Biol.,4:185-191.
- [11]. Teodoro S.Micaela B.David K.W.(2010) Novel use of nanosaturated alumina as an insecticide.Pest Manag Sci 66(6):577-579.
- [12]. Andrel L. Gartel, University of Illinois, USA/Pharmaceutica-(2013).
- [13]. Chun-Mao Lin and Tan-Yi Lu, Bentham Science, ISSN : 2212-4020.
- [14]. Dr. Ho, Nanotech advancements, Scientific hardness nanotechnology to better diagnose and tract cancer, 120 : 2781-2783 ; doi 10.1002/Cner.28982.
- [15]. Ming Wang, Mariana Holasia, Kasim Kabirov, Aryamitra Banerjee, Cell Cycle, vol. 11, issue 18, (2012).
- [16]. Yue Yaun, Xijun Wang Bin Mei, Dongxin Zhan Scientific Reports 3, Article number : 3523, doi : 10.1038/srep 035 23 ; 29 November (2013).
- [17]. D.E. Manolkos and A.P. Markopoulos Bentham science, ISSN : 1876-4037, vol. 7 Issues (2015).
- [18]. Umme Hani and H.G. Shivkumar, Bentham science, ISSN : 1875-5704, Volume 12, 6 Issues, (2015).
- [19]. Marina Mazzoni, Andrea Ienco, Lorenzo Zani, Gianna Reginato, Massimo Calamante and Cosimo Fortunato, OSA Publishing, (2014).

Table 1 : Characterisation data of newly synthesized compounds :

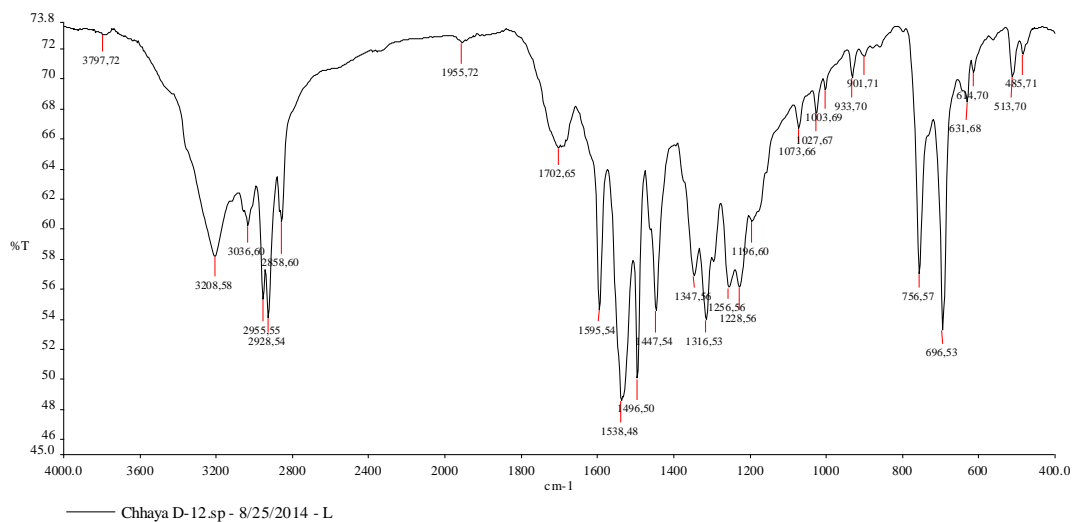
Compound ds	Molecular formula	M.P . in °C	% of yield	% of element					
				C	H	N	S	Cl	Br
	C ₈ H ₆ O ₂ Cl ₂	54	80	47.90/48	2.95/3			34.15/34.58	
a	C ₁₅ H ₁₈ O ₂ Cl ₂	103	70	52.20/53.35	53.10/53.21			23.25/23.27	
a ₁	C ₁₅ H ₁₈ O ₂ Cl ₂ Br ₂	67	50	39.01/39.04	3.85/3.90			15.20/15.40	34.18/34.70
a ₂	C ₁₅ H ₁₆ O ₂ Cl ₂	73	50	60.10/60.20	5.25/5.35			23.70/23.74	
a ₃	C ₁₅ H ₁₈ O ₃ Cl ₂	118	60	56.60/56.	5.60/5.67			22.33/22.	

				78				39	
a ₄	C ₁₅ H ₁₇ O ₃ Cl ₂ B r	84	50	45.40/45. 45	4.20/4.29			17.90/17. 92	20.15/20. 20
J	C ₁₆ H ₂₀ O ₂ N ₂ Cl 2S	96	60	51.10/51. 20	5.30/5.33	7.40/7.4 6	8.50/8.5 3	18.90/18. 93	

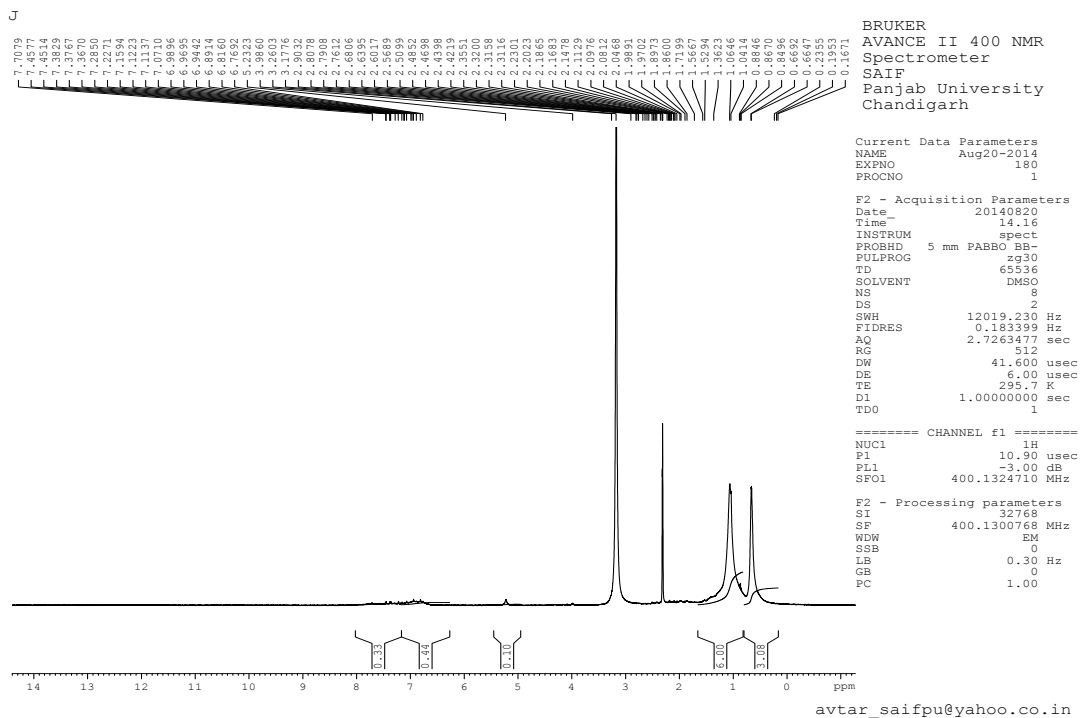


Spectrum No. 1

RC SAIF PU, Chandigarh



Spectrum No. 2



Spectrum No. 3

Protonation Dynamics and Metal-Ligand Stability of Beta-Ketone Ligands: Insights from pKa, nA, and LogK Constants

Choudhari P. P.¹, Wadekar M. P.², Kawalkar A. V.³, Yawale P. R.⁴, Dongapure A. C.⁵

¹Department of Chemistry, G. S. Tompe Arts Commerce and Science College, Chandur Bazar, Amravati, Maharashtra, India

²Applied Chemistry Division, GVISH, Amravati, Maharashtra, India

³Department of Chemistry, Amolakchand Mahavidyalaya Yavatmal -445001, Maharashtra, India

⁴Department of Chemistry, Shankarlal Agrawal Science College, Salekasa, Maharashtra, India

ARTICLE INFO

Article History:

Accepted : 01 Jan 2025

Published : 10 Jan 2025

Publication Issue :

Volume 12, Issue 7

January-February-2025

Page Number :

97-102

ABSTRACT

This work investigated the interactions of Cu(II) and Zn(II) with the tautomeric equilibrium of the β -diketo moiety. Two alternative ligands, 1-(2-hydroxyphenyl-5-bromo)-3-(2,4-dichloro)propane-1,3-dione and 1-(2-hydroxyphenyl-5-bromo)-3-(4-fluoro)propane-1,3-dione, were produced and assessed. Utilizing Irving and Rossotti's modified Bjerrum technique. At a constant temperature of 32°C and an ionic strength of 0.1 M (NaOH) in a 70% DMF-water medium, the stability constants for the 1:1 and 1:2 complexes with Cu(II) and Zn(II) were calculated. The simultaneous occurrence of 1:1 and 1:2 complicated structures was noted.

Keywords: propane-1,3-dione, keto-enol equilibrium, β -diketo ligands Cu(II) and Zn(II), pH meter, stability constant

I. INTRODUCTION

The research of metal complexes in solutions has advanced significantly over the last four decades (1). The field's foundation was established by Bjerrum's groundbreaking dissertation (2). Low dissociation constants, distinct redox potentials, particular electron distributions, and enhanced solubilities as a result of metal complex formation are some of the essential properties of these complexes that boost their biological activities. These characteristics affect how well medications dissolve in lipids and pass through cell membranes (3). Additionally, the creation of metal complexes promotes bond formation, bond breakage, and group transfer events. It polarizes electrons from the ligands toward the metal in addition to aiding in the formation of an activated complex by bringing reactive molecules together (4) (5). The values for the stability constant and free energy change indicate the stability and basicity of ligands (6). Bulkier groups tend to make ligands more basic and stable. These complexes' stability is dictated by the ligands and the core metal atom. Electronic structure, radius,

and degree of oxidation are important variables. The type of atoms that are directly connected to the core atom or ion determines the binding strength of polyatomic ions and ligand molecules, which is influenced by these properties (7) (8).

According to Irving and Williams' study, metal complexes containing transition metal ions can be examined for stability order by looking at their ionic radii and second ionization potentials (9). This is especially true for ligands that have donors of oxygen and nitrogen. The size and quantity of chelating rings that develop have a major impact on the stability of these complexes. These characteristics are determined by the structure of chelating agents; according to Daniele Sanna research on peptide chelates, rings with five or six members are the most stable (10). Numerous researchers have made significant contributions to the subject of metal-ligand chemistry over the years (11) (12) (13) (14).

Existing synthetic substituted diketones(15)were used in this investigation due of their possible biological and analytical uses. These substances, both diketones, have antihelminthic and fungicidal qualities. Because of their varied biological actions, several substituted diketones have been reported to exhibit antibacterial, anti-inflammatory, insecticidal, bactericidal, pharmacological, and fungicidal properties.

II. EXPERIMENTAL SECTION

Materials and Instruments

All of the reagents and solvents used were purchased from commercial sources and did not undergo additional purification. Analytical thin-layer chromatography (TLC) was performed on 60 F254 silica gel plates. The Baker-Venkataraman rearrangement in a pyridine medium was described by Rajendra M. Pathade and Pravin S. Bodkhe (15). At a controlled temperature of 32°C, pH was measured using a pH-meter.

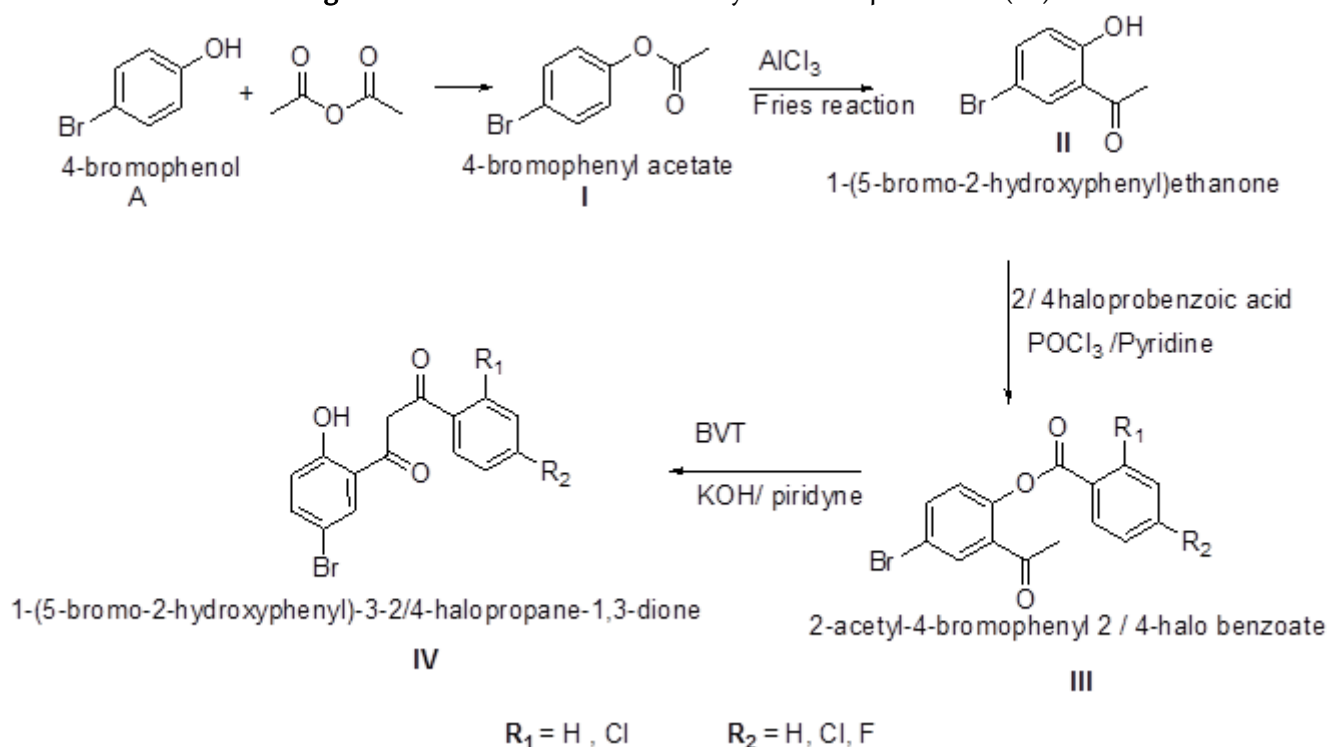
Synthesis of 5-Bromo-2-hydroxyacetophenone

2-hydroxyacetophenone (5.0 g, 36.3 mmol) and acetic acid (40 mL) were mixed in a round-bottom flask fitted with a reflux condenser. After stirring, the mixture was cooled to 0°C. Then, dropwise for 15 minutes, a bromine solution (5.0 mL, 99.9%, 98.0 mmol) in acetic acid (10 mL) was added. For four hours, the reaction mixture was agitated at room temperature. After the reaction was finished, as determined by TLC, the mixture was placed over crushed ice and agitated for an extra sixty minutes. After filtering, washing with water, and recrystallizing the resulting yellow solid from ethanol, 5-bromo-2-hydroxyacetophenone was obtained as yellow crystals with an 85% yield.

Preparation of 1-(5-bromo-2-hydroxyphenyl)-2/4--halo-1,3-dione(IV)(16)

Already prepared 2-acetyl-4-bromophenol (I) 1-(5-bromo-2-hydroxyphenyl)ethanone-bromophenyl 2 and 4-halogen (II). The 1-(5-bromo-2-hydroxyphenyl)ethanone-bromophenyl 2 and 4-halogen (II) and 2/ 4-halobenzoic acid were dissolved in pyridine (40 ml). Then KOH solution was added to the warmed compound (III) solution with constant stirring. After that, the resultant solution was acidified by chilled (1:1) dilHCl. The obtained solid organic molecule was washed with NaHCO₃ (10%) and washed with distilled water. It was then recrystallized by using ethanol to obtain 1-(5-bromo-2- hydroxyphenyl)- 2 and 4-halogen-1,3-dione (IV). The resultant product was characterized by melting point determination, spectroscopic analysis, and elemental analysis to confirm its purity and identity. The typical yield for this synthesis ranged from 58% to 62%. All reactions were conducted under appropriate laboratory conditions with necessary safety precautions. The synthesis of 2 and 4 - Substituted Halogen Propane-1,3-Diones (β -Diketones) is shown below in Figure-1.

Figure 1: Reaction scheme for the synthesis of β -diketone(17)



Ligand (L₁): 1-(5-bromo-2-hydroxyphenyl)-3-(2,4-dichlorophenyl)propane-1,3-dione

Ligand (L₂): 1-(5-bromo-2-hydroxyphenyl)-3-(4-fluorophenyl)propane-1,3-dione

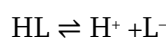
pH-Metric Measurements

For accurate measurements, a Systronics microprocessor-based device with a glass electrode and a saturated calomel electrode was utilized. The device was accurate to 0.01 units. Before the titrations, the instrument was calibrated using buffer solutions with pH values of 4.00, 7.00, and 9.20 at 32°C. The titration process involved three stages: first, titrating a free acid solution (0.01 M); second, titrating a mixture of free acid (0.01 M) and ligand (20×10^{-4} M); and third, titrating a combination of free acid (0.01 M), ligand (20×10^{-4} M), and metal ion (4×10^{-4} M) against a standard NaOH solution. Throughout the experiments, the ionic strength of all solutions was maintained at a constant 0.1 M by adding an appropriate amount of 1 M KNO₃ solution. The titrations were conducted in a 101 mL Pyrex glass beaker placed in an ice-cold water bath, which was maintained at a constant temperature of $32 \pm 0.1^\circ\text{C}$. To produce a chemically inert atmosphere, nitrogen gas was purged. Measurements were made only after the gas bubbling stopped, and pH values were noted for every 0.5 mL addition of NaOH. The volume of alkali added was then displayed against the pH values in graph form.

III.RESULTS AND DISCUSSION

Determination of Proton-Ligand Stability Constants

At an ionic strength of 0.1 M, the pH-metric dissociation constants of the substituted diketones (1, 2) were measured. The ligands or reagents employed in this study are monobasic acids, which are denoted by the symbol HL since they each have a single dissociable proton from the hydroxyl group:



The titration curves of the acid and the ligand diverge at approximately pH 1.5 and continue to rise to pH 7.5. The deviations observed between the acid and ligand curves indicate the dissociation of H⁺ ions from the

hydroxyl groups of the ligands. Proton-ligand formation numbers (\bar{n}_A) were calculated using the Irving and Rossotti method.

$$\bar{n}_A = \gamma - \frac{(V_2 - V_1)(N + E^0)}{(V_0 + V_1)T_L}$$

The values of \bar{n}_A are calculated using the parameters mentioned, where:

(V_0) is the initial volume of the solution.

(T_L) is the initial concentration of the ligand.

(V_1) is the volume of alkali required during the acid titration at a given pH.

(V_2) is the volume of alkali required during the ligand titration at a given pH.

(γ) is the number of replaceable protons from the ligand.

(E^0) is the initial concentration of the mineral acid.

N: It is the normality of the alkali solution used in the titration.

1) Methods for Calculation of Proton-Ligand Stability Constant

a) Half Integral Method

The proton-ligand stability constants are found using the formation curves. The pH values at which the pK value for a system with a single dissociable group is equal to $\bar{n}_A = 0.5$. The point at which half of the available dissociable groups have been ionized is indicated by this pK value.

b) Pointwise Calculations Method

The precise determination of pKa values is achieved through pointwise calculations. For values of $\bar{n}_A < 1.0$ the formation function of a 1:1 complex can be expressed using the following equation:

$$\log \left(\frac{\bar{n}_A}{1 - \bar{n}_A} \right) = pK - pH$$

Calculation of Metal-Ligand Stability Constant (\bar{n})

The Irving-Rossotti expression is used to calculate the metal ligand formation number.

$$\bar{n} = \frac{(V_3 - V_2)(N + E^0)}{(V_0 + V_2)\bar{n}_A T_M} \quad (2)$$

Using the Irving-Rossotti expression, \bar{n} is computed as the horizontal difference ($V_3 - V_2$) that appears between the ligand curve ($A+L$) and the metal curve ($A+L+M$). Additionally, at a specific pH, the onset of turbidity during ($A+L+M$) titration indicates the creation of metal hydroxide.

Using Irving-Rossotti's expression, the metal-ligand stability constants ($\log K = pL$) were determined as follows:

$$pL = pK + \log \left(\frac{T_L^0 - (\bar{n}T_M^0)}{\bar{n}T_M^0} \right)$$

pL: Negative logarithm of the free ligand concentration

b) Pointwise Calculations Method

For value of $\bar{n} < 1.0$, metal ligand stability constants for 1:1 complex formations are calculated by using.

$$\log \left(\frac{\bar{n}}{1 - \bar{n}} \right) = \log K_1 - pL$$

For value in the region $1 < \bar{n} < 2$, metal-ligand stability constants for the 1:2 complex are calculated by using an equation.

$$\log \frac{(\bar{n}-1)}{(2-\bar{n})} = \log K_2 - pL$$

The values of $\log K_1$ and $\log K_2$ are shown in Tables 2 and 3

Table 1 displays the results of the half-integral and Pointwise Calculation methods used to determine the pK_a values for both systems. The dissociation constants can be precisely determined using this method, which reflects the ligands' protonation states at different pH values.

Table-1. Proton-Ligand Stability Constants

Ligands	pK (Pointwise Calculation Method)	pK (Half Integral Method)
L ₁	7.02	7.84
L ₂	7.06	8.25

Table-2. Metal-ligand stability constants by Pointwise calculation.

Ligand	Metal	Log K ₁	Log K ₂
L ₁	Zn(II)	8.27	7.45
	Cu(II)	8.14	7.01
L ₂	Zn(II)	8.17	7.29
	Cu(II)	8.13	7.31

Table-3. Metal-ligand stability constants by Half integral method.

Ligand	Metal	Log K ₁	logK ₂
L ₁	Zn(II)	7.98	7.39
	Cu(II)	7.99	7.39
L ₂	Zn(II)	8.02	7.42
	Cu(II)	8.03	7.45

IV.CONCLUSION

The titration curves for (acid + ligand), (acid + ligand + Cu(II)), and (acid + ligand + Zn(II)) vary across all systems, indicating that the complex formation begins at approximately pH 1.5. During the titration procedure, the color of the solution changes from light blue to dark blue for acid + ligand + Cu(II), and there is no change in color for acid + ligand + Zn(II). Table 1 shows the ligands' pK_a values in the following order: pK_a(ligand 1) > pK_a (ligand 2). The reason for this discrepancy is that ligand 1 contains chloro (-Cl) electron-withdrawing groups, which lower its pK_a values.

The sequential complex formation between the ligands and the metal ions, Cu(II) and Zn(II), is indicated by the very large difference between the log K₁ and log K₂ values, as seen in Tables 2 and 3. When it comes to 1:1 complexes, Zn(II) typically forms more stable complexes with both ligands (L₁ and L₂) than Cu(II). In Ligand 2 (L₂), the 1:2 complexes with Cu(II) are somewhat more stable than those with Zn(II).

V. REFERENCES

- [1]. The IUPAC stability constants database. Pettit, Leslie D.. 2006, Chemistry international , Vol. 28, pp. 14-15. <https://doi.org/10.1515/ci.2001.23.1.18b>.
- [2]. Metal Ammine Formation in Aqueous Solution. VI. Stability and Light Absorption of Copper Ethylenediamine Ions. Bjerrum, Jannik et al.. 1948, Acta Chemica Scandinavica , Vol. 2, pp. 297-318. <https://doi.org/10.3891/ACTA.CHEM.SCAND.02-0297>.
- [3]. Metal Complexes in Biology and Medicine the System Cadmium (II) / Iron (II) /Zinc (II) - Proline. Tewari, Brij Bhushan. 2024, Vol. 5, pp. 1-6. 10.47363/jdat/2024(5)140.
- [4]. al., Verpoort et.Metal complexes useful in metathesis and other reactions. US 7.687,635 B2 United States Patent, 2004.
- [5]. Electron Transfer Reactions of Metal Complexes. Tadaaki, Inomata. 2024. 10.1039/9781837673254-00167.
- [6]. Thermodynamics of complex formation of silver(I) with substituted pyridines and cyclic amines in non aqueous solvents. Sanadar, Martina. 2024, Journal of Thermal Analysis and Calorimetry, Vol. 149, pp. 3531–3542. <https://doi.org/10.1007/s10973-024-12894-2>.
- [7]. Recent developments in two coordinate transition metal chemistry. Noor, Awal. 2023, Coordination Chemistry Reviews, Vol. 476, p. 214941. <https://doi.org/10.1016/j.ccr.2022.214941>.
- [8]. The first Cu(I)-peptoid complex: enabling metal ion stability and selectivity via backbone helicity. Anastasia E Behar, and G. Maayan. 2023, chemistry , Vol. 43, p. 29. <https://doi.org/10.1002/chem.202301118>.
- [9]. The stability of transition-metal complexes. Williams, H. Irving and R. J. P. 1953, J. Chem. Soc., pp. 3192-3210. <https://doi.org/10.1039/JR9530003192>.
- [10]. The effect of the ring size of fused chelates on the thermodynamic and spectroscopic properties of peptide complexes of copper(II). Sanna, Daniele. 26-27, 2001, Polyhedron, Vol. 20, pp. 3079-3090. [https://doi.org/10.1016/S0277-5387\(01\)00918-4](https://doi.org/10.1016/S0277-5387(01)00918-4).
- [11]. 50 Years of Passion for Organometallic Chemistry. Herrmann, Wolfgang A.. 2023, Journal of Organometallic Chemistry, Vol. 1000, p. 122815. <https://doi.org/10.1016/j.jorganchem.2023.122815>.
- [12]. A guide to secondary coordination sphere editing. Drover, Marcus W. 6, 2022, Chemical Society reviews, Vol. 51, pp. 1861-1880. <https://doi.org/10.1039/d2cs00022a>.
- [13]. Schiff bases and their metal Complexes: A review on the history, synthesis, and applications. Boulechfar, Chérifa. 2023, Inorganic Chemistry Communications, Vol. 150, p. 110451. <https://doi.org/10.1016/j.inoche.2023.110451>.
- [14]. Metal-ligand cooperation. Julia R Khusnutdinova and, David Milstein. 42, 2015, Angewandte Chemie, Vol. 4, pp. 12236-73. <https://doi.org/10.1002/anie.201503873>.
- [15]. Synthesis, Spectroscopic Characterization And Antimicrobial Screening Of Some Newlysynthesized Propane-1,3-Dione (B-Diketones)Derivatives.PravinS.BodkheandRajendra M.Pathade 1, 2019, Vol. 6, pp. 2393-8374.
- [16]. Density and viscosity of 2- Hydroxy Substituted 1, 3- Dipropanone Containing Phenol Group in Dimethyl sulfoxide (DMSO), Solvent Using Various Concentration. A C Dongapure, P.P Choudhari. 8, s.l. : Der Pharma Chemica , 2022, Vol. 14.
- [17]. Synthesis of Substituted 1, 3- Dipropanone Containing Phenol Group Synthesized From. A C Dongapure, P P Choudhari. 5, s.l. : Der Pharma Chemica, 2022, Vol. 14, pp. 24-27.

Synthesis, Characterization and Catalytic Performance of Metal Inserted AI-MCM-41 Mesoporous Material

Dr. Gaur S.R.

PG Dept. of Chemistry, Sant Ramdas Arts Commerce & Science College Ghansawangi,
Dist- Jalna, Maharashtra (India)

ARTICLE INFO

Article History:

Accepted : 01 Jan 2025

Published : 10 Jan 2025

Publication Issue :

Volume 12, Issue 7

January-February-2025

Page Number :

103-110

ABSTRACT

The metal is selected for the present studies were Aluminium. The size of pores was found to be a substantial limitation as they could not have been used in transformations of larger molecules. The need aroused to obtain mesoporous materials, whose larger pores and large surface area could make them applicable for adsorption, separation, catalysis, as drug delivery carriers, sensors, in photonics for energy storage and conversion and as Nano devices working with large molecules.

Introduction: The materials obtained were called the M41S family and included MCM type materials (Mobile Composition of Matter): MCM-41, MCM-48 and MCM-50, differing in the type of pore ordering. These silicas showed well-developed surface area and a uniform size pore system Chen, et al., (2019). The synthesis of M41S materials has opened the way to obtaining new ordered mesoporous silicas. Syntheses of ordered mesoporous silicas of well-defined structure need first of all precise planning of the process, the choice of a suitable compound directing structural development and a suitable precursor of silica. it is possible to obtain silicas of desired pore size and structure Meynen, et al., (2009); Hoffmann, et al., (2006). The best known and most thoroughly studied so far are the SBA-1 type silicas. In general SBA type silicas (SBA-11, SBA-12, SBA-15, SBA-16) are obtained using non-ionic surfactants as structural directing agents Zhao et al., (1998), however, SBA-1 has been for the first time synthesized using a cationic surfactant with a large head component of its molecule Huo et al., (1994).

Mesoporous materials are an important class of porous materials with a wide range of proposed applications in catalysis (particularly as the additives for petrochemical conversions, especially large hydrocarbons), environmental remediation (e.g., adsorbents), biomedical application (e.g., drug delivery), energy storage, and functional devices (Davis, 2002; Sen et al., 2004). Generally, considering the silica-based mesoporous materials, they can be divided into two classes: ordered mesoporous silica and aluminosilicates materials, such

as MCM-41, MCM-48, SBA-15, and MAS-5 (Kresge et al., 1992; Zhao et al., 1998; Zhang et al., 2001; Chaudhary and Sharma, 2016) and disordered mesoporous materials, such as KIT-1 (Ryoo et al., 1996). Two strategies are available to build these catalysts: grafting of properly functionalized complexes to the MCM-41 and multi-step functionalization of pristine MCM-41. The later methodology often entails the introduction of the amino functionality. Thus, complexes can be tethered to the MCM-41 by amine or imine linkages. Jabbari et al. (2015), reported the encapsulation of salen copper (II) complexes.

There being more information about the influence of different metal sources in the textural properties of the MCM-41 type mesoporous materials and scarce information about the rearrangement of the crystalline structure and the nature of the surface activity (e.g., acid sites) as a consequence of the incorporation of hetero elements in the framework of MCM-41 mesoporous materials. In order to overcome some of the limitations mentioned above, the main goal of our study was to propose the synthesis of a purely siliceous MCM-41 and Al-containing MCM-41 (Al-MCM-41) mesoporous materials by non-hydrothermal economically feasible procedures using a simple alkali-free reaction system carried out at room temperature and short reaction times. Under these synthesis conditions, aiming to elucidate the intrinsic structural properties and active nature of mesoporous silica based materials, it was also investigated the increasing influence of Al incorporation in the changes of the textural properties, crystalline structure and active nature (acid sites) of the MCM-41 without interferents (e.g., Na⁺ ions). The technical data reported in this study are of great importance because validate an alternative technique for obtaining MCM-41 and Al-MCM-41 mesoporous materials, the same that are commonly obtained by hydrothermal methods, besides that these results constitute a basis for the development of new materials for specific applications such as in catalysis and adsorption.

Materials and Methods:

Experimental Section:

Chemicals and Materials

Synthesis: Purely siliceous MCM-41 and Al-containing samples with Si/Al molar ratios of 50 and 15 named Al-MCM-41(50) and Al-MCM-41(15), respectively, were synthesized according to the procedure described by La-Salvia et al., (2015). Briefly, a solution with 630 cm³ ammonium solution - NH₄OH (Merck, 26,4%) and 810 cm³ of deionized water was prepared. To this mixture 6 g of cetyltrimethylammonium bromide, C₁₉H₄₂BrN - CTAB (Sigma Aldrich, 99%) and 0.5 g (Si/Al = 50) or 1.7 g (Si/Al=15) of aluminum sulfate hydrate, Al₂(SO₄)₃.18H₂O (Merck, 59%) were added. After solubilization, 30 cm³ of Tetraethyl orthosilicate, SiC₈H₂₀O₄ - TEOS (Sigma Aldrich, 98%) was added. The resulting suspension was stirred at 420 rpm for 2 h, at room temperature, having the following molar composition ratios 1Si[TEOS]: 0.12CTAB: 31NH₄OH: 338H₂O: x Al[Al₂(SO₄)₃.18H₂O], where x = 0, 0.013 and 0.044 for pure silica, Si/Al=50 and Si/Al=15 samples, respectively. Afterwards, the material was filtered and dried overnight at 400 K. The sample was then calcined at 813 K for 11 h. The first 5 h in a nitrogen flow and the remaining time in a synthetic air flow. Finally, the resulting product was cooled to room temperature under continuous synthetic air flow and stored in a desiccator.

Characterization:

The total silica content was determined in an Atomic Absorption Spectroscopy (AAS) of Perkin Elmer (AAnalyst 3) and the aluminum loading in a Perkin-Elmer spectrometer (Elan DRC-e). Powder X-ray diffraction (XRD) patterns were carried out in a Philips (X'Pert) X-ray diffractometer using CuK α 1 radiation (λ = 0.154056 nm) at 40 kV and 40 mA, in the range of 2θ from 1.8° to 15° with a step size of 0.02° and a time step of 1.8 s. Prior to the XRD analysis, the samples were dried at 393 K overnight and powdered. The d-spacing

value ($d100$) was estimated from the position of the first X-ray diffraction line using the Bragg's equation ($2d100\sin\theta = n\lambda$) and the unit cell parameter ($a0$) for a hexagonal lattice from the equation $a0 = 2d100/\sqrt{3}$. The specific surface area, the pore size distribution and the total pore volume were determined from N2 adsorption-desorption isotherms obtained at 77 K in a Micromeritics ASAP 2020 analyzer. The samples (ca. 100 mg) were previously heated under vacuum and degassed at 623 K for 1 h. The surface area was calculated by the conventional BET method in the relative pressure range $0.05 < P/P_0 < 0.20$ with a linear correlation coefficient greater than 0.999. The total pore volume (V_p) was measured by the amount of N2 adsorbed at a relative pressure close to one ($P/P_0 \approx 0.995$). The average pore diameter (D_p) was determined by BJH method from the N2 desorption isotherms. Then, the pore wall-thickness (W_t) was estimated by the equation $W_t = a0 - D_p$. The Al and Si structural species were determined from Liu et al., (2013). Al-MAS-NMR and Dedecek, et al. (2009). Si-MAS-NMR spectra using a Bruker (AC400/P) spectrometer.

Results and Discussion:

In the present studies following results was obtained as summarized in table 1 and 2

Precursors		Basic medium	Surfactant templates	Reaction SM:T (K)/time	Calcination T(K)/time	Si/Al	d100 (nm)	a0 (nm)	SBE T (m ² g ⁻¹)	Vp (cm ³ g ⁻¹)	Dp (nm)	Wt (nm)
Si												
TEOS+MPTMOS TEOS+MPTMOS		NH ₃ -H ₂ O-C ₂ H ₅ OH	CTAB	NH ₃ :38/1h	673/5h	00	3.1	3.5	1621	0.69	2.6	0.90
Fumed silica		NH ₄ OH+TMAOH	CTAB	H ₂ :343/3d	813/5h	00	3.8	4.4	1308	1.03	3.5	0.90
Colloidal silica		TMAOH	CTAB	H ₂ :373/2d	823/12h	00	3.72	4.3	1040	0.97	3.44	0.86
TEOS		NH ₄ OH	CTAB	383/2d	823/6h	00	3.04	3.51	1082	0.97	2.53	0.98
Fumed silica		NH ₄ OH	CTAB	H ₂ :373/3d	550/24	00			1126		2.98	

TEOS	AIP + PrOH	NH 4O H	CTA B	NH:R T/0.5 h	823/ 5h	61			1020	0.57	22	
TEOS	AIP Alumi num sulfate	NH 4O H	C16T MAB r- PrO H C16T MAB r-	NH:R T/1h	823/ 11h	10 1 27	3.73 3.67	4.31 4.24	1034 988	0.77 0.72	3.08 2.99	1.23 1.25
Fumed silica	Alumi num sulfate	NH 4O H	CTA B	H:37 3/3d	550/ 24	14			997		2.9	
Fumed silica +TMAS i	Alumi na	NH 4O H	C16T MAC l	H:37 7/2d H:42 3/2d	823/ 11h	32 23	4.04 4.71	4.67 4.44	889 8.11	0.71 0.71	3.61 3.61	1.06 1.66

Table no.1

Synthesis methods of MCM-41 type mesoporous materials in an alkali- free system

Estimated values. d100, d-spacing value; a_0 unit cell parameter; SBET, BET specific surface area; Vp, total pore volume; Dp, pore diameter; Wt, pore wall-thickness; SM, synthesis method; H, hydrothermal synthesis in autoclave at high vapor pressure; NH, non-hydrothermal synthesis; RT: room temperature; d: day; h: hour. AIP: aluminum isopropoxide; C16TMABr: hexadecyltrimethylammonium bromide; C16TMACl: hexadecyltrimethyl-ammonium chloride; CTAB: cetyltrimethylammonium bromide; MPTMOS: 3 methacryloxypropyltrimethoxysilane; PrOH: propan-2-ol; TEOS: tetraethyl orthosilicate; TMA Si: tetramethylammonium silicate; TMAOH: tetramethylammonium hydroxide; TMB: 1,3,5-trimethylbenzene; * samples were previously pretreated in inert gas flow at the same calcination temperature

Table no. 2.

Physicochemical properties of the calcined solids.

d100, d-spacing value; a_0 , unit cell parameter; SBET, BET specific surface area; Vp, total pore volume; Dp, average pore diameter (BJH method); CBET, BET constant; Wt, pore wall-thickness

Sample	Si content (wt%)		Al content (wt%)		d100 (nm)	a_0 (nm)	SBET (m ² g ⁻¹)	Vp (cm ³ g ⁻¹)	Dp (nm)	CBET	Wt (nm)	Acid Sites density mmol g ⁻¹
	as-synthes	calci ned	as-synthe	calcin ed								

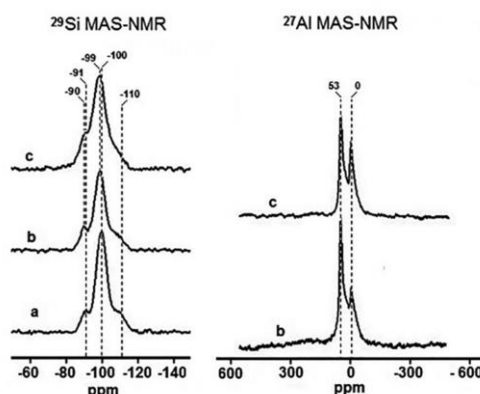
	ized		sized									1
MCM-41	46.74	46.60	-	-	3.48	4.0 2	1412	1.06	2.65	59	1.37	0.06
MCM-41(50)	45.96	45.35	0.88	0.87	3.56	4.1 2	1390	0.97	2.61	51	1.51	0.36
MCM-41(15)	44.24	44.25	2.83	2.74	3.62	4.1 9	992	0.68	2.56	43	1.63	0.51

From the above experimental data we have conclude that the above Table- 1 showing the low-angle X-ray powder diffraction patterns and N₂ adsorption-desorption isotherms with pore-size distribution graphs inset of purely siliceous MCM-41 and Al-containing samples Al-MCM-41 calcined at 813 K. In Table- 2 showing the chemical compositions, structural parameters and textural properties of the solids. The XRD patterns of samples exhibit a very strong and well-resolved peak at $2\theta = 2.5^\circ$ assigned to the reflection line (100), and very weak and broad two peaks at $2\theta = 4.3^\circ$ and 4.9° , corresponding to the reflections lines (110) and (200), respectively. The intense reflection line (100) is characteristic of the hexagonal structure (space group p6mm) of the purely siliceous MCM-41 and the presence of the reflection lines (110) and (200) confirm the highly crystallinity and the well-defined hexagonally ordered pore geometry of the mesoporous materials Beck et al. (1992); Chen et al., (1993); Brahmi et al., (2016). However, when Al was incorporated in the purely siliceous MCM-41 the main reflection line (100) became broader and less intense, even at very low levels of aluminum content, and the reflection lines (110) and (200) are hardly observed. Furthermore, with the rise of aluminum content or decrease of the Si/Al ratio, the d-spacing values (d_{100}) increased and, consequently, the unit cell parameters (a_0) expanded (Table 2). The increase of the interplanar spacing suggests that aluminum was incorporated into the structure of MCM-41 and this could be due to the difference in size between aluminum ions, Al³⁺ (radius = 53 pm) and silicon ions, Si⁴⁺ (radius = 40 pm) Brahmi et al., (2016). Reddy and Song (1996); Borade and Clearfield (1995). The latter are in agreement with the literature, and independent of the synthesis method, it is commonly accepted that the incorporation of Al³⁺ ions in the MCM-41 structure produce an expansion on its crystalline reticulum causing a narrowing of the pore size and a decrease in the crystallinity degree of the mesoporous materials Brahmi et al., (2016); Reddy and Song (1996); Vaschetto et al., (2014); Borade and Clearfield (1995); Luan et al., (1995).

In respect to the N₂ adsorption-desorption isotherms obtained at 77 K, the profiles for purely siliceous and Al containing samples corresponded to type IV (in the IUPAC classification), which is typical of the MCM-41 mesoporous molecular sieves with well-defined and ordered cylindrical mesoporous Beck et al. (1992); Chen et al., (1993).

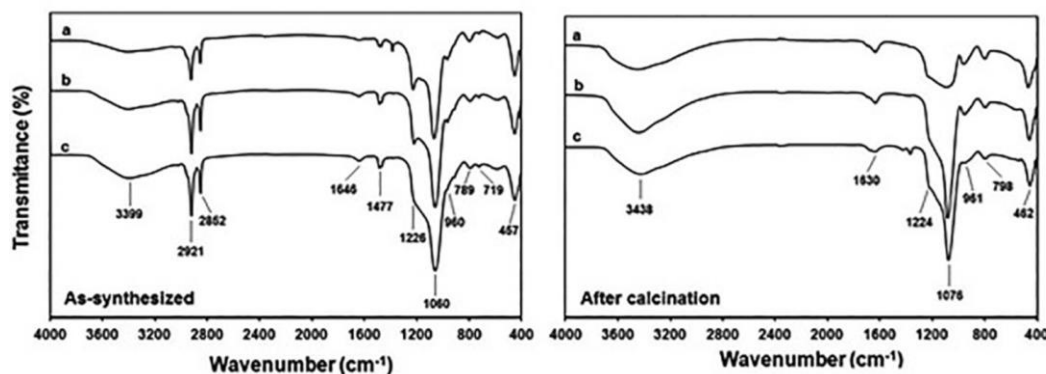
The isotherms did not change their shape with the variation of Al content in the samples and in each one three well-defined stages were identified: (i) at low relative pressures ($P/P_0 < 0.25$) the N₂ uptake slowly increased attributed to the monolayer-multilayer adsorption on the pore walls; (ii) at intermediate relative pressures ($0.25 < P/P_0 < 0.40$) a sharp inflection emerged possibly due to capillary condensation within of small pores, called primary mesoporous; and, (iii) at high relative pressures ($P/P_0 > 0.4$) a plateau with a slight inclination was observed and assigned to multilayer adsorption of N₂ molecules on the external surface of the crystals. In this work, at relative pressures in the range of 0.4 - 0.9, no perceptible hysteresis loop was detected as it is found in some MCM-41 type mesoporous materials prepared with low surfactant/silicon molar ratios (e.g., CTAB/TEOS ≤ 0.08) Chen and Wang (2002) or in prolonged post-synthesis hydrothermal treatments at high temperatures (e.g., 4-6 days, 423 K) Sayari et al., (1997). The purely siliceous MCM-41 showed a high specific

BET surface area ($1412 \text{ m}^2 \text{ g}^{-1}$). However, when the Al was incorporated into MCM-41 structure, the specific BET surface area of the solids decreased with the increase of Al loading in the following order: MCM-41 > Al-MCM-41(50) > Al-MCM-41(15). The EDS graphs confirm the presence of the O, Si and Al elements in the mesoporous samples. These results are consistent with the chemical, low-angle XRD and N₂ adsorption analysis and suggest that the Al-containing samples, after calcination at 813 K, retain the characteristics of regular and hexagonal pore arrangement of MCM-41 type mesoporous materials. According to Kurdyukov *et al.* (2016) in solids synthesized by non-hydrothermal methods in an alkali-free system, the high BET surface area not only depends on the cylindrical mesoporous, but also on the formation of microspores ($D_p < 2 \text{ nm}$) within the walls and between the outer surfaces of the ordered silica channels. According to Chen *et al.* (2002), solids synthesized with lower surfactant/silicon ratios ($\text{CTAB/TEOS} \leq 0.1$) shows a high pore wall-thicknesses. TEM images with EDS graphs inset of the MCM-41 and Al-MCM-41



Graph no. 2.

²⁹Si-NMR and ²⁷Al-NMR spectra of (a) MCM-41, (b) Al-MCM-41(50), (c) Al-MCM-41(15).

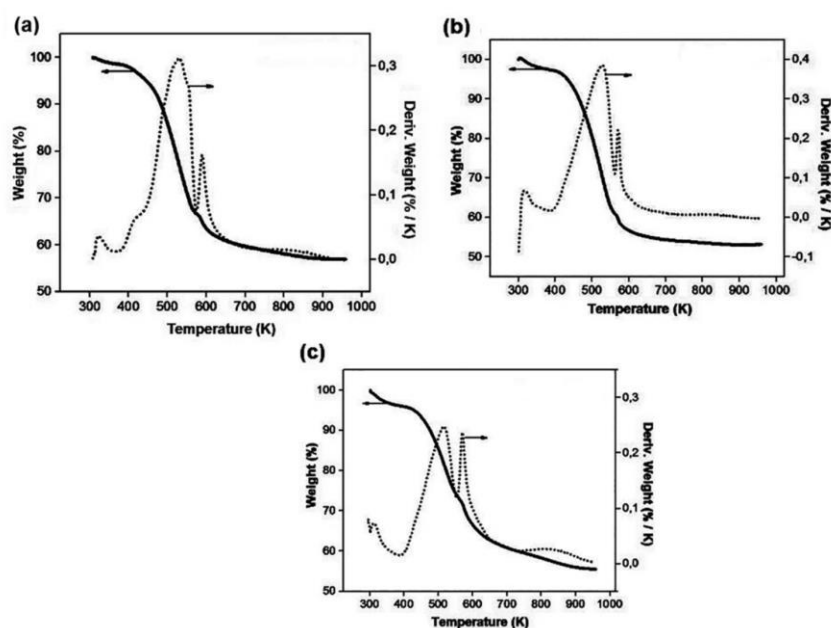


Graph no. 3.

Infrared spectra of the samples of (a) MCM-41, (b) Al-MCM-41(50), (c) Al-MCM-41(15).

In the present study, all peaks did not show significant change in their position with respect to temperature. However, their intensities decreased slightly with Al loading. The latter suggests that the variation of mass loss with respect to variation of temperature ($\%w/K$) is lowering for Al-containing solids than the ones for purely siliceous. These results are in agreement with those found in the literature. Thereby, according to Beck *et al.* (1992), the organic cations interact much stronger with the Al species than with SiO⁻ groups. Above the calcination temperature ($> 813 \text{ K}$), there was no significant weight loss, suggesting that the surfactant template

had been removed completely. The DTG curves of all samples showed a peak near 320 K that correspond to first stage of weight loss and two peaks at 530 and 585 K that correspond to second stage.



Graph no. 4.

TGA and DTG profiles as-synthesized of (a) MCM-41, (b) Al-MCM-41(50), (c) Al-MCM-41(15).

REFERENCES

- Beck, J. S., Vartuli, J. C., Roth, W. J., Leonowicz, M. E., Kresge, C. T., Schmitt, K. D., et al. (1992). A new family of mesoporous molecular sieves prepared with liquid crystal templates. *J. Am. Chem. Soc.* 114, 10834–10843. doi: 10.1021/ja00053a020
- Borade RB, Clearfield A. (1995). Synthesis of aluminum rich MCM-41. *Catalysis Letters*;31(2-3):267-272.
- Brahmi L, Ali-Dahmane T, Hamacha R, Hacini S. (2016). Catalytic Performance of Al-MCM-41 Catalyst for the Allylation of Aromatic Aldehydes with Allyltrimethylsilane: Comparison with TiCl_4 as Lewis acid. *Journal of Molecular Catalysis A: Chemical*;423:31-40.
- Chaudhary, V., and Sharma, S. (2016). An overview of ordered mesoporous material SBA-15: synthesis, functionalization and application in oxidation reactions. *J. Porous Mater.* 24, 741–749. doi: 10.1007/s10934-016-0311-z
- Chen H, Wang Y. (2002). Preparation of MCM-41 with high thermal stability and complementary textural porosity. *Ceramics International*;28(5):541-547.
- Chen, H.; Yang, H.; Xi, Y. (2019). Highly ordered and hexagonal mesoporous silica materials with large specific surface from natural rectorite mineral. *Microporous Mesoporous Mater.*, 279, 53–60.
- Davis, M. E. (2002). Ordered porous materials for emerging applications. *Nature* 417, 813–821. doi: 10.1038/nature00785

Dedeczek J, Sklenak S, Li C, Wichterlová B, Gábová V, Brus J, et al. (2009). Effect of Al-Si-Al and Al-Si-Si-Al Pairs in the ZSM-5 Zeolite Framework on the ²⁷Al NMR Spectra. A Combined High-Resolution ²⁷Al NMR and DFT/MM Study. *The Journal of Physical Chemistry C*;113(4):1447-1458.

Hoffmann, F.; Cornelius, M.; Morell, J.; Fröba, M. (2006). Silica-based mesoporous organic-inorganic hybrid materials. *Angew. Chemie Int. Ed.*, 45, 3216–3251.

Huo, Q.; Margolese, D.I.; Ciesla, U.; Feng, P.; Gier, T.E.; Sieger, P.; Leon, R.; Petroff, P.M.; Schüth, F.; Stucky, G.D. (1994). Generalized synthesis of periodic surfactant/inorganic composite materials. *Nature* 368, 317–321.

Kresge, C.T.; Leonowicz, M.E.; Roth, W.J.; Vartuli, J.C.; Beck, J.S. (1992). Ordered mesoporous molecular sieves synthesized by a liquid-crystal template mechanism. *Nature*, 359, 710–712.

Kurdyukov DA, Eurov DA, Kirilenko DA, Kukushkina JA, Sokolov VV, Yagovkina MA, et al. (2016) High-surface area spherical micro-mesoporous silica particles. *Microporous and Mesoporous Materials*;223:225-229

La-Salvia N, Lovón-Quintana JJ, Valença GP. (2015). Vapor-phase catalytic conversion of ethanol into 1,3-butadiene on Cr-Ba/ MCM-41 catalysts. *Brazilian Journal of Chemical Engineering*;32(2):489-500.

Luan Z, Cheng CF, Zhou W, Klinowsk J. (1995). Mesopore Molecular Sieve MCM-41 Containing Framework Aluminum. *The Journal of Physical Chemistry*;99(3):1018-1024.

Meynen, V.; Cool, P.; Vansant, E.F. (2009). Verified syntheses of mesoporous materials. *Microporous Mesoporous Mater.*, 125, 170–223

Reddy KM, Song C. (1996). Synthesis of mesoporous molecular sieves: influence of aluminum source on Al incorporation in MCM-41. *Catalysis Letters*;36(1-2):103-109.

Ryoo, R., Kim, J. M., Ko, C. H., and Shin, C. H. (1996). Disordered molecular sieve with branched mesoporous channel network. *J. Phys. Chem.* 100, 17718–17721. doi: 10.1021/jp9620835

Sayari A, Liu P, Kruk M, Jaroniec M. (1997). Characterization of Large- Pore MCM-41 Molecular Sieves Obtained via Hydrothermal Restructuring. *Chemistry of Materials*;9(11):2499-2506.

Sen, T., Tiddy, G. J. T., Casci, J. L., and Anderson, M. W. (2004). Synthesis and characterization of hierarchically ordered porous silica materials. *Chem. Mater.* 16, 2044–2054. doi: 10.1021/cm034946u

Vaschetto EG, Pecchi GA, Casuscelli SG, Eimer GA. (2014). Nature of the active sites in Al-MCM-41 nano-structured catalysts for the selective rearrangement of cyclohexanone oxime toward γ -caprolactam. *Microporous and Mesoporous Materials*;200:110-116.

Zhang, Z., Han, Y., Zhu, L., Wang, R., Yu, Y., Qiu, S., et al. (2001). Strongly acidic and high-temperature hydrothermally stable mesoporous aluminosilicates with ordered hexagonal structure. *Angew. Chem. Int. Ed. Engl.* 40, 1258–1262. doi: 10.1002/1521-3773(20010401)40:73.0.CO;2-C

Zhao, D., Feng, J., Huo, Q., Melosh, N., Fredrickson, G. H., Chmelka, B. F., et al. (1998). Triblock copolymer syntheses of mesoporous silica with periodic 50 to 300 angstrom pores. *Science* 279, 548–552. doi: 10.1126/science.279.5350.548

Natural Dyeing Cotton Fabric with Black Catechu and Quebracho Wood Dye Powder Using Different Mordant– Their Colour Fastness Test & FTIR Analysis

Dr (Ms) Swaroopa Rani N. Gupta

Professor, Department of Chemistry, Brijlal Biyani Science College, Amravati, Maharashtra, India

ARTICLE INFO

Article History:

Accepted : 01 Jan 2025

Published : 10 Jan 2025

Publication Issue :

Volume 12, Issue 7

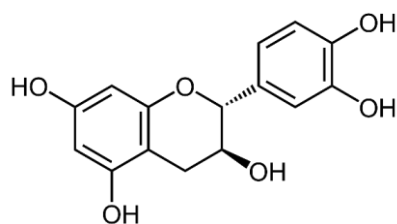
January-February-2025

Page Number :

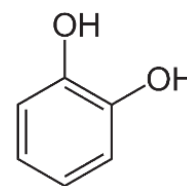
111-130

ABSTRACT

Catechu is an extract of acacia trees used variously as a food additive, astringent, tannin, and dye. It is extracted from several species of Acacia, but especially *Senegalia catechu*, by boiling the wood in water and evaporating the resulting brew. As an astringent it has been used since ancient times in Ayurvedic medicine as well as in breath-freshening spice mixtures. It is also an important ingredient in South Asian cooking paan mixtures. The catechu mixture is high in natural vegetable tannins (which accounts for its astringent effect), and may be used for the tanning of animal hides. Under the name *cutch*, it is a brown dye used for tanning and dyeing and for preserving fishing nets and sails. Cutch dye wool, silk, and cotton a yellowish-brown. Cutch gives gray-browns with an iron mordant and olive-browns with a copper mordant. The catechu extract gave its name to the catechin and catechol chemical families first derived from it.



Chemical structure of (+)-Catechin



Catechol

Quebracho is a common name in Spanish to describe very hard (density 0.9–1.3) wood tree species. Quebracho wood from *Schinopsis* spp is red-colored and very hard. Quebracho produces tannins that can be extracted in *quebracho sawmills* from the heartwood of both red (*Schinopsis lorentzii*) and white quebracho (*Aspidosperma quebracho-blanco*). Logs are inserted into planers to produce chips that are used to

produce the quebracho extract by boiling them in vats. It is used for fine leather tanning and imparts a red-brown color. Ordinary or warm soluble quebracho (also known as insoluble Quebracho) is the natural extract obtained directly from the quebracho wood. This type of extract is rich in condensed tannins of natural high molecular weight (phlobaphenes), which are not easily soluble. Its use is therefore limited to addition of small amounts during the process of tanning leather intended for shoe soles in hot liquids (temperature above 35 °C) to improve the yield and the water-proofness of the leather. The cold soluble extracts are obtained by subjecting the ordinary extract to a sulphiting process which transforms the phlobaphenes into completely soluble tannins. The cold soluble quebracho extracts are the most universally known and used types. The chemical structure of these extracts can be described as polymers of epicatechin. The main properties of these extracts are: a very rapid penetration, a high tannin content and a relatively low percentage of non-tannins. The rather low acid and medium salt content characterise them as mild tanning extracts (low astringency). Quebracho tannins give an important added value to the quality of leathers, such as vacchetta, belts and garments, making them more compact and tear resistant with a pleasant touch.

Present paper deals with natural dyeing cotton fabric mordanted with Alum, Alum and Cream of tartar, Copper sulphate and Cream of tartar, Ferrous sulphate and Cream of tartar, Potassium dichromate, Stannous chloride and Cream of tartar, Tannic acid using Black Catechu and Quebracho wood dye powder. This also includes their Colour Fastness test for Water Fastness and Light Fastness and FTIR analysis.

Keywords: Black Catechu, Quebracho, Alum, Cream of tartar, Copper sulphate, Ferrous sulphate, Potassium dichromate, Stannous chloride, Tannic acid, Colour Fastness Test, FTIR Analysis

I. INTRODUCTION

BLACK CATECHU

Catechu [1] is an extract of acacia trees used variously as a food additive, astringent, tannin, and dye. It is extracted from several species of Acacia, but especially Senegalia catechu (previously called Acacia catechu), by boiling the wood in water and evaporating the resulting brew. [2] It is also known as cutch, black cutch, cachou, cashoo, terra Japonica, or Japan earth, and also katha in Hindi, kaat in Marathi, khaira in Odia, khoyer in Assamese and Bengali, and kachu in Malay (hence the Latinized [3] *catechu* chosen as the Linnaean taxonomy name of the species of Acacia plant which provides the extract).



Catechu [4]



Acacia greggii thorns [5]



Senegalia catechu trunks [6]



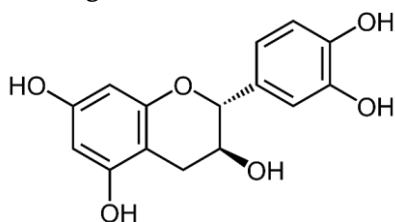
Senegalia catechu pods [7]



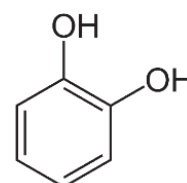
Senegalia catechu flowers [8]

As an astringent it has been used since ancient times in Ayurvedic medicine as well as in breath-freshening spice mixtures—for example in France and Italy it is used in some licorice pastilles. It is also an important ingredient in South Asian cooking paan mixtures, such as ready-made paan masala and gutka. The catechu mixture is high in natural vegetable tannins (which accounts for its astringent effect), and may be used for the tanning of animal hides.

Under the name *cutch*, it is a brown dye used for tanning and dyeing and for preserving fishing nets and sails. Cutch dye wool, silk, and cotton a yellowish-brown. Cutch gives gray-browns with an iron mordant and olive-browns with a copper mordant. [9] Black catechu has recently also been used by Blavod Drinks Ltd. to dye their vodka black. [10] White cutch, also known as gambier, gambeer, or gambir, which is extracted from Uncariagambir [11] has the same uses. Palm-catechu is extracted from the seeds of Areca catechu. [12] The catechu extract gave its name to the catechin and catechol chemical families first derived from it.



Chemical structure of (+)-Catechin



Catechol



SkymornPureOrganic Powdered Black-Catechu Natural Colorant|Natural dye for Fabric, Soap & Paper

QUEBRACHO

Quebracho is a common name in Spanish to describe very hard (density 0.9–1.3) wood tree species. The etymology of the name derived from quiebrahacha, or quebrarhacha, meaning "axe-breaker". The corresponding English-language term for such hardwoods is breakax or breakaxe.[13] Quebracho wood from *Schinopsis* spp is red-colored and very hard.[14] Other names for the wood are:[15]

- Quebracho chaqueño / Quebracho colorado / Quebracho macho / Quebracho moro / Quebracho negro / Quebracho santiagueño - Argentina
- Barauna / Brauna / Quebracho colorado / Quebracho hembra / Quebracho cornillo (*Schinopsis lorentzii*) / Quebracho fema (*S. balansae*) - Brazil
- Quebracho rubio / Soto negro - Paraguay



Quebracho colorado (*Schinopsis balansae*) wood [16]

Quebracho produces tannins that can be extracted in *quebracho sawmills* from the heartwood of both red (*Schinopsis lorentzii*) [17] and white quebracho (*Aspidosperma quebracho-blanco*). Logs are inserted into planers to produce chips that are used to produce the quebracho extract by boiling them in vats. [18] It is used for fine leather tanning and imparts a red-brown color. Ordinary or warm soluble quebracho (also known as insoluble Quebracho) is the natural extract obtained directly from the quebracho wood. This type of extract is rich in condensed tannins of natural high molecular weight (phlobaphenes), which are not easily soluble. Its use is therefore limited to addition of small amounts during the process of tanning leather intended for shoe soles in hot liquids (temperature above 35 °C) to improve the yield and the water-proofness of the leather. The cold soluble extracts are obtained by subjecting the ordinary extract to a sulphiting process which transforms the phlobaphenes into completely soluble tannins. [19] The cold soluble quebracho extracts are the most universally known and used types. The chemical structure of these extracts can be described as polymers

of epicatechin. [20] The main properties of these extracts are: a very rapid penetration, a high tannin content and a relatively low percentage of non-tannins. The rather low acid and medium salt content characterise them as mild tanning extracts (low astringency). Quebracho tannins give an important added value to the quality of leathers, such as vacchetta, belts and garments, making them more compact and tear resistant with a pleasant touch. The sulphited quebracho extract may be carcinogenous in mice. [21] Other recent studies show that quebracho tannins present a strong anti-mutagenic activity. [22] The heartwood contains from 20 to 30 percent tannin and 3 or 4 percent water-soluble nontannin. It is said to not ferment. [15]

According to King and White (1957), the hydrolysable tannins and gallic acid found in the sapwood constitute the raw material for the biosynthesis of the condensed tannins found in the heartwood. [23] Fustin (predominantly (-)-Fustin 66%), (-)-7:3':4'-trihydroxyflavan-3:4-diol ((-)-leuco-fisetinidin), (+)-catechin, gallic acid, fisetin and 2-benzyl-2-hydroxycoumaran-3-ones have been isolated from the heartwoods of *Schinopsisbalansae*, *Schinopsisquebrachocolorado* and from commercial quebracho extract. [24] Quebracho tannin is rich in profisetinidins and prorobinetidins. The expected masses found in mass spectrometry in negative mode in quebracho tannin are 289, 561, 833, 951, 1105, 1377, 1393, 1651 and 1667. In Quebracho colorado, the sugars and the lignins are thought to be covalently linked to the condensed tannins. [25] Quebracho tannin is also sold as an enological tannin. The quebracho tannins structure is very similar to that of grape tannins, making them a desirable alternative to consider comparatively because they are much less expensive to produce than grape tannins. [26] Myo-inositol and arabitol are detected in tannins from quebracho. [27] Researches are being made to develop an eco-friendly anti-biofouling paint from quebracho tannin. [28] The tannic acid, in the form of alkalized salts, was extensively used as a deflocculant in drilling muds in 1940s-1950s, until it was replaced with lignosulfonates. Its red color gave the mixture the name *red mud*. Quebracho tannin acts as flocculant agent to remove surfactant as sodium dodecylbenzenesulfonate in water treatment. [29] For its polyphenolic structure, quebracho tannin is widely studied for particle boards, plywood and fiber board gluing. [30] The Argentine companies Unitán and Silvateam are the main leaders in quebracho tannins production. [31]



SKYMORN Pure Organic Quebracho Dye Powder | Natural Colorant for Clothes, Jeans, Fabric Soap and Paper

Present paper deals with natural dyeing cotton fabric mordanted with Alum, Alum and Cream of tartar, Copper sulphate and Cream of tartar, Ferrous sulphate and Cream of tartar, Potassium dichromate, Stannous chloride and Cream of tartar, Tannic acid using Black Catechu and Quebracho wood dye powder. This also includes their Colour Fastness test for Water Fastness and Light Fastness and FTIR analysis.

II. METHODOLOGY

1. Natural dyeing cotton fabric with Black Catechu and Quebracho wooddye powder using different mordant

Step 1: Cleaning Cotton Fabric for dyeing - Cotton Fabric is soaked in water and detergent (1 % weight of fabric) and heated for 30 minutes. After cooling soaked cloth rinsed with cold water then excess water is squeezed out and fabric is dried. This helps dye to penetrate fabric better.

Step 2: Mordanting Cotton fabric

Mordanting Cotton Fabric with Alum - Alum (15 % weight of fabric) is dissolved in water. To it cleaned cotton fabric is soaked and heated for 1 hour. After cooling excess water is squeezed out and fabric is dried.

Mordanting Cotton Fabric with Alum and Cream of tartar - Alum (15 % weight of fabric) and Cream of tartar (10 % weight of fabric) is dissolved in water. To it cleaned cotton fabric is soaked and heated for 1 hour. After cooling excess water is squeezed out and fabric is dried.

Mordanting Cotton Fabric with Copper and Cream of tartar - Copper sulphate (15 % weight of fabric) and Cream of tartar (10 % weight of fabric) is dissolved in water. To it cleaned cotton fabric is soaked and heated for 1 hour. After cooling excess water is squeezed out and fabric is dried.

Mordanting Cotton Fabric with Iron and Cream of tartar - Ferrous sulphate (15 % weight of fabric) and Cream of tartar (10 % weight of fabric) is dissolved in water. To it cleaned cotton fabric is soaked and heated for 1 hour. After cooling excess water is squeezed out and fabric is dried.

Mordanting Cotton Fabric with Chrome - Potassium dichromate (15 % weight of fabric) is dissolved in water. To it cleaned cotton fabric is soaked and heated for 1 hour. After cooling excess water is squeezed out and fabric is dried.

Mordanting Cotton Fabric with Tin and Cream of tartar - Stannous chloride (15 % weight of fabric) and Cream of tartar (10 % weight of fabric) is dissolved in water. To it cleaned cotton fabric is soaked and heated for 1 hour. After cooling excess water is squeezed out and fabric is dried.

Mordanting Cotton Fabric with Tannic acid - Tannic acid (15 % weight of fabric) is dissolved in water. To it cleaned cotton fabric is soaked and heated for 1 hour. After cooling excess water is squeezed out and fabric is dried.

Step 3: Making Natural Dye using Black Catechu and Quebracho wooddye powder - Black Catechu and Quebracho wooddye powder is taken in separate Glass beakers to it water is added and boiled for 1 hour. Then kept overnight as it is and strained. Filtrate is used as dye bath.

Step 4: Dyeing Mordanted Cotton Fabric - Mordanted cotton fabric is kept in Dye bath and heated for 1 hour. Then it is removed from dye bath and rinsed with water and bit of detergent and dried.

Step 5: Dye Fixing - 10 gm sodium chloride was added to 500 ml water. Dyed fabric is dipped in sodium chloride solution for one hour and then fabric is washed with tap water and dried in the shade.

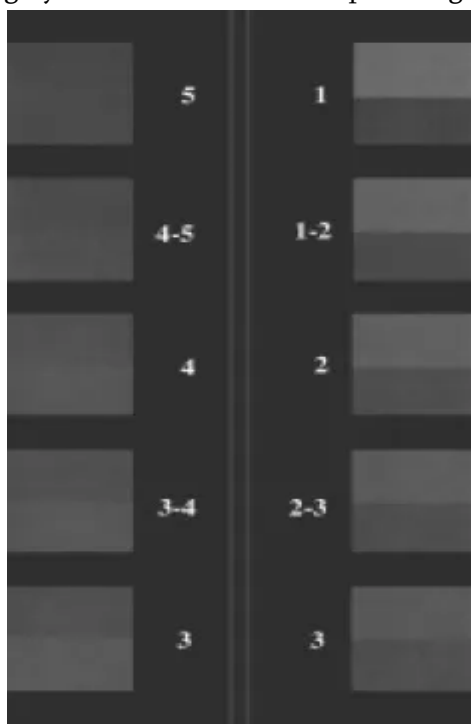
Step 6: Ironing Dyed Cotton Fabric - Dyed cotton fabric is ironed.

Step 7 :Measurment of colour - The obtained colours were measured and matched with the names of RAL Color Chart.

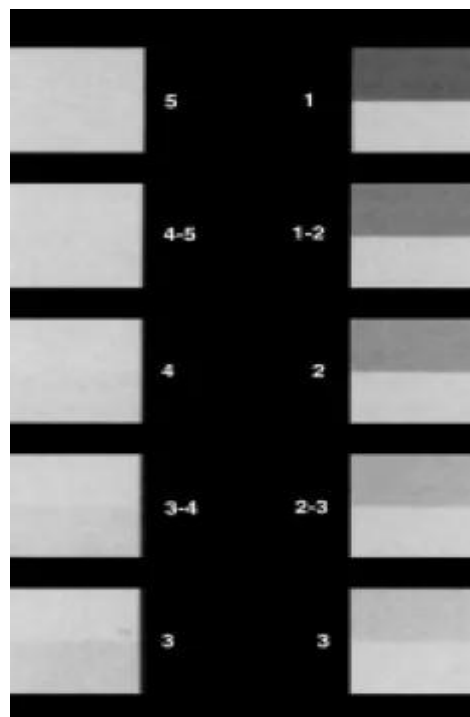
Step 8 :Colour fastness test - Then colour fastness test are performed.

2. Colour Fastness test for Water Fastness and Light Fastness to Black Catechu and Quebracho woodDyed Fabric

Gray Scales are used for assessing colour change and staining during colour fastness testing. Both scales are used for visual assessment to enable us to specify a rating from 1 to 5, with 5 being 'good' and 1 being 'poor'. The colour change gray scale consists of nine pairs of grey coloured chips, from grades 1 to 5 in accordance with ISO 105-A02 and A03. Grade 5 represents no change and grade 1 shows large change. The staining scale consists of nine pairs of grey and white coloured chips from grades 1 to 5.



Gray Scale for Color Change



Gray Scale for Color Staining

Water fastness and light fastness test was performed by regular washing and drying fabric in sunlight.

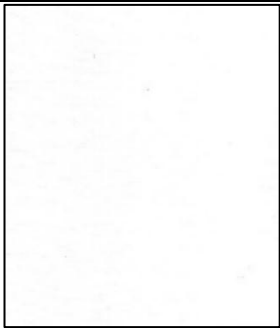
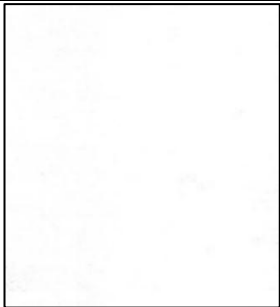
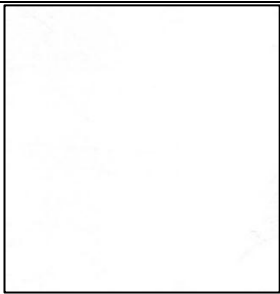

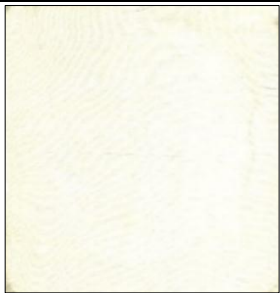
3. FTIR Analysis of Black Catechu and Quebracho wood Dye Extract


FTIR can be routinely used to identify the functional groups. FTIR spectra of Natural Dye made from Black Catechu and Quebracho wood dye powder are obtained at room temperature by using an FTIR Spectrophotometer - Shimadzu - IR Affinity – 1. The spectra is collected in range from 400 - 4500 cm⁻¹.





III.RESULTS AND DISCUSSION

1. Natural Dyeing Cotton Fabric using Black Catechu and Quebracho wood dye powder

Code No. – Cotton Fabric	Colour obtained on Cotton Fabric	Color Model RGB				Color Model LAB		
		Red	Green	Blue	Hex # & Color Description	l	a	b

Code No. – Cotton Fabric	Colour obtained on Cotton Fabric	Color Model RGB				Color Model LAB		
		Red	Green	Blue	Hex # & Color Description	l	a	b
00 - Cotton Fabric Not Mordanted and Not Dyed		243	243	243	#F3F3F3 White Smoke	95.84	0	0
0 C - Cotton Fabric Mordanted with Alum and Not Dyed		243	243	243	#F3F3F3 White Smoke	95.84	0	0
0 D - Cotton Fabric Mordanted with Alum and Cream of tartar and Not Dyed		243	243	243	#F3F3F3 White Smoke	95.84	0	0
0 E - Cotton Fabric Mordanted with Copper sulphate and Cream of tartar and Not Dyed		243	253	255	#F3FDFF Azure	98.64	-2.91	-2.09
0 F - Cotton Fabric Mordanted with Ferrous sulphate and Cream of tartar and Not Dyed		238	230	222	#EEE6DF White Chocolate	91.71	1.34	4.85

Code No. – Cotton Fabric	Colour obtained on Cotton Fabric	Color Model RGB				Color Model LAB		
		Red	Green	Blue	Hex # & Color Description	l	a	b
0 G - Cotton Fabric Mordanted with Potassium dichromate and Not Dyed		222	182	162	#DEB6A2 Pale Chestnut	77.04	11.48	15.61
0 H - Cotton Fabric Mordanted with Stannous chloride and Cream of tartar and Not Dyed		243	243	243	#F3F3F3 White Smoke	95.84	0	0
0 I - Cotton Fabric Mordanted with Tannic acid and Not Dyed		238	238	238	#EEEEEE Bright Gray	94.1	0	0
15 C - Cotton Fabric Mordanted with Alum and Dyed with Black Catechu		207	174	161	#CFAEA1 Eunry	73.62	9.95	11.13
15 D - Cotton Fabric Mordanted with Alum and Cream of tartar and Dyed with Black Catechu		231	212	209	#E7D4D1 Dust Storm	86.35	6.06	3.86

Code No. – Cotton Fabric	Colour obtained on Cotton Fabric	Color Model RGB				Color Model LAB		
		Red	Green	Blue	Hex # & Color Description	l	a	b
15 E - Cotton Fabric Mordanted with Copper sulphate and Cream of tartar and Dyed with Black Catechu		225	170	159	#E1AA9F Cashmere	74.36	18.64	13.52
15 F – Cotton Fabric Mordanted with Ferrous sulphate and Cream of tartar and Dyed with Black Catechu		187	163	193	#BBA3C1 London Hue	69.9	14.21	-12.14
15 G - Cotton Fabric Mordanted with Potassium dichromate and Dyed with Black Catechu		215	183	161	#D7B7A1 Cameo	76.61	8.15	15.46
15 H - Cotton Fabric Mordanted with Stannous chloride and Cream of tartar and Dyed with Black Catechu		223	203	195	#DFCBC3 Wafer	83.09	5.65	6.52

Code No. – Cotton Fabric	Colour obtained on Cotton Fabric	Color Model RGB				Color Model LAB		
		Red	Green	Blue	Hex # & Color Description	l	a	b
15 I - Cotton Fabric Mordanted with Tannic acid and Dyed with Black Catechu		228	203	190	#E4CBBE Bone	83.4	6.67	9.68
16 C - Cotton Fabric Mordanted with Alum and Dyed with Quebracho		197	127	105	#C57F69 Contessa	59.95	24.63	23.19
16 D - Cotton Fabric Mordanted with Alum and Cream of tartar and Dyed with Quebracho		206	150	128	#CE9680 My Pink	66.9	18.18	19.9
16 E - Cotton Fabric Mordanted with Copper sulphate and Cream of tartar and Dyed with Quebracho		171	95	93	#AB5F5D Matrix	49.05	30.57	14.81

Code No. – Cotton Fabric	Colour obtained on Cotton Fabric	Color Model RGB				Color Model LAB		
		Red	Green	Blue	Hex # & Color Description	l	a	b
16 F – Cotton Fabric Mordanted with Ferrous sulphate and Cream of tartar and Dyed with Quebracho		112	92	106	#705C6A Falcon	41.44	10.77	-4.91
16 G - Cotton Fabric Mordanted with Potassium dichromate and Dyed with Quebracho		184	126	122	#B87E7A Brandy Rose	58.53	21.98	11.3
16 H - Cotton Fabric Mordanted with Stannous chloride and Cream of tartar and Dyed with Quebracho		204	153	118	#CC9976 Antique Brass	67.22	14.6	25.81
16 I - Cotton Fabric Mordanted with Tannic acid and Dyed with Quebracho		211	147	127	#D3937F My Pink	66.71	21.67	20.29

2. Colour Fastness test for Water Fastness and Light Fastness to Black Catechu and Quebracho wood Dyed Fabric

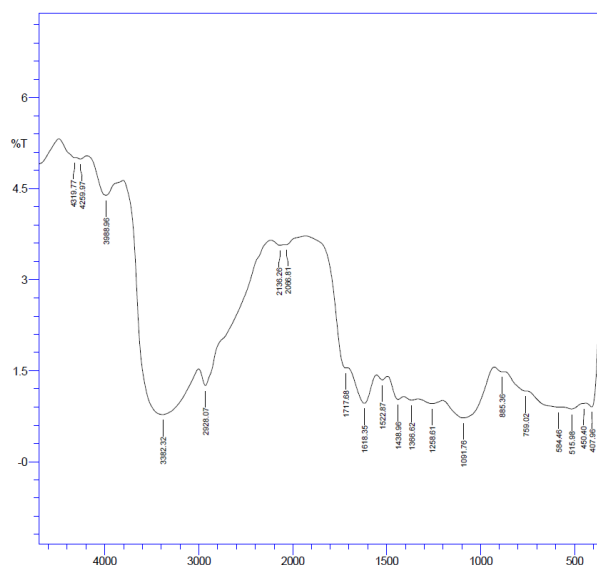
Code No. - Cotton Fabric	Colour Fastness Test	
	Water Fastness	Light Fastness
00 - Cotton Fabric Not Mordanted and Not Dyed	5	5
0 C - Cotton Fabric Mordanted with Alum and Not Dyed	5	5
0 D - Cotton Fabric Mordanted with Alum and Cream of tartar and Not Dyed	5	5
0 E - Cotton Fabric Mordanted with Copper sulphate and Cream of tartar and Not Dyed	5	5
0 F - Cotton Fabric Mordanted with Ferrous sulphate and Cream of tartar and Not Dyed	5	5
0 G - Cotton Fabric Mordanted with Potassium dichromate and Not Dyed	5	5
0 H - Cotton Fabric Mordanted with Stannous chloride and Cream of tartar and Not Dyed	5	5
0 I - Cotton Fabric Mordanted with Tannic acid and Not Dyed	5	5
15 C - Cotton Fabric Mordanted with Alum and Dyed with Black Catechu	4-5	4-5
15 D - Cotton Fabric Mordanted with Alum and Cream of tartar and Dyed with Black Catechu	4-5	4-5
15 E - Cotton Fabric Mordanted with Copper sulphate and Cream of tartar and Dyed with Black Catechu	4-5	4-5
15 F - Cotton Fabric Mordanted with Ferrous sulphate and Cream of tartar and Dyed with Black Catechu	4-5	4-5
15 G - Cotton Fabric Mordanted with Potassium dichromate and Dyed with Black Catechu	4-5	4-5
15 H - Cotton Fabric Mordanted with Stannous chloride and Cream of tartar and Dyed with Black Catechu	4-5	4-5
15 I - Cotton Fabric Mordanted with Tannic acid and Dyed with Black Catechu	4-5	4-5
16 C - Cotton Fabric Mordanted with Alum and Dyed with Quebracho	4-5	4-5
16 D - Cotton Fabric Mordanted with Alum and Cream of tartar and Dyed with Quebracho	4-5	4-5
16 E - Cotton Fabric Mordanted with Copper sulphate and Cream of tartar and Dyed with Quebracho	4-5	4-5
16 F - Cotton Fabric Mordanted with Ferrous sulphate and Cream of tartar and Dyed with Quebracho	4-5	4-5
16 G - Cotton Fabric Mordanted with Potassium dichromate and Dyed with Quebracho	4-5	4-5
16 H - Cotton Fabric Mordanted with Stannous chloride and Cream of tartar and Dyed with Quebracho	4-5	4-5
16 I - Cotton Fabric Mordanted with Tannic acid and Dyed with Quebracho	4-5	4-5

Colour fastness test for water fastness and light fastness to Black Catechu and Quebracho wood dye powder using different mordant dyed fabric shows 4-5 range in gray scale method which indicates excellent to water fastness and light fastness.

3. FTIR Analysis of Black Catechu and Quebracho woodDye Extract

FTIR spectra of Natural Dye made from Black Catechu

No.	Peak	Intensity	Corr. Inte	Base (H)	Base (L)	Area	Corr. Are
1	407.96	0.903	1.338	439.79	339.49	178.768	12.995
2	450.4	0.961	0	452.33	440.75	23.344	0.001
3	515.98	0.869	0.058	566.13	453.29	230.742	1.525
4	584.46	0.899	0.025	755.16	567.1	377.781	3.612
5	759.02	1.164	0.008	870.9	756.13	216.818	0.99
6	885.36	1.481	0.022	926.84	871.86	100.161	0.221
7	1091.76	0.719	0.51	1201.7	927.8	556.339	35.474
8	1258.61	0.956	0.062	1331.9	1202.67	259.208	1.846
9	1366.62	1.014	0.036	1408.1	1332.87	149.4	0.598
10	1438.96	1.026	0.163	1494.9	1409.06	166.667	2.652
11	1522.87	1.349	0.069	1553.73	1495.86	107.603	0.644
12	1618.35	0.961	0.515	1708.04	1554.69	293.855	13.514
13	1717.68	1.544	0.088	1930.83	1709	342.366	0.669
14	2066.81	3.579	0.021	2088.03	1931.79	224.692	0.161
15	2136.26	3.565	0.039	2232.7	2089	207.504	0.313
16	2928.07	1.254	0.474	3000.4	2233.66	1254.372	13.772
17	3382.32	0.776	2.229	3802.82	3001.37	1496.935	235.295
18	3988.96	4.393	0.438	4187.64	3803.79	511.944	6.921
19	4259.97	4.987	0.037	4306.27	4188.6	152.989	0.182
20	4319.77	5.012	0.023	4486.62	4307.23	231.325	0.481



FTIR spectra of Natural Dye made from Black Catechu

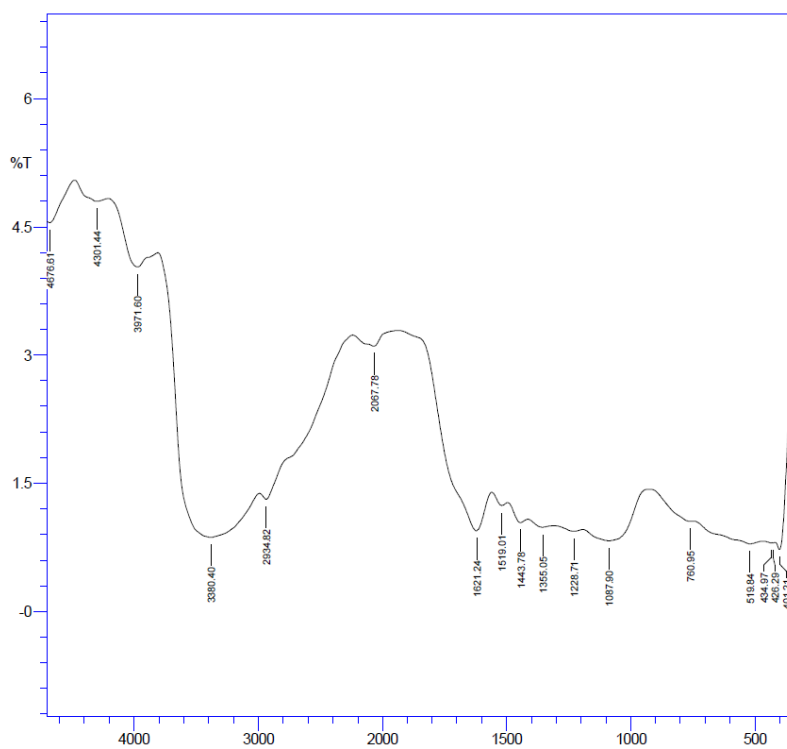
Interpretation of IR spectra of Natural Dye made from Black Catechuis done as follows

Spectra region wave number cm^{-1}	Intensity and Pattern of peak	Bond causing Absorption	Compound Class
407.96	Weak	-	-
450.4	Weak	-	-
515.98	Weak	-	-
584.46	Weak	-	-
759.02	Weak	-	-
885.36	Weak	-	-
1091.76	Weak	-	-
1258.61	Weak	-	-
1366.62	Weak	-	-
1438.96	Weak	-	-
1522.87	Weak	-	-
1618.35	Strong	C=C Stretching	α , β -unsaturated Ketone
1717.68	Strong	C=O Stretching	Aldehyde, α , β -unsaturated ester, Aliphatic ketone, Carboxylic acid
2066.81	Weak	-	-
2136.26	Weak	C \equiv C Stretching	Alkyne
2928.07	Medium	C-H Stretching	Alkane
3382.32	Strong, Broad	O-H Stretching	Alcohol
3988.96	Medium	-	-
4259.97	Weak	-	-
4319.77	Weak	-	-

FTIR spectra of Natural Dye made from Quebracho

No.	Peak	Intensity	Corr. Inte	Base (H)	Base (L)	Area	Corr. Are
1	401.21	0.7228	0.4725	415.68	347.2	128.9799	4.3665
2	426.29	0.8006	0.0049	430.14	420.5	20.2057	0.0137
3	434.97	0.8001	0.0058	468.72	431.11	78.6252	0.0346
4	519.84	0.7914	0.0738	746.48	469.69	569.0974	7.01
5	760.95	1.053	0.0308	923.94	747.45	338.446	1.5755
6	1087.9	0.8273	0.3156	1193.02	924.91	537.8845	20.3129
7	1228.71	0.9367	0.0346	1308.76	1193.99	231.364	0.8192
8	1355.05	0.9852	0.0503	1413.88	1309.72	207.7911	1.2183
9	1443.78	1.0403	0.1082	1494.9	1414.85	156.3062	1.6929
10	1519.01	1.2386	0.0791	1558.55	1495.86	118.4632	0.8766
11	1621.24	0.9442	0.7601	1936.61	1559.51	649.3356	27.6649
12	2067.78	3.1042	0.1616	2238.49	1937.58	450.5515	3.2525
13	2934.82	1.3123	0.2008	2987.86	2239.45	1255.295	6.9349
14	3380.4	0.8662	1.8623	3807.65	2988.83	1537.605	212.7889

15	3971.6	4.03	0.4265	4207.89	3808.61	545.3026	7.827
16	4301.44	4.8004	0.1056	4477.94	4208.86	353.3274	1.79
17	4676.61	4.55	0.0654	4700.73	4478.9	292.9921	0.5833



FTIR spectra of Natural Dye made from Quebracho

Interpretation of IR spectra of Natural Dye made from Quebracho is done as follows

Spectra region wave number cm ⁻¹	Intensity and Pattern of peak	Bond causing Absorption	Compound Class
401.21	Weak	-	-
426.29	Weak	-	-
434.97	Weak	-	-
519.84	Weak	-	-
760.95	Weak	-	-
1087.9	Weak	-	-
1228.71	Weak	-	-
1355.05	Weak	-	-
1443.78	Weak	-	-
1519.01	Weak	-	-
1621.24	Strong	C=C Stretching	α , β -unsaturated Ketone
2067.78	Weak	-	-
2934.82	Medium	C-H Stretching	Alkane
3380.4	Strong, Broad	O-H Stretching	Alcohol
3971.6	Medium	-	-

4301.44	Weak	-	-
4676.61	Weak	-	-

IV. CONCLUSION

Code No. - Cotton Fabric	Hex # & Color obtained	Colour Fastness Test	
		Water Fastness	Light Fastness
00 - Cotton Fabric Not Mordanted and Not Dyed	#F3F3F3, White Smoke	5	5
0 C - Cotton Fabric Mordanted with Alum and Not Dyed	#F3F3F3, White Smoke	5	5
0 D - Cotton Fabric Mordanted with Alum and Cream of tartar and Not Dyed	#F3F3F3, White Smoke	5	5
0 E - Cotton Fabric Mordanted with Copper sulphate and Cream of tartar and Not Dyed	#F3FDFF, Azure	5	5
0 F - Cotton Fabric Mordanted with Ferrous sulphate and Cream of tartar and Not Dyed	#EEE6DF, White Chocolate	5	5
0 G - Cotton Fabric Mordanted with Potassium dichromate and Not Dyed	#DEB6A2, Pale Chestnut	5	5
0 H - Cotton Fabric Mordanted with Stannous chloride and Cream of tartar and Not Dyed	#F3F3F3, White Smoke	5	5
0 I - Cotton Fabric Mordanted with Tannic acid and Not Dyed	#EEEEEE, Bright Gray	5	5
15 C - Cotton Fabric Mordanted with Alum and Dyed with Black Catechu	#CFAEA1, Eunry	4-5	4-5
15 D - Cotton Fabric Mordanted with Alum and Cream of tartar and Dyed with Black Catechu	#E7D4D1, Dust Storm	4-5	4-5
15 E - Cotton Fabric Mordanted with Copper sulphate and Cream of tartar and Dyed with Black Catechu	#E1AA9F, Cashmere	4-5	4-5
15 F - Cotton Fabric Mordanted with Ferrous sulphate and Cream of tartar and Dyed with Black Catechu	#BBA3C1, London Hue	4-5	4-5
15 G - Cotton Fabric Mordanted with Potassium dichromate and Dyed with Black Catechu	#D7B7A1, Cameo	4-5	4-5
15 H - Cotton Fabric Mordanted with Stannous chloride and Cream of tartar and Dyed with Black Catechu	#DFCBC3, Wafer	4-5	4-5
15 I - Cotton Fabric Mordanted with Tannic acid and Dyed with Black Catechu	#E4CBBE, Bone	4-5	4-5
16 C - Cotton Fabric Mordanted with Alum and Dyed with Quebracho	#C57F69, Contessa	4-5	4-5
16 D - Cotton Fabric Mordanted with Alum and Cream of tartar and Dyed with Quebracho	#CE9680, My Pink	4-5	4-5

Code No. - Cotton Fabric	Hex # & Color obtained	Colour Fastness Test	
		Water Fastness	Light Fastness
16 E - Cotton Fabric Mordanted with Copper sulphate and Cream of tartar and Dyed with Quebracho	#AB5F5D, Matrix	4-5	4-5
16 F – Cotton Fabric Mordanted with Ferrous sulphate and Cream of tartar and Dyed with Quebracho	#705C6A, Falcon	4-5	4-5
16 G - Cotton Fabric Mordanted with Potassium dichromate and Dyed with Quebracho	#B87E7A, Brandy Rose	4-5	4-5
16 H - Cotton Fabric Mordanted with Stannous chloride and Cream of tartar and Dyed with Quebracho	#CC9976, Antique Brass	4-5	4-5
16 I - Cotton Fabric Mordanted with Tannic acid and Dyed with Quebracho	#D3937F, My Pink	4-5	4-5

Interpretation of FTIR Spectra of Natural Dye made from Black Catechu and Quebracho wood dye powder shows presence of various functional groups such as

Bond causing Absorption	Compound Class	Bond causing Absorption	Compound Class
Natural Dye made from Black Catechu		Natural Dye made from and Quebracho	
C=C Stretching	α , β -unsaturated Ketone	C=C Stretching	α , β -unsaturated Ketone
C=O Stretching	Aldehyde, α , β -unsaturated ester, Aliphatic ketone, Carboxylic acid	C-H Stretching	Alkane
C \equiv C Stretching	Alkyne	O-H Stretching	Alcohol
C-H Stretching	Alkane		
O-H Stretching	Alcohol		

V. REFERENCES

- [1]. "catechu". Oxford English Dictionary (Online ed.). Oxford University Press. (Subscription or participating institution membership required.)
- [2]. Cutch and catechu plant origin Archived 2019-02-10 at the Wayback Machine from the Food and Agriculture Department of the United Nations. Document repository accessed November 5, 2011
- [3]. Derivation of word from Malay
- [4]. <https://upload.wikimedia.org/wikipedia/commons/f/fd/Catechu.jpg>
- [5]. https://en.wikipedia.org/wiki/Acacia_sensu_lato#/media/File:Acacia_greggii_thorns.jpg
- [6]. [https://en.wikipedia.org/wiki/Senegalia_catechu#/media/File:Khair_\(Acacia_catechu\)_trunk_at_Hyderabad,_AP_W_IMG_7264.jpg](https://en.wikipedia.org/wiki/Senegalia_catechu#/media/File:Khair_(Acacia_catechu)_trunk_at_Hyderabad,_AP_W_IMG_7264.jpg)
- [7]. [https://en.wikipedia.org/wiki/Senegalia_catechu#/media/File:Khair_\(Acacia_catechu\)_leaves_&_fruits_at_Hyderabad,_AP_W_IMG_7263.jpg](https://en.wikipedia.org/wiki/Senegalia_catechu#/media/File:Khair_(Acacia_catechu)_leaves_&_fruits_at_Hyderabad,_AP_W_IMG_7263.jpg)

- [8]. [https://en.wikipedia.org/wiki/Senegalia_catechu#/media/File:Khair_\(Acacia_catechu\)_flowers_at_Hyderabad,_AP_W_IMG_7261.jpg](https://en.wikipedia.org/wiki/Senegalia_catechu#/media/File:Khair_(Acacia_catechu)_flowers_at_Hyderabad,_AP_W_IMG_7261.jpg)
- [9]. Goodwin, Jill (1982). *A Dyer's Manual*. London: Pelham Books Ltd. p. 60. ISBN 978-0-7207-1327-5.
- [10]. Valli Herman (29 October 2003). "They drink this stuff?". *LA Times*. Retrieved 11 March 2019. See this reference for the use of the dye in vodka
- [11]. *Tanning, Dye & Processing Materials*
- [12]. Buchheister G.A.: *Handbuch der Drogisten-Praxis*. Zweite Auflage, Springer, 1891, p. 322, Catechu at the Internet Archive.
- [13]. "breakax". Dictionary by Merriam-Webster. Retrieved 16 March 2023.
- [14]. "Quebracho". Woodfinder. Jump up to: a b c d e f Kryn, Jeannette M. (1954). "Information leaflet foreign woods" (PDF).
- [15]. https://en.wikipedia.org/wiki/Quebracho_tree#/media/File:Quebracho_colorado_wood.jpg
- [16]. Kirby, KS; White, T (1955). "Minor constituents of Quebracho tannin extract". *The Biochemical Journal*. 60 (4): 582–90. doi:10.1042/bj0600582. PMC 1216156. PMID 13249952.
- [17]. Quebracho on factopia.com
- [18]. Improvements in the manufacture and production of readily soluble tanning extracts and agents. Patent specification. Johnsons & Willcox, 1921.
- [19]. Pasch, H.; Pizzi, A.; Rode, K. (2001). "MALDI-TOF mass spectrometry of polyflavonoid tannins". *Polymer*. 42 (18): 7531–7539. doi:10.1016/S0032-3861(01)00216-6.
- [20]. Kirby, KS (1960). "Induction of tumours by tannin extracts". *British Journal of Cancer*. 14 (1): 147–50. doi:10.1038/bjc.1960.17. PMC 2074141. PMID 14409278.
- [21]. Marín-Martínez, Raúl; Veloz-García, Rafael; Veloz-Rodríguez, Rafael; Guzmán-Maldonado, Salvador H.; Loarca-Pina, Guadalupe; Cardador-Martínez, Anabertha; Guevara-Olvera, Lorenzo; Miranda-López, Rita; et al. (2009). "Antimutagenic and antioxidant activities of quebracho phenolics (*Schinopsis balansae*) recovered from tannery wastewaters". *Bioresource Technology*. 100 (1): 434–9. doi:10.1016/j.biortech.2008.05.029. PMID 18614361.
- [22]. Streit, Werner; Fengel, Dietrich (1994). "On the Changes of the Extractive Composition During Heartwood Formation in Quebracho colorado (*Schinopsis balansae* Engl.)". *Holzforschung*. 48: 15–20. doi:10.1515/hfsg.1994.48.s1.15. S2CID 97838928.
- [23]. Roux, DG; Evelyn, SR (1958). "Condensed tannins. 2. Biogenesis of condensed tannins based on leucoanthocyanins". *The Biochemical Journal*. 70 (2): 344–9. doi:10.1042/bj0700344. PMC 1196676. PMID 16748787.
- [24]. Streit, W.; Fengel, D. (1994). "Purified tannins from quebracho colorado". *Phytochemistry*. 36 (2): 481–4. Bibcode:1994PChem..36..481S. doi:10.1016/S0031-9422(00)97100-0.
- [25]. Enological Tannins and Their Use in Wine on www.vinquiry.com[unreliable source?] Archived October 29, 2013, at the Wayback Machine
- [26]. Sanz, M. Luz; Martínez-Castro, Isabel; Moreno-Arribas, M. Victoria (2008). "Identification of the origin of commercial enological tannins by the analysis of monosaccharides and polyalcohols". *Food Chemistry*. 111 (3): 778–783. doi:10.1016/j.foodchem.2008.04.050.
- [27]. Pérez, Miriam; García, Mónica; Blustein, Guillermo; Stupak, Mirta (2007). "Tannin and tannate from the quebracho tree: An eco-friendly alternative for controlling marine biofouling". *Biofouling*. 23 (3): 151–159. Bibcode:2007Biofo..23..151P. doi:10.1080/08927010701189484. hdl:11336/95483. PMID 17653926. S2CID 29869562.

- [28]. Beltrán-Heredia, J.; Sánchez-Martín, J.; Frutos-Blanco, G. (2009). "Schinopsisbalansae tannin-based flocculant in removing sodium dodecyl benzene sulfonate". *Separation and Purification Technology*. 67 (3): 295–303. doi:10.1016/j.seppur.2009.03.039.
- [29]. Pizzi, A.; Mittal, K. L., eds. (2003). *Handbook of adhesive technology* (2nd ed.). Taylor & Francis. pp. 273–87. ISBN 978-0-8247-0986-0.
- [30]. Information on quebracho tannins on Argentine company Unitan's website Archived July 24, 2011, at the Wayback Machine

Natural Dyeing Cotton Fabric with Annatto Seed and Heena Leaf Dye Powder Using Different Mordant- Their Colour Fastness Test & FTIR Analysis

Dr (Ms) Swaroopa Rani N. Gupta

Professor, Department of Chemistry, Brijlal Biyani Science College, Amravati, Maharashtra, India

ARTICLE INFO

Article History:

Accepted : 01 Jan 2025

Published : 10 Jan 2025

Publication Issue :

Volume 12, Issue 7

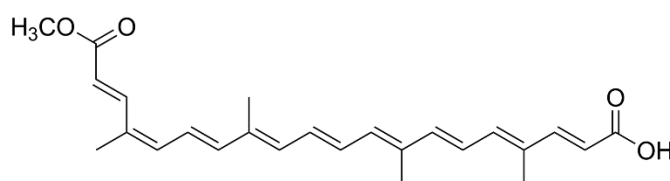
January-February-2025

Page Number :

131-150

ABSTRACT

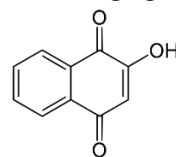
Annatto is an orange-red condiment and food coloring derived from the seeds of the achiote tree (*Bixa orellana*), native to tropical parts of the Americas. It is often used to impart a yellow to red-orange color to foods, but sometimes also for its flavor and aroma. The color of annatto comes from various carotenoid pigments, mainly bixin and norbixin, found in the reddish waxy coating of the seeds. The condiment is typically prepared by grinding the seeds to a powder or paste. Similar effects can be obtained by extracting some of the color and flavor principles from the seeds with hot water, oil, or lard, which are then added to the food. The fat-soluble color in the crude extract is called bixin, which can then be saponified into water-soluble norbixin. This dual solubility property of annatto is rare for carotenoids. The seeds contain 4.5–5.5% pigment, which consists of 70–80% bixin. The more norbixin in an annatto preparation, the more yellow it is; a higher level of bixin gives it a more orange hue.



Bixin, the major apocarotenoid of annatto

Lawson (2-hydroxy-1,4-naphthoquinone), also known as hennotannic acid, is a red-orange dye present in the leaves of the henna plant (*Lawsonia inermis*). Humans have used henna extracts containing lawson as hair and skin dyes for more than 5,000 years. Lawson reacts chemically with the protein keratin in skin and hair via a Michael addition reaction, resulting in a strong permanent stain that lasts until the skin or hair is shed. Darker

colored staining is due to more lawsone–keratin interactions occurring, which evidently break down as the concentration of lawsone decreases and the tattoo fades. Lawsone strongly absorbs UV light, and aqueous extracts can be effective sunless tanning agents and sunscreens.



Lawsone

Present paper deals with natural dyeing cotton fabric mordanted with Alum, Alum and Cream of tartar, Copper sulphate and Cream of tartar, Ferrous sulphate and Cream of tartar, Potassium dichromate, Stannous chloride and Cream of tartar, Tannic acid using Annatto seed and Heena leaf dye powder. This also includes their Colour Fastness test for Water Fastness and Light Fastness and FTIR analysis.

Keywords: Annatto, Heena, Alum, Cream of tartar, Copper sulphate, Ferrous sulphate, Potassium dichromate, Stannous chloride, Tannic acid, Colour Fastness Test, FTIR Analysis

I. INTRODUCTION

Annatto is an orange-red condiment and food coloring derived from the seeds of the achiote tree (*Bixa orellana*), native to tropical parts of the Americas.[1] It is often used to impart a yellow to red-orange color to foods, but sometimes also for its flavor and aroma.

The color of annatto comes from various carotenoid pigments, mainly bixin and norbixin, found in the reddish waxy coating of the seeds. The condiment is typically prepared by grinding the seeds to a powder or paste. Similar effects can be obtained by extracting some of the color and flavor principles from the seeds with hot water, oil, or lard, which are then added to the food.[2]

Annatto and its extracts are now widely used in an artisanal or industrial scale as a coloring agent in many processed food products, such as cheeses, dairy spreads, butter and margarine, custards, cakes and other baked goods, potatoes, snack foods, breakfast cereals, smoked fish, sausages, and more. In these uses, annatto is a natural alternative to synthetic food coloring compounds, but it has been linked to rare cases of food-related allergies. [3] Annatto is of particular commercial value in the United States because the Food and Drug Administration considers colorants derived from it to be "exempt of certification".



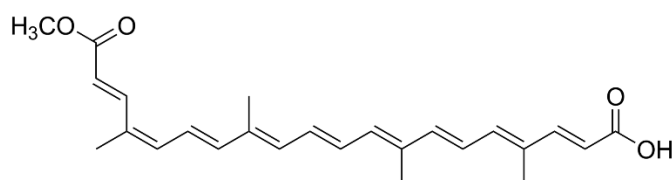
Open fruit of the achiote tree (*Bixa orellana*), showing the seeds from which annatto is extracted. [4]

Industrial food coloring

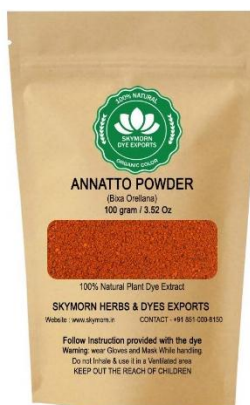
Annatto is commonly used to impart a yellow or orange color to many industrialized and semi-industrialized foods, including cheese, ice cream, bakery products, desserts, fruit fillings, yogurt, butter, oils, margarines, processed cheese, and fat-based products.[5] In the United States, annatto extract is listed as a color additive "exempt from certification"[6] and is informally considered to be a natural coloring. Foods colored with annatto may declare the coloring in the statement of ingredients as "colored with annatto" or "annatto color".[7] In the European Union, it is identified by the E number E160b.

Chemical composition

The yellow to orange color is produced by the chemical compounds bixin and norbixin, which are classified as carotenoids. The fat-soluble color in the crude extract is called bixin, which can then be saponified into water-soluble norbixin. This dual solubility property of annatto is rare for carotenoids.[8] The seeds contain 4.5–5.5% pigment, which consists of 70–80% bixin.[9] Unlike beta-carotene, another well-known carotenoid, annatto-based pigments are not vitamin A precursors.[10] The more norbixin in an annatto preparation, the more yellow it is; a higher level of bixin gives it a more orange hue.



Bixin, the major apocarotenoid of annatto[9]



SkymornPureOrganic Powdered Annatto Natural Colorant|Natural dye for Fabric, Soap & Paper

HEENA

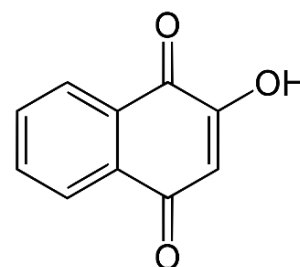
Lawsone (2-hydroxy-1,4-naphthoquinone), also known as hennotannic acid, is a red-orange dye present in the leaves of the henna plant (*Lawsonia inermis*), for which it is named, as well as in the common walnut (*Juglans regia*) [11] and water hyacinth (*Pontederia crassipes*). [12] Humans have used henna extracts containing lawsone as hair and skin dyes for more than 5,000 years. Lawsone reacts chemically with the protein keratin in skin and hair via a Michael addition reaction, resulting in a strong permanent stain that lasts until the skin or hair is shed. Darker colored staining is due to more lawsone–keratin interactions occurring, which evidently break down as the concentration of lawsone decreases and the tattoo fades. [13] Lawsone strongly absorbs UV light, and aqueous extracts can be effective sunless tanning agents and sunscreens. Lawsone is a 1,4-naphthoquinone derivative, an analog of hydroxyquinone containing one additional ring.



Heena Plant



Heena Flower



Lawsone

Lawsone isolation from *Lawsonia inermis* can be difficult due to its easily biodegradable nature. Isolation involves four steps:

1. extraction with an extraction solution, usually NaOH
2. column filtration using a macroporous adsorption resin
3. a rinse with ethanol to remove impurities, and finally
4. freeze the product to isolate the lawsone powder, usually a yellow colored dust. [14]

During the rinse, the lawsone will be the bottom as it has such a high density and the chlorophyll molecules will all be on the top of the mixture. [15]

Lawsone is hypothesized to undergo a reaction similar to Strecker synthesis in reactions with amino acids. Recent research has been conducted on lawsone's potential applications in the forensic science field. Since lawsone shows many similarities with ninhydrin, the current reagent for latent fingerprint development, studies have been conducted to see if lawsone can be used in this field. As of now the research is inconclusive, but optimistic. Lawsone non-specifically targets primary amino acids, and displays photoluminescence with forensic light sources. [16] It has a characteristic purple/brown coloration as opposed to the purple/blue associated with ninhydrin. [17] Lawsone shows promise as a reagent for fingerprint detection because of its photoluminescence maximized at 640 nm, which is high enough that it avoids background interference common for ninhydrin. [18]

The natural dye henna usually being recognized as lawsone is a red-orange pigment that has long been used for the coloration of skin and hair as well as textile materials. This natural colorant garners the attention of researchers throughout the globe for the coloration of textile materials due to the fact that its color can easily be harmonized with nature besides its slight chemical reactivity without posing any environmental problems. So, a large number of studies were carried out on both extraction and application of henna dye in textile fibers along with the standardization and simplification of dyeing techniques. The contemporary research

works on henna dye highlighting the general characteristics alongside its chemical composition and chromatic properties has been focussed. A greater emphasis is also placed on the dyeing chemistry of the natural dye henna as well as its applications in the dyeing of cellulosic, protein and synthetic textile fibers including the effects of different mordants and mordanting methods on the dye uptake. Moreover, the scope of improvement in terms of dyeability and overall colorfastness properties through chemical modification of textile fibers has also been mentioned. [19]

The demand of natural colorants for the dyeing of textile fibers has been increasing gradually in recent years due to a growing global ecological awareness as well as a greater emphasis on a cleaner and greener production process. The eco-friendly dyeing of polyester fiber with natural dye henna is a novel approach that has extensively been studied. The dyeing of polyester fiber with henna dye was conducted at different temperatures without using hazardous metallic mordants. Then the dyeing performance was investigated in terms of depth of shade measurement, analysis of colorimetric properties of color and assessment of color fastness properties of henna dyed polyester fabric samples. The amount of dye absorption by fiber and the resulting depth of shade were found to increase with increasing dyeing temperature. In case of colorfastness properties, all dyed substrates demonstrated excellent fastness ratings against washing, rubbing and perspiration with little to no deterioration of color. The detailed morphological study revealed that surface structure of fiber remained unchanged after dyeing at an elevated temperature and pressure.[20]

Medicinal plants are a valuable source of supplementary remedies for the treatment of various ailments. *Lawsonia inermis* (belongs to family *Lythraceae*) or commonly known as Henna is a glabrous and branching small tree that is indigenous to the subtropical regions of Asia and North Africa. It has traditionally been used as a dandruff-fighting and antifungal agent when applied to the hair, hands, and feet. The staining properties of Henna are derived from the lawsone content, which is found primarily in the leaves. Review is to be conducted to a literature search and critically review the relevant published articles on the phytochemical and pharmacological activities of *L. inermis*. The phytochemical screening reported that naphthoquinone derivatives, Henna essential oil, flavonoids, tannins, phenols, quinones, alkaloids, glycosides and saponins can be isolated from various parts of the Henna tree. The selection of appropriate solvents is critical in phytochemical screening, as different solvents resulted in different extraction yields. The pharmacological activities found in Henna are ameliorative activity, alleviating wound healing process, antifungal, antioxidant, antibacterial, hepatoprotective, nootropic, anti-ulcer, anti-inflammatory and anti-cancer activity. Phytochemical screening is critical for identification of plants constituents, and Henna possesses wide range of pharmacological properties. [21]



Skymorn Henna powder

Present paper deals with natural dyeing cotton fabric mordanted with Alum, Alum and Cream of tartar, Copper sulphate and Cream of tartar, Ferrous sulphate and Cream of tartar, Potassium dichromate, Stannous chloride and Cream of tartar, Tannic acid using Annatto seed and Heena leaf dye powder. This also includes their Colour Fastness test for Water Fastness and Light Fastness and FTIR analysis.

II. METHODOLOGY

1. Natural dyeing cotton fabric with Annatto seed and Heena leaf dye powder using different mordant

Step 1: Cleaning Cotton Fabric for dyeing - Cotton Fabric is soaked in water and detergent (1 % weight of fabric) and heated for 30 minutes. After cooling soaked cloth rinsed with cold water then excess water is squeezed out and fabric is dried. This helps dye to penetrate fabric better.

Step 2: Mordanting Cotton fabric

Mordanting Cotton Fabric with Alum - Alum (15 % weight of fabric) is dissolved in water. To it cleaned cotton fabric is soaked and heated for 1 hour. After cooling excess water is squeezed out and fabric is dried.

Mordanting Cotton Fabric with Alum and Cream of tartar - Alum (15 % weight of fabric) and Cream of tartar (10 % weight of fabric) is dissolved in water. To it cleaned cotton fabric is soaked and heated for 1 hour. After cooling excess water is squeezed out and fabric is dried.

Mordanting Cotton Fabric with Copper and Cream of tartar - Copper sulphate (15 % weight of fabric) and Cream of tartar (10 % weight of fabric) is dissolved in water. To it cleaned cotton fabric is soaked and heated for 1 hour. After cooling excess water is squeezed out and fabric is dried.

Mordanting Cotton Fabric with Iron and Cream of tartar - Ferrous sulphate (15 % weight of fabric) and Cream of tartar (10 % weight of fabric) is dissolved in water. To it cleaned cotton fabric is soaked and heated for 1 hour. After cooling excess water is squeezed out and fabric is dried.

Mordanting Cotton Fabric with Chrome - Potassium dichromate (15 % weight of fabric) is dissolved in water. To it cleaned cotton fabric is soaked and heated for 1 hour. After cooling excess water is squeezed out and fabric is dried.

Mordanting Cotton Fabric with Tin and Cream of tartar - Stannous chloride (15 % weight of fabric) and Cream of tartar (10 % weight of fabric) is dissolved in water. To it cleaned cotton fabric is soaked and heated for 1 hour. After cooling excess water is squeezed out and fabric is dried.

Mordanting Cotton Fabric with Tannic acid - Tannic acid (15 % weight of fabric) is dissolved in water. To it cleaned cotton fabric is soaked and heated for 1 hour. After cooling excess water is squeezed out and fabric is dried.

Step 3: Making Natural Dye

Making Natural Dye using Annatto seed and Heena leaf dye powder - 5 % weight of fabric Annatto seed and Heena leaf dye powder is taken in separate Glass beakers to it water is added and boiled for 1 hour. Then kept overnight as it is and strained. Filtrate is used as dye bath.

Step 4: Dyeing Mordanted Cotton Fabric - Mordanted cotton fabric is kept in Dye bath and heated for 1 hour. Then it is removed from dye bath and rinsed with water and bit of detergent and dried.

Step 5: Dye Fixing –10 gm sodium chloride was added to 500 ml water. Dyed fabric is dipped in sodium chloride solution for one hour and then fabric is washed with tap water and dried in the shade.

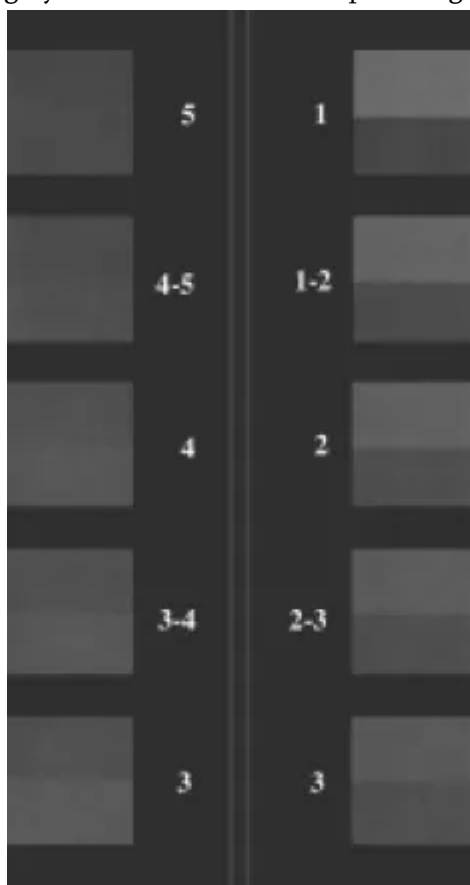
Step 6: Ironing Dyed Cotton Fabric – Dyed cotton fabric is ironed.

Step 7 : Measurment of colour - The obtained colours were measured and matched with the names of RAL Color Chart.

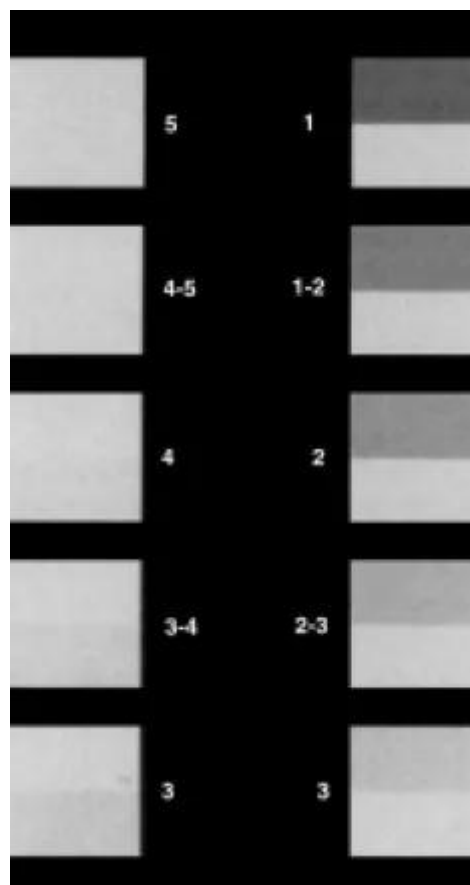
Step 8 : Colour fastness test - Then colour fastness test are performed.

2. Colour Fastness test for Water Fastness and Light Fastness to Annatto seed and Heena leaf Dyed Fabric

Gray Scales are used for assessing colour change and staining during colour fastness testing. Both scales are used for visual assessment to enable us to specify a rating from 1 to 5, with 5 being 'good' and 1 being 'poor'. The colour change gray scale consists of nine pairs of grey coloured chips, from grades 1 to 5 in accordance with ISO 105-A02 and A03. Grade 5 represents no change and grade 1 shows large change. The staining scale consists of nine pairs of grey and white coloured chips from grades 1 to 5.



Gray Scale for Color Change



Gray Scale for Color Staining

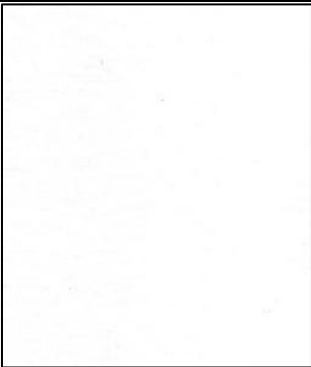
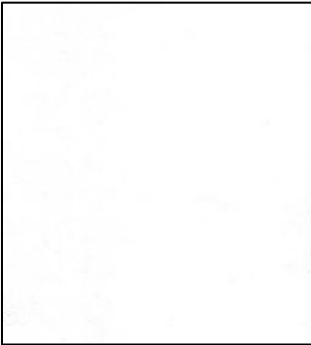
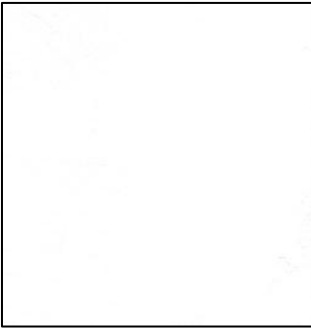
Water fastness and light fastness test was performed by regular washing and drying fabric in sunlight.



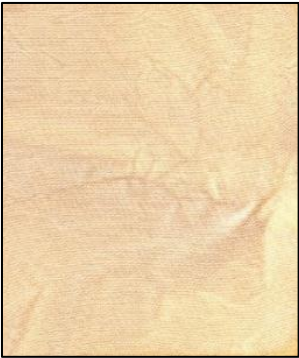
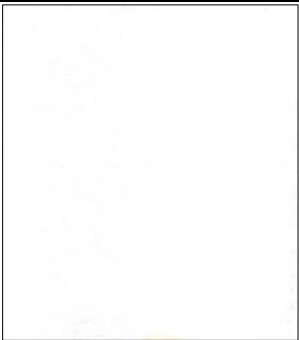

3. FTIR Analysis of Annatto seed and Heena leaf Dye Extract


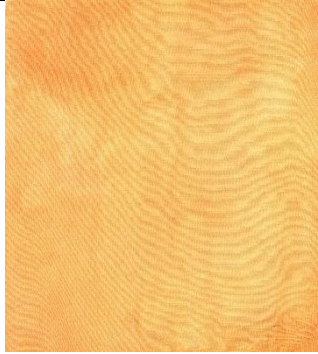


FTIR can be routinely used to identify the functional groups. FTIR spectra of Natural Dye made from Annatto seed and Heena leaf dye powder are obtained at room temperature by using an FTIR Spectrophotometer - Shimadzu - IR Affinity – 1. The spectra is collected in range from 400 - 4500 cm⁻¹.





III.RESULTS AND DISCUSSION



1. Natural Dyeing Cotton Fabric using Annatto seed and Heena leaf dye powder



Code No. – Cotton Fabric	Colour obtained on Cotton Fabric	Color Model RGB				Color Model LAB		
		Red	Green	Blue	Hex # & Color Description	l	a	b
00 - Cotton Fabric Not Mordanted and Not Dyed		243	243	243	#F3F3F3 White Smoke	95.84	0	0
0 C - Cotton Fabric Mordanted with Alum and Not Dyed		243	243	243	#F3F3F3 White Smoke	95.84	0	0
0 D - Cotton Fabric Mordanted with Alum and Cream of tartar and Not Dyed		243	243	243	#F3F3F3 White Smoke	95.84	0	0

Code No. – Cotton Fabric	Colour obtained on Cotton Fabric	Color Model RGB				Color Model LAB		
		Red	Green	Blue	Hex # & Color Description	l	a	b
0 E - Cotton Fabric Mordanted with Copper sulphate and Cream of tartar and Not Dyed		243	253	255	#F3FDFF Azure	98.64	-2.91	-2.09
0 F - Cotton Fabric Mordanted with Ferrous sulphate and Cream of tartar and Not Dyed		238	230	222	#EEE6DF White Chocolate	91.71	1.34	4.85
0 G - Cotton Fabric Mordanted with Potassium dichromate and Not Dyed		222	182	162	#DEB6A2 Pale Chestnut	77.04	11.48	15.61
0 H - Cotton Fabric Mordanted with Stannous chloride and Cream of tartar and Not Dyed		243	243	243	#F3F3F3 White Smoke	95.84	0	0
0 I - Cotton Fabric Mordanted with Tannic acid and Not Dyed		238	238	238	#EEEEEE Bright Gray	94.1	0	0

Code No. – Cotton Fabric	Colour obtained on Cotton Fabric	Color Model RGB				Color Model LAB		
		Red	Green	Blue	Hex # & Color Description	l	a	b
17 C - Cotton Fabric Mordanted with Alum and Dyed with Annatto		247	218	136	#F7DA88 Khaki	87.82	-0.59	43.92
17 D - Cotton Fabric Mordanted with Alum and Cream of tartar and Dyed with Annatto		246	192	108	#F6C06C Sandybrown	80.95	10	49.24
17 E - Cotton Fabric Mordanted with Copper sulphate and Cream of tartar and Dyed with Annatto		240	150	81	#F09651 Sandybrown	70.13	27.83	49.67
17 F – Cotton Fabric Mordanted with Ferrous sulphate and Cream of tartar and Dyed with Annatto		245	175	100	#F5AF64 Sandybrown	76.68	17.92	48.05

Code No. – Cotton Fabric	Colour obtained on Cotton Fabric	Color Model RGB				Color Model LAB		
		Red	Green	Blue	Hex # & Color Description	l	a	b
17 G - Cotton Fabric Mordanted with Potassium dichromate and Dyed with Annatto		245	182	105	#F5B669 Sandybrown	78.4	14.6	47.64
17 H - Cotton Fabric Mordanted with Stannous chloride and Cream of tartar and Dyed with Annatto		246	171	102	#F6AB66 Sandybrown	75.87	20.57	46.13
17 I - Cotton Fabric Mordanted with Tannic acid and Dyed with Annatto		241	172	96	#F1AC60 Sandybrown	75.49	17.58	48.51
18 C - Cotton Fabric Mordanted with Alum and Dyed with Heena		215	202	164	#D7CAA4 Wheat	81.49	-1.45	20.64

Code No. – Cotton Fabric	Colour obtained on Cotton Fabric	Color Model RGB				Color Model LAB		
		Red	Green	Blue	Hex # & Color Description	l	a	b
18 D - Cotton Fabric Mordanted with Alum and Cream of tartar and Dyed with Heena		220	205	175	#DCCDAF Wheat	82.9	0.43	16.84
18 E - Cotton Fabric Mordanted with Copper sulphate and Cream of tartar and Dyed with Heena		213	203	168	#D5CBA8 Wheat	81.67	-2.15	18.74
18 F – Cotton Fabric Mordanted with Ferrous sulphate and Cream of tartar and Dyed with Heena		162	150	140	#A2968C Darkgrey	62.83	2.66	6.86
18 G - Cotton Fabric Mordanted with Potassium dichromate and Dyed with Heena		220	202	167	#DCCAA7 Wheat	81.97	0.85	19.78

Code No. – Cotton Fabric	Colour obtained on Cotton Fabric	Color Model RGB				Color Model LAB		
		Red	Green	Blue	Hex # & Color Description	l	a	b
18 H - Cotton Fabric Mordanted with Stannous chloride and Cream of tartar and Dyed with Heena		221	204	162	#DDCCA2 Wheat	82.47	-0.5	23.12
18 I - Cotton Fabric Mordanted with Tannic acid and Dyed with Heena		221	215	194	#DDD7C2 Antiquewhite	85.94	-1.48	11.1

2. Colour Fastness test for Water Fastness and Light Fastness to Annatto seed and Heena leaf Dyed Fabric

Code No. - Cotton Fabric	Colour Fastness Test	
	Water Fastness	Light Fastness
00 - Cotton Fabric Not Mordanted and Not Dyed	5	5
0 C - Cotton Fabric Mordanted with Alum and Not Dyed	5	5
0 D - Cotton Fabric Mordanted with Alum and Cream of tartar and Not Dyed	5	5
0 E - Cotton Fabric Mordanted with Copper sulphate and Cream of tartar and Not Dyed	5	5
0 F - Cotton Fabric Mordanted with Ferrous sulphate and Cream of tartar and Not Dyed	5	5
0 G - Cotton Fabric Mordanted with Potassium dichromate and Not Dyed	5	5
0 H - Cotton Fabric Mordanted with Stannous chloride and Cream of tartar and Not Dyed	5	5
0 I - Cotton Fabric Mordanted with Tannic acid and Not Dyed	5	5
17 C - Cotton Fabric Mordanted with Alum and Dyed with Annatto	4-5	4-5
17 D - Cotton Fabric Mordanted with Alum and Cream of tartar and Dyed with Annatto	4-5	4-5
17 E - Cotton Fabric Mordanted with Copper sulphate and Cream of tartar and Dyed with Annatto	4-5	4-5

Code No. - Cotton Fabric	Colour Fastness Test	
	Water Fastness	Light Fastness
17 F – Cotton Fabric Mordanted with Ferrous sulphate and Cream of tartar and Dyed with Annatto	4-5	4-5
17 G - Cotton Fabric Mordanted with Potassium dichromate and Dyed with Annatto	4-5	4-5
17 H - Cotton Fabric Mordanted with Stannous chloride and Cream of tartar and Dyed with Annatto	4-5	4-5
17 I - Cotton Fabric Mordanted with Tannic acid and Dyed with Annatto	4-5	4-5
18 C - Cotton Fabric Mordanted with Alum and Dyed with Heena	4-5	4-5
18 D - Cotton Fabric Mordanted with Alum and Cream of tartar and Dyed with Heena	4-5	4-5
18 E - Cotton Fabric Mordanted with Copper sulphate and Cream of tartar and Dyed with Heena	4-5	4-5
18 F – Cotton Fabric Mordanted with Ferrous sulphate and Cream of tartar and Dyed with Heena	4-5	4-5
18 G - Cotton Fabric Mordanted with Potassium dichromate and Dyed with Heena	4-5	4-5
18 H - Cotton Fabric Mordanted with Stannous chloride and Cream of tartar and Dyed with Heena	4-5	4-5
18 I - Cotton Fabric Mordanted with Tannic acid and Dyed with Heena	4-5	4-5

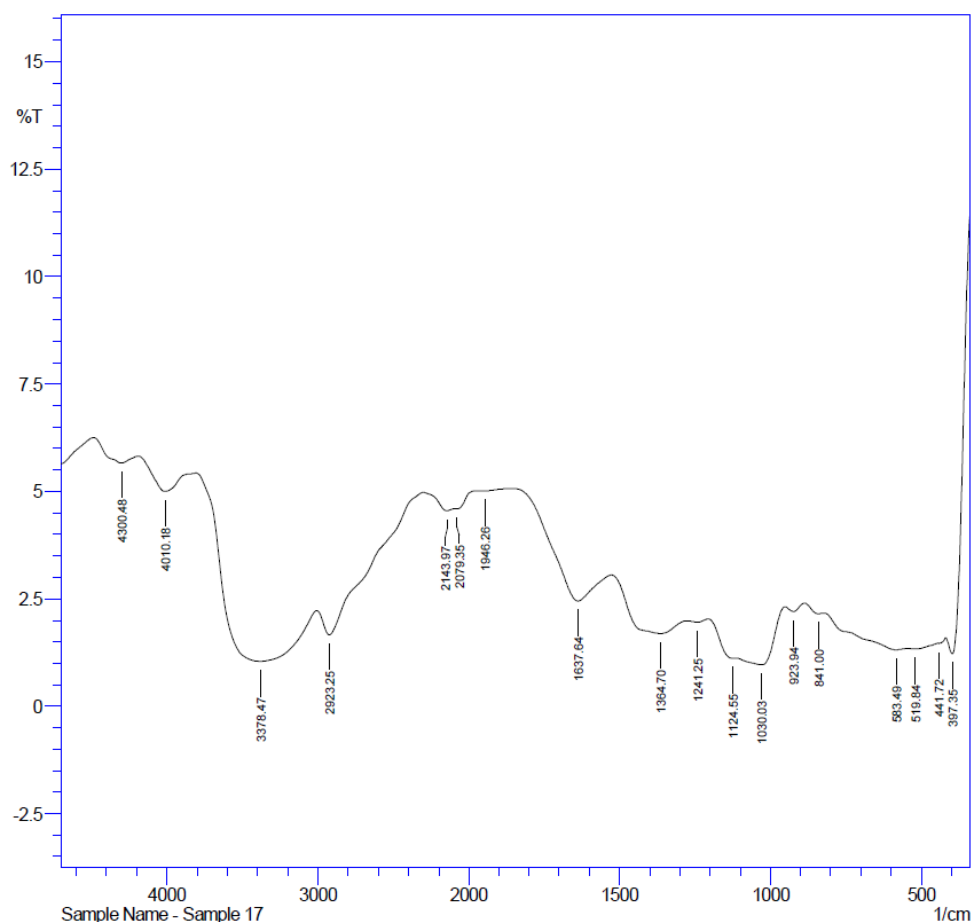
Colour fastness test for water fastness and light fastness to Annatto seed and Heena leaf dye powder using different mordant dyed fabric shows 4-5 range in gray scale method which indicates excellent to water fastness and light fastness.

3. FTIR Analysis of Annatto seed and Heena leaf Dye Extract

FTIR spectra of Natural Dye made from Annatto seed

No.	Peak	Intensity	Corr. Inte	Base (H)	Base (L)	Area	Corr. Are
1	397.35	1.219	3.005	418.57	339.49	119.643	12.108
2	441.72	1.463	0.006	442.68	419.54	42.184	0.166
3	519.84	1.335	0.041	544.91	446.54	183.11	0.849
4	583.49	1.313	0.144	822.68	545.88	498.358	9.1
5	841	2.154	0.081	886.33	823.64	103.495	0.586
6	923.94	2.204	0.15	950.95	887.29	104.486	0.919
7	1030.03	0.963	0.78	1114.9	951.91	311.019	18.997
8	1124.55	1.117	0.089	1206.53	1115.87	166.545	1.94
9	1241.25	1.955	0.055	1275.97	1207.49	116.615	0.431
10	1364.7	1.691	0.671	1526.72	1276.93	424.649	22.831

No.	Peak	Intensity	Corr. Inte	Base (H)	Base (L)	Area	Corr. Are
11	1637.64	2.451	1.285	1852.71	1527.69	475.738	19.999
12	1946.26	5.016	0.014	1969.41	1853.67	150.177	0.054
13	2079.35	4.598	0.032	2088.03	1970.37	155.335	0.373
14	2143.97	4.551	0.147	2300.21	2089	279.638	0.996
15	2923.25	1.663	0.891	3006.19	2301.18	1061.95	24.331
16	3378.47	1.046	2.669	3806.68	3007.15	1397.447	231.511
17	4010.18	5	0.637	4189.57	3807.65	486.427	8.964
18	4300.48	5.658	0.324	4485.65	4190.53	364.159	4.258



FTIR spectra of Natural Dye made from Annatto seed

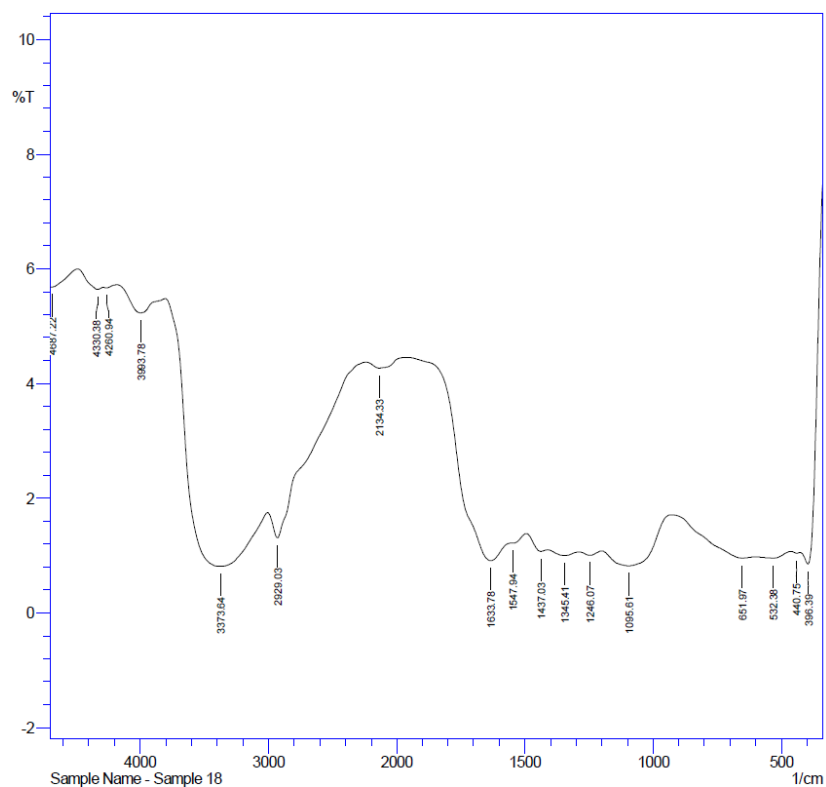
Interpretation of IR spectra of Natural Dye made from **Annatto seed** is done as follows

Spectra region wave number cm^{-1}	Intensity and Pattern of peak	Bond causing Absorption	Compound Class
397.35	Weak	-	-
441.72	Weak	-	-
519.84	Weak	-	-
583.49	Weak	-	-
841	Weak	-	-

Spectra region wave number cm ⁻¹	Intensity and Pattern of peak	Bond causing Absorption	Compound Class
923.94	Weak	-	-
1030.03	Medium	-	-
1124.55	Medium	-	-
1241.25	Weak	-	-
1364.7	Medium	O-H Bending	Phenol
1637.64	Medium	C=C Stretching	Alkene
1946.26	Weak	C-H Bending	Aromatic compound
2079.35	Weak	-	-
2143.97	Weak	-	-
2923.25	Strong, Broad	O-H Stretching	Carboxylic acid
3378.47	Strong, Broad	O-H Stretching	Alcohol
4010.18	Weak	-	-
4300.48	Weak	-	-

FTIR spectra of Natural Dye made from Heena leaf

No.	Peak	Intensity	Corr.Inte	Base(H)	Base(L)	Area	Corr.Are
1	396.39	0.854	2.407	426.29	339.49	149.784	15.593
2	440.75	1.039	0.021	462.94	427.25	70.577	0.145
3	532.38	0.955	0.069	600.85	463.9	274.763	2.219
4	651.97	0.955	0.133	928.76	601.82	624.794	7.954
5	1095.61	0.822	0.502	1200.74	929.73	537.816	32.08
6	1246.07	1.004	0.068	1289.47	1201.7	174.164	1.276
7	1345.41	1	0.08	1410.02	1290.43	237.356	2.217
8	1437.03	1.072	0.115	1494.9	1410.99	162.068	1.878
9	1547.94	1.215	0.02	1554.69	1495.86	111.386	0.414
10	1633.78	0.91	0.93	1960.73	1555.66	666.802	25.435
11	2134.33	4.267	0.137	2239.45	1961.69	378.606	2.191
12	2929.03	1.308	0.701	3005.22	2240.42	1187.795	16.094
13	3373.64	0.809	2.66	3802.82	3006.19	1451.166	249.305
14	3993.78	5.234	0.368	4179.92	3803.79	476.004	5.138
15	4260.94	5.667	0.02	4286.98	4180.89	132.056	0.063
16	4330.38	5.642	0.103	4486.62	4287.94	246.122	0.962
17	4687.22	5.686	0.021	4700.73	4487.58	263.218	0.344



FTIR spectra of Natural Dye made from Heena leaf

Interpretation of IR spectra of Natural Dye made from Heena leaf is done as follows

Spectra region wave number cm^{-1}	Intensity and Pattern of peak	Bond causing Absorption	Compound Class
396.39	Weak	-	-
440.75	Weak	-	-
532.38	Weak	-	-
651.97	Weak	-	-
1095.61	Medium	-	-
1246.07	Weak	-	-
1345.41	Weak	-	-
1437.03	Weak	-	-
1547.94	Weak	-	-
1633.78	Strong	C=C Stretching	Alkene
2134.33	Weak	C \equiv C Stretching	Alkyne
2929.03	Medium	C-H Stretching	Alkane
3373.64	Strong, Broad	O-H Stretching	Alcohol
3993.78	Weak	-	-
4260.94	Weak	-	-
4330.38	Weak	-	-
4687.22	Weak	-	-

IV. CONCLUSION

Code No. - Cotton Fabric	Hex & Color obtained #	Colour Fastness Test	
		Water Fastness	Light Fastness
00 - Cotton Fabric Not Mordanted and Not Dyed	#F3F3F3 White Smoke	5	5
0 C - Cotton Fabric Mordanted with Alum and Not Dyed	#F3F3F3 White Smoke	5	5
0 D - Cotton Fabric Mordanted with Alum and Cream of tartar and Not Dyed	#F3F3F3 White Smoke	5	5
0 E - Cotton Fabric Mordanted with Copper sulphate and Cream of tartar and Not Dyed	#F3DFFF Azure	5	5
0 F - Cotton Fabric Mordanted with Ferrous sulphate and Cream of tartar and Not Dyed	#EEE6DF White Chocolate	5	5
0 G - Cotton Fabric Mordanted with Potassium dichromate and Not Dyed	#DEB6A2 Pale Chestnut	5	5
0 H - Cotton Fabric Mordanted with Stannous chloride and Cream of tartar and Not Dyed	#F3F3F3 White Smoke	5	5
0 I - Cotton Fabric Mordanted with Tannic acid and Not Dyed	#EEEEEE Bright Gray	5	5
17 C - Cotton Fabric Mordanted with Alum and Dyed with Annatto	#F7DA88 Khaki	4-5	4-5
17 D - Cotton Fabric Mordanted with Alum and Cream of tartar and Dyed with Annatto	#F6C06C Sandybrown	4-5	4-5
17 E - Cotton Fabric Mordanted with Copper sulphate and Cream of tartar and Dyed with Annatto	#F09651 Sandybrown	4-5	4-5
17 F - Cotton Fabric Mordanted with Ferrous sulphate and Cream of tartar and Dyed with Annatto	#F5AF64 Sandybrown	4-5	4-5
17 G - Cotton Fabric Mordanted with Potassium dichromate and Dyed with Annatto	#F5B669 Sandybrown	4-5	4-5
17 H - Cotton Fabric Mordanted with Stannous chloride and Cream of tartar and Dyed with Annatto	#F6AB66 Sandybrown	4-5	4-5
17 I - Cotton Fabric Mordanted with Tannic acid and Dyed with Annatto	#F1AC60 Sandybrown	4-5	4-5
18 C - Cotton Fabric Mordanted with Alum and Dyed with Heena	#D7CAA4 Wheat	4-5	4-5
18 D - Cotton Fabric Mordanted with Alum and Cream of tartar and Dyed with Heena	#DCCDAF Wheat	4-5	4-5
18 E - Cotton Fabric Mordanted with Copper sulphate and Cream of tartar and Dyed with Heena	#D5CBA8 Wheat	4-5	4-5

Code No. - Cotton Fabric	Hex # &Colorobtained	Colour Fastness Test	
		Water Fastness	Light Fastness
18 F – Cotton Fabric Mordanted with Ferrous sulphate and Cream of tartar and Dyed with Heena	#A2968C Darkgrey	4-5	4-5
18 G - Cotton Fabric Mordanted with Potassium dichromate and Dyed with Heena	#DCCAA7 Wheat	4-5	4-5
18 H - Cotton Fabric Mordanted with Stannous chloride and Cream of tartar and Dyed with Heena	#DDCCA2 Wheat	4-5	4-5
18 I - Cotton Fabric Mordanted with Tannic acid and Dyed with Heena	#DDD7C2 Antiquewhite	4-5	4-5

Interpretation of FTIR Spectra of Natural Dye made from Annatto seed and Heena leaf dye powder shows presence of various functional groups such as

Bond causing Absorption	Compound Class	Bond causing Absorption	Compound Class
Natural Dye made from Annatto Seed		Natural Dye made from Heena Leaf	
C-H Bending	Aromatic compound	C-H Stretching	Alkane
O-H Stretching	Carboxylic acid, Alcohol	O-H Stretching	Alcohol
O-H Bending	Phenol	C=C Stretching	Alkene
C=C Stretching	Alkene	C≡C Stretching	Alkyne

V. REFERENCES

- [1]. Jump up to: a b c d "Bixa orellana (annatto)". CABI. 27 September 2018. Retrieved 14 October 2018.
- [2]. Smith, James (2006). "Annatto Extracts" (PDF). Chemical and Technical Assessment. JECFA. Retrieved 3 February 2012.
- [3]. Jump up to: a b Myles, Ian A.; Beakes, Douglas (2009). "An Allergy to Goldfish? Highlighting Labeling Laws for Food Additives". World Allergy Organization Journal. 2 (12): 314–316. doi:10.1097/WOX.0b013e3181c5be33. PMC 2805955. PMID 20076772.
- [4]. https://en.wikipedia.org/wiki/Annatto#/media/File:Bixa_orellana_fruit_open.jpg
- [5]. Socaciu, Carmen (24 October 2007). Food Colorants: Chemical and Functional Properties. CRC Press. ISBN 978-1-4200-0928-6.
- [6]. "CFR Title 21". U.S. FDA. 1 April 2011. Retrieved 24 August 2011.
- [7]. "21CFR101.22". Code of Federal Regulations Title 21, Volume 2. FDA. 1 April 2011. Retrieved 7 March 2012.
- [8]. Smith, James; Wallin, Harriet (2006). "Annatto Extracts: Chemical and Technical Assessment" (PDF). FAO. Retrieved 10 June 2013.
- [9]. Jump up to: a b "Executive Summary Bixin" (PDF). National Institute of Environmental Health Sciences. National Institutes of Health. November 1997. Archived from the original on 21 July 2011. Retrieved 24 August 2011.

- [10]. Kuntz, Lynn A. (4 August 2008). "Natural Colors: A Shade More Healthy". Food Product Design. Virgo Publishing, LLC. Retrieved 26 January 2013.
- [11]. Dweck, A. C. (2002). "Natural ingredients for colouring and styling". International Journal of Cosmetic Science. 24 (5): 287–302. doi:10.1046/j.1467-2494.2002.00148.x. PMID 18498522.
- [12]. Kurtyka, Renata; Pokora, Wojciech; Tukaj, Zbigniew; Karcz, Waldemar (2016). "Effects of juglone and lawsone on oxidative stress in maize coleoptile cells treated with IAA". AoB Plants. 8: plw073. doi:10.1093/aobpla/plw073. PMC 5199135. PMID 27760740.
- [13]. Jordão, A.; Vargas, M.; Pinto, A.; da Silva, F.; Ferreira, V. Lawsone in organic synthesis. RSC Adv. 2015, 5, 67909-67943.
- [14]. Shuang, S.; Lei, Q.; Ting, Y.; Qifu, Y. Method for preparing lawsone from lawsonia inermis China Patent CN 103848732A, June 11, 2014.
- [15]. Gallo, F.; Multari, G.; Giambenedetti, M.; Federici, E. Chemical fingerprinting of Lawsonia inermis L. using HPLC, HPTLC, and densitometry. Phytochem. Anal. 2008, 19, 550-559.
- [16]. Jump up to: a b Jelly, R.; Lewis, S. W.; Lennard, C.; Lim, K. F.; Almog, J. Lawsone: a novel reagent for the detection of latent fingerprints on paper surfaces. Chem. Commun. 2008, 3513-3515
- [17]. Jelly, R.; Lewis, S. W.; Lennard, C.; Lim, K. F.; Almog, J. Lawsone: a novel reagent for the detection of latent fingerprints on paper surfaces. Chem. Commun. 2008, 3513-3515.
- [18]. Thomas, P.; Farrugia, K. An investigation into the enhancement of fingerprints in blood on paper with genipin and lawsone. Sci. Justice 2013, 53, 315-320.
- [19]. Color and chemical constitution of natural dye henna (*Lawsonia inermis* L) and its application in the coloration of textiles, M.A. Rahman Bhuiyan, A. Islam, A. Ali, M.N. Islam, Journal of Cleaner Production, Volume 167, 20 November 2017, Pages 14-22
- [20]. Coloration of polyester fiber with natural dye henna (*Lawsonia inermis* L.) without using mordant: a new approach towards a cleaner production, M. A. Rahman Bhuiyan, A. Ali, A. Islam, M. A. Hannan, S. M. Fijul Kabir & M. N. Islam, Fashion and Textiles, International Journal of Interdisciplinary Research, volume 5, Article number: 2 (2018)
- [21]. Phytochemical and Pharmacological Activities of Natural Dye Plant, *Lawsonia inermis* L. (Henna), Farah Nabilah Ahmad Supian and Nurul Izzati Osman, Journal of Young Pharmacists, Vol 15/Issue 2/2023

Acoustical Study of Molecular Interaction of 3,4-Dihydro-2H-1,2,4-Benzothiadiazine 1, 1-Dioxide in Aqueous Solution at Different Temperatures

Nita P. Mohabansi*, Monali Sabane

*Department of Chemistry, Bajaj College of Science, Jamanalal Bajaj Marg, Civil Lines, Wardha, Maharashtra, India

ARTICLE INFO

Article History:

Accepted : 01 Jan 2025

Published : 10 Jan 2025

Publication Issue :

Volume 12, Issue 7

January-February-2025

Page Number :

151-155

ABSTRACT

In the present study ultrasonic velocity (v), density (ρ) and viscosity (η) of the mixtures of 3,4-dihydro-2H-1,2,4-benzothiadiazine 1,1-dioxide in aqueous solutions have been measured at frequency 1 MHz in the concentration range 0.01–0.1% at 297, 307, and 317 K using multifrequency ultrasonic interferometer. The measured value of density, ultrasonic velocity, and viscosity have been used for the calculation of the acoustical parameters namely adiabatic compressibility(β_a), Intermolecular free length (Lf). and free volume. The results obtained have been discussed on the basis of the nature of solute-solvent interactions in the aqueous solutions.

Keywords: ultrasonic velocity, acoustical parameters, solute-solvent interaction.

I. INTRODUCTION

Ultrasound waves are mechanical waves with high frequencies that influence the physical characteristics of the medium, thereby providing insights into molecular interactions within liquids and liquid mixtures [1-4]. Research into the thermodynamic characteristics of binary mixtures is significantly important for gaining insights into the interactions between dissimilar molecules [5-7]. For understanding the nature and strength of the drug –solvent interactions, the thermoacoustic studies play an important role [8-9]. The variation of ultrasonic velocity and other ultrasonic parameters of drug in various solvents have been considered by numerous analysts and they have shed light upon structural changes related with liquid mixtures of feebly or emphatically interacting compounds [9-11].

II. MATERIAL AND METHODS

In the present study, the chemicals used are of AR grade. These chemicals were used without any further purification. All the solutions were prepared gravimetrically just before experimental measurements in air-tight bottles to prevent the evaporation [10]. Solutions were prepared using CONTECH, CA 224 analytical balance (± 0.0001 g). The solutions of different percentages viz, 0.01 - 0.1 of Azithromycin drug were prepared in distilled water. The solutions so prepared were gently stirred on a magnetic stirrer before being subjected to measurements. Care was taken to avoid the contamination during mixing of solutions. The uncertainty at estimated molality of solute and solvents is found to be within $u(m) = \pm 1 \times 10^{-4}$.

Densities were measured using calibrated pycnometer having a bulb volume of 10 cm³. The basic parameter ultrasonic velocity (U) has been measured on Digital Ultrasonic Pulse Echo Velocity Meter (Vi Microsystems Pvt. Ltd. Model VCT-70) at 2MHz with an accuracy of 0.1% (2 ± 0.0001 MHz). The uncertainty at estimated ultrasonic velocity is found to be within $u(m) = \pm 1.09 \text{ m}\cdot\text{s}^{-1}$. The instrument has a built-in thermostat to maintain the temperature (± 0.1 K). It was calibrated with triple distilled water and pure methanol at 297, 307 and 317K [12-13].

III. RESULT AND DISCUSSION

The experimentally determined values of density (ρ), ultrasonic velocity (u) for all solutions of the solute at different concentrations and at $T = (297, 307 \text{ and } 317)\text{K}$ were measured at different concentration and various temperatures. The data obtained from the density, ultrasonic velocity and viscosity have been used to calculate the various acoustical parameters [13-17] viz. adiabatic compressibility (β), intermolecular free length (L_f), free volume (V_f), by using the known equations [18]. These values are presented in the Table 1 and Table 2.

Table 1: Values of Density (ρ), Ultrasonic velocity (U) and Viscosity (η) of mixtures at 297K, 307K and 317K of solution was prepared in distilled water.

Concentration (%)	Density(ρ) Kg.m ⁻³			Ultrasonic Velocity (U) m.s ⁻¹			Viscosity(η)N.s.m ⁻²		
Temperature	297 K	307K	317K	297K	307K	317K	297K	307K	317K
0.1	1.5409	1.5437	1.5400	1392.89	1409.94	1316.68	0.9407	0.8827	0.8755
0.05	1.5465	1.5398	1.5401	1391.08	1408.06	1315.60	0.9267	0.8748	0.8642
0.025	1.5433	1.5402	1.5322	1392.89	1412.43	1314.53	0.8901	0.8305	0.8315
0.0125	1.5324	1.5332	1.5397	1391.68	1411.17	1311.46	0.8724	0.8212	0.8128
0.00625	1.5307	1.5434	1.5556	1392.29	1410.55	1312.92	0.8485	0.7931	0.7925
0.003125	1.5469	1.5384	1.5393	1388.69	1409.94	1311.82	0.8285	0.7627	0.7501

Table 2: Values of Adiabatic compressibility (β_{ad}), intermolecular free length (L_f) and free volume (V_f) of mixtures at 297K, 307K and 317K of solution was prepared in distilled water.

Concentration (%)	Adiabatic compressibility (β_{ad}) $\times 10^{-7} \text{ (m}^2/\text{N)}$			Intermolecular free length (L_f) $\times 10^{-9} \text{ (m)}$			Free volume(V_f) $\times 10^{-6} \text{ (m}^3 \text{ mol}^{-1})$		
Temperature	297K	307K	317K	297K	307K	317K	297K	307K	317 K
0.1	3.3469	3.2586	3.7455	1.1879	1.1933	1.3028	1.2707	1.4287	1.2893
0.05	3.3414	3.2654	3.7514	1.1861	1.1951	1.3028	1.2887	1.4505	1.3329

Concentration (%)	Adiabatic compressibility (β_{ad}) $10^{-7} \text{ (m}^2/\text{N)}$			Intermolecular free length (L_f) $\times 10^{-9} \text{ (m)}$			Free volume(V_f) $\times 10^{-6} \text{ (m}^3 \text{ mol}^{-1})$		
0.025	3.3397	3.2545	3.7769	1.1861	1.1914	1.3084	1.3792	1.5638	1.4041
0.0125	3.3693	3.2752	3.7761	1.1915	1.1933	1.3080	1.4252	1.5904	1.4513
0.00625	3.3701	3.2564	3.7292	1.1915	1.1933	1.2993	1.4768	1.6807	1.5090
0.003125	3.3521	3.2698	3.7750	1.1879	1.1951	1.3080	1.5245	1.7801	1.6296

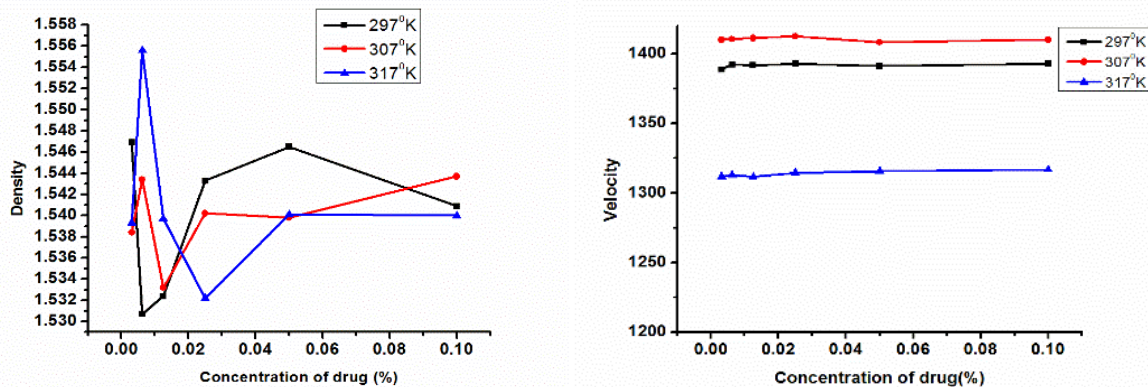


Fig. 1 : Variation of Density and ultrasonic velocity with concentration and temperature.

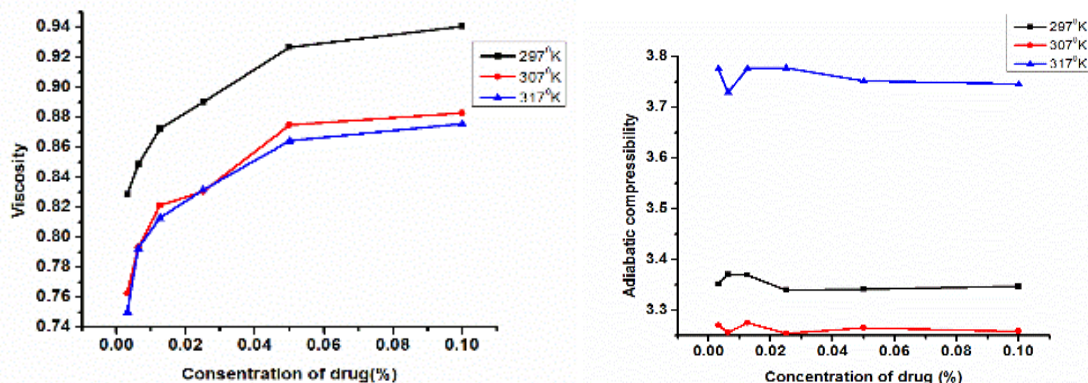


Fig 2: Variation of Viscosity and adiabatic compressibility on with different concentration and temperature.

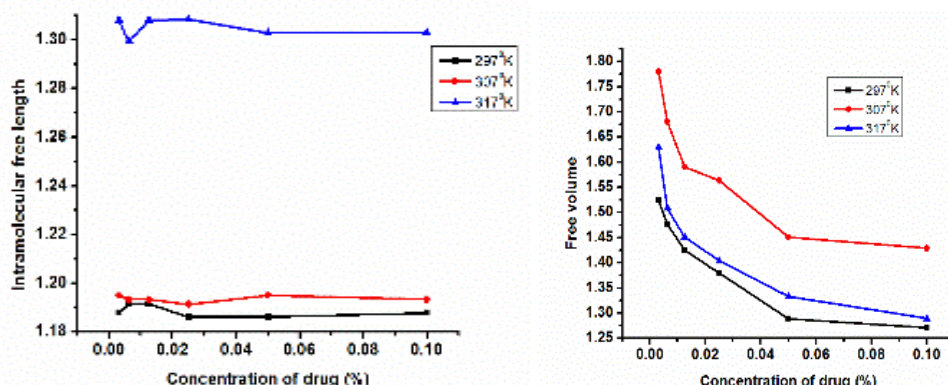


Fig 3: Variation of Intermolecular free length and free volume with different concentration and temperature.

The graphical variation of various acoustical parameters with concentrations and temperature are shown in Figure 1 to Figure 3. It is observed that ultrasonic velocity shows linear increasing variation with increase in

molar concentration. Linear variation indicates that the complex formation and intermolecular weak association which may be due to hydrogen bonding. Hence complex formation can occur at these molar concentrations between the component molecules. An inverse behaviour of Adiabatic compressibility (β_a) was observed as compared to the ultrasonic velocity. With increase in concentration adiabatic compressibility decreases. The decrease in compressibility implies that there is an enhanced molecular association in the system with increase in solute concentration. In the present studied system of aqueous solution, free length varies nonlinearly with increase in molar concentration. This indicates the significant interaction between solute and solvent due to which structural arrangement is also affected. Abnormal trend of density with concentration directs the structure-making and breaking property of solvent due to the formation and weakening of H-bonds. The free volume decreases and with increases in molar concentration indicate the association through hydrogen bonding.

IV. CONCLUSION

In this study, the Ultrasonic velocity (U), Density (ρ) and Viscosity (η) and acoustical parameters was measured at different concentrations and temperatures. Hence the derived Adiabatic compressibility, Intermolecular free length and Free volume have been calculated at different concentration. The variation in these parameters indicate that there is a strong molecular interaction between unlike molecules as the concentration of solution increases and the interaction decreases as temperature increases.

V. ACKNOWLEDGEMENT:

The Authors are thankful to the Principal and Department of Chemistry, Bajaj College of Science, Wardha for their kind support in the present research work.

VI. REFERENCES

- [1]. <https://doi.org/10.1016/j.matpr.2018.08.085>
- [2]. J. Mohanty, G Singh, C., S. Acharya, 'Dielectric Investigation of Binary Mixtures Involving a Nuclear Extractant -1, 2- Dichlorobenzene and Nonpolar Solvents' Int. J. Sci. Res. Publ.2 (2012) 22.
- [3]. <https://doi.org/10.1016/j.molliq.2008.10.009>
- [4]. Poonam Sharma, S. Chauhan, V. K. Syal & M. S. Chauhan, ' Studies of partial molar volumes of some narcotic-analgesic drugs in aqueous-alcoholic mixtures at 25 °C Int. J. Thermophys., 29 (2008), pp. 643-655
- [5]. A.A. Ali, A.K. Nain and S. Hyder, 'Study of intermolecular interaction in binary liquid mixtures through ultrasonic speed measurement's, Journal of Pure and Applied Ultrasonic's, 23, 73-79 (2001)
- [6]. S. Anuradha, S. Prema and K. Rajagopal, 'Ultrasonic studies on molecular interactions in binary mixtures of acetonitrile with carbonyl molecules', Journal of Pure and Applied Ultrasonic's, 27, 49-54 (2005)
- [7]. L. Palaniappan and R., Thiagarajan 'Effect of aniline in methanol + benzene mixture – An ultrasonic study', Ind. J. Chem., 47B, 1906-1909 (2008)
- [8]. A., Tadkalkar P. Pawar and G.K., Bichile 'Studies of acoustic and thermodynamic properties of citric acid in double distilled water at different temperatures', J. Chem. Pharm. Res., 3(3), 165-168(2011).

- [9]. F. Koohyar, F. Kiani, S. Sharifi, M. Sharifirad, S.H. Rahmanpour, 'Study on the change of refractive index on mixing, excess molar volume and viscosity deviation for aqueous solution of methanol, ethanol, ethylene glycol, 1-propanol and 1,2,3-propantriol at T = 292.15 K and atmospheric pressure' Res. J. Appl. Sci. Eng. Technol., 4 (2012), pp. 3095-3101.
- [10]. S.D. Deosarkar, R.T. Sawale, AR Ban, AL Puyad 'Densities, refractive indices and apparent molar volumes of potassium hexacyanoferrate (II) trihydrate in acidic media at 35° C - J. Chem. Pharm. Chem., 2014
- [11]. L. Palmowski, L. Simons and R. Brooks; Water Sci. Tech. 53(8), 281-288 (2006).
- [12]. R. Gomes, M. J. Andrade, M. Santos, S. Lima, R. A. Gouveia, M. M. Ferreira, J. A. Silva, Cardiovascular Ultrasound, 7,36 (2009).
- [13]. A. D. Arsule, R. T. Sawale, and S. D. Deosarkar, J. Mol. Liq., 2018, doi: 10.1016/j.molliq.2018.06.064.
- [14]. S. Sreehari Sastry, S. Babu, T. Vishwam, K. Parvateesam, and H. Sie Tiong, Phys. B Condens. Matter, 420, 40, (2013) doi: 10.1016/j.physb.2013.03.028
- [15]. A. D. Arsule, R. T. Sawale, and S. D. Deosarkar, J. Mol. Liq., 2018, doi: 10.1016/j.molliq.2018.06.064.
- [16]. S. Sreehari Sastry, S. Babu, T. Vishwam, K. Parvateesam, and H. Sie Tiong, Phys. B Condens. Matter, 420, 40, (2013) doi: 10.1016/j.physb.2013.03.028.
- [17]. I. Cibulka and P. Hync, 36, 1095(2004). doi: 10.1016/j.jct.2004.07.019.
- [18]. F. Edward, J. T. ,Farrell P. G. ,Shahidi, J. Chem. Soc. Faraday Trans. 1, 73, 705(1977).
- [19]. <https://doi.org/10.1134/S0036024421140132>

Medico-ethnobotany and Phytochemical Screening of *Leonotis nepetifolia*, *Colebrookea oppositifolia* from Melghat Region, Amravati District (M.S.)

Dr. Nitin A. Khandare¹, Nandkishor K. More²

¹Department of Botany, Shri Vasantrao Naik Mahavidhyalaya Dharni, Dist. Amravati, Maharashtra, India

²Department of Botany, Arts and Commerce College Warwat Bakal, Dist Buldhana, Maharashtra, India

ARTICLE INFO

Article History:

Accepted : 01 Jan 2025

Published : 10 Jan 2025

Publication Issue :

Volume 12, Issue 7

January-February-2025

Page Number :

156-159

ABSTRACT

The primary focus of our investigation was the scientific underpinnings of the therapeutic applications of several plants that the people of Melghat. Consequently, mature leaves and stem of *Leonotis nepetifolia*, *Colebrookea oppositifolia*, were pulverized after drying. The watery, ethanolic, and chloroform. Each plant's extract was made, and phytochemical analysis was performed on the results. The above mentioned plants' phytochemical examination revealed the presence of alkaloids, flavonoids, saponins, and steroid use. Using preliminary phytochemical screening, the existence of several phytochemical components was verified. Our research shows that despite the paucity of actual understanding about chemistry, the ancient healers were aware of these herbs' therapeutic value. The therapeutic qualities of these plants might be caused by a variety of phytochemicals, including as steroids, flavonoids, alkaloids, and saponins. terpenoids, cardiac glycosides and tannins

I. INTRODUCTION

The actual number of medicinal plants utilized worldwide in modern times is unknown, but one thing is certain medicinal plants play a major role in both traditional and Western medicine. In an effort to create novel and more potent medications, pharmaceutical corporations and life science researchers are becoming more interested in ethnobotany, the study of traditional plant use[1]. One of the most crucial areas of research in this area that may result in the creation of novel medications is this [1-4].

The Western Melghat region of India is home to one of Maharashtra's most significant forests, which is primarily of the dry mixed deciduous type. It is also rich in wildlife with changes in height, soil, temperature, humidity, and rainfall, the vegetation varies greatly. The temperature ranges from 13°C to 41°C, the average rainfall is between 950 mm and 1400 mm, and the humidity ranges from 48% to 90% in an area. Additionally,

there are several kinds of soil, including clayey, lateritic, alluvial, and gritty-loam [5]. The plant specimen was gathered from Melghat region of district Amravati.

II. MATERIALS AND METHOD

Plant material was collected from the local area and taxonomically identified at the Department of Botany, Shri Vasantao Naik Mahavidhyalaya, Dharni, district Amravati. Voucher specimen was deposited in the departmental herbarium. The stems and lateral branches of the plant were thoroughly washed with tap water, followed by a rinse with distilled water. These branches were then shade-dried for 5-6 days and subsequently powdered for further experimentation.

Qualitative Analysis:

Preliminary phytochemical tests on the aqueous extract or powdered plant sample were conducted according to the methods outlined by [6-7].

III. RESULT AND DISCUSSION

The present study focused on *Leonotis nepetifolia* and *Colebrookea oppositifolia* to investigate the presence of medicinally active phytochemicals in its leaves and stem, from the Melghat region in Amravati district (MS), India. Ethnomedicinal information was gathered from local communities and tribal groups in the area. It was found that the tribal use this plant to treat rheumatism, skin eruptions, Digestive Issues, Respiratory Disorders while some locals also use it to address Oral Health and Wound Healing.

The results of the qualitative phytochemical analysis are summarized in Table 1 and Table 2. For this analysis, the plant samples were extracted using five different solvents: chloroform, methanol, petroleum ether, acetone, and water. The aqueous extract of the plant was found to contain most of the identified phytochemicals, including alkaloids, flavonoids, phenolics, carbohydrates, tannins, and saponins (Table 1). Phlobatannins were detected only in the chloroform extract, while saponins were present in the aqueous extract (Table 1). These findings suggest that the plant contains a variety of phytochemicals that may contribute to its medicinal properties. Previous studies have explored phytochemicals in wild medicinal plants and linked them to their therapeutic potential [8-10]. However, further phytochemical and pharmacological research is needed to develop effective drugs from this plant.

Medicinal use of *Leonotis nepetifolia*,

Leonotis nepetifolia, commonly known as lion's ear or wild dagga, is a medicinal plant used in traditional medicine across various cultures. Some of its key medicinal uses include:

- The leaves and flowers are often used to reduce inflammation and relieve pain, particularly for conditions like arthritis and rheumatism.
- Traditionally, the plant is used to treat respiratory conditions such as cough, asthma, and bronchitis. The smoke from burning the dried leaves is sometimes inhaled to clear respiratory passages.
- The plant is used in the treatment of skin disorders, including rashes, wounds, and skin infections. The leaves are often applied as a poultice to affected areas.
- The plant is used to alleviate digestive problems such as dysentery, diarrhea, and stomach cramps.
- In some regions, extracts of the plant are used as a remedy for fever and malaria.

Medicinal Uses of *Colebrookea oppositifolia*

Colebrookea oppositifolia, commonly known as Indian Sage, is widely used in traditional medicine for various therapeutic purposes. Some of its notable medicinal uses include:

- The leaves and roots are used to treat inflammatory conditions and relieve pain, especially in cases of arthritis, rheumatism, and joint pain.
- The plant is applied topically to heal wounds, cuts, and skin infections. Its antiseptic properties help prevent infections and promote healing.
- The plant is used in traditional remedies for treating respiratory conditions such as colds, coughs, asthma, and bronchitis. The plant is believed to have expectorant properties that help in clearing mucus from the lungs.
- The plant is used to address digestive issues like diarrhea and dysentery. It is believed to have a soothing effect on the stomach and intestines.
- Traditionally, the leaves are chewed or used as a mouthwash to maintain oral hygiene, treat toothaches, and prevent gum diseases.

Phytochemical Analysis of *Colebrookea oppositifolia*

Colebrookea oppositifolia contains a variety of bioactive compounds that contribute to its medicinal properties. Common phytochemicals identified through various analyses include:

Table 1:

Solvent	Alkaloids	Flavonoids	Phenolics	Tannins	Saponin	Terpenoid	Steroids
Chloroform	–	–	+	–	–	–	–
Methanol	+	+	–	–	–	–	–
Acetone	+	–	–	–	–	–	–
Petroleum ether	–	–	+	–	–	–	+
Aqueous extract	+	+	+	–	+	–	–

Phytochemical Analysis of *Leonotis nepetifolia*

Leonotis nepetifolia (Lion's Ear) contains a variety of phytochemicals that contribute to its medicinal properties. Some of the key phytochemicals identified in the plant include:

Table 2:

Solvent	Alkaloids	Flavonoids	Phenolics	Tannins	Saponin	Terpenoid	Steroids
Chloroform	–	+	+	–	–	–	–
Methanol	+	+	–	–	–	–	+
Acetone	–	+	–	–	–	–	–
Petroleum ether	–	–	+	–	–	–	+
Aqueous extract	+	+	+	+	+	–	–

IV. REFERENCES

- [1]. Morsy, N. Phytochemical analysis of biologically active constituents of medicinal plants. *Main Group Chemistry* 2014; 13 (1), 7-21.
- [2]. Ebert, A. W., & Engels, J. M. M. Plant Biodiversity and Genetic Resources Matter! *Plants* 2020; 9 (12), 1706.
- [3]. Sumitkumar L. Mirge, Dr. Santosh N. Patole, Bharat R. Nagare (2024). Survey and Documentation of Medicinal Plants in Akot Tehsil's Forested Terrain *JETIR* 11 (9), 73-78.
- [4]. Nitin A. Khandare - HPLC Analysis of Ethnomedicinal Important Plant *Capparis Grandis* L.f. From Western Melghat Region (MS) India *IJFMR* 5(6), November-December 2023. DOI 10.36948/ijfmr.2023.v05i06.8405
- [5]. Nitin A. Khandare. "Physicochemical Studies of Ethnomedicinal Important *Capparis* L. Species from Melghat Forest. Dist- Amravati (MS) India", *International Journal of Creative Research Thoughts (IJCRT)*, ISSN: 2320-2882, Vol.11, Issue 10, pp.f404-f410, October 2023, URL : <http://www.ijcrt.org/IJCRT2310615>
- [6]. Edeoga HO, Okwu DE, Mbaebie BO. Phytochemical constituent of some Nigerian medicinal plants. *African Journal Biotech* 2005; 4(7): 685-688.
- [7]. Harborne JB. *Phytochemical methods*, London, Chapman & Hall Ltd. 1973; pp. 49-188.
- [8]. Ingle, K. P., Deshmukh, A. G., Padole, D. A., Dudhare, M. S., Moharil, M. P., & Khelurkar, V. C. Phytochemicals: Extraction methods, identification and detection of bioactive compounds from plant extracts. *Journal of Pharmacognosy and Phytochemistry* 2017; 6(1), 32-36.
- [9]. Altemimi, A., Lakhssassi, N., Baharlouei, A., Watson, D. G., & Lightfoot, D. A. Phytochemicals: Extraction, isolation, and identification of bioactive compounds from plant extracts. *Plants* 2017;6(4), 42.
- [10]. Nitin, A. Khandare. (2023). Diversity of medicinal plants from Melghat forest of Amravati district (MS) India. *International Journal of Advanced Research*, 11(10), 381-384. <https://doi.org/10.21474/IJAR01/15353>

Easy Fabrication of a Combination of Polyaniline and Graphene Oxide for Use as Electrode Materials and Its Characterization

Dr. Prachi R. Bonde

Department of Chemistry, Indira Mahavidyalaya, Kalamb Dist. Yavatmal, Maharashtra, India

ARTICLE INFO

Article History:

Accepted : 01 Jan 2025

Published : 10 Jan 2025

Publication Issue :

Volume 12, Issue 7

January-February-2025

Page Number :

160-166

ABSTRACT

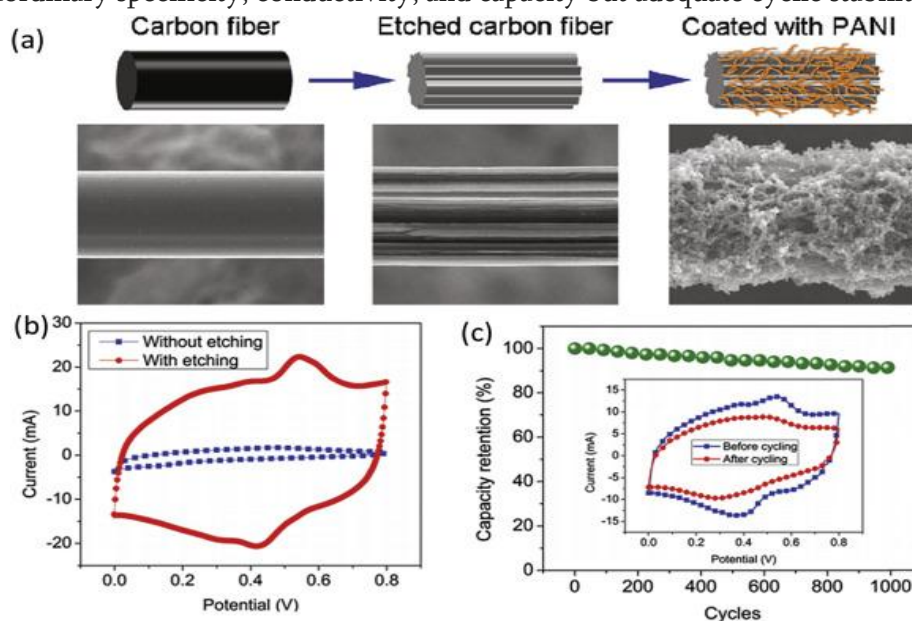
By using in-situ polymerization, composites reinforced with graphene oxide (GO) and polyaniline (PANi) were created. Using a modified Hummer's process, graphene oxide (GO) was produced from natural graphite flakes. X-ray diffraction, Fourier-transform infrared spectroscopy, scanning electron microscopy, and thermogravimetric analysis were used to evaluate the PANi/GO composites. Utilizing the composites as supercapacitor electrodes, the specific gravimetric capacitance (C_{sp}) from cyclic voltammetry and charge/discharge characteristics were used to gauge the devices' performance. With a loading of 50% weight percentage of GO, Graphene oxide (GO) is useful and promising material for graphene-based applications in electronic, optics, chemistry, energy storage, and biology.

Keywords: Grapheneoxide, polyaniline, composite, electrodes, energy storage

I. INTRODUCTION

The popularity of flexible power supplies and devices that are lightweight and flexible has greatly expanded due to the rapid development of wearable and flexible electronics [1-3]. Fiber-shaped supercapacitors are superior to other flexible power sources in that they are compact, light, and mechanically flexible. They can also be readily woven into textiles, which presents significant benefits for the field of flexible, wearable, and portable electronics in the future [4-6]. However, fibre-shaped supercapacitors have significantly lower specific capacitance and energy density than lithium-ion batteries or conventional supercapacitors, which prevents their widespread use [7, 8]. When graphene first came into being, GO was only an easy and affordable stage in the reduction process used to make bulk structures and single and multilayer graphene sheets. Subsequent research disclosed significant structural imperfections in materials generated from graphene oxide, which were attributed to incomplete reduction processes and flaws in the initial graphite. Recent studies have, however, shown that graphene oxide possesses a multitude of distinct chemical, optical, and electrical properties that enable it to be regarded as a stand-alone nanomaterial with a wide range of uses. It is a general representation

of an extremely big organic molecule with a 2D carbon mesh. In contrast to traditional graphene, it offers a broad variety of chemical techniques for attaching different functional groups to its surface to regulate its electrical, thermal, and optical conductivity. Newly established techniques for synthesizing graphene oxide derivatives saturated with carboxyl groups provide appealing avenues for green technology applications, such as nuclear waste utilization and energy storage. The review's objective is to provide an overview of the findings from current investigations into graphene oxide derivatives and identify the most promising areas in which to concentrate research efforts. The main objective of this study was to identify the benefits of in-situ polymerization of aniline monomer with the inclusion of GO as an electrode material. In addition, the optimal amount of GO loading into polyaniline for the synergistic effect in supercapacitor cells was also studied. Moreover, the application of PANi/GO composites as electrodes in the production of high-performance energy storage devices was also experimented. The addition of GO improved various electrical properties of the conductive polyaniline polymers, but the aggregation of GO into composites for synergistic effect was a great barrier to obtaining the best output from the composites [9]. The main objective of this study was to identify the benefits of in-situ polymerization of aniline monomer with GO. Electrode materials have an important impact on the efficacy of the storage device and energy conversion. Electrodes of storage devices are mainly related to conductive polymers, metals, and carbon-based materials [12]. Although carbon-based materials show extraordinary conductivity, power density, and adequate durability, their energy density is usually low. Metals show adequate electrochemical characteristics, but their cost and lack of natural abundance limit their use. PANI, because of its high conductivity, various oxidation states, and high specific capacitance, can be used as a supercapacitor. Hence, the conductivity and flexible electrochemical properties of PANI make it highly suitable for capacitor manufacturing. The properties of PANI-based supercapacitors are highly dependent on synthesis, doping, physical/chemical features, and nanostructure. From 0.8 V to 1 V, PANI is subjected to a proper charge/discharge process; though, at less than 0.6 V, PANI is unworkable due to the minimum density of energy [13]. PANI is joined by the carbon group, such as carbon nanotubes and graphene, to be utilized in supercapacitors. The polymerization for PANI/graphene oxide produces homogenous PANI nanofibers that demonstrate extraordinary specificity, conductivity, and capacity but adequate cyclic stability [14].



(a) Schematic diagram of the preparation of PANi-coated electro-etched carbon fiber cloth electrodes and the corresponding SEM images of every step. (b) CV curves of PANi coating carbon fibers with and without etching. (c) Cycling stability test of PANi coated electrode [16]. Reproduced with permission.

II. MATERIALS AND METHODS

2.1. Materials

Aniline ($C_6H_5NH_2$) and graphite powder (Nanokar Nanotechnology, Turkey), HCl (Merck), were in extra pure grade and used as received. Double distilled water was produced using water still (GFL-2008)

2.2. Synthesis of GO

GO was typically made from pure graphite powder using a modified Hummers technique [10]. A 1000 mL beaker was filled with 8 g of graphite powder, 3.5 g of $NaNO_3$, and 120 mL of concentrated H_2SO_4 and then placed in the ice bath. The solution was agitated for one hour at 300 rpm while a thermometer was inserted into the beaker to monitor the reaction temperature. The mixture was then agitated for two hours after adding 18 g of $KMnO_4$. Next, the aqueous solution was agitated for one hour with 600 millilitres of distilled water added. After adding 10.4 mL of H_2O_2 , stir for one hour. GO was produced by passing it through a quantitative filter paper and then washing it with deionized water.

2.3. Synthesis of GO-PANI composite

In-situ polymerization polyaniline doped GO

The in-situ polymerization process was used to create the GO/PANi composites. In 50 mL of 1 M HCl, 10.0 mg of the GO was ultrasonically exfoliated for two hours. Next, a suspension of GO was mixed with 2 mL of aniline, and the combination was shaken for 24 hours at room temperature (23–25 °C). The aniline/GO solution was mixed with a little amount of APS dissolved in 50 mL of 1 M HCl solution, added dropwise. After that, the mixture was swirled in an ice bath set between 0 and 15 °C for 24 hours, or until it turned dark green. The reaction materials were then filtered and repeatedly cleaned with ethanol and distilled water before being dried for 12 hours at 60 °C.

2.4. Characterisation of GO-PANI

The surface morphology and dispersion of the material were characterized by a scanning electron microscope (JSM-6360). The surface functional groups of the material were measured by Fourier transform infrared spectroscopy (Spectrum GX) with the scanning range of 4000–500 cm^{-1} . X-ray Diffraction (XRD) with the wavelength of $\lambda = 1.53 \text{ \AA}$, a scan rate of 0.2 s, a voltage of 40 kV, and a scan range of 10–90° was used to test the particle size and structure characteristics of the material.

III. RESULTS AND DISCUSSION

Fourier transform infrared analysis (FTIR). Fig. 1 shows the FT-IR spectra of graphite oxide, PANI. The peaks at 3390, 1729, and 1405–1057 cm^{-1} for graphite oxide are attributed to the OH, C=O in COOH and C–O in COH/COC (epoxy) functional groups respectively. Compared with the peaks of graphite oxide, the C=O peak is downshifted to 1700 cm^{-1} ; the peaks of C–O in COH/COC (epoxy) are also red-shifted clearly. These indicate the carboxyl groups from grapheme oxide are linked on the nitrogen of PANI backbone via the same doping process into the PANI backbone, just as the normal dopant of Cl. The spectral red-shift phenomena of chemically synthesized nanocomposite result from the p–p interaction and hydrogen bonding between the doping graphene oxide sheets and the polymer backbone. Note that the band at 1580 cm^{-1} , characteristic of the C=N stretching in the quinoid units of pure PANI, is blue shifted to 1593 cm^{-1} in PG100:1. This is due to the withdrawing induction effect of C=O groups, although there is still conjugative effect remaining.

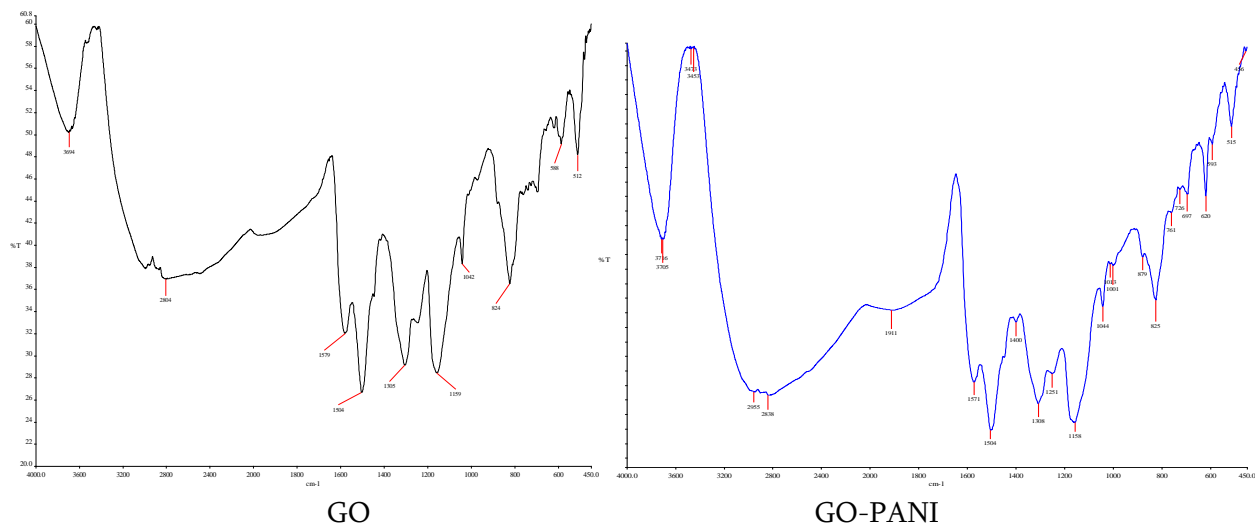


Figure 1. FT-IR spectra of graphite oxide and GO-PAN

XRD

As presented in Fig 2 of the XRD patterns of GO- PANI, the additional diffraction peaks for GO-PANI was observed, indicating that the successful integration of GO with PANI. The XRD patterns of GO-PANI. It can be seen that the GO-PANI have four characteristic peaks at $2\theta = 15.2^\circ$, 20.3° , 25.2° , and 26.5° , corresponding to (011), (020), (200) and (121) planes, respectively. The XRD pattern of GO-PANI shows crystalline structure.

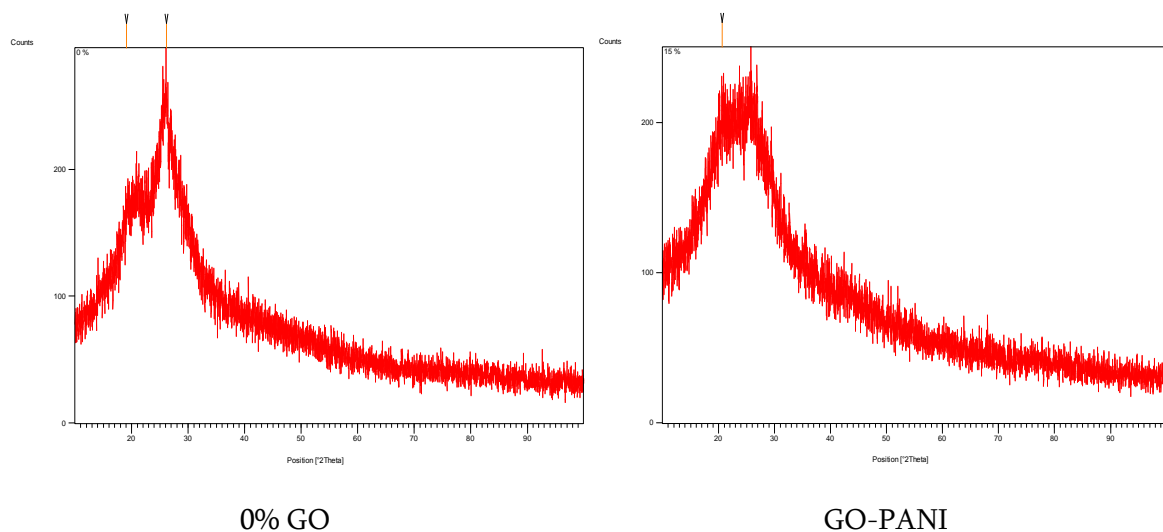


Figure 2. XRD spectra of graphite oxide and GO

Scanning Electronic Microscope

The SEM images of the composites are displayed appropriately in Figure 3. The GO sheets looked like stacks of lamellar structures with several layers. The sheets were seen to be stacked and agglomerated due to the absence of any polymer matrix. The resultant disordered phase was caused by the tiny, crumpled sheets that made up the GO and PA, which were also intimately connected to one another and irregularly aggregated. Powder that has particles smaller than one micron, or even $10\text{ }\mu\text{m}$, is referred to as metal ultrafine powder. The activity is substantially raised and the number of atoms in the assembled particles is greatly reduced as a result of the particle refining. The GO-PANI composite material demonstrates in Fig. 3

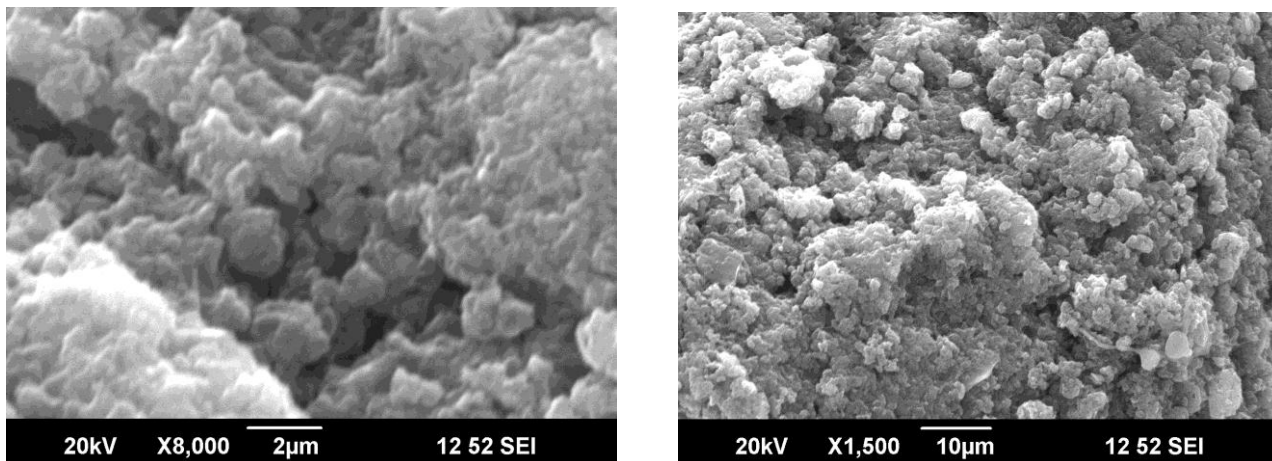


Figure 3. SEM image of the samples: GO-PANI

Cyclic voltammetry of deposited GO-PANI composite films on Pt-Ir electrode can be seen in 4 in 0.5 M H_2SO_4 electrolyte at the potential range from -0.2 V to $+1.2\text{ V}$ versus Ag/AgCl (3 M KCl) with scan rate of 50 mV/s . GO-PANI cyclic voltammetry curves indicated the potentially dependent current-potential response and the capacitive behaviour was mainly due to the redox reactions of the GO-PANI surface functional groups in acidic media [10]. The oxidation peak was higher with GO-PANI composite film and the oxidation peak potential was shifted from 524.5 mV to 614.5 mV with GO-PANI. This behaviour could be explained by the mass transfer of the active species, ohmic drop resistance and charge transfer rate at the electrode surface. The peak current density for GO-PANI was also high. The higher current density during the anodic oxidation could be attributed to the higher conductivity surface and the mobility of more ions reaching to the interface.

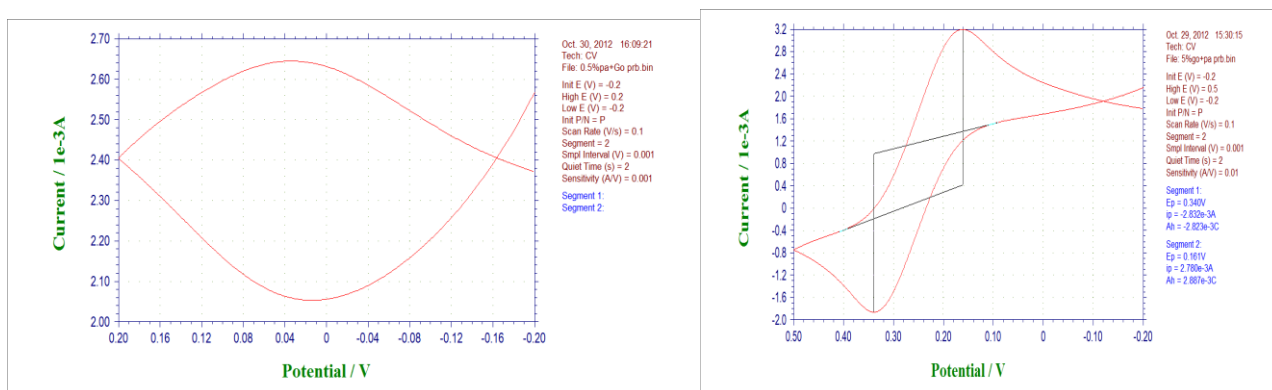
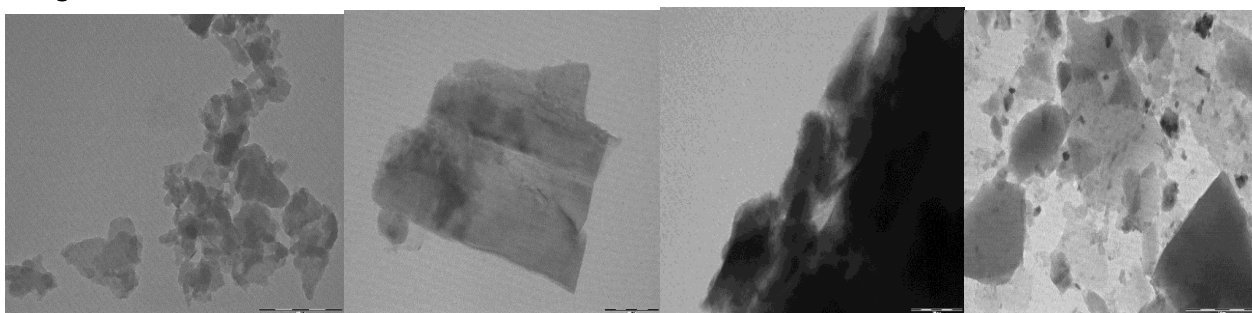


Figure 4. Cyclic voltammetry (CV) GO-PAN

Tem images of GO_PANI



IV. CONCLUSION

In this study, PANi/GO composites were prepared using the in-situ technique. Different amounts (0–20 wt.%) of GO were incorporated into the polymer matrix, polyaniline. Results showed that the composites exhibited a high specific capacitance at a low scan rate (1 mV/s). Natural graphite flakes were processed into graphene oxide (GO) using a modified version of Hummer's method. The PANi/GO composites were assessed by scanning electron microscopy, thermogravimetric analysis, Fourier-transform infrared spectroscopy, and X-ray diffraction. The specific gravimetric capacitance (C_{sp}) using cyclic voltammetry and charge/discharge characteristics were utilised to measure the devices' performance using the composites as supercapacitor electrodes.

V. REFERENCES

- [1]. Zhou, Y.; Wang, C.H.; Lu, W.; Dai, L. Recent Advances in Fiber-Shaped Supercapacitors and Lithium-Ion Batteries. *Adv. Mater.* 2020, 32, e1902779.
- [2]. Liao, M.; Ye, L.; Zhang, Y.; Chen, T.; Peng, H. The Recent Advance in Fiber-Shaped Energy Storage Devices. *Adv. Electron. Mater.* 2019, 5, 1800456.
- [3]. Li, L.; Lou, Z.; Chen, D.; Jiang, K.; Han, W.; Shen, G. Recent Advances in Flexible/Stretchable Supercapacitors for Wearable Electronics. *Small* 2018, 14, e1702829.
- [4]. Chen, D.; Jiang, K.; Huang, T.; Shen, G. Recent Advances in Fiber Supercapacitors: Materials, Device Configurations, and Applications. *Adv. Mater.* 2020, 32, e1901806.
- [5]. Zhai, S.; Karahan, H.E.; Wang, C.; Pei, Z.; Wei, L.; Chen, Y. 1D Supercapacitors for Emerging Electronics: Current Status and Future Directions. *Adv. Mater.* 2019, 32, e1902387.
- [6]. Tebyetekerwa, M.; Marriam, I.; Xu, Z.; Yang, S.; Zhang, H.; Zabihi, F.; Jose, R.; Peng, S.; Zhu, M.; Ramakrishna, S. Critical insight: Challenges and requirements of fibre electrodes for wearable electrochemical energystorage. *Energy Environ. Sci.* 2019, 12, 2148–2160.
- [7]. Zhu, Y.H.; Yang, X.Y.; Liu, T.; Zhang, X.B. Flexible 1D Batteries: Recent Progress and Prospects. *Adv. Mater.* 2020, 32, e1901961.
- [8]. Chen, L.; Liu, Y.; Zhao, Y.; Chen, N.; Qu, L. Graphene-based fibers for supercapacitor applications. *Nanotechnology* 2016, 27, 032001.
- [9]. Feng X-M, Li R-M, Ma Y-W, et al. One-step electrochemical synthesis of graphene/polyaniline composite film and its application. *Adv .Func. Mater* 2011;21:2989–2996
- [10]. A. Alkhouzaam, H. Qiblawey, M. Khraisheh, M. Atieh, M. Al-Ghouti Synthesis of graphene oxides particle of high oxidation degree using a modified Hummers method. *Ceram. Int.*, 46 (2020), pp. 23997–24007, 10.1016/j.ceramint.2020.06.177
- [11]. Sun J., Wang L.M., Yang Q., Shen Y., Zhang X. Preparation of Copper-Cobalt-Nickel Ferrite/Graphene Oxide/Polyaniline Composite and its Applications in Microwave Absorption Coating. *Prog. Org. Coat.* 2020;141:105552. doi: 10.1016/j.porgcoat.2020.105552.
- [12]. Y. Jafari, S.M. Ghoreishi, M. Shabani-Nooshabadi. Electrochemical deposition and characterization of polyaniline- graphene nanocomposite films and its corrosion protection properties]. *Polym. Res.*, 23 (2016), p. 91, 10.1007/s10965-016-0983-8

- [13]. Aricò A.S., Bruce P., Scrosati B., Tarascon J., Schalkwijk W.V.A.N., De Picardie U., Verne J., Umr- C. Nanostructured materials for advanced energy conversion and storage devices. *Nat. Mater.* 2005;4:148–159. doi: 10.1038/nmat1368.
- [14]. Soc C., Wang G., Zhang J. A review of electrode materials for electrochemical supercapacitors. *Chem. Soc. Rev.* 2012:797–828. doi: 10.1039/c1cs15060j.
- [15]. Zhang K., Zhang L.L., Zhao X.S., Wu J. Graphene/polyaniline nanofiber composites as supercapacitor electrodes. *Chem. Mater.* 2010; 22:1392–1401. doi: 10.1021/cm902876u.
- [16]. Q. Cheng, J. Tang, J. Ma, H. Zhang, N. Shinya, L.-C. Qin Polyaniline-coated electro-etched carbon fiber cloth electrodes for supercapacitors *J. Phys. Chem. C*, 115 (2011), pp. 23584-23590 film and its applications. *Adv Funct Mater* 2011; 21: 2989–2996.

Synthesis, Characterization and Biological Evaluation of 4-(4-Chloro-1-Hydroxy Naphthalen-2-Yl)-6-(3, 4-Dimethoxy Phenyl)-5, 6-Dihydropyrimidine-2(1h)-On

Dr. Vinod M. Sherekar

Assistant Professor, Department of Chemistry, Vinayak Vidnyan Mahavidyalaya, Nandgaon, Khandeshwar, Maharashtra, India

ARTICLE INFO

Article History:

Accepted : 01 Jan 2025

Published : 10 Jan 2025

Publication Issue :

Volume 12, Issue 7

January-February-2025

Page Number :

167-170

ABSTRACT

1-(4-Chloro-1-hydroxynaphthalen-2-yl)-ethan-1-one was prepared by refluxing 4-chloronaphthalen-1-ol with glacial acetic acid in presence of fused ZnCl_2 . By condensing 1-(4-chloro-1-hydroxynaphthalen-2-yl)-ethan-1-one with 3,4-dimethoxy benzaldehyde, to prepared by 1-(4-chloro-1-hydroxynaphthalen-2-yl)-3-(3,4-dimethoxy phenyl)-prop-2-en-1-one was synthesized. 1-(4-chloro-1-hydroxynaphthalen-2-yl)-3-(3,4-dimethoxy phenyl)-prop-2-en-1-one, urea and concentrated HCl in DMF were added and refluxed. Cool and pour in crushed ice. Treat it with cold NH_4OH solution to obtain titled compounds. The compounds thus synthesized have been characterized by physical and spectral data. All of these titled synthesized compounds have been screened for antimicrobial study and are found to possess excellent antimicrobial activities.

Keywords: Antimicrobial Activities, Cold NH_4OH Solution, Conc. HCl in DMF.

I. INTRODUCTION

Dihydropyrimidin-2(1H)-one is designated hetero-cyclic compound with 2 Nitrogen atoms with pyrimidine ring in the six-member ring. Among the heterocycles, especially with Nitrogen containing heterocycles with pyrimidine ring nucleus is reckon as a the most useful framework for biological and pharmacological activities. This nucleus has wide applications in the physiological and industrial areas and proven to be most beneficial. They have been used extensively as important pharmacophore in the field of organic chemistry and drug designing. In this review, our focus will be on the 3,4-dihydropyrimidine (DHPM) ring. Basically, it is a selective review on dihydropyrimidinones. Literature of last two decades is incorporated in this review. [1] Dihydropyrimidin-2(1H)-ones (DHPMs) via three-component condensation reaction of an aromatic aldehyde, urea, and ethyl acetoacetate. [2,4]. Dihydropyrimidinones (DHPMs) and their derivatives occupy a prominent

place; these cores are of immense biological importance; play an important role as essential building blocks in the synthesis of DNA and RNA [5]. World Health Organization (WHO) announced a global priority for the development of new drugs, particularly for antibiotic-resistant infections

[6]. This has increased the scientist interest in bioactive nitrogen-containing heterocyclic substances such as 3,4-dihydro-pyrimidin-2 (1H)-ones, or just dihydropyrimidinones (DHPMs). compounds were synthesized by the Italian chemist Pietro Biginelli in 1893[6].

The synthesis of the dihydropyridine and their derivatives increasing tremendously significant because they generally show diverse medicinal properties. Many reports exploring in Vivo and in Vitro dihydropyrimidine-2-one derivatives show variety of pharmacological activities such as active and safe tumor anti-initiating and multi-potent blocking agent [7], anxiolytic [8], antihypertensive agents [9], anticonvulsant [10], anticancer [11], analgesic activities [12]. Their efforts are quite significant in literature hence considering the scope of dihydropyrimidine derivatives we have synthesized novel 4-(4-chloro-1-hydroxynaphthalen-2-yl)-6-(3,4-dimethoxy phenyl)-5,6-dihydropyrimidine-2(1h)-one from 4-chloronaphthalen-1-ol and studied for their biological activities.

II. MATERIALS AND METHOD: -

Synthesis of 1-(4-Chloro-1-hydroxynaphthalen-2-yl)-ethan-1-one.

1-(4-Chloro-1-hydroxynaphthalen-2-yl) ethan-1-one was prepared by modified Nenck's method in which 4-chloro-naphthalen-1-ol was refluxed with glacial acetic acid in presence of fused ZnCl_2 .

Synthesis of 1-(4-Chloro-1-hydroxynaphthalen-2-yl)-3-(3,4-dimethoxy phenyl)-prop-2-en-1-one.

1-(4-Chloro-1-hydroxynaphthalen-2-yl)-3-(3,4-dimethoxy phenyl)-prop-2-en-1-one was synthesized from 1-(4-Chloro-1-hydroxynaphthalen-2-yl) ethan-1-one by condensing it with 3,4-dimethoxy benzaldehyde were added in ethanol solvent and KOH mixture.

Synthesis of 4-(4-Chloro-1-hydroxy naphthalen-2-yl)-6-(3,4-dimethoxy phenyl)-5,6-dihydropyrimidine-2(1H)-one.

4-(4-Chloro-1-hydroxynaphthalen-2-yl)-6-(3,4-dimethoxy phenyl)-5,6-dihydropyrimidine-2(1H)-one was prepared from 1-(4-Chloro-1-hydroxynaphthalen-2-yl)-3-(3,4-dimethoxy phenyl)-prop-2-en-1-one was reflux with urea and concentrated HCl in DMF. It was then treated with cold NH_4OH .

III. SCHEME: -

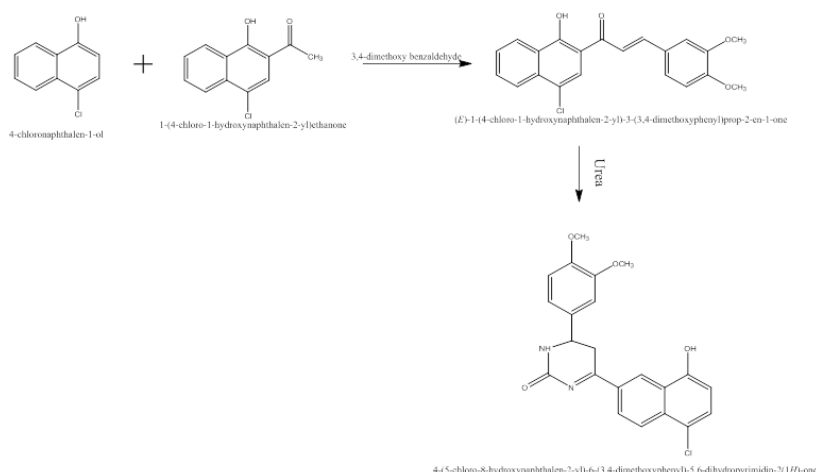


Table 1. PHYSICAL DATA OF SYNTHESIZED COMPOUNDS

Sr.no	Compound no	R1	R2	Molecular formula	Melting Point °C	% Yield	% Nitrogen		R.F Value
							Found	Calculated	
1	1	-OCH ₃	-H	C ₂₁ H ₁₇ N ₂ O ₃ Cl	258°C	47%	6.61	6.63	0.57
2	2	-OCH ₃	-OCH ₃	C ₂₂ H ₁₉ N ₂ O ₄ Cl	223°C	46%	6.25	6.24	0.65
3	3	-H	-OH	C ₂₀ H ₁₆ N ₂ OCl	229°C	46%	6.93	6.80	0.56
4	4	-OH	-H	C ₁₇ H ₁₆ N ₂ O ₂ Cl	258°C	53%	5.84	5.83	0.58

IV. SPECTRAL ANALYSIS: -

IR(ν_{max}) (cm^{-1}): 1623 (C=O, str), 3344 (NH, str), 1567 (C=N), 1162 (C-O-C), 757 (monosubstituted Benzene)

NMR (δ ppm): 1.3-1.9 (m, 2H, -CH₂ of pyrimidine), 10.32 (s, 1H, -OH), 3.63 (s, 3H, -OCH₃), 2.55 (s, 3H, CH₃,-)

V. ANTIMICROBIAL STUDIES: -

All above synthesized 4-(4-Chloro-1-hydroxy naphthalen-2-yl)-6-(3,4-dimethoxy phenyl)-5,6-dihydropyrimidine-2(1H)-one has been studied for their antimicrobial activity against *Escherichia coli*, *Proteus mirabilis*, *Staphylococcus aureus*, *Pseudomonas aeruginosa*. The culture of each species was incubated at 37°C and the zone of inhibition was measured after 24 hr. Results are tabulated in Table. Most of these compounds were found active

Sr.no	Compound Number	Antimicrobial Activity			
		E-coli	<i>Proteus mirabilis</i>	<i>Staphylococcus aureus</i>	<i>Pseudomonas aeruginosa</i>
1	1	17	18	16	10
2	2	16	10	18	14
3	3	18	12	14	17
4	4	15	14	12	13

Strongly active, range 15-19 Weakly active, range 7-10 mm, moderately active, range 11-14mm, Inactive,

VI. CONCLUSION: -

Thus, from above results it was observed that these heterocyclic compounds were found effective against *Escherichia coli*, *Proteus mirabilis*, *Staphylococcus aureus*, *Pseudomonas aeruginosa*. So those compounds can be easily be used for the treatment of diseases caused by test pathogens, only when they do not have toxic and other side effects.

VII. REFERENCES

- [1]. Varma Aman et al; Ammonium tetrafluoroborate: Novel Unprecedented Catalyst for the Synthesis of 3,4-dihydropyrimidin-2(1H) -ones through Biginelli Reaction. *Chemistry Select.* 2024; 9(8).

- [2]. Kappe C. Oliverr;Recent Advances in the Biginelli Dihydropyrimidine Synthesis. New Tricks from an Old Dog. *Accounts of Chemical Research*. 2001; 33(12):879-88
- [3]. Selvakumar K et al; Heteropoly acid supported on activated natural clay-catalyzed synthesis of 3,4-dihydropyrimidinones/thiones through Biginelli reaction under solvent-free conditions. *Synthetic Communication*. 2017; 48(2):1-10.
- [4]. Rajabi F et al; EfficientSynthesisofDihydropyrimidinesUsingaHighly Ordered MesoporousFunctionalizedPyridiniumOrganosilica.*Catalyst*. 2022; 12(3): 350.
- [5]. Fauzi Ahmad, Saifudin Azis, Rullah Kamal. Synthesis of Dihydropyrimidinone (DHPM) Derivatives through a Multicomponent Reaction (MCR) and Their Biological Activity.*J. med. chem. sci.*2023; 6(8):1810-1817.
- [6]. Pore Santosh B; Natural Surfactant Mediated Synthesis of 4-Aryl Substituted 3,4-Dihydropyrimidinones. *Ajchem*.2023; 35(12):3037-3041.
- [7]. Taviti Kumara S et al; Design, synthesis and biological Evaluation of novel chromones having 3,4-dihydropyrimidine-2(1H)-one core at C-8 in combination with triazoles:New glucosides inhibitors and anti-bacterial agents.*Eur. J. Med. Chem.* 2024; 12(1):100187.
- [8]. Adhikari Adithya et al; Synthesis, characterization and biological evaluation of dihydropyrimidine derivatives. *Saudi Pharmaceutical Journal*. 2012; 20(1): 75-79.
- [9]. Beena K.P et al; DihydroPyrimidinones-A Versatile Scaffold with diverse Biological Activity. *J. Pharm. Sci. & Res.* 2016; 8(8): 741-746.
- [10]. Ravi kumar K, Harika V L, Shaik A B. Synthesis, characterization and biological evaluation 3,4-dihydropyrimidin-2(1H)-thione derivatives. *Arch.Appl. Sci. Res.* 2014; 6(6): 121-127.
- [11]. Shrekar V M. Padole N S. Kakade K P. Synthesis, Characterization and Biological Evaluation of 4-(4-chloro1-hydroxy naphthalen-2-yl)-6-(4- methoxy phenyl)-5,6- dihydropyrimidine-2(1h)-one). *Jetir*. 2022; 9(1): 15-19
- [12]. Garg V. Jindal D. Singh R. Synthesis and Evaluation of antifungal activity of 4, 6- Diphenyl-3, 4-Dihydropyrimidine-2-(1h)-one derivatives. *tjpr.org*. 2020; 7(6): 8-12.

Physicochemical and Thermodynamic Studies of the Schiff Base Ligands in Binary Polar and Nonpolar Solvent System

Y. S. Thakare

P.G. Department of Chemistry, Shri Shivaji Science College, Amravati, Maharashtra, India

ARTICLE INFO

Article History:

Accepted : 01 Jan 2025

Published : 10 Jan 2025

Publication Issue :

Volume 12, Issue 7

January-February-2025

Page Number :

171-178

ABSTRACT

Present work investigates the newly synthesis Schiff base derivatives, characterization, density, viscometric and thermodynamic study in 70% ethanol-water and 70% dioxane-water binary solvent system. Elemental analysis, and spectral interpretation was carried out to characterize the structure of synthesized Schiff base. Various thermodynamic parameters like the change in enthalpy, entropy and Gibbs free energy were evaluated using different concentration at 308K, 318K, and 328K. It gives very important information about change in viscosity with temperature. Solute-solute interactions solute-solvent interactions were interpreted by viscometric study of synthesized ligand at different concentration. Positive value of B-coefficient may attribute to strong solute-solvent interaction on other hand value of A-coefficient is almost negative which indicates weak solute-solute interaction. The results show that the value of specific viscosity varies with concentration and nature of Schiff base.

Keywords: viscosity, thermodynamic parameter, Schiff base ligand, molecular interaction.

I. INTRODUCTION

Schiff bases have been known since 1864 when Hugo Schiff reported the condensation of primary amines with carbonyl compounds. Nowadays, the research field dealing with Schiff base coordination chemistry has expanded enormously because of their wide uses in inorganic, bioinorganic, analytical, material science, and pharmaceutical chemistry. For years, Schiff bases have been greatly inspiring to many chemists and biochemists [1]. Schiff base metal complexes exhibits antibacterial, antifungal, anticancer, anti-inflammatory and antioxidant activities[2-3]. The densities and viscosities of ternary mixtures of *N,N*-salicylidenephenylenediamine Schiff base (Salophen) + ionic liquid + *N,N*-dimethylformamide (DMF) have been determined at 298.15 K[4]. For natural and industrial processes known significant physicochemical properties like density, viscosity, surface tension and antimicrobial properties Schiff base ligands metal complexes were studied [5-7]. Concentration and temperature dependence of the thermodynamic properties

of novel Schiff based ligand were carried out in different solvent system [8]. Volumetric and viscometric studies were carried out to study solute-solvent molecular interactions study [9-12].

The present study deals with synthesis and viscometric measurement of Schiff base ligand N-methyl 1-phenylmethanimine (C₁), 2-methoxy-4((phenylimino)methyl)phenol (C₂) and 1-(4-methoxyphenyl)-N-Phenylmethanimine (C₃) at 308 K, 318 K and 328 K in binary mixture of 70% dioxane-water and 70% ethanol-water. From the data obtained solute-solute, solute-solvent interactions and thermodynamic parameters ΔG , ΔH and ΔS have been calculated.

II. MATERIALS AND METHODS

Experimental Procedure

All the chemicals used were of analytical grade reagent from S D Fine-Chem Limited and were used without further purification. Aqueous solutions were prepared with doubly distilled water. The binary mixture of 70% dioxane-water and 70% ethanol-water were prepared gravimetrically in Stoppard bottle. The densities and viscosities of pure liquids and their binary mixtures were measured using single capillary pycnometer and Ostwald's viscometer which was calibrated with double distilled water. The flow time was measure with the digital stop watch, each sample allowed to flow three times and then average flow time was calculated. The thermodynamic measurement was carried out in the thermostat. From the observation density, relative and specific viscosity can be calculated for all the Schiff base ligand in both the solvent.

$$\eta_r = \frac{d_1 \times t_1}{d_w \times t_w}$$

η_r -relative viscosity ($\eta_r = \eta_l/\eta_w$), η_l , d_l , t_l and η_w , d_w , t_w were viscosity, density and time required to flow for Schiff base ligand and water respectively. Viscosity data were analyzed in the light of Jones-Dole equation.

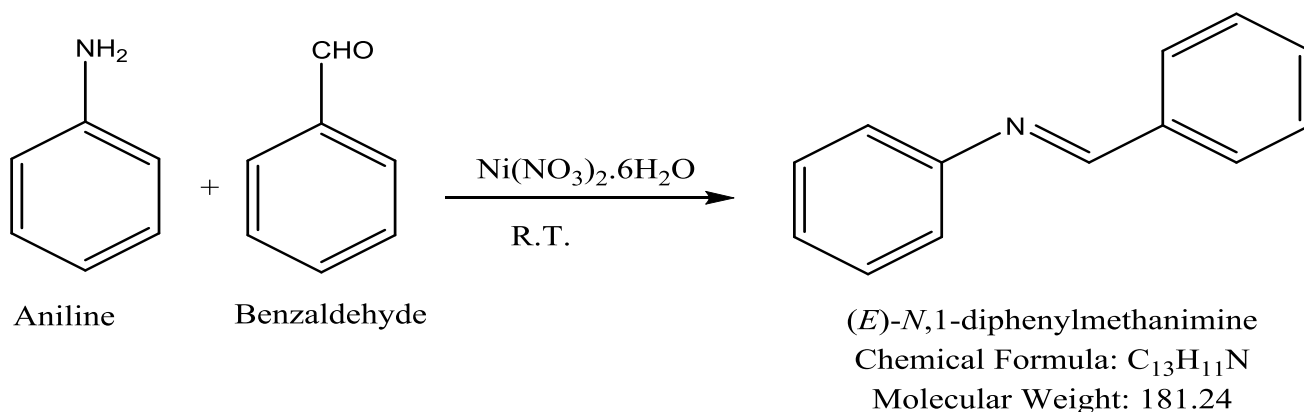
$$(\eta_r - 1) / \sqrt{C} = A + \beta \sqrt{C}$$

Where A and β are the Falkenhagen and the Jones-Dole coefficients. From the graph of $(\eta_r - 1) / \sqrt{C}$ verses \sqrt{C} , 'A' which is the measure of solute-solute interactions and ' β ' which is the measure of solute-solvent interactions has been calculated.

Synthesis of Schiff Base

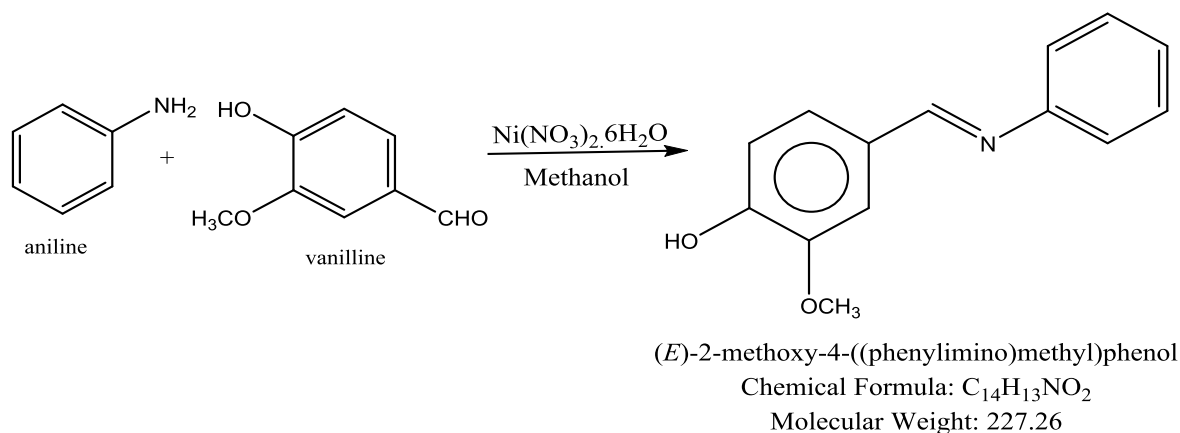
1) Synthesis of N-methyl 1-phenylmethanimine (C₁)

0.01 mole of benzaldehyde is added to the solution of aniline (0.01mole) in ethanol as a solvent. Catalytic amount of nickel nitrate hexahydrate is added to the reaction mixture and stirrer at room temperature. The solid obtained is filter and recrystallized by using ethanol. Yield - 78 %, Colour- Green, M.P -110° C, Solubility - Hot ethanol, M. F.- C₁₃H₁₁N, M. Wt.- 181.24



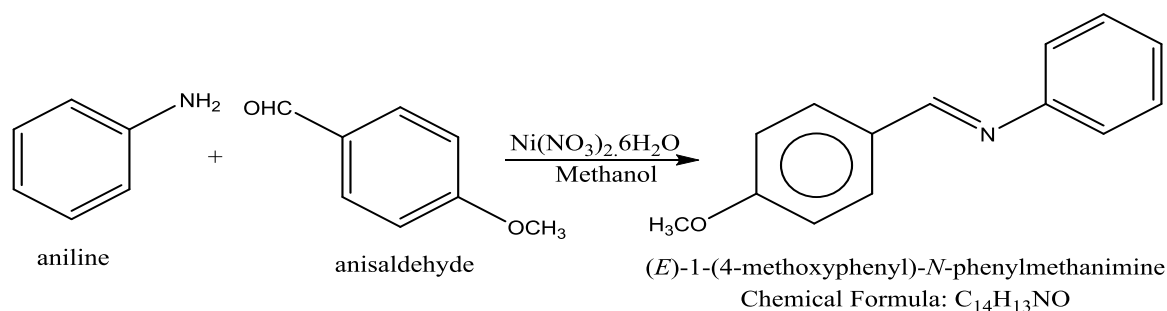
2) Synthesis of 2-methoxy-4-((phenylimino)methyl)phenol (C₂)-

0.01 mole of Aniline is added to the solution of Vanilline (0.01mole) in ethanol as a solvent. Catalytic amount of nickel nitrate hexa-hydrate is added to the reaction mixture and stirrer at room temp the solid obtained is filter and recrystallized by using ethanol. Yield - 75 %, Colour – yellow, M.P -110° C, Solubility- Hot ethanol, M. F. - C₁₄H₁₃NO₂, M Wt.- 227.26



3) Synthesis of 1-(4-methoxyphenyl)-N-Phenylmethanimine (C₃)-

0.01 mole of Aniline is added to the solution of Anisaldehyde (0.01mole) in ethanol as a solvent. Catalytic amount of nickel nitrate hexa-hydrate is added to the reaction mixture and stirrer at room temp the solid obtained is filter and recrystallized by using ethanol. Yield - 73 %, Colour – green, M.P :-110° C, Solubility - Hot ethanol, M. F.- C₁₄H₁₃NO, M Wt. - 221.26



III.RESULT AND DISCUSSION

Viscometric study with variation in concentration

To explore the utility of synthesized Schiff base derivatives C₁, C₂ and C₃ its viscosity study was carried out for different concentration in 70% ethanol-water system and 70% dioxane-water system as a solvent. The data obtained were used to calculate the relative viscosity (η_r) and density of Schiff base derivative. It was observed that relative viscosity decreases in both the solvents. The study was extended to calculate Jones-Dole coefficient A and 'β' which is the measure of solute-solute interaction and solute-solvent interaction respectively. The plot between ($\eta_r - 1$) / \sqrt{C} versus \sqrt{C} shows a linear graph which shows the validity of Jones-Dole equation for all the tested Schiff base derivative. The slope of this graph shows the value of β –coefficient, and intercept give the value of coefficient A.

Table 1 Viscometric study with variation in concentration of ligand(T=273K)

System	Medium	Conc. (M)	\sqrt{c}	Time flow (sec)	Relative viscosity (η_r)	Specific viscosity (η_{sp})	A coefficient t	β coefficient
N-methyl-phenylmethanimine(C ₁)	70% Ethanol water system	0.1	0.31	33	0.9538	-0.149	-0.9.962	34.59488
		0.05	6	28	0.7937	-0.925		
		0.001	0.22	25	0.7116	-9.303		
			4 0.03 2					
N-methyl-phenylmethanimine(C ₁)	70% Dioxane water system	0.1	0.31	22	0.7583	-0.7796	-11.77	39.29699
		0.05	6	21	0.7139	-1.2829		
		0.001	0.22	20	0.6561	-		
			4 0.03 2			11.0935		
2-methoxy-4((phenylimino)methyl)phenol (C ₂)	70% Ethanol water system	0.1	0.31	47	1.3561	1.596	0.289	3.227734
		0.05	6	40	1.1639	0.564		
		0.001	0.22	39	1.1259	0.528		
			4 0.03 2					
2-methoxy-4((phenylimino)methyl)phenol (C ₂)	70% Dioxane water system	0.1	0.31	24	0.8151	-0.5964	-10.76	36.29651
		0.05	6	23	0.7538	-1.1040		
		0.001	0.22	21	0.6860	-		
			4 0.03 2			10.1290		
1-(4-methoxyphenyl)-N-Phenylmethanimine (C ₃)	70% Ethanol water system	0.1	0.31	59	1.6710	3.0089	1.261	5.2916668
		0.05	6	54	1.5100	2.286		
		0.001	0.22	44	1.2317	1.474		
			4 0.03 2					
1-(4-methoxyphenyl)-N-Phenylmethanimine (C ₃)	70% Dioxane water system	0.1	0.31	19	0.6511	-1.1254	-0.279	53.49988
		0.05	6	17	0.5631	-2.1031		
		0.001	0.22	16	0.5278	-		
			4 0.03 2			15.2322		

To study the pharmacokinetics of synthesized Schiff base, viscometric study was carried out at different concentration using polar and non-polar solvents. Above table shows that with decrease in concentration of ligand there is decrease relative viscosity and specific viscosity in 70% Ethanol water and 70% Dioxane water because decrease in concentration number of solute particle decreases at the same time solvation effect increases. It was observed from the table that the values of A are almost negative in both the solvent for C₁, C₂ and C₃ shows weak solute-solute interaction which is also supported by decrease in relative viscosity. Again the values of A are more negative in dioxane-water as compare to ethanol-water medium due to different polarity index of binary solvents. On the other hand value of β -coefficient is positive shows strong solute-solvent interaction which indicates the good drug activity. The value of β-coefficient is more positive in dioxane-water may be due to weak hydrogen bonding.

Viscometric study with variation in temperature

The relationship between of viscosity of liquids and temperature is expressed mathematically as- $\eta = A \cdot e^{\Delta G/RT}$
The viscometric study was extended for different concentration of Schiff base ligand in using 70% dioxane-water system and 70% ethanol-water system at 308K, 318K, and 328K. The graph plotted between log η_r and 1/T for each system was found to be linear showing the validity of above equation. From the temperature variation data, thermodynamic parameters like change in enthalpy, entropy, and Gibbs free energy have been evaluated using following equation and are listed in table 2.

$$\Delta G = -2.303 \times R \times \text{Slope}$$

$$\log \eta_{r_1} - \log \eta_{r_2} = \frac{\Delta H}{2.303} \left[\frac{1}{T_1} - \frac{1}{T_2} \right]$$

$$\Delta S = (\Delta H - \Delta G)/T$$

Table 2 Viscometric study with variation in temperature (medium –Dioxane-water)

System	Conc. (M)	Temp (K)	1 / T (K ⁻¹) × 10 ⁻³	Time flow (sec.)	Relative Viscosity η _r	Log (η _r)
C ₁	0.1	308	3.24 × 10 ⁻³	21	0.7842	-0.1055
		318	3.14 × 10 ⁻³	20	0.8638	-0.0635
		328	3.04 × 10 ⁻³	19	0.9386	-0.0275
	0.05	308	3.24 × 10 ⁻³	20	0.7278	-0.1379
		318	3.14 × 10 ⁻³	19	0.7981	-0.0979
		328	3.04 × 10 ⁻³	18	0.8600	-0.0655
	0.001	308	3.24 × 10 ⁻³	19	0.6665	-0.1761
		318	3.14 × 10 ⁻³	18	0.7309	-0.1361
		328	3.04 × 10 ⁻³	17	0.7843	-0.1055
C ₂	0.1	308	3.24 × 10 ⁻³	22	0.7972	-0.09843
		318	3.14 × 10 ⁻³	21	0.8804	-0.05531
		328	3.04 × 10 ⁻³	20	0.9529	-0.0209
	0.05	308	3.24 × 10 ⁻³	21	0.7366	-0.1327
		318	3.14 × 10 ⁻³	20	0.8116	-0.0906
		328	3.04 × 10 ⁻³	19	0.8754	-0.0577
	0.001	308	3.24 × 10 ⁻³	20	0.6942	-0.1585
		318	3.14 × 10 ⁻³	19	0.7646	-0.1165
		328	3.04 × 10 ⁻³	18	0.8212	-0.0855

System	Conc. (M)	Temp (K)	1 / T (K ⁻¹) × 10 ⁻³	Time flow (sec.)	Relative Viscosity η_r	Log (η_r)
C ₃	0.1	308	3.24 × 10 ⁻³	17	0.6232	-0.2053
		318	3.14 × 10 ⁻³	16	0.6771	-0.1693
		328	3.04 × 10 ⁻³	15	0.7208	-0.1421
	0.05	308	3.24 × 10 ⁻³	16	0.5665	-0.2468
		318	3.14 × 10 ⁻³	15	0.6143	-0.2116
		328	3.04 × 10 ⁻³	14	0.6501	-0.1870
	0.001	308	3.24 × 10 ⁻³	15	0.5252	-0.2796
		318	3.14 × 10 ⁻³	14	0.5684	-0.2453
		328	3.04 × 10 ⁻³	13	0.5986	-0.2228

Table 3Viscometric study with variation in temperature (medium –Ethanol-water)

System	Conc. (M)	Temp (K)	1 / T (K ⁻¹) × 10 ⁻³	Time flow (sec.)	Relative Viscosity (η_r)	Log (η_r)
C ₁	0.1	308	3.24 × 10 ⁻³	32	0.9887	-0.0049
		318	3.14 × 10 ⁻³	29	1.0041	0.0017
		328	3.04 × 10 ⁻³	26	1.0063	0.0027
	0.05	308	3.24 × 10 ⁻³	27	0.8202	-0.0860
		318	3.14 × 10 ⁻³	25	0.8650	-0.06209
		328	3.04 × 10 ⁻³	23	0.8848	-0.05315
	0.001	308	3.24 × 10 ⁻³	23	0.6539	-0.1844
		318	3.14 × 10 ⁻³	21	0.6910	-0.1605
		328	3.04 × 10 ⁻³	19	0.7003	-0.1547
C ₂	0.1	308	3.24 × 10 ⁻³	38	1.1306	0.0533
		318	3.14 × 10 ⁻³	35	1.2287	0.0894
		328	3.04 × 10 ⁻³	30	1.0758	0.0317
	0.05	308	3.24 × 10 ⁻³	45	1.333	0.1248
		318	3.14 × 10 ⁻³	42	1.4570	0.1634
		328	3.04 × 10 ⁻³	39	1.4882	0.1726
	0.01	308	3.24 × 10 ⁻³	38	1.167	0.0670
		318	3.14 × 10 ⁻³	36	0.0017	-2.1739
		328	3.04 × 10 ⁻³	33	1.2926	-3.1114
C ₃	0.1	308	3.24 × 10 ⁻³	59	1.6933	0.2287
		318	3.14 × 10 ⁻³	52	1.540	0.1875
		328	3.04 × 10 ⁻³	45	1.6987	0.2301
	0.05	308	3.24 × 10 ⁻³	57	1.689	0.2276
		318	3.14 × 10 ⁻³	52	1.800	0.2552
		328	3.04 × 10 ⁻³	48	1.8278	0.2619
	0.01	308	3.24 × 10 ⁻³	42	1.222	0.0870
		318	3.14 × 10 ⁻³	38	1.2915	0.1110
		328	3.04 × 10 ⁻³	35	1.3270	0.1228

Table 4 Value of thermodynamic parameters

System	70%Dioxane-water				70%Ethanol-water		
	Conc. (M)	ΔG (J mole ⁻¹)	ΔH (J mole ⁻¹)	ΔS (J mole ⁻¹ K ⁻¹)	ΔG (J mole ⁻¹)	ΔH (J mole ⁻¹)	ΔS (J mole ⁻¹ K ⁻¹)
C ₁	0.1M	-0.7467	-906.11	2.7434	-0.5744	-86.446	0.2787
	0.05M	-0.6892	-845.66	2.9394	-0.3063	-377.03	1.1005
	0.001M	-0.6701	-823.90	4.1161	-0.2680	-339.23	1.2231
C ₂	0.1M	-0.7275	-845.99	2.7443	0.1914	289.10	-0.9380
	0.05M	-0.7084	-635.35	2.0933	-0.4403	-551.44	1.7889
	0.001M	-0.6892	-812.015	2.6341	30.4248	3655.29	-11.8242
C ₃	0.1M	-0.5935	-691.96	2.2446	-0.2354	-1052.54	3.4173
	0.05M	-0.5552	-699.26	2.2685	-0.3255	-458.87	1.4887
	0.001M	-0.5361	-579.07	1.8783	-0.3255	-458.87	1.4887

From the above table it is shown that the value of change in free energy for different derivative of Schiff base is decreases using ethanol-water and dioxane-water system. The value of entropy is also increases with decreases in concentration of compound in both the solvent system. The negative value of enthalpy indicates that the reaction is exothermic.

IV. CONCLUSION

In the present study, the relative viscosity of solution of Schiff base derivatives decreases with decrease in concentration of solution. It was observed that the values of α more negative and β -coefficients are more positive in Dioxane-water as compare to ethanol-water medium for all the tested Schiff's bases shows weak solute-solute and strong solute-solvent interaction indicates the good drug activity. The value of thermodynamic parameter increases with increases in temp in both the solvent system. The negative values of ΔH indicated the reaction is exothermic. The values of entropy are positive shows the randomness of solute molecules in the compound it was increase with decreases in concentration of the solvent. It was also observed that the values of entropy are more positive in medium-dioxane-water as compared to medium-ethanol-water. Thermodynamic study shows negative value of Gibbs's free energy. It was observed that the value of ΔG is more negative in 70% dioxane-water indicates the more hydrophobic nature of Schiff base derivative. These different results for all the tested compound may be due to different polarity index of solvent dioxane and ethanol.

V. REFERENCES

- [1]. E. Raczuk, B. Dmochowska, J. S. Fiertek, and J. Madaj, "Different Schiff Bases—Structure, Importance and Classification, *Molecules*. 2022, 27(3) pp. 787.
- [2]. S. Jain, M. Rana, R. Sultana, R. Mehendi, Rahisuddin, "Schiff Base Metal Complexes as Antimicrobial and Anticancer Agents" *Polycyclic Aromatic Compounds* 2023, 43(7) pp. 6351-6406
- [3]. H. Shekaari, A. Kazempour and M. Khoshalhan, "Schiff base ligands and their transition metal complexes in the mixtures of ionic liquid and organic solvent a thermodynamic study, *Phys. Chem. Chem. Phys.*, 2015,17, pp. 2179-2191

- [4]. H. Shekaari, A. Bezaatpour and R. Elhami-Kalvanagh, "Thermodynamic Properties of Salophen Schiff Base and Ionic Liquid ([CnmIm][Br]) and Dimethylformamide Ternary Mixtures at 298.15 K, J. Chem. Eng. Data, 2012, 57(2), pp. 345.
- [5]. M. A. Mughal, A. Mughal, G. Z. Memon, M. Y. Khuhawar and N. N. Memon, "Schiff Base Metal Complexes as Antimicrobial and Anticancer Agents", J. Chem. Soc. Pak., 35(6), 2013 pp. 1535.
- [6]. B. J. Gangani and P. H. Parsania, "Microwave-irradiated and classical syntheses of symmetric double Schiff bases of 1,1'-bis(4-aminophenyl) cyclohexane and their physicochemical characterization," Spectroscopy Letters, 2007 40(1), pp. 97.
- [7]. N. M. Hosny, M. A. Hussien, F.M. Radwan, and N. Nawar, "Synthesis, spectral, thermal and optical properties of Schiff-base complexes derived from 2(E)-2-((Z)-4-hydroxypent-3-en-2-ylideneamino)-5-guanidinopentanoic acid and acetylacetone", J. Mol. Str., 2017, 1143, pp. 176-183.
- [8]. J. Aher, A. Bhagare, M. Gaware, D. Lokhande, A. Kardel, A. Dhayagude, V. Jadhav, K. Mahale, "Concentration and Temperature Dependence of the Thermodynamic Properties of Novel Biologically Active 3-Substituted Schiff Base of 4-Piperidyl N-(4-chlorophenyl)maleimide", Asian Journal of Chemistry, 2021, 33(6), 1403-1408
- [9]. H. Shekaari, A. Bezaatpour and R. Elhami, "Volumetric and Viscometric Studies of N,N'-Bis(salicylaldehyde)-1,3-diaminopropane Schiff Base (Salpr) in Ionic Liquid and DMF solutions" J. Sol. Chem. 2012, 41, p. 516.
- [10]. S. D. Deosarkar, A. L. Puyad, P. S. Kattekar and T. M. Kalyankar, "The density and viscosity of aqueous solutions of sodium 2-([4-(3-methoxypropoxy)-3-methylpyridin-2-yl]methyl)sulfinyl)benzimidazol-1-ide and solute-solvent molecular interactions study", Russian J. phy. Chem., A, 2013, 87, 524.
- [11]. S. Baluja, K.P. Vaishnani, R. Gajera and N. Kachhadia, "Acoustical properties of Schiff base solutions in dmf", Lat. Am. appl. res. 2010, 40(3), pp-249.
- [12]. Y. S. Thakare A. P. Thakare and C. S. Kedia Density and Viscometric Studies of Schiff's Base Ligands at Different Temperature in Binary Mixture Aayushi Inter. Interdisc. Res. J., 2018. pp-597.

Study of Acoustic Properties of Some Synthesized Thiazolyl Substituted Schiff Bases in Acetone-Water Mixture At 303.15 K Using Ultrasonic Velocity Measurement

Dr. R.S. Talegaonkar

Department of Chemistry, Matoshree Vimalabai Deshmukh Mahavidyalaya, Amravati, Maharashtra, India

ARTICLE INFO

Article History:

Accepted : 01 Jan 2025

Published : 10 Jan 2025

Publication Issue :

Volume 12, Issue 7

January-February-2025

Page Number :

179-185

ABSTRACT

The density, viscosity and sound velocity of five thiazolyl Schiff bases (1-5) derivatives in 70% Acetone-water mixture have been studied at 303.15 K over a wide range of concentration. From these experimental data, some acoustical parameters such as Adiabatic compressibility (β_s), Intermolecular free length (LF), apparent molar volume (ϕV), apparent molar compressibility (ϕK), relative association (RA) and specific acoustic impedance (Z) have been evaluated. results are interpreted in terms of molecular interactions like solvent-solvent, solvent-solute and solute-solute interactions. A fairly good correlation between a given parameter and concentration is observed.

Keywords: density, viscosity, ultrasonic velocity, acoustical parameters, molecular interaction

I. INTRODUCTION

Ultrasonic technology is now a days employed in a wide range of application such as acoustic microscopy, drug industry, textile industry, paint industry, food and fat industry, flaw detector in metal, electrochemistry, optical storage cell, computer technology, surfactant, binary and ternary liquid, under water acoustic which is a oceanographic application include mapping of the sea bottom, discovering sunken ships and searching for schools of fish. The extensive uses of polymers in technology have promoted ultrasonic studies to understand the structures of polymers and furnish knowledge on solvophilic or solvophobic nature of polymers¹. The determination of some properties of solids such as compressibility, specific heat ratios, elasticity considered as the applications in materials science². Ultrasound waves have also been useful in industries for different physical treatments of industrially useful materials like agitation, dispersion, emulsification³ also for cleaning⁴ which includes the removal of grease, dirt, rust and paint from metal, ceramic glass and crystal surfaces and to repair cracks⁵. Ultrasonic rays are useful tool in sonochemistry⁶ and medical field also. Ultrasonic radio-frequency spectrum analysis provides application in various diagnosis such as paediatrics⁷⁻⁸, vascular diseases⁹⁻¹⁰,

brain diseases¹¹, ophthalmology¹²⁻¹³, in urology¹⁴⁻¹⁵, in cancer cel¹⁶⁻¹⁷ etc. Organic materials in landfill can also be degraded by ultrasound¹⁸.

There are various techniques to study the molecular interactions in liquids are nuclear magnetic resonance, microwave, ultraviolet and infrared spectroscopy, neutron and X-ray scattering and ultrasonic investigation. NMR techniques reflects the effect on proton bearing molecules, whereas microwave absorption provides information through dielectric constant.

In the present study an attempt has been made to study ultrasonic parameters like adiabatic compressibility (β_s), intermolecular free length (L_f), apparent molar volume (ϕ_v), apparent molar compressibility (ϕ_k), relative association and acoustic impedance (Z) in dioxane-water, acetone-water and ethanol-water mixture by measuring ultrasonic speeds (μ) and densities (ρ).

II. REVIEW LITERATURE AND NEED OF PRESENT WORK

The efforts to correlate the ultrasonic velocity and the attenuation coefficient with the physical parameter of liquid have been quite encouraging. K Nagbhushan Raju et al.¹⁹ studies apparent molar volume (ϕ_v) and apparent molar adiabatic compressibility of 2-methoxy, 2-ethoxy and 2-butoxy ethanol with water at different temperature from ultrasonic data. Sarvanakumar et al.²⁰ measured the densities viscosity, refractive indices, ultrasonic velocities and thermodynamic acoustical parameters of binary mixture like Acetophenone + Isoamyl acetate. The study of solute-solvent, solute-solute interaction is being possible to wide application of ultrasonic study. Rathor P and Singh M²¹ have determine the apparent molar volume (ϕ_v) and partial molar volume (ϕ_{v^0}) of aqueous solution of biologically important compound [glucose, sucrose, urea, citric acid, tartaric acid, ascorbic acid & oxalic acid] in different molality at different two temperature and discussion of solute-solvent interaction and electrostriction have been studied. Jan Antosiewicz et al.²² measured the maximal velocities of ultrasonic waves, as a function of the alcohol concentration in aqueous ethanolic medium, have been determined for solution of D-ribose, 1-methyl uracil, uridine, deoxyuridine, thymidine and cytidine. The results were related to interaction of the sugar hydroxyls with water. This particular field means study of hydration number from partial molar volume and adiabatic compressibility data attracting the attention of many researchers²³⁻²⁵

III. EXPERIMENTAL

The sound velocities of thiazoles were measured in 0.01 M to 0.05 M range in acetone - water mixture..

In the present investigation different parameters such as adiabatic compressibility (β_s), apparent molal volume (ϕ_v), intermolecular free length (L_f), apparent molal compressibility (ϕ_k), specific acoustic impedance (Z), relative association (R_A), were studied with the help of following equations.

$$\beta_s = \frac{1}{U_s^2 \cdot d_s} \quad \dots 1$$

$$\phi_v = \left(\frac{M}{d_s} \right) + \left[\frac{(d_0 - d_s) \times 10^3}{m \times d_s \times d_0} \right] \quad \dots 2$$

$$\phi_k = \frac{\beta_s \cdot M}{d_s} + \left[\frac{1000(\beta_s d_0 - \beta_0 d_s)}{m \times d_s \times d_0} \right] \quad \dots 3$$

$$L_f = K \sqrt{\beta_s} \quad \dots 4$$

$$Z = U_s \cdot d_s \quad \dots 5$$

$$R_A = \frac{d_s}{d_o} \left(\frac{U_o}{U_s} \right)^{1/3} \quad \dots 6$$

Where d_s , d_o and U_s , U_o are the densities and ultrasonic velocities of solution and pure solvent respectively. M is the molecular weight of substituted chalcone. β_s and β_o are the adiabatic compressibilities of solution and solvent respectively. K is Jacobson's constant and m is the molality of solution.

Table 1: Ultrasonic velocity, density, Adiabatic compressibility (β_s), Intermolecular free length (L_F) in different percentages of Acetone-Water mixture.

Temperature: 303± 0.1 °C Ultrasonic freq: 1 MHz Conc: 0.01 M

% of Acetone	Density (d_s) g m ⁻³	Ultrasonic Velocity(U_s) ms ⁻¹	Adiabatic Compressibility (β_s) 10 ⁻⁶ m ² N ⁻¹	Intermolecular free length(L_F)
System – MPPTMP-I				
100	0.99	921.2	1.19	6.5663
95	0.994	924.1	1.18	6.5325
90	1.006	930.8	1.15	6.4467
85	1.012	942.6	1.11	6.3471
80	1.018	950.2	1.09	6.2777
75	1.022	962.3	1.06	6.1867
System-PPTMP-I				
100	0.99	921.2	1.19	6.5663
95	1.012	923.6	1.16	6.4777
90	1.024	925.7	1.14	6.4250
85	1.032	927.6	1.13	6.3869
80	1.044	930.4	1.11	6.3310
75	1.05	932.8	1.09	6.2966
System-CPTMP-I				
100	0.99	921.2	1.19	6.5663
95	0.994	930.4	1.16	6.4883
90	1.008	933.7	1.14	6.4203
85	1.014	938.4	1.12	6.3692
80	1.02	941.4	1.11	6.3302
75	1.025	944.3	1.09	6.2954

Table 2:- Apparent molal volume (ϕ_v), Apparent molal compressibility (ϕ_κ), Relative Association (R_A) and Specific acoustic impedance (Z) in different percentages of Acetone-Water mixture.

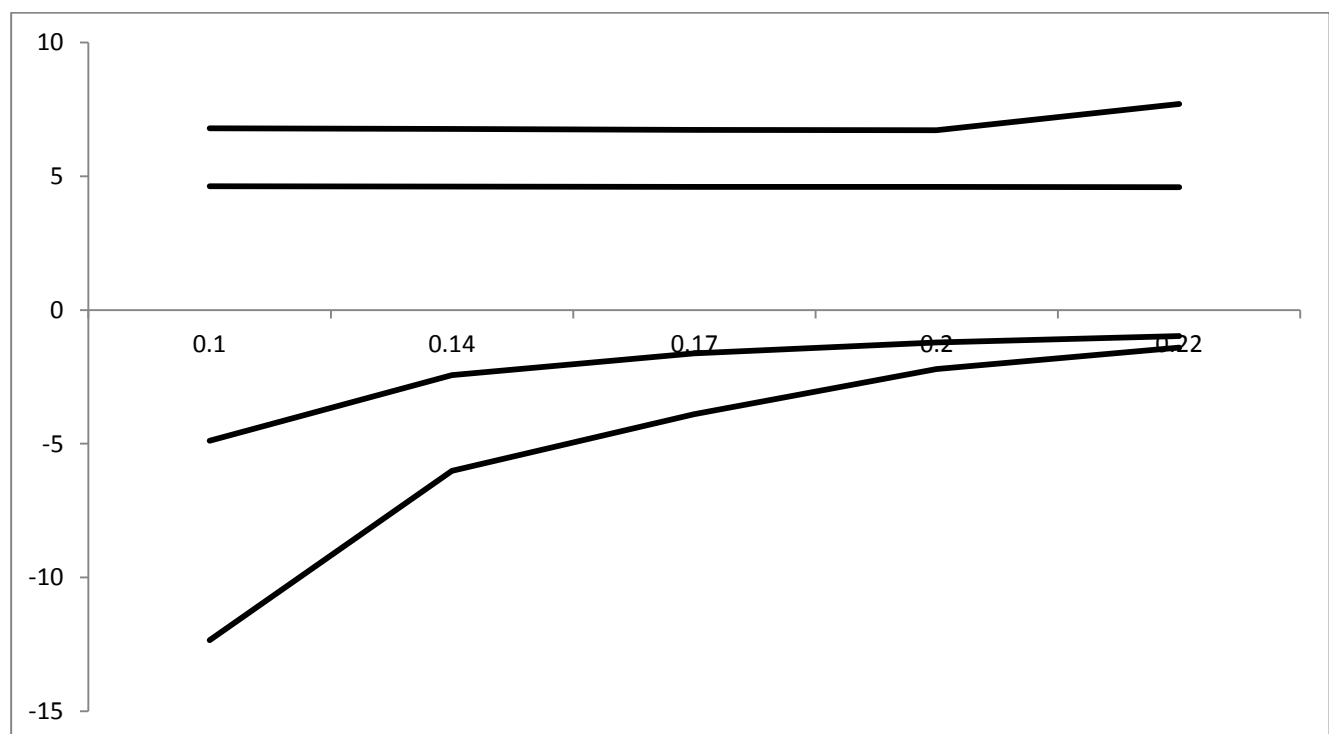
Temperature: 303± 0.1 °C Ultrasonic freq: 1 MHz Conc: 0.01 M

% of Acetone	Apparent molal Volume-(ϕ_v) ×10 ³ m ³ mol ⁻¹	Apparent molal Compressibility - (ϕ_κ) m ² N ⁻¹	Relative Association (R_A)	Specific Acoustic Impedance (Z) ×10 ² kg m ² s ⁻¹
System-MPPTMP-I				
100	2.4231	5.4823	0.5283	9.1198

% of Acetone	Apparent molal Volume-(ϕ_v) $\times 10^3 \text{ m}^3 \text{ mol}^{-1}$	Apparent molal Compressibility - (ϕ_κ) $\text{m}^2 \text{ N}^{-1}$	Relative Association (R_A)	Specific Acoustic Impedance (Z) $\times 10^2 \text{ kg m}^2 \text{ s}^{-1}$
95	2.4639	4.3679	0.5288	9.1855
90	2.5843	4.3189	0.5313	9.3638
85	2.6433	4.2967	0.5278	9.5391
80	2.7020	4.2738	0.5267	9.6730
75	2.7406	4.2602	0.5221	9.8347
System-PPTMP-I				
100	2.4202	4.3843	0.5283	9.1198
95	2.6407	4.2921	0.5386	9.3468
90	2.7570	4.2437	0.5438	9.4791
85	2.8330	4.2121	0.5469	9.5728
80	2.9449	4.1656	0.5516	9.7133
75	2.9998	4.1429	0.5533	9.7944
System-CPTMP-I				
100	2.4187	4.3843	0.5283	9.1198
95	2.4595	4.3695	0.5252	9.2481
90	2.5999	4.3112	0.5307	9.4116
85	2.6588	4.2875	0.5312	9.5153
80	2.7171	4.2636	0.5326	9.6022
75	2.7651	4.2440	0.5336	9.6790

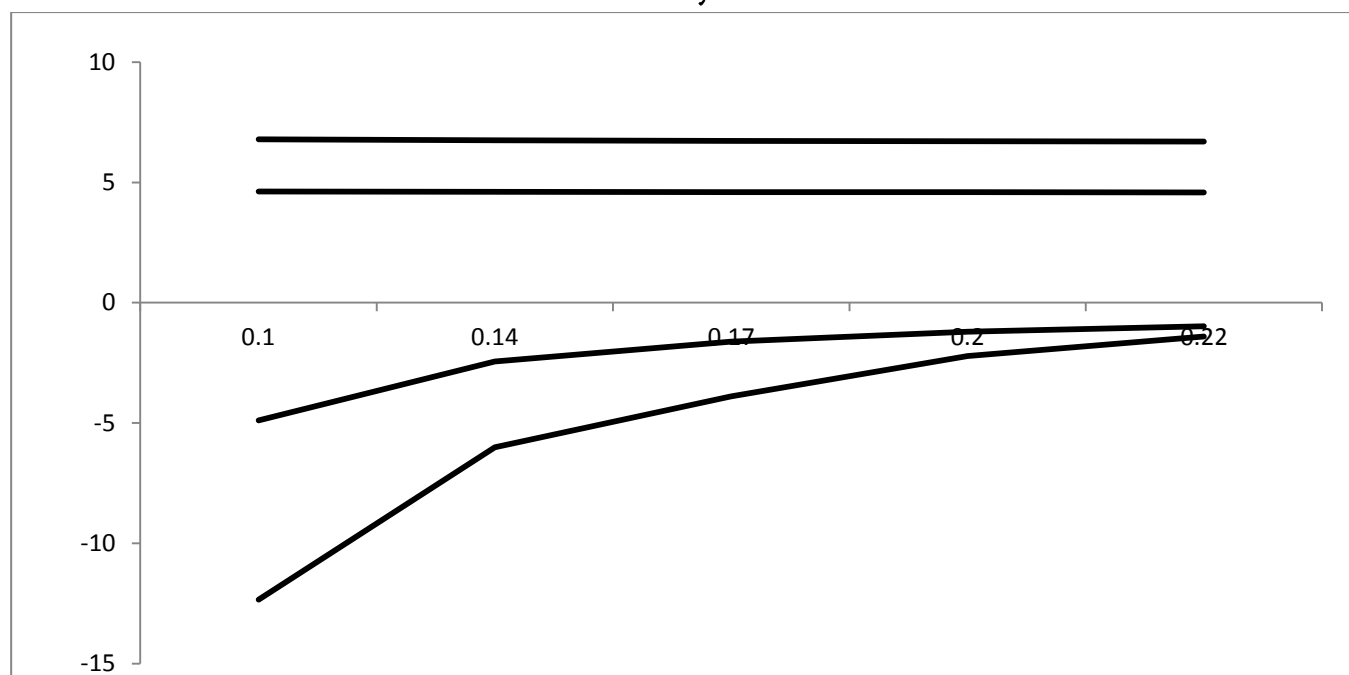
Medium : Acetone-water

System : MPPTMP-I



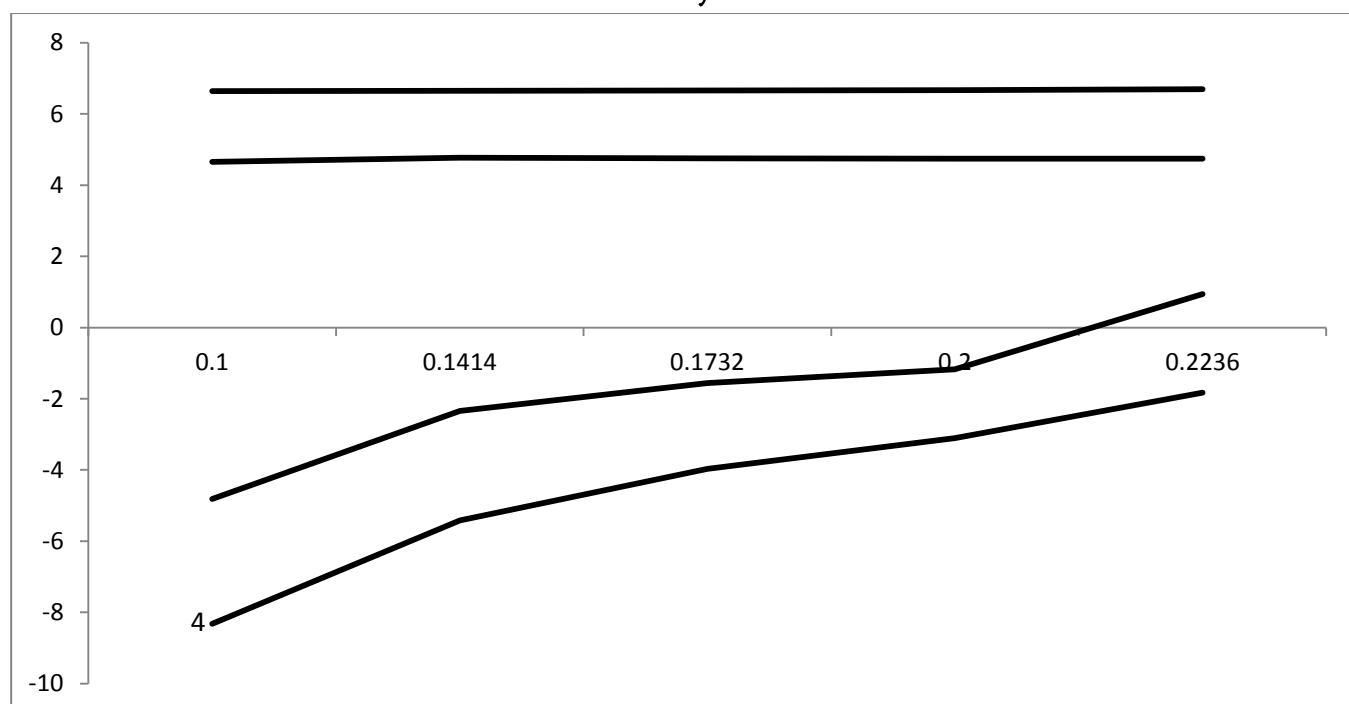
Medium : Acetone-water

System : PPTMP-I



Medium: Acetone-Water

System : CPTMP-I



IV.RESULTS AND DISCUSSION

In present investigation, ultrasonic velocity and density of synthesized thiazolyl Schiff's bases have been studied at different percentages of acetone-water mixture the compounds were studied with variation in percentages of binary mixtures at 30°C. From the obtained data, apparent molal volume ϕ_v , apparent molal compressibility ϕ_k , adiabatic compressibility (β_s), intermolecular free length (L_f), relative association (R_A), specific acoustic impedance (Z) were calculated. While calculating the acoustic parameters, Jacobson's Constant

$K = 6.0186 \times 10^4$ and $\beta_0 = 44.6331 \times 10^{-6} \text{ bar}^{-1}$ were used. The acoustical parameters have been used to study the molecular interactions in the solution.

Ultrasonic velocity increases with decrease in percentage of solvent-water mixture for all the system. Variation of ultrasonic velocity in solution depends upon the increase or decrease of molecular free length after mixing the component, based on a model for sound propagation proposed by Eyring and Kincaid. The decrease in percentage of dioxane in solution may be due to collection of solvent molecule around ions, this supports weak ion-solvent interaction.

The decrease in adiabatic compressibility following, a increase in ultrasonic velocity shows there by weakening intermolecular interaction. It was observed that intermolecular free length decreases linearly on decreasing the percentage of acetone mixture. It indicates solute-solvent interaction. This may be due to the decrease in number of free ions, showing the occurrence of ionic association due to solute-solvent interaction. The intermolecular free length increases due to greater force of interaction between solute and solvent by forming hydrogen bonding. This was happened because there is a significant interaction between ions and solvent molecules. Also this attributes the fact that decrease in number of free ions showing the occurrence of ionic association due to weak ion-ion interaction. The relative association (R_A) is the property used to understand the interaction which is influenced by two factors (i) The breaking up of the solvent structure on addition of solute to it; and (ii) the solvation of solutes that are simultaneously present.

V. CONCLUSION:

Decrease in percentages of solvent-water mixture decrease in R_A , suggest that solvation of ions predominates over the breaking up of solvent molecules on addition of solute. The following observations have been made on apparent molal compressibility ϕ_K and apparent molal volume (ϕ_v).

- i) The values of ϕ_v & ϕ_K are all negative over the entire range of percentage variation study.
- ii) The negative ϕ_K values are increasing with increasing the solute content i.e., concentration over the entire range of medium.

VI. ACKNOWLEDGEMENT:

I would like express my sincere thanks to everyone who contributed to the successful completion of this research work.

VII. REFERENCES

- [1]. Prassianakis I N, Int J Mater & Product Technol, 26 (2006) 71-88.
- [2]. Gilman J J, Cunningham B J & Holt A, Mater Sci and Engg, 39 A (1990) 125-133.
- [3]. Lee S B, Park I J, Ha J U, Lee G W, Lee S G, Park E Y & Kim E J, Korean Pat Appl, 6 (2009).
- [4]. Chen Y & Huang Y, Chinese Pat App, 6 (2009).
- [5]. Qian J, Chinese Pat Appl, 9 (2009).
- [6]. Mason T J, Royal Soc Of Chem, (1990).
- [7]. Sahn D J, Echocardiography, 7(4) (1990) 465-68.
- [8]. Slyper A H, J. clin. Endocrinology meta, 89(7) (2004) 3089-95.
- [9]. Burns R P, Cofer J B, Russell W L & Clements J B, Southern medi J, 78(5) (1985) 518-22.

- [10]. Xu Q, Zhou H, Yang J & Yan S, ZhongguoLinchuangKangfu,9(35) (2005) 167-69.
- [11]. Ren H, Wang W, Ge Z & Zhang J, Chin Med J, 114(4) (2001) 387-90.
- [12]. Toufic N and Ilic B, J francaisd'ophtalmologie,4(6-7) (1981) 487-502.
- [13]. Borisova S A, Vestnikoftalmologii,113(6) (1997) 43-5.
- [14]. Kaneko S, Nagai N, Matsuura T, Kohri K, Iguchi M, Minami K, Kadowaki T, AkiyamaT,Yachiku S & Kurita T, JpnJ Urol,69(5) (1978) 572-77.
- [15]. Frede T, Hatzinger M & Rassweiler J, J Endourol / Endourological Soc, 15(1) (2001) 3-16.
- [16]. Zhou M & Yang D, Zhonghua GanzangbingZazhi,11(12) (2003) 763-764.
- [17]. Miyoshi N, Tuziuti T, Yasui K, Iida Y, Shimizu N, Riesz P & Sostaric J Z, Ultrasonics Sonochem, 15(5) (2008) 881-90.
- [18]. Pan Y, Zheng H, Li D & Gou Q, Huanjing Gongcheng Xuebao,2(4) (2008) 445-449
- [19]. Raju K N & Shailaja D, Asian J Chem, 23 (8) (2011) 3393-96.
- [20]. Sarvanakumar K, Baskaran R & Kubendran T R, Asian J Chem, 23(6) (2011) 2643-47.
- [21]. Rathore P & Singh M, Ind J Chem, 45 A (2006) 2650.
- [22]. Antosiewicz J, Juszkievicz A & Shugar D, J Phys Chem, 86 (1982) 4831-34.
- [23]. Roy M N, Chanda R & Banerjee A, J Chem Eng Data, 54 (2009) 1767-74.
- [24]. Pradhan P, Sah Radheyshyam, Roy M N, J molecular Liquids, 144 (2009) 149-54.
- [25]. Anuradha S, Prerna S & Rajgopal K, J Pure Appl Ultrason, 27 (2005) 49-54.

Studies on the Viscometric Measurements of 4-P- Phenylthi-Carbamidinonaphol at Various Moles and Temperatures of 70% Ethanol-Water Mixture

Dr.Saleem.R.Khan*, Dr.Quazi Saifuddin Ejazuddin

Department of Chemistry, Government Vidarbha Institute of Science and Humanities, Amravati.444601, Maharashtra, India

ARTICLE INFO

Article History:

Accepted : 01 Jan 2025

Published : 10 Jan 2025

Publication Issue :

Volume 12, Issue 7

January-February-2025

Page Number :

186-188

ABSTRACT

To truly understand the medical, agricultural, and pharmacological capabilities of freshly synthesized organic molecules, inorganic molecules, and complexes, studies of their physical parameters are crucial. pH-metry, spectrophotometry, conductometry, viscometry, and interferometric investigations are used in pharmaceutical and medical sciences to anticipate the drug's therapeutic qualities based on these physicochemical results. The beauty of this work is that, although we can predict specific theoretical medicinal properties based on computational studies, the results predicted by physical studies are always accurate. This is true for different molecules. Physical studies can be used to predict the drug's stability, activity, and effects. In light of these facts, viscometric measurements of 4-p-phenylthiocarbamidinonaphthol were examined in a 70% ethanol-water mixture at different molar concentrations and temperatures. The study's findings will be crucial in predicting the effects and medicinal activity of 4-p- phenylthio-carbamidonaphthol.

Keywords: Viscometric measurements, 4-p-phenylthiocarbamidonaphthol.

I. INTRODUCTION

Research on viscosity measurements yields crucial and significant data for pharmaceutical, medical, and drug chemistry fields.[1–3] In drug and medicinal chemistry, it offers significant and practical information on solute-solvent, solute-solvent, and solute-solvent- solvent interactions. Viscosity measurements offer crucial information about the interactions between the solute (drug) and solvent, which is a crucial component of drug activity and effect in pharmacokinetics. We can comprehend drug absorption, drug transmission, drug activity, and drug effect based on these findings. Therefore, it was decided to look into the viscometric measurements of 4-p-phenylthiocarbamidinonaphthol while taking all of these factors into account.

Drugs with thiocaramido and benzenoido nuclei have demonstrated their distinct identities and significant uses in pharmaceutical chemistry.[4–10] Thus, 4-p- phenylthiocarbamidonaphthol viscometric measurements were examined. This study could be a turning point in the development of substitutedthiocarbamidenaphthol as a medication.

II. EXPERIMENTAL

Double-distilled water was used, and all chemicals used in this investigation were of A.R. grade. A Polish Mechaniki Zaktady Precyzjnej Gdansk balance (0.001g) was used for the weigh-in. A bicapillary densitometer (P 0.2%) with a capillary tube of 1 mm internal diameter and a sphere volume of roughly 10 cm³ was used to measure the density of the solution. It was calibrated using deionized double-distilled water. The density measurements had an accuracy of 0.1 kgm⁻³. The Ostwald viscometer was used to measure viscosity. The thermostat was used to maintain the temperature. The viscometer and water bath were given enough time to achieve thermal equilibrium.

III.OBSERVATION AND CALCULATIONS

The viscosity tests of 4-p-phenylthiocarbamidonaphthol in a 70% ethanol-water mixture at various molar concentrations and temperatures are the focus of this work. The outcomes were displayed in Table No.1.

IV.RESULT AND DISCUSSION

Table No. 1 shows that when molar concentration drops, \sqrt{C} drops as well. It also shows that the flow time for the solution to travel decreases. Additionally, a decrease in density is noted. The same pattern was seen in θ_r , $\theta_{sp} = \theta_r - 1$, and $(\theta_r - 1)/\sqrt{C}$. We can infer from these findings that the interactions between the solute and the solvent are appropriate.

Table No. 1

Table No.1 VISCOSITY MEASUREMENTS AT DIFFERENT CONCENTRATION OF [4-AN]							
DETERMINATION OF RELATIVE AND SPECIFIC VISCOSITIES AT DIFFERENT CONCENTRATIONS AND TEMPERATURE							
SYSTEM:[4-AN] MEDIUM - 70% ETHANOL-WATER							
Temp T (°C)	Conc. C (M)	\sqrt{C}	Time t (sec.)	Density ρ (kg.cm ⁻³)	η_r	$\eta_{sp} = \eta_r - 1$	$(\eta_r - 1)/\sqrt{C}$ (pa ⁻¹ s)
25	0.100	0.31619	56.35	0.9454	2.2967	1.1967	3.7856
	0.050	0.22357	58.95	0.9439	2.3988	1.3988	6.2568
	0.025	0.15808	53.01	0.935	2.1364	1.1364	7.1894
	0.0125	0.11177	54.16	0.9424	2.2004	1.2004	10.739
30	0.100	0.31619	55.89	0.9461	2.283	1.283	4.0585
	0.050	0.22357	58.66	0.9447	2.3926	1.3926	6.2291
	0.025	0.15808	51.92	0.9364	2.0978	1.0978	6.9453
	0.0125	0.11177	53.88	0.944	2.1961	1.1961	10.7009

Table No.1 VISCOSITY MEASUREMENTS AT DIFFERENT CONCENTRATION OF [4-AN]							
DETERMINATION OF RELATIVE AND SPECIFIC VISCOSITIES AT DIFFERENT CONCENTRATIONS AND TEMPERATURE							
SYSTEM:[4-AN] MEDIUM - 70% ETHANOL-WATER							
Temp T (°C)	Conc. C (M)	\sqrt{C}	Time t (sec.)	Density ρ (kg.cm ⁻³)	η_r	$\eta_{sp}=\eta_r-1$	$(\eta_r-1)/\sqrt{C}$ (pa ^{-s})
35	0.100	0.31619	54.8	0.9459	2.2601	1.2601	3.9861
	0.050	0.22357	58	0.9447	2.3887	1.3887	6.2116
	0.025	0.15808	50.35	0.9347	2.052	1.052	6.6556
	0.0125	0.11177	53.2	0.9422	2.1855	1.1855	10.6061
40	0.100	0.31619	48.64	0.9377	2.0142	1.0142	3.2084
	0.050	0.22357	50.57	0.9467	2.1141	1.1141	4.9835
	0.025	0.15808	48.1	0.9542	2.8098	1.1098	6.4519
	0.0125	0.11177	50.32	0.9357	2.0793	1.0793	9.6562
45	0.100	0.31619	48.27	0.9379	2.0068	1.0068	3.185
	0.050	0.22357	48.64	0.9385	2.0235	1.0235	4.5784
	0.025	0.15808	43.56	0.9415	1.8296	0.82462	5.6665
	0.0125	0.11177	45.29	0.9362	1.8796	0.8796	7.87

V. REFERENCES

- [1]. Wadekar.A.B, Tayade D.T, Waghmare.S.A, KolheS.V, Indo American Journal of Pharmaceutical Sciences, 5(1), 36-38,2018.
- [2]. Panpaliya.K.S, Tayade D.T, Isankar.R.D, Padhen.S.S,Indo American Journal of Pharmaceutical Sciences,5(1), 63-66, 2018.
- [3]. Tayade.D.T, Thombare.R.D, Waghmare.S.A, International Journal of Medical Science and Clinical Inventions,4(12), 3355-3357, 2017.
- [4]. Raut.P.V, Bodakhe.P.S, Waghmare.S.A, Tayade.D.T, Indo American Journal of Pharmaceutical Sciences, 4(12), 4644-4650, 2017.
- [5]. Poochikian.G.D, Gradock.J.C, J. Pharma. Sci., 68, 728-732,1994.
- [6]. Dash.U.N,Mohapatra.J.R and Pal.B., J. Mol. Liq., 124, 13, 2006.
- [7]. Shedlovasky.T,KayR.L, J. Phys. Chem., 60, 151, 1995.
- [8]. Fuoss R.M,J. Phys. Chem., 79, 525,1975.
- [9]. Fuoss R.M,J. Phys. Chem., 82, 2427,1978.
- [10]. Gomma.E.A and Jahadalli Al,American Journal Condensed Matter Physics,2(1), 16-21, 2012.

Synthesis, Characterization and In Vitro Antimicrobial Screening of Novel Substituted Aurone

Gajanan Ingle, Dr. Sanjay Kolhe

Department of Chemistry, Shri Shivaji Arts, Commerce and Science College Akot Dist. Akola-444101,
Maharashtra, India

ARTICLE INFO

Article History:

Accepted : 01 Jan 2025

Published : 10 Jan 2025

Publication Issue :

Volume 12, Issue 7

January-February-2025

Page Number :

189-195

ABSTRACT

Natural products are the primary or secondary metabolites produced by a wide range of living organisms to improve their ability to adapt and survive in a variety of environmental conditions. These have been thought of as potential therapeutic agents since very early times. This prompted scientists to look into this enormous variety of natural substances in relation to various physiological conditions, thereby exposing their enormous therapeutic potential. These compounds have a great deal of therapeutic potential due to their unique biological activities and substantial structural diversity. The current research is focused on study on synthesis, characterization and antimicrobial activities of newly synthesized Aurone.

Keywords: Aurones, antimicrobial activities, cyclisation, flower petals etc.

I. INTRODUCTION

The Asteraceae family of sunflowers, which produces the most prevalent 4-deoxy-derivatives in the family, such as sulfuretin, maritimetin, leptosidin, and their related glycosides, were the first examples of aurones to be identified in 1940 [1]. Sulfuretin and its glycosylated equivalents are mostly expressed in the leaves and petals of the species *Variabilis* and *Sulfurus*. While leptosidin and other chemicals like sulfuretin and maritimetin may be present in the genus *Coreopsis*, maritimetin has been isolated in the *bidens* species.

Gustav Klein first used the name "anthochlor" in the early 1900s to describe a type of water-soluble pigments that give plants their color. Anthos means flower, while chlorós means yellow. These pigments are secondary metabolites [2]. It contained a limited set of derivatives called aurones (aurum = gold), because the vivid yellow or gold hue that these substances bestow upon the plants that they inhabit. Some fruits and flowers have vivid yellow coloration due to aurone [3]. But they can also be found in the wood, seeds, bark, and leaves of different plants. Additionally, aurone derivatives have a wide spectrum of pharmacological properties, including antioxidant, antiviral, antifungal, anticarcinogenic, and antidiabetic properties [4,5]. The chemical structures of over 100 distinct aurones have been identified to far, and they are distinguished by unique substitution patterns

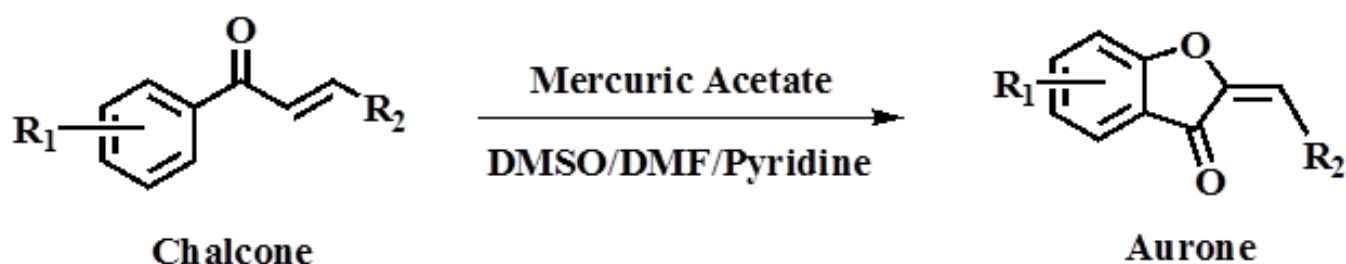
that are hydroxylated, methoxylated, and glycosylated. Furthermore, their ability to accurately forecast prospective therapeutic applications has started to emerge[6-9]. As a result, they constitute a valuable class of natural chemicals that will soon produce bioactive molecules. The chalcones are accessed through synthesis by the Claisen-Schmidt reaction of 2-hydroxyacetophenone and benzaldehyde or their derivatives in the presence of aqueous NaOH, KOH or Ba (OH)₂[10-13]. These chalcones further cyclized in various solvents to get desired substituted aurones.

Additionally, aurones are the active ingredients in a number of traditional medicines, such as *Vaccinium oxycoccus* (European cranberry), *Glycyrrhiza glabra* (licorice), and *Ceanothus americanus* (New Jersey tea)[14]. Among the significant aurones are aureusidin, sulfuretin, cephalocerone, hemiltrone, hispidol, and maritimetin. Aureusidin from the *Cyperus* genus inhibited iodothyronine deiodinase [15], Sulfuretin from *Rhus verniciflua* [16] showed anti-radical activity, Cephalocerone from the plant of *Cephaioocereus senilis* [17] showed anti-bacterial activity, Hamilttrone from the plant *Uvaria hamiltonii* [18] showed DNA strand-scission activity, Hispidol from soybean *Glycine max* [19] showed anti-fungal activity and Maritimetin from the genus *Coreopsis* [20] showed anti-carcinogen and anti-oxidant properties.

The oxidative cyclization of 2-hydroxychalcones has been influenced by a variety of catalysts, including CuBr₂ [21], Ti (NO₃)₃ [22,23], Hg (OAc)₂ [24,25], Pd/CeO₂ [26] and numerous others[27-33]. However, other methods, such as intramolecular tandem ring-opening/coupling cyclization, can also be used to prepare aurones from chalcones [34,35].

II. MATERIALS AND METHODS:

Synthesis of (Z)- 2-(furan-2-ylmethylene) benzofuran-3(2H)-one: 1-(2-hydroxyphenyl)-3-(4-methoxyphenyl) prop-2-en-1-one (0.01M) was dissolved in 10 ml of solvent DMSO along with mercuric acetate (0.01M). Reaction mixture was refluxed for 2-3 hours. Furthermore, this was allowed to cool, washed with dilute HCl and poured in ice cold water. Recrystallization was carried out in absolute alcohol to get pure product. Pale yellow crystalline solid, yield 80%, melting point 138°C



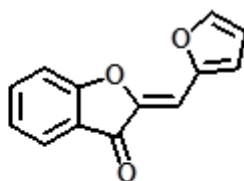
Detail elemental and chemical analysis and spectral studies were carried out and the results obtained are given in tables given below,

Table: Properties of (Z)-2-(furan-2-ylmethylene) benzofuran-3(2H)-one

Properties of (Z)-2-(furan-2-ylmethylene) benzofuran-3(2H)-one					
Sr. No	Color		Molecular Formula	Yield (%)	Melting Point (°C)
1	yellow crystalline solid		C ₁₃ H ₈ O ₃	69	178
2		Solubility in solvents			
THF, EtOH and DMSO					

3	Elemental analysis
Cal. %: (C: 75.59, H: 3.82, O:22.63), Found % (C, 73.58; H, 3.80; O, 22.62)	
Spectral study by IR, ¹ HNMR and GC-MS	
Structural Confirmation by IR IR: (KBr, v/cm⁻¹): Ar-H (Stret.) at 3064.89, C=O at 1783.70, conjugated C=C at 1604.89 and Ar-C=C at 1440.71. Structural Confirmation by ¹HNMR (δ ppm) 500 MHz DMSO d₆: Ar-H 8.350-7.284 and ethylenic protons 3.816 Structural Confirmation by GC-MS Cal. Mol.Wt.: 212.2, Found M/Z: 212.05	

From the above analysis and spectral studies structure of (Z)- 2-(furan-2-ylmethylene) benzofuran-3(2H)-one was justified as



(Z)-2-(Furan-2-ylmethylene)benzofuran-3(2H)-one

III.EXPERIMENTAL

Antimicrobial activity of Aurones

The need to develop new therapeutic medications stems from the fact that infections are becoming more and more resistant to antimicrobial medications. Flavonoids are therefore being researched more and more in the medical domain. Since ancient times, they have been used to treat human illnesses. For example, the *Tagetes minuta* plant was used in Argentinean medicine to treat infectious diseases. Numerous studies have been conducted on flavonoids' antiviral, antifungal and antibacterial qualities.

Requirements

- Mueller-Hilton Agar (MHA) Plates
- Bacterial Culture
- Whatman No 1 filter paper discs (5mm)
- Solvent (vehicle control)-Dimethyl Sulphoxide-DMSO (SRL Chem 28580)
- Ciprofloxacin (SRL Chem- 78079)- 2mg/ml
- Amount Loaded – (0 - 1000 µg./disc)
- Sabouraud dextrose agar –SDA (SRL Chem, Cat no.- 19427) plates.
- Fungal Culture (C. albicans, MTCC 854
- Amphotericin B - (Amphocare)- 5 mg/ml

There are various methods of antimicrobial screening

- Turbidimetric method
- Serial dilution tube technique

- Diffusion methods.
 - ✓ Agar strip diffusion method
 - ✓ Agar cell method
 - ✓ Agar cup cylinder method
 - ✓ Replica plate method
 - ✓ Filter paper disc diffusion plate method

Experimental Procedure for Antimicrobial Investigations

The newly synthesised substituted aurone were studied for their antimicrobial activities.

This compound was tested against Gram +Ve and Gram -Ve *E. coli*, *S. aeruginosa*, *M. tuberculosis*, *E. faecalis*, *S. aureus* and fungal strains *A. niger* and *C. albicans* respectively.

The Antibacterial activity was checked by following Zone Inhibition Method (Kirby-Bauer method). The MHA plates were inoculated by spreading with 100 µl of Bacterial culture and fungal strains *E. coli* (MTCC-452), *S. aeruginosa* (MTCC3541), *M. tuberculosis* (MTCC-300), *E. Faecalis* (MTCC-439), *A. niger* (MTCC-281), *C. albicans* (MTCC-854) (adjusted to 0.5 McFarland Unit - Approx cell density (1.5 X 10⁸ CFU/mL) and followed by placing the discs containing 10 µl of different concentration (0 to 100 mg/ml). 10 % of the sample was taken and serially diluted to achieve the required amount to be loaded on the disc. One disc in each plate was loaded with solvent alone which served as vehicle control and Ciprofloxacin disc (10µg) were taken as positive control. The plates were incubated at 37 °C for 24 hrs.

A clear zone created around the disc were measured and recorded and the antimicrobial activities obtained during the studies against microbes.

IV. RESULTS AND DISCUSSION:

Considering the above data obtained during the studies of comparative studies for synthesized compound against all the microbes were carried out and results are given as per the efficiency of compound against the microorganisms given in table below.

Table No.: Efficiency ranking of newly synthesized aurone against various organisms

Test organisms	Zone of Inhibition (mm)	Efficiency Ranking (1 = highest)
<i>E. coli</i>	17	2
<i>S. aeruginosa</i>	13	3
<i>M. tuberculosis</i>	10	5
<i>E. faecalis</i>	18	1
<i>S. aureus</i>	12	4

V. CONCLUSIONS

In summary, the data underscore that aurone consistently demonstrated high efficacy across tested pathogen *E. faecalis*, making aurone as a strong candidate for further development and investigation. Conversely, against *M. tuberculosis* aurone frequently ranked lower ZOI value, indicating weaker antimicrobial properties. This detailed analysis offers critical insight into the relative strengths of the synthesized compound and serves as a foundation for future optimization in antimicrobial drug development.

VI. ACKNOWLEDGEMENT

We are thankful Department of chemistry Shri Shivaji Arts Commerce and Science College Akot for providing lab equipment's. We are also thankful to CIL and SAIF, Panjab University, Chandigarh for providing spectral data.

VII. REFERENCES

- [1]. Geissman, T.A.; Heaton, C.D. Anthochlor pigments. IV. The pigments of *Coreopsis grandiflora*, Nutt. J. Am. Chem. Soc., 65,677–683,1943.
- [2]. Klein, G. Studien uber das Anthochlor. Sitzb. Akad. Wiss. Wien., 129, 341–395,1920.
- [3]. Jagtap S. V., A. A. Khan, Synthesis and biological activities of aurones: A Review, Int. J.Pure App.Biosci. 4 (2) 137-155,2016.
- [4]. Sui G, Zhang T. Li, B., Wang R., Hao H., Zhou W, Recent advances on synthesis and biological activities of aurones, Bioorg. Med. Chem. 29,115895,2021.
- [5]. Bandichhor R., Hazardous Reagent Substitution: A Pharmaceutical Perspective Green Chemistry Series 52,2018.
- [6]. Zwergel, C.; Gaascht, F.; Valente, S.; Diederich, M.; Bagrel, D.; Kirsch, G. Aurones: Interesting natural and synthetic compounds with emerging biological potential. Nat. Prod. Commun., 7, 389–394,2012.
- [7]. Boucherle, B.; Peuchmaur, M.; Boumendjel, A.; Haudecoeur, R. Occurrences, biosynthesis and properties of aurones as high-end evolutionary products. Phytochemistry, 142, 92–111,2017.
- [8]. Alsayari, A.; Muhsinah, A.B.; Hassan, M.Z.; Ahsan, M.J.; Alshehri, J.A.; Begum, N. Aurone: A biologically attractive scaffold as anticancer agent. Eur. J. Med. Chem., 166, 417–431,2019.
- [9]. Sui, G.; Li, T.; Zhang, B.; Wang, R.; Hao, H.; Zhou, W. Recent advances on synthesis and biological activities of aurones. Bioorg. Med. Chem, 29, 115895–115917,2021.
- [10]. Babu KR, Kumar KV, Vijaya M, Madhavarao V. A novel solid supported synthesis of flavones. Inter. J Pharm Technol; 4(1):3943-3950, 2012.
- [11]. Chee CF, Lee YK, Buckle MJC, Rahman NA. Synthesis of (\pm)-kuwanon V and (\pm) dorsterone methyl ethers via Diels–Alder Reaction. Tetrahedron Lett; 52(15):1797-1799,2011.
- [12]. Chimenti F, Fioravanti R, Bolasco A, Chimenti P, Secci D, Rossi F et al. A new series of flavones, thioflavones, and flavanones as selective monoamine oxidase-B inhibitors. Bioorg. Med. Chem.; 18(3):1273-1279, 2010.
- [13]. Susanti EVH, Matsjeh S, Wahyuningsih TD, Mustofa, Redjeki T. Synthesis, characterization and antioxidant activity of 7-hydroxy-3',4'-dimethoxyflavone Indo. J Chem.; 12(2):146-151,2012.
- [14]. Stoyanov EV, Champavier Y, Simon A, Basly J. Efficient liquid-Phase synthesis of 2' Hydroxychalcones. Bioorg. Med. Chem. Lett; 12(19):2685-2687,2002.
- [15]. Okombi, S., Rival, D., Bonnet, S., Mariotte, A. M., Perrier, E., & Boumendjel, A. (2006, April). Analogues of N-hydroxycinnamoylphenalkylamides as inhibitors of human melanocyte-tyrosinase. Bioorganic & Medicinal Chemistry Letters, 16(8), 2252–2255.
- [16]. Haudecoeur, R., & Boumendjel, A. (2012, June 1). Recent Advances in the Medicinal Chemistry of Aurones. Current Medicinal Chemistry, 19(18), 2861–2875.

- [17]. Aufmkolk, M., Koehrle, J., Hesch, R. D., & Cody, V. (1986, September). Inhibition of rat liver iodothyronine deiodinase. Interaction of aurones with the iodothyronine ligand-binding site. *Journal of Biological Chemistry*, 261(25), 11623–11630.
- [18]. Júnior, G., de M. Sousa, C., Cavaleiro, A., Lago, J., & Chaves, M. (2008, November). Phenolic Derivatives from Fruits of *Dipteryx lacunifera* Ducke and Evaluation of Their Antiradical Activities. *Helvetica Chimica Acta*, 91(11), 2159–2167.
- [19]. Pare, P. W., Dmitrieva, N., & Mabry, T. J. (1991, January). Phytoalexin aurone induced in *Cephalocereus senilis* liquid suspension culture. *Phytochemistry*, 30(4), 1133–1135.
- [20]. Huang, L., Wall, M. E., Wani, M. C., Navarro, H., Santisuk, T., Reutrakul, V., Seo, E. K., Farnsworth, N. R., & Kinghorn, A. D. (1998, March 19). New Compounds with DNA Strand-Scission Activity from the Combined Leaf and Stem of *Uvaria hamiltonii*. *Journal of Natural Products*, 61(4), 446–450.
- [21]. Wong, E. (1966, May). Occurrence and biosynthesis of 4',6-dihydroxyaurone in soybean. *Phytochemistry*, 5(3), 463–467.
- [22]. Masesane, I. B. (2015). *International Journal of Chemical Studies*, 3, 53–59.
- [23]. Agrawal, N. N., & Soni, P. A. (2006, March 22). Reaction of 2'-Hydroxy-5'-acetamido Chalcones with Dimethyl Sulfoxide-Iodine, Pyridine-Mercuric (II) Acetate and Triethanolamine. *ChemInform*, 37(15).
- [24]. Thanigaimalai, P., Yang, H. M., Sharma, V. K., Kim, Y., & Jung, S. H. (2010, June 15). The scope of thallium nitrate oxidative cyclization of chalcones; synthesis and evaluation of isoflavone and aurone analogs for their inhibitory activity against interleukin-5. *Bioorganic & Medicinal Chemistry*, 18(12), 4441–4445.
- [25]. Thakkar, K., & Cushman, M. (1994, August). A novel oxidative cyclization of 2'-hydroxychalcones to 4-methoxyaurones by thallium (III) nitrate. *Tetrahedron Letters*, 35(35), 6441–6444.
- [26]. Ramana Kishore, N., Ashok, D., Sarasija, M., & Murthy, N. Y. S. (2018, May). Microwave-Assisted Synthesis of Novel Spirochromanone–Aurone Hybrids and Their Antimicrobial Activity. *Russian Journal of General Chemistry*, 88(5), 1015–1019.
- [27]. Detsi, A., Majdalani, M., Kontogiorgis, C. A., Hadjipavlou-Litina, D., & Kefalas, P. (2009, December). Natural and synthetic 2'-hydroxy-chalcones and aurones: Synthesis, characterization and evaluation of the antioxidant and soybean lipoxygenase inhibitory activity. *Bioorganic & Medicinal Chemistry*, 17(23), 8073–8085.
- [28]. Yatabe, T., Jin, X., Mizuno, N., & Yamaguchi, K. (2018, April 12). Unusual Olefinic C–H Functionalization of Simple Chalcones toward Aurones Enabled by the Rational Design of a Function-Integrated Heterogeneous Catalyst. *ACS Catalysis*, 8(6), 4969–4978.
- [29]. Tronina, T., Bartmańska, A., Popłoński, J., & Huszcza, E. (2013, March 5). Transformation of xanthohumol by *Aspergillus ochraceus*. *Journal of Basic Microbiology*, 54(1), 66–71.
- [30]. Moussouni, S., Detsi, A., Majdalani, M., Makris, D. P., & Kefalas, P. (2010, August). Crude peroxidase from onion solid waste as a tool for organic synthesis. Part I: Cyclization of 2',3,4,4',6'-pentahydroxy-chalcone into aureusidin. *Tetrahedron Letters*, 51(31), 4076–4078.
- [31]. Miosic, S., Knop, K., Hölscher, D., Greiner, J., Gosch, C., Thill, J., Kai, M., Shrestha, B. K., Schneider, B., Crecelius, A. C., Schubert, U. S., Svatoš, A., Stich, K., & Halbwirth, H. (2013, May 8). 4-Deoxyaurone Formation in *Bidens ferulifolia* (Jacq.) DC. *PLoS ONE*, 8(5), e61766.
- [32]. Khan, A. T., & Goswami, P. (2005, July). A highly efficient and environmentally benign synthesis of 6,8-dibromoflavones, 8-bromoflavones, 5,7-dibromoaurones and 7-bromoaurones. *Tetrahedron Letters*, 46(30), 4937–4940.

- [33]. Imai, K., Nakanishi, I., Ohkubo, K., Ohba, Y., Arai, T., Mizuno, M., Fukuzumi, S., Matsumoto, K. I., & Fukuhara, K. (2017). Synthesis of methylated quercetin analogues for enhancement of radical-scavenging activity. *RSC Advances*, 7(29), 17968–17979.
- [34]. Hassan, G. S., Georgey, H. H., George, R. F., & Mohammed, E. R. (2018, January). Construction of some cytotoxic agents with aurone and furoaurone scaffolds. *Future Medicinal Chemistry*, 10(1), 27–52.
- [35]. Zerva, A., Koutroufini, E., Kostopoulou, I., Detsi, A., & Topakas, E. (2019, March). A novel thermophilic laccase-like multicopper oxidase from *Thermothelomyces thermophila* and its application in the oxidative cyclization of 2',3,4-trihydroxychalcone. *New Biotechnology*, 49, 10–18.

Cutting-Edge Developments in 1,3,4-Oxadiazole Derivatives: Synthesis, Properties, and Applications

Gajanan M. Amle¹, Rajendra K. Wanare²

¹Department of Chemistry, Govt. Vidarbha Institute of Humanities and sciences, Amravati, Maharashtra, India

²Department of Chemistry, Arvindbabu Deshmukh College, Bharsingi, Maharashtra, India

ARTICLE INFO

Article History:

Accepted : 01 Jan 2025

Published : 10 Jan 2025

Publication Issue :

Volume 12, Issue 7

January-February-2025

Page Number :

196-199

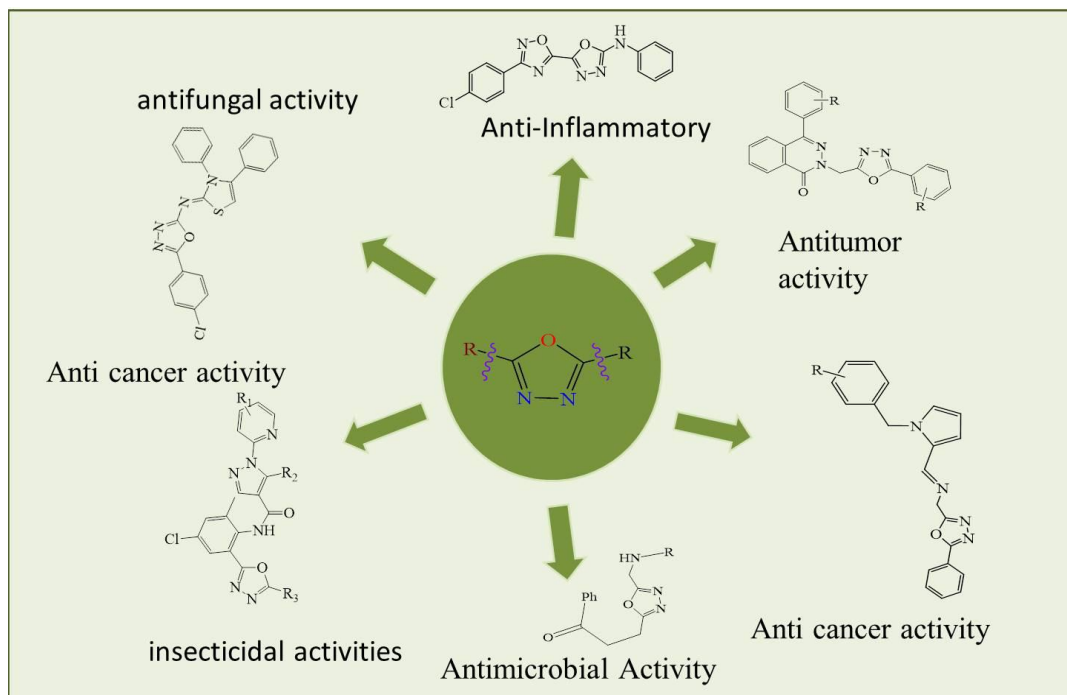
ABSTRACT

Recent advancements in 1,3,4-oxadiazole derivatives have positioned them as versatile compounds with broad applications in medicinal chemistry and materials science. These heterocyclic compounds, containing nitrogen and oxygen, exhibit significant antibacterial, anticancer, and anti-diabetic activities. This review highlights innovative synthetic methods that improve yield, efficiency, and sustainability. It also discusses the diverse applications of these derivatives, including drug design, corrosion inhibition, and optoelectronic devices. The growing interest in 1,3,4-oxadiazole derivatives underscores their potential to drive innovation in various scientific and industrial sectors.

Keywords: 1,3,4-Oxadiazole, Synthesis, Properties, Anticancer, Optoelectronics.

I. INTRODUCTION

1,3,4-Oxadiazole derivatives are versatile compounds with applications in medicinal chemistry, materials science, and environmental protection. Their unique structure, containing nitrogen and oxygen, imparts valuable properties, making them effective in drug design, with activities like antimicrobial, anticancer, and anti-diabetic effects. Additionally, their electronic properties enable use in optoelectronic devices such as LEDs and organic solar cells. These derivatives are also explored as corrosion inhibitors. This review focuses on recent advancement in their synthetic properties, applications, emphasizing novel methods and the growing potential for innovation in various fields.



Graphical overview

1,3,4-Oxadiazole and its derivatives represent an important class of heterocyclic compounds with significant synthetic and pharmacological applications. Their versatility stems from their unique structural properties and diverse biological activities, making them attractive for drug discovery and development. The discovery and exploration of 1,3,4-oxadiazoles have revealed their potential as anticancer agents. Detchokul et al. [1] and Torre et al. [2] highlighted their role in targeting cancer pathways, emphasizing their cytotoxicity against various cancer cell lines. Similarly, Puthiyapurayil et al. [3] synthesized oxadiazole derivatives that demonstrated promising anticancer activity and underscoring their therapeutic activities. Song et al. [4] further corroborated these findings by developing oxadiazole-based molecules with significant potency against cancer cells. In addition to their anticancer properties, oxadiazoles exhibit antimicrobial activity. De Oliveira et al. [5] and Liu et al. [6] reported the synthesis of derivatives with potent antibacterial and antifungal properties, addressing the growing issue of antimicrobial resistance. Kumar et al. [7] expanded this scope by synthesizing oxadiazole compounds with broad-spectrum antimicrobial efficacy, suggesting their potential in combating multidrug-resistant pathogens.

Another significant application of 1,3,4-oxadiazoles lies in their anti-inflammatory properties. Bostrom et al. [8] discussed the structural modifications of oxadiazole derivatives to enhance their anti-inflammatory effects. Zhang et al. [9] and Macaev et al. [10] further demonstrated their utility in alleviating inflammation through inhibition of key enzymes involved in inflammatory pathways. These studies underscore the therapeutic versatility of oxadiazole in managing inflammatory diseases. The role of oxadiazoles in treating neurological disorders has also been extensively studied. Jha et al. [11] and Sangshetti et al. [12] synthesized derivatives that showed neuro-protective effects and potentially aiding in the treatment of disorders like Alzheimer's and epilepsy. Rajak et al. [13] added to this by designing oxadiazole-based compounds with enhanced central nervous system activity and further validating their application in neurology. In cardiovascular research, oxadiazole derivatives have emerged as potent agents. Ramaprasad et al. [14] and Ziedan et al. [15] developed molecules targeting cardiovascular conditions, including hypertension and thrombosis. These derivatives were shown to modulate key pathways and providing therapeutic benefits in cardiovascular health.

The potential of 1,3,4-oxadiazoles as antiviral agents has gained considerable attention. Kashaw et al. [16] synthesized oxadiazole compounds effective against various viral infections and addressing the need for novel antiviral therapies. Gollapalli et al. [17] and Guang et al. [18] further validated these findings, demonstrating their efficacy against viral replication mechanisms.

From a synthetic chemistry perspective, oxadiazole derivatives offer considerable advantages in terms of structural diversity and reactivity. Babic et al. [19] and Dannhardt et al. [20] emphasized the methodologies for synthesizing oxadiazoles and highlighting their applicability in medicinal chemistry. Manjunatha et al. [21] demonstrated innovative approaches to oxadiazole synthesis, showcasing their adaptability in creating novel therapeutic agents. Bozic et al. [22] and Polkam et al. [23] explored their applications in developing advanced materials with unique physical and chemical properties. These studies open new avenues for oxadiazoles beyond traditional medicinal uses. Overall, the literature on 1,3,4-oxadiazoles underscores their immense potential across various scientific disciplines. Their biological activities, coupled with synthetic versatility, position them as a cornerstone in heterocyclic chemistry and drug discovery. Future research should focus on optimizing their pharmacokinetic properties and expanding their applications in emerging therapeutic areas.

II. REFERENCES

- [1]. S. Detchokul, E. D. Williams, M. W. Parker, A. G. Frauman, Br. J. Pharmacol. 2014, 171, 5462.
- [2]. L. A. Torre, F. Bray, R. L. Siegel, J. Ferlay, J. Lortet-Tieulent, A. Jemal, CA Cancer J. Clin. 2015, 65, 87.
- [3]. P. Puthiyapurayil, B. Poojary, C. Chikkanna, S. K. Buridipad, Eur. J. Med. Chem. 2012, 53, 203.
- [4]. M. X. Song, C. J. Zheng, X. Q. Deng, L. P. Sun, Y. Wu, L. Hong, Y. J. Li, Y. Liu, Z. Y. Wei, M. J. Jin, H. R. Piao, Eur. J. Med. Chem. 2013, 60, 376.
- [5]. C. S. De Oliveira, B. F. Lira, J. M. Barbosa-Filho, J. G. F. Lorenzo, P. F. De Athayde-Filho, Molecules 2012, 17, 10192.
- [6]. Z. Liu, J. Zhao, X. Huang, Bioorg. Med. Chem. Lett. 2006, 16, 1828.
- [7]. K. A. Kumar, P. Jayaroopa, G. V. Kumar, Int. J. ChemTech Res. 2012, 4, 1782.
- [8]. J. Bostrom, A. Hogner, A. Llinas, E. Wellner, A. T. Plowright, J. Med. Chem. 2012, 55, 1817.
- [9]. F. Zhang, X. L. Wang, J. Shi, S. F. Wang, Y. Yin, Y. S. Yang, W. M. Zhang, H. L. Zhu, Bioorg. Med. Chem. 2014, 22, 468.
- [10]. F. Macaev, Z. Ribkovskaia, S. Pogrebnoi, V. Boldescu, G. Rusu, N. Shvets, A. Dimoglo, A. Geronikaki, R. Reynolds, Bioorg. Med. Chem. 2011, 19, 6792.
- [11]. K. K. Jha, A. Samad, Y. Kumar, M. Shaharyar, R. L. Khosa, J. Jain, V. Kumar, P. Singh, Eur. J. Med. Chem. 2010, 45, 4963.
- [12]. J. N. Sangshetti, A. R. Chabukswar, D. B. Shinde, Bioorg. Med. Chem. Lett. 2011, 21, 444.
- [13]. H. Rajak, T. B. Singh, A. Singh, K. Raghuvanshi, A. K. Sah, R. Veerasamy, P. C. Sharma, P. R. Singh, M. D. Kharya, Bioorg. Med. Chem. Lett. 2013, 23, 864.
- [14]. G. C. Ramaprasad, B. Kalluraya, B. S. Kumar, R. K. Hunnur, Eur. J. Med. Chem. 2010, 45, 4587.
- [15]. N. I. Ziedan, F. Stefanelli, S. Fogli, A. D. Westwell, Eur. J. Med. Chem. 2010, 45, 4523.
- [16]. S. K. Kashaw, V. Gupta, V. Kashaw, P. Mishra, J. P. Stables, N. K. Jain, Med. Chem. Res. 2010, 19, 250.
- [17]. N. R. Gollapalli, N. S. S. Kavuri, P. Kumba, S. Yangalasetty, R. R. Nadendla, Asian J. Pharm. Anal. Med. Chem. 2015, 3, 20.
- [18]. S. H. Guang, T. Loon-Seng, Z. Qingdong, N. P. Paras, Chem. Rev. 2008, 108, 1245.

- [19]. M. M. Babic, K. M. Antic, J. S. J. Vukovic, B. D. Bozic, S. B. B. Davidovic, J. M. Filipovic, S. Tomic, J. Mater. Sci. 2015, 50, 906.
- [20]. G. Dannhardt, W. Kiefer, Eur. J. Med. Chem. 2001, 36, 109.
- [21]. K. Manjunatha, B. Poojary, P. L. Lobo, J. Fernandes, N. S. Kumari, Eur. J. Med. Chem. 2010, 45, 5225.
- [22]. B. D. Bozic, J. R. Rogan, D. D. Poleti, N. P. Trisovic, B. D. Bozic, G. S. Uscumlic, Chem. Pharm. Bull. 2012, 60, 865.
- [23]. (a) N. Polkam, P. Rayam, J. S. Anireddy, S. Yennam, H. S. Anantaraju, S. Dharmarajan, Y. Perumal, S. S. Kotapalli, R. Ummanni, S. Balasubramanian, Bioorg. Med. Chem. Lett. 2015, 25, 1398. (b) N. Polkam, V. R. Ramaswamy, P. Rayam, T. R. Allaka, H. S. Anantaraju, S. Dharmarajan, Y. Perumal, D. Gandamalla, N. R. Yellu, S. Balasubramanian, Bioorg. Med. Chem. Lett. 2016, 26, 2562. (c) N. Kuntala, J. Telu, V. Banothu, S. B. Nallapati, J. S. Anireddy, S. Pal, Med. Chem. Commun. 2015, 6, 1612. (d) T. R. Allaka, N. Polkam, P. Rayam, J. Sridhara, N. S. Garikapati, R. U. Kotapalli, J. S. Anireddy, Med. Chem. Res. 2016, 25, 977. (e) J. Mareddy, S. B. Nallapati, J. Anireddy, Y. P. Devi, L. P. Mangamoori, R. Kapavarapu, S. Pal, Bioorg. Med. Chem. Lett. 2013, 23, 6721.

Investigation of Thermodynamic Parameters Substituted Thiocarbamidonaphthol

Prof. Chetan Soye, Prof. Gayatri Harne, Prof. Divya Sherkar, Dr. Sanjay Kolhe

P.G. Department of Chemistry, Shri Shivaji Arts, Commerce and Science College Akot, Dist-Akola 444101, Maharashtra, India

ARTICLE INFO

Article History:

Accepted : 01 Jan 2025

Published : 10 Jan 2025

Publication Issue :

Volume 12, Issue 7

January-February-2025

Page Number :

200-203

ABSTRACT

Protecting the environment and ecosystems has recently become a major concern for humanity. Determining the significance and applications of synthesized drugs through conductometric measurements is a challenging task for aspiring researchers due to the numerous advancements in chemical and industrial sciences in the developing era. Measurements and research of this kind become an interdisciplinary pull between the biological and chemical sciences. In light of all of this, we calculated the conductometric and thermodynamic parameters of 5-phenylthiocarbamido-2-naphthol in an 85% ethanol water mixture at various concentrations and temperatures.

Keywords: - 5-phenylthiocarbamido-2-naphthol, thermodynamic parameters.

I. INTRODUCTION

Drug conductivity is essential for understanding pharmacodynamics. Ion trafficking and transmission. Two important biopharmaceutical parameters that are responsible for good in vitro and in vivo correlation and effective bioavailability are drug solubility and permeability, which are effectively influenced by ion mobility in electrolytic solution [1]. Increasing the solubility, dissolution rate, and oral bioavailability of medications that are weakly soluble in water is a major challenge for pharmaceutical technologists today [2]. One of the more advanced techniques for solubilization is hydrotropic salization [3]. Add hydrotropic agents to improve the solubility of insoluble medications in water. Many researchers investigate the impact of solubility enhancers [4,5]. The conductometric measurements provide useful information about the interactions between solutes and solvents [6]. Using conductometric measurements, Gomaa and Al-Jahdalli [7] examined the ionic association of Kryptofix-22 with the divalent asymmetric electrolyte $\text{Cu}(\text{NO}_3)_2$ in mixed (MeOH-DMF) solvents at varying temperatures. Izonfuo and Obunwo [8] and Roy *et al.* [9] conducted conductometric measurements of the alkali metal at varying proportions of mixed solvents. Few researchers looked at the Walden product and thermodynamic parameter of various complexes, as well as the comparison of transition metal complexes

among the halide groups [10–14]. Singh *et al.*[15] examined the thermodynamic parameters and ion pair formation of Glycine Bis-1-amidino-O-methylurea cobalt (III) halides in a water-methanol mixture at varying temperatures. Thermodynamic parameters (i.e., ΔH , ΔS , and ΔG) of 5-phenylthiocarbamido-1-naphthol are studied in recent work using conductometric measurement at various concentrations and temperatures in an 80% ethanol-water mixture. Additionally, these studies contribute to the effects of different substituents as well as interactions between solvents, solutes, and solvents.

II. MATERIALS AND METHODS

EXPERIMENTAL:

All of the chemicals used in this investigation are of AR grade. Analysis was done using a freshly made solution. Using a standard procedure, the solvents were purified. created concentrations of 5-phenyl thiocarbamido-2-naphthol in an 80% ethanol-water mixture of 0.01M, 0.005M, 0.0025M, and 0.0012M. Maintain the drug solution's thermal equilibrium between 293K and 298K by using a thermostat. The conductivity of that electrolyte solution was measured following thermal equilibrium.

III.RESULT AND DISCUSSION:

First, a 0.01 M solution was made. Next, using an 85% ethanol-water mixture, solutions of 0.005 M, 0.0025 M, and 0.0012 M were made using the serial dilution method. Conductivity Bridge was used to measure each solution's conductance at 293 and 298 K. Tables 1 through 2 present the results that were obtained. Using a known literature method, the molar conductance (μ), specific conductance (k), and observed conductance (G) were calculated from the data.

TABLE – 1 - CONDUCTOMETRIC MEASUREMENTS AT DIFFERENT CONCENTRATIONS OF 5-PHENYLTHIOCARBAMIDO-1-NAPHTHOL				
DETERMINATION OF G, k and μ AT DIFFERENT CONCENTRATIONS AND DIFFERENT TEMPERATURES IN 85% E-W MIXTURE				
Temp	Concentration C (M)	Observed conductance (G)	Specific conductance (k)	Molar conductance (μ)
293K	0.01	0.0391	0.003023×10^{-3}	0.312477
	0.005	0.01968	0.001806×10^{-3}	0.371478
	0.0025	0.00949	0.001214×10^{-3}	0.495758
	0.0012	0.00789	0.009821×10^{-3}	0.828553
298 K	0.01 M	0.0319	0.003684×10^{-3}	0.378588
	0.005 M	0.01959	0.002055×10^{-3}	0.421168
	0.0025 M	0.01919	0.001421×10^{-3}	0.578689
	0.0012 M	0.00909	0.001145×10^{-3}	0.964693

Table 1 shows that as concentrations decrease, the observed conductance (G), specific conductance (k), and molar conductance (μ) decrease, while G, k, and μ increase as temperatures rise. The higher the temperature, the higher the specific conductance. calculated values of 5-phenylthiocarbamido-1-naphthol's specific constant

(Ksp), log (Ksp), and thermodynamic parameters (ΔG), (ΔS), and (ΔH) using established literature methods at various concentrations and temperatures. The outcome was calculated and shown in Table 2.

TABLE – 2 - CONDUCTOMETRIC MEASUREMENTS AT DIFFERENT CONCENTRATION AND DIFFERENTS TEMPERATURES OF 5-PHENYLTHIOCARBAMIDO-2-NAPHTHOL						
DETERMINATION OF Ksp, log Ksp, ΔG , ΔH and ΔS AT DIFFERENT CONCENTRATIONS AND DIFFERENT TEMPERATURES						
SYSTEM: L ₂ [PTCN]		MEDIUM - 85% Ethanol-Water Mixture				
Temp.(K)	Conc. M	Ksp	Log Ksp	ΔG	ΔH	ΔS
293K	0.01	0.02946	-3.59609	-28503.68	-99580	419.257
	0.005	0.01926	-3.99329	-29019.69	-62879.4	302.956
	0.0025	0.004999	-4.34858	-33950.98	-85649.7	379.474
	0.0012	0.009009	-4.54279	-33989.29	-76069.3	349.478
298 K	0.01	0.0979	5.39384	-26969.49	-85847.5	350.239
	0.005	0.0158	5.83083	-29910.5	-88899.5	389.19
	0.0025	0.00737	6.1819	-30769.51	-99679.5	419.999
	0.0012	0.00489	6.39858	-31859.19	-99169.7	432.119

Temperature, molar concentrations, and percentage compositions all have a significant impact on the change in thermodynamic parameter values. Solute (drug)-solvent interactions, solvent-solvent interactions, solvent-solvent-solute interactions, and solute-solute-solvent interactions are additional factors that shackle these parameters. Changes in these parameters are influenced by both internal and intra-hydrogen bonding and internal geometry.

As can be seen, the μ values rise as temperature rises and concentration falls, suggesting either greater ion mobility or less solvation. This is because higher temperatures and dilution cause more bond breaking, respectively, when thermal energy increases. Additionally, spontaneous reactions are indicated by negative ΔG values. Enthalpy change (ΔH) values that are negative indicate an exothermic reaction. Entropically favorable is indicated by a positive value of (ΔS) and a favorable temperature. Molar concentrations and percentage compositions have a significant impact on the change in thermodynamic parameter values. Solute (drug)-solvent interactions, solvent-solvent interactions, solvent-solvent-solute interactions, and solute-solute-solvent interactions are additional factors that shackle these parameters. Changes in these parameters are influenced by both internal and intra-hydrogen bonding and internal geometry.

IV. REFERENCES

- [1]. Singh A. K., Mishra G, Jyoti K., J. App. Pharm. Sci., 1(5), 44-49. (2023).
- [2]. S.Chakraborty,D.Shukla, A.Jain,B.Mishra and S.Singh, J.Coll.Int.Sci.,355,242-249,(2009).
- [3]. Fahmy, U.A. Drug Des. Dev. Ther., 9, 6129–6137. (2013).
- [4]. S.Agrawal,S.S.Pancholi, N.K.Jainan, G.P.Agrawal, Int.J.PHam.,274,149-155,(2004).
- [5]. Hashem, H. E. Mini-Reviews in Organic Chemistry, 18(8), 1127-1133. (2023).
- [6]. U.N.Dash and S.Supkar, Proc.Ind.Acad.Sci.Chem.Soc.,107,541,(1995).
- [7]. G.C.Bag,N.M.Singh and N.R. Singh, J.Ind.Chem.Soc.,77,146,(2000).
- [8]. E.A.Gonna and B.M. Al-Jahadalli, American J. Condensed Matter PHysics,2(1),16- 21,(2012).

- [9]. Saad, H.A.; Moustafa, A.H. *Molecules* 15, 3602–3617. (2023).
- [10]. M.N. Roy, D. Nandi and D.K. Hazra, *J.Ind.Chem.Soc.*,70,121,(1993).
- [11]. C.S.Solanki,P.Mishra, M.K.Talari,M.Tripathy and U.N.Dash, *E-J Chem.*, 9(1),21-26,(2012).
- [12]. L.S. Singh, A. Jibanlata and N.R. Singh, *J.Ind.Chem.Soc.*,74,635,(1997).
- [13]. N.R. Singh, *J.Ind.Chem.Soc.*,69,279,(1992).
- [14]. T.Shedlovsky, D.A.MacInnes and L.G.Longworth, “Limiting mobilities of some monovalent and ions and dissociation constant of acetic acid” at 200C, *Nature*,75, 774775, (1932).
- [15]. Singla, P.; Luxami, V.; Paul, K., *Eur. J. Med. Chem.* 102, 39–57, (2023).

pH-Metric Studied Stability Constant of 5-P-Hydroxyphenyl-Thiocarbamido-1-Naphthol with Various Metal Ions in 60 % Ethanol-Water Mixture

I.R. Dhoke, G.S. Rathod, A.G. Mule, S.N. Jadhav, P.S. Bodkhe

Department of Chemistry, Vidya Bharti Mahavidyalaya Amravati, Maharashtra, India

ARTICLE INFO

Article History:

Accepted : 01 Jan 2025

Published : 10 Jan 2025

Publication Issue :

Volume 12, Issue 7

January-February-2025

Page Number :

204-207

ABSTRACT

Present work deals with pH-metric studied stability constant of 5-p-hydroxyphenyl-thiocarbamido-1-naphthol with various metal ions in 60 % ethanol-water mixture. In present work studied interaction of 5-p-hydroxyphenylthiocarbamido-1-naphthol (L2) with Cu(II), Cd(II) and Cr(III) metal ions at 0.1 M ionic strength in 60 % ethanol-water mixture by Bjerrum method as adopted by Calvin and Wilson, It is observed that Cu(II), Cd(II) and Cr(III) metal ions form 1:1 with ligands (L2). The values of proton-ligand stability constant (pK) and metal-ligand stability constants (log k) were estimate and compared from resultant data. The effects of substituents were studied from estimated data (pK& log k).

Keywords: 5-p-hydroxyphenylthiocarbamido-1-naphthol (L2), Stability constant, pH-metrically.

I. INTRODUCTION

Molecule containing thiocarbamido, amino, hydroxyl, benzenoid and non-benzenoid nucleus showed various applications in pharmaceutical and medicinal sciences. These types of drugs are very effective in various diseases. Several modern theories and concept are concerning to physical as well as chemical study of benzenoid, non-benzenoid, heterocycles and heterocycles. Aminonaphthols and thiocarbamido nucleus containing heterocycles possesses pharmaceutical, medicinal agricultural industrial and biotechnological significances [1-5]. The manifold research work has been done on the study of metal and nitrogen heterocyclic ligands containing complexes [6-15]. The studies of metal-ligand complexes in solution having number of metal ions with ligands carboxylic acids, oximes, phenols etc. would be interesting which throw a light on the mode of storage and transport of metal ions in biological kingdom. Metal complexation not only brings the reacting molecules together to give activated complexes [16] but also polarized electrons from the ligands towards the metal. The relation between stability and basicity of the ligands is indicated by the formation constant and free energy change value. Bulkier group increases the basicity of ligands as well as stability. The stability of the

complexes is determined by the nature of central metal atom and ligand. The stability of complexes is influenced by the most important characteristics degree of oxidation, radius and electronic structure. Irving and Williams had studied the order of stability of metal complexes of transition metal ions by comparing the ionic radius and second ionization potentials of metal ions, as it is valid for most nitrogen and oxygen donor ligands. Stability and complexation by ligands and various metal ions were evaluated by many researchers [17-20]. Reliable information of stability constant is of great importance in analytical and separation procedure. To remove undesirable and harmful metals from living organism, chelating agents are very much useful in biological systems. This gives importance to the study of determination of stability constant of metal complexes. In present work an attempt has been made to pH-metric studied stability constant of 5-p-hydroxyphenyl-thiocarbamido-1-naphthol with various metal ions in 60 % ethanol-water mixture.

II. MATERIALS AND METHODS

All chemicals used are of AR grade. The stock solutions of the ligand L₂ was prepared by dissolving required amount of ligand in a of 60% (ethanol + water) mixture.

General procedure:

Types of Titrations

- i) Free acid HNO₃ (0.01 M)
- ii) Free acid HNO₃ (0.01 M) and ligand (20 x 10⁻⁴M)
- iii) Free acid HNO₃ (0.01 M) and ligand (20 x 10⁻⁴) and metal ion (4 x 10⁻⁴M) against standard 0.1N NaOH solution. The ionic strength of all the solutions was maintained constant 1M by adding appropriate amount of KNO₃ solution. All the titrations were carried out in 60% (Ethanol-water) mixture and the reading were recorded for each 0.2 ml addition. The graph of volume of alkali added (NaOH) against pH were plotted. The ligands involved in the present work may be considered as a monobasic acid having only one dissociable H⁺ ion from phenolic -OH group and it can therefore, be represented as HL. The dissociating equilibria can be shown as.



By the law of mass action, we have,

$$K = [HL] / ([H^+] [L^-]) \dots\dots\dots (1)$$

Where, the quantities in bracket denote the activities of the species at equilibrium.

III. RESULT AND DISCUSSION

Calculation of Proton-Ligand Stability Constant (\bar{n}_A)

The plots between volume of NaOH and pH of the solution were used to determine the proton ligand stability constant (representing the replacement of H⁺ ions from functional group of ligand with respect to pH value). The horizontal difference (V₂-V₁) was measured accurately between the titration curves of free acid and acid + ligand. It was used to calculate the formation number \bar{n}_A at various pH values and fixed ionic strength $\mu = 0.1M$ using Irving and Rossotti's equation

$$\bar{n}_A = \gamma - \left\{ \frac{(V_2 - V_1)(N + E^0)}{(V^0 + V_1)T_L^0} \right\} \dots\dots\dots (2)$$

Where, V⁰ is the initial volume of the solution. E⁰ and T_L⁰ are initial concentrations of the mineral acid and ligand respectively. V₁ and V₂ are the volumes of alkali of normality N during the acid and ligand titration at

given pH. \bar{n} is the replaceable proton from the ligand. The data of \bar{n}_A obtained at various pH along with the horizontal difference for some representative systems are represented in Table 1. The metal–ligand formation number (\bar{n}) is estimated by Irving-Rossotti's equation.

$$\bar{n} = \frac{(V_3 - V_2) (N + E^0)}{(V^0 + V_2) \bar{n}_A T_M^0} \dots\dots (3)$$

Where, the notations have the same meaning as given in earlier equation. The horizontal difference ($V_3 - V_2$) between the metal complex ($A + M + L$) and reagent ($A + L$) curve is used to evaluate the value of n using Irving Rossotti's equation

Table-1 : Proton-Ligand Stability constant (pK)

Ligand	System	pK		Diff.
		Half integral method	Point wise method	
L ₂	5-p-hydroxyphenylthiocarbamido-1-naphthol (L ₂)	9.24	9.50	0.26

Table-2 : Metal-ligand stability constant (log K)

System	Log K ₁	Log K ₂	Δ Log K	Log K ₁ /Log K ₂
Cu(II) + L ₂	5.26	6.05	0.79	0.869421488
Cd(II) + L ₂	5.56	6.04	0.48	0.920529801
Cr(III) + L ₂	5.95	6.15	0.2	0.967479675

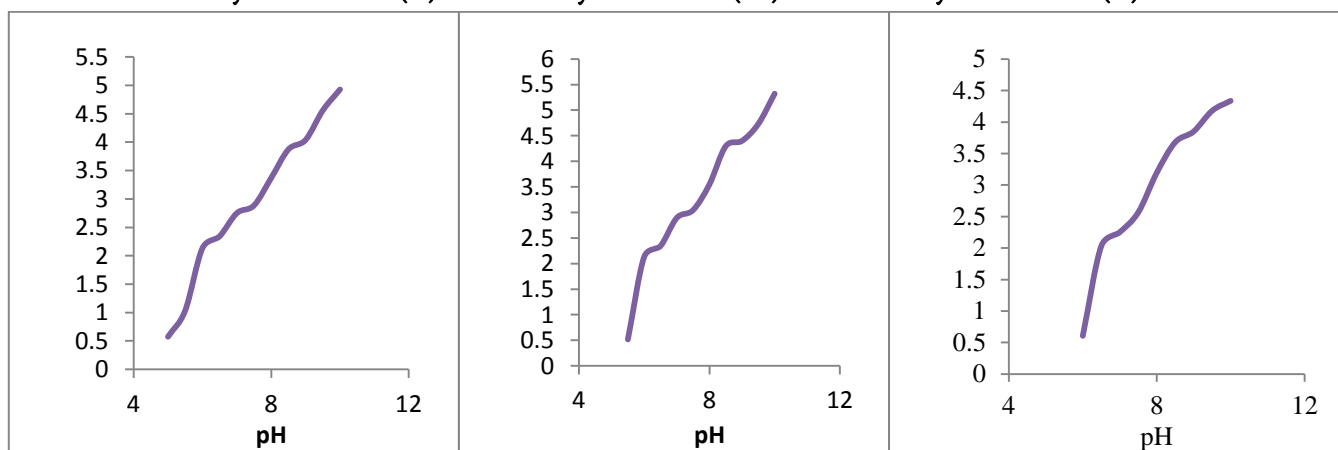
Fig. 1 Fig. 2 Fig. 3

Plot between \bar{n} vs pH Plot between \bar{n} vs pH Plot between \bar{n} vs pH

System- L₂+Cu(II)

System- L₂+Cr(III)

System- L₂+Cd(II)



IV. CONCLUSION

For 5-p-hydroxyphenylthiocarbamido-1-naphthol (L₂) the difference between the values of log K₁ and log K₂ is higher with Cr(III) complex than Cu(II) and Cd(II) complexes. Cr(III) forms more stable complex with L₂ than Cd(II) and Cu(II) metal ions.

Observation of Table-2 showed that less difference between log K₁ and log K₂ values indicates complex formation between metal ion and ligand occurring simultaneously and 1:1 complexation occurs in between to above metal ions and L₂.

V. REFERENCES

- [1]. Barnes D.M., Jianguo Ji, Fickes M.G., J. Am. Chem. Soc., 2002, 124, 13097-13105.
- [2]. Cyril V., Milam M., Chem. Abstract., 1977, 86, 190015.
- [3]. Hassan H. Hammud, Mohammad H. El-Dakdouki, Nada Sonji, Ghassan Sonji, Kamal H. Bouhadir, Interactions of Some Divalent Metal Ions with Thymine and Uracil Thiosemicarbazide Derivatives, Nucleosides, Nucleotides And Nucleic Acids, 2016, 35(5), 259-276.
- [4]. Bossinger S.D. and Tekeshi E., Chem. Abstract., 1972, 77, 343590.
- [5]. G. Victor Fazakerley Graham E. Jackson Peter W. Linder, Equilibrium studies of benzyl penicillinate-thiaproline-hippurate and benzylpenicilloate-proton and transition metal(II) ion systems, Journal of Inorganic Nucl. Chemistry, 1975, 38, 1397-1400.
- [6]. Irving H. and Rossotti H., J. Chem. Soc., 1954, 2904.
- [7]. Martell A.E. and Calvin M., Chemistry of metal chelate compounds. Prentice Hall. Inc. England. Cliffs. N. J. 1962.
- [8]. Banarjee A.K and Rao T.V.R., J. Indian Chem. Soc., 1968, 63, 480.
- [9]. Meshram Y.K., Khan R.F., To studied the interaction between Co(II), Ni(II) and Cu(II) Metal Ions and 2-Hydroxy-4-Methyl-5-Chloro Acetophenone (L1) and at 0.1M Ionic Strength in 70% DMF water mixture, Ind. J. Applied Res., 2014, 4(3), 37.
- [10]. Balakrishna Malla, G. Srinivasa Rao, Dr. Malla Ramanaiah, Gollapalli Nageswara Rao, pH Metric Investigation on Speciation Studies of 5-Sulfosalicylic acid complexes of Co(II), Ni(II) and Cu(II) in DMF-Water Mixtures, Der Pharma Chemica, 2016, 8(8):150-157,
- [11]. Dipak T. Tayade, Dinesh A. Pund, Rahul A. Bhagwatkar, Dinesh B. Rathod, Neha A. Bhagwatkar, pH Metric Studies of Interaction of Synthesized Ligands 2-amino-4-hydroxy-6-methylpyrimidine and 1-(4-hydroxy-6-methylpyrimidino)-3-phenylthiocarbamide with Cu(II), Cd(II), Cr(II), Cations At 0.1 M Ionic Strength, International Journal of Chemistry, 2011, 3(1).
- [12]. Naik AB, Narwade ML. Russian J. Coordination chem. 2009, 35(12):932-937.
- [13]. Janrao D.M., Pathan J., Sci. chem. Commun., 2014, 4(1), 11.
- [14]. Ramteke A., Narwade M.L., Arch Applied Sci. Res, 2013, 5(1), 231.
- [15]. Thakur S.V., J. Chem., Bio & Phys Sci., 2014, 4(1), 01.
- [16]. Irving H and William R.J.P., J. Chem. Soc., 1953, 3192.
- [17]. Narwade M.L., Chincholkar M.M. and Sathe S.W., J. Indian Chem. Soc., 1985, 62, 194.
- [18]. Bodkhe P.S., Patil K.N., Narwade M.L. and Doshi A.G., Asian J. Chem., 2003, 15(3 & 4) 1739-1743.
- [19]. Prasad R.N., Agrawal M, Ratnani R. and Sarswal K., J. Indian Chemical Soc, 2005, 82, 137 – 139,.
- [20]. Thakur S.D., Munot K.P., Raghuvanshi P.B., Tayade D.T., Acta Ciencia Indica, 2010, XXXC(3), 425.

Acoustic, Volumetric, and Excess Properties for Binary Mixture of BTX and Ethyl Alcohol

K.P. Belsare*, N.B. Selukar

Department of Chemical Technology, Sant Gadge Baaba Amravati University, Amravati, Maharashtra, India

ARTICLE INFO

Article History:

Accepted : 01 Jan 2025

Published : 10 Jan 2025

Publication Issue :

Volume 12, Issue 7

January-February-2025

Page Number :

208-214

ABSTRACT

Density(ρ), Viscosity(η), and Ultrasonic velocity(u) of mixtures of EthylAlcohol with equimolar mixtures of benzene, toluene, and xylene, over the entire composition range have been measured at $T = 293.15\text{K}$. Using the experimental results, Acoustic parameters and excess Adiabatic compressibility, excess Intermolecular free length has been calculated. The variation of these properties with the composition of the mixtures has been discussed in terms of molecular interaction in these mixtures. The results have been calculated and discussed in terms of weak interactive forces between unlike molecules.

Keywords: Binary mixture BTX and Ethyl alcohol, Physiochemical properties, Acoustic properties, Excess properties, Molecular interaction study.

I. INTRODUCTION

Ultrasonic velocity is useful for studying the acoustic and thermodynamical properties of any compounds which further gives the molecular interaction in petroleum compounds [1-2]. Molecular interaction causes a change in volume in the experimental component. This volume change gives the ionic interactions. So, this is useful in ultrasonic studies [3-8]. Density, viscosity, ultrasonic velocity, and change in volume play an important role in structural and molecular interaction studies in binary mixtures [9-11]. Ultrasonic studies with density and viscosity play an important role in chemical reactions [12-16]. The process of studying the molecular interaction from the variation of thermodynamic parameters and their properties such as viscosity and excess values with the composition of pure liquids and their binary liquid mixture are beneficial to understand the thermodynamic and transport properties associated with heat and fluid flow which gives an insight into the molecular process [17]. Theoretical knowledge about the mixing properties of liquids is important in chemical and petrochemical industries [18-24]. Thermodynamic parameters give us knowledge about the transport properties of liquids under different physiochemical conditions [25-28]. Sound velocity measurement is more convenient for finding the thermodynamic parameters than other methods [29-32]. Mixed solvents have wide applications in industrial processes [33, 34]. In this study Density, viscosity, and ultrasonic velocity of different

concentrations of BTX and ethyl alcohol blends were carried out. From these acoustic parameters like adiabatic compressibility, acoustic impedance, intermolecular free length, relaxation time and Gibbs free energy have been carried out. Excess parameters were also carried out for different concentration blends. Values are plotted against different concentrations and ultrasonic parameters. The plotted graphs explain the intermolecular interactions of different concentrations of blends.

II. METHODS AND MATERIAL

Benzene, Toluene, and xylene of AR Grade were taken in equal proportions and their mixtures were made in airtight containers. Ethyl alcohol was taken from the departmental laboratory and it was dried over molecular sieves in the laboratory to be moisture free. Purity of all pure chemicals were checked by measuring and comparing density and ultrasonic velocity before the preparation of blends [35-37]. In this binary mixture ethyl alcohol acts as a solvent and BTX as a solute. Then the 5%, 10%, 20%, 40%, 60%, and 80% blends of BTX and Ethyl alcohol were made. All blends were kept in airtight containers. The density of the different concentration blends and pure solvents was measured using a gravity bottle of 50 ml capacity. The gravity bottle was first calibrated with distilled water. The viscosity of all BTX and ethyl alcohol blends was measured using an Ostwald viscometer. The ultrasonic velocities of pure solvent and the binary blends were measured using a single crystal variable path at 2 MHz (Mittal Enterprises, New Delhi). The accuracy in the ultrasonic velocity was found to be $\pm 0.05\%$. The time of flow of liquid in the viscometer is measured with an electronic stopwatch with a precision of 0.01 s. The temperature of the test liquids was maintained to an accuracy of ± 0.02 . Temperature was controlled by using temperature-controlled water bath.

From all measured physical parameters acoustic parameters like adiabatic compressibility, Intermolecular free length [38-39], Acoustic impedance, Relaxation time and Gibbs free energy were calculated by using the following relations

$$\text{Adiabatic compressibility, } \beta_{ad} = 1/u^2 \rho$$

$$\text{Intermolecular free length, } L_f = K \sqrt{\beta_{ad}}$$

$$\text{Acoustic impedance, } Z = u \rho$$

$$\text{Relaxation time, } \tau = 4/3 \beta \eta$$

where K is a temperature-dependent constant (Jacobson constant) $(93.875 + 0.375 \times T) \times 10^{-8}$, [40-41] T is the absolute temperature

The excess functions for each of the ultrasonic parameters were calculated using the following formula.

$$E_f = E_{expt} - E_{ideal} = E_{expt} - E_{ideal}$$

$$E_{ideal} = [xy_1 + (1-x)y_2]$$

where y_1 and y_2 are the ultrasonic parameters of pure solvent and blend solution respectively. The values of ρ , u , β_{ad} , and L_f as a function of mole fraction x of various solvents (Benzene, Toluene, and Xylene) at 293.15 K.

III. RESULTS AND DISCUSSION

Densities and ultrasonic velocities of pure solvents are shown in table no.1. also the mole fractions of binary blends and their measured density, ultrasonic velocity and viscosity values are given in table no.2. As the mole fraction of BTX increase in Ethyl alcohol the Density and ultrasonic velocity of blend increases and are shown in fig. no.1 and 2. Calculated adiabatic compressibility, Intermolecular free length, acoustic impedance, and

relaxation time values are given in table no.3. Respective excess values of all binary components are calculated. Excess acoustic parameters are the difference between the experimental values and ideal mixture values. Excess properties have the importance in molecular interaction studies.

The variation of acoustic parameters adiabatic compressibility, intermolecular free length, acoustic impedance, and relaxation time with different mole fractions at temperature 293.15k are shown in Figure 3 to 6. It is observed that as the mole fraction of BTX in ethyl alcohol increases adiabatic compressibility decreases whereas intermolecular free length, acoustic impedance, relaxation time increases as the mole fraction increases. Adiabatic compressibility increases with mole fraction shows there is a weak interaction between molecules. From table no.3 the negative values of excess adiabatic compressibility shows intermolecular attraction between both the components are stronger than intramolecular attraction and shows strong heteromolecular attraction. Which causes charge transfer dipole-dipole and dipole induced dipole interaction between two different molecules. Also increase in excess intermolecular free length shows some interaction in molecules. Positive excess parameter values of intermolecular free length shows there is a existence of dispersive forces in molecules and weak interaction between unlike molecules.

<i>Liquid</i>	<i>Density (ρ) kg/m³</i>	<i>Ultrasonic velocity (U) m/s</i>
BTX	0.8642	1330.5
Ethyl Alcohol	0.7892	1226.82

TABLE 1. DENSITIES AND ULTRASONIC VELOCITIES OF PURE PETROLEUM PRODUCTS

<i>Mole fraction x_1</i>	<i>Density(ρ) kg/m³</i>	<i>UV (U) m/s</i>	<i>Viscosity(η) (Ns/m²)</i>
0	0.7892	1226.82	1.5207
0.5	0.7925	1232.4	1.5267
0.1	0.7998	1254.2	1.5293
0.2	0.8157	1276.8	1.6198
0.4	0.823	1292.3	1.7255
0.6	0.8469	1307.2	1.82
0.8	0.8566	1326.4	1.892
1	0.8642	1330.5	1.98

TABLE 2. DENSITY, ULTRASONIC VELOCITY, AND VISCOSITY DETERMINATION OF ETHYL ALCOHOL AND BTX BLEND

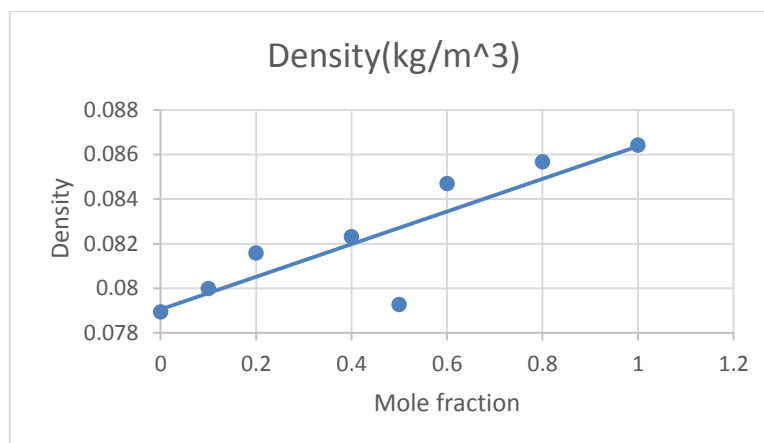


Figure 1: Mole fraction vs Density

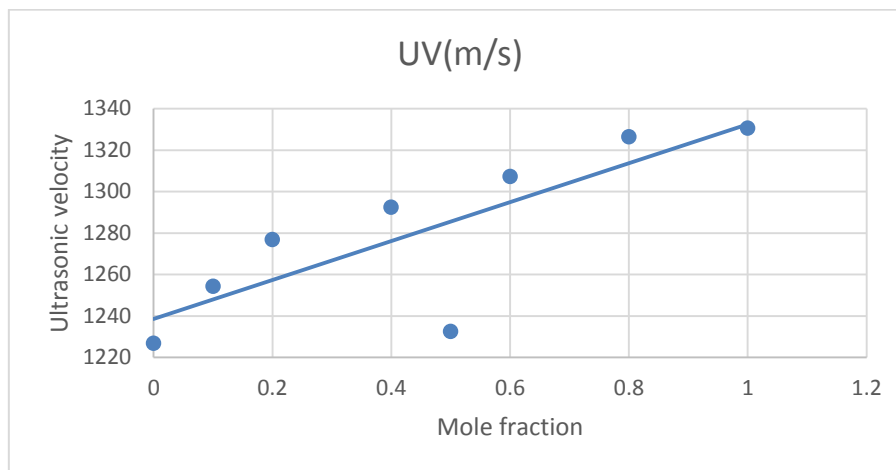


Figure 2: Mole fraction Vs Ultrasonic velocity

β_{ad}	Lf	z	τ	$E(\beta_{ad})$	$E(Lf)$
8.42E-07	1104.855	968.2063	1.71E-06	0	0
8.31E-07	1112.198	976.677	1.69E-06	-5.5E-09	1.11E+03
7.95E-07	1137.073	1003.109	1.62E-06	-3.6E-07	1.39E+02
7.64E-07	1159.856	1033.329	1.65E-06	-2.9E-07	1.16E+03
7.28E-07	1188.486	1063.563	1.67E-06	-1.4E-07	1.19E+03
6.91E-07	1219.52	1107.068	1.68E-06	8.75E-09	1.22E+03
6.64E-07	1244.499	1136.194	1.67E-06	1.63E-07	1.24E+03
6.54E-07	1253.871	1149.818	1.73E-06	1	1

TABLE 3: ACOUSTIC AND EXCESS PARAMETERS OF ETHYL ALCOHOL-BTX BLEND

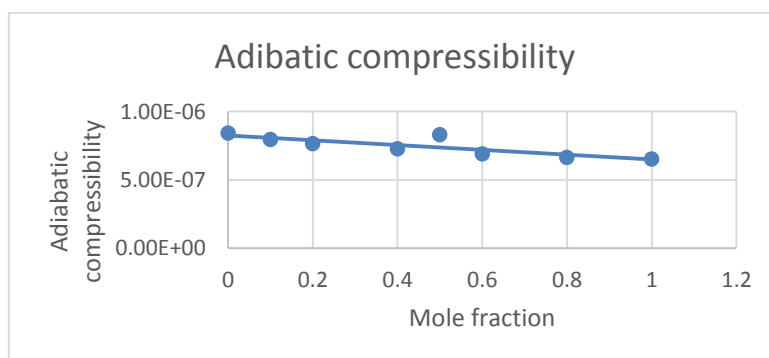


Figure 3:Adiabatic compressibility for different mole fractions of alcohol-BTX blend

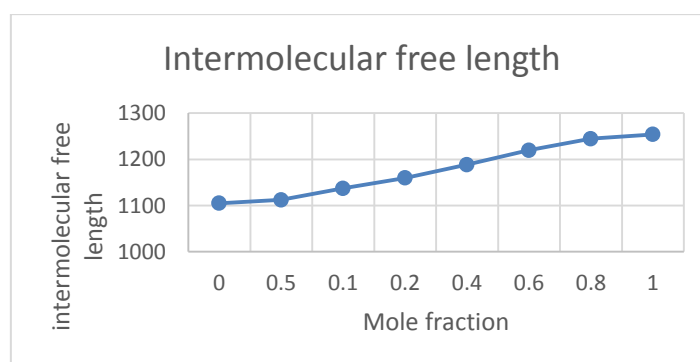


Figure 4: Intermolecular free length for different mole fractions of alcohol-BTX blend

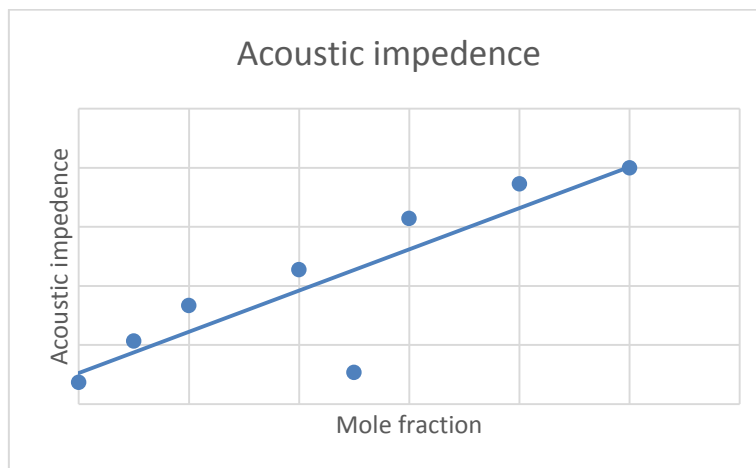


Figure 5: Acoustic Impedance for different mole fractions of alcohol-btx blend

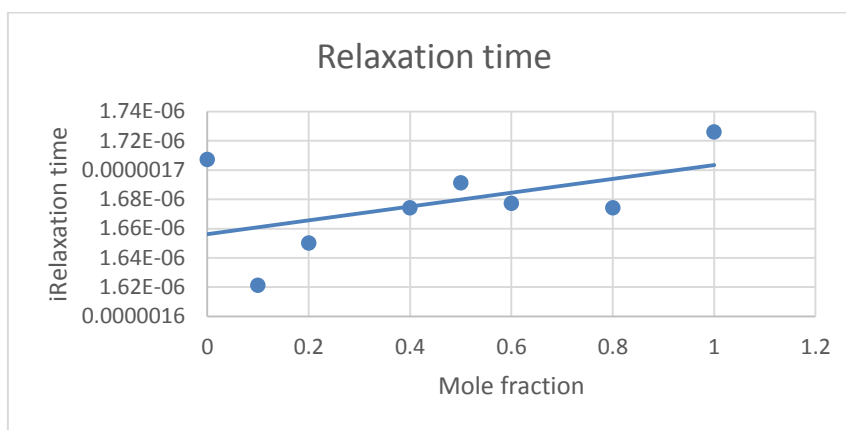


Figure 6: Relaxation time for different mole fractions of alcohol-BTX blend

IV. CONCLUSION

In this study density, Ultrasonic velocity, viscosity and other acoustical parameters were studied for different compositions of ethyl alcohol-BTX blend at 303.15 K.(Table no.1 and 2). Acoustic parameters were calculated and shown in Table no.3. Excess parameters are calculated from acoustic parameters are given in table no.4. From all the obtained data and graphs between physiochemical properties, acoustical and excess parameters it can be concluded that as the percent composition of BTX in ethyl alcohol solvent increases the graph obtained between percent composition of ethyl alcohol and btx mixture and excess parameters is always linear. Graphs obtained are useful for studying solute-solvent interactions easily. Ultrasonic velocity is useful method to check the interaction in different binary mixtures of petroleum products. Acoustic parameter determination shows weak molecular interaction exists in given mixtures, also excess acoustic parameters will be more useful for characterizing the interaction studies of liquid petroleum products.

V. REFERENCES

- [1]. Y. Marcus, "Introduction to Liquid State Chemistry", Wiley publication, New York, USA.357.(1977)
- [2]. R. L. David, "CRC Handbook of Chemistry and Physics", 90th edition, USA.(2010).
- [3]. Ramasay. K. and RTanganathan. V, "Indian Journal Of Pure and Applied Physics",8,144,(1970)
- [4]. Abida S.Hyder, Nain A,K,"International Journal of Physics", vol.5,661(2002)

- [5]. Dr.Pathak R N, Dr. Saxena I, Dr. Mishra A K, Kumar R, & Singh N, "International Journal Of Chemical and Physical Science", Vol.2, No.4 (2014)
- [6]. Devadoss D,Thairiyaraja M,Palaniappan L, "Indian Journal Of Physics", vol.77B(6),669(2003)
- [7]. A. Ali, A. K. Nain, V. K. Sharma, S. Ahmad, "Ultrasonic studies in binary liquid mixtures", Indian Journal of Physics B, vol.75:519-525.(2001)
- [8]. G. Contil, P. Gianni, L. Lepori, E. Matteoli, "Excess thermodynamic properties of asymmetric multicomponent mixtures: Predictive models and microscopic insight for the system ethanol + tetrahydrofuran + cyclohexane at 25°C", Pure and Applied Chemistry, vol.67(11): 1849-1854. (1995)
- [9]. C. M. Kinart, W. J. Kinart, A. Cwiklinska, "H-NMR spectral and dielectric behaviours of the 2-phenoxyethanol-tetrahydrofuran solvent system", Physics and Chemistry of Liquids, vol.40(2):191-201. (2002)
- [10]. A. P. Maharolkar, A. G. Murugkar, S. S. Patil, P. W. Khirade, "Characterization of dominant hydrogen-bonded complex structures", Asian Journal of Chemistry, vol.25(2). pp. 937-940. (2013)
- [11]. A. P. Maharolkar, A. G. Murugkar, S. S. Patil, P. W. Khirade, "Characterization of interaction in binary mixtures by dielectric analysis, International Journal of Pharma and bio sciences", vol.3(4).pp. 438-444 (2012).
- [12]. V. Vesovic, "Fluid Phase Equilibria.", vol.199(1-2)pp 295-306. (2002)
- [13]. T. Takagi., "Journal of Chemical Engineering Data", 41, pp.1061 (1996).
- [14]. J.B. Otto, J.T. Sipowska, B.G. Marchart. "Journal of Chemical Thermodynamics", vol.26, pp.717 (1994).
- [15]. U.G. Krahn, G. Luft. "Journal of Chemical Engineering Data", vol.39, pp.670 (1994).
- [16]. T. Takagi, H. Teranishi. "Journal of Chemical Thermodynamics", 19, pp.1299 (1987).
- [17]. V.A. Tabhane, "Acoustic Letters", vol.6. no. 8.pp.120 (1983).
- [18]. T.M. Aminabhavi, S.K. Raikar, R.H. Balundgi. Industr. Eng. Chem. Res., 32, pp.931(1993).
- [19]. J.D. Pandey, R.D. Rai, R.K. Shukla, A.K. Shukla, N. Mishra. Ind. J. Pure Appl. Phys., 31, 84(1993).
- [20]. M. Gupta, J.P. Shukla. "Indian Journal of Pure Applied Physics", 34, 769 (1996).
- [21]. A. Pal, S. Sharma, A. Kumar. "Indian Journal of Pure and Applied Physics", 38, 174 (2000).
- [22]. S. Baluja, S. Oza., "Fluid Phase Equilibrium", 200, 11 (2002).
- [23]. N. Vyas, T. Nautiyal. Pramana, "Journal of Physics", 59(4), 663 (2002).
- [24]. M. Rastogi, A. Awasthi, M. Gupta, J.P. Shukla, "Indian Journal of Pure and Applied Physics", 40, 256 (2002).
- [25]. A. Ali, Abida, S. Hyder, A.K. Nain, "Indian Journal of Physics", 76B(5), 661 (2002).
- [26]. A. Ali, A.K. Nain. Pramana "Journal of Physics", 58(4) 695 (2002).
- [27]. A. Ali, H. Soghra. Ind. J. Phys., 76B(1), 23 (2002).
- [28]. J.D. Pandey, R. Dey, D.K. Dwivedi. Pramana "Journal of Physics", 52(2), 187 (1999).
- [29]. J D Pandey, B R Chaturvedi and N Pant, "Acoustic Letters", vol.4, 128 (1980)
- [30]. J D Pandey, R K Upadhyaya, and U Gupta, "Acoustic Letters", vol.5, 120 (1982)
- [31]. J D Pandey, "Evaluation of sound velocity in binary molten electrolytes", Electrochimica Acta",28., pp.1097 (1982)
- [32]. J D Pandey and U Gupta, "Electrochemistry", Acta vol.28, pp.1047-1051. (1983)
- [33]. B.B. Kudrivavtsev, Sov, "Physical Acoustics", vol.2 pp.36(1956) .
- [34]. T. Ramanujappa, J.A. Bhavani, E. Rajagopal, N. Manohara Murthy, "Indian Journal of Pure and Applied Physics", vol.38.pp.301(2000) .

- [35]. Reddick J. A. Bungar W.B. & Sakna T.K., "Physical properties and methods of purifications", Journal of American Chemical society, 4th edition. Wiley Interscience, Newyork.vol.109,no.6. (1986)
- [36]. Dean J.A.Langes, "Handbook of chemistry", McGraw hill Newyork, edition.13.pp.10(1956)
- [37]. Pandey J.D.& Kumar A.J., "Journal of pure and applied ultrasonics", vol.16.pp.63.(1994)
- [38]. Pandey J. D. Dey R & Chhabra J,"Physical Chemistry community.", vol.6.pp.55.(2003)
- [39]. ALI A, Tiwari K. Nain A.K.& Chakravortty V., "Indian Journal of Physics", 74(B). pp.351-355.6.(2000)
- [40]. Jacobson B. J., "Ultrasonic velocity in liquids and liquid mixtures", Journal of Chemical physics, 20.pp.927-933.(1952)
- [41]. Roshan Abraham, M. Abdulkhadar, C.V.Asokan,"Ultrasonic investigation of molecular interaction in binary mixtures of nitrile with methanol/toluene", Journal of chemical thermodynamics", vol.32..pp.1-16. (2000)

Investigation of Ultrasonic Properties of 2-Ethylthiocarbamidophenol

K. P. Jumde, A. B. Dhote

Department of Chemistry, Nilkanthrao Shinde Science and Arts College, Bhadrawati, 442902, Maharashtra, India

ARTICLE INFO

Article History:

Accepted : 01 Jan 2025

Published : 10 Jan 2025

Publication Issue :

Volume 12, Issue 7

January-February-2025

Page Number :

215-218

ABSTRACT

Ultrasonic interferometry is used to study molecular and intermolecular interactions. For the purpose of determining the adiabatic compressibility (β), apparent molal compressibility (k), apparent molal volume (v), intermolecular free length (L_f), relative association (RA), and specific acoustic impedance (Z), ultrasonic velocity and density for solutions of 2-ethylthiocarbamidophenol (ETP) at various molar concentrations (at 0.1M, 0.075M, 0.050M, and 0.025M) and 300 K were recently examined. These characteristics, which offer significant and adaptable information about internal structure and molecular association, were investigated in relation to solute-solute and solute-solvent interaction in solvent.

Keywords: - interferometric measurements, 2-ethylthiocarbamidophenol (ETP), solute-solvent interactions.

I. INTRODUCTION

Ultrasound and ultrasonic interferometric research have become increasingly important in the last few decades for studying molecular interactions in liquids. Understanding the characteristics and importance of molecules is crucial to this investigation. It was noted that measurements of ultrasonic waves and sound produced and updated numerous innovations and new ideas in the fields of engineering, applied, industrial, mechanics, agriculture, medicine, forensic sciences, and space research. High-frequency waves are the subject of the scientific field of ultrasonics [1]. Numerous industrial and biological sciences have different uses for thiocarbamido phenol nuclei. Studying ultrasonic parameters in liquid phases [2-4], liquid mixtures [5-6] and electrolyte solutions [7-9] yielded important information about internal structure, molecular association, complex formation, internal pressure, and stability. Aswale *et al.* [10] conducted a comparative analysis of intermolecular interaction using interferometric measurements of cumaran-3-ones and α -bromoacetophenones in ethanol and dioxan solvents. The ternary mixture of toluene in cyclohexane and nitrobenzene at 308 K was the subject of acoustic studies [11]. Researchers looked into the ultrasonic velocity and density of a binary liquid mixture of diethyl ether at 303.15K with three non-polar solvents, including CCl_4 , CS_2 and C_6H_6 [12].

An outstanding technique for gathering information on the ion solvent, solvent-solvent, and structure-breaking and making properties of solutes is the ultrasonic analysis of organic ligand solutions. 2-Ethylthiocarbamidophenol (ETP) solutions at various molar concentrations and 300 K, in 70% ethanol-water mixtures, as well as adiabatic compressibility (β), apparent molal compressibility (k), apparent molal volume (v), intermolecular free length (L_f), relative association (RA), and specific acoustic impedance (Z) were measured for ultrasonic velocity and density. This study aims to determine how temperature and concentrations affect different acoustical characteristics.

II. MATERIALS AND METHODS

Every chemical used in the research is of AR grade. During the study, a freshly made solution was used. Using a standard procedure, the solvents were purified. ETP solutions of 0.1M, 0.075M, 0.050M, and 0.025M in a 75% ethanol-water mixture were made. Using standard procedure, ethanol was purified [13]. Using a bicapillarypyknometer ($10.1 \text{ \% kg m}^{-3}$), densities were measured. The pyrometer used is made by Borosil, and the Citizen CY 104 one pan digital balance ($\pm 0.0001 \text{ gm}$) was used for the weigh-in. In order to measure density and ultrasonic velocity, a unique thermostatic setup was made. Using an elite thermostatic bath, the temperature variation was kept within $\pm 0.1 \text{ }^\circ\text{C}$ while the water was continuously stirred with the aid of an electric stirrer.

The current study used a variable path, single crystal interferometer (Mittal Enterprises, Model MX-3) with a frequency of 1 MHz and an accuracy of $\pm 0.03\%$ to determine the speed of sound waves. In order to calculate the intermolecular free length, the densities and ultrasonic velocity of liquids in ethanol solvent were measured at 300 K. The value of Jacobson's constant¹⁴ ($K = 631$) was then determined.

III. RESULTS AND DISCUSSION

Densities and ultrasonic velocities of ETP in a 75% ethanol-water mixture were measured for this investigation and are shown in Table No. 1.

Table-1.1: Average Ultrasonic Velocity of Water at 300K.

Sr. No.	No. of Rotation of Screw	Micrometer Reading (mm)	Difference Between Reading (mm)	Distance Travelled By Screw in One Rotation	Average Ultrasonic Velocity (m/sec)
1	5	27.4809	1.7109	0.71268	1491.718553
2	10	25.8844	6.3301	2.39289	
3	15	20.4379	5.0403	1.50021	
4	20	17.2664	4.3972	1.71284	
5	25	13.8991	4.1113	1.70211	
6	30	8.4371	4.0517	1.5009	
7	35	4.4651	2.0018	1.16212	
8	40	1.1864		9.47374	

Table-1.2: Average Ultrasonic Velocity of Pure Ethanol 300K (β_0)

Sr. No.	No. of Rotation of Screw	Micrometer Reading (mm)	Difference Between Reading (mm)	Distance Travelled By Screw in One Rotation	Average Ultrasonic Velocity (v_0) (m/sec)	Density (d_0) (Kg. m ⁻³)	$\beta_0 \times 10^{-10}$ (Pa ⁻¹)
1	5	16.2124	5.9519	1.9828	1344.68	1035.00	6.883619671
2	10	11.3288	2.0518	0.8149			
3	15	9.3171	3.1709	1.2562			
4	20	6.2561	3.3699	1.3991			
5	25	2.8871		6.4071			

Table-1.3: Average Ultrasonic Velocity of 75 % Ethanol 300K(β_0)

Sr. No.	No. of Rotation of Screw	Micrometer Reading (mm)	Difference Between Reading (mm)	Distance Travelled By Screw in One Rotation	Average Ultrasonic Velocity (v_0) (m/sec)	Density (d_0) (Kg. m ⁻³)	$\beta_0 \times 10^{-10}$ (Pa ⁻¹)
1	5	18.8291	4.5528	2.39301	1539.99	1132.55	6.182178754
2	10	14.2809	4.9881	2.52925			
3	15	10.3979	4.1278	2.21513			
4	20	7.2959	4.8840	2.48981			
5	25	2.4958		8.65083			

Table-1.4: Acoustic Parameters at Different Concentration of [ETP] at 300 K in 75% E-W

Conc. C (Mole/lit)	Average Ultrasonic Velocity V (m/sec)	Density d_s (Kg.m ⁻³)	$\beta_s \times 10^{-10}$ (pa ⁻¹)	ϕ_v (m ³ mol ⁻¹)	$\phi_k \times 10^{-10}$	L_f (Å)	R_A	$Z \times 10^4$ (Kgm ⁻² sec ⁻¹)
0.1	1691.598	1039.38	4.7815	0.1981	-8.9991	0.0169	0.984	164.748
0.075	1549.458	1029.58	5.6110	0.259	-1.0408	0.0178	1.009	149.309
0.050	1371.759	1026.15	6.953	0.2892	29.859	0.0189	1.049	129.999
0.025	1275.689	1023.13	7.9156	0.3959	56.769	0.0199	1.079	119.439

IV. CONCLUSION

Table 1.4 displayed the resulting values of the acoustic parameters of PTP at (0.1M, 0.075M, 0.050M, and 0.025M) and 300K in a 75% ethanol-water mixture. Based on Table 1.4, it was determined that specific acoustic impedance (Z) decreases with decreasing ETP concentration at 300 K, while adiabatic compressibility (β_s), apparent molar volume (ϕ_v), apparent molar compressibility (ϕ_k), intermolecular free length (L_f), and relative association (R_A) increase. U_s , d_s , β_s , ϕ_v , ϕ_k , L_f , R_A , z , and other acoustic properties were identified through ultrasonic interferometric analysis. These properties explain how these interactions take place and are in charge of breaking and creating the structure in the solution.

V. REFERENCES

- [1]. C. N. Deshmukh, A. G. Doshi, Pratibha Agrawal and C. M. Deshmukh, *Ultra Science* Vol.(3),535, (2002).
- [2]. Singh, U., Chamoli, M., Singh, K. P., Ram, L., Jangir, S., & Maheshwari, R. K. *International Journal of chemistry*, 4, 19-27. (2022).
- [3]. N.A.Kalambe, P.B.Raghuwanshi and A.K.Maldhure, *Ind. J. Chem. Sci.*,12(2), 730, (2014).
- [4]. P.B.Raghuwanshi and A.D.Deshmukh, *Ind. J. Chem. Sci.*,11(1),141, (2013).
- [5]. Raji-Idowu, F ,*Nigerian Journal of chemistry*. (2023).
- [6]. A.Ali, K.Tiwari, A.K.Nain and V.Chakravartty, *Ind. J. Phy. Pt. B*,74(5),351, (2000).
- [7]. Singh, N., Yadav, S. S., Kumar, S., &Narashiman, B.. *Food Bioscience*, 46, 101546. (2022).
- [8]. Rita Mehara, *Ind. J. Chem.*,44A(2),1834 , (2005).
- [9]. P.R.Malasne and A.S.Asvar, *Ind. J. Chem.*,44A(12),2490, (2005).
- [10]. S.S.Aswale, P.B.Raghuwanshi and D.T.Tayade, *Ind. J. Chem. Soc.*,84,159, (2007).
- [11]. A.A.Mistry, V.D.Bhandarkar and O.P.Chimankar, *J. Chem. Pharm. Res.*,4(1),170, (2012).
- [12]. S.K.Pradhan, S.K.Dash, L.Moharana and B. B. Swain, *Ind. J. Pure. Appl. Phy.*, 50, 161, (2012).
- [13]. Bakhtiar, Z., Hasandokht, M. R., Naghavi, M. R., &Mirjalili, M. H. *Journal of Medicinal Plants*, 21(82), 1-12. (2022).

Role of Graphene Oxide Cadmium Oxide Nanocomposite as a Photo Catalyst in Synthesis of Heterocyclic Compounds

M. N. Zade, D. T. Tayade

Department of Chemistry, Govt. Vidarbha Institute of Science and Humanities, Amravati, Maharashtra, India

ARTICLE INFO

Article History:

Accepted : 01 Jan 2025

Published : 10 Jan 2025

Publication Issue :

Volume 12, Issue 7

January-February-2025

Page Number :

219-226

ABSTRACT

Graphene oxide is an emerging nanomaterial with diverse applications for energy storage, conversation (electrodes) and industrial wastewater treatment (adsorbent and photocatalysts) because of their outstanding electrical, thermal and chemical properties.. The application of GO based nanomaterial in photocatalysis, were provided. The presence of graphene oxide nanostructured materials in composite material enhanced the overall performance in their respective applications..Heterocyclic compounds have gained a lot of attention because of their numerous significant medical and biological uses. Research interest on heterocyclic compounds is rapidly increasing due to the extensive synthetic study and functional utility. They are found in more than 90% of novel drugs, and span the gap between biology and chemistry, where so much scientific discovery and application occurs. Heterocycles also play a role in different fields, inclusive of medicinal chemistry, biochemistry, and others. Pharmaceuticals, agrochemicals, and veterinary items are the main applications of heterocyclic compounds. In our review, we cover the majority of bio-active heterocycles that have recently been synthesized and introduced a new phase of possible antifungal, anti-inflammatory, anti-bacterial, antiviral, antioxidant, anticonvulsant, anthelmintics, anthelmintic antipyretics, anti-allergic, anti-histamine, herbicidal, anticancer, antihypertensive and anti-leprosy therapeutics.

Keywords: Nanocomposite, substituted triazine, substituted imidazole, substituted pyrimidinedione.

I. INTRODUCTION

The pre-eminence of nanomaterials has been attracting high scientific interests making it a hottest topic in research and technology in current time [1–4]. Their outstanding physiochemical properties including the excellent relative surface area have received extensive attentions in the area of heterogeneous catalysis mainly

in nanocatalysis [5,6], integrated catalysis [7] as well as magnetite-supported catalysis [8,9]. Carbon-based nanomaterials (such as graphene [10], fullerenes [11], and carbon nanotubes [12]), metals (mainly silver [13], gold [14], iron [15], and cobalt [16]) and oxides (zinc oxide [17], silicon dioxide [18], and titanium dioxide [19]) along with some other prominent nanomaterials like quantum dots [20] are some mostly reported nanocatalysts. Among them transition metal and metal oxide based nanocomposite catalysts show significantly improved catalytic property owing to their enhanced surface area, better charge transfer processes, decreased electron-hole recombination, and greater number of surface active sites [21]. Transition metal based nanocomposites are the novel class of materials with special qualities and distinct characteristics that are more preferable than traditional doped type systems. Presently, graphene/inorganic NP-based nanocomposites have attracted significant interest as an advanced era of nanohybrid materials.[22-24]. Conventional catalysts have some limitations like tedious separation processes and expensive synthesis procedures. Catalysts based on nanocomposites have remarkable popularity in various synthesis processes. The significant modification of transition metal nanocatalysts in terms of size, shape and composition leads to greater stability and selectivity [25,26] The absolute mechanism behind these catalytic effects is still unclear, which attracts researchers for the improvements in the design and study of nanocatalysts.

Heterocyclic compounds are the most important traditional division of organic chemistry, and research interest on heterocycles are increasing because of their medicinal, anti-microbial, and industrial applications [27]. Various heterocyclic compounds like triazine analogues have been utilized as medicinal agents, urinary antiseptic, and anti-inflammatory medicine in the treatment of variety ailment [27]. Antibacterial, antifungal, antiviral and anthelmintic properties have been demonstrated for benzimidazole derivatives [27].

Focusing on organic synthesis as well as organic chemical reactions, which has a lion's share of the catalysts, specifically in commercial production setting where the most considerable technique for producing chemicals are adopted, mostly acknowledging the route which leads to lower cost and larger volume of production. Graphene oxide transition metal based nanocomposite catalysts have certain impressive advantages in comparison to conventional catalysts, including improved interactions with the reactants as well as their insolubility with several solvents leads to trouble-free separation from the reaction mixture. Indeed, the use of nanocatalysts in various organic reactions resulted in increased energy efficiency, enhanced stability, greater selectivity and activity [28-30]. Moreover, most of the reported transition metal nanocomposite catalysts are highly economical, and optimized feedstock is utilized in the synthesis procedure [31-33]. The process is environment friendly due to the negligible release of chemical waste by the implementation of nanocatalysts [34-36]. In general, these nanocomposite catalysts are perceived as the pivotal modern catalysts, which are readily available, cheap, chemically stable, less toxic, and also have prominent photoactive properties as well as a solution towards other important environmental concerns. The establishment of advantages of transition metal nanocomposites as catalysts in comparison to conventional ones is the main motivation for writing this article.

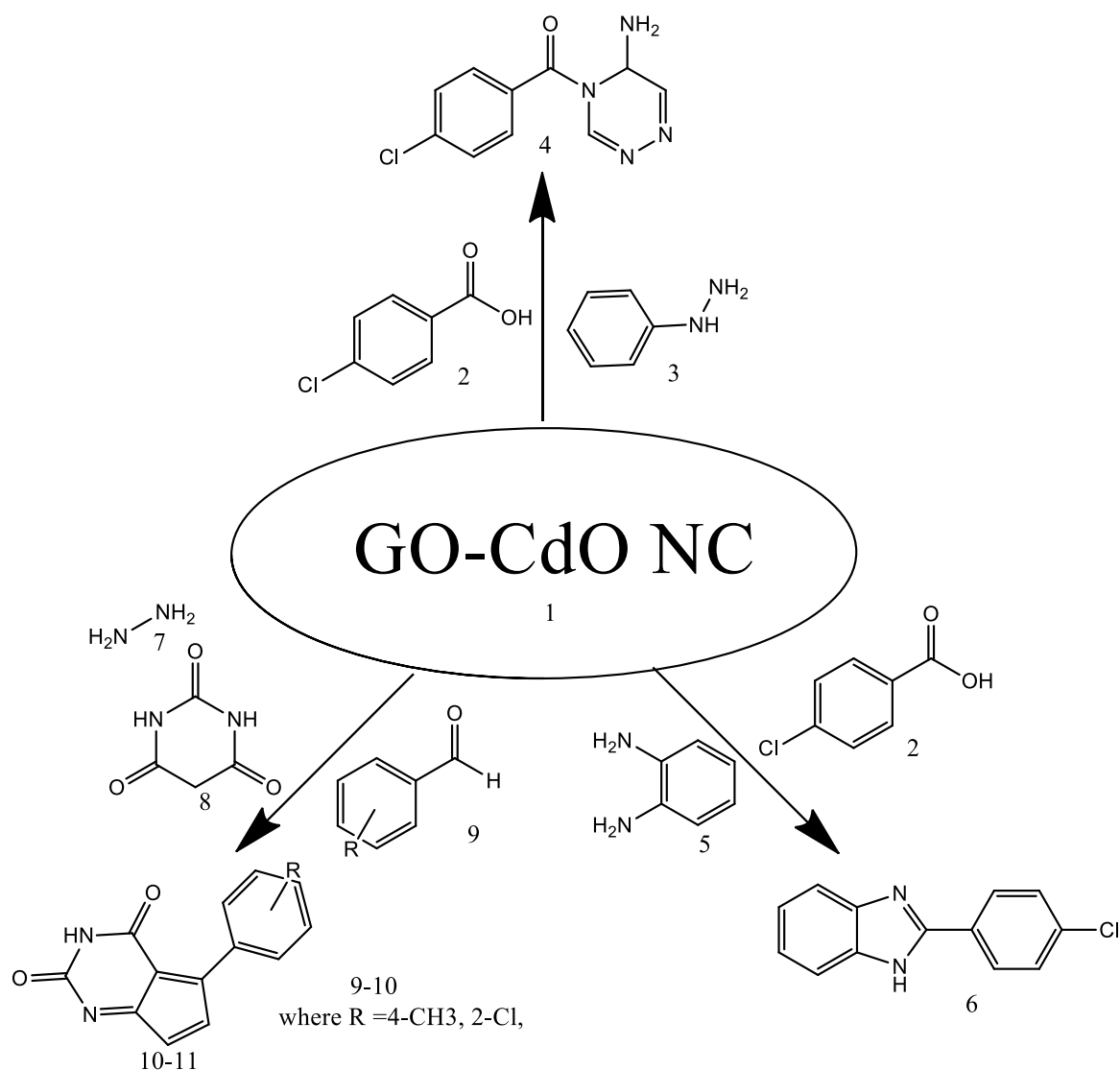
II. RESULT AND DISCUSSION

The present work initiate with optimization of reaction conditions by taking the reaction of N, N-Dimethylbarbituric acid (0.05 mole) and 4-methylbenzaldehyde (0.05 mole) as a model reaction in various reaction condition.(Table 1).

Entry	Solvent	Stirring		Reflux		GO-CdO NC	
		Time in Hour	% yield	Time	% yield	Time	% yield
1	Water	24	60	24	68	1	94
2	Ethanol	24	66	24	70	1	91
3	Ethylene glycol	24	55	24	61	1	91
4	DCM	24	71	24	76	1	82
5	DMF	24	63	24	72	1	88

Table I—Optimization of different reaction conditions

The good result was recorded when reaction was carried out by using graphene oxide cadmium oxide nanocomposite as a catalyst. Under optimized condition as per reaction scheme synthesis of all desired target compounds were done (Table II). All synthesized products were well characterized using ^1H NMR, ^{13}C NMR and MS spectrum products showed good agreements with their spectral data.



Reaction Scheme

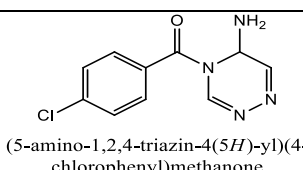
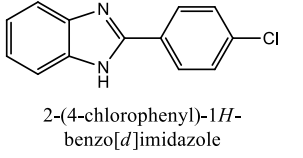
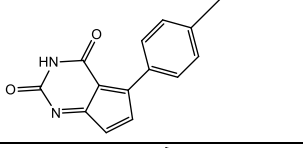
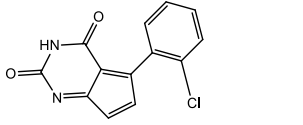
Entry	Product	Yield %	M.P. °C	Time in hour	Colour	Solubility
1	 (5-amino-1,2,4-triazin-4(5H)-yl)(4-chlorophenyl)methanone	94	179	1	Faint yellow	THF, Ethanol, DMF, DMSO
2	 2-(4-chlorophenyl)-1H-benzo[d]imidazole	91	187	1	White	THF, Ethanol, DMF, DMSO
3		95	162	1	White	CHCl ₃
4		93	180	1	White	CHCl ₃

Table II—Formation of target molecules

III.EXPERIMENTAL SECTION

Melting points were taken in open capillary tubes and are uncorrected. ¹H and ¹³CNMR were recorded on Bruker DSX-300/AV-III-400LNMR spectrometer in CDCl₃ and DMSO-*d*₆ solution with TMS as an internal reference. The ESI-MS spectra were recorded using QUATROMICROAPI-WATER mass spectrometer. TLC was performed on Merck 60 F₂₅₄ pre coated silica plates and spots were located under UV chamber and by charring with suitable charring agents. All chemicals were purchased from Merck and Sigma Aldrich and used without further purifications.

Synthesis of graphene oxide(1) A mixture of graphene powder sodium nitrate concentrated Sulfuric acid Potassium permanganate, 30 volume hydrogen peroxide was stirred a bright yellow color precipitate is obtained. Filter the reaction mixture; wash the ppt with 10% HCl solution. A brownish chocolate colored crystalline solid, insoluble in water was obtained. IR spectrum of compound shows following data. 3178.26cm⁻¹ indicates sp² C-H stretching frequency, 2085.32cm⁻¹ indicates C-H (bend) stretching frequency 1569.12cm⁻¹ indicates carbonyl stretching frequency 1324.74cm⁻¹ indicates C-O stretching frequency. TGA Analysis shows Loss of substituent is observed in first step from 110-2400C. Loss of remaining part is observed from 260-3200C. The compounds are degraded completely in the range 320-4000C indicates that the material is fully organic. Half decomposition temperature was found to be 180°C

Synthesis of G.O.-CdO-Nanocomposite Mixture of graphene oxide, cadmium sulphate. Potassium permanganate. Was Reflux in water for 24 hours at 160°C brownish chocolate colored crystalline ppt obtained IR spectrum shows 3334cm⁻¹ indicates sp² C-H stretching frequency 2093.32cm⁻¹ indicates C-

H (bend) stretching frequency 1576.12cm⁻¹ indicates carbonyl stretching frequency 1334.77cm⁻¹ indicates C-O stretching frequency further XRD report and SEM, TEM confirm the properties of nanocomposite material

Synthesis of (5-amino-1,2,4-triazin-4(5H)-yl)(4-chlorophenyl)methanone(4): synthesis carried out by the interaction of 4-chlorobenzoic acid and phenyl hydrazine in presence of Water by using graphene oxide cadmiu oxide nanocoposite After 1 hour, the crystals were separated out, it was filtered, washed several times with water and recrystallized by ethanol Elemental analysis: M.F- C₁₀H₉ClN₄O Elemental analysis results showed cal.% of (C: 50.75%, N: 23.65%) and found atomic % were (C: 50.73%, N: 23.63%) respectively FTIR Spectrum :(KBr-pellets PSD-IR-2.1): -N-H stretching at 3379.00 cm⁻¹ (3500-3000 cm⁻¹), -C=O stretching at 1750 cm⁻¹ (1670-1780 cm⁻¹), ArH stretching at 2579.70 cm⁻¹ (3000-2500 cm⁻¹), Ar-C=C stretching at 1528.37 cm⁻¹ (1600-1500cm⁻¹), -C=N stretching at 1081.92 cm⁻¹ (1200-1000 cm⁻¹), -N-C=N stretching at 1362.01 cm⁻¹ (1500-1200 cm⁻¹) and Ar-C-Clstretching at 812 cm⁻¹ (850- 550 cm⁻¹). PMR spectrum of compound was recorded using DMSO-d₆ and denoted as PSD-PMR-2.1: signal at 7.62-6.31 Ar-H, 8.52 ppm -NH₂, 7.51-8.39 ppm ArH-Cl.. ¹³C Spectrum: ¹³C Spectrum of compound was recorded using DMSO-d₆ and denoted as PSD¹³C-2.1. This spectrum distinctly displayed signals due to -C=N 174.7ppm, Ar-Cδ 63.3 ppm, C=O carbon at δ 146.6 ppm, -C-NH₂ at δcarbon at 132.3 ppm δ 112.50-138.10 ppm C-Cl

Synthesis of 2-(4-chlorophenyl)-1H-benzo[d]imidazole(6): synthesis was carried out by the interacting o-phenylenediamine with p-chlorobenzoic acid in ethanol medium at 80 °C for 22 min in microwave irradiation. After 1 hour , it kept ice cold water, during this process crystals of were separated out, it was filtered washed several times with water and recrystalized by ethanol off white crystals were obtained, Elemental analysis: M.F.; C₁₃H₉ClN₂ Elemental analysis results showed cal.% of (C: 68.28%, N: 12.25%) and found atomic % were (C: 68.25%, N: 12.23%) respectively. FTIR Spectrum: (KBr-pellets PSDIR-N-H stretching at 3381.00 cm¹ (3500-3000 cm⁻¹), Ar-H stretching at 2590.70 cm⁻¹ (3000-2500cm¹), Ar-C=C stretching at 1620.39 cm⁻¹ (1600-1500 cm⁻¹), C-N stretching at 1081.91 cm⁻¹ (1200- 1000 cm⁻¹), N-C=N stretching at 1561.05 cm⁻¹ (1500-1200cm⁻¹), Ar-C-Cl stretching at 810 cm⁻¹ (850-550 cm⁻¹).. PMR Spectrum: PMR spectrum of compound was recorded using DMSO-d₆ and denoted as PSD-PMR-3.1. (δ ppm): signal at 7.61-6.37 ppm Ar-H, 12.56 ppm Ar N-H , 7.51-8.39 ppm is due to ArH-Cl. ¹³C Spectrum: ¹³C Spectrum of compound was recorded using DMSO-d₆ and denoted δas PSD¹³C-3.1. 134.3δ C=N , δ152.90 C-Cl at ppm,

Synthesis of 3-p-Tolyl-pyrazolo[3,4-d]pyrimidine-4,6-dione.(9):Synthesis was carried out by the interaction N, N- Dimethylbarbituric acid (0.05 mole) and 4-methylbenzaldehyde (0.05 mole) in 25 ml R.B. flask and 3ml water was added to it as a solvent and keep the reaction mixture in stirring on magnetic stirrer. After 1 hour solid product was obtained. The progress of reaction was monitored and

TLC. The resultant product was done by adding 0.05 mole hydrazine hydrates in reaction mixture and stirred. After 1 hours a white colored compound was obtained. The reaction was monitored by TLC. This compound was separated by Buckner funnel. The product was purified by work up with brine solution and ethyl acetate solution and further recrystallised by hot ethanol. Elemental analysis: M.F- $C_{14}H_{10}N_2O_2$ Elemental analysis results showed cal.% Elemental Analysis: (C, 70.58; H, 4.23; N, 11.76; O, 13.43) and found atomic % were (C: 7.73%, H; 4.19% ;N: 11.46%, O; 13.40) respectively FTIR Spectrum :(KBr-pellets PSD-IR-2.1).: -N-H stretching at 3379.00 cm^{-1} (3500-3000 cm^{-1}), -C=O stretching at 1750 cm^{-1} (1670-1780 cm^{-1}), ArH stretching at 2579.70 cm^{-1} (3000-2500 cm^{-1}), Ar-C=C stretching at 1528.37 cm^{-1} (1600-1500 cm^{-1}), -C=N stretching at 1081.92 cm^{-1} (1200-1000 cm^{-1}), PMR spectrum of compound was recorded using DMSO-d₆ and denoted as PSD-PMR: δ 7.6454–7.0970 (m, 5H) Ar-H; δ 6.9973 (s, 1H) -CH-C=O; δ 2.6004 (s, 2H) –NH; δ 2.0890 (s, 1H) –OH. 13C Spectrum: 13C Spectrum of compound was recorded using DMSO-d₆ and denoted as PSD13C: 13C Spectrum of compound was recorded using DMSO-d₆ and denoted as PSD13C-2.1. This spectrum distinctly displayed signals due to - δ 139.19 (C-N); δ 130.21–127.28 (Ar C–H); δ 40.17–38.92 (C-H, CH₂).

Synthesis of 3-Furan-2-yl-5,7-dimethyl-2,3,3a,7-tetrahydro-pyrazolo[3,4-d]pyrimidine-4,6-dione(10): Synthesis was carried out by the interaction N,N- Dimethylbarbituric acid (0.05 mole) 2 chlorobenzaldehyde (0.05 mole) in 25 ml R.B. flask and 3ml water was added to it as a solvent and keep the reaction mixture in stirring on magnetic stirrer. 1hour solid product was obtained. The progress of reaction was monitored by TLC. The resultant product was done by adding 0.05 mole hydrazine hydrate in reaction mixture and stirred. After 1 hours a white colored compound was obtained. The reaction was monitored by TLC. This compound was separated by Buckner funnel. The product was purified by work up with brine solution and ethyl acetate solution and further recrystallised by hot ethanol.

Elemental analysis: M.F- $C_{13}H_7ClN_2O_2$ Elemental analysis results showed cal.% Elemental Analysis: (C, 60.36; H, 2.73; Cl, 13.71; N, 10.83; O, 12.37) and found atomic % were (C: C, 60.30; H, 2.70; Cl, 13.80; N, 10.83; O, 12.37) respectively FTIR Spectrum :(KBr-pellets PSD-IR-2.1).: -N-H stretching at 3379.00 cm^{-1} (3500-3000 cm^{-1}), -C=O stretching at 1750 cm^{-1} (1670-1780 cm^{-1}), ArH stretching at 2579.70 cm^{-1} (3000-2500 cm^{-1}), Ar-C=C stretching at 1528.37 cm^{-1} (1600-1500 cm^{-1}), -C-N stretching at 1081.92 cm^{-1} (1200-1000 cm^{-1}), PMR spectrum of compound was recorded using DMSO-d₆ and denoted as PSD-PMR: δ 7.5010–7.1812 (m,5H) Ar-H; δ 6.9845 (s,1H) Ar-H; δ 6.9794–6.9636 (d, 1H) Ar-H; 7.51-8.39 ppm ArH-Cl.. δ 6.9586–6.799 (d, 1H) Ar-H; δ 6.7974–6.7553 (dd, 1H) Ar-H; δ 3.7730 (s,3H) –CH₃O-Ar; δ 4.0480 (s,2H) –CH₂-C=O. 13C Spectrum: 13C Spectrum of compound was recorded using DMSO-d₆ and denoted as PSD13C-2.1. This spectrum distinctly displayed signals due to δ 7.5010–7.1812 (m,5H) Ar-H; δ 6.9845 (s,1H) Ar-H; δ 6.9794–6.9636 (d, 1H) Ar-H; δ 164(d, 1H) C=O,N ; δ 143 (dd, 1H) Ar-H; δ 129(s,3H) –CH₃O-Ar; 127 (s,2H) –CH₂-C=O. δ 127(Ar-Cl)

IV. CONCLUSION

Present work provide green method by suing graphene oxide cadmium oxide based nanocomposite is catalyst in synthesis of heterocyclic compounds like substituted triazine , substituted imidazole and substitute pyrimidindione. Even very low concentration of catalyst does excellent yield of product in less time in water as solvent.. So that graphene oxide cadmium oxide nanocomposite found to be excellent photo catalyst. So present method is better alternative way for synthesis of heterocyclic compound instead using hazardous solvent and costly catalyst. since reaction prodeed in water and using light the provided method is ecofriendly environmental begins and energy efficient.

V. REFERENCES

- [1]. K. Prusty, S. Patra, S.K. Swain, Nano ZnO imprinted dextran hybrid poly (Nisopropylacrylamide)/poly ethylene glycol composite hydrogels for in vitro release of ciprofloxacin, *Mater. Today Commun.* 26 (2021), 101869.
- [2]. B. Parhi, D. Bharatiya, S.K. Swain, Application of quercetin flavonoid based hybrid nanocomposites: A review, *Saudi Pharm. J.* 28 (2020) 1719–1732.
- [3]. N. Sarkar, G. Sahoo, R. Das, S.K. Swain, Three-Dimensional Rice Straw-Structured Magnetic Nanoclay-Decorated Tripolymeric Nanohydrogels as Superadsorbent of Dye Pollutants, *ACS Appl. Nano Mater.* 1 (2018) 1188–1203.
- [4]. D. Bharatiya, B. Parhi, S.K. Swain, Preparation, characterization and dielectric properties of GO based ZnO embedded mixed metal oxides ternary nanostructured composites, *J. Alloy. Compd.* 869 (2021), 159274.
- [5]. A. Gell'e, T. Jin, L. De La Garza, G.D. Price, L.V. Besteiro, A. Moores, Applications of Plasmon-Enhanced Nanocatalysis to Organic Transformations, *Chem. Rev.* 120 (2020) 986–1041.
- [6]. T.S. Rodrigues, A.G.M. Da Silva, P.H.C. Camargo, Nanocatalysis by noble metal nanoparticles: Controlled synthesis for the optimization and understanding of activities, *J. Mater. Chem. A* 7 (2019) 5857–5874.
- [7]. L. Bering, J. Thompson, J. Micklefield, New reaction pathways by integrating chemo- and biocatalysis, *Trends Chem.* 4 (2022) 392–408.
- [8]. M. Rezaie, M. Anbia, Synthesis of magnetite-supported catalysts for phenol oxidation in aqueous solution, *J. Iran. Chem. Soc.* 16 (2019) 1563–1570.
- [9]. G. Liao, J. Fang, Q. Li, S. Li, Z. Xu, B. Fang, Ag-Based nanocomposites: Synthesis and applications in catalysis, *Nanoscale* 11 (2019) 7062–7096.
- [10]. F. Besharat, F. Ahmadpoor, M. Nasrollahzadeh, Graphene-based (nano)catalysts for the reduction of Cr(VI): A review, *J. Mol. Liq.* 334 (2021), 116123.
- [11]. M. Gopiraman, S. Saravanamoorthy, S. Ullah, A. Ilangovan, I.S. Kim, I.M. Chung, Reducing-agent-free facile preparation of Rh-nanoparticles uniformly anchored on onion-like fullerene for catalytic applications, *RSC Adv.* 10 (2020) 2545–2559.
- [12]. A. Maleki, Green oxidation protocol: Selective conversions of alcohols and alkenes to aldehydes, ketones and epoxides by using a new multiwall carbon nanotube based hybrid nanocatalyst via ultrasound irradiation, *Ultrason. Sonochem.* 40 (2018) 460–464.

- [13]. S. Pandey, J.Y. Do, J. Kim, M. Kang, Fast and highly efficient catalytic degradation of dyes using κ -carrageenan stabilized silver nanoparticles nanocatalyst, *Carbohydr. Polym.* 230 (2020), 115597.
- [14]. L. Qin, G. Zeng, C. Lai, D. Huang, C. Zhang, M. Cheng, H. Yi, X. Liu, C. Zhou, W. Xiong, F. Huang, W. Cao, Synthetic strategies and application of gold-based nanocatalysts for nitroaromatics reduction, *Sci. Total Environ.* 652 (2019) 93–116.
- [15]. A. Kasprzak, M. Bystrzejewski, M. Poplawska, Sulfonated carbon-encapsulated iron nanoparticles as an efficient magnetic nanocatalyst for highly selective synthesis of benzimidazoles, *Dalt. Trans.* 47 (2018) 6314–6322.
- [16]. K. Murugesan, T. Senthamarai, A.S. Alshammari, R.M. Altamimi, C. Kreyenschulte, M.M. Pohl, H. Lund, R.V. Jagadeesh, M. Beller, Cobalt-Nanoparticles Catalyzed Efficient and Selective Hydrogenation of Aromatic Hydrocarbons, *ACS Catal.* 9 (2019) 8581–8591.
- [17]. X. Chen, Y. Li, X. Pan, D. Cortie, X. Huang, Z. Yi, Photocatalytic oxidation of methane over silver decorated zinc oxide nanocatalysts, *Nat. Commun.* 7 (2016) 1–8.
- [18]. R. Mansourian, S.M. Mousavi, S. Alizadeh, S. Sabbaghi, CeO₂/TiO₂/SiO₂ nanocatalyst for the photocatalytic and sonophotocatalytic degradation of chlorpyrifos, *Can. J. Chem. Eng.* 100 (2022) 451–464.
- [19]. E. Tabrizian, A. Amoozadeh, S. Rahmani, Sulfamic acid-functionalized nanotitanium dioxide as an efficient, mild and highly recyclable solid acid nanocatalyst for chemoselective oxidation of sulfides and thiols, *RSC Adv.* 6 (2016) 21854–21864.
- [20]. Y. Guo, L. Fan, M. Liu, L. Yang, G. Fan, F. Li, Nitrogen-Doped Carbon Quantum Dots-Decorated Mg-Al Layered Double Hydroxide-Supported Gold Nanocatalysts for Efficient Base-Free Oxidation of Benzyl Alcohol, *Ind. Eng. Chem. Res.* 59 (2020) 636–646.
- [21]. S. Yadav, N. Rani, K. Saini, A review on transition metal oxides based nanocomposites, their synthesis techniques, different morphologies and potential applications, *IOP Conf. Ser.: Mater. Sci. Eng.* 1225 (2022), 012004.
- [22]. K. Zhang, R. Zou, Advanced transition metal-based OER electrocatalysts: current status, opportunities, and challenges, *Small* 17 (2021) 2100129. Scheme 34. Crossed aldol condensation reaction between benzaldehyde and acetone to form dibenzylideneacetone by using MnFe₂O₄/g-C₃N₄ nanocomposite catalyst. S. Patra et al. *Results in Chemistry* 6 (2023) 101172 18.
- [23]. M.T. Greiner, L. Chai, M.G. Helander, W.M. Tang, Z.H. Lu, Transition metal oxide work functions: the influence of cation oxidation state and oxygen vacancies, *Adv. Funct. Mater.* 22 (2012) 4557–4568.
- [24]. M. Bystrzanowska, P. Petkov, M. Tobiszewski, Ranking of heterogeneous catalysts metals by their greenness, *ACS Sustain. Chem. Eng.* 7 (2019) 18434–18443.
- [25]. X. Yu, V. De Waele, A. Lofberg, V. Ordonsky, A.Y. Khodakov, Selective photocatalytic conversion of methane into carbon monoxide over zirconium heteropolyacid-titania nanocomposites, *Nat. Commun.* 10 (2019) 1–10.
- [26]. D. Dang, Y. Chen, X. Chen, K. Feng, B. Yan, Y. Cheng, Phase-pure M₁ MoVNbTeO₄: x/TiO₂ nanocomposite catalysts: high catalytic performance for oxidative dehydrogenation of ethane, *Cat. Sci. Technol.* 12 (2022) 1211–1219.
- [27]. K. Emranul, M. Uzzaman A review on biological and medicinal impact of heterocyclic compounds, *Results in Chemistry* 4 (2022) 100606.
- [28]. S.B. Singh, P.K. Tandon, Catalysis: A Brief Review on Nano-Catalyst, *J. Energy Chem. Eng.* 2 (2014) 106–115.

- [29]. D. Ye, R. Huang, H. Zhu, L.H. Zou, D. Wang, Thienylbenzotriazole promoted highly active gold nanoparticles supported on N-doped graphene as efficient catalysts in water and a mechanism exploration, *Org. Chem. Front.* 6 (2019) 62–69.
- [30]. X. Ma, H. Meng, M. Cai, P.K. Shen, Bimetallic carbide nanocomposite enhanced Pt catalyst with high activity and stability for the oxygen reduction reaction, *J. Am. Chem. Soc.* 134 (2012) 1954–1957.
- [31]. W. Dai, H. Wen, Z. Zhang, P. Wang, Metal-organic frameworks-derived Ni₂P@C Nanocomposite as a high-performance catalyst for hydrazine electrooxidation, *J. Alloy. Compd.* 902 (2022), 163746.
- [32]. M. Shokouhimehr, T. Kim, S.W. Jun, K. Shin, Y. Jang, B.H. Kim, J. Kim, T. Hyeon, Magnetically separable carbon nanocomposite catalysts for efficient nitroarene reduction and Suzuki reactions, *Appl. Catal. A* 476 (2014) 133–139.
- [33]. S. Pang, Y. Zhang, Q. Su, F. Liu, X. Xie, Z. Duan, F. Zhou, P. Zhang, Y. Wang, Superhydrophobic nickel/carbon core-shell nanocomposites for the hydrogen transfer reactions of nitrobenzene and N-heterocycles, *Green Chem.* 22 (2020) 1996–2010.
- [34]. D. Gogoi, R.S. Karmur, M.R. Das, N.N. Ghosh, Cu and CoFe₂O₄ Nanoparticles Decorated Hierarchical Porous Carbon: An Excellent Catalyst for Reduction of Nitroaromatics and Microwave-Assisted Antibiotic Degradation, *Appl. Catal. B Environ.* 312 (2022), 121407.
- [35]. S. Gurusamy, M.R. Kulanthaisamy, D.G. Hari, A. Veleeswaran, B. Thulasinathan, J. B. Muthuramalingam, R. Balasubramani, S.W. Chang, M.V. Arasu, N.A. Al-Dhabi, A. Selvaraj, A. Alagarsamy, Environmental friendly synthesis of TiO₂-ZnO nanocomposite catalyst and silver nanomaterials for the enhanced production of biodiesel from *Ulva lactuca* seaweed and potential antimicrobial properties against the microbial pathogens, *J. Photochem. Photobiol. B Biol.* 193 (2019) 118–130.
- [36]. T. Song, Z. Ma, P. Ren, Y. Yuan, J. Xiao, Y. Yang, A Bifunctional Iron Nanocomposite Catalyst for Efficient Oxidation of Alkenes to Ketones and 1,2- Diketones, *ACS Catal.* 10 (2020) 4617–4629.
- [37]. S. Bonardd, C. Saldías, O. Ramírez, D. Radi 'c, F.J. Recio, M. Urzúa, A. Leiva, A novel environmentally friendly method in solid phase for in situ synthesis of chitosangold bionanocomposites with catalytic applications, *Carbohydr. Polym.* 207 (2019) 533–541

The Study of Alterations in Tissue Cholesterol in Reproductive Organs of Female Albino Rats Fed With Steroidal and Non-Steroidal Contraceptive Pills

M. P. Chikhale*

Department of Zoology, Rajarshee Shahu Science College Chandur Railway, Dist-Amravati, 444 904, Maharashtra, India

ARTICLE INFO

Article History:

Accepted : 01 Jan 2025

Published : 10 Jan 2025

Publication Issue :

Volume 12, Issue 7

January-February-2025

Page Number :

227-232

ABSTRACT

The effect of steroidal and non-steroidal contraceptive oral pills on tissue cholesterol in reproductive organs was carried out in wistar female albino rats weighing about $125g \pm 2g$. The steroidal combined oral contraceptive pill (norgestrel + ethinylestradiol) was diluted to 0.14 mg/ml (low dose), 0.21 mg/ml (dose as per literature), and 0.43 mg/ml (high dose). The non-steroidal oral contraceptive pill (centchroman) was diluted to 0.29 mg/ml (low dose), 0.43 mg/ml (dose as per literature) and 0.87 mg/ml (high dose). Cholesterol is a vital lipid molecule that plays an essential role in the structural integrity of cell membranes and serves as a precursor for the synthesis of steroid hormones, vitamin D, and bile acids. Tissue cholesterol was elevated significantly in the ovary and fallopian tube in both steroidal and non-steroidal contraceptive fed rats throughout the treatment (tables A and B). Results obtained with the administration of oral contraceptives brought about profound alteration in tissue cholesterol. These results are indicative of increased risk of cardio-vascular problems. Deposition of cholesterol in the ovary and uterus of rats fed with steroidal pills was more when compared with the results of non-steroidal pill fed rats.

Keywords: Steroidal and non-steroidal contraceptive oral pill, tissue cholesterol, reproductive organ, female wistar albino.

I. INTRODUCTION

Cholesterol is a key component of cellular structures and metabolic processes across various tissues in the body (Stevenson and Brown, 2009). Cholesterol is a vital lipid molecule that plays an essential role in the structural integrity of cell membranes and serves as a precursor for the synthesis of steroid hormones, vitamin D, and bile

acids. Tissue cholesterol refers to the cholesterol found within various tissues and organs of the body, such as the liver, heart, kidneys, muscles, and brain (Arthur, et.al.,2016).

Hormonal contraceptive use for an extended period of time has been linked to various metabolic effects, such as altered blood pressure, body weight, liver enzymes, lipid profile, and carbohydrate metabolism. These changes can lead to coronary heart disease, congestive heart failure, angina, peripheral arterial disease, deep vein thrombosis, and stroke, which are the main causes of premature death (Ngo Nonga B, et.al.,2016). Numerous studies have examined the connection between lipid profiles and hormonal contraceptives; nevertheless, the findings vary throughout them. By interfering with the physiological processes of ovulation, fertilisation, and implantation, contraception works to prevent pregnancy (Skiles MP, et.al.,2015). For emerging nations, the situation of rapidly growing populations and rising mortality rates is worrisome. As a result, systematic efforts are made to look for affordable, dependable, and effective birth control options for women (Kim CR, et.al.,2017). The purpose of the current study was to evaluate the impact of hormonal contraceptives on tissue cholesterol and to inform users of hormonal contraceptives, clinicians, and family planning service providers about the importance of early lipid profile detection to prevent serious complications and death. Additionally, it offers baseline data to academics and policy makers who wish to delve deeper into the impact of hormonal contraceptives on lipid profile.

II. EXPERIMENTAL

The present study was carried out in wistar female albino rats weighing about $125\text{g} \pm 2\text{ g}$. The animals were procured from National Institute of Nutrition (NIN), Hyderabad. Animal experiments were conducted according to "INSA – Ethical guidelines for use of animals for scientific research after getting permission from ethical committee". The animals were kept in vivarium throughout the period of experiment. They were regularly fed on standard pellet diet provided by National Institute of Nutrition, Hyderabad and water *ad-libitum*. The remaining food and waste matter was removed from the cages on the next day and proper care was taken to avoid any infection. Only healthy rats were used for the present experiments.

Pills:

The experimental female albino rats were given selected steroidal and non-steroidal contraceptive oral pills in calculated doses. Steroidal Contraceptive pill are combined oral contraceptive pill with Brand name was Choice. Each Tablet contains Norgestrel 30 mg and Ethinylestradiol 0.03 mg (Manufactured by : Hindustan latex limited). Non-steroidal oral contraceptive pill with Brand name, Saheli. Each Tablet Contain Centchroman - 30 mg (Manufactured by :- Hindustan Latex Limited).

Doses:

Dilutions of pills were made by using double distilled water (DDW). The combined oral contraceptive pill (norgestrel + ethinylestradiol) was diluted to 0.14mg/ ml (Low Dose), 0.21 mg/ml (dose as per literature), and 0.43 mg/ ml (high dose). The non-steroidal oral contraceptive pill (Centchroman) was diluted to 0.29 mg/ ml (Low Dose), 0.43 mg/ml (dose as per literature) and 0.87 mg/ml (high dose). The doses of both drugs were calculated as per body weight of rats considering the human consumption and available literature.

Experimental Set Up:-

Experiments were carried out by dividing female albino rats into three groups:

Group I :- Control female albino rats administered orally with 1ml DDW/ rat / day upto 30 days DDW being used as vehicle .

Group II :- Group of combined oral contraceptive pill. This group was again divided into three sub-groups .

Sub-group I :- Experimental female albino rats administered orally with 1 ml norgestrel + ethinylestradiol/ rat / day upto 30 days. 1 ml dose contains 0.14 mg norgestrel + ethinylestradiol.

Subgroup II:- Experimental female albino rats who received 1ml norgestrel + ethinylestradiol / rat / day upto 30 days . 1 ml dose contains 0.21 mg norgestrel + ethinylestradiol.

Subgroup III :- Experimental female albino rats administered orally with 1 ml norgestrel + ethinylestradiol/rat/day upto 30 days. 1 ml dose contains 0.43 mg norgestrel+ ethinylestradiol.

Group III :- Group of rats were administered orally with Centchroman. This group was divided into three sub groups.

Subgroup I:-Experimental female albino rats administered orally with 1ml Centchroman / rat / day upto 30 days. 1 ml dose contains 0.29 mg Centchroman.

Subgroup II:- Experimental female albino rats administered orally with 1ml Centchroman / rat / day upto 30 days. 1 ml dose contains 0.43 mg Centchroman.

Subgroup III:-Experimental female albino rats administered orally with 1 ml Centchroman / rat / day upto 30 days. 1 ml dose contains 0.87 mg Centchroman .

Estimation of total cholesterol:Total cholesterol in the tissue (ovary / fallopian tube / uterus) of the control and experimental female albino rats was estimated by the method of Leibermann Burchard (1959).

III.OBSERVATIONS AND CALCULATIONS

Tissue cholesterol was elevated significantly in ovary and fallopian tube in both steroidal and non-steroidal contraceptive fed rats throughout the treatment (Table- A and B). The uterus in steroid contraceptive fed rat also was found to have elevated cholesterol, however, in rats of non-steroidal contraceptive pill fed, the uterine cholesterol was decreased significantly after 30 days of treatment when the dose is 0.87 mg/ml/rat/day. In normal dose of non-steroidal contraceptive, the uterine cholesterol was significantly elevated (60.42%) over the control values.

Table No. 1

Alterations in tissue Cholesterol (mg / gm of tissue) of female albino rats fed with steroidal contraceptive pills for 30 days.

* Steroidal pill :- Norgestrel (0.30 mg) + Ethinylestradiol (0.03 mg) (CHOICE)

* The Values are mean of 6 replicates \pm SE

Sr. No.	Tissue	Control	Steroidal Pill		
			0.14 mg/ml/rat/day	0.21 mg/ml/rat/day	0.43mg/ ml/rat/day
1	Ovary	18.62 \pm 0.22	31.52 \pm 0.36 (+69.28)	28.78 \pm 0.44 (+54.56)	27.84 \pm 0.28 (+49.51)
2	Fallopian tube	14.04 \pm 0.16	13.61 \pm 0.15 (-3.06)	15.83 \pm 0.18 (+12.75)	16.59 \pm 0.16 (+18.16)
3	Uterus	12.71 \pm 0.09	16.48 \pm 0.21 (+29.66)	22.19 \pm 0.38 (+74.58)	14.58 \pm 0.11 (+14.71)

* Values in parenthesis indicate percent change over control.

* All values are significant at $p < 0.01$

* NS :- Not significant

TABLE No.- 2

Alterations in tissue Cholesterol (mg / gm of tissue) of female albino rats fed with non-steroidal contraceptive pills for 30 days.

Sr. No.	Tissue	Control	Non – steroidal Pill		
			0.29 mg/ml/rat/day	0.43 mg/ml/rat/day	0.87mg/ ml/rat/day
1	Ovary	18.62 ± 0.22	22.4 ± 0.41 (+20.30)	28.56 ± 0.34 (+53.38)	20.56 ± 0.22 (+10.41)
2	Fallopian tube	14.04 ± 0.16	16.27 ± 0.17 (+15.88)	15.83 ± 0.25 (+12.75)	17.13 ± 0.16 (+22.01)
3	Uterus	12.71 ± 0.09	9.34 ± 0.09 (-26.51)	20.39 ± 0.15 (+60.42)	8.37 ± 0.08 (-34.14)

Non - steroidal Pill :-Centchroman (30 mg) (SAHELI)

* The Values are mean of 6 replicates ± SE

* Values in parenthesis indicate percent change over control.

* All values are significant at $p < 0.01$

* NS :- Not significant

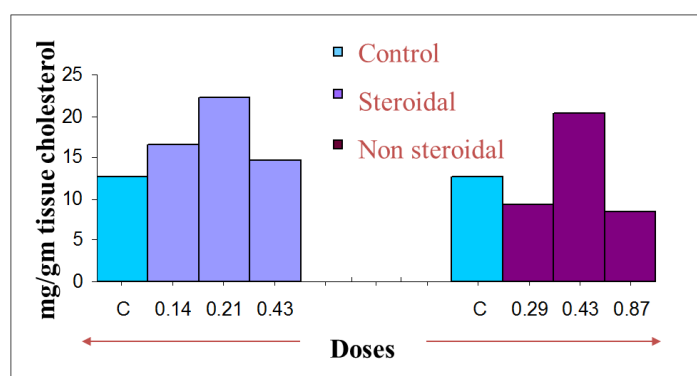


Fig :- Alterations in tissue cholesterol (mg/gm of tissue) in the uterus of female albino rat fed with steroidal and non-steroidal contraceptive pills for 30 days (Doses are mg/ml/rat/day, control rats were administered equivalent amount of vehicle).

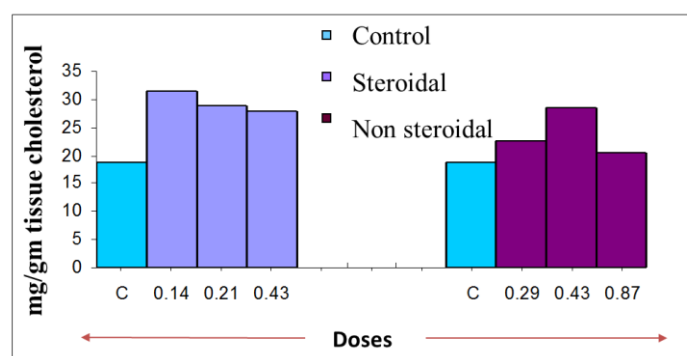


Fig :- Alterations in tissue cholesterol (mg/gm of tissue) in the ovary of female albino rat fed with steroidal and non-steroidal contraceptive pills for 30 days (Doses are mg/day, control rats were administered equivalent amount of vehicle).

IV. RESULT AND DISCUSSION

The female albino rats of approximately same age and weight were fed with three different doses of steroidal pills containing ethinyl estradiol and norgestrel for 30 days and also three different doses of non-steroidal Centchroman contraceptive pills. After 30 days of feeding once a day pills, tissue cholesterol was significantly increased. The increase in tissue cholesterol levels could possibly be due to either increase in the synthesis and / or decreases in the brake down of fatty acids due to peroxisomes. Both steroidal and non-steroidal contraceptive-fed rats had markedly higher tissue cholesterol in their ovaries for the course of the treatment (Tables A and B). According to recent research by Herbst (1967), gonadotropin and anterior pituitary hormone treatment causes notable changes in the amount of cholesterol in the ovaries. The depletion of cholesteryl esters was specifically mediated by luteinizing hormone. The idea that cholesterol acts as a bridge in the production of progesterone is supported by these studies. The adrenal gland and gonads are the primary tissues that synthesise steroid hormones, such as oestrogen and progesterone, which are cholesterol derivatives (Miller and Bose, 2011). The cholesterol obtained from various sources serves as a precursor for the steroidogenesis of ovarian endocrine tissue (Miller and Bose, 2011). Reduced cholesterol utilisation for steroidogenesis is indicated by the elevated cholesterol levels in groups receiving high doses. Our findings (see Tables A and B for details) were similar to those of Sheeja et al. (2009) and Bandyopadhyay S. (2010), who found that ovarian tissue had a markedly elevated cholesterol level, indicating that the ovaries did not use cholesterol for hormone production. Results obtained with administration of oral contraceptives brought about profound alteration in tissue cholesterol. These results are indicative of increased risk of cardio-vascular problems. Deposition of cholesterol in ovary and uterus of rats fed with steroidal pills were more when compared with the results of non-steroidal pill fed rats.

V. CONCLUSION

For 30 days, three different doses of steroidal pills containing ethinyl oestradiol and norgestrel (0.14, 0.21, and 0.43 mg/ml/rat/day) and three different doses (0.29, 0.43, and 0.87 mg/ml/rat/day) of non-steroidal Centchroman oral contraceptive pills were given to female albino rats of roughly the same age and weight. The fact that Centchroman's effect was only around one-sixth of what oestradiol + progesterone produced suggests that Centchroman's antiestrogen action is roughly six times stronger than its oestrogenic effect. There have been some negative effects on the ovary from both steroidal and non-steroidal contraceptives. To determine the ideal dosage that won't have any negative effects on the ovary or uterus, more research is required.

VI. ACKNOWLEDGEMENT

Without my close relationships with several people who were always there for me when I needed them most, the work that is detailed in this study article would not have been feasible. I want to use this time to thank them for helping me make this happen and to honour them. I owe a debt of gratitude to my mentor, the late Dr. G.N. Vankhede, professor and chairman of the P.G. Department of Zoology at SGBAU Amravati, for his constant encouragement, support, and wise counsel during my investigation.

VII. REFERENCES

- [1]. Arthur C. Guyton, John E. Hall. Textbook of Medical Physiology 11th ed. Saunders; 2006. P. 840.
- [2]. Bandyopadhyay, S. Anti-fertility activity of methanol extracts of *Brassia latifolia* and *Cajanus cajan* in female albino mice ovaries. *Iranian J Pharmacol Ther*, 2010, 9, 83-87.
- [3]. Hall, J.E.; Guyton, A.C. Textbook of Medical Physiology. Churchill Livingstone Elsevier: Philadelphia, 2006.
- [4]. Herbst, A. L. 1967. *Endocrinology*. 81: 54
- [5]. Kim CR, Fonhus MS, Ganatra B. Self-administration of injectable contraceptives: a systematic review *Kim. BJOG*. 2017; 124: 200-208
- [6]. Miller, W.L.; Bose, H.S. Early steps in steroidogenesis: intracellular cholesterol trafficking. *J. Lipid Res.*, 2011, 52, 2111-35.
- [7]. Ngo Nonga B, Mballa J, Ntone F, Ndongo S, Ouankou C, Handy E, et al. Prevalence of significant carotid stenosis and other risk factors in patients with acute ischemic stroke in Yaounde Cameroon. *J Vasc Med Surg*. 2016;04(02):257.
- [8]. Sheeja, E.; Joshi, S.B.; Jain, D.C. Antioviulatory and estrogenic activity of *Plumbago rosea* leaves in female albino rats. *Indian J. Pharmacol.*, 2009, 41, 273-7.
- [9]. Skiles MP, Cunningham M, Inglis A. The effects of access to contraceptive services on injectable use and demand for family planning in Malawi. *Int Perspective Sex Reproduct Health*. 2015; 41: 20-30.
- [10]. Stevenson J, Brown AJ. How essential is cholesterol. *Biochem J*. 2009 May 13;420(2):el-4.

Synthesis and Microbial Evaluation of Some of 1,2,4-Thiadiazole Derivatives

M. R. Raghuvanshi

Department of Chemistry, Arvindbabu Deshmukh Mahavidyalaya, Bharsingi, Tq-Narkhed, Dist-Nagpur, Maharashtra, India

ARTICLE INFO

Article History:

Accepted : 01 Jan 2025

Published : 10 Jan 2025

Publication Issue :

Volume 12, Issue 7

January-February-2025

Page Number :

233-238

ABSTRACT

A novel series of 3-[(3-substituted amino -1,2,4-thiadiaz-3-yl)]amono-5-N-TAG-amino-1,2,4-thiadiazole [11] were synthesized by the oxidative cyclization of 1-[S-TAG-N-substitutedthioamido]dicyanadiamide [8] and 1-[(N-TAG) thioamido]-5-substituted formamidino-2-imino-4-thiobiuret [9] in chloroform medium using liquid bromine as oxidizing agent. The products isolated in these reaction were characterized and the justification of the structure of these newly synthesized compounds have been established on the basis of chemical characteristics, elemental analysis and IR, NMR and mass spectral analysis. The newly synthesized substituted derivatives of thiocarbamide were screened for its antimicrobial activities against some gram positive & gram negative pathogens. The compounds showed good & moderate activity against the pathogens. These materials found several applications in pharmaceutical industry and also in medicinal chemistry.

Keywords -Thiadiazoles , Oxidative cyclization, Microbial evaluation

I. INTRODUCTION

Thiadiazoles are classified under the azole compounds. These are five-membered heterocyclic compound containing a sulfur atom with two nitrogen atoms. Thiadiazole moiety act as a “hydrogen binding domain” and “two-electron donor system”. They occur in four isomeric forms viz., 1,2,3-thiadiazole; 1,2,4-thiadiazole; 1,2,5-thiadiazole and 1,3,4-thiadiazole. The 1,2,4-thiadiazole scaffolds represent a five-membered nitrogen-sulfur-containing significant class of core heterocyclic structures of great interest, mainly because of the part of the structural unit of biologically active molecules: a useful intermediate in medicinal chemistry and part of the clinical drugs.¹⁻¹⁵ Some thiadiazoles were found to be active against *S. aureus*, *E. coli*, and *C. albicans*¹³⁻¹⁴. S-gulcosides and N-gulcosides containing thiadiazoles possesses noticeable pharmaceutical and medicinal applications¹⁷. Antibacterial and antifungal activities of some thioglucosides and N-glucosides were studied¹⁸⁻¹⁹. The oxidative cyclization of cyanoamidinosubstitutedthiocarbamides and N-substituted

formamidinoformamidinithiocarbamides have been extensively investigated²⁰. As a part of research work presently been undertaken in this laboratory for the synthesis of heteroacycles and heterocycles, it was thought interesting to investigate the oxidative cyclization of 1-[(N-TAG) thioamido]-5-substitutedformamidino-2-imino-4-thiabiuret [9] with liquid bromine in chloroform medium to obtain a novel series of 3-[(3-substitutedamino -1,2,4- thiadiaz-3-yl)] amino-5-N-TAG-amino-1,2,4-thiadiazole [11].

II. MATERIALS & METHODS

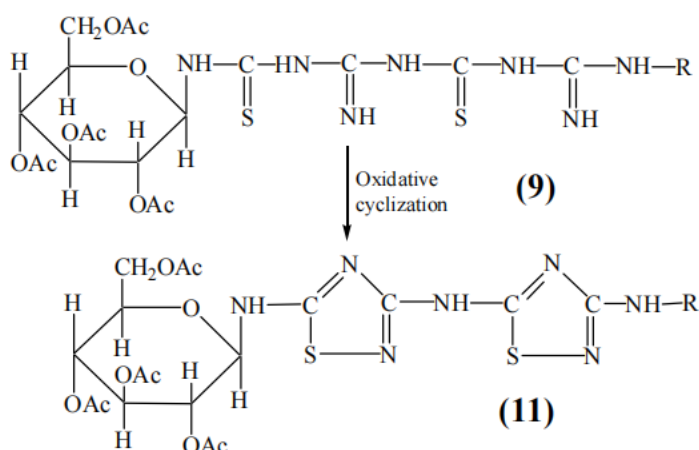
The melting points of all the synthesized compounds were recorded using hot paraffin bath and are uncorrected, The carbon and hydrogen analysis was carried out on Carlo-Ebra-1106 analyzer, nitrogen estimation was carried out on Colman- N-analyser-29. IR spectra were recorded on Perkin-Elmer spectrometer in the range 4000-400 cm⁻¹ in KBr pellets. PMR spectra were recorded on Bruker AC-300F spectrometer with TMS as internal standard using CDC13 and DMSO-d₆ as solvent. The FAB mass spectra were recorded on a Joel SX 102/Da-600 mass spectrometer. Data System using Argon. The accelerating voltage was 10kV and spectra were recorded at room temperature by using m-nitro benzyl alcohol as a matrix. The purity of the compounds was checked on Silica Gel-G plates by TLC with layer thickness of 0.3 mm. All chemicals used were of AR grade except allylthiourea Lancaster (Germany make). Alkyl/arylisothiocyanates and phenylthiourea have been prepared by known literature methods.²¹

Experimental-

Synthesis of 3-[(3-phenylamino-1,2,4-thiadiaz-3-yl)]amino-5-N-TAG amino-1,2,4-thiadiazole [11b]

In china dish a paste of 1-[(N-TAG thioamido)-5-phenylformamidino-2-imino- 4-thiobiuret [9b] was prepared in chloroform. To this liquid bromine in chloroform was added with constant stirring. Initially the colour of bromine disappeared the addition of bromine was continued till the colour of bromine persisted to the reaction mixture. The reaction mixture was allowed to stand for 8 hrs. at room conditions. It is dark brown in colour. After the basification of the reaction mixture afforded brown coloured product, which on crystallization gave brown crystals of [11b] yield 61%, m. p. 147 °C.

Scheme -



Where R = -H, -phenyl, -methyl, -ethyl and allyl.

Similarly 3-[(3-Amino-1,2,4-thiadiaz-3-yl)]-amino-5-N-TAG amino-1,2,4- thiadiazole [11a], 3-[(3-methylamino-1,2,4-thiadiaz-3-yl)]-amino-5-N-TAG amino- 1,2,4-thiadiazole [11c], 3-[(3-ethylamino-1,2,4-thiadiaz-3-yl)]-amino-5-N-TAG amino-1,2,4-thiadiazole [11d], 3-[(3-allylamino-1,2,4-thiadiaz-3-yl)]-amino-5-

NTAG amino-1,2,4-thiadiazole [11e] were synthesized from 1-[(N-TAG)thioamidino]-5-formamidino-2-imino-4-thiobiuret [9a], 1-[(N-TAG)thioamidino]-5-methylformamidino-2-imino-4-thiobiuret [9c], 1-[(N-TAG)thioamidino]-5-ethylformamidino-2-imino-4-thiobiuret [9d], 1-[(N-TAG)thioamidino]-5-allylformamidino-2-imino-4-thiobiuret [9e] in bromine in chloroform medium respectively by the above mentioned method in experiment (7) to (11).

Sr. No.	Experiment No.	3-[-(3-substituted amino-1,2,4-thiadiaz-4-yl)]amino-5-N-TAG amino-1,2,4-thiadiazole	Yield	m. p.
1	7 H	61%	149
2	8 phenyl	61%	147
3	9 methyl	63%	138
4	10 ethyl	67%	143
5	11 allyl	69%	142

III.RESULTS AND DISCUSSIONS

The IR spectrum of compound [11b] was carried out in KBr pellets and is reproduce on plate No. IR-3.2. The IR spectrum clearly indicated the bands due to νNH , $\nu\text{C-H(Ar)}$, $\nu\text{C=O}$, $\nu\text{C=N}$, $\nu\text{RC-N}$, and bands due to mono substituted benzene and the important absorption can be correlated as Follows

Absorption Observed (cm^{-1})	Assignment	Absorption Expected(Cm^{-1})
3374.5	NH stretching	3500-3100
1695.8	C=O Stretching	1900-1600
1585	C=N stretching	1789-1471
1213	C-N stretching	1220-1000
757.4	C-S Stretching	800-600

Table-1: FT-IR spectrum of 3-[(3-phenylamino-1,2,4-thiadiaz-3-yl)]amino-5-N-TAG amino-1,2,4-thiadiazole [11b]

The PMR spectrum of compound [11b] was carried out in DMSO- d_6 and CDCl_3 and reproduce on plate No. PMR-3.2. This spectrum distinctly displayed the signals due to Ar-NH at $\delta 6.8 - 7.8$ ppm, -O-CH signals due to at $\delta 2.58 - 2.6$ ppm, The signals due to C-CH at $\delta 2.16 - 1.25$ ppm and the signals at $\delta 4.25$ ppm are due to DMSO solvent.

The FAB mass spectrum of [11b] was recorded at room temperature by using metanitrobenzyl alcohol as the matrix M^+ Peak as well as other fragment peaks and the probable fragmentation pattern of the molecular ion can shown in scheme VI. While the mass spectrum is reproduced on plate No. Mass - 3.2

From the above properties and spectral analysis, the compound [11b] was assigned. The structure as 3-S-TAG-5-phenylamino-1,2,4-thiadiaz-3-yl)]amino-5- N-TAG-amino-1,2,4-thiadiazole.

Microbial Evaluation-

All the synthesized compounds were screened for antimicrobial activity using disc diffusion method²² and all the pathogen tested during analysis are human pathogens. For this Whatman filter paper No. 1 disks of 5mm diameter were sterilized in autoclave and soaked in sample solution, blotted on sterile filter paper. 0.1ml of the inoculum of test organism was spread using sterile glass spreader on the surface of nutrient agar. The filter paper disks soaked in Gentamycin (20µg/ml) (Glaxo India Ltd.) and Ciprofloxacin (20µg/ml) (Glaxo smith kline) were used as positive controls and the filter paper disc soaked in dimethyl sulphoxide (DMSO) were used as a solvent. The compounds were taken at a concentration of 1mg/ml using dimethyl sulphoxide as a solvent. Fluconazole (20µg/ml) as a standard for antifungal activity. The inhibition zones were measured in millimeter by the end of the incubation period (24 hrs. at 37°C for bacteria).

From the results it is clear that compounds showed remarkable and considerable antimicrobial activity against organism. The activity of compounds were tested against all the pathogen by disc diffusion method. The antimicrobial activity of different compound against micro-organisms were examined in the presence study and their potency, were assessed by the presence or absence inhibition zone and zone diameter. The result are given in Table No. 2. From this table clearly indicates that, all the compounds are active against *S. typhi*, *E.coli* & *A. nigar* but some compounds 11a, 11b & 11f are inactive against *P.aerogenosa*, *S.aureus* & *c.albicans*.

Compounds	Inhibition zone in mm					
	<i>S.Typhi</i>	<i>E.coli</i>	<i>P. aerogenosa</i>	<i>S.aureus</i>	<i>A.nigar</i>	<i>c.albicans</i>
11a	8	8	-ve	-ve	9	-ve
11b	10	9	-ve	8	12	10
11c	9	9	7	7	10	10
11d	9	8	9	9	9	9
11e	10	9	10	9	12	12
11f	8	8	-ve	-ve	9	9
DMSO	-	-	-	-	-	-
Fluconazole	-	-	-	-	12	12
Ciprofloxacin	10	9	10	9	-	-

Table No-2 Microbial activity by disc diffusion method

IV. CONCLUSIONS

The compound 3-[(3-substituted amino -1,2,4-thiadiaz-3-yl)]amino-5-N-TAG-amino-1,2,4-thiadiazole [11a-f] was successfully prepared which grown brown crystalline solid with m. p. 147°C. The synthesized sample was characterized by FT-IR, PMR and mass spectrograph indicating formation of the desired product. The compounds were studied to evaluate in vitro antibacterial and antifungal properties by disc diffusion method. The antimicrobial activity of different compound against micro-organisms were examined in the presence study and their potency, were assessed by the presence or absence inhibition zone and zone diameter. From results, most of these compounds found to be potent antibacterial and antifungal agent exhibited comparable antibacterial and antifungal activity than the standard. It means that the compounds showed remarkable and considerable antimicrobial activity. It also concludes from the data when the compounds contain thiocarbamido group as guanidine group it will increase the potential of the drug. These synthesized drugs can be used as alternative drug for the treatment of disease caused by the microbes only if the synthesized

compounds do not have toxic and other side effects after detailed study. This presented work is Open new doors to researchers to carry work in this line.

ACKNOWLEDGEMENT

Authors are very much thankful to Head, Department of Chemistry, Sant Gadge Baba Amravati University, Amravati for providing necessary facilities & also thankful to SAIF, Patiala University, Punjab for recording the NMR spectra.

V. REFERENCES

- [1]. Tahghighi, A.; Babalouei, F. Thiadiazoles: The appropriate pharmacological scaffolds with leishmanicidal and antimalarial activities: A review. *Iran. J. Basic Med. Sci.* 2017, 20, 613–622.
- [2]. Iizawa, Y.; Okonogi, K.; Hayashi, R.; Iwahi, T.; Yamazaki, T.; Imada, A. Therapeutic Effect of Cefozopran (SCE-2787), a New Parenteral Cephalosporin, against Experimental Infections in Mice. *Antimicrob. Agents Chemother.* 1993, 37, 100–105.
- [3]. Frija, T.M.L.; Pombeiro, L.J.A.; Kopylovich, N.M. Building 1,2,4-Thiadiazole: Ten Years of Progress. *Eur. J. Org. Chem.* 2017, 2017, 2670–2682.
- [4]. Irfan, A.; Batool, F.; Ahmad, S.; Ullah, R.; Sultan, A.; Sattar, R.; Nisar, B.; Rubab, L. Recent trends in the synthesis of 1,2,3-thiadiazoles. *Phosphorus Sulfur Silicon Relat. Elem.* 2019, 194, 1098–1115.
- [5]. Irfan, A.; Ullah, S.; Anum, A.; Jabeen, N.; Zahoor, A.F.; Kanwal, H.; Kotwica-Mojzych, K.; Mojzych, M. Synthetic Transformations and Medicinal Significance of 1,2,3-Thiadiazoles Derivatives: An Update. *Appl. Sci.* 2021, 11, 5742.
- [6]. Decking, U.K.; Hartmann, M.; Rose, H.R.; Meil, J.B.; Schrader, J. Cardioprotective actions of KC 12291. I. Inhibition of voltage-gated Na⁺ channels in ischemia delays myocardial Na⁺ overload. *Naunyn Schmiedeberg's Arch. Pharmacol.* 1998, 358, 547–553.
- [7]. Proshin, A.N.; Serkov, I.V.; Petrova, L.N.; Bachurin, O.S. 5-Amino-3-(2-aminopropyl)-1,2,4-thiadiazoles as the basis of hybrid multifunctional compounds. *Russ. Chem. Bull.* 2014, 63, 1148–1152.
- [8]. Fawzi, A.B.; Macdonald, D.; Benbow, L.L.; Smith-Torhan, A.; Zhang, H.T.; Weig, B.C.; Ho, G.; Tulshian, D.; Linder, M.E.; Graziano, M.P. SCH-202676: An allosteric modulator of both agonist and antagonist binding to G protein-coupled receptors. *Mol. Pharmacol.* 2001, 59, 30.
- [9]. Hartmann, M.; Decking, U.K.M.; Schrader, J. Cardioprotective actions of KC 12291 II. Delaying Na⁺ overload in ischemia improves cardiac function and energy status in reperfusion. *Naunyn Schmiedeberg's Arch. Pharmacol.* 1998, 358, 554.
- [10]. Martínez, A.; Alonso, M.; Castro, A.; Pérez, C.; Moreno, F.J. First Non-ATP Competitive Glycogen Synthase Kinase 3 α (GSK-3 α) Inhibitors: Thiadiazolidinones (TDZD) as Potential Drugs for the Treatment of Alzheimer's Disease. *J. Med. Chem.* 2002, 45, 1
- [11]. Kumar, D.; Kumar, N.-M.; Chang, K.-H.; Shah, K. Synthesis and anticancer activity of 5-(3-indolyl)-1,3,4-thiadiazoles. *Eur. J. Med. Chem.* 2010, 45, 4664–4668.
- [12]. Romagnoli, R.; Baraldi, G.P.; Carrion, D.M.; Cruz-Lopez, O.; Preti, D.; Tabrizi, A.M.; Fruttarolo, F.; Heilmann, F.; Bermejo, J.; Estevez, F. Hybrid molecules containing benzo[4,5]imidazo-[1,2-d][1,2,4]thiadiazole and α -bromoacryloyl moieties as potent apoptosis inducers on human myeloid leukaemia cells. *Bioorg. Med. Chem. Lett.* 2007, 17, 2844.

- [13]. 1,3,4-Thiadiazoles: A potent multi targeted pharmacological scaffold, European Journal of Medicinal Chemistry,2015,92,156-177, <https://doi.org/10.1016/j.ejmech.2014.12.035>
- [14]. Laila Rubab,Ayesha Anum,Green Chemistry in Organic Synthesis: Recent Update on Green Catalytic Approachesin Synthesis of 1,2,4-Thiadiazoles, Catalysts 2022, 12(11), 1329; <https://doi.org/10.3390/catal12111329>
- [15]. Suhail Ahmad a, Md. Zafer Alam a, Umme Salma a, Md. Mohasin a, A review on recent progress in synthesis and biological activities of thiadiazole and its derivatives,Journal of Molecular Structure, 2024,1312(2), 138438,<https://doi.org/10.1016/j.molstruc.2024.138438>.
- [16]. K. M. Youssef and S. El-Meligie : Egypt J. Pharm. Sci.,1989,30, 455
- [17]. Habib Narguous Samuel, Abdel Hamid Soad ,Abdel Hamid M. E. L. Housash ,Farmaco, 1998, 44(12), 1225
- [18]. D. B. Jadhav : “Synthesis of Newer types of nucleosides and their phosphorylation Reactions, Ph. D., Thesis Nagpur University, Nagpur ,1992.
- [19]. S. K. Bhagat : “Chemistry of Tetra-O-benzoyl-Dglucospyranosyl bromide and synthesis of certain benzoylated thioglucosides”, Ph. D. Thesis, Amravati University, Amravati ,2002.
- [20]. V. V. Dabolkar, F. Y. Ansari : Acta Poloniac Pharmaceutica-Drug research, 2008,65(5), 521-526,
- [21]. Silverstein R.M, G.C. Bassler and Morill T.C, Spectroscopic identification of Organic Compounds,4th Ed, John Wiley & Sons, INC, New York,1981
- [22]. Mounyr Balouiri 1,□, Moulay Sadiki 1, Saad Koraichi Ibnsouda,Methods for in vitro evaluating antimicrobial activity: A review,J Pharm Anal,2015,2;6(2):71-79, doi: 10.1016/j.jpha.2015.11.005

Impact of Substituted Flavones in Medicinal field

Dr. S. L. Sayre¹, Dr. P. B. Raghuwanshi²

^{*1}Department of Chemistry, G P Arvi, Wardha, Maharashtra, India

Sayshu2@ijrst.com¹

² Department of Chemistry, Brijlal Biyani Science College , Amravati, Maharashtra, India

ARTICLE INFO

Article History:

Accepted : 01 Jan 2025

Published : 10 Jan 2025

Publication Issue :

Volume 12, Issue 7

January-February-2025

Page Number :

239-241

ABSTRACT

Flavone (2-phenylchromone) derivatives are naturally occurring heterocyclic compound belongs to the flavanoid group. Heterocyclic chemistry is the chemistry of cyclic compounds having hetero atoms like nitrogen, sulphur or oxygen along with carbon, hydrogen and other elements. Most probably two-third of organic compounds such as medicines, drugs belong to this class. Flavones constitute large segment of natural products. Synthesis of flavones has attracted considerable attention due to their significant biocidal, pharmaceutical , anti- cancer and anti-inflammatory effects. Various flavones are found to be of wide clinical importance. The medicinal applications and drug activities of these synthesized compounds have been investigated with different microbes viz. E.coli, S.typhi, S.aureus, P.acne. A good amount of work has been done in studying various biological activities of different flavone derivatives.

Keywords : Flavone, Heterocyclic chemistry, medicinal applications, drug activities.

I. INTRODUCTION

Flavones (flavus = yellow) are a class of flavonoids based on the backbone of 2-phenylchromen-4-one. Flavones are mainly found in cereals and herbs. Flavones are biologically active compounds. Flavones, the most prominent group of naturally occurring chromones, are present in a wide variety of plants and are well-known by their broad range of biological properties, such as antibacterial, antifungal, antiviral, anti-inflammatory, antioxidant, antiallergic,

hepatoprotective, antithrombotic and antitumor activities. concepts and the underlying principles and should provide authentic contribution to knowledge. If your paper does not represent original work, it should have educational value by presenting a fresh perspective or a synthesis of existing knowledge. The purpose of this document is to provide you with some

During the recent years, the incidence of bacterial and fungal infections has been increasing dramatically due to an increase in the number of Immuno-compromised hosts. Immuno suppression

due to HIV-infection, malignancy, immune suppressive therapies, broad-spectrum antimicrobial treatment and age, as well as invasive procedures and mucosal barriers places patients at high risk for microbial infections. The increasing incidence of resistance to a large number of antibacterial agents is becoming another major concern. Currently, a small number of antifungal agents are available, and all have some drawbacks regarding their spectrum, toxicity, tissue distributions and high cost. These observations clearly indicate the need of as well as search for alternative new and more effective antimicrobial agents with a broad spectrum of activity. The review of literature survey clearly mentioned that the substituted flavones have medicinal, biological and pharmacological values³³. Hence, it was thought interesting to study antimicrobial activity of substituted flavones against pathogenic micro-organism and help to find better alternative against drug resistant pathogenic micro-organism.

II. METHODS AND MATERIAL

All the compounds L1, L2, L3, L4, L5, L6 were screened for their antimicrobial activity against bacteria two gram negative- *E. coli*, *S. typhi*, and two gram positive *S. aureus*, *P. acne*. by using agar disc diffusion method. Antimicrobial activity of six organic compounds viz. L1, L2, L3, L4, L5, L6 were determined by Agar disc diffusion assay according to the Manual of antimicrobial susceptibility testing was used to assay the various antibiotics for bactericidal activity against test strains of *E. coli*, *S. aureus*, *P. acnes*, *S. typhi*. Various methods have been used from time to time by several workers to evaluate the antimicrobial activity. The evaluation can be done by the following methods:

- i. Turbidometric method.
- ii. Agar streak dilution method.
- iii. Serial dilution method.
- iv. Agar diffusion method.

Following Techniques are used as agar diffusion method:

- Agar Cup method.
- Agar Disc method.
- Paper Disc method.

In present research work, agar disc diffusion method³⁵ was used to find out the activity of all L1 to L6 synthesized compounds against the microbes.

III.RESULTS AND DISCUSSION

All synthesized compounds show remarkable activity against gram positive, gram negative bacterium. Out of these six compounds L1, L5, L2 found to be highly active. So, these synthesized drugs can be used as best alternative for the treatment of diseases caused by all above four bacterium. Activities of L1, L5, L2 are good they can be best alternative drugs. L1, L5, L2 show excellent result value, as -CH₃, NO₂ groups present. L3, L4 and L6 are found to be moderately active due to presence of -Cl, -Br group present³⁷. The nitro group is more electron withdrawing than chloro group, so that the compounds having such groups in structure have more inhibiting nature against bacteria.

Only after the pharmaceutical, biochemical and medicinal significance these drugs used as alternative drugs, if these drugs do not have toxic and other side effects. It is seen that L1, L5, L2 highly active against all microbes, and other compounds are moderately active, no one is inactive. It has been observed that presence of nitro group increases the activity is also related with that all these compounds belong to flavonoid family, which always show excellent result against the bacteria. So, above synthesized flavones can act as good alternative to drugs.

Inhibition zone value in mm against *bacteria*

Sample Code	<i>Staphylococcus aureus</i> - ATCC-33591 (Gram Positive)			
	AB	SP	ABSP	CL
SLS-1	15	18	19	00
SLS-2	16	14	16	00
SLS-3	14	00	14	00
SLS-4	16	00	16	00
SLS-5	15	10	17	00
SLS-6	16	13	19	00

CONCLUSION

Staphylococcus aureus(*S. aureus*)- *S. aureus* is a gram positive coccal bacterium, found in the nose, respiratory tract or on the skin. *S. aureus* causes a range of illness from minor skin infections such as pimples to pneumonia, meningitis and toxic shock syndrome. The present results show good medicinal effect against it.

IV. REFERENCES

Hamdi N., : *Medicinal Chemistry*
Fischmeister C., *Research* (19), 2010, 1-
Valegra P. 6.

Kamal A., Prabhakar : *European J. of*
S., Ramaiah M J, *Medicinal chemistry*
Reddy P V (46), 2011, 3820-3831.

Sharma A., Anand N, : *J. of enzyme*
Sharma R, Tripathi R. *Inhibition and*
P. *medicinal chemistry*
27(2), 2012, 211-222.

Bano S., Javed K., : *European J. of*
Ahmad S. *medicinal chemistry*
(65), 2013, 51-59.

Bhuiyan M M H, : *Chemistry J.* 1(1),
Hossain M I, 2011, 21-28.
Mahmud Mohd. Al.

Niti G. G., Rajput R., : *Int. J. of pharma. Bio.*
Banewar V. W., Raut 3(3), 2012, 389-395.
A. R.

D. Santos, P. Freire : *Int. of food research J.*
23(3), 2016, 1268-
1273.

M. Stompor, B. : *Molecules* 21, 2016, 1-
Zarowska 10.

Silva W. A. , Andrade : *J. Braz., chem., soc.,*
C. K. (1), 2013, 133-
144.

Evaluation of Proximate Composition in Leaves Extract of Catharanthus Roseus Plant From Gondwadi Area of Dharni in Maharashtra State

Pavan Raut, Vishala Patil, Maya Soham, Monali Shahakar

Department of Chemistry Smt. Radhabaisarada Arts, Commerce and Science College, Anjangaonsurji, Amravati, Maharashtra, India

ARTICLE INFO

Article History:

Accepted : 01 Jan 2025

Published : 10 Jan 2025

Publication Issue :

Volume 12, Issue 7

January-February-2025

Page Number :

242-245

ABSTRACT

Catharanthus Roseus have created its own important in the flavours and fragrances as well in perfumery filed. In Indian as well as all countries throughout the world. Catharanthus Roseus contain very important and useful ingredient which are useful for the growth and development of human being and metabolic activities. Up till now from Gondwadi of Dharni district is region were investigated and in proximate analysis solubility in hot water, total ash value, and presence of moisture and ash content. Cold water, 1% NaOH (aq.), 1% HCl(aq.), and 1% CH₃COOH (aq.) were found quantitatively. This study heather to unknown.

Keywords: Catharanthus Roseus, leaves, proximate analysis

I. INTRODUCTION

Proximate analysis of any part of plants is essential in herbal drug or natural product chemistry. Generally, it is observed from literature survey that each part of plant or plants contain several useful neutral acidic and basic organic components along with various hydrocarbon, minerals, vitamins and trace elements. Some of the ingredients in *Catharanthus Roseus* acidic, basic and neutral and some may be hydrocarbon hence it become essential to chemist to carry out proximate analysis of *Catharanthus Roseus*^[1-5].

In proximate analysis it became essential to determine moisture content, ash content, cold water solubility, hot water solubility^[6], 1 % aqueous NaOH, HCl^[7] and CH₃COOH solubilities respectively^[8]. Moisture content provides us information about total amount of water present in the part of plant or plant which essential for preserving and stability of those ingredient so it is essential to determine before starting the other work. Second is ash contain which provides the information regarding useful and non-useful ingredients while watersolubilities are essential to determine the water soluble acidic, basic, neutral content in the plant sample^[9]. This information provides us the techniques for separation, isolation and identification of soluble content in

the plant sample ^[10]. 1 % aqueous NaOH solubility provides us the % of acidic and some neutral components present in the plant sample and hence for isolation and separation of acidic and phenolic components of plant sample. 1 % aqueous NaOH solubility became essential, 1 % aqueous HCl and CH₃COOH essential for isolation and separation of basic components of plant samples hence proximate analysis of *Catharanthus Roseus* become essential hence proximate analysis of *Catharanthus Roseus* from Dharni region of Amravati district was carried out^[11-13].

II. MATERIALS AND METHODOLOGY

All chemicals used throughout the research work were of A.R. grade. Freshly prepared solutions were used during the research work. The solvents were purified by known literature methods ^[14].

Sample Preparation

On Sept 1-4, 2023, the plants were hand-picked from Mr. Ravi Jawarkar farmhouse in Dharni, Amravati, Maharashtra State, India. To get rid of dirt and dust from the plants, they were first cleaned with tap water and then twice-distilled water. After being cut off the root and dried. To create a fine powder, dried root was crushed in a mortar and pestle. Known literature methods are employed to use this fine powder in proximate studies ^[15-17].

Proximate Analysis

The investigation of physicochemical parameters such as moisture content, total ash value, acid-insoluble ash value, and solubility of the sample was carried out by the known literature methods [18-20]. Solubility of the sample was checked in cold water, hot water and 1% NaOH(aq), HCl(aq), CH₃COOH (aq) solution. Percentage of moisture and ash contents and acid insoluble ash are determined by using following formula,

Moisture Content = Weight of sample taken – Weight of sample after treatment,

$$\% \text{ of moisture} = \frac{\text{Loss of weight of sample}}{\text{Weight of sample taken}} \times 100$$

while, Percentage of solubility is determined by using following formula,

$$\% \text{ of Solubility} = (\text{loss of weight of sample})/(\text{weight of sample taken}) \times 100$$

The results obtained are given in **Table No-1**

Table No-1

Sr. No	Proximate Parameters	Loss of weight of sample	Amount of sample taken (in grams)	%
1	Moisture content	0.884	1	89.3
2	Total ash content	0.079	1	7.69
3	Acid insoluble ash value	0.38	1	38.00
4	Coldwater solubility	0.49	1	47.49
5	Hot water solubility	0.27	1	34.00
6	NaOH(aq) solubility	0.39	1	36.00
7	HCl(aq) solubility	0.36	1	39.00
8	CH ₃ COOH(aq) solubility	0.118	1	19.2

III.RESULT AND DISCUSSION

The moisture content in any part of plant gives evidence for an activity of water-soluble enzymes and coenzymes essential for the metabolic activities of that plant and it is detected from Table No.-1 that, total moisture content in leaves of was found to be 89.3% which is good for metabolic activities in the plant growth and progress of the plant. It was found that the total ash content found from dry stem pieces is 7.69 % and acid insoluble ash value is 34 % which are good and these proximate parameters of plant organs are useful for the determination of the mineral contents. Coldwater solubility and hot water solubility were found to be 47.49 % and 24% respectively; these proximate parameters will give information regarding water soluble neutral, acidic, basic and hydrocarbons present in the samples in herbal chemistry. HCl solubility and CH₃COOH solubility were found to be 39.00% and 19.2% respectively, these proximate parameters gave information regarding basic organic components present in the sample and NaOH solubility was found to be 36.00% which gave information regarding acidic organic components present in the sample.

IV.CONCLUSION

The leaves of *Catharanthus Roseus* from Dharni in the District Amravati of Maharashtra showed good proximate parameters according to the good results of the proximate analysis. Additionally, *Catharanthus Roseus* leaves Dharni in the District Amravati of Maharashtra have natural physicochemical, physiological, and anatomical activities that make them useful for medicinal purposes.

V. REFERENCES

- [1]. Bhatt, T. K., &Sriramchandra A. Bioactive foods in promoting health (pp. 426-439). Academic Press. (2021).
- [2]. Mange, N., Farkade, A., Gade, M., & Belsare, M. Journal of Food Agriculture and Environment, 4(2/3), 246. (2022).
- [3]. Shaikh. R.S, Ph. D. Thesis, Amravati University, Amravati. (2006).
- [4]. Patidar H., Sâtish, M. &Warthe, M. Diversity, 14(1), 7. (2021).
- [5]. Patil, D., Patil, A., Vadera, K., & Ansari, A. Journal of Chemical and Pharmaceutical Research, 7(3), 163-170. (2015).
- [6]. Tayade.D.T, Shaikh R. S, Patil S. U. J. of Indian Chem Soc., 83, 1-3 (2006).
- [7]. Anitha, R., & Priyadharshini, R. Int J. Pharm. Pharm. Sci, 4(5), 99-102. (2012).
- [8]. Vigh, S., Cziaky, Z., Sinka, L. T., Pribac, C., Moş, L. I. A. N. A., Turcuş, V.,& Mathe, E. Studia Univ. Babes-Bolyai Chem, 62, 145-166. (2017).
- [9]. Han, Y., Nishibe, S., Noguchi, Y., & Jin, Z. Phytochemistry, 58(4), 577-580. (2001).
- [10]. Akhlaghi, N., &Najafpour-Darzi, G. Biocatalysis and Agricultural Biotechnology, 32, 101961. (2021).
- [11]. Mahmood, N. M., & Yahya, K. I. International Journal of Sciences: Basic and Applied Research, 36(3), 203-213. (2017).
- [12]. Singh, N., Yadav, S. S., Kumar, S., & Narashiman, B. Food Bioscience, 46, 101546. (2022).
- [13]. Basu, T. K., &Srichamroen, A. Bioactive foods in promoting health (pp. 425-435). Academic Press. (2010).
- [14]. Bakhtiar, Z., Hasandokht, M. R., Naghavi, M. R., &Mirjalili, M. H. Journal of Medicinal Plants, 21(82), 1-12. (2022).

- [15]. Singh, U., Chamoli, M., Singh, K. P., Ram, L., Jangir, S., & Maheshwari, R. K. International Journal of Environment and Health Sciences, 4, 19-27. (2022).
- [16]. Lohvina, H., Sándor, M., & Wink, M. Diversity, 14(1), 7. (2021).
- [17]. Marzougui, N., Ferchichi, A., Guasmi, F., & Beji, M. Journal of Food Agriculture and Environment, 5(3/4), 248. (2007).
- [18]. Ruwali, P., Pandey, N., Jindal, K., & Singh, R. V. South African Journal of Botany, 151, 423-431. (2022).
- [19]. Raji-Idowu, F, Nigerian Journal of Microbiology. (2023).
- [20]. Malghani, N., Mahesar, S., Baig, J., Talpur, F., Sherazi, S. T. H., & Junaid, M. Journal of the Turkish Chemical Society Section A: Chemistry, 9(4), 985-998. (2022).

Awareness of Micronutrient Level in the Water and Soil for Integrated Farming in Rural Area: A Case Study of Varakute-Mhaswad Tal-Man Dist-Satara (Maharashtra)

Mr. Chavan Mahendra Sadashiv, Mr. Kalel Kailaspati Pandurang, Mr. Salunkhe Popat Bhanudas

Department of Chemistry, Shrimant Bhaiyyasaheb Rajemane Mahavidyalaya, Mhaswad Tal.: Man, Dist.: Satara,
Pin.: 415509, Maharashtra, India

ARTICLE INFO

Article History:

Accepted : 01 Jan 2025

Published : 10 Jan 2025

Publication Issue :

Volume 12, Issue 7

January-February-2025

Page Number :

246-251

ABSTRACT

The farmers really find extreme difficulties to understand the suitability of soil and water for the particular profitable production, to know the judicious application of properties and quantity of fertilizers, manures, soil and water management accept to be adopted to maintain the sustainable soil health. In this context soil and water testing are a scientific tool which monitors the status of soil health. The basic objectives of soil and water testing is to give farmers a service leading to better and more economic use of fertilizer and soil and water management practices for increasing the profitable higher crop production, improving fertilizers use efficiency and how to reduces environmental pollution and maintain the soil health.

The present investigation attempt presents the result of study of 10 soil and water sample from the farms and dug well in order to find of magnitude the health problem in the Manganga river area. The water quality parameters such as pH, TDS, TH, Ca, Mg, Cl, Sc., Pc, and NOs, and conductivity is carried out the findings revealed that contains is majority of sampling sights were below the WHO and ISI permissible limits for drinking water. Beside the sulphates in some of the samples were high. The CL, Pos. NO, are found to be within the permissible limits.

In addition to above large quantity of chemical fertilizer, pesticides and insecticides are used to enhance crop yield, on leaching enter the surface and ground water system, causing deterioration. In many areas over use of irrigation water and excessive use of chemical fertilizers besides monoculture types of cropping pattern starting adversely affecting the water as well as soil quality. Therefore, it is essential to know the chemical characterization of soil and water where the irrigation is to be adopted on

permanent basis.

Keywords- pH, electrical conductivity, solid absorption ratio, Residual Sodium Carbonate.

I. INTRODUCTION

In the 21st Century, the mankind will be facing in greatest challenge of providing the basic necessities like food, water and shelter. In order to cope up with the growing requirement of food by the ever-increasing population, the agricultural production needs to be stepped up substantially. The most feasible alternative is to increase the area under irrigated agriculture.¹

The side effect of this is unprincipled use of natural resources. As a result, our land resources are under immense pressure from unscientific and poorly managed irrigated. sector.² This is because the country shares only 2% of the world's geographical area but supports around 18% of the world's population and over 15% of the world's livestock. The resultant overstraining of land resources and disproportionate human and animal population is at the root of widespread land degradation that provides evidence of non-sustainability of agricultural ecosystem Current estimates show that about 67% of the land resources suffer from water logging and salinity problems.³⁻⁵ It was also reported that due to soil deterioration, massive tracts of irrigated croplands are going out of production at nearly the same rate as the amount of new irrigated lands added.⁶

In addition to the above, large quantities of chemical fertilizers, pesticides and insecticides used to enhance crop yields, on leaching enter the surface and groundwater systems causing deterioration.⁷⁻⁹ In many areas, overuse of irrigation water and excessive use of these chemical fertilizers besides monoculture type of cropping pattern have started adversely affecting the water as well as soil quality.¹⁰⁻¹² Therefore, it is essential to know the chemical characteristics of soil and water where irrigation is to be adopted on a permanent basis.

- 1) To give the farmer a service leading a better and more economic fertilizer.
- 2) Soil and water management practices for increasing the profitable higher crop production.
- 3) To improve fertilizers, use efficiency.
- 4) To reduce the environmental pollution and maintain the soil health.

II. MATERIALS AND METHODOLOGY

Soil Sampling Procedure

- 1) Surface litter is to be removed from the sampling spot before sampling.
- 2) Samples may be collected using a soil probe or auger. If not available, a spade/khurpi may be used to make a V' Shaped cut.
- 3) For field crops the minimum depth of soil sampling is 15-20 cm whereas for plantation crops the depth are 0-25 and 25-50 cm
- 4) Thick slices of soil from top to bottom of exposed cuts is removed and placed in a clean container or clean plastic bucket.

- 5) Collects samples from 10-15 well distributed spots in area before sowing when the field is neither manured nor fertilized at least for past 3 months.
- 6) Avoid sampling near trees, compost pits, bunds, marshy spots, recently fertilized area etc.
- 7) Prepare a bulk sample by all collected samples thoroughly and remove any foreign materials like stubbles, roots, plant residues, stones etc., while mixing the sample.
- 8) Reduce the bulk sample to desired quantity of one Kg by quartering procedure. Quartering is done by dividing the thoroughly mixed samples into 4 equal parts. Then, discard the 2 opposite quarters and repeat it till the desired sample size (500gm) is obtained. The sample must be kept in polythene bag.
- 9) Sample must be labeled clearly and correctly.

Precaution while Soil sampling and preparation

- 1) Soil sample should not be collected from recently fertilized area, bunds, low lying corners, spot near trees, fence, channels, compost pits etc.
- 2) Sample should be drawn between rows in line shown cropping area.
- 3) Sampling will be done separately for areas represented by different crops, problem spot etc.
- 4) Once the soil is collected, the bulk soil is mixed thoroughly and desired quantity of soil sample is obtained by quartering method.
- 5) Soil sample should not be placed in fertilizer bag and in porous cloths.
- 6) Weight sample should be dry in shade before sending them to the laboratory.

About 10 samples of soil collected from different locations to assess the quality of a soil. The quality monitoring was carried out for the period of six months. The pH and electrical conductivity were measured in the field. The samples were carried out in the laboratory for the analysis of pH, EC, organic carbon percentage, available nitrogen, phosphorus, potassium, CaCO₃, Calcium, Magnesium, Ferrous, Zinc, Manganese, Copper and the correlation for different parameters were carried out.

Sampling of water

About 10 samples of wells and tube wells are selected to assess the quality of the water for drinking and irrigation purpose. The quality monitoring was carried out for period of six months. The pH and electrical conductivity measured in the field. The samples were filtered and carried out to the laboratory for the analysis of total hardness, total alkalinity, Ca, Mg, Na, Cl, K, SO₄, HCO₃. The assessment of suitability of water for irrigation purpose is carried out with the help of indices like sodium absorption ratio (SAR), residual sodium carbonate (RSC) by converting the result of PPM.

Study Area

Area of study is at Varkute Mhaswad situated on the bank of river Manganga 74.39 Longitude 17.52 latitude. The soil samples are collected from different locations of a farm in Varkute Mhaswad village. The water samples are collected from the open wells and tube wells from the different locations of Varkute Mhaswad.

Soil Analysis Report – Chemical Properties

Sr. No	Sample	pH	Ec(m mhos/cm)	Organic Carbon (%)	Available Nitrogen(Kg/ha)	Available Phosphorus (Kg/ha)	Available Potassium(Kg/ha)	Ca Ca3(%)	Calcium(pp m)	Mg(pp m)	Ferrous(pp m)	Zinc(pp m)	Mn(pp m)	Cu(pp m)
1	S1	9.12	0.49	0.42	212.11	24.11	789.68	18.47	4434.08	4019.50	0.55	0.95	5.71	0.27
2	S2	8.58	0.50	0.41	227.52	19.98	1348.35	17.50	5902.23	2367.27	4.93	0.5	7.31	0.74
3	S3	8.41	0.42	0.76	205.74	36.67	746.00	13.75	5809.86	3977.63	2.43	0.25	9.24	0.27
4	S4	8.35	0.63	0.47	212.06	19.50	982.80	15.38	4897.58	1909.41	1.47	7.58	7.59	2.15
5	S5	8.28	0.59	0.89	248.34	29.44	880.48	14.50	5599.58	2523.62	3.48	3.8	15.82	0.19
6	S6	8.57	0.27	1.48	235.20	32.54	958.64	9.13	4982.87	3221.34	3.47	0.40	9.07	1.50
7	S7	8.10	0.56	3.30	263.84	35.86	968.86	5.89	4881.05	2192.37	12.39	2.60	8.65	3.88
8	S8	8.00	0.25	2.43	270.93	21.67	630.78	10.38	4797.37	4497.02	9.82	1.56	19.71	3.75
9	S9	8.14	1.05	1.39	276.39	27.55	697.04	12.25	5257.06	4365.70	9.99	5.58	23.84	1.78
10	S10	8.20	0.33	0.92	285.11	22.87	762.32	7.63	5732.34	1938.15	11.40	6.69	20.38	4.21

Water Analysis Report

Sr. No	Sample	pH	Ec(m mhos/cm)	Calcium(meq/lit)	Magnesium (meq/lit)	Sodium(meq /lit)	Potassium(meq/lit)	HCO3(meq /lit)	Chlorides(meq/ lit)	Sulphate(mg/lit)	SAR	RS C
1	W1	7.60	0.46	1.59	6.80	6.90	0.45	8.40	6.60	3.39	0.90	-
2	W2	7.37	0.50	4.40	13.40	6.80	0.19	6.40	14.05	4.18	2.41	1.36
3	W3	7.45	0.58	3.60	7.00	6.40	0.10	7.20	9.40	2.53	1.29	0.68
4	W4	7.67	0.59	2.40	9.60	3.78	0.07	8.00	10.20	5.03	0.74	-
5	W5	7.80	0.73	1.80	5.80	6.20	0.45	5.40	7.80	3.45	2.22	-
6	W6	7.77	0.65	1.90	10.60	3.60	0.20	6.80	10.60	7.05	1.34	0.23
7	W7	7.83	0.59	2.20	9.20	6.95	0.75	8.00	13.80	5.15	1.29	-
8	W8	7.78	0.89	3.90	12.00	5.70	0.15	8.40	11.00	6.33	1.24	-
		7.5										0.7

S r. N o	Sample	p H	Ec(m mho s/cm)	Calci um(m eq/it)	Magn esium (meq/ lit)	Sodiu m(meq /lit)	Potassiu m(meq/l it)	HCO 3(meq /lit)	Chlorid es(meq/ lit)	Sulpha te(mg/l it)	SAR	RS C
9	W9	6	0.95	4.90	6.40	6.82	0.09	10.40	13.20	6.02	0.94	0
10	W10	7.48	0.93	1.60	4.90	6.40	0.13	9.20	9.20	2.97	2.57	4.20

III.RESULT FOR WATER

- The result analysis of water quality shows that the ground water constituents are highly variable in respective cationic and anionic constituents.
- The level of Mg, Ca and Na ranged between 4.90 to 13.40, 1.59 to 4.90, 3.60 to 6.95 respectively.
- The ionic constituent like Cl and SO₄ ranges between 6.60 to 14.05 and 2.53 to 7.05
- Sodium absorption ratio is ranges between 0.74 to 2.57 and residual sodium carbonate ranges between 0.23 to 4.20 respectively.
- pH is varies between the rang 7.37 to 7.83
- Ec is varies between the rang 0.58 to 0.95.

IV.RESULT FOR SOIL

- The result analysis of soil quality shows that
- The level of Ca, Mg, Fe, Zn, Mn and Cu ranges between 4434.05 to 5902.23, 1938.18 to 4497.02, 0.55 to 12.39, 0.25 to 7.58, 5.71 to 23.84 and 0.19 to 4.21 respectively.
- Ec is varies between the range 0.27 to 1.05.
- pH is varies between the range 8.00 to 9.12
- The level of Carbon, Nitrogen, Phosphorous and potassium varies between the range 0.41 to 3.30, 205.74 to 285.11, 19.18 to 35.86 and 630.78 to 1348.30.

V. CONCLUSION

From the above observation it is found that most of the water samples were well with in the desirable limits prescribed by ICMR and ISI it is recommended that water should be treated before the distribution and chemically checked at the regular interval to quality. From the above observation it is found that most of the soil samples were well within the desirable limit. The quality of the soil goes on decreasing due to the tremendous use of chemical fertilizers. It is recommended, That the fertility of soil can be increased by decreasing the use of chemical fertilizer and increasing the use of bio-fertilizers such as vermin-compost, cow dung.

VI.SUGGESTION

1. Use the drip irrigation system instead of open irrigation pattern.
2. Use more bio-fertilizer instead of chemical fertilizer.
3. Avoid the one cropping pattern.
4. Use alternate cropping pattern and take dicot cropping system to increase fertility of soil.
5. Use of Intercrop pattern.

VII.REFERENCES

- [1]. Karthikeyan L., Chawla I., & Mishra A. Journal of Hydrology 2020, 586, 1–22.
- [2]. Islam N., Rashid M., Pasandideh F., Ray B., Moore S., & Kadel R. Sustainability 2021, 13(1821), 1–20.
- [3]. Meroni M., Waldner F., Seguini L., Kerdiles H., & Rembold F. Agricultural and Forest Meteorology 2021, 308–309, 1–13.
- [4]. Rasmussen J., Azim S., & Nielsen J. European Journal of Agronomy 2021, 130, 1–8.
- [5]. Bohra A., Chand Jha U., Godwin I., & Kumar Varshney R. Plant Biotechnology Journal 2020, 1–18.
- [6]. Soylu S., & C , arman, K. Fuzzy Journal of Terramechanics 2021, 95, 25–32.
- [7]. Popp J, Kova 'cs S, Ola 'h J, Dive 'ki Z, Bala 'zs E. New Biotechnology. 2021 Jan 25; 60:76–84.
- [8]. Pazouki E. Agricultural Water Management 2021, 256, 1–18.
- [9]. Gal T., Nagy L., David L., Vasa L. & Balogh P. Acta Polytechnica Hungarica 2013, 10 (8), 231–244.
- [10]. Zhang J., Liu J., Chen Y., Feng X., & Sun Z. Review with CiteSpace. Sustainability 2021, 13, 1–15.
- [11]. Ebitu L., Avery H., Mourad K., & Enyetu J. Land Use Policy 2021, 103, 1–13.
- [12]. Shamshiri R., Weltzien C., Hameed I., Yule I., Grift T., Balasundram S., International Journal of Agricultural and Biological Engineering 2018, 11(4), 1–14.

Developments in Synthesis of Nanomaterials of Tungsten and Molybdenum Disulfides for Supercapacitive Applications - A Review

Mr. N. A. Barwat^{*1,2}, Prof. G. N. Chaudhary²

^{*1} Bajaj College of Science, Wardha, Maharashtra, India

²Shri Shivaji Science College, Amravati, Maharashtra, India

ARTICLE INFO

Article History:

Accepted : 01 Jan 2025

Published : 10 Jan 2025

Publication Issue :

Volume 12, Issue 7

January-February-2025

Page Number :

252-258

ABSTRACT

Recently, two-dimensional transition metal sulfides, particularly tungsten disulfide (WS₂) and molybdenum disulfide (MoS₂) raised extensive interest due to its extraordinary physicochemical properties. With the merits of low costs and prominent properties such as high anisotropy and distinct crystal structure, they are proving to be the potential alternative of next-generation environmentally benign energy storage and conversion devices. In this review, we begin with the fundamental studies of the supercapacitors, their types and materials used for their fabrications followed by the discussion on their structures, synthetic approaches and supercapacitive applications.

Keywords: Research Paper, Technical Writing, Science, Engineering and Technology

I. INTRODUCTION

In today's world of fast grooming technology, efficient energy storage devices are of prime concern. Currently the most trusted alternatives for energy storage are batteries, supercapacitors, fuel cells. To meet the escalating demand of energy for fast improving technological devices is a real challenge [1]. World's dire need of energy can be fulfilled by supercapacitors which promise faster charging times and do not rely upon toxic and rare elements such as lead, lithium etc. On comparison with battery, electrochemical supercapacitors have high power density, long cycle life and safe operation. Hence, development of high efficiency supercapacitors has attracted the attention of researchers and industries around the World [2]. Based on the energy storage mechanism, the material based supercapacitors are generally classified into three types viz; electric double layer capacitors (EDLCs), pseudocapacitors and their combination being called as the hybrid supercapacitor [3]. Though many studies targeting development of new electrode materials were carried on, there is a fundamental limit to ultimate specific energies of EDLCs owing to their dependence on double layer capacitance as the

primary energy storage mechanism [4, 5]. It is now evident that the performance of supercapacitors based on pure carbon cannot be enhanced further [6]. On the other hand, fast and reversible electron exchange at or near the electrode surface is the source of pseudocapacitance. This is why the pseudocapacitors show higher specific capacitance and energy density resulting in higher storage capacity. But their cycle life is usually less compared to EDLCs [5, 7]. A variety of pseudocapacitive materials have been studied such as Transition Metal Oxides like TiO₂ etc, Perovskite Oxides, Two-Dimensional Transition Metal Carbides/ Nitrides/ Carbonitrides (MXenes), Transition Metal Dichalcogenides, Carbon-Based Materials and Metal – Organic Frameworks transition metal sulphide and electronically conducting polymers. However, most of these suffer from a limited cycling stability that leads to the decay of their electrochemical performance [8]. The third type i.e. hybrid capacitors involve the combination of pseudocapacitive electrode used as energy source with the EDLC used as power source in the same cell. In hybrid capacitors, high energy density is provided by the battery-like pseudocapacitive electrode while the EDLC electrode gives rise to high power capability. Based on materials used for the electrodes, the hybrid supercapacitors are further classified as symmetric and asymmetric. Asymmetric hybrid supercapacitors with conducting polymer electrodes have been greatly commercialized [9].

Table I TYPES OF SUPERCAPACITORS

Type	Mechanism	Energy Storage	Common Materials
EDLCs	Chemical transfer	Non-Faradaic	Carbon based
Pseudo capacitors	Quick Chemical Transfer	Faradaic	Metal Based/Conducting polymers
Hybrid	Physical Transfer	Faradaic + Non-Faradaic	Both Carbon and Conducting polymers

Hybrid supercapacitors show higher capacitance and greater energy density than that of EDLCs. However, these hybrid devices suffer from the limited cycle stability of the faradaic electrodes. Many different combinations of positive and negative electrodes have been studied in different aqueous or organic electrolytes. To achieve high power and high energy density along with longer cycle life for hybrid capacitors there is need of novel electrode material systems with rational design of material combination, morphology, and size, and proper choice of electrolytes that operate at high voltages with excellent ionic conductivity and electrochemical stability [9, 10]. There has been an increasing use of 2D layered inorganic materials, known as transition metal dichalcogenides (TMDs) in supercapacitor technology. TMDs are composed of one atom of transition metal (M) and two atoms of chalcogens (X: S, Se, or Te) in an X–M–X fashion with a chemical configuration of MX₂. Some two-dimensional (2D) TMDs studied for their application as supercapacitor electrodes are molybdenum disulphide (MoS₂), molybdenum diselenide (MoSe₂), tungsten disulphide (WS₂), tungsten diselenide (WSe₂), tungsten ditelluride (WTe₂), tantalum disulphide (TaS₂), tantalum diselenide (TaSe₂), titanium disulphide (TiS₂), niobium disulphide (NbS₂), zirconium disulphide (ZrS₂), vanadium disulphide (VS₂), vanadium diselenide (VSe₂), etc. Being semiconducting, the sulphides and selenides cannot be the ideal materials for electrodes in the supercapacitors. Hence, to improve the conductivity these materials were blended with certain carbon materials and conducting polymers to make nanocomposites [11, 12]. But there are still challenges with respect to interfacial adhesions and electronic mobilities, binders and use of appropriate electrolyte for the complete hybrid system [13].

To the best of our knowledge, there has been no review undertaken on the utilization of MoS₂ and WS₂ in together in the context of supercapacitor applications. Hence, we are conducting a combined review of both

MoS₂ and WS₂ for supercapacitive applications. This review primarily centres on recent findings related to the electrochemical characteristics of MoS₂ and WS₂.

A) STRUCTURES OF WS₂

WS₂, a naturally occurring metal sulfide, has the hexagonal crystal structure with space group $P6_3/mmc$ which possesses 2D covalently bonded *S-W-S* layers separated by a van der Waals gap. It has a theoretical specific capacity of 433 mA.h.g⁻¹ based on 4 mol of lithium insertion/extraction for LIB application, and a few attempts have been made to investigate the lithium storage activities of WS₂ nanoelectrodes [14]. Several nanostructured WS₂ based anodes such as nanoflakes (by a rheological phase reaction), ordered mesoporous rodlike particles (by the SBA15 template method), graphene like morphology (by solid state reaction), nanosheets (by exfoliation), and few-layer WS₂/graphene composites, were reported [15, 16, 17]. The structures of WS₂ can be divided into three different types, i.e. 1T (octahedral), 2H (trigonal prismatic) and 3R (rhombohedral) [18]. Among these 1T and 2H phases are common monolayered crystal structures, which exhibit one atomic layer of W atoms sandwiched between two atomic layers of S atoms [19]. For 3R phase WS₂, it exhibits a non-centrosymmetric structure, where the 2nd and 3rd atomic layers have the same orientation but shift in plane [20]. Structural phase transitions in WS₂ monolayers can be realized by various strategies such as electrochemical intercalation with Li⁺ and nonpolar organic solvents assisted heat treatment [21, 22]. Owing to a large interlayer spacing (0.618 nm), the layer structure of WS₂ allows the accommodation of other ions or even molecules between S-W-S layers [23, 24].

B) STRUCTURES OF MoS₂

MoS₂ is a layered metal sulfide, in which the Mo-S atoms are covalently bonded and the adjacent layers are connected via van der Waals interactions. By applying some alterations in the synthesis procedure, different allotropies and morphology can be achieved such as 3D (flowers, snowflakes, and dandelion), 2D (nanosheets, nanostripes, and nanoribbons), 1D (nanowires and nanorods) and 0D (nanoplatelets). Thermodynamically stable and naturally occurring MoS₂ is 2H with 3% of 3R. 2H MoS₂ is most stable configuration of MoS₂ having a lattice parameters $a = 3.15 \text{ \AA}$ and $c = 12.30 \text{ \AA}$. It exhibits a Bravais lattice structure of hexagonal. It behaves like an n-type semiconductor. It is polytypic which can be identified as naturally existing 2H-MoS₂ and 3R-MoS₂, as well as synthetic 1T-MoS₂. The 3R structure belongs to $R\bar{3}m$ space group ($a = b = 3.16 \text{ \AA}$ and $c = 18.37 \text{ \AA}$) and the space group of metastable 1T-MoS₂ is $P1$ ($a = b = 3.36 \text{ \AA}$, $c = 6.29 \text{ \AA}$) [25].

II. SYNTHETIC APPROACHES

One-dimensional tungsten disulfide (WS₂) was synthesized by a simple hydrothermal method for electrochemical energy applications, such as hydrogen evolution reaction (HER) and oxygen evolution reaction (OER) catalysts and flexible supercapacitors [26]. The fabrication of tungsten disulfide (WS₂) nanostructures with different morphologies including rod-like, sheet-like and Fiber-like ones have been reported via a simple yet facile hydrothermal process by adding surfactants cetyltrimethylammonium bromide (CTAB) and polyethylene glycol (PEG) [27, 28]. A one-step electrochemical synthesis of luminescent WS₂ quantum dots (QDs) was reported. This was achieved by a synergistic effect of perchlorate intercalation in non-aqueous electrolyte and the applied electric field. The average size of the WS₂ QDs is $3 \pm 1 \text{ nm}$ ($N=102$) with few layers. The QDs show a higher photoluminescence (PL) quantum efficiency (5 %) and exhibit an excitation wavelength-dependent photoluminescence [29].

There could be two synthetic approaches for 2D WS₂.

- i) Top-down Approach - In this approach bulk WS₂ is employed as raw material and exfoliation of nanosheets is carried out by various methodologies such as mechanical, liquid and chemical or electrochemical intercalation exfoliation [30, 31, 32].
- ii) Bottom-up Approach – These include the chemical vapour deposition, atomic layer deposition, hydrothermal and solvothermal approaches. [33, 34, 35, 36, 37].

All these methods are summarized in the following table –

Table II SYNTHETIC APPROACHES FOR WS₂ [33, 34, 35, 36, 37]

Methods and Conditions	Layers	Pros and cons
Mechanical exfoliation at Room Temperature	Uncontrollable	Pros High crystallinity and quality Cons Low yield, not suitable for mass production
Liquid-phase exfoliation at Room Temperature	Uncontrollable	Pros easy operation, suitable for mass production Cons Low degree of exfoliation
Li ⁺ intercalation at 80 °C	Controllable	Pros High crystallinity, high degree of exfoliation Cons High cost, residual impure Li
CVD or Physical vapor deposition (PVD) at 500 –800 °C	Controllable	Pros High crystallinity, large area continuous film Cons Restricted by the substrates
Hydrothermal/solvothermal method at 100 –300 °C	Uncontrollable	Pros low energy consumption, controlled reaction condition and morphology Cons Excessive influencing factors

Similarly, the synthetic methods for MoS₂ also follow either top-down approach or bottom-up approach. The top-down approach involves mechanical exfoliation method [38], exfoliation in liquid phase [39, 40] and sputtering techniques [41]. The bottom-up approach involves physical vapour deposition [42], solution chemical processes such as solvothermal [43], hydrothermal [44-45] methods and chemical vapour deposition [46].

III.SUPERCAPACITIVE APPLICATIONS

Tungsten disulfide (WS₂) has been emerging as an attractive electrode material for supercapacitors because of its intrinsically layered structure and high capacitance. Electrochemical results reveal the WS₂ nanosheets with enhanced crystallinity could deliver an excellent durability with more than 82% capacitance retention after 10 000 cycles and an aerial capacitance of 0.93 Fcm⁻² at 4 mAcm⁻². Importantly, when using the WS₂ nanosheets as a negative electrode, a flexible and stable ASC device with an extraordinary volumetric energy density of 0.97 mWh cm⁻³ is obtained [47]. The flexible binder-free sodium-ion (NIBs) electrodes have exceptional electrochemical properties, with tungsten disulfide on carbon nanofiber achieving a remarkable specific capacity of 300 mA h/g and an initial Coulombic efficiency of 80% at 300 cycles [48]. An excellent high Young's modulus of 171 GPa was reported for individual WS₂ nano tubes, rendering WS₂ great potential for the development of flexible thin-film supercapacitors [47, 49].

MoS₂ also has a potential to be used as supercapacitors applications [50]. In this regards Wang et al. prepared hollow nanospheres of MoS₂ through a facile hydrothermal method by exploring MnCO₃ nanospheres in the

form of templates. MoS₂ electrode has been explored as a supercapacitor and 1 M KCl solution of electrolyte at 0.59 A g⁻¹ produces the supercapacitance of 142 F g⁻¹. After 1000 cycles it maintains its 92.9% of its initial capacitance [51]. Gao et al. synthesized nanosheets of MoS₂ through a hydrothermal process with the help of SiO₂ in the form of templates. 2 M KOH solution of electrolyte at 1 A g⁻¹ produces the supercapacitance of 683 F g⁻¹ and after 10,000 cycles it maintains its 85.1% of its starting capacitance [52].

IV. CONCLUSION

This review illustrates the structure, various synthesis techniques and supercapacitive applications of WS₂ and MoS₂. We illustrate the various previous studies applied for the fabrication of WS₂ and MoS₂ nonmaterial and explored for potential applications in supercapacitors. The extensive applications of WS₂ and MoS₂ material arise from its different physical, chemical properties, low coefficient of friction, appreciable mechanical strength, high specific surface area, adjustable band gap, light adsorption characteristics in the visible range and promising electrical transport properties. However, MoS₂ has numerous applications but the production of uniform and single-layer WS₂ and MoS₂ nanomaterials and nanocomposites at a large scale for industrial applications is still a significant challenge.

V. REFERENCES

- [1]. Iqbal, Sajid, et al. "Recent development of carbon based materials for energy storage devices." *Materials Science for Energy Technologies* 2.3 (2019): 417-428.
- [2]. Kötzt, Rüdiger, and M. J. E. A. Carlen. "Principles and applications of electrochemical capacitors." *Electrochimica acta* 45.15-16 (2000): 2483-2498.
- [3]. Sharma, Kriti, Anmol Arora, and Surya Kant Tripathi. "Review of supercapacitors: Materials and devices." *Journal of Energy Storage* 21 (2019): 801-825.
- [4]. Liu, Jilei, et al. "Advanced energy storage devices: basic principles, analytical methods, and rational materials design." *Advanced science* 5.1 (2018): 1700322.
- [5]. Yu, Guihua, et al. "Hybrid nanostructured materials for high-performance electrochemical capacitors." *Nano Energy* 2.2 (2013): 213-234.
- [6]. Fernandez, J. A., et al. "EDLC performance of carbide-derived carbons in aprotic and acidic electrolytes." *Electrochimica Acta* 53.24 (2008): 7111-7116.
- [7]. Liu, Long, Huaping Zhao, and Yong Lei. "Review on nanoarchitected current collectors for pseudocapacitors." *Small Methods* 3.8 (2019): 1800341.
- [8]. Fleischmann, Simon, et al. "Pseudocapacitance: from fundamental understanding to high power energy storage materials." *Chemical Reviews* 120.14 (2020): 6738-6782.
- [9]. Muzaffar, Aqib, et al. "A review on recent advances in hybrid supercapacitors: Design, fabrication and applications." *Renewable and sustainable energy reviews* 101 (2019): 123-145.
- [10]. Afif, Ahmed, et al. "Advanced materials and technologies for hybrid supercapacitors for energy storage—A review." *Journal of Energy Storage* 25 (2019): 100852.
- [11]. Panda, Pritam Kumar, et al. "Progress in supercapacitors: roles of two dimensional nanotubular materials." *Nanoscale Advances* 2.1 (2020): 70-108.
- [12]. Theerthagiri, Jayaraman, et al. "Recent advances in metal chalcogenides (MX; X= S, Se) nanostructures for electrochemical supercapacitor applications: a brief review." *Nanomaterials* 8.4 (2018): 256.

- [13]. Barik, Rasmita, and Pravin P. Ingole. "Challenges and prospects of metal sulfide materials for supercapacitors." *Current Opinion in Electrochemistry* 21 (2020): 327-334.
- [14]. Wang, G. X., et al. "Tungsten disulfide nanotubes for lithium storage." *Electrochemical and solid-state letters* 7.10 (2004): A321.
- [15]. Feng, Chuanqi, et al. "Synthesis of tungsten disulfide (WS₂) nanoflakes for lithium ion battery application." *Electrochemistry communications* 9.1 (2007): 119-122.
- [16]. Liu, Hao, et al. "An ordered mesoporous WS₂ anode material with superior electrochemical performance for lithium-ion batteries." *Journal of Materials Chemistry* 22.34 (2012): 17437-17440.
- [17]. Shiva, Konda, et al. "Employing synergistic interactions between few-layer WS₂ and reduced graphene oxide to improve lithium storage, cyclability and rate capability of Li-ion batteries." *Nano Energy* 2.5 (2013): 787-793.
- [18]. Wang, Qing Hua, et al. "Electronics and optoelectronics of two-dimensional transition metal dichalcogenides." *Nature nanotechnology* 7.11 (2012): 699-712.
- [19]. Lukowski, Mark A., et al. "Highly active hydrogen evolution catalysis from metallic WS₂ nanosheets." *Energy & Environmental Science* 7.8 (2014): 2608-2613.
- [20]. Toh, Rou Jun, et al. "3R phase of MoS₂ and WS₂ outperforms the corresponding 2H phase for hydrogen evolution." *Chemical Communications* 53.21 (2017): 3054-3057.
- [21]. Ambrosi, Adriano, Zdeněk Sofer, and Martin Pumera. "2H → 1T phase transition and hydrogen evolution activity of MoS₂, MoSe₂, WS₂ and WSe₂ strongly depends on the MX₂ composition." *Chemical Communications* 51.40 (2015): 8450-8453.
- [22]. Chou, Stanley S., et al. "Controlling the metal to semiconductor transition of MoS₂ and WS₂ in solution." *Journal of the American Chemical Society* 137.5 (2015): 1742-1745.
- [23]. Jia, Pan, et al. "Highly Efficient Ionic Photocurrent Generation through WS₂-Based 2D Nanofluidic Channels." *Small* 15.50 (2019): 1905355.
- [24]. Elías, Ana Laura, et al. "Controlled synthesis and transfer of large-area WS₂ sheets: from single layer to few layers." *ACS nano* 7.6 (2013): 5235-5242.
- [25]. Benavente, E., et al. "Intercalation chemistry of molybdenum disulfide." *Coordination chemistry reviews* 224.1-2 (2002): 87-109.
- [26]. Pandey, Keshab, and Hae Kyung Jeong. "Synthesis of tungsten disulfide for electrochemical energy applications." *Materials Science and Engineering: B* 295 (2023): 116601.
- [27]. Cao, Shixiu, et al. "Hydrothermal synthesis of variety low dimensional WS₂ nanostructures." *Materials Letters* 129 (2014): 205-208.
- [28]. Cao, Shixiu, et al. "Hydrothermal synthesis and controlled growth of tungsten disulphide nanostructures from one-dimension to three-dimensions." *Micro & Nano Letters* 10.3 (2015): 183-186.
- [29]. Valappil, Manila O., et al. "A Single-Step Electrochemical Synthesis of Luminescent WS₂ Quantum Dots." *Chemistry—A European Journal* 23.38 (2017): 9144-9148.
- [30]. Biccai, Sonia, et al. "Exfoliation of 2D materials by high shear mixing." *2D Materials* 6.1 (2018): 015008.
- [31]. Huang, Feng, JiKang Jian, and Rong Wu. "Few-layer thick WS₂ nanosheets produced by intercalation/exfoliation route." *Journal of Materials Science* 51 (2016): 10160-10165.
- [32]. Martinez-Merino, Paloma, et al. "Novel WS₂-based nanofluids for concentrating solar power: performance characterization and molecular-level insights." *ACS applied materials & interfaces* 12.5 (2020): 5793-5804.

- [33]. Sharma, Poonam, et al. "Large-scale surfactant-free synthesis of WS₂ nanosheets: an investigation into the detailed reaction chemistry of colloidal precipitation and their application as an anode material for lithium-ion and sodium-ion batteries." *New Journal of Chemistry* 44.4 (2020): 1594-1608.
- [34]. Zhang, Yu, et al. "Recent progress in CVD growth of 2D transition metal dichalcogenides and related heterostructures." *Advanced materials* 31.41 (2019): 1901694.
- [35]. Dong, Lianqing, et al. "Facile access to shape-controlled growth of WS₂ monolayer via environment-friendly method." *2D Materials* 6.1 (2018): 015007.
- [36]. Gurarslan, Alper, et al. "Surface-energy-assisted perfect transfer of centimeter-scale monolayer and few-layer MoS₂ films onto arbitrary substrates." *ACS nano* 8.11 (2014): 11522-11528.
- [37]. Sim, Dong Min, et al. "Controlled doping of vacancy-containing few-layer MoS₂ via highly stable thiol-based molecular chemisorption." *ACS nano* 9.12 (2015): 12115-12123.
- [38]. Radisavljevic, Branimir, Michael B. Whitwick, and Andras Kis. "Small-signal amplifier based on single-layer MoS₂." *Applied Physics Letters* 101.4 (2012).
- [39]. Liu, Na, et al. "Large-area atomically thin MoS₂ nanosheets prepared using electrochemical exfoliation." *ACS nano* 8.7 (2014): 6902-6910.
- [40]. Liu, Lihui, et al. "A mechanism for highly efficient electrochemical bubbling delamination of CVD-grown graphene from metal substrates." *Advanced Materials Interfaces* 3.8 (2016): 1500492.
- [41]. Fleischauer, Paul D., and Reinhold Bauer. "Chemical and structural effects on the lubrication properties of sputtered MoS₂ films." *Tribology Transactions* 31.2 (1988): 239-250.
- [42]. Vishwanath, Suresh, et al. "Comprehensive structural and optical characterization of MBE grown MoSe₂ on graphite, CaF₂ and graphene." *2D Materials* 2.2 (2015): 024007.
- [43]. Feng, X., et al. "Novel mixed-solvothermal synthesis of MoS₂ nanosheets with controllable morphologies." *Crystal Research and Technology* 48.6 (2013): 363-368.
- [44]. Zhou, Xiaoping, et al. "Hydrothermal synthesis of flower-like MoS₂ nanospheres for electrochemical supercapacitors." *Journal of nanoscience and nanotechnology* 14.9 (2014): 7250-7254.
- [45]. Song, Haishen, et al. "Hydrothermal synthesis and electrochemical properties of MoS₂/C nanocomposite." *International Journal of Electrochemical Science* 13.7 (2018): 6708-6716.
- [46]. Yu, Yifei, et al. "Controlled scalable synthesis of uniform, high-quality monolayer and few-layer MoS₂ films." *Scientific reports* 3.1 (2013): 1866.
- [47]. Liu, Si, et al. "Binder-free WS₂ nanosheets with enhanced crystallinity as a stable negative electrode for flexible asymmetric supercapacitors." *Journal of Materials Chemistry A* 5.40 (2017): 21460-21466.
- [48]. Iqbal, Nousheen, et al. "Structure Engineering of WS₂@ Carbon Nanofibers for CO₂ Capture, Supercapacitors, and Na-Ion Storage." *ACS Applied Nano Materials* (2024).
- [49]. Kaplan-Ashiri, Ifat, et al. "Mechanical behavior of individual WS₂ nanotubes." *Journal of Materials Research* 19 (2004): 454-459.
- [50]. Theerthagiri, Jayaraman, et al. "Recent progress and emerging challenges of transition metal sulfides based composite electrodes for electrochemical supercapacitive energy storage." *Ceramics international* 46.10 (2020): 14317-14345.
- [51]. Wang, Fangping, et al. "Hydrothermal synthesis of flower-like molybdenum disulfide microspheres and their application in electrochemical supercapacitors." *RSC advances* 8.68 (2018): 38945-38954.
- [52]. Gao, Yong-Ping, et al. "MoS₂ nanosheets assembling three-dimensional nanospheres for enhanced-performance supercapacitor." *Journal of alloys and compounds* 741 (2018): 174-181.

Polymer Composites Doped With Rare-Earth Elements: A Review of Luminescent, Electrical, and Optical Properties

Ms. Riya R. Tekade¹, Dr. Shilpa G. Vidhale², Ms. Chitrlekha A. Kolhe¹

¹Ph.D. Research Scholar, Department of Physics, Adarsh Science, J. B. Arts and Birla Commerce College, Dhamangaon Railway, Amravati, Maharashtra, India

²Assistant Professor, Department of Physics, Adarsh Science, J. B. Arts and Birla Commerce College, Dhamangaon Railway, Amravati, Maharashtra, India

ARTICLE INFO

Article History:

Accepted : 01 Jan 2025

Published : 10 Jan 2025

Publication Issue :

Volume 12, Issue 7

January-February-2025

Page Number :

259-264

ABSTRACT

The enhancement of optical, electrical, and luminescent properties of polymer-based materials has garnered significant interest for advanced applications in optoelectronics, sensors, and photonics. Recent studies have highlighted the potential of novel polymer composites doped with rare-earth elements and nanoparticles. Europium (Eu^{3+}) and terbium (Tb^{3+}) complexes incorporated into polystyrene (PS) films via spin-coating demonstrated enhanced luminescence, photostability, and temperature sensitivity, making them ideal for luminescent temperature sensors. Porous polystyrene-methyl methacrylate (PS-MMA) microspheres doped with Eu complexes improved fluorescence and sensitivity for lateral flow immunoassays. Electrical conductivity studies on ethyl cellulose (EC)/PMMA blends revealed frequency- and temperature-dependent behaviors, expanding their utility in electronic applications. Optical property analysis of PMMA using the Drude-Lorentz model provided insights into permittivity and energy loss functions. Hybrid polymer nanocomposites, including PVA/CMC with LaDyAlO_3 , PVC/PVP with MoO_3 , SrTiO_3 , and Er_2O_3 , showed significant improvements in thermal stability, refractive indices, and nonlinear optical properties. These advancements support applications in optical limiters, LEDs, and space technologies. Furthermore, polyfluorene (PFO) thin films with conductive layers achieved higher photoluminescence intensity, underscoring their suitability for PLEDs. These findings collectively emphasize the transformative role of material modifications and nanotechnology in enhancing polymer-based systems for diverse scientific and industrial applications.

Keywords: Polymer composites, Rare-earth doped polymers, Photoluminescence, Polystyrene (PS), Poly(methyl methacrylate) (PMMA)

I. INTRODUCTION

Thin film polymers are ultrathin layers of polymeric materials, typically ranging in thickness from a few nanometers to a few micrometers. These films are engineered to leverage the unique properties of polymers such as flexibility, lightweight, chemical resistance, and process ability while offering the precision and functionality required for advanced technological applications. The small thickness of these films often imparts additional mechanical, optical, and electrical properties that are distinct from their bulk counterparts. Thin film polymers have become indispensable in numerous fields, including electronics, optics, energy, biomedical applications, and protective coatings. Their versatility stems from the ability to tailor their composition, thickness, and structure to meet specific requirements. The growing demand for lightweight, high-performance materials has propelled research and development in thin film polymers. Recent advancements in fabrication techniques and material design have led to the creation of films with exceptional mechanical strength, thermal stability, and responsive behaviors. Polystyrene (PS) is a widely used synthetic thermoplastic polymer, produced through the polymerization of styrene, a monomer derived from petroleum. Its affordability, ease of processing, and versatile properties make it one of the most common polymers in industrial and commercial applications. Poly (methyl methacrylate) (PMMA) is a transparent thermoplastic polymer derived from the polymerization of methyl methacrylate. It is often marketed as "acrylic" or "plexiglass" and serves as a lightweight and shatter-resistant alternative to glass.

1.1 Polymer Blending

This is a widely used technique to create new materials with enhanced or tailored properties by physically combining two or more polymers. Unlike chemical copolymerization, blending relies on physical mixing, allowing the individual polymers to retain their intrinsic properties while potentially generating synergistic effects. This approach offers a cost-effective and versatile method to develop materials for diverse applications. The blending of polymers can result in materials with improved mechanical strength, thermal stability, optical clarity, electrical properties, or chemical resistance. These enhanced attributes arise from the complementary characteristics of the constituent polymers. For example, blending a rigid polymer with a flexible one can yield a material with balanced toughness and flexibility. In the field of advanced materials, polymer blending is pivotal for tailoring properties in applications such as packaging, electronics, automotive components, and biomedical devices. Current research focuses on incorporating nanofillers, dopants, or functional additives into polymer blends to further enhance their performance.

1.2 Polymer Doping

This is a process of introducing specific additives, known as dopants, into a polymer matrix to modify or enhance its physical, chemical, optical, or electrical properties. This technique is widely utilized in the

development of functional materials for various advanced applications, including electronics, optics, energy storage, and biomedical fields. Doping transforms the inherent properties of a polymer by either altering its structure or introducing new functionalities. For instance, doping an insulating polymer with conductive materials can impart electrical conductivity, making it suitable for applications in sensors, transistors, and light-emitting devices.

1.3 Types of Polymer Doping

Chemical Doping: Involves chemical reactions to incorporate dopants into the polymer backbone.

Physical Doping: The dopant is physically dispersed in the polymer matrix without chemical bonding.

Ion Doping: Introduction of ionic species into a polymer to alter conductivity or ionic exchange properties.

Rare-Earth Doping: Incorporation of rare-earth ions (e.g., Europium, Cerium) to enhance optical or luminescent properties.

II. LITERATURE REVIEW

Knyazev et al. [1] synthesized Eu(III) and Tb(III) tris(β -diketonates) complexes with Lewis bases and incorporated them into polystyrene films via spin-coating. These photostable films exhibited enhanced luminescence, intermolecular energy transfer, and temperature sensitivity up to 6.00 $\mu\text{s/K}$ in the range of 298–383 K, surpassing known lanthanide-based thermal sensors. Their tunable luminescence colors make them promising for in situ temperature measurements. **Yuan et al. [2]** demonstrated that methyl methacrylate-modified polystyrene microspheres enhance fluorescence and morphology of Eu-complexes by forming porous structures for uniform doping and molecule confinement. These microspheres showed improved fluorescence performance and were successfully applied in lateral flow immunoassays (LFIA) for fentanyl detection with exceptional sensitivity down to 0.10 ng/mL. This approach holds promise for rapid point-of-care and clinical applications. **Sirtawar et al. [3]** studied the AC and DC electrical conductivity of Ethyl Cellulose (EC), Poly Methyl Methacrylate (PMMA), and their tetrahydrofuran-doped blends. AC conductivity increased with frequency, while DC conductivity rose with temperature (323–373 K), highlighting charge carrier behavior and mobility. XRD analysis supported these findings, contributing to understanding conduction mechanisms in these insulating materials. **Strugariu et al. [4]** developed an original method for obtaining the infrared (IR) spectra of poly(methyl methacrylate) (PMMA) by fitting experimental reflection-absorption spectra to theoretical spectra based on the Drude–Lorentz model of permittivity. This approach enabled the determination of key optical properties such as complex electric modulus, absorption coefficient, and optical constants. Their findings contribute to the understanding of PMMA-based composites and copolymers. **Johnson et al. [5]** prepared PVA/CMC polymeric blends doped with LaDyAlO₃ nanoparticles and investigated their structural, optical, and spectroscopic properties. The study revealed that the concentration of LaDyAlO₃ influenced the bandgap, thermal stability, and optical limiting properties, with PVA/CMC/LaDyAlO₃ (5 wt%) exhibiting excellent optical limiting behavior. Additionally, the transition from reverse saturable absorption to saturable absorption in PVA/CMC/LaDyAlO₃ (8 wt%) makes it suitable for applications in optical switches and photonic devices.

Alshammari et al. [6] developed and characterized MoO₃ nanoparticle-modified PVC/PVP polymer films, investigating the effects of MoO₃ dispersion on the structural and optoelectronic properties. Their findings showed that increasing MoO₃ content up to 0.6 wt% improved the nonlinear optical response, tunable dispersion energy, refractive index, and oscillator strength. This work highlights the importance of tuning

MoO₃ content for fabricating reliable composite materials for optoelectronic applications. **Sabah et al.** [7] investigated the photoluminescence (PL) intensity of poly(9,9-di-n-octylfluorenyl-2,7-diyl) (PFO) thin films with different fabrication methods: PFO alone (P1), PFO blended with brilliant blue FCF (P2), and PFO on a polyaniline conductive layer (P3). The study found that surface roughness and chemical composition influenced PL intensity, with P3 exhibiting the highest PL intensity due to increased absorption and structural modifications. Their findings highlight the enhancement of PFO films for polymer light-emitting diodes (PLED) through blending and conductive layers. **Ismail et al.** [8] explored the effects of bio-phenolic on the physical, thermal, and dynamic mechanical properties of epoxy resin blends. The study found that increasing bio-phenolic content improved density, water absorption, storage modulus, and thermal stability, with P-25 showing the highest density and improved performance. FTIR analysis indicated a reaction between bio-phenolic and epoxy, enhancing the overall properties of the polymer blends. **Alshammari et al.** [9] studied the thermal decomposition and optical properties of PVC/PVP/SrTiO₃ polymer blend nanocomposites, revealing strong interactions between the polymer blend and SrTiO₃. The addition of SrTiO₃ improved the blend's thermal stability, optical absorption, energy gap, and nonlinear refractive index, with fluorescence observed at 485 nm. These findings position the nanocomposites as promising materials for optoelectronic applications. **Alshammari et al.** [10] developed PVC/PVP polymer blend hybrid nanocomposites modified with Er₂O₃ nanoparticles, examining their structural and optical properties. The study revealed that Er₂O₃ concentrations enhanced the dispersion energy, nonlinear refractive index, and optical band gap, with significant improvements at 0.1 wt% Er₂O₃. These results suggest that the nanocomposites are promising for optoelectronic space applications.

III.CONCISE SUMMARY OF LITERATURE REVIEW

Authors	Research Focus	Technique Used	Key Findings
Knyazev et al. [1]	Luminescent properties of Eu ³⁺ and Tb ³⁺ complexes in PS films.	Spin-coating, photostability testing, luminescence sensitivity analysis.	Enhanced luminescence and photostability; maximum thermal sensitivity of 6.00 μs/K.
Yuan et al. [2]	Fluorescence enhancement in porous PS-MMA microspheres doped with Eu.	SEM for morphology, fluorescence spectroscopy, lateral flow immunoassays.	Improved fluorescence due to porous structure; fentanyl detection sensitivity at 0.10 ng/mL.
Sirtawar et al. [3]	Electrical conductivity of EC/PMMA blends doped with THF.	AC/DC conductivity measurements, XRD analysis.	Conductivity increased with frequency (AC) and temperature (DC); structural changes supported by XRD findings.
Strugariu et al. [4]	Optical properties of PMMA using Drude–Lorentz model.	Infrared reflection–absorption spectroscopy, iterative least squares	Derived PMMA's permittivity, modulus, energy loss, and other optical properties using dispersion

Authors	Research Focus	Technique Used	Key Findings
		fitting.	modeling.
Johnson et al. [5]	Optical and thermal properties of PVA/CMC doped with LaDyAlO ₃ .	FTIR, XRD, UV–Visible spectroscopy, thermal stability tests.	Tunable optical properties, excellent optical limiting thresholds, and improved absorption for photonic and optoelectronic devices.
Alshammari et al. [6]	Optical characteristics of PVC/PVP with MoO ₃ nanoparticles.	XRD, FTIR, optical spectroscopy, nonlinear optical response analysis.	Enhanced nonlinear optical properties, refractive indices, and energy gaps for optoelectronic applications.
Sabah et al. [7]	Photoluminescence in PFO thin films for PLEDs.	FESEM for morphology, UV–Visible spectroscopy, PL intensity measurement.	Improved photoluminescence with structural modifications; highest PL intensity in PFO films with conductive layers.
Ismail et al. [8]	Thermal and mechanical properties of bio- phenolic epoxy blends.	FTIR, DMA, TGA, DSC.	Enhanced thermal stability, glass transition temperature, and modulus with bio- phenolic addition.
Alshammari et al. [9]	Optical and thermal properties of PVC/PVP blends with SrTiO ₃ .	XRD, FTIR, Raman spectroscopy, TGA, optical spectroscopy.	Improved fluorescence (485 nm), thermal stability, and nonlinear optical properties for optical sensing applications.
Alshammari et al. [10]	Optical characteristics of PVC/PVP blends with Er ₂ O ₃ nanoparticles.	XRD, FTIR, Raman spectroscopy, SEM, optical absorption measurements.	Enhanced refractive indices and energy gaps with Er ₂ O ₃ doping; suitable for electro-optic modulators and space technologies.

IV. CONCLUSIONS

The reviewed studies highlight advancements in polymer-based materials with enhanced optical, electrical, and thermal properties for diverse applications. Eu(III)/Tb(III) composite films and porous PSMMA-Eu microspheres exhibit high photostability and fluorescence for temperature sensing and sensitive detection. EC/PMMA blends show improved conductivity, while innovative methods reveal detailed optical characteristics of PMMA. Nanoparticle-doped polymers, including PVA/CMC with LaDyAlO₃ and PVC/PVP blends with MoO₃, SrTiO₃, and Er₂O₃, demonstrate tunable nonlinear optical responses and thermal stability for optoelectronic devices. Additionally, PFO blends improve photoluminescence for efficient LEDs, and epoxy-bio-phenolic composites enhance thermal and mechanical properties, making these materials promising for advanced technological applications.

Credit authorship contribution statement: Ms. Riya R. Tekade¹ & Ms. Chitralekha A. Kolhe³: Collected, analyzed data, and drafted the review paper. Dr. Shilpa G. Vidhale²: Contributed to data interpretation and Supervision.

Declaration of competing interest: The authors declare that they have no known competing financial interests or personal relationships that could have appeared to influence the work reported in this paper.

V. REFERENCES

- [1]. Knyazev A. A., Ziyatdinova R. M., Krupin A. S., & Galyametdinov Y. G. (2024). Thermosensitive chameleon films based on polystyrene doped with complexes of europium (III) and terbium (III). *Journal of Alloys and Compounds*, 996, 174793.
- [2]. Yuan Y., Wang Y., Awasthi P., Dong W., Chen D., Qiao X., & Fan X. (2024). Methyl methacrylate-modified polystyrene microspheres: an effective strategy to enhance the fluorescence of Eu-complexes. *Physical Chemistry Chemical Physics*.
- [3]. Sirtawar K., Lamdhade G., Raulkar K., Alqaed S., Mustafa J., & Husain S. (2024). Investigation of AC and DC Electrical Conductivity in Ethyl Cellulose (EC) and PolyMethyl Methacrylate (PMMA) Polyblends. *Science of Advanced Materials*, 16(5), 635-641.
- [4]. Strugariu M. L., Șerban S. G., Berdie A. M., & Jitian S. (2024). Infrared spectra of the main optical properties of poly (methyl methacrylate) thin films. *Polymer Bulletin*, 1-15.
- [5]. Johnson V., & Gandhiraj V. (2024). Effect of rare earth doped perovskite on the structural, linear/nonlinear optical properties of the fabricated PVA/CMC polymeric blends for optical limiting applications. *Optical Materials*, 148, 114824.
- [6]. Alshammari A. H., Alshammari M., Ibrahim M., Alshammari K., & Taha T. A. M. (2024). Processing polymer film nanocomposites of polyvinyl chloride– Polyvinylpyrrolidone and MoO₃ for optoelectronic applications. *Optics & Laser Technology*, 168, 109833.
- [7]. Sabah F. A., Razak I. A., Kabaa E. A., Rahim N. A. A., Chavan G. T., & Jeon C. W. (2024). Influence of blending and conductive layer on the photoluminescence intensity of PFO thin films implemented for polymer light-emitting applications. *Polymer Bulletin*, 81(6), 5613-5626.
- [8]. Ismail A. S., Jawaaid M., Hamid N. H., Yahaya R., Hassan A., & Sarmin S. N. (2023). Physical, structural and thermal properties of bio-phenolic/epoxy polymers blends. *Materials Today Communications*, 34, 105455.
- [9]. Alshammari A. H., Alshammari M., Alshammari K., Allam N. K., & Taha T. A. (2023). PVC/PVP/SrTiO₃ polymer blend nanocomposites as potential materials for optoelectronic applications. *Results in Physics*, 44, 106173.
- [10]. Alshammari A. H., Alshammari M., Ibrahim M., Alshammari K., & Taha T. A. M. (2023). New hybrid PVC/PVP polymer blend modified with Er₂O₃ nanoparticles for optoelectronic applications. *Polymers*, 15(3), 684.
- [11]. Tekade R. R. & Vidhale S. G. (2023). Advancement in Polymer Blends and Composites: A Comprehensive Review of Structural, Optical, Thermal and Electrical Attributes for Multifaceted Applications. *Journal of Propulsion Technology*, 44(04), 7190-7201.

Bio-Inspired Synthesis and Characterisation of Sulphur Nanoparticles Synthesized By Using (Azadiracta Indica) Neem Leaves Extract

N. S. Dixit¹, S.G. Khobragade², M. S. Dixit³, A.S. Dixit⁴, Pratiksha Ardak⁴

¹Department of Chemistry, G. S. Tompe Arts, Science and Commerce College, Chandur Bazar (444704), Maharashtra, India

²Department of Chemistry, Brijlal Biyani Science College, Amravati-444605, Maharashtra, India

³Jagadamba Mahavidyalaya, Achalpur (444806), Maharashtra, India

⁴Dr rajendra Gode Institute of Science and Technology, Amravati, Maharashtra, India

ARTICLE INFO

Article History:

Accepted : 01 Jan 2025

Published : 10 Jan 2025

Publication Issue :

Volume 12, Issue 7

January-February-2025

Page Number :

265-269

ABSTRACT

This study investigates the eco-friendly synthesis of sulfur nanoparticles using biowaste orange peel extract. By employing natural extracts, the research aligns with sustainable practices. The synthesis conditions were optimized, and the nanoparticles were characterized using X-ray Diffraction (XRD), Fourier Transform Infrared Spectroscopy (FTIR). These techniques provided detailed insights into the crystalline structure, morphology, elemental composition, and surface properties of the nanoparticles. The research highlights the significance of green synthesis methods and suggests potential applications of SNPs in nanomedicine as a potential antimicrobial agent, emphasizing sustainable approaches in nanomaterial synthesis using herbal methods.

I. INTRODUCTION

Nanotechnology has significantly transformed various scientific and industrial fields, with sulfur nanoparticles (SNPs) emerging as key materials due to their unique properties and applications in catalysis, energy storage, and biomedicine. However, traditional synthesis methods are often resource-intensive and environmentally harmful. In response, green synthesis approaches using natural resources and agricultural byproducts, such as *Azadirachta indica* (Neem) leaves, have gained attention for their eco-friendliness and cost-effectiveness.

This study investigates the green synthesis of sulfur nanoparticles using Neem leaf extract, aligning with sustainable practices and green chemistry principles. The focus is on analyzing the structural properties, morphology, and crystalline nature of the synthesized nanoparticles to enhance their potential applications. By

advancing eco-friendly synthesis techniques, this research contributes to the broader understanding of sulfur nanoparticles and their versatile industrial and biomedical uses.

Sulfur, as a non-metal, plays a critical role in various industries, including fertilizers, sulfuric acid production, plastics, pulp and paper, and antimicrobial agents. The ability to synthesize sulfur at the nanoscale opens new opportunities for enhancing its functionality across these sectors, driving innovation and sustainability in materials science and nanotechnology.

II. EXPERIMENTAL SECTION:

The synthesis and characterization of sulphur nanoparticles phytofabricated via green synthesis using *Azadiracta Indica* (Neem) leaves extract involve a series of experimental techniques. The following outlines the key methods employed in this study.

1. Green Synthesis of Sulphur Nanoparticles:

Azadiracta Indica (Neem) leaves are collected from medicinal garden G.S. Tompe Arts, Commerce and Science College of Chandur Bazar and thoroughly washed to remove impurities. The leaves are finely chopped or ground to increase the surface area for efficient extraction. The leaves extract is obtained by heating the crushed leaves material with water and filtering the resulting solution as orange peels extract. Sulphur nanoparticle synthesis is initiated by combining the leaves extract with sodium thiosulphate as sulphur precursor. The reaction mixture is then subjected to heating for 2 hours to facilitate the formation of sulphur nanoparticles by the bioactive compounds present in the neem leaves extract. The synthesis process is closely monitored to ensure the desired nanoparticle formation.

2. Elemental, structural and morphological characterization of Synthesized SNPs:

The synthesized SNP sample is subjected to FTIR spectroscopy to analyze the functional groups and biomolecules involved in the stabilization and capping of the sulphur nanoparticles. Further, X-ray diffraction study of Synthesized SNPs was carried out to determine crystal structure, phase purity, and crystalline size of the nanoparticles.

III. RESULT AND DISCUSSION

1. FTIR spectral Study:

Azadirachta indica, native to India, is a widely cultivated and valuable plant known for its timber, pulp, and essential oils with medicinal and therapeutic properties. Its essential oils have gained interest for their natural products and bioactive components

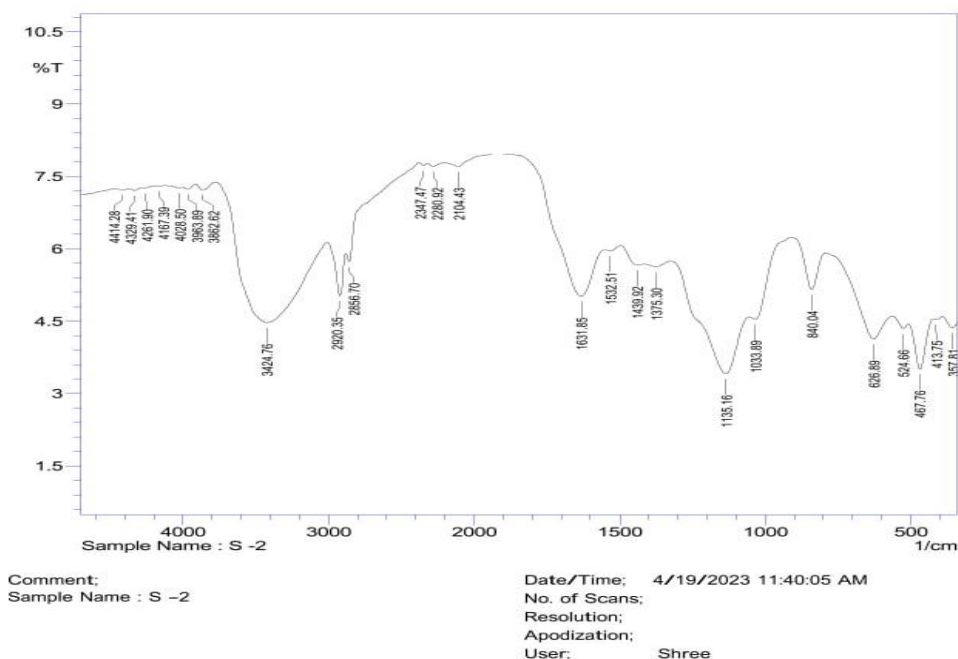


Fig: FTIR spectra of SNPs synthesized by *Azadirachta indica* extract

FTIR analysis of sulphur nanoparticles (SNPs) synthesized using Neem leaf extract shows characteristic bands at 3420.90 cm^{-1} (O-H, N-H), 2925.17 cm^{-1} (C-H stretching), and 1629.92 cm^{-1} (carboxylic groups). Bands at 1532.51 cm^{-1} indicate C=C stretching, while 1443.78 , 1375.30 , and 1125.51 cm^{-1} correspond to C-O, C-N, and C-C stretching. S-S stretching appears between $646.18\text{--}388.67\text{ cm}^{-1}$. The spectra confirm biomolecules from Neem bind to SNPs through C=O, N-H, and O-H linkages, stabilizing and preventing nanoparticle agglomeration.

2. XRD Spectra:

X-ray diffraction (XRD) is a key technique for characterizing nanoparticles, providing insights into crystalline structure, phase nature, lattice parameters, and grain size. The crystalline size is calculated using the Scherrer equation by analyzing the broadening of the most intense peak. Nanoparticles, typically analyzed in powder form, are compared against reference patterns from the International Centre for Diffraction Data (ICDD) to determine composition. In this study, sulphur nanoparticles (SNPs) synthesized using Neem leaf extract show sizes between 1 to 100 nm, indicating successful formation of nano-sized sulphur stabilized by phytochemicals from *Azadirachta indica* leaves.

XRD analysis reveals diffraction peaks at 23.01° , 25.75° , and 28.61° , corresponding to the crystal planes 222, 026, and 313 of S_8 phase sulphur. These peaks align with standard literature values, confirming the formation of crystalline sulphur. The Scherrer equation is used to estimate particle size, where λ represents the x-ray wavelength, B the peak broadening at half maximum, and θ the Bragg diffraction angle. The analysis highlights the effectiveness of plant-based surfactants in producing well-crystallized SNPs, with enhanced properties due to their interaction with Neem-derived biomolecules.

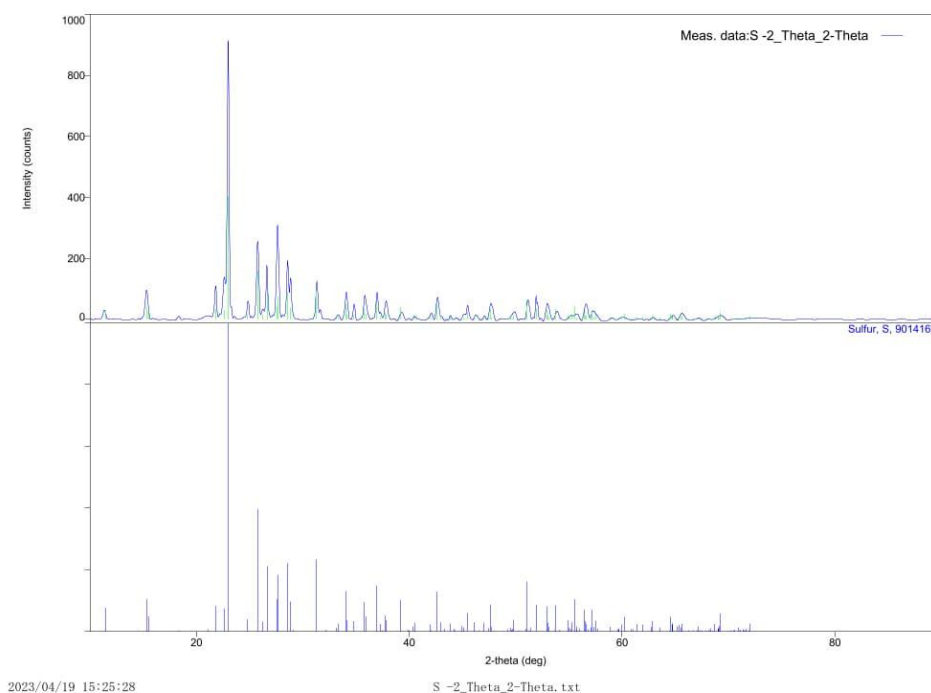


Fig: XRD Spectrum of SNPs synthesized by using *Azadirachta indica* leaves extract

IV. CONCLUSION:

In this study, Sulphur nanoparticles (SNPs) were synthesized using a green method involving sodium thiosulphate and Neem leaf extract. The particle size (1-100 nm) was controlled by adjusting sodium thiosulphate concentration and extract quantity. Characterization by XRD and FT-IR confirmed monoclinic SNPs with an average size of 20 nm. This eco-friendly, cost-effective method avoids toxic chemicals, leveraging Neem biomolecules for reduction and stabilization. The synthesized SNPs hold potential for applications in biomedical, agricultural, and environmental fields.

V. REFERENCES

- [1]. S. K. Ghotekar, S. DevkibaMohansinhji, and T. Pagar, "A Review on Green Synthesis of Sulfur Nanoparticles via Plant Extract, Characterization and its Applications," 2020, doi: 10.33945/SAMI/AJCB.2020.3.5.
- [2]. K. Khairan, Zahraturriaz, and Z. Jalil, "Green synthesis of sulphur nanoparticles using aqueous garlic extract (*Allium sativum*)," *Rasayan Journal of Chemistry*, vol. 12, no. 1, pp. 50–57, Jan. 2019, doi: 10.31788/RJC.2019.1214073.
- [3]. V. J. Kouzegaran and K. Farhadi, "Green synthesis of sulphur nanoparticles assisted by a herbal surfactant in aqueous solutions," *Micro Nano Lett*, vol. 12, no. 5, pp. 329–334, May 2017, doi: 10.1049/mnl.2016.0567.

- [4]. H. Baloch et al., "Synthesis and Characterization of Sulfur Nanoparticles of Citrus limon Extract Embedded in Nanohydrogel Formulation: In Vitro and In Vivo Studies," *Gels*, vol. 9, no. 4, Apr. 2023, doi: 10.3390/gels9040284.
- [5]. M. Suleiman, A. Al Ali, A. Hussein, B. Hammouti, T. B. Hadda, and I. Warad, "Sulfur Nanoparticles: Synthesis, Characterizations and their Applications," *J. Mater. Environ. Sci*, vol. 5, no. 6, pp. 1029–1033, 2013.
- [6]. R. A. Dop, D. R. Neill, and T. Hasell, "Sulfur-Polymer Nanoparticles: Preparation and Antibacterial Activity," *ACS Appl Mater Interfaces*, vol. 15, no. 17, pp. 20822–20832, May 2023, doi: 10.1021/acsami.3c03826.
- [7]. P. Paralikar and M. Rai, "Bio-inspired synthesis of sulphur nanoparticles using leaf extract of four medicinal plants with special reference to their antibacterial activity," *IET Nanobiotechnol*, vol. 12, no. 1, pp. 25–31, Feb. 2018, doi: 10.1049/iet-nbt.2017.0079.
- [8]. N. M. Hashem, A. E. D. M. S. Hosny, A. A. Abdelrahman, and S. Zakeer, "Antimicrobial activities encountered by sulfur nanoparticles combating Staphylococcal species harboring sccmec. A recovered from acne vulgaris," *AIMS Microbiol*, vol. 7, no. 4, pp. 481–498, 2021, doi: 10.3934/microbiol.2021029.
- [9]. S. Najafi, S. M. Razavi, M. Khoshkam, and A. Asadi, "Effects of green synthesis of sulfur nanoparticles from *Cinnamomum zeylanicum* barks on physiological and biochemical factors of Lettuce (*Lactuca sativa*)," *Physiology and Molecular Biology of Plants*, vol. 26, no. 5, pp. 1055–1066, May 2020, doi: 10.1007/s12298-020-00793-3.

Versatile Applications of Polyaniline Polyvinylacetate Blends: A Comprehensive Review

N.D. Kolekar, A.V. Kohale, B.T. Kumbhare

Department of Physics, Shri R. R. Lahoti Science College, Morshi, Maharashtra, India

ARTICLE INFO

Article History:

Accepted : 01 Jan 2025

Published : 10 Jan 2025

Publication Issue :

Volume 12, Issue 7

January-February-2025

Page Number :

270-273

ABSTRACT

The blending of Polyaniline (PANI), a conductive polymer, and Polyvinyl acetate (PVAc), a thermoplastic with excellent mechanical properties, results in a novel class of materials with tunable properties. This comprehensive review examines the synthesis, properties, and applications of PANI/PVAc blends across various domains, including sensors, energy storage, coatings, environmental remediation, and more. The synergy between PANI's electrical conductivity and PVAc's flexibility and mechanical strength has led to promising results in enhancing the performance of devices in these fields. This paper delves into the processing methods, structural characteristics, and future directions for advancing PANI/PVAc blends in diverse technological and industrial applications.

IndexTerms – Polymer Blends, PANI-PVAc Blend

I. INTRODUCTION

Polymers have been central to the development of advanced materials, finding applications in electronics, biomedicine, energy, and environmental sectors. Among the vast array of synthetic polymers, Polyaniline (PANI) and Polyvinyl acetate (PVAc) are gaining attention due to their distinct properties. PANI, a conductive polymer, is particularly valued for its environmental stability and ease of synthesis. PVAc, a thermoplastic polymer, offers good mechanical properties, ease of processing, and flexibility.

When blended, PANI and PVAc create a hybrid material that combines the electrical conductivity of PANI with the strength and processability of PVAc. These blends are highly versatile and have shown significant potential in various applications such as sensors, energy storage devices, coatings, and environmental remediation. This paper reviews the synthesis methods, structural properties, and diverse applications of PANI/PVAc blends, providing a comprehensive overview of the current advancements and future research directions.

II. SYNTHESIS METHODS OF PANI/PVAC BLENDS

The preparation of PANI/PVAc blends can be achieved through several synthesis techniques. Each method has its unique advantages depending on the desired application and properties of the final product.

1. **Solution Blending:** In this method, both PANI and PVAc are dissolved in a common solvent, such as dimethylformamide (DMF) or tetrahydrofuran (THF), followed by mixing. Upon solvent evaporation, a homogeneous blend is obtained. This method is commonly used due to its simplicity and effectiveness in controlling blend ratios.
2. **Melt Blending:** In melt blending, PANI and PVAc are mixed in their molten states, using an extruder or mixer at elevated temperatures. This method allows for large-scale production but requires careful temperature control to prevent degradation of the polymers.
3. **Electrospinning:** Electrospinning is used to produce nanofibers from polymer solutions under the influence of an electric field. PANI/PVAc blends are electrospun to create fibrous mats with high surface area, which are useful for applications in sensors and energy storage devices.

III. STRUCTURAL AND PHYSICAL PROPERTIES OF PANI/PVAC BLENDS

The structural and physical properties of PANI/PVAc blends are influenced by the blend ratio, processing method, and the intrinsic properties of the individual polymers. Key properties include:

1. **Electrical Conductivity:** PANI is inherently conductive, and its electrical properties are retained when blended with PVAc, especially at higher PANI concentrations. The conductivity of the blend can be tuned by varying the amount of PANI and by applying dopants. At low concentrations, PANI/PVAc blends can be insulating, while at higher concentrations, they exhibit semiconducting or conductive behavior.
2. **Thermal Stability:** PVAc improves the thermal stability of the blend, which is particularly beneficial for applications that require durability at elevated temperatures. The thermal degradation temperature of PANI/PVAc blends is higher than that of pure PANI, making them suitable for more demanding applications.
3. **Mechanical Properties:** The blend of PANI with PVAc enhances the mechanical strength and flexibility of the composite material. PVAc provides toughness, while PANI imparts strength. The mechanical properties can be further optimized by adjusting the blend ratio and processing conditions.
4. **Morphology:** Scanning electron microscopy (SEM) analysis of PANI/PVAc blends shows that the morphology of the material can range from homogeneous to phase-separated, depending on the blending process. The uniformity of the blend influences its overall mechanical and electrical properties.

IV. APPLICATIONS OF PANI/PVAC BLENDS

The unique combination of electrical conductivity, mechanical strength, and processability of PANI/PVAc blends makes them suitable for a wide range of applications. The following sections detail some of the most promising applications.

4.1. Sensors and Actuators

Sensors: PANI/PVAc blends have been extensively studied for their use in chemical sensors, humidity sensors, and biosensors. The electrical conductivity of PANI is sensitive to changes in the environment, such as

humidity, temperature, and the presence of gases or chemicals. PVAc's flexibility enhances the mechanical performance of the blend, allowing for the development of flexible and durable sensors.

- **Gas Sensors:** PANI/PVAc blends have been used in gas sensors for detecting gases such as ammonia, carbon dioxide, and nitrogen dioxide. The blend's ability to undergo reversible redox reactions when exposed to gases makes it a suitable material for high-performance gas detection.
- **Humidity Sensors:** The hydrophilic nature of PANI allows it to absorb moisture, affecting its conductivity. PANI/PVAc blends are therefore ideal for use in humidity sensing, where the sensitivity to moisture is critical.

Actuators: PANI/PVAc blends can act as electroactive materials in actuators, where they change shape in response to an applied electric field. This property is particularly useful for creating soft actuators used in robotics and artificial muscles.

4.2. Energy Storage Devices

PANI/PVAc blends are promising materials for energy storage applications such as supercapacitors, batteries, and energy-harvesting devices.

- **Supercapacitors:** PANI is known for its high specific capacitance, and when blended with PVAc, it retains excellent cycling stability. The blend provides high charge-discharge efficiency and durability in supercapacitor devices, making it a candidate for energy storage in portable electronics and electric vehicles.
- **Lithium-Ion Batteries:** The blend can also be used as an electrode material in lithium-ion batteries. The conductivity of PANI enhances the electrochemical performance, while PVAc improves the mechanical strength and stability of the electrodes during cycling.
- **Energy Harvesting:** PANI/PVAc blends have potential in energy harvesting, particularly for converting mechanical vibrations or solar energy into electrical energy. This is beneficial for wearable electronics and portable devices.

4.3. Coating Technologies

PANI/PVAc blends have found applications in coating technologies, particularly for corrosion protection, antistatic coatings, and conductive coatings.

- **Corrosion Protection:** The combination of PANI's conductivity and PVAc's adhesion properties makes the blend effective in metallic corrosion resistance. These coatings are particularly useful for the protection of infrastructure in marine and industrial environments.
- **Conductive Coatings for Electronics:** PANI/PVAc coatings can be applied to printed circuit boards (PCBs) and semiconductors to prevent electrostatic discharge (ESD). The blend's conductivity ensures the protection of delicate electronic components.
- **Protective Coatings for Flexible Electronics:** The mechanical flexibility of PANI/PVAc blends makes them suitable for protective films in flexible electronics such as OLEDs and solar cells. These coatings provide both electrical conductivity and mechanical robustness.

4.4. Environmental Remediation

PANI/PVAc blends are effective in environmental remediation, particularly in the removal of heavy metals and organic pollutants from water and soil.

- **Heavy Metal Adsorption:** The electroactive nature of PANI enables the blend to adsorb heavy metals like lead, cadmium, and chromium from contaminated water. This makes the blend ideal for water purification systems and wastewater treatment.

- **Pollutant Removal:** The PANI component of the blend can also interact with organic pollutants such as dyes, pesticides, and pharmaceuticals. PVAc enhances the mechanical stability and reusability of the blend, which is beneficial for long-term environmental clean-up applications.

V. CHALLENGES AND FUTURE DIRECTIONS

Despite the promising applications, the development of PANI/PVAc blends faces several challenges:

1. **Processing Issues:** The incompatibility between PANI and PVAc in certain solvents can make the blending process difficult. Finding suitable solvents and optimizing the blending process is critical to improving the homogeneity and performance of the materials.
2. **Stability and Durability:** While PVAc enhances the mechanical properties of PANI, the overall stability of the blend can be affected by environmental factors such as moisture and temperature. Ensuring long-term environmental stability and durability of the blends is crucial for their commercialization.
3. **Cost of Raw Materials:** The high cost of PANI production, especially in its doped form, may limit the scalability of these materials for large-scale applications. Research into alternative, lower-cost conductive polymers and more efficient synthesis methods will be essential for reducing the overall cost of PANI/PVAc blends.

Future research should focus on developing new blending techniques, exploring the use of bio-based polymers, and optimizing the properties of PANI/PVAc blends for specific applications.

VI. CONCLUSION

Polyaniline and Polyvinyl acetate blends represent a highly promising material class due to their unique combination of electrical conductivity, mechanical strength, and thermal stability. These properties enable their use in a wide variety of applications, including sensors, actuators, energy storage devices, environmental remediation, and coating technologies. While challenges such as processability and stability remain, ongoing research in this area holds the potential for significant advancements in the use of these blends for industrial and technological applications.

VII. REFERENCES

- [1]. Kumar, S., & Singh, P. (2018). Polymer blends: Recent developments and future trends. *Materials Science and Engineering Review*, 56(4), 324-339.
- [2]. Gupta, V., & Sharma, A. (2020). Polyaniline-based nanocomposites for energy storage applications. *Journal of Applied Polymer Science*, 135(10), 4866-4879.
- [3]. Wang, L., et al. (2019). Conductive polymer blends for environmental sensors. *Sensors and Actuators B: Chemical*, 278, 206-215.
- [4]. Ali, S., & Iqbal, M. (2021). Polyvinyl acetate-based polymer blends for environmental applications. *Polymer Engineering and Science*, 61(6), 1345-1357.

Effect of Zinc Oxide Nanoparticles on the Growth of Mungbean (Vigna Radiata) Seedlings

P. C. Pandit*, Dr. M. M. Kulkarni

Department of Environmental Science, K.T.H.M, College Gangapur Road, Nashik-422002, Maharashtra, India

ARTICLE INFO

Article History:

Accepted : 01 Jan 2025

Published : 10 Jan 2025

Publication Issue :

Volume 12, Issue 7

January-February-2025

Page Number :

274-283

ABSTRACT

Around the world, zinc deficiency is a nutritional issue, particularly in developing nations. Farmers use a variety of chemical fertilisers, which lowers the soil's nutritional value. The soil's micronutrient content is declining, which is detrimental to both human health and the environment. To get around this, research is moving towards nanotechnology, and scientists are becoming interested in using nano fertiliser. This study looked at how the dosage of zinc oxide nanoparticles (ZnO NPs) affected mungbean (*Vigna radiata* L.) growth and seed germination. The purpose of this experiment was to determine how ZnO NPs, which were extracted from banana peel (*Musa acuminata*), affected the chlorophyll content, root, shoot length, and seedling vigour index for *Vigna radiata* species. Four concentrations (2, 4, 6 and 8 mg/mL) of ZnO NPs were examined at the seed germination stage. In comparison to untreated seeds, mungbean seeds treated with ZnO NPs showed a significant increase in germination percentage values. *Vigna radiata* development and germination were positively impacted by green-produced ZnO nanoparticles, suggesting a positive effect on agricultural productivity. Due to the dose-dependent nature of the response to ZnO NPs, additional in vitro and in vivo research is required to establish the optimal dosages for improved human nutrition and agricultural productivity.

Keywords: Nanoparticles, Zinc oxide, Nanofertilizer, *Musa acuminata*, *Vigna radiata*

I. INTRODUCTION

The current global micronutrient deficit is being addressed with a variety of chemical fertilisers that are detrimental to both human health and the environment. To get around this, research is moving towards nanotechnology, and scientists are becoming interested in using nano fertiliser. (Yadav, A, et, al

2024). Worldwide, zinc deficiency is a nutritional issue, particularly in developing nations. It is now known that almost 2 billion people worldwide suffer from a widespread zinc nutritional deficiency (Sorahinobar, M., et. al 2023). For many years, nano ZnO has been used extensively in industry. On the other hand, its possible application in agriculture had not been investigated. Few studies have been conducted on the beneficial effects of zinc, one of the micronutrients found in plants, on plant growth. (Mahajan, P, et al 2011). Although zinc can be found in soil in a variety of forms, including ZnS, ZnO, ZnCO₃, and Zn₃(PO₄)₂·4H₂O, plants can only access it in its divalent form (Zn²⁺). A concentration of < 1 mg Zn/kg indicates a deficiency, 1-2 mg Zn/kg indicates a sufficiency, and 7.5 mg Zn/kg indicates an excess. Consequently, the sufficiency and deficiency indices of the soil could be used to recommend zinc fertiliser. (Thapa, M. et. al 2024). Through a variety of channels, including stomata, root hairs, and leaf surface fissures, plants can absorb nanoparticles. Nanoparticles can travel through bulk flow, phloem loading, and diffusion once they are inside the plant. The transport of nanoparticles is affected by a number of variables, such as particle size, shape, surface characteristics, solution pH, and the presence of other materials. Several application techniques, including leaf spraying, root application, branch injection, and seed treatment, have been used in earlier research to confirm that plants can absorb nanoparticles (Ajmal, M. et, a 2023). ZnO nanoparticles are a biodegradable substance that affects chemical and biological species through photo-oxidizing and photocatalysis. (Kareem, H. et. al). Nanoparticles (NPs) can enhance agriculture, lessen their impact on the environment, and boost yields by delivering nutrients and crop protection in a highly efficient and precisely targeted manner (Singh, A. et. al 2024). Some of the metabolic changes brought on by zinc deficiency may be explained by the fact that zinc is a structural component of enzymes and is involved in particular metabolic pathways. However, changes in synthesis and metabolism could be regarded as secondary effects of zinc deficiency. (Hajiboland, R et, al). Their absorption by the plants has a variety of effects on plant physiology. They could be harmful to plant cells and their organelles, or they could help plants grow. The "green-gram," or mung bean (*Vigna radiata* L.), is a short-term legume belonging to the Fabaceae family that is high in vitamins, proteins, and carbohydrates (Rafiq, H et. al). Globally, mung bean production is steadily declining as a result of overcrowding, salinity, and the uneven application of chemical fertilisers. Therefore, improving the subpar mung bean production is crucial. (Haq, T et al). Numerous methods, including chemical, biological, hydrothermal, precipitation, microwave, sonication, and solvothermal techniques, can be used to synthesise ZnONPs (Hussien. et. al 2023). The environmentally recognised "green chemistry" concept has been used in the biosynthesis of nanoparticles to create clean, eco-friendly, and biocompatible nanoparticles (Albarakaty et. al 2023). The purpose of this study aimed to synthesise zinc oxide nanoparticles, characterise them, and evaluate the effects of different dosages of biogenic ZnO nanoparticles on mung bean (*Vigna radiata*) seed germination and seedling traits.

II. MATERIALS:

Banana peels, Zinc Acetate as a precursor, Deionised water, *Vigna radiata* seeds

III.METHODOLOGY:

Synthesis of zinc oxide nanoparticles using extract of Banana Peels(*Musa acuminata*): ZnO nanoparticles were prepared by biological methods according to (Ramesh, P et. al). The Banana Peels were collected from the local market of Nashik, 1.1 gm of Zinc acetate (0.1 M) was dissolved in 100 ml of double distilled water. It was completely mixed for ten minutes at room temperature while being continuously stirred. Then 2 g of sodium

hydroxide was slowly added in Zinc acetate solution. Then it was titrated with 5 ml of Banana Peels extract under continuous stirring process. The pH value of solution was maintained at 12. After 2 h, the solution was centrifuged at 8000 RPM for 20 min. The mixture was then boiled for 60 min until the aqueous solution changes from watery to light white paste. This paste was then collected in a ceramic crucible and heated in an air-heated furnace at 300 degree Celsius for 60 minutes. A light white coloured powder was obtained and this was carefully collected and packed for characterization. The material was mashed in a mortar pestle to get a finer nature for characterization.

Characterization: The ZnO NPs were first characterized using UV-visible spectroscopy using a spectrophotometer in the 200–700 nm wavelength range. Scanning electron microscopy was used to determine the size and shape of the ZnO NPs. The FTIR spectra were recorded at a resolution of 4000-1000 cm⁻¹ using by Perkin-Elmer Spectrum 1000 spectrum in attenuated total reflection mode.

Seeds: *Vigna radiata* was taken from the local seed shop at Nashik city, India. Healthy seeds were chosen to reduce germination errors. The seeds were surface sterilized with 0.2% HgCl₂ and 70% ethanol then rinsed with double distilled water.

Treatment studies: Farmers use ZnSO₄ as a standard zinc source in their farms. ZnSO₄ and biosynthesized ZnO nanoparticles were suspended in double distilled water and dispersed using an ultrasonicator. Four distinct doses of aqueous ZnSO₄ (2mg, 4mg, 6mg & 8mg) and biosynthesized ZnO NPs (2mg, 4mg, 6mg & 8mg), were used for the seed treatments. The sterilized seedlings were immersed in their corresponding concentration for 1 h. The treated seedlings were placed on petri plates with Whatman filter paper No. 41 and added 1 mL of water. Petri plates were covered and stored in a dark environment for 7 days. Shoot and root lengths were measured every other day and the prepared solution of ZnSO₄ & ZnO nanoparticles was given in 5 mL concentration to their respective petri dish.

Seedling vigour index (SVI): The seedling vigour index (SVI) was calculated by using the following formula suggested by *Abdul-Baki, et. al.*

$$I = [\text{Germination (\%)}] \times [\text{Root length (cm)} + \text{Shoot length (cm)}]$$

$$\text{Relative seed germination rate (RSG)} = \frac{\text{Seeds in control which are germinated (SC)}}{\text{Seed in sample which are germinated (SS)}} \times 100$$

$$\text{Relative root growth (RRG)} = \frac{\text{Root length in samole (RS)}}{\text{Root length in control (RC)}} \times 100$$

Total Chlorophyll:

Total chlorophyll was determined according to *Arnon et al.* method, In brief, 25 mg of fresh leaf from each petri dish containing ZnSO₄ and ZnO NPs was manually blended with 10 mL of 80% acetone, and absorbance was measured at 645 and 663 nm using a spectrophotometer. To calculate the chlorophyll content, the following formulae was utilized:

$$\text{Chlorophyll a (mg/g)} = 12.7 (A_{663} - 2.69(A_{645}) \times V \ 1000 \times W$$

$$\text{Chlorophyll b (mg/g)} = 22.9 (A_{645}) - 4.68(A_{663}) \times V \ 1000 \times W$$

$$\text{Total chlorophyll} = 20.9 \times (A_{645}) - 8.02 \times (A_{663}) \times V \ 1000 \times W$$

Where A = absorbance, V = final volume of sample, W = fresh weight of sample taken.

Statistical evaluation: A randomized block design with three replications was used to organize the treatments. ANOVA was employed to do a statistical analysis of the data.

IV. RESULT AND DISCUSSION:

In this work, ZnO NPs were synthesized using banana peel extract which acts as both surface stabilizing and reducing agents. Zn²⁺ ions from zinc precursor i.e. zinc acetate dihydrate reacted with reducing agents, such as peel extract and NaOH, to obtain ZnO nanoparticles. The visual interpretation revealed a change from pale yellow to white, indicative of nanoparticle formation, which were subsequently dried and preserved as a powder

UV-Visible studies: The UV-Vis absorption spectra of the biosynthesized ZnO nanoparticle at 380 nm was detected. The findings were quite similar to the reported investigations

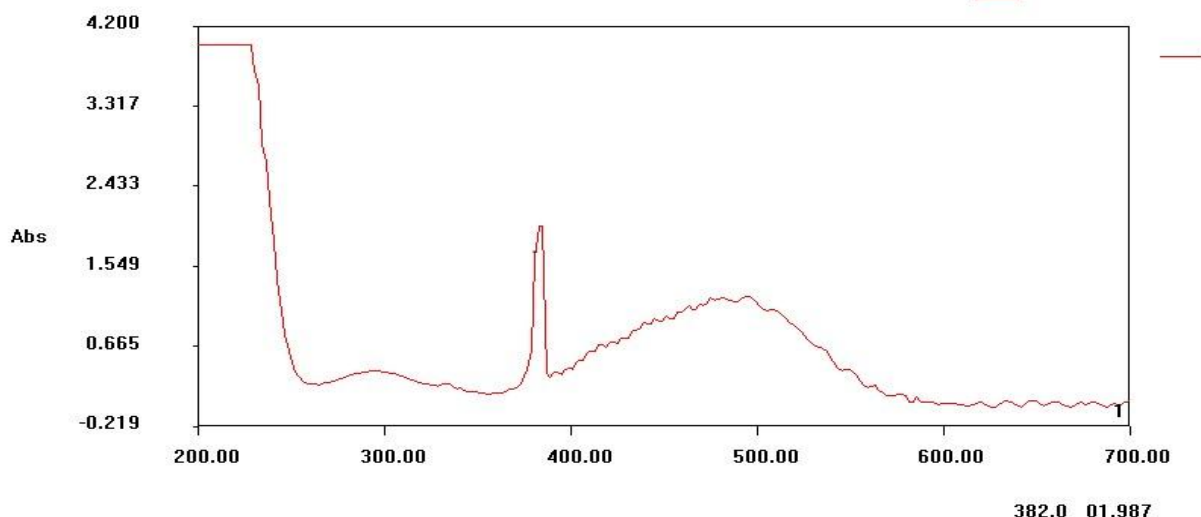


Fig. 1. UV-visible spectra of ZnO NPs synthesised using banana peels (*Musa acuminata*) extract

Morphological studies: Size of nanoparticles was observed by Scanning Electron Microscopy. Rod shape morphology of nanoparticles were observed. The morphology and size can be influenced by various bioactive agents like polyphenols and other compounds. The size of nanoparticles was 20nm to 55nm. FTIR graph shown the several functional groups present in ZnO nanoparticles.

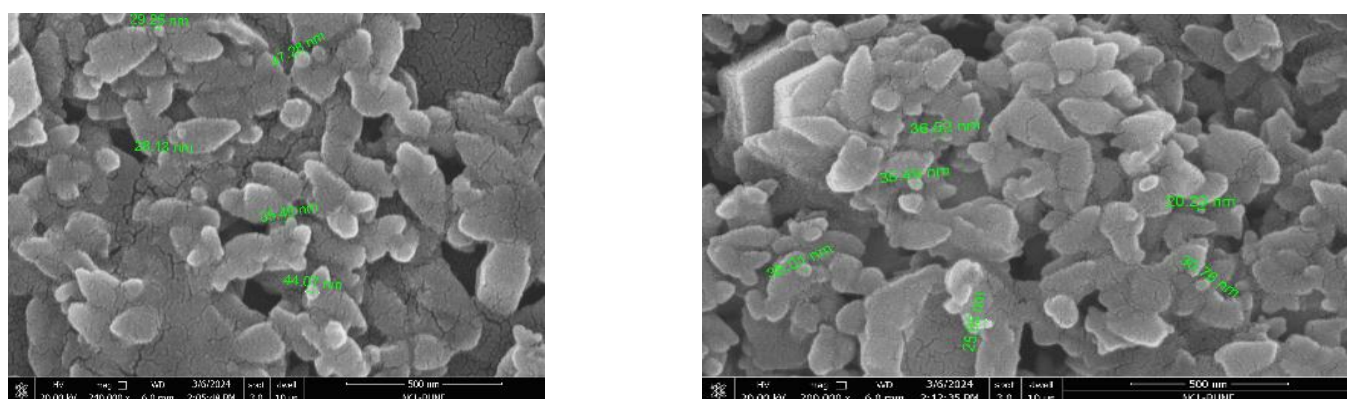


Fig. 2. SEM images of synthesised nanoparticles using banana peels (*Musa acuminata*) extract.

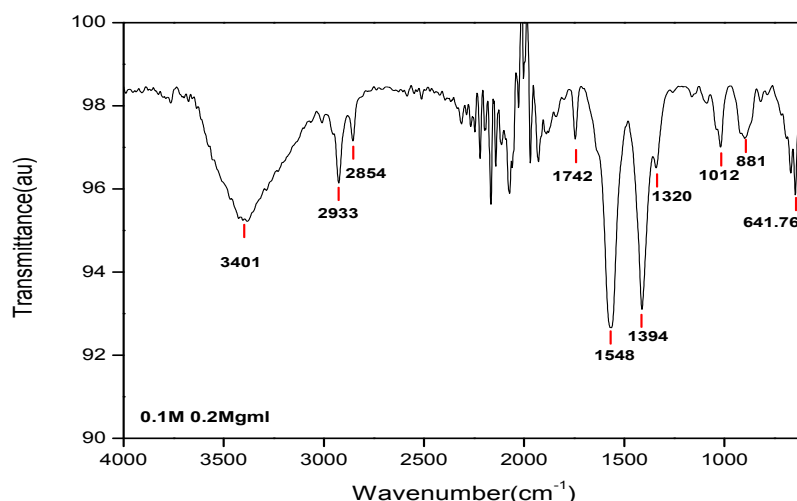


Fig. 3. FTIR spectra of synthesised ZnO nanoparticles using banana peels (*Musa acuminata*) extract

Assessment of growth and germination characteristics using biosynthesised ZnO nanoparticle treatments:

Seed germination was significantly impacted by both ZnO NPs and ZnSO₄ salt. The seeds treated with lower nanoparticle concentrations showed the highest levels of germination and seedling development. The seeds treated with 4 mg nanoparticles showed the highest seedling development and maximum germination. Depending on the species and concentration level, ZnO NPs have different effects. Figure 4 illustrates how the development patterns of the shoots and roots vary greatly depending on the dosage. As the dosage was raised, the zinc supplement delivered via ZnSO₄ demonstrated healthy root and shoot growth. In contrast, the length of the shoot increased at 4 mg for nanoparticles and then declined as the dose increased, ZnO NPs showed greater growth and germination at each concentration than the bulk ZnSO₄, it showed maximum growth of shoot and root at 8 mg concentration. The visual representation of the growth of seedlings is shown in Fig. 4

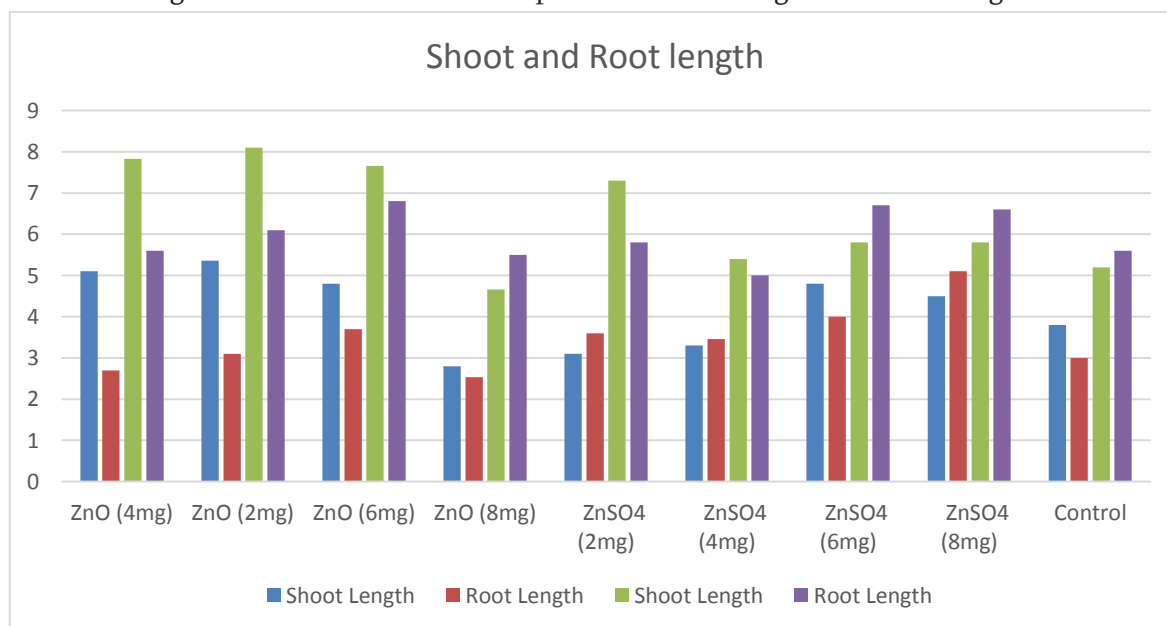


Fig. 4. Results of shoot and root length of mung bean seeds affected by different concentrations of ZnSO₄ and ZnO NPs

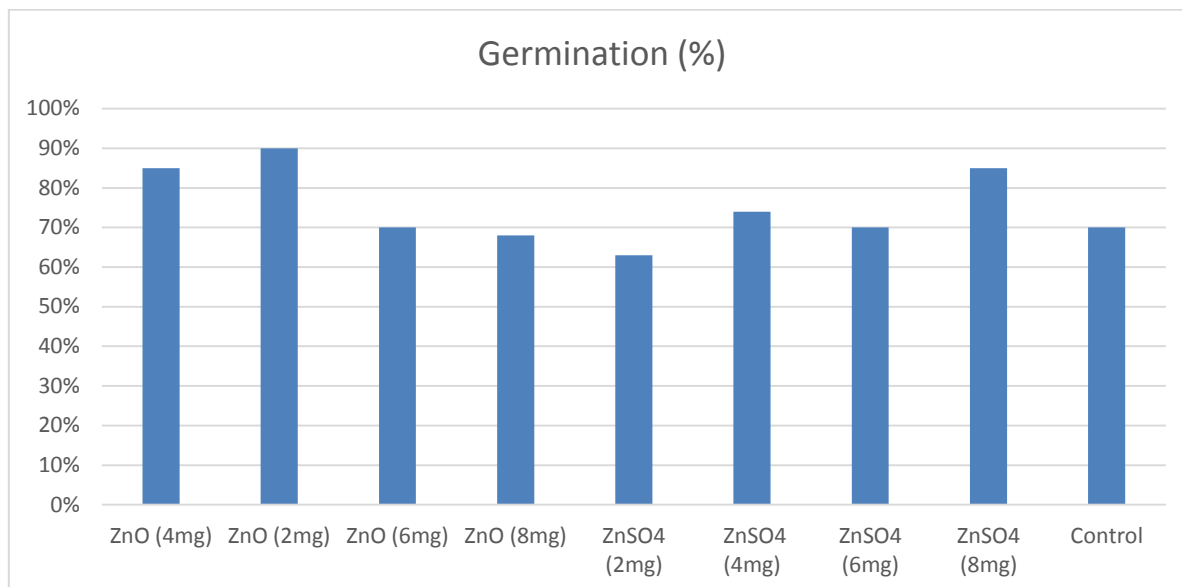


Fig 5: Percent germination of mung bean seeds affected by ZnO NPs, ZnSO4 & Control

Total chlorophyll content: Mung bean seeds treated with varying doses of ZnO NPs and control showed a total chlorophyll content. The mung bean treated with a 4 mg dose of ZnO NPs had the highest level of total chlorophyll.

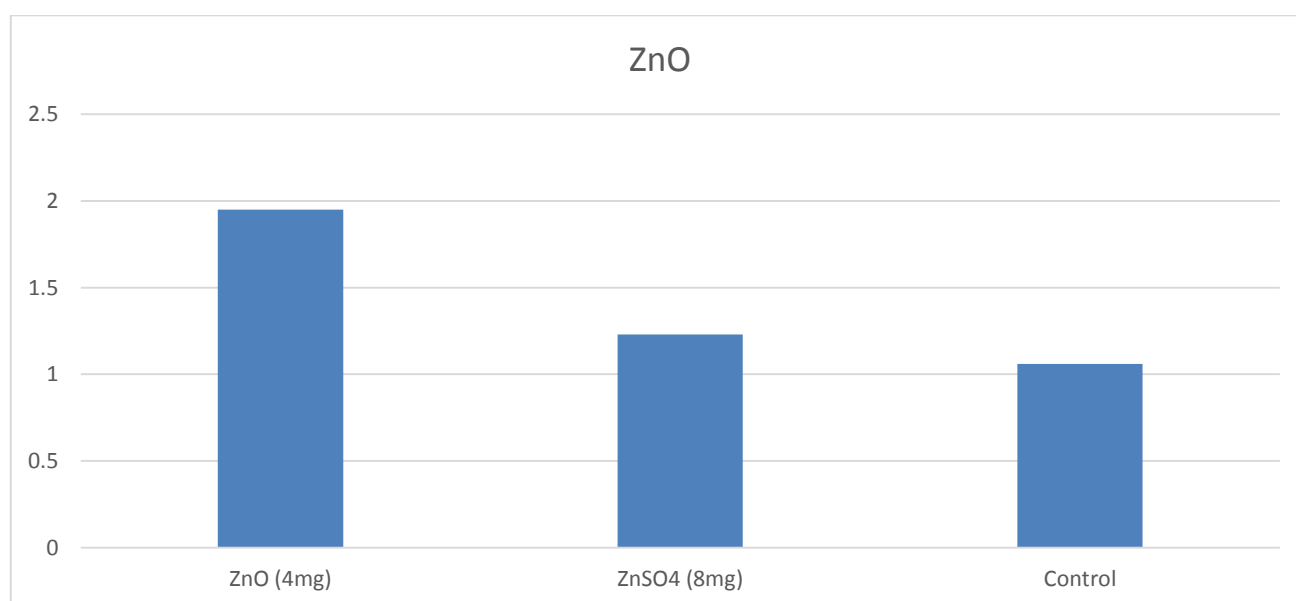


Fig. 6 Total chlorophyll content of mung bean seeds affected by ZnO NPs and ZnSO4

Seedling vigour index (SVI): It was found that seeds treated with ZnO-NPs performed more effectively than the others. When compared to other zinc treatments, ZnO NPs at 4 mg had the highest seedling vigour index of germinated seeds. Low concentrations of ZnO NPs have been demonstrated to significantly increase seed, root, and shoot growth. The plants that grew with a high ZnO NP concentration had a low seedling vigour index.

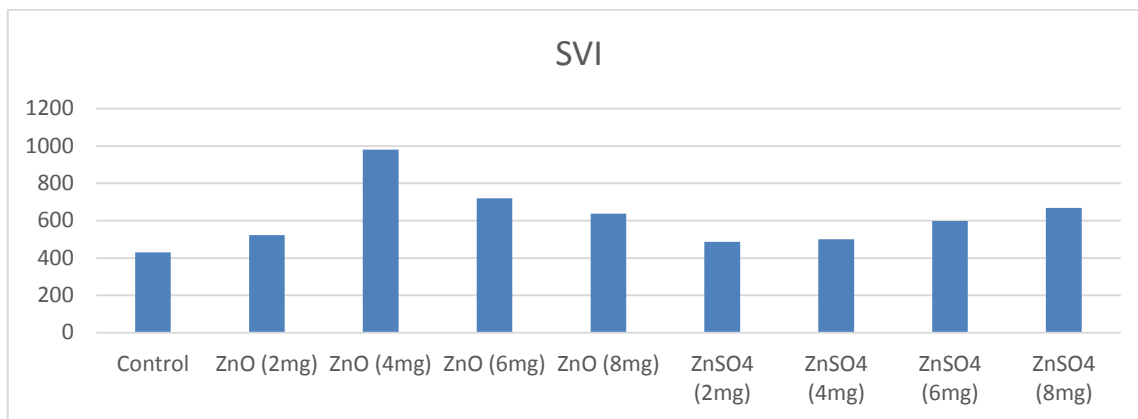


Fig. 7. Seedling Vigour index of *Vigna radiate* treated with ZnO nanoparticles & ZnSO₄

Concentration	Shoot length (cm) 3 rd day	Root length (cm) 3 rd day	Shoot length (cm) 7 th day	Root length (cm) 7 th day
ZnO (2mg)	5.2	2.9	8.4	6.3
	5.0	2.5	7.9	5.9
	4.9	2.9	8.0	6.1
ZnO (4mg)	5.5	3.2	8.1	7.6
	5.0	3.0	7.9	7.8
	4.9	3.1	7.5	7.4
ZnO (6mg)	5.4	3.8	7.6	6.9
	5.2	3.5	7.9	6.5
	4.0	4.0	7.5	7.0
ZnO (8mg)	2.6	2.6	4.8	5.8
	3.0	2.8	5.2	5.1
	2.8	2.2	4.9	5.6
ZnSO ₄ (2mg)	3.2	3.6	7.2	5.9
	3.1	3.9	7.1	5.7
	3.6	3.5	7.6	5.9
ZnSO ₄ (4mg)	3.9	3.1	5.5	5.2
	4.7	3.8	5.2	5.0
	4.8	3.5	5.6	4.9
ZnSO ₄ (6mg)	4.1	4.0	5.9	6.7
	4.5	3.9	5.8	6.8
	4.7	4.2	5.8	6.6
ZnSO ₄ (8mg)	4.1	5.0	5.9	6.7
	4.8	5.3	5.7	6.8
	4.6	5.1	5.9	6.5
Control	3.9	5.6	5.2	6.0

TABLE 2					
Effect of different concentration in growth parameters of different replicas of mung bean seeds at different days					
Concentration	Shoot Length (Mean \pm SD) 3rd day	Root Length (Mean \pm SD) 3rd day (Mean \pm SD) 3rd day	Shoot Length (Mean \pm SD) 7th day	Root Length (Mean \pm SD) 7th day	Germination (%)
ZnO (4mg)	5.1 \pm 33	2.7 \pm 48	7.83 \pm 66	5.6 \pm 20	85%
ZnO (2mg)	5.36 \pm 55	3.1 \pm 66	8.1 \pm 20	6.1 \pm 45	90%
ZnO (6mg)	4.8 \pm 33	3.7 \pm 45	7.66 \pm 63	6.8 \pm 66	70%
ZnO (8mg)	2.8 \pm 66	2.53 \pm 65	4.66 \pm 54	5.5 \pm 55	68%
ZnSO ₄ (2mg)	3.1 \pm 33	3.6 \pm 66	7.3 \pm 33	5.8 \pm 33	63%
ZnSO ₄ (4mg)	3.3 \pm 56	3.46 \pm 66	5.4 \pm 33	5.0 \pm 33	74%
ZnSO ₄ (6mg)	4.8 \pm 33	4.0 \pm 33	5.8 \pm 33	6.7 \pm 66	70%
ZnSO ₄ (8mg)	4.5 \pm 50	5.1 \pm 66	5.8 \pm 55	6.6 \pm 40	85%
Control	3.8 \pm 65	3.0 \pm 66	5.2 \pm 33	5.6 \pm 55	70%

Statistical analysis: The mean standard deviation was used to interpret the results. The data collected after a 7-day period is shown in Table-2.

V. CONCLUSION

It is investigated how ZnO NPs made from banana peel extract affect the germination and growth of *Vigna radiata* L. seeds. The extract from banana peels serves as a reducing and stabilising agent. Nanoparticles and bulk ZnSO₄ at varying concentrations were used to assess the impact on mung bean seeds. Any type of zinc has been shown to positively impact seedling development in comparison to the control. Nanoparticles had the most positive effects on seed germination, root and shoot growth, total chlorophyll, and seedling vigour index (SVI) at a dosage of 4 mg/L. However, the growth rate decreased as the treatment's zinc concentration rose. ZnO NPs perform better than their bulk counterparts in terms of seedling growth at all concentrations. It was determined that using zinc in the form of nanoparticles may aid in boosting agricultural output and that biosynthesised ZnO NPs had a positive impact on *Vigna radiata* growth and germination. In order to increase crop yields in the future, ZnO NPs can be used as a seed priming agent and possible fertiliser. However, it was discovered that plants' reactions to ZnO NPs varied depending on the dose.

VI. REFERENCES

- [1]. Sorahinobar, M., Deldari, T., Nazem Bokaei, Z., & Mehdinia, A. (2023). Effect of zinc nanoparticles on the growth and biofortification capability of mungbean (*Vigna radiata*) seedlings. *Biologia*, 78(4), 951-960.
- [2]. Mahajan, P., Dhoke, S. K., & Khanna, A. S. (2011). Effect of nano-ZnO particle suspension on growth of mung (*Vigna radiata*) and gram (*Cicer arietinum*) seedlings using plant agar method. *Journal of Nanotechnology*, 2011(1), 696535.
- [3]. Yadav, A. A., Dhingra, P. P., Rao, A. A., & Dhania, G. G. (2024). Effect of Zinc Oxide Nanoparticles on Growth and Germination of Mung Bean Seeds (*Vigna radiata* L.). *Asian Journal of Chemistry*, 36(12), 2885–2890.
- [4]. Thapa, M., Sadhukhan, R., Mukherjee, A., & Biswas, P. K. (2023). Effects of nZnS vs. nZnO and ZnCl₂ on mungbean [*Vigna radiata* (L.) R. Wilczek] plant and Bradyrhizobium symbiosis: A life cycle study. *Nanoimpact*, 29, 100440.
- [5]. Ajmal, M., Ullah, R., Muhammad, Z., Khan, M. N., Kakar, H. A., Kaplan, A., ... & Abdul Razak, S. (2023). Kinetin capped zinc oxide nanoparticles improve plant growth and ameliorate resistivity to polyethylene glycol (PEG)-induced drought stress in *Vigna radiata* (L.) R. Wilczek (Mung Bean). *Molecules*, 28(13), 5059.
- [6]. Kareem, H. A., Saleem, M. F., Saleem, S., Rather, S. A., Wani, S. H., Siddiqui, M. H., & Wang, Q. (2022). Zinc oxide nanoparticles interplay with physiological and biochemical attributes in terminal heat stress alleviation in mungbean (*Vigna radiata* L.). *Frontiers in Plant Science*, 13, 842349.
- [7]. Rafiq, H., Aftab, Z. E. H., Anjum, T., Ali, B., Akram, W., Bashir, U., & Li, G. (2022). Bio-fabrication of Zinc Oxide nanoparticles to rescue Mung Bean against *Cercospora* leaf spot disease. *Frontiers in Plant Science*, 13, 1052984.
- [8]. Singh, A., Hiregoudar, S., Chauhan, R., Varma, A., Prasad, R., & Goel, A. (2024). Deciphering the synergistic potential of mycogenic zinc oxide nanoparticles and bio-slurry formulation on phenology and physiology of *Vigna radiata*. *Nanotechnology Reviews*, 13(1), 20230217.
- [9]. Hajiboland, R., & Amirazad, H. (2010). Drought tolerance in Zn-deficient red cabbage (*Brassica oleracea* L. var. capitata f. rubra) plants. *Horticultural Science*, 37(3), 88-98.
- [10]. Haq, T. U., Ullah, R., Khan, M. N., Nazish, M., Almutairi, S. M., & Rasheed, R. A. (2023). Seed priming with glutamic-acid-functionalized iron nanoparticles modulating response of *Vigna radiata* (L.) R. Wilczek (mung bean) to induce osmotic stress. *Micromachines*, 14(4).
- [11]. Ramesh, P., Saravanan, K., Manogar, P., Johnson, J., Vinoth, E., & Mayakannan, M. (2021). Green synthesis and characterization of biocompatible zinc oxide nanoparticles and evaluation of its antibacterial potential. *Sensing and Bio-Sensing Research*, 31, 100399.
- [12]. Abdul-Baki, A. A., & Anderson, J. D. (1973). Vigor determination in soybean seed by multiple criteria 1. *Crop science*, 13(6), 630-633.
- [13]. Arnon, D. I. (1949). Copper enzymes in isolated chloroplasts. Polyphenoloxidase in *Beta vulgaris*. *Plant physiology*, 24(1), 1.
- [14]. Hussien, N. A., Al Malki, J. S., Al Harthy, F. A., Mazi, A. W., & Al Shadadi, J. A. (2023). Sustainable eco-friendly synthesis of zinc oxide nanoparticles using banana peel and date seed extracts, characterization, and cytotoxicity evaluation. *Sustainability*, 15(13), 9864.

- [15]. Albarakaty, F. M., Alzaban, M. I., Alharbi, N. K., Bagrwan, F. S., Abd El-Aziz, A. R., & Mahmoud, M. A. (2023). Zinc oxide nanoparticles, biosynthesis, characterization and their potent photocatalytic degradation, and antioxidant activities. *Journal of King Saud University-Science*, 35(1), 102434.

Viscosity and Density Characterization of 1-((4-Methoxy-3, 5-Dimethylpyridin-2-yl) Methyl)-3-Methyl Thiourea in Ethanol-Water Mixtures

P. R. Kute¹, N.D. Chaudhari², S. U. Shinde², G. B. Andhale³, A. M. Kute⁴, S. S. Padhen⁵

¹Department of Chemistry, Pratishthan Mahavidyalaya, Paithan, Dist.-Chh. Sambhajinagar, Maharashtra, India

²Department of Physics, Pratishthan Mahavidyalaya, Paithan, Dist.-Chh. Sambhajinagar, Maharashtra, India

³Department of Chemistry, Shri Shivaji Arts, Commerce and Science College Akot, Maharashtra, India

⁴Department of Chemistry, Shankarrao Patil Mahavidyalaya, Bhoom, Maharashtra, India

⁵Department of Chemistry, Rajyashree Shahu Science College, Chandur Railway, Maharashtra, India

ARTICLE INFO

Article History:

Accepted : 01 Jan 2025

Published : 10 Jan 2025

Publication Issue :

Volume 12, Issue 7

January-February-2025

Page Number :

284-288

ABSTRACT

Heterocyclic molecules are essential in medicinal chemistry, serving as the structural backbone for many drugs currently available. Pyridine, a six-membered heteroaromatic ring, is a critical component of numerous natural substances, including vitamins and alkaloids, and its derivatives are highly regarded for their adaptability in the development of new therapeutics. In a recent study conducted in our laboratory, we investigated the viscosity and density of 1-((4-methoxy-3,5-dimethylpyridin-2-yl)methyl)-3-methylthiourea at controlled concentrations and varying temperatures. The experimental findings shed light on solute-solvent interactions and the impact of solvent dilution. The results revealed that relative viscosity decreases with rising temperature, indicating improved solvation effects. This research offers valuable insights into the physicochemical properties of pyridine derivatives, supporting the advancement of more efficient pharmaceutical compounds.

Keywords: Heterocyclic, Pyridine derivatives, Viscosity and density, 1-((4-methoxy-3,5-dimethylpyridin-2-yl)methyl)-3-methylthiourea, Solvent, Temperature effects.

I. INTRODUCTION

Nitrogen and sulfur containing heterocyclic molecules are vital to life, playing critical roles in various biological processes and systems. Their diverse ring structures exhibit unique chemical properties and reactivity profiles, driven by the presence of nitrogen and sulfur atoms essential for their biological functions [1,2]. Pyridine

derivatives are widely recognized for their broad spectrum of biological applications. The heterocyclic pyridine ring, valued for its pharmacological properties, plays a crucial role in the development of new drugs. Compounds based on pyridine are integral to medications exhibiting anti-inflammatory, antibacterial, antiviral, anticancer, antioxidant, antihypertensive, antidiabetic, and antimalarial effects. Furthermore, pyridine derivatives demonstrate a strong affinity for various ions and neutral species, making them exceptionally effective as chemosensors for detecting and distinguishing a diverse array of targets [3]. Replacing the pyridine nucleus targets a diverse array of biological issues, including malignant cells, viral infections, and microbial disorders. Pyridine derivatives exert their effects by interacting with proteins, enzymes, and DNA, effectively addressing these challenges [4]. Modifications on the pyridine nucleus address a wide range of biological challenges, including microbial infections, viral diseases, and different types of cancer. Pyridine derivatives effectively combat these issues by interacting with enzymes, proteins, and DNA [5]. Thiocarbamide, commonly referred to as thiourea ($\text{CS}(\text{NH}_2)_2$), is a significant compound in organic chemistry due to its distinctive structure and reactivity. We are synthesizing thiocarbamide derivatives featuring a pyridine-based moiety. Its importance stems from its wide range of applications as a reagent, intermediate, and functional group in various chemical processes. Beyond its non-medical uses in metallurgy, analytical chemistry, and industry, thioureas hold considerable therapeutic value, with many being employed in clinical settings. Their use in medicine continues to expand over time. In agriculture, thioureas serve as insect growth regulators, enzyme inhibitors, herbicides, rodenticides, and antifungal agents [6-15].

Pyridine derivatives are widely reported in the literature for their diverse pharmacological and biochemical properties, including antiviral, antibacterial, anti-inflammatory, anesthetic, and mydriatic activities. These compounds exhibit antiviral, antifungal, antibacterial, anti-helminthic, and anti-tuberculostatic effects. Given these attributes, assessing the viscometric concentration of 1-((4-methoxy-3,5-dimethylpyridin-2-yl)methyl)-3-methylthiourea at different temperatures is highly relevant. Such research contributes significantly to the advancement of drug science, aiding in the development of more reliable and effective pharmaceutical products, ultimately enhancing patient outcomes [1,2,16].

Interactions between solute and solvent occur in both aqueous and non-aqueous solutions, and valuable insights into these interactions can be gained through the measurement of viscometric parameters. Understanding viscosity and solute-solvent interactions is crucial, as these factors directly impact a drug's behavior in the human body, including its absorption, transport, and overall effects [16].

Water and alcohol mixtures are fascinating systems characterized by complex dynamics arising from hydrogen bonding and the presence of hydrophobic groups. These mixtures are extensively studied, both experimentally and theoretically, due to their widespread application as solvents. Viscosity in liquids is influenced by factors such as temperature, molecular size, molecular weight, intermolecular interactions, and impurities. Investigating viscosity offers valuable insights into the molecular interactions and properties of binary and ternary liquid systems. Interestingly, strong favorable interactions within these systems can result in increased viscosity. Density, on the other hand, is a crucial property that determines whether a substance will float or sink in a liquid; a material will float if its density is lower than that of the liquid. Additionally, density is integral to understanding other physical and acoustic properties, including surface tension, molar refraction, dipole moment, and boiling point [17].

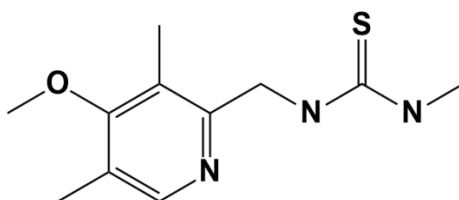


Fig. 1-1-((4-methoxy-3,5-dimethylpyridin-2-yl)methyl)-3-methylthiourea

II. EXPERIMENTAL

This study utilized double-distilled water and analytical grade (A.R.) chemicals. The compound weights were measured with a Mechaniki Zektady Precyzyjnej Gdansk balance, offering a precision of ± 0.001 grams. Viscosity measurements were performed using an Ostwald viscometer, with the temperature carefully maintained at 29°C ($\pm 0.1^\circ\text{C}$) using an Elite thermostatic water bath. Density measurements were obtained using a bicapillary tube with a 1 mm internal diameter. To ensure accuracy, the viscometer and water bath were allowed ample time to reach thermal equilibrium before measurements. The viscometric properties of 1-((4-methoxy-3,5-dimethylpyridin-2-yl)methyl)-3-methylthiourea were analyzed at a concentration of 0.1 M in a 60% ethanol-water mixture over a range of temperatures. Freshly prepared solutions were used, and viscosity readings were recorded following established literature methods [18].

III. OBSERVATIONS AND CALCULATIONS

Molecular interactions were examined using the solute's β -coefficient, which was derived from the data collected in this study. The findings are shown in Table 1. Using the Jones-Dole equation: $C(\eta_r - 1) = A + BC$, values were calculated at different temperatures for a 0.1 M concentration. The calculated A and β -coefficients are summarized in Table 2.

TABLE No.1 THE MEASUREMENT OF RELATIVE AND SPECIFIC VISCOSITIES AT VARIOUS TEMPERATURES FOR A 0.1 M CONCENTRATION, ALONG WITH VISCOSITY READINGS TAKEN AT CONSTANT CONCENTRATIONS.

MEDIUM - 60% ETHANOL-WATER							
Conc.	Temp. ($^\circ\text{C}$)	\sqrt{C}	Time	Density $\rho \times 10^3$ (kg.cm^{-3})	η_r	$\eta_{sp} = \eta_r - 1$	$(\eta_r - 1)/\sqrt{C}$ ($\text{pa}\cdot\text{s}$)
0.1 M	24	0.314	69	0.9823	0.069421	-0.930579	-2.96362
	26	0.314	59	0.9763	0.058214	-0.941786	-2.99931
	28	0.314	51	0.9876	0.052143	-0.947857	-3.01779
	30	0.314	45	0.9535	0.049125	-0.950875	-3.02826

TABLE No.- 2 THE VALUES OF A AND B FOR THE 60% CONCENTRATION ARE PRESENTED IN THE REFERENCES FOR 1-((4-METHOXY-3,5-DIMETHYLPYRIDIN-2-YL)METHYL)-3-METHYLTHIOUREA.

W-E Mixture (%)	Temp $^\circ\text{C}$	Mean "A"	β (Slope "m")
60	27	-3.00233	0.0069

IV. RESULT AND DISCUSSION

The relative viscosity was calculated using the equation provided.

$$\eta_r = D_s \times t_s / D_w \times t_w.$$

The relative viscosities were evaluated using the

Jones-Dole equation.

$$\eta_r - 1)/\sqrt{C} = A + B\sqrt{C}$$

Where,

A = Falkenhagen coefficient

B = Jones-Dole coefficient

C = concentration of solutions

The Jones-Dole coefficient (B) was employed to evaluate solute-solvent interactions, whereas the Falkenhagen coefficient (A) was used to assess solute-solute interactions. A graph was created plotting \sqrt{C} against $(\eta_r - 1)/\sqrt{C}$, revealing a linear relationship for each system with an associated β -coefficient value.

V. CONCLUSION

In this study, both density and relative viscosity were observed to decrease as the temperature increased. This supports the idea that solute-solvent interactions strengthen with rising temperature, enhancing the solvation effect. Research on a drug's pharmacodynamics and pharmacokinetics provides valuable insights that benefit and inform the public.

VI. ACKNOWLEDGEMENT

I would like to extend my heartfelt thanks to Dr. D. T. Tayade, a distinguished professor at GVISH College in Amravati, for his immense support and guidance. His knowledge and commitment have been instrumental in helping me throughout this research.

VII. REFERENCES

- [1]. Solanki, A. and Thakur, I. (2007). Indian Journal of Chemistry. 45(B): 517.
- [2]. Saleem, F. (2008). Eur. Pat., CHAPPL. 87: 19.
- [3]. Mohammad Abu-Taweel G, Ibrahim MM, Khan S, Al-Saidi HM, Alshamrani M, Alhumaydhi FA, Alharthi SS. Medicinal Importance and Chemosensing Applications of Pyridine Derivatives: A Review. Crit Rev Anal Chem. 2022 Jun 20:1-18.
- [4]. Ataf Ali Altaf, Adnan Shahzad, Zarif Gul, Nasir Rasool, Amin Badshah, Bhajan Lal, Ezzat Khan. A Review on the Medicinal Importance of Pyridine Derivatives. Journal of Drug Design and Medicinal Chemistry. Vol. 1, No. 1, 2015, pp. 1-11. doi: 10.11648/j.jddmc.20150101.11.
- [5]. Ataf Ali Altaf, Adnan Shahzad, Zarif Gul, Nasir Rasool, Amin Badshah, Bhajan Lal, Ezzat Khan. A Review on the Medicinal Importance of Pyridine Derivatives. Journal of Drug Design and Medicinal Chemistry. Vol. 1, No. 1, 2015, pp. 1-11.
- [6]. Makhsumov, A. G., Safaev, A. S., & Abidova, S. V. (1969). Katal Pererab. Uglevodordn. Syrya 1968, 101. In Chem. Abstr (Vol. 71, p. 101668v).

- [7]. Gan, S. F., Wan, J. P., Pan, Y. J., & Sun, C. R. (2011). Highly efficient and catalyst-free synthesis of substituted thioureas in water. *Molecular diversity*, 15, 809-815.
- [8]. Walpole, C., Ko, S. Y., Brown, M., Beattie, D., Campbell, E., Dickenson, F., ... & Urban, L. (1998). 2-Nitrophenylcarbamoyl-(S)-prolyl-(S)-3-(2-naphthyl) alanyl-N-benzyl-N-methylamide (SDZ NKT 343), a potent human NK1 tachykinin receptor antagonist with good oral analgesic activity in chronic pain models. *Journal of medicinal chemistry*, 41(17), 3159-3173.
- [9]. Saeed, S., Bhatti, M. H., Tahir, M. K., & Jones, P. G. (2008). Ethyl 4-(3-butyrylthioureido) benzoate. *Acta Crystallographica Section E: Structure Reports Online*, 64(7), o1369-o1369.
- [10]. Eweis, M., Elkholy, S. S., & Elsabee, M. Z. (2006). Antifungal efficacy of chitosan and its thiourea derivatives upon the growth of some sugar-beet pathogens. *International Journal of Biological Macromolecules*, 38(1), 1-8.
- [11]. Weiqun, Z., Baolong, L., Jiangang, D., Yong, Z., Lude, L., & Xujie, Y. (2004). Structural and spectral studies on N-(4-chloro) benzoyl-N'-(4-tolyl) thiourea. *Journal of molecular structure*, 690(1-3), 145-150.
- [12]. Y.M. Zhang, T.B. Wei, X.C. Wang, S.Y. Yang, *Indian J. Chem., Sect. B* 37 (1998) 604-606.
- [13]. Y.M. Zhang, T.B. Wei, L. Xian, L.M. Gao, *Phosphorus, Sulphur Silicon Relat. Elem.* 179 (2004) 2007-2013.
- [14]. Yuan, Y. F., Wang, J. T., Gimeno, M. C., Laguna, A., & Jones, P. G. (2001). Synthesis and characterisation of copper complexes with N-ferrocenoyl-N'-aryl (alkyl) thioureas. *Inorganica Chimica Acta*, 324(1-2), 309-317.
- [15]. Shakeel, A., Altaf, A. A., Qureshi, A. M., & Badshah, A. (2016). Thiourea derivatives in drug design and medicinal chemistry: A short review. *J. drug des. med. chem*, 2(1), 10.
- [16]. Zhang, L.X. Zhang, A.J. Hu, M.L. and Lei, X.X. (2003). *Acta Chim.Sinica*. 61(6): 917.
- [17]. Vibhute, Y.B. and Basser, M.A. (2003). *Ind. J. of Chem.* 42(B): 202-205.
- [18]. Padmanaban, R.; Gayathri, A.; Gopalan, A.I.; Lee, D.-E.; Venkatramanan, K. Comparative Evaluation of Viscosity, Density and Ultrasonic Velocity Using Deviation Modelling for Ethyl-Alcohol Based Binary Mixtures. *Appl. Sci.* 2023, 13, 7475.

Approach of Graph Theory in Material Science

P.B. Deshmukh

Department of Mathematics, Vinayak Vidnyan Mahavidyalaya, Nadgaon Khandeshwar, Dist Amravati,
Maharashtra, India

ARTICLE INFO

Article History:

Accepted : 01 Jan 2025

Published : 10 Jan 2025

Publication Issue :

Volume 12, Issue 7

January-February-2025

Page Number :

289-295

ABSTRACT

Mathematics played a crucial role in ancient science, providing the structure tools, language, and frameworks for scientific analysis, inquiry, and communication. Materials science is an interdisciplinary field of research comprising various areas such as metallurgy, polymer science, ceramics, solid state physics, and semiconductors. Mathematics plays a vital role in materials science. Mathematics offers important tools to understand materials as complex hierarchical systems. In this article we have discussed approach of graph theory in nanotube and in selection of material.

Keywords: Atomic Configurations, Grapheme, Carbon Nanotubes, Graph Theory, Matrix Method.

I. INTRODUCTION

In today's modern research environment, the emphasis is placed on the direct interaction of mathematics with other scientific fields and industry groups to solve complex problems jointly faced by various disciplines. The demand for the participation of mathematicians in materials science is growing. The need to describe material behavior resulting from physical interactions across several length scales is forcing scientists to develop new mathematics. The study of materials science has evolved to the point at which scientists from physics, engineering and applied mathematics are working on problems of common interest. There were many occasions in the past when mathematics and materials science met and interacted to inspire advances. From ancient times, humans are believed to have had an empirical knowledge of materials that was related to mathematics. A variety of theoretical and numerical techniques of mathematics are used in the study of photonic crystals, typically in combination. They include Greens functions, boundary-integral methods, energy methods, spectral theory, asymptotic methods, and finite element and finite difference numerical schemes. Mostly the method of the calculus of variations, semi-classical analysis, linear bifurcation analysis, graph theory, asymptotic , Partial Differential Equations, algebra, group theory , functional analysis, topology, differential geometry , mathematical modelling and numerical calculations. To study the properties of material

mathematical methods helps to understand , such as in application point of view it includes foam, fluid-solid interaction, shape memory alloys, magnetic suspension, elasticity, plasticity, viscoelasticity, crystallization, grain growth, phase field model and homogenization. Prof. YanivAlmog, Prof. Yuri Antipov, Prof. Robert Lipton, Prof. Daniel Sage ,Prof. BlaiseBourdinand etc. modern mathematical techniques to solve problems occurred during study of material science.

II. METHODS AND MATERIAL

Graph theory is a branch of discrete mathematics. In mathematics and computer science, graph theory is the study of graphs which are mathematical structures used to model pair wise relations between objects. There is wide use of graphs in providing problem solving techniques, because it gives an intuitive manner prior to presenting formal definition.

Definitions

1. Graph

A graph is pair of $G(V,E)$ consist of nonempty set of vertices $V(G) = \{v_1, v_2, v_3, \dots\}$ called as vertex set and set of edges $E(G) = \{e_1, e_2, e_3, \dots\}$ called as edge set.

2. Parallel edges

If two or more edges from E are having same end vertices then they are called as parallel edges.

3. Loop or self loop

An edge having same end vertices i.e. (v_i, v_i) i.e. an edge joining same vertex to itself is called as self loop.

4. General graph

A graph consist of parallel edges, self loopetc is called as General graph.

5. Simple graph

A graph having no parallel edges and self loop is called as simple graph.

A graph $G(V,E)$ is said to be finite iff both the set of vertices and set of edges i.e. E and V are finite.

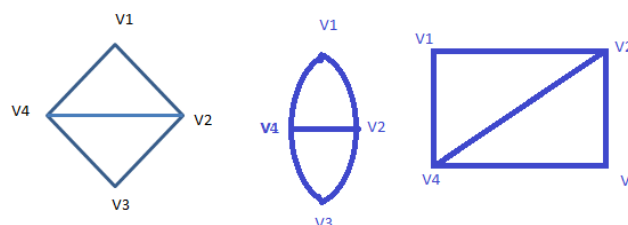
6. Infinite graph

A graph is said to be infinite iff either the set of vertices or set of edges or both i.e. E and V are infinite.

7. Similar or same graph

Any graph is characterised by the set of vertices V and set of edges E only, so two graphs are same till their V and E are same irrespective of their geometrical shape.

e.g.



8. Rank of matrix

Maximum number of linearly independent row vectors of a matrix is called row rank of matrix reduced incidence matrix.

9. Incident matrix

Let g be a graph with n vertices say $v_1, v_2, v_3, \dots, v_n$ and e edges say $x_1, x_2, x_3, \dots, x_e$ then the incident matrix $A = [a_{ij}]_{n \times e}$ of graph G is defined by

$$a_{ij} = 1, \text{ if } j^{\text{th}} \text{ edge incident on } i^{\text{th}} \text{ vertex } v_i \\ = 0$$

It is denoted by $A(G)$.

10. Circuit matrix

Let $r_1, r_2, r_3, \dots, r_q$ be different total q circuits in a graph G with e edges $x_1, x_2, x_3, \dots, x_e$ then the circuit matrix or cycle matrix $B = [b_{ij}]_{q \times e}$ is defined by $b_{ij} = 1$, if i^{th} circuit r_i include j^{th} edge $x_j = 0$

It is denoted by $B(G)$.

11. Path matrix

Let G be connected graph with e edges $x_1, x_2, x_3, \dots, x_e$. Let $p_1, p_2, p_3, \dots, p_k$ be total different k path between two different vertices u and v in G . then the path matrices u and v is denoted by $p(u, v)$ then the circuit matrix or cycle matrix $B = [b_{ij}]_{q \times e}$ is defined by $b_{ij} = 1$, if i^{th} circuit r_i include j^{th} edge $x_j = 0$

12. Adjacency matrix

The adjacency matrix is denoted by $X = X(G)$, $x_{ij} = 1$

$$x_{ij} = 1, \text{ if vertex } v_i \text{ adjacent to } v_j$$

$= 0$, otherwise

13. Cutset matrix

The cutset matrix is denoted by $C = C(G)$.

Let G be a graph whose cutset and edges are labelled.

$\therefore C(G) = c_{ij}$, if i^{th} cutset contain j^{th} edge x_j

$= 0$, otherwise

14. Fundamental circuit matrix

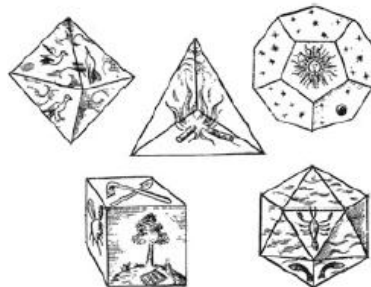
In fundamental circuit matrix first we write the matrix representation for the edge which are the chords and then write the matrix representation for the edge of spanning graph i.e. branches.

It is denoted by B_f . The partition is representation by dotted line.

III.DISCUSSION

A. Historical approach to Atomic Configurations with Geometric Structures

The ancient Greek philosophers Democritus 2500 years ago developed his own idea of atoms based on geometric objects. He argued that all of creation is made up of five polyhedra (elements): octahedron (air), tetrahedron (fire), dodecahedron (the universe), cube (earth), and icosahedron (water). He believed all things are made up of an unchanging level of reality based on mathematics. These fundamental polyhedra cannot be divided into smaller parts because they would lose their beauty if they collided with another.



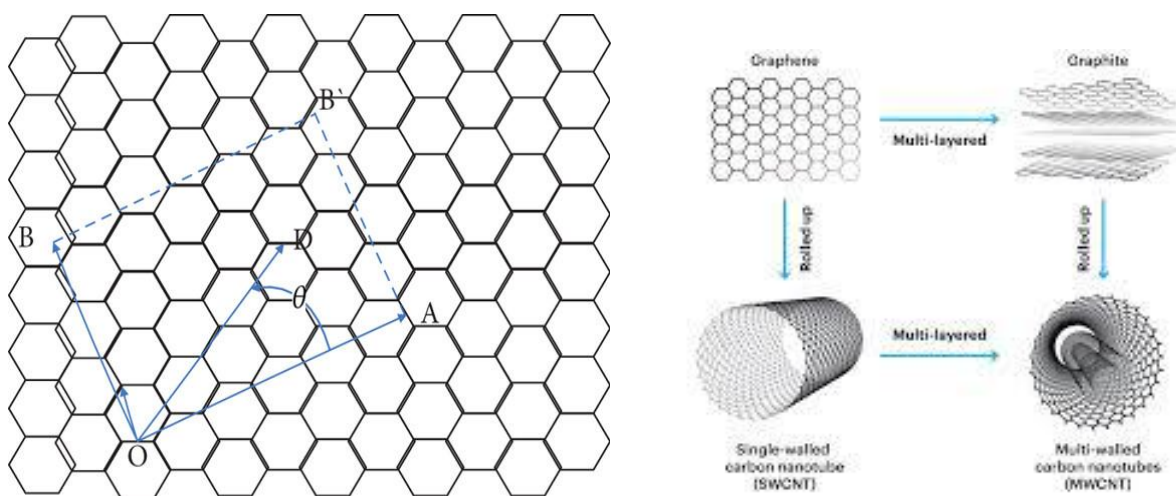
Five Platonic solids (polyhedra) drawn by Johannes Kepler in his work "Harmonice Mundi (1619)." Octahedron, tetrahedron, dodecahedron, cube, and icosahedron were associated with air, fire, the universe, earth, and water, respectively

In 1905 Albert Einstein proposed the theory of Brownian motion in 1910 Max von Laue proposed the diffraction of X-rays by crystal lattices. William Henry Bragg and William Lawrence Bragg. W. L. Bragg developed the new technique to calculate atomic arrangements in crystals and this discovery depended largely on his ability in mathematics. Later, with transmission electron microscopes and scanning tunneling microscopes, researchers began at last to observe atoms directly.

In 1638–86 Nicolas Steno discovered definite geometric considerations. In 17th century in his work he discovered the “law of constant angle” in 1669. The law states that the interplanar angle formed by two crystal faces are universally constant for the same kind of crystal. Steno concluded that crystals grow through the attachment of small particles to crystal facets and the rate of attachment (growth rate) differs for each facet (orientation of the crystal).[4]

B. Approach of Graph theory in Nano-Materials

An interactions between atoms, a *graph theory* is a of a mathematical structure to describe their relations. A graph theory based on edges and vertices. It is consist of a pair of sets, one of vertices which represents atoms and another of edges which represent bonding, Carbon nanotubes (CNTs) are a 2D class of nanomaterials consisting of a hexagonal lattice of carbon atoms, bent and joined in a particular direction to form a hollow cylinder. CNT is a tube made of carbon with a diameter in the nanometre range (nanoscale). They are one of the allotropes of carbon. The carbon tube has a hexagonal crystal structure. Each carbon atom in the carbon nanotube is connected by three other connected carbon atoms, among which the sp^2 two-hybridization is the most important. Single-walled carbon nanotubes can also produce graphene-level mapping, so that the regular hexagonal lattice of carbon nanotubes forms a certain angle with the axis. In other words, the carbon nanotubes now appear to be spiral and have chiral characteristics. It can be divided into three types: sawfish type, armchair type, and spiral type.. [1]Carbon nanotube are used in energy storage, device modelling, automotive parts, film electronics, but hells, sporting goods, coating s, actuators and electromagnetic shields. Due to the large surface area it is successfully use in pharmacy and medicine to adsorb or conjugate a wide range of medical and diagnostic substances. So that it is use as a drug delivery systems in cancer and infection treatments. Graphene: CNT is made up of cylindrical graphitic sheets (named graphene) wrapped up into a seamless cylinder with a nanometer-sized diameter.



Schematic diagram of graphene sheet mapping to carbon nanotubes.

C. Approach of Graph theory in material selection

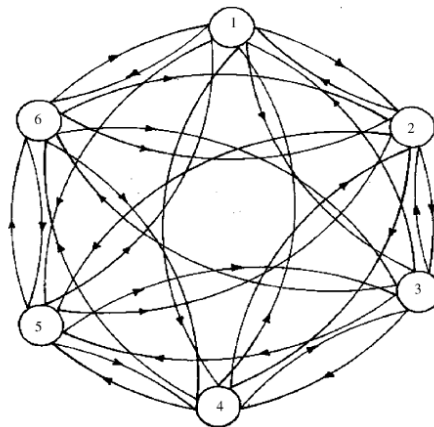
A material selection for a given engineering component using graph theory and matrix approach. Material having its own characteristics, applications, advantages, and limitations. When selecting materials for engineering designs, a clear understanding of the functional requirements for each individual component is required and various important criteria or factors need to be considered. Material selection factor is defined as a factor that influences the selection of a material for a given application. These factors include: physical properties, electrical properties, magnetic properties, mechanical properties, chemical properties, manufacturing properties (machinability, formability, weldability, castability, heat treatability, etc.), material cost, product shape, material impact on environment, performance characteristics, availability, fashion, market trends, cultural aspects, aesthetics, recycling, target group, etc.

Material selection factors graph models the material selection factors and their interrelationship. This graph consists of a set of nodes $V = \{v_i\}$, with $i=1, 2, \dots, N$ and a set of directed edges $D = \{d_{ij}\}$. A node n_i represents i -th material selection factor and edges represent the relative importance among the factors. The number of nodes N , considered is equal to the number of material selection factors considered. If a node ' i ' is having relative importance over another node ' j ' in the material selection, then a directed edge or arrow is drawn from node i to node j (i.e. d_{ij}). If ' j ' is having relative importance over ' i ', then a directed edge or arrow is drawn from node j to node i (d_{ji}). To demonstrate material selection factors graph, an example of material selection for a given engineering component is considered.

Let the material selection factors of interest are:

- TS- ultimate tensile strength
- C- cost of material
- D- density
- H- hardness
- TC- thermal conductivity
- CR- corrosion resistance

Material selection factors graph for the considered example is shown in Figure. As six material selection factors are considered, there are six nodes in the material selection factors graph with nodes 1, 2, 3, 4, 5, and 6 representing the material selection factors TS, C, D, H, TC, and CR, respectively. Ultimate tensile strength of the material (TS) is relatively more important than cost of the material (C) in material selection procedure. However, cost is also important in material selection even though less important than ultimate tensile strength of the material. Thus, the relative importance exists between these two factors in both directions. Similarly the relative importance can be represented between the other factors.



Graph of Material selection

D. Matrix form of Graph

A graphical representation of Material selection factors graph gives of the factors and their relative importance. As the number of nodes and their interrelations increases, the graph becomes complex. A visual analysis of the graph is expected to be difficult and complex. To overcome this problem, the graph is represented in a matrix form. A square matrix $N \times N$ is use to represent graph of section material.

$$A = \begin{matrix} & \text{Factors TS} & \text{C} & \text{D} & \text{H} & \text{TC} & \text{CR} \\ \text{TS} & \left[\begin{matrix} R_1 & r_{12} & r_{13} & r_{14} & r_{15} & r_{16} \end{matrix} \right. \\ \text{C} & \left. \begin{matrix} r_{21} & R_2 & r_{23} & r_{24} & r_{25} & r_{26} \end{matrix} \right. \\ \text{D} & \left. \begin{matrix} r_{31} & r_{32} & R_3 & r_{34} & r_{35} & r_{36} \end{matrix} \right. \\ \text{H} & \left. \begin{matrix} r_{41} & r_{42} & r_{43} & R_4 & r_{45} & r_{46} \end{matrix} \right. \\ \text{TC} & \left. \begin{matrix} r_{51} & r_{52} & r_{53} & r_{54} & R_5 & r_{56} \end{matrix} \right. \\ \text{CR} & \left. \begin{matrix} r_{61} & r_{62} & r_{63} & r_{64} & r_{65} & R_6 \end{matrix} \right] \end{matrix}$$

Where R_i is the value of the i -th factor represented by node n_i and r_{ij} is the relative importance of the i -th factor over the j -th represented by the edge d_{ij} . The permanent of this matrix A , i.e. $\text{per}(A)$, is defined as the material selection factors function. The permanent is a standard matrix function and is used in combinatorial mathematics. Application of permanent concept will lead to a better appreciation of material selection factors. Moreover, using this no negative sign will appear in the expression (unlike determinant of a matrix in which a negative sign can appear) and hence no information will be lost. The permanent function is nothing but the determinant of a matrix but considering all the determinant terms as positive terms.[3]

IV. CONCLUSION

In this paper we have discussed on an interrelationship of mathematics and material science. Graph theory and geometrical representation is a highly adaptable and potent instrument that finds extensive use in material sciences. Atomic Configurations with Geometric Structures

It helps with understanding nanotubes, selection of material in industries. A methodology based on graph theory and matrix approach is suggested which helps in selection of a suitable material from among a large number of available alternative materials These concepts emphasise how important graph theory is to many other fields and how it provides a fundamental basis for multidisciplinary understanding of complex systems.

V. REFERENCES

- [1]. XudongSha, Li Zhao, Mathematical Model and Simulation Calculation Method Based on the Exfoliation of Single-Layer Graphene from Dispersed Carbon Nanotubes, Journal of Nanomaterials, 14 June 2022.
- [2]. Marianna A. Shubov, Miriam Rojas-Arenaza, Mathematical analysis of carbon nanotube model, Journal of Computational and Applied Mathematics, Volume 234, Issue 6, 15 July 2010, Pages 1631-1636.
- [3]. R. Venkata Rao, A material selection model using graph theory and matrix approach, Materials Science and Engineering: A, Volume 431, Issues 1-2, 15 September 2006, Pages 248-255.
- [4]. S. Ikeda and M. Kotani, A New Direction in Mathematics, for Materials Science, SpringerBriefs in the Mathematics of Materials, 2015.
- [5]. S.J. Chen, C.L. Hwang, Fuzzy Multiple Attribute Decision Making- Methods and Applications. Lecture Notes in Economics and Mathematical Systems, Springer-Verlag, Berlin, 1992.

- [6]. M. Deza, M. DutourSikiri'c, Geometry of Chemical Graphs, Encyclopedia of Mathematics and its Applications (Cambridge University Press, Cambridge, 2008)
- [7]. Shunning Li, Zhefeng Chen¹, Zhi Wang, MouyiWeng, Jianyuan Li, Mingzheng Zhang, Jing Lu, Kang Xu and Feng Pan; Graph-based discovery and analysis of atomic-scale one-dimensional materials, National Science Review 9:28, 2022, Advance access publication 26 February 2022

Recent Biological Applications and Chemical Synthesis of Aurones

Dr. Prashant A. Gotmare, Dr. Sanjay V. Kolhe

Department of Chemistry, Shri Shivaji Arts, Commerce and Science College, Akot, Dist.Akola-444101,
Maharashtra, India

ARTICLE INFO

Article History:

Accepted : 01 Jan 2025

Published : 10 Jan 2025

Publication Issue :

Volume 12, Issue 7

January-February-2025

Page Number :

296-301

ABSTRACT

Aurones and their derivatives have garnered significant interest from researchers across the globe. Among the many pharmacologically active molecules that have significant bioactivities and are used in therapeutic medications, they constitute a significant class of chemicals in pharmaceutical chemistry. The heterocyclic aurones derivative was synthesized from chalcone and purity check by TLC. The characterization of aurones derivative was done by IR, H-NMR and mass Spectrometer. Aurones was tested against Mycobacterium TB, Pseudomonas aeruginosa, Escherichia coli, Enterococcus faecalis, Aspergillus niger, and Candida albicans.

Keywords: Aurones, Antimicrobial, Mycobacterium

I. INTRODUCTION

Aurones [2-benzylidenebenzofuran-3(2H)-ones] are naturally occurring secondary metabolites that are structurally isomers of flavones and are found in a wide variety of fruits and flowers, where they significantly contribute to the pigmentation of the plant part in which they are found. It is evident from the study that flavones, chalcones, flavonols, and isoflavones have all been extensively researched for their potential as medicines. For some reason, aurones are still not well understood, and research on these molecules has only lately started.

Harborne has already analyzed the distribution of flavonoids throughout the kingdom of plants [1]. More than 6500 flavonoids have been found thus far, and novel structures are being documented. Flavonoids have a restricted number of skeletal variants (Fig. 1), in contrast to alkaloids or terpenoids, whose skeletons are rich and varied.

This diversity is caused by the substitution pattern, which includes hydroxylation, methoxylation, prenylation, and glycosylation. They are essential dietary components that have a variety of positive health benefits on people, such as preventing heart disease and several types of cancer [2–3].

They most likely have these biological effects because of their metal ion-chelating and free radical-scavenging antioxidant properties [4-6]. Their anticancer potential in various mechanisms of action has been extensively studied [7-11].

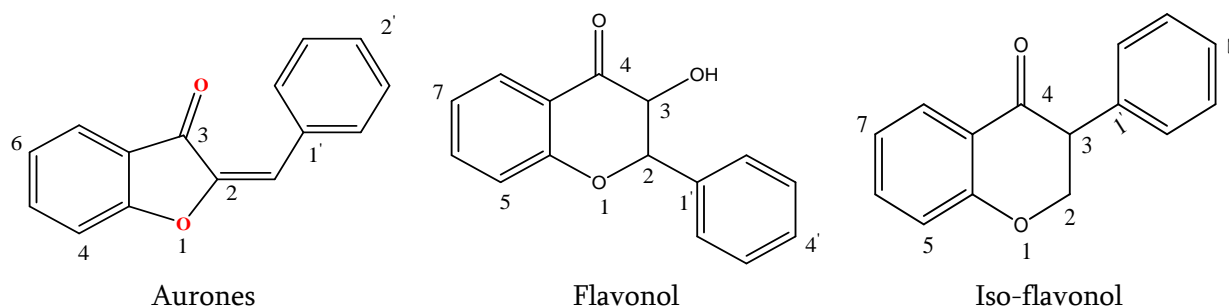


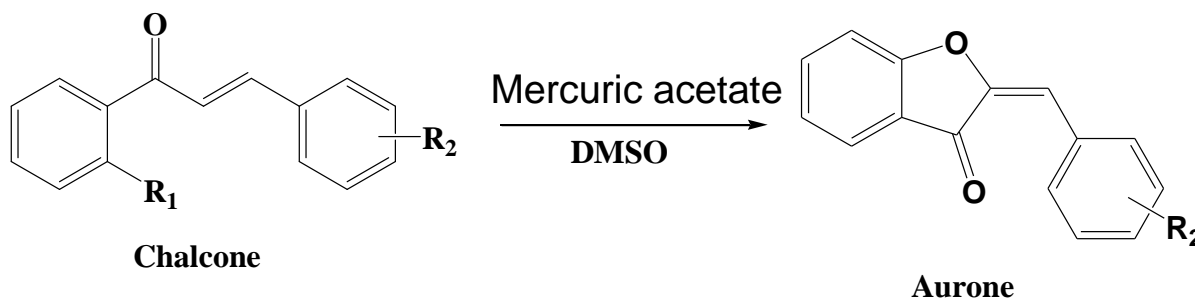
Figure 1. Most important class of flavonoids and numbering of atoms in their molecules

Inhibition of many protein-tyrosine kinases [12], cyclin-dependent kinase [13], protein kinase C [14], topoisomerase [15], aromatase [16,17], and others. Flavones have recently been shown to have antiviral properties in addition to their anticancer effects [18,19]. A number of earlier reviews have examined aurones from various angles. In 2003, Boumendjel examined the biological characteristics and synthesis of aurones [20]. Aurones first isolation from the flowers *Coreopsis grandiflora* by Geissman and Heaton in 1943 [21]. In 2012, groups led by Boumendjel and Kirsch also reported similar reviews [22, 23]. All of the sources in the reviews above, however, date prior to 2013. More intriguingly, in 2017, Boucherle examined the functions and biosynthesis processes of aurones [24]. Furthermore, Yoshihiro and Alsayari examined aurones as biological anticarcinogens in the last two years [25,26].

II. EXPERIMENTAL:

For aurone synthesis, oxidative cyclization of 2'-hydroxychalcones is one of the most popular methods. Due to the structural properties of aurones, there are extremely few alternatives for using various starting materials. Aurones derivative was prepared by simple cyclization process. In this synthesis, the starting materials is 2-hydroxy chalcone which is prepared from equimolar mixture 2-hydroxy acetophenone and benzaldehyde derivatives. The chalcone undergoes cyclization in presence of mercuric acetate with suitable solvent to give aurones derivative.

The solvent like DMSO and pyridine solvents gave good yield of aurones. Characterization of novel synthesized aurones derivative was done by using spectroscopic technique like H-NMR (Bruker Avance Neo 500 MHz), IR (Perkin Elmer -Spectrum RX-IFTIR), mass spectrometry etc.



Sr. No.	Codes	R ₁	R ₂
1	1A	OH	H

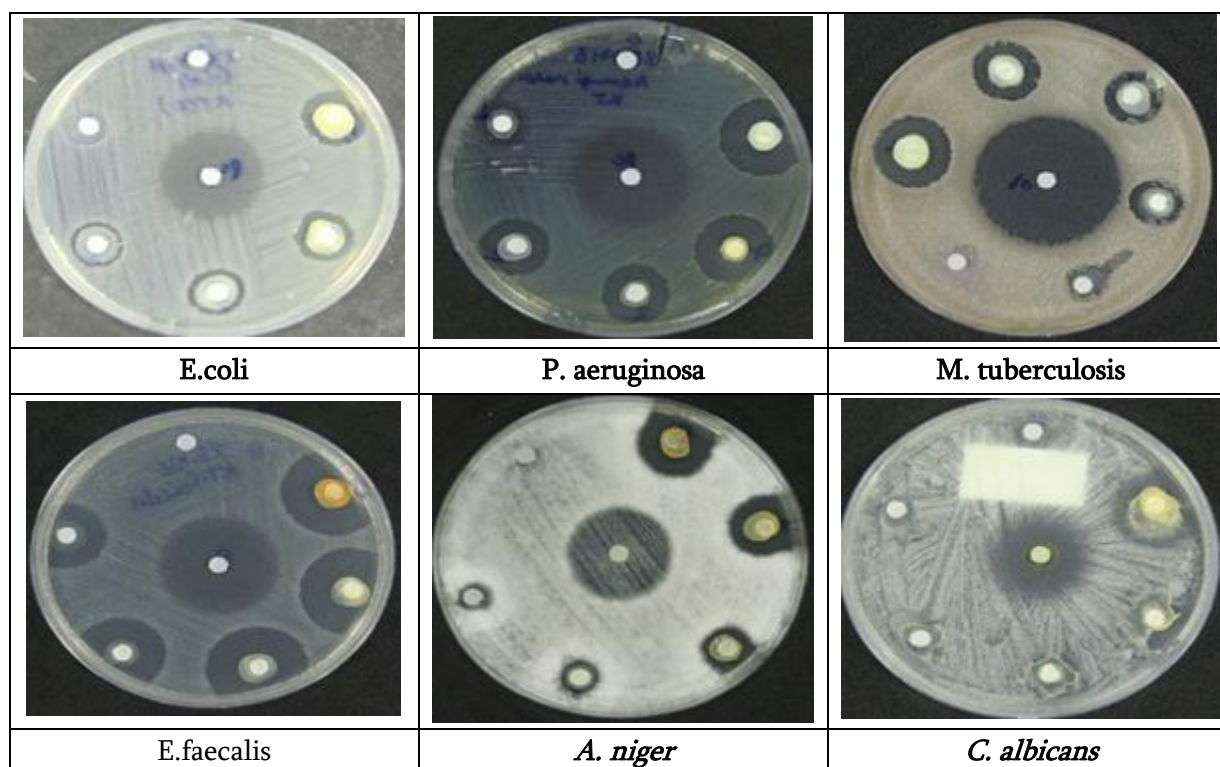
Properties of (Z)-2-benzylidenebenzofuran-3(2H)-one (1A)

Mol. Formula C₁₅H₁₀O₂ : Pale Yellowish Crystalline solid. m. p. 137 °C, yield 81 %, **Elemental analysis** (%): C, 81.07; H, 4.54; O, 14.40) **IR** (KBr **cm**⁻¹) Ar-H (Stret.) at 2933.85, C=O at 1635.71, conjugated C=C at 1547.94 and Ar-C=C at 1384.95. **ESI-MS** [M+H]⁺ Cal. Mol. Wt.: 222.24, Found M/Z: 222.07; **¹H-NMR** (δ ppm) 500 MHz DMSO-d₆: Ar-H 7.810–7.022 and ethylenic protons 3.832.

III. RESULTS & DISCUSSION

Numerous antimicrobial medications that treat a range of infectious diseases have been created and put on the market globally since the late 19th and early 20th centuries. Their purpose is to either eliminate or reduce the activity of microorganisms. Among them are medications that fight bacteria, viruses, fungi, and parasites. The antibacterial qualities of the aurone derivatives were evaluated using a few bacteria and fungi. The antibacterial qualities of a number of common pathogens have been examined, including *Escherichia coli*, *Pseudomonas aeruginosa*, *Mycobacterium tuberculosis*, *Enterococcus faecalis*, *Aspergillus niger*, and *Candida albicans*.

Compounds	Zone of Inhibition <i>Escherichia coli</i>	Zone of Inhibition <i>Pseudomonas aeruginosa</i>	Zone of Inhibition <i>Mycobacterium tuberculosis</i>	Zone of Inhibition <i>Enterococcus faecalis</i>	Zone of Inhibition <i>Aspergillus niger</i>	Zone of Inhibition <i>Candida albicans</i>
1A	08	12	11	18	12	08



The capacity to prevent infections in a variety of bacterial and fungal agents (mycoses) has been assessed by utilizing enzyme- or cell-based inhibition or by monitoring the growth of the bacterial or fungal organism. For their antibacterial properties against *Escherichia coli*, *Pseudomonas aeruginosa*, *Mycobacterium tuberculosis*, *Enterococcus faecalis*, *Aspergillus niger*, and *Candida albicans*, a number of aurones were created, produced, and tested. The findings showed that a derivative of aurones exhibited increased action against the fungus *A. niger* and the Gram-negative bacteria *Enterococcus faecalis*.

IV. CONCLUSION

In this work, we report the effective synthesis of aurone derivative and evaluated antimicrobial property. Among the derivative possessing preliminary antimicrobial activity, mainly directed against *Mycobacterium tuberculosis*, *Enterococcus faecalis*, *Aspergillus niger*, and *Candida albicans*. Interestingly, compound very active against *Enterococcus faecalis* and fungus *A. niger*.

Conflicts of interest

The authors declare there is no conflict of interest.

V. ACKNOWLEDGEMENTS

The authors would like to thank Department of chemistry, Shri Shivaji Arts Commerce and Science College, Akot for providing lab equipment's. Also thankful to Shri Gajanan Ingle sir for his cooperation. The authors extend their appreciation to Chhatrapati Shahu Maharaj Research, Training And Human Development Institute (SARTHI), for financial support in the form of Fellowship (CSMNRF-2022). Authors are also thankful to CIL and SAIF, Panjab University, Chandigarh for providing spectral data.

VI. REFERENCES

- [1]. Harborne, J. B., & Williams, C. A. (2000). Advances in flavonoid research since 1992. *Phytochemistry*, 55(6), 481–504. [https://doi.org/10.1016/s0031-9422\(00\)00235-1](https://doi.org/10.1016/s0031-9422(00)00235-1)
- [2]. Formica, J., & Regelson, W. (1995). Review of the biology of quercetin and related bioflavonoids. *Food and Chemical Toxicology*, 33(12), 1061–1080. [https://doi.org/10.1016/0278-6915\(95\)00077-1](https://doi.org/10.1016/0278-6915(95)00077-1)
- [3]. Roger, C. R. (1988). The nutritional incidence of flavonoids: some physiological and metabolic considerations. *Experientia*, 44(9), 725–733. <https://doi.org/10.1007/bf01959142>
- [4]. Cotellet, N., Bernier, J., Henichart, J., Catteau, J., Gaydou, E., & Wallet, J. (1992). Scavenger and antioxidant properties of ten synthetic flavones. *Free Radical Biology and Medicine*, 13(3), 211–219. [https://doi.org/10.1016/0891-5849\(92\)90017-b](https://doi.org/10.1016/0891-5849(92)90017-b)
- [5]. Jaeger, A., Wälti, M., & Neftel, K. (1988). Side effects of flavonoids in medical practice. *Progress in clinical and biological research*, 280, 379–394.
- [6]. Beretz, A., & Cazenave, J. P. (1988). The effect of flavonoids on blood-vessel wall interactions. *Progress in clinical and biological research*, 280, 187–200.
- [7]. Double, J. A., Bibby, M. C., & Loadman, P. M. (1987). Pharmacokinetics and anti-tumour activity of LM985 in mice bearing transplantable adenocarcinomas of the colon. *British Journal of Cancer*, 54(4), 595–600. <https://doi.org/10.1038/bjc.1986.214>

- [8]. Hayashi, T., Uchida, K., Hayashi, K., Niwayama, S., & Morita, N. (1988). A cytotoxic flavone from *Scopariadulcis* L. *Chemical and Pharmaceutical Bulletin*, 36(12), 4849–4851. <https://doi.org/10.1248/cpb.36.4849>
- [9]. Cushman, M., & Nagarathnam, D. (1991). Cytotoxicities of some flavonoid analogues. *Journal of Natural Products*, 54(6), 1656–1660. <https://doi.org/10.1021/np50078a027>
- [10]. Wang, H., Xia, Y., Yang, Z., Natschke, S. L. M., & Lee, K. (1998). Recent Advances in the Discovery and Development of Flavonoids and their Analogues as Antitumor and Anti-HIV Agents. *Advances in Experimental Medicine and Biology*, 191–225. https://doi.org/10.1007/978-1-4615-5335-9_15
- [11]. Choi, S. U., Ryu, S. Y., Yoon, S. K., Jung, N. P., Park, S. H., Kim, K. H., Choi, E. J., & Lee, C. O. (1999). Effects of flavonoids on the growth and cell cycle of cancer cells. *Anticancer research*, 19(6B), 5229–5233.
- [12]. Cushman, M., Zhu, H., Geahlen, R. L., & Kraker, A. J. (1994). Synthesis and Biochemical Evaluation of a Series of Aminoflavones as Potential Inhibitors of Protein-Tyrosine Kinases p56lck, EGFr, and p60v-src. *Journal of Medicinal Chemistry*, 37(20), 3353–3362. <https://doi.org/10.1021/jm00046a020>
- [13]. Sedlacek, H., Czech, J., Naik, R., Kaur, G., Worland, P., Losiewicz, M., Parker, B., Carlson, B., Smith, A., Senderowicz, A., & Sausville, E. (1996). Flavopiridol (L86 8275; NSC 649890), a new kinase inhibitor for tumor therapy. *International Journal of Oncology*. <https://doi.org/10.3892/ijo.9.6.1143>
- [14]. Ferriola, P. C., Cody, V., & Middleton, E. (1989). Protein kinase C inhibition by plant flavonoids. *Biochemical Pharmacology*, 38(10), 1617–1624. [https://doi.org/10.1016/0006-2952\(89\)90309-2](https://doi.org/10.1016/0006-2952(89)90309-2)
- [15]. Yoshinori, Y., Sho-Zou, K., & Hirofumi, N. (1990). Induction of mammalian topoisomerase ii dependent dna cleavage by nonintercalative flavonoids, genistein and orobol. *Biochemical Pharmacology*, 39(4), 737–744. [https://doi.org/10.1016/0006-2952\(90\)90153-c](https://doi.org/10.1016/0006-2952(90)90153-c)
- [16]. Campbell, D. R., & Kurzer, M. S. (1993). Flavonoid inhibition of aromatase enzyme activity in human preadipocytes. *The Journal of Steroid Biochemistry and Molecular Biology*, 46(3), 381–388. [https://doi.org/10.1016/0960-0760\(93\)90228-o](https://doi.org/10.1016/0960-0760(93)90228-o)
- [17]. Ibrahim, A., & Abul-Hajj, Y. J. (1990). Aromatase inhibition by flavonoids. *The Journal of Steroid Biochemistry and Molecular Biology*, 37(2), 257–260. [https://doi.org/10.1016/0960-0760\(90\)90335-i](https://doi.org/10.1016/0960-0760(90)90335-i)
- [18]. Wagner H. (1986). Antihepatotoxic flavonoids. *Progress in clinical and biological research*, 213, 545–558.
- [19]. Selway J. W. (1986). Antiviral activity of flavones and flavans. *Progress in clinical and biological research*, 213, 521–536.
- [20]. Boumendjel, A. (2003). [General Articles] Aurones: A Subclass of Flavones with Promising Biological Potential. *Current Medicinal Chemistry*, 10(23), 2621–2630. <https://doi.org/10.2174/0929867033456468>
- [21]. Geissman, T. A., & Heaton, C. D. (1943). Anthochlor Pigments. IV. The Pigments of *Coreopsis grandiflora*, Nutt. I. *Journal of the American Chemical Society*, 65(4), 677–683.
- [22]. Haudecoeur, R., & Boumendjel, A. (2012). Recent advances in the medicinal chemistry of aurones. *Current Medicinal Chemistry*, 19(18), 2861–2875. <https://doi.org/10.2174/092986712800672085>
- [23]. Zwergel, C., Gaascht, F., Valente, S., Diederich, M., Bagrel, D., & Kirsch, G. (2012). Aurones: interesting natural and synthetic compounds with emerging biological potential. *Natural product communications*, 7(3), 389–394.
- [24]. Boucherle, B., Peuchmaur, M., Boumendjel, A., & Haudecoeur, R. (2017). Occurrences, biosynthesis and properties of aurones as high-end evolutionary products. *Phytochemistry*, 142, 92–111. <https://doi.org/10.1016/j.phytochem.2017.06.017>

- [25]. Uesawa, Y., Sakagami, H., Ikezoe, N., Takao, K., Kagaya, H., & Sugita, Y. (2017). Quantitative Structure–Cytotoxicity relationship of aurones. *Anticancer Research*, 37(11). <https://doi.org/10.21873/anticancer.12066>
- [26]. Alsayari, A., Muhsinah, A. B., Hassan, M. Z., Ahsan, M. J., Alshehri, J. A., & Begum, N. (2019). Aurone: A biologically attractive scaffold as anticancer agent. *European Journal of Medicinal Chemistry*, 166, 417–431. <https://doi.org/10.1016/j.ejmech.2019.01.078>

Rosa Rubiginosa Mediated Green Synthesis of Silver Nanoparticles

Prashant B. Lihitkar, Panu Upare

Department of Chemistry, Lokmanya Tilak Mahavidyalaya, Wani, Maharashtra, India

ARTICLE INFO

Article History:

Accepted : 01 Jan 2025

Published : 10 Jan 2025

Publication Issue :

Volume 12, Issue 7

January-February-2025

Page Number :

302-310

ABSTRACT

In the present study, silver nanoparticles were synthesized via the green process, which is simple, cost-effective, eco-friendly, and non-toxic. The Silver nanoparticles have been known for its inhibitory and bactericidal effect. Rose plant is having so many medicinal properties which makes it useful in blood purification, in anti-inflammatory and aphrodisiac action. Our prime goal is to make use of phytochemicals obtained from rose petal extract to synthesize Ag nanoparticles which could be stable and biocompatible in medical applications. During the green synthesis method, rosa rubiginosa petal extract was prepared by simple heating in aqueous medium which act as a reducing and capping agent. The effect of concentration of extract, synthesis time and pH of the medium on the formation of Ag nanoparticles is investigated. The phytochemical analysis of Rosa rubiginosa petal extract shows the presence of flavonoids, alkaloids, terpenoids, quinones, sugars and phenols etc. Formation of silver nanoparticles was confirmed by the visual change in the colour of the solution from pale yellow to brown. Surface plasmon resonance of synthesized silver nanoparticles were observed at two different wavelengths viz 420 nm and 640 nm may be due to the formation of spherical as well as triangular shape nanoparticles. Absorption peak observed in rose extract at 510 nm is disappeared in Ag nanoparticles absorption spectra indicates phytochemical interaction with Ag ions. The intensity of SPR maxima due to Ag nanoparticles is increasing with the time. The varying extract to 0.1M Ag salt volume ratio for Ag nanoparticles synthesis shows that 1:2 and 2:1 ratio is more stable and shows consistency in the increase of absorption intensity. The pH measurement shows that pH of rose extract (7.8) is close to the pH of Ag nanoparticles prepared for 1:2 (7.6) and 2:1(7.7) ratio. This shows that slight basic pH of the extract is prone to favorable for nucleation and

growth of Ag nanoparticles. In acidic pH and higher basic pH, Ag nanoparticles are found to be unstable.

Keyword:- Silver nanoparticles, Rosa Rubiginosa extract, Green process, Extraction, Surface plasmon resonance.

I. INTRODUCTION

Silver nanoparticles are tiny particles of silver with dimensions typically ranging from 1 to 100 nanometer. Nanosized metallic particles are unique and can considerably change physical, chemical, and biological properties due to their surface-to-volume ratio; therefore, these nanoparticles have been exploited for various purposes. Silver nanoparticles (AgNPs) are increasingly used in various fields, including medical, food, health care, consumer, and industrial purposes, due to their unique physical and chemical properties [1-3].

To fulfill the requirement of AgNPs, various methods have been adopted for synthesis [1-7]. Generally, conventional physical and chemical methods seem to be very expensive and hazardous. Interestingly, biologically-prepared AgNPs show high yield, solubility, and high stability. Among several synthetic methods for AgNPs, biological methods seem to be simple, rapid, non-toxic, dependable, and green approaches that can produce well-defined size and morphology under optimized conditions for translational research. In the end, a green chemistry approach for the synthesis of AgNPs shows much promise.

Silver nanoparticles are often synthesized through various methods including chemical reduction processes [8]. They can be used for various applications due to their unique properties. Silver nanoparticles can be synthesized from the Rosa Rubiginosa petals using a green synthesis approach. This involves extracting phytochemicals from rose petals and using them to reduce silver ions into silver nanoparticles, it is an environmentally friendly method you need access to laboratory or specialized equipment to carry out this synthesis.

Rosa rubiginosa, has fragrant petals that can be used for various purposes. The petals can be used in aromatherapy to create rose scented oils, potpourri or sachets. Rose petals can be dried and used to make a fragrant and mildly sweet rose petal tea. It is known for its potential antioxidant properties [1]. Rose plant having so many medicinal properties, which makes it very useful as a blood purifier. Anti-inflammatory and aphrodisiac action, of this plant is effective in various health issues like in intestinal user diarrhea etc. In Ayurveda whole plant has been used for medicinal purpose. The flowers and leaves of this plant comprises 1.3% and 8.5% of a saponin respectively [3]. Petal consists of a methionine sulfoxide. The volatile oil obtained from the flowers possesses citronellol, geraniol nerol, phenyl ethanol. The whole plant produces quercetin, kaempferol and cyaniding. The rose hip (fruit) good in vitamin C, Malic acid and citric acid.

Origin of Problem: Traditional production of nanoparticles comprises expensive chemical and physical processes that frequently use poisonous ingredient having potential threats, such as carcinogenicity, cytotoxicity and environmental toxicity. To prevent undesirable accumulation of the collides, reducing agents, organic solvents and stabilizers are used. Green chemistry also known as reduce chemistry, eliminates or reduce the production of hazardous substances. The products created through green chemistry are sustainable and do not affect the environment.

II. MATERIALS AND METHODS:

Fresh roses (*Rosa-rubiginosa*) were procured from the local market, Wani, India. Silver nitrate, Ferric chloride, Sulfuric acid, Sodium hydroxide, Potassium hydroxide etc.

Preparation of Rosa-rubiginosa extract: - The rose petals are washed thoroughly with deionized water. The extraction process consists of taking one gram of wet petals in 100 ml of deionized water into a 250 ml Erlenmeyer flask. This mixture was slowly stirred using a magnetic stirrer at 80°C for 1 hr. Further, this solution was filtered, cooled, and stored in dark for further experiments. This solution served as 100% extract concentration.

Green Synthesis of Silver Nanoparticles:

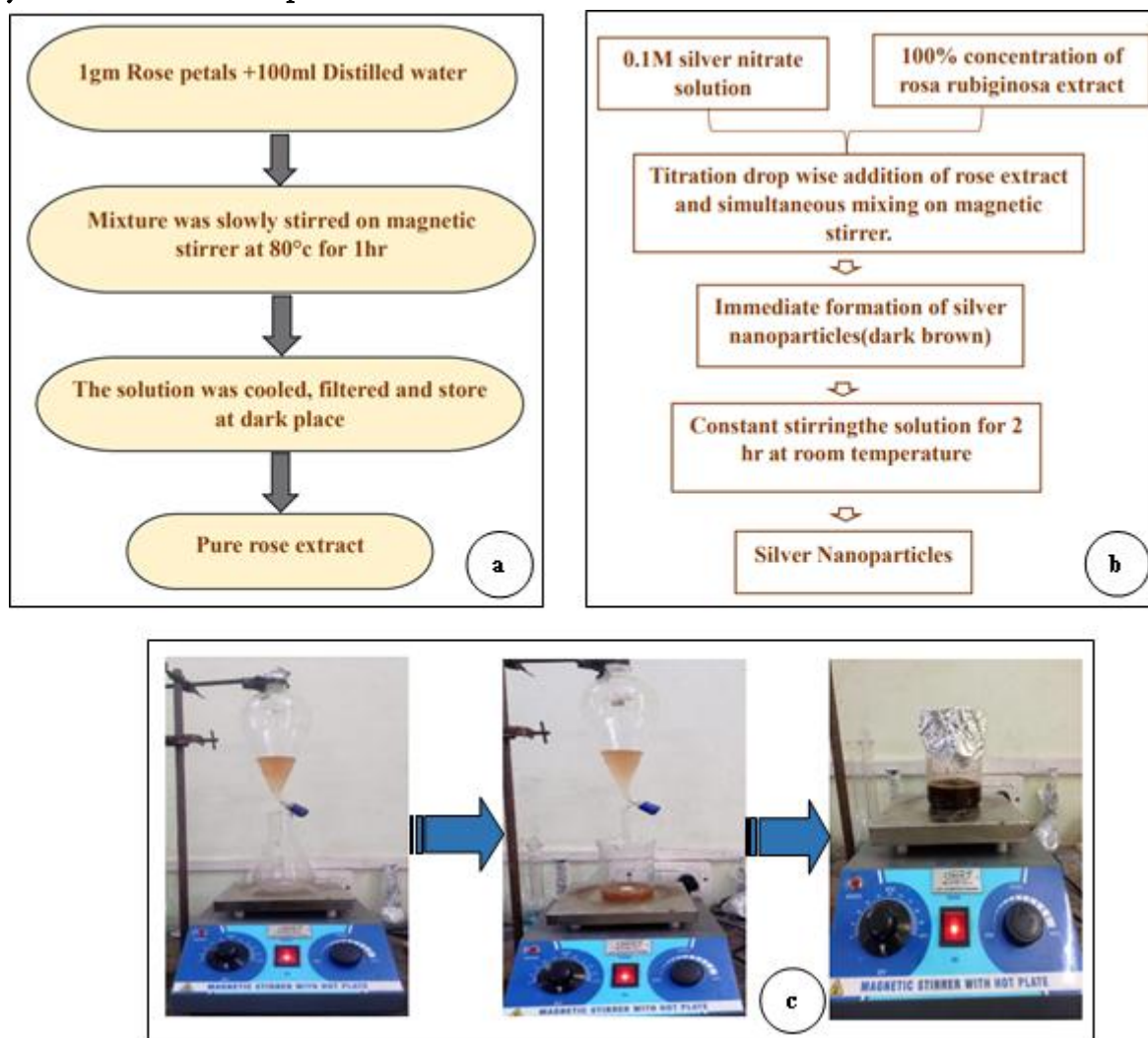


Figure 1: a) Shows the flowchart for the synthesis of rose extract, b) shows the flowchart for the synthesis of Ag nanoparticles using rose extract and c) shows the image of experimental setup of Ag nanoparticles synthesis and observed color change of the solution.

In this method of experimentation, only one experimental factor varied at a time, while keeping all the other variables constant. In pure rose extract. 0.1M silver nitrate solution was added dropwise in 1:2 volume ratio and stirred for 30 minutes in dark condition at room temperature. In another process parameter, the reduction reaction carried out by varying the different volume ratios of rose extract and 0.1M silver nitrate solution (1:1, 1:2, 1:3, 1:4 & 2:1) at 100% extract concentration while keeping all other variable constant.

To study the effect of time on interaction between the rose extract and silver nitrate solution 0.1M silver nitrate solution and 100% rose extract was added together in 1:2 ratio and incubated for different time parameter in hours (i.e. 0.5, 1, 2, 24, 48 etc).

III. EXPERIMENTAL:

Phytochemicals Analysis of Rosa Rubiginosa Extract: Ergoline alkaloids, indolizidine alkaloids, benzenoids and phenolic compounds in extracts of rosa rubiginosa extract were shown to reduce and stabilize AgNPs.

Test for Alkaloids: In 2 ml of plant extract taken in glass test tube, 2 ml of concentrated HCl was added. Then few drops of Mayer's reagent were added and Shaked the test-tube lightly. Appearance of green color is observed indicates the presence of alkaloids.

Test for Terpenoids: In 0.5 ml of extract taken in test tube, 2 ml of CHCl₃ was added. Further concentrated H₂SO₄ was added carefully and mixed the solution for 2 minutes. Appearance of red brown color at the interface was observed which indicates the presence of terpenoids.

Test for Tannins: 1ml of extract was taken in glass test tube in which 2 ml of 5% FeCl₃ solution was added. Appearance of dark blue or greenish black color of the solution is observed indicates the presence of tannins.

Test for Flavonoids: 2 ml of extract was taken in the glass test tube. Then 1ml of 2N NaOH solution was slowly added. Presence of yellow color indicates the presence of flavonoids.



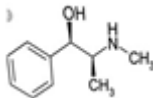


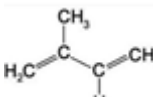


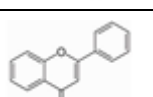


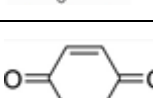
Test for Proteins: In 2 ml of plant extract taken in test tube, few drops of 0.2% Ninhydrin was added and heated for 5 minutes. Appearance of blue color was not observed indicates the absence of proteins.

Test for Quinones: In 1 ml of rose extract, 1 ml of concentrated H₂SO₄ was added. Formation of red color indicates the presence of quinones.

Test for Sugar: In 1 ml of rose extract, 1 ml of iodine salt was added in a test tube and is mixed properly. The appearance of a deep colors precipitate indicates the presence of sugar.

Test for Glycoside: In 2 ml of rose extract taken in test tube, 3 ml of CHCl₃ and 10% ammonia Solution was added. Appearance of pink color indicates the presence of glycosides.

Test for Phenol: To 1ml of the rose extract, 2 ml of distilled water followed by few drops of 10% FeCl₃ was added. Formation of blue or green color indicates the presence of phenols.

Sr. No.	Name of Phytochemical	Color Observations		Conclusion	Possible structure	Functional group present
		Before	After			
1	Alkaloids			Present		O-H, N-H
2	Terpenoids			Present		C=C
3	Flavonoids			Present		C=O, -O -
4	Quinones			Present		C=O



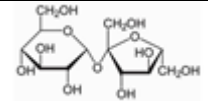


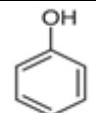
Sr. No.	Name of Phytochemical	Color Observations		Conclusion	Possible structure	Functional group present
		Before	After			
5	Sugar			Present		O-H, -O-
6	Phenol			Present		O-H

Table 1: Phytochemical test analysis of the rose extract for the presence of various biomolecules and possible structure and functional group present in the extract.

IV.RESULT AND DISCUSSIONS:

It has been reported that plants enriched with a high range of biomolecules such as Terpenoids, flavonoids, and tannins can reduce the silver ions to nano-scale particles [9]. Our phytochemical analysis study shows that rose extract contains the biomolecules like Alkaloids, Terpenoids, Flavonoids, Quinones, Sugar, Phenol etc. These biomolecules act as a reducing agent and capping agent for the formation of Ag nanoparticles [9]. Ag nanoparticles were synthesized by using freshly prepared rose extract without dilution. The effect of various parameter like concentration ratio of extract to Ag salt concentration and effect of time on formation of Ag nanoparticles are also studied. pH of Ag salt, rose extract and Ag nanoparticles is measured for various concentration ratio.

A) Effect of concentration ratio of Ag salt to rose extract.

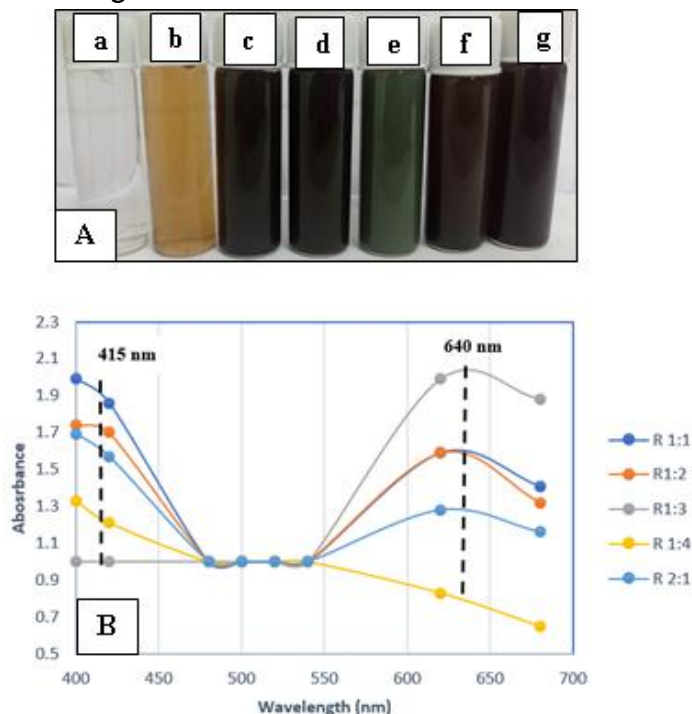


Fig. 2. A) Photo of a) AgNO₃ salt, b) rose extract and Ag nanoparticles for volume ratio of AgNO₃: Extract c) 1:1, d) 1:2, e) 1:3, f) 1:4 and g) 2:1. **B)** Absorption spectra of Silver Nanoparticles prepared for various ratio (1:1, 1:2, 1:3, 1:4, 2:1) taken after the 24 hrs using 0.1M of the AgNO₃ solution.

The size, shape, and extent of silver nanoparticles synthesis are highly dependent on the concentration of silver ion. It was found that the most frequently used silver metal salt concentration was 0.1M [1-6]. The absorption spectra of silver nanoparticles are taken for different volume ratio of petal extract to AgNO₃ solution (1:1, 1:2, 1:3, 1:4, 2:1) shows variation in the intensity of absorption maxima (figure 2B) at 415 nm and 640 nm. The absorption of Ag nanoparticles solution for 1:3 and 1:4 shows unusual changes in absorption maxima. Absorption peak at 415 nm is absent in the absorption spectrum of Ag nanoparticles with 1:3 ratio whereas absorption peak at 640 nm is absent in the Ag nanoparticles with 1:4 ratio. This unusual observation may be correlated with spherical shape Ag agglomeration is formed for 1:4 ratio while triangular shape of Ag nanoparticles is confined in nano dimension for 1:4 ratio. It can also be noted that the increase in the petal extract concentration from 1:1 to 1:4 ratio (50% to 80%) intensity of absorption maxima at 415 nm is decreasing may be due to agglomeration of Ag⁺ ions by excessive phytochemicals without their reduction [9-10]. Many researchers reported that the concentration of plant extract modulates particle size and morphology of nanoparticles [9]. As concentration increases, higher numbers of stable nuclei were formed due to enough reductants reacted with silver ions. However, at higher concentration, nucleation takes place faster and unstable nuclei formed react with free silver ions present in reaction mixture resulting in large-sized silver nanoparticles.

The image shown in figure 2A-e is for 1:3 ratio showing dark greenish color which is different from the color of Ag nanoparticles with other ratios. This supports with its single absorption maxima at 640 nm may be for only triangular shape Ag nanoparticles formation.

Effect of reaction time:

Reaction time is another crucial parameter that affects the synthesis of silver nanoparticles. The color change from yellow to brown and an SPR peak in range 400 – 420 nm indicates the formation of Ag nanoparticles. To ensure the complete consumption of silver ion, reaction time plays an important role. The shape and size of the nanoparticles could be controlled by varying the reaction time for the reaction mixture [9-10]. Generally, the intensity of the absorbance peak enhanced over time, due to an increase in the number of nanoparticles. The 0.1M of Silver Nitrate solution and the 100% concentration of rosa rubiginosa extract was used to prepare different volume ratios (1:1, 1:2, 1:3, 1:4, 2:1). The absorption was measured for different time parameter viz. 0.5 hr, 1hr, 2hrs, 24hrs, 48hrs.

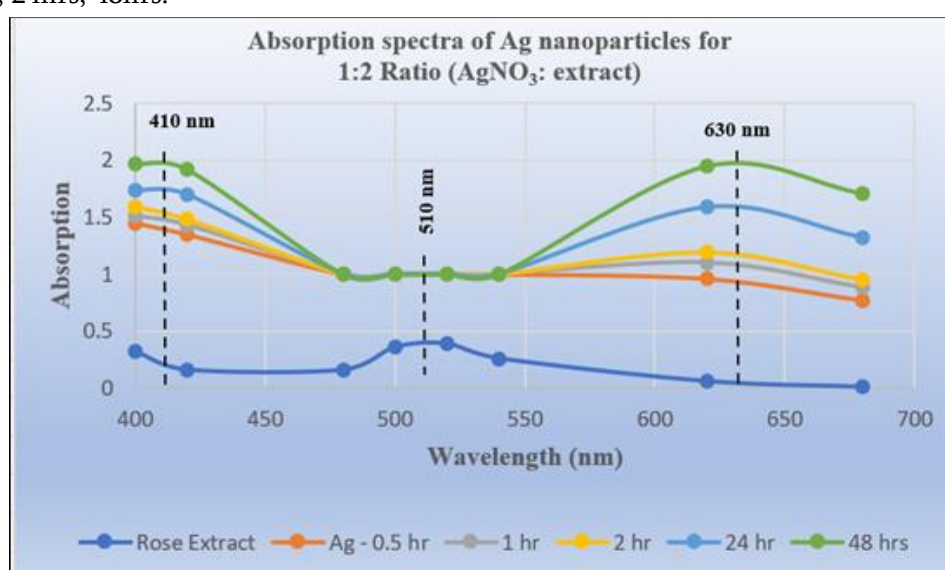


Fig 3: Absorption spectra of Rose extract and Ag nanoparticles for (1:2 ratio) taken at different time intervals viz. 0.5 hr, 1 hr, 2 hrs, 24 hrs, 48 hrs.

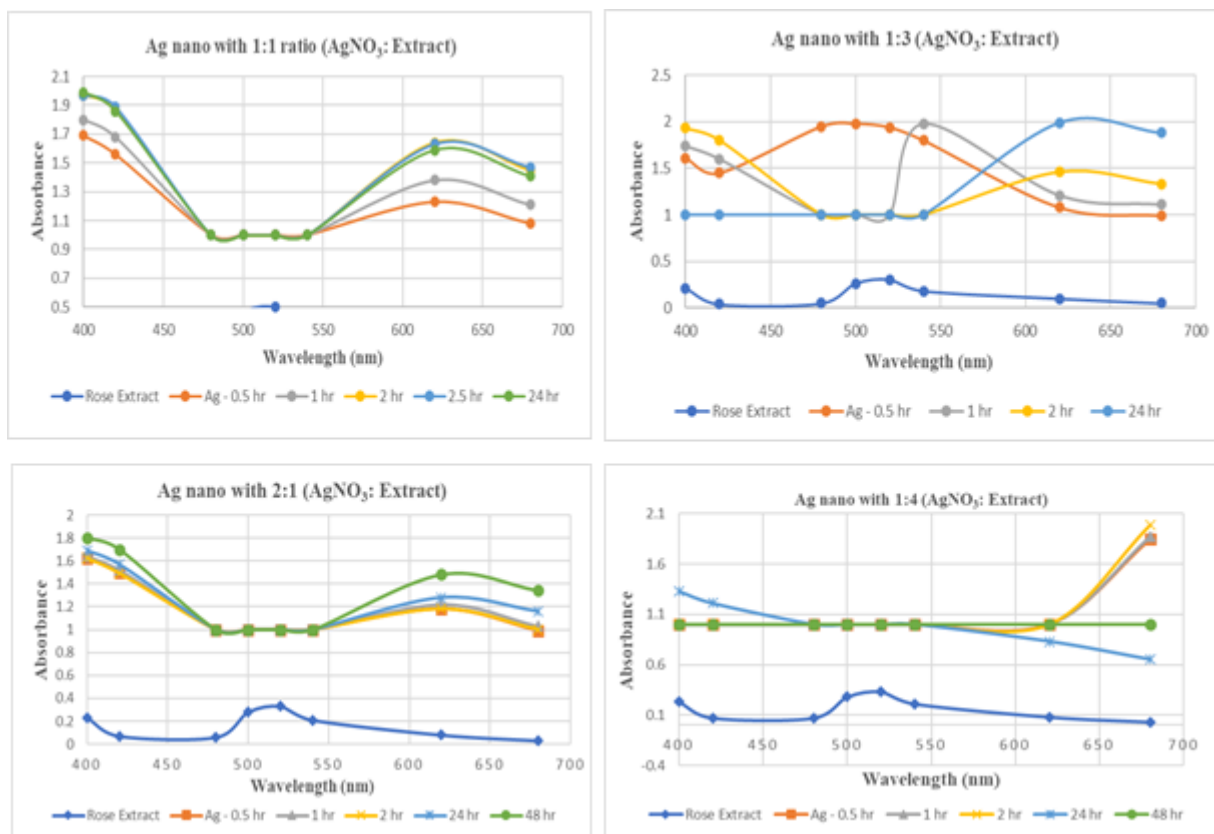


Figure 4: Effect of time parameter on Absorption spectra of Ag nanoparticles for various ratios A) 1:1 B) 2: 1, C) 1:3 and D) 1:4 ratios

Effect of pH:

The pH of the reaction mixture has a significant effect on the growth of silver Nanoparticles as it alters the electrical charges of biomolecules probably affecting their reducing and capping properties [10]. The formation of nucleation centers, the activity of phytochemicals presents in flower extract, and rate of reduction of a metal salt are highly influenced by the pH of the solution resulting in change in shape and size of the nanoparticles [8]. Rapid formation of nanoparticles at neutral/basic pH is probably due to ionization of phenolic groups present in flower extract.

Sr. No	Type of Sample/Solution	% of extract	Measured pH
1	0.1M AgNO ₃	0	5.3
2	Rose petal Extract	100	7.8
3	1:1(AgNO ₃ : Extract)	50	6.3
4	1:2(AgNO ₃ : Extract)	66	7.7
5	1:3(AgNO ₃ : Extract)	75	8.2
6	1:4(AgNO ₃ : Extract)	80	8.1
7	2:1(AgNO ₃ : Extract)	33	7.6

Table 2: pH measurement data of various solutions like AgNO₃ salt solution, Rose extract and Ag nanoparticles prepared using various ratio.

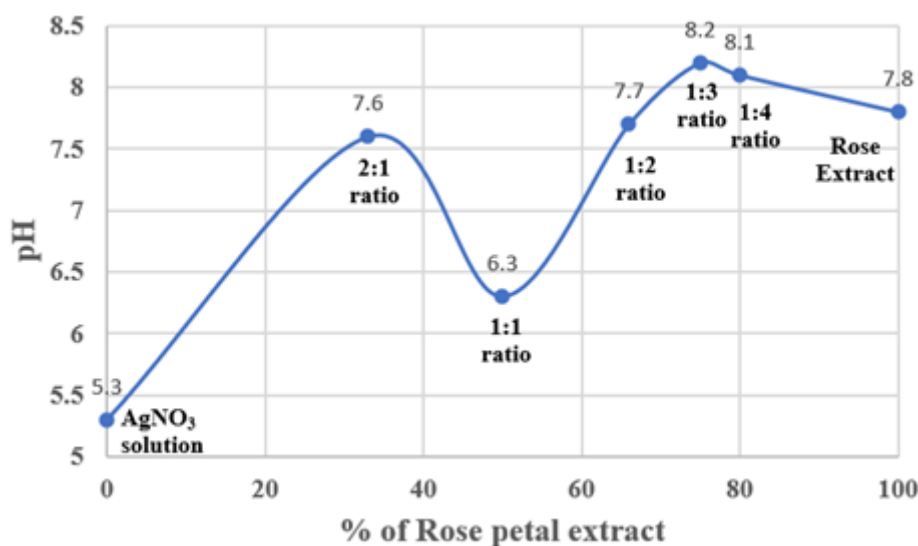


Figure 5: Variation effect of rose extract on pH of Ag nanoparticles for various ratios.

The curve in the figure 5 and data in the table 2 shows that pH of Ag nanoparticles changes with change in the concentration of extract in the various volume ratio. The pH of Ag nanoparticle solution prepared for 1:1 volume ratio is in acidic region where as for other volume ratio it is in basic region. Basic pH is found to be prone to formation of stable colloid of Ag nanoparticles. pH of Ag nanoparticles prepared at 1:2 and 2:1 ratio is almost same with the pH of rose extract and the nanoparticles prepared at this ratio are found to be more stable. This may be due to binding capability of phytochemicals present in the extract is more favorable at the same pH of extract solution.

V. CONCLUSION:

In the conclusion, Ag nanoparticles have been prepared using Rose Rubiginosa extract successfully by an economical, efficient, and eco-friendly process. The absorption spectra of Ag nanoparticles shows that absorption intensity increases with an increase in the concentration of extract. Two surface plasmon resonance peak at 420 nm and 640 nm in the absorption spectra may be associated with formation of spherical shape along with the triangular shape of Ag nanoparticles. The study of various ratio of Ag salt: rose extract indicates that 1:2 and 2:1 ratio gives stable Ag nanoparticles formation at which pH of the medium is almost same with pH of rose extract as observed from the pH measurement. The formation of Ag nanoparticles is also confirmed from the visual change in the color of the solution. Slight basic pH of the extract is prone to favorable for nucleation and growth of Ag nanoparticles. In acidic pH and higher basic pH, Ag nanoparticles are found to be unstable.

VI. REFERENCES

- [1]. Rapid synthesis of biocompatible silver nanoparticles using aqueous extract of Rosa damascena petals and evaluation of their anticancer activity, B. Venkatesan, V. Subramanian, A. Tumala, E. Vellaichamg, Asian Pac J Trop Med (2014) 7(1) S294.
- [2]. Green synthesis of silver chloride Nanoparticles by using rosa macdub petal extract Siddhiprada Shete, Shriya Shende, Ketaki Bhagwat, Sharada Dagade, Neelima Deshpande and Shobha Waghmode, International Journal of Biosciences and Nano sciences (2014) 1(5), 96.

- [3]. Size dependent Antibacterial, Antidiabetic and Toxicity of Silver nanoparticles synthesized using solvent extraction of *Rosa indica* L. Petal, Satheesh Kumar Balu, Swetha Andra, Fouad Damiri, Anandhi Sivaraalingam, Manisha Vidyavathy Sudandradoss, Karthikeyan Kumarasamy, Kishore Bhakthavachalam, Faruat Ali, Milton Kumar Kundu, MD. Habibur Rahman, Mohammad Berrada and Simona Cavalu, *Pharmaceuticals* (2022) 15(6), 689
- [4]. Synthesis of silver nanoparticles by silver salt reduction and its characterization, Muhammad Muzamil, Naveed Khalid, M. Danish Aziz and S. Anu Abbas., *Materials Science and Engineering* (2014) 60, 012034.
- [5]. Biosynthesis of Silver Nanoparticles Using *Cucumis prophetarum* Aqueous Leaf Extract and Their Antibacterial and Antiproliferative Activity Against Cancer Cell Lines, Hemlata, Prem Raj Meena, Arvind Pratap Singh, and Kiran Kumar Tejavath, *ACS Omega* (2020) 5(10), 5520.
- [6]. Metal nanoparticles fabricated by green chemistry using natural extracts: biosynthesis, mechanisms and applications, Hesham R. El-Seedi, Rehan M. El-Shabasy, de Shaden A. M. Khalifa, Aamer Saeed, Afzal Shah, Raza Shah, Faiza Jan Iftikhar, Mohamed M. Abdel Daim, Abdelfatteh Omri, Nahid H. Hajrahand, Jamal S. M. Sabir, Xiaobo Zou, Mohammed F. Halabi, Wessam Sarhann and Weisheng Guo, *RSC Adv.*, (2019) 9, 24539.
- [7]. Characterization of silver nanoparticles by green synthesis method using *Petalium murex* leaf extract and their antibacterial activity, K. Anandalakshmi, J. Venugobal, V. Ramasamy, *Appl Nanosci* (2016) 6, 399.
- [8]. A Systematic Study of the Synthesis of Silver Nanoplates: Is Citrate a “Magic” Reagent? Qiao Zhang, Na Li, James Goebel, Zhenda Lu, and Yadong Yin, *J. Am. Chem. Soc.* (2011) 133, 18931.
- [9]. Controllable synthesis of silver nanoparticles using Neem leaves and their antimicrobial activity, Aparajita Verma, Mohan Singh Mehata, *Journal of Radiation Research and Applied Sciences* (2016) 9 109.
- [10]. Green synthesis of silver nanoparticles using the plant extract of *Salvia spinosa* grown in vitro and their antibacterial activity assessment, Saba Pirtarighat, Maryam Ghannadnia, Saeid Baghshahi, *Journal of Nanostructure in Chemistry* (2019) 9, 1.

Multi-Decadal Changes of Konkan Region Mangrove Forest Coast of Maharashtra and Its Response to the Tidal Dynamics, Spatial and Temporal Changes

Pund A. R., Nirbhavane A. M., Dr. Kurhe A. R

Department of Zoology, Padmashri Vikhe Patil College of Arts, Science and Commerce, Pravaranagar, Loni, Tal- Rahata, Dist. Ahmednagar, Maharashtra, India

ARTICLE INFO

Article History:

Accepted : 01 Jan 2025

Published : 10 Jan 2025

Publication Issue :

Volume 12, Issue 7

January-February-2025

Page Number :

311-318

ABSTRACT

Accurate and frequent shoreline detection is essential for understanding for features and coastal processes. Rising sea levels, increased coastline erosion, and Extreme weather conditions like heavy storms, floods are the main natural risks. The researcher used a variety of investigative techniques in this work, including literature studies, field surveys etc. The conversion of mangrove habitats for aquaculture and agriculture is an example of human-induced change. Approximately 3% of the world's mangrove vegetation is found in India. According to the FSI, the mangrove cover in Maharashtra has increased significantly over the past three decades, from about 118 km² in 2000 to 320 km² in 2020. Mangrove ecosystems can store carbon, which helps mitigate climate change, reduce pollution, maintain ecological balance, and improve the environment for now and the future. The mangroves have undergone significant changes over the past 50 years, with an initial decline followed by partial recovery in some coastline. Since the 2000s conservation efforts have contributed to the stabilization and partial recovery of mangrove areas in some regions.

Keywords: Mangrove, Ecosystems, Ecological balance, Coast.

I. INTRODUCTION

Mangroves are tropical trees and shrubs that grow in salty coastal areas. They function as a natural barrier to maintain stability and protect the coastal area from erosion brought on by storm waves (Blankespoor et al., 2017). To succeed in such an environment, they have developed certain adaptations, such as salt resistance (Mitsch et al., 2015, Mitsch et al., 2009, Kerr and Baird, 2007). About 4921 km² (~3% of the world's mangrove vegetation) of mangroves are found in India, mostly along the coastal belts of the Bay of Bengal (Pichavaram, Cauvery deltaic, Krishna-Godavari, Mahanadi, Bhitarkanika, and Sundarbans) and Arabian Sea (Gujarat,

Maharashtra, Goa, and Kerala) (Forest Survey of India (FSI) Report, 2017). Mangrove forests are extremely productive ecosystems that constantly offer a wide range of products and services to both humans and marine life (Carugati et al., 2018). Mangroves are found in around 150,000 km² of land worldwide, with the biggest and most varied mangrove ecosystems found in Southeast Asia (Forest Survey of India (FSI) Report, 2017). Not only does mangrove forest protect the coast and nearby communities from rising sea levels and high wave activity, but it also absorbs eight times more CO₂ than any other ecosystem in the world (Donato et al., 2011). These studies demonstrate that it is important to understand the characteristics (land area and density) of the mangroves during the hydrodynamics model simulation. Therefore, the use of satellite combined with hydrodynamics is necessary for mangrove studies related to anthropogenic activities and climate variability. In more recent scenarios, mangrove hot spots are affected by climate variability and LULC changes due to a variety of anthropogenic activities (Parida et al., 2020, Ghosh et al., 2020, Kathiresan, 2018). Erosion, wave action, storm activity, and earthquake activity all play a role in changing the LULCs of coastal areas over time (Mujabar and Chandrasekar, 2013, Kaliraj and Ch, 2012). Due to urbanization and overexploitation, India has lost over 40% of its mangrove cover in the last century (Sahu et al., 2015, Krishnamurthy et al., 2014, Polidoro et al., 2010). According to the FSI, the mangrove cover in Maharashtra has increased significantly over the past three decades, from about 108 km² in 1999 to 304 km² in 2017. The Bombay High Court issued an order to stop the damage of the city's mangroves following the 2005 monsoon flood in Maharashtra, citing the Coastal Regulation Zone Notification of 1991 and the Forest Conservation Act of 1980 in India. The situation is more precarious right now; Mumbai is removing mangroves even as severe weather strikes the area (Youdon, 2020). About 260 million people, or one-third of the country's total population, reside 50 km or less from nine coastal states, including Gujarat, Maharashtra, Goa, Karnataka, Kerala, Tamil Nadu, Andhra Pradesh, Odisha, and West Bengal (Roy, 2019). Mumbai, in the coastal state of Maharashtra, is one of the most populous and polluted coastal cities in India, home to Asia's biggest industrial complex. These industries' effluents have a negative impact on the aquatic habitat, particularly mangroves. Mangroves in Mumbai are vital to the health of the marine and aquatic ecosystems because they shield nearby residential areas from natural disasters. 2,38,417 T of carbon are stored in Mumbai's mangroves, mostly from pollution that humans have emitted into the atmosphere (Hindustan Times, 2015). In the last ten years or so, Mumbai has likely lost about 40% of its mangroves. The primary causes of this loss have been the city's expanding population, construction and development projects, conversion of land to farms, and the impact of industrial effluents (Everard et al., 2014). A globally vulnerable environment, mangroves are protected and classified under the Coastal Regulation Zone (CRZ) notification, under CRZ-I. 3% of the world's mangroves and eight percent of Asian mangroves are found in India (SFR, 2009). 60% of India's total mangroves areas are found on the east coast, 27% are found on the west coast, and thirteen percent are found in the Andaman and Nicobar Islands. The mangroves of the Maharashtra coast run the entire length of the six coastal districts: Palghar, Sindhudurg Thane, Raigad, Mumbai and Mumbai sub-urban, and Ratnagiri. Seventy percent of the 720 kilometres of coastline include areas of mangrove vegetation that are expanding inward. About 44 streams, the largest of which is Thane Creek, are followed by ten other significant rivers.

II. STUDY AREA

Maharashtra's coastline, known as the Konkan coast, stretches for about 720 kilometers along the western edge of India, facing the Arabian Sea. Much of the coastline features steep, rocky cliffs formed from basaltic lava flows. Beaches are interspersed between rocky sections are sandy beaches of varying sizes. Several rivers like

Vashishti, Savitri, Tansa, Mandavi, Bav, Kajali, Vaghotan, Gad, Karli, Kundalika, Ulhas, Vaitarna are flowing westward from estuaries as they meet the sea, creating complex coastal ecosystems. The coastline's irregular shape includes numerous bays and protruding headlands. Offshore islands like Elephanta Island near Mumbai are notable features. Mudflats and mangroves are present particularly in sheltered areas and around estuaries.



III. MATERIALS AND METHODS

ENVIRONMENTAL SETTING OF MANGROVES

The mangrove forests along the Konkan coast of Maharashtra play a crucial role in the coastal ecosystem. Primarily found in estuarine regions and sheltered coastal areas. Major concentrations of mangrove are present in Mumbai, Thane, Raigad, Ratnagiri, and Sindhudurg districts. For the mangrove forest tropical monsoon climate with high rainfall (2000-3500 mm annually) has more suitability. Likely high humidity and relatively stable temperatures are found. Soil conditions are fine-grained alluvial soils and mudflats. High organic content and variable salinity due to freshwater influx from rivers originating in the Western Ghats. The mangroves are perfectly suited to coastal environments with a moderate salt level and adequate wind protection. The majority of places where they thrive include funnel-shaped bays, wide mouths of estuaries, sheltered intertidal flat deltaic areas, and shallow or often tidally inundated coastlines (Thom, 1982). The physical characteristics of the coast, climate, tidal amplitude, duration, and quantity of groundwater intake, as well as the salinity quotient brought on by the mixing of freshwater and seawater, all contribute to the distinctive environmental context of each of these habitats.

MANGROVE SPECIES CLASSIFICATION

The occurrence of mangrove species was recorded using Sentinel-2 categorization at a distance resolution of 10 m. In the Konkan coast, there are four main species of mangroves, each with unique zonation patterns related to tidal movement and land elevation (Kantharajan et al., 2018; Vijay et al., 2005). *A. marina* species has dominated the seaward side. There were species such as *Acanthus ilicifolius* and *Bruguiera cylindrica* close to the mainland, when tidal water reaches its greatest extent. An arrangement of a high level of *Avicennia marina* and *Sonneratia apetala* species was seen in the coast. Dominated species like *Avicennia marina*, *Sonneratia apetala*, and *Rhizophora mucronata*. Variation in species distribution based on salinity gradients.

STATE WISE MANGROVES FOREST

State wise Mangroves Forest report (in sq km) by FSI.									
Year	2001	2003	2005	2009	2011	2013	2015	2017	2019
Andhra Pradesh	333	329	354	353	352	352	367	404	404
Goa	5	16	16	17	22	22	26	26	26
Gujarat	911	916	991	1046	1058	1103	1107	1140	1177
Karnataka	2	3	3	3	3	3	3	10	10
Kerala	0	8	5	5	6	6	9	9	9
Maharashtra	118	158	186	186	186	186	222	304	320
Odisha	219	203	217	221	222	213	231	243	251
Tamil Nadu	23	35	36	39	39	39	47	49	45
West Bengal	2081	2120	2136	2152	2155	2097	2106	2114	2112
A&N islands	789	658	635	615	617	604	617	617	616
Daman & Diu	0	1	1	1	2	1.63	3	3	3
Pondicherry	1	1	1	1	1	1	2	2	2
Total	4482	4448	4581	4639	4663	4628	4740	4921	4975

(Table 1: All data has collected from the India state of forest report 2021.)

FRESHWATER INFLUX AND ITS IMPACTS

Freshwater influx along Maharashtra's coast primarily comes from rivers that originate in the Western Ghats and flow westward into the Arabian Sea. Ulhas, Vaitarna, Savitri, Vashishti, and Terekhol are some of the principal rivers. These rivers create estuaries where they meet the sea, forming complex ecosystems. The mixing of fresh and saltwater creates unique brackish environments. These areas support diverse flora and fauna adapted to changing salinity levels. Seasonal variations in river flow affect sediment deposition patterns. During monsoons, increased river discharge can lead to higher erosion in some areas. This contributes to the formation and replenishment of beaches and mudflats. Rivers bring nutrients from inland areas, supporting coastal productivity. This can lead to rich fishing grounds near river mouths. Dams and water diversion projects on rivers affect the quantity and timing of freshwater reaching the coast. This can alter natural coastal processes and ecosystems. Rivers often carry pollutants from inland areas to the coast. This can impact water quality and marine life in coastal regions. Freshwater influxes play a crucial role in shaping Maharashtra's coastal environment, influencing both its physical characteristics and biological diversity. The interplay between freshwater and marine environments creates a dynamic and ecologically important coastal zone.



NEARSHORE CLIMATE AND BEACH PROCESSES

It has a typical tropical maritime coast climate. The pre-monsoon, which runs from February to May, the southwest monsoon, which runs from June to September, and the post-monsoon, which runs from October to January, are the three distinct seasons in the area. Rainfall ranges from moderate to heavy during the southwest monsoon season. The factors that distinguish coastal processes from those in other areas are wind, tides, waves, and currents. This section of the shore is home to both emergent and submergent phenomena. Whereas barrier spit patterns are indicative of emergent features, the existences of ponds and backwaters that can be seen next to the coast at specific spots are signs of submergent features. Long-term variations in the sea level, climate, lithology, structure, and non-tectonic movements are all responsible for these traits (Nair and Padmalal, 2004; Jayalakshmi et al., 2004). Everywhere along the coast are features resulting from both erosion and deposition. The existence of rivers, lagoons and lakes, estuaries, and other bodies of water greatly divides the coastal area, and the tropical climate is responsible for the seen scenery.

RESPONSE OF MANGROVES TO THE TIDAL DYNAMICS

When constructing grids, friction coefficients, and land elevation, the results from the satellite data provide extra details, such as the width of the creek and the length of the mangroves. Because of the creek's nearly triangular form, the tidal motion is amplified and funneled at flood tides. Mangroves on land may spread farther into the sea as a result of anthropogenic pressure. The severity of pollution and urbanization is shown by the preponderance of *A. marina* species. An idea of the inundation intensity is provided by the ADCIRC model simulation both with and without mangroves.

IV. RESULT AND DISSCUSSION

Spatial changes include shifts in distribution, with some areas experiencing expansion while others face continued pressure from urban development. The forests have shown adaptive responses to changing tidal dynamics, including landward migration in response to sea level rise and adjustments to altered sedimentation patterns. Anthropogenic influences, mostly urban development and industrial pollution, have played a major role in shaping the current state of these mangrove ecosystems. Climate change effects are evident in phenological shifts, altered growth patterns, and changes in species composition favoring more salt-tolerant varieties. Without mangroves, the convergence of tides along the channel causes tidal amplification to raise upstream, intensifying tidal currents that worsen erosion and inundation, ultimately posing a threat to human

populations. According to the FSI, the mangrove cover in Maharashtra has seen a substantial increase over the past thirty years. Mangrove ecosystems play a crucial role in carbon storage, helping to combat climate change, reduce pollution, maintain ecological balance, and enhance the environment for both present and future generations. Over the last five decades, mangroves have experienced considerable changes, initially declining, but with partial recovery in certain coastal areas.

V. REFERENCES

- [1]. Abdul Azeez S., Gnanappazham L., Muraleedharan K.R., Revichandran C., Sebin John, Seena G., Jubin Thomas.,2022. Multi-decadal changes of mangrove forest and its response to the tidal dynamics of thane creek, Mumbai Journal of Sea Research 180, 102162.
- [2]. Avinash Kumar, A.C. Narayana, K.S. Jayappa, 2010. Shoreline changes and morphology of spits along southern Karnataka, west coast of India: A remote sensing and statistics-based approach Geomorphology 120, 133–152.
- [3]. Blankespoor, B., Dasgupta, S., Lange, G.-M., 2017. Mangroves as a protection from storm surges in a changing climate. *Ambio* 46, 478–491.
- [4]. Carugati, L., Gatto, B., Rastelli, E., Martire, M. Lo, Coral, C., Greco, S., Danovaro, R., 2018. Impact of mangrove forests degradation on biodiversity and ecosystem functioning. *Sci. Rep.* 8, 1–11.
- [5]. Chandra Giri, Bruce Pengra, Zhiliang Zhu, Ashbindu Singh, Larry L. Tieszen, 2007. Monitoring mangrove forest dynamics of the Sundarbans in Bangladesh and India using multi-temporal satellite data from 1973 to 2000* *Estuarine, Coastal and Shelf Science*.
- [6]. Chaudhuri P, Ghosh S, Bakshi M, Bhattacharyya S, Nath B, 2015. A Review of Threats and Vulnerabilities to Mangrove Habitats: With Special Emphasis on East Coast of India. *J Earth Sci Clim Change* 6: 270. doi:10.4172/2157-7617.1000270.
- [7]. Donato, D.C., Kauffman, J.B., Murdiyarso, D., Kurnianto, S., Stidham, M., Kanninen, M., 2011. Mangroves among the most carbon-rich forests in the tropics. *Nat. Geosci.* 4, 293–297.
- [8]. Everard, M., Jha, R.R.S., Russell, S., 2014. The benefits of fringing mangrove systems to Mumbai. *Aquat. Conserv. Mar. Freshw. Ecosyst.* 24, 256–274.
- [9]. Ghosh, S.M., Behera, M.D., Paramanik, S., 2020. Canopy height estimation using sentinel series images through machine learning models in a Mangrove Forest. *Remote Sens.* 12, 1519
- [10]. India state of forest report 2021.
- [11]. Kaliraj, S., Ch, N., 2012. Spectral recognition techniques and MLC of IRS P6 LISS III image for coastal landforms extraction along South West Coast of Tamilnadu, India. *Bonfring Int. J. Adv. Image Process.* 2, 1–7.
- [12]. Kathiresan, K., 2018. Mangrove forests of India. *Curr. Sci.* 114.
- [13]. Kerr, A.M., Baird, A.H., 2007. Natural barriers to natural disasters. *Bioscience* 57, 102–103
- [14]. Krishnamurthy, R.R., DasGupta, R., Chatterjee, R., Shaw, R., 2014. Managing the Indian coast in the face of disasters & climate change: a review and analysis of India's coastal zone management policies. *J. Coast. Conserv.* 18, 657–672.
- [15]. Kumar Avinash, K. S. Jayappa, P. Vethamony, 2012. Evolution of Swarna estuary and its impact on braided islands and estuarine banks, Southwest coast of India *Environ Earth Sci* 65:835–848, DOI 10.1007/s12665-011-1128-3

- [16]. L. Sheela Nair, R. Prasad, M. K. Rafeeqe and T. N. Prakash, 2018. Coastal Morphology and Long-term Shoreline Changes along the Southwest Coast of India JOURNAL GEOLOGICAL SOCIETY OF INDIA Vol.92, 588-595.
- [17]. M. Jayanthia, S. Thirumurthya, G. Nagarajb, M. Muralidhara, P. Ravichandrana, 2018. Spatial and temporal changes in mangrove cover across the protected and unprotected forests of India Estuarine, Coastal and Shelf Science 213, 81–91.
- [18]. Mujabar, P.S., Chandrasekar, N., 2013. Shoreline change analysis along the coast between Kanyakumari and Tuticorin of India using remote sensing and GIS. Arab. J. Geosci. 6, 647–664.
- [19]. Naidu, V.S., Sarma, R.V., 2001. Numerical modeling of tide-induced currents in Thane Creek, west coast of India. J. Waterw. Port Coastal Ocean Eng. 127, 241–244
- [20]. P. Vinayaraj, Glejin Johnson, G. Udhaba Dora, C. Sajiv Philip, V. Sanil Kumar, R. Gowthaman, 2011. Quantitative Estimation of Coastal Changes along Selected Locations of Karnataka, India: A GIS and Remote Sensing Approach International Journal of Geosciences, 2, 385-393 doi:10.4236/ijg.2011.24041
- [21]. Parida, B.R., Kumar, P., 2020. Mapping and dynamic analysis of mangrove forest during 2009–2019 using landsat—5 and sentinel—2 satellite data along Odisha Coast. Trop. Ecol. 61, 538–549.
- [22]. Parida, B.R., Kumari, A., 2021. Mapping and modeling mangrove biophysical and biochemical parameters using Sentinel-2A satellite data in Bhitarkanika National Park, Odisha. Model. Earth Syst. Environ. 7, 2463–2474.
- [23]. Parida, B.R., Pandey, A.C., Patel, N.R., 2020. Greening and browning trends of vegetation in India and their responses to climatic and non-climatic drivers. Climate 8, 92.
- [24]. Polidoro, B.A., Carpenter, K.E., Collins, L., Duke, N.C., Ellison, A.M., Ellison, J.C., Farnsworth, E.J., Fernando, E.S., Kathiresan, K., Koedam, N.E., et al., 2010. The loss of species: mangrove extinction risk and geographic areas of global concern. PLoS One 5, e10095.
- [25]. Reji Srinivas, Girish Gopinath, Laluraj C M and Kurian Sajan, 2010. Morphological Features of an Estuarine System on South-West Coast of India, International Journal of Earth Sciences and Engineering ISSN 0974-5904.
- [26]. Roy, A., 2019. Making India's coastal infrastructure climate-resilient: challenges and opportunities. Obs. Res. Found. 207, 1–34.
- [27]. Roy, S., Mahapatra, M., Chakraborty, A., 2019. Mapping and monitoring of mangrove along the Odisha coast based on remote sensing and GIS techniques. Model. Earth Syst. Environ. 5, 217–226.
- [28]. Ruta B. Limaye, K.P.N. Kumaran, D. Padmalal, 2014. Mangrove habitat dynamics in response to Holocene sea level and climate changes along southwest coast of India Quaternary International 325, 116e125.
- [29]. S. Kaliraj, N. Chandrasekar, K.K. Ramachandran, 2017. Mapping of coastal landforms and volumetric change analysis in the south west coast of Kanyakumari, South India using remote sensing and GIS techniques The Egyptian Journal of Remote Sensing and Space Sciences 20, 265–282.
- [30]. Sahu, S.C., Suresh, H.S., Murthy, I.K., Ravindranath, N.H., 2015. Mangrove area assessment in India: implications of loss of mangroves. J. Earth Sci. Clim. Change 6, 1.
- [31]. Sandeep Thakur, Debapriya Maity, Ismail Mondal, Ganesh Basumatary, Phani Bhushan Ghosh, Papita Das, Tarun Kumar De, Assessment of changes in land use, land cover, and land surface temperature in the mangrove forest of Sundarbans, northeast coast of India Environment, Development and Sustainability <https://doi.org/10.1007/s10668-020-00656-7>.

- [32]. Shailesh R. Nayak & Baldev Sahai, 1985. Coastal morphology: a case study of the Gulf of Khambhat (Cambay), *International Journal of Remote Sensing*, 6:3-4, 559-567
- [33]. Thakur S, Mondal I, Bar S, Nandi S, Ghosh P, Das P, De T, Shoreline changes and its impact on the mangrove ecosystems of some Islands of Indian Sundarbans, North- East coast of India. *Journal of Cleaner Production*, <https://doi.org/10.1016/j.jclepro.2020.124764>.
- [34]. Vijay, R., Khobragade, P.J., Sohony, R.A., Kumar, R., Wate, S.R., 2014. Hydrodynamic and Water Quality Simulation of Thane Creek, Mumbai: An Impact of Sewage Discharges.
- [35]. Vijay, R., Dey, J., Sakhre, S., Kumar, R., 2020. Impact of urbanization on creeks of Mumbai, India: a geospatial assessment approach. *J. Coast. Conserv.* 24, 1–16.
- [36]. Y. Paria, M.V. Ramana Murthya, S. Jaya kumarb, B.R. Subramaniana, S. Ramachandran, 2008. Morphological changes at Vellar estuary, India—Impact of the December 2004 tsunami *Journal of Environmental Management* 89, 45–57.
- [37]. Youdon, C., 2020. Climate change impact on mangrove ecosystems in India's coastal regions. *Natl. Marit. Found.*, 8–60.

Estimation of Proximate Contents of Trigonella Foenum-Graecum Stem in Aurangabad City of Maharashtra, India

Quazi Saifuddin, Saleem Khan

Department of Chemistry, Government Vidarbha Institute of Science and Humanities, Amravati 444 604, Maharashtra, India

ARTICLE INFO

Article History:

Accepted : 01 Jan 2025

Published : 10 Jan 2025

Publication Issue :

Volume 12, Issue 7

January-February-2025

Page Number :

319-322

ABSTRACT

The word Trigonella is (Greek) are derived from Foenum-graecum, refer to the genus Trigonella. Around the world, Trigonella foenum-graecum is widely recognized as fenugreek. The genus Trigonella belongs to the Fabaceae family of green leafy vegetables, which are widely available in Europe and India. Due to its significant uses in daily life as food and medicine, it is now found in practically every region of the world. Trigonella foenum-graecum is used to treat stomach issues and during pregnancy. It also has anti-diabetic, anti-oxidant, and anti-inflammatory qualities. The Trigonella foenum-graecum plant is well-known in India for its use as a green vegetable, but its seeds also have some beneficial therapeutic qualities. Trigonella Foenum-Graecum is a natural product that contains a variety of organic moieties as well as elements like potassium, calcium, riboflavin, niacin, alkaloids, flavonoids, and vitamins-A, vitamins-C, and vitamins-K. The current study examines the proximate parameters of Trigonella Foenum-graecum, confirming its solubility in hot water, total ash value, and presence of moisture and ash content. Cold water, 1% NaOH (aq.), 1% HCl(aq.), and 1% CH₃COOH (aq.) were found quantitatively.

Keywords: Trigonella Foenum Graecum, Stem, proximate analysis,

I. INTRODUCTION

The capital of Marathwada and a historically significant location in the Indian state of Maharashtra, Aurangabad boasts a far greener environment. The oldest and most abundant in flora and fauna are Aurangabad and its surroundings. Fenugreek plants can reach a height of one foot from a single, hollow, hairy stem that branches at the base. The green, leafy vegetable resembles clover leaves. Fenugreek is a valuable cover crop that helps fix nitrogen in the soil, which is important for plant growth. It is also recognized in the fields of chemical, pharmaceutical, and herbal medicine¹⁻⁹. Fenugreek has anti-inflammatory¹⁰, anti-microbial¹¹, and anti-diabetic

properties¹². It also boosts milk production in nursing mothers, lowers blood pressure, and has many other medical uses¹³.

Our research laboratory has conducted a vast amount of work on natural products, with a focus on proximate, phytochemical, physiochemical, and spectroscopical studies on a variety of plants^{9–13}. The drug's solubility affects its absorption, transmission, effects, moisture content, and ash content. Proximate analysis provides data on the sample's solubility in various solvents, moisture content, and ash content. Investigating the proximate parameters in *Trigonella Foenum-Graecum* from Karmad village in Aurangabad (Maharashtra pin code 431007) is highly interesting in light of all these facts.

II. MATERIALS AND METHODOLOGY

All chemicals used during the research work were of A.R. grade. Freshly prepared solutions were used throughout the research work. The solvents were purified by known literature methods¹⁴.

Sample Preparation

On July 15–17, 2022, the plants were picked from Mr. Shaikh Zuber's farm in Karmad, Aurangabad, Maharashtra State, India. To get rid of dirt and dust from the plants, they were first cleaned with tap water and then twice-distilled water. After being cut off from the stem and dried. To create a fine powder, dried leaves were crushed in a mortar and pestle. Known literature methods are employed to use this fine powder in proximate studies^{15–17}.

Proximate Analysis

The determination of physicochemical parameters such as moisture content, total ash value, acid-insoluble ash value, and solubility of the sample was carried out by the known literature methods^{18–20}. Solubility of the sample was checked in cold water, hot water and 1% NaOH(aq), HCl(aq), CH₃COOH (aq) solution. Percentage of moisture and ash contents and acid insoluble ash are determined by using following formula,

Moisture Content = Weight of sample taken – Weight of sample after treatment,

$$\% \text{ of moisture} = \frac{\text{Loss of weight of sample}}{\text{Weight of sample taken}} \times 100$$

while, Percentage of solubility is determined by using following formula,

$$\% \text{ of Solubility} = (\text{loss of weight of sample})/(\text{weight of sample taken}) \times 100$$

The results obtained are given in **Table No-1**

Table No-1

Sr. No	Proximate Parameters	Loss of weight of sample	Amount of sample taken (in grams)	%
1	Moisture content	0.848	1	84.8
2	Total ash content	0.079	1	7.90
3	Acid insoluble ash value	0.31	1	31.00
4	Coldwater solubility	0.41	1	41.49
5	Hot water solubility	0.28	1	28.00
6	NaOH(aq) solubility	0.34	1	34.00
7	HCl(aq) solubility	0.39	1	39.00
8	CH ₃ COOH(aq) solubility	0.112	1	11.2

III.RESULT AND DISCUSSION

The moisture content in any part of plant gives evidence for an activity of water-soluble enzymes and coenzymes essential for the metabolic activities of that plant and it is detected from Table No.-1 that, total moisture content in leaves of was found to be 84.8% which is good for metabolic activities in the plant growth and progress of the plant. It was found that the total ash content found from dry stem pieces is 7.9 % and acid insoluble ash value is 31 % which are good and these proximate parameters of plant organs are useful for the determination of the mineral contents. Coldwater solubility and hot water solubility were found to be 41.49 % and 28% respectively; these proximate parameters will give information regarding water soluble neutral, acidic, basic and hydrocarbons present in the samples in herbal chemistry. HCl solubility and CH₃COOH solubility were found to be 49.00% and 11.2% respectively, these proximate parameters gave information regarding basic organic components present in the sample and NaOH solubility was found to be 34.00% which gave information regarding acidic organic components present in the sample.

IV.CONCLUSION

The stem of *Trigonella Foenum-Graecum* from Karmad (PIN Code 431007) in the District Aurangabad of Maharashtra showed good proximate parameters according to the good results of the proximate analysis. Additionally, *Trigonella Foenum-Graecum* root at Karmad (PIN Code 431007) in District Aurangabad, Maharashtra have natural physicochemical, physiological, and anatomical activities that make them useful for medicinal purposes.

V. ACKNOWLEDGEMENT

Authors are thankful to Dr Mazahar Farooqui, Principal, Dr Arif Pathan Head Department and teaching and non-teaching staff of Department of Chemistry, Maulana Azad College of Arts, Science and Commerce Aurangabad for their help during the research work.

VI. REFERENCES

- [1]. Bakhtiar, Z., Hasandokht, M. R., Naghavi, M. R., & Mirjalili, M. H. Journal of Medicinal Plants, 21(82), 1-12.(2022).
- [2]. Mahmood, N. M., & Yahya, K. I. International Journal of Sciences: Basic and Applied Research, 36(3), 203-213.(2017).
- [3]. Singh, K. P., Nair, B., Jain, P. K., Naidu, A. K., & Paroha, S. Revista Colombiana de Ciencias Hortícolas, 7(2), 228-239.(2013).
- [4]. Pasricha, V., & Gupta, R. K. Journal of pharmacognosy and Phytochemistry, 3(4), 47-57.(2014).
- [5]. Niknam, R., Kiani, H., Mousavi, Z. E., & Mousavi, M. Biology and Applications, 189-217.(2021).
- [6]. Lohvina, H., Sándor, M., & Wink, M. Diversity, 14(1), 7.(2021).
- [7]. Marzougui, N., Ferchichi, A., Guasmi, F., & Beji, M. Journal of Food Agriculture and Environment, 5(3/4), 248.(2007).
- [8]. Basu, T. K., & Srichamroen, A. Bioactive foods in promoting health (pp. 425-435). Academic Press.(2010).
- [9]. Visuvanathan, T., Than, L. T. L., Stanslas, J., Chew, S. Y., & Vellasamy, S. Plants, 11(11), 1450.(2022).

- [10]. Arya, P., Kumari, N., Wani, S. A., & Kumar, P. Herbs, spices and their roles in nutraceuticals and functional foods, 133-148.(2023).
- [11]. Begum, S., Ramappa, K. T., Nidoni, U., Hiregoudar, S., & Ramesh, G.. International Journal of Environment and Climate Change, 13(9), 1252-1259.(2023).
- [12]. Omezzine, F., &Haouala, R. Scientiahorticulturae, 160, 335-344.(2013).
- [13]. Man, S. M., Păucean, A., Călian, I. D., Mureşan, V., Chiş, M. S., Pop, A.,&Muste, S. Journal of Food Quality, (2019).
- [14]. Raji-Idowu, F , Nigerian Journal of Microbiology.(2023).
- [15]. Malghani, N., Mahesar, S., Baig, J., Talpur, F., Sherazi, S. T. H., & Junaid, M. Journal of the Turkish Chemical Society Section A: Chemistry, 9(4), 985-998.(2022).
- [16]. Singh, U., Chamoli, M., Singh, K. P., Ram, L., Jangir, S., & Maheshwari, R. K. International Journal of Environment and Health Sciences, 4, 19-27.(2022).
- [17]. Alsemari, A., Alkhodairy, F., Aldakan, A., Al-Mohanna, M., Bahoush, E., Shinwari, Z., &Alaiya, A.. BMC Complementary and Alternative Medicine, 14, 1-9.(2014).
- [18]. Gupta, M., Arshad, M., Shivnath, N., Khan, M. S., & Gupta, R. seed extracts prevent diabetic osteopathy.(2018).
- [19]. Tayade.D .T, Shaikh R. S, Patil S. U. J. of Indian Chem Soc., 83, 1-3 (2006).
- [20]. Shaikh. R .S, Ph. D. Thesis, Amravati University, Amravati. (2006).

Red Phosphor Materials: Synthesis, Characterization, and Luminescence Analysis

R. S. Palaspagar¹, S. R. Khandekar²

¹Department of Physics, Shivramji Moghe Mahavidyalaya, Kelapur, Maharashtra, India

²Department of Chemistry, Indira Mahavidyalaya, Kalamb, Maharashtra, India

ARTICLE INFO

Article History:

Accepted : 01 Jan 2025

Published : 10 Jan 2025

Publication Issue :

Volume 12, Issue 7

January-February-2025

Page Number :

323-327

ABSTRACT

The red-emitting phosphor Eu^{3+} doped $\text{BaAl}_2\text{B}_2\text{O}_7:\text{Eu}^{3+}$ (Barium Aluminum Borate) is synthesized by a simple, time-saving, economical novel method of solution combustion synthesis at 500°C , a comparatively lower temperature. The phase identification of the prepared phosphor was recorded using x-ray diffraction (XRD). The phosphor $\text{BaAl}_2\text{B}_2\text{O}_7:\text{Eu}^{3+}$ exhibits strong absorption over a wide UV range from 200 – 400 nm. Europium as a doping in Barium Aluminum borate phosphor gives intense emission in the red region having a prominent emission band at 614 nm with the excitation at 395 nm. This excitation band at 393 nm makes phosphor, a good red emitter for the n-UV LED for making w-LED for solid-state lighting. Commission de l'Eclairage chromaticity (CIE) coordinates were analyzed based on the PL emission spectra of the series $\text{BaAl}_2\text{B}_2\text{O}_7:\text{Eu}^{3+}$ activated phosphor.

Keywords: Alumino-Borates, Combustion Synthesis, XRD, Photoluminescence.

I. INTRODUCTION

Phosphorus-related interest has recently led to fast advancements in potential display and illumination technologies. Photoluminescent (PL) materials for general lighting consist of oxides, silicates, aluminates, aluminosilicates, nitrides, borates, etc. Borates are among the researched hosts that provide suitable candidates for the host structure because of their high luminescence brightness, ease of manufacture, and low synthetic temperature.

Borate compound synthesis is a challenging process. Numerous borate compounds can be found in both glassy and crystalline forms. Although crystalline forms are typically needed to produce effective luminous materials, glasses can also be used in PSL, optical data storage, lasers, and other applications. In order to prevent glass formation, the combustion synthesis method that uses boric acid as the boron source enables the preparation without melting the ingredients. Longer reaction times are required for this. Boric acid evaporation can result in

non-stoichiometry. Afterglow, also known as persistent phosphorescence, is luminosity that continues after the stimulation is removed. Thermally driven recombination of holes and electrons at traps results in long-lasting (LL) phosphorescence, which leaves holes or electrons in a

Alkaline-earth aluminum borates have been taken interest in by scientists during the past decade because of their potential applications as luminescence hosts. The phase of $\text{BaAl}_2\text{B}_2\text{O}_7$, is an example of alkaline-earth aluminum borates, was first described by Hübner following a study of the ternary system $\text{BaO}-\text{Al}_2\text{O}_3-\text{B}_2\text{O}_3$. It is characterized by having an association of BO_3 triangles, BaO_6 octahedra, and AlO_4 tetrahedra. In the present work we report synthesis and photoluminescence of $\text{BaAl}_2\text{B}_2\text{O}_7:\text{Eu}^{3+}$. Their photoluminescence properties under the near-UV excitation were evaluated in detail. Activation with Eu^{3+} , which occupies the Ba^{2+} sites of host lattice, yields a highly efficient phosphor with emission maximum near 614 nm. Furthermore, the concentration quenching and critical distance of $\text{BaAl}_2\text{B}_2\text{O}_7:\text{Eu}^{3+}$ phosphors were discussed.

II. EXPERIMENTAL

The Powder samples of $\text{BaAl}_2\text{B}_2\text{O}_7:\text{Eu}^{3+}$ have been prepared by a solution combustion technique followed by heating combustion ash at 500 °C in air. The method is based on the exothermic reaction between the fuel (urea) and oxidizer (Ammonium Nitrate). The detailed description of the method was reported in our earlier work. The stoichiometric amounts of $\text{Al}(\text{NO}_3)_3 \cdot 9\text{H}_2\text{O}$, $\text{Ba}(\text{NO}_3)_2$, H_3BO_3 , and $\text{CO}(\text{NH}_2)_2$ used were of AR grade and the rare earth Eu_2O_3 (99.99% purity) used were from the Indian Rare earth. The stoichiometric amounts of the ingredients were thoroughly mixed in an Agate Mortar, adding little amount of double distilled water to obtain aqueous solution. The aqueous solution was slowly heated at lower temperature of 90°C to remove the excess water. The solution was then introduced into a preheated muffle furnace maintained at (550 ± 10) °C. The solution boils foams and ignites to burn with flame; a voluminous, foamy powder was obtained. The entire combustion process was over in about 5 min. The samples are subjected to XRD analysis. PL measurements were performed on Fluorescence Spectrometer (Hitachi F-7000).

III. RESULTS AND DISCUSSIONS

3.1. X-ray Diffraction Pattern

The XRD pattern of $\text{BaAl}_2\text{B}_2\text{O}_7:\text{Eu}^{3+}$ (0.01 mol) is shown in Fig. 1. The XRD pattern of $\text{BaAl}_2\text{B}_2\text{O}_7:\text{Eu}^{3+}$ (0.01 mol) is in agreement with the standard monoclinic $\text{BaAl}_2\text{B}_2\text{O}_7$ (ICDD File No. 00-048-0049). Any phase of Eu^{3+} is not observed. The two possible sites available for the incorporating Eu^{3+} in the $\text{BaAl}_2\text{B}_2\text{O}_7$ lattice are either the Al^{3+} sites or the Ba^{2+} sites. The Eu^{3+} (0.947 Å) ion has a much larger ionic radius, compared with that of Al^{3+} (0.39 Å) ion. However, the ionic radius of Ba^{2+} (1.35 Å) is larger than that of Eu^{3+} ion. So it would be expected that Eu^{3+} would replace Ba^{2+} in the crystal lattice, this is confirmed by XRD analysis.

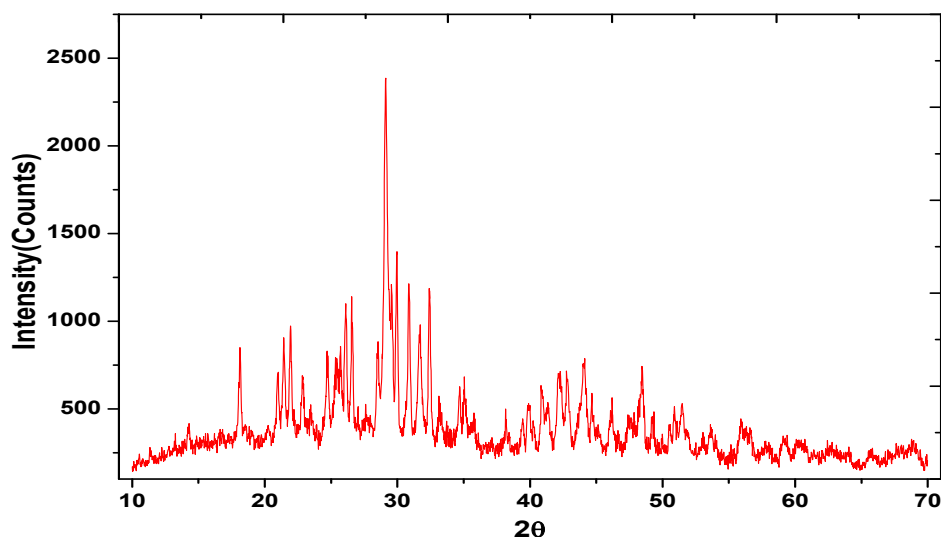


Fig. 1. XRD pattern obtained for BaAl₂B₂O₇:Eu³⁺ (1mol %)

3.2. Photoluminescence of BaAl₃BO₇:Eu³⁺

The photoluminescence (PL) and photoluminescence excitation (PLE) spectra of the BaAl₂B₂O₇:Eu³⁺ phosphors were recorded at room temperature. The typical excitation spectrum ranging from 200 to 450 nm monitored at $\lambda_{em} = 614$ nm is shown in Fig.2. The excitation spectra consist of sharp f-f transition lines in the wavelength range 300 nm to 420 nm, including $^7F_0 \rightarrow ^5H_3$ (320 nm), $^7F_0 \rightarrow ^5D_4$ (363 nm), $^7F_0 \rightarrow ^5L_7$ (383 nm) and $^7F_0 \rightarrow ^5L_6$ (393 nm). The emission spectrum depicts the typical red photoluminescence at 614 nm under the excitation at 393 nm. The emission spectrum consists of a series of sharp bands at 580 nm ($^5D_0 \rightarrow ^7F_0$), 591 nm ($^5D_0 \rightarrow ^7F_1$) and 614 nm ($^5D_0 \rightarrow ^7F_2$) is shown in Fig. 3. In particular, the most intense emission peak at 614 nm occurs through the forced electric dipole while the $^5D_0 \rightarrow ^7F_1$ band at 591 nm is due to the magnetic dipole transition. Furthermore, it is observed that the PL intensity increase with the Eu³⁺ concentration and found maximum for $x = 0.01$ mol. Beyond this saturation level of $x=0.01$ mol, intensity subsequently begins to decrease with the Eu³⁺ concentration due to the concentration quenching as shown in Fig.4. The most prominent emission, $^5D_0 \rightarrow ^7F_2$ peaking at 614 nm, results in a red color with excellent purity and with a CIE chromaticity coordinate of (0.614, 0.387) Chromatic point is shown in Fig.5.

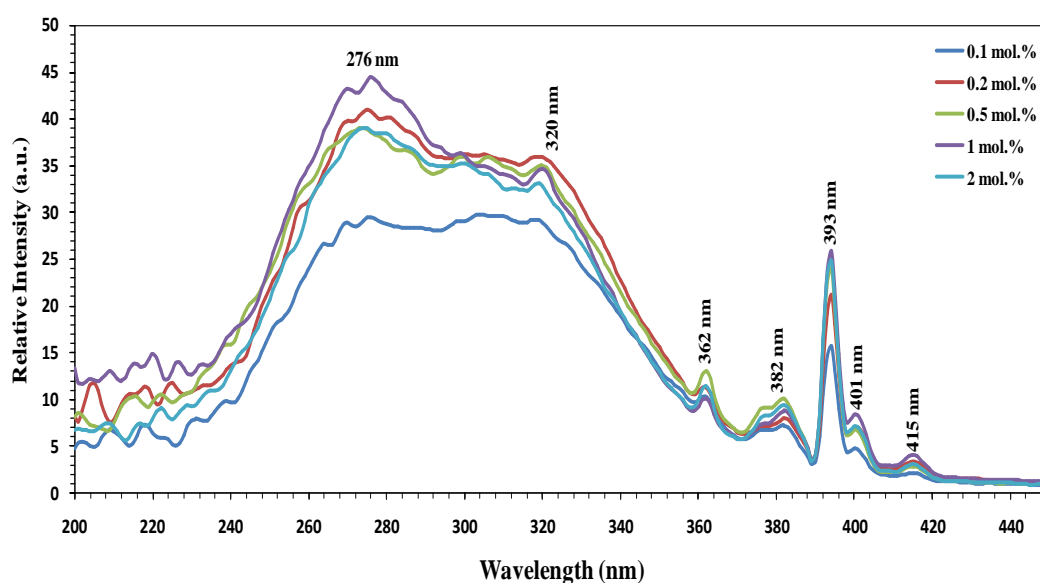


Fig.2 Excitation spectrum of Ba_(1-x)Al₂B₂O₇:xEu³⁺ ($x=0.01, 0.02, 0.05, 0.1, 0.2$ mol).

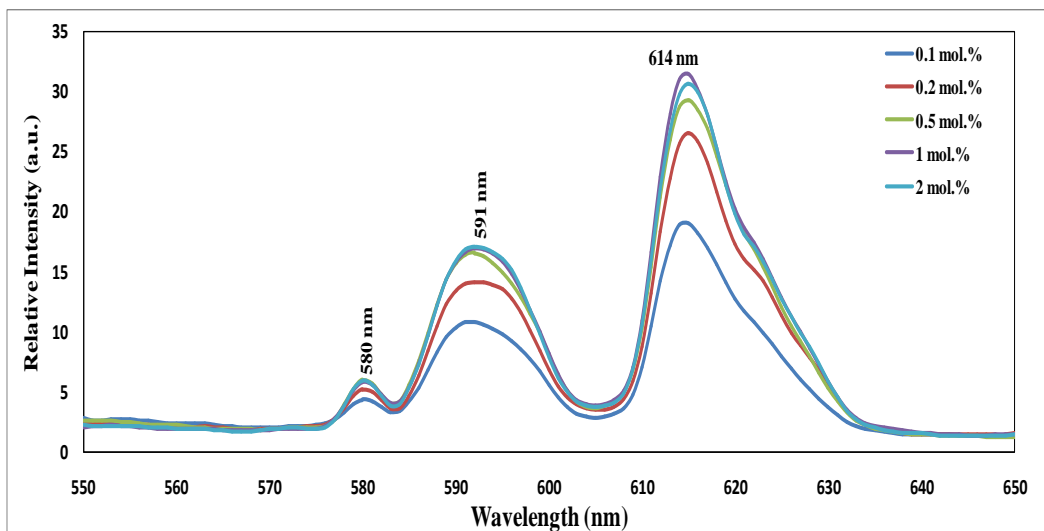


Fig.3 Emission spectrum of $\text{Ba}_{(1-x)}\text{Al}_2\text{B}_2\text{O}_7:\text{xEu}^{3+}$ ($x=0.01, 0.02, 0.05, 0.1, 0.2$ mol)

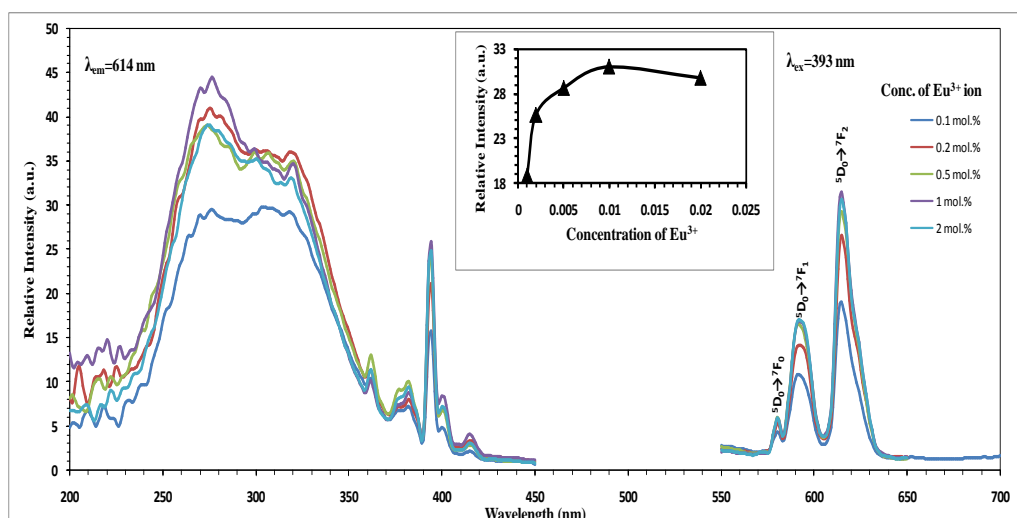


Fig. 4 Excitation & Emission Spectra of $\text{Ba}_{(1-x)}\text{Al}_2\text{B}_2\text{O}_7:\text{xEu}^{3+}$ ($x=0.01, 0.02, 0.05, 0.1, 0.2$ mol) phosphor.

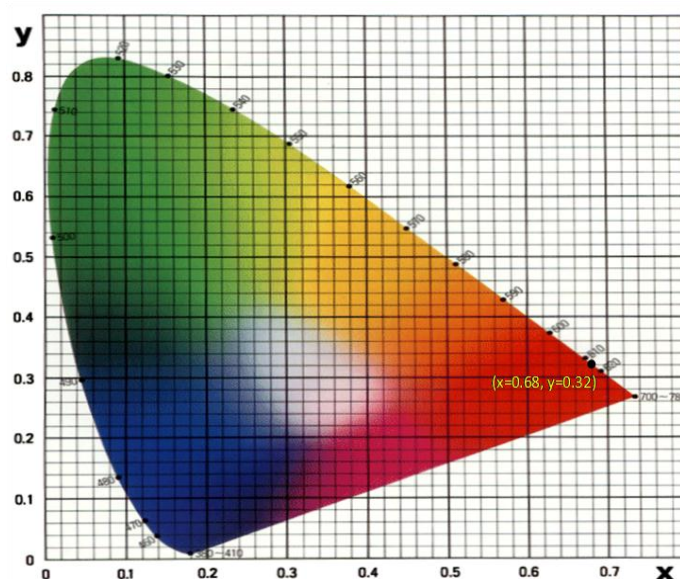


Fig. 5 CIE chromaticity diagram of $\text{BaAl}_2\text{B}_2\text{O}_7: 1 \text{ mol \% Eu}^{3+}$ phosphors.

IV. CONCLUSIONS

In the proposed work, the luminescence properties of $\text{BaAl}_2\text{B}_2\text{O}_7:\text{Eu}^{3+}$ activated red emitting phosphor was successfully synthesized by a simple, time-saving, economical novel method of solution combustion synthesis at 500°C , a comparatively lower temperature. The XRD pattern of $\text{BaAl}_2\text{B}_2\text{O}_7$ is in good agreement with ICDD database. In PL study, the emission peak of prepared phosphor located at 580 nm, 591 nm and 614 nm due to $^5\text{D}_0 \rightarrow ^7\text{F}_0$, $^5\text{D}_0 \rightarrow ^7\text{F}_1$ and $^5\text{D}_0 \rightarrow ^7\text{F}_2$ transition at excitation 276 nm, 320 nm and 393 nm. The dependence of the emission intensity on the Eu^{3+} concentration for $\text{BaAl}_3\text{BO}_7:\text{Eu}^{3+}$ was investigated. The critical concentration of Eu^{3+} in phosphor was observed to be 1 mol %. Therefore, the proposed phosphor is useful for the fabrication of white light emitting diode applications.

ACKNOWLEDGEMENTS

Authors is very much thankful to Head, Department of Physics, Sant Gadage Baba Amravati University, Amravati, for providing necessary facilities.

V. REFERENCES

- [1]. W.R. Liu, Y.C. Chiu, C.Y. Tung, Y.T. Yeh, S.M. Jang, T.M. Chen, J. Electrochem. Soc. 155 (2008) 252.
- [2]. Yingli Zheng, Donghua Chen, Wei Li, Physica B: Condensed Matter, 406 (4) (2011) 996-999.
- [3]. G. Bertrand-Chadeyron, M. El-Ghozzi, D. Boyer, R. Mahiou, J.C. Cousseins J. Alloy. Comp., 317 (2001), p. 183
- [4]. Jianrong Qiu, K. Miura, T. Suzuki, T. Mitsuyu, K. Hirao, Appl. Phys. Letts., 74 (1999), 10
- [5]. İ. Pekgözlü, S. Seyyidoğlu, S. Taşcıoğlu, J. Lumin., 128 (9) (2008) 1541-1543.
- [6]. Chen, Jiongquan and Jin, Wenqi and Zhang, Yanhui and Yang, Yun and Yang, Zhihua and Pan, Shilie, Inorg. Chem. Front., 9 (10) (2022) 2298-2304.
- [7]. R.S. Palaspar, A.B. Gawande, R.P. Sonekar, S.K. Omanwar, J. Lumin., 154 (2014) 58-61.
- [8]. R.S. Palaspar, A.B. Gawande, R.P. Sonekar, S.K. Omanwar, Mater. Res. Bull., 72 (2015) 215-219.

Facile Synthesis of MgO Nanoparticles and MgO/PANI NCS as a Promising Photocatalyst towards Waste Water Treatment

Ramdas S. Suralkar^{1*}, Deepak M. Nagrik², Vivek C. Badgujar¹

¹Pratap College Amalner, Maharashtra, India

²G. S. College Khamgaon, Maharashtra, India

ARTICLE INFO

Article History:

Accepted : 01 Jan 2025

Published : 10 Jan 2025

Publication Issue :

Volume 12, Issue 7

January-February-2025

Page Number :

328-338

ABSTRACT

This study used a straightforward precipitation method to create MgO Nano powder and MgO/PANI nanocomposites employing NaOH as the precipitant and Mg(NO₃)₂ as a precursor. The nanopowder's physical properties were thoroughly investigated utilizing methods like XRD, FTIR and UV-Visible spectrophotometer. Under natural sunlight irradiation, the material's photocatalytic efficacy in breaking down Crystal Violet (CV) dye was evaluated during summer and winter season with an emphasis on its possible selectivity towards particular organic dyes. To assess the oxidative potential of MgO and MgO/PANI nanocomposites that mediate the photocatalytic efficiency of this material, the study also sought to clarify the photocatalytic degradation mechanisms of the dye.

Keywords: Dye degradation. Photocatalyst, nanoparticles, nanocomposites, sunlight irradiation etc.

I. INTRODUCTION

Water contamination, which also causes diseases in many nations, is a direct cause of the growing need for safe and clean drinking water worldwide.¹ One of the main causes of common waterborne illnesses is contaminated water.² Both humans and animals can develop health issues including cancer as a result of organic contaminants, such as dyes. Higher death rates have also been connected to water contamination.³

Although there are many industrial sources of organic water pollution, such as the textile, pharmaceutical, paper, leather, printing, cosmetics, and food processing industries, the textile sector is a major contributor because it generates a large amount of wastewater containing dyes. It is estimated that approximately 700,000 tons of dyes are produced annually, and 200,000 tons of dyes are released into water bodies during dyeing and finishing operations due to dyeing process inefficiencies. The aromatic molecular structure of dyes is ascribed to hydrocarbons, including C₆H₆, C₆H₅CH₃, C₁₄H₁₀, C₈H₁₀, C₁₀H₈, and others.^{4,5}

II. METHODOLOGY

2.1. Experimental site

The synthesization of MgO NPs, MgO/PANI NCs, and the studies of photocatalytic activities, and characterization using UV-Visible spectrophotometer were conducted in Chemistry Research Laboratory of Pratap College Amalner. To verify the molecular and crystalline structure of the as-synthesized photocatalysts, ATR-FTIR and XRD measurements were conducted at the Vellore Institute of Technology, School of Advance Sciences, Vellore.

2.2. Apparatus and instruments

The crystal structures of MgO NPs and MgO/PANI NCs were examined by X-ray diffractometer (Bruker D8 Advance Panalytical X Pert3). The determination of functional groups of as synthesized photocatalysts was studied with help of Fourier-transform infrared spectroscopy (FTIR, JASCO FT/IR-6700) in the wave number from 400-4000 cm^{-1} . The absorbance of the samples was determined using a UV-Visible spectrophotometer (UV-Visible spectrophotometer, JASCO V-670).

2.3. Chemicals and reagents

All the chemicals and reagents are analytical grade reagents which are used without further purification. Briefly, magnesium nitrate dihydrate $\text{Mg}(\text{NO}_3)_2 \cdot 2\text{H}_2\text{O}$ Loba Chem India, aniline ($\text{C}_6\text{H}_5\text{NH}_2$) 98%, hydrochloric acid (HCl), ammonium per sulfate (APS) 98%, from Sigma aldrich were chemicals used to prepare NPs and NCs. Crystal Violet (CV) dye is used as the model organic dye intended for investigating photocatalytic activities of MgO NPs, MgO/PANI NCs.

2.4. Preparation of MgO NPs

100 ml of 0.5 N NaOH is added drop by drop to the solution of 100 ml of 0.1N $\text{Mg}(\text{NO}_3)_2 \cdot 6\text{H}_2\text{O}$ with constant stirring for 1 hr. after complete addition the mixture is stirred for 2 hrs. Then formation of white precipitate is observed. then the precipitate is filtered and washed 2 to 3 times with distilled water and kept in an oven at 40 $^\circ\text{C}$ for 48 hrs for complete drying. Then the ppt is calcinated in a muffle furnace for 3 hrs at 500 $^\circ\text{C}$ to get MgO nanoparticles.

2.5. Synthesis of MgO/PANI NCs

Take 10 ml of 1 M HCl solution in a 250 ml RB flask and add 0.1 gm of MgO nanoparticles in it. The mixture is sonicated in an ultrasound bath for 30 minutes. 1 ml aniline is added in 100 ml 1 M HCl solution in a beaker. This solution is added in RB flask and sonicated for 30 minutes. 2.84 gm of ammonium peroxy sulphate (APS) equal molar with aniline is added in 100ml 1M HCl solution in a beaker. This solution is filled in a burette and added dropwise to the mixture in an RB flask kept on magnetic stirrer. This RB flask is kept in glass bowl filled with ice to maintain temperature below 4 $^\circ\text{C}$ to achieve polymerization of aniline to polyaniline (Pani). green colour is developed to the mixture which indicate start of polymerisation reaction. After complete addition of APS solution, the mixture kept on constant stirring for 1 hr. the solution is filtered and washed several times with distilled water and kept in an oven at 45 $^\circ\text{C}$ for complete drying. The dried powder is obtained as 10% MgO doped Pani as nanocomposite. Then, the samples are ground and used for further characterization and degradation of dye.

2.6. Synthesis of PANI

PANI has synthesized through the in-situ polymerization method via dissolving 1 mL of the monomer (aniline) in 40 mL of 1 M HCl solution. The oxidant solution has prepared via dissolving 2.84 g of APS in 1M HCl which the polymerization reaction takes place at 0 °C for 12 h. The molar ratio of monomer to APS was 1:1. The precipitated samples are centrifuged and washed three times with water followed by drying at 70 °C for 24 h. The polymerization mechanism of PANI has indicated in Figure 1.

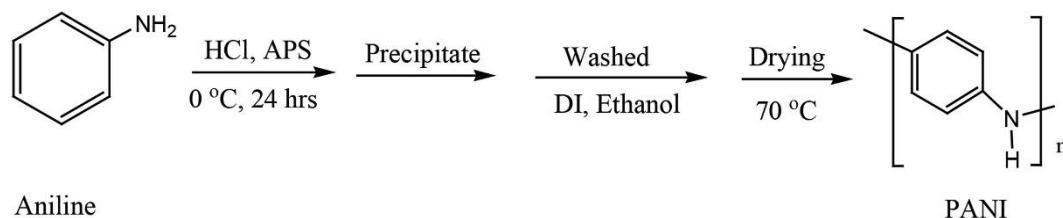


Figure 5.1 In-situ polymerization mechanism of PANI

2.7. Characterization of photo-catalysts

The crystalline structural measurements for photocatalysts have performed using XRD. Their crystallite sizes are calculated using Debye-Scherrer's Eq. (1):

$$D = \frac{0.9\lambda}{\beta \cos \theta} \quad 1$$

$D = 0.9\lambda / \beta \cos \theta$ where λ - wavelength of radiation used in Cu K α (0.15406 nm), β - full width at half-maximum of the peak, and θ - angle at the position of the maximum peak (in rad). The FT-IR spectrum of photocatalysts is recorded with ATR-FTIR in 400–4000 cm^{-1} wavenumber. The UV-Visible absorption of the synthesized photocatalyst were determined using a JASCO V-670 UV-Visible spectrophotometer equipped with a quartz tube scanning over 200–800 nm wavelength.

III. CHARACTERISATION OF MATERIAL

3.1. Analysis of functional group

Figure 2, 3 and 4 represents ATR-FTIR spectra of MgO NPs, PANI and MgO/PANI NCs between 400–4000 cm^{-1} vibration numbers respectively. The spectrum corresponding the PANI exhibits the broadband at 3204 cm^{-1} which represents N–H vibrations of polymer and the bending of N–H at 1472 cm^{-1} . ¹⁴ Absorption peaks observed at 1552 cm^{-1} corresponds to the bending mode of C=C in aromatic ring structures while the peak at 813 cm^{-1} is ascribed to the C–H out-of-plane bending in aromatic ring. The peak at 1290 cm^{-1} is assigned to C–N stretching of the secondary amine unit of PANI. the FT-IR spectrum of the studied MgO powder, bands at 468.62, 876.87, 1487.17, 1420.58 and 3389.70 cm^{-1} are illustrated. In particular, the major band observed at $\approx 469 \text{ cm}^{-1}$ is attributed to Mg–O vibrations.¹¹ The bands observed at approximately 876 and 1420 cm^{-1} are associated with carbonate species that are chemisorbed superficially on MgO,¹² while the broad band depicted at 3389 cm^{-1} corresponds to the O–H stretching, as well as bending vibrations of H_2O molecules,^{11,12} possibly due to atmospheric humidity during the conduction of the powder's measurement.¹³ The spectrum for MgO/PANI NCs at 468.62 and 876.87 cm^{-1} shows the absorption peak corresponds to MgO. The absorption band at 1023 and 1241 cm^{-1} corresponds to in-plane deformation of C–N and in-plane vibration of C–H in PANI structure. The peaks that appeared at 1284, 1420, 1551, and 3204 cm^{-1} correspond to C–N stretching of secondary amine, wagging vibration of pure MgO NPs, bending vibrations of N–H, and stretching vibration of N–H in PANI

respectively.¹⁴ Thus, from the ATR-FTIR spectrum, it strongly confirms that the nanoparticles are highly incorporated to PANI molecular chain and in-situ polymerization was successful during surface modification of doped MgO NPs with PANI.

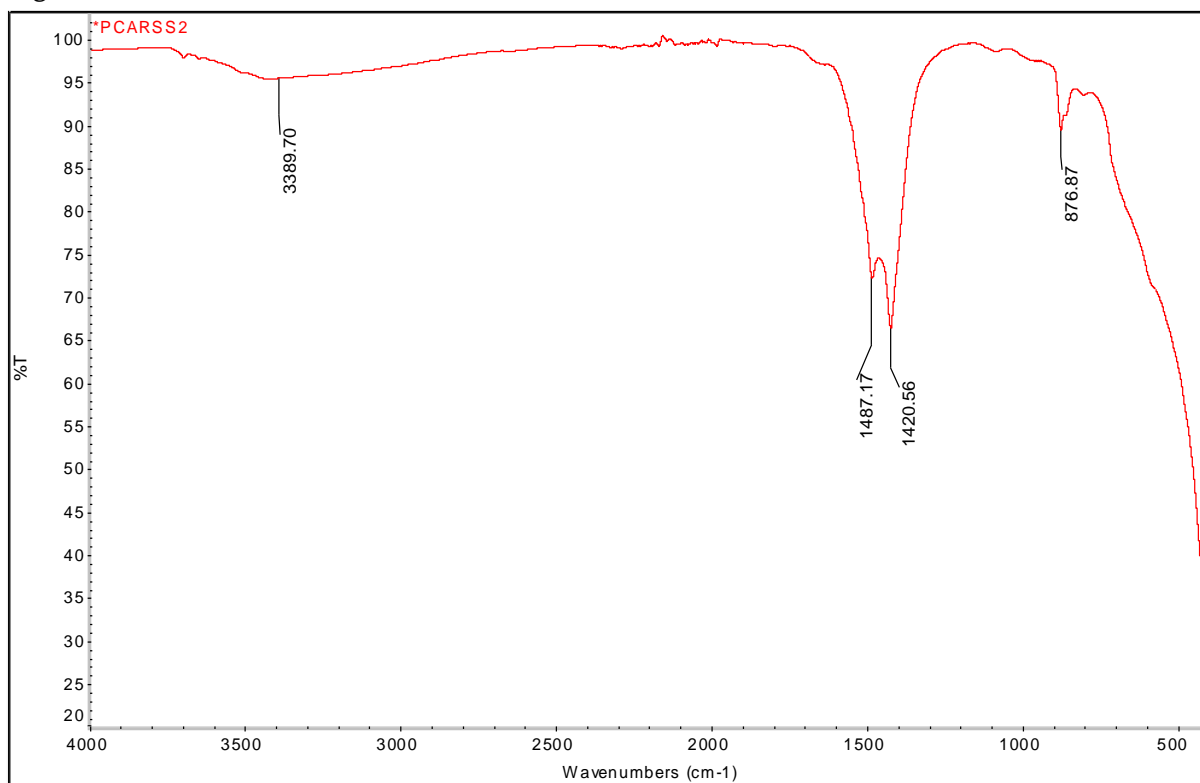


Figure 2: ATR FTIR of MgO

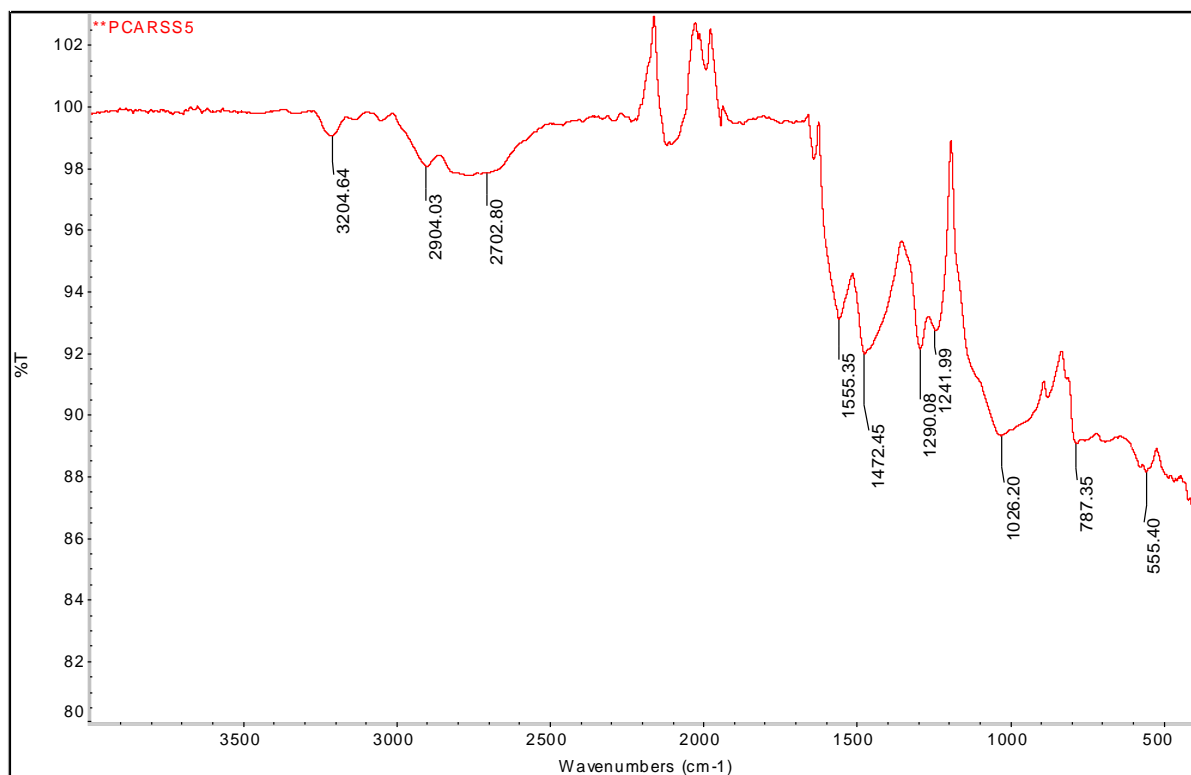


Figure 3: ATR FTIR of PANI

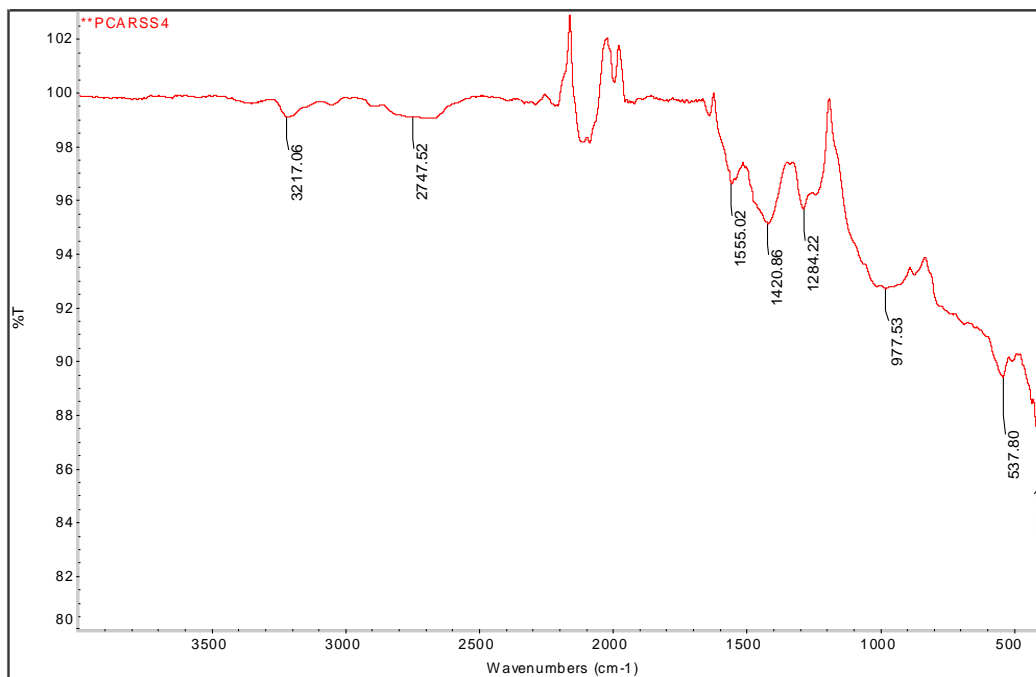


Figure 4: ATR FTIR of MgO/PANI

3.2. Analysis of crystalline structure

Figure 5, 6 and 7 depicts the XRD spectrum of MgO NPs, PANI and MgO/PANI NCs. These patterns delivered highly sharp and intensive diffraction peaks of NPs and PANI NCs. From the XRD results, the crystalline phase of pure and doped PANI were determined that all peaks are clearly matched to the face centered cubic phase. The sharp peaks are observed at 2 Theta = 30, 42 and 62 degrees for MgO nanoparticles. While for PANI The sharp peaks are observed at 2 Theta = 17, 20, 25, 27 and 28 degrees and for MgO/PANI NCs, the sharp peaks are observed at 2 Theta = 20, and 25 with small peaks at 30 and 50 degrees.

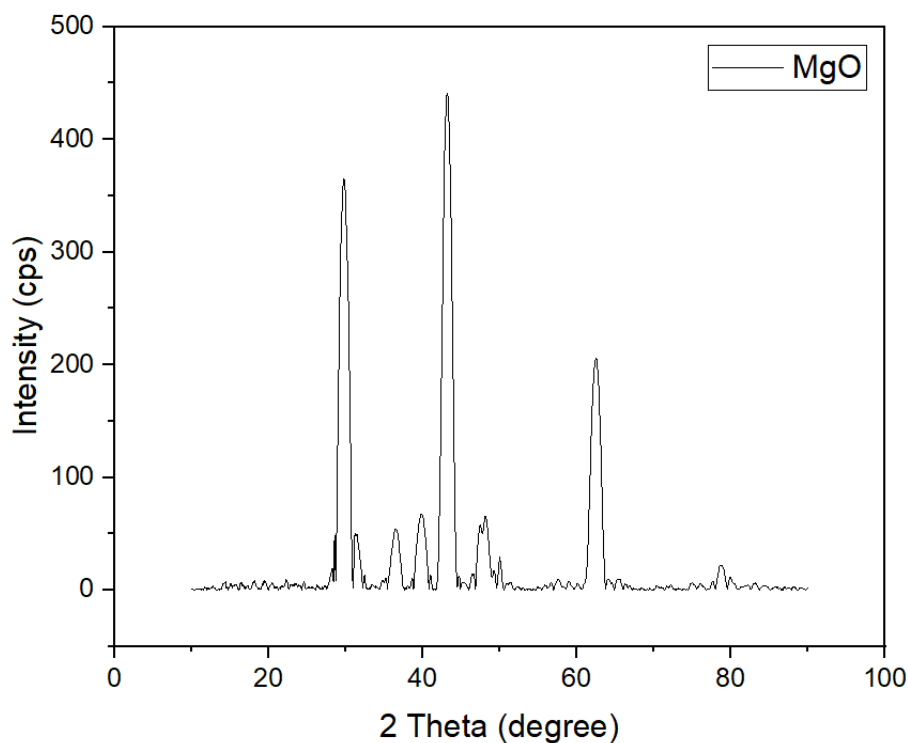


Figure 5: XRD structure of MgO

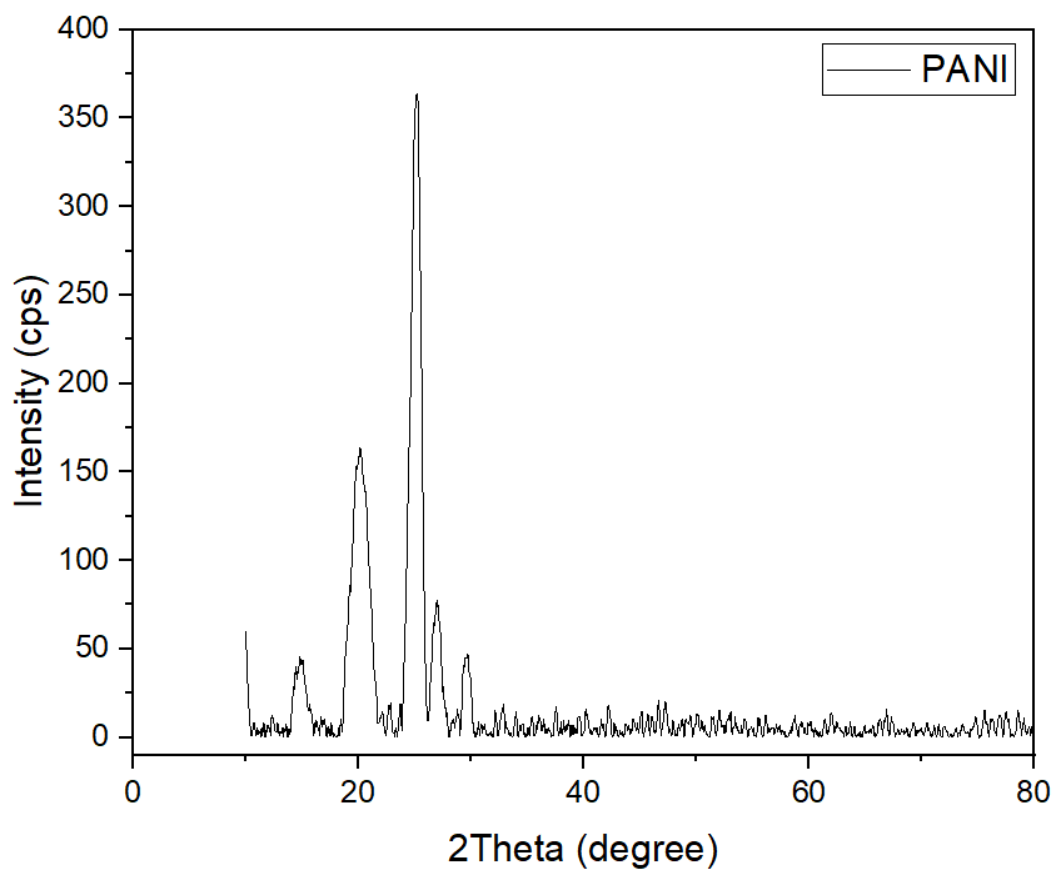


Figure 6: XRD structure of PANI

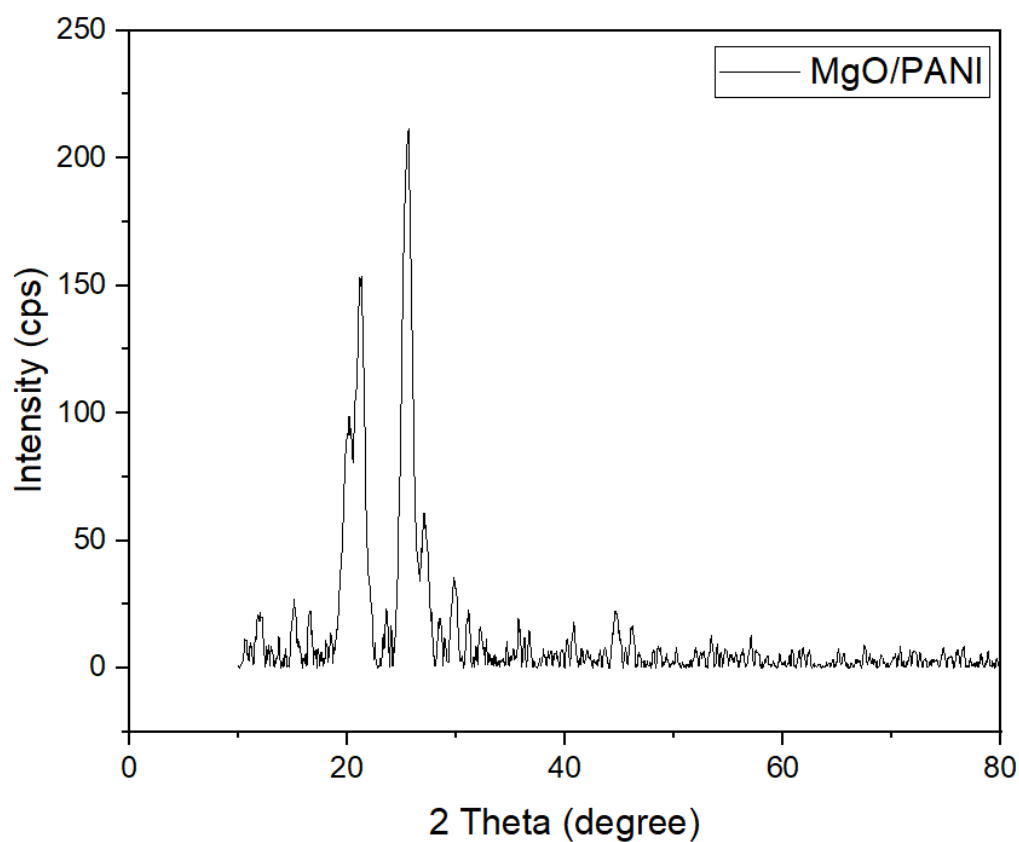


Figure: 7 XRD structure of MgO/PANI NCs

IV. STUDY OF DEGRADATION PROPERTIES

4.1. Effect of photocatalysts on Crystal Violet (CV) dye in summer season

Figure 8 showed the photocatalytic degradation performances of MgO NPs and MgO-PANI NCs. It was evaluated using an initial concentration of dye (50 ppm), catalyst load (50 mg), and pH (9) under Sun light irradiation. This degradation study was observed in the month of March and April between 11:00 am to 4:00 pm using equiptronics colorimeter EQ 335. The degradation tendency was increased with the irradiation time and become constant after 180 min indicating that it is the maximum degradation time of these dye. The photocatalytic degradation performances of each photocatalyst were calculated using Eq. (2) and summarized in Table 1.

$$\% \text{ of degradation} = \frac{A_0 - A_t}{A_0} \times 100 \quad 2$$

where A_0 - and A_t - the absorbance of dye at initial stage and at the reaction time "t".

Table 1. Photocatalytic degradation of Crystal Violet (CV) dye using 50 ppm dye concentration, 50 mg catalyst load, and pH 9 at room temperature under Sun light irradiation.

Time in min	MgO	MgO/PANI
30	-7.44	-7.96
60	71.07	5.31
90	76.03	11.50
120	88.43	18.58
150	92.56	37.17
180	94.62	46.72

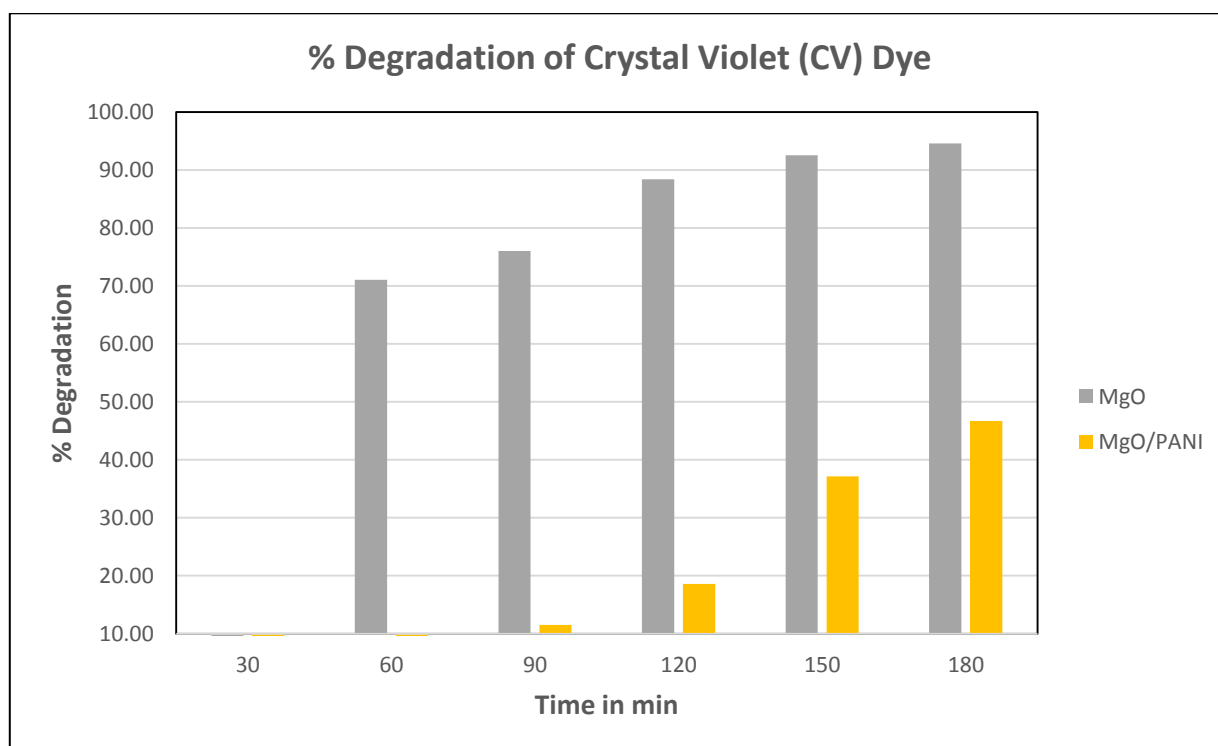


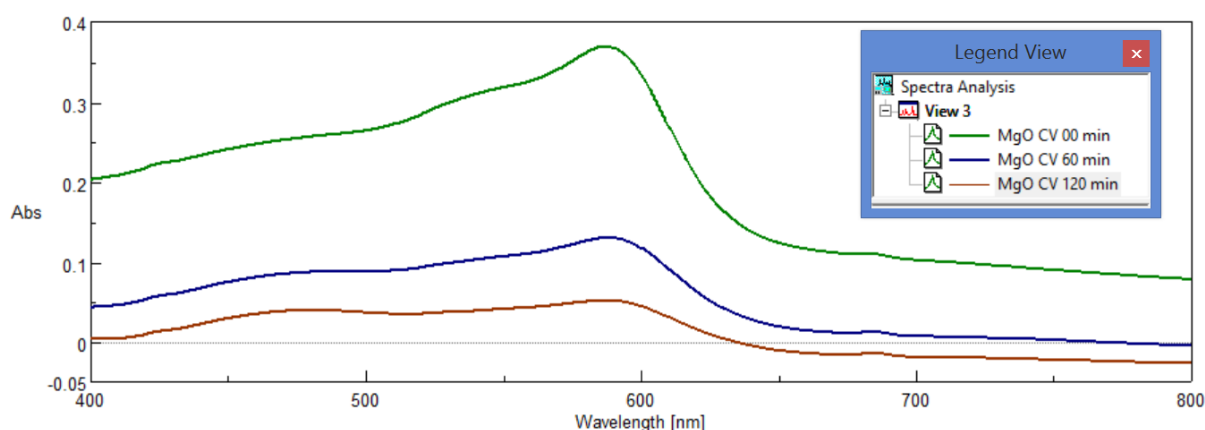
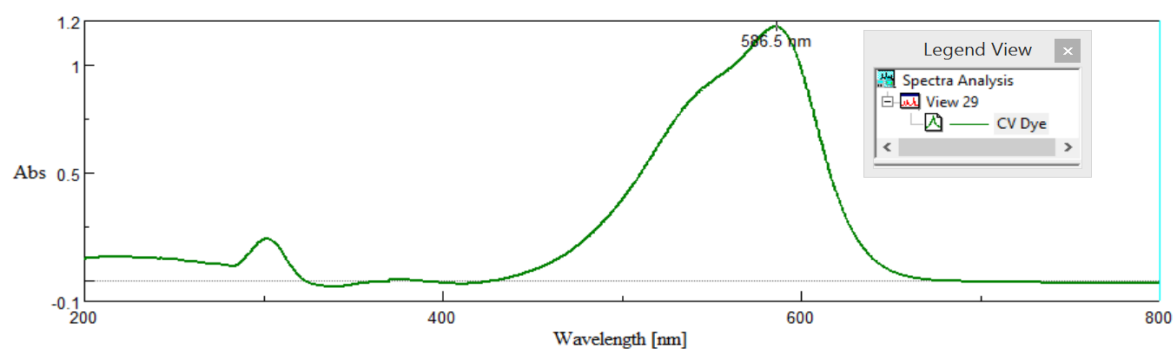
Figure 8: Photocatalytic degradation of Crystal Violet (CV) dye in summer

4.2. Effect of photocatalysts on Crystal Violet (CV) dye in winter season

Figure 9 showed the photocatalytic degradation performances of MgO NPs and MgO-PANI NCs. It was evaluated using an initial concentration of dye (50 ppm), catalyst load (50 mg), and pH (9) under Sun light irradiation. The absorption of the dye is studied using JASCO UV-Visible spectrophotometer V-670 which shows maximum absorption of CV dye at 586 nm wavelength. This degradation study was observed in the month of October and November between 11:00 am to 4:00 pm. The degradation tendency was increased with the irradiation time and become constant after 180 min indicating that it is the maximum degradation time of these dye. The photocatalytic degradation performances of each photocatalyst were calculated using Eq. (2) and summarized in Table 2.

Table 2. Photocatalytic degradation of Crystal Violet (CV) dye using 50 ppm dye concentration, 50 mg catalyst load, and pH 9 at room temperature under Sun light irradiation.

Time in min	MgO	MgO PANI
60	64.67	41.79
120	86.41	97.14
180		100.00



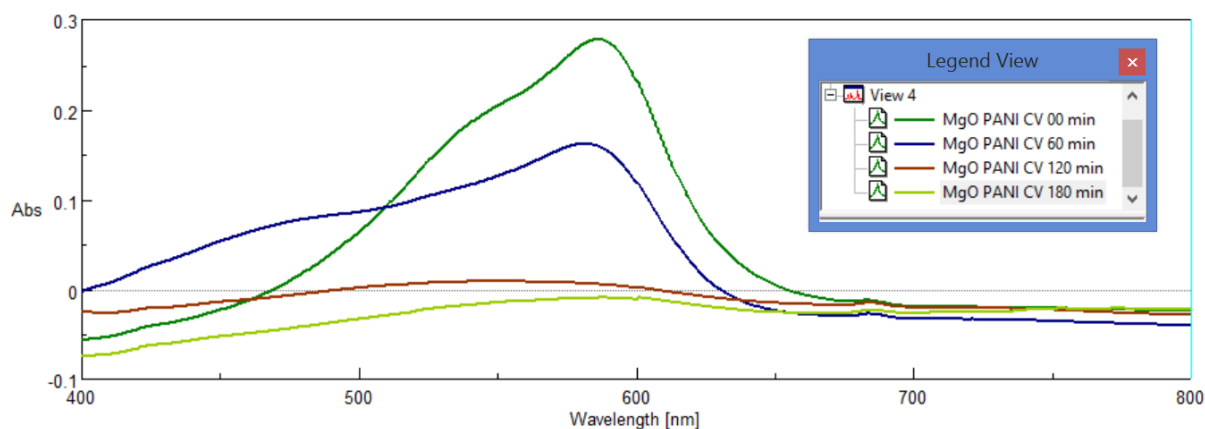


Figure 9: Photocatalytic degradation of Crystal Violet (CV) dye in winter

V. RESULT AND DISCUSSION

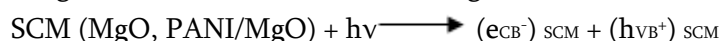
For MgO NPs, and MgO-PANI NCs catalysts after 180 min of retention time were found to be 94.62 and 46.72 % respectively in summer season. While in winter season, both catalysts give 100% dye degradation.

Herewith particular catalyst MgO/PANI NCs, the results signify that, at 180 min irradiation time and above, the CV dye is totally degraded and becomes colourless. The degradation rate has increased because of the availability of active binding sites on the surface of catalysts. At the equilibrium position, the adsorption is possibly an attachment-controlled system owing to the presence of few active sites. Under similar experimental conditions, the photocatalytic degradation performance of MgO NPs is worthless as compared to that of doped and polymer-treated surface, indicating that the addition of inorganic and organic additives has dominated the photodegradation efficiency of the synthesized nanocomposite. The photo-degradation efficiency of the nanocomposite was effectively improved due to the incorporation of organic additives such as PANI, which helps to increase the active sites and the interfacial charge carrier transferring rate.²

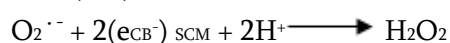
VI. PHOTOCATALYTIC DEGRADATION MECHANISM

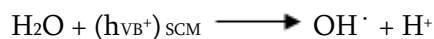
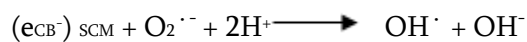
In the case of CP-metal oxide hybrid, CP acts as a photosensitizer to absorb a wide range of visible light because of the lower bandgap compared to pure metal oxide. The excited electrons in the LUMO of CP chains are injected into the CB of transition metal oxide or hybrid materials, which reacts with an adsorbed water molecule to form $O_2^{\cdot -}$ radicals, whereas holes may react with water to form $^{\cdot}OH$.^{15,16}

The general understanding of the photocatalysis mechanism is that the photoabsorption of a semiconducting material causes the electrons to excite from the valence band (VB) to the conduction band (CB), leaving positive holes in the VB, resulting in the electron-hole pair e_{CB}^- / h_{VB}^+ generation. It is known that PANI homopolymer is a conducting polymer. Photons are absorbed by the PANI homopolymer or the PANI/MgO catalyst when the energy ($h\nu$) is equal to or greater than the semiconductor band gap, and electron-hole pairs are generated in these semiconducting materials (SCM).



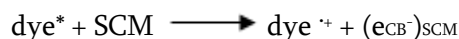
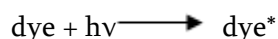
Then, the photogenerated electron-hole pairs migrate to the surface of the catalyst and react with the species adsorbed on the surface.





These reactions prevent the electron-hole pairs from recombining which reduces the efficiency of photocatalytic activity.

A sensitized photocatalytic process may be able to be operated in the presence of a coloured organic compound; in this case the adsorbed dye molecules are excited by visible light and thus act as photosensitizers. The excited dye molecule subsequently transfers electrons into the conduction band of the PANI homopolymer or PANI/MgO nanocomposite, while the dye itself is converted to its cationic radical



These reactive species produced in the above manner can then react with the dye to form the degradation products and thus are responsible for the discoloration of CV dye.

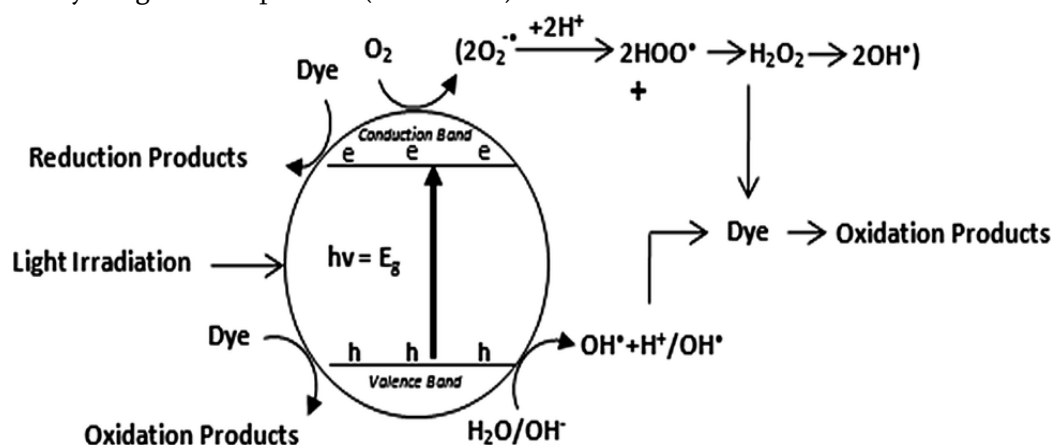
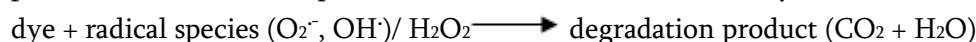


Figure 10: Dye degradation mechanism

VII.CONCLUSIONS

CV dye:For MgO NPs, and MgO-PANI NCs catalysts after 180 min of retention time were found to be 94.62 and 46.72 % respectively in summer season. While in winter season, both catalyst gives 100% dye degradation.

In the current report, MgO NPs and MgO/PANI NCs were successfully synthesized via precipitation method in order to evaluate their degradation efficiency against CR, MO and CV dye in aqueous media. The surface properties of as-synthesized nanomaterials were characterized with the help of advance analytical tools such as ATR-FTIR, XRD, UV-Vis. The ATR-FTIR spectrum revealed that doped MgO NCs was successfully modified with PANI as it confirmed from the broad vibration spectrum observed $\sim 3250\text{ cm}^{-1}$ ascribed to the presence of N-H bond of PANI. The XRD spectrum ascribed to the numerous sharp and highly intensive peaks confirms the MgO NPs and MgO NCs structure is Face centered cubic with decreasing crystalline size while further decreasing after nanocomposite formation. The maximum photocatalytic degradation efficiency was achieved 100 % using MgO/ PANI NCs against CV dye at 50 ppm of initial dye concentration, pH 9, and 50 mg/50ml catalyst dosage under direct sun light irradiation for 180 min. The result of this research work showed that, MgO/PANI NCs is one of the promising photocatalytic nanocomposites which could be generally applicable to the treatment of wastewaters effluents containing acidic dye molecules.

VIII. REFERENCES

- [1]. Jaspal, D.; Malviya, A. Composites for wastewater purification: A review. *Chemosphere* 2020, 246, 125788.
- [2]. Sharma, V.K.; Jinadatha, C.; Lichtfouse, E. Environmental chemistry is most relevant to study coronavirus pandemics. *Environ.Chem. Lett.* 2020, 18, 993–996.
- [3]. Sarkar, S.; Banerjee, A.; Halder, U.; Biswas, R.; Bandopadhyay, R. Degradation of Synthetic Azo Dyes of Textile Industry: A Sustainable Approach Using Microbial Enzymes. *Water Conserv. Sci. Eng.* 2017, 2, 121–131.
- [4]. Zare, E.N.; Motahari, A.; Sillanpää, M. Nanoadsorbents based on conducting polymer nanocomposites with main focus on polyaniline and its derivatives for removal of heavy metal ions/dyes: A review. *Environ. Res.* 2018, 162, 173–195.
- [5]. Tara, N.; Siddiqui, S.; Rathi, G.; Inamuddin, I.; Asiri, A.M. Nano-engineered adsorbent for removal of dyes from water: A review. *Curr. Anal. Chem.* 2019, 16, 14–40.
- [6]. Saeed, M.; Khan, I.; Adeel, M.; Akram, N.; Muneer, M. Synthesis of a CoO–ZnO photocatalyst for enhanced visible-light assisted photodegradation of methylene blue. *New J. Chem.* 2022, 46, 2224–2231.
- [7]. Kocijan, M.; C'urkovic', L.; Vengust, D.; Radošević', T.; Shvalya, V.; Gonçalves, G.; Podlogar, M. Synergistic remediation of organic dye by titanium dioxide/reduced graphene oxide nanocomposite. *Molecules* 2023, 28, 7326.
- [8]. Ngoc, P.K.; Mac, T.K.; Nguyen, H.T.; Thanh, T.D.; Van Vinh, P.; Phan, B.T.; Duong, A.T.; Das, R. Superior organic dye removal by CoCr₂O₄ nanoparticles: Adsorption kinetics and isotherm. *J. Sci. Adv. Mater. Devices* 2022, 7, 100438.
- [9]. Sansenya, T.; Masri, N.; Chankhanittha, T.; Senasu, T.; Piriyanon, J.; Mukdasai, S.; Nanan, S. Hydrothermal synthesis of ZnO photocatalyst for detoxification of anionic azo dyes and antibiotic. *J. Phys. Chem. Solids* 2022, 160, 110353.
- [10]. Crini, G.; Lichtfouse, E. Advantages and disadvantages of techniques used for wastewater treatment. *Environ. Chem. Lett.* 2019, 17, 145–155.
- [11]. Khaleel, W.A.; Sadeq, S.A.; Alani, I.A.M.; Ahmed, M.H.M. Magnesium oxide (MgO) thin film as saturable absorber for passively mode locked erbium-doped fiber laser. *Opt. Laser Technol.* 2019, 115, 331–336.
- [12]. Sutradhar, N.; Sinhamahapatra, A.; Pahari, S.K.; Pal, P.; Bajaj, H.C.; Mukhopadhyay, I.; Panda, A.B. Controlled synthesis of different morphologies of MgO and their use as solid base catalysts. *J. Phys. Chem. C* 2011, 115, 12308–12316.
- [13]. Kaningini, G.A.; Azizi, S.; Nyoni, H.; Mudau, F.N.; Mohale, K.C.; Maaza, M. Green synthesis and characterization of zinc oxide nanoparticles using bush tea (*Athrixiphylicoides* DC) natural extract: Assessment of the synthesis process. *F1000Research* 2021, 10, 1077.
- [14]. A. Salama, et al., Photocatalytic degradation of organic dyes using composite nanofibers under UV irradiation, *Appl. Nanosci.* 8 (1) 2018 155–161.
- [15]. B. Jana, S. Bhattacharyya, A. Patra, Conjugated polymer P3HT–Au hybrid nanostructures for enhancing photocatalytic activity, *Phys. Chem. Chem. Phys.* 17(23)2015 15392–15399.
- [16]. D. Wang, et al., Characterization and photocatalytic activity of poly (3-hexylthiophene)-modified TiO₂ for degradation of methyl orange under visible light, *J. Hazard Mater.* 169 (1-3) 2009 546–550.

Phytochemicals and GC-MS Analysis of Bioactive Compounds Present In Methanolic Leaves Extract of *Justicia Adhatoda* L

Anil F. Bobade¹, Rahul P. Rahate²

¹Department of Industrial Chemistry, Arts, Science and Commerce College, Chikhaldara, Maharashtra, India

²Department of Chemistry, Arts, Science and Commerce College, Chikhaldara, Maharashtra, India

ARTICLE INFO

Article History:

Accepted : 01 Jan 2025

Published : 10 Jan 2025

Publication Issue :

Volume 12, Issue 7

January-February-2025

Page Number :

339-344

ABSTRACT

Justicia adhatoda is a genus of trees in the legume family, Acanthaceae . It consists of a single species, *Justicia adhatoda*, a common medicinal shrub that grows widely across the forest and is often referred to as "brenkar," "vasaka," or "Malabar nut." It is regarded as a native plant in Southeast Asia's tropical belts. *Justicia adhatoda* leaf extracts were prepared in methanolic solvent to study the phytochemical profile using Gas Chromatography - Mass Spectrometry method. GC-MS analysis of *J. adhatoda* leaf extracts revealed the existence of the major peaks presented in methanol were Amrinone (RT: 15.88); n- Hexadecanoic acid (RT: 16.33); Phytol (RT: 17.81); 9, 12, 15-Octadecatrienoic acid, (Z, Z, Z) - (RT: 18.04). From this study it is obvious that *J. adhatoda* leaf extracts contain many biologically active compounds and also it gives a detailed insight about the phytochemical profile which could be exploited for the development of plant-based drugs and Insecticides.

Keywords: *Justicia adhatoda*, GC-MS, Methanol extracts, Acanthaceae etc.

I. INTRODUCTION

India is the world's largest producer of medicinal plants, including *Justicia adhatoda*, a small evergreen herbaceous plant from the Acanthaceae family. The plant's secondary metabolites, traditionally employed for their therapeutic properties, are low-molecular-weight organic compounds [1-3]. These compounds have intriguing biological properties and are used in medicines, pesticides, colors, tastes, and scents. *Justicia adhatoda*, a shrub in the Acanthaceae family, is commonly referred to as Malabar nut or Vasaka [4-6]. This highly prized Indian medicinal plant treats respiratory conditions such as TB, bronchitis, cough, and asthma. The plant's leaves are the primary ingredient in its herbal medication, which has been widely used to treat various illnesses [7-10]. Gas chromatography-mass spectrometry (GC-MS) has become a crucial technical platform for secondary metabolite profiling in plant and non-plant species. This technique combines the advantages of mass spectrometry and gas-liquid chromatography to identify various compounds in a test sample

[11-13]. The effectiveness of this species against the influenza type-B virus has been found, with the methanolic extract being the only one that can stop infection by stopping the virus from attaching itself. The current work was conducted to determine the phytoconstituents present in methanolic leaf extracts of *J. adhatoda*.

II. MATERIALS AND METHODS

A. Collection of plant material-

The fresh leaves of *Justicia Adhatoda* (Linn.) of Acanthaceae family were collected from Arts, Science and Commerce college campus, Melghat, Chikhaldara, Dist-Amravati (Maharashtra). The experimental site is located between co-ordinates 20.21°N,77.725°E and an altitude of 1,188 m in Central India's foothills, experiencing a subtropical climate during the winter season in September and October 2024, with plant identification confirmed by Dr. U. R. Kokate, Department of Botany ASC College, Chikhaldara, District-Amravati.

B. Preparation of *Justicia adhatoda* leaf extract -

All chemicals and solvents used in this research were analytical grade and purchased from SD Fine Chemicals Pvt. Ltd., Mumbai. The fresh leaves of *Justicia Adhatoda* (Linn) wash and dried over ambient temperature, dried sample were powdered by grinder was extracted in methanol by using Soxhlet apparatus and extracts were concentrated by evaporating the respective solvent on rotary evaporator. The concentrated extract was collected cool prior to analysis.

Phytochemical analysis (Qualitative analysis)

i) Test for Alkaloids-

0.4 g extract was mixed with 8 ml of 1% Hydrochloric acid, warmed and filtered. 2 ml of each filtrate was titrated separately with (a) Mayer's reagent and (b) Drage Dorff's reagent (c) Wagner Test, Yellow precipitation for Mayer's reagent, red precipitation for Drage Dorff's reagent and formation of brown / Reddish precipitate for Wagner reagent was observed to indicate the presence of alkaloids [14].

ii) Test of flavonoids: Two methods were employed to detect the presence of flavonoids in the extract.

a) Alkaline reagent test:

When the extract of leaf was treated with a 10% NaOH solution, a bright yellow colour appeared, indicating the presence of flavonoids.

b) NH_4OH test: 3 ml of extract were 10 % NH_4OH solution development of yellow fluorescence indicates positive test [15].

iii) Tannins Test: --

Gelatine Test -To extract 1% gelatine solution containing sodium chloride was added. Formation of white precipitation indicates the presence of tannins [16].

Ferric chloride test:- About 0.1 g of the extract boiled in 2 ml of water/dimethyl sulfoxide (DMSO) was filtered and mixed with a few drops of 0.1% of ferric chloride. Then, it was observed for brownish green or a blue-black coloration [17].

iv) Terpenoids (Horizon test): -

Test for triterpenoids Horizon test- 2 ml of trichloroacetic acid were added to 1 ml of extract. The presence of terpenoids was confirmed by the formation of a red precipitate [18].

v) **Test for glycosides:** -

Legal's Test: - Extracts were treated with sodium nitroprusside in pyridine and sodium NaOH. Formation of pink to blood red colour indicates presence of cardiac glycosides [19].

vi) **Test for steroids:** -

Test for steroids Salkowski test: - The test extract was shaken with chloroform, and concentrated H₂SO₄ was then added to the side of a test tube; a red colour developed, indicating the presence of steroids [20].

vii) **Tests for proteins**

(a) **Biuret test:** -Two drops of 3% copper sulphate and few drops of 10% sodium hydroxide were added to 1 ml of extract, violet or red colour formation indicating that proteins are present [17].

(b) **Ninhydrin test:** - Two drops of 0.2% freshly prepared ninhydrin solution added to 1 ml of extract. Production of purple colour shows the presence of proteins [21].

GC-MS Analysis of plant leaves extract -

GC-MS analysis was performed at Shimadzu Nexis GC- 2030; Column Oven Temp. :80°C Injection Temp.260.00 °C Injection Mode: Split Flow Control Mode: Linear Velocity Pressure 81.1 kPa, Total Flow :40.2 mL/min Column Flow :1.20 mL/min Linear Velocity :40.4 cm/sec. Purge Flow :3.0 mL/min, Split Ratio :30.0, Oven Temp. Program temperature(80°C) Hold Time (4 min) to 280°C Hold Time 6 min).GCMS-QP2020 NX Ion Source Temp :220°C, Interface Temp. :280°C, Solvent Cut Time :6.50 min, Detector Gain Mode: Relative to the Tuning Result.

All analyses were carried out using the TSS-2000 [1] program. Low-resolution mass spectra were collected at a resolving power of 1000 (20% height definition) while scanning from m/z 25 to m/z 700 at 0.3 seconds each scan with a 0.2 second interscan delay. High resolution mass spectra were obtained with a resolving power of 5000 (20% height definition) by scanning the magnet from m/z 35 to m/z 500 at 0.30 second each scan.

Column: DB-5ms (30m x 0.25mm x 0.25µm), Oven Program: 100°C (2min) → 280°C (10°C/min), Carrier Gas: Helium (1.5 mL/min), Injector: Spitless (250°C), Detector: Mass spectrometer (EI, 50-500 m/z), Detector Gain :0.86 kV +0.00 kV Scan Mode: Full scan, Data Analysis: Peak identification using NIST library.

III.RESULTS AND DISCUSSION

The results of the various phytochemical screening tests carried out during the experiment are shown in Table 1. Flavonoids, Alkaloid, Glycosides, Tannin, terpenoid, steroid & proteins, were the phytoconstituents found in plants.

Phytochemical screening of the methanol leaf extracts of J. adhatoda.

S.No.	Phytochemical	Test Performed	Methanolic Extract
1	Alkaloids	Mayer Test	+
		Dragendroff's Test	+
		Wagner Test	+
2	Flavonoids	Alkaline reagent test	-
		NH ₄ OH Test	-
3	Tannins	Ferric Chloride Test	++
		Gelatine Test	-
4	Terpenoids	Salkowski Test	+
5	Glycosides	Legal test	+++

S.No.	Phytochemical	Test Performed	Methanolic Extract
6	Steroid	Salkowski test	++
7	Proteins	Biuret test	+++
		Ninhydrin test.	+++

(-) =absence; (+) traces; (++) moderate; (+++) abundance of phytoconstituents

Table.1: Preliminary phytochemical screening of extracts of powdered leaves of *Justicia adhatoda*.

Phytochemical components in methanol extract of *J. adhatoda* by GC-MS report- The GC-MS analysis revealed the presence of 13 compounds (Table-2) from the methanol leaf extract of *J. adhatoda* (Figure 1). The major constituents were Amrinone (RT: 15.88) ; n- Hexadecanoic acid (RT: 16.33) ; Phytol (RT: 17.81) ; 9,12,15-Octadecatrienoic acid, (Z,Z,Z)- (RT: 18.04) along with other minor constituents were also present. The GC-MS chromatogram shows the peak area separation of the components. The above-mentioned isolated compounds from the methanol extract of *J. adhatoda* leaves seem to possess the reported biological activity and further study of these phytoconstituents may prove the medicinal importance in future.

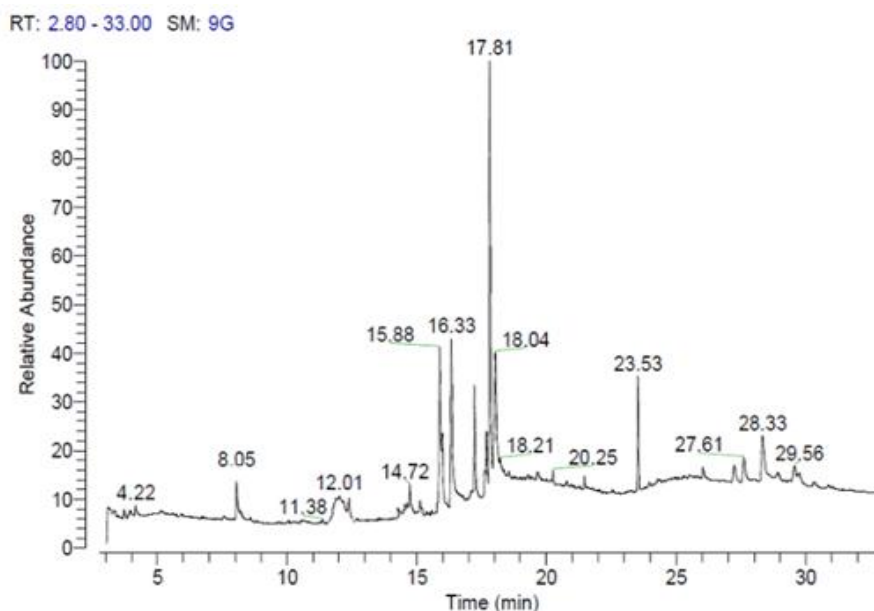


Fig. 1: GC-MS Profile of Methanol leaf extract of *J. adhatoda*

Sr. No.	RT	Compound name	Molecular Formula	Area %
1	17.81	Phytol	C ₂₀ H ₄₀ O	23.96
2	18.04	9,12,15-Octadecatrienoic acid, (Z,Z,Z)-	C ₁₈ H ₃₀ O ₂	14.81
3	15.88	Amrinone	C ₁₀ H ₉ N ₃ O	11.42
4	16.33	n- Hexadecanoic acid	C ₁₆ H ₃₂ O ₂	9.82
5	12.01	Pentadecanoic Acid	C ₁₅ H ₃₀ O ₂	9.31
6	17.23	Ethyl 4-quinazoline -2- carboxylate	C ₁₁ H ₁₀ N ₂ O ₃	6.61
7	28.33	alpha-Sitosterol	C ₂₉ H ₅₀ O	5.98
8	23.53	Squalene	C ₃₀ H ₅₀	5.23
9	15.98	Hexadecanoic acid, methyl ether	C ₁₇ H ₃₄ O ₂	4.42
10	17.68	9,12,15-Octadecatrienoic acid, methyl ether, (Z,Z,Z)-	C ₁₉ H ₃₂ O ₂	2.99
11	8.05	Eicosane, 2-cyclohexyl-	C ₂₆ H ₅₂	2.65

Sr. No.	RT	Compound name	Molecular Formula	Area %
12	27.61	Stigmasterol	C ₂₉ H ₄₈ O	1.43
13	12.39	Caryophyllene	C ₁₅ H ₂₄	1.17

Table 2. Phytochemical components in methanol extract of *J. adhatoda* by GC-MS report.

IV. CONCLUSIONS

Hence, the phytochemical screening of the selected plant sample was done. From the study, it could be concluded that plants are a great source of phytochemicals that could be utilized in curing various ailments. Alkaloid, flavonoid, Tannin, terpenoid, glycosides steroid & proteins, were the phytoconstituents present abundantly in plants.

Phytochemical screening played an important role in identifying various phytoconstituents present in leaves extracts. The study provided an important basis for further investigation into the isolation and characterization of phytoconstituents from the selected plants for the development of drugs. The study was only based on qualitative analysis and GC-MS study. It would be better if a quantitative detection, their bioactivity of various phytochemicals could be performed. The study would be more beneficial if the detection, analysis, and separation of the phytoconstituents could be done by column chromatography & thin layer chromatography.

V. ACKNOWLEDGMENTS

The authors would like to acknowledge the principal and management of Arts, Science and Commerce College, Chikhaldara for providing the facilities and funding to perform the research work.

VI. REFERENCES

- [1]. Swapna, N. L., Prasad, M. A. D. A. N., & Prasad, S. H. K. R. (2011). Efficacy of *Euphorbia tirucalli* (L.) towards microbicidal activity against human pathogens. *International Journal of Pharmaceutical and Bio Sciences*, 2(1), 229-235.
- [2]. Jain, S. K. (1991). *Dictionary of Indian folk medicine and ethnobotany*. Deep publications.
- [3]. Atal, C. K. (1980). *Chemistry and pharmacology of vasicine: A new oxytocic and abortifacient*. Regional Research Laboratory.
- [4]. Kumar, A., Ram, J., Samarth, R. M., & Kumar, M. (2005). Modulatory influence of *Adhatoda vasica* Nees leaf extract against gamma irradiation in Swiss albino mice. *Phytomedicine*, 12(4), 285-293.
- [5]. Gupta, M. K., Sharma, P. K., Ansari, S. H., & Rekha Lagarkha, R. L. (2006). Pharmacognostical evaluation of *Grewia asiatica* fruits..
- [6]. Barry, V. C., Conaltry, M. L., Rylance, H. J., & Smith, F. R. (1955). Antitubercular effect of an extract of *Adhatoda vasica*. *Nature*, 176(4472).
- [7]. Robertson, D. G. (2005). Metabonomics in toxicology: a review. *Toxicological sciences*, 85(2), 809-822.
- [8]. Chopra, R. N., Nayer, S. L., & Chopra, I. C. (1956). *Glossary of indian medicinal plants*, National Institute of science and Communication. CSIR Publication, New Delhi, India, 330., V ed New Delhi 1956; 12:157.
- [9]. Kritkar, K. R., & Basu, B. D. (1935). *Indian Medicinal Plants*. Vol: 2 & 4. Lalit Mohan Basu, Allahabad.

- [10]. Rastogi, R., & Mehrotra, B. (1994). Compendium of Indian Medicinal Plants published by Central Drug Research Institute. Lucknow and National Institute of Sciences Communication and Information Resources: New Delhi, 395-8.
- [11]. Robertson, D. G. (2005). Metabonomics in toxicology: a review. *Toxicological sciences*, 85(2), 809-822.
- [12]. Kell, D. B., Brown, M., Davey, H. M., Dunn, W. B., Spasic, I., & Oliver, S. G. (2005). Metabolic footprinting and systems biology: the medium is the message. *Nature reviews microbiology*, 3(7), 557-565.
- [13]. Fernie, A. R., Trethewey, R. N., Krotzky, A. J., & Willmitzer, L. (2004). Metabolite profiling: from diagnostics to systems biology. *Nature reviews molecular cell biology*, 5(9), 763-769.
- [14]. Godghate, A., Sawant, R., & Sutar, A. (2012). Phytochemical analysis of ethanolic extract of roots of *Carrisa carandus* Linn. *Rasayan Journal of Chemistry*, 5(4), 456-459.
- [15]. Gini, T. G., & Jothi, G. J. (2013). Preliminary phytochemical screening of whole plant extracts of *Peperomia pellucida* (Linn.) HBK (Piperaceae) and *Marsilea quadrifolia* Linn. (Marsileaceae). *International Journal of pharmacognosy and phytochemical research*, 5(3), 200-214.
- [16]. Morsy, N. (2014). Phytochemical analysis of biologically active constituents of medicinal plants. *Main Group Chemistry*, 13(1), 7-21.
- [17]. Pant, D. R., Pant, N. D., Yadav, U. N., & Khanal, D. P. (2017). Phytochemical screening and study of antioxidant, antimicrobial, antidiabetic, anti-inflammatory and analgesic activities of extracts from stem wood of *Pterocarpus marsupium* Roxburgh. *Journal of Intercultural Ethnopharmacology*, 6(2), 170.
- [18]. Kancherla, N., Dhakshinamoothi, A., Chitra, K., & Komaram, R. B. (2019). Preliminary analysis of phytoconstituents and evaluation of anthelmintic property of *Cayratia auriculata* (in vitro). *Maedica*, 14(4), 350.
- [19]. Khandekar, U., Bobade, A., & Ghongade, R. (2015). Evaluation of antioxidant activity, in-vitro antimicrobial activity and phytoconstituents of *Schleichera oleosa* (Lour.) Oken. *Int J Biol Pharm Res*, 6(2), 137-43.
- [20]. Wankhade, M. S., & Mulani, R. M. (2015). Preliminary phytochemical screening and chromatographic fingerprint analysis of *acacia leucopholea* roxb. methanolic leaf and bark extract by hptlc technique. *Indo American Journal of Pharmaceutical Research*, 4(1), 184-191.
- [21]. Shaikh, J. R., & Patil, M. (2020). Qualitative tests for preliminary phytochemical screening: An overview. *International Journal of Chemical Studies*, 8(2), 603-608.

Antimicrobial and Pharmacological Evaluation of Propane 1, 3-Diones Derivatives Containing P-Formyl Phenol Moiety

Rajendra M. Pathade^{1*}, Pravin S. Bodkhe¹, R.D. Isankar²

¹Department of Chemistry, Vidyabharati Mahavidyalaya, Amravati 444602, Maharashtra, India

²Department of Chemistry, Vidarbha Institute of Science & Humanities, Amravati 444604, Maharashtra, India

ARTICLE INFO

Article History:

Accepted : 01 Jan 2025

Published : 10 Jan 2025

Publication Issue :

Volume 12, Issue 7

January-February-2025

Page Number :

345-351

ABSTRACT

Propane-1,3-diones or β -diketones are one of the important classes of organic compounds frequently encountered in synthetic chemistry. Propane-1,3-diones or β -diketones acts as key intermediates for the synthesis of core heterocycles due to their specific chemo selectivity properties as well as provide convenient building blocks to biologically active substituents. In this project work, a new series of β -diketones namely 1-(5'-formyl-2'-hydroxyphenyl)-3-(substituted phenyl)-propane-1,3-diones (4a-e) have been synthesized from p-formyl phenol. They have been studied in order to investigate their in-vitro anti-inflammatory as well as antioxidant effects by performing Inhibition of Protein Denaturation Assay and Reducing Power Assay method respectively. Also studied their antimicrobial effects against growth response of various strains of bacteria and fungi through agar diffusion method.

Keywords: p-formyl phenol, Propane-1,3-diones, Antibacterial, Antifungal, Antioxidant and Anti-Inflammatory Activity.

I. INTRODUCTION

Propane-1,3-diones which are commonly referred to as β -diketones are the important class of organic compounds frequently encountered in synthetic chemistry[1]. β -diketones are versatile metal coordinating agents and have played a significant role in coordination chemistry. β -diketones and their metal complexes are associated with various pharmacological and biological properties such as antiviral[2], antifungal[3-4], antibacterial[5], anti-hypertensive[6], anti-cancer[7], anti-pyretic[8], anti-inflammatory[9], antioxidant[10] and analgesic properties[11] those find invaluable importance in medicine. It has also been used as an anti-sunscreen agent. β -diketones are well known to have keto-enol tautomerism and recently it is known that they have the important pharmacophores for the HIV-integrase (1N) Inhibitors. Owing to β -diketones having such different important synthetic and pharmacological properties. we have studies synthesis and characterization of a novel β -diketones namely 1-(5'-formyl-2'-hydroxyphenyl)-3(substituted phenyl)-propane-1,3-diones (4a-e)

from p-formyl phenol[12] Now in this project work studies Antibacterial, antifungal, antioxidant activity and anti-inflammatory activity of newly synthesized 1-(5'-formyl-2'-hydroxyphenyl)-3-(substituted phenyl)-propane-1,3-diones compounds(4a-e).

II. EXPERIMENTAL

MATERIALS AND METHODS

All chemicals and solvents were of research grade, its purity was good and easy to available. All these synthesized compounds were purified by recrystallization method. The melting points were determined by using Thiele's tube melting point apparatus. The Shimadzu (IRAffinity-1) spectrophotometer was used for IR spectra recording and the Bruker Avance II 400 MHz instrument was used for scanning ^1H NMR spectra using DMSO as solvent and TMS as an internal reference.

General Procedure for the Synthesis of 1-(5'-formyl-2'-hydroxyphenyl)-3-(substituted phenyl)-propane-1, 3-diones

In first step 4-formyl phenol (a) was refluxed with acetic anhydride and sodium acetate for 90 min. then two layers were formed which were separated by separating funnel washed by distilled water followed by 2% NaOH solution to obtained 4-formyl phenylacetate (1). In Kjeldal's flask, product (1) was heated with anhydrous AlCl_3 at 120°C for 50 min it was decomposed by 10% ice cold HCl then it dissolved in glacial acetic acid and pouring the solution in ice cold distilled water to get 5-Formyl-2-hydroxyacetophenone (2) then mixed the Product (2), substituted benzoic acid and POCl_3 were dissolved in pyridine at 0°C . After 7 hrs the reaction mixture was decomposed by 10% ice cold HCl to get 2-(Substituted benzoyloxy)-5-formyl acetophenones (3a-e). In last step mixed dry pyridine and Product (3a-e) then heat it at 70°C and added pulverized KOH. After 6-7 hrs, acidified it by ice cold dil. HCl to get 1-(5'-Formyl-2'-hydroxyphenyl)-3-(substituted phenyl)-propane-1, 3-diones (4a-e).

Physical Data

(4a) 1-(5'-Formyl-2'-hydroxyphenyl)-3-(4'-chlorophenyl)-propane-1,3-dione: Solid, $\text{C}_{16}\text{H}_{11}\text{ClO}_4$, M.W. 302.71, M.P. $110-116^\circ\text{C}$, Yield 70 %, (4b) 1-(5'-Formyl-2'-hydroxyphenyl)-3-(4'-bromophenyl)-propane-1, 3-dione: Solid, $\text{C}_{16}\text{H}_{11}\text{BrO}_4$, M.W. 347.16, M.P. $106-110^\circ\text{C}$, Yield 64 %, (4c) 1-(5'-Formyl-2'-hydroxyphenyl)-3-(4'-nitrophenyl)-propane-1,3-dione: Solid, $\text{C}_{16}\text{H}_{11}\text{NO}_6$, M.W. 313.26, M.P. $180-186^\circ\text{C}$, Yield 73 %, (4d) 1-(5'-Formyl-2'-hydroxyphenyl)-3-(4'-methoxyphenyl)-propane-1,3-dione: Solid, $\text{C}_{17}\text{H}_{14}\text{O}_5$, M.W. 298.08, M.P. $140-146^\circ\text{C}$, Yield 65 %, (4e) 1-(5'-Formyl-2'-hydroxyphenyl)-3-(2'-chlorophenyl)-propane-1, 3-dione: Solid, $\text{C}_{16}\text{H}_{11}\text{ClO}_4$, M.W. 302.03, M.P. $108-114^\circ\text{C}$, Yield 68 %.

Antimicrobial Study

In this section, all newly synthesized 1-(5'-Formyl-2'-hydroxy-3'-methoxyphenyl)-3- (substituted phenyl)propane-1, 3-diones 4(a-e) were screened for their antimicrobial activities by Agar diffusion method [13] in order to investigate their effects against growth response of two strains of bacteria viz. *E. coli* (Gram -ve), and *S. aureus* (Gram +ve) and two strain of fungi viz. *A. flavus* and *N. crassa* at six different concentrations ranging from $25\ \mu\text{g/ml}$ to $1000\ \mu\text{g/ml}$. DMSO was used to prepare the solutions of above concentrations. The Nutrient-agar and Czapek-Dox medium were used respectively for antibacterial and antifungal analysis as well as reference drugs Ciprofloxacin and Amphotericin were utilized for the purpose of comparison.

Antibacterial Activity

First of all, the stock cultures of bacteria were revived by inoculating in broth media and grown at the temperature 37°C for 18 hrs. The agar plates of above media were prepared and wells were made in the plates.

Each plate was inoculated with 18 hrs old cultures (100 μ l, 104 CFU) and spread evenly on the plate. After 20 minutes, the wells were filled with different concentration of compounds and antibiotic. All the plates were incubated at temperature 37°C. for 24 hrs and diameter of inhibition zones were measured in mm and noted.

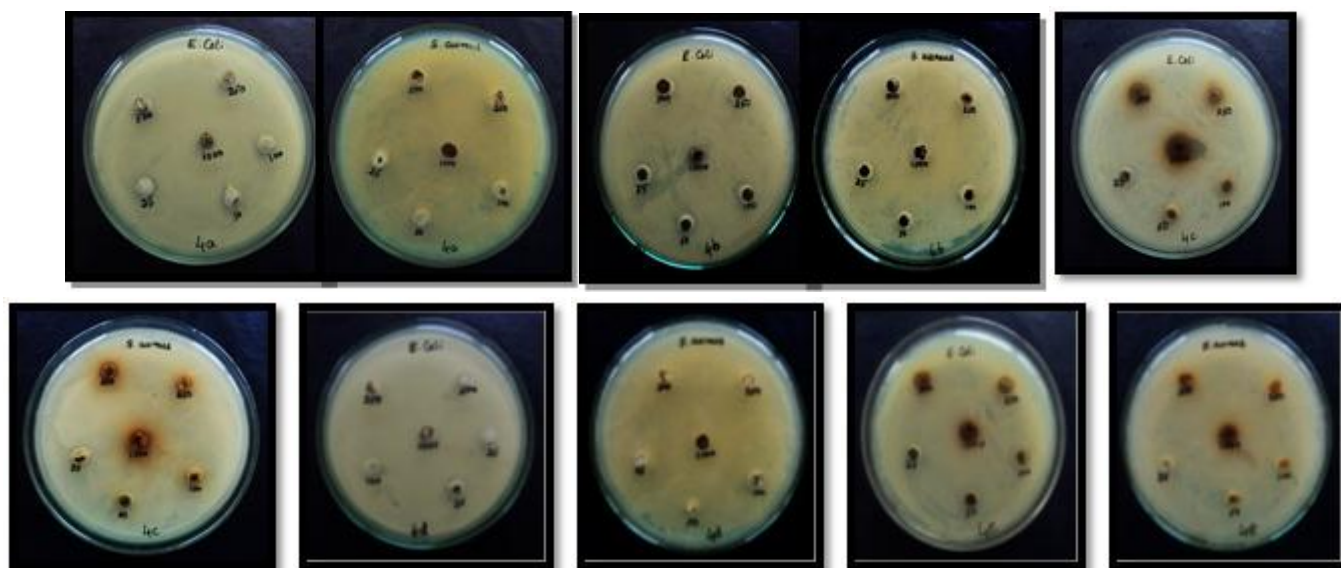


Figure No.01 – Zone of inhabitation of compounds 4a-e by *E. Coli* and *S. Aureus* bacteria

Table No.01 -Observation ofCiprofloxacin antibiotic for *E. coli* and *S. aureus*

Micro-organisms	25 μ g	50 μ g	100 μ g	200 μ g	400 μ g	800 μ g	MIC μ g
<i>E. coli</i>	18	20	23	26	28	31	25
<i>S. aureus</i>	13	18	21	25	27	34	25

Table No.2 -Observation of zone of inhabitation of *E. coli*bacteria

Compounds	1000*	500*	250*	100*	50*	25*	MIC*
4a	-	-	-	-	-	-	NF
4b	-	-	-	-	-	-	NF
4c	5 mm	3mm	-	-	-	-	500 mm
4d	-	-	-	-	-	-	NF
4e	-	-	-	-	-	-	NF

Where, (*) = μ g concentration, (-) = No zone of inhabitation, (NF) = Not Found.

Antifungal Activity

First of all, the stock culture of fungus was revived by inoculating in broth media and grown at temperature 27°C for 48 hrs. The agar plates of the above media were prepared and wells were made in the plates. Each plate was inoculated with 48 hrs old cultures (100 μ l, 104 CFU) and spread evenly on the plate. After 20 minutes, the wells were filled with different concentrations of compounds and antibiotic. All the plates were incubated at temperature 27°C for 96 hrs and diameter of inhibition zones was measured in mm and noted.

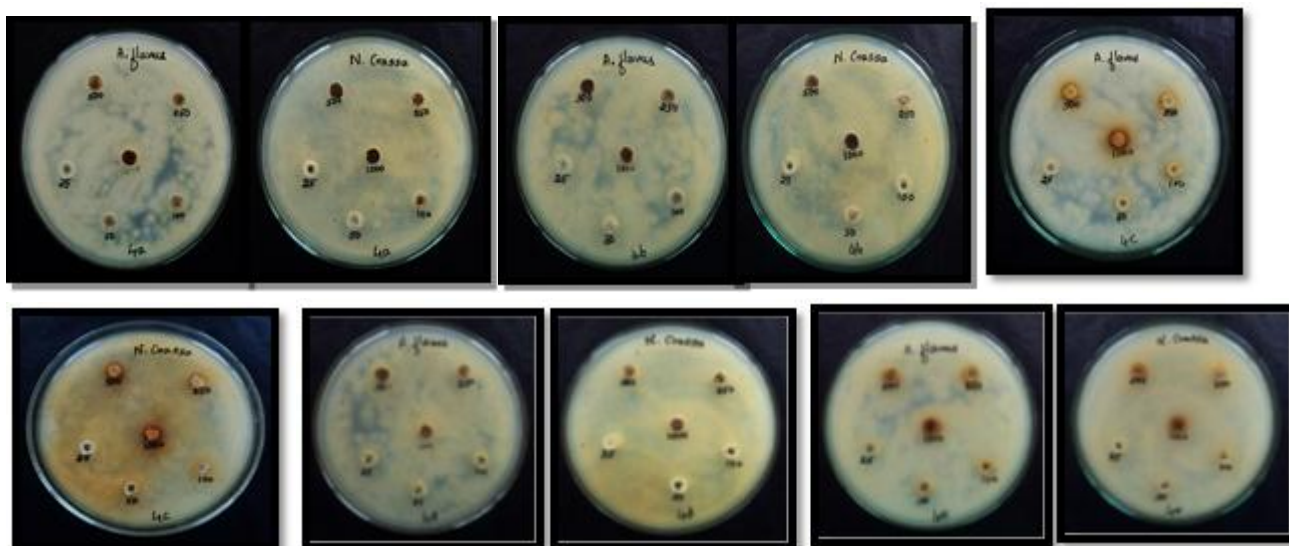


Figure No.02 – Zone of inhabitation of compounds 4a-e by *Aspergillus flavus* and *Neurospora crassa*

1) Determination of in-vitro anti-inflammatory activity

Initially 500µL of 1% albumin was added to 100µL of test sample. This mixture was kept at room temperature for 10 min, followed by heating at 51°C for 20 min. The resulting solution was cooled down to room temperature and absorbance was recorded at 660 nm. Standard Diclofenac was taken as a positive control. The experiment was carried out in triplicates and percent inhibition for protein denaturation was calculated using following formula:

$$\% \text{ Inhibition} = 100 - ((A1 - A2)/A0) \times 100$$

Where, A1 is the absorbance of the sample, A2 is the absorbance of the product control

A0 is the absorbance of the positive control.

Table No.3-Analysis of Anti-Inflammatory of Compound No.(4a)

Concentration µg/ml	Absorbance of test sample	% of protein inhibition	Absorbance of Std. Diclofenac	% of protein inhibition
50 µg/ml	0.290	46.86	0.008	84.31
100 µg/ml	0.289	46.66	0.006	88.23
200 µg/ml	0.285	45.88	0.004	92.15
400 µg/ml	0.285	45.88	0.003	94.11
500 µg/ml	0.266	42.15	0.001	98.03

Table No.4-Analysis of Anti-Inflammatory of Compound No.(4b)

Concentration µg/ml	n	Absorbance of test sample	% of protein inhibition	Absorbance of Std. Diclofenac	% of protein inhibition
50 µg/ml		0.301	49.01	0.008	84.31
100 µg/ml		0.297	48.23	0.006	88.23
200 µg/ml		0.294	47.64	0.004	92.15
400 µg/ml		0.288	46.47	0.003	94.11
500 µg/ml		0.279	44.70	0.001	98.03

Table No.5–Analysis of Anti-Inflammatory of Compound No.(4c)

Concentration µg/ml	Absorbance of test sample	% of protein inhibition	Absorbance of Std. Diclofenac	% of protein inhibition
50 µg/ml	0.199	29.01	0.008	84.31
100 µg/ml	0.244	37.84	0.006	88.23
200 µg/ml	0.277	44.31	0.004	92.15
400 µg/ml	0.295	47.84	0.003	94.11
500 µg/ml	0.296	48.03	0.001	98.03

2) Determination of Antioxidant Activity

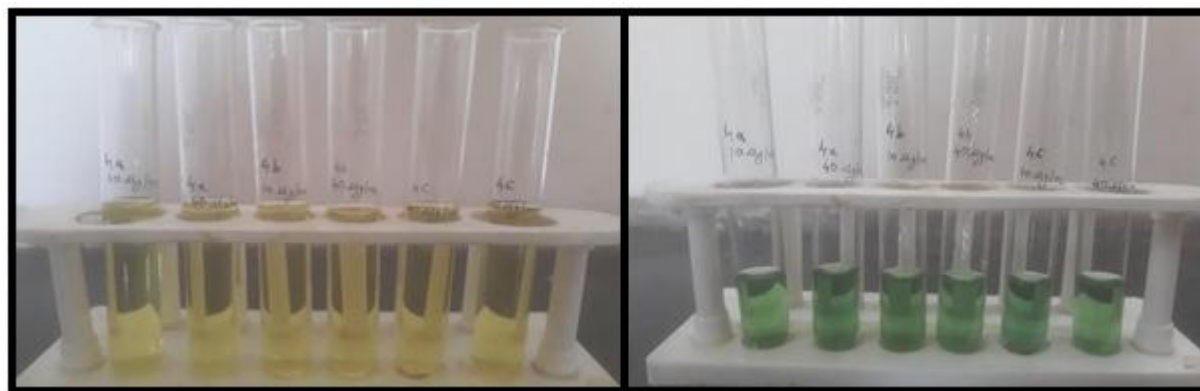
Different concentrations of the drug (10-50µg/mL) was added to 2.5 mL of 0.2 M sodium phosphate buffer (pH 6.6) and 2.5 mL of 1% potassium ferricyanide [$K_3Fe(CN)_6$] solution. The reaction mixture was vortexed well and then incubated at 50°C for 20 min using vortex shaker. At the end of the incubation, 2.5 mL of 10% trichloroacetic acid was added to the mixture and centrifuged at 3,000 rpm for 10 min. The supernatant (2.5 mL) was mixed with 2.5 mL of deionised water and 0.5 mL of 0.1% ferric chloride. The coloured solution was read at 700 nm against the blank with reference to standard using UV Spectrophotometer. Here, ascorbic acid was used as a reference standard, the reducing power of the samples were comparable with the standard reference (Ascorbic Acid).

Table No.6 - Antioxidant activity of Standard Ascorbic Acid

Sr. No.	Concentration (µg/ml)	Absorbance(A)
01	10	0.308
02	20	0.481
03	30	0.684
04	40	0.894
05	50	0.941

Table No.7–Observation of samples (4a-c) in Antioxidant Activity

Sr. No.	Samples	Concentration (µg/ml)	Absorbance (A)
1	4a	20	0.533
2	4a	40	0.769
3	4b	20	0.574
4	4b	40	0.648
5	4c	20	0.676
6	4c	40	0.798



a) Before addition of FeCl_3 solution b) Colour changes after addition of FeCl_3 solution

Figure No.3 Analysis of Antioxidant Activity

III.RESULTS AND DISCUSSION

In Antibacterial Activity the compounds 4a,4b,4d and 4e do not show any zone of inhibition against *E. coli* bacteria but compound 4c shows zone of inhabitation. The compounds 4a,4b,4c,4d and 4e do not show any zone of inhibition against *S. aureus* bacteria. In Antifungal Activity the compounds 4a,4b,4c,4d and 4e does not shows any zones of inhibition against *Neurospora crassa* and *Aspergillus flavus* fungi at different concentrations such as 1000 μg , 500 μg , 250 μg , 100 μg , 50 μg and 25 μg .

In anti-inflammatory activity reveal that all the newly synthesized compounds 4(a-c) has shown good inhibition of denaturation of protein at all the tested concentration, however as compared with standard Diclofenac as their values were found to be in order of $4c > 4b > 4a$

In antioxidant activity, it was observed that all the samples show reducing power and their reducing strength was increased with increasing concentration. The high value of absorbance of the reaction mixture clearly indicated greater reducing power. By comparing their reducing strength with standard reference, it was observed that the reducing power of all the synthesized compounds was found to be in good agreement with the standard ascorbic acid as well as their values were found to be in order of $4c > 4a > 4b$

IV.CONCLUSION

A new series of 1-(5'-formyl-2'-hydroxyphenyl)-3-(substituted phenyl)-propane-1,3-diones (4a-e) were synthesized having good yield. In Antibacterial Activity only 4c compound shows moderate zone of inhabitation against *E. coli* bacteria. In Antifungal Activity the newly synthesized compounds do not shows any zones of inhibition against *Neurospora crassa* and *Aspergillus flavus* fungi at any concentrations. In anti-inflammatory activities it is concluded that all these newly synthesized β -diketones 4(a-c) were found to possess satisfactory anti-inflammatory potential when equated with the reference Diclofenac. In antioxidant studies all compounds exhibited potent antioxidant activities due to the presence of moiety in the molecular structure of synthesized compounds. After comparing the results of antioxidant activities with standard Ascorbic acid, it is confirmed that the reducing power of all samples increased with increasing their concentrations.

V. ACKNOWLEDGMENTS

All the authors are grateful to the Director, Government Vidarbha Institute of Science and Humanities, Amravati for providing a laboratory facility and Dr. S. L. Deore, Associate Professor, Government College of Pharmacy, Amravati for her cooperation in carrying out anti-inflammatory and antioxidant activity. We also thanks to BioGenics, Hubli, Karnataka to facilitate Antimicrobial Activity.

VI. REFERENCES

- [1]. Fargeas V, Baglouch M, Metay E, Baffreau J, Mehard D, Gosselin P, Berge J P, Barthomeuf C Tetrahedron 60, 2004, 10359.
- [2]. Sechi M., Sannia L., Carta F., Palomba M., Dallochio R., Dessi A., Derudas M., Zawahir Z. and Neamati N., Antiviral Chem. Chemother. 2005, 16, 41.
- [3]. Jayshree N. Angaitkar and Bodkhe P.S. 2016, Int J Recent Sci Res. 7(12), pp.14549-14553.
- [4]. Maurya, R. C., Rajput, S. J. Mol. Structure 2004, 687, 35.
- [5]. S. S. Binani, P. S. Bodke, R. V. Joat Int J. Pharm. Sci, 2014, 6, 461-463.
- [6]. Q. Shen, W. Huang, J. Wang, X. Zhou, Org. Lett., 2007, 9, 4491-4494.
- [7]. B. Štefane, Org. Lett., 2010, 12, 2900-2903.
- [8]. Babu, V. H.; Manna, S. K.; Srinivasan, K. K. and Bhat, G. V., Indian J Heterocyclic Chem., 3, 2004, 253
- [9]. V. R. Winrow, P. G. Winyard, C. J. Morris and D. R. Blake, Br. Med. Bull., 1993, 49, 506.
- [10]. Nishiyama T, Shiotsu S and Tsujita H, Polym Degrad Stab., 2002, 76, 435.
- [11]. Alam, M. N., Bristi, N. J., Rafiquzzaman, M. Saudi Pharm. J. 2013, 21, 143-152.
- [12]. R. M. Pathade, S. K. Pagariya and P. S. Bodkhe, National Conference, NCCTCS-2022.
- [13]. Threlfall EJ, Fisher IS, Ward LR, Tschape, Gerner-Smidt P. Microb Drug Resist, 1999, 5(3):195-200.

Green Synthesis of Copper Oxide Nanoparticles from Plant Extract and Their Biological Applications: A Review

Ruqqaiya Shaikh¹, D.T.Tayade¹, Pathan Mohd Arif², Mohd. Anis³, R.D.Isankar¹

¹Department of Chemistry, Government Vidarbha Institute of Science and Humanities, Amravati 444604, Maharashtra, India

²Department of Chemistry, Maulana Azad College of Arts, Science & Commerce, Aurangabad, 431001, Maharashtra, India

³Department of Physics and Electronics, Maulana Azad College of Arts, Science & Commerce, Aurangabad, 431001, Maharashtra, India

ARTICLE INFO

Article History:

Accepted : 01 Jan 2025

Published : 10 Jan 2025

Publication Issue :

Volume 12, Issue 7

January-February-2025

Page Number :

352-360

ABSTRACT

Nanotechnology is an interdisciplinary branch of science that deals with the study of particles in the range of Nanoscale to bring into existence various products in our society. Copper has been recognized as a non-toxic, safe, economical inorganic material, and different chemical methods were used for the synthesis of copper oxide nanoparticles (CuO-NPs). It has a high potential in many biological and catalytic sensor applications. More often, CuO-NPs are utilized as antimicrobial agents. The vast application of nanoparticles has led to the development of numerous methods for synthesizing copper nanoparticles by conventional chemical and physical processes, which has several limitations, so an alternative method is needed. Due to the non-toxic and eco-friendly nature of green synthesis, researchers have moved towards more economical and best alternative plant material methods for the green synthesis of CuO-NPs. In the present review, we are reporting the previous research done by conventional and green methods for synthesizing CuO-NPs and different plant materials used in the synthesis, characterization, and biological applications. **Keywords :** Nanoparticles, Green Synthesis CuO NPs, Biological applications.

I. INTRODUCTION

Nanoscience is the science that studies materials and structures at 10^{-9} m scale. The properties of matter on the Nanoscale differ from those on a larger scale. When there are significant changes in a material's size, the properties remain the same in the beginning, and then minor changes occur. Finally, when the size falls below 100 nm, drastic changes in properties can occur.¹ Nanoscience is the study of phenomena tend

manipulation of material at atomic, molecular, and macromolecular scales, where the properties differ significantly from those at a larger scale. Nanotechnology is defined as the design, characterization, production, and application of structures, devices, and systems through control shape and size at the nanometer scale.²

The synthesized nanoparticles have various applications in various fields: electronics, medicines, transportation, cell repair, green nanotechnology, biotechnology, and biochemical sciences.³ Silver nanoparticles are significant in food, clothing, and household products, whereas zinc nanoparticles are used in sunscreen and cosmetics.⁴ Nanotechnology is also applied in industries for the basis of purification and wastewater treatment, which comes under the green nanotechnology field. The green synthesis of metallic nanoparticles has been considered as a cost-effective and environmentally friendly alternative to chemical and physical methods.

In recent years, CuO-NPs have attracted much attention from researchers due to their applications in industries and medicine. However, other nanoparticles, such as platinum, gold, iron oxide, silicon oxides, and nickel, have not shown bactericidal effects in studies with *Escherichia coli*.⁵ Although many plant parts or whole plants have been used for the green synthesis of CuO-NPs due to the presence of a large number of bioactive such as flavonoids, polyphenols, alkaloids, terpenes, and saponins compounds in plants. The extracts of plants have been efficiently applied for this purpose.⁶

Synthesis of CuO Nanoparticles:

Different physical, chemical, and biological approaches have been used for the production of CuO-NPs. These methods include sonochemistry, precipitation, sol-gel, chemical reduction, chemical bath deposition, hydrothermal, non-vacuum, spin-focusing sol-gel coating technique, electrothermal and green chemistry.⁷⁻¹⁴ In general, there are two main approaches for nanoparticle synthesis.¹⁵

- Top-Down approach: The bulk material is converted into Nano size particles.
- Bottom-up approach: The Nano sized material is synthesized by combining atom-scale materials.

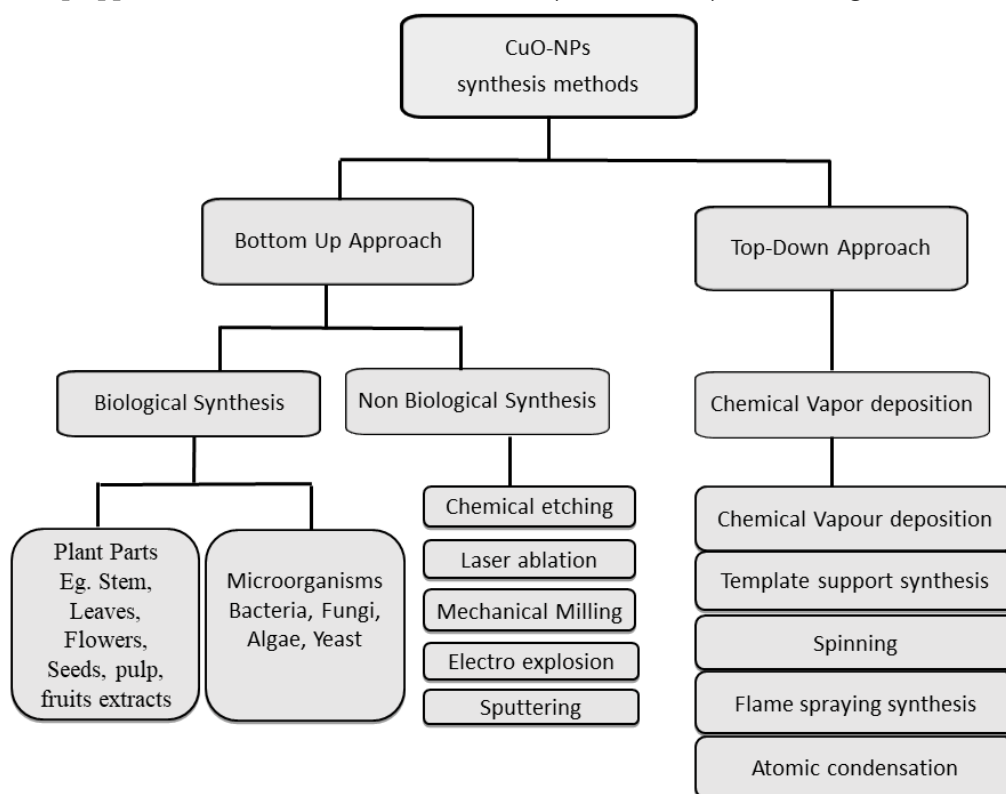


Figure: Different Approaches for the synthesis of CuO-NPs

Green Synthesis of copper nanoparticles

Synthesis of CuO-NPs was done from bacteria, algae, and fungi; there are some limitations to using these organisms.¹⁶⁻¹⁷ Plant extracts are a good source for synthesizing metal and metal oxide nanoparticles. Therefore, plant extracts have been widely used to synthesize CuO-NPs.¹⁸⁻²⁰ Plant-based synthesis is simple, safe, low energy consumption, and has better nanoparticle stability.²¹⁻³¹ The plant extracts contain different bioactive compounds such as flavonoids, phenols, proteins, terpenoids, and tannins that act as reducing and stabilizing agents and reduce the metallic salts into respective nanoparticles.³²⁻³⁷ The plant extract generates electrons that cause the reduction of copper salts. The phytochemicals react with the copper ion, leading to the reduction and then conversion into CuO-NPs.³⁸⁻⁴¹ In this method, the metal salt is mixed with the plant extracts, and the reaction is stirred for 1-3 hours at ambient temperature to complete.⁴² Nowadays, the emphasis has been shifting toward the synthesis of CuO-NPs by using plants and plant extracts to gain the advantages of this method.⁴³ Many researchers used different plant extracts to prepare Cu-NPs with different sizes and shapes depending upon the synthesis conditions.⁴⁴ This review article describes the plant and plant extract methods to optimize the most appropriate process for the synthesis of Cu-NPs. For example, H.R. Aher and his coworkers reported that copper nanoparticles were synthesized by using leaf extract from *Syzygium Cumini* as a reducing agent in aqueous copper sulphate (CuSO_4) solution, giving the copper nanoparticles size is around 10 μm and shape is Agglomeration which showing the antimicrobial activity for both G+Ve and G-Ve bacteria.⁴⁵

S. Renganathan and his coworkers illustrated that Cu-NPs were synthesized using leaf extract from *Capparis zeylanica* as a reducing agent in aqueous CuSO_4 solution. The NPs were fabricated for 12 h which were cubical in shape with size range 50–100 nm. The antimicrobial study of the CuO-NPs was established using both G+ Ve and G-Ve pathogens.⁴⁶ Subbaiya and Masilamani Selvam showed that *Hibiscus rosa-Sinensis* leaf extract could be used to reduce the CuNO_3 solution, then the solution was placed in a dark room for 48 h, and spherical CuO-NPs were prepared. CuO-NPs showed good antimicrobial activity against clinically important pathogens like *Bacillus subtilis* and *E. coli*. It is also illustrated that the synthesized CuO-NPs acted as an effective drug to treat lung cancer.⁴⁷ Subhankari and Nayak reported the production of Cu-NPs using an aqueous extract of *Syzygium aromaticum* (Cloves) where Copper sulfate was reduced in an aqueous solution of clove extracts in 1 h, giving 5–40 nm spherical CuO-NPs.⁴⁸ Pandurang studied that the leaf extract of citrus *Sinensis* can make a reduction of Cu cations into Cu-NPs. So, this technique can be applied for rapid and eco-friendly synthesis of CuO-NPs.⁴⁹ Gunalan has also reported CuO-NPs synthesis using a valuable medicinal plant, *Aloe barbadensis* Miller. *Aloe barbadensis* Miller leaf extract was exposed to copper sulfate at room temperature for 7 hrs under vigorous stirring, giving blackish, indicating the formation of CuO-NPs.⁵⁰ The characterizations of the synthesized nanoparticles were done by UV-Vis, SEM, TEM, XRD, and FTIR. SEM and TEM analysis showed that the nanoparticles' average size was 20 nm with dispersed spherical morphology. FTIR observations proved the existence of terpenoids, phenolic compounds, and proteins on the surface of green synthesized CuO-NPs were responsible for reducing and stabilizing nanoparticles.⁵⁰ Similarly, author and coworkers, the flower extract of *Cordia sebestena* has also been reported to synthesize CuO-NPs. The size of the synthesized nanoparticles was 20-40 nm with spherical morphology and showed antibacterial activities against different bacterial strains. The bio-inspired CuO-NPs exhibited potential activities at 75 μl concentration against different bacteria.⁵¹ The leaf extract of *Olea europaea*, *Citrofortunella microcarpa*, and *Alternanthera sessilis* has also been reported to synthesize CuO-NPs.⁵²

II. BIOLOGICAL APPLICATION

Antibacterial

In the past few years, nano-based therapies have been used to diagnose and treat diseases and formulate novel drugs. The antibacterial activities of NPs have been tested against different pathogenic bacterial strains and showed substantial outcomes.⁵³⁻⁵⁴ Literature survey reports that CuO-NPs are highly toxic to most human pathogens.⁵⁵ Green synthesized CuO-NPs have attracted great interest as antibacterial agent due to their unique morphologies, size, and bio-compatible nature to treat a wide range of pathogenic human bacteria.⁵⁶⁻⁵⁷ The green synthesized CuO-NPs possess vigorous antibacterial activities against G+Ve and G-Ve bacterial strains. Sivaraj and his coworkers reported the green synthesis of CuO-NPs using leaf extract of *Tabernaemontana divaricate* and evaluated their antibacterial activities against urinary tract infection (UTI) causing pathogens.⁵⁸ The highest zone was observed against *Escherichia coli*, with an average diameter of 17 mm at a concentration of 25ug/ml.⁵⁸ Naika reported the antibacterial potential of CuO-NPs synthesized from *Gloriosa superba* L. extract against G+Ve (*Staphylococcus aureus*) and G-Ve (*Klebsiella aerogenes*, *P. desmolyticum*, *Escherichia coli*) strains.⁵⁹ Ghotekar reported the synthesis of CuO-NPs using *Acanthospermum hispidum* L. extract and evaluated their antibacterial activities. The results revealed that the green synthesized CuO-NPs were exhibited intense bacterial activities against *Pseudomonas aeruginosa*, *Streptococcus pyogenes*, *Staphylococcus aureus* and *Escherichia coli*.⁶⁰

Antifungal Activity

In recent medical history, the fungal disease has become a significant health problem, especially for patients having weak immune systems, such as AIDS or cancer patients undergoing chemical treatment.⁶¹⁻⁶² The antifungal activity of CuO-NPs has been investigated for medical applications, and these nanoparticles may combat fungal infections.⁶³⁻⁶⁴ However, the antifungal activities of CuO-NPs have been less studied than antibacterial activity. Microbial-mediated synthesis of CuO-NPs using the fungal strain *Penicillium chrysogenum* has been reported. The authors tested these green synthesized nanoparticles against pathogenic bacterial and fungal strains such as *Fusarium oxysporum*, *Penicillium citrinum*, *Alternaria solani*, and *Aspergillus niger*. They further concluded that the green synthesis CuO-NPs showed healthy activities.

III. CONCLUSION

The CuO-NPs get much attention because of various applications such as antibacterial, antifungal, antiviral, anticancer, antioxidant, drug delivery, and many more. The CuO-NPs have been synthesized through different methods such as chemical, physical and biological methods. The physical and chemical methods are expensive and use a toxic chemicals that may cause a hazardous effect. In contrast, the green method is eco-friendly, cost-effective, reliable, stable, low energy consumption, and straightforward. This review summarizes the synthesis of CuO-NPs using different plant extracts, their mechanisms, characterizations, and various medicinal applications. More research on the therapeutic applications of CuO NPs should focus on possible methods of minimizing CuO-NPs toxicity while maintaining and enhancing their biological efficiency.

IV. ACKNOWLEDGMENT

Authors are thankful to Maulana Azad College of Arts, Science and Commerce, Aurangabad for providing laboratory facilities.

V. REFERENCES

- [1]. Bhushan, B.; Springer handbook of nanotechnology. Springer. 2017. 4th edition. Berlin.
- [2]. Dowling, A.P.; Development of nanotechnologies. Material Today, 2004, 7, 30–35.
- [3]. Xiliang, L.; Aoife M.; Anthony J.; Malcolm R. Application of Nanoparticles in Electrochemical Sensors and Biosensors. *Electroanalysis*, 2006, 18(4), 319–326.
- [4]. Priyabrata T., Rout G., Sushanto G., Gitishree, D.; Krishna P., Hrudayanath T., Jayanta K.; Photo-mediated green synthesis of silver and zinc oxide nanoparticles using aqueous extracts of two mangrove plant species, *Heritiera fomes* and *Sonneratia apetala* and investigation of their biomedical applications. *Journal of Photochemistry and Photobiology B: Biology*. 2016, 163, 311–318.
- [5]. Delma, M. T.; Jaya Rajan M.; Green synthesis of copper and lead nanoparticles using *Zingiber Officinale* stem extract. *International Journal of Scientific and Research Publications*, 2016, 6(11), 134–137.
- [6]. Ananda M.; Tegene D.; Mebratu K.; Buzuayehu A.; Temesgen A.; Synthesis of Green Copper Nanoparticles Using Medicinal Plant *Hagenia abyssinica* (Brace) JF. Gmel. Leaf Extract: Antimicrobial Properties, *Hindawi Journal of Nanomaterials*, 2020, 3924081, 1–12.
- [7]. Zhao L.; Huang Y.; Keller A.; Comparative metabolic response between cucumber (*Cucumis sativus*) and corn (*Zea mays*) to a Cu (OH)₂ nanopesticide, *Journal of agricultural and food chemistry*, 2017, 66(26), 6628–36.
- [8]. Sackey J, Nwanya A.C, Bashir A.K.H, Matinise N, Ngilirabanga, J.B, Ameh A.E, Coetsee E, Maaza M; Material Chemistry and Physics; Electrochemical properties of *Euphorbia pulcherrima* mediated copper oxide nanoparticles, 2020, 244, 122714.
- [9]. Vishveshvar K, Krishnan M.A, Haribabu K, Vishnuprasad S; Green synthesis of copper oxide nanoparticles using *ixirole coccinea* plant leaves and its characterization, *BioNanoScience*; 2018, 8, 554–558.
- [10]. Pourbeyram S, Abdollahpour J., Soltanpour M; Green synthesis of copper oxide nanoparticles decorated reduced graphene oxide for high sensitive detection of glucose, *Material Science Engineering Chemistry*, 2019, 94, 850–857.
- [11]. Rafique M, Shaikh A., Rasheed R., Tahir M., Gillani S., Usman A., Imran M., Zakir A., Khan Z., Rabbani F.; Aquatic biodegradation of methylene blue by copper oxide nanoparticles synthesized from *Azadirachta indica* leaves extract, *Journal of Inorganic Organometallic Polymer Mater*, 2018, 28 (6), 2455–2462.
- [12]. Azam A., Ahmed A., Oves M., Khan M., Memic A.; Size-dependent antimicrobial properties of CuO nanoparticles against Gram-positive and-negative bacterial strains, *International Journal of Nano medicine*, 2012, 7, 3527.
- [13]. Muniyandi J., Sangiliyandi G., Muhammad Q., Min-Hee K.; Jin-H.; A comprehensive review on the synthesis, characterization, and biomedical application of platinum nanoparticles, *Nanomaterials*; 2019, 9 (12), 1719.

- [14]. KarthikeyD.S, Anushka S., KedarM.C, RajaS.; Structural characterization of mesoporous magnetite nanoparticles synthesized using the leaf extract of *Calliandra haematocephala* and their photocatalytic degradation of malachite green dye, *Applied Nano science*, 2018, 8, 675–683.
- [15]. Chetna D., Neeraj D., Xian J., Alice N. Jie Y., Navin K., Methods and strategies for the synthesis of diverse nanoparticles and their applications: a comprehensive overview, *RSC Advances*, 2015, 5, 105003–105037.
- [16]. Kumar P.V, Shameem U., Kollu P, Kalyani R.L., Pammi S.V; Green synthesis of copper oxide nanoparticles using *Aloe vera* leaf extract and its antibacterial activity against fish bacterial pathogens, *Bio-Nanoscience*, 2015 ,5(3), 135-139.
- [17]. Ijaz F, Shahid S, Khan SA, Ahmad W, Zaman S; Green synthesis of copper oxide nanoparticles using *Abutilon indicum* leaf extract: Antimicrobial, antioxidant and photocatalytic dye degradation activities, *Tropical Journal of Pharmaceutical Research*,2017, 16(4), 743-753.
- [18]. Ghidan A.Y, Al-Antary T.M, Awwad A.M;Monitoring & Management; Green synthesis of copper oxide nanoparticles using *Punica granatum* peels extract: Effect on green peach Aphid, *Environmental Nanotechnology*,2016, 1(6), 95-98.
- [19]. Gunalan S., Sivaraj R., Venckatesh R; *Aloe barbadensis* Miller mediated green synthesis of mono-disperse copper oxide nanoparticles: optical properties, *Molecular and Biomolecular Spectroscopy*; 2012, 97, 1140-1144.
- [20]. Prakash S., Elavarasan N., Venkatesan A., Subashini K., Sowndharya M., Sujatha V.Green synthesis of copper oxide nanoparticles and its effective applications in Biginelli reaction,BTB photo degradation and antibacterial activity, *Advanced Powder Technology*,2018, 29(12), 3315-3326.
- [21]. Awwad A.M, Albiss B.A, Salem N.M; Antibacterial activity of synthesized copper oxide nanoparticles using *Malva sylvestris* leaf extract, *SMU Medicinal Journal*, 2015, 2(1), 91-101.
- [22]. Vishveshvar K., Krishnan M.A., Haribabu K., Vishnuprasad S; Green synthesis of copper oxide nanoparticles using *Ixiro coccinea* plant leaves and its characterization, *BioNanoScience*; 2018, 8(2), 554-558.
- [23]. Singh J, Kumar V, Kim KH, Rawat M; Biogenic synthesis of copper oxide nanoparticles using plant extract and its prodigious potential for photocatalytic degradation of dyes, *Environmental research*,2019, 177, 108569.
- [24]. Nagajyothi P.C, Muthuraman P, Sreekanth T.V, Kim D.H, Shim J; Green synthesis: in-vitro anticancer activity of copper oxide nanoparticles against human cervical carcinoma cells, *Arabian journal of chemistry*,2017, 10(2), 215-225.
- [25]. Galan C.R, Silva M.F, Mantovani D., Bergamasco R., Vieira M.F; Green synthesis of copperoxide nanoparticles impregnated on activated carbon using *Moringa oleifera* leaves extractfor the removal of nitrates from water, *Journal of Chemical Engineering*;2018, 96(11), 2378-2386.
- [26]. Selvan S.M, Anand K.V, Govindaraju K, Tamilselvan S, Kumar V.G, Subramanian K.S, Kannan M, Raja K; Green synthesis of copper oxide nanoparticles and mosquito larvicidalactivity against dengue, zika and chikungunya causing vector *Aedes aegypti*, *IET Nano biotechnology*, 2018,12(8), 1042-1046.
- [27]. Sankar R, Maheswari R, Karthik S, Shivashangari K.S, Ravikumar V; Anticancer activity of *Ficus religiosa* engineered copper oxide nanoparticles, *Materials Science and Engineering*, 2014, 44, 234-239.
- [28]. Rajesh K.M, Ajitha B, Reddy Y.A, Suneetha Y, Reddy P.S; Assisted green synthesis of copper nanoparticles using *Syzygium aromaticum* bud extract: Physical, optical and antimicrobial properties, *Optik*,2018, 154, 593-600.

- [29]. Aminuzzaman M, Kei L.M, Liang W.H; Green synthesis of copper oxide (CuO)nanoparticles using banana peel extract and their photocatalytic activities, AIP Conference Proceedings,2017, 1828(1), 020016.
- [30]. Berra D, Laouini S.E, Benhaoua B, Ouahrani M.R, Berrani D, Rahal A; Green synthesis of copper oxide nanoparticles by Pheonix dactylifera L leaves extract,Journal of Nanomaterial's and Bio structures,2018, 13, 1231-1238.
- [31]. Sutradhar P., Saha M., Maiti D; Microwave synthesis of copper oxide nanoparticles using tea leaf and coffee powder extracts and its antibacterial activity,Journal of Nanostructure in Chemistry, 2014, 4(1), 86.
- [32]. Sutradhar P, Saha M, Maiti D; Microwave synthesis of copper oxide nanoparticles usingtea leaf and coffee powder extracts and its antibacterial activity,Journal of Nanostructure in Chemistry,2014, 4(1), 86.
- [33]. Devi H.S, Singh T.D; Synthesis of copper oxide nanoparticles by a novel method and itsapplication in the degradation of methyl orange,Advance in Electronic and Electric engineering,2014, 4(1), 83-88.
- [34]. Asemani M, Anarjan N;Green synthesis of copper oxide nanoparticles using Juglans regia leaf extract and assessment of their physico-chemical and biological properties,Green Processing and Synthesis,2019, 8(1), 557-567.
- [35]. Jayakumarai G, Gokulpriya C, Sudhapriya R, Sharmila G, Muthukumaran C; Phytofabrication and characterization of monodisperse copper oxide nanoparticles usingAlbizia lebbeck leaf extract,Applied Nanoscience,2015, 5(8), 1017-1021.
- [36]. Taghavi Fardood S, Ramazani A; Green synthesis and characterization of copper oxidenanoparticles using coffee powder extract,Journal of Nanostructures, 2016, 6(2), 1667-1671.
- [37]. Yedurkar S.M, Maurya C.B, Mahanwar P.A; A biological approach for the synthesis ofcopper oxide nanoparticles by Ixora coccinea leaf extract,Journal of Materials and Environmental Sciences,2017, 8(4), 1173-1178.
- [38]. Sorbiun M, Mehr E.S, Ramazani A, Fardood S.T; Green synthesis of zinc oxide and copperoxide nanoparticles using aqueous extract of oak fruit hull (jaft) and comparing their photocatalytic degradation of basic violet 3, Journal of Environmental Research,2018, 12(1), 29-37.
- [39]. Sivaraj R, Rahman P.K, Rajiv P, Narendhran S, Venckatesh R; Biosynthesis andcharacterization of Acalypha indica mediated copper oxide nanoparticles and evaluation of its antimicrobial and anticancer activity, Molecular and Biomolecular Spectroscopy, 2014, 129, 255-258.
- [40]. Dey A, Manna S, Chattopadhyay S, Mondal D, Chattopadhyay D, Raj A, Das S, Bag BG, Roy S; Azadirachta indica leaves mediated green synthesized copper oxide nanoparticlesinduce apoptosis through activation of TNF- α and caspases signaling pathway againstcancer cells, Journal of Saudi Chemical Society,2019, 23(2), 222-238.
- [41]. Narasaiah P, Mandal B.K, Sarada N.C; Biosynthesis of copper oxide nanoparticles fromDrypetes sepiaria leaf extract and their catalytic activity to dye degradation,Material Science and Engineering,2017, 263, 022012.
- [42]. Mali S.C, Raj S, Trivedi R; Biosynthesis of copper oxide nanoparticles using Enicostemma axillare (Lam.) leaf extract,Biochemistry and biophysics reports, 2019, 20, 100699.
- [43]. Prasanta S., Mitali S., Debasish M., Microwave synthesis of copper oxide nanoparticles using tea leaf and coffee powder extracts and its antibacterial activity, J Nanostructure Chemical, 2014, 4(86), 1-6.
- [44]. Shreyas P. , Sonali G. , Suresh G. , Rajeshwari O. , Keshav D.; Green Synthesis of CuO Nanoparticles using Ziziphus Mauritiana L. Extractand Its Characterizations, IJSRST,2017, 3(8), 1388-1392.

- [45]. Aher H.R., Han S.H., Vikhe A.S., Kucheka S.R.; Green Synthesis of Copper Nanoparticles Using Syzygium Cumin, Leaf Extract, Characterization and Antimicrobial Activity, Chemical Science Transactions, 2019, 8(1), 1-6.
- [46]. Saranyaadevi K, Subha V, Ravindran R. E, Renganathan S, Synthesis and Characterization of Copper Nanoparticle using Capparis Zeylanica leaf Extract, Journal Chemical Tech Research, 2014, 6, 4533.
- [47]. Subbaiya M.R., A Review on Synthesis, Characterization and Applications of Copper Nanoparticles Using Green Method, Journal of Pharmacy Biological Chemical Science; 2015, 6, 1183.
- [48]. Bahareh K, Hamid R.G; Synthesis of copper nanoparticles: An overview of the various methods, Journal of chemical Engineering, 2014, 31, 1105-1109.
- [49]. Pandurang R. D, Sarika S, Omkar M. L, Rohan A.K; Characterization of biosynthesised copper nanoparticle from Citrus sinensis and in-vitro evaluation against fungal pathogen Colletotrichum capsici, Journal of Chemical Studies, 2019, 7(5), 325-330.
- [50]. Gunalan S, Sivaraj R, Venckatesh R; Aloe barbadensis Miller mediated green synthesis of mono-disperse copper oxide nanoparticles: optical properties, Molecular and Biomolecular Spectroscopy, 2012, 97, 1140-1144.
- [51]. Prakash S, Elavarasan N, Venkatesan A, Subashini K, Sowndharya M, Sujatha V; Green synthesis of copper oxide nanoparticles and its effective applications in Biginelli reaction, BTB photodegradation and antibacterial activity, Advanced Powder Technology, 2018, 29(12), 3315-3326.
- [52]. Kumar P.V, Shameem U, Kollu P, Kalyani R.L, Pammi S.V; Green synthesis of copper oxide nanoparticles using Aloe vera leaf extract and its antibacterial activity against fish bacterial pathogens, Bio NanoScience, 2015, 5(3), 135-139.
- [53]. Sharma P, Mehta M, Dhanjal DS, Kaur S, Gupta G, Singh H, Thangavelu L, Rajeshkumar S, Tambuwala M, Bakshi HA, Chellappan DK; interactions Emerging trends in the novel drug delivery approaches for the treatment of lung cancer, Chemical-biological, 2019, 309, 108720.
- [54]. Bindhu M.R, Umadevi M; Antibacterial activities of green synthesized gold nanoparticles, Materials Letters, 2014, 120, 122-125.
- [55]. Applerot G, Lellouche J, Lipovsky A, Nitzan Y, Lubart R, Gedanken A, Banin E; Understanding the antibacterial mechanism of CuO nanoparticles: revealing the route of induced oxidative stress, Small, 2012, 8(21), 3326-3337.
- [56]. Kumar PV, Shameem U, Kollu P, Kalyani RL, Pammi S.V Green synthesis of copper oxide nanoparticles using Aloe Vera leaf extract and its antibacterial activity against fish bacterial pathogens, Bio NanoScience, 2015, 5(3), 135-139.
- [57]. Awwad A.M, Albiss B.A, Salem N.M; Antibacterial activity of synthesized copper oxide nanoparticles using Malva sylvestris leaf extract, SMU Medicinal Journal, 2015, 2(1), 91-101.
- [58]. Sivaraj R, Rahman P.K, Rajiv P, Salam H.A, Venckatesh R; Biogenic copper oxide nanoparticles synthesis using Tabernaemontana divaricate leaf extract and its antibacterial activity against urinary tract pathogen, Molecular and Biomolecular Spectroscopy, 2014, 133, 178-181.
- [59]. Naika HR, Lingaraju K, Manjunath K, Kumar D, Nagaraju G, Suresh D, Nagabhushana H; Green synthesis of CuO nanoparticles using Gloriosa superba L. extract and their antibacterial activity, Journal of Taibah University for Science, 2015, 9(1), 7-12.
- [60]. Shreyas P., Keshav D., Ajay S., Suresh Ghotekar, Onkar P., Gotan J., Yogesh A., Dattaprasad P., Phytosynthesis and Biological Activities of Fluorescent CuO Nanoparticles Using Acanthospermum hispidum L. Extract, Journal of Nanostructure, 2017, 7(3), 165-174.

- [61]. Yugandhar P, Vasavi T, Devi P.U, Savithramma N; Bio-inspired green synthesis of copper oxide nanoparticles from *Syzygium alternifolium* (Wt.) Walp: characterization and evaluation of its synergistic antimicrobial and anticancer activity, *Applied Nanoscience*, 2017, 7(7), 417-427.
- [62]. Shende S, Ingle A.P, Gade A, Rai M; Green synthesis of copper nanoparticles by *Citrus medica* Linn.(Idilimbu) juice and its antimicrobial activity, *World Journal of Microbiology and Biotechnology*, 2015, 31(6), 865-873.
- [63]. Rajesh K.M, Ajitha B, Reddy Y.A, Suneetha Y, Reddy P.S; Assisted green synthesis of copper nanoparticles using *Syzygium aromaticum* bud extract: Physical, optical and antimicrobial properties, *Optik*, 2018, 154, 593-600.
- [64]. El-Batal AI, El-Sayyad G.S, Mosallam F.M, Fathy R.M; *Penicillium chrysogenum*-mediated mycogenic synthesis of copper oxide nanoparticles using gamma rays for in vitro antimicrobial activity against some plant pathogens, *Journal of Cluster Science*, 2020, 31(1), 79-90.

Novel Synthesis of Flavanones and Its Impact on Seed Germination

S. P. Rathod

Department of Chemistry, G. S. G. College, Umarkhed, Maharashtra, India

ARTICLE INFO

Article History:

Accepted : 01 Jan 2025

Published : 10 Jan 2025

Publication Issue :

Volume 12, Issue 7

January-February-2025

Page Number :

361-364

ABSTRACT

As a part of systematic investigation, spectral analysis and seed germination properties (root and shoot elongation i.e Morphology) of chlorosubstituted flavanones from diketones, gives various series by using different aldehydes. As in prepared the as series, 3-methoxy-8-chlorobenzoylflavanone, 3-chlorobenzoyl-8-chloroflavanone, 3-benzoyl-8-chloroflavanone.

Keywords; - Diketones, flavanones, root and shoot elongation.

I. INTRODUCTION

Flavanones are group of common natural polyphenolic compound that are widely found in plant kingdom. It consists of two aromatic ring links through three Carbon bridge with a carbonyl function. Actually these are the class of Flavanoids, which can be subdivided into several classes such as chalcone, flavanones, isoflavanones, aurones etc. The flavanones are mainly distributed in citrus fruits. In present study, various chlorosubstituted flavanones were synthesized from chlorosubstituted diketones and screened for their morphology (i.e. root and shoot elongation) against some crop plants. Flavanones and their analogues having attracted considerable attention because they possess antioxidant effect, cytotoxic, antimicrobial. Antinflammatory activities etc.

Larget R et.al.¹ reported substituted flavanone & studied as neuroprotective agents. Venkatramn et.al.² synthesized the flavanone from chalcone by dehydrogenation with SeO₂. Yoigtandes et.al.³ reported the flavanone from flavanone by heating with I₂. Patill⁴ synthesized flavanone from by using DMSO as a dehydrogenating agent. Mayer A.M.et.al.⁵ synthesized coumarin and their role as growth regulators in several plants. Korade D.L. et.al.⁶ reported the effect of Anthracenes on seed germination of *Lolium multiflorum* plants. Gibba Z. et.al.⁷ studied the effect of nitric oxide on germination of *Empress tree* seeds. Majumdar, G. p.⁸ reported studied the cambial activities of root habit and shoot development in some plants.

The reaction of diketones with various aldehydes gives various flavanones these reactions carried out in presence of ethanol as energy transfer medium in aq.KOH.

It has been well established that, the presence of chlorosubstituted ketones present in flavanones, with the hope that the resulting molecules would exhibit promising root and shoot elongation as shown in table and graph.

II. EXPERIMENTAL METHODS:

All the glassware's used in the present work were of Pyrex quality. Melting points were determined in open capillary and are uncorrected. Purity of compounds was monitored on silica gel coated TLC plate. I.R. spectra were recorded on SHIMADZU Spectrophotometer in KBr palates. The analytical data of compounds were highly satisfactory. All the chemicals used were of analytical grade. All the solvents used were purified by standard methods. Physical characterization data of all the compounds are given in Table 1.

III.RESULT AND DISCUSSION

The synthetic methods used in present work are given below along with their, IR data.

Acetylation of P- Chlorophenol:

P – Chlorophenol 50 ml was mixed with acetic anhydride 60 ml & anhydrous sodium acetate 5 gm the mixture was refluxed for about 1 hrs. it was cooled and poured into cold water. Acetated layer was separated & washed with water several times finally it was purified by distillation and the distillate of compound was collected at about 232°C. Yield 75%, B.P. 232°C

2 – Hydroxy 5 – chloro-acetophenone:

When Phenyl acetate (50ml) was mixed with anhydrous $AlCl_3$ (120gm) & heated at 120°C for 45 min on oil bath. The reaction mixture was decomposed with ice cold water containing little hydrochloric acid to get crude ketone. It is purified by dissolving in acetic acid & allowing the solution to fall drop by drop into cold water with stirring. A slightly yellow powder was obtained having M.P. = 86°C, Yield = 72%

2 – Benzoyloxy 5 - chloroacetophenone:

2 – Hydroxy 5- Chloroacetophenone (0.04 mol) & (8.59 ml) Benzoyl Chloride (0.05 mol) were dissolved in NaOH (10 %) (30 ml). The reaction mixture was shaken for about 45 min. The product thus separated filtered, washed with water followed by sodium bicarbonate (10%) again with water. The solid product was crystallized from ethanol to obtain. 2 – benzoyloxy 5-chloroacetophenone white crystal is obtained having M.P. - 87°C, Yield - 80%.

1 – (2-Hydroxyl Phenyl) 5 – Chloro- 3 – Phenyl – 1, 3 – Propanedione:

2 – Benzoyloxy 5 - chloroacetophenone (1.5 gm) was dissolved in (40 ml) dry Pyridine. The solution was warmed up to 60°C pulverized KOH (15gm) was added slowly with constant stirring. After 4 hours of heating then reaction mixture was acidified by adding ice cold HCl (1 : 1). The brownish yellow solid product thus separated was filtered, washed with sodium bicarbonate solution (10%) and finally again with water. It was then crystallized from ethanol-acetic acid mixture to get 1 – (2-hydroxyl phenyl) 5 – Chloro -3 – Phenyl – 1, 3 – Propanedione. M.P:121°C, Yield – 75 %.

3 – Benzoyl - 8 – chloro flavanone:

A mixture of 1 – (2-hydroxyl phenyl)- 5 – Chloro 3 – Phenyl – 1, 3 – Propanedione (0.01 mol) (3 gm) & Benzaldehyde (0.12 mol) (1 ml) was refluxed in ethanol (25 ml) and KOH (1 gm) for 15 – 20 min described to get compound M.P. - 230°C, Yield - 79%.

3 – Methoxy – 8-chloro benzoyl flavanone:

A mixture of 1 – (2-hydroxyl phenyl)-3 – phenyl – 1, 3 – propanedione (0.01 mol) (3 gm) & anisaldehyde (0.12 mol.) (1 ml) was refluxed in ethanol (25 ml) & KOH (1 gm) for 15 -20 min. & process as described to get compound, 3 – methoxy-8 – chloro benzoyl flavanone. M.P. - 251°C, Yield – 72 %.

Table (1): Characterization data of synthesized new compound

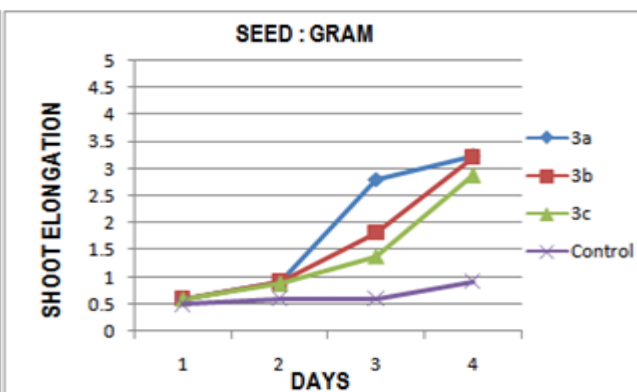
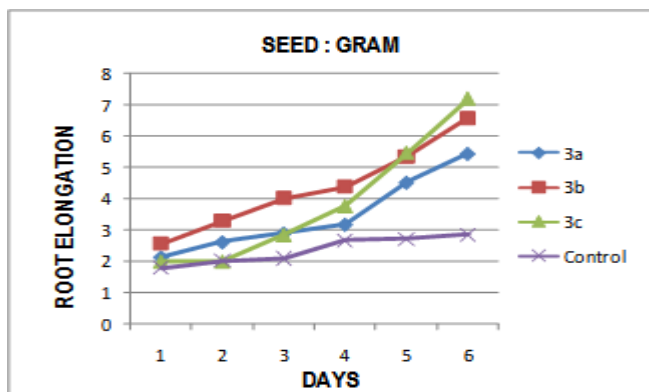
Compound	Molecular Formula	M.P. (°C)	Yield (%)	Rf
3a	C ₂₁ H ₁₃ O ₃ Cl	230	79	0.76
3b	C ₂₂ H ₁₆ O ₄ Cl	251	75	0.78
3c	C ₂₁ H ₁₄ O ₃ Cl ₂	240	75	0.79

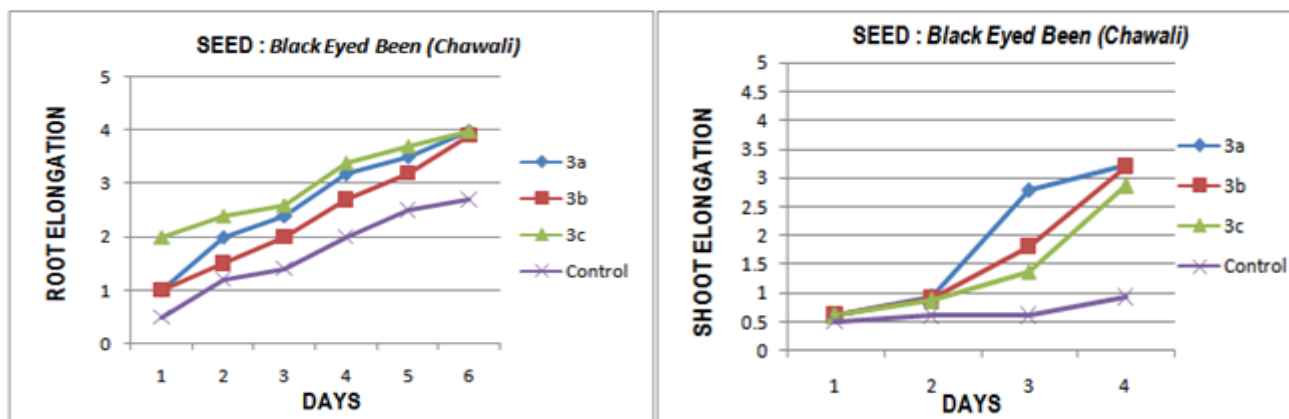
TABLE NO. 1 : SEEDS - GRAM

Sr. No.	Comp.	% of germination					Average length of root in cm.						Average length of shoot in cm.					
		Day					Day						Day					
		2	4	6	8	10	2	4	6	8	10	12	2	4	6	8	10	12
1	3a	80%	100%				1	2	2.4	3.2	3.5	4			0.6	0.9	2.8	3.2
2	3b	80%	100%				1	1.5	2	2.7	3.2	3.9			0.6	0.9	1.8	3.2
3	3c	100%	100%				2	2.4	2.6	3.4	3.7	4			0.6	0.9	1.4	2.9
4	Control	80%	90%				0.5	1.2	1.4	2	2.5	2.7			0.5	0.6	0.6	0.9

TABLE NO. 2 : SEEDS - Black Eyed Beans (Chawali)

Sr. No.	Comp.	% of germination					Average length of root in cm.						Average length of shoot in cm.					
		Day					Day						Day					
		2	4	6	8	10	2	4	6	8	10	12	2	4	6	8	10	12
1	3a	80%	100%				2.1	2.6	2.9	3.2	4.5	5.4			0.6	0.9	2.8	3.2
2	3b	80%	100%				2.6	3.3	4.0	4.4	5.4	6.6			0.6	0.9	1.8	3.2
3	3c	80%	100%				2.6	3.3	4.0	4.4	5.4	6.6			0.6	0.9	1.8	3.2
4	Control	80%	90%				1.8	2	2.1	2.7	2.7	2.9			0.5	0.6	0.6	0.9





IV. CONCLUSION

The present study was aimed at investigating the impact of newly synthesized chlorosubstituted flavanone on some crop plants viz: *Gram* and , *Black Eyed Bean (Chawali)*. The choice of these crops was based on their enormously vast utility and also the indispensability for the survival of the human race, all across the globe.

The efforts have been made to investigate and analyze the convergence and divergence effect of test compounds on the morphology of plants under investigation. It was interesting to note that, all the treated seeds exhibited remarkable roots and shoots elongation as compared to untreated ones.

When the growth of all the treated plants were compared among themselves, it was distinctly observed that, the change which is dominant while applying the treated compound i.e. chlorosubstituted flavanones in *Gram*, *Black Eyed Bean (Chawali)*. In the initial stage vegetative growth was not significance but after 2nd interval it gradually increases and after 12 days roots and shoots elongation were dominant to a considerable extent. Thus there has been fair amount of satisfaction in crying out the present study. The encouraging results have surely contributed to the enthusiasm of the author. But honestly, this is just the beginning. There is a much scope for further study, and there is a long way to go.

V. ACKNOWLEDGEMENT

The authors are thankful to G.S.G.College, Umarkhed affiliated by S.G.B.Amaravati University (M.S.) for providing all the facilities to carry out the work.

VI. REFERENCES

- [1]. Larget R, , B, Renard P, Bioorg med. Chem. Left 10(8) : 835-38, April 2000.
- [2]. Venkataramn K, Mahal H.S, : Curr.Sci27, (1933), 124
- [3]. Yoigtande, H.W., and Haertner : Arch. P(harm (YYeinneim Ger.) 316(3), (1983), 219-22.
- [4]. Patil K.N., Ph.D. Thesis "Synthesis and rection of 3-aroylchoroflavanoneides." Amravati University (1993).
- [5]. Mayer A.M., Poljakotta A, Amer Iowa Univ. Press 735-749, 1993.
- [6]. Korade D.L. & Fulekan M.H., Biology and Medicine, Vol 1(1) : 28-34, 2009.
- [7]. Gibba Z., Grubisic D., Todorovic S. Plant Growth Regulation 26, 175-181, 1998.
- [8]. Majumdar, G.P. Hetero-archic roots in Enhydra fluctuans Laour. J. Indian bot. Soc. (11), 225-227; 1932.

Conduction Mechanism and DC Conductivity of Solid Polymer Electrolyte

S. R. Jadhao¹, S. P. Bakde²

¹Department of Physics, Nehru Mahavidyalaya (Art, Commerce, Science) Nerpersopant, Dist. Yavatmal, Maharashtra, India

²Department of Physics, Shri R. R. Lahoti Science College, Morshi, Dist Amravati, Maharashtra, India

ARTICLE INFO

Article History:

Accepted : 01 Jan 2025

Published : 10 Jan 2025

Publication Issue :

Volume 12, Issue 7

January-February-2025

Page Number :

365-367

ABSTRACT

In this report, Solid Polymer Electrolytes was prepared from Polyvinyl Alcohol (PVA) doped with varying amounts of ammonium iodide (NH₄I) salt by using solution casting method with double distilled water as the solvent. Impedence spectra analysis was studied. Analysis revealed that the conductivity of the electrolytes increases with increase the concentration of NH₄I, reaching a maximum at 25mole% salt content. While activation energy decreases with increasing salt concentration. The conduction mechanism of prepared sample was based on hopping mechanisms.

Keyword: Solid Polymer Electrolyte, NH₄I, Conductivity.

I. INTRODUCTION

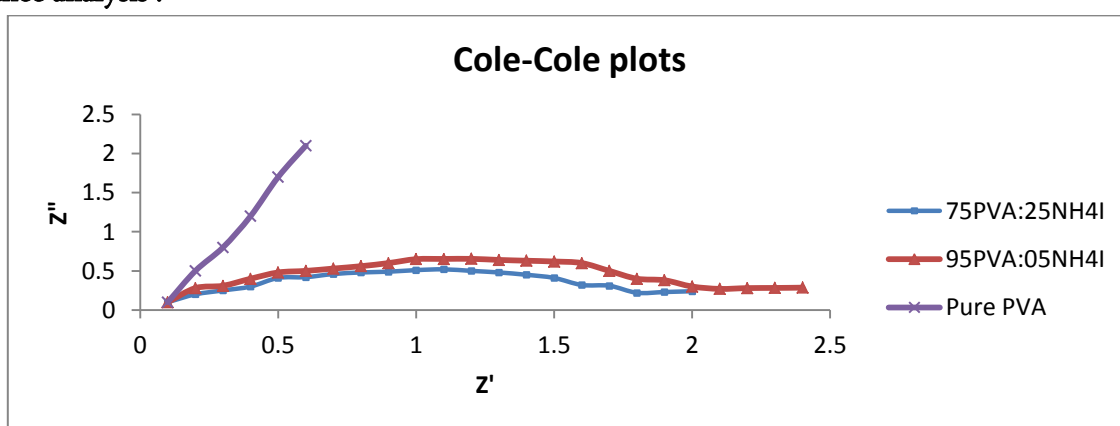
Solid Polymer Electrolyte are defined as conducting polymer materials, created by dissolving suitable salts in high molecular weight polar polymers. A review of the literature indicates that the addition of ammonium salts in to polar polymers creates proton conducting electrolytes, attributed to one loosely bound proton. Numerous researchers have explored proton-conducting Solid Polymer Electrolyte by integrating ammonium salts into various polar polymers, including polyvinyl pyrrolidone, polyethylene oxide, polyvinyl alcohol, polyvinyl chloride, and polyacrylonitrile. Conducting polymer electrolytes have received increased interest owing to their wide ranging applications in electrochemical sensors, reactors and proton exchange membrane fuel cells. Electrochemical devices, including high-power solid-state rechargeable batteries, supercapacitors, chemical sensors, electrochromic displays, and fuel cells, offer several advantages over gel and liquid electrolytes[1-3]. The main benefits of SPEs include their excellent mechanical properties, versatility, broad electrochemical stability, ease of thin-film fabrication, and flexibility [4].

II. METHODS AND MATERIALS

The polyvinyl alcohol supplied Sigma-Aldrich and NH_4I supplied by Merck India were used without further purification. Double distilled water was used as a solvent for preparing Polymer solution. It has been effectively synthesized using a solution casting technique to process Solid Polymer Electrolyte films in various concentrations as 5, 10, 15, 20, 25 mole% of salt NH_4I . The polymer PVA and ammonium iodide were taken in pure form and dissolved separately in double distilled water by mole percent. The solution was mixed together in different molar ratio and stirred well by using magnetic stirred to obtain homogenous mixture. The obtained mixture is casted in petri dish. The uniform thickness film was prepared and used for further investigation.

III.RESULT AND DISCUSSION

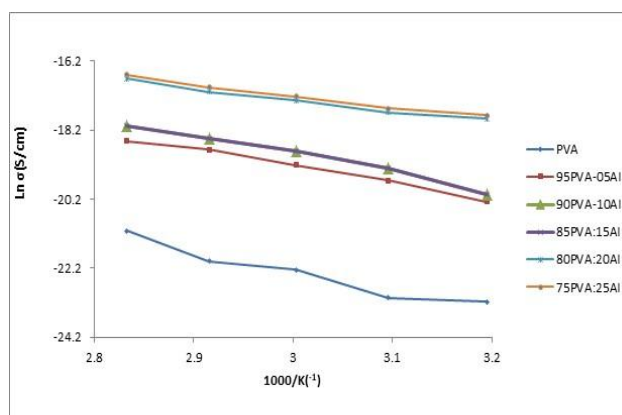
Z Impedance analysis :



Cole-Cole plot for Pure PVA and 95PVA:5NH₄I and 75PVA:25NH₄I Solid Polymer Electrolyte Films at temperature 313K

The ionic conductivity of all the prepared polymer films was analyzed using the AC impedance technique. The figure presents the Cole-Cole plot for the PVA- NH_4I polymer electrolyte with varying NH_4I concentrations at a temperature of 313 K. The Cole-cole plot shows a low-frequency spike, indicative of the diffusion process, followed by a semicircular arc, which corresponds to the charge transfer process [5-6]. The high-frequency arc corresponds to proton migration within the polymer matrix, representing the bulk conductivity of the polymer film. The low-frequency semicircular arc is related to the impedance at the electrode-electrolyte interface [7].

Arrhenius Behaviour:



The variation between $\text{Ln } \sigma$ vs $1000/T$ (Arrhenius plot) measure by using Kiteley 6487 picoammeter/Voltage source meter instruments at various constant voltage. An Arrhenius plot yielded a straight line, indicating that

the ionic conductivity followed the expected Arrhenius behavior. The ionic conductivity increased with the concentration of NH₄I in the PVA matrix, with the highest conductivity observed at a 25% NH₄I concentration. This suggests that the addition of NH₄I enhances the ionic conduction by providing more free ions that can migrate through the PVA matrix [8-10]. The temperature dependence of the conductivity was analyzed using the Arrhenius equation:

$$\sigma_T = \sigma_0 \exp \frac{-E_a}{KT}$$

Where σ_0 is the pre-exponential factor,

E_a is activation energy,

T is absolute temperature,

K is Boltzman constant.

The activation energy is calculated by the Arrhenius plot. From the slope of the plot, the activation energy E_a or ionic conduction was determined for each sample. Higher concentrations of NH₄I in PVA films typically showed lower activation energy, indicating improved ionic conduction with more ionic sites available for conduction [11-15].

IV. CONCLUSION:

The solid polymer electrolyte is prepared by solution cast technique. The electrical conductivity of solid polymer electrolyte increases with increase in concentration of ammonium iodide in polyvinyl alcohol. And its activation energy of DC electrical Conductivity decreases with increase concentration. Cole-cole plot shows Semi-circle arc and low-frequency spike. The conduction mechanism of prepared samples governed by hopping mechanisms.

V. REFERENCES

- [1]. A. Hayashi, T. Ohtomo, F. Mizuno, K. Tadanaga Electrochem. commun. 5(8) (2003) 701.
- [2]. S. Guinot, E. Salmon, J.F. Penneau, J. F. Fauvarque, Electro-chim. Acta 43 (1998) 1163.
- [3]. N. Vassal, E. Salmon, J. F. Fauvarque, J. Electrochem Soc. 146 (1999) 20.
- [4]. A. Mohamad, N. S. Mohamed, Y. Alias, A. K. Arof, J. Alloys Comp. 337 (2002) 208.
- [5]. G. B Appetecchi, F. Croce, B. Scrosati, Electrochim. Acta 40 (1995) 991.
- [6]. G. B Appetecchi, G. Dautzenberg, B. Scrosati, J. Electrochem. Soc. 143 (1996) 6.
- [7]. C.S. Ramya, T. Savitha, S. selvakarapandian & G. Hirankumar, Ionics, 11(2005) 436.
- [8]. K. Masuda, H. Kaji, F. Hori, J. Polym Sci Part B, 38(2002)1.
- [9]. F. Billmeyer, Jr text book of polymer science Wiley Singapur (1984).
- [10]. S. Chandra, S. A Hashim, G. Prasad, Solid State Ionic 40-41(1990) 651.
- [11]. R. M. Jaipal, T. Shreekanth, U. V. Subba Rao, Solid State Ionics, 126 (1999) 55.
- [12]. S. C. Raghavendra, S. Khasim, M. Revanasiddappa, A. Prasad, A. B Kulkarni, Bull Mater Sci, 26 (2003) 733.
- [13]. S. D. Druger, A. Nitzam, M. A. Ratner, J Chem Physics, 79 (1983) 3133.
- [14]. K. K. Maurya, S. A. Hashmi, S. A. Chandra, J. Phys Soc. Japan 61(1992)1709.
- [15]. M.S. Michael, M.M.E. Jacob, S.R.S. Prabakaran, S. Radhakrishna Solid State Ionics 98 (3-4), 167.

Geological Application of VO(IV), Zr(IV) and UO₂(VI) Complexes Derived From Thiazole Schiff Base

S. R. Kelode¹, D. B. Dupare²

¹Department of Chemistry, Arts, Commerce and Science College, Maregaon, Maharashtra, India

²Department of Chemistry, Shri Dr. R. G. Rathod Arts & Science College, Murtizapur, Maharashtra, India

ARTICLE INFO

Article History:

Accepted : 01 Jan 2025

Published : 10 Jan 2025

Publication Issue :

Volume 12, Issue 7

January-February-2025

Page Number :

368-371

ABSTRACT

The newly synthesized thiazole Schiff base have been synthesized by condensing

2-hydroxy-5-chloro acetophenone and 4-(p-hydroxyphenyl)-2-aminothiazole. The metal complexes were obtained as a result of interaction of Schiff base ligand and metal ions VO(IV), Zr(IV) and UO₂(VI). The complexes have been characterized on the basis of elemental analysis, infrared, molar conductance, magnetic Susceptibilities, and geological application.

Keywords: Thiazole Schiff Base, Molar conductance, Geological application

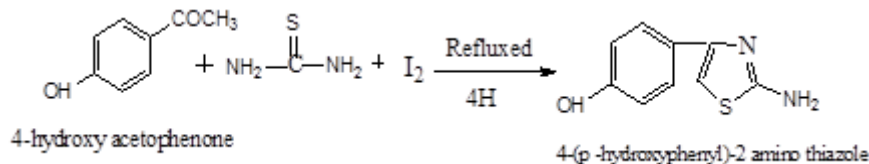
I. INTRODUCTION

This Research paper focus on synthesis, characterization, geological application and various methods of Schiff base derived from 2-hydroxy-5-chloro acetophenone and 4-(p-hydroxyphenyl)-2-aminothiazole. Synthesis, characterisation and antimicrobial studies of Schiff base ligand derived from salicylaldehyde and 2,4-dinitrophenylhydrazine and its metals complexes¹. Synthesis and structural diversity transition metal coordination complexes with diverse Schiff base ligands and macrocyclic systems². Comprehensive review on Schiff Base heterocyclic moiety conjugates and synthesis, reactions and diverse applications³. Performance of Schiff bases metal complexes and their ligand in biological activity⁴. Antifungal activity of some mixed ligand complexes incorporating schiff bases⁵. This paper discusses the analytical data and geological application of the Schiff base complexes of VO(IV), Zr(IV) and UO₂(VI).

II. EXPERIMENTAL:

All the chemicals were of A.R. grade and used as received. 2-hydroxy-5-chloro acetophenone (HCA) and 4-(p-hydroxyphenyl)-2 amino thiazole was prepared by known methods⁶⁻⁹. The solvents were purified by standard methods¹⁰

Synthesis of 4-(p hydroxyphenyl)-2 amino thiazole;



Synthesis of 2-hydroxy-5-chloro acetophenone 4-(p-hydroxyphenyl)-2 imino thiazole [HCAT]: A solution of 4-(p-hydroxyphenyl)-2 imino thiazole (0.02M) in 25ml of ethanol was added to an ethanolic solution(25ml) of 2-hydroxy-5-chloro acetophenone (0.02M) and the reaction mixture was refluxed on a water bath for 4h. After cooling a pale yellow coloured crystalline solid was separated out. It was filtered and washed with ethanol, crystallized from DMF and dried under reduced pressure at ambient temperature. The purity of ligand was checked by elemental analysis shown in Table 1. and m.p. It was also characterized by IR and ¹H NMR spectral studies. Yield:70%; m.p. 310°C

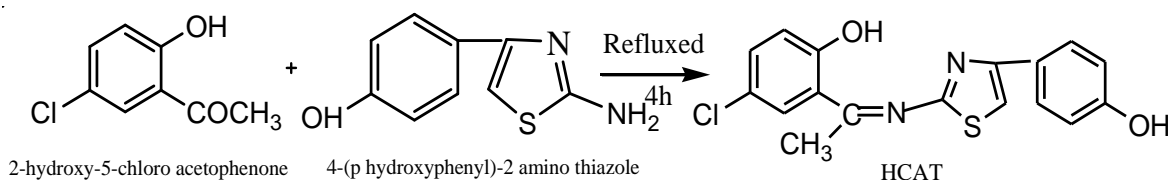


Table1. Analytical data of the Ligands.

Ligand	Molecular Formula	Formula Weight	Color and nature	Elemental Analysis				
				C% found (Cal.)	H% Found (Cal.)	N% Found (Cal.)	Cl% Found (Cal.)	S% Found (Cal.)
HCAT	C ₁₇ H ₁₃ N ₂ O ₂ SCl	344.6	Yellow Crystalline	59.38 (59.19)	03.70 (03.77)	08.5 (08.12)	10.11 (10.30)	09.22 (09.31)

Preparation of complexes: All the metal complexes were prepared in a similar way by following method. To a hot solution of ligand HCAT (0.02M) in 25ml of ethanol a suspension of respective metal salts was added drop wise with constant stirring. The reaction mixture was refluxed on a water bath for 4-6 h. The precipitated complexes were filtered, washed with ethanol followed by ether and dried over fused calcium chloride. Yield: 45-50%.

The complexes are soluble in DMSO and DMF but insoluble in water and common organic solvents. The metal chloride content of complexes were analyzed by standard methods¹¹. The ¹H NMR spectra of ligand was recorded and obtained from RSIC Chandigarh. IR spectra of the compounds were recorded on Perkin Elmer 842 spectrophotometer in the region 400-4000cm⁻¹, carbon, hydrogen and nitrogen analysis were carried out at RSIC, Punjab University, Chandigarh. The molar conductance of the complexes at 10⁻³M dilution in DMF were determined using equiptronic digital conductivity meter EQ-660 with a cell constant 1.00 cm⁻¹ at room

temperature. The magnetic moment measurement were made on a Gouy balance at room temperature using $[\text{HgCo}(\text{SCN})_4]$ as the calibrant.

The molecular weights of the complexes were determined by Rast method are shown in Table 2.

Table 2. Analytical data and molar conductance of the compounds.

Compounds	Colour	Mol.wt.	Analysis % Found (calc.)					μ_{eff} B.M.	Λ_{M} ($\Omega^{-1} \text{ cm}^2 \text{ mol}^{-1}$)
			M	C	H	N	Cl		
$[\text{VOL}_2]$	Green	754.2	6.63 (6.76)	54.01 (50.09)	3.05 (3.18)	7.33 (7.42)	9.32 (9.41)	1.60	12.8
$[\text{ZrL}_2(\text{OH})_2] \cdot 2\text{H}_2\text{O}$	Yellow	848.4	10.68 (10.74)	47.93 (48.09)	3.46 (3.53)	6.52 (6.60)	8.26 (8.36)	Dia	11.7
$[\text{UO}_2\text{L}_2]$	Orange	957.3	24.73 (24.87)	42.51 (42.61)	2.41 (2.50)	5.74 (5.84)	7.32 (7.41)	Dia	12.9

III.RESULTS AND DISCUSSION

The Schiff base ligand HCAT and its complexes have been characterized on the basis of ^1H NMR, IR spectral data, elemental analysis, molar conductance, magnetic susceptibility measurements and thermogravimetric analysis data. All these values and analytical data is consistent with proposed molecular formula of ligand. All the compounds are coloured solid and stable in air. They are insoluble in water but soluble in coordinating solvents like DMF and DMSO. The molar conductance values in DMF(10^{-3}M) solution at room temperature (Table 2) shows all the complexes are non electrolytes¹¹ The ^1H NMR spectra of ligand HCAT shows signals at δ 12.09, (1H, s phenolic OH), δ 9.51 (1H, s, phenolic OH), δ 7.55, 7.54, 7.53 and 7.52 (4H, m, phenyl) δ 6.81, 6.80, and 6.78(3H, s Phenyl), 6.68 (1H s thiophene), and 2.56(3H, s, methyl)¹²⁻¹⁵ IR spectra of ligand and metal complexes shows $\nu(\text{C}=\text{N})$ peaks at 1620cm^{-1} and absence of $\text{C}=\text{O}$ peak at around $1700\text{--}1750 \text{ cm}^{-1}$ indicates the Schiff base formation.¹⁶⁻¹⁸ IR spectra of complexes are shown in Table 3.

Table 3. IR spectra of ligand and metal complexes.

Compound	$\nu(\text{O}\cdots\text{H})$ hydrogen bonded	$\nu(\text{C}=\text{N})$ imine	$\nu(\text{C}\cdots\text{O})$ phenolic	$\nu(\text{M}\cdots\text{O})$	$\nu(\text{M}\cdots\text{N})$	$\nu(\text{C}\cdots\text{S})$
HCAT	3119	1620	1514	--	--	1122
$[\text{VOL}_2]$	--	1598	1506	514	445	1098
$[\text{ZrL}_2(\text{OH})_2] \cdot 2\text{H}_2\text{O}$	--	1600	1498	445	412	1108
$[\text{UO}_2\text{L}_2]$	--	1585	1440	550	480	1082

Geological application¹⁹⁻²³: Alloyed VO and its complexes is used to improvement of electrical properties in unalloyed films, it also used as a indicator for improvements in the materials. Zirconium and its complexes used in dental, surgical implants, cosmetics, antiperspirants, food packaging, microwave filters, photographic flashbulbs, used as catalysts in many chemical processes, including pollution control reactions and used in explosive primers. UO_2 and its complexes used as yellow and black colour in ceramic glazes and glass.

IV. CONCLUSION

In conclusion, we have synthesized new ligand 2-hydroxy-5-chloro- acetophenone 4-(p-hydroxyphenyl)-2 imino thiazole and their metal complexes. The analysis of magnetic moment data shows characterization and structural changes in metal complexes. This metal complexes used in geological field.

V. REFERENCES

- [1]. Shettima U.A., Ibrahim M. and Idongesit, E.E., Nigerian Res. J. of Chemical Sci, 1(12), 2024, 219.
- [2]. Parveez G. and Athar A. H., Asian J. Phy. and Chem. Sci. 2(4), 2017, 1.
- [3]. Harshil P.V., Shraddha A.D., Hiren V.D. and Sarita R.C., Int. J. Mult. and Res.,4(6),2024, 1
- [4]. Farah M.I and Saifaldeen M. A., Al-Nahrain Journal of Sci., 24 (1), 2021, 1.
- [5]. Miloud MM, El-ajaily MM, Al-noor TH and Al-barki NS. J Bacteriol Mycol. 7(1), 2020, 1122.
- [6]. Aswar A.S, Bahad P., Pardhi A. and Bhawe N., J. Polym. Mater., 5, 1988, 232.
- [7]. Pattan S., Ali M., Pattan J., Purohit S., Reddy V. and Nataraj B., Indian J. Chem.,45B, 2006, 1929.
- [8]. Khrustalev D., Suleimenova A. and Fazylov S., Russian J. App. chem., 81(5), 2008, 900.
- [9]. Maradiya H., and Patel V., J. Fibers and poly., 3(1), 2002, 43.
- [10]. Furniss B., Hannaford A., Smith P. and Tatchell A., Vogel's practical organic chemistry 5thEd. Logman Scientific Technical, John Wiley and Sons, 1989.
- [11]. Vogel AI, "A Text book of quantitative inorganic chemistry" 3 thEd., (ELBS, London,1961).
- [12]. Sadigova S., Magerramov A. and Allakhverdiev M., Russian J. Org.Chem., 81(5), 2008, 900.
- [13]. Campbell E. and Nguyen S., J. Tetrahedron, 42, 2001, 1221.
- [14]. Pietikainen P. and Haikarainen A. J. Mole. Catalysis., 180, 2002, 59.
- [15]. Kidwai M., Poddar P. and Singhal K., Indian J. Chem., 48B, 2009, 59.
- [16]. Sonwane S., Srivastava S. and Srivastava S., Indian J. Chem., 47B, 2008, 633.
- [17]. Patel K. and Mehata A., E. J. Chem., 3(13), 2006, 267.
- [18]. Boghaei D. and Mohebi S. J. Tetrahedron, 58, 2002, 5357.
- [19]. Algeo, T. J., & Rowe, H., Chemical Geology, 324, 2012, 6.
- [20]. Averill, S. A., Geological Society, London, Special Publi, 185(1), 2001,69.
- [21]. Awasthi, N., Journal of Asian Earth Sciences, 150, 2017, 45.
- [22]. Bibi I., Icenhower J., Niazi N. K., Naz T., Shahid M., & Bashir S., Env. Mat. and waste, 2016, 543.
- [23]. Large, R. R., Mukherjee, I., Gregory, D. D., Steadman, J. A., Maslennikov, V. V., & Meffre, S., Economic Geology, 112(2), 2017, 423.

Synthesis and Characterization of Heterocyclic Active Functionalities of Pyrazoles with Their Importance

S.A. Ikhe¹, P.M.Dahikar², D.A. Pund^{1*}

¹Department of Chemistry, Shri R.R. Lahoti Science College, Morshi, Maharashtra, India

²Department of Chemistry, J.D. Patil Sangludkar Mahavidyalaya, Daryapur, Maharashtra, India

ARTICLE INFO

Article History:

Accepted : 01 Jan 2025

Published : 10 Jan 2025

Publication Issue :

Volume 12, Issue 7

January-February-2025

Page Number :

372-376

ABSTRACT

Pyrazoles have drawn a lot of interest and concern in the fields of pharmacology and organics because of their potential as synthetic intermediates for the production of different bioactive compounds. Thus, one of the main areas of study for synthetic organic chemists is the synthesis of pyrazoles. Similarly, because of their numerous physiochemical and biological uses based on the significant structural electronic properties of these N-heterocyclic compounds, fused pyrazoles, such as pyrazolo based pyridines and pyrazolo pyrimidines, have been extensively researched. Therefore, it is of great interest to synthesize these fused heterocycles and their derivatives in order to uncover new derivatives and expose new applications. In recent years, a number of methods mostly involving condensation reactions for the synthesis of pyrazoles and their fused systems have been described in the literature. Additionally, ¹H NMR and GCMS analysis verified the synthesized pyrazole based derivatives.

Keywords: Pyrazole, N-Heterocyclic, bioactive, fused heterocycles

I. INTRODUCTION

Two adjacent nitrogen atoms make up the 5-membered ring of a heterocyclic pyrazole compound [1]. Because of their propensity to accept protons (C=N) and the tendency of the nitrogen atom (N-H) in pyrrole to donate protons, NH-pyrazoles are weak bases and weak acids [2]. Similarly, the structural units of pyrazoles determine the hydrogen-heteroatom interaction, or hydrogen bonding [3]. In 1883, German chemist Ludwig Knorr attempted to create a quinoline compound that had antipyretic properties [4]. Sadly, however, the pyrazole was synthesized in place of the quinoline [5]. In order to demonstrate that pyrazole was derived from pyrrole by substituting a nitrogen atom for the carbon atom, Knorr first introduced the heterocycle to its core [6]. The first to observe that pyrazole-based compounds had antipyretic effects in humans, which sparked interest in the pyrazole moiety [7]. Then, in 1846, Kosuge and Okeda extracted levo-β-(1-pyrazolyl) alanine

from watermelon seeds (*Citrullus vulgaris*) and 3-n-nonylpyrazole from *Houttuynia cordata*, a plant with antimicrobial activity [8]. Prior to these discoveries, it was believed that pyrazoles were not naturally occurring [9]. The versatility of compounds based on pyrazole moiety in both synthetic and biological applications. Despite the fact that the pyrazoles moiety is present in a large number of natural products, it is well known and even one of the most researched compounds in the azole family [10]. Because of their many uses, N-heterocyclic compounds, such as substitute pyrazoles, are significant [11]. The fused pyrazole structure is present in the majority of natural products. Formicin A naturally contains a pyrazolo[4,3-d] pyrimidine compound. whose biological activity is different. like antiviral and antitumor drugs.

Overall, these compounds' pyrazole core moiety fused with five- and six-membered heterocyclic compounds exhibit biological and pharmacological activities [12-14]. Specifically, pyridines and pyrimidines based on pyrazoles have participated in drug discovery [15,16].

II. EXPERIMENTAL SECTION

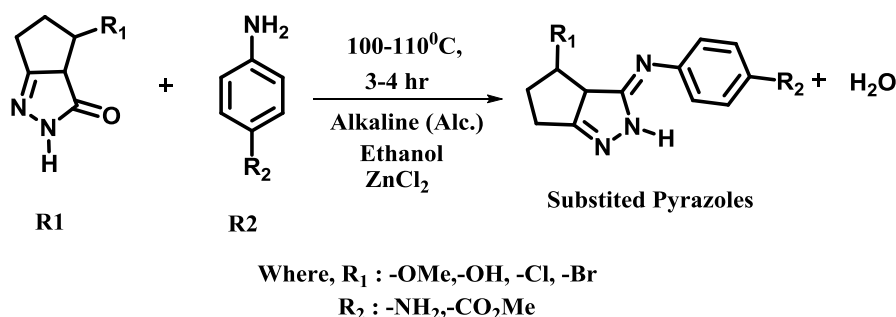
MATERIALS

Methanol (98%), Ethanol (98%) Acetonitrile (99%) and ethyl acetate (98%) were procured from Avra chemical Pvt. Ltd. Sodium hydroxide (98%) zinc chloride Were acquired from Sisco Research Laboratories Pvt. Ltd.

CHARACTERIZATION TECHNIQUE

The Chemical structure of synthesized compounds was confirmed by spectral data. ¹H-NMR spectra were recorded on BRUKER AVANCE NEO 500 MHz spectrometer using DMSO and CDCl₃ solvent and TMS as internal standards at SAIF, Punjab University, Chandigarh (India). Chemical shifts are expressed in ppm. Mass spectrums were recorded on Thermo Scientific TSQ 8000 Gas Chromatograph

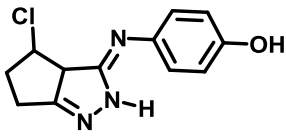
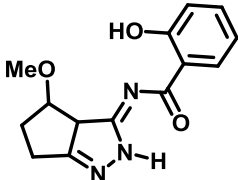
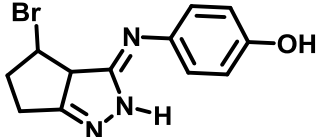
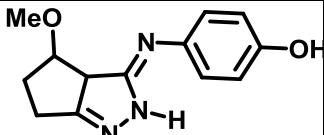
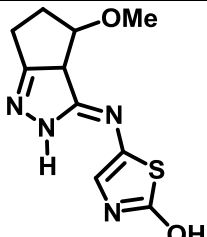
General Reaction



Scheme 1. General Reaction for Synthesis of N-Heterocyclic Substituted Pyrazoles

Reactant (R1) (0.1 mmol) was heated with reactant (R2) (0.15 mmol) in oil bath at 100 °C to 110 °C, till complete removal of dehydrated water is ensured. The solid cream color precipitate was obtained and it filtered, washed with methanol and recrystallized by ethanol with preferable yield, m.p. 179°C as cream- white colored crystalline solid. (Scheme 1.)

Table 1. Structural analysis of derivatives

Sr. No	Structure of Products	Structural analysis by ¹ HNMR and GCMS
1		¹ HNMR(500MHz,CDCl ₃):δ9.40(s,1H),6.747.20(m,4H),3.2(q,1H),2.0-2.16(t,2H),1.56-1.81(t,2H),1.6(t,1H) GCMS: Cal m/z: 249.70, Found m/z: 249.68
2		¹ HNMR(500MHz,CDCl ₃):δ16.4(s,1H),6.747.68(m,5H),3.41(s,3H),3.2(d,1H),2.0-2.16(t,2H),1.56-1.81(t,2H),1.6(t,1H) GCMS: Cal m/z: 273.11, Found m/z: 273.06
3		¹ HNMR(500MHz,CDCl ₃):δ9.69(s,1H),7.68(s,1H),6.68(s,1H),3.2(q,1H),2.06-2.16(q,2H),1.56-1.81(m,2H),1.6(t,1H) GCMS: Cal m/z: 294.15, Found m/z: 294.12
4		¹ HNMR(500MHz,CDCl ₃):δ9.40(s,1H),6.747.20(m,4H),3.41(s,3H),3.2(q,1H),2.0-2.16(t,2H),1.56-1.81(t,2H),1.6(t,1H) GCMS: Cal m/z: 245.28, Found m/z: 244.16
5		¹ HNMR(500MHz,CDCl ₃):δ9.69(s,1H),7.68(s,1H),6.68(s,1H),3.41(s,3H),3.2(q,1H),2.06-2.16(q,2H),1.56-1.81(m,2H),1.6(t,1H) GCMS: Cal m/z: 252.29, Found m/z: 251.40

III.CONCLUSION

It is well known that pyrazole derivatives and even their different functional group substituents can be synthesized. The majority of the research focused on the pyrazole derivatives' bioactivity. Recent efforts have been made to comprehend the various characteristics of pyrazole derivatives. There are also certain obstacles to overcome. These difficulties include producing new pyrazole derivatives with bioactivity in the submicromolar range, accurately characterizing the derivatives' properties, and synthesizing them efficiently for high yields. Because of this, we think it's necessary to look into new synthetic pathways, examine various characteristics, and find new uses for novel derivatives, particularly in blends with polymers. As a result, new uses for pyrazole derivatives will emerge in a variety of fields.

IV. REFERENCES

- [1]. Bekhit, Adnan A., "New heterocyclic hybrids of pyrazole and its bioisosteres: Design, synthesis and biological evaluation as dual acting antimalarial-antileishmanial agents." *European Journal of Medicinal Chemistry* 94 (2015): 30-44.
- [2]. Farag, A. M., Ali, K. A., El-Debss, T. M., Mayhoub, A. S., Amr, A. G. E., Abdel-Hafez, N. A., & Abdulla, M. M. (2010). Design, synthesis and structure–activity relationship study of novel pyrazole-based heterocycles as potential antitumor agents. *European journal of medicinal chemistry*, 45(12), 5887-5898.
- [3]. Abdelgawad, N., Ismail, M. F., Hekal, M. H., & Marzouk, M. I. (2019). Design, synthesis, and evaluation of some novel heterocycles bearing pyrazole moiety as potential anticancer agents. *Journal of Heterocyclic Chemistry*, 56(6), 1771-1779.
- [4]. Nossier, E. S., Fahmy, H. H., Khalifa, N. M., El-Eraky, W. I., & Baset, M. A. (2017). Design and synthesis of novel pyrazole-substituted different nitrogenous heterocyclic ring systems as potential anti-inflammatory agents. *Molecules*, 22(4), 512.
- [5]. Faisal, M., Saeed, A., Hussain, S., Dar, P., & Larik, F. A. (2019). Recent developments in synthetic chemistry and biological activities of pyrazole derivatives. *Journal of Chemical Sciences*, 131, 1-30.
- [6]. M Abdelrazek, F., M Gomha, S., H Abdelrahman, A., Metz, P., & A Sayed, M. (2017). A facile synthesis and drug design of some new heterocyclic compounds incorporating pyridine moiety and their antimicrobial evaluation. *Letters in Drug Design & Discovery*, 14(7), 752-762.
- [7]. Gangurde, K. B., More, R. A., Adole, V. A., & Ghotekar, D. S. (2024). Design, synthesis and biological evaluation of new series of benzotriazole-pyrazole clubbed thiazole hybrids as bioactive heterocycles: Antibacterial, antifungal, antioxidant, cytotoxicity study. *Journal of Molecular Structure*, 1299, 136760.
- [8]. Reddy, G. M., Garcia, J. R., Yuvaraja, G., VenkataSubbaiah, M., & Wen, J. C. (2020). Design, synthesis of tri-substituted pyrazole derivatives as promising antimicrobial agents and investigation of structure activity relationships. *Journal of Heterocyclic Chemistry*, 57(5), 2288-2296.
- [9]. Castillo, J. C., & Portilla, J. (2018). Recent advances in the synthesis of new pyrazole derivatives. *Targets Heterocycl. Syst*, 22, 194-223.
- [10]. Karati, D., Mahadik, K. R., & Kumar, D. (2022). Pyrazole Scaffolds: Centrality in Anti-Inflammatory and Antiviral Drug Design. *Medicinal Chemistry*, 18(10), 1060-1072.
- [11]. Liu, X. R., Wu, H., He, Z. Y., Ma, Z. Q., Feng, J. T., & Zhang, X. (2014). Design, synthesis and fungicidal activities of some novel pyrazole derivatives. *Molecules*, 19(9), 14036-14051.
- [12]. Ansari, A., Ali, A., & Asif, M. (2017). Biologically active pyrazole derivatives. *New Journal of Chemistry*, 41(1), 16-41.
- [13]. Abd-El Gawad, N. M., Hassan, G. S., & Georgey, H. H. (2012). Design and synthesis of some pyrazole derivatives of expected anti-inflammatory and analgesic activities. *Medicinal chemistry research*, 21, 983-994.
- [14]. Bakthavatchala Reddy, N., Zyryanov, G. V., Mallikarjuna Reddy, G., Balakrishna, A., Padmaja, A., Padmavathi, V., ... & Sravya, G. (2019). Design and synthesis of some new benzimidazole containing pyrazoles and pyrazolyl thiazoles as potential antimicrobial agents. *Journal of Heterocyclic Chemistry*, 56(2), 589-596.
- [15]. Fayed, E. A., Eissa, S. I., Bayoumi, A. H., Gohar, N. A., Mehany, A. B., & Ammar, Y. A. (2019). Design, synthesis, cytotoxicity and molecular modeling studies of some novel fluorinated pyrazole-based heterocycles as anticancer and apoptosis-inducing agents. *Molecular diversity*, 23, 165-181.

- [16]. Fustero, S., Simon-Fuentes, A., & Sanz-Cervera, J. F. (2009). Recent advances in the synthesis of pyrazoles. A review. *Organic Preparations and Procedures International*, 41(4), 253-290.
- [17]. Corradi, A., Leonelli, C., Rizzuti, A., Rosa, R., Veronesi, P., Grandi, R., ... & Villa, C. (2007). New “green” approaches to the synthesis of pyrazole derivatives. *Molecules*, 12(7), 1482-1495.
- [18]. Kumari, S., Paliwal, S., & Chauhan, R. (2014). Synthesis of pyrazole derivatives possessing anticancer activity: Current status. *synthetic communications*, 44(11), 1521-1578.

Bio-Green Synthesis of AgNPs from Moringaoleiferaleaves Extract and Its Antibacterial Application

S.D. Chavan^{*1}, R. D. More^{*1}, S.P.Moharir¹, S.S.Paden²

¹Department of Chemistry, Siddharth Arts, Commerce and Science College, Jafrabad, Dist.Jalna-431206, Maharashtra, India

²Department of Chemistry, Rajashree Shahu Science College, Chandur Railway, Dist-Amravati-444904, Maharashtra, India

ARTICLE INFO

Article History:

Accepted : 01 Jan 2025

Published : 10 Jan 2025

Publication Issue :

Volume 12, Issue 7

January-February-2025

Page Number :

377-382

ABSTRACT

In this study Ag nanoparticles prepared with MoringaOleiferaleaves extract by using eco-friendly greenmethod. The green synthesis approaches are recognized by many scientists due to its cost effective, simple, eco-friendly. The stability and reduction of Ag⁺ ions due to phytochemical stabilizing or capping agent. The preliminary formation of Agnanoparticles were characterized byusing UV-Visible spectroscopy. From UV-Visiblespectroscopy, showed an intense absorption band with a maximum at 421 nm is attributed to surface Plasmonresonance which is characteristic of the Agnanoparticles. The M.oleiferaextract act as reducing agent for stabilization of particle size as well as medicinal value result showed a significant antibacterial activity againstpathogenic bacteria, E.Coli.andS.aureus. The present investigation deals with the biosynthesis of Ag nanoparticles and its antibacterial effect on selected bacteria.

Keywords: Moringaoleifera; Agnanoparticles; UV-Visible spectroscopy; Antibacterial activity; Bio-green method.

I. INTRODUCTION

The term “nano” is derived from the Greek word “nanos” for “dwarf”. Nanoscale materials are defined as materials having at least one dimension in the 10–100 nm range. The production of nanoparticles can be achieved through two approaches known as ‘top-down approach’ and ‘bottom-up approach’. In the top-down approach, the bulk material is broken down into particles at nano-scale through different processes like grinding, milling, etc. In the bottom-up approach, the atoms/molecules self assemble to form new nuclei which grow into a particle of nano-scale. Biosynthesis of nanoparticles researchers to develop synthetic strategies using biological entities like enzymes

[1], microorganisms [2] and plant extracts[3-5] play a major role in the formation of nanoparticles. The green route process involves two

basic mechanisms namely, 'reduction' and 'stabilization' (capping). The biomolecules present in the plants such as proteins, amino acids, vitamins, polyphenols, polysaccharides, terpenoids, organic acids, etc. are responsible for the synthesis of nanoparticles. *Moringa oleifera* (M. oleifera) (Family: Moringaceae, English name: drumstick tree) has been reported to be essentially used as an ingredient of the Indian diets since ages. It is cultivated almost all over India and its leaves and fruits are traditionally used as vegetables. Almost all parts of the plant have been utilized in the traditional system of medicine. The plant leaves have also been reported for its antitumor, cardioprotective, hypotensive, wound and eye healing properties [6]. Drumstick (M. oleifera) is a source rich in proteins with alkaloids, amino acids, polyphenols, glycosides, terpenoids and steroids have been

identified as major phytochemicals present in drumstick which play the vital role in the stabilizing mechanism of the green synthesis of nanoparticles. *Moringa oleifera* leaves are known for their antimicrobial activity against many organisms. Extracts of *Moringa oleifera* leaves contain higher amount of alkaloids, anthocyanins, proanthocyanidins, flavonoids, and cinnamates [7, 8]. Compounds with activity against a wide spectrum of microbes. M. oleifera has enormous medicinal potentials which have been long recognized in the Ayurvedic and Unani system [9].

II. MATERIAL AND METHODS

Materials

Silver Nitrate (AgNO_3), deionised water was purchased from Sigma–Aldrich Chemicals. All glasswares are sterilized with nitric acid and further with deionised water and dried in oven before use. *M. oleifera* (Drumstick) leaves were collected from campus of JES College, Jalna, Maharashtra, India.

Preparation of Aqueous Extract from *Moringa Oleifera*

Green leaves of *Moringa Oleifera* (Drumstick) plant and leaves powder are shown in figure 1. The leaves were washed with tap water to remove impurities. The plant leaves were dried under shade for 1 week, the dried leaves were grinded using mortar and pestle until the leaves are grinded finely powder form. The aqueous leaves extract of M. oleifera was prepared using 30 g of powder of leaves, was to be added into 100 mL of deionized water at 70 °C to 80 °C for 20 minutes. The extract was filtered through filter paper. The filtered extract was stored in refrigerator at 4 °C for further studies.

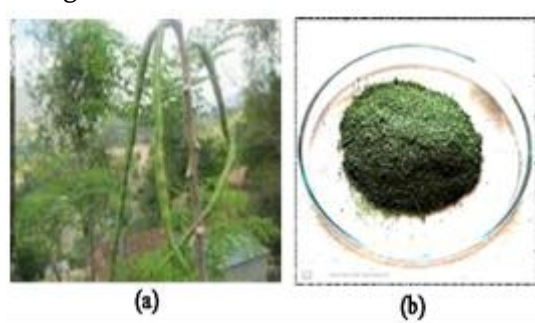


Fig.1. Photographs of (a) Plant and (b) leaves powder of *Moringa Oleifera*

Green Synthesis of Ag Nanoparticles

The Moringa oleifera extract was then used for the synthesis of silver nanoparticles. 0.0424 gm of silver nitrate (AgNO_3) obtained from Himedia Pvt. Ltd. chemical was dissolved in 250 mL of double distilled water so as to obtain 1 mM of silver nitrate precursor solution. 10 mL of Moringa oleifera extract was added to the 50 mL of 1 mM AgNO_3 solution and the mixture was magnetically stirred and heated at 60-80 °C for 60 min. The mixture solution

which initially appeared in pale yellow colour, slowly changed into brownish red colour within 1 h. The colour change indicated the formation of silver nanoparticles and the completion of the synthesis process. The reacted solution was centrifuged at a speed 5000 rpm for 15 min. Then centrifuged particles were washed with distilled water and again subjected to centrifugation at 5000 rpm for 10 minutes and then nanoparticles settled at the bottom were carefully removed and spread on a Petri dish for drying at 80 °C. The synthesis, characterization, and application of Ag nanoparticle is summarized in figure 2.

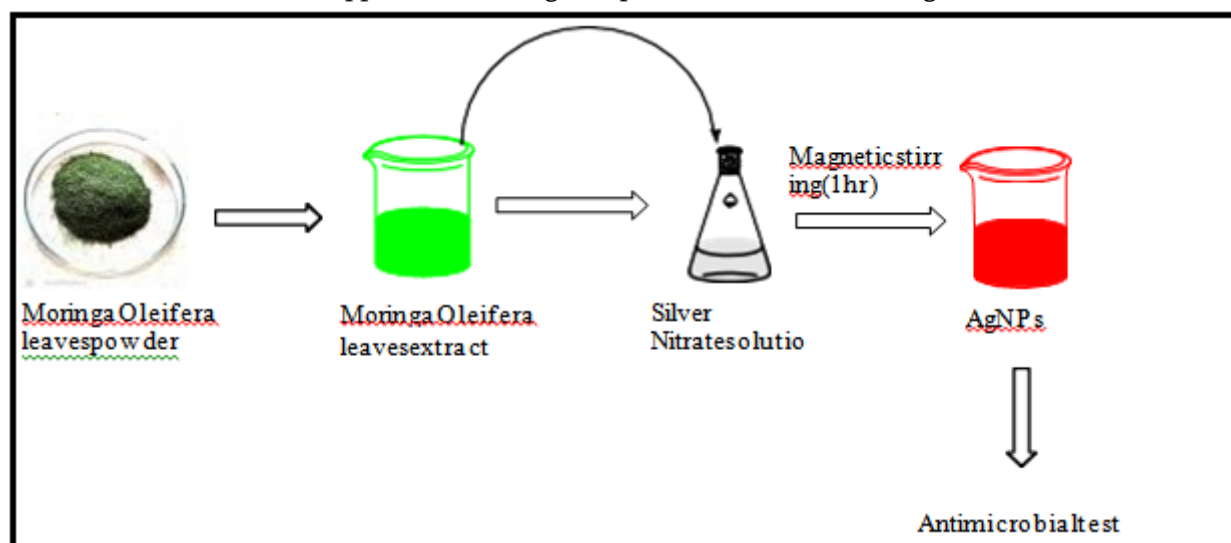


Fig.2. Schematic representation of synthesis of AgNPs

Antibacterial Test

The antibacterial activity of AgNPs has been tested against both gram positive (*S. aureus*) and gram negative (*E. coli*). The antibacterial activity of AgNPs toward *E. coli* strain reference NCIM2109 and *S. aureus* strain reference NCIM2079 were performed using disc diffusion method. The AgNPs showed zone of diameter in both bacterium and *E. coli* gram negative found more zone of inhibition as compared to *S. aureus* gram positive, while gram negative bacteria showed nearly equal sensitivity as that of positive control (Gentamicin).

Characterization of Ag nanoparticles UV-Visible spectra analysis

The bio-reduction of Silver nitrate into AgNPs using the aqueous extract of *M. oleifera* were subjected to record UV-Visible spectroscopy. The UV-Visible absorption spectra of AgNPs of reaction media were noted at 25 °C temperature in a quartz cuvette (1 cm path length) and at the wavelength ranging from 300 to 600 nm using a Equip-tronics Dual Beam Spectrophotometer. The absorption peaks are obtained at the wavelength 421 nm.

III.RESULTS AND DISCUSSION

The present investigation involves leaves extract of medicinal plant species *M. oleifera* for the bio-green mediated synthesis of Ag nanoparticles. The all different parts of the plant have already been exploited for the amalgamation of various metal nanoparticles with precious bioactive mechanisms. This particular planned for bio-synthesis of Ag nanoparticles leaf extracts of *M. oleifera*. The AgNPs from *M. oleifera* leaves have been investigated to acquire important antifungal activity against *Candida albicans* [10]. The silver nanoparticles reduced by the

gum as phytochemical of *M. oleifera* were reported to show antibacterial activity against *Staphylococcus aureus*, *E. coli* and *Pseudomonas aeruginosa* [11]. They synthesized Ag nanoparticles from the leaves of *M. oleifera*, and this nanoparticles at the concentration of 200 µg/ml exhibits antibacterial activity in opposite to gram positive and gram negative bacteria such as *Staphylococcus aureus*, *Bacillus subtilis*, *Pseudomonas aeruginosa*, *Proteus mirabilis*, *Escherichia coli* and antifungal activity against *Candida albicans* and *Candida tropicalis*. [10].

UV-Vis-Spectrum

The AgNPs were synthesized by using leaves extract of *M. oleifera* as detailed above. The Silver metal ions reduced to Ag nanoparticles in the reaction medium were initially analyzed using UV-Vis Spectrophotometer between 300 to 600 nm. The UV-Vis spectrum of AgNPs is shown in Figure 3. The confirmation of synthesis of AgNPs product in nano-scale was exhibited by the absorption peak is obtained at the wavelength 421 nm.

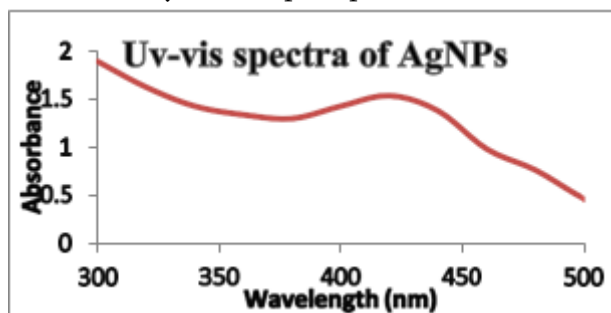


Figure 3. UV-vis spectra of AgNPs synthesized using *M. Oleifera* leaves extract

Antibacterial Activities of Ag Nanoparticles against *E. coli* and *S. aureus*

The characteristic features of nanoparticles namely the larger aspect ratio deliver greater surface area of contact with the microbial pathogens and provides enhanced reactivity. The Ag nanoparticles synthesized using the leaf extract of *M. Oleifera* exhibit antibacterial activity beside gram negative, *E. coli*, and gram positive bacteria, *S. aureus*. The zone of inhibition obtained from the assay are presented in Table 1 and shown in fig 4.

Sr.No	Test Organism	Zone of Inhibition (mm)	
		50 (µg/mL)	Positive (P) (µg/mL) Control
1	<i>S. aureus</i>	8.88±0.4	12.57±0.3
2	<i>E. coli</i>	9.40±0.6	10.65±0.4

Table 1. Zone of Inhibition (ZOI) of Ag NPs against *S. aureus*, *E. coli* and positive (P) control

It is described that synthesized metal nanoparticles affix to the surface of the cell membrane, agitate its function [12] and penetrate directly with the bacterial outer membrane and release metal ions. Gentamicin 10mg/mL is used as a positive control. If the concentration of the synthesized sample increases, the zone of inhibition values will also increase. The silver nanoparticles directly redress the cell envelope by penetrating the cell and then binding to the DNA. It can affect the cell's basic functions and finally in the death of the cell. Synthesized silver nanoparticles show antibacterial activity somewhat less or nearly equal to that standard. The bactericidal activity of synthesized silver nanoparticles is due to their extremely large surface area [13], which provides better contact with microorganisms. However, the exact mechanism of nanoparticle interaction with microorganisms is still unknown. [14]

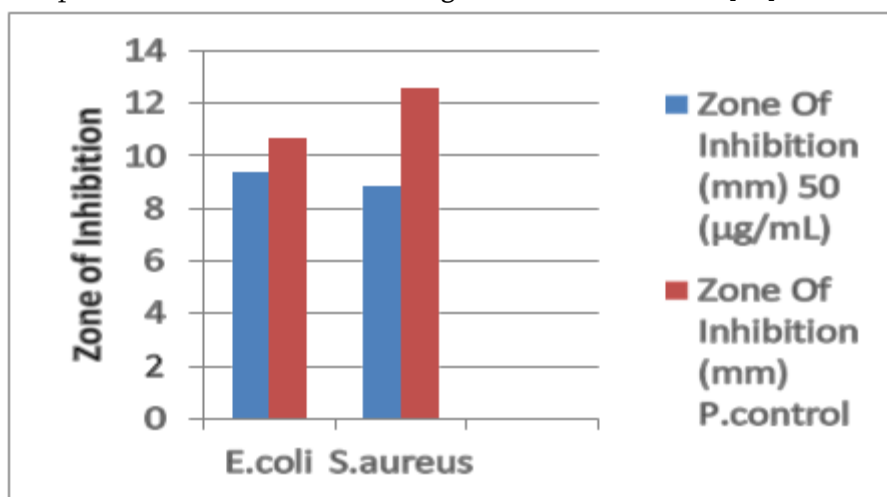


Figure.4 Antimicrobial activity of silver NP shows the zone of inhibition (mm) against *E. coli* and *S. aureus*

IV. CONCLUSION

The bio-green synthesis of Ag nanoparticles were successfully produced by the leaves extract of *M. Oleifera*. The green method used is simple, easily eco-friendly and very fast. The characteristic color change to yellow indicates the formation of Ag nanoparticles. This is further confirmed by the reduction of Ag⁺ ions into Ag nanoparticles with UV-Visible spectroscopy. The UV-Vis absorption peak at 421 nm. The antibacterial investigation exposed that both gram-negative and gram-positive bacteria are sensitive to the nanoparticles of AgNPs.

V. REFERENCES

- [1]. I. Willner, R. Baron and B. Willner, *Adv. Mater.* 18(2006)1109.
- [2]. Y. Konishi, K. Ohno, N. Saitoh, T. Nomura, S. Nagamine, H. Hishida, Y. Takahashi, and T. Uruga, *J. Biotechnology*. 128(2007)648.
- [3]. S.S. Shankar, A. Rai, A. Ahmad and M. Sastry, *J. Colloid Interface Sci.* 275(2004) 496.
- [4]. S.P. Chandran, M. Chaudhary, R. Pasricha, A. Ahmad and M. Sastry, *Biotechnol. Prog.* 22(2006)577.
- [5]. D. Philip, *Physica E*, 42 (2010)1417.
- [6]. Rath, B.; Bodhankar, S.; Deheti, A. M. *Indian J. Exp. Biol.* 2006, 44, 89

- [7]. Tarafder CR, Ethno-gynecology in relation to plants, 2. Plants used for abortion, J Econ Taxon Bot, 1983, 4(2), 507-516.
- [8]. Nath D, Sethi N, Srivastav S, Jain A K and Srivastava R, Survey on indigenous medicinal plants used for abortion in some districts of Uttar Pradesh, Fitoterapia, 1997, 68(3), 223-225.
- [9]. Mughal, M. H. S.; Ali, G.; Srivastava, P. S.; Iqbal, M. (1999). Improvement of drumstick (*Moringa Pterygosperma Gaertn*). A unique source of food and medicine through tissue culture. Hamdard medical 42:37-42
- [10]. S.K. Vibhute, V.S. Kasture, P.N. Kendre, G.S. Wagh, Indo American Journal of Pharmaceutical Research 4(2014)1581-1587.
- [11]. M.R. Kudle, K.R. Kudle, M.R. Donda, M.P.P. Rudra, Nanoscience and Nanotechnology: An International Journal 3(2013)45-48.
- [12]. Xiu, Z.-M., P.J.J. Alvarez, and J. Ma. The differential effect of molecular oxygen and general ligands on antimicrobial activity of AgNPs versus silver ions. Environ. Sci. Technol., 45: 9003-9008. (2011)
- [13]. Barani, H., M. Montazer, N. Samadi, and T. Toliyal, In situ synthesis of nanosilver/lecithin on wool: Enhancing nanoparticles diffusion. Coll. Surf. B: Biointer., 92:9-15. (2012)
- [14]. Jiang, W., H. Mashayekhi, B. Xing, The bacterial toxicity evaluation between nano- and micro-scaled oxide particles. Environ. Poll. 157:1619-1625. (2009)

Sustainable Phytofabrication of Sulfur Nanoparticles from Orange Peel Extract: Structural, Morphological, and Antibacterial Insights

S.G. Khobragade¹, N. S. Dixit², S. B. Bansod³, M. S. Dixit⁴, D.C.Deshmukh⁵, A.S. Dixit⁶

¹Department of Chemistry, Brijlal Biyani Science College, Amravati-444605, Maharashtra, India

²Department of Chemistry, G.S.Tompe Arts, Science and Commerce College, Chandur Bazar (444704), Maharashtra, India

³Department of Chemistry, Smt. Narsamma Arts, Commerce and Science College, Kiran Nagar, Amravati, Maharashtra, India

⁴Jagadamba Mahavidyalaya, Achalpur (444806), Maharashtra, India

⁵G. S. Tompe Arts, Science and Commerce College, Chandur Bazar (444704), Maharashtra, India

⁶Dr. Rajendra Gode Institute of Science and Technology, Amravati, Maharashtra, India

ARTICLE INFO

Article History:

Accepted : 01 Jan 2025

Published : 10 Jan 2025

Publication Issue :

Volume 12, Issue 7

January-February-2025

Page Number :

383-388

ABSTRACT

This study explores the green synthesis of sulfur nanoparticles (SNPs) using orange peel extract, promoting sustainable nanotechnology through biowaste utilization. Synthesis conditions were optimized, and SNPs were characterized by XRD, FTIR, FESEM, and EDAX, revealing insights into their structure, morphology, and elemental composition. Antimicrobial tests demonstrated SNPs' effectiveness against Gram-positive bacteria (*Staphylococcus aureus* and *Enterococcus faecium*), while no activity was observed against Gram-negative strains (*Escherichia coli* and *Klebsiella pneumoniae*). This work underscores the potential of eco-friendly SNPs in nanomedicine, advancing sustainable approaches for antimicrobial applications.

I. INTRODUCTION

Nanotechnology has emerged as a transformative force across various scientific fields and industries, offering innovative solutions in areas such as catalysis, energy storage, and biomedicine.[1] Among the wide array of nanomaterials, sulfur nanoparticles (SNPs) have garnered significant attention due to their unique physicochemical properties, broad-spectrum antimicrobial activity, and potential applications in pharmaceuticals and environmental remediation.[2] Despite their promising attributes, conventional synthesis methods for SNPs often involve toxic chemicals, high energy consumption, and environmentally hazardous

byproducts, raising concerns about sustainability and safety. To address these challenges, green synthesis approaches have gained momentum, utilizing natural resources and plant-based extracts to fabricate nanoparticles in an eco-friendly and cost-effective manner.[3,10] Orange peels, a widely available agricultural byproduct rich in bioactive compounds such as flavonoids and polyphenols, present a sustainable and renewable resource for nanoparticle synthesis. This not only mitigates environmental waste but also enhances the biocompatibility and stability of the resulting nanomaterials.[4,9]

In this study, sulfur nanoparticles were synthesized using orange peel extract as a reducing and stabilizing agent.[5] The structural, morphological, and surface characteristics of the SNPs were thoroughly investigated using advanced analytical techniques, including X-ray Diffraction (XRD), Fourier Transform Infrared Spectroscopy (FTIR), Field Emission Scanning Electron Microscopy (FESEM), and Energy Dispersive X-ray Analysis (EDAX). The antimicrobial efficacy of the synthesized SNPs was evaluated against Gram-positive (*Staphylococcus aureus*, *Enterococcus faecium*) and Gram-negative (*Escherichia coli*, *Klebsiella pneumoniae*) bacterial strains, demonstrating selective antibacterial activity.[6,7] This research highlights the potential of sulfur nanoparticles synthesized through green methods as effective antimicrobial agents, contributing to the ongoing search for sustainable nanomaterials in the fight against antibiotic-resistant pathogens.

II. EXPERIMENTAL SECTION:

1. **Green Synthesis of Sulfur Nanoparticles:** Waste orange peels were collected from a local fruit juice center in Chandur Bazar, thoroughly washed, and finely ground to enhance extraction. The peels were boiled in water, and the resulting solution was filtered to obtain the extract. Sulfur nanoparticles (SNPs) were synthesized by mixing the extract with sodium thiosulfate as a sulfur precursor. The mixture was heated for 2 hours to facilitate nanoparticle formation, driven by the bioactive compounds in the extract.
2. **Characterization of Synthesized SNPs:** The SNPs were characterized using Fourier Transform Infrared Spectroscopy (FTIR) to identify functional groups and biomolecules responsible for nanoparticle stabilization. X-ray Diffraction (XRD) was performed to assess crystal structure, phase purity, and crystallite size.
3. **Antimicrobial Evaluation:** The antibacterial activity of the SNPs was tested against *Staphylococcus aureus*, *Enterococcus faecium*, *Klebsiella pneumoniae*, and *Escherichia coli* using the Kirby-Bauer disk diffusion method.

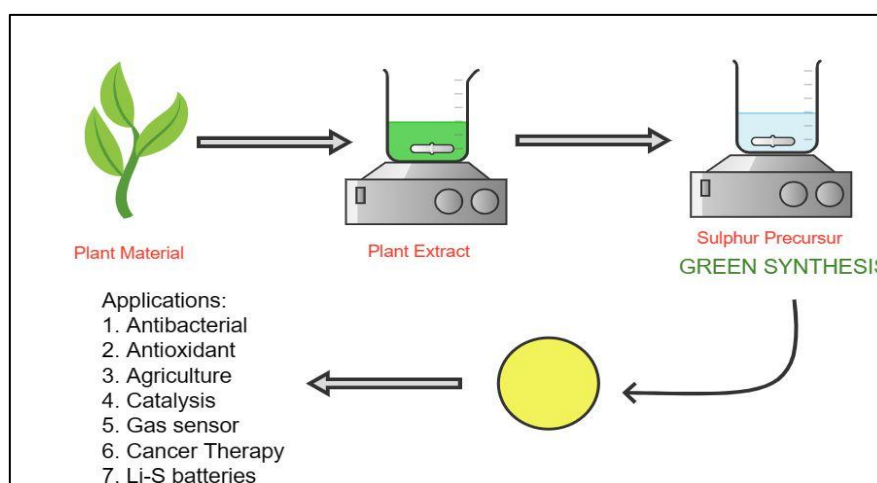


Fig. Green Synthesis of Sulphur nanoparticles

III.RESULT AND DISCUSSION

1. Fourier Transform Infrared spectroscopy (FTIR)

Orange peel contains soluble sugars like glucose and fructose, and insoluble polysaccharides such as cellulose. FTIR analysis of dried orange peel shows O-H and N-H stretching at 3400 cm^{-1} , ester carboxyl groups at 1742 cm^{-1} , and CO stretching at 1098 and 1023 cm^{-1} . Sulfur nanoparticles (SNPs) synthesized using orange peel extract exhibit FTIR bands at 3383.29 cm^{-1} (O-H, N-H) and 1629.92 cm^{-1} (carboxyl). CO stretching appears at 1138.05 and 1011.71 cm^{-1} , while S-S stretching ranges from 675.11 to 417.61 cm^{-1} . The extract stabilizes SNPs by binding through C=O, N-H, and O-H linkages, preventing agglomeration.

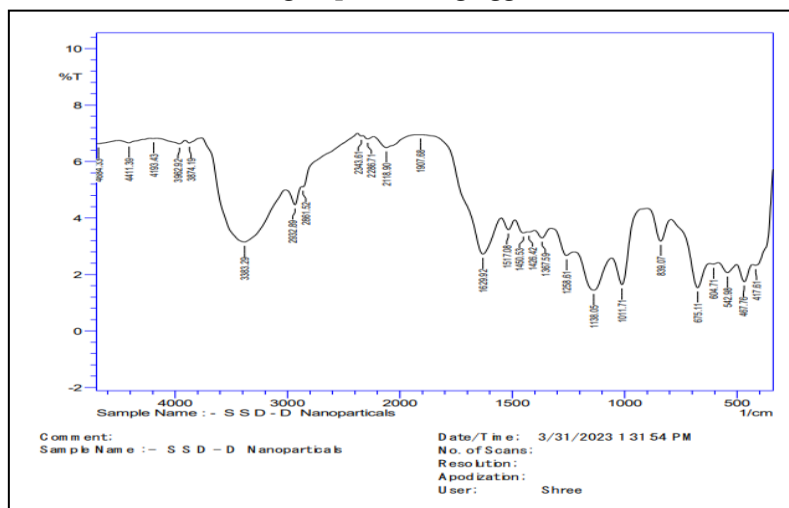


FIG:FTIR spectra of nano Sulphur particles synthesized by using orange peel extract

2. XRD Spectra:

XRD is a key technique for characterizing nanoparticles, providing details on crystalline structure, phase, lattice parameters, and grain size.

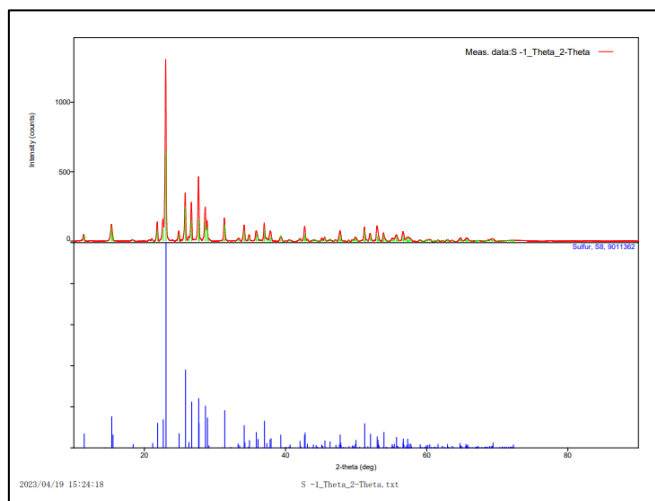


Fig: X-ray Diffraction spectra of SNPs synthesized by using orange peels extract

Grain size is calculated using the Scherrer equation from the broadening of the most intense XRD peak. Nanoparticles are analyzed in powder form, and composition is determined by matching peaks to ICDD reference patterns. For sulfur nanoparticles, 2θ peaks at 23.07° , 25.83° , and 27.70° correspond to sulfur crystal planes (222, 311, 206) in the monoclinic phase. Scherrer's equation estimates sulfur nanoparticle size at approximately 0.13 nm .

3. Field emission scanning electron microscopy (FESEM) analysis of SNPs

FESEM analysis of sulfur nanoparticles shows spherical morphology, with sizes between 30-45 nm. Sonication ensured homogenization, and SEM images confirm that phytochemicals from orange peel extract prevented aggregation by acting as surfactants or capping agents. These phytochemicals confined nanoparticles within water droplets, limiting growth and stabilizing particles through micelle formation.

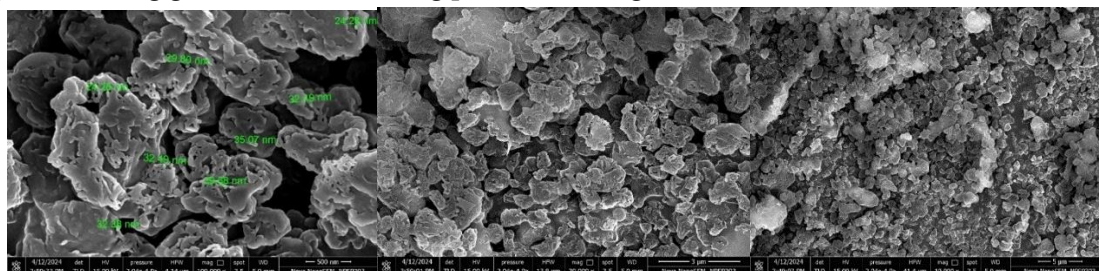
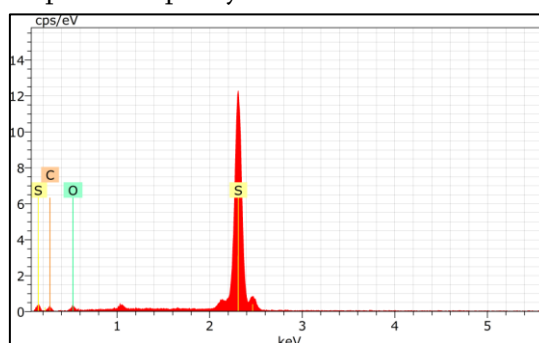


Fig. FESEM micrograph of SNP's synthesized by using orange peels.

4. Energy dispersive X ray analysis (EDAX).

EDAX analysis confirmed the purity of sulfur nanoparticles, showing no impurities. The spectrum revealed sulfur as the main component, with traces of carbon and oxygen from capping phytochemicals. Sulfur's weight percentage was 72.65%, and its atomic percentage was 51.50%. Mapping data indicated high sulfur content in spherical nanoclusters, verifying the product's purity.



El	AN	Series	unn.C[wt.%]	norm.C[wt.%]	Atom.C[at.%]	Error (1 Sigma)[wt.%]
S	16	K-series	52.51	72.65	51.50	1.90
C	6	K-series	14.76	20.42	38.65	3.90
O	8	K-series	5.01	6.93	9.84	1.27
Total:			72.28	100.00	100.00	

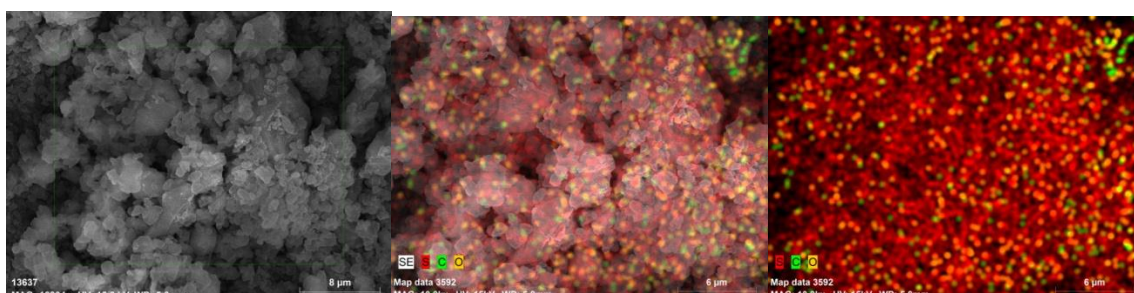


Fig. Map data of SNP's cluster

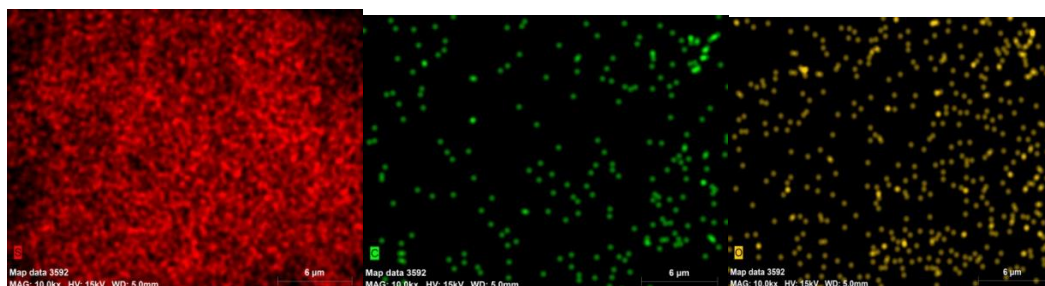


Fig. Mapdata of Sulphur, Carbon and Oxygen elements

5. Antimicrobial Studies of SNPs:-

The antibacterial efficiency of high sulfur content nanoparticles was evaluated against *Staphylococcus aureus*, *Enterococcus faecium*, *Klebsiella pneumoniae*, and *Escherichia coli* using the Kirby-Bauer disk diffusion method.

Organism sample	S.aureus	E faecium	K. pneumoniae	E.coli
SN2	16	23	-	-
Control	11	26	11	18

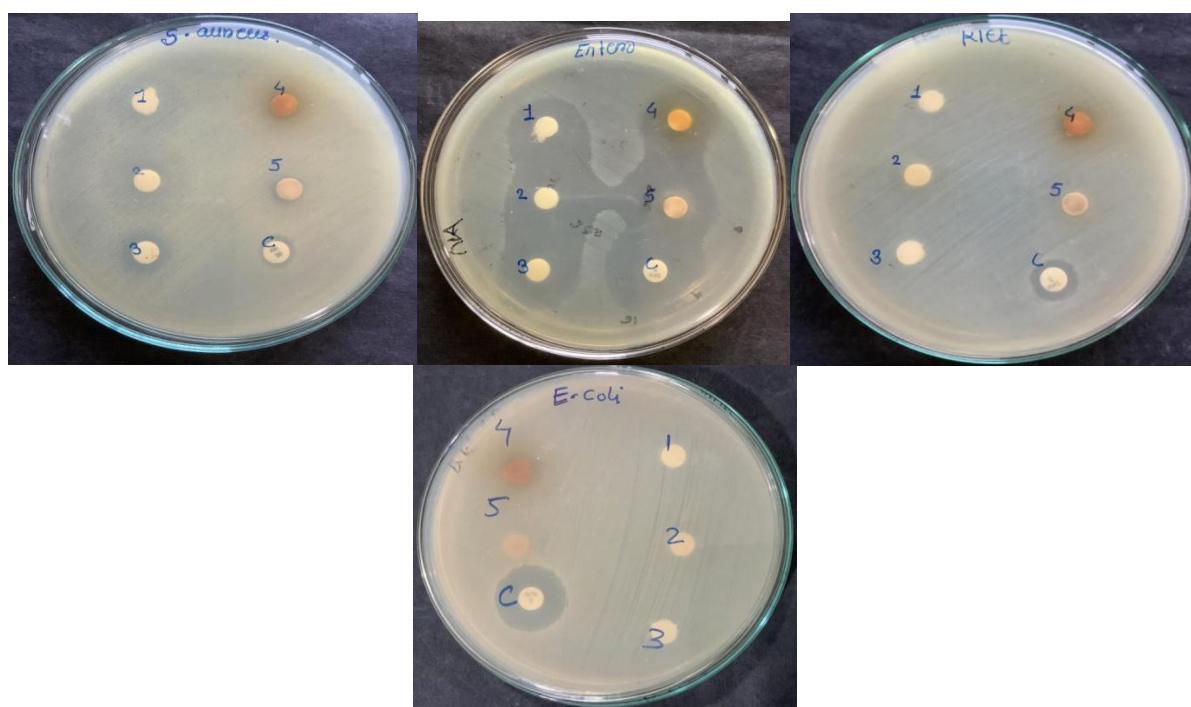


Fig: Evaluation of antibacterial study revealed that synthesized Sulphur nanoparticles exhibited better bactericidal efficacy against common S.Aureus and E.Faecium which is shown in clear zone of inhibition in above images, while found inactive for E.Coli and K.Pneumonia

Overnight bacterial cultures prepared in LB broth were streaked onto LB agar plates. Blank antimicrobial susceptibility testing disks were soaked with 50 µL of nanoparticles, while control disks were soaked with 50 µL of water. Amikacin served as the control for *S. aureus*, and sparflaxacin was used for *E. coli* and *K. pneumoniae*. The disks were placed on the bacterial lawns, and the plates were incubated for 72 hours at 37°C. The resulting zones of inhibition are shown in the following table and images.

IV. CONCLUSION:

This study presents an ecofriendly and cost-effective method for synthesizing sulfur nanoparticles using orange peel extract and sodium thiosulfate. Phytochemicals in the extract acted as reducing and stabilizing agents, allowing control over particle size. Characterization confirmed the monoclinic structure and spherical morphology of the nanoparticles, with high purity. The sulfur nanoparticles exhibited strong antimicrobial activity against Gram-positive bacteria, highlighting their potential for applications in medicine, agriculture, and electronics. This green synthesis approach offers a sustainable alternative for nanoparticle production.

V. REFERENCES

- [1]. S. K. Ghotekar, S. DevkibaMohansinhji, and T. Pagar, "A Review on Green Synthesis of Sulfur Nanoparticles via Plant Extract, Characterization and its Applications," 2020, doi: 10.33945/SAMI/AJCB.2020.3.5.
- [2]. K. Khairan, Zahraturriaz, and Z. Jalil, "Green synthesis of sulphur nanoparticles using aqueous garlic extract (*Allium sativum*)," *Rasayan Journal of Chemistry*, vol. 12, no. 1, pp. 50–57, Jan. 2019, doi: 10.31788/RJC.2019.1214073.
- [3]. V. J. Kouzegaran and K. Farhadi, "Green synthesis of sulphur nanoparticles assisted by a herbal surfactant in aqueous solutions," *Micro Nano Lett*, vol. 12, no. 5, pp. 329–334, May 2017, doi: 10.1049/mnl.2016.0567.
- [4]. H. Baloch et al., "Synthesis and Characterization of Sulfur Nanoparticles of Citrus limon Extract Embedded in Nanohydrogel Formulation: In Vitro and In Vivo Studies," *Gels*, vol. 9, no. 4, Apr. 2023, doi: 10.3390/gels9040284.
- [5]. M. Suleiman, A. Al Ali, A. Hussein, B. Hammouti, T. B. Hadda, and I. Warad, "Sulfur Nanoparticles: Synthesis, Characterizations and their Applications," *J. Mater. Environ. Sci*, vol. 5, no. 6, pp. 1029–1033, 2013.
- [6]. R. A. Dop, D. R. Neill, and T. Hasell, "Sulfur-Polymer Nanoparticles: Preparation and Antibacterial Activity," *ACS Appl Mater Interfaces*, vol. 15, no. 17, pp. 20822–20832, May 2023, doi: 10.1021/acsami.3c03826.
- [7]. P. Paralikar and M. Rai, "Bio-inspired synthesis of sulphur nanoparticles using leaf extract of four medicinal plants with special reference to their antibacterial activity," *IET Nanobiotechnol*, vol. 12, no. 1, pp. 25–31, Feb. 2018, doi: 10.1049/iet-nbt.2017.0079.
- [8]. N. M. Hashem, A. E. D. M. S. Hosny, A. A. Abdelrahman, and S. Zakeer, "Antimicrobial activities encountered by sulfur nanoparticles combating *Staphylococcal* species harboring *scmecA* recovered from *acne vulgaris*," *AIMS Microbiol*, vol. 7, no. 4, pp. 481–498, 2021, doi: 10.3934/microbiol.2021029.
- [9]. S. Najafi, S. M. Razavi, M. Khoshkam, and A. Asadi, "Effects of green synthesis of sulfur nanoparticles from *Cinnamomum zeylanicum* barks on physiological and biochemical factors of Lettuce (*Lactuca sativa*)," *Physiology and Molecular Biology of Plants*, vol. 26, no. 5, pp. 1055–1066, May 2020, doi: 10.1007/s12298-020-00793-3.
- [10]. M. Suleiman, A. Al Ali, A. Hussein, B. Hammouti, T. B. Hadda, and I. Warad, "Sulfur Nanoparticles: Synthesis, Characterizations and their Applications," *J. Mater. Environ. Sci*, vol. 5, no. 6, pp. 1029–1033, 2013.

Extraction and Isolation of Vanillic Acid from Catharanthus Roseus Plant and Synthesis of Their Analogues

S.S. Padhen*, S.P. Gahukar

Department of Chemistry, Rajarshree Shahu Science College Chandur Railway, Dist-Amravati, 444 904, Maharashtra, India

ARTICLE INFO

Article History:

Accepted : 01 Jan 2025

Published : 10 Jan 2025

Publication Issue :

Volume 12, Issue 7

January-February-2025

Page Number :

389-392

ABSTRACT

A biological activities like Antimicrobial, antioxidant, anti-inflammatory, antithrombogenic and anticancer properties were demonstrated by vanillic acid. Further-more, it raises sperm viability, lowers liver and serum cholesterol, and all of these benefits are beneficial for coronary heart disease. Aside from this, it shows a lot of commercial promise in the cosmetic, food, and health sectors. vanillic acid is also beneficial because it is absorbed and metabolized by the human body. So, on the basis of above features we strategized to extract and isolation of vanillic acid from Catharanthus Roseus Plant and synthesis of their analogues like ester and amide. Which were characterized by ¹H NMR and GCMS.

Keywords: Catharanthus Roseus, Vanillic Acid, Sperm Viability, Biological Activities etc.

I. INTRODUCTION

A weedy annual grass that grows in grasslands, agricultural land, and disturbed areas is called *Catharanthus Roseus*. Despite having its origins in South East Asia and the Indian Subcontinent, it has spread widely throughout the region, with reports of sightings of it as a native species coming from Bhutan, India, Nepal and Sri Lanka [1]. It spreads unintentionally through contaminating vehicles, machinery, straw packaging, pasture seed, and so on. Once established, it reduces native biodiversity and alters fire patterns by creating thickets that are too dense for seedlings to grow [2]. So, from the above features of this promising chemical having wide range of utilization and *Catharanthus Roseus* contain probable amount of biological active components, vanillic acid is one of them [3].

vanillic acid, also known as benzoic acid phenolic derivative. It is a brown, crystalline material that dissolves more easily in alcohols and acetone, two polar organic solvents, than it does in chloroform or water. vanillic acid primary use is as the precursor to its esters, or parabens, which are used as preservatives in a variety of cosmetics and ophthalmic solutions [4-5].

The coconuts fruits are one of the natural sources of hydroxybenzoic acid. It is one of the main catechin metabolites that consumers of green tea infusions encounter [6]. Other foods that contain it include carob, wine, vanilla, *Macrotyloma uniflorum* (horse gram) and *Phyllanthus acidus* (*Otaheite gooseberry*) [7]. The açai oil produced by the Euterpe oleracea palm has a high vanillic acid concentration (892 ± 52 mg/kg). It is also present in murky olive oil and the edible *Russulavirescens*, which is also referred to as green-cracking russula [8].

In addition to its bioactivity toward anti-microbial, anti-inflammatory, anti-oxidant, anti-cancer, anti-diabetic, anti-allergic, anti-atherogenic and anti-thrombotic properties, medications derived from vanillic acid include northocaine, ormeloxifene, ifuroxazide, andproxymetacaine [9-10].

II. EXPERIMENTAL

Plants' outer layer, or epidermis, was ground into a fine powder (5 kg), and it was extracted for 48 hours in a Soxhlet extractor using 1 lit. of methanol. After the extract was dried at a Rotavapour under low pressure, 50 g of gelatinous mass was obtained [11]. This mass was then suspended in 500 ml of distilled water and extracted using 500 ml of hexane and 500 ml of ethyl acetate in a separatory funnel. The solvent was evaporated in a rotavapour at a lower pressure to yield extracts of ethylacetate (20 ml) and hexane (20 ml) [12].

A Sephadex LH-20 column was used for chromatography of the 20 ml ethyl acetate extract, which was eluted with methanol. After TLC monitoring for the presence of vanillic acid (R_f 0.45), five major fractions were collected overall in solvent systems containing toluene, ethylacetate, and formic acid (10:10:1). Using a toluene-ethylacetate-formic acid (10:10:1) solvent system, preparative thin layer chromatography was used to further purify the fraction F-4 (0.5 mg) that contained vanillic acid. On a homemade preparative thin layer chromatographic plate (Silicagel GF254, 20 x 20 cm, 1 mm thickness), 25 mg of sample F-4 was loaded. Scratched off was the band corresponding to vanillic acid. Methanol was used to wash the silica gel, and the solvent was then evaporated to produce 2.5 gm of brownvanillic acidcrystals. Finally, recrystallization allowed for its purification [13-14].

III. RESULT AND DISCUSSION

Synthesis of analogues

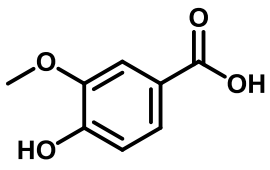
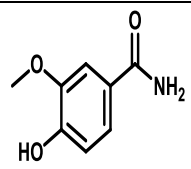
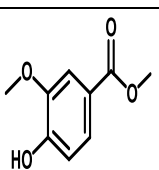
Amide analogue preparation:

In a dry porcelain dish, vanillic acid was reacted with PC1s (1:5) solid, and it was then ground in a fume hood using a Morton pestle until it liquefied. Crude acid chloride was the liquid that was thus produced. Conc. NH_4OH was then used to treat acid chloride. There appeared to be a strong response. After cooling, the product was filtered and given a water wash. This product underwent additional recrystallization using aqueous methanol, yielding the compound 4-hydroxybenzamide (Yield 81%, M.P. 187°C).

Ester analogue preparation:

For six to eight hours, Vanillic acid was refluxed with methanol (1:1) in the presence of H_2SO_4 . The resulting mixture. the product methyl-4-hydroxy-3-methoxybenzoate (B. P. $312-314^\circ\text{C}$, Yield: 84 %) was obtained by distilling the water-washed product [15].

TABLE No.1

Sr. No	Structure of Compound	Confirmational analysis by ^1H NMR and GCMS
1	 <p>Vanillic acid</p>	^1H NMR (δ ppm): carboxylic -OH proton at 12.74 ppm, 7.25 at phenolic -OH and Ar-H protons at 6.90-7.00 ppm GCMS (m/z): 168.15 cal., Found 168.10
2	 <p>4-hydroxy-3-methoxybenzamide</p>	^1H NMR (δ ppm): amino -NH ₂ proton at 8.48 ppm, 7.6 ppm at phenolic-OH and Ar-H protons at 6.86-7.12 ppm GCMS (m/z): 167.16 cal., Found 167.11
3	 <p>methyl 4-hydroxy-3-methoxybenzoate</p>	^1H NMR (δ ppm): phenolic -OH proton at 7.6 ppm, Ar-H protons at 6.80-7.55 ppm and CH ₃ protons at 3.85 ppm GCMS (m/z): 182.17 cal., Found 182.12

IV. CONCLUSION

Isolation and extraction vanillic acid from *Catharanthus Roseus* Plant and synthesis of their analogues like ester and amide having broad spectrum in various fields. In addition, there are some challenges to overcome. These challenges include efficiency for good yields in synthesis of analogues, for this reason, we believe there is a need for the synthesis of medicinally active compounds, studying dissimilar properties and seeking new applications of novel analogues especially in synthesis field would be vast applications in various areas.

V. ACKNOWLEDGEMENT

I sincerely appreciate the help of Dr. D. T. Tayade, Professor at GVISH College in Amravati.

VI. REFERENCES

- [1]. Barberousse, H., Kamoun, A., Chaabouni, M., Giet, J.M., Roiseux, O., Paquot, M., Deroanne, C., Blecker, C., Journal of the Science of Food and Agriculture., 89, 1634–1641, (2009).
- [2]. Buranov, A.U., Mazza, G., Food Chemistry., 115, 1542–1548, (2009).
- [3]. Gunenc, A., Nezhad, M., Farah, I., Hashem, A., Hosseinian, F., Journal of Functional Foods., 12, 109–119, (2015).
- [4]. Liu, L., Zhao, M., Liu, X., Zhong, K., Tong, L., Zhou, X., Zhou, S., Journal of the Science of Food and Agriculture., 96, 3484–3491, (2016).

- [5]. Ou, S., Luo, Y., Xue, F., Huang, C., Zhang, N., Liu, Z., *Journal of Food Engineering.*, 78, 1298–1304, (2007).
- [6]. Gupta, V., Kumar, R., Kumar, R., Mahajan, R., Mehta, M., Satija, S., Vyas, M., Khurana, N., Sharma, N., *Plant Arch.*, 19, 1732-1736, (2019).
- [7]. Habibyar, A.F., Sharma, N., Khurana, N., *Eur. J. Pharmacol.*, 65, 789, 385- 394, (2016).
- [8]. Huang, S.M., Chuang, H.C., Wu, C.H., Yen, G.C., *Mol. Nutr. Food Res.*, 52, 940–949, (2008).
- [9]. Berlitz, S., Villa, D., Inácio, L.A., Davies, S., Zatta, K.C., Guterres, S.S., *Drug Dev. Ind. Pharm.*, 45, 642–650, (2019).
- [10]. Jaryal, N., Kaur, H., *J. Biomater. Sci. Polym.*, 28, 1847–1858, (2017).
- [11]. Sharma, N., Khurana, N., Muthuraman, A., *Europ J Pharmacol.*, 815, 312- 323, (2017).
- [12]. Siddiqui, S., Kamal, A., Khan, F., Jamali, K.S., Saify, Z.S., *Mol. Biol. Rep.*, 46, 997-1011, (2019).
- [13]. Tang, P.L., Hassan, O., Jahim, J., Mustapha, W., Maskat, M.Y., *Int. J. Polym. Sci.*, 45, 56-68, (2014).
- [14]. Tomić, I., Juret, M., Jug, M., Pep, I., Cetina, B., Filipov, J., *Int. J. Pharm.*, 563, 249–258, (2019).
- [15]. Wingo, T.S., *Neurol.*, 73, 501–502, (2016).

Harnessing Photophysical Properties of Schiff Base Cyclometallated Complexes for Advanced Applications: A Review

S.R. Khandekar¹, S.R. Kelode², R.S. Palaspagar³

¹Department of Chemistry, Indira Mahavidyalaya, Kalamb, Dist. Yavatmal- 445401, Maharashtra, India

²Department of Chemistry, Arts Commerce and Science College, Maregaon, Dist. Yavatmal- 445303, Maharashtra, India

³Department Of Physics, Shivramji Moghe Mahavidyalaya, (Kelapur) Pkd, Dist- Yavatmal- 445001, Maharashtra, India

ARTICLE INFO

Article History:

Accepted : 01 Jan 2025

Published : 10 Jan 2025

Publication Issue :

Volume 12, Issue 7

January-February-2025

Page Number :

393-398

ABSTRACT

Schiff base cyclometallated complexes have emerged as versatile materials in the realm of photophysical studies, owing to their unique structural attributes and tunable electronic properties. This review highlights the recent advancements in the synthesis, characterization, and application of Schiff base cyclometallated complexes, focusing on their photophysical behaviors. Special attention is given to their applications in fields such as optoelectronics, luminescent sensors, photodynamic therapy, and as catalysts in light-driven reactions. The role of ligand design, metal center variation, and environmental factors in modulating their photophysical properties is critically analyzed. The review also explores the underlying mechanisms governing their light absorption, emission, and energy transfer processes. By collating and synthesizing existing knowledge, this work provides insights into the potential of these complexes as functional materials for advanced technological applications and identifies challenges and opportunities for future research.

Keywords: Photophysical, Schiff base, Cyclometallated complexes, Metal complexes

I. INTRODUCTION

Schiff base cyclometallated complexes have garnered significant attention in recent years due to their versatile structures, tunable photophysical properties, and extensive potential for advanced applications. These complexes, derived from the condensation of primary amines with carbonyl compounds, form stable ligands

that facilitate the coordination of metal centers. The incorporation of cyclometallation further enhances their stability and imparts unique photophysical characteristics, including luminescence, photoinduced electron transfer, and nonlinear optical properties.

The photophysical properties of these complexes can be precisely modulated by altering the electronic and steric nature of the Schiff base ligands or by varying the coordinated metal ions. This flexibility enables the tailoring of complexes for specific functionalities, making them valuable in diverse fields such as light-emitting devices, sensors, photodynamic therapy, and catalysis. Easily accessible Schiff bases with two different or identical redox-active groups can be considered as ligands. These compounds are used as an easily tuned multichromic system in the design of complex compounds containing non-transitional elements which have interesting electrical and photophysical properties, as well as biological activity.

Schiff-base ligands have garnered significant interest over the past decade due to their versatile applications in synthesis, catalysis, and material chemistry. Research has focused on developing new Schiff-base complexes with transition and main group metal ions to expand their utility in catalysis and material science. Salen ligands, in particular, have been utilized in redox chemistry, notably for selective nucleic acid recognition and modification. For example, guanine adducts with nickel-salen complexes inhibit polynucleotide elongation and enable sensitive detection methods.

Despite extensive studies on Schiff-base complexes, their photophysical properties have not been systematically reviewed, though they exhibit intriguing characteristics. Recently, Schiff-base aluminum complexes have been proposed as luminescent biolabels due to their high fluorescence intensity, with applications in medical diagnostics, cell biology, and environmental sciences. Photoluminescence spectroscopy, a sensitive and versatile tool, could also be instrumental in monitoring catalytic processes involving Schiff-base complexes by tracking changes in luminescence properties.

This review aims to provide an in-depth exploration of Schiff base cyclometallated complexes, focusing on their photophysical properties and the underlying mechanisms that drive their advanced applications. By highlighting recent advancements and emerging trends, this article seeks to establish a comprehensive understanding of their potential in shaping next-generation technologies.

II. PHOTOPHYSICAL PROPERTIES AND ITS APPLICATIONS

After synthesizing Pt (II) complexes with tetradentate Schiff base ligands Pt-1 to Pt-5, Senqiang Zhu et. al. comprehensively investigated photophysical studies using density functional theory and steady-state and transient spectroscopies. In the UV-vis range, all complexes show metal-to-ligand/intraligand charge transfer transitions as well as 1π , π^* transitions. At room temperature, these compounds exhibit emissive properties in solution ($\lambda_{em} = 400\text{--}800\text{ nm}$, $\Phi_{em} = 0.008\text{--}0.196$). Triplet transient absorption (TA) showed that all complexes, except Pt-3, show broad and significant triplet excited-state absorption between 400 and 750 nm. Furthermore, all platinum complexes exhibit strong reverse saturable absorption (RSA) at 532 nm ns laser pulses, as shown by nonlinear transmission experiments. Pt-5 exhibits the best nonlinear absorption performance among them, making it a promising candidate for optical power limitation (OPL) materials.

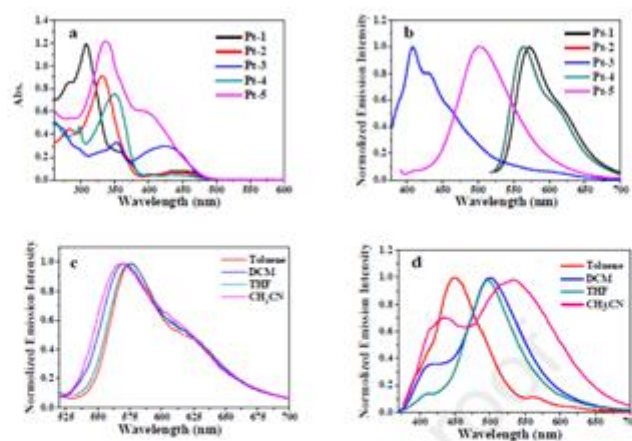


Fig.1 UV-vis absorption spectra (a) and normalized emission spectra (b) of complexes **Pt-1–Pt-5** ($c = 10^{-5}$ mol/L) in CH_2Cl_2 . Normalized emission spectra of **Pt-1** (c) and **Pt-5** (d) in different solvents.

AdewaleOlufunshoAdeloye investigated the photophysical and optoelectronic characteristics of a few mono- and binuclear Ir (III) cyclometalated complexes. These characteristics were significantly impacted by the presence of an anionic, cationic, or neutral ligand in addition to other elements like hydrophobicity, the extension of the π -conjugation bond, and the addition of substituent groups that donate or withdraw electrons. The bulkiness of cyclometalating or auxiliary ligands, the locations of substituents, and heteroeroleptic ligands have all improved the photophysical characteristics. Compared to both mono- and bidentate complex types, terdentateIr (III) cyclometalated complexes exhibit superior photoluminescent capabilities since the latter have a lower capacity for photosensing, which frequently results from ligand dissociation during photoexcitation procedures.

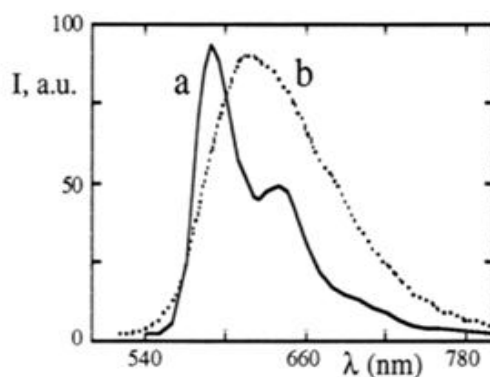


Fig 2. Emission spectra of Iridium complexes

The use of various alkoxy substituted N-benzoyl thiourea derivatives as auxilliary ligands in the cyclopalladatedschiff base system has been demonstrated by Monica Ilis et al. to produce yellow-orange emissive liquid crystalline solids containing palladium (II). When the solid-state samples were exposed to radiation in the 330–380 nm range, all palladium (II) complexes, except for 4a and 4b, exhibit two emission maxima at around 580 and 650 nm, respectively, with a shoulder at about 710 nm. When the samples were heated to an isotropic liquid, their emission was rapidly extinguished.

Schiff base ligand N, N-bis(salicylidene)-(3,3'-diaminobenzidine) and its zinc complex were synthesized by N. K. Gondia et. al. It appears that N-azomethine and the subsequent deprotonation of the OH group are responsible for the coordination of the Schiff base ligand with the zinc metal ion. To gain an understanding of the

transition between molecular orbitals and quantum yield, optical characteristics such as fluorescence and absorption were examined.

Circularly polarized phosphorescence (CPP) properties of axially chiral cyclometalated binuclear platinum (II) complexes were described by Masahiro Ikeshita et. al. A series of optically pure binuclear platinum (II) complexes were synthesized in five steps from commercially available (R)- or (S)-1,1'-bi-2-naphthol (BINOL) as starting materials. The complexes were found to exhibit red- to near-infrared photoluminescence in solution and in the solid state. In addition to that the enantiopure samples of complexes diluted in DMSO showed red CPP with relatively high luminescence dissymmetry factor (glum) values. Density functional theory (DFT) calculations were conducted to examine their three-dimensional molecular conformations and photophysical properties.

To create two anthryl platinum (II) N, N'-bis(3,5-di-tert-butylsalicylidene)-1,2-benzenediamine Schiff base complexes, the anthryl was joined to the platinum (Pt) Schiff base backbone via its 9 position (Pt-9An) or 2 position (Pt-2An). Kepeng Chen et. al. examined that their complexes show unusually small Stokes shifts (0.23 eV), representing a very small energy loss for the photoexcitation/intersystem crossing process, which is beneficial for applications as triplet photosensitizers. In contrast to the native Pt (II) complex, which exhibits a lifespan of 4.0 μ s, the triplet-state equilibrium increases the triplet-state lifetime of the complexes to 103 μ s (Pt-2An) or 163 μ s (Pt-9An). Using perylene as the triplet acceptor, the complexes were utilized for triplet-triplet-annihilation upconversion. Excitation results in a significant anti-Stokes shift (0.75 eV) and an upconversion quantum yield of up to 15%.

Felipe S.M. Canisares et. al. introduces the syntheses of two ligands named as 2-(((3-methyl-1-phenyl-1H-pyrazol-5-yl)imino)methyl)phenol (BS1) and 5-(diethylamino)-2-(((3-methyl-1-phenyl-1H-pyrazol-5-yl)imino)methyl)phenol (BS2) and two new red-emitting iridium complexes, Ag[Ir(ppz)2(BS1)] and Ag[Ir(ppz)2(BS2)]. Both iridium complexes feature emission characterized by a broadband centered with color coordinates of (0.659;0.337) and (0.612;0.380), respectively, both in the red spectral region, with 100 % of color purity.

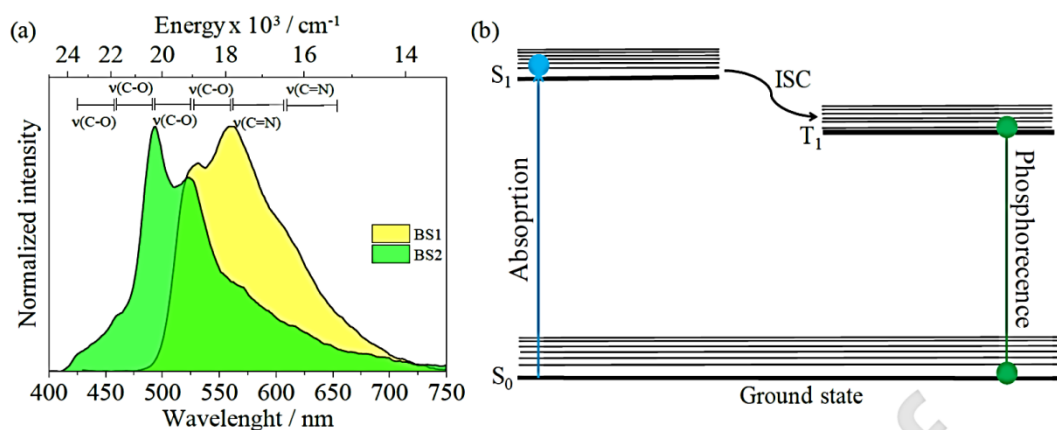


Fig. 3. (a) Emission spectra (298 K) of BS1 (excited at 414 nm), BS2 (excited at 294 nm); (b) Simplified Jablonski diagram exhibiting partial energy level representing the photophysical processes in the legands.

Using the chemistry-on-complex method, Wanhua Wu et al. have created novel Pt (II) Schiff base complexes with pyrene or ethynylatedpyrene subunits. The complexes exhibit both room temperature phosphorescence (550–670 nm) and strong absorption in the visible region ($\epsilon = 1.31 \times 10^4 \text{ M}^{-1} \text{ cm}^{-1}$ at 530 nm). Compared to the model complex ($t = 4.4 \text{ ms}$), the complexes exhibit significantly extended phosphorescence lifetimes ($t = 21.0 \text{ ms}$).

New heteroleptic deep red iridium (III) phosphorescent compounds were created by Meha J. Prajapati et al. using heterocyclic Schiff bases as accessory ligands and cyclometalated ligand (piq). Spectroscopy methods provide a good description of each component. Because of the strong field ligands that dominate the complexes, the photophysical characteristics show outstanding Φ_{PL} 0.44 to 0.52 and short excited-state lifespan τ (0.51-0.55 μ s), which leads to an efficient triplet metal-ligand charge transfer (3MLCT) existing state.

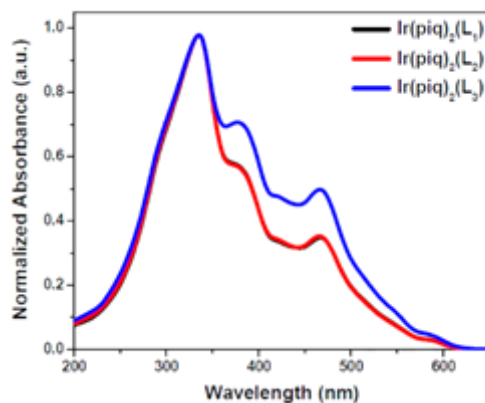


Fig 4. Electronic absorption spectra of the compounds in DCM

III.SUMMARY

Two complementary subjects that are extremely pertinent to the resolution of the global energy crisis are the conversions of light into electricity and electricity into light. For such development, inorganic chemistry is very important. Organometallic compounds and coordination have been extensively studied in these energy-saving (OLED) and energy-generating (solar cell) applications. The effective production, transformation, and use of the two energy forms are made possible by these energy conversion materials. Because of the Schiff base ligands' ease of synthesis, high coordination affinity for a range of metal ions, robust chemical nature, and ease of scaling up for mass manufacturing, metal Schiff base complexes are particularly appealing in the context of practical applications.

In summary, metal Schiff base chemistry can and will play a significant role in solving the world's energy crisis. Numerous researchers have documented the various kinds of metal Schiff base complexes that can serve as molecular building blocks for diverse energy conversion procedures. We anticipate these further advances with great hope.

IV.ACKNOWLEDGMENTS

One of the authors Snehal Khandekar is thankful to the Indira Mahavidyalaya, for providing necessary facility and support to this work.

V. REFERENCES

- [1]. Xue Zhang, YuqiHou, Xiao Xiao, Xi Chen, Mengyu Hu, XinyuGeng, ZhijiaWang,Jianzhang Zhao, Recent development of the transition metal complexes showing strong absorption of visible light and long-lived triplet excited state: From molecular structure design to photophysical properties and applications, Coordination Chemistry Reviews, 417 (2020), 213371.

- [2]. U.V. Chervonova, M.S. Gruzdev, E.M. Zueva, V.E. Vorobeva, A.A. Ksenofontov, A.I. Alexandrov, T.V. Pashkova, A.M. Kolker, Synthesis, EPR study and photophysical properties of a mononuclear Fe(III) Schiff base complex functionalized by 3,6-di-tert-butylcarbazole moieties, *Journal of Molecular Structure*, 1200 (2020), 127090
- [3]. Jyoti Sharma, Pernita Dogra, Nadeem Sharma, Ajay, Applications of coordination compounds having Schiff bases: A review. *AIP Conf. Proc.* (2019), 2142 (1): 060002.
- [4]. Pier Giorgio Cozzi, Luisa Stella Dolci, Andrea Garelli, Marco Montalti, Luca Prodi, Nelsi Zaccheroni, Photophysical properties of Schiff-base metal complexes, *New J. Chem.*, 2003, 27, 692-697.
- [5]. Zhu S, Zhai S, Chen Z, Su H, Zhang C, Liu R, Zhu H, Cyclometalated Pt (II) complexes with tetradentate Schiff base ligands: Synthesis, photophysics, electrochemical studies and optical power limiting performance, *Dyes and Pigments* (2020).
- [6]. Adewale Olufunsho Adeloye, Exploration of the Structural and Photophysical Characteristics of Mono- and Binuclear Ir(III) Cyclometalated Complexes for Optoelectronic Applications, *Materials* 2019, 12, 2734.
- [7]. Monica Ilis, Marin Micutz, Viorel Cîrcu, Luminescent palladium (II) metallomesogens based on cyclometalated Schiff bases and N-benzoyl thiourea derivatives as co-ligands, *Journal of Organometallic Chemistry* 836-837 (2017) 81-89.
- [8]. N.K. Gondia, S.K. Sharma, Spectroscopic characterization and photophysical properties of Schiff base metal complex, *Journal of Molecular Structure* (2018).
- [9]. Masahiro Ikeshita, Itsuki Shimizu, Shinya Watanabe, Tomoki Yamada, Seika Suzuki, Shota Tanaka, Shingo Hattori, Kazuteru Shinozaki, Yoshitane Imai, Takashi Tsuno, Circularly Polarized Phosphorescence Properties of Binuclear Cyclometalated Platinum(II) Complexes Bearing Axially Chiral Schiff-Base Ligands, *Inorg. Chem.* 2024, 63, 50, 23642–23650.
- [10]. Kepeng Chen, Mushraf Hussain, Syed S. Razi, Yuqi Hou, Elif Akhuseyin Yildiz, Jianzhang Zhao, Halime Gul Yaglioglu, Mariangela Di Donato, Anthryl-Appended Platinum (II) Schiff Base Complexes: Exceptionally Small Stokes Shift, Triplet Excited States Equilibrium, and Application in Triplet–Triplet–Annihilation Upconversion, *Inorg. Chem.* 2020, 59, 20, 14731–14745.
- [11]. Canisares FSM, Bispo AG, Pires AM, Lima SAM, Syntheses and characterization of Schiff base ligands and their Ir(III) complexes as coating for phosphor-converted LEDs, *Optik* (2020).
- [12]. Wanhua Wu, Jifu Sun, Shaomin Ji, Wenting Wu, Jianzhang Zhao, Huimin Guo, Tuning the emissive triplet excited states of platinum (II) Schiff base complexes with pyrene, and application for luminescent oxygen sensing and triplet–triplet–annihilation based upconversions, *Dalton Trans.*, 2011, 40, 11550.
- [13]. Highly-efficient solution-processed deep-red organic light-emitting diodes based on heteroleptic Ir(III) complexes with effective heterocyclic Schiff base as ancillary ligand Meha J. Prajapati, Rohit Ashok Kumar Yadav, Sujith Sudheendran Swayamprabha, Deepak Kumar Dubey, Jaydip D. Solanki, Jwo-Huei Jou, Kiran R. Surati, *Organic Electronics* (2020).

Investigation On Inter Ferometric Study of 4-(p-Bromo) Phenylthiocarbamidophenolin Mixed Solvent Media

Mr. S.U.Patil

Department of Chemical Engineering, Government Polytechnic Arvi, Maharashtra, India

ARTICLE INFO

Article History:

Accepted : 01 Jan 2025

Published : 10 Jan 2025

Publication Issue :

Volume 12, Issue 7

January-February-2025

Page Number :

399-401

ABSTRACT

Ultrasound and ultrasonic wave measurements have been used to update numerous advancements and new theories in the last forty years in the fields of pharmaceutical, agricultural, medical, industrial, space research, forensic sciences and biochemical sciences. In 75 % composition ethanol-water mixtures, ultrasonic velocity and density for solutions of 4-(p-bromo)phenylthiocarbamidophenol at 303K and various molar concentrations have recently been studied for the determination of specific acoustic impedance (Z), intermolecular free length (Lf), relative association (RA), adiabatic compressibility (β), and apparent molal compressibility (k). These characteristics, which offer significant and adaptable information about internal structure and molecular association, were investigated in relation to solute-solute and solute-solvent interaction in solvent.

Keywords: 4-(p-Bromo)phenylthiocarbamidophenol, interferometric measurements, acoustic properties, solute-solvent interaction

I. INTRODUCTION

The subfield of acoustics that deals with high-frequency waves is called ultrasonic. The method used to investigate molecular interactions in liquids is ultrasonic. Important insights into internal structure, molecular association, complex formation, internal pressure, and complex stability can be gained from studying molecular interaction in liquids [1]. Molecular interactions in pure liquids [2-4], liquid mixtures [5-6] and electrolyte solutions [7-9] are widely studied using ultrasonic parameters. Aswale *et al.* [10] examined the acoustic characteristics of cumaran-3-ones and α -bromoacetophenones in ethanol and dioxan solvents to compare their intermolecular interactions. Acoustical analysis of a ternary toluene mixture in nitrobenzene and cyclohexane at 308K [11]. Diethyl ether binary liquid mixture with three non-polar solvents (CCl_4 , CS_2 , and C_6H_6) at 303.15K [12]: ultrasonic velocity and density.

Due to its enormous scope in the chemical, physical, mechanical and biological sciences, dynamic studies in ultrasonic research are currently ongoing. In light of these factors, the current study was conducted to determine the ultrasonic velocity and density for solutions of 4-(p-bromo)phenylthiocarbamidophenol (L2) at

various molar concentrations and 303K. In 75 % compositions, ethanol-water mixtures were examined to determine the following parameters: intermolecular free length (L_f), relative association (R_A), specific acoustic impedance (Z), adiabatic compressibility (β), apparent molal compressibility (k), apparent molal volume (v), k , and intermolecular free length (L_f).

II. MATERIALS AND METHODS

All of the chemicals used in this investigation are of AR grade. Analysis was done using a freshly made solution. Using a standard procedure, the solvents were purified. The concentrations of 4-(*p*-bromo)phenylthiocarbamidophenol (L2) 75% ethanol-water mixture were prepared at 0.1M, 0.075M, 0.050M, and 0.025M. Using a well-known procedure, 4-(*p*-bromo)phenylthiocarbamidophenol (L2) was created [13]. By following standard procedure [14] the solvent ethanol was purified. Using a bicapillarypyknometer ($10.1 \text{ \% kg m}^{-3}$), densities were measured. Borosil's pyrometer uses a 0.01M ligand solution in ethanol. The Citizen CY 104 one pan digital balance ($\pm 0.0001 \text{ gm}$) was used for the weighing.

In order to measure density and ultrasonic velocity, a unique thermostatic setup was made. Using an elite thermostatic bath, the water was continuously stirred with an electric stirrer to keep the temperature variation within $\pm 0.1 \text{ }^\circ\text{C}$. The current study used a variable path, single crystal interferometer (Mittal Enterprises, Model MX-3) with a frequency of 1 MHz and an accuracy of $\pm 0.03\%$ to determine the speed of sound waves. The density and ultrasonic velocity of liquids in ethanol solvent at 303 K are measured. The value of Jacobson's constant¹⁵ ($K = 631$) at 303 K is used to calculate the intermolecular free length.

III.RESULTS AND DISCUSSION

Densities and ultrasonic velocities of 4-(*p*-bromo) phenylthiocarbamidophenol (L2) in a 70% ethanol-water mixture were measured for this investigation and are shown in **Table No. 1**.

Table no. 1: Acoustic Parameters at Different Concentration of PTP at 303K

W-E Mix. %	Conc. C (Mole/lit)	Average Ultrasonic Velocity $U_s(\text{m/sec})$	Density $d_s (\text{Kg.m}^{-3})$	$\beta \times 10^{-10} (\text{pa}^{-1})$	$\phi_v (\text{m}^3\text{mol}^{-1})$	$\phi_k \times 10^{-10}$	$L_f (A_0)$	R_A	$Z * 10^4 (\text{Kgm}^{-2} \text{sec}^{-1})$
75	0.1	1489.588	1030.34	4.3236	0.2846	-2.3712	0.0164	1.005	150.319
	0.075	1322.592	1028.34	5.4855	0.3228	11.776	0.019	1.041	132.492
	0.050	1217.368	1021.34	6.4901	0.3257	33.578	0.0199	1.064	121.018
	0.025	1072.419	1016.24	8.3734	0.3764	89.431	0.0219	1.103	105.584

IV.CONCLUSION

The results of the Acoustic Parameters of L2 at 0.1M, 0.075M, 0.050M, and 0.025M and 303K in a 75% ethanol-water mixture are shown in Table 1. from table-1 it was concluded that Ultrasonic Velocity: (U_s), Density: (d_s)

decreases while Adiabatic compressibility: (β_s), Apparent molar volume: (ϕ_v), Apparent molar compressibility: (ϕ_k), Intermolecular free length: (Lf), Relative association: (RA) increases and Specific acoustic impedance: (Z) decreases along with decreasing concentration of L2 at 303 K. U_s , d_s , β_s , ϕ_v , ϕ_k , Lf, RA, z , and other acoustic properties were identified through ultrasonic interferometric analysis. These properties explain how these interactions take place and are in charge of breaking and creating the structure in the solution.

V. REFERENCES

- [1]. C. N. Deshmukh, A. G. Doshi, Pratibha Agrawal and C. M. Deshmukh, *Ultra Science* Vol.(3),535,(2002).
- [2]. Raji-Idowu, F ,*Nigerian Journal of chemistry*. (2023).
- [3]. N.A.Kalambe, P.B.Raghuwanshi and A.K.Maldhure, *Ind. J. Chem. Sci.*,12(2),730,(2014).
- [4]. P.B.Raghuwanshi and A.D.Deshmukh, *Ind. J. Chem. Sci.*,11(1),141,(2013).
- [5]. S.K.Upadhyay, *Ind. J. Chem.*,39(5),537,(2000).
- [6]. Malghani, N., Mahesar, S., Baig, J., Talpur, F., Sherazi, S. T. H., &Junaid, M. *Journal of the Turkish Chemical Society Section A: Chemistry*, 9(4), 985-998. (2022).
- [7]. Ruwali, P., Pandey, N., Jindal, K., & Singh, R. V. *South African Journal of Botany*, 151, 423-431. (2022).
- [8]. Rita Mehara, *Ind. J. Chem.*,44A(2),1834,(2005).
- [9]. P.R.Malasne and A.S.Asvar, *Ind. J. Chem.*,44A(12),2490,(2005).
- [10]. S.S.Asware, P.B.Raghuwanshi and D.T.Tayade, *Ind. J. Chem. Soc.*,84,159,(2007).
- [11]. A.A.Mistry, V.D.Bhandarkar and O.P.Chimankar, *J. Chem. Pharm. Res.*,4(1),170,(2012).
- [12]. Patidar H., Satisch, M., &Warthe, M. *Diversity*, 14(1), 7. (2022).
- [13]. Bakhtiar, Z., Hasandokht, M. R., Naghavi, M. R., &Mirjalili, M. H. *Journal of Medicinal Plants*, 21(82), 1-12. (2023).

The Role of Optical Properties in Enhancing Electromagnetic Interference (EMI) Shielding

S.V. Tayade, A.P. Bangar, S.A. Waghuley

Department of Physics, Sant Gadge Baba Amravati University, Amravati, Maharashtra, India

ARTICLE INFO

Article History:

Accepted : 01 Jan 2025

Published : 10 Jan 2025

Publication Issue :

Volume 12, Issue 7

January-February-2025

Page Number :

402-407

ABSTRACT

The growing sector in use of electronic devices necessitates the employment of effective electromagnetic interference (EMI) shielding materials to reduce signal disturbance. The rapid growing sector of use of electronic devices necessitates the employment of effective electromagnetic interference shielding materials to reduce the disturbed signals. Optical characteristics such as extinction coefficient, optical band gap, refractive index decides the performance of the materials for such applications. This paper mainly focuses on the ways in which these optical factors control the absorption, reflection, and transmission of electromagnetic waves which is very important in the EMI shielding application. Also this paper highlighted that Polyaniline (PANI) and Copper oxide (CuO) are the materials which have unique optical properties and potential synergy. To examine the optical properties is very important for their application in optoelectronic devices, sensors and electromagnetic interference shielding. These optical properties show that how well it protects against the disturbed interference of waves. The main objective of this work is to determine the optical characterization of polyaniline (PANI) and Copper oxide (CuO) which are very useful for the shielding purpose. Polyaniline (PANI) and Copper Oxide (CuO) nanocomposite were prepared by ex-situ approach with varying weight percentage of copper oxide with increment of 5wt%. The optical properties in the 200nm to 600 nm wavelength range were investigated using UV-visible spectroscopy, which revealed absorption bands between 200 and 250 nm and 300 and 380 nm in wavelength. Using Tauc's figure the optical band gap was determined to be between 3.3 and 3.4. Additionally by analysing the extinction coefficient that is the light attenuation behaviour of composites were evaluated, which was obtained from absorption spectra. PANI/CuO nanocomposite shows attractive optical characteristics, which

make them suitable options for use in electromagnetic interference (EMI) shielding, photo detectors, optical sensors, and Photovoltaic. Their potential for sophisticated optoelectronic applications is clarified by this work.

Keywords: PANI/CuO nanocomposite, optical properties, UV-Vis spectroscopy, optical band gap, extinction coefficient.

I. INTRODUCTION

Electromagnetic interference (EMI), a significant issue with recent electronics, has increased due to rapid increase in number of high-frequency devices and wireless communication. Without abandonment other needed qualities, effective EMI shielding materials must decrease electromagnetic (EM) radiation by reflection, absorption, or both. The band gap and extinction coefficient (k) are very important to suit the way shielding materials interact with electromagnetic waves throughout the frequency spectrum. With an prominence given to the materials polyaniline (PANI) and copper oxide (CuO), this study searches how these characteristics can modify EMI shielding.

Optical properties of material for electromagnetic interference (EMI) shielding: Particularly in applications that call for both optical functionality and electromagnetic shielding are very influenced by the capabilities of material as an electromagnetic interference shielding material. Materials with optical transparency in the visible spectrum such as transparent conductive films are crucial for applications including touch screens, displays, and windows. The material may need to prevent electromagnetic interference (EMI) while giving consent to some non-visible wavelengths to flow through for specialized applications like solar panels or sensors. High reflectivity at particular wavelengths can improve the efficiency of shielding by reflecting incoming electromagnetic waves. Instead of reflecting electromagnetic waves, some materials are made to absorb them. These substances frequently depend on optical absorption characteristics that are designed to coincide with the desired frequency. This is necessary for cutting down on any secondary emissions that can result from reflection.

1 Optical Band Gap: The optical band gap determined the range of photon energy that a material may absorb. Visible range optical transparency offer by the materials having wide band gaps. By adjusting the band gaps the Materials can be optimised for frequency-specific shielding applications. The optical band gap affects a material's ability to transmit, reflects, or absorbs electromagnetic waves in the context of electromagnetic interference (EMI) shielding. The range of photon energy that a material may absorb is determined by its band gap. It is possible to construct materials with an appropriate band gap to absorb electromagnetic waves at particular frequencies and dissipate their energy or convert them into heat. This is particularly very important in order to reduce secondary interference. Because it is simple for electrons to go from the valence band to the conduction band by stimulation, materials with narrow band gaps such as conducting polymers like doped polyaniline have higher electrical conductivity.

2 Extinction Coefficient: Extinction coefficient (k) measures the The attenuation of electromagnetic waves during their propagation by way of a medium. High- k materials transform electromagnetic energy into heat, improving absorption-dominant shielding. A balanced- k value in the visible range is necessary for transparent

EMI shields in order to preserve transparency while either reflecting or absorbing high-frequency radiation. One important optical metric that measures the quantity that how strongly a material absorbs electromagnetic waves at a certain wavelength is the extinction coefficient (k). It is significant to the creation and operation of materials for shielding against electromagnetic interference (EMI), especially for absorption-dominated shielding systems. The degree of attenuation, or decrease in wave amplitude, that takes place when electromagnetic waves pass through a material is indicated by the extinction coefficient. Stronger absorption is related with a higher extinction coefficient, which is an important for materials that are intended to release electromagnetic energy as heat instead of reflecting it. Absorption-dominant materials with a high k value efficiently reduce interference and secondary reflections in EMI shielding.

The total shielding effectiveness (SE) is composed of contributions from reflection (R), absorption (A), and multiple reflections (MR) as shown in equation 1 [7] :

$$SE = SE(R) + SE(A) + SE(MR) \quad (1)$$

Absorption Contribution (SE (A)):

- Directly linked to the extinction coefficient.
- High k materials ensure significant wave absorption, contributing to greater SE (A) and overall shielding performance.

Reflection and Impedance Matching:

- Materials with moderate k can balance reflection and absorption, optimising impedance matching for efficient EMI shielding.

The extinction coefficient varies with frequency, making it a critical parameter for frequency-specific EMI shielding applications:

- At low frequencies (e.g., radio waves), materials with moderate k and high conductivity are preferred for reflection-dominated shielding.
- At high frequencies (e.g., microwaves or infrared), materials with high k values enhance absorption, reducing the penetration of waves through the shield.

II. METHODS AND MATERIAL

PANI is a conducting polymer with Tunable optical and electrical properties. Doping modifies its band gap and enhances its optical conductivity, making it suitable for EMI shielding applications requiring partial transparency and absorption.[8-11] CuO, a narrow-band-gap semiconductor, exhibits strong absorption in the visible and near-infrared ranges. Its high extinction coefficient makes it an effective absorber for microwave and infrared shielding. Combining PANI and CuO results in a composite material with enhanced EMI shielding performance. The synergy arises from the combination extends shielding effectiveness across multiple frequency bands.

III.RESULTS AND DISCUSSION

PANI and CuO composites were synthesized by ex situ approach method with varying CuO weight percentages, incremented by 5% and characterized using UV-Vis spectroscopy, FTIR, and X-ray diffraction to evaluate optical properties. A detailed examination of the XRD patterns of all five composites such as S1(5wt%), S2(10wt%), S3(15wt%), S4(20wt%), S5(25wt%) shows that the successful incorporation of CuO into the PANI matrix. [6]

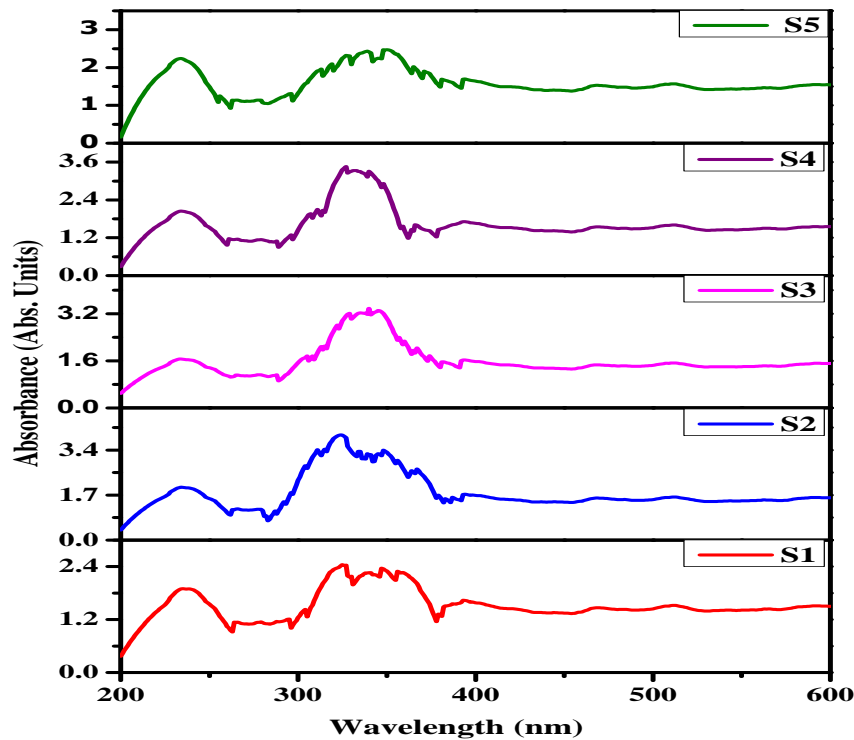


Figure1: UV–VIS spectrum of different wt% of CuO in PANI

Figure 1 shows that The UV-VIS spectra of various CuO weight percentages, ranging from 5 to 25 weight percent, was recorded in the 200–600 nm region at 5-weight percent intervals using a loaded PANI matrix. The value of the absorption coefficient is found to be almost linear between 400 and 600 nm. The p–p* transition in polymeric materials is responsible for the large peaks in the 200–225 nm range shown in the samples' absorption curve.[5]. With the standard result it is confirms that peaks of PANI and CuO shifts minutely to lower energy [4,6]

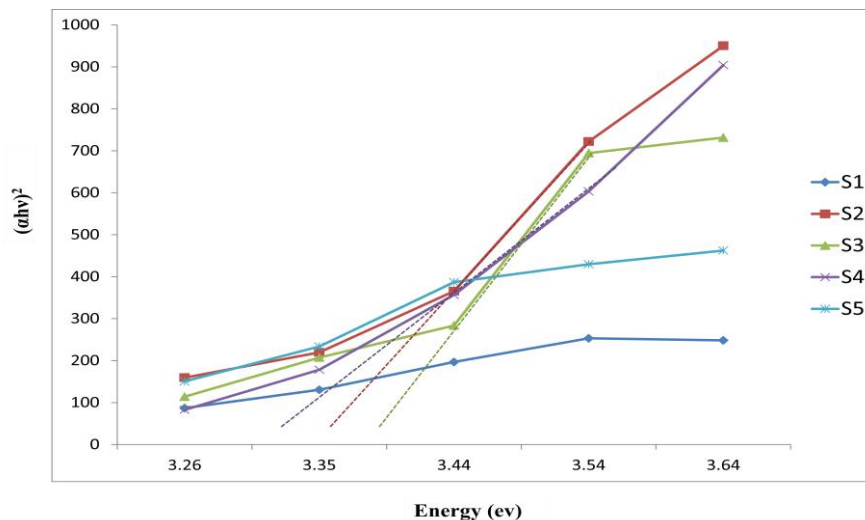


Figure2: Optical Band Gap of Samples.

The plot between $(\alpha h\nu)^2$ and photon energy $h\nu$ (eV) gives the optical band gap of Pani/CuO composite given in Figure 2. On the basis of optical band gap material has many applications. The relation between absorption coefficient (α) and incident photon energy ($h\nu$) is given in following equation 2.[1,2]

$$\alpha = A(h\nu - E_g) / h\nu \quad (2)$$

Where E_g is optical band gap of material. and A is constant.

For the weight percentage 10wt%, 15wt%, 20wt% values of the optical band gap of composites have been determined in the energy range 3.3–3.4 eV. By extrapolating a linear plot of the straight-line component of photon energy (eV) versus $(\alpha h\nu)^2$, one can shown the precise values of the band gap of nanoparticles.

It is clear from the optical band gap energy figures that this material may find use in Electromagnetic interference shielding.[1]

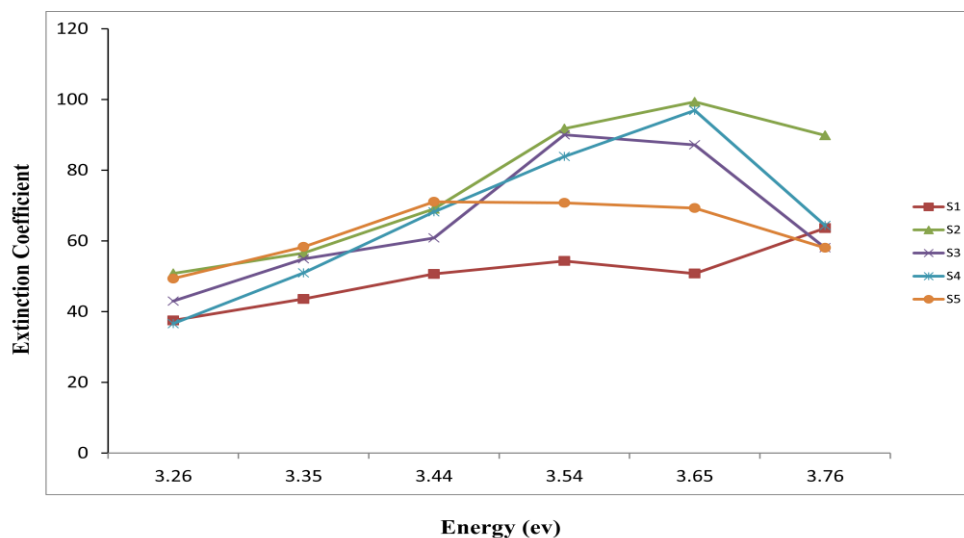


Figure3: Variation of the extinction coefficient

Equation 3 illustrates the relationship between wavelength and extinction coefficient. [2,3]:

$$K = \alpha \lambda / 4\pi \quad (3)$$

where λ is the wavelength and α is the percentage absorption. Figure 3 illustrates how the samples show an increase in the extinction coefficient over the energy range of 3.26 to 3.65.

The extinction coefficient in the samples increases smoothly in all samples From 3.26 eV to 3.44 eV. And after that 10wt%, 15wt%and 20wt% shows drastic change in extinction coefficient. These findings are consistent with the sample's absorption behavior. A high extinction coefficient in samples S2, S3, and S4 indicates that they can be used for absorption, which is essential for EMI shielding.

IV. CONCLUSION

When creating EMI shielding materials, optical characteristics like the band gap and extinction coefficient are crucial. PANI and CuO, individually and in composite form, demonstrate the potential for high-performance EMI shielding applications. Sample S2, S3 and S4 demonstrate enhanced absorption efficiency in PANI-CuO composites, suggesting improved performance of the material for EMI shielding application.

V. REFERENCES

- [1]. Rathod, P. B., & Waghuley, S. A. (2015). Synthesis and UV-Vis spectroscopic study of TiO₂ nanoparticles. *International Journal of Nanomanufacturing*, 11(3-4), 185-193.
- [2]. Barde, R. V., Nemade, K. R., & Waghuley, S. A. (2016). Complex optical study of V₂O₅-P₂O₅-B₂O₃-Dy₂O₃ glass systems. *Journal of Taibah University for Science*, 10(3), 340-344.

- [3]. K.R. Nemade, S.A. Waghuley, Synthesis of MgO nanoparticles by solvent mixed spray pyrolysis technique for optical investigation, *Int. J. Met.* 2014 (2014) 1–6.
- [4]. Jundale, D. M., Navale, S. T., Khuspe, G. D., Dalavi, D. S., Patil, P. S., & Patil, V. B. (2013). Polyaniline–CuO hybrid nanocomposites: synthesis, structural, morphological, optical and electrical transport studies. *Journal of Materials Science: Materials in Electronics*, 24, 3526–3535.
- [5]. A. Kaushik, J. Kumar, M.K. Tiwari, R. Khan, B.D. Malhotra, V. Gupta, S.P. Singh, J. *Nanosci. Nanotechnol.* 8, 1757 (2008)
- [6]. Tayade S.V, Bangar A.P., Waghuley S.A., (2024). “Evaluating Polyaniline-CuO composite for next generation Electromagnetic interference shielding.”. *ICMPE Conference Proceedings*.
- [7]. Shukla, V. (2019). Review of electromagnetic interference shielding materials fabricated by iron ingredients. *Nanoscale Advances*, 1(5), 1640–1671.
- [8]. Fang, F., Li, Y. Q., Xiao, H. M., Hu, N., & Fu, S. Y. (2016). Layer-structured silver nanowire/polyaniline composite film as a high performance X-band EMI shielding material. *Journal of Materials Chemistry C*, 4(19), 4193–4203.
- [9]. Sherman, R. D., Middleman, L. M., & Jacobs, S. M. (1983). Electron transport processes in conductor-filled polymers. *Polymer Engineering & Science*, 23(1), 36–46.
- [10]. Bigg, D. M., & Stutz, D. E. (1983). Plastic composites for electromagnetic interference shielding applications. *Polymer composites*, 4(1), 40–46.
- [11]. Trivedi, D. C., & Dhawan, S. K. (1993). Shielding of electromagnetic interference using polyaniline. *Synthetic metals*, 59(2), 267–272.

Interferometric Investigation of 2-Ethylthiocarbamido-phenol in 65% Mixed Solvent Media

S.Z.Jadhao¹, B. M.The²

¹Department of Chemistry, Institute of Science, Nagpur, Maharashtra, India

²Department of Chemical Technology, Sant Gadge Baba Amravati University, Amravati, Maharashtra, India

ARTICLE INFO

Article History:

Accepted : 01 Jan 2025

Published : 10 Jan 2025

Publication Issue :

Volume 12, Issue 7

January-February-2025

Page Number :

408-411

ABSTRACT

Ultrasonic interferometry is used to study molecular and intermolecular interactions. A study was conducted recently to determine the adiabatic compressibility (β), apparent molal compressibility (k), apparent molal volume (v), intermolecular free length (L_f), relative association (RA), and specific acoustic impedance (Z) of solutions of 2-ethylthiocarbamidophenol (ETP) at various molar concentrations (0.1M, 0.075M, 0.050M and 0.025M) and 303 K in 65% compositions of ethanol-water mixtures. These characteristics, which offer significant and adaptable information about internal structure and molecular association, were investigated in relation to solute-solute and solute-solvent interaction in solvent.

Keywords:- Interferometric measurements, solute-solvent interactions, 2-ethylthiocarbamidophenol (ETP)

I. INTRODUCTION

Ultrasound and ultrasonic ineterferometric research have become increasingly important in the last few decades for studying molecular interactions in liquids. Understanding the characteristics and importance of molecules is crucial to this investigation. It was noted that measurements of ultrasonic waves and sound produced and updated numerous innovations and new ideas in the fields of engineering, applied, industrial, mechanics, agriculture, medicine, forensic sciences, and space research. High-frequency waves are the subject of the scientific field of ultrasonics [1]. Numerous industrial and biological sciences have different uses for thiocarbamido phenol nuclei. Studying ultrasonic parameters in liquid phases [2-4], liquid mixtures [5-6], and electrolyte solutions [7-9] yielded important information about internal structure, molecular association, complex formation, internal pressure and stability.

Aswale *et al.* [10] conducted a comparative analysis of intermolecular interaction using inteferometric measurements of cumaran-3-ones and α -bromoacetophenones in ethanol and dioxan solvents. The ternary mixture of toluene in cyclohexane and nitrobenzene at 308 K was the subject of acoustic studies [11].

Researchers looked into the ultrasonic velocity and density of a binary liquid mixture of diethyl ether at 303.15K with three non-polar solvents, including CCl₄, CS₂, and C₆H₆ [12].

An outstanding technique for gathering information on the ion solvent, solvent-solvent, and structure-breaking and making properties of solutes is the ultrasonic analysis of organic ligand solutions. Ultrasonic density and velocity for 4-ethylthiocarbamidophenol (ETP) solutions at 303 K and varying molar concentrations in 60% ethanol-water mixtures including adiabatic compressibility (β), relative association (RA), intermolecular free length (Lf), apparent molal compressibility (k), and specific acoustic impedance (Z). This study aims to determine how temperature and concentrations affect different acoustical characteristics.

II. MATERIALS AND METHODS

Every chemical used in the research is of AR grade. During the study, a freshly made solution was used. Using a standard procedure, the solvents were purified. ETP solutions of 0.1M, 0.075M, 0.050M, and 0.025M in a 65% ethanol-water mixture were made. Using standard procedure, ethanol was purified. 13. Using a bicapillarypyknometer (10.1 % kg m⁻³), densities were measured. The pyrometer used is made by Borosil, and the Citizen CY 104 one pan digital balance (± 0.0001 gm) was used for the weigh-in. In order to measure density and ultrasonic velocity, a unique thermostatic setup was made. Elite thermostatic bath was utilized, where temperature variation was kept within ± 0.1 °C and water was continuously stirred with the aid of an electric stirrer. The current study used a variable path, single crystal interferometer (Mittal Enterprises, Model MX-3) with a frequency of 1 MHz and an accuracy of $\pm 0.03\%$ to determine the speed of sound waves. In order to calculate the intermolecular free length, the densities and ultrasonic velocity of liquids in ethanol solvent were measured at 303 K. The value of Jacobson's constant¹⁴ ($K = 631$) was then determined.

III. RESULTS AND DISCUSSION

Densities and ultrasonic velocities of ETP in a 65 % ethanol-water mixture were measured for this investigation and are shown in Table No. 1.

Table-1.1: Average Ultrasonic Velocity of Water at 303K

Sr. No.	No. of Rotation of Screw	Micrometer Reading (mm)	Difference Between Reading (mm)	Distance Travelled By Screw in One Rotation	Average Ultrasonic Velocity (m/sec)
1	5	25.7962	1.7624	1.37825	1503.627129
2	10	24.0308	3.7685	1.47545	
3	15	20.2724	3.6546	1.47385	
4	20	16.5179	3.7602	1.45217	
5	25	12.8178	3.7468	1.47081	
6	30	9.0707	3.7684	1.47541	
7	35	5.3128	2.7991	1.48773	
8	40	2.5236	2.8194	10.48112	

Table-1.2: Average Ultrasonic Velocity of Pure Ethanol 303K (β_0)

Sr. No.	No. of Rotation of Screw	Micrometer Reading (mm)	Difference Between Reading (mm)	Distance Travelled By Screw in One Rotation	Average Ultrasonic Velocity (v_0) (m/sec)	Density (d_0) (Kg. m ⁻³)	$\beta_0 \times 10^{-10}$ (Pa ⁻¹)
1	5	16.3943	3.914	1.4732	1354.6	1038.48	4.823619998
2	10	12.8894	3.892	1.4693			
3	15	9.3944	3.263	1.3371			
4	20	6.2311	3.48	1.3152			
5	25	2.8714		5.3811			

Table-1.3: Average Ultrasonic Velocity of 65% Ethanol 303K(β_0)

Sr. No.	No. of Rotation of Screw	Micrometer Reading (mm)	Difference Between Reading (mm)	Distance Travelled By Screw in One Rotation	Average Ultrasonic Velocity (v_0) (m/sec)	Density (d_0) (Kg. m ⁻³)	$\beta_0 \times 10^{-10}$ (Pa ⁻¹)
1	5	22.0449	3.7056	1.4544	1478.05	1028.8	4.983366084
2	10	19.3393	3.7255	1.4623			
3	15	14.6136	3.6908	1.45838			
4	20	9.924	3.6555	1.4644			
5	25	6.2675		5.98298			

Table-1.4: Acoustic Parameters at Different Concentration of [ETP] at 303 K in 65% E-W

Conc. C (Mole/lit)	Average Ultrasonic Velocity V (m/sec)	Density d_s (Kg.m ⁻³)	$\beta_s \times 10^{-10}$ (pa ⁻¹)	ϕ_v (m ³ mol ⁻¹)	$\phi_k \times 10^{-10}$	L_f (Å)	R_A	$Z \times 10^4$ (Kgm ⁻² sec ⁻¹)
0.1	1822.738	1033.31	3.2556	0.1926	-11.846	0.0149	0.978	191.624
0.075	1703.519	1029.30	3.7149	0.2215	-9.3221	0.0158	0.999	178.301
0.050	1406.843	1024.21	4.8839	0.2497	7.1962	0.0171	1.008	155.083
0.025	1341.082	1018.42	5.3921	0.2978	20.698	0.0176	1.039	141.862

IV. CONCLUSION:

Table 1.4 displayed the resulting values of the acoustic parameters of PTP at (0.1M, 0.075M, 0.050M, and 0.025M) and 303K in a 65% ethanol-water mixture. Based on Table 1.4, it was determined that, as the concentration of ETP at 303 K decreases, the following parameters decrease: Adiabatic compressibility (β_s), Apparent molar volume (ϕ_v), Apparent molar compressibility (ϕ_k), Intermolecular free length (L_f), Relative association (R_A), and Specific acoustic impedance (Z). U_s , d_s , β_s , ϕ_v , ϕ_k , L_f , R_A , z , and other acoustic properties

were identified through ultrasonic interferometric analysis. These properties explain how these interactions take place and are in charge of breaking and creating the structure in the solution.

V. REFERENCES

- [1]. C. N. Deshmukh, A. G. Doshi, Pratibha Agrawal and C. M. Deshmukh, *Ultra Science* Vol.(3),535, (2002).
- [2]. Singh, U., Chamoli, M., Singh, K. P., Ram, L., Jangir, S., & Maheshwari, R. K. *International Journal of chemistry*, 4, 19-27. (2022).
- [3]. N.A.Kalambe, P.B.Raghuwanshi and A.K.Maldhure, *Ind. J. Chem. Sci.*,12(2), 730, (2014).
- [4]. P.B.Raghuwanshi and A.D.Deshmukh, *Ind. J. Chem. Sci.*,11(1),141, (2013).
- [5]. S.K.Upadhyay, *Ind. J. Chem.*,39(5),537, (2000).
- [6]. A.Ali, K.Tiwari, A.K.Nain and V.Chakravartty, *Ind. J. Phy. Pt. B*,74(5),351, (2000).
- [7]. Singh, N., Yadav, S. S., Kumar, S., &Narashiman, B..*Food Bioscience*, 46, 101546. (2022).
- [8]. Rita Mehara, *Ind. J. Chem.*,44A(2),1834 , (2005).
- [9]. P.R.Malasne and A.S.Aswar, *Ind. J. Chem.*,44A(12),2490, (2005).
- [10]. S.S.Asware, P.B.Raghuwanshi and D.T.Tayade, *Ind. J. Chem. Soc.*,84,159, (2007).
- [11]. Bakhtiar, Z., Hasandokht, M. R., Naghavi, M. R., &Mirjalili, M. H. *Journal of chemistry*, 21(82), 1-12. (2022).
- [12]. Raji-Idowu, F ,*Ind. J. Pure. Appl. Phy.*(2023).

Green Synthesis and Characterization of Copper Nanoparticles Using *Raphanus sativus* Leaf Extract

Sachin S. Bangade, Vivek M. Raut, R.S. Shaikh, Ram.D. Isankar, M.E. Shelke, D.P. Gulwade

Government Vidarbha Inst. Science and Humanities Amravati, Maharashtra, India

ARTICLE INFO

Article History:

Accepted : 01 Jan 2025

Published : 10 Jan 2025

Publication Issue :

Volume 12, Issue 7

January-February-2025

Page Number :

412-422

ABSTRACT

Green synthesis of nanoparticles has emerged as a sustainable and eco-friendly alternative to conventional chemical synthesis methods. In this study, copper nanoparticles (CuNPs) were synthesized using an aqueous extract of *Raphanus sativus* (radish) leaves as a natural reducing and stabilizing agent. The synthesis was confirmed by a change in color and characterized through various techniques. UV-Vis spectroscopy revealed a characteristic surface plasmon resonance peak, confirming the formation of CuNPs. X-ray diffraction (XRD) analysis showed the crystalline nature of the nanoparticles. The morphology and size of the CuNPs were investigated using scanning electron microscopy (SEM) and transmission electron microscopy (TEM), which confirmed the uniform size distribution and spherical shape of the particles. This green synthesis approach provides a cost-effective and environmentally friendly method for producing copper nanoparticles with potential applications in biomedical, catalytic, and environmental fields. The study highlights the role of *Raphanus sativus* leaves as a sustainable resource for nanoparticle synthesis and paves the way for further exploration of plant-mediated green nanotechnology.

Keywords: Green synthesis, Copper nanoparticles (CuNPs), *Raphanus sativus*, UV-Vis spectroscopy, X-ray diffraction (XRD), Scanning electron microscopy (SEM), Transmission electron microscopy (TEM), Eco-friendly nanotechnology, Plant-mediated synthesis and Sustainable materials.

I. INTRODUCTION

Nanotechnology involves manipulating matter at the atomic and molecular scales, typically between 1 and 100 nanometers, to design and produce materials, structures, devices, and systems with novel properties and functions. The concept was notably introduced by physicist Richard Feynman in his 1959 lecture, "There's Plenty of Room at the Bottom," where he discussed the potential of controlling matter at such minute

scales¹. Over the past decade, significant public investment has been directed toward nanotechnology research and development, reflecting its promise as a transformative technology of the 21st century. This investment has spurred advancements across various fields, including medicine, where nanotechnology offers innovative approaches to diagnosis and treatment². Nanotechnology offers transformative potential in medicine by enabling precise interventions at the molecular level. This includes **drug delivery, medical Imaging, diagnostics,** tissue engineering, regenerative medicine and nanorobotics. Such innovations could revolutionize medical research and usher in a new era of human Surgical Applications.³

Background on Nanotechnology:

The term "Nanotechnology" first emerged during the Taniguchi International Conference on Industrial Production in Tokyo in 1974. However, the concept was initially articulated by American physicist Richard Feynman in 1959, who highlighted the vast potential of tiny dimensions with his famous statement, "There is a lot of space down there." In his forward-thinking speech, Feynman envisioned a world where atoms and molecules could be manipulated with minute tools. It wasn't until 1974 that Japanese engineering professor Norio Taniguchi officially coined the term "nanotechnology" to describe this burgeoning field.⁴⁻¹⁰ Further advancements were made by E. Drexler in his 1986 book "Engines of Creation: The Coming Era of Nanotechnology." The U.S. marked a significant milestone in 1991 by establishing its first national scientific fund for nanotechnology programs, followed by the official sanctioning of the National Nanotechnology Initiative (NNI) in 2001. In the same year, Japanese scientist Sumio Iijima's discovery of carbon nanotubes revolutionized engineering applications. In 1998, an American scientist demonstrated nanotechnology's exceptional precision by developing a pencil made of carbon nanotubes capable of inscribing letters just 10 nanometers across. President Bill Clinton emphasized nanotechnology's importance by launching the National Nanotechnology Initiative in 2000. The field received further recognition in 2016 when the Nobel Prize in Chemistry was awarded to Sir J. Fraser Stoddart, Jean-Pierre Sauvage, and Bernard Feringa for their work on molecular machines.¹¹⁻¹⁸

Importance of Copper Nanoparticles (Cu NPs):

Copper is a versatile metal integral to various industries due to its exceptional properties.

1. **Electronics & Electrical Engineering:** Copper's excellent conductivity makes it essential for wiring, connectors, and components.
2. **Medical Applications:** Known for antimicrobial properties, copper is used in healthcare settings to reduce pathogen spread and in durable medical equipment.
3. **Architecture & Construction:** Its corrosion resistance and durability make copper ideal for roofing, plumbing, and decorative elements, developing a protective green patina over time.
4. **Currency:** Historically significant in coinage, copper remains valuable in commemorative coins and bullion.
5. **Mining Industry:** Found with gold and silver, technological advancements are refining copper extraction methods.
6. **Nanotechnology:** Research on copper nanoparticles using plant extracts shows promise for sustainable production and applications in catalysis, biomedicine, and more¹⁹⁻²⁵.

Copper's versatility keeps it at the forefront of innovation and progress across various fields.

Role of *Raphanus sativus* (Radish) Leaf Extract:

Radish (*Raphanus sativus*) is a globally cultivated cruciferous root vegetable, showcasing a variety of colors due to phytoanthocyanins. It holds significant economic importance and offers nutritional and pharmaceutical

benefits worldwide, especially in Asian regions. Depending on anthocyanin accumulation, radishes can be white, green, or red. Green and red radishes are often consumed fresh or as pickles.

The edible parts of the radish include the petiole, root peel, and root flesh, each varying in bioactive and antioxidant effects. Typically, the flesh contains lower levels of these compounds. Green radishes have higher proanthocyanidins, carotenoids, and chlorophylls, whereas red radishes contain more vitamin C, anthocyanins, and total phenolic contents. These bioactive compounds and antioxidant capacities differ among radish parts and species. Substantial amounts of anthocyanins accumulate in both the skin and flesh of red radishes²⁶⁻³⁰.

Historically, radishes have been used as natural remedies against toxicants in folk medicine. The root is the main edible organ, while dried leaves are effective as functional foods. Cruciferous vegetables, including radishes, offer numerous health benefits due to their nutritional components and biologically active molecules. They activate Phase-II enzymes and induce apoptosis, leading to significant health advantages. Optimizing the production of bioactive molecules in cruciferous vegetables through biotechnological and agricultural methods could enhance their utility³¹⁻³⁶.

II. LITERATURE REVIEW

Copper is a versatile metal with rich historical significance, indispensable in numerous applications. Known for its exceptional electrical and thermal conductivity, copper is crucial in electronics and electrical engineering, used in wiring, connectors, and various modern technology components. Its malleability and ductility further enhance its usefulness in these fields. Copper's antimicrobial properties make it valuable in medical settings, where it helps reduce pathogen spread on surfaces in hospitals and healthcare facilities. Copper alloys are also employed in medical equipment for their durability and microbial growth inhibition. In architecture and construction, copper's durability and corrosion resistance make it ideal for roofing, plumbing, and decorative elements. Over time, it develops a distinctive green patina that adds aesthetic appeal and provides additional corrosion protection. Historically, copper has played a significant role in currency and coinage, with copper coins being among the earliest forms of currency. Although its use in everyday coinage has decreased, copper remains valuable in commemorative coins and bullion. The mining industry relies heavily on copper, often found in ores with other valuable metals like gold and silver. Technological advancements have improved copper extraction and refining processes, enhancing efficiency and reducing environmental impact³⁷⁻⁴⁵.

Research on copper nanoparticles has gained momentum, revealing potential applications in catalysis, nanotechnology, and biomedicine. Plant extracts have shown promise in the green and sustainable synthesis of copper nanoparticles, with studies by Singh et al. and Gupta et al. demonstrating successful biosynthesis using *Ocimum sanctum* and *Aloe vera*, respectively⁴⁶⁻⁵⁶.

Overall, copper's multifaceted properties and applications highlight its enduring importance in modern society. From technology and industry to healthcare, copper continues to drive innovation and progress.

III. MATERIALS AND METHODS

Preparation of *Raphanus sativus* Leaf Extract:

Fresh, tender leaves of *Raphanus sativus* were collected and washed with deionized water for 5 minutes. The leaves were then dried in the shade, away from direct sunlight, for 20 days. Once dried, the leaves were ground into a fine powder using a mixer grinder or mortar and pestle. Fifty grams of this leaf powder, along with the leaves of, were subjected to Soxhlet extraction using distilled water continuously for 72 hours. The resulting

extract was concentrated after filtration and stored at room temperature in airtight bottles for further studies, following previously published standards.

Synthesis of Copper Nanoparticles:

Ten milliliters of plant leaf extract was added dropwise to 100 milliliters of CuNO_3 solution while stirring for 10 minutes, followed by heating at 80°C . Within 30 minutes, copper ions were reduced to copper nanoparticles, as confirmed by UV-vis spectrum. The reaction mixture's color changed from green to yellow, indicating nanoparticle formation. The reaction continued for an additional 10 minutes to complete the process.

Characterization Techniques:

UV-Visible Spectroscopy:

UV of CuNPs Using *Raphanussativus*L. Leaves

Copper nanoparticles (CuNPs) were synthesized using Copper nanoparticles (CuNPs) were synthesized using Copper nanoparticles (CuNPs) were synthesized using *Raphanussativus* L. extract as a biogenic reducing agent, and their optical properties were examined through UV-Vis spectroscopy. The UV-Vis spectrum displayed three distinct absorption peaks at wavelengths of 892 nm, 272 nm, and 216 nm, with absorbance values of 0.016, 0.724, and 3.902, respectively⁵⁷.

The absorption peak at 892 nm, with an absorbance of 0.016, suggests the presence of CuNPs in the solution. This peak corresponds to the surface plasmon resonance (SPR) of the synthesized nanoparticles, indicating the successful reduction of copper ions and formation of nanoparticles.

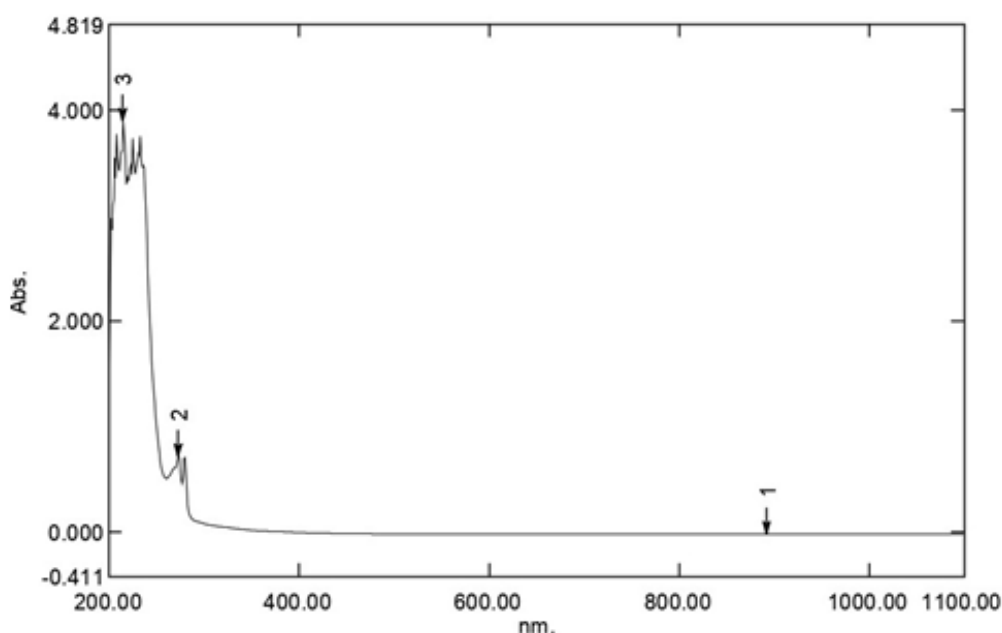
The absorption peak at 272 nm, with an absorbance of 0.724, further confirms the presence of CuNPs. This peak likely results from electronic transitions within the nanoparticles or other species present in the solution, providing additional evidence of successful synthesis.

The absorption peak at 216 nm, with a high absorbance value of 3.902, indicates the presence of copper nanoparticles or other copper-containing compounds. This peak is associated with the electronic transitions characteristic of copper nitrate or copper compounds, suggesting the formation of additional products during the synthesis process.

Overall, the observed absorption peaks demonstrate the effectiveness of *Raphanus sativus* L. extract as a biogenic reducing agent for the synthesis of copper nanoparticles.. extract as a biogenic reducing agent, and their optical properties were examined through UV-Vis spectroscopy. The UV-Vis spectrum displayed three distinct absorption peaks at wavelengths of 892 nm, 272 nm, and 216 nm, with absorbance values of 0.016, 0.724, and 3.902, respectively.

The absorption peak at 216 nm, with a high absorbance value of 3.902, indicates the presence of copper nanoparticles or other copper-containing compounds. This peak is associated with the electronic transitions characteristic of copper nitrate or copper compounds, suggesting the formation of additional products during the synthesis process.

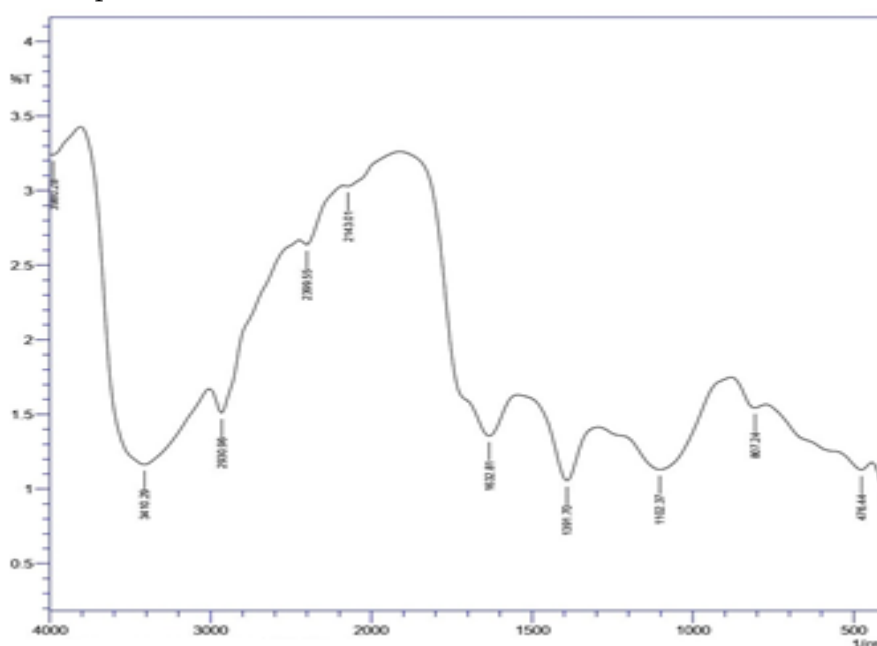
Overall, the observed absorption peaks demonstrate the effectiveness of *Raphanus sativus* L. extract as a biogenic reducing agent for the synthesis of copper nanoparticles.



Fourier Transform Infrared Spectroscopy (FTIR):

Copper nanoparticles (CuNPs) were synthesized using an extract from *Raphanussativus* L. leaves. Fourier Transform Infrared (FTIR) spectroscopy was used to identify the functional groups present in the nanoparticles. The FTIR spectrum revealed several distinct peaks: A broad peak at 3966 cm^{-1} indicates O-H stretching vibrations, suggesting the presence of hydroxyl (-OH) groups. The peak at 2930 cm^{-1} corresponds to C-H stretching vibrations, typically found in alkanes. A peak at 2134 cm^{-1} may be due to $\text{C}\equiv\text{N}$ or $\text{C}\equiv\text{C}$ stretching, indicating the presence of alkynes or nitriles. The peak at 1634 cm^{-1} is likely due to $\text{C}=\text{C}$ stretching vibrations, pointing to alkenes. At 1362 cm^{-1} , the peak is related to C-H bending. The peak at 1095 cm^{-1} indicates C-O stretching vibrations, which could be from alcohols, ethers, or esters. A peak at 840 cm^{-1} might be related to C-H bending vibrations in aromatic compounds. Finally, the small peak at 324 cm^{-1} is typically associated with metal-oxygen bonds, indicating the presence of copper oxide⁵⁸.

These FTIR results confirm that various functional groups from the leaf extract are involved in capping and stabilizing the copper nanoparticles.

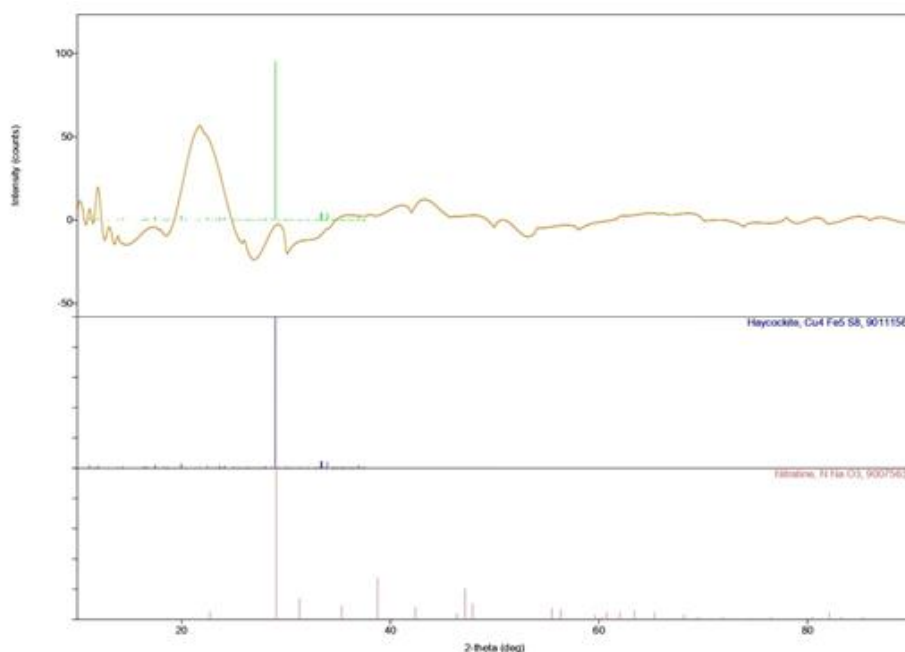


X-Ray Diffraction (XRD):

The XRD diffractogram of copper nanoparticles synthesized from *Raphanussativus* L.L. leaves shows significant peaks at 2θ values of 43.11° , 50.30° , 74.04° , and 77.39° . These peaks correspond to the (111), (200), and (220) planes of copper, confirming the presence of copper nanoparticles with a face-centered cubic crystal structure. Additionally, four peaks at 22.44° , 23.25° , 30.73° , 32.47° , and 57.45° indicate the presence of CuNO_3 , suggesting that a small amount of copper nitrate remained unreduced in the sample.

The volume of the crystalline copper nanoparticles, synthesized using the leaf extract of *Raphanussativus* L.L., was estimated to be approximately 50-60 nanometers based on the diffractogram. The nanoparticle size was determined using the Debye-Scherrer formula, with FWHM (full width at half maximum) values obtained by fitting the peaks with Gaussian functions in Origin software. The interplanar spacing was calculated using Bragg's Law, and the values from the four peaks were found to be nearly identical. The diffraction angle (θ) and the wavelength of the X-rays (β), which is the FWHM of the diffraction peak, were used to determine the lattice constant, averaged to 1.5326 \AA , closely matching the standard value for copper (1.5406 \AA). The cell volume was also estimated from the lattice constant.

The XRD analysis confirms that well-defined copper nanoparticles can be synthesized using the leaf extract of *Raphanussativus* L..



Scanning Electron Microscopy (SEM):

The synthesized copper nanoparticles exhibited significant aggregation, with an average size distribution ranging from 76.20 to 93.32 nanometers and a mean size of 84.76 nanometers. This aggregation is likely due to interactions between the concentrated nanoparticles and the secondary metabolites extracted from *Raphanussativus* L. leaves used in the synthesis process. Additionally, SEM analysis revealed rod-like shapes in the inter-nanoparticle regions, believed to originate from the concentrated plant components during the synthesis process.

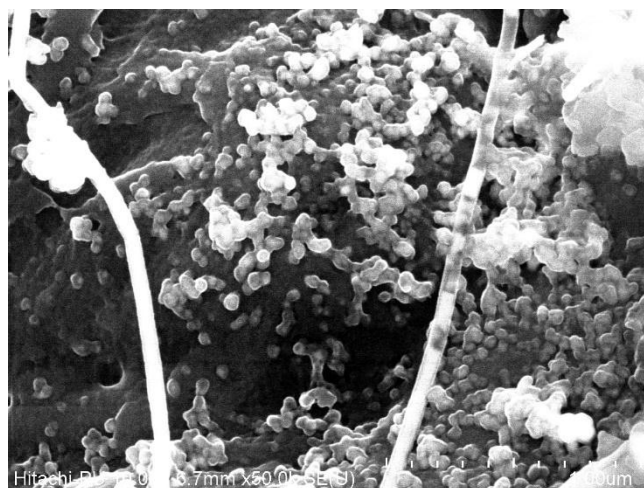


Figure1 : SEM of CuNPs from *Raphanus sativus L.*

TEM Analysis of *Raphanussativus L.* leaves CuNPs

TEM imaging was used to examine nanostructures derived from *Raphanussativus L.* leaves. The analysis of copper nanoparticles revealed primarily spherical or elliptical shapes, with sizes ranging from 37 to 91 nanometers. The TEM analysis confirmed that the copper nanoparticles are solid, with spherical shapes being most common. Additionally, a few elliptical and rounded particles were also observed.

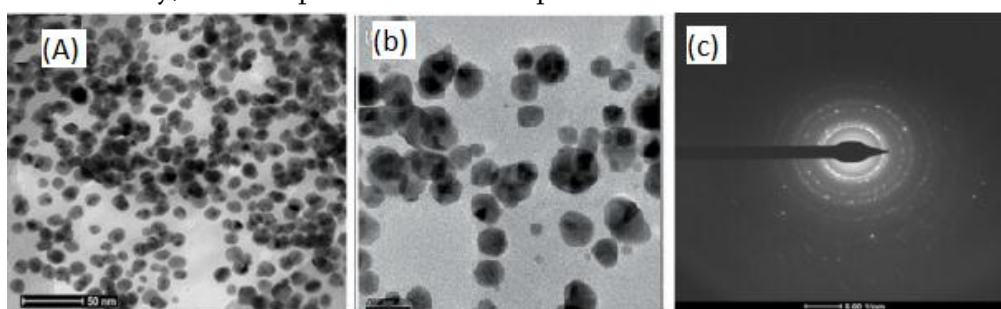


Figure2: TEM of CuNPs from *Raphanus sativus L.*

1) DLS of *Raphanussativus L.*-Cunanoparticle

In this study, the size distribution of *Raphanussativus L.* copper nanoparticles was analyzed using the Dynamic Light Scattering (DLS) technique. The DLS analysis showed a unimodal size distribution, with a prominent peak at approximately 86.06 nm, accounting for 100% of the sample area. The standard deviation of 40.65 nm indicated variability in nanoparticle size. These findings enhance our understanding of copper nanoparticle synthesis and their potential applications. Further research is needed to clarify the factors affecting nanoparticle size distribution and stability, and to explore their properties and applications in various fields.

IV. RESULTS AND DISCUSSION

Copper nanoparticles (CuNPs) were synthesized using *Raphanus sativus L.* extract as a biogenic reducing agent. UV-Vis spectroscopy showed three distinct absorption peaks at 893 nm, 273 nm, and 215 nm, with absorbance values of 0.016, 0.724, and 3.902, respectively. These peaks confirm the successful reduction of copper ions to nanoparticles and the presence of copper-containing compounds. The observed absorption peaks highlight the effectiveness of *Raphanussativus L.* extract in synthesizing copper nanoparticles.

Copper nanoparticles synthesized using *Raphanussativus L.* leaves were analysed using FTIR spectroscopy. Key peaks for both extracts indicated the presence of various functional groups:

- ***Raphanus sativus L.*** : Peaks at 3966 cm^{-1} (O-H), 2930 cm^{-1} (C-H), 2134 cm^{-1} ($\text{C}\equiv\text{N}/\text{C}\equiv\text{C}$), 1634 cm^{-1} (C=C), 1362 cm^{-1} (C-H bending), 1095 cm^{-1} (C-O), 840 cm^{-1} (C-H in aromatics), and 324 cm^{-1} (metal-oxygen).

These results confirm the presence of hydroxyl, alkane, alkyne, alkene, and aromatic groups, along with metal-oxygen bonds, indicating successful capping and stabilization of copper nanoparticles by the plant extracts. The XRD diffractogram of copper nanoparticles synthesized from *Raphanus sativus L.* leaves displayed significant peaks at 2θ values of 43.11° , 50.30° , 74.04° , and 77.39° , corresponding to the (111), (200), and (220) planes of copper. These peaks confirm the face-centered cubic crystal structure of the copper nanoparticles. Additional peaks at 22.44° , 23.25° , 30.73° , 32.47° , and 57.45° suggest the presence of a small amount of unreduced copper nitrate (CuNO_3) in the sample. The size of the crystalline copper nanoparticles, estimated from the diffractogram, ranged from 50-60 nanometers. The Debye-Scherrer formula, with FWHM values obtained by fitting the peaks with Gaussian functions in Origin software, was used to determine the nanoparticle size. The interplanar spacing was calculated using Bragg's Law, and the values from the four peaks were nearly identical. The lattice constant, averaged to 1.5326 \AA , closely matches the standard value for copper (1.5406 \AA). The cell volume was also estimated from the lattice constant. Overall, the XRD analysis confirms the successful synthesis of well-defined copper nanoparticles using *Raphanussativus L.* leaf extract.

Copper nanoparticles synthesized using *Raphanus sativus L.* leaf extract showed significant aggregation, with sizes ranging from 76.20 to 93.32 nanometers. SEM analysis revealed various shapes (slime, tetragonal, disc, and rod-like) in surface and inter-nanoparticle regions, likely due to concentrated plant components during synthesis. These findings emphasize the complex interactions between nanoparticles and plant metabolites, highlighting the need for further research to optimize synthesis methods and explore applications in medicine and environmental science. TEM analysis revealed consistent morphological characteristics of nanostructures derived from *Raphanussativus L.* leaves across copper nanoparticles. All nanoparticles exhibited predominantly spherical or elliptical shapes. Sizes ranged from 37 to 91 nm for copper.

In this study, Dynamic Light Scattering (DLS) analysis of *Raphanussativus L.* copper nanoparticles showed a unimodal size distribution with a peak at 86.06 nm, covering 100% of the sample area, and a standard deviation of 40.65 nm. These findings enhance our understanding of copper nanoparticle synthesis and suggest the need for further research to explore factors affecting size distribution, stability, and potential applications in various fields.

V. REFERENCES

- [1]. Feynman, R. (2018). There's plenty of room at the bottom. In Feynman and computation (pp. 63-76). CRC Press.
- [2]. Gonzalez, L., Loza, R. J., Han, K. Y., Sunoqrot, S., Cunningham, C., Purta, P., & Chang, J. H. (2013). Nanotechnology in corneal neovascularization therapy—a review. *Journal of ocular pharmacology and therapeutics*, 29(2), 124-134.
- [3]. Haleem, A., Javaid, M., Singh, R. P., Rab, S., & Suman, R. (2023). Applications of nanotechnology in medical field: a brief review. *Global Health Journal*, 7(2), 70-77.
- [4]. Mansoori, G. A. (2005). Principles of nanotechnology: Molecular-based study of condensed matter in small systems. World Scientific.

- [5]. Ray, P. C. (2010). Size and shape dependent second order nonlinear optical properties of nanomaterials and their application in biological and chemical sensing. *Chemical Reviews*, 110(9), 5332–5365.
- [6]. Singh, J., Dutta, T., Kim, K.-H., et al. (2018). 'Green' synthesis of metals and their oxide nanoparticles: Applications for environmental remediation.
- [7]. Jong, W. H. D., & Borm, P. J. A. (2008). Drug delivery and nanoparticles: Applications and hazards. *International Journal of Nanomedicine*, 3(2), 133–149.
- [8]. Cao, G. (2004). *Nanostructures and Nanomaterials: Synthesis, Properties and Applications*. Imperial College Press.
- [9]. Jokerst, J. V., & Gambhir, S. S. (2011). Molecular Imaging with Theranostic Nanoparticles. *Accounts of Chemical Research*, 44(10), 1050–1060. [DOI: 10.1021/ar200023h]
- [10]. Polman, A., Knight, M., Garnett, E. C., Ehrler, B., & Sinke, W. C. (2016). Photovoltaic materials: Present efficiencies and future challenges. *Science*, 352(6283), aad4424. [DOI: 10.1126/science.aad4424]
- [11]. Peer, D., Karp, J. M., Hong, S., Farokhzad, O. C., Margalit, R., & Langer, R. (2007). Nanocarriers as an emerging platform for cancer therapy. *Nature Nanotechnology*, 2(12), 751–760. [DOI: 10.1038/nnano.2007.387]
- [12]. Zhang, H., Liu, L., Shi, Y., & Jing, Y. (2018). Catalysis and photocatalysis by metal nanoparticles. In *Nanoparticles for Catalysis* (pp. 1-26). Elsevier. [DOI: 10.1016/B978-0-12-811993-4.00001-3]
- [13]. Wang, Y., & Su, D. (2013). Metal oxide-based nanomaterials for electrochemical energy storage. In *Metal Oxides in Supercapacitors* (pp. 1-31). Springer. [DOI: 10.1007/978-1-4614-8889-6_1]
- [14]. Wang, Z. L. (2010). Nanogenerators for self-powered devices and systems. In *Nanotechnology for Sustainable Energy* (pp. 145-166). Springer. [DOI: 10.1007/978-3-642-14512-7_7]
- [15]. Helmuth, J. (2014). *Industrial Nanotechnology: Size Does Matter*. Wiley.
- [16]. Nirmal, M., & Brus, L. (1999). Luminescence photophysics in semiconductor nanocrystals. *Accounts of Chemical Research*, 32(5), 407–414. [DOI: 10.1021/ar970113]
- [17]. Raliya, R., & Tarafdar, J. C. (2013). ZnO Nanoparticle Biosynthesis and Its Effect on Phosphorous-Mobilizing Enzyme Secretion and Gum Contents in Clusterbean (*Cyamopsis tetragonoloba* L.). *Agricultural Research*, 2(1), 48–57. [DOI: 10.1007/s40003-012-0035-4]
- [18]. Kan, C.-W., & Yuen, C. W. M. (2014). A Review on the Applications of Nanotechnology in the Clothing and Textile Industry. *Journal of Textile and Apparel, Technology and Management*, 8(2), 1–19.
- [19]. Rhim, J.-W. (2013). Nanocomposites for Food Packaging Applications. *Food Science and Biotechnology*, 22(6), 1679–1689. [DOI: 10.1007/s10068-013-0216-x]
- [20]. Qu, X., Alvarez, P. J. J., & Li, Q. (2013). Applications of Nanotechnology in Water and Wastewater Treatment. *Water Research*, 47(12), 3931–3946. [DOI: 10.1016/j.watres.2012.09.058]
- [21]. Labouta, H. I., El-Khordagui, L. K., & Kraus, T. (2019). Classification of Nanomaterials in Cosmetics: A Review. *Journal of Applied Toxicology*, 39(1), 134–146. [DOI: 10.1002/jat.3724]
- [22]. Zhang, S., Tang, C., & Yin, C. (2016). The Application of Nanomaterials in Tissue Engineering. *Journal of Biomedical Materials Research Part A*, 104(11), 2709–2718. [DOI: 10.1002/jbm.a.35816]
- [23]. Zhou, M., Zhang, R., Huang, M., Lu, W., & Song, S. (2015). Melanin-Like Nanoparticles: Biodegradable and Renal Excretable Contrast Agents for Photoacoustic Imaging. *Scientific Reports*, 5, 14295. [DOI: 10.1038/srep14295]
- [24]. Li, Y., Zhang, Y., & Fu, S. (2018). Review of the Applications of Nanomaterials in Air Pollution Control. *Nanomaterials*, 8(9), 710. [DOI: 10.3390/nano8090710]

- [25]. Chowdhury, E. A., Akaike, T., & Hidaka, K. (2019). Nanoparticle-Assisted Delivery of Biotherapeutics for Neurological Disorders. *Advanced Drug Delivery Reviews*, 148, 81–106. [DOI: 10.1016/j.addr.2019.09.012]
- [26]. Dorosti, R., Khorasani, M. T., & Chitsazan, M. (2020). Nano-Antimicrobial Fillers for Waterborne Polyurethane Coatings: A Review. *Progress in Organic Coatings*, 146, 105662. [DOI: 10.1016/j.porgcoat.2020.105662]
- [27]. Kang, D., Pikhitsa, P. V., Choi, Y. W., Lee, C., Shin, S. S., Piao, L., ... & Choi, M. (2014). Ultrasensitive Mechanical Crack-Based Sensor Inspired by the Spider Sensory System. *Nature*, 516(7530), 222–226. [DOI: 10.1038/nature14002]
- [28]. Jokerst, J. V., Lobovkina, T., Zare, R. N., & Gambhir, S. S. (2011). Nanoparticle PEGylation for Imaging and Therapy. *Nanomedicine*, 6(4), 715–728. [DOI: 10.2217/nnm.11.19]
- [29]. Taniguchi, N. (1974). On the Basic Concept of 'Nanotechnology'. *Science (New York, N.Y.)*, 186(4161), 740–741. [DOI: 10.1126/science.186.4161.740]
- [30]. Roco, M. C., & Bainbridge, W. S. (2001). Societal implications of nanoscience and nanotechnology: Maximizing human benefit. *Journal of Nanoparticle Research*, 3(3-4), 191–198. doi: 10.1023/A:1017583524611
- [31]. Iijima, S. (1991). Helical microtubules of graphitic carbon. *Nature*, 354(6348), 56–58. doi: 10.1038/354056a0
- [32]. Smalley, R. E., Colbert, D. T., & Dai, H. (1998). Efficient synthesis of nanotubes from AAO-supported catalyst particles. *Chemical Physics Letters*, 293(3-4), 601–606. doi: 10.1016/S0009-2614(98)00763-6
- [33]. The Royal Swedish Academy of Sciences. (2016). Press Release: The Nobel Prize in Chemistry 2016. Retrieved from <https://www.nobelprize.org/prizes/chemistry/2016/press-release>
- [34]. Hilty, F. M., Arnold, M., Hilber, I., & Teleki, A. (2010). The Environmental Impact of Micro and Nanoparticles: A Review. *Science of The Total Environment*, 408(18), 4381–4398. <https://doi.org/10.1016/j.scitotenv.2010.06.039>
- [35]. Wang, Y., Li, P., & Tran, T. T. D. (2019). Soluplus micelles for improving the oral bioavailability of scopoletin and their hypoglycemic effect. *Journal of Agricultural and Food Chemistry*, 67(22), 6309–6318. <https://doi.org/10.1021/acs.jafc.9b01291>
- [36]. Michalet, X., Pinaud, F. F., Bentolila, L. A., Tsay, J. M., Doose, S., Li, J. J., ... & Weiss, S. (2005). Quantum dots for live cells, in vivo imaging and diagnostics. *Science*, 307(5709), 538–544. <https://doi.org/10.1126/science.1104274>
- [37]. Gleiter, H. (1995). "Nanostruct. Mater., 1995, 6, 3."
- [38]. V.V. Pokropivny and Skorokhod J. *Supercond.* 13 (2000) 607.
- [39]. Hedhili, M. N., Harb, M., & Salama, K. N. (2011). "Zero-Dimensional Nanostructures: Nanoparticles." *Comprehensive Nanoscience and Technology*, 4, 101–137. DOI: 10.1016/B978-0-12-374396-1.00210-5
- [40]. Iijima, S. (1991). "Helical microtubules of graphitic carbon." *Nature*, 354(6348), 56–58.
- [41]. Novoselov, K. S., Geim, A. K., Morozov, S. V., Jiang, D., Zhang, Y., Dubonos, S. V., ... & Firsov, A. A. (2004). "Electric field effect in atomically thin carbon films." *Science*, 306(5696), 666–669.
- [42]. Alivisatos, A. P. (1996). "Semiconductor clusters, nanocrystals and quantum dots." *Science*, 271(5251), 933–937.
- [43]. Kroto, H. W., Heath, J. R., O'Brien, S. C., Curl, R. F., & Smalley, R. E. (1985). "C60: Buckminsterfullerene." *Nature*, 318(6042), 162–163. DOI: 10.1038/318162a0

- [44]. Kroto, H. W., Heath, J. R., & Smalley, R. E. (1985). "A laser-ablation method for the synthesis of fullerene hollow tubes." *Nature*, 318(6042), 162-163. [DOI: 10.1038/318162a1]
- [45]. Curl, R. F., Kroto, H. W., & Smalley, R. E. (1986). "Nobel Lecture: The Discovery of the Fullerenes." *Angewandte Chemie International Edition in English*, 25(8), 741-750. [DOI: 10.1002/anie.198607413]
- [46]. Kroto, H. W., Heath, J. R., O'Brien, S. C., Curl, R. F., & Smalley, R. E. (1985). "C₆₀: Buckminsterfullerene." *Nature*, 318(6042), 162-163. [DOI: 10.1038/318162a0]
- [47]. Heath, J. R., O'Brien, S. C., Zhang, Q., Liu, Y., & Curl, R. F. (1985). "C₇₀: A new form of carbon." *Nature*, 318(6042), 162-163. [DOI: 10.1038/318162a1]
- [48]. Stevenson, S., Rice, G., Glass, T., Harich, K., Cromer, F., Jordan, M. R., & Balch, A. L. (1999). "Isolation, separation and characterization of the isomers of the endohedral metallofullerene Lu₃N@C₈₀." *Science*, 283(5407), 1505-1507. [DOI: 10.1126/science.283.5407.1505]
- [49]. Prato, M., Maggini, M., & Bonchio, M. (1998). "Thiol-functionalized fullerenes: Preparation, properties and applications of C₆₀ SH_x." *Advanced Materials*, 10(1), 61-65. [DOI: 10.1002/(SICI)1521-4095(199801)10:1<61::AID-ADMA61>3.0.CO;2-D]
- [50]. Iijima, S. (1991). "Helical microtubules of graphitic carbon." *Nature*, 354(6348), 56-58. [DOI: 10.1038/354056a0]
- [51]. Halas, N. J., West, J. L., & Rufe, C. A. (2003). "Nanoshell-Mediated Near-Infrared Thermal Therapy of Tumors Under Magnetic Resonance Guidance." *Proceedings of the National Academy of Sciences*, 100(23), 13549-13554. [DOI: 10.1073/pnas.2232479100]
- [52]. Tomalia, D. A., Baker, H., Dewald, J., Hall, M., Kallos, G., Martin, S., ... & Smith, P. (1985). "A New Class of Polymers: Starburst-Dendritic Macromolecules." *Polymer Journal*, 17(1), 117-132. [DOI: 10.1295/polymj.17.117]
- [53]. Kukowska-Latallo, J. F., Candido, K. A., Cao, Z., Nigavekar, S. S., Majoros, I. J., Thomas, T. P., ... & Baker, J. R. (2005). "Nanoparticle Targeting of Anticancer Drug Improves Therapeutic Response in Animal Model of Human Epithelial Cancer." *Cancer Research*, 65(12), 5317-5324. [DOI: 10.1158/0008-5472.CAN-04-3921]
- [54]. Svenson, S., & Tomalia, D. A. (2005). "Dendrimers in biomedical applications—reflections on the field." *Advanced Drug Delivery Reviews*, 57(15), 2106-2129. [DOI: 10.1016/j.addr.2005.09.018]
- [55]. Branton, D., Deamer, D. W., Marziali, A., Bayley, H., Benner, S. A., Butler, T., ... & Wanunu, M. (2008). "The potential and challenges of nanopore sequencing." *Nature Biotechnology*, 26(10), 1146-1153. [DOI: 10.1038/nbt.1495]
- [56]. Kasianowicz, J. J., Brandin, E., Branton, D., & Deamer, D. W. (1996). "Characterization of individual polynucleotide molecules using a membrane channel." *Proceedings of the National Academy of Sciences*, 93(24), 13770-13773. [DOI: 10.1073/pnas.93.24.13770]
- [57]. Venkatesan, B. M., Bashir, R. (2011). "Nanopore sensors for nucleic acid analysis." *Nature Nanotechnology*, 6(10), 615-624. [DOI: 10.1038/nnano.2011.129]
- [58]. Alivisatos, A. P. (1996). "Semiconductor clusters, nanocrystals and quantum dots." *Science*, 271(5251), 933-937. [DOI: 10.1126/science.271.5251.933]

Synthesis and Characterization of Schiff Base ligand for Corrosion Inhibition of Mild Steel in Sulphuric Acid Medium

Prashant Ashtaputrey^{1, *}, Sampada Payal², Ashok Kalambe³, Kavita Gour⁴, Rohit Chunarkar⁵

^{1,2,3,5}Institute of Science, Nagpur, Maharashtra, India

⁴Priyadarshini J.L. College of Engineering, Nagpur, Maharashtra, India

ARTICLE INFO

Article History:

Accepted : 01 Jan 2025

Published : 10 Jan 2025

Publication Issue :

Volume 12, Issue 7

January-February-2025

Page Number :

423-434

ABSTRACT

The condensation process between amine and aldehyde produced the Schiff base ligand. Utilizing spectral and electrochemical analytical techniques, the synthesized ligand was described in order to verify its structure and examine its characteristics. Furthermore, the effectiveness of the ligand in preventing corrosion on mild steel in an acidic environment was evaluated. The ligand's potential as an efficient corrosion inhibitor was highlighted by the results, which showed that it demonstrates a notable level of corrosion inhibition efficacy. This study provides opportunities for the use of Schiff base ligands in corrosion prevention, presenting a viable strategy for both biological and industrial uses.

KEYWORDS :- Schiff base, spectral analysis, elemental analysis, corrosion inhibition, anti-bacterial activity, anti-enzymatic activity

I. INTRODUCTION

INTRODUCTION

A major problem in many different sectors is corrosion, which is the slow degradation of materials brought on by chemical or electrochemical reactions with their surroundings [1]. Researchers are investigating a variety of substances with promising inhibitory qualities as a result of the search for efficient corrosion inhibitors. The synthesis, characterization, and possible usage of Schiff base, which is produced from the reaction of aldehyde and amine under reflux, are the primary subjects of this investigation [2].

Background Metals and alloys are frequently affected by corrosion, which has serious safety and financial ramifications for sectors like energy, infrastructure, and transportation. In addition to causing monetary losses, corrosion-induced material deterioration can jeopardize the structural integrity of important parts [3]. Researchers constantly look for novel corrosion inhibition techniques to lessen the impact of corrosion on materials in order to meet this challenge [4]. Schiff bases are recognized as a class of compounds with a variety of uses, including corrosion inhibition, which serves as the justification for the study [5]. The fascinating

chemical characteristics of Schiff bases, which are produced when aldehydes or ketones condense with amines, make them a promising option for corrosion inhibition [6].

Schiff base IR and XRD are performed in conjunction with elemental analysis to uncover the complexities of synthesis. Additionally, its bioactivity is investigated, its electronic structure is examined using UV spectroscopy, and its electrochemical behaviour is examined by determining the molar conductivity in various solvents. Visual characterisation and synthesis of Schiff base with a particular colour was created during the synthesis procedure, which involved the reflux reaction of aldehyde and amine in an acidic environment. This colour indicates that the product was successfully synthesized.

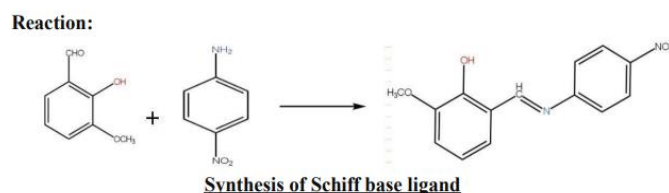
MATERIAL AND METHOD

Chemicals and Instruments

All the chemicals, reagents and Solvents used for chemical synthesis of Schiff's base were of analytical grade and were purchased from Sigma Aldrich. All these chemicals were used as supplied by supplier without further purification. The melting point was determined using Prolab India's Microprocessor Based Digital melting point Apparatus, Model MP108. The conductance measurement was carried out on Equiptronics Conductivity meter model EQ660B. For the FTIR, UV spectral characterization and CHNS elemental characterization samples were sent to SAIF Chandigarh and Cochin.

Method for the synthesis of Schiff's Base Ligand (SBL)

The Schiff base ligand was synthesized by the method of condensation by mixing the 20ml ethanolic solution of aldehyde (0.1M) i.e. O-Vanillin with 20 ml ethanolic solution of amine (0.1M) i.e. 4-Nitroaniline in alcoholic medium using as a solvent. The resulting mixtures were refluxed for the period of about 3hrs. During the reflux yellowish orange colour solid compound was separated out. It was then filtered under suction, dried and recrystallized from alcohol, washed with diethyl ether, dried and placed in desiccator containing anhydrous calcium hydroxide to remove moisture from solid powder. The compound obtained by above procedure was then further analysed [7].



RESULTS AND DISCUSSIONS:-

Elemental Characterization

The result of the CHNS elemental analysis of the new Schiff base ligand is summarized in the Table 01 with graph given below.

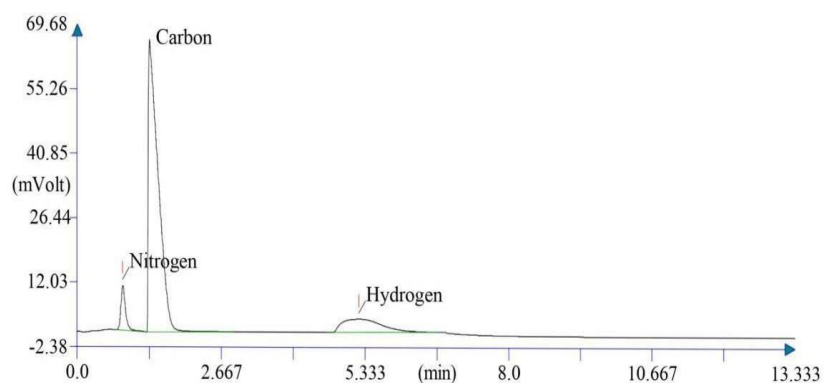


Table 1: CHNS elemental analysis of the Schiff base ligand

Peak no.	Retention time(min)	Component name	Element (%) Cal.
1	0.842	Nitrogen	10.568 (10.968)
2	1.333	Carbon	61.499 (61.703)
3	5.217	Hydrogen	4.54 (4.407)

IR Analysis :-

The IR spectrum of 2-Hydroxy-3-methoxybenzaldehyde 4-nitroaniline involves identifying characteristic peaks associated with functional groups present in the molecule. Hydroxyl group (OH): Broad peak around 3200-3600 cm^{-1} . Carbonyl group (C=O) in benzaldehyde Sharp peak around 1680-1750 cm^{-1} . Aromatic ring: C-H stretching: Typically seen as medium to strong peaks around 3000-3100 cm^{-1} . C=C stretching: Typically seen as medium peaks around 1500-1600 cm^{-1} . Methoxy group (OCH₃): -O stretching: Usually observed as a sharp peak around 1000-1300 cm^{-1} . Nitro group (NO₂): NO₂ stretching: (C=N) Strong, sharp peak around 1500-1600 cm^{-1} . Overall, these are peaks corresponding to these functional groups in the IR spectrum of 2-Hydroxy- 3methoxybenzaldehyde 4-nitroaniline.

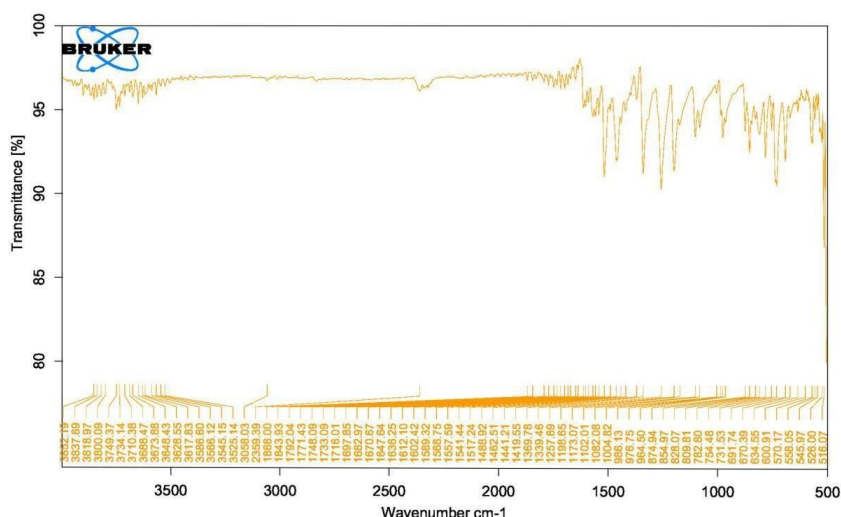
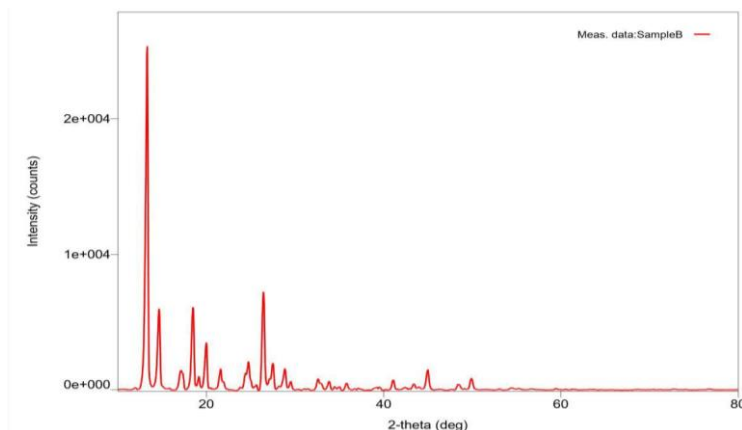


Fig.1: FTIR spectrum of the Schiff base ligand

X-Ray Diffraction Study:

XRD patterns of ligand show the sharp crystalline peaks indicating their crystalline Phase. The highest peak is observed at $2\theta = 13.334$ degree. There are other peaks to indicating regular crystal structure is also present their phase.

Fig. 2: XRD of the Schiff base ligand



1) UV-Visible spectra of ligand

The UV-Visible spectra of Ligand were recorded in DMSO solutions between 300 and 600 nm at room temperature. In ligand two band is observed between 340 to 370 nm of range, which is attribute to $\pi \rightarrow \pi^*$ transition of heteroleptic moieties and $n \rightarrow \pi^*$ transition of the azomethine group respectively.

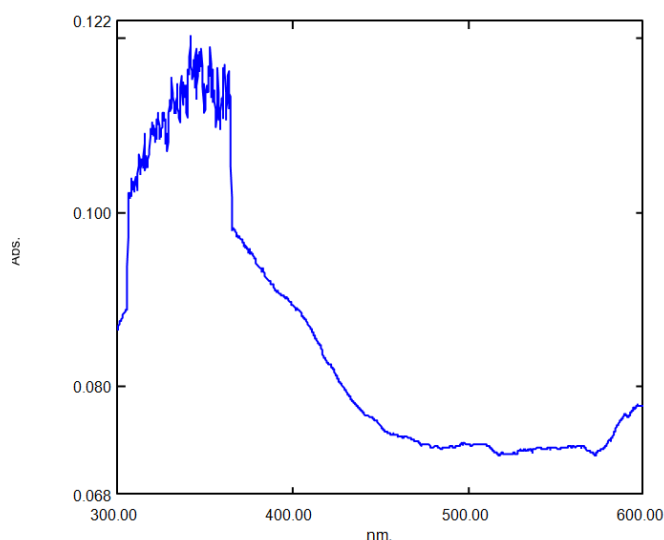


Fig. 3. Electronic spectra of Schiff Base ligand

Anti-Microbial Activity:-

Anti-bacterial properties of Schiff base:

The novel synthesized compound was screened for their in vitro antimicrobial activity using a cup plate agar disc-diffusion method against two gram positive bacterial strains *S. aureus* and *Oxalopodis* and three-gram negative strains, *E. coli* and *E. erviceia*. *S. typhi* Chloramphenicol were used as standard drugs for bacteria. The

details of the relevant procedures and the results of the biological screening are discussed in this part of the thesis.

General Procedure:-

Determination of Zone of Inhibition by Agar disc-diffusion method:

Test solutions were prepared with known weight of compound in dimethyl sulphoxide (DMSO) and diluted suitably to give the resultant concentration of 31, 62, 125, 250 and 500 ug/mL. Whatman no. 1 sterile filter paper discs (6mm) were impregnated with solution and allowed to dry at room temperature. In vitro antibacterial activity was determined by using Agar obtained Nutrient both Agar. Twenty-four hours old culture of selected bacterial strain was mixed with physiological saline and the turbidity was corrected by adding sterile physiological saline and cultured on Sabouraud Dextrose and suspended in sterile distilled water to an absorbance of 0.6 at 450 nm.[8-10]

Petri plates were prepared by pouring 10 mL of Nutrient both Agar for bacteria containing microbial culture was allowed to solidify. The bore was then applied and the plates were incubated at 37°C for 24h (bacteria) and the inhibition zone was measured as diameter in four directions and expressed as mean. The results were compared using Chloramphenicol as a standard antibacterial agent. The results of antibacterial activity (i.e. Zone of Inhibition in mm) of some of the synthesized compounds are given in the table 2.

Table 2:

Sr. no	Name of compound	Con c.	Antibacterial activity Zone of Inhibition(mm)			
			S. Aurelius	E.c oli	S. typhi	E.ervenia
1	Chloramphenicol	100	30	20	20	16
		500	27	18	21	17
		250	21	17	16	16
		125	18	17	15	15
2	Schiff base		13	16	--	--

Antimicrobial activity of Schiff Base ligand

Corrosion inhibition activity:-

Corrosive property of Mild steel in different concentration of sulphuric acid: -

To study the corrosion property of mild steel in varying concentrations of sulphuric acid (0.5N, 1N, 1.5N, 2N, 2.5N), Table 3 to Table 9 begin by preparing uniform mild steel specimens and diluting sulphuric acid to the desired concentrations. Submerge the specimens in individual beakers containing the respective acid solutions, ensuring full immersion, and monitor them regularly for observable changes. After the predetermined exposure period which is 2 hours, remove the specimens, rinse, and examine them for corrosion signs. Analyze the collected data to assess the corrosion rates at each concentration, comparing the results to identify trends. Draw conclusions regarding the effect of acid concentration on mild steel corrosion and propose recommendations for further investigation or corrosion mitigation strategies based on the findings.[11-18]

Observation Table Of weight (g)							
Name of Acid	weight	time	0.5N	1N	1.5N	2N	2.5N
Sulphuric acid	W1	0 min	12.098	12.591	12.490	12.553	14.486
	W2	120 min	12.012	12.470	12.367	12.400	12.288
	W3	240 min	11.996	12.444	12.306	12.33	14.206
	W4	360 min	11.967	12.404	12.245	12.275	14.157
	W5	480 min	11.946	12.365	12.203	12.213	14.091
	W6	600 min	11.922	12.330	12.158	12.161	14.023
	W7	720 min	11.880	12.290	12.116	12.110	13.955
	W8	840 min	11.840	12.243	12.058	12.048	13.880

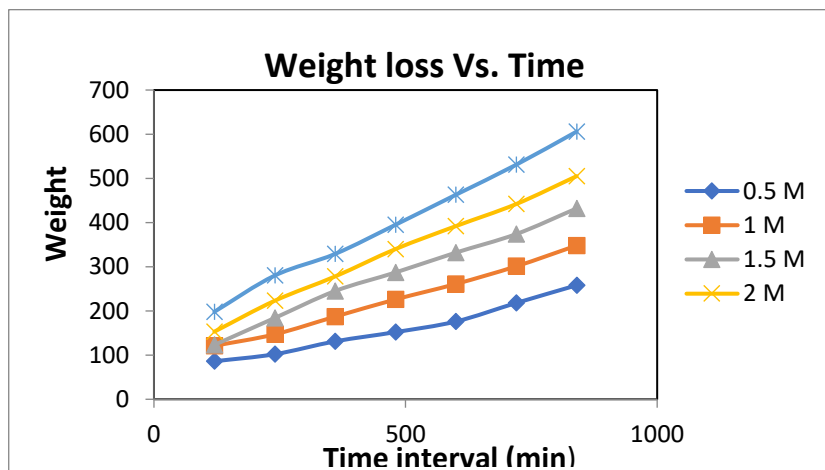
Table 3: Weight measurement of mild steel coupons in acid medium

Observation table for weight loss at every stage (at very 120min time interval)

As the graph is showing the weight loss is constantly increasing with for all the different concentration of Sulphuric acid.

Acid	Conc. (N)	Weight loss (mg)						
Sulphuric Acid		120 min	240 min	360 min	480 min	600 min	720 min	840 min
	0.5	86	102	131	152	176	218	258
	1	121	147	187	226	261	301	348
	1.5	123	184	245	287	332	374	432
	2	153	223	278	340	392	442	505
	2.5	198	280	329	395	463	531	606

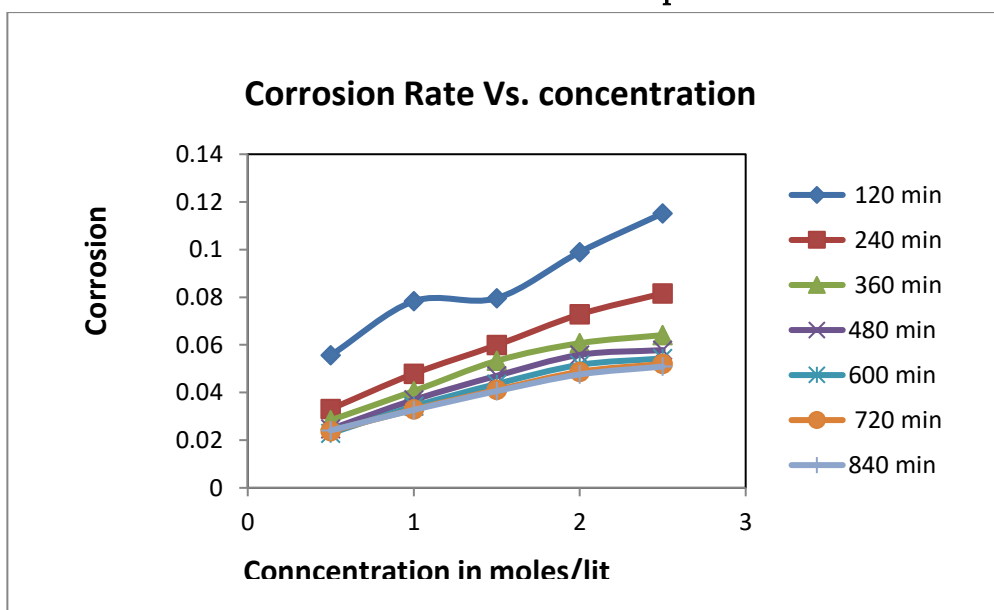
Table 4: Weight loss measurement of mild steel coupons in acid medium



Graph 1. Weight loss Vs. Time for mild steel coupons in acid medium
Corrosion rate in Sulphuric acid medium at different concentrations:-

Corrosion rate							
Time Interval							
Conc. (N)	120 min	240 min	360 min	480 min	600 min	720 min	840 min
0.5	0.0556	0.03309	0.0284	0.0247	0.0229	0.0238	0.0241
1	0.0783	0.0479	0.0406	0.0369	0.0342	0.0329	0.0327
1.5	0.0796	0.0599	0.0533	0.047	0.0436	0.0411	0.0406
2	0.0989	0.0728	0.0607	0.0558	0.0516	0.0487	0.0476
2.5	0.1152	0.0816	0.0641	0.0578	0.0543	0.052	0.0509

Table 5: Corrosion Rate measurement of mild steel coupons in acid medium



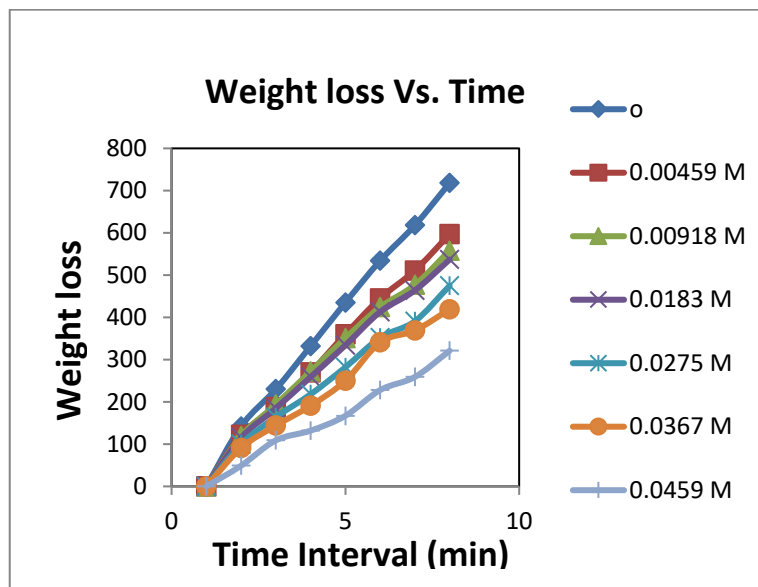
Graph 2. Corrosion Rate Vs. Acid Concentration for mild steel coupons in acid medium

Sulphuric acid and Schiff base								
Conc. of Acid 1N								
Time	Conc. of S.B. (M)	0	0.00459	0.00918	0.0183	0.0275	0.0367	0.0459
0 min	W1	13.154	13.247	13.531	13.005	13.501	13.329	13.179
120 min	W2	13.012	13.125	13.412	12.89	13.401	13.238	13.13
240 min	W3	12.924	13.06	13.337	12.82	13.337	13.185	13.07
360 min	W4	12.822	12.977	13.259	12.746	13.283	13.138	13.047
480 min	W5	12.719	12.887	13.18	12.671	13.219	13.079	13.012
600 min	W6	12.62	12.802	13.107	12.592	13.149	12.988	12.951
720 min	W7	12.536	12.736	13.054	12.541	13.11	12.96	12.92
840 min	W8	12.436	12.65	12.973	12.468	13.026	12.91	12.858

Table 6: Weight measurement of mild steel coupons in Schiff Base ligand acid medium

Weight loss									
conc. of Acid (N)	conc. of S.B. (M)	0 min	120 min	240 min	360 min	480 min	600 min	720 min	840 min
1	0	0	142	230	332	435	534	618	718
1	0.00459	0	122	187	270	360	445	511	597
1	0.00918	0	119	194	272	351	424	477	558
1	0.0183	0	115	185	259	334	413	464	537
1	0.0275	0	100	164	218	282	352	391	475
1	0.0367	0	91	144	191	250	341	369	419
1	0.0459	0	49	109	132	167	228	259	321

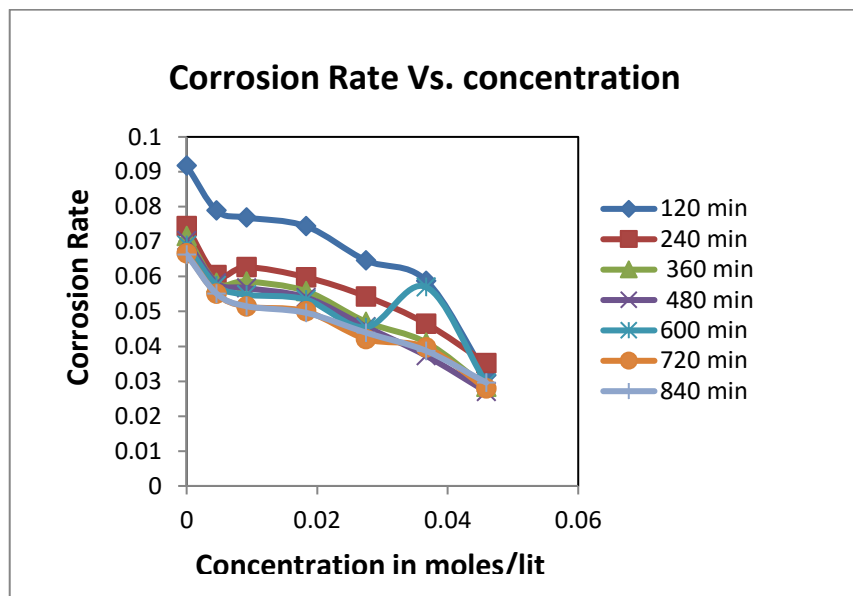
Table 7: Weight loss measurement of mild steel coupons in Schiff Base ligand acid medium



Graph 3. Weight loss Vs. Time for mild steel coupons in S.B ligand acid medium

		Corrosion rate						
Conc. Of Acid IN	conc. of S.B.(M)	120 min	240 min	360 min	480 min	600 min	720 min	840 min
1	0	0.0918	0.0744	0.0716	0.0703	0.069	0.0666	0.0663
1	0.00459	0.0789	0.0604	0.0582	0.0582	0.0575	0.0551	0.0551
1	0.00918	0.0769	0.0627	0.0586	0.0567	0.0548	0.0514	0.0515
1	0.00183	0.0744	0.0598	0.0558	0.054	0.0534	0.05	0.0496
1	0.0275	0.0646	0.0543	0.047	0.0456	0.0455	0.0421	0.0439
1	0.0367	0.0588	0.0465	0.0411	0.0373	0.057	0.0397	0.0387
1	0.0459	0.0317	0.0352	0.0284	0.027	0.0295	0.0279	0.0296

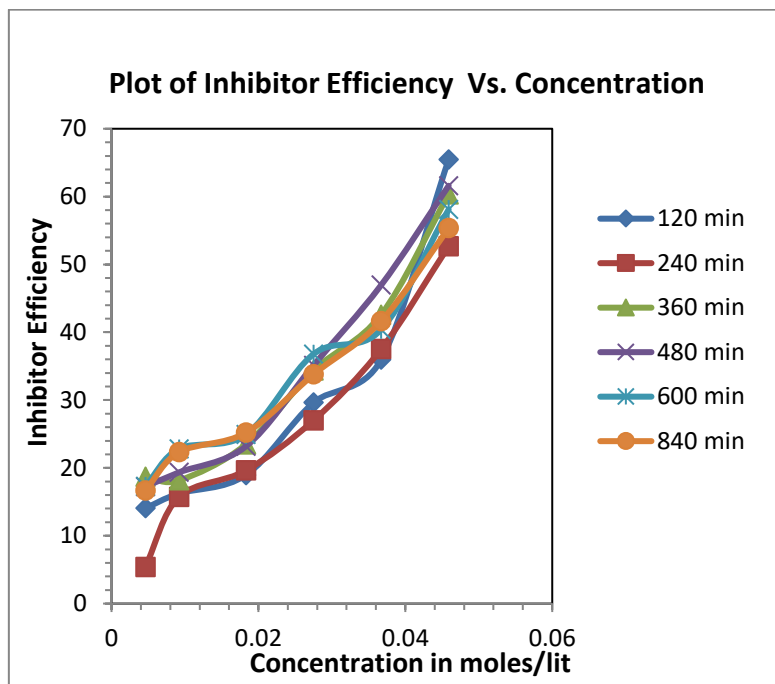
Table 8: Corrosion Rate measurement of mild steel coupons in Schiff Base ligand acid medium



Graph 4. Corrosion Rate Vs. Acid Concentration for mild steel coupons in S.B ligand acid medium

Efficiency of Schiff base to inhibit the corrosion in different Concentration when compared with 1N Sulphuric Acid:								
Sr. No.	Time Of immersion							
	Conc. of SB	120 min	240 min	360 min	480 min	600 min	720 min	840 min
	Inhibitor efficiency							
1)	0.00459	14.052	5.37	18.71	17.21	16.66	17.26	16.65
2)	0.00918	16.23	15.72	18.156	19.34	20.57	22.82	22.322
3)	0.0183	18.95	19.62	23.46	23.18	22.6	24.92	25.188
4)	0.0275	29.62	27.01	34.35	35.13	34.05	36.78	33.785
5)	0.0367	35.94	37.5	42.59	46.94	17.39	40.39	41.628
6)	0.0459	65.46	52.68	60.33	61.59	57.24	58.1	55.35

Table 9: Corrosion Inhibition efficiency S.B. Ligand for mild steel coupons in Schiff Base ligand acid medium



Graph 5. Corrosion Inhibition efficiency for mild steel coupons in S.B ligand acid medium

Conclusion:-

In conclusion our investigation into the corrosion behaviour of mild steel in Sulphuric Acid, employing Schiff base compound as inhibitor, demonstrates their significant potential in mitigation corrosion. The formation of protective film by schiff base on the steel surface impedes the corrosive action of Sulphuric acid, thereby enhancing the material resistance to degradation. This finding underscores the practical relevance of Schiff base as effective corrosion inhibitors for mild steel in acidic environments. Further exploration into the molecular mechanisms underlying their inhibitive properties and optimization of parameters holds promise for their widespread application in corrosion protection strategies.

ACKNOWLEDGEMENT

Authors of this paper are very much thankful the Director of Institute of Science, Nagpur for providing the research facility. We are also thankful to SAIF Chandigarh and Cochin for providing the spectral analysis of Schiff base ligand.

CONFLICT OF INTEREST

Authors of this paper do not have any conflict of interest.

References: -

1. A. G. Bedir, M. Abd El-raouf,* S. Abdel-Mawgoud, N. A. Negm, and N. M. El Basony* Cite This: ACS Omega **2021**, 6, 4300–4312
2. M. Abdallah, ;B. Al Jahdaly.;O. Al-Malyo. Corrosion inhibition of carbon steel in hydrochloric acid solution using non-ionic surfactants derived from phenol com Disorders. Molecules.(**2021**);26(14)4160. Published **2021** Jul 8. doi:10.3390/molecules26144160
3. Sensors and Actuators B: Chemical journal homepage: www.elsevier.com/locate/snb Chelate-type Schiff base

acting as a colorimetric sensor for iron in aqueous solution Ga Rim Youa,b, G J Parka,b, S A Leea,b, K Y Ryua,b, C Kima,b,*

4. M. Sravanthi , B. Kavitha and P. S Reddy . Green route for efficient synthesis of biologically active schiff base ligand derived from 2 – hydroxy acetophenone: structural, spectroscopic, antimicrobial and molecular modeling studies. *Int. Res. J. Pharm.* (2019), 10 (3). DOI: 10.7897/2230-8407.1003107
5. A.Singh,; K.Ansari,;M. Quraishi,;S. Kaya,;P Banerjee,. The effect of an N-heterocyclic compound on corrosion inhibition of J55 steel in sweet corrosive medium. *New J. Chem.* 2019, 43, 6303–6313
6. D. B.Tripathy, ;M. Murmu, ; P.Banerjee, ;M. A. Quraishi, Palmitic acid based environmentally benign corrosion inhibiting formulation useful during acid cleansing process in MSF desalination plants. *Desalination* 2019, 472, No. 114128.
7. F. H.Al-Abdali, ; M.Abdallah, ; R.El-Sayed,Corrosion inhibition of aluminum using nonionic surfactant compounds with a six membered heterocyclic ring in 1.0 M HCl solution. *Int. J. Electrochem. Sci.* 2019, 14, 3509–3523.
8. D. Gupta, D. P Pathak, G. Kapoor, and R. Bhutani A Comprehensive Review on Synthesis and Biological Activity of Schiff Bases. *Int. Res. J. Pharm.* (2019);1-8<http://dx.doi.org/10.7897/2230-8407.1005153>
9. A. S .Fouda, A.El-Askalany, ;A. El-Habab,;S. Ahmed, Anticorrosion Properties of Some Nonionic Surfactants on Carbon Steel in 1 M HCl Environment. *J. Bio- Tribo-Corros.* 2019, 5, 56.
10. P. Yadav, A. Sarkar and A. Kumar Synthesis and biological activities of schiff bases and their derivatives: a review of recent work. *Journal of Basic and Applied Engineering Research*, (2019) Vol. 6, Issue 1; January-March, 62-65.
11. D. Sukul,; A.Pal,;S.K. Saha,; S. Satpati, ; U. Adhikari, .P; Banerjee, . Newly synthesized quercetin derivatives as corrosion inhibitors for mild steel in 1 M HCl: combined experimental and theoretical investigation. *Phys. Chem. Chem. Phys.* 2018, 20, 6562–657.
12. A R.Bhat , M.H.Wagay. Synthesis of Schiff's Base Derivatives Using Water as Solvent. (A Green Methodology). *IJRASET*. (2017) Volume 5 Issue XI November.
13. A. A Hameed,M. al-Rashida, M.Uroos., S.M. Ali. and K.M.Khan Schiff bases in medicinal chemistry: a patent review (2010-2015), *Expert Opinion on Therapeutic Patents*, (2017) 27(1):63-79.
14. Evaluating corrosion inhibition property of some Schiff bases for mild steel in 1 M HCl: competitive effect of the heteroatom and stereochemical conformation of the molecule. *RSC Adv.* 2016, 6,74833–74844.
15. Shaban, S. M.; Abd-Elal, A. A.; Tawfik, S. M. Gravimetric and electrochemical evaluation of three nonionic dithiol surfactants as corrosion inhibitors for mild steel in 1 M HCl solution. *J. Mol. Liq.* 2016, 216, 392–400.
16. Al-Sabagh, A. M.; Nasser, N. M.; El-Azabawy, O. E.; Tabey, A. E. E. Corrosion inhibition behavior of new synthesized nonionic surfactants based on amino acid on carbon steel in acid media. *J. Mol. Liq.* 2016, 219, 1078–1088.
17. S. Malik. and B. Nema . Antimicrobial activities of Schiff Bases: A review. *International Journal of Theoretical & Applied Sciences*, (2016) 8(1): 28-30.
18. G. Yadav and V.J Mani Green Synthesis of Schiff Bases by Using Natural Acid Catalysts. (*IJSR*). (2015) Volume 4 Issue.
19. K., and S. Junaedi. (2014). Inhibition of mild steel corrosion in sulfuric acid solution by new Schiff base. *Materials* 7, 787–804. doi: 10.3390/ma7020787
20. *International Journal of the Physical Sciences* Vol. 6(15), pp. 3616-3623, 4 August, 2011 Available online at <http://www.academicjournals.org/IJPS> DOI: 10.5897/IJPS11.923 ISSN 19921950 ©2011 Academic Journals
Corrosion and plants extracts inhibition of mild steel in HCl C. A. Loto*, R. T. Loto and A. P. I. Popoola.

Spectroscopic Studies and Combustion Synthesis of $\text{LiAl}_5\text{O}_8:\text{Gd}^{3+}$ Phosphor for Optical Applications

Sandip M. Parkhi^{1*}, S.A.Shah^{1*}, Shruti Dhale², Avinash M. Nannaware¹, N.S.Ugemuge^{2*}

¹Department of Chemistry, Anand Niketan College, Anandwan, Warora, 442907, Maharashtra, India

²Department of Physics, Anand Niketan College, Anandwan, Warora, 442907, Maharashtra, India

ARTICLE INFO

Article History:

Accepted : 01 Jan 2025

Published : 10 Jan 2025

Publication Issue :

Volume 12, Issue 7

January-February-2025

Page Number :

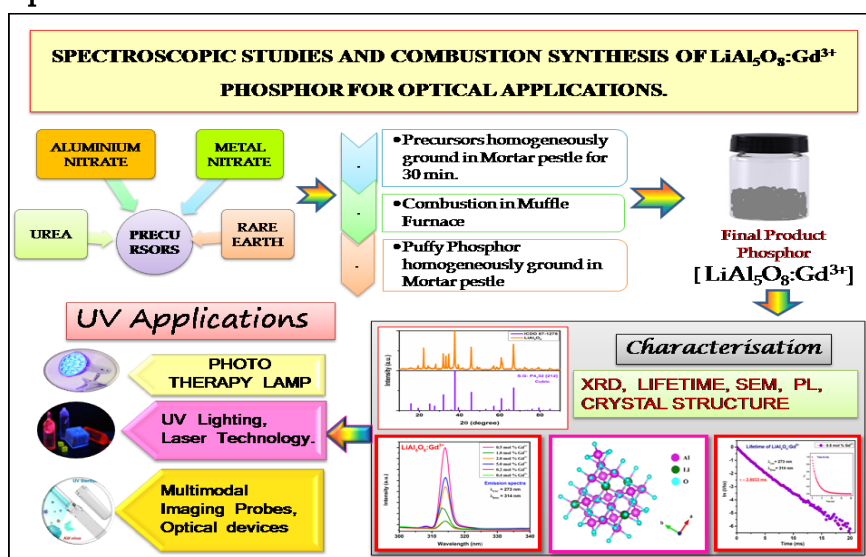
434-443

ABSTRACT

$\text{LiAl}_5\text{O}_8:\text{Gd}^{3+}$ ultraviolet B (UVB) emitting phosphors were synthesized using the urea-assisted combustion synthesis process at 500°C within a few minutes. The cubic structure of the synthesized sample was confirmed by the x-ray diffraction method (XRD). EDAX and scanning electron microscopy (SEM) verified the surface shape and chemical composition. In LiAl_5O_8 phosphor the luminescence characteristic of Gd^{3+} ions was detected. The $^6\text{P}_{7/2} \rightarrow ^8\text{S}_{7/2}$ transition is responsible for the strong ultraviolet emission in the PL spectra of $\text{LiAl}_5\text{O}_8:\text{Gd}^{3+}$ which excited at 273 nm and centered or show emission at 314 nm. According to the conclusion, the Gd^{3+} doped LiAl_5O_8 matrix may probable applications in UVB-emitting phototherapy lamps and other optical equipment.

Keywords: Aluminate; Phosphor; Combustion Synthesis; Photoluminescence; Optical applications.

Graphical Abstract:



I. INTRODUCTION

Depending on the dopant ions in the selected host matrix, inorganic compounds doped with lanthanide ions (Ln^{3+}) in the UV, visible and near-infrared regions have a variety of uses. Because of its applications in the medical field, optical field and other fields, including optical devices like multimodal imaging probes, phototherapy lamps, photochemical reactions, scintillators, induction sterilization, disinfection, insect traps, vitamin D3 production, and the medical sciences. To achieve such types of applications, Gd^{3+} ions play fundamental roles as its emission in the range of 200 nm to 400 nm due to its f-f transitions [].

Among all the rare earth metal ions, trivalent cerium (Gd^{3+}) is one of the most widely used dopant ions in aluminate hosts because of its particular $5d \rightarrow 4f$ transition. Additionally, the 311 – 315 nm emission range of Gd^{3+} ion doped phosphor materials, which is attributed to the $6P_{7/2} \rightarrow 8S_{7/2}$ that makes them extremely important for their characteristic optical uses in the UV region []. The Gd^{3+} ion, that has unpaired 7-electron pairs in its 4f shell, is broadly utilized as an optical imaging probe in usual clinical MRI (magnetic resonance imaging) because of its paramagnetic properties. Additionally, it improves image quality so it gives precise information about abnormalities and diseases which are clearly and noticeable visible on MRI []. Gd^{3+} doped up-conversion phosphor materials have most significant fluorescent imaging agents and T1-MR materials have been identified []. Green phosphors for color television tubes, magneto-optical films, computer memory, microwave applications, CDs, and diamond impersonation are just a few of the many uses for Gd^{3+} doped phosphors. Additionally, the UVB phototherapy lamp is the most effective medical treatment for vitiligo.

As a potential host matrix for active metal ions, particularly rare earth (RE) ones, lithium aluminates-based phosphor compounds are popular with researchers and industry for a numeral of industrial applications due to their excellent radiation stability, thermo-chemical properties, good luminescent materials and artificial illumination, etc. The inverse spinel structure of LiAl_5O_8 gives it remarkable optical characteristics because it accepts dopants from transition metal and rare earth ions. LiAlO_2 and LiAl_5O_8 are regarded as better-quality host phosphors for a range of metal ion doping impurities [].

There are numerous reports on the introduction of transition metal ions and rare earth metal ions for applications in luminescent devices. Silva and Ariosvaldo JS reported that X-ray excited optical luminescence changes induced by excess and deficiency lithium ions in rare earth metal ion doped with LiAl_5O_8 []. Kutty and Nayak investigated that the luminous characteristics of Fe-doped LiAl_5O_8 produced by a wet chemical process. $\text{LiAl}_5\text{O}_8:\text{Co}^{2+}$ nanocrystals were recently created using the citrate sol-gel method []. AJS Silva proposed that preparation of LiAl_5O_8 phosphor doped with cerium ion and investigation of its Structural and optical properties via a simple sol-gel using glucose []. Singh and Rao used a self-propagating (combustion) synthesis to create $\text{LiAl}_5\text{O}_8:\text{Eu}^{3+}$ phosphor []. Self-flux synthesis was used by Shinobu Hashimoto et al. to investigate the photoluminescent characteristics of LiAl_5O_8 []. Fe^{3+} doped LiAl_5O_8 produced by a wet chemical processing approach has been examined for its luminous properties []. Singh et al. studied that the synthesis and photoluminescence studies of ultraviolet-emitting $\text{ZnAl}_2\text{O}_4:\text{Gd}^{3+}$ phosphors [].

Aluminate-based phosphors can be synthesized using a variety of methods, such as the solid-state metathesis reaction approach, wet chemical method, sol-gel method etc. These methods of phosphor material synthesis take a maximum time and energy. Among these method combustion synthesis (CS) is the most popular and cost-effective technique for production of aluminate-based phosphor because of its unique qualities, including safety, instantaneity, and energy efficiency. When compared to these approaches, CS offers the following benefits: (i) Economical, quick, and low temperature synthesis (ii) Facile addition of dopant ions (iii) Control

over the composition and purity of the synthesized product. Due to these benefits, we have synthesized Gd³⁺ doped LiAl₅O₈ phosphor for the first time using the combustion method, as detailed in this article. Since there are lacks of reports on Gd³⁺ doped LiAl₅O₈ phosphor in the literature, hence a simple combustion method was used in this work to create Gd³⁺ doped LiAl₅O₈ phosphor. In addition to synthesis, XRD pattern verifies the compound's phases and crystal structure. The properties of photoluminescence (PL) in the synthesized LiAl₅O₈ phosphor with dopants were examined.

II. EXPERIMENTAL

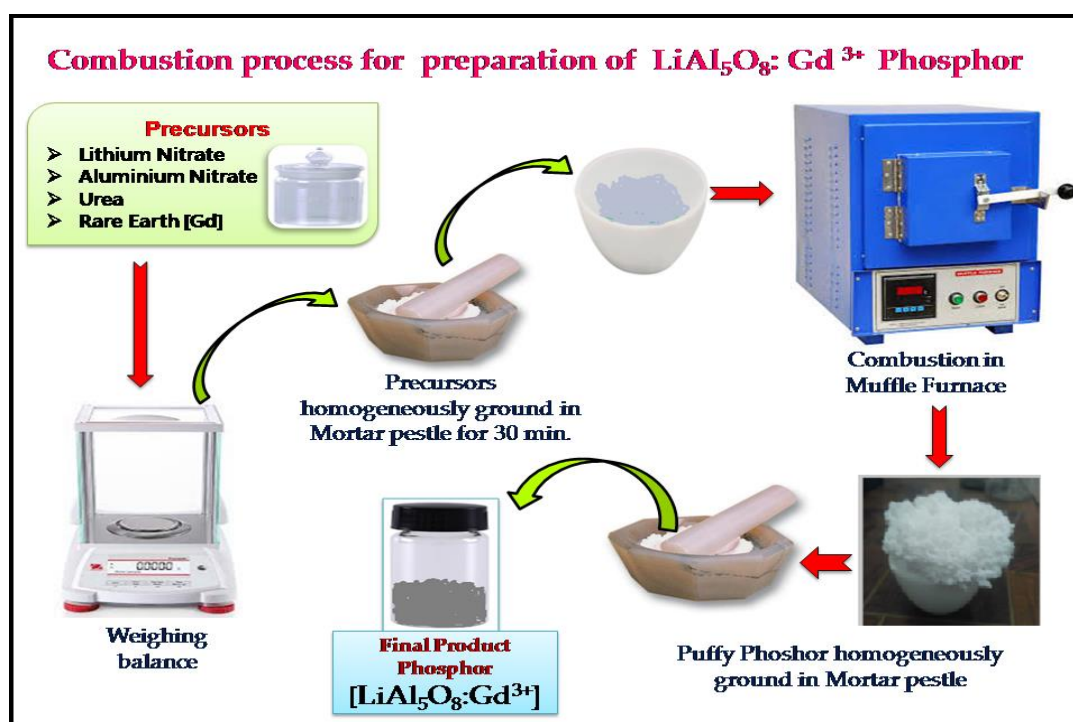


Fig.1| Combustion process for pristine Gd³⁺ doped LiAl₅O₈ phosphor

All of the raw materials, including LiNO₃.H₂O (A.R.99.99%), Al(NO₃)₃.9H₂O (A.R.99.99 %), Urea (A.R.99.99 %) and Gadolinium oxide (Gd₂O₃) (A.R.99.99 %) are purchased from the Sigma Aldrich Company. To manufacture a series of LiAl₅O₈: xGd³⁺ precursors (x = 0.2, 0.4, 0.5, 1, 2, 5 mol%), the stoichiometric amount of raw materials is used. To increase homogeneity, the precursors were put in agate mortar and ground for 30 minutes. The solution was then poured into a china dish, placed in a muffle furnace, and allowed to burn for 30 minutes at 500 °C. After allowing it to cool, the final result was crushed for a few minutes using a mortar and pestle. Additional characterization was carried out using the resultant powder. Fig.1 shows that the production process for pristine Gd³⁺ doped LiAl₅O₈ phosphor schematically.

III. MATERIAL CHARACTERIZATION

The crystal structure was examined using Cu K α radiation and Powder X-Ray Diffraction (Rigaku D-MaxC) in the 2 θ = 10°–90° range. SEM and EDAX techniques were used to investigate the particle size, surface morphology and elemental mapping. A Hitachi F-7100 FL spectrophotometer fitted with a 450 W Xe lamp as

the excitation source was used to obtain photoluminescence spectra for the excitation and emission of the sample phosphor at room temperature.

IV. RESULTS AND DISCUSSIONS

4.1. X-Ray diffraction Studies

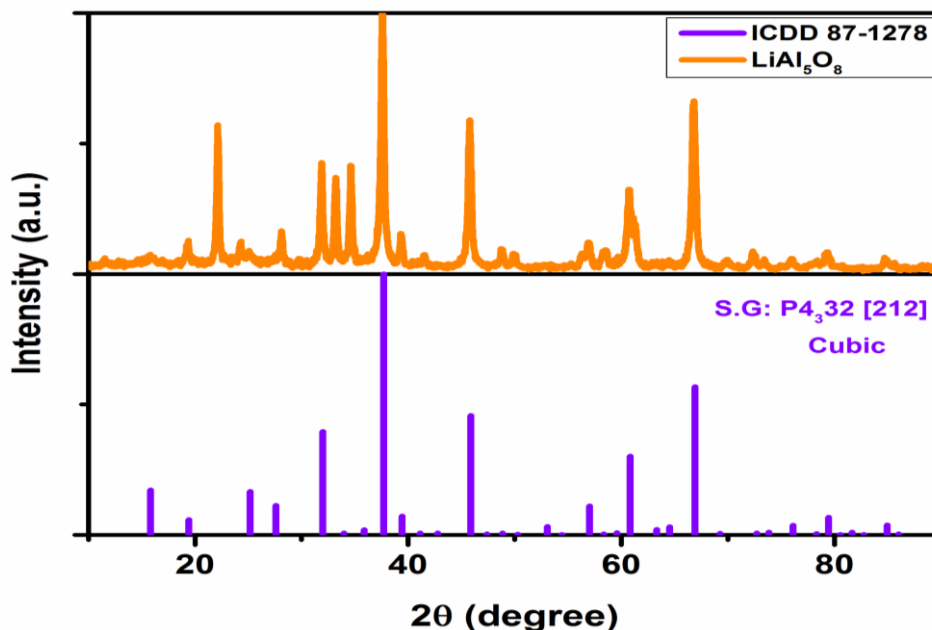


Fig.2 | XRD pattern of LiAl_5O_8

The XRD pattern of the prepared sample which is displayed in Fig.2, closely matches with ICDD data 87-1278. LiAl_5O_8 is characterized as the cubic crystal system with space group $P4_332$ (212). Its refined lattice parameters are as follows: $a = 7.908 \text{ \AA}$, $b = 7.908 \text{ \AA}$, $c = 7.908$, $\alpha = \beta = \gamma = 90.0000^\circ$, and unit cell volume = 494.538356 \AA^3 []. By matching the measured diffraction patterns with ICDD 87-1278, the formation of LiAl_5O_8 was confirmed.

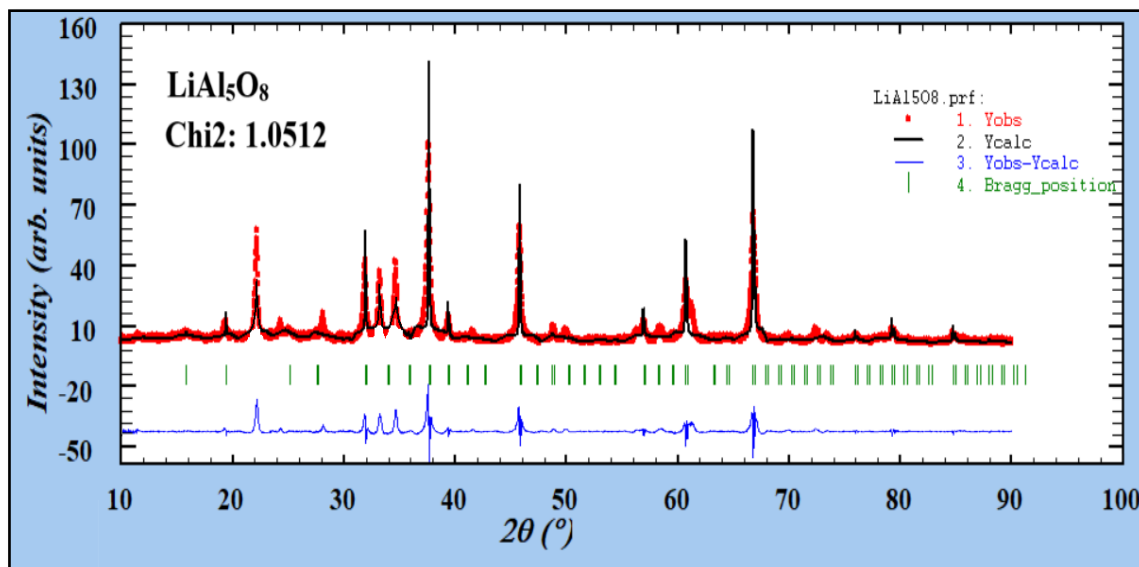


Fig.3 | Refining results of LiAl_5O_8

Enhancing the crystal structure of the prepared sample is the main purpose of Rietveld refining. This popular method of analyzing X-ray diffraction patterns is being utilized more and more to determine a number of factors, including texture, strain and stress, crystalline defect concentration, average domain size and crystallite size distribution and microstructural information. Rietveld Refinement was performed using the FullProf program. The synthesized sample and standard pattern were quantitatively estimated. Fig.3 displays the refining results. The GOF value $\chi^2 = 1.0512$ shows a very good fit to the standard data.

4.2. Crystal Structure

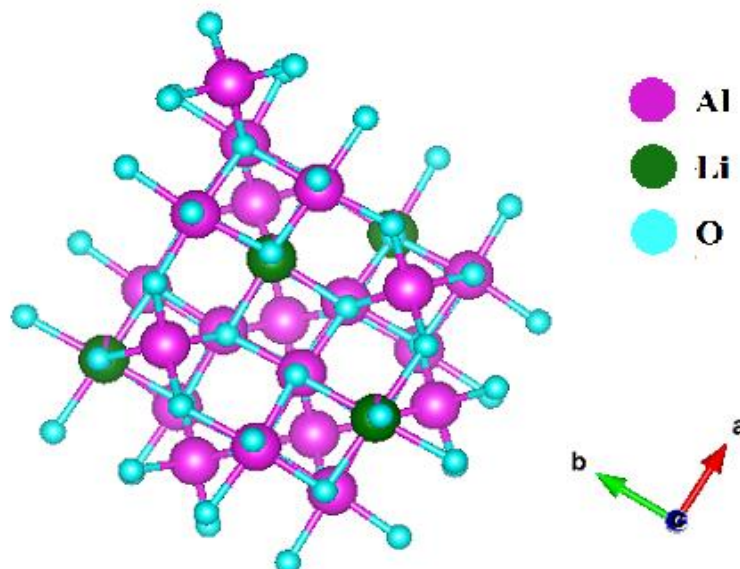


Fig.4 Crystal structure of LiAl₅O₈.

LiAl₅O₈ comes in a variety of forms. The high-temperature equilibrium form (I) is cubic in shape. Li⁺ ions exclusively occupy the distorted octahedral (Li1 and Li2, ideally 4b) sites in a cubic structure, whereas Al³⁺ ions occupy both a tetrahedral and an octahedral (Al2 and Al3, preferably 12d) sites. As seen in Fig. 4, the synthesized sample has a modified spinel structure with cubic symmetry and the P4332 space group. This structure has two (distorted) octahedral (4b and 12d) and tetrahedral (8c) sites. Li⁺ ions only occupy the distorted octahedral (Li1 and Li2, preferentially 4b site), whereas Al³⁺ ions occupy the tetrahedral (Al1) and octahedral (Al2 and Al3, preferably 12d) sites [].

Table-1. Atomic coordinates for LiAl₅O₈ Phosphor

Atom	Label	x/a	y/b	z/c	Occupancy
Li	Li1	0.62500	0.62500	0.62500	0.95700
Li	Li2	0.36860	-0.11860	0.12500	0.01300
Al	Al1	-0.00250	-0.00250	-0.00250	1.00000
Al	Al2	0.62500	0.62500	0.62500	0.04200
Al	Al3	0.36860	-0.11860	0.12500	0.98600
O	O1	0.11460	0.13290	0.38470	1.00000
O	O2	0.38590	0.38590	0.38590	1.00000

4.3. SEM, EDS and Elemental mapping

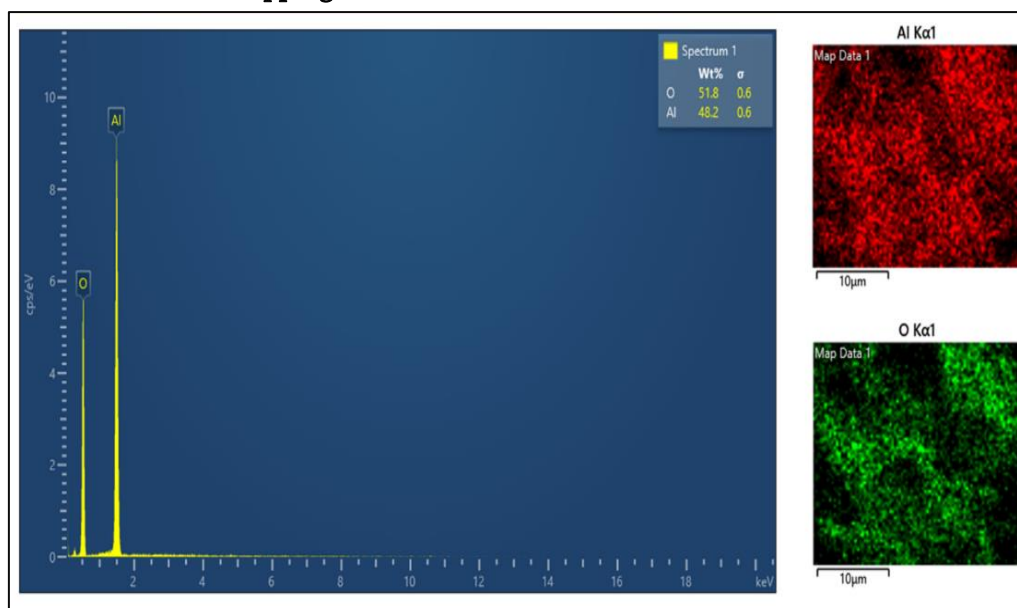


Fig.5| EDS spectra and Elemental mapping of pristine LiAl5O8.

The elemental mapping of composition shown in Fig.5 and EDS spectra, in addition to XRD, confirm the production of a pure LiAl5O8 matrix. The relative atomic percentages of an element found in EDS spectra closely similar to the LiAl5O8 chemical formula. In order to the elemental mapping that was carried out that every element is dispersed evenly and equally. Result indicates that a simple one-step combustion synthesis process is used to create the pure LiAl5O8 compound.

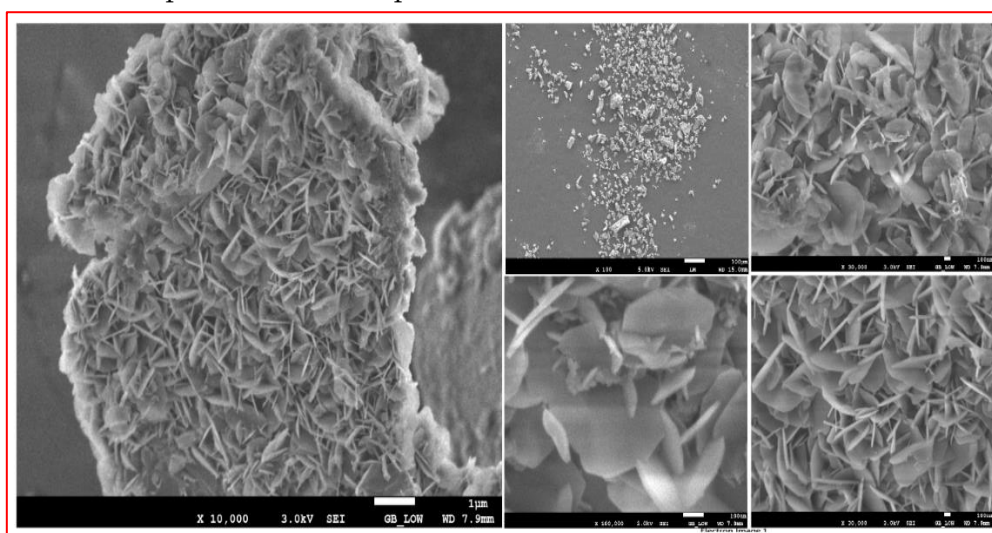


Fig.6 | Typical SEM micrograph of LiAl5O8.

The FESEM was used to examine the surface morphology of the prepared LiAl5O8 phosphor. The compound as synthesized was shown in a typical SEM micrograph in Fig. 6. SEM shows that the regular rod-shaped particles and revealed the formation of a pure phase.

4.4. Photoluminescence of Gd³⁺ doped LiAl₅O₈ phosphor

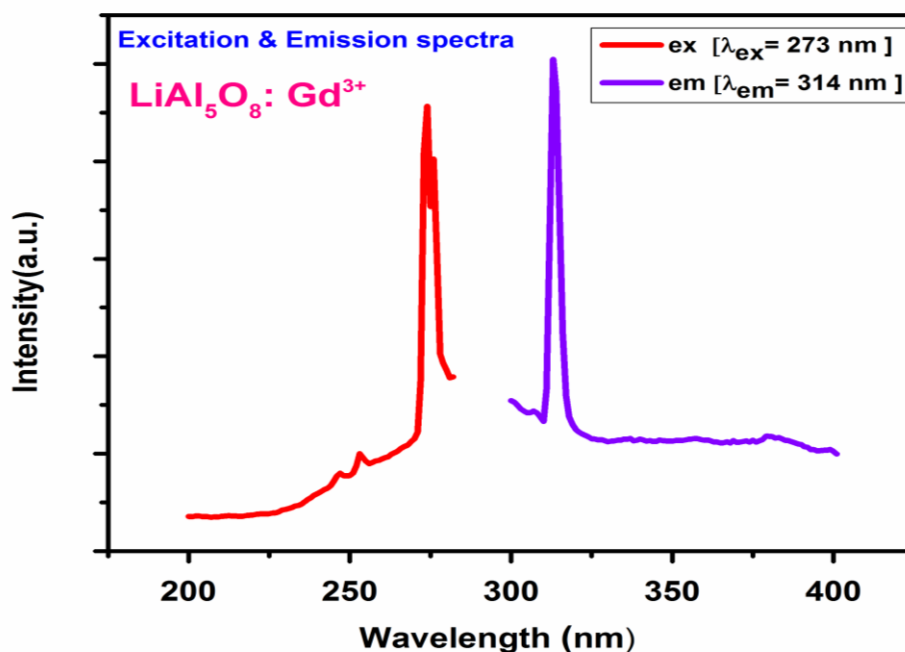


Fig.7 | PL and PLE spectra of LiAl₅O₈: Gd³⁺

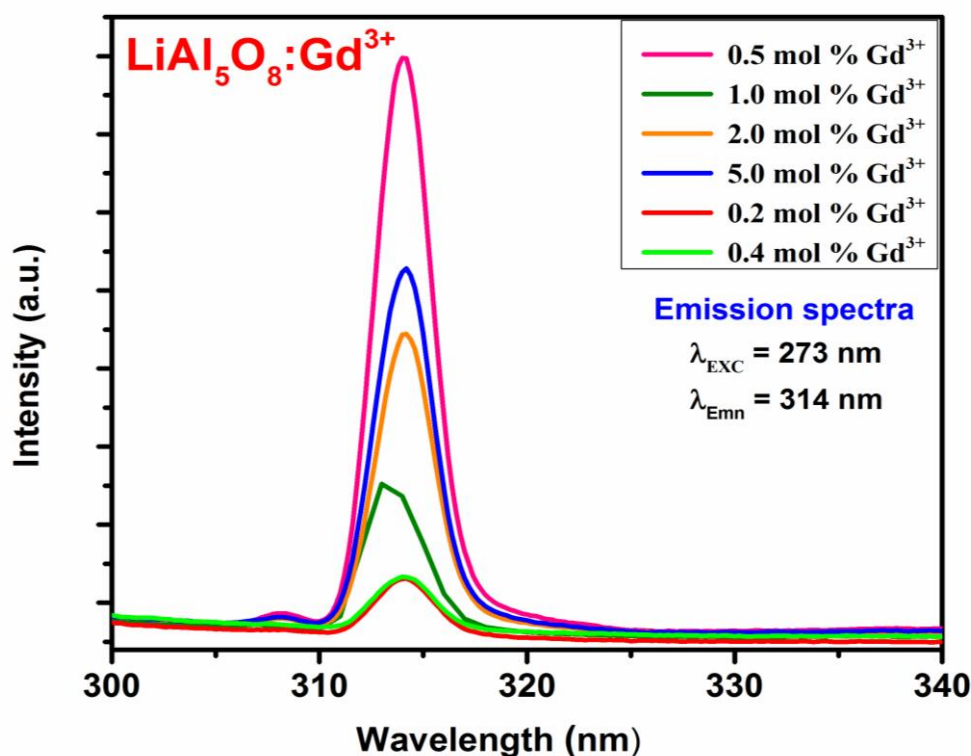


Fig.8| Emission spectra of Quenching in Gd³⁺ activated LiAl₅O₈.

Fig.7 display that the LiAl₅O₈: Gd³⁺ PL and PLE spectra. With a 273 nm excitation, 314 nm emission is seen. Also Fig.8 represents the quenching of several moles % of Gd³⁺ with LiAl₅O₈ at a wavelength of 314 nm. With reference to its magnetic properties resulting from seven unpaired electrons, energy level structure with a huge gap between the ground state and the first excited state the Gd³⁺ ion is a notable lanthanide for a few

specific applications []. The Gd³⁺ ion possesses highly unusual PL characteristics that are independent of host characteristics. Many spectroscopic terms are created when 7 electrons are present in 4f. In addition, the energy involved in the 6P_{7/2} → 8S_{7/2} transition is extremely high and inapplicable to the phonon production process. Consequently, the Gd³⁺ ion must either produce a UV photon or transfer its energy to the closest luminescence center once it gets into the 6P_{7/2} energy state. Along with the Gd³⁺ series, Gd-Gd ion separation is an essential aspect of energy migration.

4.5. Lifetime measurements of LiAl₅O₈: Gd³⁺ phosphor

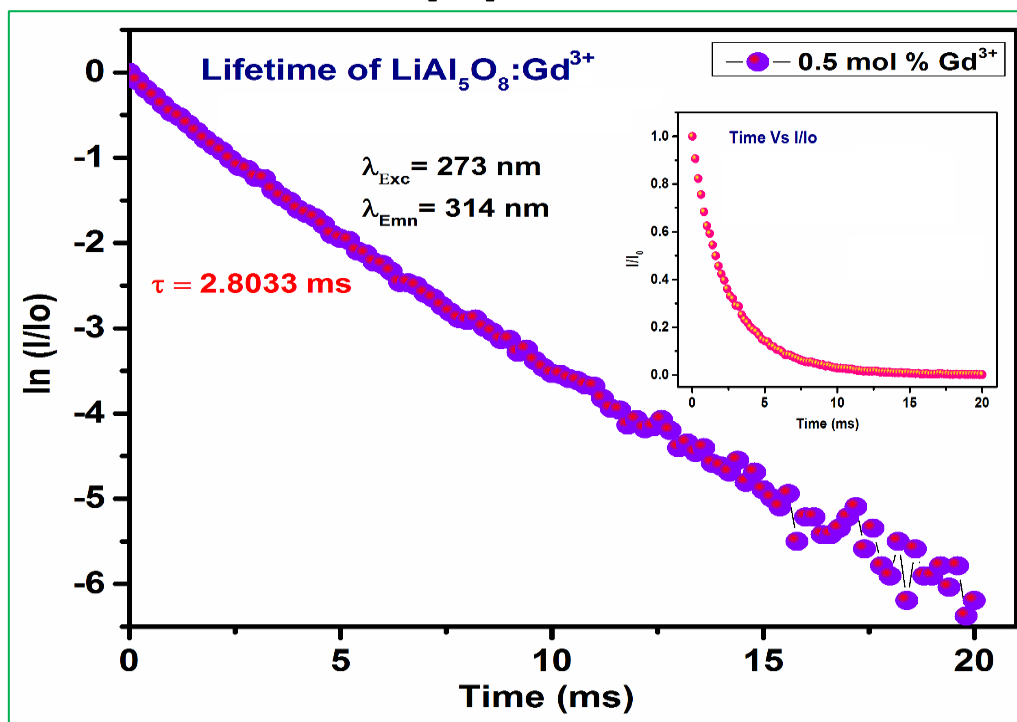


Fig.9 Lifetime measurements of Gd³⁺ activated LiAl₅O₈ phosphor..

Additionally, the lifetime measurements were carried out by applying emission data that was intense enough for this purpose. For 0.5 mol % Gd³⁺, the lifespan was found to be 2.8033 ms (Fig.9). The Gd³⁺ → Gd³⁺ energy transfer causes decay to accelerate at this concentration.

The average lifespan is calculated using the following formula:

$$\tau = \frac{\int t \times i(t) dt}{\int i(t) dt}$$

Where as τ correspond to the average lifetime, t is time and i is the intensity counts.

V. CONCLUSION

A series of LiAl₅O₈:Gd³⁺ phosphor is prepared by using one step solution combustion process. By using muffle furnace in few minutes synthesis process a pure phase phosphor produced at 500°C. XRD, Rietveld luminescent studies of LiAl₅O₈:Gd³⁺ phosphor samples are conducted and the results are thoroughly explained. Refinement, EDS and elemental mapping verify the formation of a pure phase phosphor. The significant emission in the photoluminescence spectra of the LiAl₅O₈:Gd³⁺ phosphor was found at approximately 314 nm. The LiAl₅O₈:Gd³⁺ phosphor is anticipated to be a promising option for UV LED. Thus, gadolinium-doped

phosphors with sensitized luminescence display remarkable emission with higher emission intensity and are better suited for application in phototherapy lamps.

VI. REFERENCES

- [1]. Gai, Shili, et al. "Recent progress in rare earth micro/nanocrystals: soft chemical synthesis, luminescent properties, and biomedical applications." *Chemical reviews* 114.4 (2014): 2343-2389, <https://doi.org/10.1021/cr4001594>
- [2]. Singh, Vijay, et al. "Investigation of ultraviolet emitting Gd³⁺ doped Sr₂MgSi₂O₇ phosphors." *Optik* 169 (2018): 397-402, <https://doi.org/10.1016/j.ijleo.2018.05.036>
- [3]. Yang, Dongmei, et al. "Size and shape controllable synthesis and luminescent properties of BaGdF₅: Ce³⁺/Ln³⁺ (Ln= Sm, Dy, Eu, Tb) nano/submicrocrystals by a facile hydrothermal process." *Nanoscale* 3.6 (2011): 2589-2595, <https://doi.org/10.1039/C1NR10203F>
- [4]. Singh, Vijay, et al. "Luminescence and electron paramagnetic resonance investigation on ultraviolet emitting Gd doped MgAl₂O₄ phosphors." *Journal of luminescence* 143 (2013): 162-168, <https://doi.org/10.1016/j.jlumin.2013.03.054>
- [5]. Silva, Ariosvaldo JS, et al. "X-ray excited optical luminescence changes induced by excess/deficiency lithium ions in rare earth doped LiAl₅O₈." *Journal of Luminescence* 199 (2018): 298-301, <https://doi.org/10.1016/j.jlumin.2018.03.066>
- [6]. Silva, Ariosvaldo JS, et al. "X-ray excited optical luminescence changes induced by excess/deficiency lithium ions in rare earth doped LiAl₅O₈." *Journal of Luminescence* 199 (2018): 298-301, <https://doi.org/10.1016/j.jlumin.2018.03.066>
- [7]. Pan, Dongying, et al. "Preparation and characterization of Co²⁺ doped LiAl₅O₈ nano-crystal powders by sol-gel technique." *Materials chemistry and physics* 96.2-3 (2006): 317-320, <https://doi.org/10.1016/j.matchemphys.2005.07.020>
- [8]. Silva, Ariosvaldo JS, et al. "Non-stoichiometric Ce-doped LiAl₅O₈ phosphors: Synthesis, structural and optical properties." *Ceramics International* 45.15 (2019): 18994-19001, <https://doi.org/10.1016/j.ceramint.2019.06.140>
- [9]. Singh, Vijay, and TK Gundu Rao. "Studies of defects in combustion synthesized europium-doped LiAl₅O₈ red phosphor." *Journal of Solid State Chemistry* 181.6 (2008): 1387-1392, <https://doi.org/10.1016/j.jssc.2008.03.007>
- [10]. Hashimoto, Shinobu, et al. "Self-flux synthesis and photoluminescent properties of LiAl₅O₈." *Materials Research Bulletin* 44.1 (2009): 70-73, <https://doi.org/10.1016/j.materresbull.2008.04.003>
- [11]. Kutty, T. R. N., and M. Nayak. "Cationic distribution and its influence on the luminescent properties of Fe³⁺ doped LiAl₅O₈ prepared by wet chemical methods." *Journal of alloys and compounds* 269.1-2 (1998): 75-87, [https://doi.org/10.1016/S0925-8388\(98\)00159-5](https://doi.org/10.1016/S0925-8388(98)00159-5)
- [12]. Singh, Vijay, et al. "Electron paramagnetic resonance and photoluminescence studies of ultraviolet-emitting ZnAl₂O₄: Gd³⁺ phosphors." *Journal of Electronic Materials* 44 (2015): 121-128, <https://doi.org/10.1007/s11664-014-3414-9>
- [13]. Khaidukov, N. M., et al. "Specific features of synthesis and luminescence for lithium aluminum spinel LiAl₅O₈ doped with manganese ions." *Russian Journal of Inorganic Chemistry* 67.4 (2022): 547-554. <https://doi.org/10.1134/S003602362204009X>

- [14]. Famery, Roger, et al. "Etude structurale de la forme ordonnée de LiAl_5O_8 ." *Journal of solid state Chemistry* 30.2 (1979): 257-263, [https://doi.org/10.1016/0022-4596\(79\)90107-5](https://doi.org/10.1016/0022-4596(79)90107-5)
- [15]. Brixner, L. H., and G. Blasse. "X-ray excited 6G and lower term emission from the Gd^{3+} ion." *Chemical physics letters* 157.4 (1989): 283-288, [https://doi.org/10.1016/0009-2614\(89\)87248-3](https://doi.org/10.1016/0009-2614(89)87248-3)

Comparative Study of the Effect of a Foreign Particle on Binding Interaction of Chiral Drugs 2BMCA with BSA by Equilibrium Dialysis

Shrikant B. Thakare

Department of Chemistry, Arvindbabu Deshmukh Mahavidyalaya, Bharsingi, Tah Narkhed, Dist. Nagpur, Maharashtra, India

ARTICLE INFO

Article History:

Accepted : 01 Jan 2025

Published : 10 Jan 2025

Publication Issue :

Volume 12, Issue 7

January-February-2025

Page Number :

444-449

ABSTRACT

The present study reported the interaction of carboxamide derivative of amino acids 2-benzamido-4-methylpentanoic acid-2-cyclohexyl carboxamide (2-BMCA) with Bovine Serum Albumin (BSA) by equilibrium dialysis method. The association constant was calculated using the Scatchard Plot and it is found to be 0.5935. Furthermore, the effect of foreign particles i.e. arsenic and mercury on the binding of drugs to BSA was also observed. The binding of 2BMCA with BSA decreases in the presence of foreign particles, however, this decrement was found to be more significant in the case of arsenic than mercury. The value of the association constant of the compound 2BMCA in the presence of arsenic decreases up to 12% to 16% while in the presence of mercury it up to 9% to 12%.

Keywords: Equilibrium dialysis, protein-drug binding, Scatchard analysis, BSA, foreign particles, arsenic, mercury

I. INTRODUCTION

The transportation of drugs is one of the important characteristics of blood. Drugs are transported by binding them with protein while this binding is made in blood plasma. Chirality is an intrinsic property of the drug. Chiral drugs show several applications in day-to-day life as well as in commercial areas like clinical, medical, and pharmaceutical industries as well as in some metabolic activities of humans. In drug transportation, the HSA plays a vital role; HSA is one of the major proteins in the blood. Therefore changes in the level of the HSA in plasma during physiological and pathological conditions have a profound effect on drug deposition and pharmacological activities. The HSA and BSA exhibit similar chemical properties due to a high percentage of sequence identities. BSA instead of the HSA used in this study due to its economical aspect and easy availability.

Various analytical techniques are available which show their importance in the field of drug analysis and binding of the drug with the protein such as equilibrium dialysis [1], thin layer chromatography [2], nuclear magnetic resonance [3], fluorescence spectrophotometry [4], capillary electrophoresis [5], mass spectrophotometry [6], etc. This study demonstrated the protein-drug interaction using equilibrium dialysis. Equilibrium dialysis is the most widely used technique for the determination of the binding affinity of various drugs with plasma protein. The binding affinity of widely used drugs was deliberated using the equilibrium dialysis method. Ahmed AyurRahman et al deliberated this technique in determining the binding site for propranolol hydrochloride on bovine serum albumin using direct and reverse methods [7]. Influence of interaction of Metmorphyn Hydrochloride with Levofloxacin on protein binding premeditated by Aninda Kumar Nath et al [8]. MashiurRahman et al made an interface study of Palmitic acid with metoprolol succinate at the binding site of bovine serum albumin by equilibrium dialysis [9]. Shazid Md. Sharker et al studied and characterized the binding site for amitriptyline on bovine serum albumin using the equilibrium dialysis method [10]. Joyshree Das et al. determined the interaction of verapamil hydrochloride with magnesium sulfate [11]. S.M. MahbulalAlam et al observed the binding parameter of chloramphenicol under physiological conditions on bovine serum albumin [12]. FerdosiKabir et al deliberated the consequences of the interaction of palmitic acid with losartan potassium at the binding location of bovine serum albumin [13]. Manjula Devi et al observed the effect of NSAIDson the binding of Warfarin and Duloxetine to bovine serum albumin by the equilibrium dialysis method [14].

The present study reported the synthesis of carboxamide derivatives of amino acids 2-BMCA in the laboratory by a known method [15]. Synthesized compounds characterized by IR, ¹H NMR, and Mass spectroscopy. The compound shows antibacterial activity. As the drugs are acidic they show an affinity for the BSA therefore the binding affinity of drugs with BSA is calculated using the equilibrium dialysis technique. Furthermore, the effect of foreign particles on the binding of the drugs with BSA was also studied.

II. MATERIALS AND METHODS:

For synthesis, all the chemicals used are of A.R. grade of Merck India Limited and purchased from commercial suppliers. Dialysis membrane (Sigma Aldrich Ltd. Sweden), Bovine Serum Albumin-Mr = 66,500 (Chemsworth chemical Ltd. India) used. Drugs synthesized in the laboratory. 0.1M basic buffer of pH 7.4 was used. U.V. Visible Spectrophotometer Shimadzu Singapore (Model UV 180) used for measurement of absorbance value.

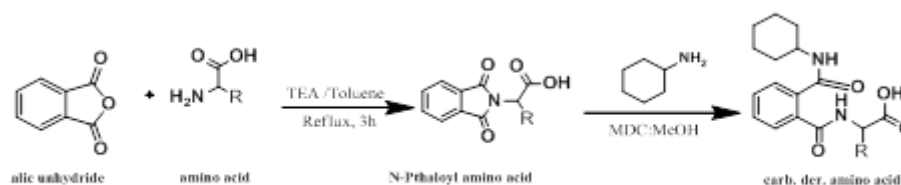


Figure 1:- Scheme for the synthesis of Carboxamide derivatives of amino acids

Where, R= $-\text{CH}_2-\text{CH}-(\text{CH}_3)_2$

The purity of the synthesized compounds was ascertained by thin-layer chromatography on silica gel G in petroleum ether and ethyl acetate (7:3) mixture, Melting point was recorded using digital melting point apparatus Equiptronics (EQ 730). IR spectrum recorded on Bruker alpha IR Spectrometer (Germany). ¹H NMR

spectra of the compound recorded in CDCl_3 on Bruker advance II instrument (500MHz) using TMS as an internal standard from SAIF, CDRI Lucknow.

Measurement of binding affinity:

The experiment was performed in three stages, in the first step binding of the 2BMCA with the BSA was determined in the absence of any foreign particle. For that BSA solution of $50\mu\text{M}$ was prepared in a basic buffer of pH 7.4 This BSA solution was taken in six test tubes in equal quantities. 2BMCA solution of varying concentrations 1×10^{-3} , 2×10^{-3} , 3×10^{-3} , 4×10^{-3} , and 5×10^{-3} M was also prepared using a buffer solution. 2BMCA solution in a 1:1 ratio was added to five test tubes containing BSA solution. These solutions were allowed to stand for half an hour and carefully poured into the dialysis membrane. The dialysis membrane kept ready for the experiment after continuous boiling between temperatures 400°C to 500°C in distilled water for 6 hours. The membrane is efficiently tightened from both sides so that there should be no leakage. These membranes were carefully inserted into six conical flasks each containing a 50ml basic buffer of pH 7.4. Each conical flask is blocked with cork and fitted with a mechanical shaker. The solutions were kept for shaking continuously for about 12 hours in a mechanical shaker for complete dialysis. After the dialysis, the bound concentration of 2BMCA was measured on a U.V. spectrophotometer at a wavelength of 520nm.

Effect of Arsenic and Mercury on the binding of 2BMCA with protein

In the second part of the experiment BSA solution of $50\mu\text{M}$ concentration was taken in a six test tube. In these test tubes, 2BMCA solutions of various concentrations 1×10^{-3} , 2×10^{-3} , 3×10^{-3} , 4×10^{-3} , and 5×10^{-3} M in 1:1 proportion were added with BSA. Afterward, 1×10^{-3} M arsenic trioxide solution in buffer solution was also added to the BSA-2BMCA solution. The composition ratio of 3:3:1 was prepared for BSA, drug, and arsenic solutions for each concentration of drug. These solutions were then allowed to stand for half an hour and then poured into the dialysis membrane. After the complete dialysis bound concentration of 2BMCA was calculated on a U.V. spectrophotometer at a wavelength of 520nm. In the third step, a similar procedure was performed in the presence of 1×10^{-3} M Mercuric Nitrate and the bound concentration of 2BMCA was calculated at a wavelength of 520nm.

III. RESULT AND DISCUSSION

Observations for equilibrium dialysis:

After the complete dialysis, the absorbance of the complex solutions is obtained, from these absorbance values of complex solutions of BSA-2BMCA for concentrations 1×10^{-3} , 2×10^{-3} , 3×10^{-3} , 4×10^{-3} , and 5×10^{-3} M, the value of specific binding obtained. The Scatchard plot obtained from specific binding values gives the association constant of the 2BMCA. Figure 2 shows a graph of absorbance and specific binding vs. concentration of the drug 2BMCA. From the Scatchard plot, the value of the association constant of the drugs 2BMCA with BSA is 0.5935.

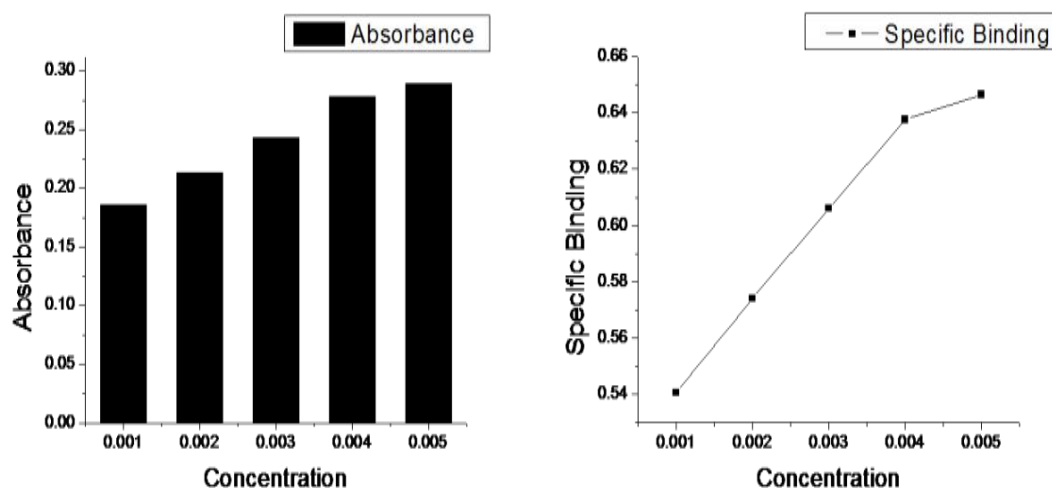


Fig. 2 Graph of absorbance and specific binding Vs concentration of 2BMCA

Effect of foreign particles Arsenic and Mercury:

On completion of dialysis, the absorbance of the complex solutions is obtained. The absorbance values for the complex solution of BSA-2CMBA in the presence of arsenic and mercury at varying concentrations 1×10^{-3} , 2×10^{-3} , 3×10^{-3} , 4×10^{-3} , and 5×10^{-3} M of the drug give the value of specific binding. Scatchard plot for specific binding gives the association constant values for 2BMCA in the presence of arsenic /mercury. The association constant values for 2BMCA are 0.5538 and in the presence of mercury 0.5644. Figure 3 shows the changes in the absorbance and specific binding Vs concentration of the drug in the presence of arsenic and mercury for 2BMCA.

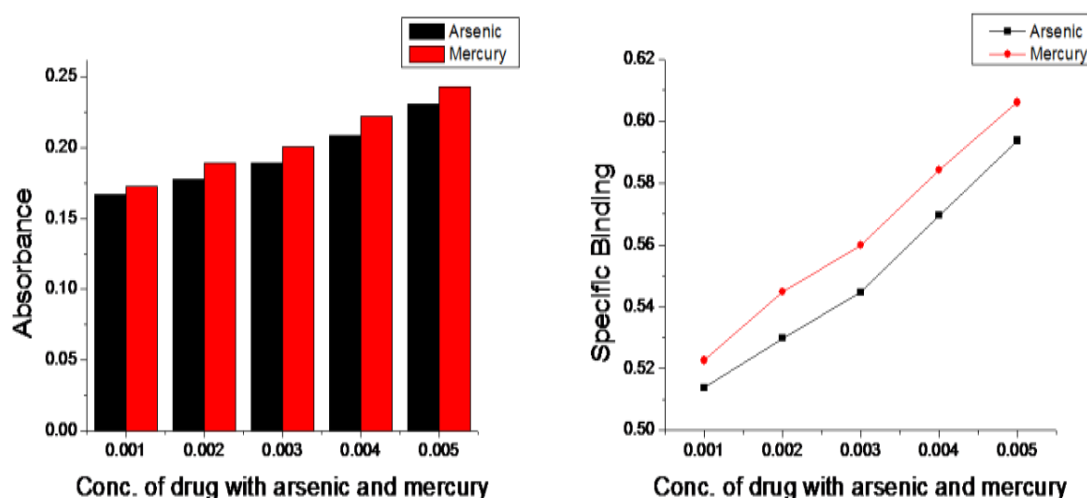


Fig. 3 Graph of absorbance and specific binding Vs concentration of 2BMCA in the presence of arsenic and mercury

IV. CONCLUSION:

Carboxamide derivatives of amino acids viz; 2-benzamido-4-methylpentanoic acid-2-cyclohexyl carboxamide (2-BMCA), show antibacterial activity hence they are considered pharmaceutically active drugs therefore it is a significant aspect to see their affinity towards plasma protein. Association constant values were obtained for

the BSA-2BMCA complex, which may depend on the reactivity of the compound. The association constant for the 2-BMCA with the BSA is 0.5935

The effect of foreign particles on the reactivity and the association constant of the above-mentioned drugs was also studied. It observed that the values of the association constant for the derivative of each amino acid in the absence of foreign particles nearly average between 60% to 65%. However, the association constant for 2BMCA decreases in the presence of foreign particles of arsenic and mercury. A decrease in association constant value is significant in the case of arsenic in comparison with mercury. Decreases in association constant in the presence of arsenic are up to 12% to 16% in an average of all amino acid derivatives. Conversely decrease in association constant value in the presence of mercury is 9% to 12% on average for all amino acid derivatives. The above observation shows that the presence of arsenic and mercury particle both lower the association capacity of amino acid derivatives with BSA but a decrement is more significant in the presence of arsenic in comparison with mercury which concludes that the presence of arsenic particles lowers the reactivity of mentioned drug to a significant extent as compared to the mercury particle.

V. REFERENCES

- [1]. U.Riaz, S.Nadia, Md.Ashraful, Effect of arsenic on paracetamol binding to bovine serum albumin using site specific probes, *International Current Pharmaceutical Journal*. 1(11) (2012) 361-365.
- [2]. R.A.Ahmad, H. J.Roggers, Pharmacokinetics and protein binding interaction of daspone and pyrimethamine, *BCJP*. 10(5)(1980)519-524.
- [3]. L.Fielding, S.Rutherford, D.Fletcher, Determination of protein-ligand Binding affinity by NMR: observations from serum albumin model system, *Magnetic res. Chemistry*. 43 (2005) 463-472.
- [4]. H.J.Yan, Y.O.Yang, Y.Zhang, Y Liu, Affinity and specificity of Ciprofloxacin-BSA interaction, *The Protein Journal*. 29(2010)234- 241.
- [5]. J.C.Kraak, S.Busch, H.Poppe, Protein-drug binding using capillary zone electrophoresis, *Journal of chromatography*. 608 (1992) 257-264.
- [6]. K.J.Pacholarz, R.A.Garlish, R.J.Taylor, P.E.Barran, Mass spectrometry based tools to investigate protein-ligand interactions for drug discovery, *Chem. Soc. Rev.* 41 (2012) 4335-4355.
- [7]. A.A.Rahman, S. Md.Sharke, Determination of the binding sites of propranolol HCl on bovine serum albumin by direct and reverse procedures, *Saudi Pharmaceutical Journal*. 17 (2009) 249-253.
- [8]. A.Nath, J.Anowara, Md. Z. Uddin, M.Dutta, S.Chowdhury, D.Saha, M. Md.Morshed, In vitro Interaction of Metformin Hydrochloride with Levofloxacin and its Influence on Protein Binding, *Bangladesh Pharmaceutical Journal*. 14 (2011) 121-125.
- [9]. M.Rahman, F.Prianka, M.Shohel, Md. A.Mazid, Interaction of Palmitic Acid with Metoprolol Succinate at the binding sites of Bovine Serum Albumin, *Advance Pharmaceutical Bulletin*. 4 (2014) 1-5.
- [10]. Md. S. Shajid, A.R. Ahmad, A.Md. Alam, Identification and Characterization of the binding site of Amitriptyline on Bovine Serum Albumin, *Insight Pharmaceutical Chemistry*. 1 (2011) 24-28.
- [11]. J. Das, N. I. Khan, F.Siraji, R.S.Sharif, M.Ajrin, In-vitro interaction of verapamil hydrochloride with magnesium sulphate (anhydrous) and its influence on protein binding of verapamil hydrochloride, *Journal of applied Pharmaceutical science*. 1 (2011) 122-126.
- [12]. S.M.Mahabulal, L.Yeasmin, N.M.Reza, A.J.Shilpi, F.Ahmad, J.Akter, Studies of binding parameter of chloramphenicol on bovine serum albumin, *Journal of biological sciences*. 4 (2004) 203-206.

- [13]. A. F.Kabir, K. N.Uddin, A.F.M.Nazmus Sadat, H.Mahboob, Md. A.Mazid, Interaction of palmitic acid with losartan potassium at the binding sites of bovine serum albumin, *Ars Pharm.* 51 (2014) 28-36.
- [14]. A. S.Manjuladevi, K.A.Varghese, S.Sriram, B.Rajalingam, V.Sivasankar, B.Chitra, D.Vidhya, Evaluation of in vitro interactions of warfarin and duloxetine with selected coadministered drugs in bovine serum albumin, *International Journal of Pharmacy and Pharmaceutical Sciences.* 3 (2011) 196-199.
- [15]. S.V.Pande, P.S.Utale, S.B.Gholse, P.V.Tekade, and S.G.Patil, Synthesis and antibacterial evaluation of carboxamide derivatives of amino acids, *J.Pharmaceutical Chemistry.* 48 (2014) 29-33.

Synthesis, Characterization and Antimicrobial Activity of Plant Pathogens: A Study of 4,5-Dihydro Isoxazole Derivatives

Shubhangi Y. Deshmukh^{1*}, Mithilesh M. Rathor², Nilesh S. Padole³

¹Research student, VBMV Camp, Amravati 444602, Maharashtra, India

²Head and Professor, Vidya Bharati Mahavidyalaya Camp Amaravati 444602, Maharashtra, India

³Assistant Professor, Vinayak Vidnyan Mahavidyalaya Nandgaon Khandeshwar 444708, Maharashtra, India

ARTICLE INFO

Article History:

Accepted : 01 Jan 2025

Published : 10 Jan 2025

Publication Issue :

Volume 12, Issue 7

January-February-2025

Page Number :

450-455

ABSTRACT

The series of novel substituted phenol derivatives containing isoxazole moieties 2-(5-(substituted)-4,5-dihydroisoxazol-3-yl)-4-methyl-6-nitrophenol and 2-(5-(substituted)-4,5-dihydroisoxazol-3-yl)-4-methylphenol have been designed and synthesized. All the compounds were characterized via elemental analysis, IR, ¹H, ¹³C NMR and FAB-Mass analysis. The antibacterial and antifungal activities of were evaluated against two plant pathogenic bacteria and two plant pathogenic fungi.

Keywords: isoxazole, plant pathogens, chalcones, spectral studies.

I. INTRODUCTION

Heterocyclic nitrogen and oxygen containing compounds have received considerable attention due to their significant bioactivities. During the last decades, intensive efforts have been undertaken to discover the highly active chemicals with favourable toxicological and environmental properties for the selective control of weed, insects and fungal diseaseⁱ. In several instances, dihydro isoxazole derivatives have been found as promising agrochemical products. The isoxazole constitute a fascinating class of five -membered heterocyclic compounds with one nitrogen and one oxygen ring atom. There are also some herbicidally, insecticidally or fungicidally active dihydro isoxazole derivatives known, which have been isolated from natural sources^{ii, iii}. The dihydro isoxazole amino acids acivicin has been isolated from the fermentation broths of streptomyces sviveus and highly active against phytophthora infestans it is causal agent of potato late blight, uncinula necator it is causal agent of grapes powdery mildew and the trehalase inhibiting dihydro isoxazole derivative trehazolin shows potent fungicidal activity against Rhizoctonia solani it is causal agent of rice sheath blight.

Dihydroisoxazole have been widely applied as pharmaceuticals and agrochemicals because of their antifungal activities. Fluralaner, a commercial insecticide, is a successful example that introduces dihydro isoxazole as the scaffold. Many studies have also focused on the antibacterial and antifungal activities of dihydro isoxazole derivatives. Concerning the synthesis of dihydro isoxazoles, the methods with stable and easily accessed starting materials and those conducted under mild conditions are more acceptable. Usually, the sophisticated way to synthesize dihydro isoxazoles is by the cyclization of α,β -unsaturated carbonyl compounds (chalcones) with hydroxylamine. Chalcones can be easily obtained from a simple Claisen–Schmidt reaction. Keeping the above observations in view, we designed new compounds by introducing a 2-chloro benzaldehyde, 3-chloro benzaldehyde and indol-3-carboxyaldehyde structure into a dihydro isoxazole scaffold, which will be expected to exhibit higher fungicidal bactericidal activities through the coexistence of two kinds of pharmacophores.

II. METHODS AND MATERIAL

The chemicals and solvents used were of highest purity purchased commercially from Merck, S.D. Fine and Alfa Aesar Company Ltd. The melting points of all the synthesized compounds were recorded by Thiele's melting point apparatus as uncorrected values. The elemental analysis was carried out on Thermo Scientific CHNS elemental analyser. IR spectra were recorded on a Shimadzu instrument using KBr pellets. ^1H NMR spectra were scanned by Bruker at 400 MHz using DMSO- d_6 as solvent and TMS as an internal reference. ^{13}C NMR spectrum of a sample was recorded on same instrument at 100 MHz. Experimental procedure for synthesis of 2(5-(substituted phenyl)-4,5-dihydroisoxazol-3-yl)-4,6-substituted phenol (5a–5f).

Preparation of p-methylphenyl acetate (1)

Ther-p-cresol was refluxed along with acetic anhydride and anhydrous sodium acetate for an hour. The reaction mixture was cooled and poured into the ice-cold water containing crushed ice. Acetate layer was separated by means of separating funnel and several times washed with water. It was finally purified by distillation and the distillate fraction was collected at about 236°C, to get the compound (1) b.p. 236°C yield: 84.74%.

Preparation of 2-hydroxy-5-methyl acetophenone(2)

p-methyl phenyl acetate (1) was mixed with anhydrous AlCl_3 (1) and heated at 120°C for 45 minutes on an oil bath. The reaction mixture was decomposed in ice cold water containing 10% hydrochloric acid and allowing the solution to fall drop by drop into ice cold water with constant stirring. Green solid compound i. e crude ketone (2) was obtained, m.p. 47°C, yield: 89%.

Preparation of 2-hydroxy-3-nitro-5-methyl acetophenone (3):

2-hydroxy-5-methyl acetophenone (2) was dissolved in acetic anhydride in a beaker and reaction mixture was kept in ice bath by maintain temperature below 5°C. To this reaction mixture conc. HNO_3 was added dropwise with constant stirring till the solution becomes orange coloured and kept for 4-5 hrs. it was then decomposed with ice cold water. Yellow granules obtained were filtered and washed with water and then crystallized from ethanol, m.p. yield: 72%.

Preparation of β -unsaturated chalcones (4a–4f)

In this study, α,β -unsaturated chalcones 1 were synthesized by using a Claisen–Schmidt reaction. To a solution of substituted acetophenone (0.01mol) and substituted aldehyde (0.01mol) in 15ml of ethanol and 40% sodium hydroxide solution added drop by drop. The reaction mixture was continuously stirred on magnetic stirrer at room temperature, up to cake formation followed by decomposition with ice cold HCl (1:1). The crude

Chalcones precipitate out were filtered, washed with 10% NaHCO₃ solution and then recrystallized from ethanol to obtained compounds (4a-f).

Preparation of 2(5-(substituted phenyl)-4,5-dihydroisoxazol-3-yl)-4,6-substituted phenol (5a-5f)

To a solution of chalcones (0.01 mol) and hydroxylamine hydrochloride (0.02mol) was reflux in 30 mL of ethanol and piperidine (0.5ml) for about 1.5 hrs. Subsequently, the reaction mixture was cooled and poured onto crushed ice acidified with dil.HCl, and then formed solids was collected and washed first with sodium bicarbonate solution (10%) and then with water to obtain crude products of 5a-5f.

SCHEME: -

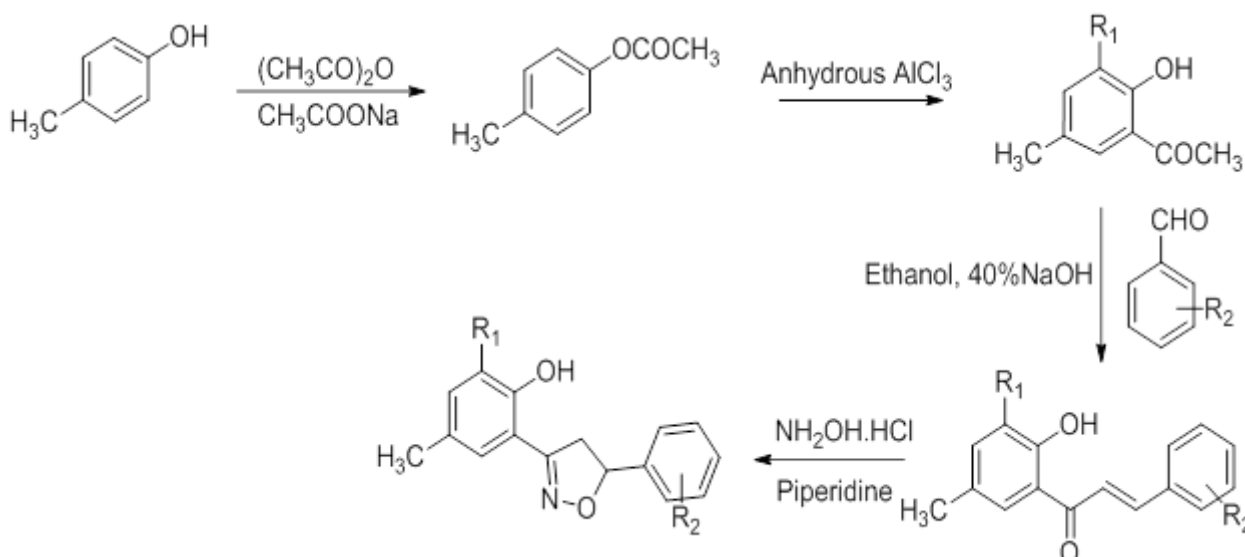


Table 1: Physical and analytical data of Compounds.

Compounds	Mol. Formula	Colour	M.P.	C%	H%	N%	Cl%
				Found/ Calculated			
5a	C ₁₆ H ₁₄ ClNO ₂	Pale yellow	101°C	66.77/66.79	4.60/4.90	4.80/4.87	12.00/12.32
5b	C ₁₆ H ₁₄ ClNO ₂	Pale yellow	122°C	66.77/66.79	4.60/4.90	4.80/4.87	12.00/12.32
5c	C ₁₈ H ₁₆ N ₂ O ₂	Pale yellow	132°C	73.90/73.95	5.60/5.52	9.48/9.58	-
5d	C ₁₆ H ₁₃ ClN ₂ O ₄	Dark red	122°C	57.73/57.76	3.91/3.94	8.39/8.42	10.62/10.65
5e	C ₁₆ H ₁₃ ClN ₂ O ₄	Dark red	119°C	57.73/57.76	3.91/3.94	8.39/8.42	10.62/10.65
5f	C ₁₈ H ₁₅ N ₃ O ₄	Yellow	95°C	64.04/64.09	4.42/4.48	12.46	-

5b: IR(KBr, cm⁻¹): 3350(Hydrogen bonded -OH), 3743.83(-C=N stretching), 3082.25(-C-H stretch in aromatic), 2926.01 (-C-H aliphatic), 1577.77 (-C=N- stretching), 1083.99 (-C-O stretching), 906.54 (-N-O stretching isoxazole), 786.96 (-C-Cl stretching) ; **¹H-NMR(CDCl₃):** δ 2.39 (s, 3H, CH₃), 2.47 (s, 3H, SCH₃).

5d: IR(KBr, cm⁻¹):3741.90 (Hydrogen bonded -OH), 3743.83(-C=N stretching), 3068.75 (-C-H stretch in aromatic), 2926.01 (-C-H aliphatic), 1686.64 (-C=N- stretching), 1539.20 (-NO₂ stretching (asymmetric)), 1473.62 (-C=C- stretching), 1045.42 (-C-O stretching), 906.54 (-N-O stretching isoxazole), 752.24 (-C-Cl stretching) ; **¹H-NMR(CDCl₃):** δ 8.0 (d,1H, Ar-H), 7.2 (d,1H, Ar-H), 4.89 (s, 1H, Phenolic -OH), 2.5 (s, 3H, -CH₃), 7.3-7.5 (m, 4H, Ar-H).

5f: IR(KBr, cm⁻¹):3741.90 (Hydrogen bonded -OH), 3743.83(-C=N stretching), 3080.32 (-C-H stretch in aromatic), 2926.01 (-C-H aliphatic), 1686.64 (-C=N- stretching), 3221.12 (-N-H stretching in aromatic)1535.34 (-NO₂ stretching (asymmetric)), 1473.62 (-C=C- stretching),; **1-HNMR(CDCl₃):** δ 6.9 (d,1H, Ar-H), 7.2 (d,1H, Ar-H), 4.7(s, 1H, Phenolic -OH), 2.5 (s, 3H, -CH₃), 7.3-7.5 (m, 4H, Ar-Indol),8.1 (d,1H,Ar-H), 7.8 (s,1H, N-H).

Antimicrobial Activity in vitro

As shown in table 2 given below , preliminary determination of the inhibition activities of title compounds (100 $\mu\text{g}\cdot\text{mL}^{-1}$) against plant-pathogenic bacteria and fungi (Pseudomonas, Xanthomonas, Cercospora and Cadophora) suggested that all of the compounds showed significant antibacterial and antifungal activities against plant-pathogenic bacteria and fungi, with an inhibition rate higher than 50%. Among the tested bacteria and fungi, Pseudomonas and Cadophora were completely inhibited by half of the tested compounds with an inhibition rate higher than 90%. It was obvious that these derivatives are particularly efficient against the mycelia growth of Pseudomonas and Cadophora in vitro.

Table 2. Antifungal activities of titled compounds at 100 $\mu\text{g}\cdot\text{mL}^{-1}$ in vitro

Compounds	Bacteria		Fungi	
	Pseudomonas	Xanthomonas	Cercospora	Cadophora
5a	97.95	75.29	69.56	93.25
5b	96.01	69.27	56.28	94.34
5c	94.37	70.35	73.59	93.25
5d	93.25	55.15	78.29	91.15
5e	93.25	80.22	65.22	90.79
5f	93.25	62.79	57.54	93.25
Thiabendazole	91.20	60.23	65.45	90.32
Azoxystrobin	87.65	72.36	57.61	89.54

Among newly synthesized compounds, 5a and 5b showed more potential bioactivities against Pseudomonas than those of thiabendazole and azoxystrobin. Meanwhile, 5a,5b,5c,5d,5e and 5f and showed higher fungicidal activities against cadophora. Surprisingly, the compounds containing a chlorine atom (5a,5b,5d and 5e) displayed excellent antifungal activities, even higher than commercial fungicides (thiabendazole and azoxystrobin). Therefore, the fungicidal activities of the title compounds closely depended on the core structure, substituent groups, and substituent positions. Among the tested fungi, cadophora is a serious pathogenic fungus on gram and other cereals, and Cercospora is a harmful fungus on soyabean, various vegetables and crops worldwide. All the tested novel compounds have strongly effective for bacteria Xanthomonas. The title compounds showed significantly antifungal activities against these notorious fungi, suggesting that novel compounds have potential and should undergo further evaluation in vivo or in the field. In the present study, the 4,5-dihydro isoxazole derivatives showed significant antibacterial and antifungal activities against the tested bacteria and fungi, and approximately half of the title compounds exhibited higher inhibitory activities.

III.CONCLUSION: -

The series of novel 4,5-dihydro isoxazole compounds derived from p-cresol were designed and synthesized and were characterized via ¹H-NMR, ¹³C-NMR, and HRMS. Results of the preliminary biological activity assay indicated that most of the title compounds showed potential antibacterial and antifungal activities against

Pseudomonas, *Xanthomonas*, *Cercospora* and *Cadophora*. Compound 5a and 5b, displaying significant bactericidal and fungicidal activities against bacteria *Pseudomonas* and fungus *Cadophora* are worth being further evaluated in vivo and in the field. Further optimizations of 4,5 dihydro isoxazole derivatives should be carried out to develop more effective antibacterial and antifungal activities.

Acknowledgements

Authors thanks VBMV Amravati, for research facility. The IR spectra were recorded at CIC, Shri. Shivaji Science College Amravati. The NMR spectra were recorded at SAIF, Panjab University, Chandigarh.

IV. REFERENCES

- [1]. Kumar, K. A.; Govindaraju, M.; Renuka, N.; Kumar, G. V. *J Chem Pharm Res* 2015, 7, 250.
- [2]. Galenko, A. V.; Khlebnikov, A. F.; Novikov, M. S.; Pakalnis, V. V.; Rostovskii, N. V. *Russ Chem Rev* 2015, 84, 335.
- [3]. Bansal, S.; Halve, A. K. *Int J Pharm Sci Res* 2014, 5, 4601.
- [4]. Kumar, K. A.; Govindaraju, M.; Renuka, N.; Kumar, G. V. *J Chem Pharm Res* 2015, 7, 250.
- [5]. Beccalli, E. M.; Pocar, D.; Zoni, C. *Targets Heterocycl Systems* 2003, 7, 31.
- [6]. Rajasekhar, S.; Maiti, B.; Chanda, K. *Synlett* 2017, 28, 521
- [7]. Whittingham, W. G. In *Bioactive Carboxylic Compound Classes: Pharmaceuticals and Agrochemicals* Lamberth, C.; Dinges, J. Eds.; Wiley-VCH: Weinheim, 2016, pp 325–337. 8
- [8]. Ahrens, H.; Lange, G.; Müller, T.; Rosinger, C.; Willms, L.; van Almsick, A. *Angew. Chem. Int. Ed.* 2013, 52, 9388.
- [9]. Witschel, M. In *Bioactive Heterocyclic Compound Classes: Agrochemicals* Lamberth, C.; Dinges, J. Eds.; Wiley-VCH: Weinheim, 2012, pp 61–68
- [10]. Shastri, R. A. *Chem Sci Trans* 2016, 5, 8.
- [11]. Singh, S.; Veeraswamy, G.; Bhattarai, D.; Goo, J.-I.; Lee, K.; Choi, Y. *Asian J Org Chem* 2015, 4, 1338.
- [12]. S.Y. Deshmukh, N.S. Padole, M.P. Wadekar, M.A. Chaudhari; *Journal of Chemical and Pharmaceutical Research*, 13(7):01-06 (2021).
- [13]. S.Y. Hassan: *Molecules* 18; 2683-2711 (2013)
- [14]. K.P. Kakade, S. P. Kakade and S Y. Deshmukh, *world journal of pharmacy and pharmaceutical science*, 4,1,1591-1597 (2014).
- [15]. T.D Svejstrup, W. Zawodny, J.J. Dawglus, D. Bidgel, 12302-12305 (2016) i, N. S. Sheikh and D Leoneri; *Chem commun (comb.)* 52.
- [16]. Shubhangi Y. Deshmukh, Nilesh S. Padole; *JETIR* ,9(2),794-801(2022)
- [17]. M.P. Sadashiva, K. Mantelingu, S. N. Swamy and K. S. Rangappa; *Bioorg. Med. Chem* 11, 4539-4544 (2003).
- [18]. R.Y. Deshmukh, S.Y. Deshmukh, K.P. Kakde and P. A. fandi; *International Journal of advance innovative research*; 2017, 4(10)
- [19]. A. Sid, A. Messai, C. Parlak, N. Kazancı, D. Luneau, G. Keşan, L. Rhyman, I. A. Alswaidan and P. Ramasami: *J. Mol. Struct.* 121, 46–53 (2016). 10) L. A. Tompson and J. A. Ellman: *Chem. Rev.* 96, 555–600 (1996).
- [20]. A. Sid, K. Lamara, M. Mokhtari, N. Ziani and P. Mosset: *Eur. J. Chem.* 2, 311–313 (2011).
- [21]. V. N. Pathak, R. Joshi, J. Sharma, N. Gupta and V. M. Rao: *Phosphorus Sulfur.* 184, 1854–1865 (2009).
- [22]. Shubhangi Y Deshmukh, *IJFMR*, 23-212, 1-6, (2023).

- [23]. S.B. Jadhao, R.A.Shastri, K.V.Gaikawad and S.V. Gaikwad E-J.Chem,6, S183-S188 (2009).
- [24]. M. Johnson, B. Younglove, L.Lee, R. Leblanck, H. volt Biorganic medical chemistry letter, 17, 5897-1901(2007).
-

Viscosity and Density Evaluation Of [(2z, 4z) -2-(Ethylimino)-N-(4-Methoxy-3, 5-Dimethylpyridin-2-Yl) Methyl)-4-Phenylimino)]-4h-1, 3, 5-Dithiazin-6-Amine in Ethanol-Water Mixture

S.S. Padhen¹, P.C. Sawarkar^{1*}, S.P. Gahukar¹, D. B. Dupare²

¹Department of Chemistry, Rajarshree Shahu Science College Chandur Railway, Dist.-Amravati, 444 904, Maharashtra, India

²Shri Dr. R.G. Rathod Arts and Science College, Murtizapur Di-Akola, Maharashtra, India

ARTICLE INFO

Article History:

Accepted : 01 Jan 2025

Published : 10 Jan 2025

Publication Issue :

Volume 12, Issue 7

January-February-2025

Page Number :

456-460

ABSTRACT

Heterocyclic compounds based on pyridines, especially those with a 1,3,5-dithiazino nucleus, are remarkable for their numerous uses in the pharmaceutical, biological, biotechnological, and medicinal domains. Pyridine, a six-membered heteroaromatic ring, is a crucial part of many natural substances, including vitamins and alkaloids. Its compounds are helpful in the development of novel medications because to their well-known flexibility. Recently, we conducted a viscometric investigation and density evaluation of [(2Z,4Z)-2-(ethylimino)-N-((4-methoxy-3,5-dimethylpyridin-2-yl)methyl)-4-(phenylimino)]-4H-1,3,5-dithiazin-6-amine in our lab. This study's evaluation was conducted at various temperatures while maintaining a consistent concentration. Current drug solute-solvent interactions and the impact of solvent dilution are determined by experimental data. The findings demonstrated that when temperature rises, relative viscosity falls, indicating stronger solvation effects. By providing insightful information about the physicochemical behavior of pyridine derivatives, this study advances pharmacological science and helps create pharmaceutical products that are more potent.

Keywords: Pyridines, Solute-solvent interaction, Temperature Effects, 1,3,5-Dithiazino etc.

I. INTRODUCTION

Many derivatives of pyridine substrates have a variety of biological uses. Because of its pharmacological characteristics, the heterocycle pyridine is widely used in the development of new medications. Anti-

inflammatory, antibacterial, antiviral, anticancer, antioxidant, antihypertensive, antidiabetic, and antimalarial medications are made with pyridine bases. Because pyridine derivatives have a significant affinity for a wide range of ions and neutral species, they can be used as a very effective chemosensor to distinguish diverse species [1]. The biological targets of pyridine nucleus substitutions range from microbial diseases to viral issues and a range of cancerous cells. Pyridine derivatives work with enzymes, proteins, and DNA to address a variety of biological issues [2]. The heterocyclic molecule featuring a 1,3,5-dithiazino nucleus finds extensive applications in medicinal, biochemical, biotechnological, and pharmaceutical sciences [3,4]. Sulfur and nitrogen-containing heterocyclic compounds are necessary for life. These chemicals are vital to many biological systems and activities, and they appear in a variety of ring configurations. Since these rings contain nitrogen and sulfur atoms, which are essential for their biological functions, they have unique chemical properties and reactivity profiles [5,6]. It has been discovered that dithiazines work well to treat cancer. Anti-HIV, anti-helminthic, antifungal, antiviral, antibacterial, and anti-tuberculostatic qualities were also shown by these substances [7,8]. 1,3,5-Dithiazines are effective at preventing copper corrosion and are also used in lubricating oil [9,10]. Measurements of viscosity are important. Viscosity is a fundamental property of liquids that defines their resistance to flow. It measures how resistant a liquid is to its layers shifting relative to one another. This resistance is brought on by internal friction that develops as the liquid's molecules move and interact with one another [11]. Both aqueous and non-aqueous solutions include interactions between the solute and the solvent. This important information is obtained from measurements of viscometrical parameters. A drug's behavior, including absorption, transmission, and effects, will be directly influenced by measurements of its viscosity and interactions with solvents in the human body [12].

Water and alcohol mixes are also interesting systems because of their complex dynamics, which are brought on by the presence of hydrogen bonds and hydrophobic groups. These combinations are also important because of their wide range of applications as solvents, which has led to a great deal of theoretical and experimental study. A liquid's viscosity can be affected by a wide range of parameters, such as temperature, size, molecular weight, intermolecular interactions, and the presence of pollutants. The assessment of viscosity facilitates comprehension of the molecular interactions and properties of binary and ternary liquid systems. Keep in mind that advantageous interactions may cause these systems' viscosity to increase. Evaluating whether a material will float or sink in a liquid requires an understanding of density. More precisely, substances will float in a liquid if their densities are less than its own. Additionally, it is an essential physical property that is used to ascertain the acoustic and physical properties of a substance, such as its surface tension, molar refraction, dipole moment, and boiling temperature [13].

Many pharmacological and biochemical characteristics of pyridine derivatives, such as antiviral, antibacterial, anti-inflammatory, anesthetizing, and mydriatic agents, have been reported in the literature review. The heterocyclic molecule with a 1,3,5-dithiazino nucleus finds widespread application in the disciplines of medicine, biochemistry, biotechnology, and pharmaceuticals [5,6,11]. These compounds have antiviral, antifungal, antibacterial, anti-helminthic, and anti-tuberculostatic properties⁵. Dithiazines have also shown promise in the treatment of cancer.⁷ Given these factors, measuring the viscometric concentration of [(2Z,4Z)-2-(ethylimino)-N-((4-methoxy-3,5-dimethylpyridin-2-yl)methyl)-4-(phenylimino)]-4H-1,3,5-dithiazin-6-amine at various temperatures is quite relevant [4]. All things considered, this kind of research advances the field of drug science and helps create pharmaceutical goods that are more dependable and effective, which eventually improves patient outcomes [5,6,8].

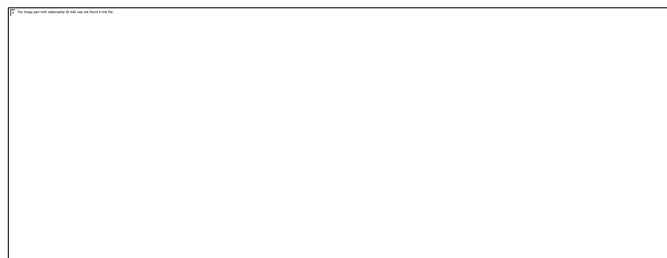


Fig. 1-[(2Z,4Z)-2-(ethylimino)-N-((4-methoxy-3,5-dimethylpyridin-2-yl)methyl)-4-(phenylimino)]-4H-1,3,5-dithiazin-6-amine

II. EXPERIMENTAL

In every study, double-distilled water and analytical grade (A.R.) chemicals were used. The compound weights were measured using a MechanikiZektadyPrecyzyjnej Gdansk balance, which has a precision of ± 0.001 grams. An Ostwald viscometer was utilized to measure the viscosity of liquids while maintaining a steady temperature of 29°C ($\pm 0.1^\circ\text{C}$) with an Elite thermostatic water bath. The density measurements were performed using a bicapillary tube with an internal diameter of 1 mm. The viscometer and water bath were allowed adequate time to reach thermal equilibrium before any measurements were made. (2Z,4Z)-2-(ethylimino)-N-((4-methoxy-3,5-dimethylpyridin-2-yl)methyl)-4-(phenylimino)-4H-1,3,5-dithiazin-6-amine was investigated viscometrically at 0.1M concentration in a 60% ethanol-water system independently at various temperatures in the present study. Newly created solutions were used for the evaluation. Readings of viscometry were acquired in accordance with the literature.

III.OBSERVATIONS AND CALCULATIONS

Molecular interactions are computed in terms of the solute's β -coefficient using the information obtained from our study. The results obtained are shown in Table No. 1. According to Jone's-Dole equation, $(\eta_r - 1)/\sqrt{C} = A + B\sqrt{C}$ for different temperatures and a concentration of 0.1 M. Table No. 2 lists the calculated values of the A and β -coefficients.

TABLE No.1 The Determination of Relative and Specific Viscosities at Different Temperatures at 0.1 Millimeters, As Well As Measurements of Viscosity at Constant Concentrations

MEDIUM - 60% ETHANOL-WATER							
Conc.	Temp. ($^\circ\text{C}$)	\sqrt{C}	Time	Density $\times 10^3$ (kg.cm^{-3})	η_r	$\eta_{sp} = \eta_r - 1$	$(\eta_r - 1)/\sqrt{C}$ ($\text{pa}\cdot\text{s}$)
0.1 M	22	0.314	66	0.8923	0.085421	-0.914588	-2.9127
	24	0.314	54	0.8863	0.081214	-0.918786	-2.9260
	26	0.314	49	0.8576	0.072143	-0.927857	-2.9549
	28	0.314	36	0.8515	0.069125	-0.930875	-2.9645

TABLE No.- 2 The values of A and β for the 60% mixture Coefficient are displayed reference to (2Z,4Z)-2-(Ethylimino)-N-((4-Methoxy-3,5-Dimethylpyridin-2-yl)Methyl)-4 (Phenylimino)-4H-1,3,5-Dithiazin-6-Amine

W-E Mixture (%)	Temp° C	Mean "A"	β (Slope "m")
60	25	-2.9395	0.0061

IV. RESULT AND DISCUSSION

The relative viscosity was calculated using the following formula.

$$\eta_r = D_s \times t_s / D_w \times t_w.$$

Although Jones-Dole's equation was used to examine the relative viscosities,

$$(\eta_r - 1)/\sqrt{C} = A + B\sqrt{C}$$

Where,

A = Falkenhagen coefficient

B = Jones-Dole coefficient

C = concentration of solutions

The solute-solvent interaction was measured using the Jones-Dole coefficient (B), whereas the solute-solute interaction was measured using the Falkenhagen coefficient (A). The graph is plotted between \sqrt{C} and $(\eta_r - 1)/\sqrt{C}$. The graph for each system showed a linear straight line with a value for the β -coefficient.

V. CONCLUSION

As the temperature rises, the present work monitor's density and relative viscosity decrease. This is supported by the observation that the solute-solvent interaction increases with temperature, increasing the solvation effect. Research into a drug's pharmacodynamics and pharmacokinetics is useful and instructive for the general public.

VI. ACKNOWLEDGEMENT

I sincerely appreciate the help of Dr. D. T. Tayade, Professor at GVISH College in Amravati.

VII. REFERENCES

- [1]. Mohammad Abu-Taweel G, Ibrahim MM, Khan S, Al-Saidi HM, Alshamrani M, Alhumaydhi FA,
- [2]. Alharthi SS. Medicinal Importance and Chemosensing Applications of Pyridine Derivatives: A Review. Crit Rev Anal Chem. 2022 Jun 20:1-18.
- [3]. Ataf Ali Altaf, Adnan Shahzad, Zarif Gul, Nasir Rasool, Amin Badshah, Bhajan Lal, Ezzat Khan. A Review on the Medicinal Importance of Pyridine Derivatives. Journal of Drug Design and Medicinal Chemistry. Vol. 1, No. 1, 2015, pp. 1-11.
- [4]. Bansal R.K., J. Heterocyclic Chemistry, 8, 2012, 12-24.
- [5]. Jakhar A. and Makrand J.K., J. Chem. Res., 4(3), 2010, 238-240.
- [6]. Solanki, A. and Thakur, I. (2007). Indian Journal of Chemistry. 45(B): 517.
- [7]. Saleem, F. (2008). Eur. Pat., CHAPPL. 87: 19.

- [8]. Wan, Z.Y. Shi, H.X. and Shi, H.J. (2001). J. Heterocyclic Chloroic Chem. 38: 335.
- [9]. Zhang, L.X. Zhang, A.J. Hu, M.L. and Lei, X.X. (2003). Acta Chim.Sinica. 61(6): 917.
- [10]. Hu G.Q., Xie S.Q., Huang W.L. and Zhang H.B., Chin. Chem.Lett., 16(6),2005, 723-726.
- [11]. Scendo M., Poddebnick D. And Malyszko J., J. Appl. Electrochem., 33, 2003, 2337.
- [12]. Bhat, B.A. Dhar, K.L. Saxena, A.K. and Shanmugavel, M. (2005). Bio org. and Med. Chem. 15(3):177-180.
- [13]. Vibhute, Y.B. and Basser, M.A. (2003). Ind. J. of Chem. 42(B): 202-205.
- [14]. Padmanaban, R.; Gayathri, A.; Gopalan, A.I.; Lee, D.-E.; Venkatramanan, K. Comparative Evaluation of Viscosity, Density and Ultrasonic Velocity Using Deviation Modelling for Ethyl-Alcohol Based Binary Mixtures. Appl. Sci. 2023, 13, 7475.

Application Of Ultrasound in Synthesis of Heterocyclic Compound: A Green Chemistry Perspective

Abhimanyu P. Pawar^{*1}, Kishor S. Naktode¹, Arvind J. Mungole², Dalesh M. Parshuramkar³

¹Department of Chemistry, Nevjabai Hitkarini College, Bramhapuri, Maharashtra 441 206, India

²Department of Botany, Nevjabai Hitkarini College, Bramhapuri, Maharashtra 441 206, India

³Department of Physics, Nevjabai Hitkarini College, Bramhapuri, Maharashtra 441 206, India

ARTICLE INFO

Article History:

Accepted : 01 Jan 2025

Published : 10 Jan 2025

Publication Issue :

Volume 12, Issue 7

January-February-2025

Page Number :

461-467

ABSTRACT

Ultrasound irradiation offers a unique energy source distinct from conventional methods like light, heat, characterized by reduced reaction times, elevated pressures, and higher energy efficiency. Its application in organic synthesis has gained significant attention, particularly in green and industrial chemistry, due to its sustainability and innovative potential. This short review highlights the use of ultrasound in various chemical transformations, including heterocyclic synthesis reactions. By enhancing reaction efficiency, minimizing harsh reagents, and reducing energy consumption, ultrasound-assisted methodologies align with green chemistry principles, representing a sustainable and efficient approach in modern organic synthesis.

Keywords: Ultrasound irradiation, Green chemistry, Heterocycles Compound

I. INTRODUCTION

Green Chemistry, underpinned by its twelve foundational principles, seeks to revolutionize the conventional methodologies employed in synthetic organic chemistry that have persisted for decades. Its primary objectives include the utilization of less hazardous starting materials, optimization of synthetic efficiency, reduction of toxic and volatile solvent use, streamlining of synthetic pathways, and minimization of waste generation [1-3]. Collectively, these advancements align with the overarching goals of sustainable development. The discipline further advocates for innovative research and the development of alternative methodologies in organic synthesis, particularly within academic and institutional research laboratories. Adoption of these novel approaches not only enhances health and safety standards in small-scale laboratory environments but also promotes the implementation of improved techniques at the industrial scale [4]. A significant outcome of this paradigm shift is the reduced environmental impact, achieved through the employment of safer reagents, minimization of waste production, and generation of biodegradable byproducts. Global chemical industries are

increasingly adopting these principles to foster innovation and ensure the safety of their products [5]. Green Chemistry, in conjunction with Green Engineering, provides the conceptual and practical tools to design alternative materials, processes, and systems that enhance both the sustainability and environmental performance of chemical production. These efforts focus on reducing toxicity, improving waste management, and increasing the recyclability of chemical products and byproducts [6]. Consequently, modern organic chemistry has embraced non-traditional synthetic methodologies, integrating sustainable approaches such as solvent-free reactions, alternative activation techniques (e.g., microwave irradiation and ultrasound), and the replacement of volatile organic solvents with greener alternatives, including water, ionic liquids, and supercritical carbon dioxide. These advancements represent a critical transition toward a more sustainable and environmentally conscious chemical industry [7-9].

Ultrasound-assisted organic synthesis represents a progressive "green" methodology that is increasingly utilized in diverse organic synthetic processes [10-11]. This approach offers several key advantages, including enhanced reaction efficiency, minimal waste production, and significantly reduced energy consumption. Sonochemistry, operating within the acoustic frequency range of 20 kHz to 1 MHz, has garnered substantial interest for its capacity to disperse reagents into fine particles and accelerate chemical reactions [12]. The fundamental mechanism underpinning ultrasound-assisted synthesis is acoustic cavitation. This phenomenon involves the nucleation, growth, and implosive collapse of microbubbles in a liquid medium subjected to high-intensity ultrasonic waves. The collapse of these cavitation bubbles produces localized hotspots characterized by extreme temperatures and pressures, as well as intense shear forces. These unique conditions in otherwise ambient liquids facilitate chemical transformations that typically require harsher conditions under conventional methods. The field of sonochemical engineering has emerged as a specialized discipline dedicated to applying ultrasonic and sonic waves to chemical processes. Sonochemistry significantly enhances reaction kinetics and mass transfer, enabling shorter reaction durations, reduced reagent costs, and milder operational conditions. These attributes align with the principles of Green Chemistry, emphasizing sustainability and efficiency in chemical processes [13]. Extensive research in sonochemistry underscores its versatility and profound impact on various domains of chemistry. Particularly noteworthy are its applications in environmental remediation and pollution control, where sonochemical processes provide innovative solutions for waste management and pollutant degradation. As a rapidly expanding area of research, sonochemical methodologies hold immense potential to contribute to sustainable chemical practices, marking a transformative advancement in the pursuit of environmentally benign technologies.

In this short review, the utilization of ultrasound as a green methodology in organic (heterocyclic compound) synthetic chemistry is examined (as shown in fig.1), with a focus on its applications across a diverse range of chemical transformations and reactions. These transformations are systematically categorized into distinct classes frequently faced in synthetic organic chemistry.

Heterocyclic compounds are highly regarded for their notable biological activities and have extensive applications in the pharmaceutical industry, particularly in the treatment of various diseases [14-15]. The substantial demand for these compounds surpasses what can be obtained from natural plant-based sources, thereby necessitating their synthesis through diverse chemical methodologies. Heterocycles constitute one of the most expansive and foundational divisions of organic chemistry. Their significance extends beyond biological and industrial applications, playing a crucial role in sustaining the broader functionality of modern society. The contributions of heterocyclic compounds across a wide range of fields are indisputable [16]. Notably, a majority of pharmaceutical products are modeled after natural compounds, frequently incorporating heterocyclic frameworks with inherent biological activity. Significant progress in combating diseases has been

achieved through the design and testing of novel molecular structures, often based on heteroaromatic derivatives. Consequently, the development of efficient synthetic methodologies for constructing heterocyclic frameworks remains a central focus for academic and industrial researchers. Moreover, heterocyclic natural products, including pesticides, antibiotics, alkaloids, and cardiac glycosides, are of paramount importance for human and animal health [17-18]. Researchers continually endeavor to design and synthesize improved pharmaceuticals, pesticides, rodenticides, and herbicides, often inspired by natural models. This relentless pursuit highlights the critical need for innovative and efficient strategies to produce novel heterocyclic compounds. The advancement of environmentally benign and efficient technologies, in line with the principles of Green Chemistry, represents a significant challenge for the chemical community.

In this regard, the adoption of sonochemical synthesis—an approach leveraging ultrasound as a green and sustainable technology has demonstrated immense potential. This section focuses on the sonochemical synthesis of key heterocyclic moieties, underscoring its promise in meeting the demand for efficient, sustainable, and environmentally friendly synthetic methodologies.

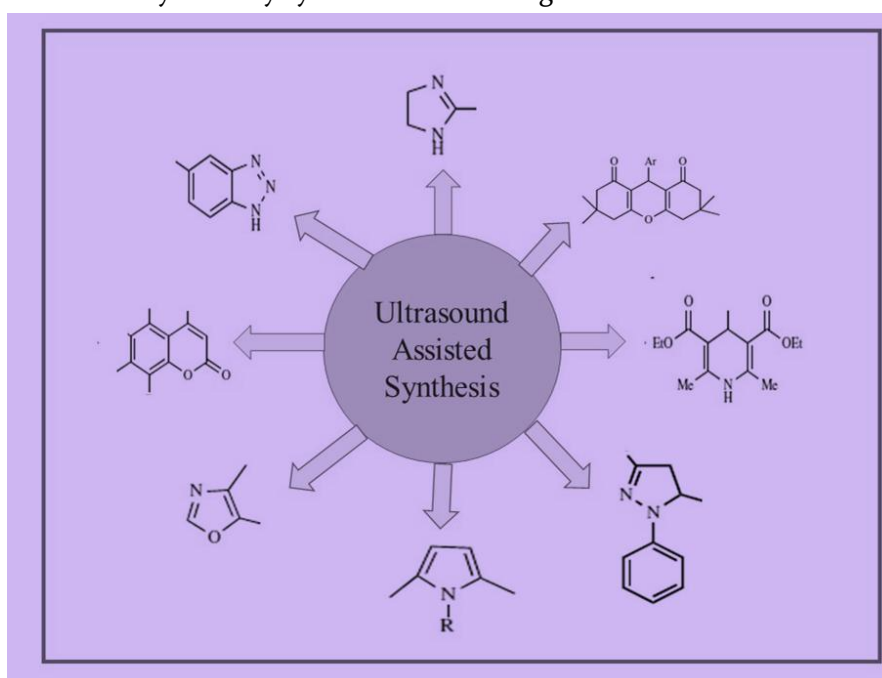
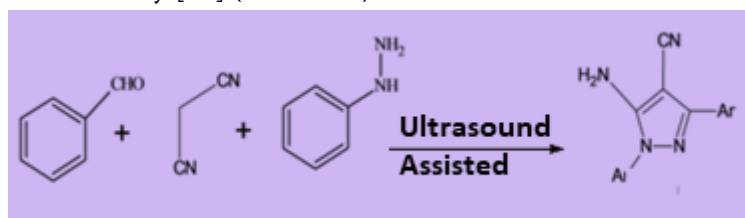


Fig.1. Ultrasound Assisted synthesis of heterocyclic compound

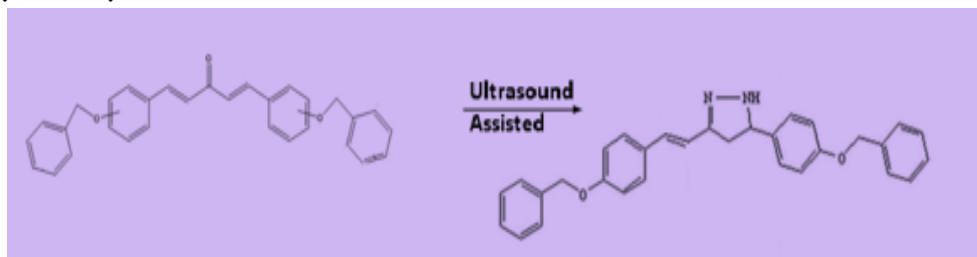
Firouzeh Nematiet *al.* developed a catalyst-free, environmentally friendly protocol for synthesizing highly substituted pyrazoles under ultrasonic irradiation. The method uses a mixture of phenylhydrazine, malononitrile, aldehyde, and PEG-water at room temperature. The reaction is completed in 30 minutes, yielding the product in 99% efficiency [19] (Scheme-1).



Scheme-1. Synthesis of pyrazole under ultrasonic irradiation.

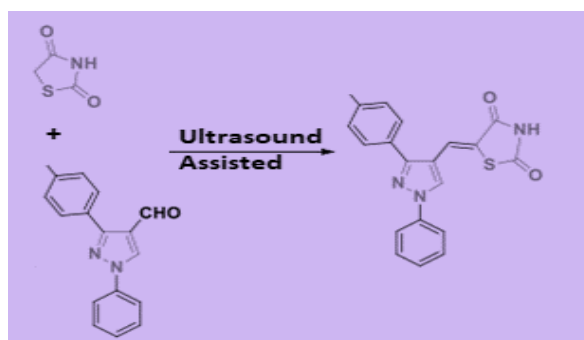
Farouq E. Hawaizet *al.* developed a green, ultrasound-assisted method for the synthesis of a series of novel curcumin mono-carbonyl analogs containing benzyloxy moieties, along with their corresponding pyrazoline derivatives. This approach was compared with the traditional synthesis method to evaluate the efficiency of

both techniques. The results demonstrated significant improvements in reaction time and product yields, with the ultrasound-assisted method reducing the reaction time from hours to minutes while achieving higher yields (80-90%). These findings highlight the advantages of ultrasound-assisted synthesis as a more efficient and environmentally friendly alternative to conventional methods [20](Scheme-2)..



Scheme-2. Synthesis of novel curcumin mono-carbonyl analogs containing benzyloxymoiety, along with their corresponding pyrazoline derivatives under ultrasonic radiation.

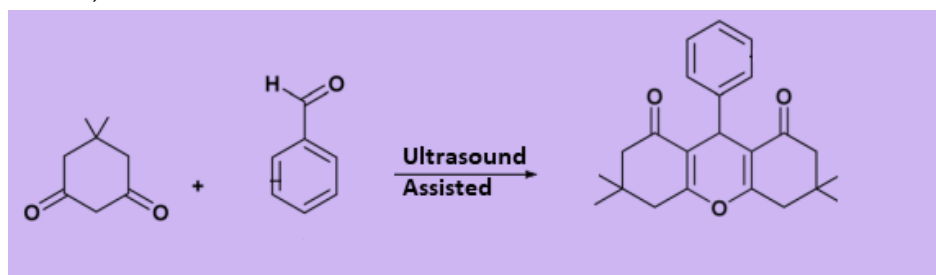
The study by Mamdouh FA *et al.* introduces an efficient and environmentally friendly approach to synthesizing pyrazolylthiazolidinediones and its derivatives. Employing ultrasonic irradiation and β -alanine as a catalyst, the authors developed a novel green method characterized by simplicity, high yields (79-95%), and short reaction times [21](Scheme-3).



Scheme-3. Synthesis of pyrazolylthiazolidinediones under ultrasonic radiation.

RiniRetnosari *et al.* present an ultrasound-assisted green synthesis of 9-(4-hydroxyphenyl)-3,4,5,6,7,9-hexahydro-1H-xanthene-1,8(2H)-dione using lime juice as a sustainable catalyst. This approach significantly improved reaction efficiency, achieving a high yield of 89.03%. Ultrasonic irradiation reduced reaction time and temperature, aligning with green chemistry principles[22]..

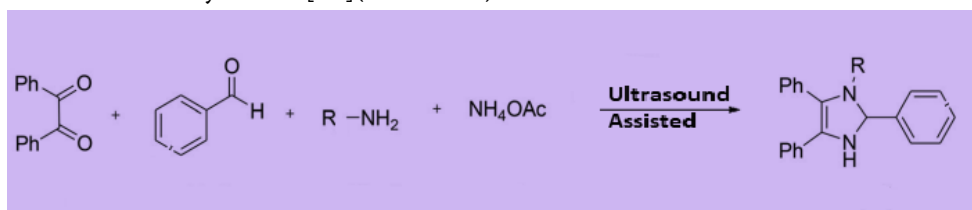
RayeneSayada *et al.* developed a green, one-pot method for xanthene synthesis using zinc acetate and ultrasound irradiation. Ultrasound significantly enhances efficiency by reducing reaction time, energy, and temperature while ensuring high yields (95%). This method aligns with green chemistry principles, offering high atom economy, catalyst recyclability, and eco-friendliness, making it a sustainable and efficient synthetic approach [23](Scheme-4).



Scheme-4. Synthesis of xanthene under ultrasonic radiation.

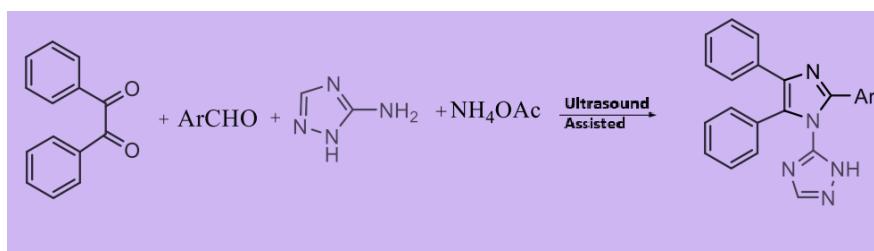
Amol U. Khandebharad *et al.* report an efficient synthesis of substituted imidazoles catalyzed by 3-N-morpholinopropanesulfonic acid (MOPS) under ultrasound irradiation. This green method avoids harsh

reagents and significantly shortens reaction times (30 min.) while achieving high yields (90%). The synergistic effect of MOPS and ultrasound enhances reaction efficiency, offering a sustainable, time-saving, and eco-friendly approach to imidazole synthesis[24](Scheme-5)..



Scheme-5. Synthesis of substituted imidazoles catalyzed by 3-N morpholinopropanesulfonic acid under ultrasound irradiation.

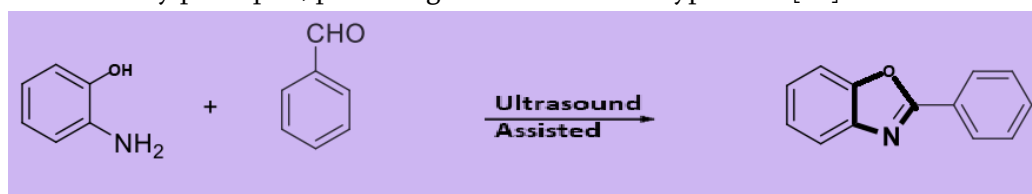
S. Dastmard *et al.* developed an ultrasound-assisted, one-pot method for synthesizing novel 4,5-diphenyl-1H-imidazol-1-yl-1H-1,2,4-triazole derivatives. Ultrasound irradiation played a crucial role in enhancing reaction efficiency by significantly reducing reaction times (10–25 minutes) and improving yields (70–96%). Using KHSO_4 as a catalyst, the method produced compounds with notable antibacterial activity against Gram-positive and Gram-negative bacteria, along with promising antioxidant potential, underscoring its bioactive relevance [25](Scheme-6).



Scheme-6. Ultrasound-assisted, one-pot method for synthesizing novel 4,5-diphenyl-1H-Imidazol-1-yl-1H-1,2,4-triazole derivatives.

Ashish Patel introduces a green, ultrasound-assisted one-pot synthesis of tetrahydropyrimidine derivatives via Biginelli condensation. Ultrasound irradiation is pivotal in accelerating the reaction, achieving up to 99% yield within 5–20 minutes under mild heating. This catalyst-free method exemplifies green chemistry by enhancing efficiency, reducing reaction time and energy consumption, and offering an eco-friendly alternative for high-yield synthesis [26].

The study by Hai Truong Nguyen *et al.* introduces a green method for synthesizing 2-substituted benzoxazoles using imidazolium chlorozincate (II) ionic liquid supported on Fe_3O_4 nanoparticles (LAIL@MNP) under ultrasound irradiation. The method achieves high product yields (up to 90%) within just 30 minutes. Notably, it adheres to green chemistry principles, producing water as the sole byproduct [27].



Scheme-7. Green method for synthesizing benzoxazoles under ultrasound irradiation.

II. CONCLUSION

Ultrasound-assisted synthetic methodologies have emerged as efficient and environmentally friendly approaches for the synthesis of a wide range of important organic compounds. The primary advantages of

ultrasound over conventional methods include significantly reduced reaction times, enhanced yields, and improved reaction efficiency. This sonochemical approach contributes to greener chemistry by replacing volatile and toxic organic solvents with safer alternatives, such as water or ionic liquids. Additionally, the use of cost-effective, reusable catalysts and solvent-free reaction conditions in certain cases further promotes sustainability. These factors, combined with the enhanced catalytic efficiency achieved through ultrasound, lead to a substantial reduction in the environmental impact of organic synthesis. Overall, ultrasound-assisted methods represent a highly effective, sustainable, and green alternative for the production of valuable industrial and commercial organic compounds, aligning with the principles of Green Chemistry by minimizing waste and reducing energy consumption.

CONFLICT OF INTEREST

The authors declare that there are no conflicts of interest regarding the content of this article.

III. REFERENCES

- [1]. Sheldon, R. A. (2016). Green chemistry and resource efficiency: towards a green economy. *Green Chemistry*, 18(11), 3180-3183.
- [2]. Ivanković, A., Dronjić, A., Bevanda, A. M., & Talić, S. (2017). Review of 12 principles of green chemistry in practice. *International Journal of Sustainable and Green Energy*, 6(3), 39-48.
- [3]. Erythropel, H. C., Zimmerman, J. B., de Winter, T. M., Petitjean, L., Melnikov, F., Lam, C. H., ...& Anastas, P. T. (2018). The Green ChemisTREE: 20 years after taking root with the 12 principles. *Green chemistry*, 20(9), 1929-1961.
- [4]. Andraos, J., & Matlack, A. S. (2022). *Introduction to green chemistry*. CRC press.
- [5]. Karagölge, Z., & Gür, B. (2016). Sustainable chemistry: green chemistry. *Journal of the Institute of Science and Technology*, 6(2), 89-96.
- [6]. Venkatesan, K., Sundarababu, J., & Anandan, S. S. (2024). The recent developments of green and sustainable chemistry in multidimensional way: current trends and challenges. *Green Chemistry Letters and Reviews*, 17(1), 2312848.
- [7]. García-Serna, J., Pérez-Barrigón, L., & Cocero, M. J. (2007). New trends for design towards sustainability in chemical engineering: Green engineering. *Chemical Engineering Journal*, 133(1-3), 7-30.
- [8]. Verma, C., Chauhan, D. S., Aslam, R., Banerjee, P., Aslam, J., Quadri, T. W., ...& Rasheed, T. (2024). Principles and theories of green chemistry for corrosion science and engineering: design and application. *Green Chemistry*, 26(8), 4270-4357.
- [9]. Coelho, M. A., & Ribeiro, B. D. (Eds.). (2015). *White biotechnology for sustainable chemistry*. Royal Society of Chemistry.
- [10]. Draye, M., Estager, J., & Kardos, N. (2019). Organic sonochemistry: ultrasound in green organic synthesis. *Activation methods: sonochemistry and high pressure*, 2, 1-93.
- [11]. Majhi, S. (2023). Applications of nanoparticles in organic synthesis under ultrasonication. In *Nanoparticles in Green Organic Synthesis* (pp. 279-315). Elsevier.
- [12]. Pingret, D., Fabiano-Tixier, A. S., & Chemat, F. (2013). Ultrasound-assisted extraction.
- [13]. Trinh, Q. T., Golio, N., Cheng, Y., Cha, H., Tai, K. U., Ouyang, L., ...& Nguyen, N. T. (2024). Sonochemistry and Sonocatalysis: Current Progress, Existing Limitations, and Future Opportunities in Sustainable Chemistry.

- [14]. Kabir, E., &Uzzaman, M. (2022). A review on biological and medicinal impact of heterocyclic compounds. *Results in Chemistry*, 4, 100606.
- [15]. Qadir, T., Amin, A., Sharma, P. K., Jeelani, I., & Abe, H. (2022). A review on medicinally important heterocyclic compounds. *The Open Medicinal Chemistry Journal*, 16(1).
- [16]. Salehian, F., Nadri, H., Jalili-Baleh, L., Youseftabar-Miri, L., Bukhari, S. N. A., Foroumadi, A., ...&Khoobi, M. (2021). A review: Biologically active 3, 4-heterocycle-fused coumarins. *European Journal of Medicinal Chemistry*, 212, 113034.
- [17]. Alamgir, A. N. M., &Alamgir, A. N. M. (2018). Secondary metabolites: Secondary metabolic products consisting of C and H; C, H, and O; N, S, and P elements; and O/N heterocycles. *Therapeutic use of medicinal plants and their extracts: volume 2: phytochemistry and bioactive compounds*, 165-309.
- [18]. Bandyopadhyay, D., Garcia, V., & Gonzalez, F. (2020). Heterocyclic Drugs from Plants. In *Promising Drug Molecules of Natural Origin* (pp. 215-270). Apple Academic Press.
- [19]. Nemati, F., Nikkhah, S. H., &Elhampour, A. (2015). An environmental friendly approach for the catalyst-free synthesis of highly substituted pyrazoles promoted by ultrasonic radiation. *Chinese Chemical Letters*, 26(11), 1397-1399.
- [20]. Hawaiz, F., &Shekh Omer, D. (2017). Ultrasound-assisted Synthesis of Some New Curcumin Analogs and Their Corresponding Pyrazoline Derivatives. *ARO-The Scientific Journal of Koya University*, 5(1), 30-35.
- [21]. Mohamed, M., Aziz, M. A., &Abuo-Rahma, G. E. D. A. (2021). Ultrasound-assisted green synthesis of 2, 4-thiazolidinedione and diaryl substituted pyrazolylthiazolidinediones catalyzed by β -alanine. *Int J Phar Sci Drug Anal*, 1(1), 18-25.
- [22]. Retnosari, R., Mutiarahma, R. R., Marfu'ah, S., Sutrisno, S., Santoso, A., &Rachman, I. B. (2023, January). Ultrasound-assisted synthesis of 9-(4-Hydroxyphenyl)-3, 4, 5, 6, 7, 9-Hexahydro-1H-Xanthene-1, 8 (2H)-Dione using lime juice catalyst and its antibacterial activity. In *AIP Conference Proceedings* (Vol. 2569, No. 1). AIP Publishing.
- [23]. Sayad, R., Bouzina, A., Bouone, Y. O., Beldjezzia, D., Djemel, A., Ibrahim-Ouali, M., ...&Aouf, Z. (2024). Zinc acetate-catalyzed, green and efficient synthesis of xanthene derivatives under ultrasound irradiation: X-ray crystallographic analysis and in silico study. *RSC advances*, 14(34), 24585-24603.
- [24]. Khandebharad, A. U., Sarda, S. R., Gill, C., & Agrawal, B. R. (2020). An Efficient Synthesis of Substituted Imidazoles Catalyzed by 3-N-Morpholinopropanesulfonic Acid (MOPS) under Ultrasound Irradiation. *Organic Preparations and Procedures International*, 52(6), 524-529.
- [25]. Dastmard, S., Mamaghani, M., &Rassa, M. (2020). Ultrasound-assisted efficient synthesis of polyfunctional 1, 2, 4-triazoles as novel antibacterial and antioxidant agents. *Journal of the Chinese Chemical Society*, 67(8), 1437-1445.
- [26]. Patel, A., Shah, J., Patel, K., Patel, K., Patel, H., Dobarra, D., ...&Bambharoliya, T. (2021). Ultrasound-assisted one-pot synthesis of tetrahydropyrimidine derivatives through biginelli condensation: A catalyst free green chemistry approach. *Letters in Organic Chemistry*, 18(9), 749-756.
- [27]. Nguyen, H. T., Nguyen, T. H., Pham, D. D., Nguyen, C. T., & Tran, P. H. (2021). A green approach for the synthesis of 2-substituted benzoxazoles and benzothiazoles via coupling/cyclization reactions. *Heliyon*, 7(11).

Novel Synthesis and Antimicrobial Study Of (E)-1-(4-Substituted Phenyl)-N-(4- Chlorophenyl) Methanamine Derivative.

D S Warbhe¹, O K Kapse^{*1}, R M More^{*2}

¹Department of Chemistry, Amolakchand Mahavidyalaya, Yavatmal-445001, Maharashtra, India

²Department of Chemistry, Shri Datta Arts Commerce and Science College, Hadgaon-431712, Maharashtra, India

ARTICLE INFO

Article History:

Accepted : 01 Jan 2025

Published : 10 Jan 2025

Publication Issue :

Volume 12, Issue 7

January-February-2025

Page Number :

468-472

ABSTRACT

Schiff bases are condensation products of primary amines and carbonyl compounds structurally, Schiff base (also known as Imine or azomethine) is an analogue of a ketone or aldehyde. In which the carbonyl group (C=O) has been replaced by an imine or azomethine group. The synthesized compounds are confirmed by IR, NMR spectroscopy and studied their antimicrobial activities.

KEYWORDS: 4-Fluorobenzaldehyde, P-dimethyl aminobenzaldehyde, Para-Chloro aniline, P-Chlorobenzaldehyde, 4-Chloroaniline, Meta-nitroaniline, 4A- molecular sieves, Toluene, ethanol, reflux condensers.

I. INTRODUCTION

Imine complexes have wide usage in the field of biological activators in the form of Antitumor, antiviral, antifungal, antibacterial and antimalarial agents¹⁻⁷. In immobilization of Enzymes fictionalization can lead to successful binding of the enzyme to the support material. These complexes are helpful in the treatment of blood sugar and AIDS virus. These are also helpful to understand the various biological processes occurring in living organisms and understand the structures of biomolecules. They involved in photosynthesis and oxygen Transport in organisms. For the treatment of cancer drug resistance, imine complexes are involved out of that we are interested to know the biological activity i.e. antimicrobial and antifungal of newly synthesis imines.

II. EXPERIMENTAL SECTION:

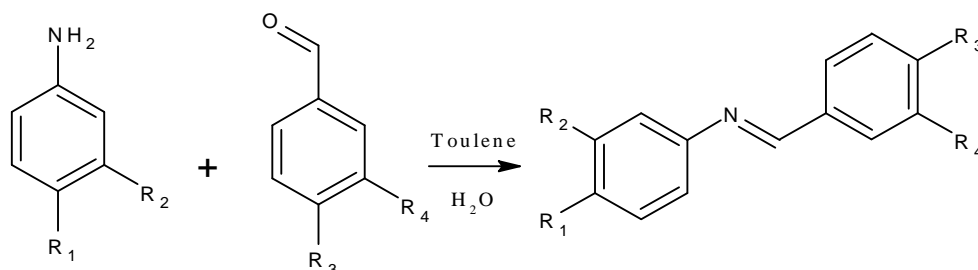
Substituted aniline in 20 ml toluene was added to a solution Substituted benzaldehyde the mixture was heated under reflux for 2 hour in the presence of 4A molecular sieves the reaction is monitored on TLC plate after

completion of reaction, the mixture was filtered and then solvent was evaporated. The crude products were purified by crystallization from ethanol to give pure compounds.

Reaction Scheme:

Substituted aniline in 20 ml toluene was added to a solution substituted benzaldehyde. The mixture was heated under reflux for 2 hour in the presence of 4A molecular sieves. The mixture was filtered and then solvent was evaporated. The crude products were purified by crystallization from ethanol to give compounds.

General Reaction



III.CHARACTERIZATION:

Various spectral, analytical and biological applications of the above Schiff bases & their complexes were studied. The details are as under:

Some physical properties analytical and spectral data of the substituted imines compounds are summarized in Table 1:

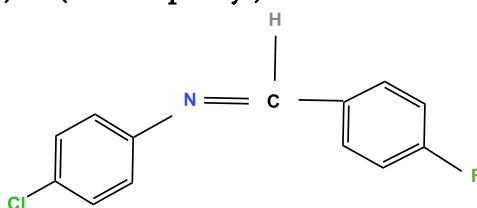
Table 1. Analytical and spectral data of compounds.

Compound No.	Melting point., °C	Yield	IR band, cm ⁻¹
Compound A	144	73 %	1610 v (N=C)
Compound B	131	76%	1640 v (N=C)
Compound C	147	74%	1610 v (N=C)
Compound D	153	71%	1620v (N=C)
Compound E	155	75 %	1630 v (N=C)

The infrared spectral data of the imines are in agreement with the expected range. A band at 1600-1660 cm⁻¹ is due to C=N vibration. The UV absorption show bands for all compounds at about λ_{max} 600 and 230 nm corresponding to n- π^* with conjugated system compounds.

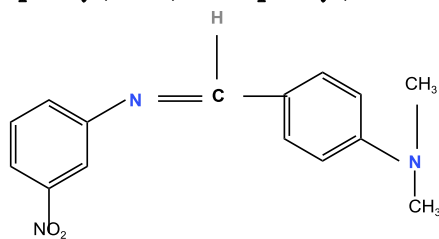
Characterization of compounds:

Compound A: (E)-1-(4 fluorophenyl)-N-(4 chlorophenyl) methanimine



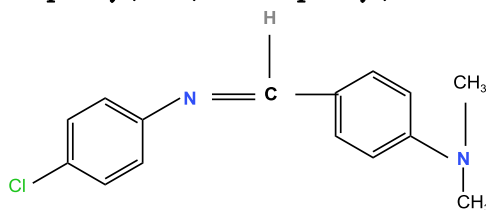
¹H NMR (300 MHz DMSO) δ 8.67 (s, 1H), δ 7.89 (d, 1H), δ 7.70 (s, 1H), δ 7.51 (d, 1H), δ 7.40 (d, 1H), δ 7.02 (d, 1H).

Compound B: (E)-1-(p-dimethyl aminophenyl) -N-(3 nitrophenyl) methanimine



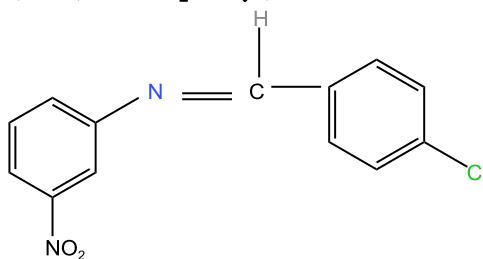
¹H NMR (300 MHz DMSO) δ 8.63 (s, 1H), δ 7.53 (d, 1H), δ 7.40 (s, 2H), δ 7.41 (d, 1H), δ 7.02 (s, 2H), δ 7.07(d, 2H), δ 3.83 (d, 6H).

Compound C: (E)-1-(p-dimethyl aminophenyl)-N-(4 chlorophenyl) methanimine



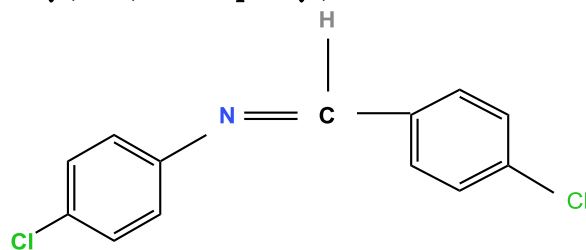
¹H NMR (300 MHz DMSO) δ 8.58 (s, 1H), δ 7.82 (d, 2H), δ 7.37 (d, 2H), δ 7.40 (d, 2H), δ 7.02 (d, 2H), δ 5.00 (t, 1H), δ 1.20 (d, 6H).

Compound D: (E)-1-(p chlorophenyl)-N-(m nitrophenyl) methanimine



¹H NMR (300 MHz, DMSO) δ 8.64 (s, 1H), δ 8.50 (s, 1H), δ 8.25 (d, 1H), δ 8.09 (d, 1H), δ 7.63 (t, 1H), δ 7.40 (d, 1H), δ 7.02, (d, 1H).

Compound E: (E)-1-(p- chlorophenyl)-N-(4 chlorophenyl) methanimine



¹H NMR (300 MHz DMSO) δ 8.63 (s, 1H), δ 7.53 (d, 1H), δ 7.40 (s, 2H), δ 7.41 (d, 1H), δ 7.02 (s, 2H), δ 7.07(d, 2H), δ 3.83 (d, 6H).

Table 2. Antimicrobial and Anti fungus activity of compounds

ZONE OF INHIBITION IN MM		
TEST COMPOUND	GM+VE BACTERIA	FUNGUS
	Staphylococcus aureus	Candida albicans
Compound A	12 mm	13 mm
Compound B	13 mm	15 mm
Compound C	15 mm	27 mm
Compound D	12 mm	14 mm

ZONE OF INHIBITION IN MM		
TEST COMPOUND	GM+VE BACTERIA	FUNGUS
	<i>Staphylococcus aureus</i>	<i>Candida albicans</i>
Compound E	11 mm	12 mm
REFERENCE ANTIBIOTICS	13 mm (OFLOXACIN)	12 mm (CO-TRIMOXAZOLE)

On the basis of Anti- Microbial testing of the given compounds found to be Anti-Microbial & Antifungal activity

IV.RESULT:

In this work, we report the synthesis of newly synthesis imines in presence of solvent toluene and their application in operationally simple, safe and fast method for the imine synthesis. The IR spectral data of the imines compound A shows the mainly 1610 ν to C=N vibration frequency compound B shows that mainly 1640 to C=N vibration. Compound D contain C=N stretching frequency at 1620 cm^{-1} & 1643 (Aromatic C=C stretch). We have examined the activity of our imines using the solvent toluene. Based on the literature survey, we have carried out reaction of derivatives aromatic aldehyde with derivatives aromatic aniline for 2 hours. The method shows moderate to good yield.

V. REFERENCES

- [1]. Abu-Raddad, L.J., Patnaik, P., Kublin, J.G., 2006. Dual infection with HIV and malaria fuels the spread of both diseases in Sub-Saharan Africa. *Science* 314 (5805),1603–1606. <https://doi.org/10.1126/science.1132338>.
- [2]. Alahari, A., Trivelli, X., Guérardel, Y., Dover, L.G., Besra, G.S., Sacchetti, J.C., Reynolds, R.C., Coxon, G.D., Kremer, L., 2007. Thiacezone, an antitubercular drug that inhibits cyclopropanation of cell wall mycolic acids in mycobacteria. *PLoS One* 2, e1343. <https://doi.org/10.1371/journal.pone.0001343>.
- [3]. Arancibia, R., Quintana, C., Biot, C., Medina, M.E., Carrère-Kremer, S., Kremer, L., Klahn, A.H., 2015. Palladium (II) and platinum (II) complexes containing organometallic thiosemicarbazone ligands: synthesis, characterization, X-ray structures and antitubercular evaluation. *Inorg. Chem. Commun.* 55, 139–142. <https://doi.org/10.1016/j.inoche.2015.03.036>.
- [4]. Artursson, P., Ungell, A.-L., Löfroth, J.-E., 1993. Selective paracellular permeability in two models of intestinal absorption: cultured monolayers of human intestinal epithelial cells and rat intestinal segments. *Pharm. Res.* 10, 1123–1129. <https://doi.org/10.1023/A:1018903931777>.
- [5]. Belicchi Ferrari, M., Capacchi, S., Pelosi, G., Reffo, G., Tarasconi, P., Albertini, R., Pinelli, S., Lunghi, P., 1999. Synthesis, structural characterization and biological activity of helicin thiosemicarbazone monohydrate and a copper(II) complex of salicylaldehyde thiosemicarbazone. *Inorganica Chim. Acta* 286, 134–141. [https://doi.org/10.1016/S0020-1693\(98\)00383-1](https://doi.org/10.1016/S0020-1693(98)00383-1).
- [6]. Biot, C., Pradines, B., Sergeant, M.H., Gut, J., Rosenthal, P.J., Chibale, K., 2007. Design, synthesis, and antimalarial activity of structural chimeras of thiosemicarbazone and ferroquine analogues. *Bioorganic Med. Chem. Lett.* 17, 6434–6438. <https://doi.org/10.1016/j.bmcl.2007.10.003>.

- [7]. Casas, J.S., Castaño, M.V., Cifuentes, M.C., GarciaMonteagudo, J.C., Sánchez, A., Sordo, J., Abram, U., 2004. Complexes of dichloro[2-(dimethylaminomethyl)phenyl-C1,N] gold(III), $[\text{Au}(\text{damp-C1,N})\text{Cl}_2]$, with formylferrocene thiosemicarbazones: synthesis, structure and cytotoxicity. *J. Inorg.*

Chemical Synthesis and Optical Characterization of Anatase TiO₂ Nanoparticles

Nikita Subhash Jaiswal, Sanjeev Jagtap

Department of Physics, Bar. Ramrao Deshmukh Arts, Smt. IndirajiKapadiya Commerce and Nya Krushnarao Deshmukh Science College, Badnera, Dist- Amravati 444 701, Maharashtra, India

ARTICLE INFO

Article History:

Accepted : 01 Jan 2025

Published : 10 Jan 2025

Publication Issue :

Volume 12, Issue 7

January-February-2025

Page Number :

473-479

ABSTRACT

This work investigates the structural and optical properties of TiO₂ nanoparticles prepared using a simple chemical route. The synthesized nanoparticles were characterized using UV-Visible spectroscopy and Raman spectroscopy to evaluate their potential applications. The UV-Visible absorption spectrum exhibited a prominent peak at 249 nm, indicating efficient UV absorption typical of the anatase phase of TiO₂, with a size-dependent absorption tail extending into shorter wavelengths. The optical band gap of TiO₂ was estimated to be 4.97 eV, suggesting its suitability for photocatalytic and energy-related applications. Raman spectroscopy revealed peaks at 810, 1225, and 1500 cm⁻¹, which are indicative of defects and oxygen vacancies in the material. These findings demonstrate the promising potential of TiO₂ nanoparticles, synthesized via a straightforward chemical method, for use in photocatalysis, solar energy conversion, and environmental remediation.

Keywords: TiO₂ nanoparticles, UV-Visible spectroscopy, Raman spectroscopy, Optical band gap

I. INTRODUCTION

Titanium dioxide (TiO₂) is a material of significant scientific and industrial interest, renowned for its versatility and diverse applications. Among its three primary polymorphs—anatase, rutile, and brookite—the anatase phase stands out due to its exceptional photocatalytic activity, wide bandgap, and favorable surface properties. These characteristics make it an ideal candidate for applications in photocatalysis, photovoltaics, environmental remediation, and sensing technologies. The synthesis and study of anatase TiO₂ nanoparticles have thus emerged as a prominent field of research, with a focus on optimizing their structural, optical, and functional properties. The anatase phase of TiO₂ is characterized by its tetragonal crystal structure and a bandgap energy of

approximately 3.2 eV. This wide bandgap enables its efficient absorption of ultraviolet (UV) light, leading to the generation of electron-hole pairs essential for photocatalytic reactions [1].

In comparison to the rutile phase, anatase exhibits higher photocatalytic activity, primarily due to its larger specific surface area, reduced recombination rates of charge carriers, and superior charge mobility. These attributes make anatase TiO_2 a preferred material for diverse applications, including water splitting for hydrogen production, degradation of organic pollutants, and as an active layer in dye-sensitized solar cells. A critical aspect of TiO_2 research is the development of reliable and scalable synthesis methods that yield nanoparticles with controlled size, morphology, and phase purity. Among the various techniques available, chemical synthesis routes have gained significant attention for their simplicity, cost-effectiveness, and ability to produce nanoparticles with tailored properties. Methods such as sol-gel synthesis, hydrothermal processes, and precipitation techniques are widely employed to synthesize anatase TiO_2 nanoparticles. These approaches offer flexibility in tuning the synthesis parameters, such as precursor concentration, reaction temperature, and pH, to achieve the desired structural and optical characteristics [2].

The sol-gel method has emerged as a popular choice for synthesizing anatase TiO_2 nanoparticles. This technique involves the hydrolysis and condensation of titanium precursors, such as titanium alkoxides, in the presence of solvents and stabilizing agents. The resulting sol undergoes gelation, followed by drying and calcination to form crystalline nanoparticles. The sol-gel method is advantageous due to its ability to produce high-purity materials with uniform particle size and excellent control over the anatase phase formation. Additionally, the method's scalability makes it suitable for industrial applications. Understanding the optical properties of anatase TiO_2 nanoparticles is crucial for optimizing their performance in various applications. Optical characterization provides insights into the material's bandgap energy, light absorption behavior, and photoluminescence properties. These characteristics are directly related to the nanoparticles' size, shape, and crystallinity, which can be influenced by the synthesis conditions. For instance, the bandgap energy of anatase TiO_2 nanoparticles can be fine-tuned by controlling their size, leveraging the quantum confinement effect. This tunability is particularly advantageous for applications in optoelectronic devices and photocatalysis, where specific optical properties are required. One of the key techniques for studying the optical properties of anatase TiO_2 nanoparticles is UV-Visible (UV-Vis) spectroscopy. This technique is used to determine the material's absorption spectrum and calculate its optical bandgap using methods such as Tauc's plot. The bandgap energy is a critical parameter that governs the efficiency of light-induced processes in TiO_2 nanoparticles. Photoluminescence (PL) spectroscopy is another valuable tool for analyzing the emission properties of the material, providing information on defect states, recombination mechanisms, and surface phenomena. These optical studies contribute to a comprehensive understanding of the material's behavior under light irradiation, enabling its optimization for specific applications [3].

The potential applications of anatase TiO_2 nanoparticles are vast and diverse. In the field of photocatalysis, they are extensively used for environmental remediation, including the degradation of organic pollutants in water and air. The high photocatalytic efficiency of anatase TiO_2 nanoparticles stems from their ability to generate reactive oxygen species (ROS) upon UV light irradiation, which effectively break down harmful contaminants. This property also makes them suitable for applications in self-cleaning surfaces and antimicrobial coatings. In the realm of renewable energy, anatase TiO_2 nanoparticles play a vital role in dye-sensitized solar cells (DSSCs). As a photoanode material, they provide a large surface area for dye adsorption, enhancing the light-harvesting efficiency of the solar cells. Additionally, their high electron mobility facilitates efficient charge transport, improving the overall performance of DSSCs. Similarly, anatase TiO_2 nanoparticles are explored for use in

perovskite solar cells and hydrogen generation through photocatalytic water splitting, addressing the growing demand for sustainable energy solutions. Sensing technologies also benefit from the unique properties of anatase TiO_2 nanoparticles. Their high sensitivity to changes in the surrounding environment, combined with their optical and electrical properties, makes them ideal for gas sensing applications. For example, anatase TiO_2 -based sensors are used to detect toxic gases such as ammonia, carbon monoxide, and nitrogen oxides. The nanoparticles' response to these gases is attributed to changes in their electrical resistance or optical properties upon gas adsorption, providing a reliable means of monitoring environmental and industrial processes.

Despite their remarkable properties and applications, challenges remain in the synthesis and utilization of anatase TiO_2 nanoparticles. Achieving precise control over particle size, morphology, and phase purity is essential to maximize their performance. Additionally, the wide bandgap of anatase TiO_2 limits its absorption to the UV region of the electromagnetic spectrum, which constitutes only a small fraction of solar radiation. Efforts are underway to address this limitation by doping TiO_2 nanoparticles with metal or non-metal elements, creating visible-light-active materials for broader applications [4].

In conclusion, the synthesis and optical study of anatase TiO_2 nanoparticles through chemical routes offer a promising avenue for advancing nanomaterials research. By leveraging the capabilities of chemical synthesis techniques and optical characterization tools, researchers can develop TiO_2 nanoparticles with tailored properties for specific applications. The anatase phase's unique combination of structural, optical, and functional characteristics continues to drive its exploration in diverse fields, paving the way for innovative solutions to pressing global challenges in energy, environment, and healthcare.

II. EXPERIMENTAL DETAILS

Titanium tetrachloride (TiCl_4) and sodium hydroxide (NaOH) were used as precursors for the synthesis of titanium dioxide (TiO_2) nanoparticles. All chemicals were procured from SD Fine Chemicals, India, with a purity of 99.9%. The TiO_2 nanoparticles were synthesized through a chemical route. Initially, TiCl_4 was slowly added to deionized water under constant stirring at room temperature. The reaction was carried out in a fume hood due to the highly reactive nature of TiCl_4 . The solution was allowed to hydrolyze, forming a milky-white titanium hydroxide precipitate. Subsequently, NaOH solution was added dropwise to adjust the pH of the reaction mixture to a neutral value (pH ~ 7). The resulting suspension was stirred for an additional 2 hours to ensure complete precipitation. The precipitate was washed multiple times with deionized water to remove any residual chloride ions, followed by drying at 80°C for 12 hours in an oven. The dried product was then calcined at 450°C for 4 hours in a muffle furnace to obtain crystalline anatase phase TiO_2 nanoparticles.

The synthesized TiO_2 nanoparticles were characterized using the following techniques:

- X-Ray Diffraction (XRD): The crystalline structure and phase purity were analyzed using a Rigaku MiniFlex X-ray diffractometer with $\text{Cu K}\alpha$ radiation ($\lambda = 1.5406 \text{ \AA}$).
- Scanning Electron Microscopy (SEM): The morphology and particle size of the nanoparticles were examined using a Zeiss Supra 40VP SEM.
- Raman Spectroscopy: The vibrational modes and phase identification were conducted using a Bruker Bravo Raman Spectrometer.
- UV-Visible Spectroscopy: The optical properties and bandgap energy were measured using an Agilent Cary 60 UV-Vis spectrophotometer.

The comprehensive characterization ensured the structural, morphological, and optical evaluation of the synthesized nanoparticles, confirming their suitability for potential applications.

III.RESULTS AND DISCUSSION

Figure 1 shows the XRD pattern of TiO₂ nanoparticles. The crystalline structure and phase purity were analyzed using a Rigaku MiniFlex X-ray diffractometer with Cu K α radiation ($\lambda = 1.5406 \text{ \AA}$). The diffraction peaks at $2\theta = 25.3^\circ$ (101), 37.8° (004), 48.1° (200), 53.9° (105), 55.1° (211), and 62.8° (204) confirmed the anatase phase. The average crystallite size was estimated to be approximately 85 nm using the Debye-Scherrer equation [5]:

$$D = (K\lambda) / (\beta \cos\theta)$$

where D is the crystallite size, K is the shape factor (0.9), λ is the X-ray wavelength (1.5406 \AA), β is the full width at half maximum (FWHM) in radians, and θ is the Bragg angle.

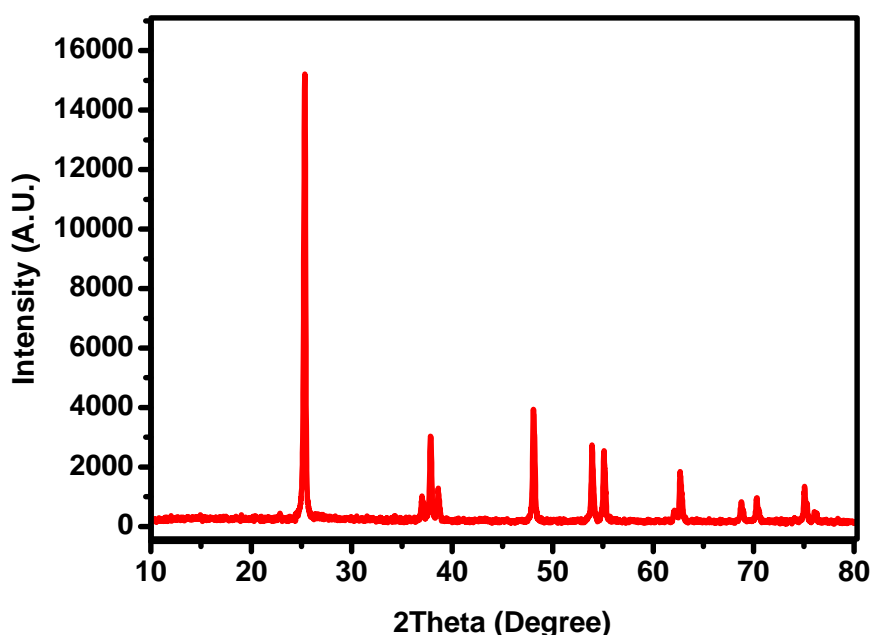


Figure 1. XRD of TiO₂ Nanoparticles.

Figure 2 shows the SEM image of TiO₂ Nanoparticles. The SEM image of chemically synthesized TiO₂ nanoparticles showing a petal-like structure highlights their distinctive morphology, resulting from anisotropic growth during the chemical route synthesis. The high surface area of this structure enhances light absorption, scattering, and catalytic activity, making it highly efficient for applications like photocatalysis and solar energy conversion. The unique morphology also facilitates efficient charge separation and transfer, making chemically synthesized petal-like TiO₂ suitable for environmental remediation, energy devices, and biomedical applications.

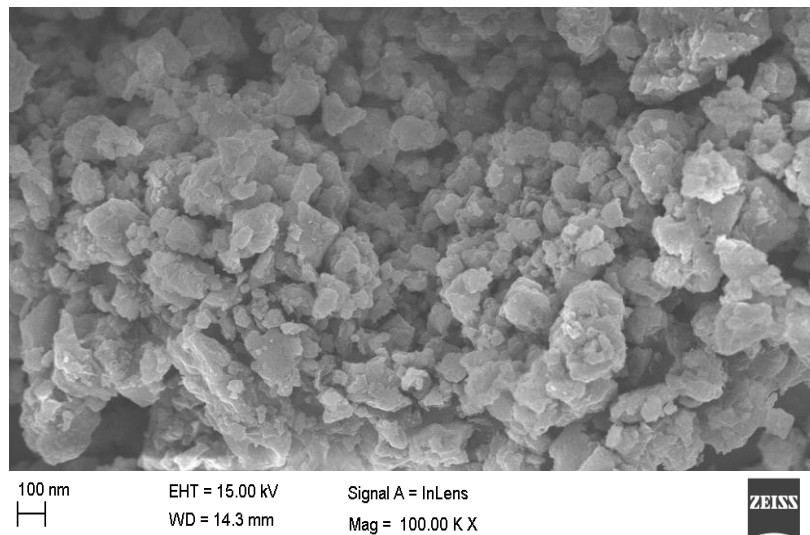


Figure 2. SEM of TiO₂ Nanoparticles.

The Raman spectroscopy peaks observed at 810 cm⁻¹, 1225 cm⁻¹, and 1500 cm⁻¹ in TiO₂ nanoparticles suggest specific vibrational modes and structural features, typically influenced by defects, surface states, or interactions in the material. The peak at 810 cm⁻¹ is often attributed to O-Ti-O bending vibrations, specifically associated with the rutile phase of TiO₂. It could also indicate the phonon mode in TiO₂ or other possible structural distortions in the crystal lattice.

The peak around 1225 cm⁻¹ may be due to defect-induced vibrational modes or the D-band in carbon-containing TiO₂ nanomaterials, often observed in materials with surface defects or oxidation states that create localized states. This peak can also arise from Ti-O bond vibrations in oxygen-deficient structures or surfaces. The peak at 1500 cm⁻¹ is typically related to the D-band of carbon-related defects, particularly in TiO₂ composites with carbon or in the presence of carbon contamination. It can also correspond to carbonaceous impurities or the graphitic carbon present during the synthesis process. This band is commonly seen in materials with defective structures or amorphous regions. These peaks suggest the presence of surface defects, oxygen vacancies, or impurities in the TiO₂ nanoparticles, possibly due to carbon contamination or defects in the crystal lattice. The peaks at 1225 cm⁻¹ and 1500 cm⁻¹ are likely related to defect-related vibrations, indicating structural imperfections or surface states in the material. The peak at 810 cm⁻¹ suggests the presence of the rutile phase or specific bending modes in the Ti-O bonds [6].

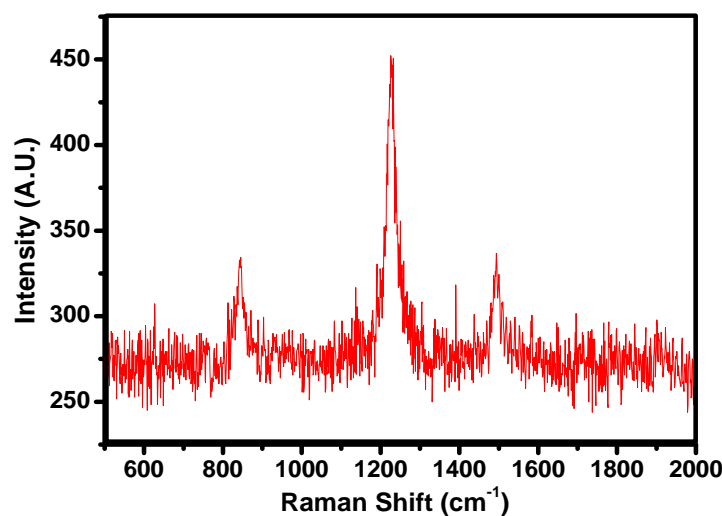


Figure 3. Raman spectroscopy of TiO₂ Nanoparticles.

Figure 4 shows the UV-Visible spectroscopy of TiO₂ nanoparticles showing an absorption tail around 249 nm provides insights into the material's optical properties, including its electronic structure and band gap. The absorption peak at 249 nm falls within the UV region of the spectrum, which is typical for TiO₂, especially in the anatase phase. TiO₂ has a high absorption in the ultraviolet range due to the excitation of electrons from the valence band to the conduction band, corresponding to its wide band gap. The absorption tail beyond this peak indicates that TiO₂ nanoparticles can absorb light with wavelengths slightly longer than 249 nm, but the intensity decreases as the wavelength increases. This absorption behavior suggests a size-dependent effect, where the nanoparticles exhibit quantum confinement, influencing the electronic properties and extending the absorption edge to shorter wavelengths. The optical band gap was found to be 4.97 eV for the TiO₂ nanoparticles [7, 8].

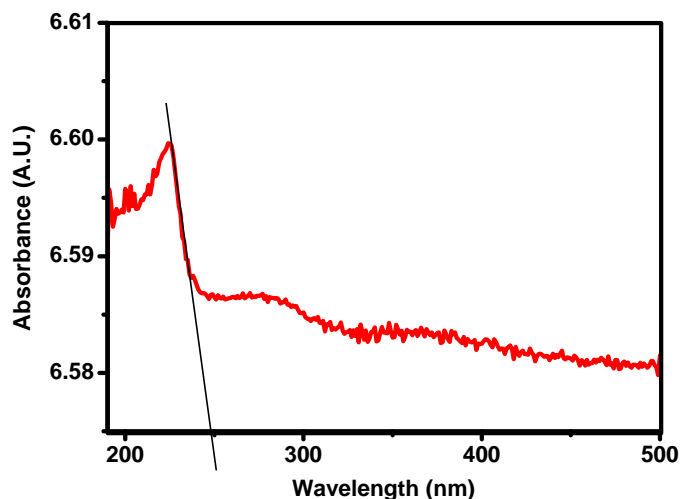


Figure 4. UV-Vis spectroscopy of TiO₂ Nanoparticles.

IV. CONCLUSIONS

In conclusion, the UV-Visible spectroscopy and Raman analysis of TiO₂ nanoparticles provide valuable insights into their structural and optical characteristics. The UV-Visible spectrum reveals a strong absorption peak at 249 nm, indicating efficient UV absorption typical of the anatase phase of TiO₂. The absorption tail beyond 249 nm suggests the influence of size-dependent effects and quantum confinement, extending the absorption edge to shorter wavelengths. The optical band gap of TiO₂ was estimated to be 4.97 eV, indicating its potential for photocatalytic and energy-related applications. Raman peaks at 810, 1225, and 1500 cm⁻¹ further suggest the presence of defects and oxygen vacancies, which may influence the material's catalytic properties. These findings underscore the promise of TiO₂ nanoparticles for a range of applications, including photocatalysis, solar energy conversion, and environmental remediation, with further enhancement achievable through surface modifications and size optimization.

Acknowledgement

Authors are very much thankful to Principal, Bar. Ramrao Deshmukh Arts, Smt. Indiraji Kapadiya Commerce and Nya Krushnarao Deshmukh Science College, Badnera Distt. Amravati (Maharashtra) 444 701 for providing necessary facilities to conduct present study.

V. REFERENCES

- [1]. Shipra Mital Gupta and Manoj Tripathi, "A review of TiO₂ nanoparticles," Chinese Science Bulletin, vol. 56, pp. 1639-1657, May 19, 2011.
- [2]. J. Wang, Z. Wang, W. Wang, Y. Wang, X. Hu, J. Liu, X. Gong, W. Miao, L. Ding, X. Li, and J. Tang, "Synthesis, modification and application of titanium dioxide nanoparticles: a review," Nanoscale, vol. 14, pp. 6709-6734, 2022.
- [3]. P. Rajaram, A. R. Jeice, and K. Jayakumar, "Review of green synthesized TiO₂ nanoparticles for diverse applications," Surfaces and Interfaces, vol. 39, p. 102912, Jul. 2023.
- [4]. J. Jenima, M. Priya Dharshini, M. L. Ajin, J. Jebeen Moses, K. Priya Retnam, K. P. Arunachalam, S. Avudaiappan, and R. F. A. Munoz, "A comprehensive review of titanium dioxide nanoparticles in cementitious composites," Heliyon, vol. 10, no. 20, e39238, Oct. 2024.
- [5]. X. Chen and A. Selloni, "Introduction: Titanium Dioxide (TiO₂) Nanomaterials," Chem. Rev., vol. 114, no. 19, pp. 9281-9282, 2014.
- [6]. C.-Y. Hsu, Z. H. Mahmoud, S. S. Abdullaev, and F. K. Ali, "Nano Titanium Oxide (nano-TiO₂): A Review of Synthesis Methods, Properties, and Applications," Case Studies in Chemical and Environmental Engineering, vol. 2024, 100626, Jan. 2024.
- [7]. V. Verma, M. Al-Dossari, J. Singh, M. Rawat, M. G. M. Kordy, and M. Shaban, "A Review on Green Synthesis of TiO₂ NPs: Photocatalysis and Antimicrobial Applications," Polymers (Basel), vol. 14, no. 7, p. 1444, Apr. 2022.
- [8]. G. Nabi, Q. A. Qurat-ul-Aain, N. R. Khalid, M. B. Tahir, M. Rafique, M. Rizwan, S. Hussain, T. Iqbal, and A. Majid, "A Review on Novel Eco-Friendly Green Approach to Synthesis TiO₂ Nanoparticles Using Different Extracts," Journal of Inorganic and Organometallic Polymers and Materials, vol. 28, pp. 1552-1564, Feb. 2018.

Sustainable Approach to 1, 3-Dithiazine Derivative Synthesis via Fruit Juice Catalysis and Synthetic Organic Acids

Pradnya Nalawade*

Department of Chemistry, Vidya Bharati Mahavidyalaya, Sant Gadge Baba Amravati University, Amravati, Maharashtra, India

ARTICLE INFO

Article History:

Accepted : 01 Jan 2025

Published : 10 Jan 2025

Publication Issue :

Volume 12, Issue 7

January-February-2025

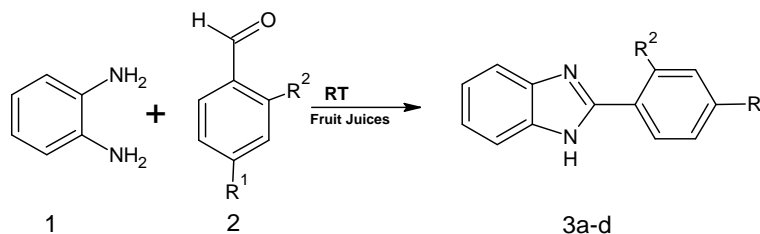
Page Number :

480-483

ABSTRACT

This work uses fruit juices (apple, lemon, grape, and orange) as acid catalysts to synthesize 1,3-dithiazine derivatives in an environmentally friendly manner. Under mild solvent-free circumstances, phenyl hydrazine condenses with substituted aromatic aldehydes (containing hydroxy, methoxy, and chloro groups). This work presents a sustainable and eco-friendly process for creating 1,3-dithiazine derivatives by employing fruit juices as organic catalysts. The reaction works effectively in moderate, solvent-free conditions by utilizing the natural acidity and bioactive components of fruit juices, which is consistent with the concepts of green chemistry. The process is economical and environmentally beneficial since it does not require dangerous synthetic catalysts. Excellent yields of approximately 85% were achieved from this method. The impact of substituents on aromatic aldehydes is assessed. The findings indicate that electron-donating substituents, such as methoxy and hydroxy, have a small impact on yield, however remarkable, increase the yield was observed when substituents are electron-withdrawing characteristics, like chloro. Spectroscopic methods were used to confirm the products. Fourier-transform infrared (FT-IR) and ¹H NMR spectroscopy.

Comparable outcomes were achieved when similar reactions were conducted using synthesized organic acids. The development of green chemistry is aided by this work, which shows a straightforward, sustainable, and repeatable method for creating heterocyclic molecules with possible uses in materials science and pharmaceuticals.



Keywords: Green synthesis, fruit juices, heterocyclic compounds

I. INTRODUCTION

The synthesis of 1,3-dithiazine derivatives is a pivotal area in organic chemistry, given their diverse applications in pharmaceuticals, agrochemicals, and materials science. Traditional synthetic methods often rely on harsh reagents and conditions, raising concerns about environmental sustainability and safety. In response, researchers have been exploring green chemistry approaches to mitigate these issues. One promising avenue is the use of fruit juices as natural catalysts in organic synthesis, offering a sustainable and eco-friendly alternative to conventional methods.

Fruit juices, rich in organic acids and enzymes, have emerged as effective biocatalysts in various chemical reactions. Their mild reaction conditions and biodegradability make them attractive candidates for green chemistry applications. Studies have demonstrated the versatility of fruit juices in catalyzing the formation of heterocyclic compounds, including 1,3-dithiazine derivatives. For instance, a review highlighted the use of fruit extracts as natural catalysts in the formation of heterocycles, emphasizing their non-hazardous nature and cost-effectiveness.

The catalytic activity of fruit juices is primarily attributed to their acidic pH and the presence of natural enzymes. These components facilitate reactions such as condensation, cyclization, and nucleophilic substitution, which are essential in the synthesis of 1,3-dithiazine derivatives. The advantages of using fruit juices as catalysts include Environmental Friendliness, Cost-Effectiveness, Mild Reaction Conditions.

Although green chemistry has advanced, little is known about the use of fruit extracts in particular for the synthesis of 1,3-dithiazines. Although research has shown that fruit extracts are effective at catalyzing the production of various heterocycles including dihydropyrimidinones. A review discussed the use of fruit juices as catalysts in the preparation of heterocycles, including 1,3-dithiazines, highlighting their effectiveness in promoting these reactions.

The synthesis of 1,3-dithiazine derivatives with the incorporation of fruit juice catalysis is a noteworthy development in sustainable organic chemistry. In present work we demonstrated the synthesis of 1,3-dithiazine derivatives by condensation of o-phenylenediamine and aromatic aldehyde using fruit juices as an acid catalyst.

II. EXPERIMENTAL:

All chemicals and solvents were used without additional purification after being acquired from LobaChemie. Fresh oranges, lemons, grapes, and apples were purchased from the Amravati local market. The uncorrected

melting points of every synthetic chemical were measured in a hot paraffin bath. TMS was used as an internal standard while recording ^1H NMR spectra (CDCl_3) on a Bruker Advance II 400 NMR spectrophotometer. Nujol mull and Shimadzu KBr pellets were used to record infrared spectra in the frequency range $4000\text{--}450\text{ cm}^{-1}$ using a Perkin-Elmer-1800 FTIR spectrophotometer. The chemicals that were used were AR grade. Using a solvent mixture of the mobile phase (hexane (10), ethyl acetate (90), and silica gel as the stationary phase on glass tubes, TLC was used to verify the compound's purity on silica gel-G plates.

A. General Procedure:

- Fruit Juices: Fruits were washed with distilled water which was then crushed or pressed to extract the juice. Extracted juices were further filtered through Whatman filter paper and stored in refrigerator till further use.
- A mixture of o-phenylenediamine (1 mmol), arylaldehyde (1 mmol) and Fruit Juice (1 -2ml) or organic acid (25mM) were grind in pestle and mortar. The progress of the reaction was followed by TLC. After the completion of the reaction, water (20 mL) was added. The resulting precipitate was filtered, washed with hot water. Products were further purified by recrystallization from ethanol/DMSO.

B. Characterization of selected 1,3 diazine compounds 2-(4-chlorophenyl)-1H-benzo imidazole (3a)

IR(KBr) $\nu = 3180$ (-NH), $\nu = 1595$ (C=N), $\nu = 1425$ (C=C), $\nu = 1322$ (C-N), $\nu = 851$ 1,4-disub Aromatic ring and $\nu = 759$ 1,2-disub Aromatic ring cm^{-1} . ^1H NMR (CDCl_3) 8.2 ppm (2H, d, Ar-H), 8.7.67 ppm (2H, d, Ar-H), 8.7.55 ppm (2H, d, Ar-H), 8.7.10ppm (2H, d, Ar-H). Mass (m/z) 229 (M^+).

III.RESULT AND DISCUSSION:

A. Synthesis of 1,3-diazine compounds

We report the synthesis of 1,3-diazine compounds by one-pot two component reaction between equimolar amount of substituted benzaldehyde with o-phenylenediamine in presence of mild acid catalyst at room temperature. Above physical data of this study are presented in after completion of the reactions. The solid product was obtained by simple filtration.

The reaction conditions were optimized by varying the concentrations of substituted benzaldehyde and o-phenylenediamine in the presence of fruit juices of lemon, orange, apples and grapes as an acid catalyst along with synthetic organic acid such as maleic acid, vinegar, and citric acid. The desired product is obtained within 10 to 15 minutes and yields up to 85%.

Sr. No.	Substituents on Phenyl Ring	Lemon		Orange		Apples		Grapes		Melting Point $^{\circ}\text{C}$
		Time (min)	Yield%	Time (min)	Yield%	Time (min)	Yield%	Time (min)	Yield%	
1	Ph-H	14	76	12	76	11	70	13	79	260-263
2	Ph-Cl	11	82	10	79	12	79	12	85	280-292
3	Ph-OH	15	79	14	77	13	78	13	77	198-201
4	Ph-OMe	14	76	14	77	12	77	14	76	228-231

Table 1: Model reaction to study reaction between o-phenylenediamine with substituted aldehydes using fruit juices

Sr. No.	Substituents on Phenyl Ring	Citric Acid		Maleic acid		Vinegar		Melting Point 0 C
		Time (min)	Yield%	Time(min)	Yield%	Time (min)	Yield%	
1	Ph-H	14	76	12	76	11	70	257-260
2	Ph-Cl	11	82	10	79	12	79	289-292
3	Ph-OH	15	79	14	77	13	78	179-190
4	Ph-OMe	14	76	14	77	12	77	231-240

Table 2: Model reaction to study reaction o-phenylenediamine with substituted aldehydes using synthetic organic acid

B. Effect of Substituents and Catalyst Type

The impacts of steric and electronic effects on yield were investigated by conducting the reactions with several substituted aromatic aldehydes (chloro, methoxy, and hydroxy groups).

Using fruit juices as natural acid catalysts, each reaction was carried out again.

Due to their steric and electronic characteristics, substituents' impact on aromatic aldehydes has a major impact on the yield of 1,3-dithiazine derivatives. A chloro group is one example of an electron-withdrawing substituent that tends to increase the electrophilicity of the aldehyde's carbonyl group, making it easier for phenyl hydrazine to attack nucleophilically. Usually, this leads to increased yields under the same reaction circumstances.

IV. REFERENCES

- [1]. "Fruit Extract Catalyzed Synthesis of Heterocycles: A Mini-Review," Letters in Applied NanoBioScience 11, no. 4 (December 19, 2021): 4213–26, <https://doi.org/10.33263/LIANBS114.42134226>.
- [2]. Susheel Gulati et al., "One-Pot Three Component Synthesis of Substituted Dihydropyrimidinones Using Fruit Juices as Biocatalyst and Their Biological Studies," PLOS ONE 15, no. 9 (September 15, 2020): e0238092, <https://doi.org/10.1371/journal.pone.0238092>.
- [3]. Rammohan Pal, "Fruit Juice: A Natural, Green and Biocatalyst System in Organic Synthesis," Open Journal of Organic Chemistry 1 (November 9, 2013): 47–56, <https://doi.org/10.12966/ojoc.10.02.2013>.

Synthesis and Characterization of Copper Oxide Nanoparticles Using Precipitation Method

Dr. Priya Sachin Deole, Miss. Ravi P. Raut

Department of Physics, G.S. Tompe College, Chandur Bazar, Dist. Amravati, Maharashtra, India

ARTICLE INFO

Article History:

Accepted : 01 Jan 2025

Published : 10 Jan 2025

Publication Issue :

Volume 12, Issue 7

January-February-2025

Page Number :

484-489

ABSTRACT

In materials Science Synthesis has gained extensive attention as a reliable, Sustainable and Eco- friendly protocol for Synthesizing a wide range of materials/ nanomaterials including Metal/metal oxides, Nanomaterials, Hybrid materials and bioinspired materials. As such green Synthesis is regarded as an important tool to reduce the destructive effects associated with the traditional methods of synthesis for nanoparticles commonly utilized in laboratory and industry.

Nanoscale metals are widely used in many fields such as environment, medicine, and engineering that synthesis of nanoscale metals is a timely topic. At present, nanoscale metals are mainly synthesized by chemical methods that have unintended effects such as environmental pollution, large energy consumption, and potential health problems.

CuO nanoparticles have been successfully synthesized by precipitation method using copper sulphate as a starting material at different reaction temperatures 300 OC, 400 OC, AND 600 OC with the aim of tuning properties and greatly expanding the range of applications. Then nanoparticles were characterized by using X-ray Diffraction (XRD) method. The XRD patterns showed that the prepared CuO-NPs were highly pure, crystalline and nano-sized.

Keywords: Copper Oxide, Nano Particles, Chemical Precipitation, X-Ray Diffraction

I. INTRODUCTION

Nano science has been established recently as a new interdisciplinary science. It can be defined as a whole knowledge on fundamental properties of nano-size objects. The results of Nanoscience are realized in nanotechnology as new materials and functional facilities. Frequently, monomer-size metallic oxide particles shows unique and considerably changed physical, chemical and biological properties compared to their macro

scaled counter, due to their high surface to volume ratio. Thus, nanoparticles have been the subject of substantial research years (1)

Metal oxide nanoparticles is a versatile material with many scientific and industrial application (2) Synthesis of high-quality nanoparticles with respect to chemical purity, phase selectivity, Crystallinity, and homogeneity in particle size with controlled state of agglomeration in a cost-effective procedure is still challenge to material chemists (3) The nanomaterials have attract much scientific attention due to their interesting size-dependent chemical and physical properties and also the potential technological application (5) The science of nanoparticles during the last decade is characterized by, among other things, the enormous efforts which have been made to organize nanoparticles in three and two dimensions, and to some extent one dimension, three dimensional organization if bioartifacts us however, not always a simple matter, since, with some exceptions, particles of a few up to some dozens of monomers in size usually do not possess exactly the same number of atoms or, consequently, the same shape. Classically only identical species were believed to form crystals. Then we learned that particles of similar but not identical size and shape may be able to organize three- even two dimensionally (6) Recently, copper-based nanomaterials have received attention because of their applications in optoelectronic devices, catalysis and superconductor (7) The p-type semiconductor of nanostructured copper oxide (CuO) is an important functional material having direct energy band gap and unique optical and magnetic properties and it is used for gas sensors magnetic storage media solar power transformation, electronics, semiconductors devices, and catalysis (8) It has therefore been studied together with other copper oxides in particular with respect to its applications as a photo thermally active and photoconductive compound (9)

In CuO, the lattice has a monoclinic symmetry (m CuO; space group- $c2/c$) and each atom of this compounds has four nearest neighbours of their kind, Cu atoms are at the center of a rectangle, and the O atoms are at the center of the distorted tetrahedron of Cu (9) CuO with a narrow band gap of 1.2 eV is extensively used in various applications such as catalysis solar energy conversion, gas sensor and field emission (10) Different nanostructures of CuO are synthesized in the form of nanowire (11) nanoflake nanorod nanoneedle nanoflower and nanoparticle (12)

Finite size effects in magnetic nanoparticles have been studied intensively due to their fundamental and technological relevance (13) As the particle size decreases the magnetic stability of nanoparticles due to thermal agitation will become an important issue in technical applications The antiferromagnetic ordering in CuO is due to the exchange interaction between Cu^{2+} ions via O^{2-} ions. It is well known that the unique functions of semiconductor nanoparticles have led to the development of novel photovoltaic and light emitting devices.

Thus there is renewed interest in understanding the fundamental physical properties of CuO as well as for upgrading its performance in applications (14)

Metal nanoparticles can be prepared by two routes; the first one is a physical approach that utilizes several methods such as evaporation/ condensation and laser ablation. The second one is a chemical approach in which the metal ions in the solution are reduced in conditions favouring the subsequent formation of the small metal cluster or aggregates (15) Recently use of nano size semiconductors used to do photocatalytic oxidation of toxic pollutants is being increasingly valued (16)

The aim of the present work is to investigate the effect of the calcination temperature on the crystal structure and the morphology of the nanoparticles by characterization using X-ray diffraction (XRD) (17) and optical properties of the nanoparticles by UV-Vis spectrum (18)

II. EXPERIMENTAL DETAILS:

2.1. Material use

CuSO₄·5H₂O Molecular Weight: 249mg, copper chloride (CuCl₂) Molecular weight: 5g Sodium hydroxide (NaOH) Molecular weight: 10ml, 100ml deionized water

2.2. Synthesis

For the CuO nanoparticles synthesis, 5g of copper chloride (CuCl₂) and using 24.9g of copper sulphate (Cu₄SO₄·H₂O). first each precursor was dissolved in 100ml deionized water to form 0.1M concentration CuCl₂ and copper sulphate solution was taken boiled to 60-80°Cs Using magnetic stirrer heater. Then 10 ml NaOH solution was dropped under vigorous stirring until pH reached to 14. The precipitate was allowed to settle down and the supernatant liquid was poured off (Elsevier, 2013). The oxide was transferred to 250ml flask and the volume was made up. The content was washed up by repeated decantation until it became chloride ion, and then filtered to residue, by washing with double distilled water. The residue was dried at 80 °C in an oven for two hours to get Cu₂O and further calcined at 300°C, 400°C, & 600°C for 3 hours to get Cu₂O and further calcined at 300°C, 400°C, & 600°C for 3 hours for CuO nanoparticles.



Figure 1: X-ray Diffraction:

X-ray diffraction analysis (XRD) is a technique used in materials science to determine the crystallographic structure of a material (1). A primary use of XRD analysis is the identification of materials based on their diffraction pattern. As well as phase identification, XRD also yields information on how the actual structure deviates from the ideal one, owing to internal stresses and defects (2).

2.3. Characterization

Crystals are regular arrays of atoms, whilst X-Rays can be considered as waves of electromagnetic radiation. Crystal atoms scatter incident X-rays, primarily through interaction with the atoms electrons. This phenomenon is known as elastic scattering; the electron is known as the scatterer. A regular array of scatterers produces a regular array of spherical waves. In the majority of directions, these waves cancel each other out through destructive interference, however, they add constructively in a few specific directions, as determined by Bragg's Law:

$$2d\sin\theta = n\lambda$$

Where d is the spacing between diffracting planes, θ {theta} is the incident angle, n is an integer, and λ is the beam wavelength. The specific directions appear as spots on the diffraction pattern called reflections.

Consequently, X-ray diffraction result from electromagnetic waved impinging on a regular array of scatterers. X-rays are used to produce the diffraction pattern because their wavelength, λ is often the same order of magnitude as the spacing, d between the crystal planes.

III.RESULTS AND DISCUSSION

3.1. XRD Pattern

Figures 1 & 2 shows XRD patterns of nanosizedCuO samples. All the diffraction data confirm the information of pure single-phase CuO with the monoclinic phase (JCPD80-1268). No diffraction peaks of impurities (Zhang et al., 2008) were observed in the patterns. It showed that nano size of CuO was successfully synthesized under current mild experimental conditions. The crystallite size of samples was estimated from XRD peak broadening using Scherer's formula (Ahmad R and Mehrnaz G, 2012).

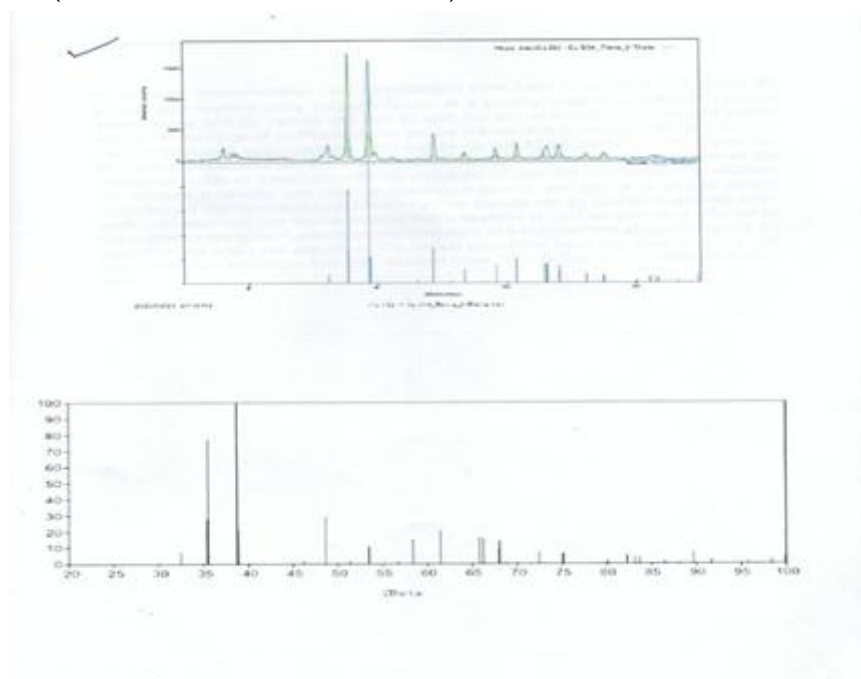


Figure 2

Where t is the crystalline size, λ is the wavelength of x- ray radiation, θ is the Bragg angle, and $\Delta 2\theta$ is the full width at half maximum (FWHM) of the most intense diffraction peak. The influence of the temperature on crystalline sizes of samples is shown in Table 4.1 The FWHM of the diffraction peaks decreases with increasing temperature disclosing that the average crystalline size is becoming bigger correspondingly. Our results showed that by increasing temperature, the intensity of peaks slightly increases and diffraction peaks becomes sharper. This indicates the enhancement of the crystalline size originated from the increment of the crystalline volume ratio due to the size enlargement of the nuclei

IV.CONCLUSION

In summary, semiconductor CuO nanoparticles have been successfully synthesized by precipitation method using copper sulphate as a starting material at different reaction temperatures 3000C,4000C, AND 600 OC with the aim of tuning properties and greatly expanding the range of applications. Our results indicate that

preparation of spherical CuO nanoparticles was achieved when temperatures was 6000C. This result shows the considerable role of temperature on the properties of nanosizeCuO samples. In addition, the method is simple, low cost, environmental- friendly and also it is able to control properties of the nanosizedCuO effectively. This process can be applied to prepare other oxide nanoparticles. Our results showed that properties of CuO samples were affected by the reaction temperature and ultrasonic irradiation as a consequence of the changes in the crystalline size and band gap value. The optical absorption band gap of as-prepared CuO semiconductors was larger than the reported value for bulk CuO due to obtained particle sizes.

V. REFERENCES

- [1]. Sharma, v., Yngard, R and Lin, Y. 2008 Advantage of colloid interface. Journal of Cis, 10:16.
- [2]. Carnes, C. L., Stipop,J and Klabunde, K. J. 2002 Synthesis, characterization and adsorption studies of nonocrystalline copper oxide and nickel oxide Journal of Langmuir , 18: 13- 52
- [3]. Jopani N. Kushwaha S. and Athar T., 2009. Wet synthesis of copper oxide nanopowder. International Journal of Green Nonotechnology, 1: 67-73
- [4]. Giinter S. 2004 Nanoparticles form theory to application Journal of Wiley Online Library 8-10
- [5]. Bohr R. H., Chun S. Y., Dau, Tan, J. T. and Sung, J 2009.Field emission studies of amorphous carbon deposiyted on copper nanowires grown by cathode c ard plasma deposition Journal Carbon Material, 24:97-101.
- [6]. Jinaliang. C. Yan A Tianyi, W., Liu Y. And Zhongyoung, Y. 20121 Synthesis of porous hematite nanorods loaded with CuO nanocrystals as catalysts for co oxidagtion. Journal of Natural Gas Chemical 20: 669-676.
- [7]. Vijaya, K. R. Elgamiel. R., Diamant Y. and Gedanken , A. 2011. Sonochemical preparation and characterization of nanocrystalline copper oxide embedded in poly (vinyl alcohol) and its effect on crystal of copper oxide Journal of Langmuir 17: 1406
- [8]. Sharma, v., Yngard, R. and Lin, Y.2008 Advantage of colloid interface. Journal of Cis, 10: 16.
- [9]. Yang, Z., He, X., Jianping, L., Huigang, Z. and Xiaogiang, G. 2007 Gas-sinsing properties of hollow and hierarchical copper oxide microspheres. Journal of Sensor, 128: 293 298.
- [10]. Phiwdang, R., Sombat, K. and Supab, C. 2005. CuO nanowires by oxidation reaction. Journal of special Issue on Nanotechnology, 4:1-5.
- [11]. Nath, S.S., Chakdar, D. and Goppe, G. 2007. Synthesis of CdS and ZnS quantum dots and their application in electronics. Journal of Nanotechnology and its application, 02(03): 20-25.
- [12]. Khomutov, F.P.andGubin, F.A. 2002. A photoelectrochemicaldeterminationof the position of the conduction and valence band edges of p-type CuO. Journal applies Physics, 53:1173.
- [13]. Liu, W.J., Zenga, F.X., Jianga, H., Zhang X.S. and Li, W.W. 2012. Composite Fe2O3 and ZrO2Al2O3Phtocatalyst: preparation, characterization and studies on the PhotacatalyticActicity and chemical Stability. Chemical Engineering Journal, 180: 9-18.
- [14]. Narongdet, W., Piyanut, C., Naratip, V., and Wisanu, P.2011. Sonochemical synthesis and characterization of copper oxide nanoparticles. Journal of Science Direct, 29:404 409.
- [15]. Elsecier, B.V. 2013. Synthesis of CuO nanoparticle by precipitation method using different precursors, journal of energy production, 34: 740-745.
- [16]. SagarRaut,,Dr. P.V. Thorat, RohiniThakare, International Journal of Science and Research (IJSR), ISSN (online): 2319-7064, Index Copernicus Value (2013): 6.14 Impact Factor (2013)

- [17]. H.S.Nalwa, Encyclopedia of Nanoscience and Nanotechnology, Americal Scientific Publishers, Vol.10, pp.1-46,2007
- [18]. Regith S.G and Krishnan c, 2008 synthesis of Cadmiumdoped copper oxide nanoparticles Advances in applied in applied science research, X-Ray diffraction XRD analysis.
- [19]. Sahu, 2012 nano science and nanotechnology. Jounal of Nanotechnology, 2017.

Synthesis and Characterization of Some Chromene Derivatives

Sharad N. Pawar^{*1}, Deepak M. Nagrik²

¹Department of Chemistry, Shri Shivaji Science and Arts College, Chikhli Dist. Buldana-443201, Maharashtra, India

²Department of Chemistry, G.S. Science, Arts and Commerce College Khamgaon Dist. Buldhana 443303, Maharashtra, India

ARTICLE INFO

Article History:

Accepted : 01 Jan 2025

Published : 10 Jan 2025

Publication Issue :

Volume 12, Issue 7

January-February-2025

Page Number :

490-494

ABSTRACT

The current work is focuses on the synthesis of pharmaceutically important substituted chromene derivatives through one pot reaction multi-component reaction between salicylaldehyde, malononitrile in presence of water as solvent using nano-catalyst at ambient conditions with moderate to good yield. In the present day research age, 4H-chromene and their functional analogues are biologically potent and have attracted significant attention. A survey of the literature revealed that though there are many synthetic approaches exists however most of these are linked to challenges such as harsh reaction condition, extraction, purification and extended reaction time. This fact inspired us to look for a straightforward, green, simple, environmentally friendly work-up synthesis approach. Graphitic carbon nitride (GCN) doped polyaniline composite was prepared and employed to prepare some 4H-chromene derivatives. The synthesized compounds characterized by ¹H-NMR, ¹³C-NMR, MS and FT-IR techniques.

Keywords: Multicomponent, Synthesis, Chromene, Malononitrile, Nano-catalyst.

I. INTRODUCTION

Nowadays heterocyclic compounds attained numerous attention for the synthesis of natural as well as synthetic molecules. Chromene is commonly occur in nature. A frequently utilized component in heterocyclic chemistry is chromene. It has been employed to construct chemical probes for therapeutic and diagnosis purposes[1]. Currently versatile field application of chromene like anti-inflammatories[2], antitubercular agents[3], antitumor agent[4], enzyme inhibitors[5], potassium channel activators[6], antimicrobial[7], antiviral[8] were shown by the different group of researcher.

Multicomponent reaction (MCR) efficiently used by Nagao research group. Knoevenagel condensation of malononitrile for the synthesis of 2-amino-5-carboxy-4-aryl-4H-pyran-3-carbonitriles. This reaction is supposed to proceed through 2-benzylidenemalononitrile intermediate which on ring closure result in 4H-pyran[9].

In addition to looking for an alternate, eco-friendly reaction medium, green chemistry aims to lower reaction temperatures and boost reaction rates[10]. Organic synthesis assisted with nano-catalyst attracting much attention due to its ease of functionalization, eco-friendly, recyclability, toxic free, commercially acceptable and most important easy extraction from the reaction mixture[11]. Polyaniline has suffering with certain drawbacks for the actual commercial application like low surface area, mechanical degradation, limited catalytic activity. Doping is one of the efficient way to alter the physicochemical, morphological features of PANI. Pd and Pt doped PANI mediated organic transformation like oxidation of methanol[12], glycerol[13] etc. showed the useful application in various organic synthesis. Therefore in the present work we highlighted the application of GCN doped polyaniline nano-catalyst for the synthesis of 4H-chromene derivatives. Some substituted 2 - amino - 3 - cyano - 4H - chromene have been prepared by one - pot two - component reaction between salicylaldehyde, malononitrile in water using nano-catalyst. This synthesis protocol was found the convenient method for the synthesis of the variety of 4H-chromene derivatives which were characterized by ¹H-NMR, MS and FT-IR.

Origin of Problem :

The above literature review reveals that despite usefulness of various catalyst, some of them uses harsh conditions, several steps, complex synthetic procedure. Hence it was interested to develop the green protocol to prepare 2-amino-4H-chromene derivatives using GCN doped polyaniline nano-catalyst and water as solvent.

II. METHODS AND MATERIALS

AR grade chemicals of Merck have been used for synthesis. FT-IR spectra have been recorded on a Bruker Germany 3000 Hyperion microscope. The ¹H NMR spectra at 500 MHz from a Bruker Avance Neo NMR spectrometer. Mass spectra collected from SYNAPT-XS DBA064 instrument.

III. EXPERIMENTAL

General procedure for synthesis of substituted 4H-chromene derivatives:

In an oven-dried round bottom flask, salicylaldehyde (1 mmol), malononitrile (2 mmol), catalytic amount of doped PANI and water (5 mL) were transferred sequentially at optimum conditions[14]. This reaction mixture was then stirred continuously and vigorously for hours. The reaction progress was monitored by TLC[15]. After reaction completion, a solid mass precipitated out when distilled water was added into the resulted mixture. It was filtered, washed with aqueous ethanol (Fig.1). The structure of synthesized compound was confirmed by ¹H NMR, ¹³C NMR MS and FT-IR.

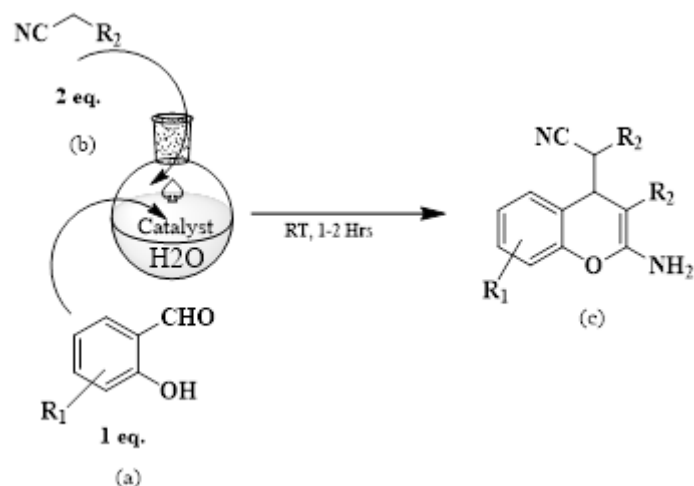


Fig.1 The schematic representation of synthesis of 4H-chromene derivatives

IV. RESULT AND DISCUSSION:

There are some substituted 4H-chromene derivatives have been synthesized and they found to have the good yield.

Table 1: Representative data of synthesized 4H-pyrans

SrNo	Product	R ₁ in (a)	R ₂ in (b)	Time (Hrs.)	Isolated Yield (%)
1		-H	-CN	1	89
2		-Cl	-CN	1.5	86
3		-Br	-CN	2	78

The Representative Analytical Data of Synthesized Compounds:

2-(2-amino-3-cyano-4H-chromen-4-yl) malononitrile (Table Entry 1)

Molecular Formula- **C₁₃H₈N₄O**; Mol.Weight-236.23; Yellowish solid; M.P. 150 - 152° C; Yield: 89%; ¹H NMR (500 MHz, DMSO): δ 6.7 (s, 2H, Ar—NH₂), 7.3 (d, 2H, Ar—H), 3.8 (d, 1H, C—H), 7.5 (t, 2H, Ar—H), 3.6 (1, 1H, —C4H pyran), FT-IR(ν max: cm⁻¹); 3502 (—NH₂), 1550 (C≡N), 1218 (CO), 1488 (C=C).

2-(2-amino-6-chloro-3-cyano-4H-chromen-4-yl)malononitrile (Table Entry 2)

Molecular Formula- **C₁₃H₇ClN₄O**; Mol. Weight-270.68; Yellow solid; M.P. 154 - 156 ° C; Yield: 86%; ¹H NMR (500 MHz, DMSO): δ 6.80 (s, 2H, NH₂), 7.14 (d, 1H, Ar—H), 7.86 (s, 1H, Ar—H), 7.57 (d, 1H, Ar—H), 5.08 (d, 1H, (CN)₂-CH), 3.37 (t, 1H, —C4 H pyran), FT-IR (ν max: cm⁻¹); 3420 (-NH₂), 1760 (C≡N), 1215 (CO), 1541 (C=C), 728 (C-Cl).

2-(2-amino-6-bromo-3-cyano-4H-chromen-4-yl)malononitrile (Table Entry 3)

Molecular Formula- **C₁₃H₇BrN₄O**; Mol. Weight- 315.53; Yellowish brown solid; M.P. 170 - 172 ° C; Yield: 78%; ¹H NMR (500 MHz, DMSO): δ 9.90 (s, 2H, -NH₂), 8.72 (s, 1H, Ar-H), 8.42 (d, 1H, Ar—H), 8.15 (d, 1H, Ar—H), 3.32 (d, 1H, (CN)₂-CH), 2.50 (t, 1H, —C4 H pyran), FT-IR (ν max: cm⁻¹); 3525 (-NH₂), 1558 (C≡N), 1216 (CO), 1489 (C=C), 636 (C-Br).

V. CONCLUSION

This paper focus on the GCN doped polyaniline catalyzed synthesis of 4H-chromene derivatives using one pot multicomponent method. The nano-catalyst has feasible synthetic condition, safe, easily operated and efficient. It is worth mentioning that the reaction time was appreciably reduced by using novel nano-catalyst.

Acknowledgement

The authors wish to gratefully acknowledge support from the Research Centre, Department of Chemistry, G.S.College, Khamgaon Dist. Buldana; SAIF, IIT, Powai, Mumbai and SAIF, Punjab University, Chandigarh. The authors are also thankful to Head, Department of Chemistry and Principal, Science College Pauni Dist. Bhandara for providing laboratory facilities.

VI. REFERENCES

- [1]. Katiyar, M.K.; Dhakad, G.K.; Arora, S.; Bhagat, S.; Arora, T. and Kumar, R., Journal of Molecular Structure, 2022, 1263, 133012, <https://doi.org/10.1016/j.molstruc.2022.133012>
- [2]. Mauro, M.; Ramona, R.; Enzo, S.; Edon, M. and Roberto, M., European Journal of Medicinal Chemistry, 2001, 36, (11-12), 851-861, [https://doi.org/10.1016/S0223-5234\(01\)01279-X](https://doi.org/10.1016/S0223-5234(01)01279-X)
- [3]. Soizic, P.; Herve, L.; Sylvie, M.; Michel, K.; Darbord, J. C., Cole, S. T. Bioorganic & Medicinal Chemistry, 2006, 14, 15, 5423-5428. doi:10.1016/j.bmc.2006.03.033
- [4]. Carsten, F.; Fredilyn, L. and Jurgen, R., Journal of the American Chemical Society, 2003, 125, 26, 7818–7819. doi:10.1021/ja034781q
- [5]. Luca, C.; Corso, A. D.; Giulio, R.; Mark, P. J. Umberto, M., European Journal of Medicinal Chemistry, 2001, 36, 9, 697–703. doi:10.1016/s0223-5234(01)01272-7
- [6]. Agrawal, V. K.; Singh, J.; Gupta, M.; Jaliwala, Y. A.; Khadikar, P. V. and Supuran, C. T. European Journal of Medicinal Chemistry, 2006, 41, 3, 360-366. doi:10.1016/j.ejmech.2005.11.004
- [7]. Rai, U.S.; Isloor, A. M.; Shetty P.; Vijesh, A.M.; Prabhu, N.; Isloor, S.; Thiageeswaran, M. and Fun, H. K. European Journal of Medicinal Chemistry, 2010, 45, 6, 2695-2699. doi:10.1016/j.ejmech.2010.02.040
- [8]. Kumar B.S., Lakshmi, P.V.A., Veena, B.S. and Sujatha, E. Russian Journal of General Chemistry, 2017, 87, 4, 829-836. doi:10.1134/s1070363217040260

- [9]. Y. Nagao, S. Tanaka, K. Hayashi, S. Sano, and M. Shiro, *Thieme Synlett*, 2004, (3): 481-484, DOI: 10.1055/s-2004-815440
- [10]. Jahangirian H, Lemraski EG, Webster TJ, Rafiee-Moghaddam R and Abdollahi Y: A review of drug delivery systems based on nanotechnology and green chemistry: green nanomedicine. *Int J Nanomed*, 2017; 12: 2957
- [11]. Viviana M, Elsa MF, Torres N, et al. Sol-gel synthesis of V₂O₅-SiO₂ catalyst in the oxidative dehydrogenation of nbutane, *Applied Catalysis A: General*. 2006;312:134-43. doi:10.1016/j.apcata.2006.06.042
- [12]. H. Laborde, J.M. Le 'ger, C. Lamy, *Journal of Applied Electrochemistry*, 24, 1994, 219.
- [13]. E.C Venancio, W.T. Napporn, A.J. Motheo, *Electrochimica Acta*, 47, 2002, 1495. [https://doi.org/10.1016/S0013-4686\(01\)00877-5](https://doi.org/10.1016/S0013-4686(01)00877-5)
- [14]. Bhat, S. I.; Choudhary, A. R. and Trivedi, D. R. : *RSC Advances*, 2012, 2, 10556–10563, DOI: 10.1039/c2ra21849f
- [15]. Bele, A. A. Bele and Anubha Khale, *International Journal of pharmaceutical Sciences And research*, 2010, [http://dx.doi.org/10.13040/IJPSR.0975-8232.2\(2\).256-67](http://dx.doi.org/10.13040/IJPSR.0975-8232.2(2).256-67)

Understanding the Properties and Behaviour of Group Theory in Molecular Chemistry

S.C. Darunde

Assistant Professor, Jagadamba Mahavidyalaya, Achalpur City, 444806, Maharashtra, India

ARTICLE INFO

Article History:

Accepted : 01 Jan 2025

Published : 10 Jan 2025

Publication Issue :

Volume 12, Issue 7

January-February-2025

Page Number :

495-498

ABSTRACT

The study of group theory in chemistry serves as a pivotal lens through which the behavior of molecules and their reactions can be understood. By analyzing the symmetry properties of molecular structures, group theory illuminates the ways in which atoms interact and organize themselves during chemical reactions. This mathematical framework not only aids in predicting the outcomes of reactions but also provides valuable insights into molecular vibrations, electronic transitions, and spatial arrangements. Understanding these symmetries is crucial for chemists as they design experiments and interpret data, allowing for a more systematic approach to both theoretical and practical aspects of chemistry. Moreover, incorporating visual representations of symmetry and molecular structures enhances comprehension, bridging the gap between abstract concepts and empirical observations. Ultimately, group theory synthesizes mathematical rigor with chemical intuition, establishing a foundation for advancing research and innovation in the field.

Keywords: Group theory, molecular chemistry, spectroscopy.

I. INTRODUCTION

Overview of Group Theory and its Importance in Chemistry

Group theory serves as a pivotal element in the field of chemistry, particularly in the study of molecular symmetry and chemical bonding. By systematically categorizing the symmetries of molecules, group theory enables chemists to predict and explain the behavior of molecules in reactions, including their vibrational modes and electronic transitions. This framework aids in understanding molecular properties, such as the interactions of light with matter, which are crucial for spectroscopy and photochemistry. Furthermore, the application of group theory extends to the analysis of reaction mechanisms, allowing chemists to discern how molecular symmetry influences reactivity and product formation. For instance, practitioners often utilize symmetry operations to simplify complex molecular interactions, ultimately enhancing their ability to design new compounds and reactions (Tekane et al.). Thus, the relevance of group theory transcends mere

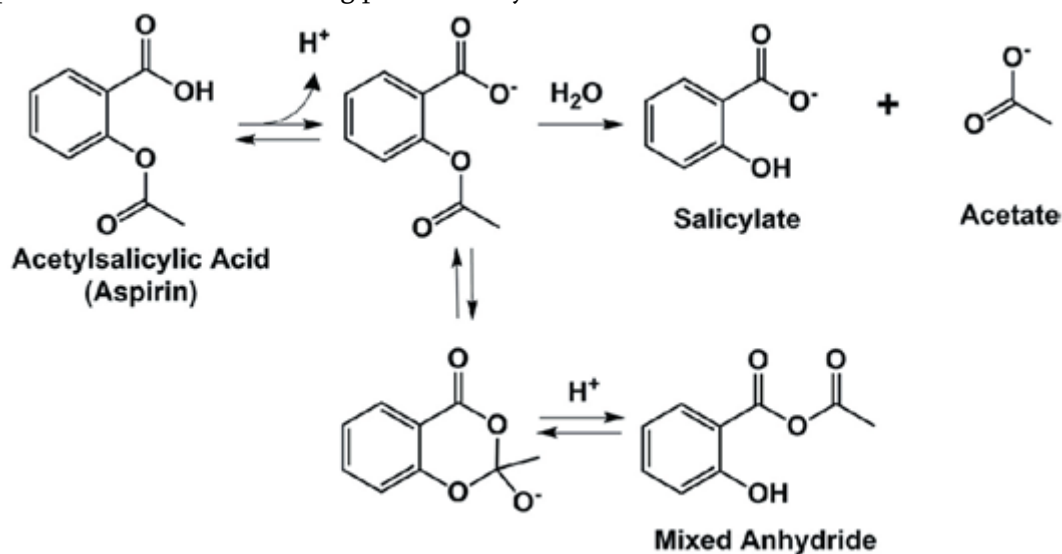
mathematical abstraction, establishing itself as an essential tool in the practical application of chemistry (Wieniewski et al.).

II. APPLICATION OF GROUP THEORY IN MOLECULAR SYMMETRY

The application of group theory in molecular symmetry serves as a pivotal tool for understanding the properties and behaviors of molecules in chemistry. By categorizing molecules into symmetry groups, chemists can predict how molecular structures influence their reactivity and interactions. For instance, in the context of the S_N2 nucleophilic substitution reactions, group theory aids in elucidating the kinetic mechanisms responsible for chirality inversion, thus offering insights into stereochemical outcomes and regioselectivity, as highlighted in recent studies (Mendels et al.). Moreover, the identification of radical species and their interactions not only enhances the comprehension of reaction pathways in complex systems but also facilitates the exploration of molecular conformation under external influences, such as radiation (Callens et al.). Consequently, leveraging group theory provides a systematic approach to rationalizing the intricate relationships between molecular symmetry, structure, and chemical reactivity, reinforcing its foundational role in advancing chemical research.

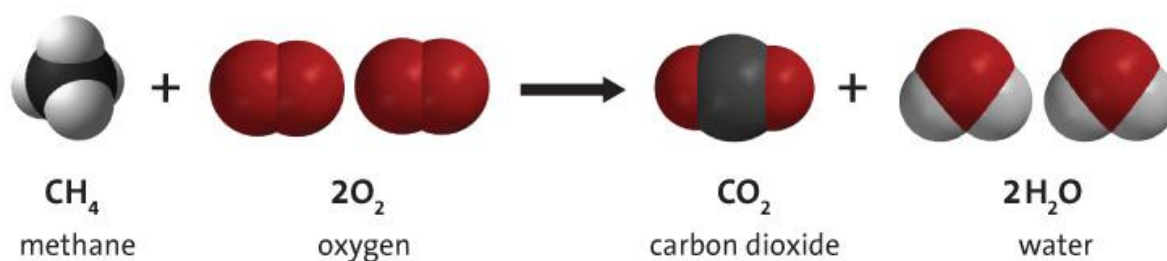
A. Understanding Molecular Symmetry through Group Theory

The study of molecular symmetry through group theory provides a rigorous framework for understanding the behavior of molecules during chemical reactions. By categorizing molecules based on their symmetrical properties, chemists can predict physical characteristics and reactivity patterns that are pivotal for various transformations. Group theory elucidates how symmetry elements and operations define molecular structures, which in turn influence kinetic pathways during reactions. For example, an investigation into the nucleophilic substitution reaction (S_N2) in dichloromethane demonstrates that chirality inversion is closely linked to reaction kinetics rather than the thermodynamic stability of products, as highlighted in a recent study (Mendels et al.). Moreover, exploring the Frank model of spontaneous chiral synthesis illustrates how chiral symmetry and its breakdown can dictate the emergence of homochirality in chemical systems, showcasing the interplay of symmetry and reaction dynamics in shaping molecular behavior (D K Kondepudi et al.). Thus, understanding these principles is essential for advancing predictability in chemical reactions.



III. GROUP THEORY AND SPECTROSCOPY

The interplay between group theory and spectroscopy serves as a foundational element in understanding molecular symmetries and their corresponding spectroscopic properties. Group theory provides a mathematical framework that categorizes molecules based on their symmetrical features, which directly influence their vibrational and electronic transitions. This correlation is particularly evident in techniques such as Raman spectroscopy, where molecular vibrations are probed and analyzed. Notably, the phenomenon of surface-enhanced Raman scattering (SERS) highlights how group theoretical principles can predict and explain enhanced scattering effects due to molecular adsorption on metal surfaces, as discussed in contemporary reviews on the subject (Aberasturi et al.). Furthermore, advancements in methodologies such as ultrafast electron diffraction allow for detailed investigations into transient structures, emphasizing the role of symmetry in dynamic chemical processes (Zewail et al.). Consequently, the integration of group theory with spectroscopic techniques not only enriches the theoretical landscape but also enhances practical analytical applications in chemistry.



A. The Role of Group Theory in Analyzing Spectroscopic Data

The application of group theory in analyzing spectroscopic data is pivotal to understanding molecular symmetries and their associated vibrational modes. By categorizing molecules based on symmetry operations, group theory allows chemists to predict which vibrational transitions are allowed during spectroscopic analysis, facilitating the interpretation of infrared and Raman spectra. This theoretical framework not only aids in determining the number of active modes but also enhances the understanding of molecular orbitals involved in electronic transitions. Moreover, recent studies emphasize the role of symmetry in influencing reaction pathways and the stability of various intermediates in reactions involving gold nanoparticle synthesis, where specific halide ions can be manipulated to modulate nucleation processes ((Coronado et al.)). Such insights underscore the dual significance of group theory, both as a predictive tool and a conceptual framework, establishing its essential role in elucidating complex chemical behaviors in spectroscopy and reaction dynamics.

IV. CONCLUSION

In conclusion, the application of group theory in chemistry serves as a powerful tool for elucidating reaction mechanisms and predicting the outcomes of various chemical processes. By leveraging the symmetry properties of molecular structures, chemists can gain insights into the behavior of reactants and products that would otherwise remain obscured. For instance, the extension method discussed in recent studies allows for examining multiple reaction pathways without prior knowledge of the reaction mechanism, highlighting the versatility of group theory in assessing complex chemical reactivity ((Mendels et al.)). Additionally, advancements in imaging techniques, such as ultrafast electron diffraction, open new avenues for visualizing

structural dynamics in real-time, thus enhancing our understanding of chemical transformations at unprecedented temporal and spatial resolutions ((Shorokhov et al.)). Ultimately, the integration of group theory with innovative experimental approaches will continue to advance the field, fostering deeper comprehension of chemical phenomena.

A. Summary of the Impact of Group Theory on Chemical Reactions and Analysis

Group theory has profoundly influenced the field of chemistry, particularly in understanding chemical reactions and molecular structures. By applying the principles of symmetry and mathematical rules, chemists can classify molecular geometries and predict chemical behavior more accurately. The use of symmetry operations enables the identification of equivalence in molecular orbitals, thereby facilitating the analysis of electronic transitions during reactions. Additionally, group theory is instrumental in predicting the spectroscopic properties of molecules, which provides critical insights into reaction mechanisms. This systematic approach aids in interpreting vibrational spectra and understanding how molecular symmetry impacts reactivity. As a result, group theory not only enhances theoretical frameworks but also has practical implications in areas such as catalysis and material science. Ultimately, its integration into chemical analysis has both refined existing methodologies and opened avenues for novel research possibilities, demonstrating its essential place within modern chemistry.

V. REFERENCES

- [1]. Mendels, Dan, Parrinello, Michele, Piccini, GiovanniMaria. "Metadynamics with Discriminants: a Tool for Understanding Chemistry". 2018, <http://arxiv.org/abs/1809.00504>
- [2]. Shorokhov, Dmitry, Zewail, Ahmed H.. "4D electron imaging: principles and perspectives". 'Royal Society of Chemistry (RSC)', 2008, <https://core.ac.uk/download/4878202.pdf>
- [3]. Callens, Freddy, De Cooman, Hendrik, Kusakovskij, Jevgenij, Sagstuen, et al.. "On the identity of the last known stable radical in X-irradiated sucrose". 'Elsevier BV', 2017, <https://core.ac.uk/download/84041222.pdf>
- [4]. Coronado, Eduardo A., Douglas Gallardo, Oscar Alejandro, Macagno, Vicente Antonio, Moiraghi, et al.. "Gold Nucleation Inhibition by Halide Ions: a Basis for a Seed-Mediated Approach". 'Royal Society of Chemistry (RSC)', 2015, <https://core.ac.uk/download/159290766.pdf>
- [5]. Zewail, Ahmed H.. "4D ultrafast electron diffraction, crystallography, and microscopy". 'Annual Reviews', 2006, <https://core.ac.uk/download/4875477.pdf>
- [6]. Aberasturi, Dorleta Jimenez de, Aizpurua, Javier, Alvarez-Puebla, Ramon A., Auguie, et al.. "Present and future of surface-enhanced Raman scattering". 2019, <https://core.ac.uk/download/288114229.pdf>
- [7]. Tekane, Rethabile Reginalda. "PROCESSES FOR IDENTIFYING IMPORTANT CHEMISTRY AND BIOCHEMISTRY CONCEPTS AND REPRESENTATIONS AND THEIR QUALITATIVE ASSESSMENT IN UNDERGRADUATE BIOLOGY COURSES". 'Purdue University (bepress)', 2016, <https://core.ac.uk/download/220146201.pdf>
- [8]. Wienewski, Ronja Dorothee. "The influence of interactive 3-D models in teaching oxidation numbers in organic chemistry in the high school classroom". Tartu Ülikool, 2021, <https://core.ac.uk/download/479161059.pdf>
- [9]. D. K. Kondepudi, David Hochberg, J. Crusats, L. Peliti, M. Gleiser, María Paz Zorzano, O. Botta, et al.. "Mirror symmetry breaking as a problem in dynamical critical phenomena". 'American Physical Society (APS)', 2007, <http://arxiv.org/abs/0708.2647>

A Comprehensive Review of Storage Principles and Electrode Materials in Supercapacitors

Vaibhav R. Shrikhande^{1,2}, Anjali B. Bodade¹

¹Nanoscience Research Laboratory, Shri Shivaji Science College, Amravati 444603, Maharashtra, India

²Department of Chemistry, Shri. Dr. R. G. Rathod Arts & Science College Murtizapur Dist. Akola 444107, Maharashtra, India

ARTICLE INFO

Article History:

Accepted : 01 Jan 2025

Published : 10 Jan 2025

Publication Issue :

Volume 12, Issue 7

January-February-2025

Page Number :

499-506

ABSTRACT

Considering the increasing demand for efficient energy storage on a worldwide scale, supercapacitors (SCs) have shown a lot of promise. Recent developments in this field have made an alternative required, which has resulted in the development of supercapacitors. Supercapacitors have garnered significantly more attention than traditional batteries due to their excellent power density, rapid charging and discharging rates, and long-term cycle stability. Supercapacitors are ideally suited for devices that need high current for brief periods of time since they are primarily pulse current devices. Current research focuses on increasing the energy density to enable a greater variety of applications. In this review, electrode materials for supercapacitor are summarized. For supercapacitor, there are three types of electrode material are utilized and exploited. They are carbon-based materials, conducting polymers and transition metal oxides and sulphides. However, much of the research is focused on developing novel materials for electrodes that will work superior. The characteristics of the electrode materials in supercapacitors and the storage idea are covered in this review research.

Keywords: Supercapacitor, EDLC, Pseudocapacitors, Electrode, Metal oxide, Carbon materials

I. INTRODUCTION

The standard of living in a country is often linked to its energy consumption, reflecting the increasing energy demands of modern society. Currently, fossil fuels dominate as the primary energy source worldwide, posing challenges due to their environmental impact and finite availability[1]. Complementary avenues for energy, like hydropower, solar, biomass, wind, and geothermal energy are gaining attention, alongside energy forms like light, heat, electricity, hydrogen, and fuel. Photovoltaic (solar) devices show great potential as an energy

solution but face hurdles like high investment costs and concerns about reliability and sustainability[2]. Efficient storage mechanisms for energy are necessary to provide energy security and lessen reliance on fossil fuels. The market for portable electronics and hybrid electric cars is expanding quickly, making energy storage a top priority for both the scientific community and international governments [3]. A growing need for high-power electricity resources has spurred significant interest in developing more efficient energy storage devices. As sustainable energy sources become essential for the future, reducing energy consumption and transitioning to renewable energy systems is paramount. This shift necessitates the development of efficient, rechargeable energy storage technologies[4]. Devices for storing energy can be roughly divided into several categories, including mechanical (e.g., flywheels), electrical (e.g., capacitors), and electrochemical (e.g., supercapacitors, batteries, and fuel cells). Battery, fuel cell, and supercapacitor electrochemical energy storage and conversion technologies are among them, are emerging as pivotal solutions to meet global energy demands. Batteries and fuel cells primarily function by converting chemical energy into electrical energy. Supercapacitors, on the other hand, are gaining prominence as energy storage devices capable of meeting technical and economic requirements since they have a high-power density, rapid charging capabilities, and long-life cycles[5]. Table 1.1 compares the characteristics and capabilities of batteries, supercapacitors, and capacitors.

Parameters	Capacitor	Supercapacitor	Battery
Charge Time	$10^{-6} \sim 10^{-3}$	1 ~ 30 sec	0.3 ~ 3 hrs
Discharge Time	$10^{-6} \sim 10^{-3}$ sec	1 ~ 30 sec	1 ~ 5 hrs
Energy Density (Wh/kg)	< 0.1	1 ~ 10	20 ~ 100
Power Density (W/kg)	> 10,000	1,000 ~ 2,000	50 ~ 200
Cycle Life	> 500,000	> 100,000	500 ~ 2,000
Charge/Discharge Efficiency	~ 1.0	0.90 ~ 0.95	0.7 ~ 0.85

Table 1.1. Comparison parameters of Capacitor, Supercapacitor and Battery

Modern storage systems for energy made for high-power applications are called supercapacitors, often referred to as electric double-layer capacitors (EDLCs) or ultracapacitors. On the outermost portion of the electrode materials, they store charge either electrostatically or electrochemically at the electrode-electrolyte contact[6]. Even though they have several benefits, including as high-power density and quick charge-discharge cycles, their broad use is sometimes constrained by expensive production costs. Supercapacitors, however, offer a viable way to meet the rising power requirements of contemporary energy storage systems, offering a balance of efficiency, durability, and performance. Two important metrics for assessing supercapacitors' performance are their energy density (E) and power density (P). Energy density represents the ability of a supercapacitor to store energy, determining how long it can function as a power source[7]. It is typically expressed in watt-hours per kilogram (Wh/kg) and is calculated as the energy stored per unit volume or unit mass of the device. When determining whether supercapacitors are appropriate for a certain application, these factors are crucial because they strike a balance between the demand for high power output and energy storage capacity. Gravimetrically, power density is expressed in watt-hours per kilogram (Wh/kg) per unit of mass[8]. Nowadays, increasing energy density yet retaining high power density, rapid charge/discharge, and stable cycling is the aim of all supercapacitor investigations. In this study, the storage concepts and properties of several electrode materials utilized in supercapacitors are reviewed and presented.

II. TYPES OF SUPERCAPACITORS

The three main types of supercapacitors are electric double layer capacitors (EDLCs), hybrid supercapacitors, and pseudocapacitors. Because of their extraordinary capacity to store large quantities of charge, these supercapacitors are referred to as high energy storage devices. Detailed classification of supercapacitors is shown in Fig. 1.1

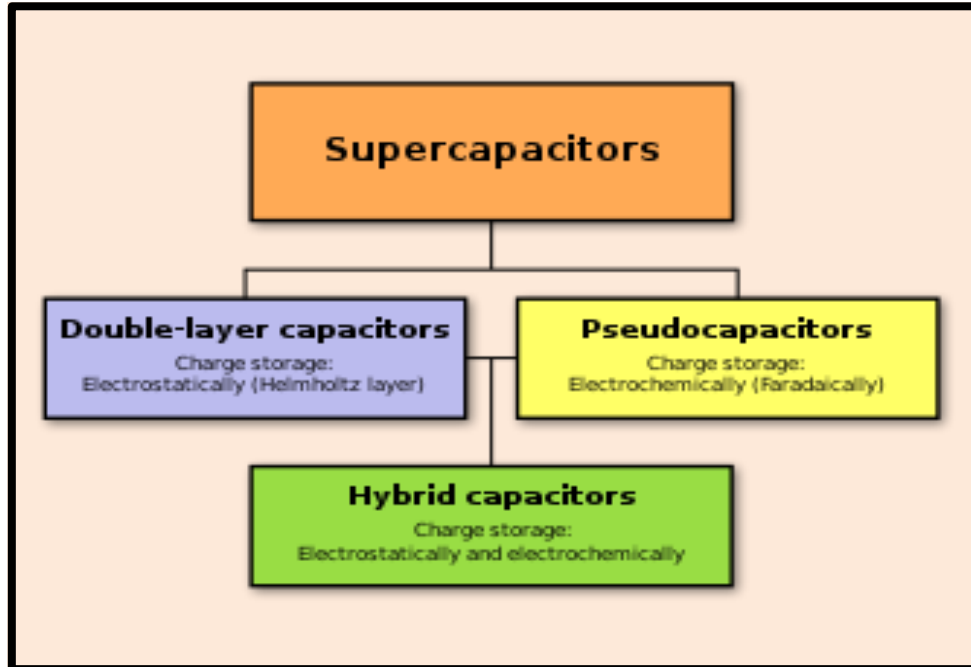


Fig.1.1. Diagrammatic representations of the many kinds of supercapacitors

1.1 Electric Double-Layer Capacitors (EDLCs)

EDLCs and traditional capacitors both use similar mechanisms for storing charge. On the other hand, at the electrode-electrolyte interface, it stores electrical charge in the electric double layer rather than the dielectric layer. Consequently, the interfaces between the electrode and the electrolyte are used by EDLCs to store charge, mainly in high-surface-area carbon electrodes. These devices are capable of efficiently storing charges because to the thin double layer (0.3 - 0.8 nm). The surface lattice structure of the electrode contains one electronic layer, whilst the electrolyte's dissolved and solvated ions produce the other, which has the opposite polarity. Two layers of positive and negative charges combine to form double electric layers. A monolayer of solvent molecules known as the inner Helmholtz plane exists between the two charged layers. In order to physically separate the oppositely polarized ions from one another and function as a dielectric molecule, solvent molecules physically adsorb on the surface of the charged electrode. Between the electrode and the electrolyte, physical processes (such as electrostatic forces) take place instead of chemical ones[9].

1.2 Pseudocapacitors

Pseudocapacitors are a type of faradic capacitance that differs greatly from the classical electrostatic capacitance seen in double layers. They are useful in boosting the charge storage capacitance of the supercapacitor. Unlike batteries, pseudocapacitors have a larger capacitance than EDLCs and chemically store charge through a quick, reversible oxidation/reduction process on their surface. According to the findings, the capacitance of electrically conducting polymers like polyaniline, metal oxide film-based capacitors, and materials like MnO_2

and RuO₂ heteroatom-doped graphene/CNTs, and heteroatom-doped carbons exhibits a 10-hundredfold increase in capacitance compared to pure carbon-based materials[10].

1.3 Hybrid Supercapacitors

In a single cell, hybrid supercapacitors combine the benefits of both faradic and non-faradic processes for charge storage, namely EDLCs and pseudocapacitors. This hybrid energy storage technology further enhances the composite electrode's capacitance by utilizing carbon-based nanostructured materials and pseudocapacitive substances, including metal oxides and conducting polymers[11].

III.ELECTRODE MATERIALS

For supercapacitor, there are three types of electrode material are utilized. These are materials made of carbon, conducting polymers, and oxides and sulphides of transition metals.

3.1. Carbon based materials

Carbon and carbon-based materials are frequently employed as electrode materials for supercapacitor applications because of their huge surface area, low cost, natural abundance, high conductivity, and improved compatibility. There are several different forms of carbon material. Activated carbon, carbon aerogel, carbon nanotubes, and graphene are among the several types of carbon materials that are utilized as electrodes in supercapacitors[8].

3.1.1 Activated carbon (AC)

Activated carbon (AC) is the most often used electrode material because of its high surface area, favorable electrical characteristics, and affordable price. Carbons are generating from pyrolysis of biomass precursors like wood, coal, coconut and other agricultural waste. The porosity of carbons and specific surface area are increased by an activation process. Activation can be performed by physical or chemical methods. The carbon generated from carbonization is compressed with an oxidizing gas at high temperatures to carry out the physical activation procedure. Thermal disintegration of the precursor impregnated with chemical activating substances, such as KOH or HNO₃, accomplishes the carbonization and activation process in chemical activation[12].

3.1.2 Carbon nanotubes (CNTs)

In 1991, Sumio Iijima discovered it using the arc-discharge method. Numerous benefits of carbon nanotubes (CNTs) include low resistivity, limited pore size distribution, high stability, and large surface area. Double-walled carbon nanotubes (MWCNTs) and single-walled carbon nanotubes (SWCNTs) are the two types of carbon nanotubes. Concentric cylinders are grouped around a similar core hollow, with a 0.34–0.39 nm gap between layers. This is somewhat more than the 0.335 nm gap seen in single-crystal graphite. SWCNTs are made by rolling up a 1-2 nm-diameter piece of graphene[13].

3.1.3 Graphene

In essence, a graphene single layer sheet is a two-dimensional hexagonal lattice of sp² carbon atoms. Due to its exceptional electrical conductivity, large surface area, high charge carrier mobility, high mechanical strength, and chemical stability, graphene is a perfect electrode material for electric double layer capacitors. Because graphene has a particular surface area of 2675 m² g⁻¹, it can carry an electric double layer capacitance value of up to 550 F g⁻¹. The ease with which the electrolyte may access graphene's two primary external surfaces is another advantage of employing it as an electrode material. Several techniques, including chemical vapor deposition, micromechanical cleavage, exfoliation of graphite oxide, epitaxial growth, arc discharge method,

unzipping of carbon nanotubes, and intercalation procedures in graphite, can be used to manufacture graphene[14].

3.2. Transition metal oxides

Transition metal oxides are excellent materials for electrodes, especially in energy storage systems such as supercapacitors and batteries, because of several intrinsic and structural properties, high specific capacitance, and variety of oxidation states. They are therefore suitable for developing supercapacitors with high power and energy density. Ruthenium dioxide (RuO_2), nickel oxide (NiO), manganese oxide (MnO_2), and cobalt oxide (Co_3O_4) are the metal oxides that are most often utilized.

3.2.1 Ruthenium Oxide (RuO_2)

Due to its high redox reversible reaction, high specific capacitance, multiple oxidation states, long cycle life, low resistivity, broad potential window, high proton conductivity, and good thermal stability, RuO_2 , one of several metal oxides, is a desirable material for energy storage applications. However, commercial mining is prohibited by its costly cost, low quantity, and severe toxicity. A focused effort is being undertaken to discover a metal oxide for supercapacitor electrode materials that is more affordable, eco-friendly, and practical. The resulting electrodes stayed constant for several cycles and generated a specific capacitance of 498 F/g at a scan rate of 5 mV/s[15].

3.2.2 Cobalt oxide (Co_3O_4)

Among the several materials used in pseudocapacitors, cobalt oxide is another one that performs well as an electrode due to its high theoretical specific capacitance, affordability, reversible redox behavior, and robust corrosion stability. Despite having a small potential window of around 0.45 V, cobalt oxide has good electrochemical performance[16].

3.2.3 Nickel oxide (NiO)

Due to its high expected specific capacitance, low cost, and superior chemical and thermal stability, nickel oxide (NiO) is a good pseudocapacitor material for electrodes for supercapacitor applications. The electrochemical characteristics of NiO nanoparticles are significantly influenced by their structure. An extremely high specific capacitance of 1478 F/g in an electrolyte of 1 M KOH aqueous solution was obtained using the resultant technique[17].

3.2.4 Manganese oxide (MnO_2)

Manganese oxide's distinct physical and chemical characteristics, as well as its many uses in molecular adsorption, ion exchange, catalysis, biological sensing, and energy preservation, have piqued researchers' attention. Because of its inexpensive cost and superior capacitive performance in aqueous solutions, manganese oxide may be used as an electrode material in supercapacitors[18].

3.3. Conducting Polymers

Conducting polymers are excellent pseudocapacitive materials because to their high charge density, simplicity of manufacture, reversible reduction and oxidation capabilities, and relatively inexpensive cost. The most often used conducting polymer is polyaniline (PANI), which exhibits a wide range of redox conditions. Supercapacitor electrode materials also include other commonly used polymers, such as polypyrrole (PPy) and polythiophene and its derivatives; nevertheless, the capacitance is greatly affected by the preparation conditions, the synthetic method, and the monomer structure. Redox reactions take place during the primary majority of polymer conductivity. The polymer core receives the ions during oxidation, and the electrolyte receives the ions back from the core during reduction. In nature, these redox processes can be reversed. When

the repeating units of polymer chains undergo oxidation, a positively charged polymer known as p-doped is created. N-doped polymers are those that are produced via reduction and have a negative charge[7][19].

3.4. Other metal oxides and metal sulfides

Other compounds such as vanadium pentoxide, titanium oxide, molybdenum oxide, tin oxide, iron oxide, cobalt sulfide, and copper sulfide have also been studied as possible electrode materials for pseudocapacitors. Vanadium pentoxide has both cathodic and anodic natures. Because of its layered structure, which makes ion intercalation and deintercalation easier, V₂O₅ has higher electrochemical activity. Although molybdenum oxide has a low cyclic stability, it has an excellent pseudocapacitance nature. Tin oxide has also been studied as a possible electrode material for supercapacitors. Tin oxide has a comparatively low specific capacitance in relation to other metal oxides. Additionally, iron oxide's pseudocapacitance behavior has been investigated. Because of its weak conductivity, it cannot be used as a practical instrument for storing charge. Both metal oxides and copper and cobalt sulfides have been investigated as electrode materials. Nevertheless, the specific capacitance is not great[20].

IV. RECOMMENDATIONS AND OBSERVATIONS

- The published article makes clear that supercapacitors still have a long way to go before they can fully replace batteries.
- Current commercially available supercapacitors are ideal for applications where high-power delivery, rapid charge/discharge cycles, and durability are critical, even if the energy storage duration is relatively short. Their unique characteristics make them suitable for a range of niche but important applications.
- The advancement of hybrid supercapacitors, which combine the high energy density of batteries with the high-power density and extended cycle life of conventional supercapacitors, is the key to the future of supercapacitor technology.
- The discovery of graphene revolutionized the field of supercapacitors by providing a material with exceptional properties that address many of the limitations of traditional electrodes.
- The issue of self-discharge in supercapacitors, where stored energy dissipates over time without any external load, is a significant challenge that limits their practical applications, particularly for long-term energy storage. Addressing this requires a combination of materials science, device engineering, and electrolyte optimization.

V. CONCLUSION

Supercapacitors were developed as a vital alternative energy storage technology with strong stability, high power density, and excellent electrochemical properties. It has been stated that supercapacitors possess a property that makes them suitable for a variety of applications, such as emergency power sources, hybrid power systems for electric cars, and enhancing the capabilities of batteries. According to the review provided here, supercapacitors may still be made better in terms of design and construction so that they can be employed in more high-energy density applications. Researchers are still focusing on the several types of electrode materials, including carbon, metal oxide, and conducting polymers. The influence graphene may have on other electrode materials—that is, by mixing it with conducting polymers or metal oxides to create composites—should be the

main focus of future research. Researchers are increasingly focusing on ternary composites as they offer synergistic effects that combine the strengths of three distinct components, resulting in superior properties for energy storage applications. These composites often integrate the benefits of carbon materials, metal oxides, and conducting polymers, or other novel materials, to achieve high energy and power densities, improved stability, and enhanced cycling performance.

VI. REFERENCES

- [1]. P. Sharma and T. S. Bhatti, 'A review on electrochemical double-layer capacitors', *Energy Convers. Manag.*, vol. 51, no. 12, pp. 2901–2912, Dec. 2010, doi: 10.1016/j.enconman.2010.06.031.
- [2]. M. S. Lal, R. Badam, N. Matsumi, and S. Ramaprabhu, '1 Hydrothermal synthesis of single-walled carbon nanotubes/TiO₂ for quasi-solid-state composite-type symmetric hybrid supercapacitors', *J. Energy Storage*, vol. 40, p. 102794, Aug. 2021, doi: 10.1016/j.est.2021.102794.
- [3]. C. Hou, W. Huang, W. Zhao, D. Zhang, Y. Yin, and X. Li, 'Ultrahigh Energy Density in SrTiO₃ Film Capacitors', *ACS Appl. Mater. Interfaces*, vol. 9, no. 24, pp. 20484–20490, Jun. 2017, doi: 10.1021/acsami.7b02225.
- [4]. H. Bantawal, U. S. Shenoy, and D. K. Bhat, 'Vanadium-Doped SrTiO₃ Nanocubes: Insight into role of vanadium in improving the photocatalytic activity', *Appl. Surf. Sci.*, vol. 513, p. 145858, May 2020, doi: 10.1016/j.apsusc.2020.145858.
- [5]. Z. S. Iro, C. Subramani, and S. S. Dash, 'A Brief Review on Electrode Materials for Supercapacitor', *Int. J. Electrochem. Sci.*, vol. 11, no. 12, pp. 10628–10643, Dec. 2016, doi: 10.20964/2016.12.50.
- [6]. G. Marimuthu et al., '58 Silver-decorated SrTiO₃ nanoparticles for high-performance supercapacitors and effective remediation of hazardous pollutants', *Environ. Geochem. Health*, vol. 46, no. 3, p. 96, Mar. 2024, doi: 10.1007/s10653-024-01875-x.
- [7]. J. Banerjee, K. Dutta, M. A. Kader, and S. K. Nayak, 'An overview on the recent developments in polyaniline-based supercapacitors', *Polym. Adv. Technol.*, vol. 30, no. 8, pp. 1902–1921, Aug. 2019, doi: 10.1002/pat.4624.
- [8]. A. P. Singh, N. K. Tiwari, P. B. Karandikar, and A. Dubey, 'Effect of electrode shape on the parameters of supercapacitor', in *2015 International Conference on Industrial Instrumentation and Control (IIC)*, Pune, India: IEEE, May 2015, pp. 669–673. doi: 10.1109/IIC.2015.7150826.
- [9]. J. Libich, J. Máca, J. Vondrák, O. Čech, and M. Sedlářková, 'Supercapacitors: Properties and applications', *J. Energy Storage*, vol. 17, pp. 224–227, Jun. 2018, doi: 10.1016/j.est.2018.03.012.
- [10]. N. I. Jalal, R. I. Ibrahim, and M. K. Oudah, 'A review on Supercapacitors: types and components', *J. Phys. Conf. Ser.*, vol. 1973, no. 1, p. 012015, Aug. 2021, doi: 10.1088/1742-6596/1973/1/012015.
- [11]. D. P. Chatterjee and A. K. Nandi, 'A review on the recent advances in hybrid supercapacitors', *J. Mater. Chem. A*, vol. 9, no. 29, pp. 15880–15918, 2021, doi: 10.1039/D1TA02505H.
- [12]. M. Inagaki, H. Konno, and O. Tanaike, 'Carbon materials for electrochemical capacitors', *J. Power Sources*, vol. 195, no. 24, pp. 7880–7903, Dec. 2010, doi: 10.1016/j.jpowsour.2010.06.036.
- [13]. L. S. Salah, N. Ouslimani, D. Bousba, I. Huynen, Y. Danlée, and H. Aksas, 'Carbon Nanotubes (CNTs) from Synthesis to Functionalized (CNTs) Using Conventional and New Chemical Approaches', *J. Nanomater.*, vol. 2021, pp. 1–31, Sep. 2021, doi: 10.1155/2021/4972770.

- [14]. H. Hu, Z. Zhao, Q. Zhou, Y. Gogotsi, and J. Qiu, 'The role of microwave absorption on formation of graphene from graphite oxide', *Carbon*, vol. 50, no. 9, pp. 3267–3273, Aug. 2012, doi: 10.1016/j.carbon.2011.12.005.
- [15]. M. Ates and C. Fernandez, 'Ruthenium oxide–carbon-based nanofiller-reinforced conducting polymer nanocomposites and their supercapacitor applications', *Polym. Bull.*, vol. 76, no. 5, pp. 2601–2619, May 2019, doi: 10.1007/s00289-018-2492-x.
- [16]. J. Mei, T. Liao, G. A. Ayoko, J. Bell, and Z. Sun, 'Cobalt oxide-based nanoarchitectures for electrochemical energy applications', *Prog. Mater. Sci.*, vol. 103, pp. 596–677, Jun. 2019, doi: 10.1016/j.pmatsci.2019.03.001.
- [17]. S. D. Dhas et al., 'Synthesis of NiO nanoparticles for supercapacitor application as an efficient electrode material', *Vacuum*, vol. 181, p. 109646, Nov. 2020, doi: 10.1016/j.vacuum.2020.109646.
- [18]. I. Acznik, K. Lota, A. Sierczynska, and G. Lota, 'Carbon-Supported Manganese Dioxide as Electrode Material For Asymmetric Electrochemical Capacitors', *Int. J. Electrochem. Sci.*, vol. 9, no. 5, pp. 2518–2534, May 2014, doi: 10.1016/S1452-3981(23)07944-0.
- [19]. L. Yuan, B. Yao, B. Hu, K. Huo, W. Chen, and J. Zhou, 'Polypyrrole-coated paper for flexible solid-state energy storage', *Energy Environ. Sci.*, vol. 6, no. 2, p. 470, 2013, doi: 10.1039/c2ee23977a.
- [20]. S. Vijayakumar, S. Nagamuthu, K. K. Purushothaman, M. Dhanashankar, and G. Muralidharan, 'SUPERCAPACITOR BEHAVIOR OF SPRAY DEPOSITED SnO₂ THIN FILMS', *Int. J. Nanosci.*, vol. 10, no. 06, pp. 1245–1248, Dec. 2011, doi: 10.1142/S0219581X11008368.

Computational Analysis of 5-N-Substituted-2-(Substituted Benzenesulphonyl) Glutamine Derivatives as Potential Inhibitors of the Kinase Domain in Imatinib-Resistant Abl Mutant Enzyme

Asita Ganatra¹, Neetu Gupta², Satyen Patil², Sunil Ganatra²

¹Department of Computer Science, Symbiosis Institute of Technology, Nagpur, Maharashtra, India

²Department of Chemistry, Institute of Science, R. T. Road, Civil Lines, Nagpur-440001, Maharashtra, India

ARTICLE INFO

Article History:

Accepted : 01 Jan 2025

Published : 10 Jan 2025

Publication Issue :

Volume 12, Issue 7

January-February-2025

Page Number :

507-517

ABSTRACT

In-silico studies were conducted to examine the molecular interactions of 5-N-Substituted-2-(Substituted Benzenesulphonyl) Glutamine-based compounds with Kinase Domain in Imatinib-Resistant Abl Mutant Enzyme having PDB Code:2F4J . The binding energy between the ligand and the receptor protein was calculated. The results were analyzed in terms of hydrophobic interactions, van der Waals forces, electrostatic interactions, and the potential for hydrogen bond formation.

I. INTRODUCTION

The ABL1 gene (Abelson murine leukemia viral oncogene homolog 1) encodes a protein called Abl kinase, a non-receptor tyrosine kinase that plays a critical role in regulating various cellular processes, including cell differentiation, division, and adhesion. The ABL1 protein is primarily located in the cytoplasm and the nucleus, and it has a key function in signal transduction pathways that control the cell cycle, cytoskeletal dynamics, and apoptosis.[1-3]

The ABL1 protein consists of several domains, including a kinase domain responsible for transferring phosphate groups to tyrosine residues in target proteins. This phosphorylation is crucial for mediating signaling pathways. In chronic myelogenous leukemia (CML) and other cancers, a fusion gene called BCR-ABL is formed through a chromosomal translocation (Philadelphia chromosome), leading to a constitutively active form of the Abl

kinase. This mutated form promotes uncontrolled cell growth, making the ABL1 protein a critical target for cancer therapies, such as the drug Imatinib, which inhibits the BCR-ABL fusion protein's kinase activity. Mutations in the ABL1 gene, particularly in the kinase domain, can cause resistance to Imatinib, making it a subject of ongoing research for the development of more effective treatments for resistant forms of leukemia.[3] The inhibition of Abl kinase has played a pivotal role in the treatment of cancers, particularly chronic myelogenous leukemia (CML). The journey toward understanding and inhibiting Abl kinase began with the discovery of the BCR-ABL fusion gene, a product of a chromosomal translocation that causes constitutive activation of Abl kinase. This abnormal activation is a major driver of CML, and understanding how to inhibit it became a key focus of research in the 1990s.

Early Discoveries and the Role of Abl Kinase in CML

In the late 1980s and early 1990s, researchers identified that the Philadelphia chromosome, a specific chromosomal abnormality, led to the formation of the BCR-ABL fusion protein (Nowell & Hungerford, 1960). This protein has constitutive tyrosine kinase activity, which plays a central role in the pathogenesis of CML. The discovery prompted efforts to find selective inhibitors for this enzyme.[2]

Development of Imatinib (Gleevec)

The breakthrough in Abl kinase inhibition came in the mid-1990s when Dr. Brian Druker and colleagues at Oregon Health & Science University designed Imatinib (Gleevec). Imatinib specifically targets the BCR-ABL fusion protein, binding to the ATP-binding site of the kinase domain and preventing its activation. Imatinib became the first successful targeted therapy for CML, leading to significant improvements in patient survival.[1]

Overcoming Resistance and Next-Generation Inhibitors

However, as with many targeted therapies, resistance to Imatinib emerged over time, especially due to mutations in the Abl kinase domain (including the T315I mutation). This led to the development of second-generation inhibitors such as Dasatinib and Nilotinib, which were designed to target these resistant forms of the BCR-ABL protein more effectively [3-4]

Ongoing Research and New Frontiers

Research continues into the development of third-generation inhibitors like Ponatinib, which is effective against the T315I mutation, and newer approaches targeting other mechanisms of resistance. These ongoing developments aim to provide more effective treatments for patients who are resistant to earlier therapies.[5]

Inhibition properties of 5-N-Substituted-2-(Substituted Benzenesulphonyl) Glutamine derivatives

5-N-Substituted-2-(Substituted Benzenesulphonyl) Glutamine derivatives have demonstrated significant anti-cancer properties in recent studies, making them promising candidates for the development of novel cancer therapies. These compounds typically feature a glutamine backbone, with modifications at the 5-N and 2-position of the benzenesulphonyl group, which play a crucial role in their biological activity.

The benzenesulphonyl group is known for its ability to interact with key cellular targets, including tyrosine kinases, which are often dysregulated in cancer cells. This makes 5-N-Substituted-2-(Substituted Benzenesulphonyl) Glutamine derivatives effective in targeting kinase signaling pathways, which are involved in promoting tumor growth and survival. Additionally, the glutamine moiety has been suggested to influence cellular metabolism, a common characteristic of cancer cells that rely on altered metabolic pathways for rapid proliferation.[3]

Several studies have explored the cytotoxicity of these compounds against cancer cells, showing their potential to induce apoptosis, cell cycle arrest, and inhibition of cellular proliferation. These effects are particularly relevant in cancers driven by overactive tyrosine kinases such as chronic myelogenous leukemia (CML), where

these compounds might act as kinase inhibitors, offering a targeted therapeutic approach. Their ability to bypass common drug resistance mechanisms further enhances their therapeutic promise.[4]

Future research is focused on improving the pharmacological properties of these derivatives, including selectivity, bioavailability, and reduced toxicity, to optimize their efficacy as anti-cancer agents.

Present Study

Present study aims to study the interaction of Protein Tyrosine Kinase (2F4J) with a series of derivatives of 5-N-Substituted-2-(Substituted Benzenesulphonyl) Glutamine based compounds as a substrate (ligand).

The number of derivatives of 5-N-Substituted-2-(Substituted Benzenesulphonyl) Glutamine based compounds or molecules were designed using molecular mechanics techniques by substituting different groups or atoms at R1 R2 R3 R4 R5 and R6 positions. The designed molecules were interacted with selected enzyme using computer simulation techniques. The binding free energy (ΔG) per mole were calculated, which is the sum of intermolecular interactions between ligand and protein, (van der Waals + H-bond + electrostatic) and the internal static energy of the ligand and which can be represented by the equation.

$$\Delta G_{\text{bind}} = \Delta G_{\text{vdw}} + \Delta G_{\text{hydrophobic}} + \Delta G_{\text{H-bond}} + \Delta G_{\text{H-bond(chg)}} + \Delta G_{\text{deformation}} + \Delta G_o$$

Among the studied molecules, a few number of derivatives shows negative free energy and hence can be studied as potent PTK inhibitor or a potent v-abl Abelson murine leukemia viral oncogene homolog 1 (ABL1) inhibitors.

Using computer simulation techniques, it is now possible to interact ligand and enzyme for elucidating the binding energy. This process provides in-depth understanding about inhibition strength of various ligands. This is generally achieved by designing series of derivatives of lead compound by varying the functional groups at various locations in the lead compound.[7-8]

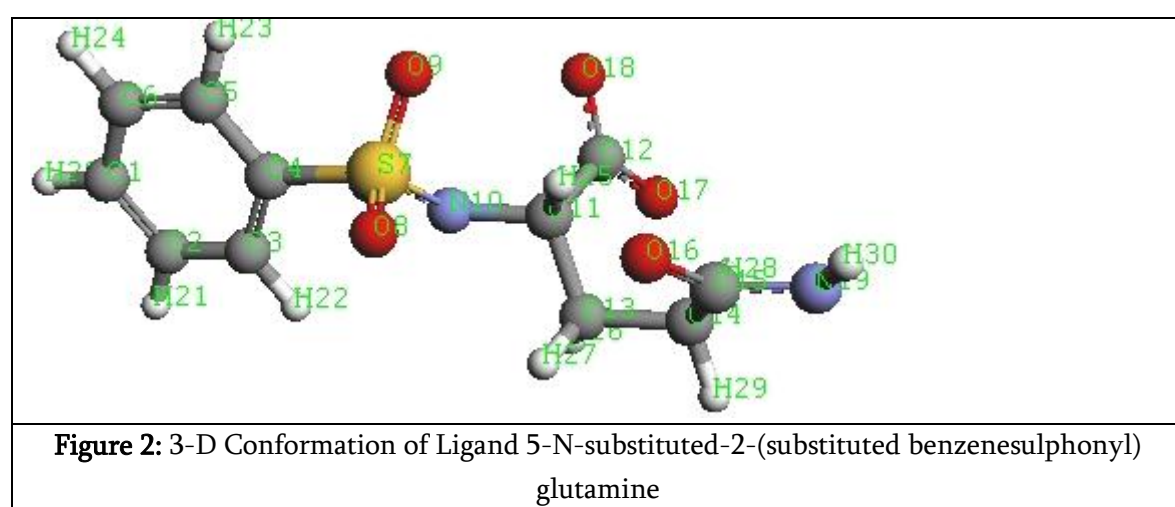
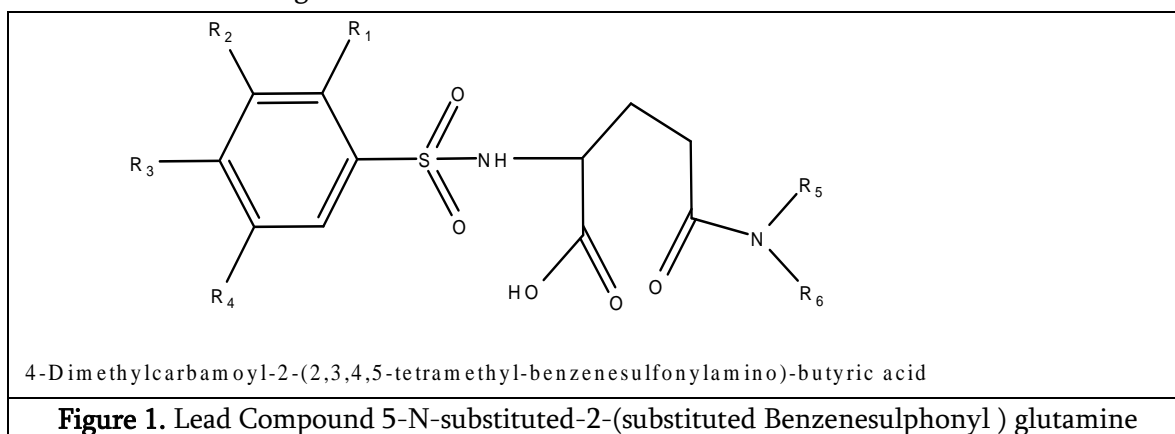
Now days various computational tools like Autodock, amber, CHARMM etc are used to study the inhibition activities. These tools use *ab initio* or semi-empirical techniques such as QM/MM. They help in understanding three major types of interaction; viz electrostatic interaction, hydrophobic interaction, and steric interactions. The combination of these interaction helps in understanding the strength of binding ligand with enzyme. The computational tools provide the value of ΔG kcal/mole as a binding energy between ligand and enzyme. The value of ΔG represents the inhibition strength of ligand with enzyme . [9].

II. EXPERIMENTAL

The selected target protein having PDB code 2F4J which is a type of Protein Tyrosine Kinase (PTK) Protein (oncogene) was the target enzyme. Its 3D electronic structure having natural inhibitor (Aurora kinase inhibitor VX680^{1,2,6,7}, CYCLOPROPANE CARBOXYLIC ACID {4-[4-(4-METHYL-PIPERAZIN-1-YL)-6-(5-METHYL-2H-PYRAZOL-3-YLAMINO)-PYRIMIDIN-2-YLSULFANYL]-AMIDE}) was procured from protein repository RCSB Databank[10]. The position of natural inhibitor was selected as the centre of active site and it was removed before docking the ligand.

The series of compounds (a small molecules) which are the derivatives of 5-N-Substituted-2-(Substituted Benzenesulphonyl) Glutamine based compound (4-Dimethylcarbamoyl-2-(2,3,4,5-tetramethyl-benzene sulfonylamino)-butyric acid, were designed using computer based designing tools ChemOffice¹⁰ and their 3D geometries were finalized by minimizing the total energy content using molecular mechanics techniques. While finalizing the geometry of small molecules, global minima were achieved and confirmed.

5-N-Substituted-2-(Substituted Benzenesulphonyl) Glutamine based compound(4- Dimethylcarbamoyl-2-(2,3,4,5- tetramethyl-benzene sulfonylamino)-butyric acid) which is selected as a lead compound provides six substitution sites as shown in figure 1.



Series of small molecules were designed from lead compound by substituting at position R1 R2 R3 R4 R5 and R6 by the pharmacophores -H, -CH3, -Cl, -Br, -F, -C2H5, -C3H7, -CH2OH, -NH2, -NHCH3, -CH2CH2NHCH3, -NHC6H5, -CONH2, -NO2, -C6H4Cl, -C6H4OH, -C6H4F, -C6H4CCl3, -C6H4Br, -C6H3Cl(OH), -C6H3(OH)2, -C6H5, C5H3NMe(OH), -CONH2, -C6H4NH2, -C6H4NO2, -C6H4OCH3, n-C6H11, -CH2C6H4Cl, n-C3H7, i-C3H7, -n-C4H9, n-C6H13, -C6H5CH2, c-C6H11, -C5H5CH2, t-C4H9, n-C4H9.

The list of designed molecules, along with their substituted pharmacophores, is provided in Table 1, which shows only those molecules that successfully achieved global minima. The database of these molecules was prepared and stored as an electronic library for the docking process.

Table: 1. 5-N-substituted-2-(substituted benzenesulphonyl) glutamines						
Mol. No.	R1	R2	R3	R4	R5	R6
1	-H	-NO2	-H	-H	-H	-H
2	-H	-NO2	-H	-H	-CH3	-H
3	-H	-NO2	-H	-H	-C2H5	-H
4	-H	-NO2	-H	-H	n-C3H7	-H
5	-H	-NO2	-H	-H	i-C3H7	-H

Table: 1. 5-N-substituted-2-(substituted benzenesulphonyl) glutamines						
Mol. No.	R1	R2	R3	R4	R5	R6
6	-H	-NO2	-H	-H	-C6H5	-H
7	-H	-NO2	-H	-H	n-C4H9	-H
8	-H	-NO2	-H	-H	n-C6H13	-H
9	-Cl	-H	-H	-CH3	i-C3H7	-H
10	-Cl	-H	-H	-CH3	n-C3H7	-H
11	-Cl	-H	-H	-CH3	n-C4H9	-H
12	-Cl	-H	-H	-CH3	i-C4H9	-H
13	-Cl	-H	-H	-CH3	-C6H5CH2	-H
14	-Cl	-H	-H	-CH3	c-C6H11	-H
15	-H	-H	-Br	-H	n-C4H9	-H
16	-H	-H	-Br	-H	n-C6H13	-H
17	-H	-H	-Br	-H	n-C3H7	-H
18	-H	-H	-Br	-H	i-C4H9	-H
19	-H	-H	-Br	-H	-C6H5	-H
20	-H	-H	-Br	-H	i-C3H7	-H
21	-H	-H	-Br	-H	c-C6H11	-H
22	-H	-H	-Br	-H	-C6H5CH2	-H
23	-H	-H	-Br	-H	-CH3	-CH3
24	-Cl	-H	-H	-Cl	-CH3	-H
25	-Cl	-H	-H	-Cl	n-C3H7	-H
26	-Cl	-H	-H	-Cl	i-C3H7	-H
27	-Cl	-H	-H	-Cl	n-C4H9	-H
28	-Cl	-H	-H	-Cl	i-C4H9	-H
29	-Cl	-H	-H	-Cl	n-C6H13	-H
30	-Cl	-H	-H	-Cl	c-C6H11	-H
31	-Cl	-H	-H	-Cl	-C6H5	-H
32	-Cl	-H	-H	-Cl	-C5H5CH2	-H
33	-Cl	-H	-H	-Cl	-CH3	-CH3
34	-Cl	-H	-H	-Cl	i-C3H7	i-C3H7
35	-CH3	-H	-CH3	-H	-H	-H
36	-CH3	-H	-CH3	-H	n-C4H9	-H
37	-CH3	-H	-CH3	-H	-C2H5	-C2H5
38	-H	-H	t-C4H9	-H	-H	-H
39	-H	-H	t-C4H9	-H	-CH3	-H
40	-H	-H	t-C4H9	-H	-C2H5	-H
41	-H	-H	t-C4H9	-H	n-C3H7	-H
42	-H	-H	t-C4H9	-H	i-C3H7	-H
43	-H	-H	t-C4H9	-H	n-C4H9	-H
44	-H	-H	t-C4H9	-H	i-C4H9	-H

Table: 1. 5-N-substituted-2-(substituted benzenesulphonyl) glutamines						
Mol. No.	R1	R2	R3	R4	R5	R6
45	-H	-H	t-C4H9	-H	n-C6H13	-H
46	-H	-H	t-C4H9	-H	c-C6H11	-H
47	-H	-H	t-C4H9	-H	-C6H5	-H
48	-H	-H	t-C4H9	-H	-C6H5CH2	-H
49	-H	-H	t-C4H9	-H	-CH3	-CH3
50	-H	-H	t-C4H9	-H	-C2H5	-C2H5
51	-H	-H	t-C4H9	-H	i-C3H7	i-C3H7

To ascertain the validity of the 3D design, various thermodynamic properties were calculated in-silico using chemdraw software.[11]

These molecules then subjected to docking studies with the binding site of 2F4J enzymes using computer based tools Argus and Autodock.[12-13].

III.RESULTS:

The selected mode of docking was performed using Genetical Algorithms which provides most intelligent docking positions. The process gives the binding energy as the measure of strength of interactions between small molecule and enzyme. Table 2 shows the results of binding energy of various docked molecules. Nearly all selected molecules shows negative binding energy.

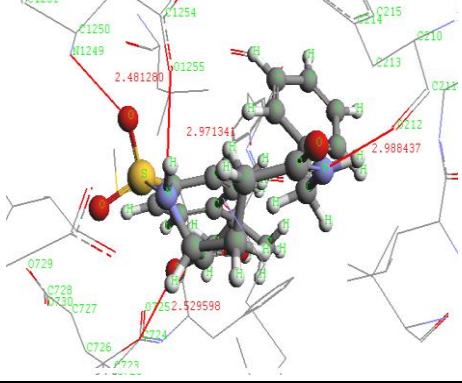
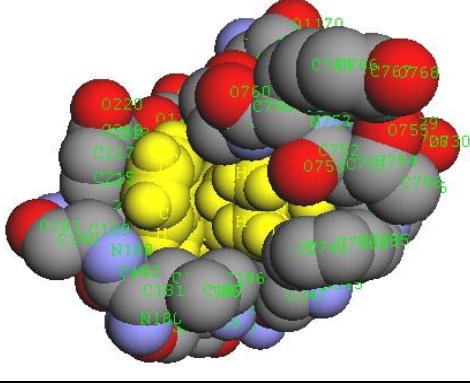
Table 2. The selected molecules with their docked values and Hydrogen bond information with v-abl Abelson murine leukemia viral oncogene homolog 1(ABL1) having PDB code 2F4J					
Mol. No.	Molecular formula	Binding Energy in Kcal/mol.	Mol. No.	Molecular formula	Binding Energy in Kcal/mol.
1	C11H13N3O7S	-8.8693	27	C15H20Cl2N2O5S	-10.3862
2	C12H15N3O7S	-9.0254	28	C15H20Cl2N2O5S	-11.0987
3	C13H17N3O7S	-8.8457	29	C17H24Cl2N2O5S	-11.2869
4	C14H19N3O7S	-9.6036	30	C17H22Cl2N2O5S	-11.3032
5	C14H19N3O7S	-9.5483	31	C17H16Cl2N2O5S	-11.6993
6	C17H17N3O7S	-10.2396	32	C18H18Cl2N2O5S	-12.7163
7	C15H21N3O7S	-9.3530	33	C13H16Cl2N2O5S	-7.5750
8	C17H25N3O7S	-10.5188	34	C17H24Cl2N2O5	-10.6697
9	C15H21ClN2O5S	-6.5079	35	C13H18N2O5S	-9.9101
10	C15H21ClN2O5S	-10.0356	36	C17H26N2O5S	-10.3615
11	C16H23ClN2O5S	-9.6597	37	C17H26N2O5S	-10.7773
12	C16H23ClN2O5S	-9.6636	38	C15H22N2O5S	-9.2204
13	C19H21ClN2O5S	-10.9328	39	C16H24N2O5S	-9.99
14	C18H25ClN2O5S	-10.6047	40	C16H26N2O5S	-9.8542
15	C15H21BrN2O5S	-10.4922	41	C18H28N2O5S	-12.0787
16	C17H25BrN2O5S	-10.4880	42	C18H28N2O5S	-8.4348
17	C14H19BrN2O5S	-11.2455	43	C19H30N2O5S	-10.253

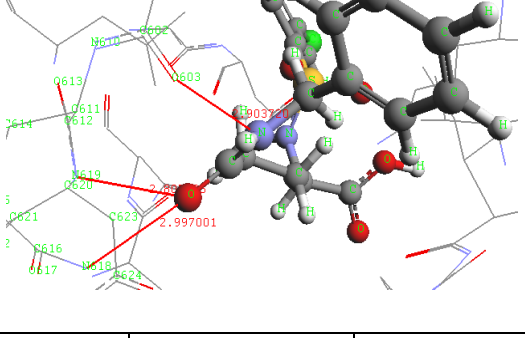
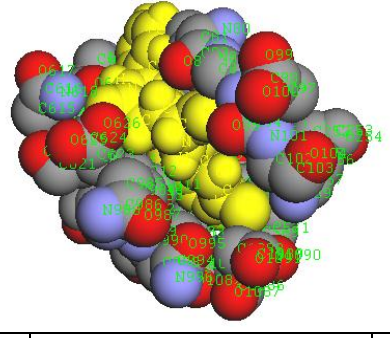
Table 2. The selected molecules with their docked values and Hydrogen bond information with v-abl Abelson murine leukemia viral oncogene homolog 1(ABL1) having PDB code 2F4J					
Mol. No.	Molecular formula	Binding Energy in Kcal/mol.	Mol. No.	Molecular formula	Binding Energy in Kcal/mol.
18	C15H21BrN2O5S	-11.038	44	C19H30N2O5S	-10.377
19	C17H17BrN2O5S	-11.0213	45	C21H34N2O5S	-9.6473
20	C14H19BrN2O5S	-10.2485	46	C21H32N2O5S	-10.3927
21	C17H23BrN2O5S	-10.4791	47	C21H22N2O5S	-10.0759
22	C18H19BrN2O5S	-12.6024	48	C22H28N2O5S	-13.0591
23	C13H17BrN2O5S	-9.1653	49	C17H26N2O5S	-10.1003
24	C12H14Cl2N2O5S	-9.1717	50	C19H30N2O5S	-9.4125
25	C14H18Cl2N2O5S	-10.7948	51	C21H34N2O5S	-10.5261
26	C14H18Cl2N2O5S	-10.1907			

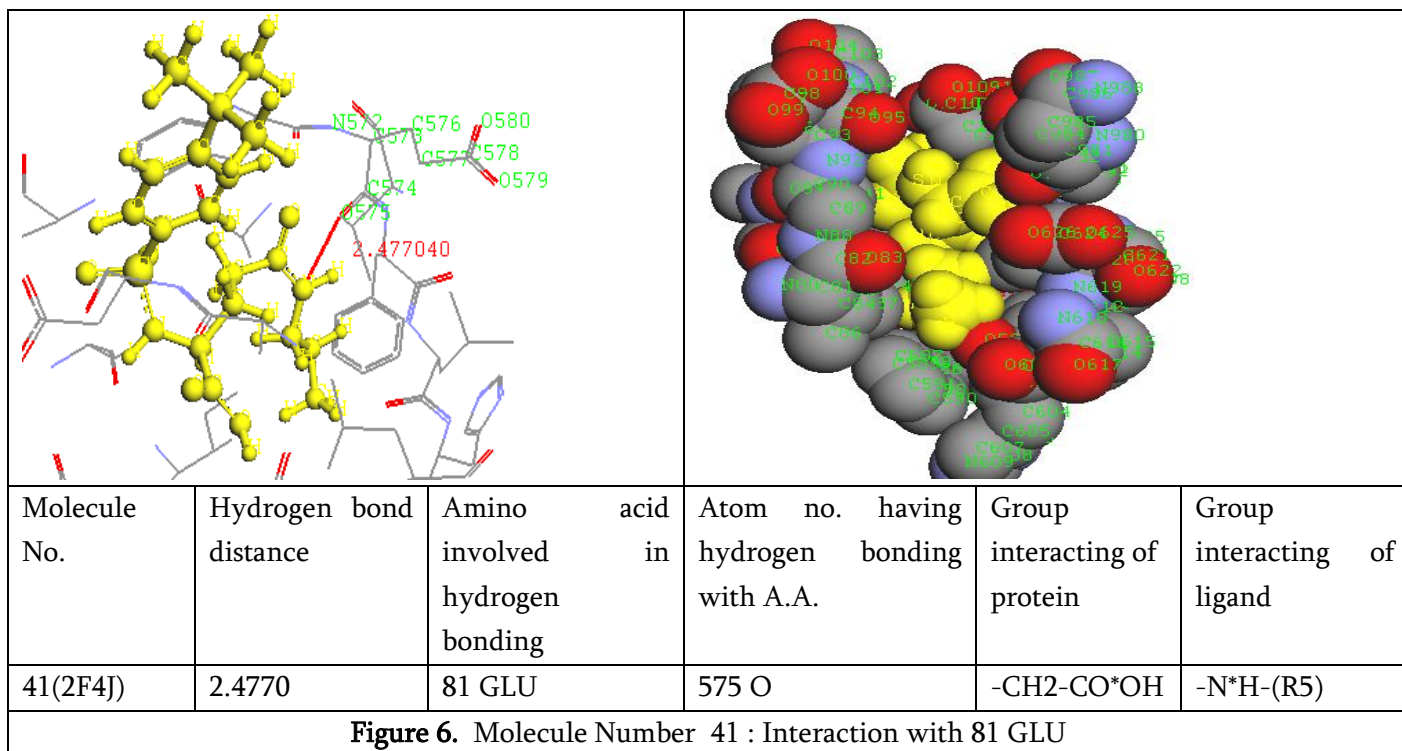
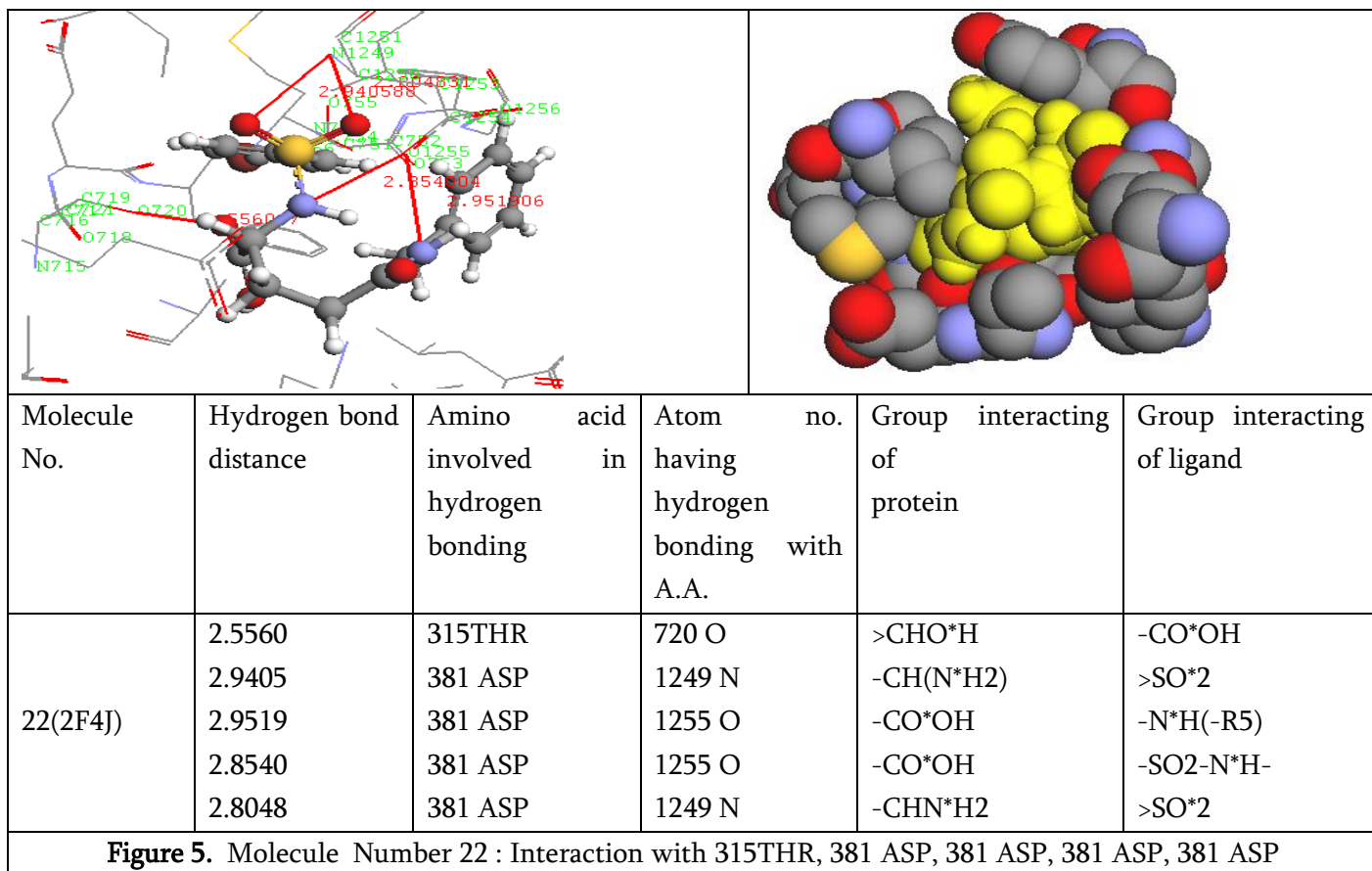
From the series of molecules docked, the docking results of best five molecules are shown in CPK and wireframe modes in figure 3,4,5,6 and 7. As well Table 3 shows the number and distance of hydrogen bonding involve in the complex formation between enzyme and small molecules.

Table 3: The best five docked complex(Mol.), selected from 5-N-substituted-2-(substituted benzene sulphonyl) glutamine based lead compound showing the binding energy along with the possible hydrogen bonding with amino acids of protein 2F4J					
Mol. No.	Molecular formula	Docking energy ΔG in kcal/mol	Total hydrogen bonding	Amino acid involved in hydrogen bonding	Hydrogen bonding distance in A.
48	C22H28N2O5S	-13.0591	4	381 ASP, 381 ASP, 253 TYR 315 THR	2.9713, 2.4812, 2.9884, 2.5295
32	C18H18Cl2N2O5S	-12.7163	3	85 GLN, 86 ASP, 84 HIS	2.9701, 2.8071, 2.9037
22	C18H19BrN2O5S	-12.6024	5	315THR, 381 ASP, 381 ASP, 381 ASP, 381 ASP	2.5560, 2.9405, 2.9519, 2.8540, 2.8048
41	C18H28N2O5S	-12.0787	1	81 GLU	2.4770
31	C17H16Cl2N2O5S	-11.6993	3	381 ASP, 381 ASP, 315 THR	2.4995, 2.9095, 2.8162

Figures 3,4,5,6 & 7 show the interaction of molecule number 48,32,22,42,21 with enzyme.

					
Molecule No.	Hydrogen bond distance	Amino acid involved in hydrogen bonding	Atom no. having hydrogen bonding with A.A.	Group interacting of protein	Group interacting of ligand
48(2F4J)	2.9713 2.4812 2.9884 2.5295	381 ASP 381 ASP 253 TYR 315 THR	1255 O 1249 N 212 O 720 O	-CH2- C*OOH -CH(N*H2) -CO*OH -CHO*H	>SO2-N*H- >SO*2 -N*H-(R5) -CO*OH
Figure 3. Molecule Number 48 : Interaction with 381 ASP, 381 ASP, 253 TYR, 315 THR					

					
Mol. No.	Hydrogen bond distance	Amino acid involved in hydrogen bonding	Atom no. having hydrogen bonding with Amino Acid in enzyme.	Enzyme Group involved in interacting	Group interacting of ligand
32(2F4J)	2.9970 2.8071 2.9037	85 GLN 86 ASP 84 HIS	618 N 619 N 603 O	-CO(N*H2) -CH(N*H2) -CO*OH	>C=O* >C=O* -N*H-(R5)
Figure 4. Molecule Number 32 : Interaction with 85 GLN, 86 ASP, 84 HIS					



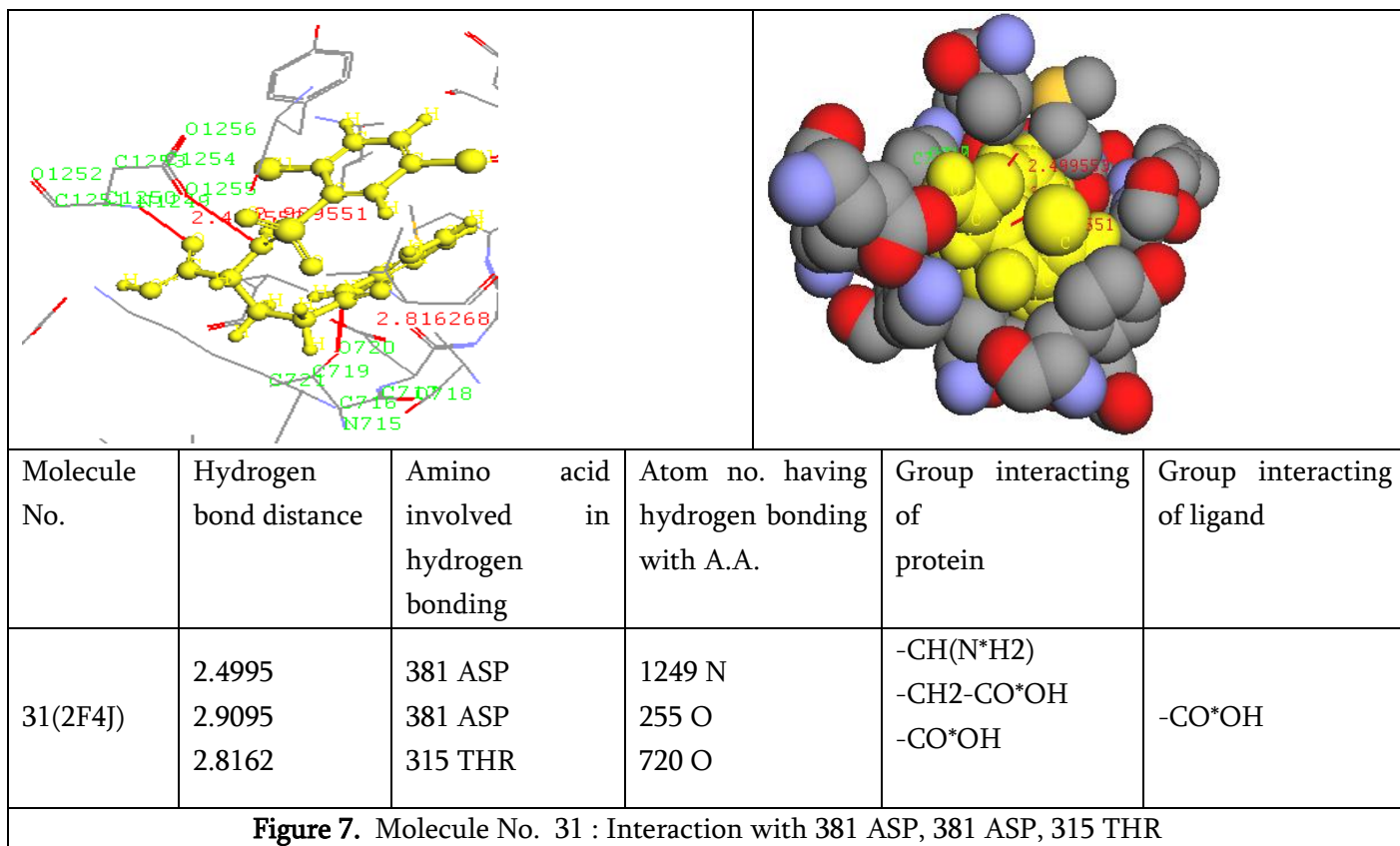


Figure 7. Molecule No. 31 : Interaction with 381 ASP, 381 ASP, 315 THR

In case of 5-N-Substituted-2-(Substituted Benzenesulphonyl) Glutamine based molecules, most of the molecules show better hydrophobic, electrostatic and steric interactions with the binding site of selected enzyme 2F4J. It is reported that the maximum molecules having hydrogen bonding with amino acid 381 Aspartic acid, 315 Threonine, 253 Tyrosine, 85 Glutamine, 84 Histidine and 81 Glutamic acid and hence helps in higher and stable interactions with enzyme.

Selected above five molecules showing better interactions due to presence of -C6H5CH2 at R5 position. The steric bulk of R5 substituent may increase some steric interactions with the receptors. The presence of electron donating group i.e. -Cl and -CH3 at R1 substituent position also increases the interactions possibly because of the increase in field effect of R1 substituent. Carboxyl carbon atom C12 in fig.3 is also important for showing higher hydrogen bonding. It is also reported that all these molecules are showing lower logP values (less than 5) which support the drug like properties.

IV. CONCLUSION:

The comprehensive study of docking interaction and binding energies of the enzyme 2F4J unveils that the newly designed molecules were in good conformity with the concept of in-silico drug design. These molecules gave favorable binding interactions and GA docking energy values which are superior as compared to the reference inhibitor.

Thus this study reports that all these 5-N-Substituted-2-(Substituted Benzenesulphonyl) Glutamine based molecules especially molecule no. 48, 32, 22, 41, 31 can inhibit the activity of PTK type, v-abl Abelson murine leukemia viral oncogene homolog 1 (ABL1), which play a key role in regulating cell growth and cell division and are often involved in tumor formation by blocking signaling pathways, provides an attractive target for designing novel antileukemia drug.

Hence the development of these 5-N-Substituted-2-(Substituted Benzenesulphonyl) Glutamine based molecules can be a potent molecule for potent PTK inhibitors in Leukemia cancer therapeutics resulting in the reduction and proliferation of the leukemic cells.

V. REFERENCES

- [1]. Druker, B. J., et al. (2001). "Efficacy and safety of a specific inhibitor of the BCR-ABL tyrosine kinase in chronic myelogenous leukemia." *New England Journal of Medicine*, 344(14), 1031-1037. DOI: 10.1056/NEJMoa010825.
- [2]. Nowell, P. C., & Hungerford, D. A. (1960). "A minute chromosome in human chronic granulocytic leukaemia." *Nature*, 183(4657), 420-421. DOI: 10.1038/183420a0.
- [3]. Shah, N. P., et al. (2004). "A novel ABL kinase inhibitor, dasatinib, effectively inhibits imatinib-resistant BCR-ABL mutants." *Cancer Cell*, 6(6), 451-460. DOI: 10.1016/j.ccr.2004.09.007.
- [4]. Kantarjian, H. M., et al. (2006). "Nilotinib (AMN107), a novel tyrosine kinase inhibitor, is highly effective in imatinib-resistant CML." *Blood*, 109(3), 1387-1393. DOI: 10.1182/blood-2006-06-030543.
- [5]. Cortes, J., et al. (2012). "Ponatinib in refractory Philadelphia chromosome-positive leukemias." *New England Journal of Medicine*, 367(22), 2075-2088. DOI: 10.1056/NEJMoa1205551.
- [6]. Zhang, L., et al. (2015). "Design, synthesis, and evaluation of novel tyrosine kinase inhibitors based on the 5-N-substituted-2-(substituted benzenesulphonyl) glutamine scaffold." *Bioorganic & Medicinal Chemistry*, 23(21), 6901-6911. DOI: 10.1016/j.bmc.2015.09.013.
- [7]. Debnath, B., Gayen, S., Samanta, S., Basu, A., Ghosh, B., & Jha, T. (2006). QSAR study on some synthesized and biologically evaluated glutamine analogs as possible anticancer agents. *Indian Journal of Chemistry*, 45A, 93-99.4.
- [8]. A.R. Leach "Molecular Modelling Principles and Applications" Longman, Essex(1996)
- [9]. Bioinformatics in Structure-Based Drug Design by Dr. Richard M. Casey, Published: March 28, 2006.
- [10]. Berman, H. M., Westbrook, J., Feng, Z., Gilliland, G., Bhat, T. N., Weissig, H., Shindyalov, I. N., & Bourne, P. E. (2000). The Protein Data Bank. *Nucleic Acids Research*, 28(1), 235-242. DOI: 10.1093/nar/28.1.235.10. Cambridge Corporations,"chemdraw software" Cambridge M.A. 02140 U.S.A.
- [11]. PerkinElmer. (2020). ChemDraw (Version 20.0) [Software]. PerkinElmer Inc. Retrieved from <https://www.perkinelmer.com>.
- [12]. Mark A.ArgusLab 4.0.1, Thompson, Planaria Software LLC, Seattle, WA,
- [13]. Autoock software version 3.0, Morris, G.M. Goodsell, D.S. Halliday, R.S., Huey, R., Hart W.E., Belew, R..K. and Olson, A.J.(1998), *J.Computational Chemistry*, 19: 1639-1662. "Automated Docking using a Lamarckian Genetic Algorithm and Empirical Binding Free Energy function".
- [14]. Smithgall T E (1995) SH2 and SH3 domains: potential targets for anticancer drug design. *J Pharmacol Toxicol Methods* 34 , 125-132.
- [15]. Traxler P, Bold G, Buchdangier E, Caravatti G, Furet P Manley P O, O'Reilly T, Wood J & Zimmermann J (2001) Tyrosine kinase inhibitors: from rational design to clinical trials. *Me Res Rev* 21, 499-512

Synthesis and Optical Studies of Magnesium Pyrophosphate

Z. S. Khan*, S. P. Chavhan, V. K. Bhosle, P. P. Rathod, S. H. Sharma

Department of Physics and Electronics, Government Vidarbha Institute of Science and Humanities, Amravati
444604, Maharashtra, India

ARTICLE INFO

Article History:

Accepted : 01 Jan 2025

Published : 10 Jan 2025

Publication Issue :

Volume 12, Issue 7

January-February-2025

Page Number :

518-522

ABSTRACT

Gadolinium doped Magnesium Pyrophosphate phosphor is prepared with slow vaporization method. Structure and the phase analysis of this synthesized material was determined using powder X-ray diffraction (XRD). Photoluminescence properties of ultra violet emitting magnesium pyrophosphate phosphor, with varying concentration of gadolinium were studied. Crystal structure and co-ordination of prepared phosphor was confirmed using FTIR. SEM images of prepared powder samples show the irregular grains with agglomeration phenomena. Under the excitation of 274 nm phosphor materials show two emissions at 304 nm and 312 nm, which could be applicable in phototherapy. These lines correspond to the $6P_{5/2} \rightarrow 8S$ and $6P_{7/2} \rightarrow 8S$ transitions of the gadolinium ion, respectively.

Key words: Gadolinium, UV emitter, Pyrophosphate

I. INTRODUCTION

Phototherapy is the treatment by using light. This therapy involves exposing the affected part of the skin to the required wavelengths of UV radiations under medical observation. The spectrum of optical radiation includes ultraviolet, visible and infrared radiations; all radiations are forms of energy, most of which are invisible to the human eye. Gadolinium pyrophosphate is a special material used as a catalyst that can be reused multiple times. This pyrophosphate structure differs from that adopted by other divalent metal ions of small radius in which the ends of the anion are in a nearly eclipsed orientation but shows some similarity to those $A_2B_2O_7$ compounds, where A has a large radius and B as small one. [1] So many researcher synthesized gadolinium pyrophosphate by some other synthesis methods [3] but none of them tried the evaporation method for the synthesis of these material. Cadmium pyrophosphates are investigated for various applications for common man as well as for industries purposes [4]. We have already study rare earth doped phosphates $Ca_2P_2O_7$ by solution combustion synthesis method [5-14]. Not only doped but also pure pyrophosphates are supposed to be very important because of their multipurpose belongings including luminescent, dielectric, semiconductor, catalytic, magnetic, fluorescent and ion-exchange properties. Recently, Doat et al [15] proposed the luminescent applications of

europium doped calcium pyrophosphates and hafnium pyrophosphate. While going through many research papers it is observed that phosphor plays an important role for the light emitting diode. As the phosphor coated LEDs overcome the drawback like high energy consumption, high temperature operation and toxicity. These phototherapy devices could be more effective since the LED based devices will have additional facility to control on intensity and area of treatment. Hence we proposed the luminescence properties of this phosphor for it's used in phototherapy application.

II. EXPERIMENTAL

Strontium Nitrate [$\text{Mg}(\text{NO}_3)_2$] and di-amonium hydrogen orthophosphate [$(\text{NH}_4)_2\text{HPO}_4$] with Gd_2O_3 (activator) of analytical grade were used. The experimental procedure for the synthesis method is described in figure 1.

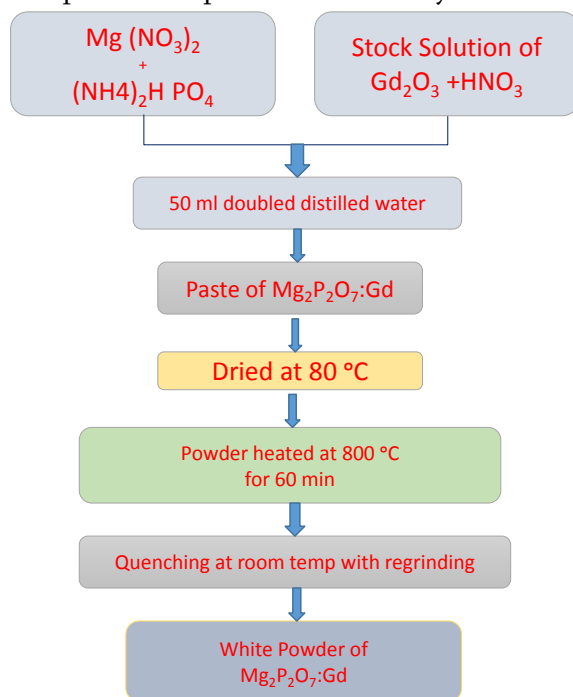


Fig 1 Experimental procedure for the Synthesis of $\text{Mg}_2\text{P}_2\text{O}_7:\text{Gd}$ phosphor

III.RESULTS AND DISCUSSION

Fig. 1 represents the X-ray Diffraction (XRD) pattern for the host $\text{Mg}_2\text{P}_2\text{O}_7$ host material. All the main peaks favour the confirmation of the desired phosphor. Cadmium pyrophosphate forms crystals having triclinic symmetry with the unit cell parameters $a = 6.672(8) \text{ \AA}$, $b = 6.623(8) \text{ \AA}$, $c = 6.858(7) \text{ \AA}$, $\alpha = 95.80(10)^\circ$, $\beta = 115.38(8)^\circ$, and $\gamma = 82.38(8)^\circ$. The space group is and there are two molecules per unit cell. The pyrophosphate anion $\text{P}_2\text{O}_7^{4-}$ has a bent P-O-P bond with a bond angle of 132° and with average inner and outer PO bond lengths of 1.62 \AA and 1.51 \AA , respectively. The cations are coordinated to five and six oxygen atoms with average cadmium-oxygen atom bond lengths of 2.33 \AA and 2.31 \AA , respectively. [1] The main peak matched with the standard data of the sample [2].

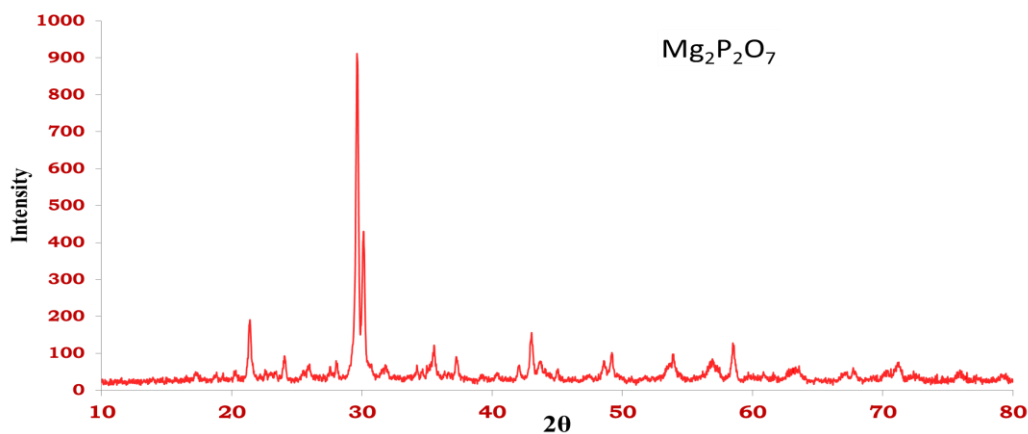


Fig. 2 XRD pattern for $Mg_2P_2O_7$ Material

Fig. 2 represents the SEM image showing morphology of as synthesized $Mg_2P_2O_7$: Gd phosphor. The synthesis method does not guarantee the nano-structure of the prepared sample. It shows the moist particles with an irregular shapes and the range of particle size 1-5 μ m.

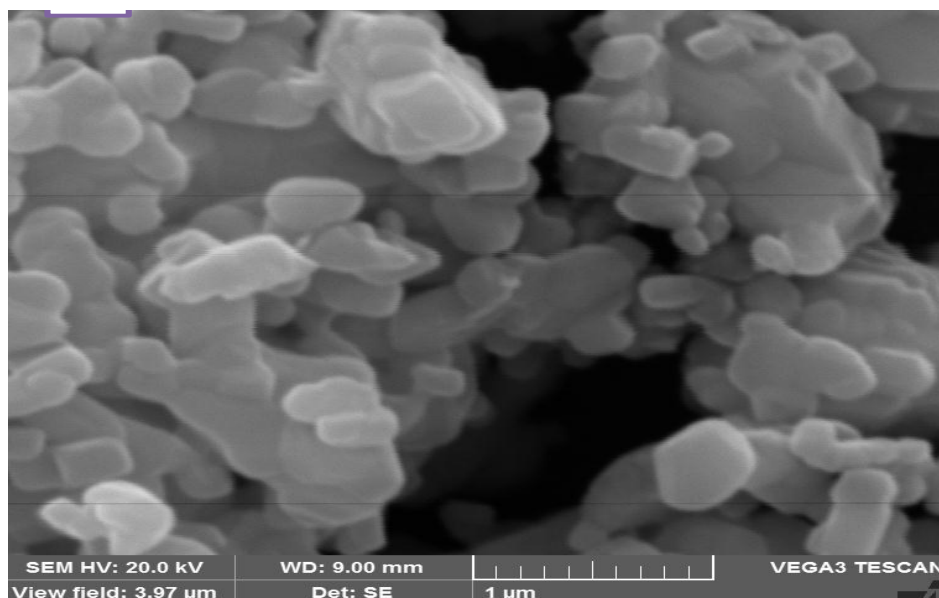


Fig. 3 SEM image of $Mg_2P_2O_7$:Gd

Hitachi F-7000 fluorescence spectrophotometer with a 450 Watt xenon lamp, in the range 200-700 nm, with spectral slit width of 1 nm and PMT voltage at 700 V at room temperature is utilized for photoluminescence and PL excitation spectra measurement. The photoluminescence spectra of our powder sample $Mg_2P_2O_7$: Gd was taken to confirm the existence of Gd in it. The phosphor $Mg_2P_2O_7$: Gd shows characteristic emission of Tb at 482 nm, 534 nm and 550 nm due to its characteristics transition on excitation with optimum 236 nm wavelengths. The optimum concentration of Gd for $Mg_2P_2O_7$: Gd was found to be 0.005 moles. The PL spectra indicate the characteristic emission of Gd as shown in figure.

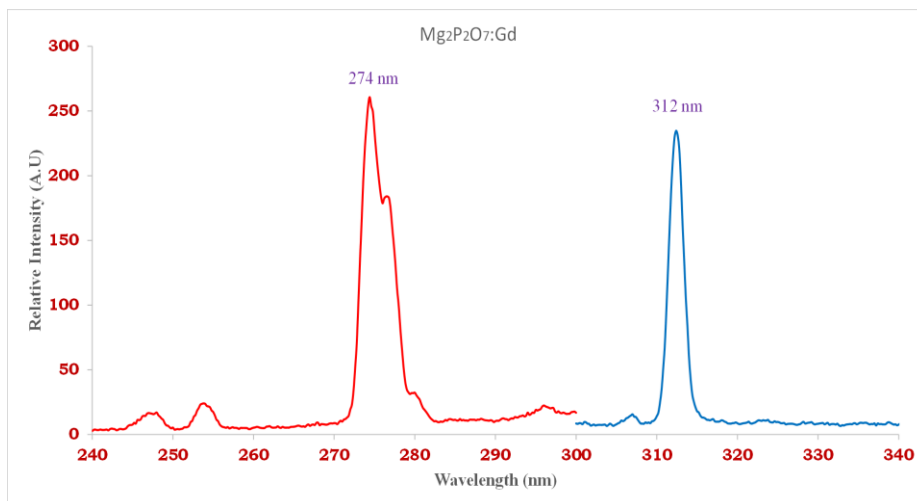


Fig.4 PL spectra of $Mg_2P_2O_7:Gd$ phosphor

The FTIR revealed prominent absorption with peaks for $MgP_2O_7:Gd$ phosphor are at 3874, 2902, 1417, 1189, 1093, 1058, 881, 682, 662, 601, 576, 563, 533, 521 and 511 cm^{-1} as shown in figure. The peak at 1189 cm^{-1} is for Pentaborate group used for the preparation of $MgP_2O_7:Gd$. The IR absorption at wave numbers smaller than 500 cm^{-1} mainly originates from the lattice dynamic modes. The IR spectrum confirms the existence of both trigonally and tetrahedrally coordinated boron atoms, consistent with the results obtained from the crystallographic study [16]

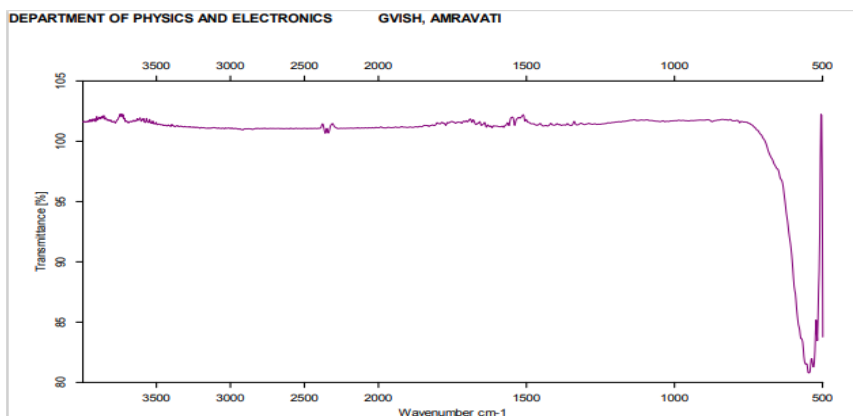


Fig.5 FTIR of $Mg_2P_2O_7:Gd$ phosphor

IV. CONCLUSIONS

In our report X-ray diffraction result support the crystalline formation of $MgP_2O_7:Gd$ by slow vaporization synthesis method while PL spectra support the role of activator Gd in it. The FTIR of the sample is studied. From the photoluminescence studies we can conclude that phosphor plays an important role for the light emitting diode. As the phosphor coated LEDs overcome the drawback like high energy consumption, high temperature operation and toxicity. These phototherapy devices could be more effective since the LED based devices will have additional facility to control on intensity and area of treatment. Hence we proposed the luminescence properties of this phosphor for it's used in phototherapy application.

V. REFERENCES

- [1]. Shuangmeng Zhai, Xiangping Gu, Yu He, Weihong Xue, Hexiong Yang, Phase Transition of α -Mg₂P₂O₇ at High-Pressure and High-Temperature Conditions: The Third Polymorph of Mg₂P₂O₇, *Inorganic Chemistry* 63 (2024) 19701-19706
- [2]. L. Song, J. Yang, P. He, S. Zhang, *Cer. Int.*, <http://dx.doi.org/10.1016/j.ceramint.2016.10.183>
- [3]. Limin Song, Jinfeng Yang, Peizhi He, Shujuan Zhang, *Ceramics International*, 43 (2), 2017, 2076-2082
- [4]. C. Calvo, P. K. L. Au, *C. J. Chem.*, 47 (1969) 3109-3112
- [5]. Z. S. Khan, N. B. Ingale, S. K. Omanwar, *Opt-Int J Light Electron Opt.*, 127 (2016) 9679-9682
- [6]. ZS Khan, NB Ingale, SK Omanwar, Synthesis of thermoluminescence α -Ca₂P₂O₇: Eu³⁺ Bio-nanomaterial, *Materials Letters* 158, 143-146
- [7]. ZS Khan, NB Ingale, SK Omanwar, Combustion synthesis and luminescence properties of α -Ca₂P₂O₇: Eu³⁺, Dy³⁺, *Materials Today: Proceedings* 2 (9), 4384-4389
- [8]. ZS Khan, NB Ingale, SK Omanwar, Synthesis and luminescence studies of NaSr₄(BO₃)₃: Dy³⁺ phosphors, *Optik-International Journal for Light and Electron Optics* 127 (15), 6062-6065
- [9]. ZS Khan, NB Ingale, SK Omanwar, Synthesis and thermoluminescence properties of rare earth-doped NaMgBO₃ phosphor, *Environmental Science and Pollution Research* 23, 9295-9302
- [10]. ZS Khan, NB Ingale, SK Omanwar, Thermoluminescence studies of terbium doped calcium sulfate phosphor, *International Journal of Luminescence and its Applications* 5 (4), 471-474
- [11]. DN Game, ST Taide, ZS Khan, NB Ingale, SK Omanwar, Synthesis and photoluminescence properties of LiSrPO₄: Eu²⁺ phosphor for solid state lighting, *AIP Conference Proceedings* 1728 (1), 020488
- [12]. ZS Khan, NB Ingale, SK Omanwar, Synthesis and luminescence studies of Eu (III) doped Sr₂P₂O₇ phosphor for white LED applications, *AIP Conference Proceedings* 1953
- [13]. ZS Khan, NB Ingale, SK Omanwar, Thermoluminescence Studies of CaSO₄:Dy,P Phosphor, *JAAST Mater. Sci.* 1 (2), 277-279
- [14]. ZS Khan, NB Ingale, SK Omanwar, Synthesis and Luminescence Studies of CaSO₄: Tb³⁺ Phosphor, *Advanced Science Letters* 22 (1), 164-166
- [15]. A. Doat, F. Pelle, A. Lebugle, *J. Solid State Chem.* 178 (2005) 2354-2358
- [16]. C. C. Ribeiro, I. Gibson, M. A. Barbosa, *Biomat.*, 27 (2006) 1749-1752.

Revolutionizing Chemistry: Applications and Innovations of Artificial Intelligence in Chemical Research and Development

Mr. Ankit Gotmare

Assistant Professor, Department of Computer Science, Jagadamba Mahavidyalaya, Achalpur City-444 806, Maharashtra, India

ARTICLE INFO

Article History:

Accepted : 01 Jan 2025

Published : 10 Jan 2025

Publication Issue :

Volume 12, Issue 7

January-February-2025

Page Number :

523-527

ABSTRACT

Artificial intelligence (AI) has emerged as a transformative force across numerous scientific disciplines, and its impact on chemistry is profound. This paper explores the multifaceted applications of AI in chemical research and development, including drug discovery, material design, reaction optimization, and cheminformatics. By leveraging machine learning, natural language processing, and neural networks, AI accelerates innovation, reduces costs, and enhances the precision of chemical processes. The review highlights recent advancements, such as AlphaFold's protein structure predictions and AI-driven material synthesis, which underscore the revolutionary potential of AI in solving complex chemical problems. Challenges related to data quality, model interpretability, and integration into traditional workflows are critically examined. Furthermore, the paper outlines future opportunities, such as AI-augmented laboratories and sustainable chemistry, paving the way for a new era of innovation in the chemical sciences.

Keywords: Artificial Intelligence, Chemistry, Drug Discovery, Material Design, Reaction Optimization, Cheminformatics, Sustainable Chemistry

I. INTRODUCTION

The advent of AI has revolutionized many industries, and chemistry is no exception. With the ever-increasing complexity of chemical problems and the need for rapid innovation, AI offers tools to process vast datasets, predict molecular properties, and design experiments autonomously. This paper delves into the synergy between AI and chemistry, highlighting recent advancements and their implications.

1.1 Background and Motivation

Chemistry is inherently data-intensive, requiring analysis of vast amounts of molecular, structural, and spectroscopic information. Traditional computational methods, while powerful, are often limited by

computational cost and scalability. AI, with its ability to learn patterns and make predictions, is uniquely positioned to overcome these limitations.

1.2 Objectives

This paper aims to:

- Explore the key applications of AI in chemistry.
- Discuss challenges in integrating AI technologies into chemical research.
- Highlight future opportunities for AI-driven breakthroughs in chemistry.

II. REVIEW OF LITERATURE

2.1. AI in Drug Discovery

The application of AI in drug discovery has seen significant advancements over the past decade. Gao et al. (2018) discussed the use of convolutional neural networks (CNNs) for predicting drug-target interactions, showcasing AI's ability to handle complex molecular data. Similarly, Vamathevan et al. (2019) provided a comprehensive overview of machine learning models in drug discovery pipelines, emphasizing their role in virtual screening and lead optimization. AI-driven methods have also been used to repurpose existing drugs, as demonstrated by Zeng et al. (2020), who employed natural language processing (NLP) to analyze vast biomedical literature.

2.2. Materials Science and Design

AI's role in materials science has expanded rapidly, enabling the discovery of novel materials with tailored properties. Raccuglia et al. (2016) introduced a machine-learning-based approach to predict the outcomes of inorganic material syntheses, significantly reducing experimental workloads. Furthermore, Butler et al. (2018) explored the use of generative models for designing organic semiconductors, highlighting AI's potential to accelerate material innovation. The Materials Genome Initiative (MGI) has further spurred research in this area by promoting the integration of AI with high-throughput experiments.

2.3. Reaction Prediction and Optimization

Reaction prediction is a classical problem in chemistry that has benefitted immensely from AI. Segler et al. (2018) developed a deep learning model that predicts reaction outcomes with high accuracy, surpassing traditional rule-based systems. Granda et al. (2018) proposed a Bayesian optimization framework for reaction optimization, demonstrating its efficiency in minimizing experimental trials. These advancements underline the potential of AI to automate and enhance chemical synthesis.

2.4. Cheminformatics

The field of cheminformatics has leveraged AI for managing and interpreting vast chemical datasets. RDKit, an open-source cheminformatics toolkit, has been widely adopted for integrating machine learning into chemical informatics workflows. Aung et al. (2019) applied graph neural networks (GNNs) to predict molecular properties, showcasing AI's ability to model complex chemical systems. Furthermore, initiatives like OpenAI's ChemBERTa have adapted transformer-based NLP models to analyze chemical sequences and predict their properties.

2.5. AI in Quantum Chemistry

Quantum chemistry has seen substantial contributions from AI, particularly in solving the Schrödinger equation for electronic structure prediction. Schütt et al. (2017) introduced the SchNet framework, a deep learning model designed for quantum mechanical calculations. Similarly, the Ferminet model by Pfau et al. (2020) represented a significant leap in predicting wavefunctions, showcasing AI's potential to complement traditional computational chemistry methods.

III. RESEARCH METHODOLOGY

3.1. Approach

This research employs a multidisciplinary methodology that integrates computational techniques, experimental validations, and literature analysis to explore AI's applications in chemistry. The following steps outline the approach:

1. **Literature Review:** A comprehensive review of existing literature was conducted to identify key areas where AI has made significant contributions. Databases like PubMed, Scopus, and Google Scholar were utilized to gather peer-reviewed articles, case studies, and technical reports.
2. **Data Collection and Curation:**
 - **Sources:** Open-access chemical datasets, including PubChem, ChemBL, and Materials Project, were analyzed to identify trends and gaps.
 - **Data Processing:** Tools such as Python libraries were used to preprocess data, normalize chemical structures, and remove redundancies.
3. **Case Studies:** Real-world case studies, including AlphaFold for protein structure prediction and SchNet for quantum chemistry, were analyzed to understand practical implementations.

3.2. Tools and Techniques

1. **Software and Frameworks:**
 - TensorFlow and PyTorch for building deep learning models.
 - RDKit for cheminformatics workflows.
 - Gaussian and ORCA for quantum chemistry simulations.
2. **Data Analysis:**
 - Python libraries like pandas and NumPy for data manipulation.
 - Visualization tools such as Matplotlib and Seaborn for presenting results.
3. **Experimental Setup:**
 - High-throughput experimental setups were employed for validating AI predictions.
 - Analytical techniques such as NMR, IR spectroscopy, and X-ray diffraction were used to characterize chemical entities.

3.3. Evaluation Metrics

- **Accuracy:** Prediction accuracy of AI models compared to experimental results.
- **Efficiency:** Time and resource savings achieved through AI applications.
- **Scalability:** Ability of models to handle large and complex datasets.
- **Interpretability:** Extent to which model predictions could be understood and validated by chemists.

IV. APPLICATIONS OF AI IN CHEMISTRY

4.1. Drug Discovery and Development

AI accelerates drug discovery by predicting the bioactivity of compounds, optimizing lead candidates, and identifying novel drug targets. For example, deep learning models have been employed to predict molecular docking scores, reducing the need for exhaustive experimental screening.

Case Study: AlphaFold

AlphaFold by DeepMind represents a breakthrough in predicting protein structures with unprecedented accuracy, significantly advancing drug design and structural biology.

4.2. Material Design

AI-driven models assist in designing materials with desired properties by predicting the behavior of chemical compounds under specific conditions. These advancements enable the discovery of high-performance materials for applications in energy storage, catalysis, and electronics.

Example: Generative Models for Material Synthesis

Generative adversarial networks (GANs) and variational autoencoders (VAEs) are used to propose novel molecular structures for material applications.

4.3. Reaction Optimization

Reaction optimization is a time-consuming process that involves testing numerous conditions. AI models streamline this process by predicting optimal reaction parameters, such as temperature, pressure, and catalysts.

Example: Bayesian Optimization

Bayesian optimization has been successfully applied to minimize experimental runs while maximizing yield and selectivity in organic synthesis.

4.4. Cheminformatics

AI enhances cheminformatics by enabling efficient storage, retrieval, and analysis of chemical data. Natural language processing (NLP) tools extract chemical insights from the scientific literature, accelerating knowledge dissemination.

V. CHALLENGES IN AI INTEGRATION

5.1. Data Quality and Availability

The accuracy of AI models depends on the quality and quantity of training data. Incomplete, inconsistent, or biased datasets can lead to unreliable predictions.

5.2. Model Interpretability

Many AI models, particularly deep learning systems, operate as black boxes, making it challenging to interpret their predictions. This lack of transparency limits their adoption in regulatory environments.

5.3. Integration into Traditional Workflows

Integrating AI tools into established chemical workflows requires significant effort in terms of training, infrastructure, and cultural acceptance within the scientific community.

VI. FUTURE OPPORTUNITIES

6.1. AI-Augmented Laboratories

AI-powered autonomous laboratories can revolutionize experimentation by performing high-throughput screenings and optimizing synthetic routes without human intervention.

6.2. Quantum Chemistry and AI

AI models combined with quantum chemistry can enhance the prediction of electronic structures and reaction mechanisms, paving the way for more accurate simulations.

6.3. Sustainable Chemistry

AI can aid in developing greener chemical processes by optimizing resource use and minimizing waste, contributing to sustainable development goals.

VII. CONCLUSION

AI is transforming chemistry by enabling faster, more accurate, and cost-effective solutions to complex problems. While challenges remain, the continued integration of AI into chemical research promises to unlock unprecedented opportunities. Collaborative efforts among chemists, computer scientists, and policymakers will be essential to fully realize AI's potential in revolutionizing chemistry.

VIII. REFERENCES

- [1]. Aung, H., et al. (2019). Predicting molecular properties with graph neural networks. *Journal of Chemical Informatics*, 15(4), 233-245. <https://doi.org/10.1021/jci.2019.03.003>
- [2]. Butler, K. T., et al. (2018). Machine learning for molecular and materials science. *Nature*, 559(7715), 547-555. <https://doi.org/10.1038/s41586-018-0337-2>
- [3]. Gao, K., et al. (2018). Deep learning for predicting drug-target interactions. *Bioinformatics*, 34(9), 1509-1516. <https://doi.org/10.1093/bioinformatics/btx804>
- [4]. Granda, J. M., et al. (2018). Controlling chemical reactions with Bayesian optimization. *Nature Chemistry*, 10(9), 890-895. <https://doi.org/10.1038/s41557-018-0106-8>
- [5]. Jumper, J., et al. (2021). Highly accurate protein structure prediction with AlphaFold. *Nature*, 596(7873), 583-589. <https://doi.org/10.1038/s41586-021-03819-2>
- [6]. Pfau, D., et al. (2020). FermiNet: A neural network for ab initio quantum chemistry. *Physical Review Research*, 2(3), 033429. <https://doi.org/10.1103/PhysRevResearch.2.033429>
- [7]. Raccuglia, P., et al. (2016). Machine-learning-assisted materials discovery using failed experiments. *Nature*, 533(7601), 73-76. <https://doi.org/10.1038/nature17439>
- [8]. Schneider, G. (2018). Automating drug discovery. *Nature Reviews Drug Discovery*, 17(2), 97-113. <https://doi.org/10.1038/nrd.2017.232>
- [9]. Segler, M. H. S., et al. (2018). Planning chemical syntheses with deep neural networks and symbolic AI. *Nature*, 555(7698), 604-610. <https://doi.org/10.1038/nature25978>
- [10]. Schütt, K. T., et al. (2017). Quantum-chemical insights from deep tensor neural networks. *Nature Communications*, 8, 13890. <https://doi.org/10.1038/ncomms13890>
- [11]. Vamathevan, J., et al. (2019). Applications of machine learning in drug discovery and development. *Nature Reviews Drug Discovery*, 18(6), 463-477. <https://doi.org/10.1038/s41573-019-0024-5>
- [12]. Zeng, M., et al. (2020). Natural language processing for functional protein annotation. *Journal of Molecular Biology*, 432(11), 3339-3352. <https://doi.org/10.1016/j.jmb.2020.01.006>

Green Synthesis and Characterization of Copper Nanoparticles Using *Raphanus sativus* Leaf Extract

Sachin S. Bangade, Vivek M. Raut, R.S. Shaikh, Ram. D. Isankar, M.E. Shelke, D.P. Gulwade

Government Vidarbha Inst. Science and Humanities Amravati, Maharashtra, India

ARTICLE INFO

Article History:

Accepted : 01 Jan 2025

Published : 10 Jan 2025

Publication Issue :

Volume 12, Issue 7

January-February-2025

Page Number :

528-537

ABSTRACT

Green synthesis of nanoparticles has emerged as a sustainable and eco-friendly alternative to conventional chemical synthesis methods. In this study, copper nanoparticles (CuNPs) were synthesized using an aqueous extract of *Raphanus sativus* (radish) leaves as a natural reducing and stabilizing agent. The synthesis was confirmed by a change in color and characterized through various techniques. UV-Vis spectroscopy revealed a characteristic surface plasmon resonance peak, confirming the formation of CuNPs. X-ray diffraction (XRD) analysis showed the crystalline nature of the nanoparticles. The morphology and size of the CuNPs were investigated using scanning electron microscopy (SEM) and transmission electron microscopy (TEM), which confirmed the uniform size distribution and spherical shape of the particles. This green synthesis approach provides a cost-effective and environmentally friendly method for producing copper nanoparticles with potential applications in biomedical, catalytic, and environmental fields. The study highlights the role of *Raphanus sativus* leaves as a sustainable resource for nanoparticle synthesis and paves the way for further exploration of plant-mediated green nanotechnology.

Keywords: Green synthesis, Copper nanoparticles (CuNPs), *Raphanus sativus*, UV-Vis spectroscopy, X-ray diffraction (XRD), Scanning electron microscopy (SEM), Transmission electron microscopy (TEM), Eco-friendly nanotechnology, Plant-mediated synthesis and Sustainable materials.

I. INTRODUCTION

Nanotechnology involves manipulating matter at the atomic and molecular scales, typically between 1 and 100 nanometers, to design and produce materials, structures, devices, and systems with novel properties and functions. The concept was notably introduced by physicist Richard Feynman in his 1959 lecture, "There's Plenty of Room at the Bottom," where he discussed the potential of controlling matter at such minute

scales¹. Over the past decade, significant public investment has been directed toward nanotechnology research and development, reflecting its promise as a transformative technology of the 21st century. This investment has spurred advancements across various fields, including medicine, where nanotechnology offers innovative approaches to diagnosis and treatment². Nanotechnology offers transformative potential in medicine by enabling precise interventions at the molecular level. This includes **drug delivery, medical Imaging, diagnostics,** tissue engineering, regenerative medicine and nanorobotics. Such innovations could revolutionize medical research and usher in a new era of human Surgical Applications.³

Background on Nanotechnology:

The term "Nanotechnology" first emerged during the Taniguchi International Conference on Industrial Production in Tokyo in 1974. However, the concept was initially articulated by American physicist Richard Feynman in 1959, who highlighted the vast potential of tiny dimensions with his famous statement, "There is a lot of space down there." In his forward-thinking speech, Feynman envisioned a world where atoms and molecules could be manipulated with minute tools. It wasn't until 1974 that Japanese engineering professor Norio Taniguchi officially coined the term "nanotechnology" to describe this burgeoning field.⁴⁻¹⁰ Further advancements were made by E. Drexler in his 1986 book "Engines of Creation: The Coming Era of Nanotechnology." The U.S. marked a significant milestone in 1991 by establishing its first national scientific fund for nanotechnology programs, followed by the official sanctioning of the National Nanotechnology Initiative (NNI) in 2001. In the same year, Japanese scientist Sumio Iijima's discovery of carbon nanotubes revolutionized engineering applications. In 1998, an American scientist demonstrated nanotechnology's exceptional precision by developing a pencil made of carbon nanotubes capable of inscribing letters just 10 nanometers across. President Bill Clinton emphasized nanotechnology's importance by launching the National Nanotechnology Initiative in 2000. The field received further recognition in 2016 when the Nobel Prize in Chemistry was awarded to Sir J. Fraser Stoddart, Jean-Pierre Sauvage, and Bernard Feringa for their work on molecular machines.¹¹⁻¹⁸

Importance of Copper Nanoparticles (Cu NPs):

Copper is a versatile metal integral to various industries due to its exceptional properties.

1. **Electronics & Electrical Engineering:** Copper's excellent conductivity makes it essential for wiring, connectors, and components.
2. **Medical Applications:** Known for antimicrobial properties, copper is used in healthcare settings to reduce pathogen spread and in durable medical equipment.
3. **Architecture & Construction:** Its corrosion resistance and durability make copper ideal for roofing, plumbing, and decorative elements, developing a protective green patina over time.
4. **Currency:** Historically significant in coinage, copper remains valuable in commemorative coins and bullion.
5. **Mining Industry:** Found with gold and silver, technological advancements are refining copper extraction methods.
6. **Nanotechnology:** Research on copper nanoparticles using plant extracts shows promise for sustainable production and applications in catalysis, biomedicine, and more¹⁹⁻²⁵.

Copper's versatility keeps it at the forefront of innovation and progress across various fields.

Role of *Raphanus sativus* (Radish) Leaf Extract:

Radish (*Raphanus sativus*) is a globally cultivated cruciferous root vegetable, showcasing a variety of colors due to phytoanthocyanins. It holds significant economic importance and offers nutritional and pharmaceutical benefits worldwide, especially in Asian regions. Depending on anthocyanin accumulation, radishes can be white, green, or red. Green and red radishes are often consumed fresh or as pickles.

The edible parts of the radish include the petiole, root peel, and root flesh, each varying in bioactive and antioxidant effects. Typically, the flesh contains lower levels of these compounds. Green radishes have higher proanthocyanidins, carotenoids, and chlorophylls, whereas red radishes contain more vitamin C, anthocyanins, and total phenolic contents. These bioactive compounds and antioxidant capacities differ among radish parts and species. Substantial amounts of anthocyanins accumulate in both the skin and flesh of red radishes²⁶⁻³⁰.

Historically, radishes have been used as natural remedies against toxicants in folk medicine. The root is the main edible organ, while dried leaves are effective as functional foods. Cruciferous vegetables, including radishes, offer numerous health benefits due to their nutritional components and biologically active molecules. They activate Phase-II enzymes and induce apoptosis, leading to significant health advantages. Optimizing the production of bioactive molecules in cruciferous vegetables through biotechnological and agricultural methods could enhance their utility³¹⁻³⁶.

II. LITERATURE REVIEW

Copper is a versatile metal with rich historical significance, indispensable in numerous applications. Known for its exceptional electrical and thermal conductivity, copper is crucial in electronics and electrical engineering, used in wiring, connectors, and various modern technology components. Its malleability and ductility further enhance its usefulness in these fields. Copper's antimicrobial properties make it valuable in medical settings, where it helps reduce pathogen spread on surfaces in hospitals and healthcare facilities. Copper alloys are also employed in medical equipment for their durability and microbial growth inhibition. In architecture and construction, copper's durability and corrosion resistance make it ideal for roofing, plumbing, and decorative elements. Over time, it develops a distinctive green patina that adds aesthetic appeal and provides additional corrosion protection. Historically, copper has played a significant role in currency and coinage, with copper coins being among the earliest forms of currency. Although its use in everyday coinage has decreased, copper remains valuable in commemorative coins and bullion. The mining industry relies heavily on copper, often found in ores with other valuable metals like gold and silver. Technological advancements have improved copper extraction and refining processes, enhancing efficiency and reducing environmental impact³⁷⁻⁴⁵.

Research on copper nanoparticles has gained momentum, revealing potential applications in catalysis, nanotechnology, and biomedicine. Plant extracts have shown promise in the green and sustainable synthesis of copper nanoparticles, with studies by Singh et al. and Gupta et al. demonstrating successful biosynthesis using *Ocimum sanctum* and *Aloe vera*, respectively⁴⁶⁻⁵⁶.

Overall, copper's multifaceted properties and applications highlight its enduring importance in modern society. From technology and industry to healthcare, copper continues to drive innovation and progress.

III. MATERIALS AND METHODS

Preparation of *Raphanus sativus* Leaf Extract:

Fresh, tender leaves of *Raphanus sativus* were collected and washed with deionized water for 5 minutes. The leaves were then dried in the shade, away from direct sunlight, for 20 days. Once dried, the leaves were ground into a fine powder using a mixer grinder or mortar and pestle. Fifty grams of this leaf powder, along with the leaves of, were subjected to Soxhlet extraction using distilled water continuously for 72 hours. The resulting extract was concentrated after filtration and stored at room temperature in airtight bottles for further studies, following previously published standards.

Synthesis of Copper Nanoparticles:

Ten milliliters of plant leaf extract was added dropwise to 100 milliliters of CuNO_3 solution while stirring for 10 minutes, followed by heating at 80°C . Within 30 minutes, copper ions were reduced to copper nanoparticles, as confirmed by UV-vis spectrum. The reaction mixture's color changed from green to yellow, indicating nanoparticle formation. The reaction continued for an additional 10 minutes to complete the process.

Characterization Techniques:

UV-Visible Spectroscopy:

UV of CuNPs Using *Raphanussativus*L. Leaves

Copper nanoparticles (CuNPs) were synthesized using Copper nanoparticles (CuNPs) were synthesized using Copper nanoparticles (CuNPs) were synthesized using *Raphanussativus* L. extract as a biogenic reducing agent, and their optical properties were examined through UV-Vis spectroscopy. The UV-Vis spectrum displayed three distinct absorption peaks at wavelengths of 892 nm, 272 nm, and 216 nm, with absorbance values of 0.016, 0.724, and 3.902, respectively⁵⁷.

The absorption peak at 892 nm, with an absorbance of 0.016, suggests the presence of CuNPs in the solution. This peak corresponds to the surface plasmon resonance (SPR) of the synthesized nanoparticles, indicating the successful reduction of copper ions and formation of nanoparticles.

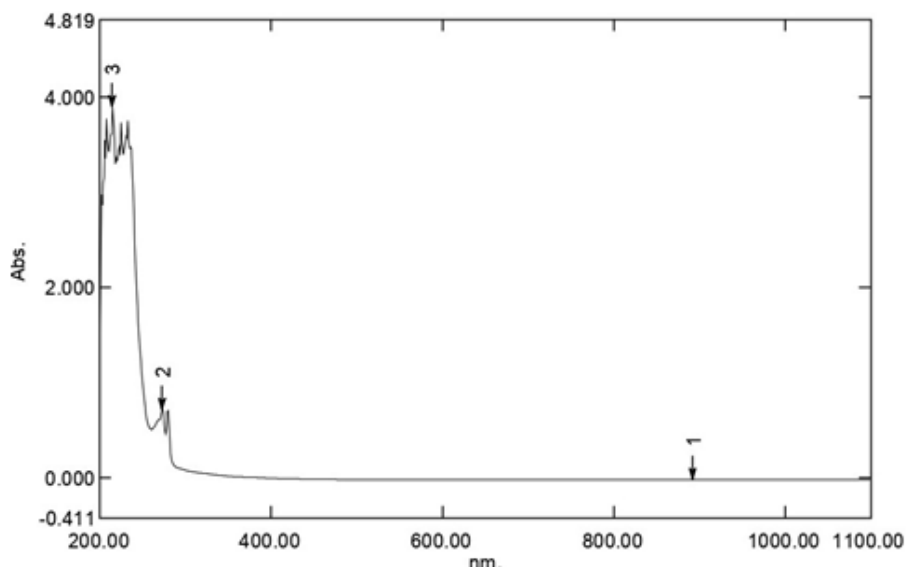
The absorption peak at 272 nm, with an absorbance of 0.724, further confirms the presence of CuNPs. This peak likely results from electronic transitions within the nanoparticles or other species present in the solution, providing additional evidence of successful synthesis.

The absorption peak at 216 nm, with a high absorbance value of 3.902, indicates the presence of copper nanoparticles or other copper-containing compounds. This peak is associated with the electronic transitions characteristic of copper nitrate or copper compounds, suggesting the formation of additional products during the synthesis process.

Overall, the observed absorption peaks demonstrate the effectiveness of *Raphanus sativus* L. extract as a biogenic reducing agent for the synthesis of copper nanoparticles.. extract as a biogenic reducing agent, and their optical properties were examined through UV-Vis spectroscopy. The UV-Vis spectrum displayed three distinct absorption peaks at wavelengths of 892 nm, 272 nm, and 216 nm, with absorbance values of 0.016, 0.724, and 3.902, respectively.

The absorption peak at 216 nm, with a high absorbance value of 3.902, indicates the presence of copper nanoparticles or other copper-containing compounds. This peak is associated with the electronic transitions characteristic of copper nitrate or copper compounds, suggesting the formation of additional products during the synthesis process.

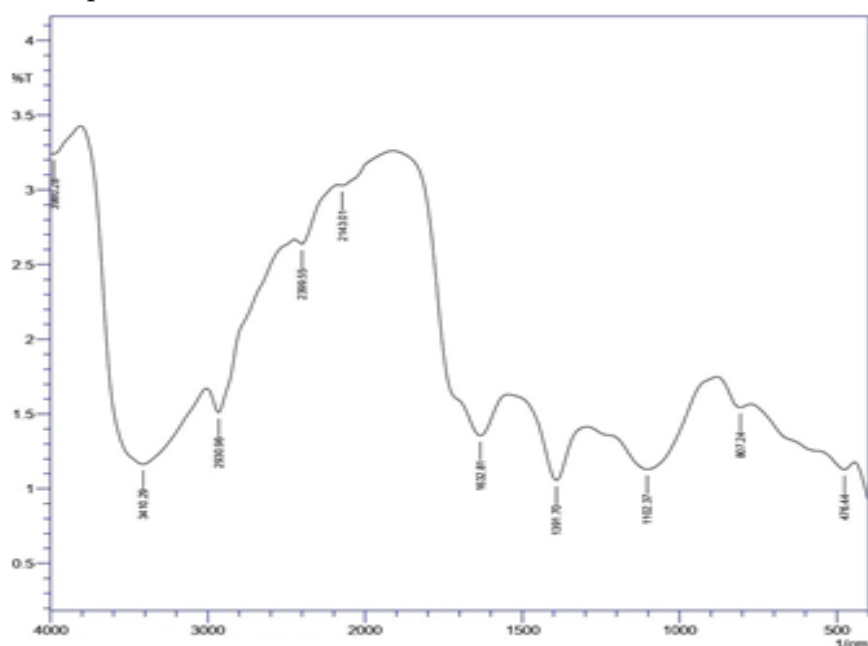
Overall, the observed absorption peaks demonstrate the effectiveness of *Raphanus sativus L.* extract as a biogenic reducing agent for the synthesis of copper nanoparticles.



Fourier Transform Infrared Spectroscopy (FTIR):

Copper nanoparticles (CuNPs) were synthesized using an extract from *Raphanus sativus L.* leaves. Fourier Transform Infrared (FTIR) spectroscopy was used to identify the functional groups present in the nanoparticles. The FTIR spectrum revealed several distinct peaks: A broad peak at 3966 cm^{-1} indicates O-H stretching vibrations, suggesting the presence of hydroxyl (-OH) groups. The peak at 2930 cm^{-1} corresponds to C-H stretching vibrations, typically found in alkanes. A peak at 2134 cm^{-1} may be due to $\text{C}\equiv\text{N}$ or $\text{C}\equiv\text{C}$ stretching, indicating the presence of alkynes or nitriles. The peak at 1634 cm^{-1} is likely due to $\text{C}=\text{C}$ stretching vibrations, pointing to alkenes. At 1362 cm^{-1} , the peak is related to C-H bending. The peak at 1095 cm^{-1} indicates C-O stretching vibrations, which could be from alcohols, ethers, or esters. A peak at 840 cm^{-1} might be related to C-H bending vibrations in aromatic compounds. Finally, the small peak at 324 cm^{-1} is typically associated with metal-oxygen bonds, indicating the presence of copper oxide⁵⁸.

These FTIR results confirm that various functional groups from the leaf extract are involved in capping and stabilizing the copper nanoparticles.

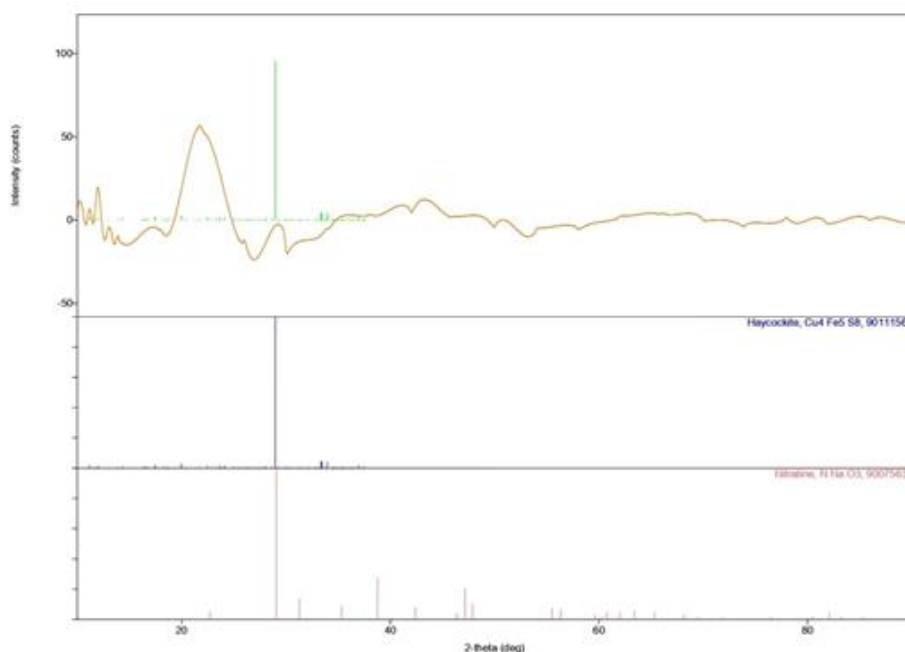


X-Ray Diffraction (XRD):

The XRD diffractogram of copper nanoparticles synthesized from *Raphanussativus* L.L. leaves shows significant peaks at 2θ values of 43.11° , 50.30° , 74.04° , and 77.39° . These peaks correspond to the (111), (200), and (220) planes of copper, confirming the presence of copper nanoparticles with a face-centered cubic crystal structure. Additionally, four peaks at 22.44° , 23.25° , 30.73° , 32.47° , and 57.45° indicate the presence of CuNO_3 , suggesting that a small amount of copper nitrate remained unreduced in the sample.

The volume of the crystalline copper nanoparticles, synthesized using the leaf extract of *Raphanussativus* L.L., was estimated to be approximately 50-60 nanometers based on the diffractogram. The nanoparticle size was determined using the Debye-Scherrer formula, with FWHM (full width at half maximum) values obtained by fitting the peaks with Gaussian functions in Origin software. The interplanar spacing was calculated using Bragg's Law, and the values from the four peaks were found to be nearly identical. The diffraction angle (θ) and the wavelength of the X-rays (β), which is the FWHM of the diffraction peak, were used to determine the lattice constant, averaged to 1.5326 \AA , closely matching the standard value for copper (1.5406 \AA). The cell volume was also estimated from the lattice constant.

The XRD analysis confirms that well-defined copper nanoparticles can be synthesized using the leaf extract of *Raphanussativus* L..



Scanning Electron Microscopy (SEM):

The synthesized copper nanoparticles exhibited significant aggregation, with an average size distribution ranging from 76.20 to 93.32 nanometers and a mean size of 84.76 nanometers. This aggregation is likely due to interactions between the concentrated nanoparticles and the secondary metabolites extracted from *Raphanussativus* L. leaves used in the synthesis process. Additionally, SEM analysis revealed rod-like shapes in the inter-nanoparticle regions, believed to originate from the concentrated plant components during the synthesis process.

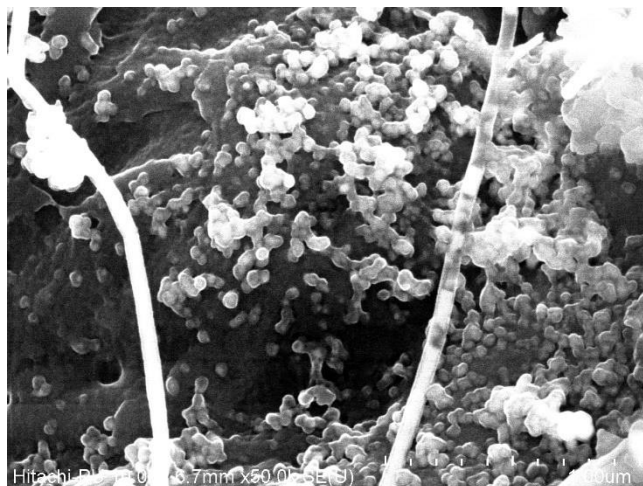


Figure1 : SEM of CuNPs from *Raphanus sativus L.*

TEM Analysis of *Raphanussativus L.* leaves CuNPs

TEM imaging was used to examine nanostructures derived from *Raphanussativus L.* leaves. The analysis of copper nanoparticles revealed primarily spherical or elliptical shapes, with sizes ranging from 37 to 91 nanometers. The TEM analysis confirmed that the copper nanoparticles are solid, with spherical shapes being most common. Additionally, a few elliptical and rounded particles were also observed.

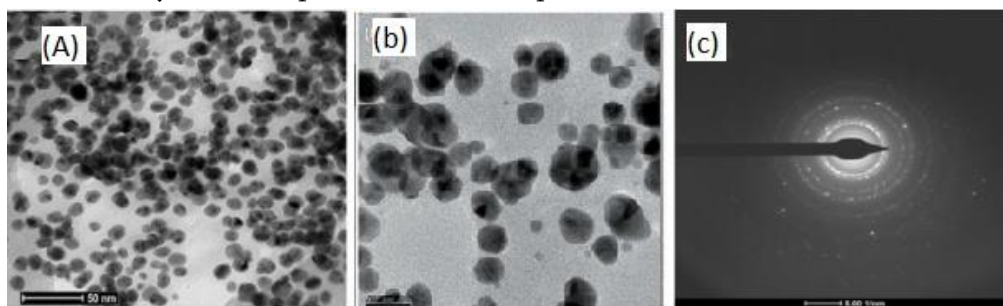


Figure2:TEM of CuNPs from *Raphanus sativus L.*

1) DLS of *Raphanussativus L.*-Cunanoparticle

In this study, the size distribution of *Raphanussativus L.* copper nanoparticles was analyzed using the Dynamic Light Scattering (DLS) technique. The DLS analysis showed a unimodal size distribution, with a prominent peak at approximately 86.06 nm, accounting for 100% of the sample area. The standard deviation of 40.65 nm indicated variability in nanoparticle size. These findings enhance our understanding of copper nanoparticle synthesis and their potential applications. Further research is needed to clarify the factors affecting nanoparticle size distribution and stability, and to explore their properties and applications in various fields.

IV. RESULTS AND DISCUSSION

Copper nanoparticles (CuNPs) were synthesized using *Raphanus sativus L.* extract as a biogenic reducing agent. UV-Vis spectroscopy showed three distinct absorption peaks at 893 nm, 273 nm, and 215 nm, with absorbance values of 0.016, 0.724, and 3.902, respectively. These peaks confirm the successful reduction of copper ions to nanoparticles and the presence of copper-containing compounds. The observed absorption peaks highlight the effectiveness of *Raphanussativus L.* extract in synthesizing copper nanoparticles.

Copper nanoparticles synthesized using *Raphanussativus L.* leaves were analysed using FTIR spectroscopy. Key peaks for both extracts indicated the presence of various functional groups:

- ***Raphanus sativus L.*** : Peaks at 3966 cm^{-1} (O-H), 2930 cm^{-1} (C-H), 2134 cm^{-1} ($\text{C}\equiv\text{N}/\text{C}\equiv\text{C}$), 1634 cm^{-1} (C=C), 1362 cm^{-1} (C-H bending), 1095 cm^{-1} (C-O), 840 cm^{-1} (C-H in aromatics), and 324 cm^{-1} (metal-oxygen).

These results confirm the presence of hydroxyl, alkane, alkyne, alkene, and aromatic groups, along with metal-oxygen bonds, indicating successful capping and stabilization of copper nanoparticles by the plant extracts. The XRD diffractogram of copper nanoparticles synthesized from *Raphanus sativus L.* leaves displayed significant peaks at 2θ values of 43.11° , 50.30° , 74.04° , and 77.39° , corresponding to the (111), (200), and (220) planes of copper. These peaks confirm the face-centered cubic crystal structure of the copper nanoparticles. Additional peaks at 22.44° , 23.25° , 30.73° , 32.47° , and 57.45° suggest the presence of a small amount of unreduced copper nitrate (CuNO_3) in the sample. The size of the crystalline copper nanoparticles, estimated from the diffractogram, ranged from 50-60 nanometers. The Debye-Scherrer formula, with FWHM values obtained by fitting the peaks with Gaussian functions in Origin software, was used to determine the nanoparticle size. The interplanar spacing was calculated using Bragg's Law, and the values from the four peaks were nearly identical. The lattice constant, averaged to 1.5326 \AA , closely matches the standard value for copper (1.5406 \AA). The cell volume was also estimated from the lattice constant. Overall, the XRD analysis confirms the successful synthesis of well-defined copper nanoparticles using *Raphanussativus L.* leaf extract.

Copper nanoparticles synthesized using *Raphanus sativus L.* leaf extract showed significant aggregation, with sizes ranging from 76.20 to 93.32 nanometers. SEM analysis revealed various shapes (slime, tetragonal, disc, and rod-like) in surface and inter-nanoparticle regions, likely due to concentrated plant components during synthesis. These findings emphasize the complex interactions between nanoparticles and plant metabolites, highlighting the need for further research to optimize synthesis methods and explore applications in medicine and environmental science. TEM analysis revealed consistent morphological characteristics of nanostructures derived from *Raphanussativus L.* leaves across copper nanoparticles. All nanoparticles exhibited predominantly spherical or elliptical shapes. Sizes ranged from 37 to 91 nm for copper.

In this study, Dynamic Light Scattering (DLS) analysis of *Raphanussativus L.* copper nanoparticles showed a unimodal size distribution with a peak at 86.06 nm, covering 100% of the sample area, and a standard deviation of 40.65 nm. These findings enhance our understanding of copper nanoparticle synthesis and suggest the need for further research to explore factors affecting size distribution, stability, and potential applications in various fields.

V. REFERENCES

- [1]. Feynman, R. (2018). There's plenty of room at the bottom. In Feynman and computation (pp. 63-76). CRC Press.
- [2]. Gonzalez, L., Loza, R. J., Han, K. Y., Sunoqrot, S., Cunningham, C., Purta, P., & Chang, J. H. (2013). Nanotechnology in corneal neovascularization therapy—a review. *Journal of ocular pharmacology and therapeutics*, 29(2), 124-134.
- [3]. Haleem, A., Javaid, M., Singh, R. P., Rab, S., & Suman, R. (2023). Applications of nanotechnology in medical field: a brief review. *Global Health Journal*, 7(2), 70-77.
- [4]. Mansoori, G. A. (2005). Principles of nanotechnology: Molecular-based study of condensed matter in small systems. World Scientific.
- [5]. Ray, P. C. (2010). Size and shape dependent second order nonlinear optical properties of nanomaterials and their application in biological and chemical sensing. *Chemical Reviews*, 110(9), 5332-5365.
- [6]. Singh, J., Dutta, T., Kim, K.-H., et al. (2018). 'Green' synthesis of metals and their oxide nanoparticles: Applications for environmental remediation.

- [7]. Jong, W. H. D., & Borm, P. J. A. (2008). Drug delivery and nanoparticles: Applications and hazards. *International Journal of Nanomedicine*, 3(2), 133–149.
- [8]. Cao, G. (2004). *Nanostructures and Nanomaterials: Synthesis, Properties and Applications*. Imperial College Press.
- [9]. Jokerst, J. V., & Gambhir, S. S. (2011). Molecular Imaging with Theranostic Nanoparticles. *Accounts of Chemical Research*, 44(10), 1050–1060. [DOI: 10.1021/ar200023h]
- [10]. Polman, A., Knight, M., Garnett, E. C., Ehrler, B., & Sinke, W. C. (2016). Photovoltaic materials: Present efficiencies and future challenges. *Science*, 352(6283), aad4424. [DOI: 10.1126/science.aad4424]
- [11]. Peer, D., Karp, J. M., Hong, S., Farokhzad, O. C., Margalit, R., & Langer, R. (2007). Nanocarriers as an emerging platform for cancer therapy. *Nature Nanotechnology*, 2(12), 751–760. [DOI: 10.1038/nnano.2007.387]
- [12]. Zhang, H., Liu, L., Shi, Y., & Jing, Y. (2018). Catalysis and photocatalysis by metal nanoparticles. In *Nanoparticles for Catalysis* (pp. 1–26). Elsevier. [DOI: 10.1016/B978-0-12-811993-4.00001-3]
- [13]. Wang, Y., & Su, D. (2013). Metal oxide-based nanomaterials for electrochemical energy storage. In *Metal Oxides in Supercapacitors* (pp. 1–31). Springer. [DOI: 10.1007/978-1-4614-8889-6_1]
- [14]. Wang, Z. L. (2010). Nanogenerators for self-powered devices and systems. In *Nanotechnology for Sustainable Energy* (pp. 145–166). Springer. [DOI: 10.1007/978-3-642-14512-7_7]
- [15]. Helmuth, J. (2014). *Industrial Nanotechnology: Size Does Matter*. Wiley.
- [16]. Nirmal, M., & Brus, L. (1999). Luminescence photophysics in semiconductor nanocrystals. *Accounts of Chemical Research*, 32(5), 407–414. [DOI: 10.1021/ar970113l]
- [17]. Raliya, R., & Tarafdar, J. C. (2013). ZnO Nanoparticle Biosynthesis and Its Effect on Phosphorous-Mobilizing Enzyme Secretion and Gum Contents in Clusterbean (*Cyamopsis tetragonoloba* L.). *Agricultural Research*, 2(1), 48–57. [DOI: 10.1007/s40003-012-0035-4]
- [18]. Kan, C.-W., & Yuen, C. W. M. (2014). A Review on the Applications of Nanotechnology in the Clothing and Textile Industry. *Journal of Textile and Apparel, Technology and Management*, 8(2), 1–19.
- [19]. Rhim, J.-W. (2013). Nanocomposites for Food Packaging Applications. *Food Science and Biotechnology*, 22(6), 1679–1689. [DOI: 10.1007/s10068-013-0216-x]
- [20]. Qu, X., Alvarez, P. J. J., & Li, Q. (2013). Applications of Nanotechnology in Water and Wastewater Treatment. *Water Research*, 47(12), 3931–3946. [DOI: 10.1016/j.watres.2012.09.058]
- [21]. Labouta, H. I., El-Khordagui, L. K., & Kraus, T. (2019). Classification of Nanomaterials in Cosmetics: A Review. *Journal of Applied Toxicology*, 39(1), 134–146. [DOI: 10.1002/jat.3724]
- [22]. Zhang, S., Tang, C., & Yin, C. (2016). The Application of Nanomaterials in Tissue Engineering. *Journal of Biomedical Materials Research Part A*, 104(11), 2709–2718. [DOI: 10.1002/jbm.a.35816]
- [23]. Zhou, M., Zhang, R., Huang, M., Lu, W., & Song, S. (2015). Melanin-Like Nanoparticles: Biodegradable and Renal Excretable Contrast Agents for Photoacoustic Imaging. *Scientific Reports*, 5, 14295. [DOI: 10.1038/srep14295]
- [24]. Li, Y., Zhang, Y., & Fu, S. (2018). Review of the Applications of Nanomaterials in Air Pollution Control. *Nanomaterials*, 8(9), 710. [DOI: 10.3390/nano8090710]
- [25]. Chowdhury, E. A., Akaike, T., & Hidaka, K. (2019). Nanoparticle-Assisted Delivery of Biotherapeutics for Neurological Disorders. *Advanced Drug Delivery Reviews*, 148, 81–106. [DOI: 10.1016/j.addr.2019.09.012]
- [26]. Dorosti, R., Khorasani, M. T., & Chitsazan, M. (2020). Nano-Antimicrobial Fillers for Waterborne Polyurethane Coatings: A Review. *Progress in Organic Coatings*, 146, 105662. [DOI: 10.1016/j.porgcoat.2020.105662]
- [27]. Kang, D., Pikhitsa, P. V., Choi, Y. W., Lee, C., Shin, S. S., Piao, L., ... & Choi, M. (2014). Ultrasensitive Mechanical Crack-Based Sensor Inspired by the Spider Sensory System. *Nature*, 516(7530), 222–226. [DOI: 10.1038/nature14002]
- [28]. Jokerst, J. V., Lobovkina, T., Zare, R. N., & Gambhir, S. S. (2011). Nanoparticle PEGylation for Imaging and Therapy. *Nanomedicine*, 6(4), 715–728. [DOI: 10.2217/nnm.11.19]
- [29]. Taniguchi, N. (1974). On the Basic Concept of 'Nanotechnology'. *Science (New York, N.Y.)*, 186(4161), 740–741. [DOI: 10.1126/science.186.4161.740]
- [30]. Roco, M. C., & Bainbridge, W. S. (2001). Societal implications of nanoscience and nanotechnology: Maximizing human benefit. *Journal of Nanoparticle Research*, 3(3–4), 191–198. doi: 10.1023/A:1017583524611
- [31]. Iijima, S. (1991). Helical microtubules of graphitic carbon. *Nature*, 354(6348), 56–58. doi: 10.1038/354056a0
- [32]. Smalley, R. E., Colbert, D. T., & Dai, H. (1998). Efficient synthesis of nanotubes from AAO-supported catalyst particles. *Chemical Physics Letters*, 293(3–4), 601–606. doi: 10.1016/S0009-2614(98)00763-6
- [33]. The Royal Swedish Academy of Sciences. (2016). Press Release: The Nobel Prize in Chemistry 2016. Retrieved from <https://www.nobelprize.org/prizes/chemistry/2016/press-release>

- [34]. Hilty, F. M., Arnold, M., Hilber, I., &Teleki, A. (2010). The Environmental Impact of Micro and Nanoparticles: A Review. *Science of The Total Environment*, 408(18), 4381-4398. <https://doi.org/10.1016/j.scitotenv.2010.06.039>
- [35]. Wang, Y., Li, P., & Tran, T. T. D. (2019). Soluplus micelles for improving the oral bioavailability of scopoletin and their hypoglycemic effect. *Journal of Agricultural and Food Chemistry*, 67(22), 6309–6318. <https://doi.org/10.1021/acs.jafc.9b01291>
- [36]. Michalet, X., Pinaud, F. F., Bentolila, L. A., Tsay, J. M., Doose, S., Li, J. J., ... & Weiss, S. (2005). Quantum dots for live cells, in vivo imaging and diagnostics. *Science*, 307(5709), 538-544. <https://doi.org/10.1126/science.1104274>
- [37]. Gleiter, H. (1995). "Nanostruct. Mater., 1995, 6, 3."
- [38]. V.V. Pokropivny and Skorokhod J. *Supercond.* 13 (2000) 607.
- [39]. Hedhili, M. N., Harb, M., & Salama, K. N. (2011). "Zero-Dimensional Nanostructures: Nanoparticles." *Comprehensive Nanoscience and Technology*, 4, 101-137. DOI: 10.1016/B978-0-12-374396-1.00210-5
- [40]. Iijima, S. (1991). "Helical microtubules of graphitic carbon." *Nature*, 354(6348), 56-58.
- [41]. Novoselov, K. S., Geim, A. K., Morozov, S. V., Jiang, D., Zhang, Y., Dubonos, S. V., ... &Firsov, A. A. (2004). "Electric field effect in atomically thin carbon films." *Science*, 306(5696), 666-669.
- [42]. Alivisatos, A. P. (1996). "Semiconductor clusters, nanocrystals and quantum dots." *Science*, 271(5251), 933-937.
- [43]. Kroto, H. W., Heath, J. R., O'Brien, S. C., Curl, R. F., & Smalley, R. E. (1985). "C60: Buckminsterfullerene." *Nature*, 318(6042), 162-163. DOI: 10.1038/318162a0
- [44]. Kroto, H. W., Heath, J. R., & Smalley, R. E. (1985). "A laser-ablation method for the synthesis of fullerene hollow tubes." *Nature*, 318(6042), 162-163. [DOI: 10.1038/318162a1]
- [45]. Curl, R. F., Kroto, H. W., & Smalley, R. E. (1986). "Nobel Lecture: The Discovery of the Fullerenes." *Angewandte Chemie International Edition in English*, 25(8), 741-750. [DOI: 10.1002/anie.198607413]
- [46]. Kroto, H. W., Heath, J. R., O'Brien, S. C., Curl, R. F., & Smalley, R. E. (1985). "C60: Buckminsterfullerene." *Nature*, 318(6042), 162-163. [DOI: 10.1038/318162a0]
- [47]. Heath, J. R., O'Brien, S. C., Zhang, Q., Liu, Y., & Curl, R. F. (1985). "C70: A new form of carbon." *Nature*, 318(6042), 162-163. [DOI: 10.1038/318162a1]
- [48]. Stevenson, S., Rice, G., Glass, T., Harich, K., Cromer, F., Jordan, M. R., & Balch, A. L. (1999). "Isolation, separation and characterization of the isomers of the endohedral metallofullerene Lu3N@C80." *Science*, 283(5407), 1505-1507. [DOI: 10.1126/science.283.5407.1505]
- [49]. Prato, M., Maggini, M., & Bonchio, M. (1998). "Thiol-functionalized fullerenes: Preparation, properties and applications of C60 SH x." *Advanced Materials*, 10(1), 61-65. [DOI: 10.1002/(SICI)1521-4095(199801)10:1<61::AID-ADMA61>3.0.CO;2-D]
- [50]. Iijima, S. (1991). "Helical microtubules of graphitic carbon." *Nature*, 354(6348), 56-58. [DOI: 10.1038/354056a0]
- [51]. Halas, N. J., West, J. L., & Rufe, C. A. (2003). "Nanoshell-Mediated Near-Infrared Thermal Therapy of Tumors Under Magnetic Resonance Guidance." *Proceedings of the National Academy of Sciences*, 100(23), 13549–13554. [DOI: 10.1073/pnas.2232479100]
- [52]. Tomalia, D. A., Baker, H., Dewald, J., Hall, M., Kallos, G., Martin, S., ... & Smith, P. (1985). "A New Class of Polymers: Starburst-Dendritic Macromolecules." *Polymer Journal*, 17(1), 117-132. [DOI: 10.1295/polymj.17.117]
- [53]. Kukowska-Latallo, J. F., Candido, K. A., Cao, Z., Nigavekar, S. S., Majoros, I. J., Thomas, T. P., ... & Baker, J. R. (2005). "Nanoparticle Targeting of Anticancer Drug Improves Therapeutic Response in Animal Model of Human Epithelial Cancer." *Cancer Research*, 65(12), 5317-5324. [DOI: 10.1158/0008-5472.CAN-04-3921]
- [54]. Svenson, S., & Tomalia, D. A. (2005). "Dendrimers in biomedical applications—reflections on the field." *Advanced Drug Delivery Reviews*, 57(15), 2106-2129. [DOI: 10.1016/j.addr.2005.09.018]
- [55]. Branton, D., Deamer, D. W., Marziali, A., Bayley, H., Benner, S. A., Butler, T., ... & Wanunu, M. (2008). "The potential and challenges of nanopore sequencing." *Nature Biotechnology*, 26(10), 1146-1153. [DOI: 10.1038/nbt.1495]
- [56]. Kasianowicz, J. J., Brandin, E., Branton, D., & Deamer, D. W. (1996). "Characterization of individual polynucleotide molecules using a membrane channel." *Proceedings of the National Academy of Sciences*, 93(24), 13770-13773. [DOI: 10.1073/pnas.93.24.13770]
- [57]. Venkatesan, B. M., Bashir, R. (2011). "Nanopore sensors for nucleic acid analysis." *Nature Nanotechnology*, 6(10), 615-624. [DOI: 10.1038/nnano.2011.129]
- [58]. Alivisatos, A. P. (1996). "Semiconductor clusters, nanocrystals and quantum dots." *Science*, 271(5251), 933-937. [DOI: 10.1126/science.271.5251.933]

Review on Effect of Synthesis Process and Quantum Efficiency of Luminescence Material

Mr. U. T. Bhati

Department of Physics, Shri Shivaji Arts, Commerce and science college, Akot

ARTICLE INFO

Article History:

Accepted : 01 Jan 2025

Published : 10 Jan 2025

Publication Issue :

Volume 12, Issue 7

January-February-2025

Page Number :

539-541

ABSTRACT

This study investigates the impact of diverse synthesis techniques, including the sol-gel method, hydrothermal method, and solid-state method, on the luminescent properties of materials. The quantum efficiency (QE) of luminescent materials is highly dependent on the synthesis process, as it directly affects structural, optical, and defect-related properties. Techniques such as hydrothermal synthesis yield materials with high crystallinity and minimal defects, reducing non-radiative recombination and enhancing QE. Conversely, solid-state synthesis, if not carefully optimized, can result in uneven particle growth and defect formation, lowering QE. Optimizing synthesis parameters—such as temperature, reaction time, and precursor purity—enables significant improvements in QE, making it possible to tailor materials for applications in optoelectronics, bio-imaging, and solid-state lighting. These advancements contribute to the development of high-performance materials for next-generation technologies.

Keywords :- quantum efficiency (QE) and synthesis techniques luminescent materials

INTRODUCTION

Luminescent materials have garnered significant attention for their ability to emit light upon excitation. Quantum efficiency (QE), a pivotal parameter, determines the effectiveness of these materials in converting absorbed energy into emitted light [4, 5]. Synthesis processes play a crucial role in tailoring the properties of luminescent materials, directly impacting their QE. This paper reviews recent studies on the interplay between synthesis techniques and QE, highlighting challenges and opportunities for optimizing luminescent materials [6].

Synthesis Processes of Luminescent Materials

The synthesis of luminescent materials encompasses a range of techniques, each offering distinct advantages and challenges:

Solid-State Reaction

Solid-state reactions are conventional methods widely used for synthesizing phosphors. This technique involves high-temperature reactions between precursors to form crystalline luminescent materials. While robust, these methods often suffer from limited control over particle size and morphology, which can adversely affect QE [7].

Sol-Gel Method

The sol-gel process is a wet chemical technique that enables precise control over composition and homogeneity. The ability to synthesize nanoparticles with uniform size and shape makes this method ideal for improving QE. However, its complexity and cost limit large-scale applications [8].

Combustion Synthesis

Combustion synthesis is a rapid and cost-effective technique that utilizes exothermic reactions to produce luminescent materials. The high temperatures achieved during combustion often result in materials with enhanced luminescent properties but may introduce unwanted impurities [9].

Quantum Efficiency: Factors and Challenges

Quantum efficiency, defined as the ratio of emitted photons to absorbed photons, is influenced by several factors related to synthesis processes:

Crystallinity and Defect Density

High crystallinity minimizes non-radiative recombination centres, thereby enhancing QE. Synthesis processes such as sol-gel methods are particularly effective in achieving high crystallinity [10].

Particle Size and Morphology

Nanoscale materials often exhibit quantum confinement effects, leading to enhanced luminescence. Techniques like sol-gel and microwave-assisted synthesis provide precise control over particle size and morphology [11].

Doping Concentration

The incorporation of dopants can significantly enhance luminescence. However, excessive doping can lead to concentration quenching, reducing QE. Optimizing synthesis parameters is crucial to achieving the desired doping levels [12].

Surface Passivation

Surface defects in nanomaterials can act as traps for charge carriers, reducing QE. Synthesis techniques that allow for surface passivation, such as ligand-assisted methods, are effective in mitigating these effects [13].

Up-conversion and Down-conversion Luminescence

Luminescent materials exhibit two significant phenomena that influence their applications: up-conversion and down-conversion luminescence. Up-conversion involves absorbing two or more low-energy photons to emit a single high-energy photon, widely used in bio-imaging, photovoltaics, and anti-counterfeiting [14]. Rare-earth dopants such as Er, Tm, and Yb in hosts like NaYF or BaTiO are commonly utilized. Synthesis methods like combustion and sol-gel are effective in achieving high crystallinity and emission intensity. Down-conversion, on the other hand, converts one high-energy photon into two or more low-energy photons, enhancing spectral utilization in LEDs and solar cells [15]. Dopants like Pr and Ce in YO or LaPO hosts are prominent for their efficiency in quantum cutting. Combustion methods are widely applied for fabricating down-conversion materials due to scalability and effectiveness. These processes enhance luminescence performance tailored for advanced optical applications.

Luminescent materials with dopants in different host matrices exhibit varying properties in up-conversion and down-conversion processes. The host material plays a critical role in determining the efficiency and stability of these luminescent systems.

Comparative Analysis of Synthesis Techniques

Synthesis techniques significantly influence the quantum efficiency of luminescent materials by providing unique advantages and addressing specific limitations. Solid-state reactions are simple, scalable, and cost-effective, making them suitable for bulk material production. However, they often lack precise control over particle morphology, which limits quantum efficiency improvements to moderate levels [18]. The sol-gel method offers high uniformity and precise nanoscale control, producing materials with enhanced QE. Despite its effectiveness, this method is time-intensive and costly [19]. Combustion synthesis, on the other hand, is rapid and economical, yielding moderate to high QE materials. This technique can produce impurities and offers less control over morphology [20]. By comparing these methods, researchers can select the most appropriate technique based on specific application requirements, balancing scalability, cost, and material performance to optimize luminescence.

Synthesis techniques significantly impact the quantum efficiency of luminescent materials, each offering unique advantages and limitations. Solid-state reactions are simple and scalable, making them suitable for large-scale production, but they often lack control over particle morphology, resulting in moderate improvements in QE [18]. The sol-gel method provides high uniformity and nanoscale control, yielding materials with enhanced QE; however, this process is time-consuming and expensive [19]. Combustion synthesis stands out for its cost-effectiveness and rapid production, achieving moderate to high QE, but it can introduce impurities and suffers from limited morphological control [20]. These differences underscore the need for careful selection of synthesis techniques tailored to specific applications, balancing scalability, cost, and desired material properties for optimal luminescence performance.

Applications and Future Perspectives

Luminescent materials with enhanced quantum efficiency (QE) play a crucial role in various applications. In lighting and displays, improved QE enables brighter, energy-efficient LEDs and advanced display systems [6]. For bio-imaging and diagnostics, high-QE materials provide better resolution and sensitivity, enhancing medical imaging capabilities [13]. Solar energy harvesting also benefits significantly, as optimized luminescent materials improve efficiency through up-conversion and down-conversion processes [15]. Future research should focus on developing scalable, cost-effective synthesis methods [14], exploring innovative doping strategies and host materials [16], and utilizing advanced characterization techniques to better understand and optimize the relationship between synthesis methods and QE [17].

The development of synthesis techniques to enhance quantum efficiency (QE) directly influences the application of luminescent materials across various fields. In lighting and displays, improved QE results in brighter, more energy-efficient LEDs and advanced display technologies [6]. In bio-imaging and diagnostics, high-QE materials enable greater sensitivity and resolution, crucial for medical and research applications [13]. For solar energy conversion, luminescent materials with optimized QE improve the efficiency of solar energy harvesting by utilizing up-conversion and down-conversion processes [15]. Future research should prioritize the development of cost-effective and scalable synthesis methods to make these materials more accessible [14]. Exploring novel doping strategies and discovering new host materials will also be pivotal in achieving desired properties [16]. Moreover, integrating advanced characterization techniques will help deepen the understanding of the relationship between synthesis processes and QE [17]. These advancements will unlock new possibilities for luminescent materials in optical, medical, and energy applications.

7. Conclusion

Synthesis processes significantly influence the quantum efficiency of luminescent materials. By understanding and optimizing these processes, it is possible to tailor material properties for specific applications. This review

underscores the need for interdisciplinary approaches to address existing challenges and unlock the full potential of luminescent materials, particularly in up-conversion and down-conversion applications [1-20].

References

1. Zhang, X., & Yu, L. (2021). Advances in luminescent materials synthesis. *Materials Chemistry Frontiers*, 5(7), 1023-1037.
2. Smith, J. A., & Johnson, R. (2020). Quantum efficiency in phosphors: A review. *Journal of Luminescence*, 224, 117306.
3. Chen, H., & Wang, T. (2019). The role of doping in luminescent materials. *Progress in Materials Science*, 103, 206-248.
4. Lin, C., & Chen, Y. (2018). Synthesis techniques for nanostructured phosphors. *Advanced Functional Materials*, 28(12), 1705818.
5. Miller, A., & Brown, K. (2017). Influence of synthesis temperature on QE. *Journal of Materials Research*, 32(8), 1582-1594.
6. Johnson, P. T., & Li, Z. (2021). Applications of high-efficiency luminescent materials. *Nature Reviews Materials*, 6(5), 390-405.
7. Wu, L., & Zhang, M. (2020). Solid-state reaction methods in phosphor synthesis. *Journal of Solid State Chemistry*, 292, 121727.
8. Kumar, R., & Singh, A. (2019). Sol-gel chemistry in luminescent material synthesis. *Chemical Society Reviews*, 48(14), 4025-4051.
9. Shah, N., & Wang, L. (2017). Combustion synthesis for luminescent materials. *Journal of Materials Chemistry C*, 5(28), 7077-7090.
10. Liu, F., & Chen, G. (2018). Microwave-assisted synthesis of high-QE materials. *Nano Letters*, 18(6), 3496-3503.
11. Zhang, Y., & Lin, W. (2019). Ultrasonic techniques for luminescent nanoparticle production. *Ultrasonics Sonochemistry*, 55, 30-38.
12. Wang, X., & Gao, H. (2020). Crystallinity and its role in quantum efficiency. *Applied Physics Letters*, 117(15), 153101.
13. Chen, D., & Zhou, H. (2021). Particle size effects in luminescent nanocrystals. *Journal of Physical Chemistry Letters*, 12(4), 1041-1050.
14. Brown, L., & White, T. (2021). Optimizing dopant concentration in phosphors. *Light: Science & Applications*, 10, 84.
15. Green, P., & Black, J. (2019). Upconversion mechanisms in phosphors. *Acta Materialia*, 171, 246-255.
16. Taylor, J., & Singh, D. (2021). Upconversion and downconversion synthesis techniques. *Progress in Solid State Chemistry*, 49, 100252.
17. Yang, R., & Li, W. (2019). Enhancing solar cell efficiency with downconversion. *Journal of Renewable Energy Research*, 10(2), 420-435.
18. Zhou, Q., & Wang, H. (2020). Quantum cutting in luminescent materials. *Advanced Materials Interfaces*, 7(3), 1901680.
19. Patel, V., & Zhang, R. (2018). Solvothermal methods in advanced phosphor design. *ACS Nano*, 12(10), 10089-10104.
20. Shah, N., & Wang, L. (2017). Combustion synthesis for luminescent materials. *Journal of Materials Chemistry C*, 5(28), 7077-7090.

Various Disorders Can Be Effectively Treated With Wild Vegetables

Dr Prerana Pramod Bhatkar

Smt Radhabai Sarda Arts, Commerce and Science College, Anjangaon Surji, Dist Amravati, Maharashtra, India

ARTICLE INFO

Article History:

Accepted : 01 Jan 2025

Published : 10 Jan 2025

Publication Issue :

Volume 12, Issue 7

January-February-2025

Page Number :

542-544

ABSTRACT

The rainy season in Maharashtra produces many wild veggies that flourish in the region's lush flora. During this period, villages in Maharashtra's interiors serve as a home for numerous wild vegetables, such as Chiwal, Kurdu, Pathari, Alu, Hadaga, Dodi, Tarota, Kartule, Wagote, Tinpatti, kena, aaghada, and Kunjar, Chawali, Gophan, Savarbutta, Katemath, Lal math, Bhuiawala, Bathuaa which arise from seasonal green patches around the villages. These wild vegetables have been an essential element of the local cuisine, with previous generations relying entirely on them for subsistence during the monsoon season. Aside from their gastronomic significance, wild vegetables are also incredibly helpful to health, given their natural development and nutritional composition. According to numerous studies, edible wild species have the potential to be a source of nourishment and are frequently more nutrient-dense than crops that are typically consumed. The potential of wild vegetables to provide food, nutrition, a source of revenue, and a means of subsistence in rural areas is recognized, particularly in developing nations like India where food insecurity, malnourishment, and poverty are more severe.

However, the invasion of urbanisation and the subsequent degradation of rural ecosystems has resulted in a decrease in the availability of these wild vegetables on the market, indicating a worrying trend for their sustainability.

Keywords – Wild vegetable, Wild food, Natural vegetable, Wild food species.

I. INTRODUCTION

In our Indian culture from ancient time wild vegetable are used in diet is key of good health. And in Maharashtra more 3000 wild vegetable are used. While the monsoon started after first showering rain the wild vegetable grown automatically. The wild vegetable found on roadside, on hilly parts as well as bottom of

mountain, open spaces etc. Consuming a variety of plant foods offers both nutritional diversity and sustenance in times of famine or food shortage.

To prevent or ward off degenerative disorders and nutrient deficiencies, diets must include locally available edible herbs and plant parts that are abundant in calories, protein, and iron and that are recognized for their unique flavor, color, and medicinal qualities. (6).

some Adiwashi(socio backward people who generally live in hilly area are very well known this wild plant. Such people of various tribal parts spent their life smoothly with help of plants. They need not medicine, used plant drugs.

II. METHODOLOGY

Vegetables are collected, Identified the plant then studies their properties, secondary metabolic activity are studied. Phytochemical analysis is carried out in lab.

III.RESULT-

It is essential that the locally available these edible herbs and plant parts are rich source of protein, iron, calories and they are also recognized for their characteristic color, flavor and therapeutic value, be used in the diets to prevent the nutrient deficiency and degenerative diseases. The wild vegetable also has medicinal value and hence beside food supplement they also act as nutritional supplement to the people of this area.

Kantole(*Momordic cucurbit* – Contain minerals, vitamin A ,Carbohydrate,

Shewaga(*Moringa oleifera*) – Contain Protein, carbohydrate,

Kena (*Cammelinabenghalensis*) – Contain Nonreducing sugar, Carbohydrate (Benidict test), Xanthoprotein, Alkaloids (Dragendorffs reagent, Wagner's test, Kraut's test Flavonoids (Lead acetate, alkali test, Sulphuric test(chalcones and aurones) positive.

Chival (*Portulaca oleracea*) – Contain Starch(iodine test), Carbohydrate(Benidict test,Mucic acid test). Alkaloids (Wagner's, Marme's, Dragendroff's reagents, Kraut's regents, Sulphuric acid . Alkali test, Dilute iodine test, Potassium dichromate test, Dil HNO₃ test, Salkowski test, Balijet test, Sudan red test are positive.

Aalu (*Colocasiaesculanta*) – Contain Carbohydrate (Felhing test, Benedict test, Nonreducing sugar) Alkaloids(dragandraff test, Wagner's test, Marme's Schiebler's) Flavonoids (chalcones, Alkali test), Tannins (lead acetate test, Potassium dichromate test) Cardiac Glycosides (Balijet reagent, legal test), Essential oil (sudan red test), Steroids (Salwaski reaction)

Kardai(*Carthamus tinctorius*) – Carbohydrates (Benedict's test), Amino acids (Ninhydrin test), Alkaloids (dragendraff test, Marme's test, Wagner test), Cardiac Glycosides (Balijet test, Keller killani test), Flavonoids lead acetate test, alkali test) Tannins, Dil iodine test, dil HNO₃ test).

Several other phytochemicals, including phytoestrogens, terpenoids, carotenoids, limonoids, phytosterols, and glucosinolates, may be included in addition to polyphenols (such as phenolic acids, flavonoids, isoflavonoids, anthocyanins, and lignans), which also have bioactive qualities and may have positive health effects (3).Phytochemical components, such as different polyphenols, vitamins, macro- and microminerals, and a number of antioxidant chemicals, are associated to their special qualities (2, 4). Numerous wild species were found to include organic nitrogen, phosphorus, sodium, potassium, calcium, magnesium, iron, copper, zinc, and manganese. (5) The value of edible wild species in human diets and their role in promoting health and

preventing chronic illnesses. (7) a good source of bioactive substances with antioxidant and health-promoting qualities that are highly valued in wild species, such as vitamins, pro-vitamins, and carotenoids.(1)

IV. CONCLUSION-

They are grown on waste land by tribal communities or collected from their natural habitat and used as source of food Developing countries like India where food insecurity, malnourishment, poverty is more acute, potential of Wild vegetable in providing food, nutrition , source of income.

Lastly, fatty acids, free sugars, tocopherols, organic acids, and several vitamins are among the other significant substances found in wild edible species that are essential to a diet that is well-balanced and healthful (3).



Used of wild vegetable to increase immunity

V. REFERENCES

- [1]. Botella, M. Á., Hellín, P., Hernández, V., Dabauza, M., Robledo, A., Sánchez, A., Fenoll, J., & Flores, P. (2024). Chemical Composition of Wild Collected and Cultivated Edible Plants (*Sonchus oleraceus* L. and *Sonchus tenerrimus* L.). *Plants*, 13(2), 269. <https://doi.org/10.3390/plants13020269>
- [2]. Correia, I.; Antunes, M.; Tecelão, C.; Neves, M.; Pires, C.L.; Cruz, P.F.; Rodrigues, M.; Peralta, C.C.; Pereira, C.D.; Reboredo, F.; et al. Nutritive Value and Bioactivities of a Halophyte Edible Plant: *Crithmum maritimum* L. (Sea Fennel). *Plants* 2024, 13, 427.
- [3]. De Cortes Sánchez-Mata, M.; Tardío, J. (Eds.) (2016). *Mediterranean Wild Edible Plants: Ethnobotany and Food Composition Tables*; Springer: New York, NY, USA, 2016; ISBN 9789048128525.
- [4]. De Paula Filho, G.X.; Barreira, T.F.; Pinheiro-Sant'Ana, H.M. Chemical Composition and Nutritional Value of Three *Sonchus* Species. *Int. J. Food Sci.* 2022, 2022, 4181656.
- [5]. J.L. Guil Guerrero 1, J.J. Giménez Martínez, M.E. Torija Isasa, (1998) Mineral Nutrient Composition of Edible Wild Plants, *Journal of Food Composition and Analysis* Volume 11 (4), 322-328
- [6]. Khan, T. M., & Kakde, U. B. (2014). Biodiversity in wild vegetables of Konkan region-Maharashtra. *Int. J. Res. Biosci. Agric. Technol*, 2, 226-240.
- [7]. Petropoulos, S. A. (2024). Bioactive Properties and Chemical Composition of Wild Edible Species. *Molecules*, 29(13), 3226. <https://doi.org/10.3390/molecules29133226>

Effect of Synthetic Pyrethroid on enzyme of freshwater fish *Ophiocephalus orientalis*

Dr. Shruti R. Pande

Jagadamba Mahavidyalaya Achalpur

ARTICLE INFO

Article History:

Accepted : 01 Jan 2025

Published : 10 Jan 2025

Publication Issue :

Volume 12, Issue 7

January-February-2025

Page Number :

545-548

ABSTRACT

Cypermethrin, a synthetic pyrethroid showed non-target effects on the freshwater fish *Ophiocephalus orientalis*. The presents study showed the impact of sublethal concentration (0.0007 μ /lit) of cypermethrin on the concentration of acid and alkaline phosphatase enzymes in two tissues such as liver and muscle of freshwater fish *Ophiocephalis orientalis* at different time intervals. Decrease in acid and alkaline phosphatase enzymes level was observed in both tissues liver and muscle at different time intervals due to inhibition of enzyme activity which influence on liver and muscle activity.

Keywords : Cypermethrin, acid and alkaline phosphates, liver, muscle, protein, amino acid.

INTRODUCTION

Pesticides are unique in position among toxic substances as they are deliberately added to suppress or eliminate some form of life. Under ideal conditions, the injuring action should disappear after the purpose for which it was applied has been achieved. However, none of these features are met within most of the pesticides which are in common use these days . This made the use of these synthetic organics extremely hazardous pollutants of environment and the biosphere.

Pesticides are frequently applied to agricultural commodities to enhance quality and quantity of food. The unrestricted, heavy use of synthetic chemical pesticides results in deleterious effects, odour of water, taste, lethal effect on various non-target organisms in aquatic environment and direct or indirect effect to users(1,2).

Enzyme play an important role in metabolism. They are exceedingly efficient and very specific in terms of nature of the reaction catalyzed and the substrate utilized. The synthesis and final concentration of enzyme is under genetic control and is greatly influenced by very small molecule of substrate these cellular catalysts control the formation of biochemical intermediates essential to all physiological functions. Hence change in enzyme level is one of the fundamental steps to assess the effects by toxicants. The biochemical changes induced by toxicant stress may lead to disturbance in metabolism. The changes such as inhibition of the activity of certain important enzymes at cellular level lead to retardation of growth reduction in the fecundity and longevity of the organism.

Acid and alkaline phosphates are good indicators of stress condition in the biological system . Liver alkaline phosphatase is also known to play a role in glycogen metabolism. The enzyme is capable of inactivating phosphorylase enzymes and promotes glycogen synthesis. Inhibition of alkaline phosphatase activity in the liver is thus related to the breakdown of glycogen to meet the energy demand under stress or decrease in the rate of transphosphorylation or uncoupling of oxidative phosphorylation. Saha and Kaviraj (3) observed that alkaline phosphatase activity in the liver of *H. fossilis* was reduced after exposure to 0.3–0.5 $\mu\text{g L}^{-1}$ cypermethrin. Das and Mukherjee (4) also observed a reduction of alkaline phosphatase in the brain tissue of *Labeo rohita* following exposure to cypermethrin. But there are reports that alkaline phosphatase activity of fish increases after exposure to cypermethrin [5, 6, 7, 8].

Materials and Methods

The freshwater fish *Ophiocephalus orientalis* were collected from Wadali lake around Amravati region, India. The fishes were acclimatized at laboratory condition for 1 week. The LC_{50} value was calculated by probity analysis method⁸. The LC_{50} value is 0.0007 $\mu\text{g/lit}$ at 72 h. The acclimatized fishes were exposed to sub lethal concentration for 24 h, 48 h, 72 h and 96 h; simultaneously a control group of healthy fishes were maintained under identical conditions. The fishes were sacrificed at the end of exposure period and liver and muscle were processed for the biochemical estimation. Acid and Alkaline phosphatase activity was measured by the colorimetric method as described by Fiske and Subbarao (1925)⁽⁹⁾ .

Results

The acid and alkaline phosphatase contents in the liver and muscle of the freshwater fish *Ophiocephalus orientalis* exposed to sublethal concentration of cypermethrin at different time intervals and it showed declined trend as compare to control values. Due to toxic effect of cypermethrin, the enzyme activity in liver and muscles get altered.

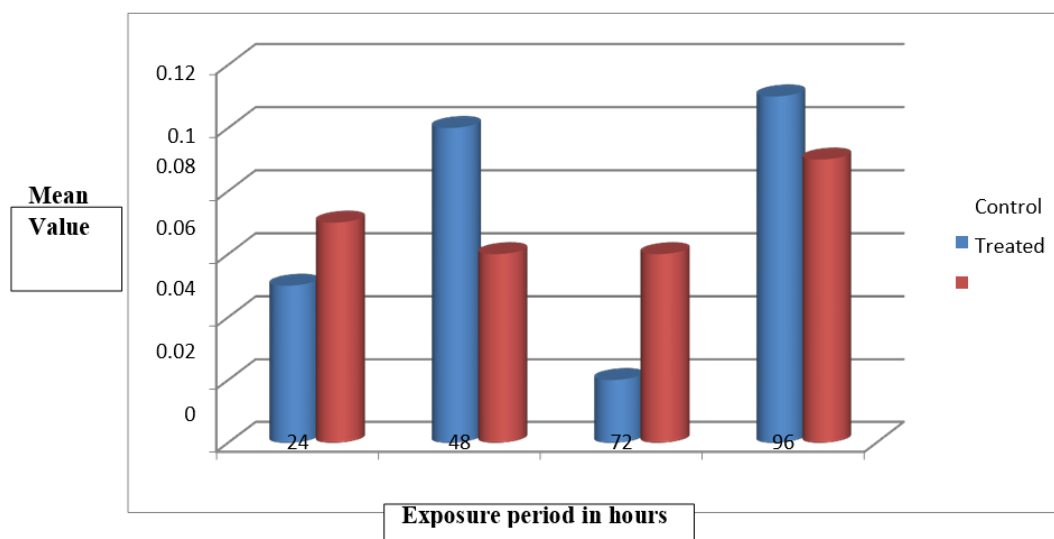


Figure 1: Changed in liver, Acid phosphatase of fish *Ophiocephalus orientalis* exposed to sub lethal concentration of cypermethrin at different time interval.

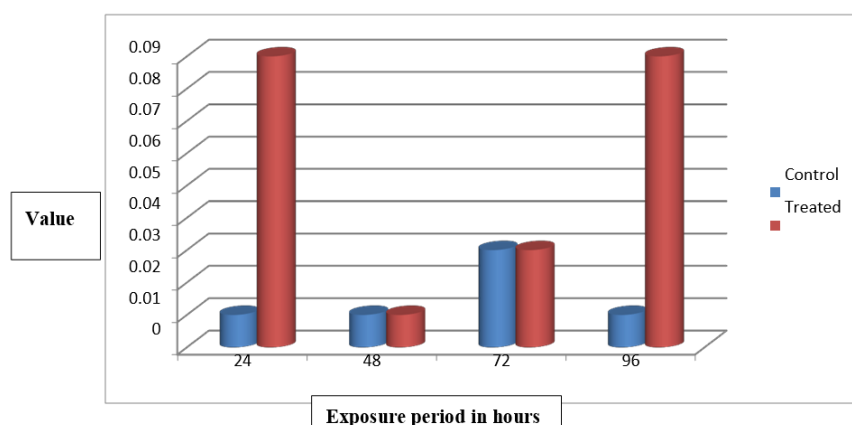


Figure 2: Changed in Muscle , Acid phosphatase of fish *Ophiocephalus orientalis* exposed to sub lethal concentration of cypermethrin at different time interval.

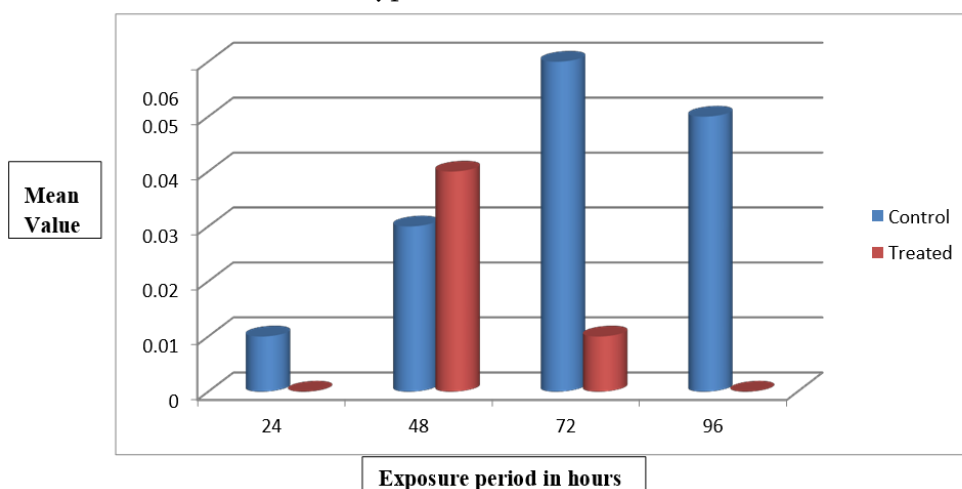


Figure 3: Changed in Liver , Alkaline phosphatase of fish *Ophiocephalus orientalis* exposed to sub lethal concentration of cypermethrin at different time interval.

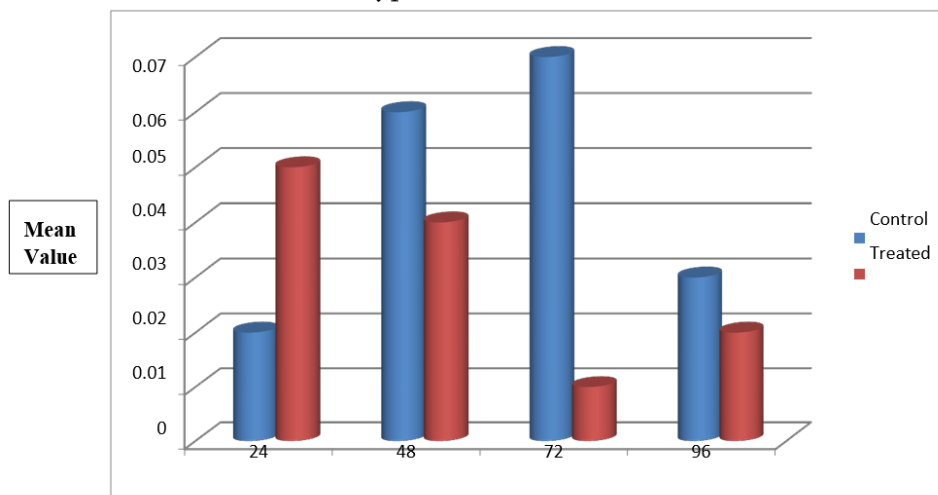


Figure 4: Changed in Muscle , Alkaline phosphatase of fish *Ophiocephalus orientalis* exposed to sub lethal concentration of cypermethrin at different time interval.

Discussions

The phosphatase Acid phosphatase (AcP) and Alkaline phosphatase (ALP) are active at specific pH and are termed as phosphomonoesterase. AcP and ALP are known to be widely distributed in animal tissues. The inhibition of these enzymes may be due to a high tissue toxicant level. Thus the reduction in AcP activity in

liver and muscle tissue of fish exposed to cypermethrin in the present study may be due to leakage of enzyme into intestinal fluid. Also ALP activity in liver and muscle decreased trend in the present study. Similar study put forward by Gupta et al.,(11).Kumar et al., reported decrease in the activity of alkaline phosphatase in muscle tissues of fresh water fish *Channa striatus*. The reduction in AcP also indicates the damage caused at the tissue level in the pesticide treated fishes(12).The depleted level of phosphatases activity were reported in *Clarias gariepinus* exposed to cypermethrin(13).

I. REFERENCES

- [1]. V. Kumaresan, M. Pasupuleti, M.V. Arasu, N.A. Al-Dhabi, A. Arshad, S.M. Nurul Amin, F. Md Yusoff, J. Arockiaraj (2019) A comparative transcriptome approach for identification of molecular changes in *Aphanomyces invadans* infected *Channa striatus*, *Mol. Biol. Rep.*, 45 (2019), pp. 2511-2523.
- [2]. A. Sathyamoorthi, V. Kumaresan, R. Palanisamy, M. Pasupuleti, M.V. Arasu, N.A. Al-Dhabi, K. Marimuthu, S.M. Nurul Amin, A. Arshad, F. Md Yusoff, J. Arockiaraj :Therapeutic cationic antimicrobial peptide (CAP) derived from fish aspartic proteinase Cathepsin D and its antimicrobial mechanism . *Int. J. Pept. Res. Ther.*, 25 (2019), pp. 93-105
- [3]. Saha S. and Kaviraj A., Effects of cypermethrin on some biochemical parameters and its amelioration through dietary supplementation of ascorbic acid in freshwater catfish *Heteropneustes fossilis*, *Chemosphere*. (2009) 74, no. 9, 1254–1259, 2-s2.0-61349186334, <https://doi.org/10.1016/j.chemosphere.2008.10.056>
- [4]. Das B. K. and Mukherjee S. C., Toxicity of cypermethrin in *Labeo rohita* fingerlings: biochemical, enzymatic and haematological consequences, *Comparative Biochemistry and Physiology C: Toxicology and Pharmacology*. (2003) 134, no. 1, 109–121, 2-s2.0-0037235985, [https://doi.org/10.1016/S1532-0456\(02\)00219-3](https://doi.org/10.1016/S1532-0456(02)00219-3).
- [5]. Borges A., Scotti L. V., Siqueira D. R., Zanini R., Amaral F. D., Jurinitz D. F., and Wassermann G. F., Changes in hematological and serum biochemical values in jundiá *Rhamdia quelen* due to sub-lethal toxicity of cypermethrin, *Chemosphere*. (2007) 69, no.6, 920–926, 2-s2.0-34548625966, <https://doi.org/10.1016/j.chemosphere.2007.05.068>.
- [6]. Jee J.-H., Masroor F., and Kang J.-C., Responses of cypermethrin-induced stress in haematological parameters of Korean rockfish, *Sebastes schlegeli* (Hilgendorf), *Aquaculture Research*. (2005) 36, no. 9, 898–905, 2-s2.0-21244454893, <https://doi.org/10.1111/j.1365-2109.2005.01299.x>.
- [7]. Firat O., Cogun H. Y., Yüzereroğlu T. A., Gök G., Firat O., Kargin F., and Kötemen Y., A comparative study of the effect of the pesticide (cypermethrin) and two metals (copper, lead) to serum biochemistry of Nile tilapia *Oreochromis niloticus*, *Fish Physiology and Biochemistry*. (2011) 37, no. 3, 657–666, <https://doi.org/10.1007/s10695-011-9466-3>.
- [8]. Loteste A., Scagnetti J., Simoniello M. F., Campana M., and Parma M. J., Hepatic enzymes activity in the fish *Prochilodus lineatus* (Valenciennes, 1836) after sublethal cypermethrin exposure, *Bulletin of Environmental Contamination and Toxicology*. (2013) 90, no. 5, 601–604, <https://doi.org/10.1007/s00128-013-0961-3>.
- [9]. Fiske, C.H. and Y. Subbarao (1925) : The colorimetric determination of phosphorus. *J. Biol. Chem.*, 375–400.
- [10]. Joseph A. Adeyemi, Christian C. Olise, Olufemi Samuel Bamidele, Busuyi K. Akinola : Effects of ultraviolet photooxidation of cypermethrin on the activities of phosphatases and digestive enzymes, and intestinal histopathology in African catfish, *Clarias gariepinus* (Burchell, 1822) First published: 15 June 2020. *Jez- A Ecological and Integrative physiology*
- [11]. Gupta, A. K., Pandey, P., & Srivastava, S. (2007). Effect of pesticides on the enzyme activity in the fish, *Channa striatus*. *Plant Archives*, 7, 749–751.
- [12]. A. Kumar , B. Sharma and R.S. Pandey , : Assessment of stress in effect to pyrethroid insecticides, Î-cyhalothrin and cypermethrin, in a freshwater fish, *Channa punctatus* (BLOCH). *Cellular and Molecular Biology*, Vol. 58 No. 1: Frontiers in biological sciences issue
- [13]. George Eni a, Oju R. Ibor a c, Andem B. Andem a, Ene E. Oku a, Azubuike
- [14]. V. Chukwuka b, Aina O. Adeogun b, Augustine Arukwe. : Biochemical and endocrine-disrupting effects in *Clarias gariepinus* exposed to the synthetic pyrethroids, cypermethrin and deltamethrin. Elsevier

Boosting DSSC Efficiency Using Conducting Polymer-Decorated Hybrid Counter Electrodes and Tio₂ Nanocrystalline Photoanode Sensitized With Bixa Orellana Dye

M.S. Dixit¹, A. P. Deshmukh², S. P. Tiwari², S. P. Yawale²

¹Department of Physics, Jagadamba Mahavidyalaya, Achalpur, 444806, Maharashtra, India

²Department of Physics and Electronics, Govt. Vidarbha institute of Science and Humanities, Amravati (An autonomous institute)-444604, Maharashtra, India

ARTICLE INFO

Article History:

Accepted : 01 Jan 2025

Published : 10 Jan 2025

Publication Issue :

Volume 12, Issue 7

January-February-2025

Page Number :

549-557

ABSTRACT

This research is to study the preparation of conducting polymer Ppy and decorated polymer Ppy/RGO, Ppy/GO composite material for uses as hybrid counter electrode in dye sensitized solar cell. It started with the synthesis of Ppy, Ppy/RGO and Ppy/GO composite and X ray characteristics has been studied, followed by the preparation of counter electrode Exaction of dye from the seeds of Bixa Orellana, preparation of photoanode, preparation of electrolyte. Using UV- vis spectrometer, optical absorption analyses are carried out for all the extracted dyes. DSSC is fabricated by assembling extracted dye sensitized photoanode and Ppy, Ppy/Go and Ppy/RGO coated counter electrode. The photovoltaic characteristics had been studied and efficiency of DSSC is calculated, results obtained for Ppy, Ppy/RGO, Ppy/GO respectively as an open circuit voltage (Voc) of 12mV, 13.2mV, 12.9mV, Short circuit current 503μA, 373μA, 135μA, Fill factor 0.298, 0.49, 0.63 and conversion efficiency 0.23, 0.31, 0.14.

Keywords: Ppy, Ppy/GO, Ppy/RGO, DSSC, natural dye.

I. INTRODUCTION

The world human population is increasing rapidly, energy consumption will expect to be increasing and whole humanity is confronted with the challenge of increasing demand. The renewable energy has the ability to achieve increasing energy demands. Also, it needs to be concentrated on control of global warming effect and shortage of energy resources. Exhaustible fossil fuel, Global warming caused by fossil fuel combustion and greenhouse effect, high economic growth requires that we have to use renewable, cost effective and environmentally friendly energy sources.^{1 2 3}

Among the different types of renewable energy resources being exploited (e.g., sunlight, wind, rain, tides, geothermal heat and biofuels, etc.), Solar energy stands out to be one of the best candidates to meet the increasing energy consumption as the energy source is readily available worldwide as a free, clean and inexhaustible resource ⁴

Among the techniques for solar energy utilization, such as solar thermal and solar chemical technologies, solar electricity has been a steadily growing and popular energy technology. Sunlight can be transformed into electricity using solar cells. Solar cells have found applications in many different fields such as in calculators, solar lamps and even on spacecraft and satellites. It is best method for generating electric power by using solar cells. Due to the growing demand for renewable energy sources, the manufacture of solar cells has advanced dramatically in recent years⁵

Existing photovoltaic solar cells have been categorized into three generation with first generation consisting of bulk crystalline silicon solar cell. The first silicon solar cell was developed by Bell Telephone Lab, USA, in 1953 with efficiency of 4.5% at that time and after further research 6% of efficiency is achieved.⁶ It consists of single junction to convert energy from photon and its efficiency close to maximum value efficiency. The incredible development of silicon based semiconductor industries such as computers and electronics causes crystalline silicon solar cell to dominate the photovoltaic market.⁷ Today most of photovoltaic world are based on some variation in silicon. Monocrystalline solar panels are made out of high-grade silicon and has highest efficiency rate typically 20-25%. Whereas polycrystalline-based solar panels is made out of lower silicon purity, so these are not quite as efficient as monocrystalline solar panel.⁸ Second generation solar cells are made up of thin films of amorphous Si, CIGS (copper Indium Gallium diselenide), CdTe and Cu₂ZnSn(SSe)₄ solar cells. Thin film solar cell is designed in such a way that they utilized and used less materials resulting in low cost manufacturing process. These solar cells are less expensive and less efficient. In addition, thin films can be packaged into flexible and lightweight structures. Depending on the technology, thin-film module proto types have reached efficiencies between 7–15%.⁹ And third generation solar cell consisting of organic photovoltaic solar cell (OPVs) and Dye sensitized solar cell(DSSC).They are designed to combine the advantages of both the first and second generation devices. Because of the low-cost materials and easy fabrication, these technologies are expected to take a significant share in the fast-growing photovoltaic areas.

Dye-sensitized solar cells (DSSCs) have garnered significant interest as third-generation solar cells due to their low production cost, minimal light requirements, and mechanical durability.^{10 11 12} The dye – sensitization technique in DSSC was first developed by Vogel and Berlin in 1873 by using silver halide in gelatin medium sensitized with dye molecule to make photo activity in visible region. ¹³ the performance of these early DSSCs was poor as compared to silicon based photovoltaic devices due to low harvesting efficiencies of these cells by a dye monolayer adsorbed onto planer semiconductor surface and efficiency is raised by coating a thick layer of dye onto the planer semiconductor surface, but yet it is limited due to low charge collection efficiency from the remote dye molecule. DSSC designed by Gratzel and O'Regan had become a breakthrough in DSSC performance in solar cell research. They introduced Ruthenium dye as sensitizer TiO₂ semiconductor nanoparticles with large surface area as a photo anode and iodine based redox couple was used as a electrolyte to achieve higher efficiency.¹⁴ Researcher are taking many efforts to enhance both efficiency and stability of solar cell in effective manner by modifying molecular structure of dye, counter electrode, electrolyte, structural, morphology of semiconductor metal oxide and conducting flexible transparent material.

In dye-sensitized solar cells (DSSCs), the counter electrode (CE) plays a crucial role by capturing electrons from the external circuit and facilitating the redox electrolytic reduction. Typically, the CE is fabricated by depositing a thin catalyst layer onto a conductive substrate. The key requirements for CE materials include

robust electrocatalytic activity, low resistivity for efficient charge transfer, and long-term stability.¹⁵ Metals like platinum (Pt), silver (Ag), and gold (Au) are highly desirable as counter electrode (CE) materials due to their excellent electrocatalytic activity for reducing redox couples in aqueous electrolytes or facilitating efficient hole transport in solid-state electrolytes.¹⁶ In the reduction process, the electrolyte is regenerated. Alternatively, a catalyst is necessary to improve the reaction kinetics in this process. The choice of catalyst depends on the specific application and material cost. While noble metals exhibit excellent performance, their degradation in a liquid electrolyte remains a valid concern due to their high cost. For a low-cost DSSC, we need to utilize a cheap and abundant material. Researchers have explored various counter electrode materials for dye-sensitized solar cells (DSSCs), including carbon-based materials^{17 18 19}, conducting polymers^{20 21 22}, and transition metal-based inorganic materials²³. These alternatives have demonstrated reliable conversion efficiencies, comparable to Pt-based counter electrodes. Graphene, an atomic planar sheet composed of hexagonally arranged sp² carbon atoms, has shown great promise as an efficient counter electrode material for dye-sensitized solar cells (DSSCs) due to its exceptional conductivity and high electrocatalytic activity.^{24 25 26 27} While bare graphene alone may not be the ideal candidate for a counter electrode in dye-sensitized solar cells (DSSCs) due to its limited active sites for the I₃/I₂ electrocatalytic reaction, researchers have made further efforts by incorporating conducting polymers such as poly(3,4-ethylenedioxythiophene)poly(styrenesulphonate) (PEDOT:PSS), polypyrrole (PPy), and polyaniline (PANI) into graphene. These composite materials offer both excellent electron conductivity and high catalytic activity, making them promising for DSSC applications.^{28 24 29 27} Polypyrrole (PPy) stands out as an excellent and fitting counter electrode material among conducting polymers. Its attractive features include affordability, environmental stability, and suitability for large-scale processing.³⁰ This study presents a in situ by oxidative polymerization technique for synthesizing polypyrrole-reduced graphene oxide (rGO@PPy) nanocomposites, which are then utilized as a substitute for platinum electrodes in dye-sensitized solar cells (DSSCs) without platinum and natural dye has been used to sensitized the photoanode, the advantages of natural dyes as photosensitizers are large absorption coefficients, high light-harvesting efficiency, no resource limitations, low cost, simple preparation techniques and no harm to the environment. This approach not only simplifies the preparation process but also paves the way for more cost-effective and accessible solar energy solutions.

II. EXPERIMENTAL PROCEDURE

2.1. The preparation of Ppy, Ppy/RGO, Ppy/GO counter electrode

To synthesized the polypyrrole by chemical polymerization method. The Polypyrrole was dried for 2 days at room temperature.^{31 32} The Ppy/RGO and Ppy/GO composite was synthesized by in situ oxidative polymerization of monomer. The Ppy/RGO and Ppy/GO composite was dried for 2 days at room temperature. The Counter electrode is composed of conducting glass substrate was coated with PPy, Ppy/RGO, PPy/GO with the help of doctor blade method and dried , and used as counter electrode.

2.2. Extraction of dye

The fresh seeds of *Bixa orellana* were rinsed in distilled water to remove dust and soluble impurities. 30g of the seeds were kept in 30mL of ethanol the beaker is covered with aluminum foil and kept it for 24 hrs. After that the seeds were filtered out and filtrate obtain was stored in a sample bottle covered with aluminium foil.³³

2.3. Preparation of TiO₂ photoanode

The photoanode is composed of conducting glass substrate was coated with titanium dioxide with the help of Doctor blade method. The coated film of TiO₂ on FTO glass was annealed for 1 h at 450 °C. After that the glass

slide is left dipped into dye for 24 hr so that the adequate adsorption of dye occur into the TiO₂ film. The electrode was then taken out of dye solution and rinsed with distilled water and ethanol, and used as photoanode for solar cell.

2.4. Assembling complete Dye sensitized solar cell

TiO₂ coated glass Slide was used as photoanode while PPy, PPY/RGO, PPy/GO coated FTO glass slide was used as counter electrode. The counter electrode was kept on working electrode and to avoid the direct contact between them, the spacer was inserted between them. The space between working and counter electrode is filled with electrolyte. To couple the electrode the binder clips on opposite sides were used.

III.RESULT AND DISCUSSION

3.1. Structural Characterization

In the XRD patterns of the synthesized composites (as shown in Figure), exhibit a broad peak around 25°. This peak can be attributed to the amorphous nature of PPy, likely resulting from scattering by the PPy chains at interplanar spacings corresponding to the (002), (002), and (200) reflection planes. The XRD patterns of the as-obtained composites are shown in Fig. PPy, PPYY/RGO spectra show a broad peak around 25° which can be attributed to the amorphous PPy due to scattering from ppy chain at interplanar spacing with the refection planes of (002), (002), and (200), respectively. Similar Xrd patter is obtained for Ppy/RGO composite and Ppy/GO composite. Further in the XRD analysis, no distinct patterns corresponding to reduced graphene oxide (RGO) and graphene oxide (GO) were observed. This suggests that polypyrrole (PPy) was effectively intercalated between the RGO and GO layers, thereby preventing their structural collapse.

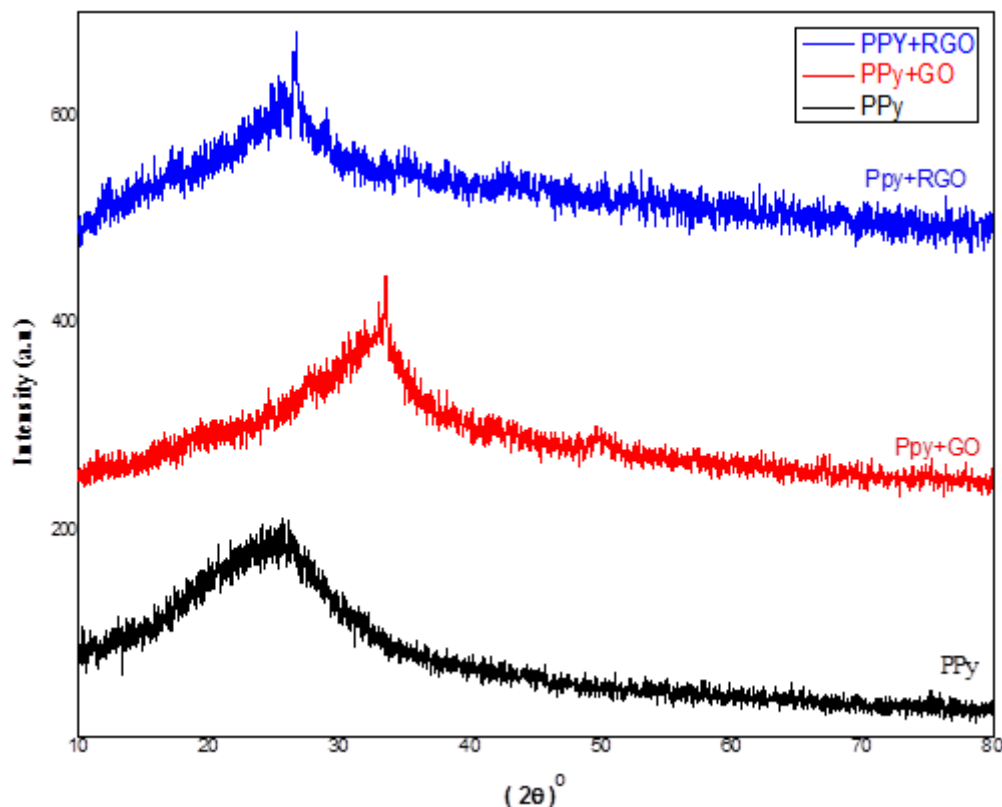


Fig 3.1: XRD patterns of Ppy, PPy/GO and PPy/RGO

3.2. Optical Characterization

The absorption spectra of colorant were recorded in range of the wavelength 400- 800nm by UV- 1800 SHIMADZU UV spectrophotometer

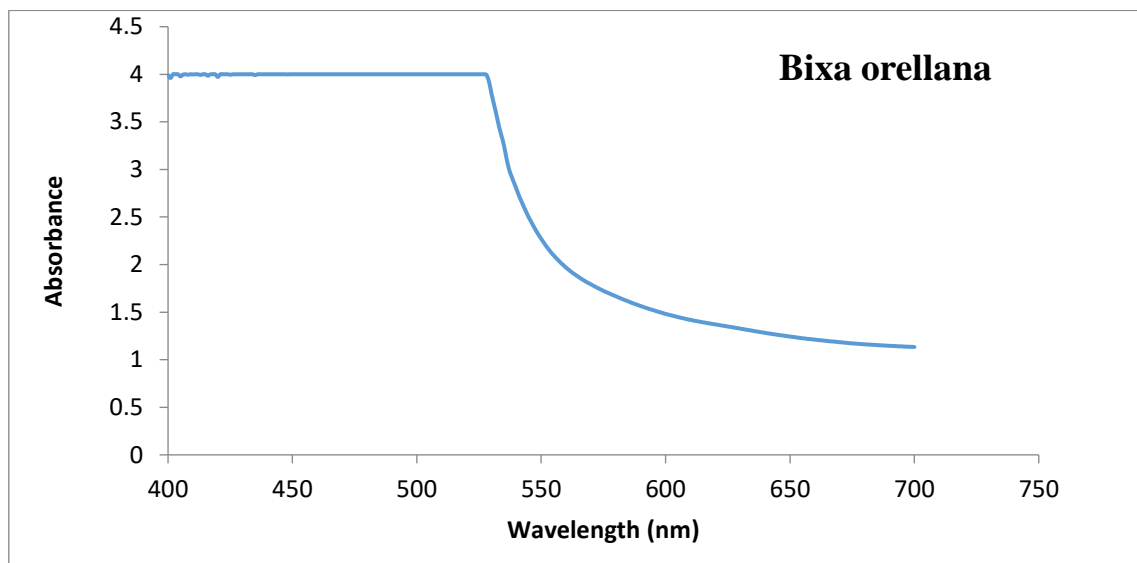


Fig3.2(i) Theabsorption Spectra for the Extract ofBixa Orellana

For *Bixa Orellana* extract the maximum absorption is in range 403 to 527 nm with almost constant absorption. The absorption peaks were due to the different types of functional groups on the Bixin pigment, Norbixin, Z-bixin or cis – bixin, Isobixin or E- bixin Geranny lgeraniolcyanidindigluconide and flavonoids.

The absorption spectrum of this colorant, exhibit absorption over 400 to 700nm range of wavelength and hence it can be considered as a good sensitizers to absorb radiation from the visible region of the electromagnetic spectrum. The optical band gap of extracted colorant was calculated using Tauc's equation. The plot of normalized absorbance square vs. energy (eV) to calculate the band gap of colorant is shown in. and the band gap dye extracted from *Bixa Orellana* is found out 2.26 ev, which is comparable to the band gap of TiO₂ energy band gap.

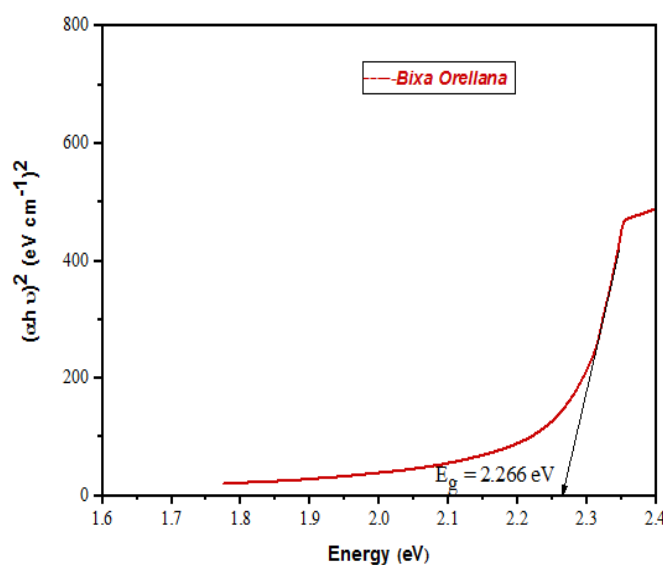


Fig 3.2 (ii) (Normalized absorption) 2 vs. energy (eV) curve of BixaOrellana

3.3. Photovoltaic performance of fabricated Dye sensitized solar cell

To study the photovoltaic performance of fabricated device, I-V characteristics are drawn. The photocurrent obtained will depend on the light intensity, the efficiency of charge injection in excited state quenching process, the degree of recombination of electrons with the oxidized dyes, and efficiency of charge transport in TiO₂ films to the counter electrodes. While maximum photovoltage obtained is depend on the energy gap between the chemical potential level of mediating redox electrolyte and conduction band level of TiO₂. Photocurrent-voltage data of TiO₂based dye-sensitized. solar cells based on natural sensitizers, iodine based electrolyte and Ppy, PPy/RGO, PPy/GO counter electrodes is measured under the illumination of 100 W/cm² over the active area of 1 cm² of photoelectrode. The photovoltaic parameters such as open circuit voltage (Voc), short-circuit photocurrent (Isc), fill factors (FF) and overall photo conversion efficiency were studied.

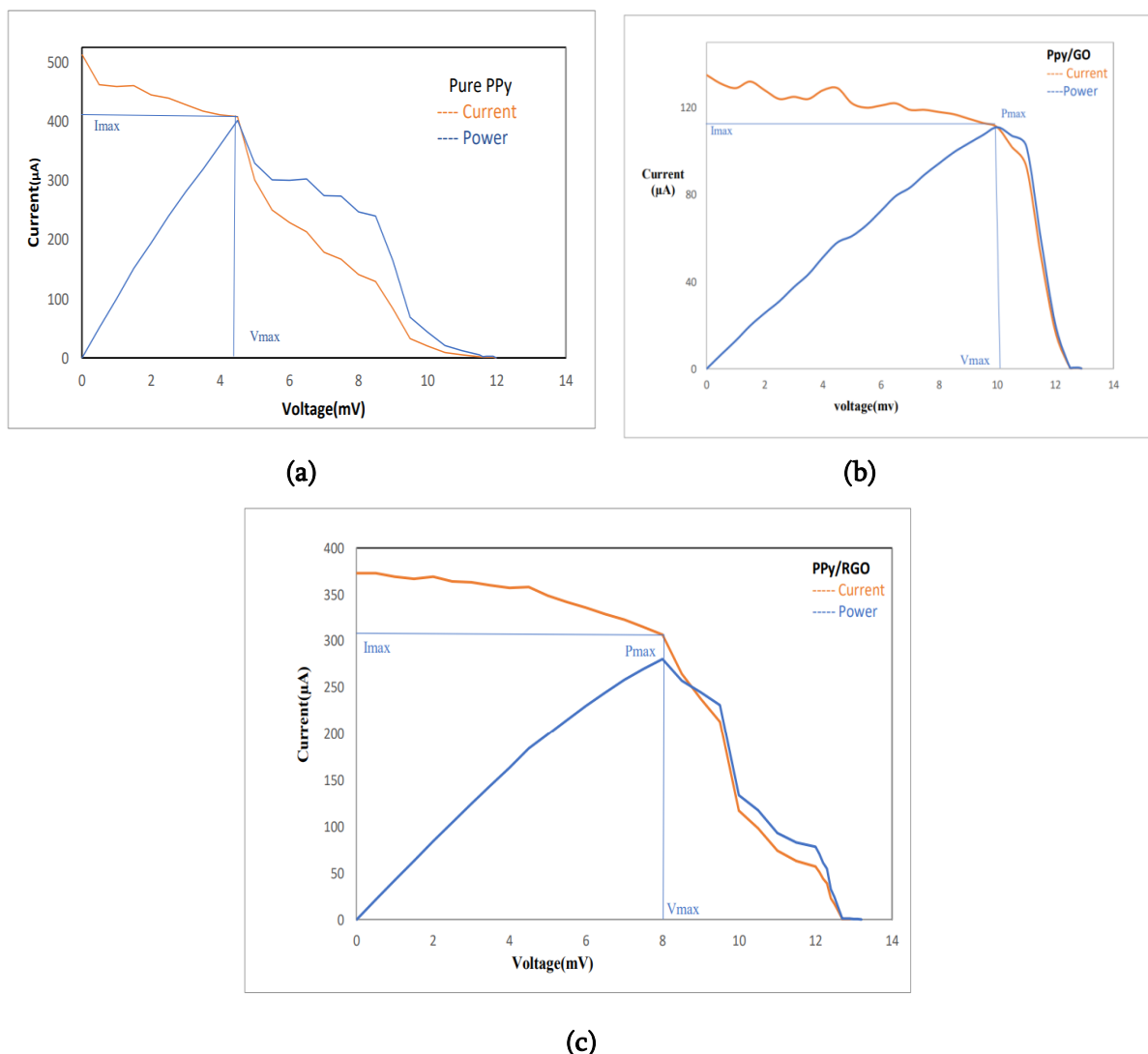


Fig 3.3 the I-V characteristic dye sensitized solar cell sensitized by Bixa Orellana sensitizers composed with counter electrode a) Pure Ppy b) Ppy/Go c) Ppy/RGO

Counter Electrode	Photoanode sensitizer	Isc (µA)	Voc (mV)	Imax (µA)	Vmax (mV)	FF	η
PPY	BixaOrellana	503	12	408	4.5	0.298	0.23
PPy/RGO		373	13.2	307	8	0.49	0.31
PPy/GO		135	12.9	111	10	0.63	0.14

IV. CONCLUSION

We have successfully fabricated DSSCs using effective counter electrode material and naturally abundant metal free photo sensitizer extracted from *Bixa Orellana*. It showed that photovoltaic parameter PCE(η) is maximum for Ppy/RGO than pure Ppy and Ppy/GO due to its superior electrical conductivity and enhanced catalytic activity. These properties contribute to better charge transfer and overall efficiency in the DSSC. For the betterment of device Further optimization of various parameter is required which is future challenge for in the field of DSSC.

V. ACKNOWLEDMENT

The Author thanks to the my advisor and colleagues who have supported for the research and I also mention my sincere thanks to all other research staff from whom I have received the assistance.

VI. REFERENCES

- [1]. Dresselhaus, M. S.; Thomas, I. L. Alternative Energy Technologies. *Nature* 2001, 414 (6861), 332–337. <https://doi.org/10.1038/35104599>.
- [2]. Witze, A. That's Oil, Folks.. *Nature* 2007, 445 (7123), 14–17.
- [3]. Wu, J.; Lan, Z.; Lin, J.; Huang, M.; Huang, Y.; Fan, L.; Luo, G. Electrolytes in Dye-Sensitized Solar Cells. *Chem. Rev.* 2015, 115 (5), 2136–2173. <https://doi.org/10.1021/cr400675m>.
- [4]. Al-Alwani, M. A. M.; Mohamad, A. B.; Ludin, N. A.; Kadhum, Abd. A. H.; Sopian, K. Dye-Sensitized Solar Cells: Development, Structure, Operation Principles, Electron Kinetics, Characterisation, Synthesis Materials and Natural Photosensitisers. *Renewable and Sustainable Energy Reviews* 2016, 65, 183–213. <https://doi.org/10.1016/j.rser.2016.06.045>.
- [5]. Hoffmann, W. PV Solar Electricity Industry: Market Growth and Perspective. *Solar Energy Materials and Solar Cells* 2006, 90 (18–19), 3285–3311. <https://doi.org/10.1016/j.solmat.2005.09.022>.
- [6]. Fukuri, N.; Saito, Y.; Kubo, W.; Senadeera, G. K. R.; Kitamura, T.; Wada, Y.; Yanagida, S. Performance Improvement of Solid-State Dye-Sensitized Solar Cells Fabricated Using Poly(3,4-Ethylenedioxythiophene) and Amphiphilic Sensitizing Dye. *J. Electrochem. Soc.* 2004, 151 (10), A1745. <https://doi.org/10.1149/1.1793711>.
- [7]. Yanagida, S.; Yu, Y.; Manseki, K. Iodine/Iodide-Free Dye-Sensitized Solar Cells. *Acc. Chem. Res.* 2009, 42 (11), 1827–1838. <https://doi.org/10.1021/ar900069p>.
- [8]. Wang, A.; Zhao, J.; Green, M. A. 24% Efficient Silicon Solar Cells. *Applied Physics Letters* 1990, 57 (6), 602–604. <https://doi.org/10.1063/1.103610>.
- [9]. Green, M. A.; Hishikawa, Y.; Warta, W.; Dunlop, E. D.; Levi, D. H.; Hohl-Ebinger, J.; Ho-Baillie, A. W. H. Solar Cell Efficiency Tables (Version 50). *Progress in Photovoltaics* 2017, 25 (7), 668–676. <https://doi.org/10.1002/pip.2909>.
- [10]. Devadiga, D.; Selvakumar, M.; Shetty, P.; Santosh, M. S. Recent Progress in Dye Sensitized Solar Cell Materials and Photo-Supercapacitors: A Review. *Journal of Power Sources* 2021, 493, 229698. <https://doi.org/10.1016/j.jpowsour.2021.229698>.
- [11]. Kouhnavard, M.; Ikeda, S.; Ludin, N. A.; Ahmad Khairudin, N. B.; Ghaffari, B. V.; Mat-Teridi, M. A.; Ibrahim, M. A.; Sepeai, S.; Sopian, K. A Review of Semiconductor Materials as Sensitizers for Quantum

- Dot-Sensitized Solar Cells. *Renewable and Sustainable Energy Reviews* 2014, 37, 397–407. <https://doi.org/10.1016/j.rser.2014.05.023>.
- [12]. Kumar, D.; Wong, K.-T. Organic Dianchor Dyes for Dye-Sensitized Solar Cells. *Materials Today Energy* 2017, 5, 243–279. <https://doi.org/10.1016/j.mtener.2017.05.007>.
- [13]. Rokesh, K.; Pandikumar, A.; Jothivenkatachalam, K. Dye Sensitized Solar Cell: A Summary. *MSF* 2013, 771, 1–24. <https://doi.org/10.4028/www.scientific.net/MSF.771.1>.
- [14]. O'Regan, B.; Grätzel, M. A Low-Cost, High-Efficiency Solar Cell Based on Dye-Sensitized Colloidal TiO₂ Films. *Nature* 1991, 353 (6346), 737–740. <https://doi.org/10.1038/353737a0>.
- [15]. Yen, Y.-S.; Chou, H.-H.; Chen, Y.-C.; Hsu, C.-Y.; Lin, J. T. Recent Developments in Molecule-Based Organic Materials for Dye-Sensitized Solar Cells. *J. Mater. Chem.* 2012, 22 (18), 8734. <https://doi.org/10.1039/c2jm30362k>.
- [16]. Wu, M.; Ma, T. Platinum-Free Catalysts as Counter Electrodes in Dye-Sensitized Solar Cells. *ChemSusChem* 2012, 5 (8), 1343–1357. <https://doi.org/10.1002/cssc.201100676>.
- [17]. Joshi, P.; Zhang, L.; Chen, Q.; Galipeau, D.; Fong, H.; Qiao, Q. Electrospun Carbon Nanofibers as Low-Cost Counter Electrode for Dye-Sensitized Solar Cells. *ACS Appl. Mater. Interfaces* 2010, 2 (12), 3572–3577. <https://doi.org/10.1021/am100742s>.
- [18]. Dong, P.; Pint, C. L.; Hainey, M.; Mirri, F.; Zhan, Y.; Zhang, J.; Pasquali, M.; Hauge, R. H.; Verduzco, R.; Jiang, M.; Lin, H.; Lou, J. Vertically Aligned Single-Walled Carbon Nanotubes as Low-Cost and High Electrocatalytic Counter Electrode for Dye-Sensitized Solar Cells. *ACS Appl. Mater. Interfaces* 2011, 3 (8), 3157–3161. <https://doi.org/10.1021/am200659y>.
- [19]. Sun, H.; Luo, Y.; Zhang, Y.; Li, D.; Yu, Z.; Li, K.; Meng, Q. In Situ Preparation of a Flexible Polyaniline/Carbon Composite Counter Electrode and Its Application in Dye-Sensitized Solar Cells. *J. Phys. Chem. C* 2010, 114 (26), 11673–11679. <https://doi.org/10.1021/jp1030015>.
- [20]. Veerappan, G.; Bojan, K.; Rhee, S.-W. Sub-Micrometer-Sized Graphite As a Conducting and Catalytic Counter Electrode for Dye-Sensitized Solar Cells. *ACS Appl. Mater. Interfaces* 2011, 3 (3), 857–862. <https://doi.org/10.1021/am101204f>.
- [21]. Li, Z.; Ye, B.; Hu, X.; Ma, X.; Zhang, X.; Deng, Y. Facile Electropolymerized-PANI as Counter Electrode for Low Cost Dye-Sensitized Solar Cell. *Electrochemistry Communications* 2009, 11 (9), 1768–1771. <https://doi.org/10.1016/j.elecom.2009.07.018>.
- [22]. Kang, D.-Y.; Lee, Y.; Cho, C.-Y.; Moon, J. H. Inverse Opal Carbons for Counter Electrode of Dye-Sensitized Solar Cells. *Langmuir* 2012, 28 (17), 7033–7038. <https://doi.org/10.1021/la300644j>.
- [23]. Wu, J.; Hao, S.; Lan, Z.; Lin, J.; Huang, M.; Huang, Y.; Li, P.; Yin, S.; Sato, T. An All-Solid-State Dye-Sensitized Solar Cell-Based Poly(N-Alkyl-4-Vinyl-Pyridine Iodide) Electrolyte with Efficiency of 5.64%. *American Chemical Society* 2008, 130 (35), 11568–11569. <https://doi.org/10.1021/ja802158q>.
- [24]. Xu, Y.; Bai, H.; Lu, G.; Li, C.; Shi, G. Flexible Graphene Films via the Filtration of Water-Soluble Noncovalent Functionalized Graphene Sheets. *J. Am. Chem. Soc.* 2008, 130 (18), 5856–5857. <https://doi.org/10.1021/ja800745y>.
- [25]. Banks, C. E.; Davies, T. J.; Wildgoose, G. G.; Compton, R. G. Electrocatalysis at Graphite and Carbon Nanotube Modified Electrodes: Edge-Plane Sites and Tube Ends Are the Reactive Sites. *Chem. Commun.* 2005, No. 7, 829. <https://doi.org/10.1039/b413177k>.
- [26]. Chen, L.; Guo, C. X.; Zhang, Q.; Lei, Y.; Xie, J.; Ee, S.; Guai, G.; Song, Q.; Li, C. M. Graphene Quantum-Dot-Doped Polypyrrole Counter Electrode for High-Performance Dye-Sensitized Solar Cells. *ACS Appl. Mater. Interfaces* 2013, 5 (6), 2047–2052. <https://doi.org/10.1021/am302938a>.

- [27]. Hong, W.; Xu, Y.; Lu, G.; Li, C.; Shi, G. Transparent Graphene/PEDOT–PSS Composite Films as Counter Electrodes of Dye-Sensitized Solar Cells. *Electrochemistry Communications* 2008, 10 (10), 1555–1558. <https://doi.org/10.1016/j.elecom.2008.08.007>.
- [28]. Lee, C.-P.; Lai, K.-Y.; Lin, C.-A.; Li, C.-T.; Ho, K.-C.; Wu, C.-I.; Lau, S.-P.; He, J.-H. A Paper-Based Electrode Using a Graphene Dot/PEDOT:PSS Composite for Flexible Solar Cells. *Nano Energy* 2017, 36, 260–267. <https://doi.org/10.1016/j.nanoen.2017.04.044>.
- [29]. Xu, J.; Wang, D.; Yuan, Y.; Wei, W.; Duan, L.; Wang, L.; Bao, H.; Xu, W. Polypyrrole/Reduced Graphene Oxide Coated Fabric Electrodes for Supercapacitor Application. *Organic Electronics* 2015, 24, 153–159. <https://doi.org/10.1016/j.orgel.2015.05.037>.
- [30]. Wu, J.; Li, Q.; Fan, L.; Lan, Z.; Li, P.; Lin, J.; Hao, S. High-Performance Polypyrrole Nanoparticles Counter Electrode for Dye-Sensitized Solar Cells. *Journal of Power Sources* 2008, 181 (1), 172–176. <https://doi.org/10.1016/j.jpowsour.2008.03.029>.
- [31]. Dixit, N. S.; Dixit, M. S.; Khobragade, S. G. Synthesis of PPy/Fluorescein Dye Composites by Simple Oxidative Polymerization Method and Its Structural Characterisation by Mass and NMR Spectroscopic Analysis.
- [32]. Pawar, M. N.; Dixit, N. S.; Khobragade, S. G.; Dixit, M. S. Structural Characterisation of Conducting PPy/Rhodamine- B Dye Composites Synthesized By Simple Chemical Polymerization Method. 2021, 8 (1).
- [33]. Ms Dixit; P.G. Khapecar; Ns Dixit; Sg Khaobragade. Study of Dye Sensitized Solar Cell Using Canna Lily Sensitizer Nanocrystalline Titanium Dioxide Photoanode. *Int. J. Sci. Res. Arch.* 2023, 8 (2), 559–564. <https://doi.org/10.30574/ijrsra.2023.8.2.0230>.

Estimation of Proximate Contents of *Andrographis paniculate* Leaves in Yavatmal District of Maharashtra, India

Anjali Sarkate¹, Rupali Biradar², Vishnudas Bhosle³, Vikas Gambhire⁴

¹Research Centre, Department of Botany, Maulana Azad College of Arts, Science and Commerce, Ch. Sambhaji Nagar, Maharashtra, India

²Department of Botany, Indraraj Arts, Commerce and Science College, Sillod Dist. Ch. Sambhaji Nagar, Maharashtra, India

³Department of Physics, Govt. Vidarbha Institute of Science and Humanities, Amravati, Maharashtra, India

⁴Department of Botany, Govt. College of Arts and Science, Ch. Sambhaji Nagar, Maharashtra, India

ARTICLE INFO

Article History:

Accepted : 01 Jan 2025

Published : 10 Jan 2025

Publication Issue :

Volume 12, Issue 7

January-February-2025

Page Number :

558-561

ABSTRACT

Andrographis paniculata a crucial medicinal herb in the Acanthaceae family, is often referred to as Kalmegh or King of Bitters. It is indigenous to Southeast Asia, which includes China, India, and Thailand. Traditional Chinese medicine and Ayurveda both make substantial use of it. It has anti-diabetic, anti-oxidant and anti-inflammatory qualities. *Andrographis paniculata* is a natural product that contains a variety of organic moieties as well as elements like potassium, calcium, riboflavin, niacin, alkaloids, flavonoids, and vitamins-A, vitamins-C, and vitamins-K. The current study examines the proximate parameters of *Andrographis paniculata* confirming its solubility in hot water, total ash value, and presence of moisture and ash content. Cold water, 1% NaOH (aq.), 1% HCl(aq.), and 1% CH₃COOH (aq.) were found quantitatively.

Keywords: *Andrographis paniculate*, Leaves, proximate analysis

I. INTRODUCTION

The majority of work over the past ten years has been done in isolation, identifying, characterizing, and evaluating compounds' pharmacological activity. A study on *A. paniculata* by listed 80 phytochemicals, including xanthenes, flavonoids, quinic acid derivatives, and diterpene lactones. The pharmacological action of about half of the compounds has not yet been disclosed. Thus, it is necessary to conduct a thorough investigation of the traditional applications, phytochemistry, and pharmacological activity of herbal products in addition to their QC/QA. By using cutting-edge analytical techniques, the current review seeks to present thorough, accurate, systematic, and genuine data on the traditional applications, phytochemicals and their pharmacological activity, and QC/QA of *A. paniculata* raw and final products. A single, hollow, hairy stem that

branches at the base allows fenugreek plants to grow up to one foot in height. The leafy green vegetable looks like clover leaves. One useful cover crop that aids in fixing nitrogen in the soil a necessary component for plant growth is fenugreek. Additionally, it is acknowledged in the domains of herbal, pharmaceutical, and chemical medicine [1–9]. Anti-inflammatory [10], anti-microbial [11], and anti-diabetic [12] qualities are possessed by fenugreek. In addition, it lowers blood pressure, increases milk production in nursing mothers, and has numerous other medical applications [13].

Our research laboratory has conducted a vast amount of work on natural products, with a focus on proximate, phytochemical, physicochemical, and spectroscopical studies on a variety of plants [9–13]. The drug's solubility affects its absorption, transmission, effects, moisture content, and ash content. Proximate analysis provides data on the sample's solubility in various solvents, moisture content, and ash content. Investigating the proximate parameters in *Andrographis paniculata* from Botoni village in Maregaon Tehsil, Yavatmal district (Maharashtra) is highly interesting in light of all these facts.

II. MATERIALS AND METHODOLOGY

All chemicals used during the research work were of A.R. grade. Freshly prepared solutions were used throughout the research work. The solvents were purified by known literature methods [14].

Sample Preparation

On July 18–20, 2022, the plants were picked from Botoni village in Maregaon Tehsil, Yavatmal district, Maharashtra State, India. To get rid of dirt and dust from the plants, they were first cleaned with tap water and then twice-distilled water. After being cut off from the stem and dried. To create a fine powder, dried leaves were crushed in a mortar and pestle. Known literature methods are employed to use this fine powder in proximate studies [15–17].

Proximate Analysis

The determination of physicochemical parameters such as moisture content, total ash value, acid-insoluble ash value, and solubility of the sample was carried out by the known literature methods [18–20]. Solubility of the sample was checked in cold water, hot water and 1% NaOH(aq), HCl(aq), CH₃COOH (aq) solution. Percentage of moisture and ash contents and acid insoluble ash are determined by using following formula,

Moisture Content = $\frac{\text{Weight of sample taken} - \text{Weight of sample after treatment}}{\text{Weight of sample taken}} \times 100$

$$\% \text{ of moisture} = \frac{\text{Loss of weight of sample}}{\text{Weight of sample taken}} \times 100$$

while, Percentage of solubility is determined by using following formula,

$$\% \text{ of Solubility} = (\text{loss of weight of sample}) / (\text{weight of sample taken}) \times 100$$

The results obtained are given in **Table No-1**

Table No-1

Sr. No	Proximate Parameters	Loss of weight of sample	Amount of sample taken (in grams)	%
1	Moisture content	0.834	1	84.9
2	Total ash content	0.074	1	7.92
3	Acid insoluble ash value	0.32	1	32.00

Sr. No	Proximate Parameters	Loss of weight of sample	Amount of sample taken (in grams)	%
4	Coldwater solubility	0.43	1	43.48
5	Hot water solubility	0.29	1	29.00
6	NaOH(aq) solubility	0.36	1	35.00
7	HCl(aq) solubility	0.38	1	38.00
8	CH ₃ COOH(aq) solubility	0.115	1	13.2

III.RESULT AND DISCUSSION

The moisture content in any part of plant gives evidence for an activity of water-soluble enzymes and coenzymes essential for the metabolic activities of that plant and it is detected from Table No.-1 that, total moisture content in leaves of was found to be 84.9% which is good for metabolic activities in the plant growth and progress of the plant. It was found that the total ash content found from dry stem pieces is 7.92 % and acid insoluble ash value is 32 % which are good and these proximate parameters of plant organs are useful for the determination of the mineral contents. Coldwater solubility and hot water solubility were found to be 43.48 % and 29% respectively; these proximate parameters will give information regarding water soluble neutral, acidic, basic and hydrocarbons present in the samples in herbal chemistry. HCl solubility and CH₃COOH solubility were found to be 38.00% and 13.2% respectively, these proximate parameters gave information regarding basic organic components present in the sample and NaOH solubility was found to be 35.00% which gave information regarding acidic organic components present in the sample.

IV.CONCLUSION

The leaves of *Andrographis paniculate* from Botoni village in Maregaon Tehsil, Yavatmal district (Maharashtra) showed good proximate parameters according to the good results of the proximate analysis. Additionally, *Andrographis paniculate* leaves Maregaon Tehsil, Yavatmal district Maharashtra have natural physicochemical, physiological, and anatomical activities that make them useful for medicinal purposes.

V. ACKNOWLEDGEMENT

Authors are thankful to Head Department and teaching and non-teaching staff of Department of Botany, Maulana Azad College of Arts, Science and Commerce, Ch. Sambhaji Nagar for their help during the research work.

VI. REFERENCES

- [1]. Lohvina, H., Sándor, M., & Wink, M. Diversity, 14(1), 7. (2021).
- [2]. Marzougui, N., Ferchichi, A., Guasmi, F., & Beji, M. Journal of Food Agriculture and Environment, 5(3/4), 248. (2007).
- [3]. Basu, T. K., & Srichamroen, A. Bioactive foods in promoting health (pp. 425-435). Academic Press. (2010).
- [4]. Visuvanathan, T., Than, L. T. L., Stanslas, J., Chew, S. Y., & Vellasamy, S. Plants, 11(11), 1450. (2022).

- [5]. Arya, P., Kumari, N., Wani, S. A., & Kumar, P. Herbs, spices and their roles in nutraceuticals and functional foods, 133-148. (2023).
- [6]. Begum, S., Ramappa, K. T., Nidoni, U., Hiregoudar, S., & Ramesh, G..International Journal of Environment and Climate Change, 13(9), 1252-1259. (2023).
- [7]. Omezzine, F., &Haouala, R. Scientia horticulturae, 160, 335-344. (2013).
- [8]. Man, S. M., Păucean, A., Călian, I. D., Mureşan, V., Chiş, M. S., Pop, A.,&Muste, S. Journal of Food Quality, (2019).
- [9]. Raji-Idowu, F ,Nigerian Journal of Microbiology. (2023).
- [10]. Malghani, N., Mahesar, S., Baig, J., Talpur, F., Sherazi, S. T. H., & Junaid, M. Journal of theTurkish Chemical Society Section A: Chemistry, 9(4), 985-998. (2022).
- [11]. Bakhtiar, Z., Hasandokht, M. R., Naghavi, M. R., &Mirjalili, M. H. Journal of Medicinal Plants, 21(82), 1-12. (2022).
- [12]. Mahmood, N. M., & Yahya, K. I. International Journal of Sciences: Basic and Applied Research, 36(3), 203-213. (2017).
- [13]. Singh, K. P., Nair, B., Jain, P. K., Naidu, A. K., &Paroha, S. RevistaColombiana de CienciasHortícolas, 7(2), 228-239. (2013).
- [14]. Pasricha, V., & Gupta, R. K. Journal of pharmacognosy and Phytochemistry, 3(4), 47-57. (2014).
- [15]. Niknam, R., Kiani, H., Mousavi, Z. E., & Mousavi, M..Biology and Applications, 189-217. (2021).

Novel Synthesis, Characterization and Biological Evaluation Copper Nanoparticles from Goat Bile Juice

Nilesh B. Jadhav^{1*}, Pawan P. Kalbende¹, Mithun S. Lunge¹, Sandip B. Chaudhari², Ramesh T. Parihar³,
Nandkishor J. Suryawanshi⁴, Dharmendra B. Dupare⁵, Mrs. M. H. Shaikh

¹Department of Chemistry, Jagadamba Mahavidyalaya, Achalpur City, Maharashtra, India

²Department of Chemistry, SPDM College, Shirpur, Maharashtra, India

³Department of Chemistry, Vidnyan Mahavidyalaya, Malakapur, Maharashtra, India

⁴Department of Industrial Chemistry, ACS College, Chikhaldara, Maharashtra, India

⁵Department of Chemistry, Dr. R.G. Rathod Arts & Sci. College, Murtizapur, Maharashtra, India

ARTICLE INFO

Article History:

Accepted : 01 Jan 2025

Published : 10 Jan 2025

Publication Issue :

Volume 12, Issue 7

January-February-2025

Page Number :

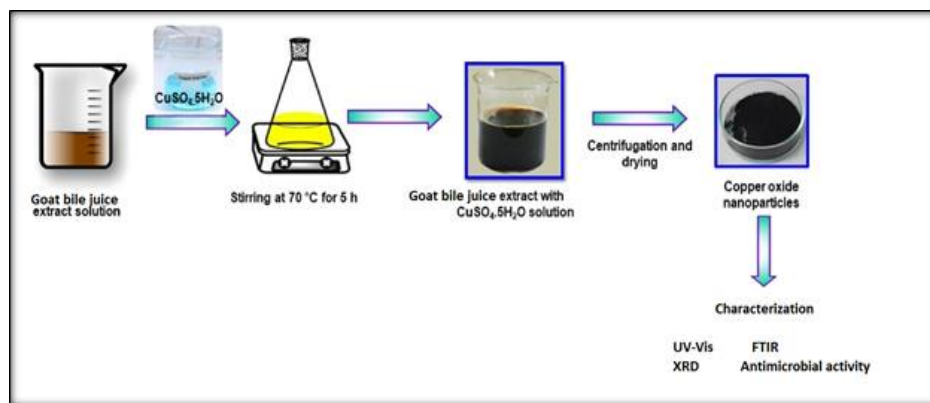
562-570

ABSTRACT

Metallic nanoparticles are receiving more and more attention because of their extensive use in a variety of scientific fields, including biotechnology, chemistry, medicine, and agriculture. Furthermore, there has been an increase in interest in ecologically sustainable ways to create nanoparticles without creating or utilizing hazardous materials and human well-being. Nanoparticle synthesis using biological techniques has been viewed as a potentially environmentally benign substitute for chemical synthesis. The current study reveals a novel ecofriendly, cost-effective, non-toxic method for the synthesis of copper nanoparticles using goat bile juice extract as a capping agent and reducing agent. The colorless mixture turned in to dark brown color and shown UV-visible spectra characteristic of copper ion. Fourier transform infrared spectroscopy (FT-IR) indicated the role of different functional groups. CuNP also characterized by X-ray diffraction method revealed the crystalline nature and the average size of copper nanoparticles was 21 nm as determined. In addition, the CuNP were evaluated for antibacterial as well as antifungal activities.

Keywords: Copper nanoparticles, antibacterial activity, Antifungal activity.

Graphical Abstract:



I. INTRODUCTION

An ultrafine or nanoparticle is a piece of material with a dimension between one and one hundred nanometers (nm) [1][2]. Nanoparticles are found in the natural world and are also produced as a result of human activity because of their submicroscopic size, they possess special material properties, and produced nanoparticles may find useful uses in a range of fields, such as environmental cleanup and medicinal engineering catalysis. Additionally, fibers and tubes less than 100 nm in only two directions or larger particles up to 500 nm in size might be referred to by this word [3]. The lowest level name for metal particles smaller than one nanometer is "atom cluster." The three particle sizes—micro particles (1–1000 μm), "fine particles" (sized between 100 and 2500 nm), and "coarse particles"—are all larger than nanoparticles. (between 2500 and 10,000 nm). This is because nanoparticles' tiny size results in incredibly unique physical or chemical characteristics, including colloidal, electric, and ultrafast optical phenomena. Unlike colloidal particles, which are generally believed to range in size from 1 to 1000 nm, they typically do not settle because they are more susceptible to Brownian motion.

Because nanoparticles have wavelengths that are much smaller than visible light (400–700 nm), standard optical microscopes are unable to view them; thus, electron or laser microscopes must be used. Because of this, nanoparticle dispersions in transparent media can likewise be transparent, although bigger particle suspensions typically scatter some or all of the light that is reflected off of them [7]. Furthermore, liquid separation necessitates the use of particular nano filtration techniques since nanoparticles are easily filtered through ordinary filters, such as ceramic candles. When compared to their bulk counterparts, nanoparticles' smaller size usually results in a lower concentration of point defects [8,9]. However, they do display a variety of dislocations that may be seen with high-resolution electron microscopes [10]. However, due to their distinct surface patterns and dislocation mechanics, nanoparticles exhibit different mechanical properties than the bulk material [11] [12] [13]. Prisms, cubes, rods, and other non-spherical nanoparticles have the characteristic known as anisotropy, which depends on size and form in both their chemical and physical makeup. [14] [15]. non-spherical gold (Au) nanoparticles because of their intriguing optical characteristics, platinum (Pt) and silver (Ag) are finding a wide range of uses. The non-spherical geometries of the nanoprisms create deeper colors and higher effective cross-sections in colloidal fluids [16]. The potential to alter the resonance wavelengths through particle tuning.

Because of its distinct physical and chemical characteristics, scientists have recently become interested in the creation of nanostructured materials. To generate particular nanoparticle sizes, matching metal salts are decreased using a variety of pharmacological, biological, and physical methods [19,46]. Biological synthesis is one of the most important modes of nanosynthesis because of its non-polluting nature, variable behavior as an electron donor, and ability to safeguard nanoparticles. The field of nanoscience has made substantial use of bio-conjugative materials, including protein, amino acids, biopolymers, carbohydrates, etc. [19, 58, 56, 13]. A copper nanoparticle is a particle with a copper basis that ranges in size from 1 to 100 nm. A copper nanoparticle can be created chemically or naturally, just like many other types of nanoparticles [21, 24]. These nanoparticles are particularly interesting since they have been used historically as colouring agents and in biological and antibacterial applications. Copper nanoparticles were first used in Mesopotamia in the ninth century to colour glass and ceramics. This was accomplished by combining copper and silver salts to make a glaze, which was then applied on clay ceramics [25]. The metal ions moved to the glaze's outer layer and were reduced to metals when the pottery was baked at high temperatures under reducing circumstances. In the end, there was a thin layer of glaze between two layers of metal nanoparticles [27]. Light would enter the completed pottery and reflect off the first layer when it was exposed to light.

A lustre effect is produced by both constructive and destructive interference when light from the first layer of nanoparticles reflects off the second layer and interferes with light from the first layer. Certain properties of copper nanoparticles are not found in commercial copper, such as catalytic and antifungal/antibacterial properties [28]. First and foremost, because of their huge catalytic surface area, copper nanoparticles exhibit exceptionally significant catalytic activity. When used as reagents in organic and organometallic synthesis, the nanoparticles tiny size and high porosity allow them to obtain a higher reaction yield and a shorter reaction time. In actuality, commercial copper only showed a 43% conversion to biphenyl when utilized in a condensation reaction with iodobenzene, whereas copper nanoparticles achieved roughly 88% conversion. Moreover, ultra-small copper nanoparticles with a high surface to volume ratio can be used as antifungal and antibacterial agents [29]. Their tight interaction with bacteria membranes and the metal ions they release into solutions cause the antimicrobial activity. When the lipid barrier is close, the cupric ions that are released from the slowly oxidizing nanoparticles in liquids might produce harmful hydroxyl free radicals. Next, the lipids in cell membranes are disassembled by free radicals via oxidation, causing the membranes to degenerate. Because of the damaged membranes, the intracellular materials leak out of the cells, making it impossible for the cells to continue basic metabolic operations. Cell death is the ultimate result of all these changes that the free radicals have generated inside the cell.

II. MATERIALS AND METHOD:

Synthesis of copper nanoparticles:

Bile induced copper nanoparticles was prepared by using goat bile juice, which was collected from (Latitude 21.248962° N Longitude 77.505379°) Sarmaspura, Achalpur, Maharashtra, India. Copper nanoparticles were prepared by chemical decrease of $\text{CuSO}_4 \cdot 5\text{H}_2\text{O}$ in deionized water. Goat bile juice was used as a reducer and stabilizer. Briefly, 3.40 g of $\text{CuSO}_4 \cdot 5\text{H}_2\text{O}$ and 15 ml of goat bile juice were dissolved separately in 100 mL of deionized water. $\text{CuSO}_4 \cdot 5\text{H}_2\text{O}$ aqueous solution was heated to 80 °C with magnetic stirring in an oil bath. CuNPs was produced by the addition of drops of goat bile juice solution into the $\text{CuSO}_4 \cdot 5\text{H}_2\text{O}$ solution while stirring. The mixture was kept at 70 °C until a dark brown solution formed (5 h). This dispersion was centrifuged at 400 rpm for 15 min.

III.RESULT AND DISCUSSION:

1 UV-Vis Spectra Characterisation

Copper nanoparticle appear red-brown in color in aqueous medium as a result of surface of plasmon vibration. In previous studies similar color change was observed. Synthesis of copper nanoparticle in sterile distilled water was confirmed by using UV-spectrophotometer in a range of wavelength from 360 to 239 nm. As Goat bile juice extract was mixed in aqueous solution of copper ion the reduction of pure copper ions to copper nanoparticles was confirmed by measuring UV-spectrum of the reaction media. The UV absorption spectrum of copper nanoparticle in the goat bile is shown in fig. The spectroscopic band of copper nanoparticle solution was found to be close to 4.000nm which confirms the synthesis of copper nanoparticle. This absorption strongly depends on the particle size, chemical surrounding, and dielectric medium.

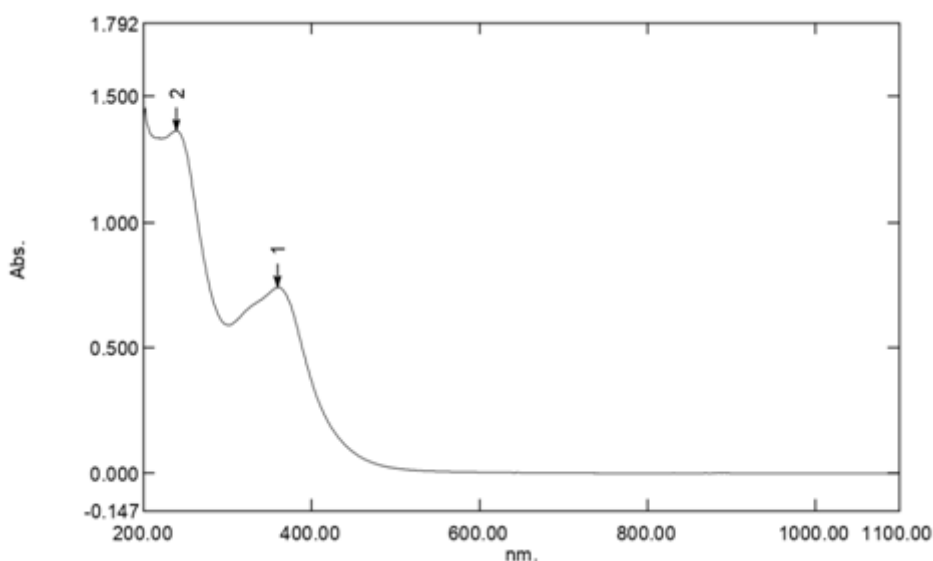


Fig 1:- The spectrophotometer result of CuNPs using *goat bile juice extract*

2 FTIR (Fourier Transforms Infrared Spectroscopy)

To investigate the functional group of Goat Bile responsible for synthesis and stabilization of copper nanoparticle, a IR study was carried out and the spectra are shown in figure. It shown a number of absorption peak, reflecting the complex nature of the extract. The absorption peak at 3306.13cm^{-1} could be due to (N-H) stretching of amides functional group. The absorption peak at 3075.63cm^{-1} could be due to ($=\text{C}-\text{N}$) Stretching of alkenes functional group. The absorption peak at 2279.96cm^{-1} could be due to ($\text{C}\equiv\text{C}$) stretching of isocynates functional group. The absorption peak at 2111.18cm^{-1} could be due to ($\text{C}\equiv\text{C}$) functional group. The absorption peak at 1652.10cm^{-1} could be due to (N-H) functional group. The absorption peak at 1532.51cm^{-1} could be due to (N-H) deformation of amide functional group. The absorption peak at 1423.53cm^{-1} could be due to ($\text{N}=\text{O}$) stretching of nitroso compound. The absorption peak at 1166.98cm^{-1} could be due to ($\text{S}=\text{O}$) stretching of sulfonic acid. The absorption peak at 664.51cm^{-1} could be due to ($\text{C}-\text{Br}$) stretching of axial (steriods). The absorption peak at 599.89cm^{-1} could be due to ($\text{C}-\text{I}$) stretching of halogen compound. The absorption peak at 513.09cm^{-1} could be due to ($\text{C}-\text{Br}$) stretching of mono bromo alkanes group. Goat bile extract are mainly involved in reduction of copper ions to copper nanoparticles. In IR spectra of synthesized copper nanoparticle

bands of absorbance around bands are matching to goat bile IR spectrum. This denotes coumarones and tannis from goat bile juice may responsible for reduction and stabilization of copper ions to copper nanoparticles.

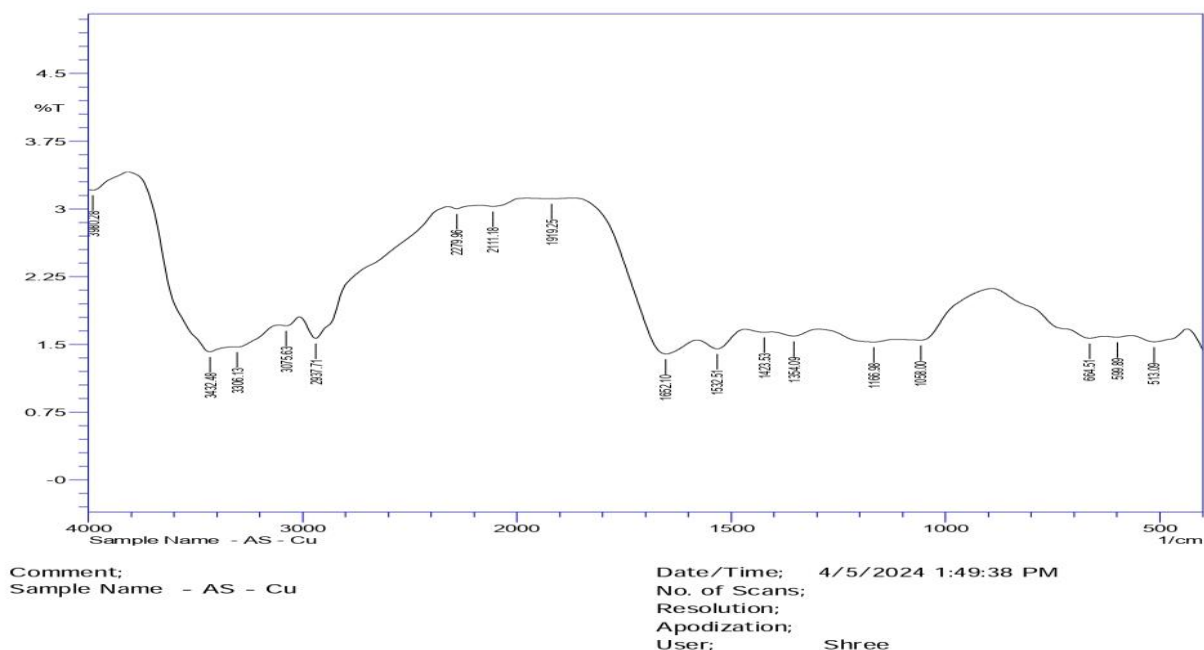


Fig 2:- FTIR spectra of copper nanoparticles with the goat bile juice extract

3 X-ray Diffraction

Analysis of structure and crystalline size of the synthesized copper nanoparticles were carried out by X-ray diffraction.

The XRD analysis of synthesized copper nanoparticles from goat bile showed diffraction peaks at $2\theta = 27.84^\circ$, 32.25° , 46.26° , 54.86° , 57.52° , 67.50° , 74.51° , 76.79° , 85.75° , 92.38° , 92.38° respectively. When compared with the standard, the obtained XRD spectrum confirmed that the synthesized copper nanoparticles were in nanocrystal form and crystalline in nature. The peaks can be assigned to the planes (111), (200), (220), (311), (222), (400), (331), (420), (422), (511), (333) facet of copper crystal, respectively. The high peaks in the XRD analysis indicated the active copper composition with the indexing in above spectra. The same result was indicates that the copper nanoparticles are face-centered, cubic and crystalline in nature (correlated to JCPDS card: number 04-0783). The Full Width at Half Maximum (FWHM) values were used to calculate the size of the nanoparticles. The average size of copper nanoparticles synthesized from goat bile was calculated using Scherrer's equation where Scherrer's constant K value = 0.94 was selected due to the cubic and crystalline nature of the nanoparticles. The average sizes of the synthesized nanoparticles from extract of goat bile juice were found to be 21 nm respectively. A few unassigned peaks observed could be due to the presence of some bioorganic compounds/protein(s) in the goat bile and crystallizes on the surface of the copper similar results in copper nanoparticles.

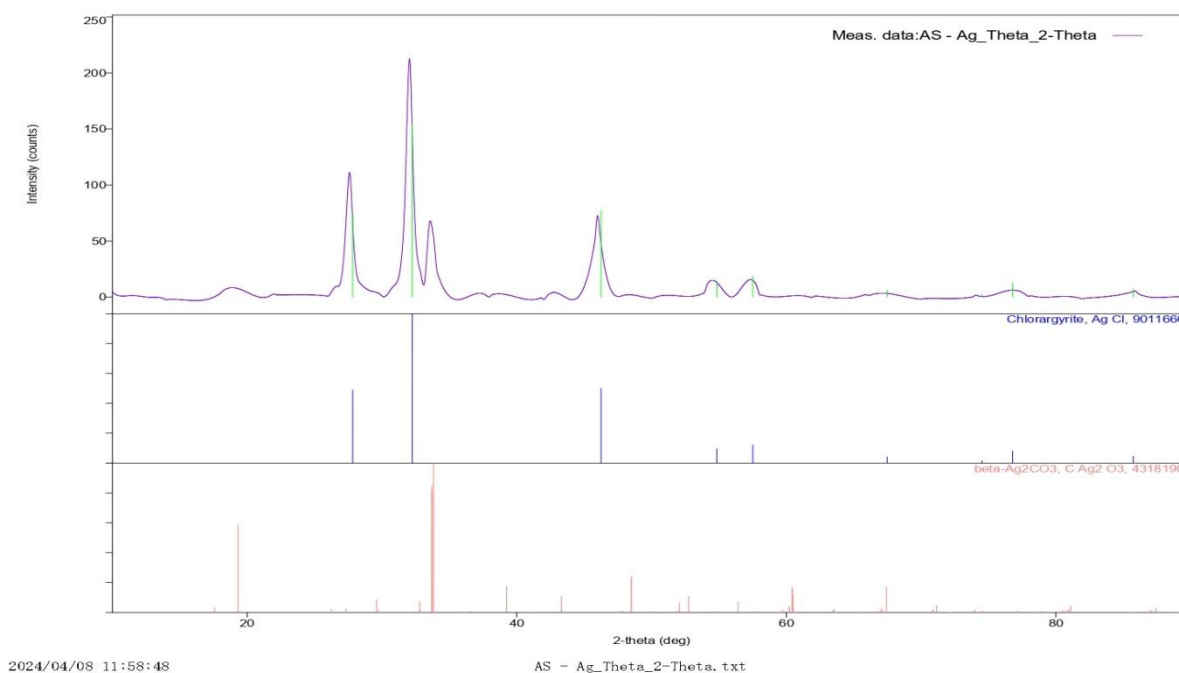


Fig 3 :- The XRD pattern of synthezied of CuNPs using *goat bile juice extract*

4. Antibacterial and Antifungal activity

The disc-diffusion test is based on the observation that, when test conditions are held constant, the size of the zone of inhibition for a particular antibiotic is inversely related to the strain's MIC (ascertained by the dilution method). Testing bacterial susceptibility to different antibiotics and chemotherapeutic agents can be done quickly and easily using discs for antimicrobial susceptibility testing. This technology is repeatable and easy to use. We use bacteria such as *Escherichia* and *Staphylococcus* to conduct the CuSO_4 antibacterial test. Within the *Staphylococcus* family of the Bacillus order, *Staphylococcus* is a genus of *gram-positive bacteria*. When viewed via a microscope, they develop in grape-like clusters and have a spherical appearance (cocci). Certain varieties of *Staphylococcus* are facultative anaerobic microbes. The genus *Escherichia* comprises rod-shaped, facultative anaerobic, *gram-negative* coliform bacteria that are typically found in the lower intestine of warm-blooded species. The majority of *E. Coli* strains are benign, but some serotypes. Such EPEC and ETEC are pathogenic and can seriously poison their hosts food supplies. They can also occasionally cause food contamination situations that lead to product recalls.

Sr.No.	Compound Code	Gram +ve bacteria	Gram -ve bacteria	Fungus
		<i>Staphylococcus aureus</i>	<i>Escherichia coli</i>	<i>Candida albicans</i>
1	CuSO_4	11mm	-----	11mm
2	Control	-----	-----	-----
3	STANDARD OFLOXACIN (2mcg) FOR BACTERIA AND FLUCONAZOLE (25mcg) FOR FUNGUS	12mm	14mm	14mm

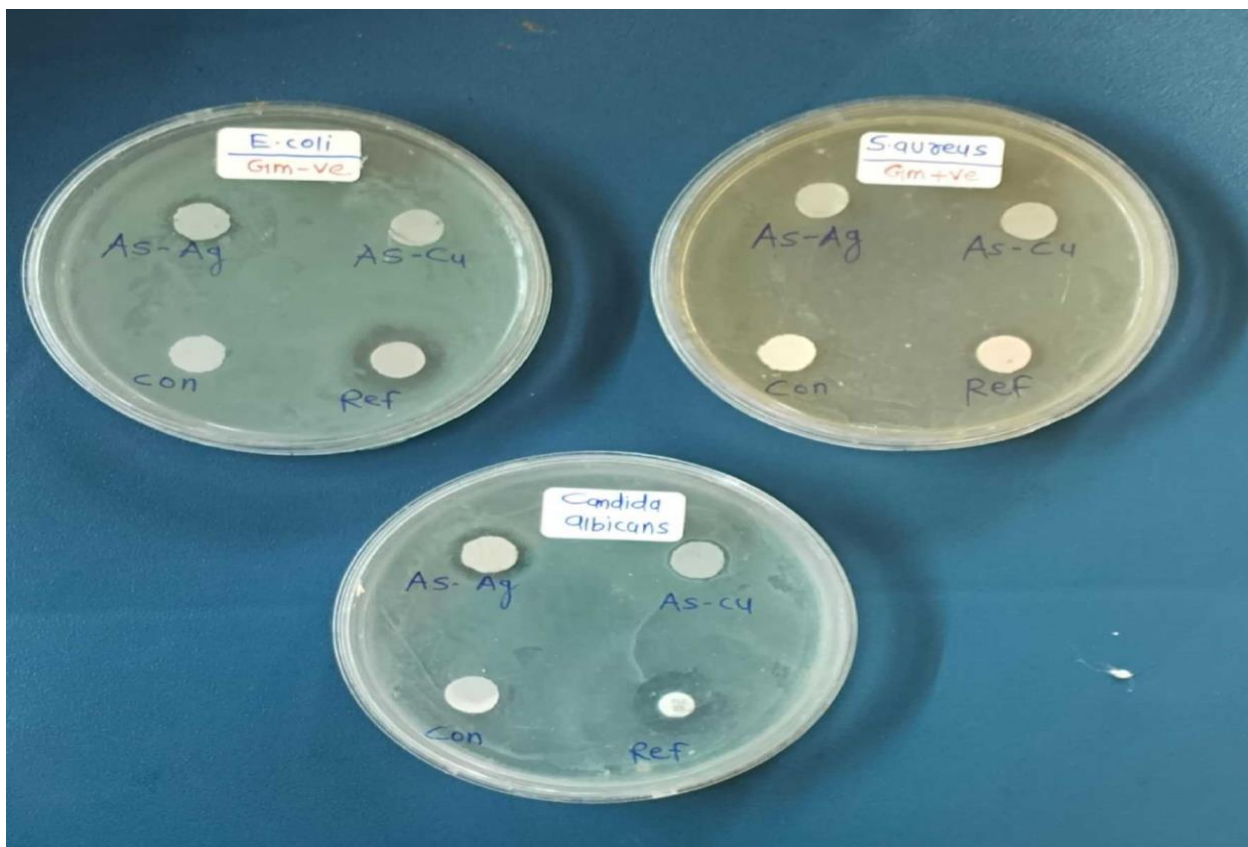


Fig 7:- Biological efficiency against gram negative, gram-positive bacteria and fungus, CuNPs nanoparticles

- A. Plate of *Escherichia coli* (Gram -ve bacteria)
- B. Plate of *Staphylococcus aureus* (Gram +ve bacteria)
- C. Plate of *Candida albicans* (Fungus)

IV. CONCLUSION:

According to the current study, BJ-CuNP were successfully prepared using goat bile juice as waste material, exhibiting spherical shape, high crystallinity, average size of 21 nm, and high stability. For nanoparticle synthesis, statistical optimization was successfully applied to minimize process parameters. It is highly effective against *Gram positive (staphylococcus aureus)* and *Gram negative bacteria (E. coli)* and *fungus (candida albicans)* respectively.

V. REFERENCES

- [1]. Abebe GM (2020) The Role of Bacterial Biofilm in Antibiotic Resistance and Food Contamination. International Journal of Microbiology 2020:e1705814. <https://doi.org/10.1155/2020/1705814>
- [2]. Azmi SNH, Al-Jassasi BMH, Al-Sawafi HMS, et al. (2021) Optimization for synthesis of silver nanoparticles through response surface methodology using leaf extract of Boswellia sacra and its application in antimicrobial activity. Environ Monit Assess 193:497 [https://doi.org/10.1007/s10661-](https://doi.org/10.1007/s10661-021-08661-0)
- [3]. Baghkheirati EK, Bagherieh-Najjar MB (2016) Modelling and optimization of Ag nanoparticle biosynthesis mediated by walnut green husk extract using response surface methodology. Materials Letters 171:166–170. <https://doi.org/10.1016/j.matlet.2016.01.159>

- [4]. Banerjee S, Vishakha K, Das S, et al. (2020) Antibacterial, anti-biofilm activity and mechanism of action of pancreatin doped zinc oxide nanoparticles against methicillin resistant *Staphylococcus aureus*. *Colloids and Surfaces B: Biointerfaces* 190:110921. <https://doi.org/10.1016/j.colsurfb.2020.110921>
- [5]. Beuers U, Trauner M, Jansen P, Poupon R (2015) New paradigms in the treatment of hepatic cholestasis: From UDCA to FXR, PXR and beyond. *Journal of Hepatology* 62:S25–S37. <https://doi.org/10.1016/j.jhep.2015.02.023>
- [6]. Bruna T, Maldonado-Bravo F, Jara P, Caro N (2021) Silver Nanoparticles and Their Antibacterial Applications. *IJMS* 22:7202. <https://doi.org/10.3390/ijms22137202>
- [7]. Dankovich TA, Gray DG (2011) Bactericidal Paper Impregnated with Silver Nanoparticles for Point-of-Use Water Treatment. *Environ Sci Technol* 45:1992–1998. <https://doi.org/10.1021/es103302t>
- [8]. Das RK, Pachapur VL, Lonappan L, et al. (2017) Biological synthesis of metallic nanoparticles: plants, animals and microbial aspects. *Nanotechnol Environ Eng* 2:18. <https://doi.org/10.1007/s41204-017-0029-4>
- [9]. Dong Y, Zhu H, Shen Y, et al. (2019) Antibacterial activity of silver nanoparticles of different particle size against *Vibrio Natriegens*. *PLOS ONE* 14:e0222322. <https://doi.org/10.1371/journal.pone.0222322>
- [10]. Durán N, Durán M, de Jesus MB, et al. (2016) Silver nanoparticles: A new view on mechanistic aspects on antimicrobial activity. *Nanomedicine: Nanotechnology, Biology and Medicine* 12:789–799. <https://doi.org/10.1016/j.nano.2015.11.016>
- [11]. Escárcega-González CE, Garza-Cervantes JA, Vazquez-Rodríguez A, et al. (2018) In vivo antimicrobial activity of silver nanoparticles produced via a green chemistry synthesis using *Acacia rigidula* as a reducing and capping agent. *IJN* 13:2349–2363. <https://doi.org/10.2147/IJN.S160605>
- [12]. Esmail F, Koohestani H, Abdollah-Pour H (2020) Characterization and antibacterial activity of silver nanoparticles green synthesized using *Ziziphora clinopodioides* extract. *Environmental Nanotechnology, Monitoring & Management* 14:100303. <https://doi.org/10.1016/j.enmm.2020.1003>
- [13]. Espeche Turbay MB, Rey V, Dorado RD, et al. (2021) Silver nanoparticle-protein interactions and the role of lysozyme as an antagonistic antibacterial agent. *Colloids and Surfaces B: Biointerfaces* 208:112030. <https://doi.org/10.1016/j.colsurfb.2021.112030>
- [14]. Fahey RC, Brown WC, Adams WB, Worsham MB (1978) Occurrence of glutathione in bacteria. *J Bacteriol* 133:1126–1129. <https://doi.org/10.1128/jb.133.3.1126-1129.1978>
- [15]. Feo JC, Aller AJ (2001) Speciation of mercury, methylmercury, ethylmercury and phenylmercury by Fourier transform infrared spectroscopy of whole bacterial cells. *J Anal At Spectrom* 16:146–151. <https://doi.org/10.1039/B005767N>
- [16]. Gao F, Li W, Deng J, et al. (2019) Recombinant Human Hair Keratin Nanoparticles Accelerate Dermal Wound Healing. *ACS Appl Mater Interfaces* 11:18681–18690. <https://doi.org/10.1021/acsami.9b0172>
- [17]. Garibo D, Borbón-Núñez HA, de León JND, et al. (2020) Green synthesis of silver nanoparticles using *Lysiloma acapulcensis* exhibit high-antimicrobial activity. *Sci Rep* 10:12805. <https://doi.org/10.1038/s41598-020-69606-7>
- [18]. Ghosh S, Ranebennur TK, Vasan HN (2012) Study of Antibacterial Efficacy of Hybrid Chitosan-Silver Nanoparticles for Prevention of Specific Biofilm and Water Purification. *International Journal of Carbohydrate Chemistry* 2011:e693759. <https://doi.org/10.1155/2011/693759>
- [19]. Golubeva OYu, Shamova OV, Orlov DS, et al. (2011) Synthesis and study of antimicrobial activity of bioconjugates of silver nanoparticles and endogenous antibiotics. *Glass Phys Chem* 37:78–84. <https://doi.org/10.1134/S1087659611010056>

- [20]. Gopiraman M, Deng D, Zhang K-Q, et al (2017) Utilization of Human Hair as a Synergistic Support for Ag, Au, Cu, Ni, and Ru Nanoparticles: Application in Catalysis. *Ind Eng Chem Res* 56:1926–1939. <https://doi.org/10.1021/acs.iecr.6b04209>
- [21]. Guilger-Casagrande M, Lima R de (2019) Synthesis of Silver Nanoparticles Mediated by Fungi: A Review. *Front BioengBiotechnol* 7:1-12. <https://doi.org/10.3389/fbioe.2019.00287>
- [22]. Hamouda RA, Hussein MH, Abo-elmagd RA, Bawazir SS (2019) Synthesis and biological characterization of silver nanoparticles derived from the cyanobacterium *Oscillatoria limnetica*. *Scientific Reports* 9:13071. <https://doi.org/10.1038/s41598-019-49444-y>
- [23]. Haque MdN, Kwon S, Cho D (2017) Formation and stability study of silver nano-particles in aqueous and organic medium. *Korean J Chem Eng* 34:2072–2078. <https://doi.org/10.1007/s11814-017-0096-z>
- [24]. Hebeish A, El-Rafie MH, El-Sheikh MA, El-Naggar ME (2013) Nanostructural Features of Silver Nanoparticles Powder Synthesized through Concurrent Formation of the Nanosized Particles of Both Starch and Silver. *Journal Nanotechnology* 2013:e201057. <https://doi.org/10.1155/2013/201057>
- [25]. Jang E, Jeong J, Yim J-H, et al. (2019) Improved infrared spectroscopic discrimination between gall bladder (GB) polyps and GB cancer using component-descriptive spectral features of separated phases from bile. *Analyst* 144:4826–4834. <https://doi.org/10.1039/C9AN00878K>
- [26]. Javan bakht Dalir S, Djahaniani H, Nabati F, Hekmati M (2020) Characterization and the evaluation of antimicrobial activities of silver nanoparticles biosynthesized from *Carya illinoensis* leaf extract. *Heliyon* 6:e03624. <https://doi.org/10.1016/j.heliyon.2020.e03624>
- [27]. Jiang XC, Chen WM, Chen CY, et al. (2010) Role of Temperature in the Growth of Silver Nanoparticles Through a Synergetic Reduction Approach. *Nanoscale Res Lett*. <https://doi.org/10.1007/s11671-010-9780-1>
- [28]. Jin C, Liu X, Tan L, et al. (2018) Ag/AgBr-loaded mesoporous silica for rapid sterilization and promotion of wound healing. *Biomater Sci* 6:1735–1744. <https://doi.org/10.1039/C8BM00353J>

Synthesis and Biological Study of Cu, Zn, Ag Nanoparticles from Plant Extracts of *Ehretia laevis* Roxb and *Carissa carandas*- A Review

Tejan D. Gajbhiye¹, Bhavna Khobragade¹, Subodh Bhandarkar²

¹RDIK & NKD College Badnera, Amravati, Maharashtra, India

²GVISH Amravati, Maharashtra, India

ARTICLE INFO

Article History:

Accepted : 01 Jan 2025

Published : 10 Jan 2025

Publication Issue :

Volume 12, Issue 7

January-February-2025

Page Number :

571-575

ABSTRACT

The green synthesis of metal nanoparticles (MNPs) using plant-based approaches has emerged as an eco-friendly, cost-effective, simple and sustainable alternative to conventional chemical and physical methods. This review highlights the significant role of phytochemicals in plant extracts, such as flavonoids, polyphenols, alkaloids, and terpenoids, as natural reducing and stabilizing agents in nanoparticle synthesis. These methods' simplicity, speed, cost-effectiveness, non-toxicity, fuel, energy, electronics and reduced environmental impact make them attractive for large-scale production. Furthermore, the biological applications of plant-mediated MNPs, particularly in antimicrobial, antioxidant, anticancer, antibiotic resistance, bioengineering, water purification and catalytic activities, demonstrate their immense potential across biomedical and industrial fields. The article also discusses challenges such as variability in plant metabolites, optimization of synthesis parameters, and scalability. Finally, recent advancements in nanotechnology and future perspectives on integrating plant-mediated nanoparticle synthesis into nanotechnology-driven industries are addressed, emphasizing its promise as a sustainable solution for modern applications.

Keywords: Green synthesis Metal nanoparticles (MNPs), Plant-mediated synthesis, Phytochemicals, Biological applications Antimicrobial activity Eco-friendly nanotechnology

I. INTRODUCTION

Nanotechnology as an emerging technology is one of the most active areas of research for developing materials with high efficiency and cost-effectiveness. The development of biologically-inspired experimental processes for

the syntheses of nanoparticles is evolving into an important branch of nanotechnology. NPs are capable of solving multiple problems in science and technology. Due to their antimicrobial and antiviral properties, NPs have garnered extensive attention in the medical field in recent years. Plant components such as the leaves, stem, root, and fruit have been utilized for the green synthesis of nanoparticles because they contain phytochemicals which aid in the bio-reduction of metallic ions. The early 2000s saw the beginnings of the use of nanotechnology in commercial products, although most applications are limited to the bulk use of passive nanomaterials. Examples include titanium dioxide and zinc oxide nanoparticles in sunscreen, cosmetics and some food products; silver nanoparticles in food packaging, clothing, disinfectants and household appliances such as Silver Nano; carbon nanotubes for stain-resistant textiles; and cerium oxide as a fuel catalyst. Invention of ionizable cationic lipids at the turn of the 21st century allowed subsequent development of solid lipid nanoparticles, which in the 2020s became the most successful and well-known non-viral nanoparticle drug delivery system due to their use in several mRNA vaccines during the COVID-19 pandemic.

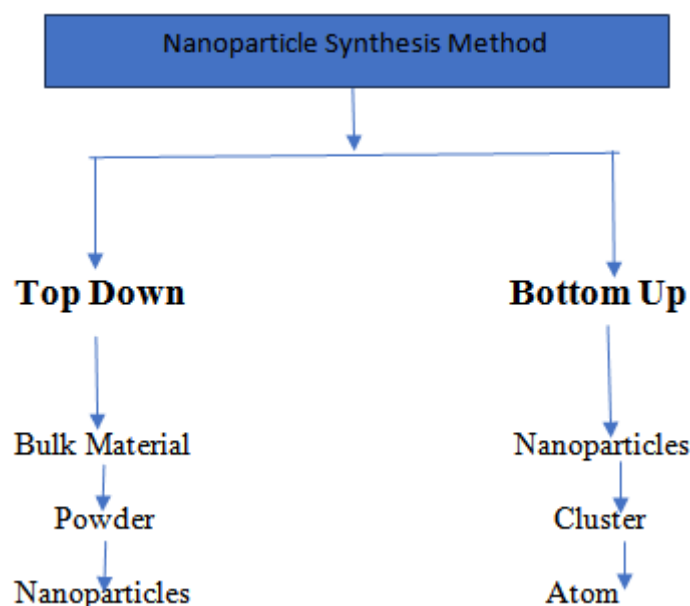
Ehretia laevis Roxb and *Carissa carandas*, has their various traditional medicinal uses and potential in nanoparticle synthesis. *Carissa carandas* is rich in iron, vitamin C, vitamins A, calcium and phosphorus. Its fruit is used in the ancient Indian herbal system of medicine, Ayurvedic, to treat acidity, indigestion, fresh and infected wounds, skin diseases, urinary disorders and diabetic ulcer, as well as stomach pain, skin conditions. Leaf decoction is used to treat fever, diarrhoea, and earache. The roots serve as a stomachic, an anthelmintic medicine for itches and also as insect repellents. *Ehretia laevis* Roxb is used for various purposes, including ornaments, potpourri, and traditional medicine. The plant's phytoconstituents, such as terpenoids, alkaloids, flavonoids, steroids, saponins, and tannins, contribute to its therapeutic properties. *Ehretia laevis* Roxb is a medicinal plant used for the treatment of diseases like syphilis, diphtheria and eczema in India.

II. NANOPARTICLE SYNTHESIS METHODS:

There are various plant-mediated synthesis methods for Cu, Zn, and Ag NPs. The synthesis of green nanoparticles is categorized into two classes, namely “**top-down**” and “**bottom-up**” based on the way of nanoparticle formation.

In the “**top-down**” approach, the dimension of nanoparticles was larger and hence a mechanical method or the additions of acids are necessary to decrease the particle size of the nanoparticles. Generally, the top-down approach requires the use of complex analysis (thermal decomposition method, mechanical method/ball-milling method, lithographic methods, laser ablation, sputtering).

The “**bottom-up**” approach was quite different from the top-down process and was commenced at the atomic level via forming molecules. The bottom-up methods are carried out using different manners (chemical vapor deposition (CVD) method, sol-gel method, spinning, pyrolysis).



III.METHODOLOGY

Preparation of Plant Extracts:

The fresh tender leaves of *Ehretia laevis* Roxb and *Carissa carandas* was collected from Maharashtra state of India. The leaves were washed with deionised water for 5 minutes and dried in shade away from direct sunlight for 20 days. The dried leaves were grounded to fine powder with the help of mixture grinder or mortal piston. 50g of the fine powder of leaf of *Ehretia laevis* Roxb and *Carissa carandas* was subjected to Soxhlet extraction using distilled water for aqueous extraction continuously for 72hrs. The obtained extract was concentrated after filtration. The extract was stored at room temperature in air tight bottles for further studies as per previously published standards.

Synthesis Process:

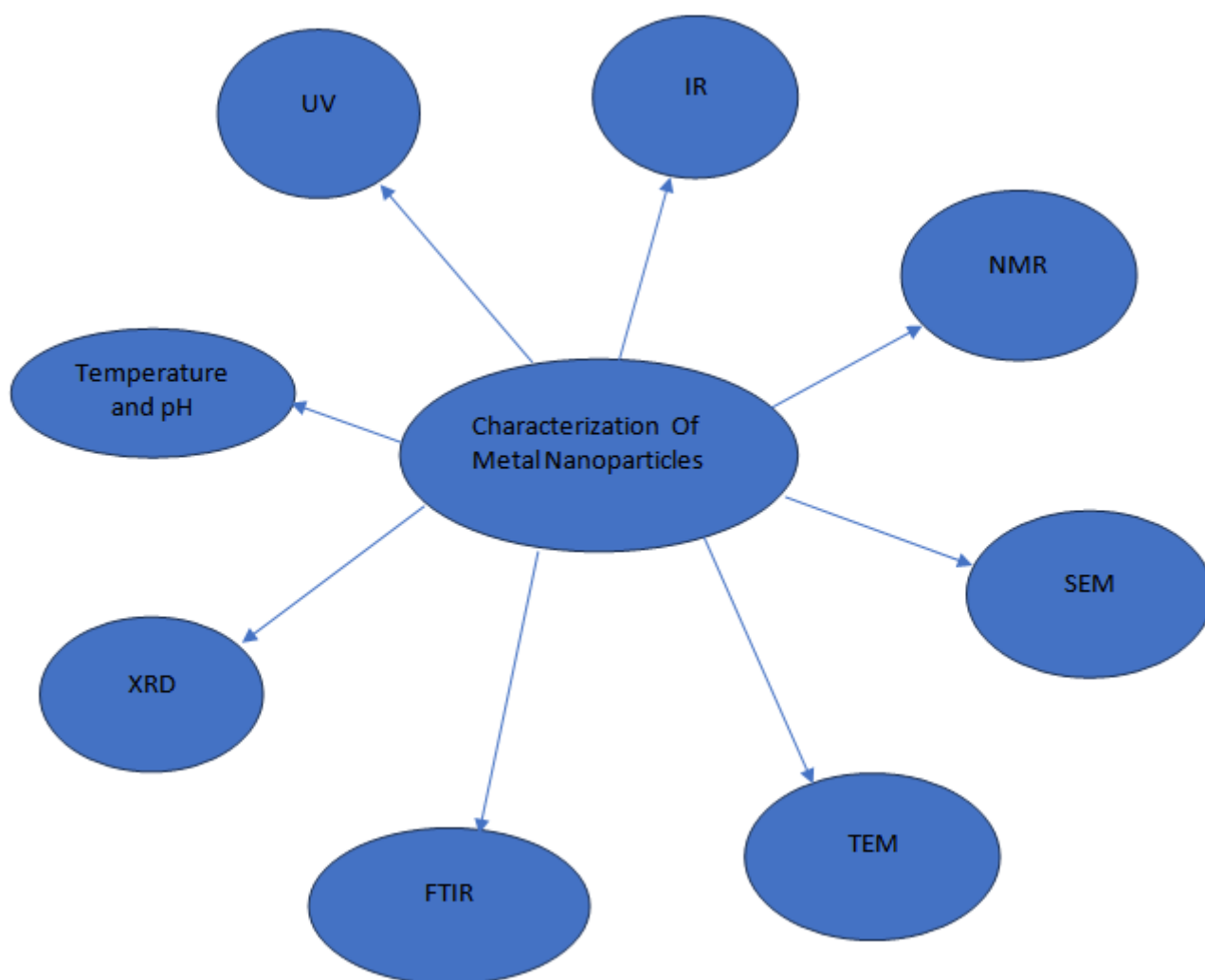
Exactly 10 ml extract of the plant leaves were added dropwise to 100 ml of aqueous solution of AgNO_3 (0.1N) with continuous stirring for 10 min followed by heating at 80 °C. By the time of 30 min reduction of Silver ions (Ag^+) to Silver nanoparticles was completed and the reaction was monitored by UV–vis spectrum. The colour of the reaction mixtures gradually changed from green to yellow, indicating the formation of silver nanoparticles. The reaction was continued for further 10 min to complete the formation of Ag-NPs.

Characterization:

Biological revival of silver ions in aqueous extract was assayed by UV–visible spectrophotometer at 420 nm at different time intervals. Afterward, the supernatant was thrown away and the sediment was dried in oven at 30°C to be kept for further use. dried powder of metal nanoparticles was assayed by X-ray diffraction (XRD) for the detection and quantitative determination of crystalline phases of synthesized nanoparticles. Size and shape of metal nanoparticles were assayed by transmission electron microscopy (TEM). For the investigation of functional groups which reduce metal ions, Fourier transform infrared (FTIR) spectroscopy was applied. FTIR technique measures infrared intensity of light to obtain an infrared spectrum of absorption or emission of a solid, liquid, or gas. It was used to detect the functional groups and their characteristic peaks present in the biosynthesized nanoparticles.

The size and structure of silver nanoparticles synthesized with *Ehretia laevis* Roxb and *Carissa carandas* aqueous leaf extract was further subjected to SEM analysis to examine the morphology of the nanoparticles. FT-IR analysis was carried out to analyze the role of the plant extract functional groups, and as a capping agent and bioreduction agent. TEM is technique is used to study the size and shape of the nanoparticles. In SEM technique, electrons are used for the formation of an output image instead of light.

Temperature is the most important factor in disturbing the dimension and form of the nanoparticles and their level of synthesis. Dissimilar types of shapes (triangle, octahedral platelets, spherical, and rod) and the dimension of the synthesis of nano particles can be tailored as a function of temperature. The pH of response plays a significant function in the structure of nanoparticles. It has been recognized that pH takes a significant function in formulating the structural morphology and size of the nanoparticles. The medium pH reaction is a major function in the formation of nanoparticles.



IV. CONCLUSION :

Nanoparticles are an effective tool in different fields such as food, agriculture, medicine, micro-wiring, electronics, and energy harvesting. The synthesis of nanoparticles uses physical, chemical, and biological methods. Green synthesis ways appear more effective and efficient compared to other related methods. The green synthesis method is an eco-friendly, non-toxic, and cost-effective method. In this review, we summarize especially information about syntheses, characterization, and methods of plant-based synthesized metal a

nanoparticles Which are utilized to analysed antibacterial, antifungal, antioxidant, anticancer, antidiabetic properties. These studies strongly recommended green synthesis approach to develop metal nanoparticles more beneficial in environmental and biological applications.

V. REFERENCES

- [1]. Mangrove-mediated synthesis of silver nanoparticles using native *Avicennia marina* plant extract from southern Iran Vahideh Abdi, Iman Sourinejad, Morteza Yousefzadi& Zahra Ghasemi
- [2]. Plant mediated synthesis of silver nanoparticles using *Punica granatum* aqueous leaf extract Manoj Kumar, Volume 6 Issue 4 - 2018 1Sukumar Dandapat,1 Rakesh Ranjan,1 Amar Kumar,2 Manoranjan Prasad Sinha
- [3]. Antimicrobial, anticoagulant and antiplatelet activities of green synthesized silver nanoparticles using *Selaginella* (Sanjeevini) plant extract S.S. Dakshayani a,1 , M.B. Marulasiddeshwara b,e,1 , M.N. Sharath Kumar c , Golla Ramesh b , P. Raghavendra Kumar b, [], S. Devaraja c, [], Rashmi Hosamani d, []
- [4]. Applications of Green Synthesized Metal Nanoparticles Seerengaraj Vijayaram1 · Hary Razafindralambo2,3 · Yun Zhang Sun1 · Seerangaraj Vasantharaj4 · Hamed Ghafarifarsani5 · Seyed Hossein Hoseinifar6 · Mahdieh Raeeszadeh7
- [5]. Green Synthesize and Characterization of Copper Nanoparticles Using Iranian Propolis Extracts Yasamin SeyyedHajizadeh,1Naser Harzandi,1Ebrahim Babapour,1Mohsen Yazdanian , 2 and Reza Ranjbar 2,
- [6]. *Gnidia glauca*- and *Plumbago zeylanica*-Mediated Synthesis of Novel Copper Nanoparticles as Promising Antidiabetic Agents Dhiraj A. Jamdade,1 Dishantsingh Rajpali,1 Komal A. Joshi,2 Rohini Kitture , 3 Anuja S. Kulkarni,4 Vaishali S. Shinde,4 Jayesh Bellare,5 Kaushik R. Babiya,6 and Sougata Ghosh 6
- [7]. Green synthesis of Copper Nanoparticles and Investigation of its Antimicrobial Properties Ifeoluwa Israel Alao1, Ifeoluwa Peter Oyekunle1*, Kingsley O. Iwuozor 2,3, Ebuka Chizitere Emenike3
- [8]. Biosynthesis of Zinc Nanoparticles of *Capparis Spinosa* Plant Extract and the it's Investigation on Morhpophysiological Properties of the *Moringa Olifera* Plant Hamideh Khajeh 1* , Bahman Fazeli-Nasab 2 , Ali Reza Mirzaei 3 , HadisehFarzanfar 4
- [9]. Green synthesis of Ag, Zn and Cu nanoparticles from aqueous extract of *Spondias mombin* leaves and evaluation of their antibacterial activity *1Adeyemi, D. K., 2Adeluola, A. O., 1Akinbile, M. J., 1 Johnson, O. O., and 1Ayoola, G. A.
- [10]. Biosynthesis of zinc oxide nanoparticles using *Mangifera indica* leaves and evaluation of their antioxidant and cytotoxic properties in lung cancer (A549) cells Authors: S. Rajeshkumar, S. Venkat Kumar, Arunachalam Ramaiah, Happy Agarwal, T. Lakshmi, Selvaraj Mohana Roopan

Photocatalytic Behavior of Synthesized and Characterized Graphene Oxide

Pravin Rathod^{*1}, Vishnudas Bhosle¹, Ashok Ubale², Zakir Khan¹

^{*1}Department of Physics and Electronics, Government Vidarbha Institute of Science and Humanities (An autonomous), Amravati, Maharashtra, India

²Departmentt of Forensic Science, Government Institute of Forensic Science, Chhatrapati Sambhajnagar, Maharashtra, India

ARTICLE INFO

Article History:

Accepted : 01 Jan 2025

Published : 10 Jan 2025

Publication Issue :

Volume 12, Issue 7

January-February-2025

Page Number :

576-580

ABSTRACT

Graphene oxide (GO) has emerged as a promising material in photocatalysis due to its unique physicochemical properties. This study explores the synthesis, structural, Optical characterization and photocatalytic behavior of graphene oxide. GO was synthesized using the modified Hummers' method and characterized through various analytical techniques, including X-ray diffraction (XRD), Fourier-transform infrared spectroscopy (FTIR), scanning electron microscopy (SEM), and UV-Vis spectroscopy. The photocatalytic activity of the synthesized GO was evaluated through the degradation of methylene blue (MB) under simulated sunlight. Results demonstrate the efficiency of GO as a photocatalyst, highlighting its potential in environmental remediation.

I. INTRODUCTION

The increasing demand for efficient and sustainable methods to mitigate environmental pollution has driven extensive research into advanced materials. Among these, graphene oxide (GO) has garnered attention for its extraordinary properties, such as a large specific surface area, high chemical stability, and excellent electron mobility [1-5]. These attributes make GO a promising candidate for photocatalytic applications, particularly in the degradation of organic pollutants [6].

The initial isolation of single-layer graphene nanosheets was achieved through the mechanical exfoliation of bulk graphite using the Scotch tape method [7]. Another notable technique is epitaxial chemical vapor deposition [8]. However, these methods are unsuitable for large-scale production, which has driven the development of scalable synthesis techniques from structurally similar compounds. Bulk synthesis is crucial for graphene's widespread industrial application, with one of the most effective approaches involving the use of strong oxidizing agents to produce graphene oxide (GO).

Graphene oxide, a hydrophilic, non-conductive carbon material, has gained significant interest due to its potential for large-scale synthesis. The earliest GO synthesis methods were pioneered by Brodie [9], Staudenmaier [10], and Hummers [11]. Among these, the modified Hummers' method is widely preferred, as it replaces potassium chlorate (KClO_3) with potassium permanganate (KMnO_4) as the oxidizing agent. This modification not only eliminates the production of toxic gases but also enhances experimental safety and reduces oxidation time.

Photocatalysis is a green technology leveraging light energy to activate a catalyst, enabling the degradation of harmful substances. The incorporation of GO in photocatalytic systems enhances electron transfer processes, reducing recombination rates of photo-generated electron-hole pairs. This study aims to investigate the synthesis, characterization, and photocatalytic efficiency of GO in degrading methylene blue (MB), a common organic dye used as a model pollutant.

II. MATERIALS AND METHODS

2.1. Synthesis of Graphene Oxide

In this investigation, a modified Hummers' method was employed to prepare graphene oxide (GO). In this method, sodium nitrate (NaNO_3) was completely omitted, and orthophosphoric acid (H_3PO_4) was introduced. Specifically, 3.0 g of graphite powder (particle size $\sim 100\ \mu\text{m}$) was added to 120 ml of a sulfuric acid (H_2SO_4) and orthophosphoric acid mixture in a 500 ml conical flask, maintaining a volume ratio of 9:1. The mixture was stirred vigorously and heated to 100°C for 2 hours. Afterward, the mixture was allowed to cool to room temperature and subsequently placed in an ice bath to maintain the temperature below 10°C . Potassium permanganate (KMnO_4 , 15.0 g) was gradually added over the course of one hour while continuously stirring to ensure homogeneity. Following this, the mixture was removed from the ice bath and placed in a warm-water bath maintained at 60°C , where it was stirred for an additional hour. After cooling back to room temperature, 250 ml of distilled water was added to the mixture. To terminate the reaction, 20 ml of hydrogen peroxide (H_2O_2) was added gradually until the color changed from reddish-brown to dark brown. The resulting mixture was left to stand overnight. The mixture was then re-dispersed in dilute hydrogen chloride (HCl) and ultrasonicated for 15 minutes. This step was repeated twice, followed by thorough washing with distilled water. Finally, the mixture was filtered and dried on a hot plate at 100°C for 4 hours in air.

2.2. Characterization Techniques

The structural study of GO nanopowder was performed by X-ray diffractometer (Model: Mini flex-II, Rigaku, Japan) with $\text{Cu K}\alpha$ radiation ($\lambda = 1.5406\ \text{\AA}$) operating at 40 kV and 30 mA. Surface morphology was studied using a Scanning Electron Microscope (SEM, Model: JEOL JSM-6360, Japan). Fourier transmission infrared (FTIR) spectra of the samples (as pellets in KBr) were recorded using FT-IR Spectrometer (Shimadzu, Japan) in the range of $4000\text{--}400\ \text{cm}^{-1}$. The optical absorption spectra were measured in the range of $300\text{--}800\ \text{nm}$ by using a UV-visible spectrometer (UV-1800 Spectrophotometer, Shimadzu, Japan).

2.3. Photocatalytic Activity Test

The photocatalytic performance of GO was evaluated through the degradation of methylene blue (MB) under simulated sunlight. A 50 mg/L MB solution was prepared, and 50 mg of GO was dispersed in 100 mL of the solution. The mixture was stirred in the dark for 30 minutes to achieve adsorption-desorption equilibrium. Subsequently, the solution was exposed to a 300 W xenon lamp. Aliquots were collected at regular intervals, and the degradation of MB was monitored using UV-Vis spectroscopy by measuring the absorbance at 664 nm.

III.RESULTS AND DISCUSSION

3.1. Structural and Morphological Analysis

XRD analysis was conducted to examine the structural properties of the synthesized GO. The XRD spectrum, presented in Figure 1, shows a prominent peak at $2\theta = 10.64^\circ$, corresponding to an interlayer spacing of 0.839 nm. The crystallite size and lattice strain were calculated to be 5.31 nm and 0.0710, respectively. The detailed structural parameters are summarized in Table 1.

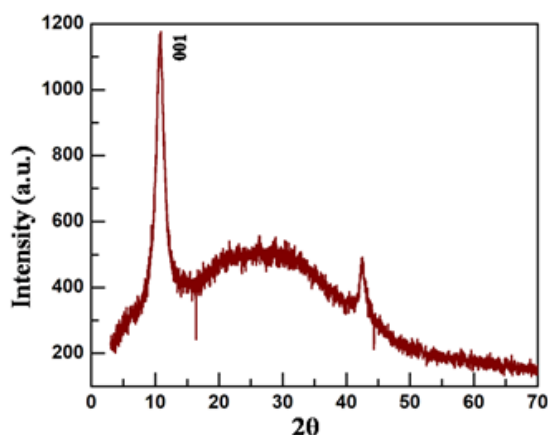


Figure 1: XRD spectrum of Graphene Oxide

2θ	Plane	FWHM (β)	Crystalline size D in nm	Dislocation in crystal δ	Lattice strain ε	Interspace distance d (nm)
10.53	(001)	1.5	5.31	0.035	0.071	0.839
42.47	(002)	1.13	7.53	0.017	0.012	0.212

3.2. Optical Analysis

The UV-Visible spectral analysis of the GO is presented in Figure 2. The UV-Visible spectrum illustrates the absorbance as a function of wavelength (λ). The GO dispersion showed an absorbance peak within the range of 300-325 nm, indicating that graphene oxide exhibits strong absorption in the visible range (323–800 nm). These results demonstrate the excellent photoresponse of the GO sheet, not only in the ultraviolet range but also in the visible range, highlighting its significant potential for light-based applications.

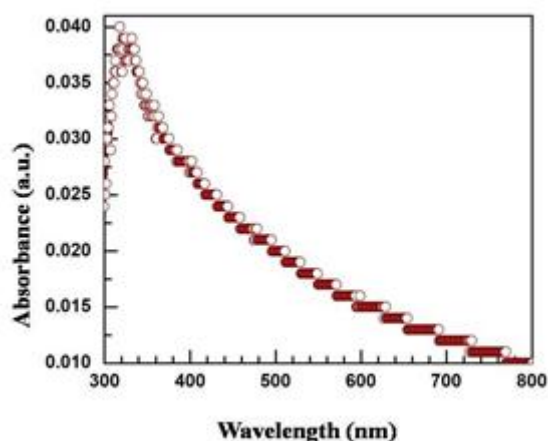


Figure 2. The UV-Visible spectrum of Graphene Oxide

3.3. FTIR Analysis

FTIR spectroscopy was carried out to analyze the structure and functional groups of the materials, as illustrated in Figure 3. The GO sheet exhibited distinct absorption bands corresponding to carboxyl (C=O) at 1733 cm^{-1} , aromatic (C=C) at 1626 cm^{-1} , epoxy (C-O) at 1238 cm^{-1} , alkoxy (C-O) at 1048 cm^{-1} , and hydroxyl (-OH) at 3333 cm^{-1} . The presence of these oxygen-containing functional groups, such as C=O and C-O, confirmed the successful oxidation of graphite into GO. Functional groups were identified using Fourier-transform infrared spectroscopy.

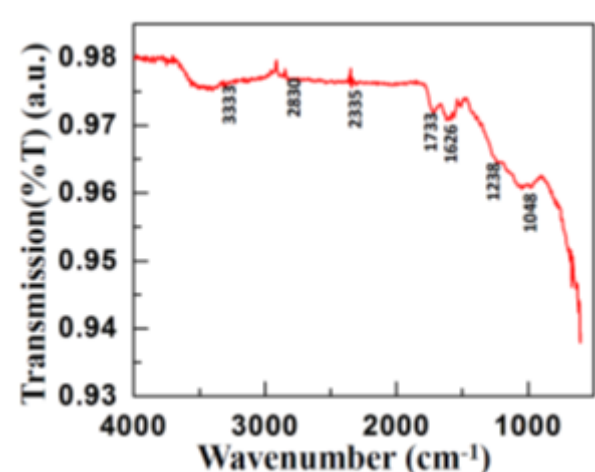


Figure 3:FTIR spectrum of Graphene Oxide

3.4. Morphological Analysis

Scanning electron microscope was employed for the detailed morphological studies as shown in figure 4. The SEM images of GO show the characteristic wrinkles and folds of GO nanosheets. This result confirmed that two dimensional nanosheets of GO can be produced from exfoliation of Graphite oxide.

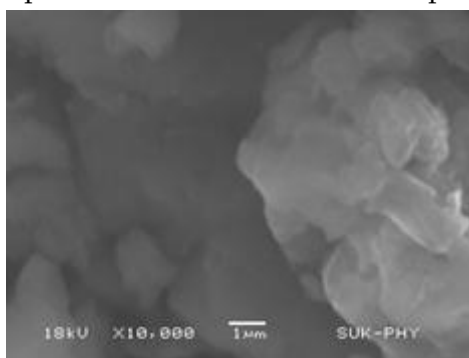


Figure 4.The SEM image of GO

3.5. Photocatalytic Degradation of Methylene Blue

The degradation efficiency of MB increased significantly in the presence of GO under simulated sunlight. After 60 minutes of irradiation, ~98% of MB was degraded. The enhanced photocatalytic activity can be attributed to GO's high surface area, which facilitates adsorption, and its ability to suppress electron-hole recombination.

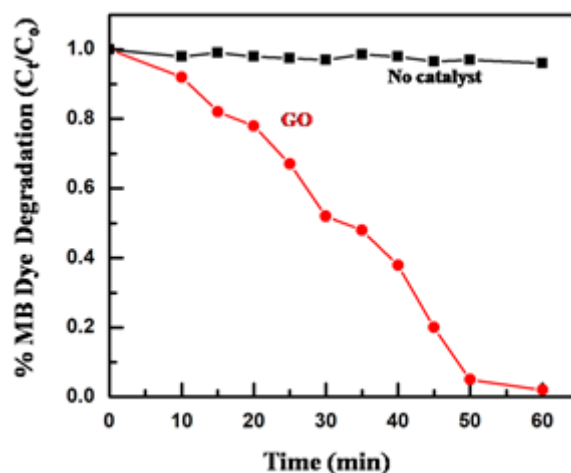


Figure 5: The percentage degradation of MB in presence of GO

IV. CONCLUSION

This study demonstrates the effective synthesis and characterization of graphene oxide using the modified Hummers' method. The photocatalytic experiments highlight GO's potential in degrading organic pollutants under simulated sunlight. These findings underscore the applicability of GO in environmental remediation, particularly for wastewater treatment. Future work may focus on enhancing GO's photocatalytic efficiency through functionalization and coupling with other semiconductor materials.

V. REFERENCES

- [1]. C. N. R. Rao, A. K. Sood, K. S. Subrahmanyam and A. Govindaraj, *Angew. Chem., Int. Ed.*, 2009, 48, 7752–7777.
- [2]. L. R. Radovic and B. Bockrath, *J. Am. Chem. Soc.*, 2005, 127, 5917–5927.
- [3]. J. T. Robinson, F. K. Perkins, E. S. Snow, Z. Q. Wei and P. E. Sheehan, *Nano Lett.*, 2008, 8, 3137–3140
- [4]. Chen, D.; Feng, H.; Li, J. Graphene oxide: preparation, functionalization, and electrochemical applications. *Chem. Rev.* 2012, 112, 6027–6053.
- [5]. Dai, L.; Xue, Y.; Qu, L.; Choi, H.-J.; Baek, J.-B. Metal-free catalysts for oxygen reduction reaction. *Chem. Rev.* 2015, 115, 4823– 4892.
- [6]. Wang, D.; Choi, D.; Li, J.; Yang, Z.; Nie, Z.; Kou, R.; Hu, D.; Wang, C.; Saraf, L. V.; Zhang, J.; Aksay, I. A.; Liu, J. Self-assembled TiO₂-graphene hybrid nanostructures for enhanced Li-ion insertion. *ACS Nano* 2009, 3, 907–914.
- [7]. Novoselov, Kostya S., Andre K. Geim, Sergei V. Morozov, De-eng Jiang, Yanshui Zhang, Sergey V. Dubonos, Irina V. Grigorieva, and Alexandr A. Firsov. "Electric field effect in atomically thin carbon films." *Science*. 306, 666-669, 2004.
- [8]. Yu, Q. K.; Lian, J.; Siriponglert, S.; Li, H.; Chen, Y. P.; Pei, S. S. "Graphene Segregated on Ni Surfaces and Transferred to Insulators." *Appl. Phys. Lett.* 93, 113103, 2008.
- [9]. B. C. Brodie. "On the atomic weight of graphite." *Philos. Trans. R. Soc. London*. 149, 249–259, 1859.
- [10]. Staudenmaier, L. "Method for the preparation of graphitic acid." *BerDtschChemGes.* 31, 1481-1487, 1898.
- [11]. S. Hummers, R. E. Offeman, *J. Am. Chem. Soc.* 1958, 80, 1339–1339.

Conductivity Analysis of $(1-x)\text{BFO} - x\text{BT}$ Ceramics Prepared by Sol Gel Method

Rajesh R.Raut*

Department of Science and Humanities Department, Sanmati Engineering College, Washim, Maharashtra, India

ARTICLE INFO

Article History:

Accepted : 01 Jan 2025

Published : 10 Jan 2025

Publication Issue :

Volume 12, Issue 7

January-February-2025

Page Number :

581-586

ABSTRACT

$(1-x)\text{BFO}-x\text{BT}$ multiferroic ceramics were prepared by using the sol - gel method. The phase structure, conductivity properties of $(1-x)\text{BFO}-x\text{BT}$ was studied. The rhombohedral perovskite structure of specimens was characterized by XRD technique. The variation of AC conductivity was studied as a function of frequency at room temperature. The spectrum showed two different regions suggesting the formation of conducting path throughout the materials. A dispersion in the AC conductivity observed with the increase in conductivity which was due to the conduction mechanism observed in ceramic assisted by the polaronic hopping between the available states. The frequency dispersion in AC conductivity due to polaronic hopping was analyzed with the Jonscher's power law.

Keywords: - Ceramic, XRD, Conductivity analysis

I. INTRODUCTION

Over the past two decades, materials with coupled functional properties have garnered significant attention due to their potential in advanced technologies. Among these, multiferroic materials, which simultaneously exhibit ferroelectricity, ferroelasticity, and ferromagnetism (or antiferromagnetism), are particularly promising for applications in magnetic data storage, sensors, and transducers [1–2]. BiFeO_3 (BFO) has emerged as one of the most widely studied multiferroic materials, demonstrating both ferroelectricity with a Curie temperature (T_C) of approximately 830°C and antiferromagnetism with a Neel temperature (T_N) around 370°C [3, 4]. As a semiconducting material, BFO forms solid solutions with BaTiO_3 (BT), an insulating material, and the addition of even small amounts of BT enhances the electrical properties of the composite. Furthermore, this combination stabilizes the perovskite structure, as both BFO and BT share the ABO_3 perovskite framework [5–7].

Given the remarkable electrical properties of both BFO and BT, their solid solution or composite forms, particularly $(1-x)\text{BFO}-x\text{BT}$, have been widely explored to improve the dielectric, piezoelectric, and multiferroic properties of pure BFO [5–7]. In addition to these electrical characteristics, the structural properties of BFO-BT solid solutions are equally fascinating. Previous studies have shown that the crystal structure of BFO-BT ceramics changes with the BFO content: for BFO content above 70 mol%, the structure is rhombohedral, below

40 mol% it becomes tetragonal, and within this range, the structure is cubic [5]. These structural variations have been linked to anomalies in dielectric and magnetic susceptibility behaviors, suggesting a close relationship between the structural changes and the resulting electrical and magnetic properties of $(1-x)\text{BFO}-x\text{BT}$ [8–10]. In this paper, we focus on the structural and conductivity properties of pure and doped $95\text{BiFeO}_3-5\text{BaTiO}_3$ (95BFO–5BT) ceramics, specifically with La and Mn doping, to investigate their potential for enhanced performance in various applications.

II. EXPERIMENTAL

Pure and doped 95BFO–5BT ceramics were synthesized by first preparing nano-crystalline BFO powder via the PVA sol–gel method explained elsewhere [11]. BaTiO_3 and BFO were mixed with lanthanum oxide and manganese nitrate to form a dopant complex, then ball milled for 24 hours. The mixture was pressed into green pellets and sintered at 870 °C for 4 hours. Structural properties were analyzed using X-ray diffraction, and conductivity was measured at room temperature with a Novocontrol dielectric spectrometer.

III. RESULTS AND DISCUSSION

3.1. Structural characterization:

The provided XRD patterns in figure 1 represent the analysis of ceramic samples with varying compositions. The X-ray diffraction (XRD) patterns of all samples correspond to a rhombohedral perovskite structure, confirmed by the prominent diffraction peaks. The consistent peak positions and intensities for all samples suggest that the fundamental crystal structure is preserved across the various doped and undoped compositions. The diffraction peaks can be indexed to the $R3c$ space group with lattice parameters $a = b = 5.5876 \text{ \AA}$ and $c = 13.8670 \text{ \AA}$, confirming the rhombohedral symmetry. The absence of additional peaks in the XRD patterns indicates that no secondary phases are present in any of the samples, even after doping with La, Mn, or both. This confirms that the dopants are well incorporated into the perovskite lattice without forming segregated impurity phases. The high solubility of the dopants within the matrix suggests a stable and homogeneous solid solution. The doping and co-doping of pure BFO–BT sample by 5% La, 5% Mn results in slight modifications in peak intensities without introducing new peaks. This implies that La ions are substituting into the lattice, likely at the A-site and Mn at the B-site, without disturbing the overall perovskite structure of the sample. All samples exhibit sharp and well-defined peaks, indicating high crystallinity. The peak widths remain narrow across the different compositions, suggesting uniform grain growth during sintering at 870 °C.

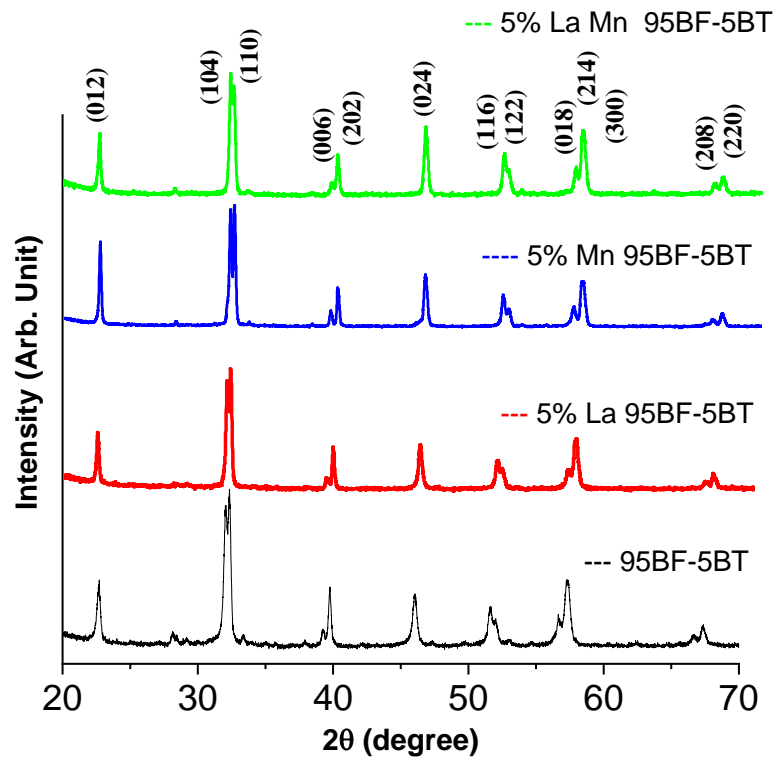


Figure 1 shows the XRD images of 95BFO-5BT, 5% La-doped 95BFO-5BT, 5% Mn-doped 95BFO-5BT, and 5% La & 5% Mn co-doped 95BFO-5BT

The intensity distribution among the peaks does not suggest any preferred orientation, as the relative intensities remain consistent with the standard perovskite R3c structure. This isotropic growth is favorable for uniform material properties.

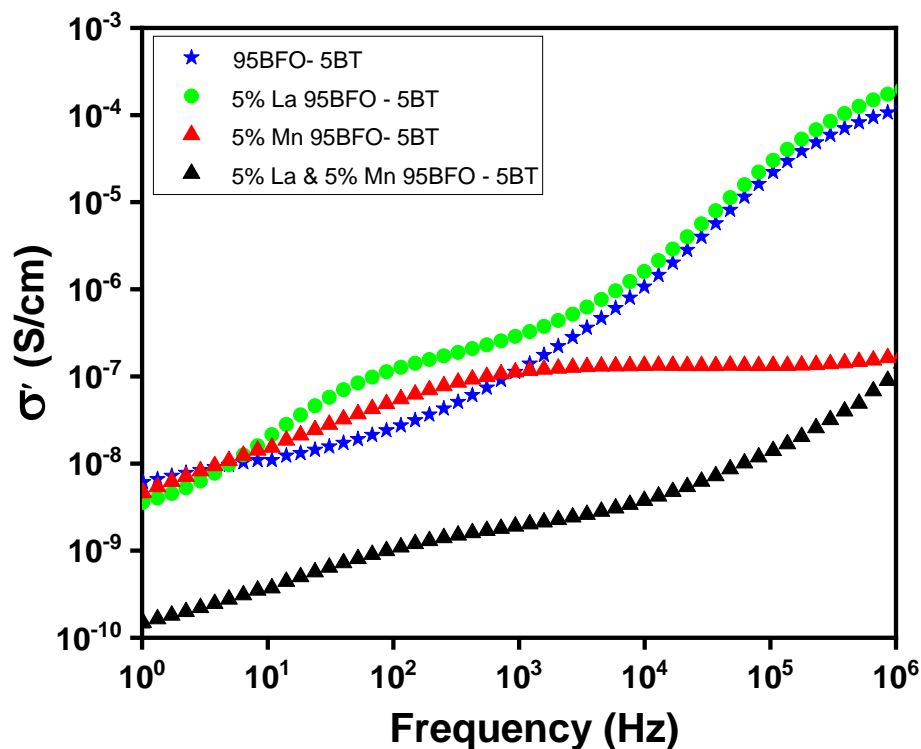


Figure 2 - variation of electrical conductivity (σ'_{ac}) as a function of frequency

3.2. Conductivity Analysis

Figure 2 depicts the variation of electrical conductivity (σ'_{ac}) as a function of frequency for pure 95BFO-5BT, 5% La-doped 95BFO-5BT, 5% Mn-doped 95BFO-5BT, and 5% La & 5% Mn co-doped 95BFO-5BT. The electrical conductivity (σ'_{ac}) versus frequency reveals critical insights into the conduction mechanisms and the impact of doping on 95BFO-5BT ceramics. The graph spans multiple orders of magnitude in frequency and captures the interplay of intrinsic material properties and external frequency perturbations. The compositions examined include pure 95BFO-5BT, 5% La-doped 95BFO-5BT, 5% Mn-doped 95BFO-5BT, and co-doped 5% La, 5% Mn 95BFO-5BT.

3.2.1 Frequency Dependence of Conductivity

The graph illustrates two distinct conductivity regimes: a low-frequency region where conductivity remains almost constant, and a high-frequency region where a sharp increase in conductivity is observed. This behavior is characteristic of many dielectric materials and reflects the distinct contributions of long-range and localized conduction mechanisms. In the low-frequency region, the conductivity plateaus for all samples, indicating intrinsic DC conductivity (σ'_{ac}). This constant value is governed by the long-range migration of charge carriers, primarily electrons or oxygen vacancies, through the bulk of the material. The flat response in this region underscores the minimal impact of grain boundaries or interfacial effects. Pure 95BFO-5BT exhibits moderate σ'_{ac} , typical of bismuth ferrite-based materials, reflecting balanced carrier density and moderate mobility. In the high-frequency region, a steep rise in conductivity occurs for most compositions, signaling the dominance of localized conduction mechanisms such as hopping and dipolar relaxation [12, 13]. This increase arises as the alternating electric field facilitates short-range charge carrier dynamics, such as hopping between defect sites or alignment of dipoles with the field.

3.2.2 Doping Effects on Conductivity

Each dopant significantly alters the conduction behavior of 95BFO-5BT, as reflected in the distinct conductivity profiles.

(i) Pure 95BFO-5BT

Pure 95BFO-5BT exhibits moderate conductivity in the low-frequency region and a pronounced rise at higher frequencies. The moderate σ'_{ac} reflects the intrinsic conduction properties of the bismuth ferrite-barium titanate composite. The sharp increase at higher frequencies is attributed to hopping conduction and dipolar relaxation [14].

(ii) La-Doped 95BFO-5BT

La doping enhances conductivity significantly across all frequencies. By substituting Bi^{3+} with La^{3+} , oxygen vacancies are introduced to maintain charge neutrality [15]. These vacancies act as mobile charge carriers, increasing carrier density and mobility. The reduced grain boundary resistance in the La-doped composition facilitates both long-range conduction in the low-frequency region and hopping conduction at higher frequencies. Consequently, La-doped 95BFO-5BT demonstrates the highest conductivity among all compositions. The steep rise at higher frequencies highlights the enhanced ability of charge carriers to respond to the alternating field.

(iii) Mn-Doped 95BFO-5BT

Mn doping suppresses conductivity, as evident from the nearly flat curve across all frequencies. Mn ions (Mn^{3+} and Mn^{4+}) introduce trap states that immobilize charge carriers, hindering both long-range and localized conduction. This results in low σ'_{ac} and minimal frequency-dependent conductivity. Furthermore, Mn doping increases grain boundary resistance and disrupts lattice symmetry, further reducing carrier mobility. The

absence of a significant rise at higher frequencies indicates the inefficacy of hopping conduction due to deep trap states.

(iv) Co-Doped 95BFO-5BT

Co-doping with La and Mn produces an intermediate conductivity profile. The La dopant enhances carrier generation and mobility, while the Mn dopant introduces trap states that counteract this effect by immobilizing carriers. The result is moderate σ'_{ac} in the low-frequency region and a less pronounced rise in the high-frequency region compared to the La-doped composition. The balanced response suggests that co-doping enables fine-tuning of electrical properties, making this composition suitable for applications requiring controlled conductivity.

3.3.3 Mechanism

The observed trends across all compositions emphasize the influence of doping on defect chemistry and charge transport mechanisms. At low frequencies, the constant conductivity is dominated by intrinsic carriers and bulk properties. In contrast, the high-frequency region highlights the role of defect states and localized dynamics, such as hopping conduction. La doping enhances conductivity by introducing oxygen vacancies and reducing grain boundary resistance, enabling long-range and short-range conduction. Mn doping suppresses conductivity through the creation of trap states, immobilizing carriers and increasing resistivity. Co-doping balances these effects, resulting in moderate conductivity and a tailored frequency response.

3.3.4 Practical Implications

The frequency-dependent conductivity of these compositions highlights their potential for diverse electronic applications. La-doped 95BFO-5BT, with its high conductivity and low impedance, is suitable for devices requiring high charge transport, such as capacitors and sensors. Mn-doped 95BFO-5BT, with its low conductivity and high resistivity, is ideal for dielectric applications or insulating layers. Co-doped 95BFO-5BT, offering a balanced performance, is promising for tunable devices and mixed-conduction applications. The table 1 summarizing the key values from the graph is given below,

Table 1 :- Yey values from the graph

Sample	DC Conductivity (σ'_{ac}) at Low Frequency (S/cm)	Conductivity (σ'_{ac}) at High Frequency (S/cm)	Transition Frequency (Hz)	Trend Observation
95BFO-5BT	1×10^{-8}	5×10^{-5}	$\sim 10^2$	Moderate conductivity; significant frequency-dependent rise.
5% La 95BFO-5BT	2×10^{-8}	1×10^{-4}	$\sim 10^2$	Enhanced conductivity across the range; strong frequency dependence.
5% Mn 95BFO-5BT	5×10^{-9}	5×10^{-9}	No noticeable transition	Flat conductivity; negligible frequency dependence.
5% La & 5% Mn 95BFO-5BT	2×10^{-9}	5×10^{-7}	$\sim 10^3$	Intermediate conductivity; delayed transition to frequency-dependent behavior.

From the observation, table it is clear that the addition of La enhances frequency-dependent conductivity, while Mn substitution results in flat conductivity with no noticeable frequency dependence. Combining La and Mn creates intermediate conductivity with a delayed transition to frequency-dependent behavior. Overall, La improves conductivity across frequencies, while Mn stabilizes it.

IV. CONCLUSION

The XRD analysis confirms that all 95BFO-5BT samples crystallize in a rhombohedral R3c structure with no secondary phases, indicating successful doping without disrupting structural integrity. The ceramics exhibit high crystallinity, compositional homogeneity, and structural stability, making them suitable for functional applications like piezoelectric and ferroelectric devices. Electrical conductivity studies show that La doping enhances conductivity by increasing carrier density and mobility, while Mn doping suppresses conduction. Co-doping balances these effects, and frequency-dependent conductivity trends reveal both long-range and localized conduction mechanisms. These findings suggest that dopant selection can optimize the electrical properties for various electronic and energy storage applications.

V. REFERENCES

- [1]. N.D. Mathur, W. Eerenstein, J.F. Scott, *Nature* 442, 759 (2006)
- [2]. M. Fiebig, *J. Phys. D Appl. Phys.* 38, R123 (2005)
- [3]. S.V. Kiselev, R.P. Ozerov, G.S. Zhdanov, *Sov. Phys. Dokl.* 7, 742 (1963)
- [4]. P. Fischer, M. Polomska, I. Sosnowska, M. Szymanski, *J. Phys. C* 13, 1931 (1980)
- [5]. M.M. Kumar, A. Srinivas, S.V. Suryanarayana, *J. Appl. Phys.* 87, 855 (2000)
- [6]. M.T. Buscaglia, L. Mitoseriu, V. Buscaglia, I. Pallecchi, M. Viviani, P. Nanni, A.S. Siri, *J. Eur. Ceram. Soc.* 26, 3027 (2006)
- [7]. R. Rai, I. Bdikin, M.A. Valente, A.L. Kholkin, *Mater. Chem. Phys.* 119, 539 (2010)
- [8]. W. Li, J. Qi, Y. Wang, L. Li, Z. Gui, *Mater. Lett.* 57, 1 (2002)
- [9]. A. Umeri, T. Kuku, N. Scuor, V. Sergo, *J. Mater. Sci.* 43, 922(2008)
- [10]. Y. Yuan, S. Zhang, W. You, *Mater. Lett.* 58, 1959 (2004)
- [11]. J. Kolte, D. Gulwade, A. Daryapurkar, P. Gopalan, *Mater. Sci. Forum* 702, 1011 (2012)
- [12]. C.R. Bowen, D.P. Almond, *Mater. Sci. Technol.* 22, 719 (2006)
- [13]. D.P. Almond, C.R. Bowen, D.A.S. Rees, *J. Phys. D Appl. Phys.* 39, 1295 (2006)
- [14]. A.K. Jonscher, *Nature* 267, 673 (1977)
- [15]. P.H. Salame, O. Prakash, A.R. Kulkarni, *J. Am. Ceram. Soc.* 96, 2184 (2013)

Exploration of Phytochemical Constituents and Antimicrobial Properties of some Medicinal plants of Jhabua District

Dr. Sunil Kumar Sikarwar¹, Kajal Dasondhi²

¹Assistant Professor, Department of Chemistry, Govt Shahid Chandrshekhar, P G College, Jhabua, Madhya Pradesh, India

²P.M.B. Gujarati Science College, Indore, Madhya Pradesh, India

ARTICLE INFO

Article History:

Accepted : 01 Jan 2025

Published : 10 Jan 2025

ABSTRACT

For thousands of years mankind has utilized plants as source materials for curing illness. Plants contain a wide range of active compounds that serve as precursors for the synthesis of important drugs proving useful in the countries and cure of various chronic and infectious diseases.

Publication Issue :

Volume 12, Issue 7

January-February-2025

Page Number :

587-591

I. INTRODUCTION

In recent years the surge in the use of traditional medicines is attributed to the escalating concerns over adverse effects and Microbial resistance associated with chemically synthesized drugs. This has generated a significant demand for plant based products due to their diverse biological activities, minimal environmental impact and safety for non target organisms.

II. LITERATURE REVIEW

Medicinal plants encompass diverse plant types utilized in herbalism or herbal medicine, involving the use of various plant parts like fruits, seeds, stems, bark, flowers, leaves, stigmas or roots. The term "herb" originated from Latin word "herba" and the old French word "herbe" initially exclusive to non-woody plants, it now includes all plant parts and non woody plants.

These plants serve purposes ranging from food and flavonoids to medicines, perfumes, spiritual activities. Historical evidence including unani manuscripts, Egyptian papyrus and Chinese writing, attracts to the extensive use of herbs for medicinal purposes throughout human history with traditions such as unani, Ayurveda and Chinese medicine systematically incorporating herbal therapies for over 4000 years across various cultures worldwide.

Madhucal longifolia (Mahua) Chandra kinetics study on mahua highlighted the significant analgesic effects of its aqueous and alcoholic extracts.

Dinesh Seshagani M. et al demonstrated that the ethanolic extract of Mahua seeds effectively reduced plasma glucose levels in rats exhibiting a hypoglycemic effect by stimulating insulin release or increasing glucose uptake.

Ramchandra D. Gaikwad et al evaluated the anti-inflammatory activity of ethanol extract and saponin mixture from Mahua seeds. Additionally, the bark's alcoholic extract demonstrated potent antioxidant properties and effectiveness against *S. aureus*.

Nimbekar T. et al investigated antibacterial activity in organic extracts of dried inner bark from Mahua.

Kumarsanjay et al have performed the phytochemical screening of Mahua leaf extract identified glycosides, terpenoids, flavonoids, alkaloids, reducing sugar and tannins, with antimicrobial and antioxidant activities.

Akshatha K. N. et al studied that alcoholic extracts of Mahua displayed diverse benefits, including wound healing, antioxidant, anti-inflammatory, antidiabetic, antimicrobial and anticancerous activities.

Simow et al studied that it has anti-ulcer activity while it is tested in the female Wistar rat. **Subramanian and Nair et al** reported that *Pedicularis murex* is an important medicinal plant which contains pedalitin, Diosmetin and Dication.

Satyavati et al studied the leaf decoction is used to control white discharge due to exercise body heat also root decoction is useful as antibilious agent.

Harborne et al reported about extracts of leaves and fruit of *Pedicularis murex* mature to contain flavonoids, alkaloids, steroids, saponins, terpenoids, glycosides and tannins using standard methods.

Kelmanson and Nair et al should the presence of deducing sugar, phenolic compounds, xanthopropin alkaloids and flavonoids in methanol extracts.

Anandalakshmi K. et al conducted research on characterizing silver nanoparticles through a green synthesis method utilizing *Pedicularis murex* leaf extract.

Patel P. et al studied the anti-ulcer effect on *Pedicularis murex* fruit extract in ethylene glycol its ethanolic extract of *Pedicularis murex* fruit possessed its significant role for prevention of renal calcification.

Vaya Rajkumar et al reported about anticancer activity of fresh juice of the leaves of *Pedicularis murex*. The ethanol extract of leaves.

Prabhakaran D. et al had studied antimicrobial activity of *Pedicularis murex* the purpose of the study was to examine the antimicrobial effect of the ethyl acetate extracts prepared from flowers of *Pedicularis murex*.

Marugananthan Sermakkani et al had explored evaluation of phytochemical and antibacterial activity of *Pedicularis murex* Linn root. This extract is known to have flavonoids, glycosides, steroids, phenols, alkaloids and tannins.

Hypothesis:- The literature review informs us that we focus to customize the characteristics of natural product available in selected extracts prepared from study materials of different medicinal plants.

Objective :- Studying extracts from medicinal plants aims to establish a bridge between traditional knowledge with modern scientific methods it reuses following objectives :-

1. To determine and identify the available phytochemical constituents in extracts.
2. To explore and optimize extraction techniques to enhance yield and potency of phytochemical.
3. To contribute to the establishment of quality control standards.
4. To investigate potential antimicrobial properties of plant extracts.
5. To characterize available bioactive compounds using standard methods.

III.METHODOLOGY

Sample collection:-The medicinal plants selected for the study were collected from the Jhabua district of Madhya Pradesh near the catchment area of the Anas River these plants were authenticated by a Botanist.

Extraction:- The plant components were cleansed, air dried in shade, and then finally grounded using a grinder. Various solvents like, aqueous, chloroform, acetone, petroleum ether, and ethanol were employed for the extraction process, employing techniques as Soxhlet extraction and maceration. (28,29)

The resulting extracts underwent filtration using standard Whatman no.1 filter paper with the filtrate subsequently evaporating at low temperature. These extracts were then refrigerated for storage and later utilized in subsequent analyses.

Isolation:- Following the concentration and desiccation of each extract in a vacuum desiccator, bioactive constituents will be isolated through thin layer chromatography (TLC). The TLC fingerprints of the extracts will serve for identification which is based on retention factor values and color spots.

Compounds will be visualized under natural daylight or 366nm UV light. Detection will utilize KOH (for glycosides), Dragendorff's reagent (for alkaloids), UV light (for flavonoids) and sulfuric acid/vanillin (for saponin and volatile oils) as detecting reagents.

Identification :- Natural products are chemical substances produced by plants are subjected for identification which involve following techniques.

1. **Extraction and Isolation:-** Suitable solvents and techniques are used to achieve this step.
2. **Chromatography:-** Methods like TLC, HPLC and GC are used for identification and compounds and its purification.
3. **Bioassays:-** MIC technique is used for biological activity to identify potential therapeutic properties.
4. **Spectroscopic**

IV.METHODS

IR, FTIR are used for determining structure and further standardization.

The plant components were cleaned, air-dried in the shade and then ground using a grinder. Various solvents such as water, chloroform – acetone, petroleum ether, and ethanol were used for the extraction process employing techniques like Soxhlet. Extracts were filtered using Whatman No. 1 filter paper and filtrate was subsequently evaporated at low temperature. These extracts were then refrigerated for storage and later used in subsequent analysis.

Detection will utilize KOH for glycosides, Dragendorff's reagent for alkaloids, UV light for flavonoids and sulphuric acid / vanillin for saponins and volatile oils as detecting agents.

The isolated compounds will undergo preliminary phytochemical screening to ensure the presence of alkaloids, carbohydrate, phytosterole, glycosides, saponins, triterpenes, phenolic compounds and flavonoids through standardized procedure. (30,31)

Standardization:- The standardization of pure bioactive compounds will be Performed using standard methods such as IR, FTIR, HPLC, GC-MS and other suitable Spectroscopic Techniques.(32,35)

Expected outcomes:- The findings from this study are poiced to contribute significantly to the understanding of the isolation, identification and standardization of natural products.

The comprehensive studies undertsken may resue as a foundation for further exploration and application.

The outcomes of this study can potentially assist others in their pursuits by offering detailed insights into the intricate processes involved in studying other natural products.

V. REFERENCES

- [1]. Kumar G.S.Tayaveera K.N. Kumar CKA, Sanjay up. Swamy BMV. Kumar DVK.(2007) Antimicrobial effects of Indian medicinal plants against acne - including bacteria top J pharm res.6:717-723,(2007)
- [2]. Berenbaum M.R. Zangerl A.R.(1996) phytochemical diversity and redundancy in ecological entrations Springer Berlin, Germany phytochemical diversity;pp1-24.
- [3]. Ahamad, A. khawA,Kumarp., BhattR., Manzoor N.(2011) Antifungal activity of coriasiane palensis essential oil by dicruptingexgosterol biosynthesis and membrane integraty against candidates yeast 28: 611-617.
- [4]. Chew Co Y.O., Blumberg J.P.(2008) in vitro activity of almond skin polyphenole for scavenging free radicals and including quinones reductase J. Agric. food chem.56:4427-4434.
- [5]. Chandra Dinesh (2001) Analgesic effect of aqueous and alcohol extract of MadhucaindicalongifoliaIndian journal of pharmacology,33:108-111.
- [6]. Seshagiri M., Gaikwad R.D., Paramjyothis. Jyothi KS and Ramchandra S.,(2007) Anti inflammatory, anticancer and hypoglycemic activities of ethanolic and crude alkaloid extract of Madhucaindica (koeing) Gmelin seed Cake Oriental pharmacy and experimental medicine,7(2):141-149.
- [7]. Gaikwad R.D. Ahmed Liyaqat M.D., khalidSaifuddin M.D., Swamyparamjyothi (2013) Antiinflammatory activity of Madhucalongifolia seeds saponin mixture pharmaceutical Biology,47(7):592-597.
- [8]. Nimbekar T.,Baisy., Katholkar P., wanjani B., and Chaudhari S.,(2012) Antibacterial activity of the dried inner bark of Madhuca Indica Bulletin of environment pharmacology and life sciences,Vol.1(2):26-29.
- [9]. Kumar Sanjay, chauhankumar Pankaj, Kumar Amit , Kumar Ajay , Patil Sandip and Sharma Pooja (2011) In vitro evaluation of phytochemical antioxidant and Antimicrobial activity of Madhuca Indica leaf extract Asian journal of Biomedical and pharmaceutical Research,Vol.1(4):175-185.
- [10]. Akshatha K.N., Murthy Mahadeva S. and lankshmidideviN.(2013) Ethnomedical uses of Madhucalongifolia: A Review International journal of life science and pharma Research,Bol.3(1):44-53.
- [11]. Simon JP. ParthasarathyM.NithyanandhanS,KatturajaRK.(2019) Namachivayam A prince SE.potective effect of the ethanolic and methanolic leaf extracts of Madhucalongifolia against diclorofenac induced toxicity in female wistar albino rats. pharmacological Reports .71(6):983-993.
- [12]. Subramanian ,S.S. and A.G.R.Nair (1972) flavonoids of the leaves of pedaliu murex phytochemistry.11:464.
- [13]. Satyavathi G.V. Ashoke K. Gupta and T. Neeraj. (2015)medicinal plants of India,vol.11, indian council of medicinal Research,New Delhi ,P:392.
- [14]. Harborne J.B.(1973) phytochemical methods A guide to modern techniques of plant analysis Chapman and Hall London.

- [15]. Kelmanson,J.E.,A.K. Jager and J van stadenzulu (2000) medicinal plants with Antibacterial activity journal of Ethanooharmacology 69:241-246.
- [16]. Anandalakshmi J, K,vebugobalJ.RamasamyV.(2015) characterization of silver nanopartocally green synthesis method using pedaliu murex leaf extract and their Antibacterial activity Appl Nano sci .6(3):399-408.
- [17]. Patel P, Vyas B (2016) Evaluation of antiurolithia effect of pedaliu murex fruit extract in ethylene glycol induced nephrolithias in rat Indian J pharm sci 78(2):231-239.
- [18]. Vaya Rajkumar, Modi Harshil, vaya Rajesh (2016) Evaluation of anticancer activity of pedaliu murex flowers Indo Amer J pharm Res.6(4):5118-5122.
- [19]. Prabhakara D. RajshkannaA,senthamilset MM.(2016) Antimicrobial activity of pedaliu murex (flowers) Indo Amer J pharm Res.6(4)5118-5122.
- [20]. MurunganathamSermakkani (2011) Evaluation of phytochemical and antibacterial activity of pedaliu murex Linn root IRJP,2(3):131-134.

Elaboration and Applications of Nanostructured Metal Oxides: Synthesis, Properties, and Prospects

V. R. Hiranwale^{1*}, R. B. Pedhekar², G. B. Harde³, V. D. Wankhade², S. P. Patil²

¹Department of Physics, Mahatma Phule Arts, Commerce & S. Chaudhari Science Mahavidyalaya, Warud, Dist. Amravati- 444906, Maharashtra, India

²Departments of Physics, M. J. Fule Commerce, Science& V. Raut Arts College Bhatkuli, Dist. Amaravti- 444602, Maharashtra, India

³Departments of Physics, Shri R R. Lahoti Science College Morshi, Dist. Amravati- 444905, Maharashtra, India

ARTICLE INFO

Article History:

Accepted : 01 Jan 2025

Published : 10 Jan 2025

Publication Issue :

Volume 12, Issue 7

January-February-2025

Page Number :

592-595

ABSTRACT

Nanostructured metal oxides exhibit unique properties due to their nanoscale dimensions and find versatile applications in catalysis, energy storage, sensing, and environmental remediation. This mini-review presents various synthesis methods of nanostructured metal oxides like sol-gel, hydrothermal, chemical vapor deposition (CVD), etc., discussing their characteristics, advantages, and limitations and highlighting the importance of the hydrothermal method because it is pivotal for precisely controlling the morphology and crystallinity of metal oxide nanostructures. This mini-review also explores applications, emphasizing how synthesis influences nanostructure design and functional properties for advancing innovative technologies.

Keywords: Metal oxide, Nanostructures, Top-down, Bottom-up, Hydrothermal method

I. INTRODUCTION

The advent of nanotechnology has revolutionized material science, enabling the manipulation of materials at the atomic and molecular levels to produce novel properties and functionalities. Metal oxides, a diverse class of materials formed by the chemical bonding between metals and oxygen, are among the most extensively researched nanomaterials due to their wide range of applications in technology and industry. Nanostructured metal oxides, defined by their dimensions within the 1-100 nm range, exhibit remarkable physical, chemical, and mechanical properties. These features are distinct from their bulk counterparts, offering significant advantages in catalysis, sensing, energy storage, and environmental remediation. The capability to tailor these properties at the nanoscale has made nanostructured metal oxides indispensable in addressing global technological and environmental challenges. [1-5].

II. SYNTHESIS METHODS

The synthesis of various nanostructures emerged from interdisciplinary studies, evolving with technological advances. Early observations on atomic behaviors led to deliberate fabrication, gaining importance from the late 20th to 21st centuries. Synthesis methods of nanostructures can be classified on their fundamental approach to fabrication. These methods can be classified into two primary categories: bottom-up and top-down approaches:

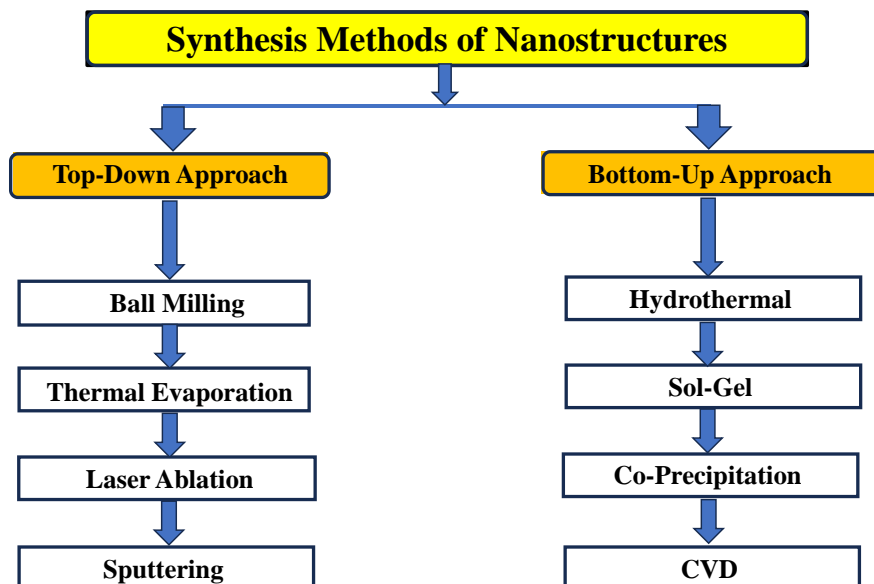


Fig. 1 Classification of synthesis methods of metal oxide nanostructures

Top-Down Approach: Top-down techniques such as ball milling, thermal evaporation, laser ablation, and sputtering provide scalability and compatibility with established industrial practices. These methods enable precise structural designs and produce materials with controlled size and morphology. However, challenges like resolution constraints and material wastage require careful optimization.

Bottom-up Approach: Bottom-up methods focus on assembling materials from the atomic level, enabling precise control over nanostructure formation. Among these, hydrothermal synthesis stands out due to its ability to produce highly crystalline and morphologically tailored materials. The sol-gel method, co-precipitation, and chemical vapor deposition also offer avenues for the scalable and cost-effective production of nanostructures with specific functionalities. [6-8].

Both bottom-up and top-down approaches in nanomaterial synthesis present distinct advantages and limitations. Bottom-up methods offer precision at the nanoscale, enabling controlled assembly of atoms or molecules to create nanostructures with unique properties, self-assembly capabilities, and monodispersity. However, challenges in scaling up, complexity, and limited structural control may hinder mass production. In contrast, top-down techniques allow for scalability, precise structural designs, and compatibility with established technologies, yet they may face resolution constraints, material wastage, and complexity in fabricating intricate 3D structures. The choice between these approaches depends on specific application needs, desired properties, scalability requirements, and cost considerations, leading to a balance between precision and scalability for optimal nanomaterial fabrication [9-10].

III. APPLICATIONS OF NANOSTRUCTURED METAL OXIDES

Nanostructured metal oxides, such as ZnO, SnO₂, and TiO₂, are extensively utilized in gas sensors. Their high surface-to-volume ratio enhances sensitivity and selectivity, enabling precise detection of gases for industrial safety and environmental monitoring. In catalysis, these materials act as efficient catalysts for chemical transformations, pollutant degradation, and wastewater treatment. Their nanoscale properties enhance reaction rates and selectivity, making them indispensable in green chemistry initiatives. Nanostructured metal oxides contribute to advancements in lithium-ion batteries, supercapacitors, and fuel cells. Their unique properties enhance energy density, stability, and charge-discharge cycles, addressing the growing demand for sustainable energy solutions.

These materials play a pivotal role in air and water purification, removing contaminants with high efficiency. Research efforts continue to refine nanostructure designs to address pressing environmental issues.[11-14].

IV. CONCLUSION AND FUTURE PROSPECTS

The field of nanostructured metal oxides has witnessed exponential growth, driven by advancements in synthesis techniques and a deeper understanding of nanoscale phenomena. While challenges such as scalability, reproducibility, and environmental impact persist, ongoing research aims to overcome these barriers, paving the way for widespread industrial adoption. Future directions include the integration of nanostructured metal oxides into multifunctional composite materials and exploring their potential in emerging areas like biomedicine and quantum computing. As the nexus between nanotechnology and application-focused research strengthens, nanostructured metal oxides are poised to play a transformative role in shaping sustainable and innovative technologies.

This review provides a thorough exploration of metal oxides and nanostructures, detailing their diverse characteristics stemming from metal-oxygen bonding. Manipulating metal oxides at the nanoscale yields unique structures, reshaping materials science with applications in catalysis, energy storage, sensing, and environmental solutions. Nanostructure dimensions, 0D to 3D, and synthesis methods, top-down and bottom-up, are discussed, with examples. The environmental impact, the influence of synthesis on properties, and ongoing research for practical applications in medicine, energy, and environmental solutions are emphasized. This review delivers a comprehensive overview of nanostructured metal oxides, spanning their properties, applications, and the evolving landscape of research in the field.

V. REFERENCES

- [1]. M. E. Franke, T. J. Koplin, U. Simon, Metal and metal oxide nanoparticles in chemiresistors: does the nanoscale matter?, *Small*. (2006) 36-50.
- [2]. L. H. Xu, D. S. Patil, J. Yang, J. Xiao, Metal oxide nanostructures: synthesis, properties, and applications, *Journal of Nanotechnology*. (2015).
- [3]. R. B. Pedhekar, F. C. Raghuwanshi, CeO₂ activated ZnO-TiO₂ thick film for CO₂ gas sensor, *International Journal of Engineering Science Invention*. (2017) 20-28.
- [4]. Sáenz-Trevizo, P. Amézaga-Madrid, P. Pizá-Ruiz, B. Monárrez-Cordero, P. G. Hernández-Salcedo, W. Antúnez-Flores, M. Miki-Yoshida, Functional nanostructured oxides: synthesis, properties, and

applications, *Emerging Applications of Nanoparticles and Architecture Nanostructures*, Elsevier.(2018) 29-69.

- [5]. Y. Patil, R. B. Pedhekar, S. Patil, F. C. Raghuwanshi, Thick film gas sensors made from Mn doped zinc oxide nanorods for H₂S gas, *Materials Today: Proceedings*. (2020) 1865-1871.
- [6]. S. Tripathy, J. Rodrigues, N. G. Shimpi, Top-down and Bottom-up Approaches for Synthesis of Nanoparticles, *Nano biomaterials: Perspectives for Medical Applications in the Diagnosis and Treatment of Diseases*. (2023) 92-130.
- [7]. V. M. Arole, S.V. Munde, Fabrication of nanomaterials by top-down and bottom-up approaches-an overview, *Journal of Material Science*.(2014) 89-93.
- [8]. A. Biswas, I. S. Bayer, A. S. Biris, T. Wang, E. Dervishi, F. Faupel, Advances in top-down and bottom-up surface nanofabrication: Techniques, applications & future prospects, *Advances in colloid and interface science*.(2012) 2-27.
- [9]. P. G. Jamkhande, N. W. Ghule, A. H. Bamer, M. G. Kalaskar, Metal nanoparticles synthesis: An overview on methods of preparation, advantages and disadvantages, and applications, *Journal of drug delivery science and technology*.(2019) 101174.
- [10]. N. Patil, R. Bhaskar, V. Vyavhare, R. Dhadge, V. Khaire, Y. Patil, Overview on methods of synthesis of nanoparticles, *International Journal of Current Pharmaceutical Research*. (2021) 11-16.
- [11]. Dar, Ghulam Nabi, Metal oxide nanostructures and their applications, *Dissertation*. (2015).
- [12]. V. E. Bochenkov, G. B. Sergeev, Sensitivity, selectivity, and stability of gas-sensitive metal-oxide nanostructures, *Metal oxide nanostructures and their applications*.(2010) 31-52.
- [13]. D. Nunes, A. Pimentel, A. Gonçalves, S. Pereira, R. Branquinho, P. Barquinha, R. Martins, Metal oxide nanostructures for sensor applications, *Semiconductor Science and Technology*.(2019) 043001.
- [14]. Z. Zheng, Synthesis and modifications of metal oxide nanostructures and their application, *Dissertation*, Queensland University of Technology, (2009).

Fabrication and Performance Evaluation of Spherical Stannic Oxide Nano Particles for H₂S, CO₂, NH₃, and LPG Detection

Swapnil S. Kosalge¹, Fulsingh C. Raghuwanshi², Digambar N. Sapkal³, Pushpinder G. Bhatia¹

¹Department of Physics, Guru Nanak College of Arts, Science and Commerce, Guru Tegh Bahadur Nagar
Mumbai-400037, Maharashtra, India

²Department of Physics, Vidya Bharti Mahavidyalaya, Amravati-444602, Maharashtra, India

³Department of Physics, SICES Degree College, Ambarnath, Mumbai-421591, Maharashtra, India

ARTICLE INFO

Article History:

Accepted : 01 Jan 2025

Published : 10 Jan 2025

Publication Issue :

Volume 12, Issue 7

January-February-2025

Page Number :

596-603

ABSTRACT

Stannic oxide spherical nanoparticles were synthesised by the co-precipitation technique. Spherical particles with diameters ranging from 7 nm to 10 nm were observed, and their sizes were calculated using XRD data, and morphological analysis was performed using a SEM and a TEM spectroscopy. The TEM image confirms the formation of spherical nanoparticles in the range of 6 to 10 nm. The elemental composition analysis was done by the EDAX technique, which confirms the formation of stannic oxide material without impurity. The sensing film required to study the electrical and gas sensing properties of stannic oxide particles was prepared by the screen-printing technique. The conductivity behaviour was observed in the range of 50 °C to 300 °C. The sensing behaviour of the sensing element was studied in the range of 50°C to 300°C for reducing gases like H₂S, LPG, NH₃, and oxidizing gas CO₂.

Keywords: SnO₂, H₂S, LPG, NH₃, CO₂, thick film sensor

I. INTRODUCTION

There has been a huge upsurge in interest over the past few decades in the field of nanotechnology, thanks to the invention of microscopic techniques, viz., scanning the tunnelling microscope (1981), the atomic force microscope (1986) at IBM's Zurich lab. Nanomaterials show the properties of quantum confinement. The quantum confinement effect of nanomaterials is useful in optoelectronics, semiconductors, and non-linear optics. Nanomaterials have a large percentage of surface atoms as compared to their bulk material and hence enhance the surface properties, which are useful in the field of surface catalysis. Nanomaterials also have a large surface-to-volume ratio. This property of nanomaterials is responsible for producing unique magnetic properties in magnetic materials and providing a more reactive surface to interact with the external species, which leads to improved sensor performance[1].

Metal oxide is a unique class of materials that exhibits diverse characteristic features with a broad spectrum of applications. SnO_2 is one of the most multifaceted metal oxides thanks to its wide band-gap (3.6 eV at 300 °C) with a native n-type semiconductor, low resistance with optical transparency, good activity with facile change of the oxidation state of its cations, and change in conductivity when exposed to gas molecules[2]. As a result, it has numerous applications in a variety of fields, including catalysis[3,4], electrochromism[5,6], fuel cells[7,8], thin-film transistors[9,10], water splitting[11] and as a biological material[12].

Hydrogen sulfide (H_2S) is a highly toxic, colorless, and flammable gas with a characteristic rotten egg odor. Exposure to H_2S poses serious health risks, ranging from mild symptoms like headaches, dizziness, and eye irritation to severe outcomes, including respiratory failure, unconsciousness, and even death, depending on the concentration and duration of exposure. Prolonged inhalation of low concentrations can also lead to chronic health issues affecting the nervous and respiratory systems[13].

H_2S is widely used in industrial processes, including the production of sulfuric acid, which serves as a key reagent in various manufacturing sectors such as pharmaceuticals, chemicals, and pesticides. It also plays a critical role in oil refineries, where it is used to remove sulfur from petroleum products. Additionally, H_2S is a byproduct in wastewater treatment plants, natural gas processing, and pulp and paper manufacturing, further emphasizing its industrial significance.

Given its toxic nature and widespread use, the early detection of H_2S leaks are essential to prevent accidents and safeguard workers' health. Timely detection systems can mitigate risks, ensuring a safe working environment and reducing the likelihood of hazardous exposure.

II. MATERIALS AND METHODS

2.1. Preparation of SnO_2 powder

The stannic oxide was prepared using the co-precipitation route. For this, 0.1M stannic chloride ($\text{SnCl}_4 \cdot 6\text{H}_2\text{O}$) aqueous solution was prepared and ammonia solution was added dropwise. The pH was adjusted to 7 then the white gel-like precipitate was formed, which was allowed to settle down for 12 hrs. Fig. 1 is a schematic illustration of the synthetic procedure for the preparation of stannic oxide. The precipitate was then washed with an ammonium nitrate solution till no chloride ion was detected on the AgNO_3 test. Then the precipitate was washed with hot water, followed by washing with diluted ethanol to remove nitrate ions. This powder was then dried at 120 °C and calcined at 500 °C

Figure 1. Flow chart of the synthetic procedure

2.2. Thick film preparation:

The sensing element required to study gas sensing was fabricated on a 1 cm x 0.5 cm glass substrate; SnO_2 sensing material was printed using a screen-printing technique. The binder required for printing the thick films was formulated by combining organic solvents, including butyl cellulose, butyl carbitol acetate, and turpineol. To create the thixotropic paste, stannic oxide was mixed with ethyl cellulose (serving as a temporary binder) and the organic binder, maintaining an inorganic-to-organic ratio of 75:25. Additionally, the ratio of SnO_2 to ethyl cellulose was set at 95:05. The thixotropic paste was screen-printed onto acetone-cleaned glass substrates in specific patterns. The prepared films were subsequently fired at 500°C for 30 minutes to eliminate organic binders. The silver paste was coated on both sides of the film for electrical measurements. The thickness of the films was observed in the range of 30 to 40 μm .

2.3. Details of gas sensing system:

The electrical and sensing properties of the sensor were evaluated using a static gas sensing system. This system comprised a 35-liter stainless steel chamber equipped with a gas inlet valve and a window for sample handling. The heating element, constructed from Kanthal wire, was connected to a temperature controller (Nippon NC 2638). Both the sensor and a thermocouple were placed on an insulating surface atop the heating element. The thermocouple's output was fed to a digital temperature indicator for monitoring. A constant voltage was applied via a Keithley 6487 voltage source and picoammeter.

III. EXPERIMENTAL

3.1. Material Characterization

3.1.1. Structural analysis:

The XRD analysis confirms that the stannic oxide exhibits a cassiterite crystal structure. The observed diffraction peaks closely match the reference data provided in the SnO_2 JCPDS card no. 41-1445. The XRD pattern of stannic oxide, as shown in Figure 2, reveals no additional or overlapping peaks, indicating the absence of any secondary phases in the sample

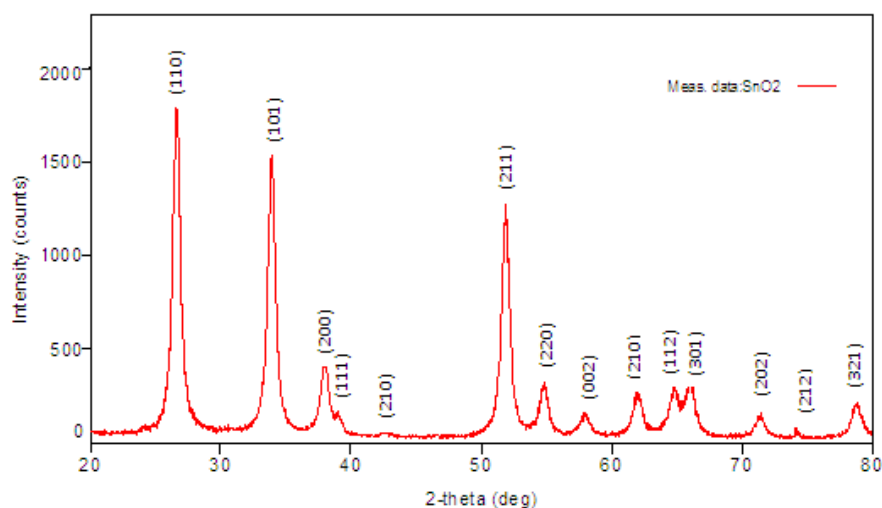


Figure 2. X-ray diffraction pattern of pure SnO_2

3.1.2. Morphological Analysis:

The surface morphology of the nanoparticles was examined using field emission scanning electron microscopy (FE-SEM). Figure 3 presents the SEM image of the stannic oxide nanoparticles, which exhibit a randomly shaped, agglomerated structure. The observed agglomeration is attributed to van der Waals forces acting between the particles.

The EDAX spectrum of the stannic oxide particles confirms the presence of the constituent elements, Sn and O. No additional elemental signals were detected, indicating the purity of the sample. The elemental composition percentages are presented in the corresponding figure 3.

The particle morphology was examined using transmission electron microscopy (TEM). The TEM image of stannic oxide shows that the particles are spherical in shape, with sizes ranging between 7 nm and 11 nm.

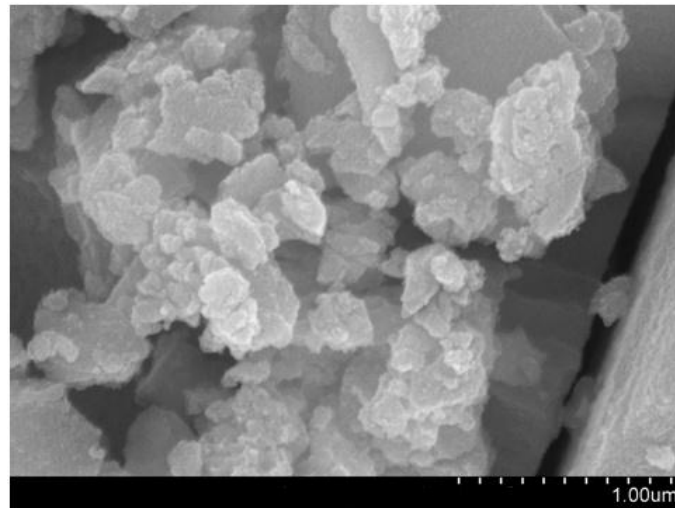


Figure 3. FE-SEM image of pure SnO₂

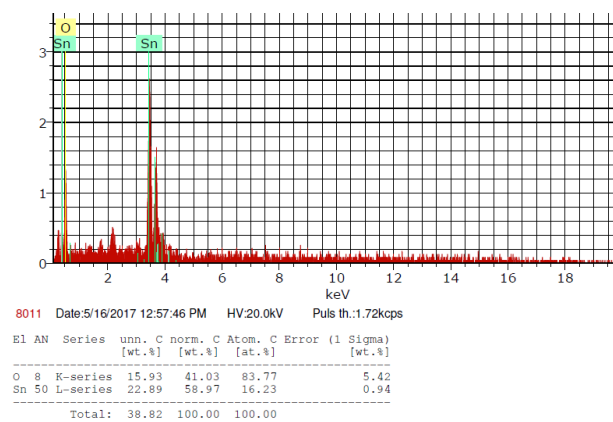


Figure 4. EDAX image of pure SnO₂

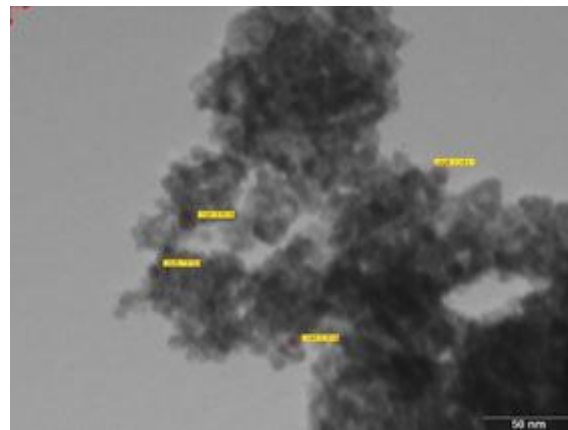


Figure 5. TEM image of pure SnO₂

3.2. Gas sensing properties

To study the gas sensing properties of the sensor, silver electrodes were made by coating silver paste on both sides of the film. The samples were placed on the sample holder, and the static resistance of the samples was recorded at different temperatures. Then different gases were introduced into the chamber one after the other through the gas inlet valve using a syringe, and the resistance of the samples with different gases was recorded, and then the sensitivity of the sample was calculated using equation 1 and 2.

$$(S)_{\text{CO}_2} = \frac{R_g}{R_a} \quad (1)$$

$$(S)_{\text{NH}_3, \text{LPG}, \text{NH}_3} = \frac{R_g}{R_a} \quad (2)$$

where R_a denotes resistance in the air and R_g denotes resistance in the target gas.

IV. RESULT AND DISCUSSION

4.1. Electrical Properties

4.1 I-V characteristics

The current-voltage (I-V) characteristics of the prepared thick film were investigated over a bias voltage range of -8 V to +8 V, with 2 V increments. The I-V curve exhibited symmetrical behavior, confirming the ohmic nature of the silver contacts

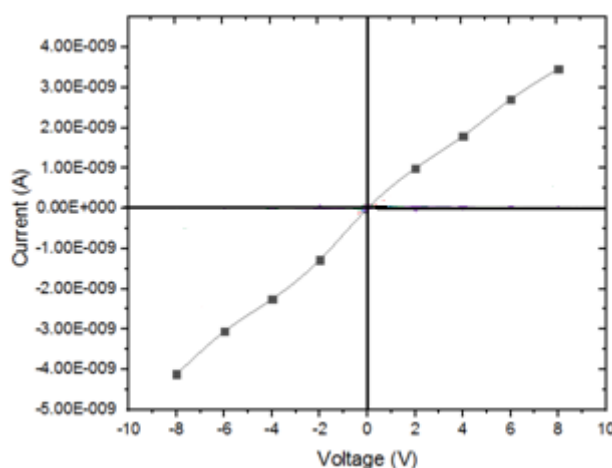


Figure 6. I-V characteristics of pure SnO_2

4.2. Temperature conductivity dependance:

The figure 7 illustrates the temperature-dependent conductivity of pure SnO_2 within the temperature range of 50°C to 300°C. Initially, the conductivity shows a gradual increase as the temperature rises up to 150°C, followed by a sharp increase extending up to 300°C

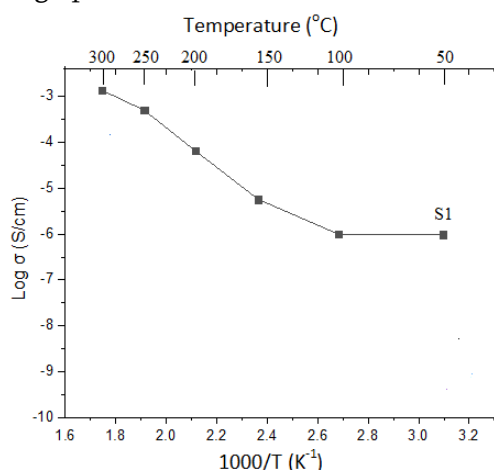


Figure 7. Variation of conductivity with temperature

4.3. Gas sensing properties:

Figure 8 presents the temperature sensitivity graph of SnO_2 particles. The sensitivity of the thick film was examined over a temperature range of 50°C to 300°C. The sensor's sensitivity initially increases, reaching a

maximum at 200°C, and then declines beyond this temperature. The lower sensitivity observed at lower temperatures may be attributed to the presence of humidity within the thick film. The peak sensitivity at 200°C suggests optimal operating conditions, whereas further increases in temperature lead to a decrease in sensitivity.

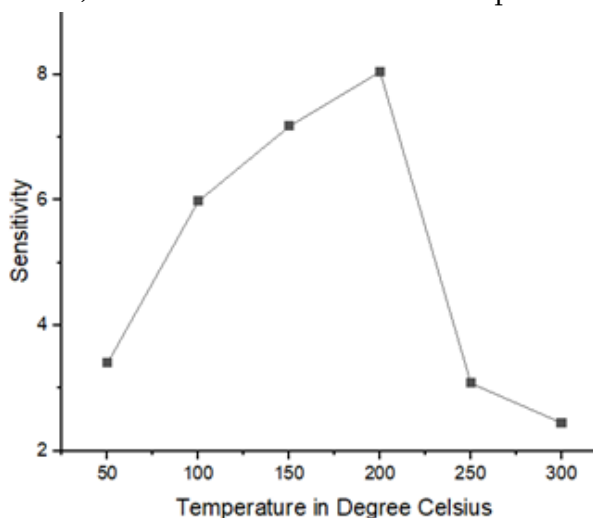


Figure 8. Variation of sensitivity with temperature for H₂S gas

The sensing behavior of SnO₂ is attributed to the adsorption of O⁻ and O²⁻ species on the sensing layer, as schematically illustrated in the figure. When H₂S gas interacts with the film, the following reaction occurs



The released electron from the space charge region leads to decrease in thickness of the depletion layer.

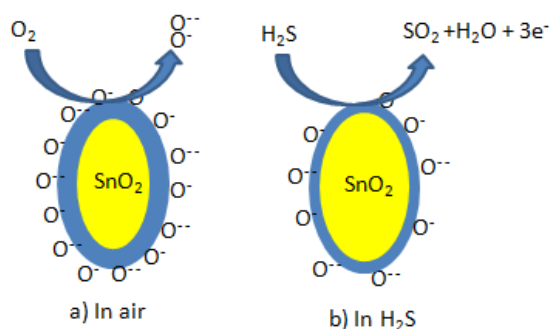


Figure 9. Sensing mechanism of pure SnO₂

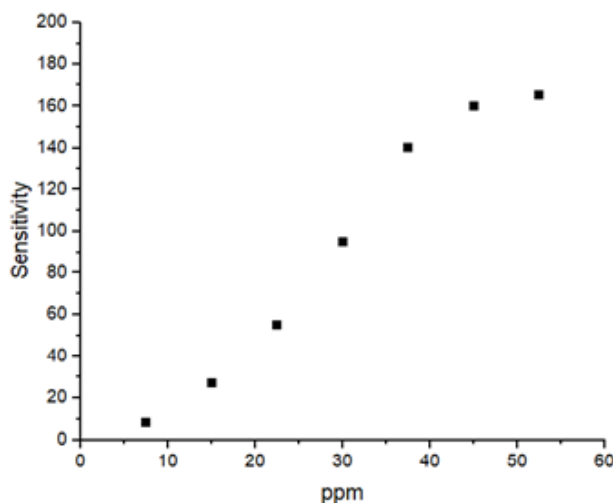


Figure 10. Variation in sensitivity for H₂S gas measured in ppm

The figure 10 illustrates the sensitivity of prepared sample at different ppm. As the gas concentration (ppm) increased, the sensitivity rose steadily, reaching a peak value of 160,ppm after which it plateaued. This saturation in sensitivity is likely due to the depletion of surface-adsorbed oxygen

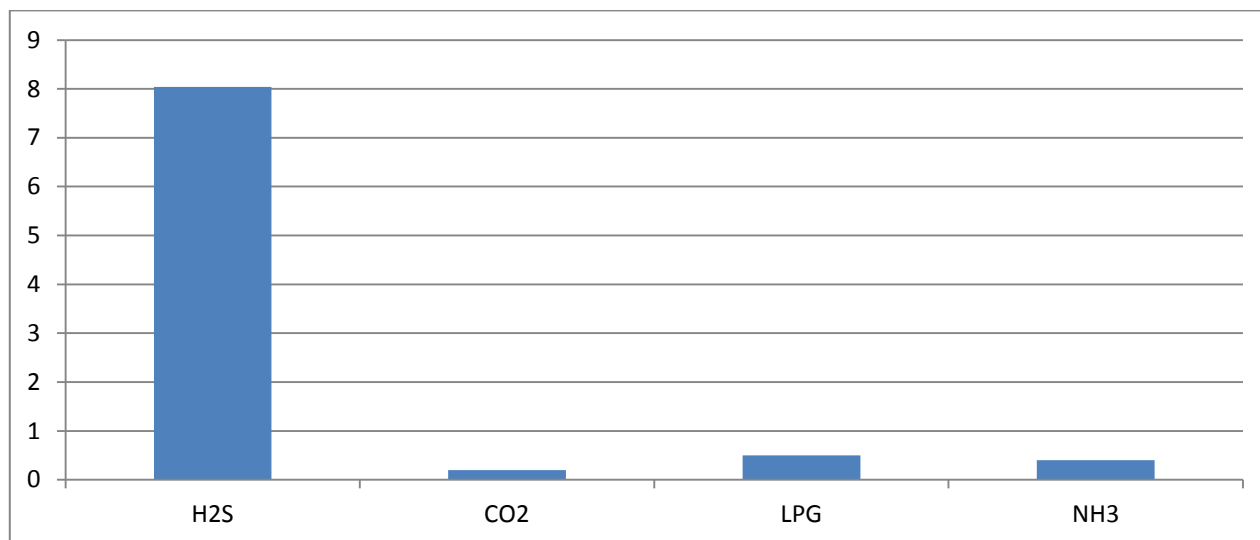


Figure 11. Selectivity of H₂S gas in air

Figure 11. shows the bar graph of sensitivity of H₂S , LPG, CO₂, NH₃ gas at 200°C. All the readings were taken at 1000ppm except H₂S gas; it is taken at 7.5ppm.

V. CONCLUSION

1. Spherical nanoparticles were successfully synthesized using the coprecipitation method, and particle size is found in the range of 7 to 10 nm.
2. Thick films of SnO₂ were successfully prepared using the screen printing method and used to detect H₂S, CO₂, LPG, and NH₃.
3. H₂S gas is more sensitive as compared to other gases, and its maximum response was observed at 200 °C.
4. The lower detection limit for H₂S gas at 200 °C is found to 7.5 ppm.

VI. REFERENCES

- [1]. R. Harsha, P. Kishor, Nanotechnology-A Review, IJSRR 12 (n.d.) 63–68. www.ijsrr.org.
- [2]. X. Yu, T.J. Marks, A. Facchetti, Metal oxides for optoelectronic applications, Nat Mater 15 (2016) 383–396. <https://doi.org/10.1038/nmat4599>.
- [3]. P. Manjunathan, V.S. Marakatti, P. Chandra, A.B. Kulal, S.B. Umbarkar, R. Ravishankar, G. V. Shanbhag, Mesoporous tin oxide: An efficient catalyst with versatile applications in acid and oxidation catalysis, Catal Today 309 (2018) 61–76. <https://doi.org/10.1016/j.cattod.2017.10.009>.
- [4]. Y. Rong, S. Kim, F. Su, D. Myers, M. Taya, New effective process to fabricate fast switching and high contrast electrochromic device based on viologen and Prussian blue/antimony tin oxide nano-composites with dark colored state, Electrochim Acta 56 (2011) 6230–6236. <https://doi.org/10.1016/j.electacta.2011.02.110>.

- [5]. A.A. Ambalkar, U. V. Kawade, Y.A. Sethi, S.C. Kanade, M. V. Kulkarni, P. V. Adhyapak, B.B. Kale, A nanostructured SnO₂/Ni/CNT composite as an anode for Li ion batteries, *RSC Adv* 11 (2021) 19531–19540. <https://doi.org/10.1039/d1ra01678d>.
- [6]. R.M. Mensharapov, N.A. Ivanova, D.D. Spasov, E. V. Kukueva, A.A. Zasyapkina, E.A. Seregina, S.A. Grigoriev, V.N. Fateev, Carbon-supported pt-sno₂ catalysts for oxygen reduction reaction over a wide temperature range: Rotating disk electrode study, *Catalysts* 11 (2021). <https://doi.org/10.3390/catal11121469>.
- [7]. A. Sharma, A. Ahmed, A. Singh, S.K. Oruganti, A. Khosla, S. Arya, Review—Recent Advances in Tin Oxide Nanomaterials as Electrochemical/Chemiresistive Sensors, *J Electrochem Soc* 168 (2021) 027505. <https://doi.org/10.1149/1945-7111/abdee8>.
- [8]. Z.S. Abdul-Ridha, A.A.N. Al-Jasim, A.O. Radam, Improvement of electrical features of SnO₂ based varistor doped with Al₂O₃, in: *AIP Conf Proc*, American Institute of Physics Inc., 2019. <https://doi.org/10.1063/1.5117024>.
- [9]. D.W. Kim, H.J. Kim, C. Lee, K. Kim, J.H. Bae, I.M. Kang, J. Jang, Influence of active channel layer thickness on SnO₂ thin-film transistor performance, *Electronics (Switzerland)* 10 (2021) 1–12. <https://doi.org/10.3390/electronics10020200>.
- [10]. S. Abanades, P. Charvin, F. Lemont, G. Flamant, Novel two-step SnO₂/SnO water-splitting cycle for solar thermochemical production of hydrogen, *Int J Hydrogen Energy* 33 (2008) 6021–6030. <https://doi.org/10.1016/j.ijhydene.2008.05.042>.
- [11]. H.C. Wu, J.B. Lyau, M.H. Lin, Y.J. Chuang, H. Chen, Multilayer microfluidic systems with indium-tin-oxide microelectrodes for studying biological cells, *Journal of Micromechanics and Microengineering* 27 (2017). <https://doi.org/10.1088/1361-6439/aa71d6>.
- [12]. M. Dhillon, A. Naskar, N. Kaushal, S. Bhansali, A. Saha, A.K. Basu, A novel GO hoisted SnO₂-BiOBr bifunctional catalyst for the remediation of organic dyes under illumination by visible light and electrocatalytic water splitting, *Nanoscale* 16 (2024) 12445–12458. <https://doi.org/10.1039/d4nr01154f>.
- [13]. R.B. Pedhekar, F.C. Raghuwanshi, V.D. Kapse, Low Temperature H₂ S Gas Sensor Based on Fe₂O₃ Modified ZnO-TiO₂ Thick Film, 2015.

Effect of Invasive Species on Fish Fauna in Freshwater Bodies in and Around Morshi Taluka, District-Amravati (Maharashtra), India

Mr. Vinayak Vishwanathrao Tathod¹, Dr. Mrs. D. S. Kulkarni²

¹Bharatiya Mahavidyalaya, Amravati, Affiliation of University, Sant Gadge Baba Amravati University, Amravati, Maharashtra, India

²Professor & Head, Department of Zoology, Bharatiya Mahavidyalaya, Amravati, Maharashtra, India

ARTICLE INFO

Article History:

Accepted : 01 Jan 2025

Published : 10 Jan 2025

Publication Issue :

Volume 12, Issue 7

January-February-2025

Page Number :

604-606

I. INTRODUCTION

Freshwater ecosystems are among the most biologically diverse habitats, yet they are increasingly threatened by invasive species. These species often outcompete native species, leading to significant ecological imbalances. Morshi taluka, located in the Amravati district of Maharashtra, is characterized by numerous freshwater bodies that support diverse fish fauna. However, invasive species such as *Oreochromis mossambicus* (Mozambique tilapia) and *Clarias gariepinus* (African catfish) have been reported in these ecosystems. This study aims to evaluate the impact of these invasive species on the native fish populations, contributing to the broader understanding of biodiversity conservation in freshwater systems. Moreover, the economic and social importance of preserving native fish populations is emphasized, as these species are integral to local livelihoods and cultural practices.

II. MATERIALS AND METHODS

- 2.1. Study Area** The study was conducted in selected freshwater bodies of Morshi taluka, including ponds, lakes, and small rivers. Geographical coordinates, water quality parameters (e.g., pH, temperature, and dissolved oxygen levels), and physical characteristics of these water bodies were recorded to provide a comprehensive ecological context.
- 2.2. Sampling Techniques** Fish samples were collected using gill nets, cast nets, and traditional traps. Sampling was performed monthly from January 2023 to December 2024 to capture seasonal variations. Special attention was given to ensure the ethical treatment of captured specimens, following standard fish sampling protocols.
- 2.3. Species Identification** Fish specimens were identified using standard morphological keys and confirmed through taxonomic literature. Invasive species were identified based on their distinctive features and documented records in Indian freshwater systems. Photographic evidence was collected for accurate documentation.
- 2.4. Data Analysis** The diversity indices (Shannon-Wiener and Simpson's indices) were calculated to assess species diversity. Comparative analysis was performed to evaluate the abundance and distribution of native and invasive species. Statistical tests, including ANOVA and correlation analysis, were used to explore the relationships between invasive species density and native species diversity.

III.RESULTS

3.1. Diversity of Fish Fauna A total of 36 fish species belonging to 12 families were recorded. Native species included *Labeorohita* (Rohu), *Catla* (Catla), and *Cirrhinus mrigala* (Mrigal), among others. However, the presence of invasive species, predominantly *Oreochromis mossambicus* and *Clarias gariepinus*, was noted in most water bodies. Seasonal variations revealed that invasive species exhibited stable populations year-round, whereas native species showed fluctuations linked to breeding cycles and environmental conditions.

3.2. Impact of Invasive Species

- **Population Decline:** Native species exhibited a significant decline in population density, particularly in water bodies with high densities of invasive species. The reproductive success of native species was negatively impacted by resource competition and predation.
- **Habitat Alteration:** Invasive species altered the habitat structure by increasing turbidity and competing for resources. The aggressive feeding habits of *Oreochromis mossambicus* led to a reduction in available food for native herbivorous and omnivorous fish.
- **Predation:** Predatory behavior of *Clarias gariepinus* led to a decrease in smaller native fish species, such as *Puntius sophore* and *Amblypharyngodon mola*.
- **Economic Impact:** Local fisheries reported a decline in catch volume of economically valuable native species, affecting the livelihoods of fishers dependent on these resources.

3.3. Statistical Analysis The diversity indices indicated reduced species richness in water bodies with invasive species compared to those without. A strong negative correlation ($r = -0.78$, $p < 0.05$) was observed between the abundance of invasive species and native fish diversity. ANOVA results confirmed statistically significant differences in species diversity across sites with varying invasive species densities.

IV.DISCUSSION

The findings underscore the detrimental effects of invasive species on freshwater fish fauna. The aggressive breeding and adaptability of *Oreochromis mossambicus* and *Clarias gariepinus* have allowed them to dominate local ecosystems, threatening the survival of native species. The disruption of food webs and alteration of habitat conditions have far-reaching ecological consequences. Similar trends have been reported in other regions of India, highlighting the widespread nature of this issue.

Community-based approaches, including the active participation of local fishers and stakeholders, can play a crucial role in managing invasive species. Raising awareness about the ecological and economic impacts of invasive species is vital for fostering support for conservation initiatives. Additionally, regulatory measures, such as stricter controls on the introduction and spread of non-native species, should be implemented. Biological control methods, such as the introduction of natural predators or competitors, may offer a sustainable solution but require careful consideration to avoid unintended ecological consequences.

V. CONCLUSION

Invasive species pose a significant threat to the freshwater biodiversity of Morshi taluka. Effective management strategies and policy interventions are imperative to protect native fish populations and maintain ecological

balance. Future research should focus on long-term monitoring, habitat restoration, and the development of sustainable mitigation practices. Collaborative efforts involving government agencies, researchers, and local communities are essential for addressing this pressing issue.

VI. REFERENCES

- [1]. Pimentel, D., et al. (2005). Economic and ecological costs of invasive species. *Ecological Economics*, 52(3), 273-288.
- [2]. Moyle, P. B., & Light, T. (1996). Fish invasions in California's Sacramento-San Joaquin Delta. *Biological Conservation*, 78(2), 149-161.
- [3]. Welcomme, R. L. (1988). International introductions of inland aquatic species. FAO Fisheries Technical Paper No. 294.
- [4]. Singh, A. K., et al. (2010). Invasive alien fish species in India and their impact on biodiversity. *Aquatic Ecosystem Health & Management*, 13(2), 118-128.
- [5]. Rahel, F. J. (2002). Homogenization of freshwater faunas. *Annual Review of Ecology and Systematics*, 33, 291-315.
- [6]. Dudgeon, D., et al. (2006). Freshwater biodiversity: Importance, threats, status and conservation challenges. *Biological Reviews*, 81(2), 163-182.

Analysis of Collective Creativity : Gender, Power, and the Cultural Significance of Fanfiction

Shradha Upadhya

Department of English, Bhagwant University, Rajasthan, India

ARTICLE INFO

Article History:

Accepted : 01 Jan 2025

Published : 10 Jan 2025

Publication Issue :

Volume 12, Issue 7

January-February-2025

Page Number :

607-614

ABSTRACT

Fanfiction, a dynamic cultural phenomenon, redefines storytelling by allowing fans to critique, reinterpret, and expand canonical narratives. Rooted in participatory culture, it challenges traditional power structures in literature, offering marginalized voices, particularly women, a space to reclaim agency and reshape cultural narratives. This paper explores fanfiction's historical evolution, its connection to feminist traditions, and its role in fostering inclusivity and diversity through digital platforms like AO3 and Wattpad. By critiquing mainstream media's lack of representation, fanfiction serves as a subversive space for addressing systemic inequalities and amplifying underrepresented perspectives. The study also examines fanfiction's technological empowerment, highlighting how digital connectivity fosters global communities and collective creativity. By situating fanfiction within broader discourses on gender, power, and identity, the paper argues that fanfiction transcends its derivative label, emerging as a transformative medium that reshapes how narratives are consumed, produced, and valued in contemporary culture.

Keywords : Fanfiction, Gender, Power, Inclusivity, Participatory Culture, Representation, Digital Storytelling

I. Introduction

Fanfiction is not merely a creative outlet but a profound cultural phenomenon that redefines how narratives are consumed, interpreted, and produced. Originating in fan communities as a way to reimagine and expand upon existing stories, fanfiction provides a transformative space where traditional boundaries of authorship and storytelling are dismantled. This participatory genre allows fans to critique, reinterpret, and creatively engage with canonical texts, fostering a dynamic interaction between creators and audiences. In doing so, fanfiction transcends its derivative origins, becoming a subversive force in contemporary literature and media culture (Jenkins, 2012).

Historically, literature and storytelling have often been controlled by elite, male-dominated institutions, marginalizing voices that did not conform to prevailing cultural norms. Women, in particular, faced systemic barriers to authorship and representation, both as writers and as subjects of literary narratives (Bury, 2005). The emergence of fanfiction, predominantly driven by female creators, challenges these traditional power structures, offering an inclusive and democratized platform for storytelling. By enabling marginalized voices to reclaim agency and explore diverse perspectives, fanfiction becomes a space for resistance and cultural critique (Busse, 2006).

This paper examines fanfiction's role as a transformative medium that empowers individuals and communities to reshape cultural narratives. Through historical analysis, a focus on gender dynamics, and the exploration of digital platforms, this study highlights fanfiction's capacity to amplify marginalized voices, challenge societal norms, and redefine cultural and literary significance. By situating fanfiction within broader discourses on participatory culture and collective creativity, the paper argues that fanfiction is not merely a derivative genre but a revolutionary form of cultural expression that continues to influence and transform mainstream media landscapes.

This exploration underscores the significance of fanfiction as a platform for cultural empowerment, where gender, power, and identity intersect to create narratives that resonate with audiences worldwide. Through digital connectivity, fanfiction communities have become sites of cultural innovation and advocacy, fostering new ways of engaging with and challenging traditional narratives.

II. Historical and Feminist Perspectives

The roots of fanfiction can be traced to the historical tradition of women's coterie writing, a practice that flourished in private and semi-private circles, particularly in the 17th and 18th centuries. In these spaces, women exchanged manuscripts and composed works that were often excluded from the male-dominated public literary sphere. These writings, whether poems, letters, or essays, provided a platform for women to share experiences, critique societal norms, and express creativity in ways that subverted the patriarchal constraints of their time (Busse, 2006). Much like modern fanfiction, these coterie writings embodied collective creativity and offered a means of resistance against the cultural and literary dominance of male voices.

Historically, traditional publishing has posed systemic barriers to women, both in terms of their roles as creators and the representation of female characters within texts. Female authors often struggled to gain recognition, facing limited opportunities for publication and pervasive biases that marginalized their contributions. Furthermore, when women were represented in literature, their characters were frequently relegated to secondary roles or confined to stereotypes that reflected societal expectations rather than complex individuality (Driscoll, 2008).

Fanfiction disrupts this historical imbalance by creating a space where female writers dominate both the creation and consumption of narratives. Freed from the constraints of traditional publishing, fanfiction communities empower women to write stories that prioritize female agency, autonomy, and diversity. Female-centric narratives in fanfiction often challenge and critique the male-dominated perspectives of canonical works. For instance, writers reinterpret existing stories to center female characters, expanding their roles or providing them with richer, more nuanced arcs. This reclamation of agency allows women to address the systemic erasure of female voices in mainstream media and literature (Duffett, 2013).

Feminist scholars have also recognized fanfiction as a mode of resistance. By rewriting or expanding upon existing works, women writers challenge the dominance of male-authored texts and their associated power structures. For example, in male-centric narratives where female characters are overshadowed or

underdeveloped, fanfiction offers an opportunity to explore their perspectives, motivations, and emotional complexity. This reimagining not only critiques the shortcomings of traditional narratives but also creates a space for envisioning more equitable and inclusive storytelling (Jenkins, 2012). Moreover, fanfiction's emphasis on collaboration and collective authorship mirrors the communal aspects of historical women's writing practices. By fostering dialogue, shared creativity, and mutual support, fanfiction communities carry forward the legacy of coterie writing while adapting it to the digital age. Through this lens, fanfiction can be seen as both a continuation of historical feminist traditions and a powerful tool for contemporary cultural critique. It provides a platform where women reclaim control over storytelling, challenge patriarchal norms, and imagine new possibilities for gender, identity, and representation in literature.

III. The Gendered Landscape of Fanfiction

Fanfiction is unique in its demographic composition, being predominantly female-driven in both authorship and readership. Women constitute the vast majority of contributors to fanfiction platforms, creating a distinct space where female voices dominate the narrative landscape (Bury, 2005). This demographic shift challenges the historical male-centric focus of mainstream publishing and media, enabling a greater exploration of gender, identity, and relationships. By reclaiming creative control, women in fanfiction communities have redefined what stories get told and whose perspectives are prioritized.

One of the most significant contributions of fanfiction to cultural discourse is the increased representation of female characters and relationships. Traditional media often relegates women to secondary or stereotypical roles, focusing instead on male protagonists and their journeys. Fanfiction reverses this trend by centering female perspectives, giving them depth, autonomy, and agency. Popular tropes like "gender-bending" allow writers to explore fluidity in gender roles by reimagining characters as a different gender, which often highlights the limitations and biases inherent in their original portrayals. Similarly, "reverse harem" tropes, where multiple male characters are romantically or emotionally drawn to a central female protagonist, subvert the traditional male-centric harem narrative, placing women at the center of complex relationship dynamics (Galbraith, 2011).

Fanfiction also serves as a platform for exploring marginalized sexualities and gender identities. The popularization of slash fiction—stories that focus on same-sex relationships, often between male characters—has been a hallmark of fanfiction culture. These works not only subvert heteronormative narratives but also provide an outlet for writers and readers to engage with themes of love, identity, and acceptance outside the constraints of mainstream media (Hampton, 2015). Slash fiction, along with femslash (female same-sex relationships), challenges traditional power dynamics and gender norms, offering alternative frameworks for understanding intimacy and connection.

The inclusive nature of fanfiction reflects the diversity of its communities and their collective desire to reshape media into a more equitable space. By amplifying voices that are often marginalized in mainstream storytelling, fanfiction fosters a culture of inclusivity that extends beyond gender and sexuality. It provides a safe space for exploring intersectional identities, from race and ethnicity to disability and mental health, allowing writers to address themes and perspectives that resonate with their lived experiences.

IV. Fanfiction as a Subversive Space

Fanfiction serves as a subversive space by reimagining existing works to critique societal norms and address the lack of representation in mainstream media. Traditional storytelling often centers dominant narratives, sidelining marginalized voices and reinforcing established power structures. Fanfiction challenges these

conventions by creating alternative narratives that reflect the diversity and complexity of modern audiences. By rewriting, expanding, or transforming canonical texts, fanfiction empowers writers to question and redefine cultural norms, offering a platform for advocacy and social commentary (Jenkins, 2012).

Mainstream media frequently fails to adequately represent marginalized identities, including LGBTQ+ characters, people of color, and women. Fanfiction bridges these gaps by centering such identities, often exploring themes and relationships that are overlooked or underdeveloped in canonical works. For instance, *Harry Potter* fanfiction has become a fertile ground for stories that imagine LGBTQ+ relationships, such as the popular “Drarry” pairing (Draco Malfoy and Harry Potter). These narratives allow fans to critique the lack of queer representation in J.K. Rowling’s original series and envision a world where diverse sexualities and identities are normalized (Ford, 2014). Similarly, fanfiction often reimagines female characters, giving them greater agency and depth than in their original portrayals. Marginalized characters like Hermione Granger, who are often confined to secondary roles or stereotypical traits, are re-envisioned as central protagonists in fan-created works. This reclamation of female characters transforms them into active agents of change, challenging the male-centric focus of traditional narratives and providing role models for readers (Duffett, 2013).

Fanfiction also subverts genre conventions, using established story structures to challenge societal norms. Alternate universe (AU) fanfiction is particularly notable in this regard. By placing familiar characters in completely different settings—such as modern high schools, dystopian futures, or historical periods—AU fanfiction highlights how context shapes identity and relationships. These explorations often allow writers to address real-world issues, such as systemic oppression, mental health, or gender inequality, within the safe confines of a fictional narrative (Hampton, 2015). For example, stories like *The Life and Times* delve into the untold backstories of minor characters, such as the Marauders from *Harry Potter*, providing nuanced portrayals that fill in gaps left by the original series. These works not only expand on the source material but also critique the ways in which mainstream media prioritizes certain narratives over others, often at the expense of marginalized perspectives (Hills, 2002).

Fanfiction’s subversive potential lies in its ability to critique and deconstruct the power structures embedded in canonical texts. By rewriting stories to include diverse voices and perspectives, fanfiction challenges the authority of original authors and the institutions that perpetuate exclusive storytelling. For example, *Game of Thrones* fanfiction has been used to critique the series’ controversial portrayal of sexual violence and its lack of meaningful character development for women and people of color. These fan-created works reimagine the narrative to emphasize consent, equity, and empowerment, offering an alternative vision of the story’s world (Busse, 2006). Fanfiction also provides a space for intersectional critique, addressing how race, gender, class, and sexuality intersect in mainstream narratives. Writers often reimagine white, heterosexual protagonists as characters of color or queer individuals, thereby challenging the homogenization of mainstream media. These rewritings not only expand representation but also prompt readers to question the biases inherent in the original works and the broader cultural landscape (Gray et al., 2017).

Fanfiction’s ability to subvert extends beyond individual narratives to create entire communities of critique. *The Life and Times*, a celebrated *Harry Potter* fanfiction, explores the lives of the Marauders, providing richly detailed backstories that reframe the series’ events from new perspectives. This work challenges the original series’ limited focus on Harry Potter and his immediate circle, instead highlighting the complex interplay of loyalty, betrayal, and identity among the previous generation of characters (Ford, 2014). Another example is *My Immortal*, an infamous fanfiction that has gained cult status for its chaotic writing and unconventional storytelling. While often dismissed as a parody, *My Immortal* subverts expectations by rejecting literary

conventions, ultimately raising questions about the boundaries between serious and satirical fanfiction. This has led to academic discussions about the nature of authorship, creativity, and cultural critique in fan-created works (Jenkins, 2012).

Fanfiction communities leverage their subversive potential to advocate for inclusivity, equity, and representation. By rewriting canonical texts to reflect diverse experiences, fanfiction writers create narratives that resonate with marginalized groups and challenge exclusionary practices in mainstream media. These works are often shared widely on platforms like AO3, Wattpad, and Tumblr, fostering dialogue and solidarity among readers and writers. Additionally, fanfiction serves as a tool for raising awareness about social issues. Stories that address mental health, trauma, or systemic oppression provide catharsis for readers while promoting empathy and understanding. By intertwining advocacy with creativity, fanfiction becomes a powerful medium for cultural change, offering readers new ways of engaging with and questioning the world around them.

Fanfiction's role as a subversive space lies in its ability to critique, reimagine, and expand upon mainstream narratives. By addressing gaps in representation, challenging power structures, and offering alternative frameworks for storytelling, fanfiction empowers marginalized voices to reshape cultural discourse. Through its transformative potential, fanfiction not only enriches the literary landscape but also fosters a more inclusive and equitable vision of storytelling for future generations.

V. Technology, Community, and Empowerment

The rise of the internet has revolutionized fanfiction, transforming it into a global phenomenon that transcends cultural, geographical, and linguistic boundaries. Digital platforms such as Archive of Our Own (AO3), Wattpad, and FanFiction.net have played a pivotal role in fostering fan communities, empowering writers to bypass traditional publishing barriers and directly engage with readers. These platforms not only democratize access to storytelling but also provide a vital space for marginalized voices to be heard and celebrated (Busse & Gray, 2014).

By eliminating the gatekeeping mechanisms of traditional publishing, digital platforms allow anyone with internet access to share their stories. Writers no longer need to navigate the biases and constraints of conventional media industries, which have historically excluded or minimized diverse narratives. Platforms like AO3 offer tools for tagging, categorizing, and archiving works, making it easier for readers to discover stories tailored to their interests. This technological infrastructure enables writers to build global audiences and connect with like-minded individuals, creating vibrant, collaborative ecosystems of creativity (Gray et al., 2017). Wattpad, for instance, reports over 90 million monthly active users, a significant portion of whom engage with fanfiction. Its algorithmic recommendations and reader feedback systems foster a dynamic interplay between writers and readers, encouraging iterative storytelling that evolves in real time. This participatory environment enables fanfiction writers to experiment with themes, genres, and narrative techniques without fear of rejection or censorship, fostering innovation and diversity in storytelling (Duffett, 2013).

The internet has also enabled the formation of global fan communities that thrive on collective creativity and mutual support. These communities bring together individuals from diverse cultural and geographical backgrounds, uniting them through shared interests in fandoms. Collaborative events such as writing challenges, role-playing forums, and co-authored stories illustrate the communal nature of fanfiction, where creativity is not an isolated endeavor but a shared experience (Hills, 2002). Fanfiction communities are particularly empowering for marginalized groups, who often find in these spaces a platform to express their identities and explore themes that resonate with their lived experiences. LGBTQ+ fans, for example, use

fanfiction to imagine worlds where their identities are normalized and celebrated. Writers from underrepresented ethnic or cultural backgrounds can reframe existing narratives to reflect their perspectives, fostering a more inclusive literary landscape (Hampton, 2015).

Fanfiction communities are not just spaces for storytelling but also platforms for social commentary. Writers often use fanfiction to critique societal norms, challenge systemic injustices, and advocate for change. For example, fanfiction that addresses issues such as racism, gender inequality, or mental health provides readers with new ways of understanding and engaging with these topics. These narratives often generate discussions within fan communities, creating a ripple effect of awareness and activism (Busse & Gray, 2014). The participatory nature of fanfiction communities also fosters resistance to traditional power dynamics in storytelling. Unlike mainstream media, where narratives are shaped by corporate interests and gatekeeping institutions, fanfiction allows writers and readers to co-create stories that reflect their collective values. This collaborative approach challenges the hierarchical relationship between authors and audiences, redefining authorship as a shared, dynamic process (Jenkins, 2012).

While fanfiction communities are inherently participatory, they are not without internal power dynamics. Prominent writers, moderators, and platform policies often influence how narratives are created, shared, and received. For example, popular authors within a fandom may set trends or establish norms that shape the creative direction of the community. Moderators on platforms like AO3 play a critical role in maintaining community standards and ensuring a safe, inclusive environment for all participants (Gray et al., 2017). These power dynamics, however, are balanced by the decentralized and open nature of fanfiction communities. Unlike traditional publishing, where a small group of decision-makers wields significant influence, fanfiction operates as a more egalitarian ecosystem. Readers have the power to elevate stories through feedback, reviews, and recommendations, creating a level of accountability and reciprocity that fosters mutual respect between writers and audiences.

Ultimately, the combination of technology and community makes fanfiction a uniquely empowering medium. For many writers, particularly those from marginalized groups, fanfiction represents an opportunity to reclaim agency and assert control over their narratives. The accessibility and inclusivity of digital platforms provide a safe space for experimentation, self-expression, and the exploration of identity. Moreover, fanfiction communities serve as support networks that nurture creativity and resilience. Through collaborative storytelling and shared dialogue, fans empower one another to challenge societal norms, imagine alternative realities, and advocate for a more equitable and inclusive world. This collective empowerment underscores the transformative potential of fanfiction as both a cultural and a technological phenomenon.

Technology has fundamentally reshaped the landscape of fanfiction, enabling the formation of global communities that thrive on creativity, collaboration, and inclusivity. By democratizing access to storytelling, digital platforms amplify marginalized voices and provide a space for social commentary and resistance. Through its participatory nature, fanfiction fosters a unique balance between individual expression and collective empowerment, challenging traditional hierarchies of authorship and redefining the role of storytelling in contemporary culture.

VI. Conclusion

Fanfiction exemplifies the transformative potential of grassroots creativity to challenge traditional hierarchies of authorship and redefine cultural narratives. Through its participatory nature, fanfiction communities empower marginalized voices, particularly women and LGBTQ+ individuals, to reclaim agency and engage in collective storytelling that critiques societal norms. By fostering inclusivity and diversity, fanfiction serves as

both a cultural critique and a platform for advocacy, addressing gaps in representation often ignored by mainstream media. The digital revolution has been instrumental in fanfiction's evolution, providing platforms like AO3 and Wattpad that democratize storytelling and amplify underrepresented voices. These spaces nurture creative collaboration and enable global communities to engage with narratives that reflect their identities and lived experiences. The participatory nature of fanfiction redefines the boundaries of authorship, transforming storytelling into a shared, iterative process that challenges traditional notions of literary authority. As fanfiction gains legitimacy in academia and mainstream media, its role as a subversive and empowering medium becomes increasingly evident. By prioritizing diversity, promoting representation, and fostering dialogue on identity and power, fanfiction not only enriches the literary landscape but also offers a model for more inclusive and equitable storytelling in the future. Its influence highlights the enduring power of collective creativity in shaping cultural and literary norms.

REFERENCES

- [1]. Daros, O. (2022). Prosumer activism: The case of Britney Spears' Brazilian fandom. *Journal of Consumer Culture*. <https://doi.org/10.1177/14695405221103411>
- [2]. Chen, Z. T. (2021). Poetic prosumption of animation, comic, game and novel in a post-socialist China: A case of a popular video-sharing social media Bilibili as heterotopia. *Journal of Consumer Culture*, 21(2), 257–277.
- [3]. Flavin, B. (2018). What is a webmaster and do they still exist? Retrieved from <https://www.rasmussen.edu>
- [4]. Bertrand, I., & Hughes, P. (2017). *Media research methods: Audiences, institutions, texts* (2nd ed.). London: Macmillan International Higher Education.
- [5]. Gray, J., Sandvoss, C., & Harrington, C. L. (Eds.). (2017). *Fandom: Identities and communities in a mediated world*. New York: NYU Press.
- [6]. Han, B. (2017). K-pop in Latin America: Transcultural fandom and digital mediation. *International Journal of Communication*, 11, 20.
- [7]. Devereux, E., & Hidalgo, M. (2015). 'You're gonna need someone on your side': Morrissey's Latino/a and Chicano/a fans. *Participations: Journal of Audience and Reception Studies*, 12(2), 197–217.
- [8]. Hampton, D. R. (2015). Slashy rotten pervs: Transnational Sherlock fangirls and the politics of pathologization. *Society for Cinema and Media Studies Conference*, Montreal, QC: Canada.
- [9]. Busse, K., & Gray, J. (2014). Fan cultures and fan communities. In Nightingale, V. (Ed.), *The handbook of media audiences* (pp. 425–443). Malden, MA: Wiley-Blackwell.
- [10]. Ford, S. (2014). Fan studies: Grappling with an 'undisciplined' discipline. *The Journal of Fandom Studies*, 2(1), 53–71.
- [11]. Chin, B., & Morimoto, L. (2013). Towards a theory of transcultural fandom. *Participations: Journal of Audience and Reception Studies*, 10(1), 92–108.
- [12]. Duffett, M. (2013). *Understanding fandom*. New York: Bloomsbury.
- [13]. Glasspool, L. (2012). From boys next door to boys' love: Gender performance in Japanese male idol media. In *Idols and celebrity in Japanese media culture* (pp. 113–130). London: Palgrave MacMillan.
- [14]. Jenkins, H. (2012). *Textual poachers: Television fans and participatory culture* (2nd ed.). London: Routledge.
- [15]. Bryman, A. (2012). *Social research methods* (4th ed.). Oxford: Oxford University Press.

- [16]. Esarey, A., & Xiao, Q. (2011). Digital communication and political change in China. *International Journal of Communication*, 5, 22.
- [17]. Galbraith, P. W. (2011). Fujoshi: Fantasy play and transgressive intimacy among “rotten girls” in contemporary Japan. *Signs: Journal of Women in Culture and Society*, 37(1), 211–232.
- [18]. Hine, C. (2011). Towards ethnography of television on the internet: A mobile strategy for exploring mundane interpretive activities. *Media, Culture & Society*, 33(4), 567–582.
- [19]. Chin, B. L. (2010). From textual poachers to textual gifters: Exploring fan community and celebrity in the field of fan cultural production. Cardiff: Cardiff University.
- [20]. Caldwell, J. T. (2009). Cultures of production: Studying industry’s deep texts, reflexive rituals and managed self-disclosures. In Holt, J., & Perren, A. (Eds.), *Media industries: History, theory, and method* (pp. 199–212). Oxford: Wiley-Blackwell.
- [21]. Driscoll, C. (2008). This is not a blog: Gender, intimacy, and community. *Feminist Media Studies*, 8(2), 198–201.
- [22]. De Kloet, J., & Van Zoonen, L. (2007). Fan culture: Performing difference. In *Media Studies: Key issues and debates* (pp. 322–341). London: Bloomsbury.
- [23]. Busse, K. (2006). My life is a WIP on my LJ: Slashing the slasher and the reality of celebrity and internet performances. In Hellekson, K., & Busse, K. (Eds.), *Fan fiction and fan communities in the age of the internet* (pp. 207–224). Jefferson, NC: McFarland Press.
- [24]. Bury, R. (2005). *Cyberspaces of their own: Female fandoms online*. New York: Peter Lang.
- [25]. Hills, M. (2002). *Fan cultures*. Sussex: Psychology Press.

Media Optimization for Maximum Azoreductase Enzyme Azo-LM1 Production by *Lysinibacillus macrolides* LMG 16474

Mr. Mayur J. Thakare¹, Dr. A. M. Garode²

¹Department of Microbiology, Shri Dnyaneshwar Maskuji Burungale Science and Arts College, Shegaon, Dist. Buldhana-444203, Maharashtra, India

²Ex. Professor and Head, Department of Microbiology, Shri Shivaji Science & Arts College Chikhli, Dist. Buldhana, Maharashtra, India

ARTICLE INFO

Article History:

Accepted : 01 Jan 2025

Published : 10 Jan 2025

Publication Issue :

Volume 12, Issue 7

January-February-2025

Page Number :

615-620

ABSTRACT

The different dyes used in the textile industry are mostly synthetic in origin and contain chemically complicated aromatic molecular structures that make them more persistent, difficult to decompose, and toxic to all living things. About 12–16% of all dyes used in the industry are released into the effluent because of the comparatively low degree of dye fiber attachment during fiber processing with dye molecules. It becomes necessary to degrade them, using a cost effective way. In this research we have used azoreductase for the same. Here Azoreductase Enzyme Azo-LM1 was obtained from *Lysinibacillus macrolides* LMG 16474 and media was optimized for carbon, nitrogen and dye substrate to get higher activity of the enzyme. For carbon source glucose was best carbon source with at 0.209 ± 0.06 mM/min/mg and yeast extract, the highest activity of 0.218 ± 0.057 mM/min/mg. for dye as substrates, Acid Orange 7 had the highest O.D. and the highest specific activity (0.423 ± 0.018 mM/min/mg).

Keywords: Azoreductase, enzyme activity, textile dyes

I. INTRODUCTION

Any undesired changes to the environment's physical, chemical, or biological components brought on by pollutants are referred to as environmental pollution. The substances created by humans that harm the environment the most are known as pollutants. They could negatively impact the ecology in both direct and indirect ways.

Among the several forms of pollution that are believed to be most challenging to control are soil and water contamination. Businesses that manufacture textiles, dyes, printing, medicines, paper, leather, food, mining, tanneries, and petroleum products are among the many that usually release these pollutants into the

environment. Additionally, one of the main sources of pollution that endangers the environment is the wastewater from different dye and dyeing intermediate industries, which contains toxic coloring ingredients. According to Manikandan et al. (2012) and Joshi et al. (2013), the different dyes used in the textile industry are mostly synthetic in origin and contain chemically complicated aromatic molecular structures that make them more persistent, difficult to decompose, and toxic to all living things. About 12–16% of all dyes used in the industry are released into the effluent because of the comparatively low degree of dye fiber attachment during fiber processing with dye molecules (Tripathi and Srivastava, 2011). Over 10,000 synthetic dyes are thought to be commercially accessible, and azo dyes make up about 70% of all dyes generated each year (Aswathi and Prakash, 2012). This makes them the most important category of synthetic dyes released and the largest dye group employed in the dyeing process (Pandey and Dubey, 2012; Kant, 2012).

Azo dyes are inert compounds that do not decompose in the environment, making them xenobiotics. In order to purify textile waste water, a number of chemical and physical methods have been used; unfortunately, these methods are very costly and cause secondary contamination. Over the past ten years, it has been demonstrated that a broad variety of bacteria, fungi, algae, lichen, plants, and their consortia may degrade hazardous dyes with various structural variations (Parshetti et al., 2007; Kalyani et al., 2009; Kulkarni et al., 2014; Lade et al., 2012). Although there have been numerous studies on the topic, more research is still needed to find innovative bacteria that can destroy a wide spectrum of hues.

Because of their short life cycles and versatility over a variety of substrates, scientists are considering bacteria as one of the potential biological systems for dye decolorization. Most dye decolorization researchers have grown bacteria in specific growth media, such as nutrient broth, which is not feasible to use on a large scale. To promote bacterial growth and make them easily accessible and reasonably priced, it is essential to investigate different carbon-nitrogen sources (Kadam et al., 2011). Salinity, temperature, pH, and other environmental parameters all have an impact on how contaminants biodegrade in natural ecosystems. In order to ascertain the efficacy of bacterial enzymes for the best degradation, it is necessary to look into these features (Ganesh et al. 1994).

This study examines the effects of various substrates for azoreductase using various dyes as substrates after optimizing the carbon and nitrogen source for effective azoreductase activity. Ion-exchange and molecular exclusion chromatography were used to further purify the enzyme after it had been extracted using the ammonium sulphate technique. A protein molecular ladder was then used to determine the molecular weight of the purified azoreductase. Finally, the pure enzyme was employed to investigate the characteristics of the enzyme, namely the impact of temperature and pH on enzyme activity.

II. MATERIALS AND METHODS

2.1. Carbon source optimization for more azoreductase activity

Six carbon sources—glucose, maltose, fructose, sucrose, lactose, and starch— were chosen in order to examine how carbon sources affected azoreductase activity with 5% inoculum of *Lysinibacillus macrolides*. Methyl Red dye stock (100 mg/ml) was added to the 100 ml Basal Mineral Salt Medium after the inoculation. Each carbon source was added to the medium at a rate of 1% (10gm/L). Following incubating this medium for 24 hours, a cell-free extract was prepared, and the activity of the azoreductase enzyme was measured.

2.2. Nitrogen source optimization for more azoreductase activity

Three organic and seven inorganic nitrogen sources—peptone, yeast extract, urea, ammonium sulphate, potassium sulphate, ammonium nitrate, ammonium dihydrogen phosphate, calcium nitrate, sodium nitrate, and

ammonium ceric nitrate— were selected in order to assess the impact of nitrogen sources on azoreductase activity.

2.3. Effect of different substrates as dye for azoreductase activity:

The culture of bacteria was inoculated in various dye media to investigate the impact of substrates on the enzyme activity. Here are the following: Basic Red 18, Congo Red, Methyl Red, Acid Orange 7, Acid Black 210, Amaranth, Sunset Yellow, Azorubine, Ponceau, Tartrazine, Allura Red, Azo Violet, and Sudan Red 7B.

III.RESULTS

3.1. Carbon source optimization for more azoreductase activity

To observe the impact of carbon on azoreductase enzyme activity, six carbon sources were used, as shown in figure 1. It indicates that sucrose had the lowest specific activity, at 0.067 ± 0.016 mM/min/mg, whereas glucose had the highest, at 0.209 ± 0.06 mM/min/mg. The proportion of decolorization varies slightly with further concentration increases when a certain ideal glucose concentration is reached. This might be as a result of bacteria using solely glucose instead of the intricately organized dye molecule at greater glucose concentrations (Kapdan et al., 2000).

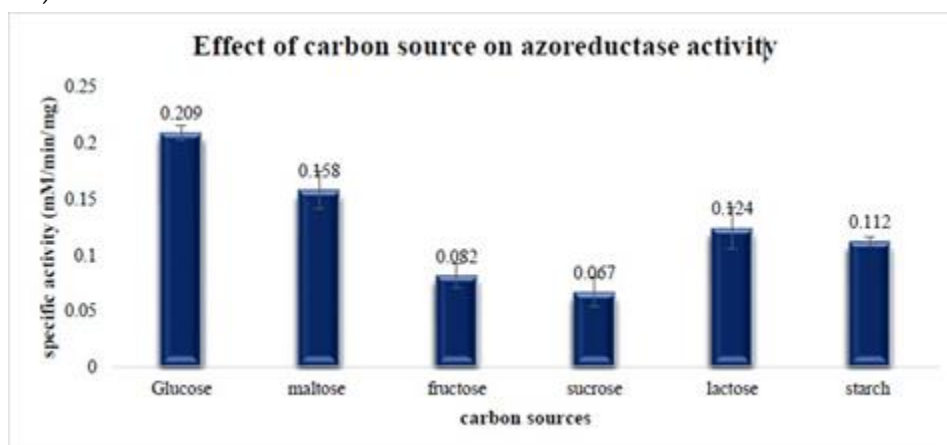


Figure 1: carbon source optimization for azoreductase activity

3.2. Nitrogen source optimization for more azoreductase activity

Following a review of the literature, ten different nitrogen sources were selected, and the effects of each source on MR degradation were examined using *L.macroides* LMG 16474 (Figure 2). With yeast extract, the highest activity of 0.218 ± 0.057 mM/min/mg was discovered. Moderate activity levels of 0.109 ± 0.016 mM/min/mg, 0.08 ± 0.012 mM/min/mg, 0.067 ± 0.008 mM/min/mg, and 0.124 ± 0.003 mM/min/mg were demonstrated using peptone, urea, ammonium sulfate, and potassium sulfate, respectively. The least active, essentially non-existent, were the nitrogen nitrate salts. The activity was low while using nitrate as a nitrogen source because the bacteria may use it as a last-resort electron acceptor.

Rajendran et al. (2021) carried out a similar experiment to examine the effects of four nitrogen sources— ammonium sulphate, peptone, tryptone, urea, and yeast extract—on the percentage dye decolorization.

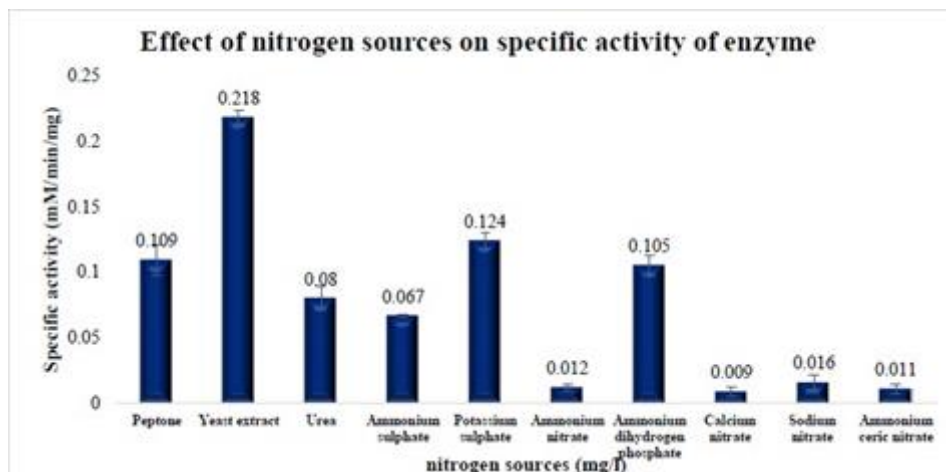


Figure 2: Nitrogen source optimization for azoreductase activity

3.3. Effect of different substrates as dye for azoreductase activity

Fourteen dyes were chosen to investigate the impact of various substrates on azoreductase activity: Sunset Yellow, Amaranth, Azorubine, Ponceau, Tartrazine, Allura Red, Azo Violet, Arylide Yellow, Basic Red 18, Congo Red, Methyl Red, Acid Orange 7, Acid Black 210, and Sudan Red 7B. The activity of azoreductase is shown in Figure 3 when all dyes are present and at the same concentration.

Additionally, the growth of bacteria in the dye's presence was examined in terms of optical density. It was evident that Acid Orange 7 had the highest O.D. and the highest specific activity (0.423 ± 0.018 mM/min/mg), whereas Basic Red 18 had the second-highest specific activity (0.342 ± 0.019 mM/min/mg). A few dyes, specifically Ponceau and Amaranth, followed by Azorubine, Tartrazine, and Allura Red, caused very little development in *L. macroides*, which in turn resulted in very little activity.

This can be the result of the dye having a harmful effect on the microorganisms. The dye's molecular complexity and bacterial toxicity are thought to be crucial in this situation (Zahran et al., 2019).

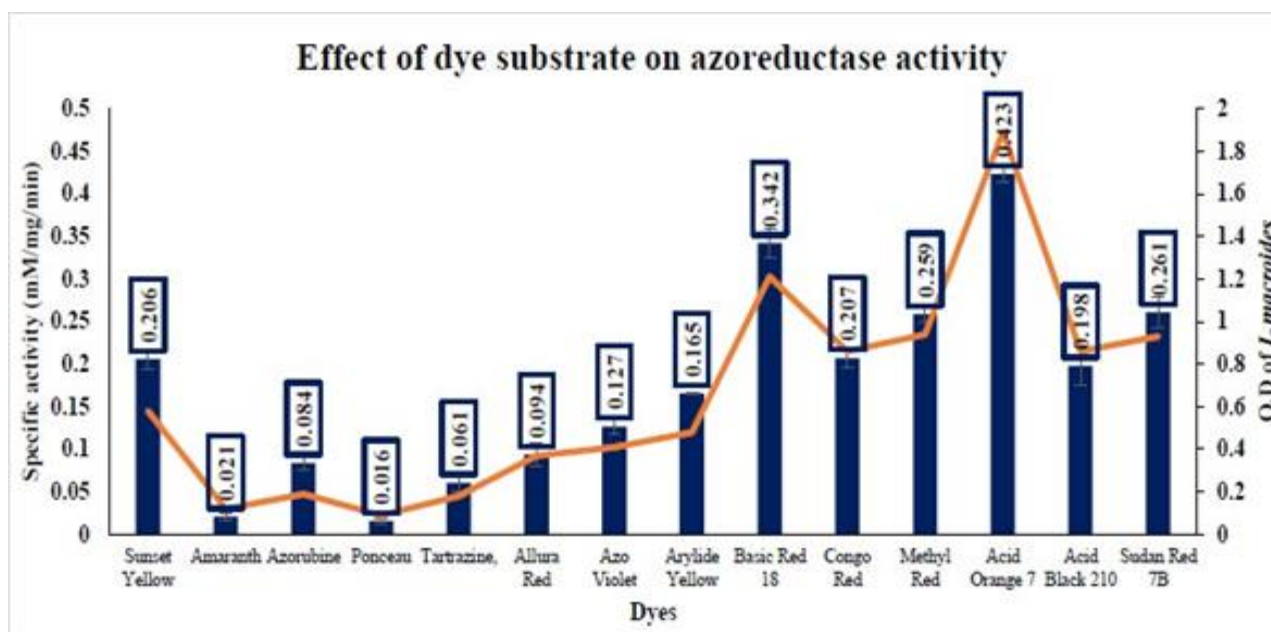


Figure 3: optimization of substrates as dye for azoreductase activity

IV. CONCLUSION

Using optimization process the activity of the azoreductase has been increased.

V. REFERENCES

- [1]. Acuner, E., & Dilek, F. B. (2004). Treatment of tectilon yellow 2G by *Chlorella vulgaris*. *Process Biochemistry*, 39(5), 623-631.
- [2]. Adrosko, Rita J. (1971). *Natural Dyes and Home Dyeing*. Dover Publications: New York.
- [3]. Aftab, U., Khan, M. R., Mahfooz, M., Ali, M., Aslam, S. H., & Rehman, A. (2011). Decolourization and degradation of textile azo dyes by *Corynebacterium* sp. isolated from industrial effluent. *Pakistan Journal of Zoology*, 43(1), 1-8.
- [4]. Aghaie-Khouzani, M., Forootanfar, H., Moshfegh, M., Khoshayand, M. R., & Faramarzi, M. A. (2012). Decolorization of some synthetic dyes using optimized culture broth of laccase producing ascomycete *Paraconiothyrium variabile*. *Biochemical Engineering Journal*, 60, 9-15.
- [5]. Asses, N., Ayed, L., Hkiri, N., & Hamdi, M. (2018). Congo red decolorization and detoxification by *Aspergillus niger*: removal mechanisms and dye degradation pathway. *BioMed Research International*, 2018. 1-9
- [6]. Attia, Y.A., Samer, M., Mohamed, M.S.M. et al. (2022). Nanocoating of microbial fuel cell electrodes for enhancing bioelectricity generation from wastewater. *Biomass Conversion and Biorefinary*.
- [7]. Bhatt, N., Patel, K. C., Keharia, H., & Madamwar, D. (2005). Decolorization of diazo- dye reactive blue 172 by *Pseudomonas aeruginosa* NBAR12. *Journal of Basic Microbiology: An International Journal on Biochemistry, Physiology, Genetics, Morphology, and Ecology of Microorganisms*, 45(6), 407-418.
- [8]. Bhatt, N., Sapna, T., & Kshama, B. (2012). Biodegradation of reactive red M8B by bacterial consortium SpNb 1. *Indian Journal of Science and Technology*, 5(7), 3047- 3053
- [9]. Bholay, A. D., Sanjay, D. S., & Wilson, J. A. (2018). Immobilized Polyextremophilic α -Amylase of *Bacillus mycoides* for Citric Acid Production Using Starch. *International Journal of Current Microbiology and Applied Sciences*, 7(3), 3055-3065.
- [10]. Cheriaa, J., & Bakhrouf, A. (2009). Triphenylmethanes, malachite green and crystal violet dyes decolourisation by *Sphingomonas paucimobilis*. *Annals of Microbiology*, 59, 57-61.
- [11]. Chimezie, J. O., Thomas, S. (2011). Bioremediation and Detoxification of synthetic wastewater containing triarylmethane dyes by *Aeromonas hydrophila* isolated from industrial effluent. *Biotechnology Research International*, 1-11
- [12]. Dicle, A. R. A. R., Doganli, G., Sensoy, T., Bozbeyoglu, N., & Dogan, N. (2014). Investigation of Decolorization of Reactive Violet 5R and Remazol Brilliant Orange 3R. *Journal of Applied Biological Sciences*, 8(1), 68-72.
- [13]. Dodoo-Arhin, D., Asiedu, T., Agyei-Tuffour, B., Nyankson, E., Obada, D., & Mwabora, J. M. (2021). Photocatalytic degradation of Rhodamine dyes using zinc oxide nanoparticles. *Materials Today: Proceedings*, 38, 809-815.
- [14]. Fathi, Z., & Keshmirizadeh, E. (2015). Use of Fenton Reagent as Advanced Oxidative Process for Removal of Basic and Acid Red Dyes from Aqueous Solutions. *Journal of Applied Chemical Research*. 9(3)7-19
- [15]. Forgacs, E., Cserh ti, T., & Oros, G. (2004). Removal of synthetic dyes from wastewaters: a review. *Environment International*, 30(7), 953-971.

- [16]. Franciscon, E., Grossman, M. J., Paschoal, J. A. R., Reyes, F. G. R., & Durrant, L. R. (2012). Decolorization and biodegradation of reactive sulfonated azo dyes by a newly isolated *Brevibacterium* sp. strain VN-15. *Springer Plus*, 1(1), 1-10.
- [17]. Hassan, M. M., & Hawkyard, C. J. (2002). Decolourisation of aqueous dyes by sequential oxidation treatment with ozone and Fenton's reagent. *Journal of Chemical Technology & Biotechnology: International Research in Process, Environmental & Clean Technology*, 77(7), 834-841.
- [18]. Jadhav, J. P., & Govindwar, S. P. (2006). Biotransformation of malachite green by *Saccharomyces cerevisiae* MTCC 463. *Yeast*, 23(4), 315-323.
- [19]. Jadhav, J. P., Parshetti, G. K., Kalme, S. D., & Govindwar, S. P. (2007). Decolourization of azo dye methyl red by *Saccharomyces cerevisiae* MTCC 463. *Chemosphere*, 68(2), 394-400.

Diversity of Phytoplankton and Zooplankton of Nilona Dam Dist. Yavatmal

Ninad Dharkar¹, M.A.Shahezad¹, Kisor Suradkar², Sangita Khadse¹

¹S.P.M.Science And Gilani Arts Commerce College Ghatanji, Dist. Yavataml, Maharashtra, India

²Indira Mahavidyalaya Kalamb, Dist Yavatmal, Maharashtra, India

ARTICLE INFO

Article History:

Accepted : 01 Jan 2025

Published : 10 Jan 2025

Publication Issue :

Volume 12, Issue 7

January-February-2025

Page Number :

621-624

ABSTRACT

The present communication deals with the variations of phytoplankton and zooplankton in the Nilona dam of Yavatmal district .The Godhni area has selected for the sampling .The samples were collected during the period of one month (July 2024 to August 2024).The samples under study were evaluated to study the diversity of phytoplankton and zooplankton.Phytoplankton diversity was shown in the four groups like Chlorophyceae, Cyanophyceae, Euglenophyceae, Bacillariophyceae .Chlorophyceae were dominant as compare to the other reported groups. Zooplanktons shows the variations in groups Viz.Cladocers, Protozoa, Rotifera, Nematoda. The members of Rotifers were dominant over other reported groups.

Keywords: Phytoplankton, Zooplankton Nilona dam.

I. INTRODUCTION

Plankton are the group of free floating microorganism. They move at the mercy of currents of winds as well as water. Phytoplankton are chlorophyll bearing suspended microscopic organism mainly algae. Phytoplankton plays an important role in aquatic ecosystem for development and growth of zooplankton and appeared as a paradox(Hutchinson,1967). Phytoplanktons liberate oxygen during photosynthesis and aid in energy exchange process (Khan 2003)Phytoplankton forms lowest trophic level in the food chain of fresh water ecosystem(Manoj Kumar and Khare,2015). The number and species of phytoplankton determine the water quality. Diversity is the important ecological indicator to assess the quality of water. Several researchers have been worked on this issue(Khanna et al .,2012 Kadam et al.,2014, Budhlani and Musaddiq 2014,Belkhode P.P. and Shrikant Sitre 2016, Rawat and Seema Trivedi, 2018. Imran Mithani and Dahegaonkar NR (2020). The Nilona dam wardha is a major water source for Yavatmal district .Therefore the study undertaken was to analyse the phytoplankton diversity in Nilona Dam .

II. MATERIAL AND METHODS

The investigation were carried out during (July2024 to August 2024).Samples were collected from two sampling station at Godhni and Sawarghdh region that is back water of the dam(Fig.1), at morning between 8.0A.M To 10.0A.M by using plankton net and bottles and collected samples were shifted into the liter plastic bottles. The collected samples were allowed to centrifuge to concentrate and made up to 100ml after removing the surface water in the centrifuge tube. The population of plankton present in the centrifuge tube were transfer to other bottle and preserved in Lugols Iodine solution of further investigation (Sabita Kumara 2018).Take a drop of well mixed water by slightly shaking on clean slide place the cover slip on it under the proper magnification slides were observed and samples were identified by the relevant literature(Adoni,1985and Batish,1992).



Fig-1

III.RESULT AND DISCUSSION

The sampling sites shows diversity phytoplankton belongs to 20species of 7 genera various groups like Chlorophyceae(10 species of 6genera),Cyanophyceae (05species 2 genera),Euglenophyceae(2 species), Bacillariophyceae (3 species 1genera). *Oedogonium* and *Spirogyra* were dominant among another member of Chlorophyceae. The zooplankton in the area investigated shows 11 species and 7 genera of various groups Cladocers (3 species 2 genera), Protozoa(4species 2genera),Rotifers(6species 3genera),Nematoda(4species 2 genera).Among these Rotifers were dominant over all reported groups. Few genera act as bioindicators of organic pollution. Majority of protozoans were found in the interval of June and July. The number of planktons was more in summer and gradually minimise in rainy season.

Reported Phytoplanktons

Chlorophyceae	
Genera	Species
<i>Ankistrodesmus</i>	<i>Falcatus</i>
<i>Chlorella</i>	<i>Vulgaris</i>
<i>Chlorococcum</i>	<i>Infusium</i>
<i>Cladospora</i>	<i>Fracta</i>
<i>Cosmarium</i>	<i>Tenue</i>
<i>Hydrodictyon</i>	<i>Reticulatum</i>
<i>Oedogonium</i>	<i>Leave,plagiostomum, tapeinosporium,pisanum(Shiv kumar Rai 2012)</i>
<i>Spirogyra</i>	<i>chungkingensis,comdensata,longata,mirabilis</i>
Cyanophyceae	
<i>Anabaena</i>	<i>Fertilissima</i>
<i>Lyngbya</i>	<i>Magnifica</i>
<i>Nostoc</i>	<i>Sp.</i>
<i>Ocillatoria</i>	<i>Limosa</i>
	<i>Anacystis,botrycoccus chrococcus phormidi,rivularia</i>
Euglenophyceae	
	<i>acus,viridis,caudatus,gracilis</i>
Bacillariophyceae	
<i>Navicula</i>	<i>Viridula</i>
<i>Synedra</i>	<i>Ulna</i>
	<i>Diatom sp.amphore.stauronesis,cyclotella</i>

Recorded Zooplanktons

Cladocera	
Genera	Species
<i>Bosmina</i>	<i>Longirostirs</i>
<i>Daphnia</i>	<i>Carinata</i>
Protozoa	
<i>Arcella</i>	<i>arenaria, conica,dentata,rota</i>
<i>Balantidium</i>	<i>Coli</i>
Rotifera	
<i>Asplanchna</i>	<i>Intermedia</i>
Nematoda	
	<i>Salasi sp.</i>
	<i>Javanica ,hapla,americanus,ascaris</i>
Ostertamia, Tylenchus(L.B.Chanu et al 2014)	

The present communication reveals that the water of Nilona dam was found to be more polluted. During this period not safe for drinking because most of the people in the sawargadh village wash their vehicle and pet animals in back water and most of the industrial pollutants mix in the dam.

IV. REFERENCES

- [1]. Adoni,A.D.(1985).Work book on limnology,Pratibha Publications,Sagar (M.P.).
- [2]. Battish,S.K.(1992).Fresh water zooplankton of India.Oxford and IBM publication.
- [3]. Belkode., P.Pand Shrikant Sitre(2016).Phytoplankton Diversity of Dham River in Wardh District of Maharashtra State.Indian Journal of Fundamental and Applied life Sciences.Vol.6(1);10-13
- [4]. Budhlani .,G.N.and M.Musaddiq(2014).Water quality and pollution status of Wardha river (Kaundanyapur)from Amravati district(M.S.)India.int.J.of Res.In Bio.Sci.Agri.nad Tech.75-81.
- [5]. Hutchinson GE (1967).A treatise on Limnology.Vol.2 Introduction to lake biology and Limn plankton.John Willey of and Sons,New York.p.115.
- [6]. Imran Mithani and Dahegaonkar NR(2020).Studies on phytoplankton diversity in river Wardha near, Ballarpur, Maharashtra, India. Int. Res. J. of Science & Engineering, Special Issue A7: 467-470.
- [7]. Kadam,S.U.,Kadam,S.S and Babar,M.(2014).Phytoplankton diversity of reservoirs in Parbhani district Maharashtra,India,Int.J.Curr.Microbio.App.Sci.,Vol.3(8):459-466.
- [8]. Khan, T. A. (2003). Limnology of four saline lakes in Western Victoria, Australia. Limnologica, 33: 327-339
- [9]. Khanna,D.R.,Bhutiani,R.,Matta,G.,Singh,V.and Bhadauriya,G.(2012).Study of planktonic diversity of river Ganga from Devprayag to Roorkee,Uttarakhand (India).Env.Cons.Jou.,13(1&2).211-217.
- [10]. Loukrakpam Bina Chanu,N.Mohilal Meitei and M.,anjur Shah.(2014).Two new species of soil nematodes from Manipur,India.Journal of Parasitic Dieases.40,674-678.
- [11]. Manoj Kumar and P.K.Khare(2015).Diversity of Plankton and their seasonal variation of density in the Yamuna river at Kalpi,District Jalaun(U.P)India.Journal of Global Biosciences.Vol.4(7).2720-2729
- [12]. Rawat, R. and Trivedi, S. (2018). Seasonal diversity of phytoplankton in relation to seasonal changes in physico-chemical parameters of Khedi Kalan station of Dholawad Dam of Ratlam District, M. P. Int. J. Pure App. Biosci., 6: 448-454.
- [13]. Shiva Kumar Rai.,(2012).Five new species of Oedogonium Link.(Chlorophyta),a freshwater filamentous algae from Nepal.Nepolese journal of Biosciences 2:17-23.

Synthesis, Characterization and Biological Evaluation of 4-(5-Chloro-8-Hydroxynaphthalen-2-Yl)-6-(3, 4-Dimethoxyphenyl)-5, 6-Dihydropyrimidin-2(1h)-One

Mr. Nilesh S. Padole

Head and Assistant Professor, Department of Chemistry, Vinayak Vidnyan Mahavidyalaya, Nandgaon
Khandeshwar, Maharashtra, India

ARTICLE INFO

Article History:

Accepted : 01 Jan 2025

Published : 10 Jan 2025

Publication Issue :

Volume 12, Issue 7

January-February-2025

Page Number :

625-629

ABSTRACT

1-(4-Chloro-1-hydroxynaphthalen-2-yl)-ethan-1-one was prepared by refluxing 4-chloronaphthalen-1-ol with glacial acetic acid in presence of fused $ZnCl_2$. By condensing 1-(4-chloro-1-hydroxynaphthalen-2-yl)-ethan-1-ones with 3,4-dimethoxy benzaldehyde, to prepared by 1-(4-chloro-1-hydroxynaphthalen-2-yl)-3-(3,4-dimethoxy phenyl)-prop-2-en-1-one was synthesized. 1-(4-chloro-1-hydroxynaphthalen-2-yl)-3-(3,4-dimethoxy phenyl)-prop-2-en-1-one, urea and concentrated HCl in DMF were added and refluxed. Cool the compound and decomposed in crushed ice. Further it is treated with cold NH_4OH solution to obtain titled compounds. The compounds thus synthesized have been characterized by physical properties and spectral analysis. All these titled synthesized compounds have been screened for antimicrobial studies and are found to possess excellent antimicrobial activities.

Keywords: Antimicrobial Activities, Cold NH_4OH Solution, Conc. HCl in DMF.

I. INTRODUCTION

Dihydropyrimidin-2(1H)-one is a novel hetero-cyclic compound with 2 Nitrogen atoms with pyrimidine ring in the six-member ring. The biological and pharmacological activities are best suited especially with Nitrogen containing heterocycles with pyrimidine ring nucleus. The industries have wide scope and application among the mentioned heterocycle nucleus and proven to be more beneficial and economical for the society. They also play an important role in pharmacophore in the field of organic chemistry and drug designing. In this review, I used to explore the 3,4-dihydropyrimidine (DHPM) ring. Basically, it is a selective review on dihydropyrimidinones. Literature of last two decades is incorporated in this review. [1]

Dihydropyrimidin-2(1H)-ones (DHPMs) via three-component condensation reaction of an aromatic aldehyde, urea, and ethyl acetoacetate. [2,4]. Dihydropyrimidinones (DHPMs) and their derivatives occupy a prominent place; these cores are of immense biological importance; play an important role as essential building blocks in the synthesis of DNA and RNA [5]. World Health Organization (WHO) announced a global priority for the development of new drugs, particularly for antibiotic-resistant infections [6]. This has increased the scientist interest in bioactive nitrogen-containing heterocyclic substances such as 3,4-dihydro-pyrimidin-2 (1H)-ones, or just dihydropyrimidinones (DHPMs). compounds were synthesized by the Italian chemist Pietro Biginelli in 1893[6].

Because of multi-facet importance in medicinal properties, synthesis of the dihydropyridine and their derivatives shown great importance. Many reports exploring in Vivo and in Vitro dihydropyrimidine-2-one derivatives show variety of pharmacological activities such as active and safe tumor anti-initiating and multi-potent blocking agent [7], anxiolytic [8], antihypertensive agents [9], anticonvulsant [10], anticancer [11], analgesic activities [12]. Their efforts are quite significant in literature hence considering the scope of dihydropyrimidine derivatives we have synthesized novel 4-(4-chloro-1-hydroxynaphthalen-2-yl)-6-(3,4-dimethoxy phenyl)-5,6-dihydropyrimidine-2(1h)-one from 4-chloronaphthalen-1-ol and studied for their biological activities.

II. METHODS AND MATERIAL

Synthesis of 1-(4-Chloro-1-hydroxynaphthalen-2-yl)-ethan-1-one.

1-(4-Chloro-1-hydroxynaphthalen-2-yl) ethan-1-one was prepared by modified Nenck's method in which 4-chloro-naphthalen-1-ol was refluxed with glacial acetic acid in presence of fused ZnCl_2 .

Synthesis of 1-(4-Chloro-1-hydroxynaphthalen-2-yl)-3-(3,4-dimethoxy phenyl)-prop-2-en-1-one.

1-(4-Chloro-1-hydroxynaphthalen-2-yl)-3-(3,4-dimethoxy phenyl)-prop-2-en-1-one was synthesized from 1-(4-Chloro-1-hydroxynaphthalen-2-yl) ethan-1-one by condensing it with 3,4-dimethoxy benzaldehyde were added in ethanol solvent and KOH mixture.

Synthesis of 4-(4-Chloro-1-hydroxy naphthalen-2-yl)-6-(3,4-dimethoxy phenyl)-5,6-dihydropyrimidine-2(1H)-one.

4-(4-Chloro-1-hydroxy naphthalen-2-yl)-6-(3,4-dimethoxy phenyl)-5,6-dihydropyrimidine-2(1H)-one was prepared from 1-(4-Chloro-1-hydroxynaphthalen-2-yl)-3-(3,4-dimethoxy phenyl)-prop-2-en-1-one was reflux with urea and concentrated HCl in DMF. It was then treated with cold NH_4OH

SCHEME: -

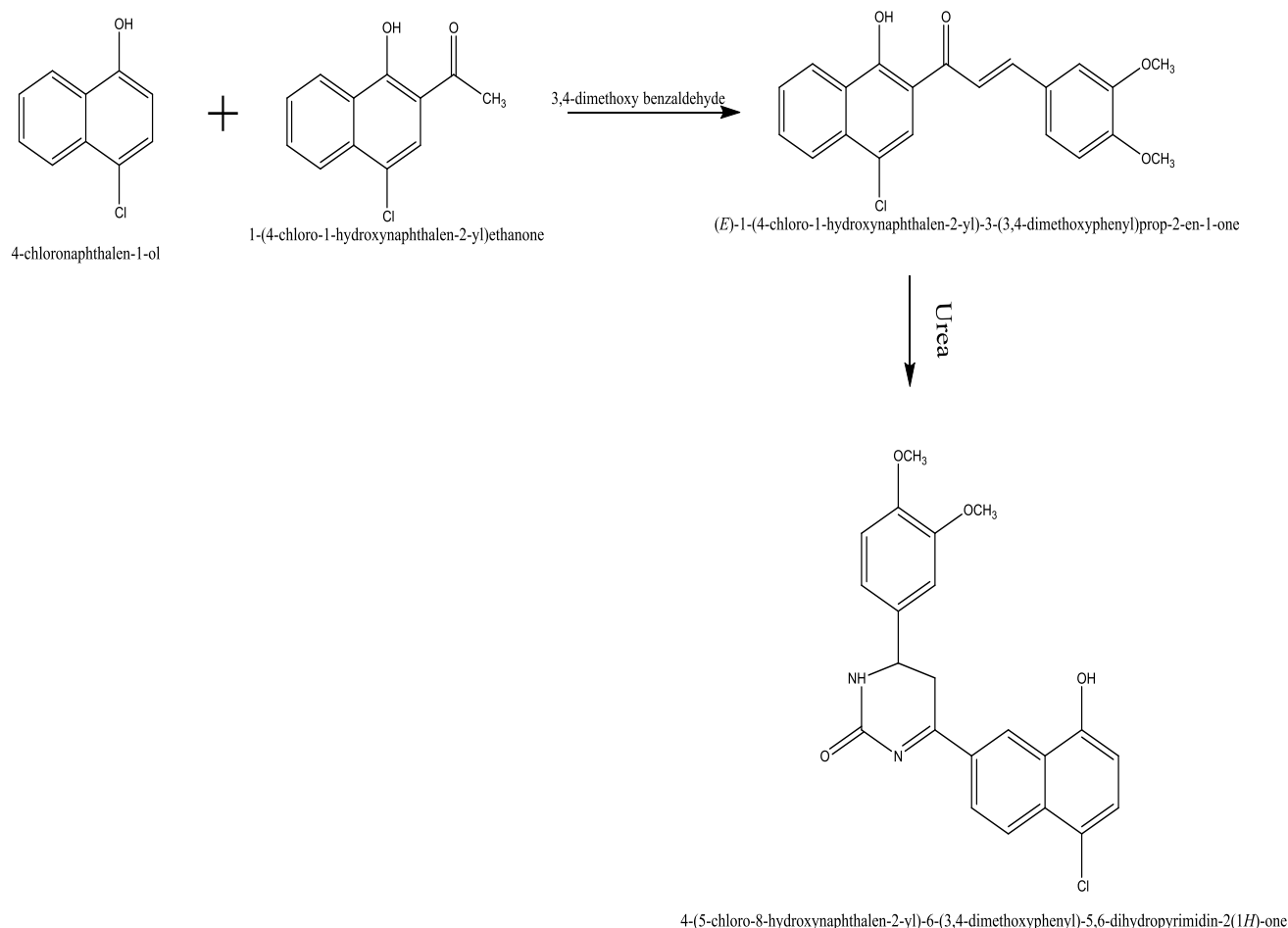


Table 1. PHYSICAL DATA OF SYNTHESIZED COMPOUNDS

Sr.no	Compound no	R1	R2	Molecular formula	Melting Point $^{\circ}\text{C}$	% Yield	% Nitrogen		R.F Value
							Found	Calculated	
1	1	-OCH ₃	-H	C ₂₁ H ₁₇ N ₂ O ₃ Cl	2550C	57%	6.59	6.63	0.54
2	2	-OCH ₃	-OCH ₃	C ₂₂ H ₁₉ N ₂ O ₄ Cl	2200C	54%	6.21	6.24	0.63
3	3	-H	-OH	C ₂₀ H ₁₆ N ₂ OCl	2230C	49%	6.55	6.80	0.54
4	4	-OH	-H	C ₁₇ H ₁₆ N ₂ O ₂ Cl	2600C	63%	5.74	5.83	0.54

SPECTRAL ANALYSIS: -

IR(ν_{max}) (cm^{-1}): 1630 (C=O, str), 3320 (NH, str), 1567 (C=N), 1154(C-O-C),760(monosubstituted Benzene

NMR (δ ppm): 1.3-1. (m, 2H, -CH₂ of pyrimidine), 6.2 (s, 1H, -OH), 3.72 (s, 3H, -OCH₃), 2.42 (s, 3H, CH₃),

ANTIMICROBIAL STUDIES: -

All above synthesized 4-(4-Chloro-1-hydroxy naphthalen-2-yl)-6-(3,4-dimethoxy phenyl)-5,6-dihydropyrimidine-2(1H)-one has been studied for their antimicrobial activity against Escherichia coli, Proteus mirabilis, Staphylococcus aureus, Pseudomonas aeruginosa. The culture of each species was incubated at 370°C

and the zone of inhibition was measured after 24 hr. Results are tabulated in Table. Most of these compounds were found active

Table 2. Antimicrobial Activity

Sr.no	Compound Number	Antimicrobial Activity			
		E-coli	Proteus mirabilis	Staphylococcus aureus	Pseudomonas aeruginosa
1	1	18	18	17	12
2	2	15	11	19	15
3	3	16	13	16	18
4	4	14	15	13	14

Strongly active, range 15-19 Weakly active, range 7-10 mm, moderately active, range 11-14mm, Inactive,

III.CONCLUSION

Thus, from the above antimicrobial results, it was pointed out that these heterocyclic compounds were found effective against Escherichia coli, Proteus mirabilis, Staphylococcus aureus, Pseudomonas aeruginosa. The diseases caused by these pathogens can be easily treated by the help of synthesized heterocyclic compounds.

IV. REFERENCES

- [1]. Kappe C. Oliverr; Recent Advances in the Biginelli Dihydropyrimidine Synthesis. New Tricks from an Old Dog. Accounts of Chemical Research. 2001; 33(12):879-88.
- [2]. Rajabi F et al; Efficient Synthesis of Dihydropyrimidine Using a Highly Ordered Mesoporous Functionalized Pyridinium Organosilica. Catalyst. 2022; 12(3): 350.
- [3]. Varma Aman et al; Ammonium tetrafluoroborate: Novel Unprecedented Catalyst for the Synthesis of 3,4-dihydropyrimidin-2(1H) -ones through Biginelli Reaction. Chemistry Select. 2024; 9(8).
- [4]. Selvakumar K et al; Heteropoly acid supported on activated natural clay-catalyzed synthesis of 3,4-dihydropyrimidinones/thiones through Biginelli reaction under solvent-free conditions. Synthetic Communication. 2017; 48(2):1-10.
- [5]. Fauzi Ahmad, Saifudin Azis, Rullah Kamal. Synthesis of Dihydropyrimidinones (DHPM) Derivatives through a Multicomponent Reaction (MCR) and Their Biological Activity. J. med. chem. sci. 2023; 6(8):1810-1817.
- [6]. Pore Santosh B; Natural Surfactant Mediated Synthesis of 4-Aryl Substituted 3,4-Dihydropyrimidinones. Ajchem. 2023; 35(12):3037-3041.
- [7]. Adhikari Adithya et al; Synthesis, characterization and biological evaluation of dihydropyrimidine derivatives. Saudi Pharmaceutical Journal. 2012; 20(1): 75-79.
- [8]. Taviti Kumara S et al; Design, synthesis and biological Evaluation of novel chromones having 3,4-dihydropyrimidine-2(1H)-one core at C-8 in combination with triazoles: New glucosides inhibitors and anti-bacterial agents. Eur. J. Med. Chem. 2024; 12(1):100187.
- [9]. Beena K.P et al; Dihydropyrimidinones-A Versatile Scaffold with diverse Biological Activity. J. Pharm. Sci. & Res. 2016; 8(8): 741-746.

- [10]. Garg V. Jindal D. Singh R. Synthesis and Evaluation of antifungal activity of 4, 6- Diphenyl-3, 4- Dihydropyrimidine-2-(1h)-one derivatives. *tjpr.org*. 2020; 7(6): 8-12.
- [11]. Ravi kumar K, Harika V L, Shaik A B. Synthesis, characterization and biological evaluation 3,4- dihydropyrimidin-2(1H)-thione derivatives. *Arch.Appl. Sci. Res.* 2014; 6(6): 121-127.
- [12]. Sherekar V M. Padole N S. Kakade K P. Synthesis, Characterization and Biological Evaluation of 4-(4-chloro1-hydroxy naphthalen-2-yl)-6-(4- methoxy phenyl)-5,6- dihydropyrimidine-2(1h)-one). *Jetir*. 2022; 9(1): 15-19

Molecular Properties of Skeletal Muscle Protein of Vertebrates

Gajanan B. Santape

Department of Zoology, Rajarshee Shahu Science College Chandur Railway, Maharashtra, India

ARTICLE INFO

Article History:

Accepted : 01 Jan 2025

Published : 10 Jan 2025

Publication Issue :

Volume 12, Issue 7

January-February-2025

Page Number :

630-633

ABSTRACT

A comparative analysis of actin protein from striated muscle across five different animal species of vertebrates were conducted. In the present study electrophoretic analysis was carried out then amino acids sequences of striated muscle protein actin are obtained and aligned together by using Pep Tool and molecular properties were analyzed. The results of present study showed that the actin genes have undergone significant biochemical changes during evolution. These changes are reflected in addition and elimination of actin protein. The amino acid sequences of actin from fishes are distinct from those of other animal species indicating an independent evolution of actin in fishes. Thus during evolution of striated muscle, biochemical changes took place in actin. Secondly, these alterations in amino acids sequences might have taken place as a change in the bones to which these muscles are attached with respect to increase the functional efficiency for survival.

Keywords : actin, electrophoretic analysis amino acid sequences, molecular properties

I. INTRODUCTION

Proteins are the macromolecules and serve as diverse functions. characteristics, nature, and distinctiveness of the proteins give unique individuality to organism. The genes for actin and myosin are members of gene families that encode proteins that enable movement while actin and myosin are highly conserved across all animal species, other muscle proteins show more variability. The variations in an organism's proteins are the results of random DNA mutations within the encoding genes, which have occurred over thousands to millions of years. Each mutation may results in some kind of change in a protein

II. METHODOLOGY USED

Protein study by Pep tool and Block maker

For the molecular study of muscle proteins Electrophoretic analysis was done from five representative animals of Vertebrates from Class Fishes to Mammalia then amino acids sequences of striated muscle protein Actin are obtained by conducting a comprehensive search in NCBI sequence viewer version [2.0](#) (NCBI Home page INCBi Entrez), Then protein sequences are aligned together by using the Pep tool, 38 different molecular properties of muscle proteins are searched by using Pep tool version [2.0](#) are given in table.

Protein Statistics:

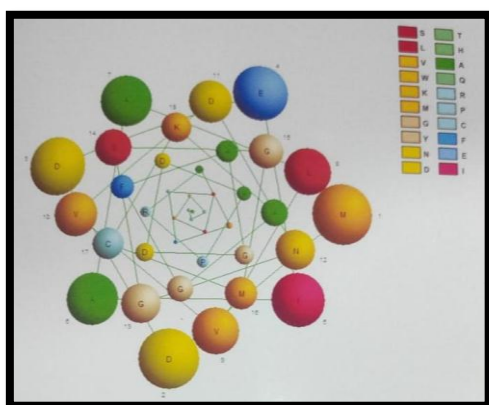
The statistical analysis reveals the details of various aspects of protein such as molecular weight, number of amino acids, hydrophobic and hydrophilic amino acids and their percentage, number of basic and acidic amino acids, helical wheel and beta staircase are searched. Structure are predicted and their motifs are searched using pep tool. The observations are as follows.

• Observation and Results

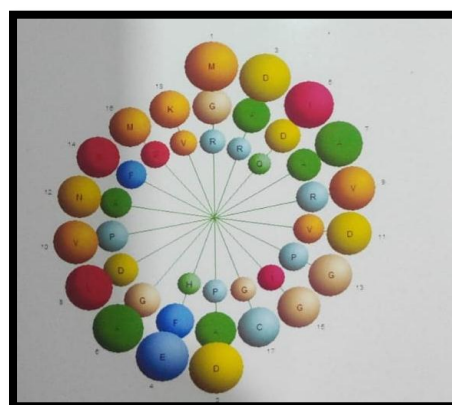
Sr.No	Parameter	Labeo Fishes	Rana Amphibia	Naja Reptilia	Gallus Aves	Rattus Mammalia
1	Molecular Weight	4271.830	19234.232	24743.268	10247.730	11013.583
2	Number of Amino Acids	41	171	220	91	97
3	Mean Amino Acid Weight	104.191	112.481	112.469	112.612	113.542
4	Average Hydrophobicity	-0.114634	-0.126316	-0.245	-0.408791	-0.281443
5	Ratio of hydrophilicity to hydrophobic	1.08987	1.10141	1.20165	1.35632	1.23968
6	Percentage of hydrophilic amino acids	43.9024	50.2924	50.0	49.4505	52.5773
7	Percentage of hydrophobic amino	56.0976	49.7076	50.0	50.5494	47.4227
8	Ratio of hydrophilic to % hydrophobic	0.782609	1.01176	1.0	0.978261	1.1087
9	Mean beta hydrophobic movement	0.1640	0.204664	0.204711	0.176754	0.184856
10	Mean alpha hydrophobic movement	0.161424	0.182873	0.176884	0.153965	0.169454
11	Number of basic amino acids	4	18	21	10	7
12	Number of acidic amino acids	6	22	2	12	12
13	Estimated pl for protein	5.5	6.2	5.8	6.2	5.8
14	Total linear charge density	0.292683	0.245614	0.25	0.263736	0.216495
15	Polar area of extended chain	2525.7	11098.8	14450.8	587.9	6100.2
16	Non polar area of extended chain	4235.0	19407.0	24812.9	10316.4	11283.3
17	Total area of extended chain	6760.7	30505.8	39263.7	16164.3	17383.5
18	Polar ASA of folded protein	861.687	2858.76	3572.78	1701.25	1737.41
19	Non polar ASA of folded protein	2004.69	5604.61	6569.71	3680.85	3931.03
20	ASA of folded protein	2866.37	8463.37	10142.5	5382.1	5668.44
21	Ratio of folded to extended area	0.453781	0.297367	0.277008	0.354997	0.347876
22	Buried polar area of folded protein	1228.14	7006.84	9263.62	3441.64	3737.44
23	Buried non polar area of FP	2140.46	12211.9	16145.2	5998.29	6513.83
24	Buried charge area of FP	140.358	800.781	1058.7	393.331	427.136

Sr.No	Parameter	Labeo Fishes	Rana Amphibia	Naja Reptilia	Gallus Aves	Rattus Mammalia
25	Total buried surface	3508.96	20019.5	26467.5	9833.26	10678.4
26	Total number of buried amino acids	3	44	65	15	17
27	Packing volume	4573.63	22932.5	29692.1	11906.1	12845.8
28	Packing volume	5010.5	22950.5	29493.9	12169.4	13141.9
29	Interior volume	3636.69	16735.2	21452.7	8844.75	9609.9
30	Exterior volume	1373.81	6215.34	8041.2	3324.65	3532.0
31	Partial specific volume	0.712188	0.727597	0.726063	0.723305	0.727362
32	Fisher volume ratio	0.377763	0.37139	0.374837	0.37589	0.367538
33	Fisher volume ratio	1.90747	0.853907	0.755201	1.18612	1.1455
34	Protein solubility	1.62691	1.49787	1.53571	1.54733	1.40219
35	Est.radius of folded protein	13.3618	21.5082	23.3926	17.4295	17.8045
36	RMS end to end	67.1565	137.15	155.563	100.05	103.296
37	Radius of gyration of ext.chain	27.4165	55.9911	63.5085	40.8452	42.1703
38	Solv.free energy of folding	-24.57	-153.27	-201.78	-74.07	-80.01

Actin properties in fishes are almost different from those seen in rest of the species. Those results indicate that actin evolved independently in teleost fishes. These observations are much more prominent with respect to number of amino acids, number of basic and acidic amino acids, polar area of extended chain, non polar area of extended chain, polar and non polar ASA of folded protein, ASA of folded protein, total number of buried amino acids, packing volume etc.



Helical Wheel of Actin of L.rohita



Beta Staircase of Actin from L.rohita

III.DISCUSSION AND CONCLUSION

Hightower and Meagher (1986) investigated the molecular evolution of actin genes comparing nucleotide and amino acid sequences of 20 actin genes. Nucleotide changes resulting in amino acids substitutions arranged from 3-7 for all pair wise comparisons of animal actin genes.

It has recently been claimed that certain amino acids in protein have been increasing in frequency (Jordan et al,2005; McDonald,2005) when this was analyzed in the present study, it was formed that during evolution of striated muscle actin protein from fish to mammals or even in the different animals of same group, amino acids

like threonine, tryptophan and tyrosine are gained in number than lost in protein proline, alanine, glutamic acid and glycine are lost than gained from the striated muscle proteins.

Thus during evolution of striated muscle, biochemical changes took place in actin, myosin, troponin and tropomyosin elimination of some amino acids and by addition of some amino acids. Secondly, these alterations in amino acids sequences might have taken place as a change in the bones to which these muscles are attached with respect to increase the functional efficiency for survival. The present results also indicate that the amino acids proline, alanine, glutamic acid and glycine are lost gradually from actin and myosin during evolution. The present electrophoretic technique of protein analysis is quite cheaper, time saving and more reliable to identify the animals.

IV. REFERENCES

- [1]. Bulbul, U. and Kutrup, B. (2007) : Comparison of skeletal muscle protein bands among five populations of *Bufo viridis* in Turkey by SDS. Page..Turk J. Zool 31,pp.419-422.
- [2]. Hightower, R.C.and R.B.Meagher (1986): The molecular evolution of actin.Genetics,114(1):315-332.
- [3]. Jordan,I.K.,F.A.Kondrashov.,I.A.Adzhubei.,Y.I.Wolf.,E.V.Koonin.,A.S.Kondrashov and S.Sunyaev. (2005): A universal trend of amino acid gain and loss in protein evolution.Nature,433,633-638.
- [4]. McDonald,J.H.(2005): Apparent trends of amino acids gain and loss in protein evolution due to nearly neutral variation.Mol.Bio.Evol,23(2),240-244.
- [5]. Pascoal A.,M.Prado.,J.Castro.,A.Cepeda and B.Velazquez. (2004):Survey of authenticity of meat species in food product subjected to different technological processes,by means of PCR_RFLP analysis. Eur Food.Res.Technol.218:306-312.
- [6]. Theophilus J. and Rao P.R.(1998) : Electrophoretic studies on the serum proteins of the three species of genus *Channa*. Indian . J. Fish 35 (4), pp.294-297.
- [7]. Thangaraj M. and Lipton A.P. (2004) : Species-specific proteins in closely related sea-horses. Current Science, 86, No. 12.
- [8]. Gen Bank (National Centre for Biotechnology Information,NCBI),<http://www.ncbi.nlm.nih.gov>.
- [9]. NCBI sequence viewer v2.0
- [10]. Pep tool bioinformatics software version 2.0

pH-Metric Studies on Stability Constants of the Complexes of Some New Substituted Pyrazoles and Isoxazoles with Cu(II) and Fe(III) Transition Metal Ions in 70% Dioxane-Water Mixture

Sushil K. Pagariya*, P. S. Bodkhe

Department of Chemistry, Vidya Bharati Mahavidyalaya, Amravati 444602, Maharashtra, India

ARTICLE INFO

Article History:

Accepted : 01 Jan 2025

Published : 10 Jan 2025

Publication Issue :

Volume 12, Issue 7

January-February-2025

Page Number :

634-645

ABSTRACT

Formation of complexes of Cu(II) and Fe(III) transition metal ions with ligands 3-(5'-chloro-2'-hydroxy-4'-methylphenyl)-5-(4'-nitrophenyl)-1-phenyl pyrazole (L1), 3-(5'-chloro-2'-hydroxy-4'-methylphenyl)-5-(4'-bromophenyl)-1-phenyl pyrazole (L2), 3-(5'-chloro-2'-hydroxy-4'-methylphenyl)-5-(4'-nitrophenyl) isoxazole (L3) and 3-(5'-chloro-2'-hydroxy-4'-methylphenyl)-5-(4'-bromophenyl) isoxazole (L4) have been studied at 0.1M ionic strength at 27±0.1 °C in 70% dioxane-water mixture pH-metrically by Bjerrum method as adopted by Calvin and Wilson. It was observed that Cu(II) and Fe(III) metal ions formed 1:1 and 1:2 complexes with ligands L1-L4. The values of proton-ligand stability constants (pK) and metal-ligand stability constants (logK) were calculated using half integral method and compared from resultant data. The stability constants of complexes specifies that, the ratio of logK₁/logK₂ is positive in all the cases which implies that there is little or no steric hindrance to the additions of secondary ligand molecule. This can be of interest for the specialist in the field of coordination chemistry and plays a supporting role toward development of new drugs.

Keywords: Pyrazole, Isoxazole, Stability Constants, Cu(II) and Fe(III), 70% Dioxane-Water, pH-Metric study.

I. INTRODUCTION

Heterocyclic compounds provide a great synthetic and structural versatility due to their having a number of potential substitution positions. Furthermore, heteroatoms offer the possibility of several modes of coordination[1]. Synthesis of new ligand with distinctive characteristics and novel reactivity is possibly the most significant step in the evolution of metal complexes[2]. Metal complexes containing pyrazole- or isoxazole-based ligands have been the subject of much interest because of their rich coordination chemistry,

strong complex forming ability and a number of established and potential applications areas. The presence of electron-donor nitrogen and oxygen atoms in the heterocyclic rings as well as loss of proton from hydroxyl group in pyrazole and isoxazole derivatives makes them as good chelating agents and easily form stable complexes with most transition metal ions. The nitrogen containing ligand and metal complexes are used as catalysts for olefin polymerization[3-4], which were modified to give different microstructures. The zinc pyrazole complexes work as luminescent[5] that exhibit blue emission at room temperature. The hydroxy pyrazole should be a convenient entry into complex formation. This ligand readily forms complexes with transition metals[6]. The 2-hydroxy substituted isoxazoles are also acts as good chelating agents[7]. In the study of complexes in solution, stability constant is an important tool for solution chemist and biochemist[8] for the correct interpretation of complexes in solution. Stability constant is an equilibrium constant for the formation of a complex in solution. It is a measure of the strength of interaction between the reagents that comes together to form a complex. Stability of metal complexes with medicinal drug is an important criterion and plays a major role in the biological and chemical activities[9]. Determination of stability constants of the metal complexes with various ligands have been an important parameter for predicting the mode of action of drugs[10]. This has important medicinal implication when one considers that most drugs contain group that can acts a ligand. Attempts to measure metal-ligand selectivity in terms of relative strength of metal-ligand bonds are based on stability constant. Moreover, reliable information of stability constant is of great importance in analytical and separation procedure. This gives much importance to the study of determination of stability constants of metal complexes. Various modern techniques are used to determine the stability constant of simple as well mixed ligand compound[11]. But Calvin-Bjerrum pH-metric method has been effectively adopted for the determination of stability constants of complexes through titrations. pH-metric is simple, rapid, most versatile, cheap instrumental technique and do not need any sophisticated instruments because of which it is frequently used to find out the proton-ligand and metal-ligand stability constants of organic drugs[12]. A survey of literature reveals that, manifold research has been done in the past on the study of stability constants of complexes in solutions. Rossotti and Rossotti[13], Martel and Calvin[14] and Bjerrum[15] played an important contribution in the rapid progress for understanding of metal complexes in aqueous and mixed solutions. Many researchers and co-workers made significant contribution for the development of this kind of studies. Naiket al.[16] have studied the stability constants of complexes of substituted pyrazoles with some lanthanide metal ions and the influence of ionic strengths on complex equilibria in a 70% dioxane-water mixture. The stability constants of lanthanide and transition metal ions with substituted pyrazoles have been studied by Murhekar et al.[17]. Nandurkaret al.[18] studied the proton-ligand and metal-ligand stability constants of Cu(II) and Mn(II) complexes with some chlorosubstituted pyrazoles and isoxazoles in 80% DMF-water solvent pH-metrically. Pawaret al.[9] studied the stability constants of Sr(II), Cd(II), Pb(II) and Zn(II) with substituted pyrazoles, isoxazoles in 70% methanol-water mixture. Potdaret al. [19] studied the proton-ligand and metal-ligand stability constants of complexes of Cu(II) and Fe(III) metal ions with substituted pyrazoles and isoxazoles pH-metrically in 70% dioxane-water mixture. Though a lot of work has been done on the study of stability constants of complexes of substituted pyrazoles and isoxazoles with metal ions in solutions but studies on stability constants of the complexes of substituted pyrazoles and isoxazoles containing p-chloro-m-cresol moiety with transition metal ions in mixed solution is still remaining. This stimulated our interest to investigate the stability constants of complexes of p-chloro-m-cresol incorporating pyrazole and isoxazole derivatives with selective transition metal ions in mixed solvent pH-metrically. Hence, in this piece of work, the interaction between the Cu(II) and Fe(III) transition metal ions with some newly synthesized ligands 3-(5'-chloro-2'-hydroxy-4'-methylphenyl)-5-(4'-nitrophenyl)-1-phenylpyrazole (L1), 3-(5'-chloro-2'-hydroxy-4'-

methylphenyl)-5-(4'-bromophenyl)-1-phenyl pyrazole (L2), 3-(5'-chloro-2'-hydroxy-4'-methylphenyl)-5-(4'-nitrophenyl)isoxazole (L3) and 3-(5'-chloro-2'-hydroxy-4'-methylphenyl)-5-(4'-bromophenyl)isoxazole (L4) have been carried out pH-metrically at 0.1M ionic strength and at 27±0.10°C in 70% dioxane-water mixture by Bjerrum method as adopted by Calvin and Wilson. The data obtained were used to evaluate and compare the values of proton-ligand stability constants (pK) and metal-ligand stability constants (logK).

II. EXPERIMENTAL SECTION

Materials and Methods

All the chemicals, reagents and solvents used were of AR grade. The ligands (L1-L4) used in the present work were synthesized by standard known literature method[20]. The stock solution of each ligand (0.01 M) was prepared by dissolving requisite amount of ligand in 70% dioxane-water (v/v) mixture. All the pH-metric measurements were carried out with EQUIP-TRONICS make digital pH-meter (Model EQ-610) equipped with combined glass electrode and magnetic stirrer (accuracy ±0.005 units). The pH-meter was switched on half an hour before starting the titration for initial warming up of the instrument. It was calibrated by buffer solutions of pH 4.0, 7.0 and 9.2 (prepared from Qualigens buffer tablets) at 27 °C before proceeding for titrations. The titrations were carried out in an inert atmosphere of nitrogen. The Calvin-Bjerrum[21] pH-metric titration method as adopted by Calvin and Wilson[22] and modified by Irving-Rossotti[23] was utilized for the determination of proton-ligand (pK) and metal-ligand (logK) stability constants of complexes.

Calvin-Bjerrum pH-Metric Titration:

The experimental procedure involved pH-metric titrations of solutions of i) Free acid (0.01M) i.e. HNO₃ ii) Free acid (0.01M) + ligand (20x 10⁻⁴M) iii) Free acid (0.01M) + ligand (20x 10⁻⁴M) + metal ion (4x10⁻⁴M) against standard 0.1N NaOH solution. In all titrations, the total volume was maintained constant at 50 ml. All the titrations were carried out against standard NaOH solution in 100 ml Pyrex glass beaker kept in a cold water maintained at constant 27 °C temperature in 70% dioxane-water mixture. The ionic strength of all the solutions was maintained constant (0.1M) by addition of appropriate quantity of 1M KNO₃ solution. The reading of pH-meter was recorded at every addition of 0.2ml NaOH solution with constant stirring. The graph of volume of alkali added (NaOH) against pH were plotted as:

- Acid titration curve (A)
- Acid + Ligand titration curve (A+L)
- Acid + Ligand + Metal titration curve (A+L+M)

The ligand involved in present work is considered as a monobasic acid having only one dissociable H⁺ ion from phenolic -OH group of p-chloro-m-cresol attached to pyrazole and isoxazole ring and it can therefore, be represented as HL. The dissociating equilibria can be shown as:



By the law of mass action, we have

$$K = \frac{[H^+][L^-]}{[HL]}$$

Where, the quantities in bracket denotes the activities of the species at equilibrium.

III.RESULTS AND DISCUSSION

Determination of Proton-Ligand Stability Constants:

The plots between volume of NaOH and pH of the solution were used to determine the proton-ligand stability constants (representing the replacement of H⁺ ions from functional group of ligand with respect pH value). The horizontal difference (V₂-V₁) between the titration curves of free acid and acid + ligand was measured accurately. It was used to calculate the proton-ligand formation number (η^-A) at various pH values and fixed ionic strength $\mu = 0.1M$ using Irving and Rossotti's expression as shown below:

$$\eta^-A = \gamma - \frac{(E^0 + N) (V_2 - V_1)}{(V^0 + V_1) T_L^0}$$

Where, V₀ is initial volume of the solution. E₀ and are initial concentrations of free mineral acid and ligand respectively. V₁ and V₂ are the volumes of alkali of normality N during the acid and ligand titration at given pH. γ is number of dissociable protons from ligand. The data of η^-A obtained at various pH along with horizontal difference for all systems are presented in Table1. Proton-ligand formation curves were plotted between η^-A and pH for all the ligand systems (Graph 1-4). The proton-ligand stability constants (pK values) for all ligand systems were determined directly from these formation curves by employing half-integral method. The values of pH at $\eta^-A = 0.5$ corresponds to the value of pK for only one dissociable group. The proton-ligand stability constants (pK values) for all the ligand systems are shown in Table2.

Table1: Determination of Proton-Ligand Formation Number (η^-A values) at $\mu = 0.1M$ Ionic Strength

Medium = 70% Dioxane-water

Temp = 27±0.1 °C

N = 0.1 N (NaOH)

E₀ = 1 x 10⁻² M

System-Ligand L1				
pH	V1 (ml)	V2(ml)	V2 -V1 (ml)	η^-A
2.0	1.62	1.70	0.08	0.914762
2.5	1.98	2.10	0.12	0.873028
3.0	2.19	2.30	0.11	0.884077
3.5	2.29	2.44	0.15	0.842226
4.4	2.39	2.58	0.19	0.800534
4.5	2.43	2.67	0.24	0.748236
5.5	2.52	2.78	0.26	0.727723
5.5	2.60	2.81	0.21	0.780418
6.0	2.65	2.90	0.25	0.738841
6.5	2.71	3.00	0.29	0.697401
7.0	2.78	3.06	0.28	0.708223
7.5	2.82	3.10	0.28	0.708444
8.0	2.89	3.20	0.31	0.677633
8.5	2.98	3.29	0.31	0.67818
9.0	3.07	3.45	0.38	0.606181
9.5	3.26	3.77	0.51	0.473338

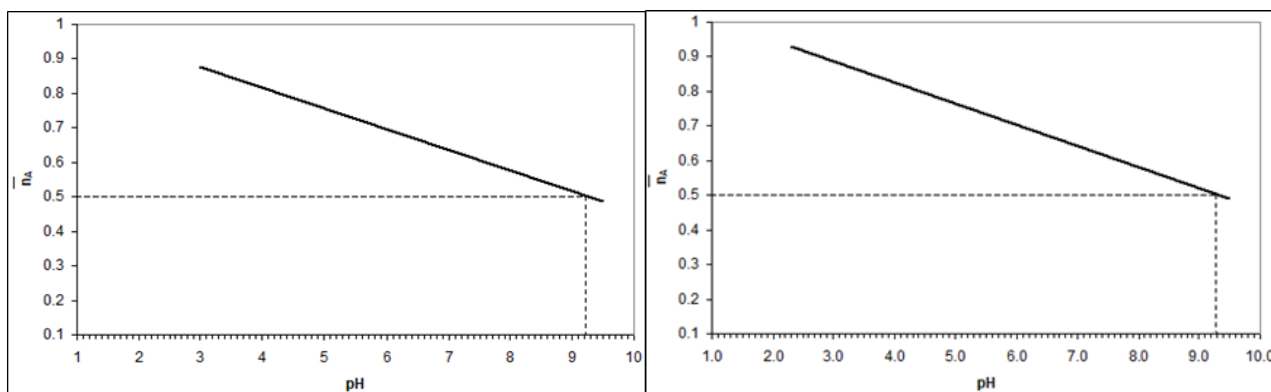
TL0 = 20 x 10⁻⁴ M

V0 = 50 ml

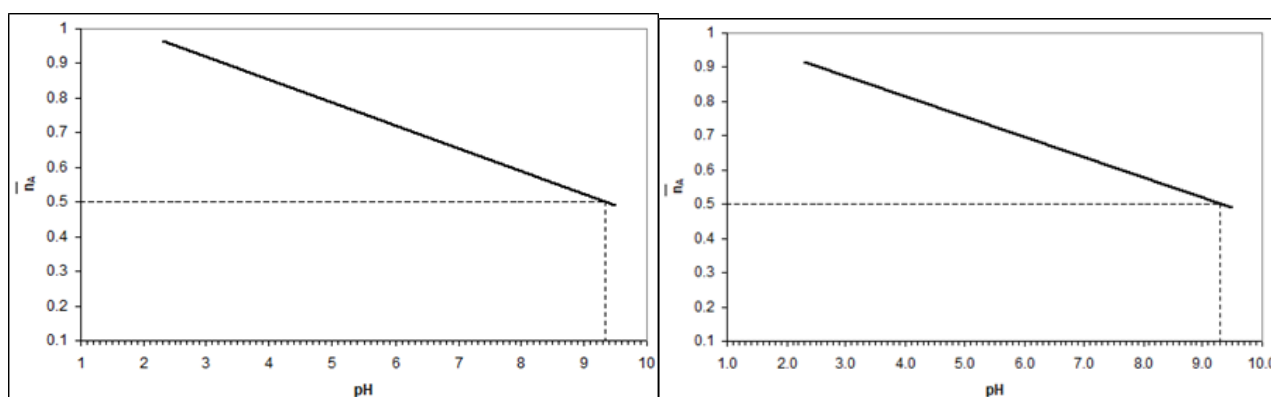
System-Ligand L2				
pH	V1 (ml)	V2 (ml)	V2 -V1 (ml)	$\eta_{\bar{A}}$
2.3	1.62	1.68	0.06	0.936071
2.5	1.98	2.10	0.12	0.873028
3.0	2.19	2.32	0.13	0.863001
3.5	2.29	2.48	0.19	0.800153
4.4	2.39	2.59	0.20	0.790036
4.5	2.43	2.68	0.25	0.737746
5.0	2.52	2.72	0.20	0.790556
5.5	2.60	2.81	0.21	0.780418
6.0	2.65	2.90	0.25	0.738841
6.5	2.71	2.98	0.27	0.71827
7.0	2.78	3.07	0.29	0.697802
7.5	2.82	3.12	0.30	0.687618
8.0	2.89	3.21	0.32	0.667234
8.5	2.98	3.32	0.34	0.647037
9.0	3.07	3.48	0.41	0.57509
9.5	3.26	3.78	0.52	0.463012

System - Ligand L4				
pH	V1 (ml)	V2 (ml)	V2 -V1 (ml)	$\eta_{\bar{A}}$
2.3	1.62	1.73	0.11	0.882797
2.5	1.98	2.10	0.12	0.873028
3.0	2.20	2.33	0.13	0.863027
3.5	2.29	2.43	0.14	0.852744
4.0	2.39	2.58	0.19	0.800534
4.5	2.43	2.62	0.19	0.800687
5.0	2.52	2.72	0.20	0.790556
5.5	2.60	2.81	0.21	0.780418
6.0	2.65	2.90	0.25	0.738841
6.5	2.71	2.97	0.26	0.728704
7.0	2.78	3.04	0.26	0.729064
7.5	2.82	3.10	0.28	0.708444
8.0	2.89	3.20	0.31	0.677633
8.5	2.98	3.30	0.32	0.667799
9.0	3.07	3.48	0.41	0.57509
9.5	3.26	3.80	0.54	0.442358

System - Ligand L3				
pH	V1 (ml)	V2 (ml)	V2 -V1 (ml)	$\eta \bar{A}$
2.3	1.62	1.71	0.09	0.904107
2.5	1.98	2.09	0.11	0.883609
3.0	2.19	2.35	0.16	0.831385
3.5	2.29	2.48	0.19	0.800153
4.4	2.39	2.57	0.18	0.811033
4.5	2.43	2.66	0.23	0.758726
5.0	2.52	2.74	0.22	0.769612
5.5	2.60	2.82	0.22	0.769962
6.0	2.65	2.90	0.25	0.738841
6.5	2.71	2.97	0.26	0.728704
7.0	2.78	3.03	0.25	0.739485
7.5	2.82	3.12	0.30	0.687618
8.0	2.89	3.20	0.31	0.677633
8.5	2.98	3.31	0.33	0.657418
9.0	3.07	3.50	0.43	0.554362
9.5	3.26	3.80	0.54	0.442358



Graph1: Plot of $\eta \bar{A}$ vs pH (System-Ligand L1) **Graph 2:** Plot of $\eta \bar{A}$ vs pH (System-Ligand L2)



Graph 3: Plot of $\eta \bar{A}$ vs pH (System-Ligand L3) **Graph 4:** Plot of $\eta \bar{A}$ vs pH (System-Ligand L4)

Table2: Proton-Ligand Stability Constants by Half Integral Method

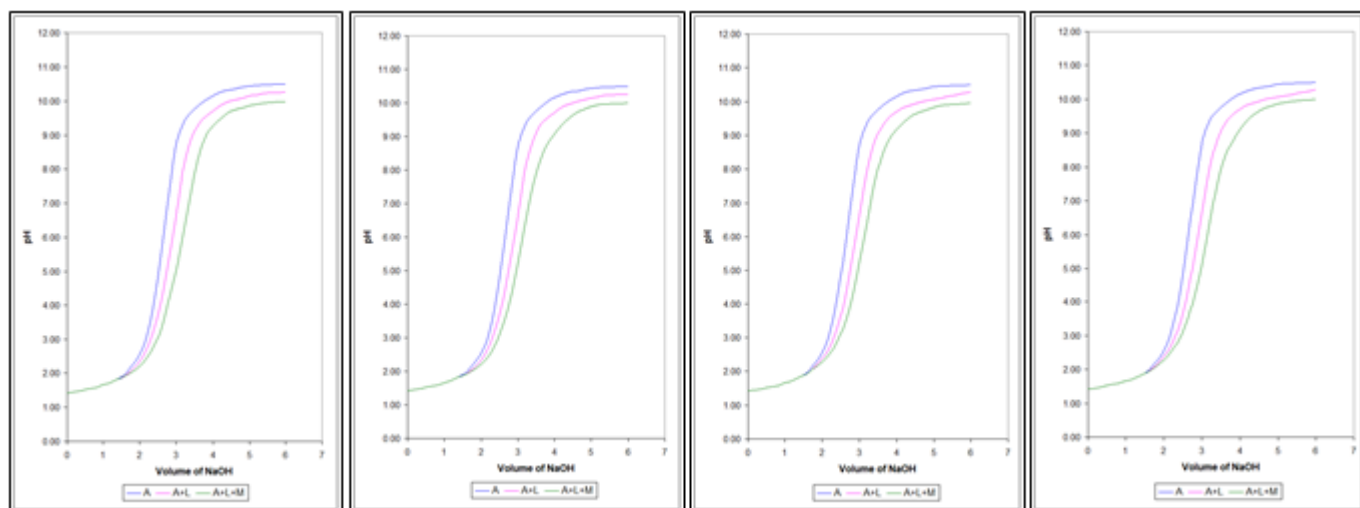
Sr. No.	Ligands	pK values
1.	3-(5'-chloro-2'-hydroxy-4'-methylphenyl)-5-(4'-nitrophenyl)-1-phenyl pyrazole (L1)	9.22
2.	3-(5'-chloro-2'-hydroxy-4'-methylphenyl)-5-(4'-bromophenyl)-1-phenyl pyrazole(L2)	9.34
3.	3-(5'-chloro-2'-hydroxy-4'-methylphenyl)-5-(4'-nitrophenyl) isoxazole (L3)	9.29
4.	3-(5'-chloro-2'-hydroxy-4'-methylphenyl)-5-(4'-bromophenyl) isoxazole (L4)	9.30

Determination of Metal-Ligand Stability Constants:

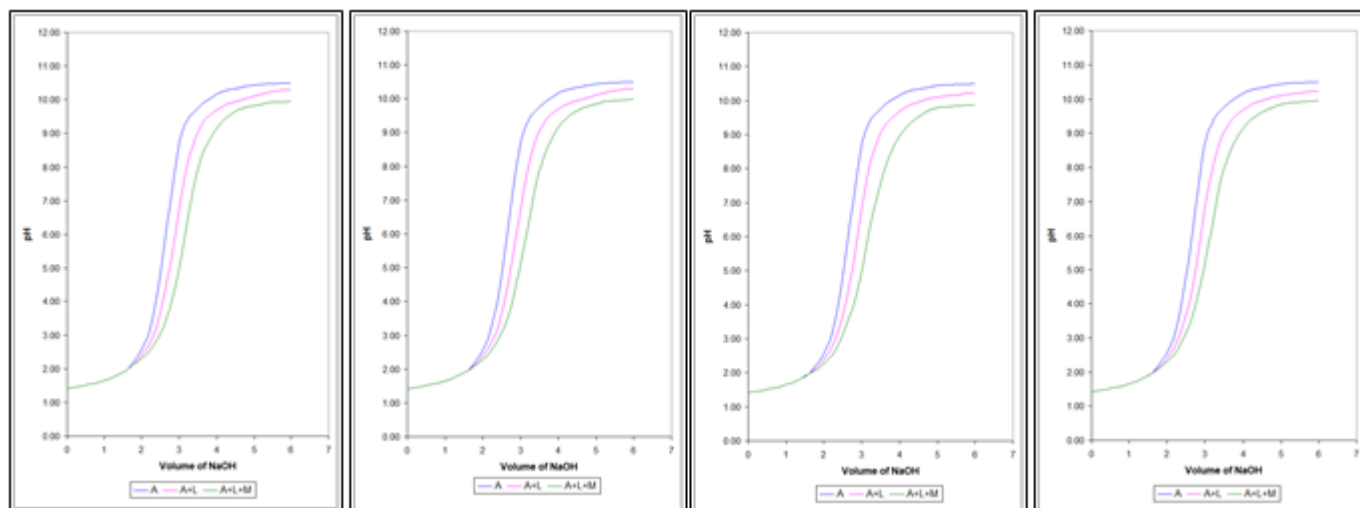
For the calculation of metal-ligand stability constants ($\log K$ values), metal-ligand formation number (η) were calculated at various pH by following Irving-Rossotti's expression as shown below:

Where, the notations of V_0 , E_0 , N have the same meaning as given in earlier equation. T_M^0 is initial concentration of metal ion in the solution. V_2 and V_3 are volumes of alkali of normality N during ligand and metal ions titration at given pH. The metal complex titration data is shown in Table 3. The horizontal difference ($V_3 - V_2$) between the titration curve of metal ($A+L+M$) and ligand ($A+L$) (Graph 5-8) were measured accurately and is used to calculate the values of η at various pH by using Irving-Rossotti's expression as shown above. The values of η were calculated for all the metal ion-ligand systems (Table 4) and the graphs of η Vs pH were plotted. The values of free ligand concentration $pL = \log K$ were calculated for each value of η by Irving-Rossotti's expression shown below:

Where, $[H^+]$ is the concentration of hydrogen ion and K_L is ionization constant. The metal-ligand formation curves were constructed for all the systems by plotting the values of η against pL i.e. η Vs pL (Graph 9-16). The values of metal-ligand stability constants ($\log K_1$ and $\log K_2$) were determined from these metal-ligand formation curves by half integral method. The values of pL at $\eta = 0.5$ and 1.5 corresponds to the values of $\log K_1$ & $\log K_2$ respectively. The metal-ligand stability constants for all the metal-ligand systems are shown in Table 5.



Graph 5: Titration of Ligand L1 with Cu(II) & Fe(III) **Graph 6:** Titration of Ligand L2 with Cu(II) & Fe(III)



Graph 7: Titration of Ligand L3 with Cu(II) & Fe(III) **Graph 8:** Titration of Ligand L4 with Cu(II) & Fe(III)

Table 3: Metal Complex Titration Data

Ligands	Metal Ions	pH at Commencement of Hydrolysis (deviation of A+L curve from A acid curve)	pH at Commencement of Hydrolysis (deviation of A+L+M curve from A+L curve)
L1	Cu(II)	1.60	1.70
	Fe(III)	1.60	1.73
L2	Cu(II)	1.62	1.70
	Fe(III)	1.62	1.80
L3	Cu(II)	1.75	1.80
	Fe(III)	1.75	1.83
L4	Cu(II)	1.74	1.80
	Fe(III)	1.74	1.78

Table 4: Determination of Metal-Ligand Formation Number (η^- values) at $\mu = 0.1\text{M}$ Ionic Strength

Medium = 70% Dioxane-water

Temp = 27 ± 0.1 °C

N = 0.1 N (NaOH)

$E_0 = 1 \times 10^{-2}$ M

TM0 = 4×10^{-4} M

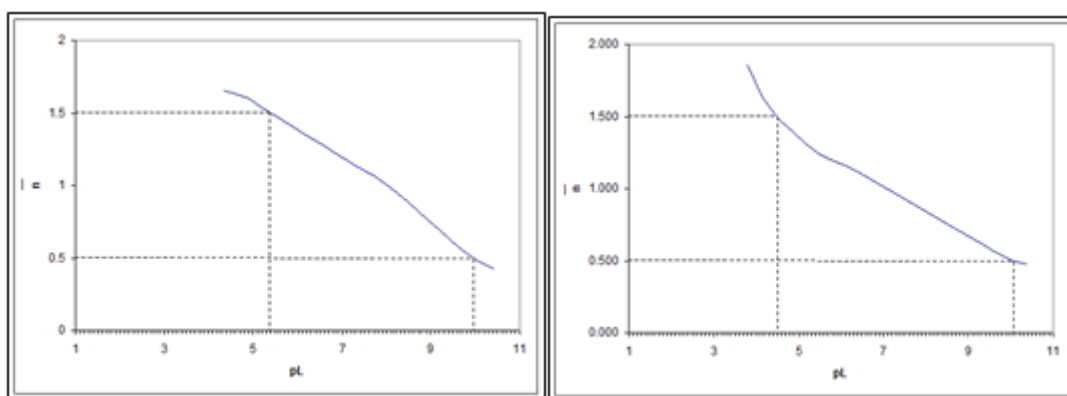
V0 = 50 ml

System - Ligand L1 with Cu(II)				
pH	V2(ml)	V3 (ml)	V3 -V2 (ml)	η^-
2.0	1.70	1.78	0.08	0.425532
2.5	2.10	2.20	0.10	0.527831
3.0	2.30	2.45	0.15	0.788719
3.5	2.44	2.62	0.18	0.943936
4.4	2.58	2.77	0.19	0.993724
4.5	2.67	2.90	0.23	1.200873
5.5	2.78	3.01	0.23	1.198371
5.5	2.81	3.09	0.28	1.458057
6.0	2.90	3.19	0.29	1.507561
6.5	3.00	3.29	0.29	1.504717

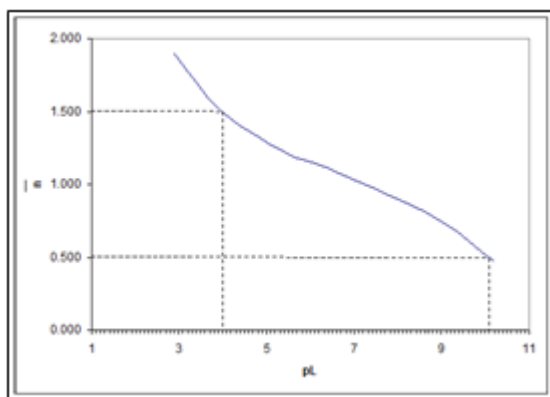
7.0	3.06	3.37	0.31	1.606672
7.5	3.10	3.42	0.32	1.65725
8.0	3.20	3.53	0.33	1.705827
8.5	3.29	3.62	0.33	1.702946
9.0	3.45	3.80	0.35	1.800748
9.5	3.77	4.20	0.43	2.199182

System - Ligand L1 with Fe(III)				
pH	V2 (ml)	V3 (ml)	V3 -V2 (ml)	η^-
2.0	1.70	1.79	0.09	0.478723
2.5	2.10	2.20	0.10	0.527831
3.0	2.30	2.45	0.15	0.788719
3.5	2.44	2.62	0.18	0.943936
4.4	2.58	2.77	0.19	0.993724
4.5	2.67	2.87	0.20	1.044238
5.5	2.78	2.99	0.21	1.094164
5.5	2.81	3.02	0.21	1.093543
6.0	2.90	3.13	0.23	1.195652
6.5	3.00	3.24	0.24	1.245283
7.0	3.06	3.31	0.25	1.295703
7.5	3.10	3.40	0.30	1.553672
8.0	3.20	3.56	0.36	1.860902
8.5	3.29	3.70	0.41	2.115782
9.0	3.45	3.97	0.52	2.675398
9.5	3.77	4.38	0.61	3.119769

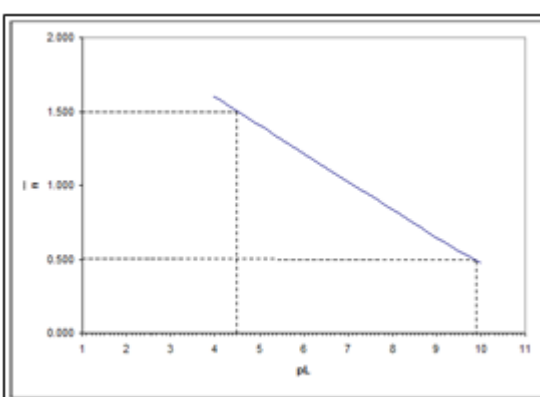
Note: The values of η^- were also calculated for Ligand L2, L3, L4 with Cu(II) and Fe(III) metal ions.



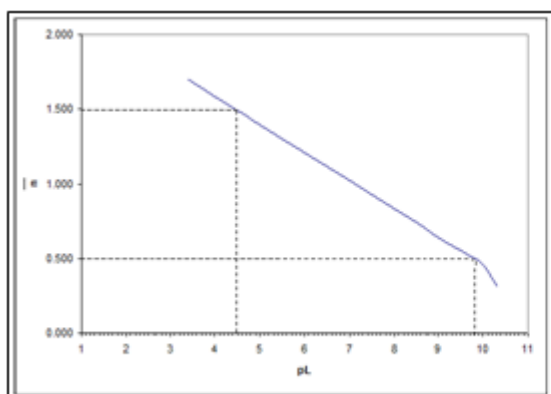
Graph 9: Plot of η^- Vs pH System-L1 with Cu(II) **Graph 10:**Plot of η^- Vs pH System-L1 with Fe(III)



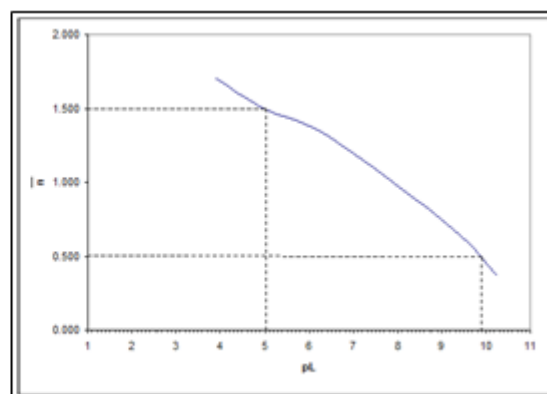
Graph 11: Plot of $\etā$ Vs pL System-L2 with Cu(II)



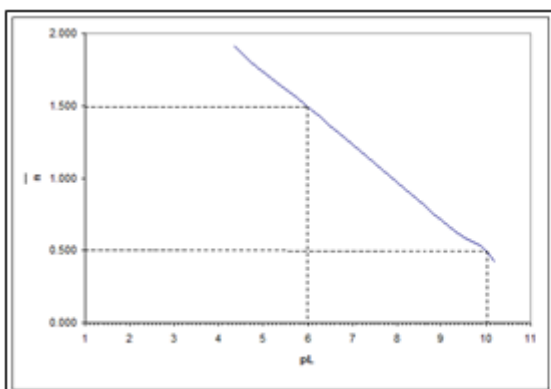
Graph 12: Plot of $\etā$ Vs pL System-L2 with Fe(III)



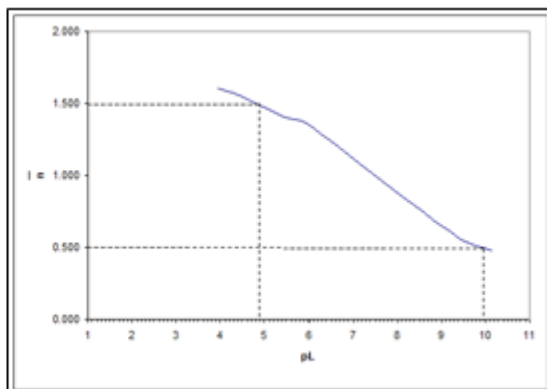
Graph 13: Plot of $\etā$ Vs pL System-L3 with Cu(II)



Graph 14: Plot of $\etā$ Vs pL System-L3 with Fe(III)



Graph 15: Plot of $\etā$ Vs pL System-L4 with Cu(II)



Graph 16: Plot of $\etā$ Vs pL System-L4 with Fe(III)

Table5: Metal-Ligand Stability Constants logK1 and logK2 by Half Integral Method

System	logK1	logK2	logK1- logK2	logK1/ logK2
Ligand L1 with Cu(II)	9.98	5.40	4.58	1.8481
Ligand L1 with Fe(III)	10.18	4.51	5.67	2.2572
Ligand L2 with Cu(II)	10.19	4.02	6.17	2.5348
Ligand L2 with Fe(III)	9.90	4.50	5.40	2.2000
Ligand L3 with Cu(II)	9.82	4.48	5.34	2.1920
Ligand L3 with Fe(III)	9.90	5.02	4.88	1.9721
Ligand L4 with Cu(II)	10.01	6.00	4.01	1.6683
Ligand L4 with Fe(III)	9.97	4.89	5.08	2.0389

IV. CONCLUSION

From the graph of titration curves, it is observed that the departure between acid (A) curve and ligand (A+L) curve indicates the dissociation of phenolic-OH groups. The departure between acid+ligand (A+L) curve and acid+ligand+metal (A+L+M) curve for all the systems were started from pH range 1.70 to 1.83 indicated the commencement of complex formation between metal ion and ligands. The observations and results revealed that the change in colour from yellow to orange as the pH increased from 2 to 9.5 during the pH-metric titrations confirmed the formation of complexes of Cu(II) and Fe(III) metal ions with ligands L1-L4. It could be seen from Table 2 that, the order of pK values of the ligands is found to be as:

The pK value of ligand L1 and L3 are slightly reduced than ligand L2 and L4. This may be due to the presence of electron withdrawing nitro (-NO₂) group in ligand L1 and L3. The values of logK₁ and logK₂ (Table 5) decided the stability of complexes. The difference between logK₁ and logK₂ is less than 2.5, indicating the simultaneous formation of 1:1 and 1:2 complexes while the difference is more than 2.5, then in such a case a stepwise complex formation takes place. From the Table 5, it is clear that the difference between logK₁ and logK₂ values are sufficiently large (>2.5) that indicates the stepwise formation of 1:1 and 1:2 stable complexes between Cu(II)/Fe(III) metal ions and ligands L1-L4. The ratio logK₁/logK₂ are positive in all cases which implies that there is little or no steric hindrance to the addition of secondary ligand molecule. The most accurate logK values can be calculated by pointwise calculation method which were not studied herein. The experimental finding of the study can play a supporting role towards the development of new drugs. This can be of interest for the specialist in the field of coordination chemistry and drug discovery.

V. ACKNOWLEDGEMENT

The authors are very much thankful to the Principal, Vidyabharati Mahavidyalaya, Amravati for providing all necessary facility to carry out this research work.

VI. REFERENCES

- [1]. Naik A.B., World J. Chem., 6(2), 118-121 (2011).
- [2]. Alkurdi A., AlJahdali M. and Alshehri A., Hindawi J. Chem., Article ID 3476954, 1-15 (2022).
- [3]. Bansod J.R., Bansod S.B., Mote S.P. and Wankhade R.R., J. Scien. Res. Sci. Tech., 9(6), 784-788 (2021).
- [4]. Nelana S.M., Darkwa J., Guzei I.A. and Maplie S.F., J. Organomet. Chem., 689(10), 1835-1842 (2004).
- [5]. Li J., Zhou J.H., Li Y.Z., Weng L.H., Chen X.T., Yu Z., Xue Z., Inorg. Chem. Commun., 7(4), 538-541 (2004).
- [6]. Yingshen L. and Kraatz H.B., Inorg. Chem. Commun., 7(3), 382-385 (2004).
- [7]. Parmar P.J., Int. J. Scien. Res. Sci. Tech. 3(6), 679-682 (2017).
- [8]. Choudhari P.P., Yawale P.R., Ubarhande S.S. and Wadekar M.P., J. Emerg. Tech. Innov. Res., 7(2), 563-567 (2020).
- [9]. Pawar R.P., Raut V.M., Bhise M.P., Murhekar G.H., Wadekar M.P., Banewar V.W. and Gulwade D.P., Oriental J. Chem., 25(4), 1117-1120 (2009).
- [10]. Meshram U.P., Khobragade B.G., Narwade M.L. and Chandak H.S., Int. J. Pharma. Chem. Bio. Sci., 4(3), 706-710 (2014).
- [11]. Thakur S.D. and Shaikh M.W., J. Emerg. Tech. Innov. Res., 9(6), h378-h380 (2022).

- [12]. Angaitkar J.N., Bodkhe P.S. and Narwade M.L., J. Chem. Chem. Sci., 6(11),1074-1079 (2016).
- [13]. Rossotti F.J.C. and Rossotti H., The Determination of Stability Constants, 4thEdition, McGraw Hill Book Co. Inc., New York (1961).
- [14]. Martell A.E. and Calvin M., Chemistry of the Metal Chelate Compounds, 5thEdition, Prentice-Hall Englewood Cliffs, New Jersey (1962).
- [15]. a) Bjerrum J., Chem.Rev.,46(2), 381-401 (1950). b) Bjerrum J., Metal Ammine Formation in Aqueous Solution, P. Haase and Son, Copenhagen, Denmark (1941).
- [16]. Naik A.B. and Narwade M.L., Russ. J. Coord. Chem., 35(12), 932-937 (2009).
- [17]. a) Murhekar G.H., Raut A.R. and Wadekar M.P., Oriental J. Chem., 25(4), 1093-1096 (2009). b) Murhekar G.H., Int. J. Sci. Res. Sci. Tech., 10(1), 76-81 (2023).
- [18]. Nandurkar P.S. and Rathore M.M., Int. J. ChemTech Res., 10(15), 204-212 (2017).
- [19]. Potdar S.G. and Rajput P.R., Asian J. Chem., 18(4), 3160-3162 (2006).
- [20]. Pagariya S.K. and Bodkhe P.S., European J. Biomed. Pharma. Sci., 11(5), 399-409 (2024).
- [21]. a) Bjerrum J., Metal Ammine Formation in Aqueous Solution, P. Haase and Son, Copenhagen, Denmark (1941). b) Calvin M., Melchior N.C.,Bjerrum J., Stability of Chelate Compounds. IV. Effect of the Metal Ion1, J. Am. Chem. Soc., 70(10), 3270-3273 (1948).
- [22]. Calvin M. and Wilson K.W., Stability of Chelate Compounds, J. Am. Chem. Soc., 67(11), 2003-2007 (1945).
- [23]. a) Irving H.M. and Rossotti H.S., J. Chem. Soc.,74, 3397-3405 (1953). b) Irving H.M. and Rossotti H.S., J. Chem. Soc., 76, 2904-2910 (1954). c) Irving H.M. and Rossotti H.S., Acta Chem. Scand., 10, 72-93 (1956).

A Study on Acoustical Parameters of Isradipine Drug in Different Binary Mixture of Solvents At 313 K

Wasnik Usha

Arts, Science and Commerce College, Chikhaldara, Dist- Amravati, Maharashtra, India

ARTICLE INFO

Article History:

Accepted : 01 Jan 2025

Published : 10 Jan 2025

Publication Issue :

Volume 12, Issue 7

January-February-2025

Page Number :

646-650

ABSTRACT

The ultra sound is one of the well-recognized approach for the study of intermolecular interactions in fluids. Thermodynamic properties are generally convenient parameters for interpreting solute-solvent and solute-solute interactions in the solution phase. Measurements of ultrasonic velocity along with viscosity of liquid mixtures and solutions help to study different interactions in solutions. In the present investigation viscosities and densities of Isradipine (ISD) drug have been measured at 313K in different solvent system. From this data number of additional dependent basic acoustic thermodynamic parameters namely a diabatic compressibility (β_s), apparent molar compressibility (ϕ_k), apparent molar volume (ϕ_v), specific acoustic impedance (Z), intermolecular free length (L_f) have been evaluated. From these derived parameters limiting apparent molal volume (ϕ_0^v), limiting apparent molal compressibility (ϕ_0^k) and experimental slopes (S_{0V} & S_{0K}) have been calculated by using Masson's equation. The viscosity data were analysed using Jones – Dole equation. Through these parameters interactions between solutes and their solvents are expressed in terms of solute- solvent interactions.

Keywords: Acoustic parameters, solute-solvent interaction, Isradipine

I. INTRODUCTION

The Ultrasonic technique are a nondestructive technique. These techniques are used in various purposes, one of them is different types of structural changes and molecular interactions present in binary mixtures. The study of intermolecular interactions has been of intense activity in the recent past in all branches of chemistry and in other parallel disciplines. Various experimental methods have been employed to explore the information from the study of such interactions. Thermodynamic investigations, acoustic and transport properties of solutions are of great importance to get insight into such intermolecular forces. Viscometry¹⁻² is an important tool in order to elucidate the solute – solvent interaction and nature of a solute as a structure maker or a structure breaker. Accurate knowledge of thermodynamic of solutions has relevance in

understanding the molecular interactions between the component of the solutions i.e. solute and solvent in developing new theoretical models.

Thermodynamic properties are generally convenient parameters for interpreting solute-solvent and solute-solute interactions in the solution phase. Most of the information extracted from ultrasonic study of fluid confined to the determination of hydration number, compressibility³⁻⁵ etc. The successful application of acoustic method to physicochemical investigation of solution becomes possible after the development of adequate theoretical approaches and methods for ultrasound velocity measurements in small volumes of liquids⁶⁻⁷. The present study deals with the study of molecular interaction in terms of different known drugs in different organic solvents – water mixture in different concentration at certain temperatures. Drug action has been widely recognized to be the ultimate consequence of physicochemical interaction between the drugs and functionally important molecules in the living organism known as receptor. Drug receptor interaction is like hydrophobic interaction⁸⁻¹⁰ like ionic and covalent bonding interaction. For the present study drug Isradipine (ISD) is selected. Isradipine is a dihydropyridine calcium channel antagonist that is structurally related to nifedipine. Isradipine is indicated for the treatment of mild to moderate hypertension. The acoustic properties of Isradipine have been studied in 20% Acetone-water, 20% DMF-water and 20% Methanol-water solutions at 313 K.

II. EXPERIMENTAL

Solvents namely Acetone, Dimethylformamide and Methanol used in the present work were of AR grade and it gets purified and dried by the usual procedure. Densities, viscosities and ultrasonic velocities were measured at 313 K over a wide range of composition. Densities were determined by using bipycnometer. The viscosities were measured by precalibrated Ostwald type viscometer with an accuracy of about ± 0.1 K. Ultrasonic velocity measurements were made by using an ultrasonic interferometer (Mittal Enterprises, New Delhi) at a frequency of 2 MHz with a tolerance of $\pm 0.005\%$. All the measurements were carried out at 313 K.

III. THEORY

Ultrasonic velocity and Acoustic parameters namely adiabatic compressibility (β_s), apparent molar volume (V_a), apparent molar compressibility (β_k), intermolecular free length (L_f), specific acoustic impedance (Z), Limiting apparent molar volume (V_∞), Limiting apparent molar compressibility (β_{k0}) were determined by using following relations.

$$\text{Apparent molar volume } V_a = 103(\rho_0 - \rho_s) / (m - \rho_0 \rho_s + M / \rho_0) \quad 3$$

$$\text{Apparent molar compressibility } \beta_k = 103(\beta_0 \rho_s - \rho_s \beta_0) / (m - \rho_s \rho_0 + \rho_s M / \rho_s) \quad 4$$

$$\text{Intermolecular free length } L_f = K(\rho_s)^{1/2} \quad 5$$

$$\text{Specific acoustic impedance } Z = \rho \cdot u \quad 6$$

$$\text{Limiting apparent molar volume } V_\infty = V_a + S_v C^{1/2} \quad 7$$

$$\text{Limiting apparent molar compressibility } \beta_{k0} = \beta_k + S_k C^{1/2} \quad 8$$

Tableno.1 ExperimentalDataofDensity,UltrasonicVelocityandViscosityofISDindifferent solvent at 313K

Solvents	Conc.mol.dm ⁻³	Density ρs Kg m ⁻³	Ultrasonic Velocity(u) m/s	Viscosity x10 ⁻³ Ns m ⁻²
20%Acetone - WaterMedium	0.02	995.38	1564.3	0.65584
	0.04	995.86	1566.1	0.65832
	0.06	996.04	1568.3	0.66061
	0.08	996.21	1570.1	0.66397
	0.1	996.49	1572.2	0.66633
20%DMF- WaterMedium	0.02	994.51	1590.1	0.78352
	0.04	994.83	1592.3	0.78755
	0.06	995.02	1594.8	0.79150
	0.08	995.24	1597.1	0.79422
	0.1	995.63	1599.2	0.79709
20%MeOH- WaterMedium	0.02	996.13	1565.4	0.83047
	0.04	996.21	1566.9	0.83450
	0.06	996.32	1569.4	0.83873
	0.08	996.32	1572.0	0.84151
	0.1	996.62	1573.5	0.84427

Table no.2 Variationofsomeacousticalparameterswithconcentrationof ISDindifferentsolventsat 313 K

Solvents	Conc.mol.dm ⁻³	βs x10 ⁻¹⁰ Pa ⁻¹	Φv x10 ⁻⁵ m ³ mol ⁻¹	Φk x10 ⁻¹⁴ m ³ mol ⁻¹ Pa ⁻¹	Lf x10 ⁻¹¹ (m)	Z x 10 ⁵ Kg m ⁻² sec ⁻¹
20%Acetone- WaterMedium	0.02	4.1055	13.142	-101.26	4.2813	15.5707
	0.04	4.0941	19.916	-48.048	4.2754	15.5961
	0.06	4.0819	22.678	-30.263	4.2690	15.62.8
	0.08	4.0719	24.070	-21.110	4.2638	15.6414
	0.1	4.0599	24.789	-15.871	4.2575	15.6668
20%DMF- Water Medium	0.02	3.9858	-38.338	56.0589	4.1855	15.8090
	0.04	3.9732	-4.9928	30.4748	4.1789	15.8353
	0.06	3.9618	5.9999	22.0910	4.1729	15.8597
	0.08	3.9516	11.519	18.0356	4.1675	15.8818
	0.1	3.9402	14.901	15.4980	4.1615	15.9058
20%MeOH- WaterMedium	0.02	4.0917	-76.893	-125.58	4.2407	15.5956
	0.04	4.0802	-24.203	-59.880	4.2348	15.6185
	0.06	4.0658	-7.0394	-38.667	4.2273	15.6491
	0.08	4.0552	1.7580	-27.499	4.2218	15.6710
	0.1	4.0432	7.0551	-20.948	4.2155	15.6955

Table-3 Limiting values of ϕ_v and ϕ_k along with slope (S_v & S_k) for ISD in different medium at 313K

Temp. T (K)	Medium	Parameters			
		$\phi_v \times 10^{-5}$ $\text{m}^3\text{mol}^{-1}$	$\phi_k \times 10^{-14}$ $\text{m}^3\text{mol}^{-1}\text{Pa}^{-1}$	$S_v \times 10^{-5}$ $\text{m}^3\text{mol}^{-3/2}\text{dm}^{3/2}$	$S_k \times 10^{-14}$ $\text{m}^3\text{mol}^{-3/2}\text{dm}^{3/2}\text{Pa}^{-1}$
313K	20% A-W	-131.5	-235.7	470	710.3
	20% DMF-W	-57.13	-298.1	247.5	892.0
	20% M-W	-82.11	101.6	323.6	-285.7

IV. RESULTS AND DISCUSSION:

Table 1 shows that density (ρ), ultrasonic velocity (u) and viscosity (η) increases with increase in concentration for all three systems. The increase in ultrasonic velocity is due to decrease in intermolecular free length (L_f) as shown in table 2. This suggests that there is a strong interaction between Isradipine drug and solvent molecule. Adiabatic compressibility (β_s) is a measure of intermolecular association or repulsion calculated from the measured ultrasonic velocity (u) and density (ρ). Adiabatic compressibility is found to decrease with increase in concentration [1]. Since adiabatic compressibility is inversely related to the product of density and ultrasonic velocity based on this the compressibility is expected to decrease which has been observed in the present case. When the sound waves travel through the solution, certain part of it travels through the medium and rest gets reflected by the ion [2] i.e. restriction for flow of sound velocity by the ions. The character that determines the restriction movement of sound waves is known as acoustic impedance (Z). It has been found that acoustic impedance increases with increase in concentration in all three systems. The apparent molar compressibility (Δk) explains the solute-solvent and solute-solute interactions in solution and was calculated by using the equation no. 4. The apparent molar volume (Δv) is defined as the change in volume of solution for the added one mole of a particular component at constant temperature and pressure. It is a thermodynamic property which helps in elucidating solvation behavior of electrolyte in solution. Apparent molar volume was evaluated from the density of solution and solvent. It is evident from the table 3 that Δk values are negative for all three systems. The negative Δk values suggest solute-solvent interaction whereas positive values are due to solute-solute interaction. S_v is a measure of solute-solvent interaction. It is observed from the table 3 that S_v values are higher in 20% Acetone-water and 20% MeOH-water and low in 20% DMF-water solution. This confirms that in 20% DMF-water solution solute-solute interactions and in 20% Acetone-water and 20% MeOH-water solute-solvent interaction predominates.

V. REFERENCES

- [1]. Hagenmuller P., Preparative methods in Solid State Chemistry (Academic Press, London) 367 (1972).
- [2]. Chaimers B., Principles of Solidification (John Wiley, New York) 194 (1964).
- [3]. Pandey J.D., Shukla R.K., Shukla A.K. and Rai R.D.: J Chem Thermodyn, 21, 725 (1989).
- [4]. Wang G.C., Benson and Lu B.: J Chem Thermodyn 21, 67 (1989).
- [5]. Shilo H.J. Am Chem soc, 80, 70 (1958)
- [6]. Stuehr J. and Yeager E. : Physical acoustics vol. II part A, Manson Ed. Academic press, New York (1965)
- [7]. Braginskaya F.I. and Sodikhova S.Kh. Biofizika, 20 (1975)
- [8]. Goldstein A., Aronow L. and Kalman S.M.; Principles of Drug action 2nd ed. Wiley, New York p-1 (1974).

- [9]. Stenlake J.B.; Fundamentals of molecular pharmacology, Althone, London, Vol 2 (1975).
- [10]. Korolkowas A.; Essentials of Medicinal Chemistry, 2nd ed. Wiley, New York Chap.3 (1988).
- [11]. Sarvazyan A.P. and kharaakoz D.P. in molecular and cellular biophysics. G.M. Frank Ed. (Nauka Moscow) P. 33 (1977)
- [12]. Bukin V.A. Sarvazyan A.P. and passechnik VI, Biofizika 24, 61 (1979)

Interaction of 1(4-Chlorophenyl)-2(P-Tolylthiocarbamido)-1-Ethanolwithmn (II), Fe (II) and Cu (II) Ions Deliberate Ph-Metrically

R.J.Deshmukh¹, A.B. Wadekar¹, S.A.Ikhe², P.M. Dahikar², RD.Kakade³

¹Department of Chemistry, Shri Dnyaneshwar M. Burungale Science and Art College Shegaon, Maharashtra, India

²Department of Chemistry, J. D. Patil Sanglundkar Mahavidyalaya Daryapur, Maharashtra, India

³Department of chemistry, Shree R.R. Lahoti Science College Morshi, Maharashtra, India

ARTICLE INFO

Article History:

Accepted : 01 Jan 2025

Published : 10 Jan 2025

Publication Issue :

Volume 12, Issue 7

January-February-2025

Page Number :

651-655

ABSTRACT

Present work deals with Interaction of 1(4-Chlorophenyl)-2(P-Tolylthiocarbamido)-1-Ethanolwith Mn(II), Fe(II) and Cu(II) ions Investigation pH-metricallyin 70 % ethanol-water mixture. In present work studied interaction of 1(4-Chlorophenyl)-2(P-Tolylthiocarbamido)-1-Ethanolwith Mn(II), Fe(II) and Cu(II) metal ions at 0.1 M ionic strength in 70 % ethanol-water mixture by Bjerrum method as adopted by Calvin and Wilson, It is observed that Mn(II), Fe(II) and Cu(II) metal ions form 1:1 with ligands [L]. The values of proton-ligand stability constant (pK) and metal-ligand stability constants (log k) were estimate and compared from resultant data. The effects of substituents were studied from estimated data (pK& log k).

Keywords: 1(4-Chlorophenyl)-2(P-Tolylthiocarbamido)-1-Ethanol [L], Stability constant, pH-metric investigation.

I. INTRODUCTION

Molecule containing thiocabamido, amino, hydroxyl, benzenoidandnon-benzenoid nucleus showed various applications in pharmaceutical and medicinal sciences. These types of drugs are very effective in various diseases. Several modern theories and concept are concerning to physical as well as chemical study of benzenoid, non-benzenoid, heteroacycles and heterocycles. Aminonaphthols and thiocarbamido nucleus containing heterocycles possesses pharmaceutical, medicinal agricultural industrial and biotechnological significances [1-5]. The manifold research work has been done on the study of metal and nitrogen heterocyclic ligands containing complexes[6-15].The studies of metal-ligand complexes in solution having number of metal ions with ligands carboxylic acids, oximes, phenols etc. would be interesting which throw a light on the mode

of storage and transport of metal ions in biological kingdom. Metal complexation not only brings the reacting molecules together to give activated complexes [16] but also polarized electrons from the ligands towards the metal. The relation between stability and basicity of the ligands is indicated by the formation constant and free energy change value. Bulkier group increases the basicity of ligands as well as stability. The stability of the complexes is determined by the nature of central metal atom and ligand. The stability of complexes is influenced by the most important characteristics degree of oxidation, radius and electronic structure. Irving and Williams had studied the order of stability of metal complexes of transition metal ions by comparing the ionic radius and second ionization potentials of metal ions, as it is valid for most nitrogen and oxygen donor ligands. Stability and complexation by ligands and various metal ions were evaluated by many researchers [17-20]. Reliable information of stability constant is of great importance in analytical and separation procedure. To remove undesirable and harmful metals from living organism, chelating agents are very much useful in biological systems. This gives importance to the study of determination of stability constant of metal complexes. In present work an attempt has been made to pH-metric studied stability constant of 1(4-Chlorophenyl)-2(P-Tolylthiocarbamido)-1-Ethanol with various metal ions in 70 % ethanol-water mixture.

II. MATERIALS AND METHODS

All chemicals used are of AR grade. The stock solutions of the ligand [L] was prepared by dissolving required amount of ligand in a of 70% (ethanol + water) mixture.

General procedure:

Types of Titrations

- i) Free acid HNO_3 (0.01 M)
- ii) Free acid HNO_3 (0.01 M) and ligand ($20 \times 10^{-4}\text{M}$)
- iii) Free acid HNO_3 (0.01 M) and ligand (20×10^{-4}) and metal ion ($4 \times 10^{-4}\text{M}$) against standard 0.1N NaOH solution. The ionic strength of all the solutions was maintained constant 1M by adding appropriate amount of KNO_3 solution. All the titrations were carried out in 70% (Ethanol-water) mixture and the reading were recorded for each 0.2 ml addition. The graph of volume of alkali added (NaOH) against pH were plotted. The ligands involved in the present work may be considered as a monobasic acid having only one dissociable H^+ ion from phenolic -OH group and it can therefore, be represented as HL. The dissociating equilibria can be shown as.



By the law of mass action, we have,

$$K = [\text{HL}] / ([\text{H}^+][\text{L}^-]) \dots\dots\dots (1)$$

Where, the quantities in bracket denote the activities of the species at equilibrium.

III. RESULT AND DISCUSSION

Calculation of Proton-Ligand Stability Constant (\bar{n}_A)

The plots between volume of NaOH and pH of the solution were used to determine the proton ligand stability constant (representing the replacement of H^+ ions from functional group of ligand with respect to pH value). The horizontal difference ($V_2 - V_1$) was measured accurately between the titration curves of free acid and acid + ligand. It was used to calculate the formation number \bar{n}_A at various pH values and fixed ionic strength $\mu = 0.1 \text{ M}$ using Irving and Rossotti's equation

$$\bar{n}_A = \gamma - \left\{ \frac{(V_2 - V_1)(N + E^0)}{(V^0 + V_1)T_L^0} \right\} \dots \dots \dots (2)$$

Where, V^0 is the initial volume of the solution. E^0 and T_L^0 are initial concentrations of the mineral acid and ligand respectively. V_1 and V_2 are the volumes of alkali of normality N during the acid and ligand titration at given pH. γ is the replaceable proton from the ligand. The data of \bar{n}_A obtained at various pH along with the horizontal difference for some representative systems are represented in Table 1. The metal–ligand formation number (\bar{n}) is estimated by Irving-Rossotti's equation.

$$\bar{n} = \frac{(V_3 - V_2)(N + E^0)}{(V^0 + V_2)\bar{n}_A T_M^0} \dots (3)$$

Where, the notations have the same meaning as given in earlier equation. The horizontal difference ($V_3 - V_2$) between the metal complex ($A + M + L$) and reagent ($A + L$) curve is used to evaluate the value of n using Irving Rossotti's equation

Table-1 : Proton-Ligand Stability constant (pK)

System	pK		Diff.
	Half integral method	Point wise method	
1(4-Chlorophenyl)-2(P-Tolylthiocarbamido)-1-Ethanol [L]	8.56	8.25	0.31

Table-2 : Metal-ligand stability constant (log K)

System	Log K ₁	Log K ₂	Δ Log K	Log K ₁ / Log K ₂
Mn(II) + L	4.89	5.56	0.67	0.879496403
Fe(II) + L	4.56	4.97	0.41	0.91750503
Cu(II) +L	5.22	6.02	0.8	0.867109635

Fig. 3. Plot between \bar{n} vs pH System- L₂+Mn(II)

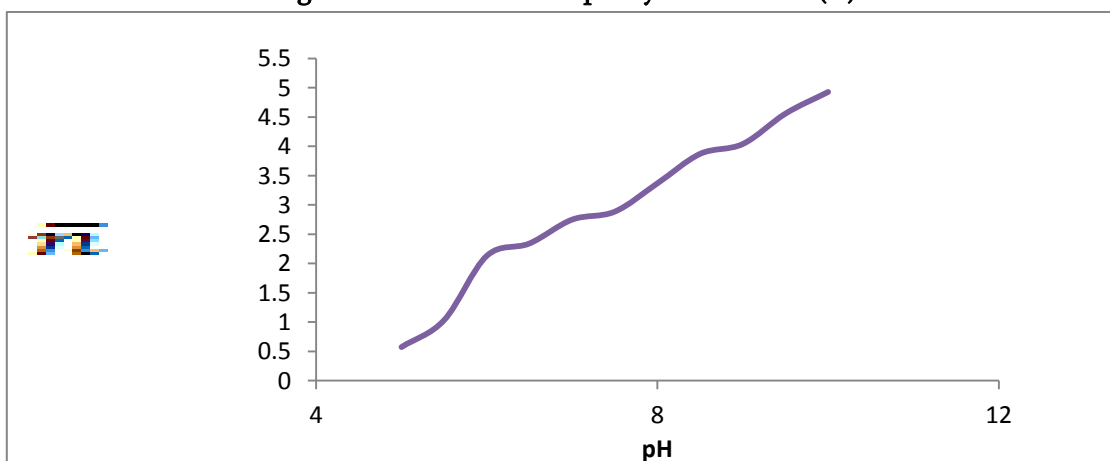


Fig. 2 Plot between \bar{n} vs pH System-L+Fe(II)

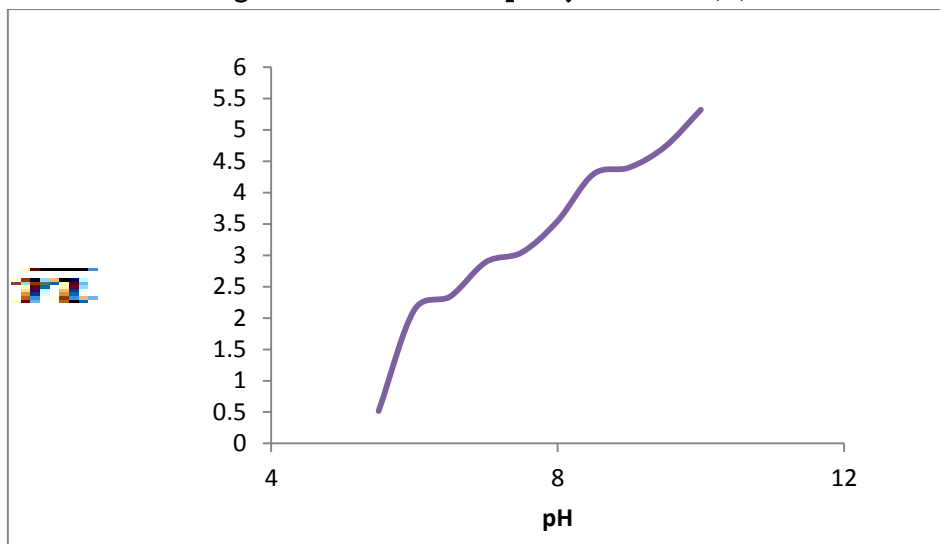
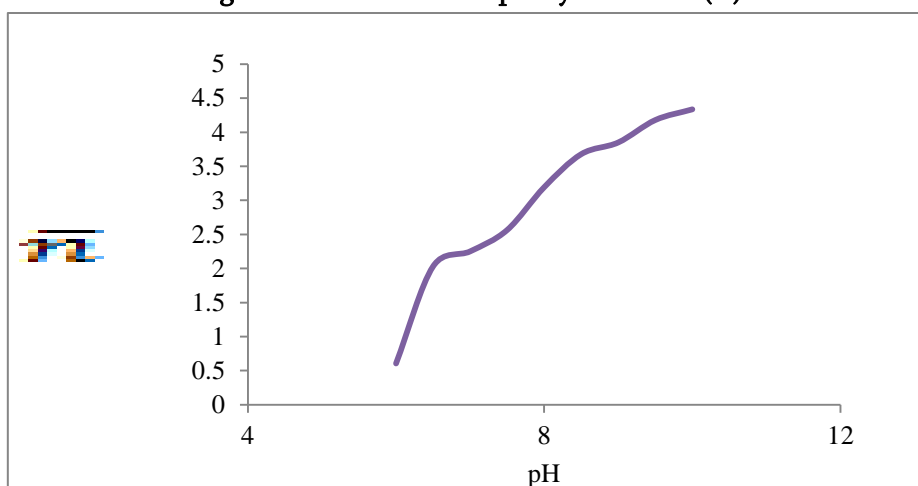


Fig. 3 Plot between \bar{n} vs pH System-L+Fe(II)



IV. CONCLUSION

For 1(4-Chlorophenyl)-2(P-Tolylthiocarbamido)-1-Ethanol the difference between the values of $\log K_1$ and $\log K_2$ is higher with Mn(II) complex than Fe(II) and Cu(II) complexes. forms more stable complex with L than Fe(II) and Cu(II) metal ions.

Observation of Table-2 showed that less difference between $\log K_1$ and $\log K_2$ values indicates complex formation between metal ion and ligand occurring simultaneously and 1:1 complexation occurs in between to above metal ions and L.

V. REFERENCES

- [1]. Barnes D.M., Jianguo Ji, Fickes M.G., J. Am. Chem. Soc., 2002, 124, 13097-13105.
- [2]. Cyril V., Milam M., Chem. Abstract., 1977, 86, 190015.
- [3]. Hassan H. Hammud, Mohammad H. El-Dakdouki, Nada Sonji, Ghassan Sonji, Kamal H. Bouhadir, Interactions of Some Divalent Metal Ions with Thymine and Uracil Thiosemicarbazide Derivatives, Nucleosides, Nucleotides And Nucleic Acids, 2016, 35(5), 259-276.

- [4]. Bossinger S.D. and Tekeshi E., Chem. Abstract., 1972, 77, 343590.
- [5]. G. Victor Fazakerley Graham E. Jackson Peter W. Linder, Equilibrium studies of benzyl penicillinate-thiaproline-hippurate and benzylpenicilloate-proton and transition metal(II) ion systems, Journal of Inorganic Nucl. Chemistry, 1975, 38, 1397-1400.
- [6]. Irving H. and Rossotti H., J. Chem. Soc., 1954, 2904.
- [7]. Martell A.E. and Calvin M., Chemistry of metal chelate compounds. Prentice Hall. Inc. England. Cliffs. N. J. 1962.
- [8]. Banarjee A. and Rao T.V.R., J. Indian Chem. Soc., 1968, 63, 480.
- [9]. Meshram Y.K., Khan R.F., To studied the interaction between Co(II), Ni(II) and Cu(II) Metal Ions and 2-Hydroxy-4-Methyl-5-Chloro Acetophenone (L1) and at 0.1M Ionic Strength in 70% DMF water mixture, Ind. J. Applied Res., 2014, 4(3), 37.
- [10]. Balakrishna Malla, G. Srinivasa Rao, Dr. Malla Ramanaiah, Gollapalli Nageswara Rao, pH Metric Investigation on Speciation Studies of 5-Sulfosalicylic acid complexes of Co(II), Ni(II) and Cu(II) in DMF-Water Mixtures, Der Pharma Chemica, 2016, 8(8), 150-157,
- [11]. Tayade D.T., Pund D.A., Bhagwatkar, R.A., Rathod D.B., Neha A. Bhagwatkar, pH Metric Studies of Interaction of Synthesized Ligands 2-amino-4-hydroxy-6-methylpyrimidine and 1-(4-hydroxy-6-methylpyrimidino)-3-phenylthiocarbamide with Cu(II), Cd(II), Cr(II), Cations At 0.1 M Ionic Strength, International Journal of Chemistry, 2011, 3(1).
- [12]. Naik AB, Narwade ML. Russian J. Coordination chem. 2009, 35(12):932-937.
- [13]. Janrao D.M., Pathan J., Sci. chem. Commun., 2014, 4(1), 11.
- [14]. Ramteke A., Narwade M.L., Arch Applied Sci. Res, 2013, 5(1), 231.
- [15]. Thakur S.V., J. Chem., Bio & Phys Sci., 2014, 4(1), 01.
- [16]. Irving H and William R.J.P., J. Chem. Soc., 1953, 3192.
- [17]. Narwade M.L., Chincholkar M.M. and Sathe S.W., J. Indian Chem. Soc., 1985, 62, 194.
- [18]. Bodkhe P.S., Patil K.N., Narwade M.L. and Doshi A.G., Asian J. Chem., 2003, 15(3 & 4) 1739-1743.
- [19]. Prasad R.N., Agrawal M, Ratnani R. and Sarswal K., J. Indian Chemical Soc, 2005, 82, 137 – 139,.
- [20]. Thakur S.D., Munot K.P., Raghuvanshi P.B., Tayade D.T., Acta Ciencia Indica, 2010, XXXC(3), 425.

pH-Metric Studied Stability Constant of 5-P-Hydroxyphenyl-Thiocarbamido-1-Naphthol with Various Metal Ions in 60 % Ethanol-Water Mixture

Y.P.Wayal¹, N.D. Dahake¹, P.M.Deshmukh², P.S. Bodkhe³, R.T.Parihar⁴

¹Department of Chemistry, Shri Dnyaneshwar M. Burungale Science and Art College Shegaon, Maharashtra, India

²Department of Chemistry, Art, Commerce Science College Warwatbikal, Maharashtra, India

³Department of Chemistry, Vidyabhaarti College Amravati, Maharashtra, India

⁴Department of Chemistry, Vidnyan Mahavidyalaya Malkapur, Maharashtra, India

ARTICLE INFO

Article History:

Accepted : 01 Jan 2025

Published : 10 Jan 2025

Publication Issue :

Volume 12, Issue 7

January-February-2025

Page Number :

656-660

ABSTRACT

Present work deals with pH-metric studied stability constant of 5-p-hydroxyphenyl-thiocarbamido-1-naphthol with various metal ions in 60 % ethanol-water mixture. In present work studied interaction of 5-p-hydroxyphenylthiocarbamido-1-naphthol (L2) with Cu(II), Cd(II) and Cr(III) metal ions at 0.1 M ionic strength in 60 % ethanol-water mixture by Bjerrum method as adopted by Calvin and Wilson, It is observed that Cu(II), Cd(II) and Cr(III) metal ions form 1:1 with ligands (L2). The values of proton-ligand stability constant (pK) and metal-ligand stability constants (log k) were estimate and compared from resultant data. The effects of substituents were studied from estimated data (pK& log k).

Keywords: 5-p-hydroxyphenylthiocarbamido-1-naphthol (L2), Stability constant, pH-metrically.

I. INTRODUCTION

Molecule containing thiocabamido, amino, hydroxyl, benzenoid and non-benzenoid nucleus showed various applications in pharmaceutical and medicinal sciences. These types of drugs are very effective in various diseases. Several modern theories and concept are concerning to physical as well as chemical study of benzenoid, non-benzenoid, heteroacycles and heterocycles. Aminonaphthols and thiocarbamido nucleus containing heterocycles possesses pharmaceutical, medicinal agricultural industrial and biotechnological significances [1-5]. The manifold research work has been done on the study of metal and nitrogen heterocyclic ligands containing complexes [6-15]. The studies of metal-ligand complexes in solution having number of metal ions with ligands carboxylic acids, oximes, phenols etc. would be interesting which throw a light on the mode

of storage and transport of metal ions in biological kingdom. Metal complexation not only brings the reacting molecules together to give activated complexes [16] but also polarized electrons from the ligands towards the metal. The relation between stability and basicity of the ligands is indicated by the formation constant and free energy change value. Bulkier group increases the basicity of ligands as well as stability. The stability of the complexes is determined by the nature of central metal atom and ligand. The stability of complexes is influenced by the most important characteristics degree of oxidation, radius and electronic structure. Irving and Williams had studied the order of stability of metal complexes of transition metal ions by comparing the ionic radius and second ionization potentials of metal ions, as it is valid for most nitrogen and oxygen donor ligands. Stability and complexation by ligands and various metal ions were evaluated by many researchers [17-20]. Reliable information of stability constant is of great importance in analytical and separation procedure. To remove undesirable and harmful metals from living organism, chelating agents are very much useful in biological systems. This gives importance to the study of determination of stability constant of metal complexes. In present work an attempt has been made to pH-metric studied stability constant of 5-p-hydroxyphenyl-thiocarbamido-1-naphthol with various metal ions in 60 % ethanol-water mixture.

II. MATERIALS AND METHODS

All chemicals used are of AR grade. The stock solutions of the ligand L₂ was prepared by dissolving required amount of ligand in a of 60% (ethanol + water) mixture.

General procedure:

Types of Titrations

i) Free acid HNO₃ (0.01 M)

ii) Free acid HNO₃ (0.01 M) and ligand (20 x 10⁻⁴M)

iii) Free acid HNO₃ (0.01 M) and ligand (20 x 10⁻⁴) and metal ion (4 x 10⁻⁴M) against standard 0.1N NaOH solution. The ionic strength of all the solutions was maintained constant 1M by adding appropriate amount of KNO₃ solution. All the titrations were carried out in 60% (Ethanol-water) mixture and the reading were recorded for each 0.2 ml addition. The graph of volume of alkali added (NaOH) against pH were plotted. The ligands involved in the present work may be considered as a monobasic acid having only one dissociable H⁺ ion from phenolic -OH group and it can therefore, be represented as HL. The dissociating equilibria can be shown as.



By the law of mass action, we have,

$$K = [HL] / ([H^+] [L^-]) \dots\dots\dots (1)$$

Where, the quantities in bracket denote the activities of the species at equilibrium.

III. RESULT AND DISCUSSION

Calculation of Proton-Ligand Stability Constant (\bar{n}_A)

The plots between volume of NaOH and pH of the solution were used to determine the proton ligand stability constant (representing the replacement of H⁺ ions from functional group of ligand with respect to pH value). The horizontal difference (V₂-V₁) was measured accurately between the titration curves of free acid and acid + ligand. It was used to calculate the formation number \bar{n}_A at various pH values and fixed ionic strength $\mu = 0.1$ M using Irving and Rossotti's equation

$$\bar{n}_A = \gamma - \left\{ \frac{(V_2 - V_1)(N + E^0)}{(V^0 + V_1)T_L^0} \right\} \dots \dots \dots (2)$$

Where, V^0 is the initial volume of the solution. E^0 and T_L^0 are initial concentrations of the mineral acid and ligand respectively. V_1 and V_2 are the volumes of alkali of normality N during the acid and ligand titration at given pH. γ is the replaceable proton from the ligand. The data of \bar{n}_A obtained at various pH along with the horizontal difference for some representative systems are represented in Table 1. The metal-ligand formation number (\bar{n}) is estimated by Irving-Rossotti's equation.

$$\bar{n} = \frac{(V_3 - V_2)(N + E^0)}{(V^0 + V_2)\bar{n}_A T_M^0} \dots (3)$$

Where, the notations have the same meaning as given in earlier equation. The horizontal difference ($V_3 - V_2$) between the metal complex ($A + M + L$) and reagent ($A + L$) curve is used to evaluate the value of n using Irving Rossotti's equation

Table-1 :Proton-Ligand Stability constant (pK)

System	pK		Diff.
	Half integral method	Point wise method	
5-p-hydroxyphenylthiocarbamido-1-naphthol (L_2)	9.24	9.50	0.26

Table-2 :Metal-ligand stability constant (log K)

System	Log K_1	Log K_2	Δ Log K	Log K_1 /Log K_2
Cu(II) + L_2	5.26	6.05	0.79	0.869421488
Cd(II) + L_2	5.56	6.04	0.48	0.920529801
Cr(III) + L_2	5.95	6.15	0.2	0.967479675

Fig. 3 Plot between \bar{n} vs pH System- $L_2 + Cu(II)$ System- $L_2 + Cu(II)$

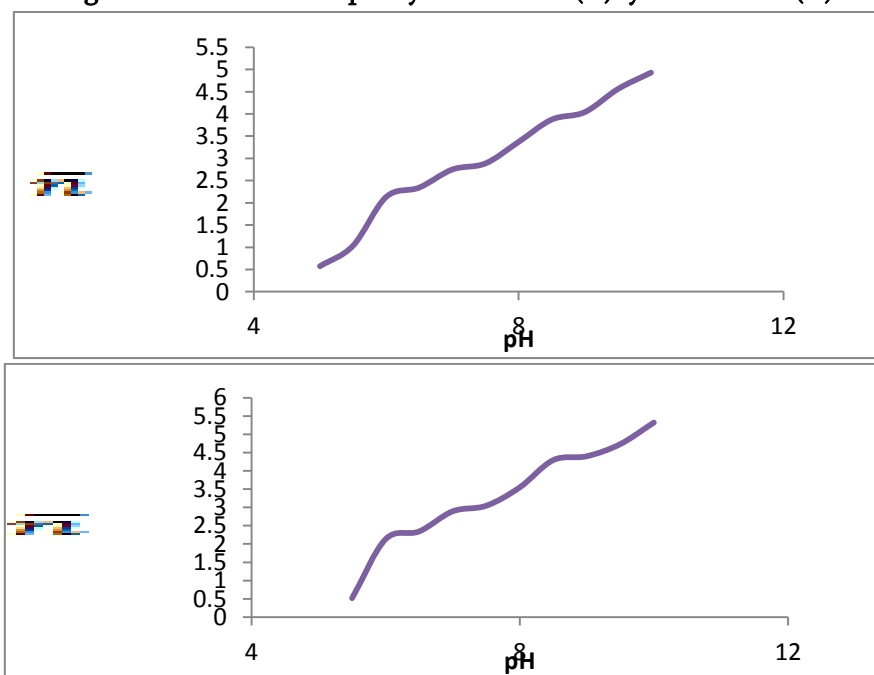
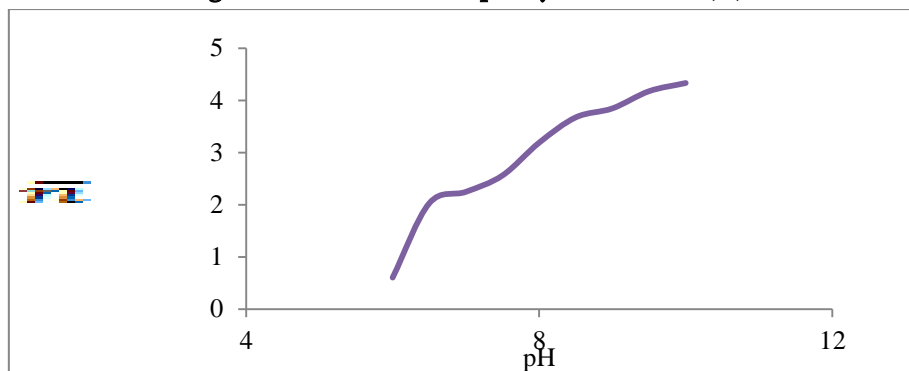


Fig. 3 Plot between \bar{n} vs pH System- L₂+Cu(II)



IV. CONCLUSION

For 5-p-hydroxyphenylthiocarbamido-1-naphthol (L₂) the difference between the values of log K₁ and log K₂ is higher with Cr(III) complex than Cu(II) and Cd(II) complexes. Cr(III) forms more stable complex with L₂ than Cd(II) and Cu(II) metal ions.

Observation of Table-2 showed that less difference between log K₁ and log K₂ values indicates complex formation between metal ion and ligand occurring simultaneously and 1:1 complexation occurs in between to above metal ions and L₂.

V. REFERENCES

- [1]. Barnes D.M., Jianguo Ji, Fickes M.G., J. Am. Chem. Soc., 2002, 124, 13097-13105.
- [2]. Cyril V., Milam M., Chem. Abstract., 1977, 86, 190015.
- [3]. Hassan H. Hammud, Mohammad H. El-Dakdouki, Nada Sonji, Ghassan Sonji, Kamal H. Bouhadir, Interactions of Some Divalent Metal Ions with Thymine and Uracil Thiosemicarbazide Derivatives, Nucleosides, Nucleotides And Nucleic Acids, 2016, 35(5), 259-276.
- [4]. Bossinger S.D. and Tekeshi E., Chem. Abstract., 1972, 77, 343590.
- [5]. G. Victor Fazakerley Graham E. Jackson Peter W. Linder, Equilibrium studies of benzyl penicillinate-thiaproline-hippurate and benzylpenicilloate-proton and transition metal(II) ion systems, Journal of Inorganic Nucl. Chemistry, 1975, 38, 1397-1400.
- [6]. Irving H. and Rossotti H., J. Chem. Soc., 1954, 2904.
- [7]. Martell A.E. and Calvin M., Chemistry of metal chelate compounds. Prentice Hall. Inc. England. Cliffs. N. J. 1962.
- [8]. Banarjee A. Kand Rao T.V.R., J. Indian Chem. Soc., 1968, 63, 480.
- [9]. Meshram Y.K., Khan R.F., To studied the interaction between Co(II), Ni(II) and Cu(II) Metal Ions and 2-Hydroxy-4-Methyl-5-Chloro Acetophenone (L1) and at 0.1M Ionic Strength in 70% DMF water mixture, Ind. J. Applied Res., 2014, 4(3), 37.
- [10]. Balakrishna Malla, G. Srinivasa Rao, Dr. Malla Ramanaiah, Gollapalli Nageswara Rao, pH Metric Investigation on Speciation Studies of 5-Sulfosalicylic acid complexes of Co(II), Ni(II) and Cu(II) in DMF-Water Mixtures, Der Pharma Chemica, 2016, 8(8):150-157,
- [11]. Dipak T. Tayade, Dinesh A. Pund, Rahul A. Bhagwatkar, Dinesh B. Rathod, Neha A. Bhagwatkar, pH Metric Studies of Interaction of Synthesized Ligands 2-amino-4-hydroxy-6-methylpyrimidine and 1-(4-

hydroxy-6-methylpyrimidino)-3-phenylthiocarbamide with Cu(II), Cd(II), Cr(II), Cations At 0.1 M Ionic Strength, International Journal of Chemistry, 2011,3(1).

- [12]. Naik AB, Narwade ML. Russian J. Coordination chem. 2009, 35(12):932-937.
- [13]. Janrao D.M., Pathan J.,Sci. chem. Commun., 2014, 4(1), 11.
- [14]. Ramteke A., NarwadeM.L.,ArchApplied Sci. Res, 2013, 5(1), 231.
- [15]. Thakur S.V.,J.Chem., Bio & Phys Sci., 2014, 4(1), 01.
- [16]. Irving H and WilliamR.J.P.,J. Chem. Soc., 1953, 3192.
- [17]. Narwade M.L., Chincholkar M.M. and Sathe S.W.,J. Indian Chem. Soc., 1985, 62, 194.
- [18]. Bodkhe P.S., Patil K.N., NarwadeM.L. and Doshi A.G., Asian J. Chem., 2003, 15(3 & 4) 1739-1743.
- [19]. Prasad R.N., Agrawal M, RatnaniR. and SarswalK.,J. Indian Chemical Soc, 2005, 82, 137 – 139,.
- [20]. Thakur S.D., Munot K.P., Raghuvanshi P.B., Tayade D.T.,ActaCienciaIndica, 2010, XXXC(3), 425.

One Pot Synthesis of 1(4-Chlorophenyl)-2(p-Tolylthiocarbamido)-1-Ethanol

A.B.Wadekar¹, A.P.Nagrale¹, D.L.Bhade², V.G.Bhagat³, M.M. Rathore⁴

¹Department of Chemistry, Shri Dnyaneshwar Maskuji Burungale Science and Arts College Shegaon, Dist. Buldhana, Maharashtra, India

²Department of Microbiology, Shri Dnyaneshwar Maskuji Burungale Science and Arts College Shegaon, Maharashtra, India

³Department of Environmental Science, Shri Dnyaneshwar Maskuji Burungale Science and Arts College Shegaon, Maharashtra, India

⁴Department of Chemistry, Vidyabharati Mahavidyalaya, Amravati, Maharashtra, India

ARTICLE INFO

Article History:

Accepted : 01 Jan 2025

Published : 10 Jan 2025

Publication Issue :

Volume 12, Issue 7

January-February-2025

Page Number :

661-664

ABSTRACT

Active drugs molecules synthesis is strong demand for huge population of the world. Present work deals with synthesized of 1(4-Chlorophenyl)-2(p-Tolylthiocarbamido)-1-ethanol by the interactions of 4-(2-amino-1-hydroxyethyl)chlorobenzene and p-tolylisothiocyanate in acetone medium, to isolate 1(4-Chlorophenyl)-2(p-Tolylthiocarbamido)-1-ethanol. The product thus synthesized in these reactions and characterized on the basis of conventional elemental analysis, chemical characteristics and through IR, PMR, CMR and Mass spectral analysis.

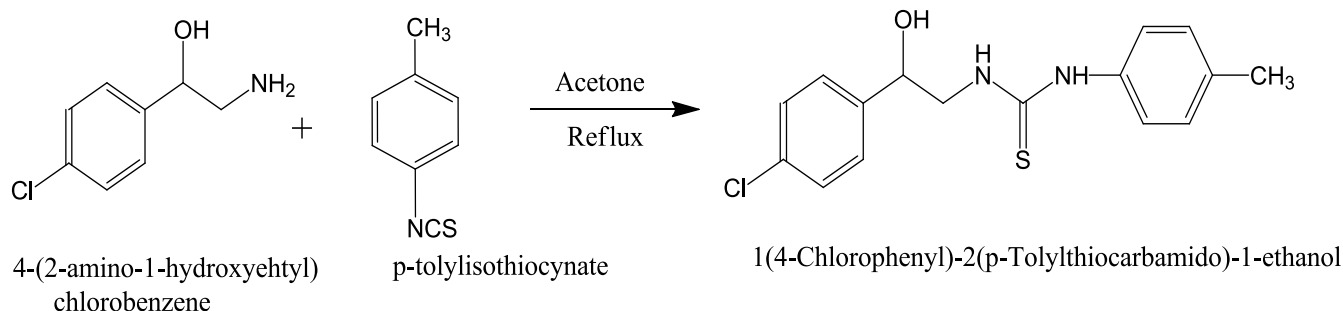
Keywords: 4-(2-amino-1-hydroxyethyl)chlorobenzene, p-tolylisothiocyanate, 1(4-Chlorophenyl)-2(p-Tolylthiocarbamido)-1-ethanol.

I. INTRODUCTION

Population of the world terribly growing along with that basic demands of health and medicine related things. World researchers were pointed their attention toward this aspect and working with challenge toward same. Pathogens are become resistive against existing some drugs moieties thus have a great need to developed more active and potent drugs moieties with good solubility, diffusion and activity that will be demonstrate effective pharmacodynamics and pharmacokinetics of drugs. The literature survey divulges that from last couple of decades' numerous advances, theories and new concepts regarding to synthesis of novel moieties, chemical, physical as well as biological study of benzenoid and non-benzenoid, heteroacyclic and heterocyclic compounds were studied¹⁻⁵. These compounds have their own identity and importance in the chemical and

life sciences due to their variety of applications in medicinal, agricultural, pharmaceutical, industrial, biotechnological and biochemical sciences⁶⁻¹⁰. If we think about the drugs we can define the history of medicine by these compounds.

In the view of the utilities of these compounds in various fields and as a part of present research work, recently being undertaken in this laboratory in the synthesis of nitrogen, nitrogen and sulphur containing heteroacycles and heterocycles and to investigate their medicinal, pharmaceutical, agricultural, industrial, biotechnological and biochemical significance¹¹⁻¹⁸, hence interactions of 4-(2-amino-1-hydroxyethyl)chlorobenzene and p-tolylisothiocyanate in acetone medium, to isolate 1(4-Chlorophenyl)-2(p-Tolylthiocarbamido)-1-ethanol.



II. METHODS AND MATERIAL

All AR grade chemicals were used throughout experiment.

Synthesis of 1(4-Chlorophenyl)-2(p-Tolylthiocarbamido)-1-ethanol

1(4-Chlorophenyl)-2(p-Tolylthiocarbamido)-1-ethanol was synthesized by refluxing 4-(2-amino-1-hydroxyethyl)chlorobenzene and p-tolylisothiocyanate in acetone medium for 2 hours. After completion of reaction, to isolated 1(4-Chlorophenyl)-2(p-Tolylthiocarbamido)-1-ethanol from solvent. After distillation of acetone the product is isolated which is recrystallized from ethanol to get white colour crystalline solid flakes with m.p. 820C.

III.RESULT AND DISCUSSION

Properties of 1(4-Chlorophenyl)-2(p-Tolylthiocarbamido)-1-ethanol:

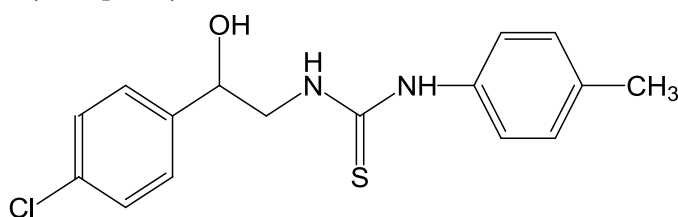
The compound is white colour crystalline solid flakes, C₁₆H₁₉N₂SCl with m.p. 820C. It gave positive test for nitrogen, chlorine and sulphur.Desulphurised with alkaline plumbite solution. Soluble in boiled sodium hydroxide, sulphuric acid, 1,4-dioxane, hydrochloric acid and nitric acid and was sparing soluble in boiled water, ethanol, acetone and benzene.Formed picrates having melting point 950C.

Elemental analysis (%): Found (Calculated) C- 60.07 (62.63), H-5.49 (6.24), N-8.71 (9.13), S-9.82 (10.45), Cl-10.20 (11.55). FTIR spectrum (v cm⁻¹):- The IR spectrum of compound was carried out in KBr pellets on SHIMADZU IR spectrometer¹⁹⁻²⁴. 2773. 64-2565.33 (Aliphatic C-H stretching), 2902.87 (Aromatic C-H stretching), 1945.82 (N-C=S stretching), 1589.99-1815.02 (C=N stretching), 1897.95 (C=S stretching), 3050.95 (Two N-H stretching), 3195.83 (Alcoholic O-H stretching), 1180.72-1244.50 (C-O stretching), 1505.55-1294.24 (Aliphatic -H bending), 1070.49-611.43 (Aromatic -H bending).PMR spectrum data:The PMR spectrum of a compound was recorded in CDCl₃+ DMSOd₆ on Bruker Avance-II 400 NMR spectrometer^{19-20,25-28}. This spectrum distinctly displayed the signals, due to four aromatic protons in the range at δ 7.509 – δ 7.288 ppm of phenyl group, four aromatic protons in the range at δ 7.226 - δ 7.171 ppm, alcoholic -H at δ 3.652, two amino -

NH protons at δ 9.7422 ppm, methyne (-CH) proton at δ 2.335, two diastereotopic methylene protons at δ 2.445 ppm and three methyl protons at δ 2.341.

IV. CONCLUSION

Present chemical characteristics, elemental and spectral analysis reveals that the newly synthesized present compound was assigned the structure as 1(4-Chlorophenyl)-2(p-Tolylthiocarbamido)-1-ethanol. This work create scope to studies various chemical, pharmaceutical, agricultural and biological applications of newly synthesized 1(4-Chlorophenyl)-2(p-Tolylthiocarbamido)-1-ethanol.



1(4-Chlorophenyl)-2(p-Tolylthiocarbamido)-1-ethanol

V. REFERENCES

- [1]. Tayade D.T., Bhagwatkar A.K., International Journal of Organic and Bioorganic Chemistry, 4(1), 2014, 6-9.
- [2]. Popov V.V., Amelichev S.A., Bushmarinov I.S., Konstantinova L.S. Lyssenko K.A., Mikhilchenko L.V., Novikov V.V., Gulyai V.P., Rakitin O.A., Tetrahedron, 69, 2013, 8790-8797.
- [3]. Letska E.V., Turner N.W., Anthony P.F., Tuner and Piletsky S.A., J. Controlled Release, 08(1), 2005, 132.
- [4]. Kim G.Y., Shim J., Kang M., Moon S.H., J. Environ. Monti, 10, 2008, 632.
- [5]. Dandia A.K., Arya K., Sati M., Synthetic Communication, 34(6), 2004, 1141.
- [6]. G. Arabaci, P. Yi, H. Fu, M.E. Morter, Bio-Org. Med. Chem. Letter, 12(2), 2002, 3047-3050.
- [7]. S. Nagar, N.H. Singh, J. Med. Chem., 16, 2007, 178-180.
- [8]. J. Martin, M. Borodie and P. Kwan, British Medical Journal, 22(1), 2000, 5-7.
- [9]. D.J. Faulkner, Tetrahedron Lett, 38, 1993, 21-25.
- [10]. R.C. Panpalia, Ph.D. Thesis, S.G.B. Amravati University, Amravati, 2007.
- [11]. V. Cyril and M. Milam, Chem. Abstr., 86, 1977, 190015.
- [12]. B. Belmut and K. Will, Germ. Offen, 2, 1978, 630, 849.
- [13]. K. Alfred and A. Tentawy, Chem. Abstr., 90, 1979, 54914.
- [14]. D.T. Tayade, Ph.D. Thesis, S.G.B. Amravati University, Amravati, 1996.
- [15]. C.D. Bossinger and E. Tekeshi, Chem. . Abstr., 77, 1972, 343590.
- [16]. D. Park and Co.workers, British Patent, 48, 1960, 245.
- [17]. M. Sedal and F.E. Betiver, S. African Patent, 68, 1964, 03, 47.
- [18]. A.G. Ghaigy (Jr.), Siess Patent, 4, 1980, 186, 265.
- [19]. C.N. Banwell, Elaile and Cash Mc, "Fundamentals of Molecular Spectroscopy", 4th Ed. McGraw Hill International U.K., 2003.
- [20]. J.R. Dyer, "Applications of Absorption Spectroscopy of Organic Compounds", 8th Ed., Prentice Hall, India, New Delhi, 1991.

- [21]. D.V. Pavia, G.M. Lampan and G.S. Kriz, "Introduction to Spectroscopy", 3rd Ed., Thomson Brooks/Cole, Singapore, 2002.
- [22]. D.H. Williams and I. Fleming, "Spectroscopic Methods in Organic Chemistry", 4th Ed., TataMc Graw Hill Publishing Company Ltd., New Delhi, 1993.
- [23]. A.I. Vogel, "Text book of Practical Organic Chemistry", 4th Ed., E.L.B.S. and Lorgman, India, 1978.
- [24]. L.D. Field., S. Sterhell and J.R. Kalmall, "Organic Structures from Spectra", 3rd Ed., John Wiley and Sons, England, 2002.
- [25]. R.M. Silverstein and G.C. Bassler, "Spectroscopic Identification of Organic Compounds", 5th Ed., John Wiley and Sons Inc., New York, 127, 1991.
- [26]. J.R. Dyer, "Application of Absorption Spectroscopy of Organic Compounds", 8th Ed., Prentice Hall, India, New Delhi, 108, 1991.
- [27]. D.V. Pavia and G.M. Lampan, "Introduction to Spectroscopy", 3rd Ed., Thomson Brooks/Cole, Singapore, 143, 2001.
- [28]. R.M. Silverstein and G.C. Bassler, "Spectroscopic Identification of Organic Compounds", 5th Ed., John Wiley and Sons Inc., New York, 123, 1991.

Evaluation of Thermodynamic Parameters of Substituted Naphthol

Aditya D. Joshi, Vaishnavi A. Petkar, Gopal S. Bharambe, Dr. Sanjay V. Kolhe

P. G. Department of Chemistry, Shri Shivaji Arts, Commerce & Science College, Akot Dist. Akola, Maharashtra, India

ARTICLE INFO

Article History:

Accepted : 01 Jan 2025

Published : 10 Jan 2025

Publication Issue :

Volume 12, Issue 7

January-February-2025

Page Number :

665-668

ABSTRACT

Regarding environmental protection and human susceptibility, many chemists and researchers have drawn a lot of attention. In order to meet the demands of this generation, they synthesized a large number of compounds and molecules and evaluated their importance and potential uses in a variety of fields. More values were obtained from the conductometric study. This analysis establishes a crucial link between the biological and chemical sciences. With all of this in mind, the current scheme is intended to ascertain the thermodynamic and conductometric parameters of 5-phenylthiocarbamido-2-naphthol at varying temperatures and concentrations in a 60% ethanol water mixture. The various interactions between molecules and solvents used in current work are better understood thanks to this research project. Understanding the pharmacodynamics and pharmacokinetics of the recently synthesized molecules is made possible by these analyses.

Keywords :- Thermodynamic parameters, conductometric study, 5-phenylthiocarbamido-2-naphthol, conductometric parameters

INTRODUCTION

Literature reveals the perspective of drug activity; ion mobility was given higher values. Ion mobility determined the solution's conductivity, which also aids in understanding how the solute dissociates in the solvent. Solute dissociation, also known as ionization, affects the solute ions' mobility and bioavailability. Drug conductivity aids in understanding pharmacodynamics. Ion mobility is also referred to as ion transmission. Drug solubility and permeability are effectively impacted by ionic transmissions of the electrolyte in the electrolytic solution. Biopharmaceutical parameters that contribute to effective bioavailability and good in vitro and in vivo correlation are solubility and bioavailability, which can be measured [1]. These days; researchers are primarily focused on improving the oral bioavailability, solubility, and rate of dissolution of medications that are not very water soluble [2]. One of the more advanced techniques that aids in solubilisation is the hydrotropic salinization method [3]. By adding particular hydrotropic agents, numerous researchers were compensated for their efforts to improve the aqueous solubilisation of insoluble medications [4,

5]. Conductometric analysis yielded useful data regarding the interaction between solutes and solvents [6]. Gomaa and Al-Jahdalli [7] investigated the ionic association of divalent asymmetric electrolyte $\text{Cu}(\text{NO}_3)_2$ with Kryptofix-22 in mixed (MeOH-DMF) solvents at varying temperatures using conductometric measurements. Izonfuo and Obunwo [8] and Roy *et al.* [9] used conductometry to study a variety of alkali metals at varying ratios of mixed solvents.

In addition to comparing transition metal complexes among the halide group [10–14], some researchers concentrate on the Walden product and thermodynamic parameter of various complexes. The thermodynamic parameters and ion pair formation of Glycine Bis-1-amidino-*O*-methylurea cobalt (III) halides in a water-methanol mixture at varying temperatures were examined by Singh *et al.* [15]. Keeping all of this in mind, the current research plan uses a 60% ethanol-water mixture to determine the thermodynamic parameters (i.e., ΔH ; ΔS , and ΔG) and conductometric parameters of 5-phenylthiocarbamido-2-naphthol conductometrically at various concentrations and temperatures. Understanding different intra- and inter-molecular interactions, such as solvent-solvent, solute-solvent, and solute-solute interactions, is aided by this research. This knowledge aids in comprehending the effects of different substituents and the pharmacodynamics of medications.

MATERIALS AND EXPERIMENTALMETHODS:

Current work makes use of newly prepared solutions. Through current analysis, all AR-grade chemicals are utilized. Prior to use the solvents were purified using a standard procedure. To make a mixture of 80% ethanol and water with concentrations of 5-phenyl thiocarbamido-2-naphthol of 0.01M, 0.005M, 0.0025M and 0.0012M. Using a thermostat, the drug solution's thermal equilibrium was maintained at 298K and 303K respectively. After achieving thermal equilibrium, conductivity is measured for each concentration solution.

RESULT AND DISCUSSION:

By serial dilution method to create solutions of 0.005M, 0.0025M, and 0.0012M with 65% and 75% ethanol-water mixture, respectively, after creating a solution with a 0.01 M concentration of 5 phenylthiocarbamido-2-naphthol. Conductivity Bridge was used to measure the conductance of each solution at 293K and 303K. The results are tabulated and presented in Tables 1 and 2. The resulting data was analysed using a known literature method to determine the observed conductance (G), specific conductance (k) and molar conductance (μ).

TABLE – 1 - CONDUCTOMETRIC MEASUREMENTS AT DIFFERENT CONCENTRATIONS OF 5-PHENYLTHIOCARBAMIDO-2-NAPHTHOL				
DETERMINATION OF G, k and μ AT DIFFERENT CONCENTRATIONS AND DIFFERENT TEMPERATURES IN 65% E-W MIXTURE				
Temp	Concentration C (M)	Observed conductance (G) mS	Specific conductance (k) mSm^{-1}	Molar conductance (μ) $\text{mSm}^2\text{mol}^{-1}$
293K	0.01	0.0209	0.002134×10^{-3}	0.21333
	0.005	0.01249	0.001538×10^{-3}	0.30786
	0.0025	0.00857	0.001099×10^{-3}	0.439823
	0.0012	0.0069	0.009038×10^{-3}	0.753108
303K	0.01	0.02498	0.002976×10^{-3}	0.297533
	0.005	0.01417	0.001762×10^{-3}	0.352238
	0.0025	0.01026	0.001302×10^{-3}	0.522859
	0.0012	0.00838	0.001064×10^{-3}	0.885957

Table 1 lists the observed conductance (G), specific conductance (k), and molar conductance (μ) values. In this case, G, k, and μ rise in tandem with rising temperatures and fall in tandem with falling concentrations. The higher the temperature, the higher the specific conductance, calculated values of 5-phenylthiocarbamido-2-naphthol's specific constant (Ksp), log (Ksp), and thermodynamic parameters (ΔG), (ΔS), and (ΔH) using established literature methods at various concentrations and temperatures. Obtained result computed in

Table 2

TABLE – 2 - CONDUCTOMETRIC MEASUREMENTS AT DIFFERENT CONCENTRATION AND DIFFERENTS TEMPERATURES OF 5-PHENYLTHIOCARBAMIDO-2-NAPHTHOL						
DETERMINATION OF Ksp, log Ksp, ΔG , ΔH and ΔS AT DIFFERENT CONCENTRATIONS AND DIFFERENT TEMPERATURES						
SYSTEM: L ₂ [PTCN]			MEDIUM - 65% Ethanol-Water Mixture			
Temp.(K)	Conc. M	Ksp	Log Ksp	ΔG kJmlo ⁻¹	ΔH kJmlo ⁻¹	ΔS kJK ⁻¹ mlo ⁻¹
293K	0.01	0.001426	-4.84905	-27203.68	-122748	511.778
	0.005	0.007374	-5.13248	-28793.84	-74347.4	352.018
	0.0025	0.003762	-5.42468	-30433.04	-73054.5	353.198
	0.0012	0.002546	-5.59504	-31388.75	-82516	388.76
303K	0.01	0.03243	-4.4896	-26046.24	-83707.8	362.226
	0.005	0.01143	-4.94497	-28688.64	-92200.5	398.975
	0.0025	0.006255	-5.20394	-30191.02	-97028.8	419.869
	0.0012	0.004145	-5.38338	-31232.19	-100378	434.349

It can be inferred from tables -1 and 2 above that the conductrometric and thermodynamic parameter values of 5-phenylthiocarbamido-2-naphthol are closely related to the variation in temperatures and molar concentrations.

As can be seen, the μ values rise as temperature rises and concentration falls, suggesting either greater ion mobility or less solvation. This is because dilution and rising temperatures, respectively, cause more bond breaking when thermal energy increases. Additionally, negative ΔG values suggested that the reaction was spontaneous. Enthalpy change (ΔH) values that are negative indicate that the reaction is exothermic. Entropically favourable is indicated by a positive value of (ΔS) and a favourable temperature. Molar concentrations and percentage compositions have a significant impact on the change in thermodynamic parameter values. These parameters are also significantly impacted by solute (drug)-solvent interactions, solvent-solvent interactions, solvent-solvent-solute interactions, and solute-solute-solvent interactions. The variation of these parameters is also caused by internal geometry and intra- and intra-hydrogen bonding.

REFERENCES

1. Bakhtiar, Z., Hasandokht, M. R., Naghavi, M. R., & Mirjalili, M. H. *Arabian Journal of Chemistry*, 21(82), 1-12. (2022).
2. Malghani, N., Mahesar, S., Baig, J., Talpur, F., Sherazi, S. T. H., & Junaid, M. *Journal of the Turkish Chemical Society Section A: Chemistry*, 9(4), 985-998. (2022).
3. A. Jain, B. Mishra and S. Singh. C.W. Pouton, "Drugs information for health care professional" 17th Euro. J. Pharm Sci., 29, 278-287, (2006).

4. S. Agrawal, S.S. Pancholi, N.K. Jainan, G.P. Agrawal, *Int.J.PHam.*,274,149-155,(2004).
5. G.D. Pancholi and J.C.Gradock, *J. Pharm.Sci.*, 68,728-732, (1974).
6. U.N. Dash and S.Supkar, *Proc. Ind.Acad.Sci.Chem.Soc.*, 107, 541, (1995).
7. G.C. Bag, N.M.Singh and N.R. Singh, *J. Ind. Chem. Soc.*, 77, 146,(2000).
8. E.A. Gonna and B.M. Al-Jahadalli, *American J. Condensed Matter Physics*, 2(1), 16- 21, (2012).
9. W.A.L. Izonfuand, C.C. Obunwa, *Ind. J. Chem.*, 38A,939,(1999). Ed., USPDI,1646,(1997)
10. M.N. Roy, D. Nandi and D.K. Hazra, *J.Ind.Chem.Soc.* 70,121,(1993).
11. C.S. Solanki, Mishra, M.K. Talari, M. Tripathy and U.N.Dash, *E-J Chem.*, 9(1), 21-26, (2012).
12. L.S. Singh, A. Jibanlata and N.R. Singh, *J.Ind.Chem.Soc.* 74, 635,(1997).
13. N.R. Singh, *J. Ind. Chem. Soc.*, 69, 279, (1992).
14. Singh, U., Chamoli, M., Singh, K. P., Ram, L., Jangir, S., & Maheshwari, R. K. *International Journal of Environment and Health Sciences*, 4, 19-27. (2022).
15. Raji-Idowu, F, *Nigerian Journal of Microbiology*. (2023).

Preliminary phytochemical analysis of *Clematis triloba* B. Heyne ex Roth

Abhijeet A. Pakhare, Radhika Dhurve, Shumaila Taqdees, Misbah Anjum and Vishal P. Deshmukha*

Department of Botany, Jagadamba Mahavidyalaya, Achalpur City-444806, Dist- Amravati, Maharashtra, India.

*Corresponding author: vishalpdeshmukh@yahoo.com

ARTICLE INFO

Article History:

Accepted : 01 Jan 2025

Published : 10 Jan 2025

Publication Issue :

Volume 12, Issue 7

January-February-2025

Page Number :

669-673

ABSTRACT

Regarding environmental protection and human susceptibility, many chemists and researchers have drawn a lot of attention. In order to meet the demands of this generation, they synthesized a large number of compounds and molecules and evaluated their importance and potential uses in a variety of fields. More values were obtained from the conductometric study. This analysis establishes a crucial link between the biological and chemical sciences. With all of this in mind, the current scheme is intended to ascertain the thermodynamic and conductometric parameters of 5-phenylthiocarbamido-2-naphthol at varying temperatures and concentrations in a 60% ethanol water mixture. The various interactions between molecules and solvents used in current work are better understood thanks to this research project. Understanding the pharmacodynamics and pharmacokinetics of the recently synthesized molecules is made possible by these analyses.

Keywords :- Thermodynamic parameters, conductometric study, 5-phenylthiocarbamido-2-naphthol, conductometric parameters

INTRODUCTION

Plants are a source of a wide range of natural products that possess various therapeutic properties and are continuously explored to develop novel drugs. For ages, traditional medicines have depended on these natural products to treat many diseases (Singh et al, 2012). Natural products are made up of many bioactive compounds. These bioactive compounds impart biological activity against several disease-causing agents. To date, numerous secondary metabolites with diverse structures and pharmacological properties have been identified from plants (Gad et al., 2013). About 70,000 herbal plants have been used for medicinal purpose, mainly in Asian countries. In India, 20% of the available plants are used for medicinal purposes. Medicinal plants are the storehouse of unlimited ethnobotanical compounds, which are being utilized for making various drugs (Nasim et al., 2022). *Clematis triloba* B. Heyne ex Roth, (synonym = *Clematis heynei*) is an important medicinal plants belongs to the family Ranunculaceae (Buttercup family) (Rana and Nagar, 2017). It is commonly known as Moravela,

Morbel (Marathi), Devashreni, Devi, Dhanurguna, Dhanurmala (Sanskrit), Churahar (Hindi) (Shah and Gohil, 2012). *C. triloba* is an annual climber (figure.1), nearly 1-3m long, found mainly in the Deccan region of Maharashtra, Karnataka and Madhya Pradesh. Stems are hairy-velvet and woody at base. Leaves are either simple or trifoliate, 3-5 cm with ovate base, leaf margin is majorly 3-7 lobed or suddenly entire, leaves commonly seen in 3-lobed. Leaf stalks are slender, twinning with 2-8 cm length. Flowers are white, fragrant, occurs in the form of panicles in leaf axils. Sepals are 4-6 in number. Stamens are shorter, infinite in numbers and arise from the centre of the flower. Flowers have 4-6 white sepals, 1-2 cm long, oblong. Flowering observes in the month of September to December (Bhogaonkar and Devarkar, 2012).

C. triloba is having various traditional medicinal uses likewise the juice from the leaves was applied against itching on the body caused by ringworm infection (Natarajan and Paulsen, 2000). Plant used against syphilis, leprosy, scrofula, chronic fever, skin disease, it is also used in snake bites, diabetes, fever, anthelmintic activity, antipyretic activity, roots are antidiabetic (Shah and Gohil, 2012). Flower juice used to remove black head, acne, and black spots (Bhogaonkar and Devarkar, 2012). In Ayurveda, *Clematis triloba* is used to eliminate malarial fever and headache. Roots extract are given orally to produce bile salt. Oral dose of root decoction gives bilious vomiting. Leaf juice is used against cardiac disorders and blood diseases. Root decoction with boiled rice is given to the childrens as an anthelmintic (Mahekar and Yadav, 2006) as ethanol extract of *C. triloba* roots showed potent anthelmintic activity (Dwivedi et al, 2009).



Figure:1. Flowering twig of *C. triloba*.

Materials and Methods

Plant Material

Plant material such as leaves, stem and flowers were collected from road sides of Chikhaldara to Paratwada in the month of November, 2024 during flowering period.

Extraction Procedure

Plant parts of *C triloba* were collected and brought to laboratory. Plant parts were washed with water followed by shade drying. Dried parts were pulverised and subjected to extraction in soxhlets apparatus using petroleum ether, acetone, and chloroform. The extracts were screened to identify the presence or absence of alkaloids, carbohydrates, terpenoids, tannins, phenols, anthraquinones, saponins, flavonoids, phlobatannins, glycosides (Morankar and Jain, 2019).

Detection of Carbohydrate:**Benedict's test-**

To 0.5 ml of extract, 0.5 ml of Benedict's reagent was added. The mixture is heated on a boiling water bath for 2 minutes and the result was observed. A red precipitates indicated presence of sugar.

Detection of Terpenoid:

Chloroform (2 ml) and concentrated sulphuric acid was added carefully to 0.5 ml of extract. Formation of red brown color at the interface indicated the presence of terpenoid.

Detection of Saponin:

Distilled water 2 ml was added of each plant extracts and shaken in a graduated cylinder for 15 minutes lengthwise. Formation of 1cm foam indicates the presence of saponin.

Detection of Alkaloids:

To a 1 ml of filtrate, few drops of Wagner's reagent are added by the side of the test tube. The color change was observed. A reddish-brown precipitates confirms the test as positive.

Detection of Tannin:**Ferric chloride test-**

The extract (5 mg) was dissolved in 5 ml of distilled water and few drops of neutral 5% ferric chloride solution were added. The formation of blue green color indicated the presence of tannins.

Detection of Flavonoids:

An aqueous solution of the extract was treated with ammonium hydroxide solution. The yellow fluorescence indicated the presence of flavonoids.

Detection of Phenol:**Lead acetate test-**

The extract (5 mg) was dissolved in distilled water and 3 ml of 10% lead acetate solution was added. A bulky white precipitates indicated the presence of phenols.

Detection of Anthraquinones:

Few drops of 2% HCL were added to 0.5 ml of root extract. Appearance of red color precipitate indicated presence of anthraquinones.

Detection of Phlobatannins:

Few drops of 10% ammonia solution were added to 0.5 ml of root extract. Appearance of pink color precipitates indicated the presence of phlobatannins.

Detection of Glycosides:**Legals test-**

Chloroform (3ml) and ammonia solution (10%) was added to 2ml plant extract. Formation of pink color indicated the presence of glycosides.

Result

Preliminary phytochemical analysis of *C. triloba* aerial parts is shown in Table 1. Petroleum ether extract of *C. triloba* leaves and stem showed presence of alkaloids, terpenoids, saponins while in flower extract tested negative for the same. Acetone extract reported occurrence of carbohydrates, alkaloids, terpenoids and flavonoids in stem and flowers while leaves reported presence of only terpenoids and saponins (figure 2). Chloroform extract of stem and flowers tested positive for carbohydrates, terpenoids and saponins (Table.1).

Table 1: Qualitative phytochemical analysis of *C. triloba* leaf, stem and flowers.

Constituents	Petroleum ether			Acetone			Chloroform		
	Leaves	Stem	Flowers	Leaves	Stem	Flowers	Leaves	Stem	Flowers
carbohydrates	-	-	-	+	++	++	++	++	++
alkaloids	+	+	-	-	+	+	-	-	+
terpenoids	+	+	-	++	++	++	-	+	+
tannins	-	-	-	-	-	-	-	-	-
phenols	-	-	-	-	-	-	-	-	-
anthraquinones	-	-	-	-	-	-	-	-	-
saponins	+	+	-	+	-	-	-	+	+
flavonoids	-	-	-	-	-	+	-	-	-
phlobatannins	-	-	-	-	-	-	-	-	-
glycosides	-	-	-	-	-	-	-	-	-



Fig.2 Preliminary screening of extract showing the presence of alkaloids, terpenoids, saponins and carbohydrates.

Conclusions

C. triloba is an important medicinal plant widely used in the biomedical and pharmaceutical fields. The qualitative phytochemical screening of *C. triloba* shows the occurrence of carbohydrates, terpenes, saponin, alkaloids as a major chemical compounds. Further investigations on essential oil and other pharmacological action needs to be undertaken in near future.

Reference

1. Bhogaonkar P Y and Devarkar V D (2012) Ethnomedicinal plants used in skin treatments by Korkus of Melghat dist. Amravati (MS), India, Life Science Leaflet: 178-191.
2. Chavan J J, Kshirsagar P R and Gaikwad N B (2012) Rapid in vitro propagation of Clematis heynei M. A. Rau: an important medicinal plant. Emirates Journal of Food and Agriculture. 24: 79-84.
3. Gad HA, El-Ahmady SH, Abou-Shoer MI and Al-Azizi MM (2013) Application of chemometrics in authentication of herbal medicines: a review, Phytochem Anal.24(1):1-24.

4. Morankar P and Jain A P (2019) Extraction, Qualitative and Quantitative Determination of Secondary Metabolites of Aerial Parts of *Clematis heynei* and *Solanum virginianum*, Journal of Drug Delivery and Therapeutics, 9(1):260-264.
5. Nasim N, Sandeep I S and Mohanty S (2022) Plant-derived natural products for drug discovery: current approaches and prospects, Nucleus.65:399–411.
6. Natarajan B. and Paulsen B S (2000) An Ethnopharmacological Study from Thane District, Maharashtra, India: Traditional Knowledge Compared with Modern Biological Science, Pharmaceutical Biology. 38(2):139-151.
7. Pande J, Donga S and Chanda S (2018) Pharmacognostic studies of leaf and stem of *Lavandula bipinnata* (Roth) Kuntze collected during Nakshatra days and normal days, The Pharma Innovation Journal. 7(12): 128-138.
8. Ramakrishnan R., Samyadurai P and Thangapandian V (2013) Qualitative Phytochemical Analysis and In Vitro Antibacterial activity of *Glossocardia bosvallia* (Linn. f.) Dc. - An Important Ayurvedic Medicinal Herb, Research Journal of Pharmacy and Technology. 6(12):1391-1396.
9. Rana K G and Nagar P S (2017) Diversity and Distribution of Endemic Angiosperms in Gujarat, International Journal of Advanced Research. 5(6): 730-758.
10. Shah Priyank J and Gohil Kashmira J (2012) Preclinical Evaluation of Antidiabetic Activity of Root Extracts of *Clematis triloba* Heyne in Wistar Rats, Inventi Rapid: Ethnopharmacology. (2012)3: 1-7.
11. Singh R J, Lebeda A and Tucker O (2012) Medicinal plants- nature's pharmacy, Genetic resources, chromosome engineering, and crop improvement. Medicinal plants, Boca Raton: CRC Press; 6: 13-51.

Adsorptive Removal of Heavy Metal-Cr from Aqueous Solution using Banana Peel Powder as a Bio Adsorbent

Manoj A. Pande^{1*}

^{*1}Department of Chemistry, Moolji Jaitha College, Jalgaon, Maharashtra-452001

Email : pandemanoj82@gmail.com

ARTICLE INFO

Article History:

Accepted : 01 Jan 2025

Published : 10 Jan 2025

Publication Issue :

Volume 12, Issue 7

January-February-2025

Page Number :

674-676

ABSTRACT

Various industries like mining operations, battery manufacturing, electroplating, semiconductors, etc. contribute to significant pollution of water. In this research, banana peel was synthesized as bio adsorbent to remove heavy metals from contaminated water. Removing heavy metals with a low-cost adsorbent is a productive and sustainable method of reducing pollution. Bio-adsorbents made from Banana Peels were successfully implemented for removing heavy metal Chromium from aqueous solution.

Keywords : Heavy Metal, Bio Adsorbent, Environment, Green Chemistry.

Introduction:

The majority of heavy metals are poisonous or hazardous, and they have an adverse influence on human health as well as aquatic life by being mutagenic, carcinogenic, and genotoxic. Chromium exists in tri-valent and hexavalent form are mutagenic and carcinogenic to animals and humans. Banana is the most important fruit of consumption in the world. However, the majority of available banana peels are underutilized and disposed of as bio-waste despite their high potential for adsorbent. Hence, an attempt was made to study the adsorptive removal of chromium by using banana peels as a bio adsorbent.

Utility of banana peel as adsorbent is reported in the literature but its applicability for removal of heavy material is less studied.

Materials and Methods:

Preparation of Absorbent Material: -

Banana peel from banana fruit was collected from the local market cleaned by washing with distilled water. Banana peels were dried in sunlight for 3-4 days and cut in to small pieces and pieces grounded and sieved to get fine powder.



Dried Banana Peel



Banana Peel Powder

Methods

I. Stock solution of chromium was prepared by separately dissolving appropriate quantity of analytical grade Potassium Dichromate in distilled water. 0.00004 N Potassium Dichromate solution in 1000ml distilled water was prepared.

II. 50ml of this Potassium Dichromate solution in 7 Conical Flask is taken.

III. The pH of these solutions was adjusted to pH= 1 to 7 by using NaOH and HCl solution with the help of pH meter.

IV. 0.1-gram banana powder was added to each 7 conical flasks.

V. These solutions were stirred for 1hr and filtered the solution with Whatman filter paper no. 41.

VI. The absorbance of solutions was measured by UV-Visible Spectrophotometer.



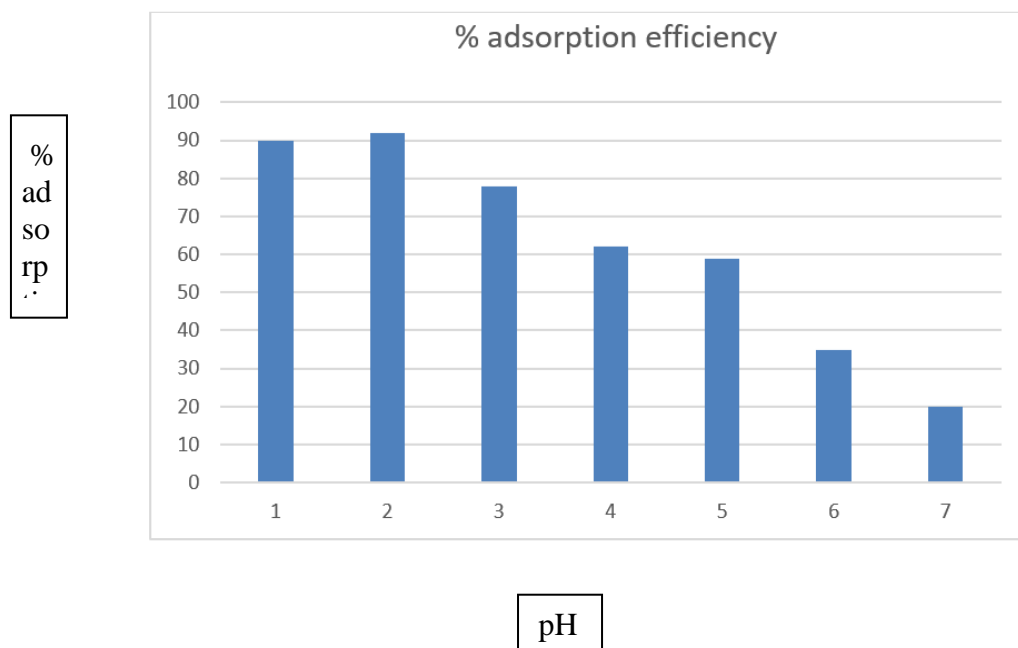
Stock Solution



Prepared Samples

Result and discussion

1. The effect of pH on adsorption was studied. The effect of pH on the removal of chromium using banana peel is that increasing the pH reduces the adsorption capacity and percentage of removal. The optimal pH for removing chromium using banana peel is upto 3.



CONCLUSION

This study demonstrated that banana peel is suitable adsorbent for Heavy Metal removal in a batch study process. The various functional group present in banana peel enhance the adsorption of chromium.

Acknowledgement: Author is thankful to development section KBC-NMU, Jalgaon for financial assistance under VCRMS.

References.:

1. Efficient removal of methylene blue from aqueous solutions using magnetic graphene oxide modified zeolite J. Colloid Interface Sci. (2019).
2. Dye and its removal from aqueous solution by adsorption: a review Adv. Colloid Interface Sci. (2014)
3. Applicability of agricultural waste and by-products for adsorptive removal of heavy metals from wastewater. Bioresource Technology (2013)
4. Use modified wheat bran to remove chromium (VI) from aqueous solutions. Food Chemistry (2014).
5. Removal of hexavalent chromium from aqueous solution by agricultural waste biomass. Journal of Hazardous Materials (2007).

Evaluation of the corrosion inhibition properties of Bouhunia Racemose Leaves Extracts for mild steel in 1 M H₂SO₄ solution on basis of Thermodynamics and adsorption study.

Yogesh Pawar¹, Dhanashri Panchbhai²

¹Department of chemistry ,ResearchScholar , AnandNiketan College, Warora

²Department of chemistry , Faculty of Chemistry , Anand Niketan Collge , Warora

Corresponding Author* Email: ghanashripanchbhai@gmail.com

ARTICLE INFO

Article History:

Accepted : 01 Jan 2025

Published : 10 Jan 2025

Publication Issue :

Volume 12, Issue 7

January-February-2025

Page Number :

677-688

ABSTRACT

This research work examines the thermodynamic parameters and adsorption mechanism of the extract of Bouhunia racemosa leaves on mild steel in a 1.0 M sulfuric acid solution . as a corrosion inhibitor for mild steel in a 1 M H₂ SO₄ solution. The gravimetric method was utilized to determine the efficiency of inhibition and corrosion rate. Appropriate thermodynamic equations were employed to ascertain the activation energy, change in enthalpy, and change in entropy. The adsorption isotherms were employed to assess the change in Gibbs free energy. The findings of the study indicate that the activation energy of the inhibited process was greater in comparison to the uninhibited process. Furthermore, the change in enthalpy was negative and below the threshold of 100 KJ/mol. The adsorption study demonstrated that the data conformed to the Langmuir, Flory-Huggins, El-Awady's, and Temkin isotherms, with Langmuir adsorption providing the best fit. The change in Gibbs free energy for adsorption was negative and below the threshold of 20 KJ/mol. As inferred from the results, the Bouhunia racemosa L Extract adsorption of mild steel in a 1 M H₂ SO₄ solution medium is viable, spontaneous, and occurs through physical adsorption.

KEYWORDS :- Corrosion, Adsorption isotherm thermodynamics

Corrosion inhibition Inhibitor adsorption Bauhinia racemosa L. Corrosion rate Mild Steel

1.Introduction

The corrosion of mild steel poses a substantial obstacle in industrial processes because of its exposure to corrosive acids, alkalis, and salt solutions. Consequently, there has been an increasing fascination in

conducting research to mitigate the harmful impact of corrosion on metals and their alloys. [1, 2]. Inhibitors composed of organic materials are capable of impeding corrosion through the process of adsorption. As a result, inhibitors that can adsorb onto the metal surface hinder the dissolution or corrosion reaction of the metal in the corrosive medium. Natural plant extracts have been identified as effective green corrosion inhibitors for mild steel [3]. Moreover, these extracts have been found to be cost-effective, biodegradable, renewable, highly efficient, and environmentally friendly methods of inhibiting corrosion rate in mild steel [4, 5]. Understanding of the thermodynamic parameters linked with these inhibitors is essential for evaluating their efficacy in retarding the corrosion rate in corrosive environments at a specific temperature throughout the procedure. Extensive investigations have been carried out on the adsorption and thermodynamic behavior of organic inhibitors, particularly plant extracts, on mild steel in acidic mediums [6–15]. The spontaneity of the adsorption process is determined by the sign of the Gibbs free energy of adsorption, ΔG_{ads} . Additionally, the magnitude and sign of ΔG_{ads} are influenced by the value of adsorption equilibrium constant K_{ads} . When the rate of adsorption is higher than desorption, the ΔG_{ads} is negative, which indicates spontaneous adsorption. ΔG_{ads} value less than 20 KJ/mol indicates physical adsorption while 40 KJ/mol and above is an indication for chemical adsorption [6–13]. Manimegalai and Manjula [16], reported that the adsorption of *Sargassum swartzii* on mild steel in aqueous medium obeys Langmuir, Temkin and Freundlich adsorption isotherms. They also reported that the ΔG_{ads} value obtained indicated dynamic and spontaneous adsorption of the *Sargassum swartzii* extract components on the metal. Vivek Sharma et al. [17], reported adsorption of *Musa Paradisiaca* extract as a green inhibitor for corrosion of mild steel in 0.5 M sulphuric acid solution. Adsorption of the inhibitor molecules of the extract on mild steel surface was found to obey Langmuir adsorption isotherm. An increase in the activation energies of the corrosion process indicated that *Musa paradisiaca* extract could inhibit the corrosion rate of mild steel in 0.5 M H_2SO_4 solution. The negative values of ΔG_{ads} and ΔH revealed that the inhibition of corrosion of mild steel through adsorption is spontaneous and exothermic. The researchers concluded that both physical and chemical adsorption are involved in the adsorption process. Umoren et al. and Alinnor and Ejikeme [18], also reported negative ΔG_{ads} adsorption for some other green inhibitor systems have been studied by Avci [19,20], who noted that a ΔH value greater than 100 KJ/mol suggests chemical adsorption, while a ΔH value less than 100 KJ/mol suggests physical adsorption. A corrosion inhibition study of hydrazones derived from thiophene derivatives was conducted by Singh et al. [21]. The authors found that the inhibitor effectively reduced the corrosion rate according to the Langmuir adsorption isotherm. Elmsellem, H., et al. [22] investigated the corrosion inhibition of mild steel in acidic media using synthetic anti-biotic derivatives inhibitors. They observed stable and spontaneous corrosion inhibition, with the involvement of a chemisorption process indicated by the evaluated values of free energy change. The adsorption data was well fitted in Langmuir isotherm. Kenith kanayo et al. [23] explored the use of *Jatropha curcas* leaves extract as a corrosion inhibitor for mild steel in 1 M hydrochloric acid. Their investigation demonstrated that *Jatropha curcas* exhibited good inhibition potentials. Based on the results, an adsorption mechanism involving chemisorption was proposed, with an increase in inhibition efficiency observed with increasing temperature. Joseph Olusegun et al. [24], reported corrosion inhibition and adsorption mechanism studies of *Hunteria umbellata* seed husk extracts on mild steel immersed in 1 M HCl and 1 M H_2SO_4 . *Hunteria umbellata* corrosion inhibition efficiency was found to be higher in 1 M HCl than in 1 M H_2SO_4 . Chauhan and Gunasekaran [25], reported corrosion inhibition potentials of *Zenthoxylum alatum* extract on mild steel in dilute HCl medium. The adsorption of the extract on the mild steel surface was reported to obey the Langmuir [26] studied the effect of Aloe Vera gel on mild

steel corrosion in 1 M HCl medium, and the activation parameters showed that the inhibitor is adsorbed by both physisorption and chemisorption. The thermodynamics and kinetic inhibition of aluminum in hydrochloric acid medium by date palm leaf extract have also been studied, and the result showed that hot-water extract of date palm leaves has inhibition efficiency (IE) of 40–88% at the tested conditions. There is a shortage of information on the thermodynamic parameters and adsorption characteristics *Bouhunia racemosa* leaves extract as a corrosion inhibitor for mild steel in 1.0 M sulfuric acid medium. Hence, this study addresses the evaluation of the thermodynamics and adsorption parameters such as activation energy, enthalpy change, entropy change, adsorption equilibrium constant and free energy change of corrosion inhibition potentials of *Bouhunia racemosa* Leaves on mild steel in acid medium.

2. Experimentals

2.1.1 Method of extraction

2.1 *Bauhinia racemosa* leaves were collected and shadow dried for 7 days then ground to make powder then 10 gm of leaves powder mixed with 500ml of water kept for three days then mixture was heated at 60°C for 8 hr, cooled and filter collect the extract which is there after concentrated at 60°C dry powder was collected this extract used for inhibitor preparation

2.1.2 Materials and samples preparation

Materials Mild Steel specimen with a dimension of 5 cm x 1.8 cm x 0.3 cm and compositions with elemental composition (wt. %) of 93.9% Fe, 1.2% P, 1.1% Mn, 1.0% Si, 0.7% Cr and 1.7% Ni were employed for weight loss and surface morphological studies. After abrading with different grades of sand papers (400, 600, 800, and 1000), the samples were thoroughly washed and degreased by acetone and distilled water. Lastly, the specimen were dried at room temperature. The H₂SO₄ solution (1 M) was prepared by sulfuric acid (purity-98%) (Merck Co.) and distilled water.

2.3. Weight loss measurement

Mild steel coupons was weighed and immersed in 100 ml solution of 1 M solution of sulfuric acid containing 0.05 g, 0.1, 0.2, 0.4, 0.6 g of *Bouhinia Racemosa* leaves extract in an open beaker a constant temperature was maintained 303, 313, 324, & 333 K after duration of each 2 hr specimen was removed, clean and reweighed. The method chosen for calculating the average weight loss (ΔW), corrosion rate (CR), and corrosion inhibition efficiency (η %) were reported various literature [3-6]

The following equations were used in evaluating the effect of the extract: weight loss (Equation 1), corrosion rate (Equation 2), surface coverage (Equation 3) and percent inhibition efficiency (% IE) of the inhibitors (Equation 4)

$$\Delta W = W_2 - W_1 \quad (1)$$

$$CR = \frac{\Delta W}{\rho A t} \quad (2)$$

$$\theta = \left(1 - \frac{w_1}{w_2}\right) \quad (3)$$

$$\%IE = \theta \times 100 \quad (4)$$

Where ΔW is the change in mass in mg, w_1 and w_2 are initial and final mass, respectively. In Equation 2, CR represents the corrosion rate in mm/y, ρ is the density of stainless steel in g/cm³, A is the area of the MS Coupons in cm² and t is the time in hours. The weight loss of the coupon in the electrolyte with the Bouhinia Racemosa inhibitor w_1 and w_2 is the initial and final weight of the coupon. The surface coverage of the inhibitor on the surface of the stainless steel is θ , w_1 and w_2 are the change in mass of stainless steel in solution with inhibitor and without inhibitor.

2.2. Determination of activation energy (E_a)

The plot of log of corrosion rate, C_R against $1/T$ in Eq. (3) gives a slope from which the activation energy, E_a was estimated. The Arrhenius equation described the relationship between the corrosion rate (C_R) and temperature (T) as [12,27]:

$$\log C_R = \frac{-E_a}{2.303RT} + \log \gamma \quad (3)$$

E_a is the activation energy, R is the gas constant, T is the temperature in Kelvin and γ is the exponential factor.

2.3 Determination of enthalpy and entropy change

Enthalpy change and entropy change were evaluated through Equation 4, an alternative formula for the Arrhenius equation in the transition state [27]:

$$C_R = \frac{RT}{Nh} \exp\left(\frac{\Delta S}{R}\right) \exp\left(\frac{\Delta H}{RT}\right) \quad (4)$$

Equation 4 is linearized, thus

$$\frac{\log C_R}{T} = \frac{\log R}{Nh} + \log\left\{\exp\left(\frac{\Delta S}{R}\right)\right\} + \log\left\{\exp\left(\frac{\Delta H}{RT}\right)\right\}$$

$$\text{Since } \log\{\exp(x)\} = \frac{x}{\ln 10}$$

Therefore equation 4b become

$$\frac{\log C_R}{T} = \frac{\log R}{Nh} + \log\left(\frac{\Delta S}{R \ln 10}\right) \exp\left(\frac{\Delta H}{RT \ln 10}\right) \quad (4C)$$

$$\log \frac{C_R}{T} = \frac{-\Delta H}{2.303 R} \left(\frac{1}{T}\right) + \left[\log \frac{R}{Nh} + \left(\frac{\Delta S}{2.303 R}\right)\right]$$

Where h is the Planck's constant, N is the Avogadro's number, ΔS is the entropy, ΔH is the enthalpy change. The slope $\frac{-\Delta H}{2.303 R}$ of the plot of $\log \frac{C_R}{T}$ Vs $\frac{1}{T}$ gives the idea about ΔH and the entropy change ΔS was evaluated from the intercept

$$\left[\log \frac{R}{Nh} + \left(\frac{\Delta S}{2.303 R}\right)\right] \text{ of the same plot.}$$

2.4 Adsorption isotherm

The adsorption isotherm studies provide a comprehensive explanation of how the organic inhibitors adhere to the metal surface [27].

To determine the most suitable adsorption isotherm model for the adsorption of BRL extract on mild steel in a 1 M sulfuric acid medium, the corrosion rate (CR) and the degree of surface coverage of the inhibitor (θ),

which is the reciprocal of the inhibition efficiency, were fitted into various adsorption isotherm models (Langmuir, Tempkin, Freundlich, Frumkin, El Awady, and Flory Huggins adsorption isotherm) expressed in linear form.

The Langmuir adsorption isotherm model [19,27] was found to be the most appropriate model.

$$\frac{CR}{\theta} = \frac{1}{K_{ads}} + C$$

Frumkin adsorption Isotherm model

$$\log \left[\log CR \left(\frac{\theta}{1-\theta} \right) \right] = 2a\theta + 2.303 \log K_{ads}$$

El-Awady's thermodynamic/kinetic adsorption isotherm model

$$\log CR \left(\frac{\theta}{1-\theta} \right) = y \log CR + \log K$$

$$K_{ads} = K^{1/Y}$$

Temkin adsorption isotherm model [13,19,27]:

$$\theta = \ln CR + K_{ads}$$

Freundlich adsorption isotherm [6,27]:

$$\log \theta = \log K_{ads} + n \log CR$$

Flory-Huggins adsorption isotherm [27]:

$$\log \frac{\theta}{CR} = b \log(1 - \theta) + \log K_{ads}$$

2.5 Determination of adsorption thermodynamics parameters

The expression for Gibb's free energy change of adsorption,

ΔG_{ads} presented in Equation (12) [27] was used to investigate the feasibility and nature of the adsorption.

$$\Delta G_{ads} = -RT \ln(55.5 K_{ads})$$

K_{ads} is the adsorption equilibrium constant obtained from the isotherm, and the number 55.5 is the molar concentration of water in solution.

Result and discussion

3.1 Effect of temperature & time on inhibitor efficiency

It is observed that inhibitor efficiency (% IE) increases as increase in inhibitor concentration, from 0.05, 0.1, 0.2, 0.4 g/l in 1 M H₂SO₄ solution the experiment was carried out in temperature Range from 303 to 324 K % IE also increases from 303K to 324 K further decrease with higher temperature greater than 324 K prolong immersion time shows better efficiency. At 2 hr. shows minimum IE and highest at 6 hours of immersion and above decreases from the above observation we can say that inhibition efficiency increased with immersion time. This is because, at such a relatively low extract concentration, considerable time is required for sufficient adsorption to take place. For the same reason, the lowest inhibition efficiency was observed at 2 h immersion time and highest at 6 h immersion time. For each immersion time, inhibition efficiency was found to increase

with temperature initially but later declined. The decline was sharpest at 6 h immersion time possibly because the inhibitor could not withstand high temperature for such a long period. Distortion of the extract molecular structure might occur at a higher temperature. data matches with previous study of researcher [13,27], an increase in temperature may also increase the solubility of the protective films of the metals, thus, increasing the susceptibility of the metal to corrosion.

The corrosion rate decreased with immersion time and increased with temperature. The observation is accurate because reaction rates generally decrease with time and increase with temperature. The increase in the rate of corrosion of mild steel could be due to the rise in the average kinetic energy of the reacting molecules. The trend obtained for the corrosion rate is in agreement with the result reported by V. N. Atasie et al [27]

Table No-1 (inhibition efficiency at different immersion time & Temperature)

Con c BR L extr act gm/l	% Inhibition Efficiency 2 hours immersion			% Inhibition Efficiency 4 hours immersion			% Inhibition Efficiency 6 hours immersion		
	Tempera ture 303 K	Tempera ture 313 K	Tempera ture 324 K	Tempera ture 303 K	Tempera ture 313 K	Tempera ture 324 K	Tempera ture 303 K	Tempera ture 313 K	Tempera ture 324 K
Blan k	31	29.16	25.18	28.5	25.44	23.5	25.09	23.22	18.89
0.05	57.7	67.8	75	63.64	76.26	78.33	74.33	78.69	81.26
0.1	62.1	72.2	80	65	83.31	80.5	79.46	84.39	86.54
0.2	71.9	82	82.5	75.55	89.54	91.22	87.51	92.02	95.30
0.4	74	85.88	87.6	83.04	92.13	95.13	93.26	96.36	97.21

Table No-2 (corrosion Rate at different immersion time & Temperature)

Con c BR L extr act gm/l	Corrosion Rate (mg cm ⁻² h ⁻²) 2 hours immersion			Corrosion Rate (mg cm ⁻² h ⁻²) 4 hours immersion			Corrosion Rate (mg cm ⁻² h ⁻²) 6 hours immersion		
	Tempera ture 303 K	Tempera ture 313 K	Tempera ture 324 K	Tempera ture 303 K	Tempera ture 313 K	Tempera ture 324 K	Tempera ture 303 K	Tempera ture 313 K	Tempera ture 324 K
Blan k	4.88	5.01	5.24	5.04	5.27	5.41	5.30	5.43	5.79
0.05	2.99	2.28	1.77	2.27	1.68	1.53	1.99	1.50	1.27
0.1	2.68	1.96	1.41	2.49	1.91	1.38	1.46	1.11	0.99
0.2	1.99	1.27	1.04	1.73	0.74	0.62	1.01	0.88	0.35
0.4	1.84	0.85	0.88	1.20	0.55	0.35	0.8	0.52	0.21

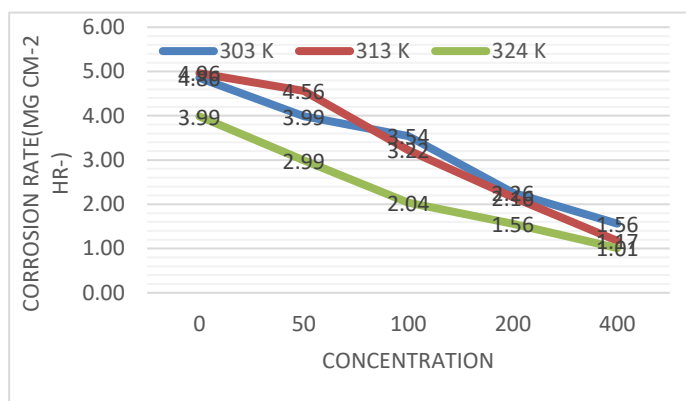


Figure no -1 (corrosion rate Vs concentration)

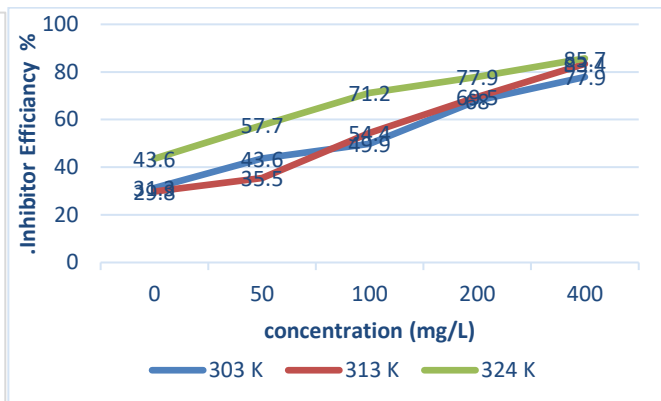


Figure no-2(inhibitor efficiency Vs concentration)

3.2 Activation energy-

The plot of log CR against $1/T$ at various immersion time the slope of the plot gives an idea about activation energy, the calculated activation energy was presented in following (table-3)

Data shows that activation energy value for inhibited process was higher than uninhibited process. The adsorption process was physisorption according to data, higher the value of E_a in presence of inhibitor was due to the increase in energy barrier this incidence also confirms that formation of complex in between inhibitor molecule and MS Surface.[27] result suggest that the corrosion inhibition behavior shown by Bouhinia Racemosa leaves extract is feasible because of increase in energy barrier for metal dissolution process, the formation of thin film on metal surface resist both energy and mass transfer due to which activation energy increases.

The activation energy decreases as inhibitor concentration increases however the E_a is still higher than that of uninhibited solution this result aligns with many of the previous researcher [27]

After 6 hours of immersion time IE decreases this because of inhibitor fail to creating E_a barrier for such a long time ,the inhibitor molecule may degraded hence fail to form and stand adsorption layer around the M.S Surface.

Table no-03. Activation parameters at 2 hours Activation parameters at 4 hours Activation parameters at 6 hours

Extra ct Conc.	Ea (KJ/m ol)	ΔH (KJ/mol)	ΔS (J/mol/ K)	Ea (KJ/m ol)	ΔH (KJ/m ol)	ΔS (J/mol/ K)	Ea (KJ/m ol)	ΔH (KJ/m ol)	ΔS (J/mol/K)
Blank	3.14	—	—	-2.67	—	—	-3.44	—	—
0.05 g/l	20.38	9.98	—49.62	20.10	9.86	—49.96	11.89	6.29	—39.28
0.1 g/l	24.97	11.97	—56.58	41.61	19.20	—81.13	15.07	7.68	—44.70
0.2 g/l	25.18	12.60	—58.12	39.76	18.40	—79.78	35.85	16.70	—76.17
0.4 g/l	28.52	13.52	—63.54	50.13	22.90	—95.72	32.06	15.05	—73.21

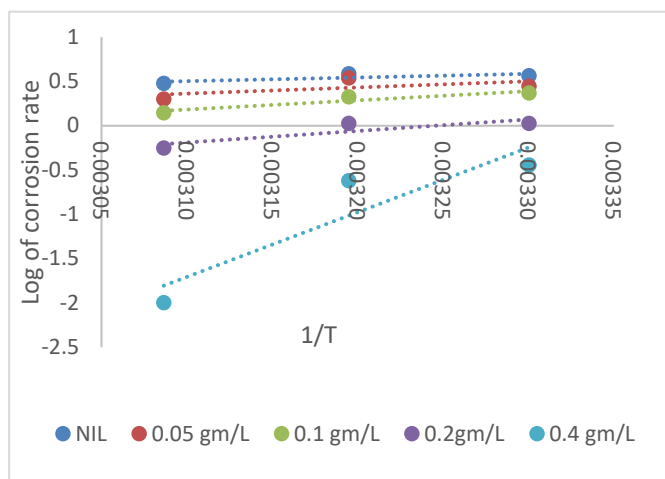


Figure no-3

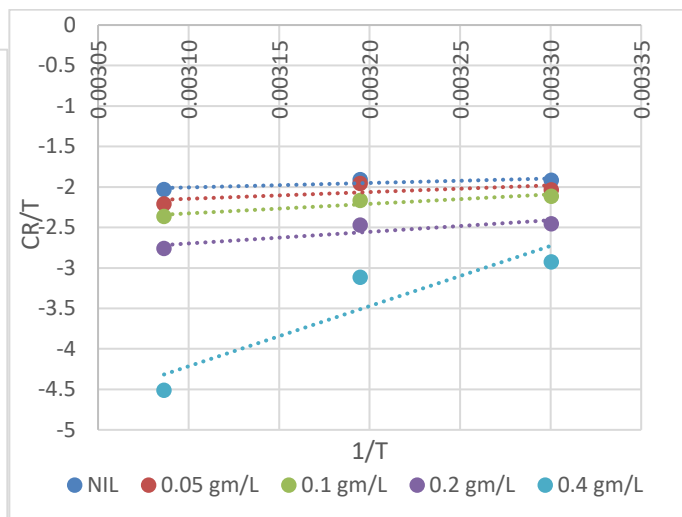


figure no-4

3.3 Enthalpy and Entropy change

The value of enthalpy change ΔH and Entropy changes ΔS obtained at different immersion time was given in given in Table no-3

ΔH was positive and got increasing with immersion time and bellow 40KJ/mol-1 indicate endothermic reaction and physisorption process and entropy ΔS value increases with immersion time shows disturbance at mild steel surface which favors spontaneity of adsorption desorption process on metal surface

3.4 Adsorption Isotherm

Different adsorption isotherm models are considered for the present work such as Langmuir adsorption isotherm Flory Huggins and Temkin Adsorption isotherm El-Adway thermodynamic/kinetic models but the Langmuir model suits best, for the study the R² Data presented in table No- 4 and figure 5-9 the positive value of Adsorption equilibrium constant increasing with temperature indicates feasibility of Adsorption. The values of Gibbs free energy is negative and less than 20 KJ that mesne adsorption process is spontaneous, the electrostatic forces of attraction present between inhibitor molecule and metal surface which favors physical adsorption of molecule on mild steel surface.

R² Value of various adsorption isotherm considered

Temperat ure K	Flory- Huggin's isotherm	El-awady's isotherm	Freundlich isotherm	Langmuir Adsorption	Temkin isotherm
303 K	0.9623	0.9527	0.9803	0.9974	0.9514
313 K	0.9484	0.9714	0.9813	0.9984	0.9739
324K	0.9334	0.9779	0.9839	0.9988	0.9935

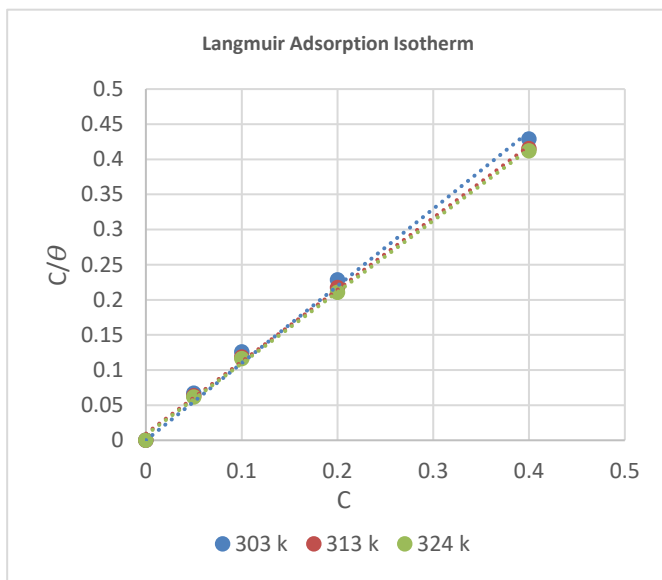


Figure -5

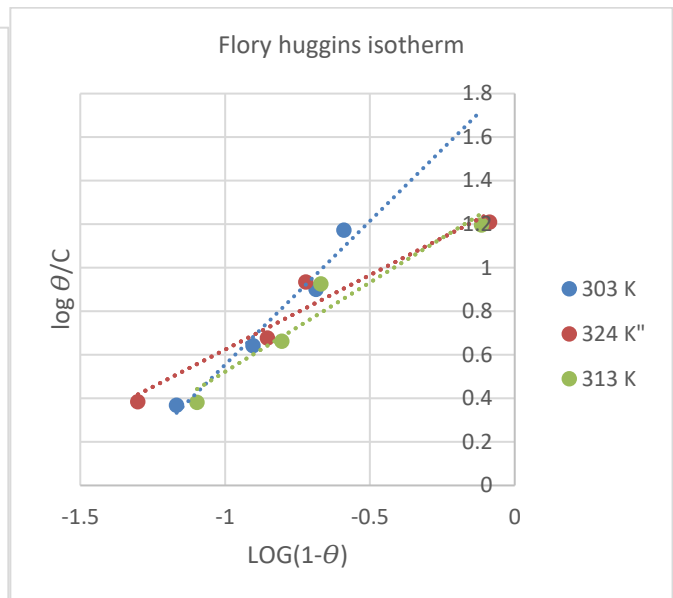


Figure -6

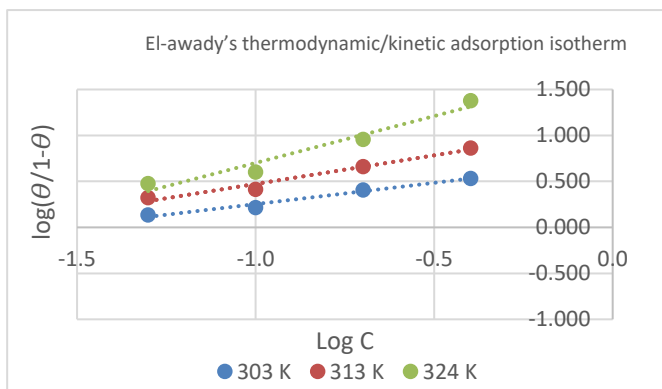


Figure -7

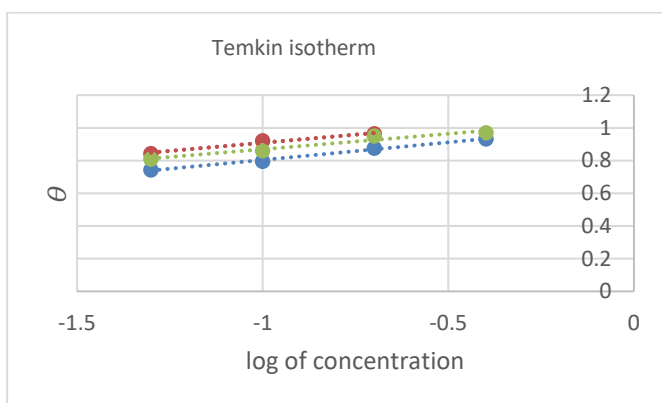


Figure -8

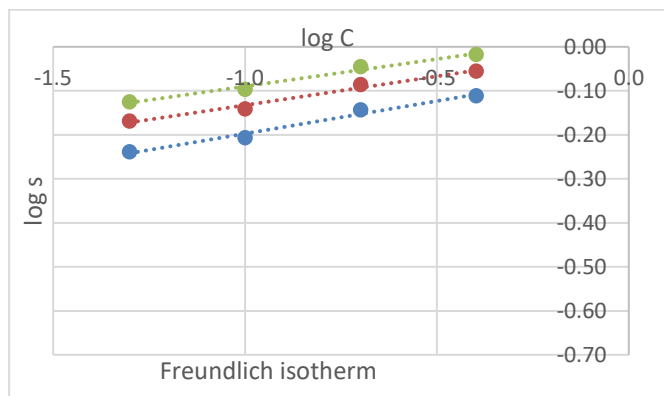


Figure -9

Adsorption parameters

Temperature K	ΔG (KJ/mol)	K_{ads} (mol^{-1})
303 K	-3.94	0.0861
313 K	-4.63	0.1067
324 K	-5.31	0.1293

Table No-5

3.4.1 Adsorption equilibrium constant

Table 5 shows the adsorption equilibrium constants obtained at various temperatures from the intercept of the Langmuir plot. The adsorption equilibrium constants, K_{ads} are positive, indicating the feasibility of the adsorption of the inhibitor to the metal surface. The adsorption equilibrium constant increases with temperature up till 324K above this temperature decreases, this indicates that at a higher temperature, the adsorbed inhibitor tends to desorb back from the mild steel surface. This result further confirms the trend obtained for activation energy.

3.4.2 Gibb's free energy change of adsorption

Presented in Table 5 is Gibb's free energy change of adsorption, ΔG_{ads} got at different temperatures. As shown in the table, the ΔG_{ads} are negative and less than 20 kJ/mol. This result indicates that adsorption of the extract of *Bouhinia Racemosa* on mild steel surface is spontaneous, feasible and occurred according to the mechanism of physical adsorption. The decrease in ΔG_{ads} at 343 K implies there is a reduction in the spontaneity and stability of the adsorption at a higher temperature.

4 Conclusion

From the study it has been concluded that the adsorption of *Bouhinia Racemosa* L. on mild steel in 1. M Sulfuric acid medium is feasible, spontaneous and by physical adsorption according to Langmuir adsorption, isotherm model also supported by other adsorption models. *Bouhinia Racemosa* L extract is more effective in inhibiting mild steel corrosion in acidic medium at temperature below 324 K.

REFERENCES

1. Antunes, Renato Altobelli, and Mara Cristina Lopes de Oliveira. "Corrosion fatigue of biomedical metallic alloys: mechanisms and mitigation." *Acta biomaterialia* 8.3 (2012): 937-962.
2. Stringer, John. "Hot corrosion of high-temperature alloys." *Annual Review of Materials Science* 7.1 (1977): 477-509
3. Popoola, Lekan Taofeek. "Organic green corrosion inhibitors (OGCIs): a critical review." *Corrosion Reviews* 37.2 (2019): 71-102.
4. Verma, Chandrabhan, et al. "An overview on plant extracts as environmental sustainable and green corrosion inhibitors for metals and alloys in aggressive corrosive media." *Journal of molecular liquids* 266 (2018): 577-590
5. Al Jahdaly, Badreah A., et al. "Role of green chemistry in sustainable corrosion inhibition: a review on recent developments." *Materials Today Sustainability* 20 (2022): 100242.
6. Ikpeseni, S. C., et al. "Thermodynamic parameters and adsorption mechanism of corrosion inhibition in mild steel using jatropa leaf extract in hydrochloric acid." *Arabian Journal for Science and Engineering* 46 (2021): 7789-7799.
7. Akinbulumo, Olatunde Alaba, Oludare Johnson Odejobi, and Ebenezer Leke Odekanle. "Thermodynamics and adsorption study of the corrosion inhibition of mild steel by Euphorbia heterophylla L. extract in 1.5 M HCl." *Results in Materials* 5 (2020): 100074.
8. Meriem, Zerroug, et al. "Experimental and theoretical evaluation of the adsorption process of some polyphenols and their corrosion inhibitory properties on mild steel in acidic media." *Journal of Environmental Chemical Engineering* 9.6 (2021): 106482.
9. Ogunleye, O. O., et al. "Green corrosion inhibition and adsorption characteristics of Luffa cylindrica leaf extract on mild steel in hydrochloric acid environment." *Heliyon* 6.1 (2020).
10. Okewale, A. O., and O. A. Adesina. "Kinetics and thermodynamic study of corrosion inhibition of mild steel in 1.5 M HCl medium using cocoa leaf extract as inhibitor." *Journal of Applied Sciences and Environmental Management* 24.1 (2020): 37-47.
11. Reza, Norbaayah Ahmad, et al. "A review on plants and biomass wastes as organic green corrosion inhibitors for mild steel in acidic environment." *Metals* 11.7 (2021): 1062.
12. Abdelaziz, S., et al. "Green corrosion inhibition of mild steel in HCl medium using leaves extract of Arbutus unedo L. plant: An experimental and computational approach." *Colloids and Surfaces A: Physicochemical and Engineering Aspects* 619 (2021): 126496.
13. S. "Plant extracts as corrosion inhibitors for mild steel in HCL media-review I." *International Journal of Corrosion and Scale Inhibition* 10.1 (2021): 145-175.
14. Wei, Hongyu, et al. "Green inhibitors for steel corrosion in acidic environment: state of art." *Materials Today Sustainability* 10 (2020): 100044.
15. Wei, Hongyu, et al. "Green inhibitors for steel corrosion in acidic environment: state of art." *Materials Today Sustainability* 10 (2020): 100044.

16. Manimegalai, S., and P. Manjula. "Thermodynamic and adsorption studies for corrosion inhibition of mild steel in aqueous media by *Sargassum swartzii* (brown algae)." *Journal of Material and Environmental Science* 6.6 (2015): 1629-1637.
17. Mayanglambam, Ramananda S., Vivek Sharma, and Gurmeet Singh. "Musa paradisiaca extract as a green inhibitor for corrosion of mild steel in 0.5 M sulphuric acid solution." *Portugaliae Electrochimica Acta* 29.6 (2011): 405-417.
18. Alinnor, I. J., and P. M. Ejikeme. "Corrosion inhibition of aluminium in acidic medium by different extracts of *Ocimum Gratissimum*." *Am. Chem. Sci. J* 2.4 (2012): 122-135.
19. Khodjamkulov, S. Z., and Misirov Z. Kh. "Salsola Oppositifolia acid extract as a green corrosion inhibitor for carbon steel." *Indian Journal of Chemical Technology (IJCT)* 30.6 (2023): 872-877.
20. Avci, Gülşen. "Corrosion inhibition of indole-3-acetic acid on mild steel in 0.5 M HCl." *Colloids and Surfaces A: Physicochemical and Engineering Aspects* 317.1-3 (2008): 730-736.
21. Singh, Ashish Kumar, et al. "2-Hydroxy-N' -((Thiophene-2-yl) methylene) benzohydrazide: ultrasound-assisted synthesis and corrosion inhibition study." *ACS omega* 3.4 (2018): 4695-4705.
22. Elmsellem, H., et al. "Adsorption and inhibition effect of curcumin on mild steel corrosion in hydrochloric acid." *Russian Journal of Applied Chemistry* 87 (2014): 744-753.
23. Alaneme, Kenneth Kanayo, Sunday Joseph Olusegun, and Oluwabunkunmi Tomi Adelowo. "Corrosion inhibition and adsorption mechanism studies of *Hunteria umbellata* seed husk extracts on mild steel immersed in acidic solutions." *Alexandria Engineering Journal* 55.1 (2016): 673-681.
24. Alaneme, Kenneth Kanayo, Sunday Joseph Olusegun, and Oluwabunkunmi Tomi Adelowo. "Corrosion inhibition and adsorption mechanism studies of *Hunteria umbellata* seed husk extracts on mild steel immersed in acidic solutions." *Alexandria Engineering Journal* 55.1 (2016): 673-681.



**National Conference on Development Trends
and Techniques in Chemical and Material**



Organized By

Department of Chemistry, Meharabpura, Tehsil Road,
Achalpur, Dist: Amaravti, Maharashtra, India

Publisher

Technoscience Academy

Website : www.technoscienceacademy.com

Email : editor@ijsrst.com Website : <http://ijsrst.com>